Dissertation zur Erlangung des Doktorgrades

der Fakultät für Chemie und Pharmazie

der Ludwig-Maximilians-Universität München

Reactivity of Oxygen and Sulfur Nucleophiles and Basicity Scales Toward Heteroatom Lewis Acids

von

Robert Josef Mayer

aus

Kempten, Deutschland

2020

Erklärung

Diese Dissertation wurde im Sinne von §7 der Promotionsordnung vom 28. November 2011 von Herrn PD Dr. Armin R. Ofial betreut.

Eidesstattliche Versicherung

Diese Dissertation wurde selbstständig und ohne unerlaubte Hilfe erarbeitet.

München, den 01.07.2020

_____

Robert J. Mayer

Dissertation eingereicht am: 26.05.2020

1. Gutachter: PD. Dr. Armin R. Ofial

2. Gutachter: Prof. Dr. Hendrik Zipse

Mündliche Prüfung am: 18.06.2020

“A discovery is said to be an accident meeting a prepared mind.”

Albert Szent-Györgyi

Acknowledgment

First, I want to express my deep gratitude to my two supervisors Dr. Armin Ofial and Prof. Herbert Mayr for the opportunity to work in their group, their constant support and mentorship. I want to thank Dr. Armin Ofial for introducing me to the methods and concepts of physical organic chemistry, his time and patience correcting all my drafts with great care and for giving me the freedom and support to follow my ideas. I'm very thankful to Prof. Herbert Mayr for all the discussions not just about chemistry, and all his suggestions to look into the important little details that often evolved into key findings of my different projects.

Furthermore, I want to thank Prof. Claude Y. Legault for his mentorship, open ear to all of my questions and being a great collaboration partner. I'm grateful to him introducing me into coding and guiding me through the field of computational chemistry.

I'm indebted to Prof. Hendrick Zipse for accepting to be reviewing this thesis and Prof. Konstantin Karaghiosoff and Dr. Dorian Didier for their willingness to participate in my defense.

I want to thank all the current and former members of the Mayr/Ofial group for the great environment in the group. First, I want to thank Prof. Guillaume Berionni, with whom I had the pleasure to share my fume hood for the first months of this thesis for great discussions and showing me a lot of tips and tricks, Dr. Daria Timofeeva and Dr. Artem Leonov for being the best possible guides through icy Moscow city, Patrick Jüstel for always having time to talk about the big and small daily challenges, Dr. Li Zhen for being a very patient collaboration partner and for teaching me my first Chinese words, Li Le for being an even better Chinese teacher and Dr. An Feng for his support when I started in the lab.

I'm extremely grateful to Nathalie Hampel, my lab partner for the past three years, who constantly helped me in all the synthetic challenges of my projects. I thank her for her open ear, and especially her introduction into the art of synthesizing all these nicely colored benzhydrylium ions that made the first part of this project possible. Special thanks also go to my F-Praktikantin Amalina Buda for great experimental support.

Finally, I want to thank all my friends and family who supported me during the time of my studies. Last but not least, I'm deeply grateful to Eva-Maria Eckl for her continuous support, love and partnership since almost the very beginning of my time at LMU.

Publications

The present work is a cumulative dissertation comprised of five publications in peer-reviewed journals and one submitted manuscript.

R. J. Mayer, A. R. Ofial,
"Nucleophilic Reactivities of Bleach Reagents",
Org. Lett. **2018**, *20*, 2816-2820.

R. J. Mayer, A. R. Ofial,
"Intramolecular Hydrogen-Bonding Modulates the Nucleophilic Reactivity of Ammonium-Peroxycarboxylates",
Eur. J. Org. Chem. **2018**, 6010-6017.

R. J. Mayer, M. Breugst, N. Hampel, A. R. Ofial, H. Mayr,
"Ambident Reactivity of Phenolate Anions Revisited: A Quantitative Approach to Phenolate Reactivities",
J. Org. Chem. **2019**, *84*, 8837-8858.

R. J. Mayer, A. R. Ofial
"Nucleophilicity of Glutathione: A Link to Michael Acceptor Reactivities",
Angew. Chem. Int. Ed. **2019**, *58*, 17704-17708; *Angew. Chem.* **2019**, *131*, 17868-17872.

R. J. Mayer, A. R. Ofial, H. Mayr, C. Y. Legault,
"Lewis Acidity Scale of Diaryliodonium Ions toward Oxygen, Nitrogen, and Halogen Lewis Bases",
J. Am. Chem. Soc. **2020**, *142*, 5221-5233

R. J. Mayer, N. Hampel, A. R. Ofial,
"Lewis Adduct Formations: Lewis Basicity Scales Towards Boranes",
submitted.

Publications originating from projects performed during the time this thesis was performed which will not be discussed herein:

D. S. Timofeeva, **R. J. Mayer**, P. Mayer, A. R. Ofial, H. Mayr,
"Which Factors Control the Nucleophilic Reactivities of Enamines?",
Chem. Eur. J. **2018**, *24*, 5901-5910.

R. J. Mayer, N. Hampel, P. Mayer, A. R. Ofial, H. Mayr,
"Synthesis, Structure and Properties of Amino-Substituted Benzhydrylium Ions - a Link Between Ordinary Carbocations and Neutral Electrophiles",
Eur. J. Org. Chem. **2019**, 412-421.

A. Eitzinger, **R. J. Mayer**, N. Hampel, P. Mayer, M. Waser, A. R. Ofial,
"Electrophilic Reactivities of Vinyl p-Quinone Methides",
Org. Lett. **2020**, *22*, 2182-2186

J. Zhang, Q. Chen, **R. J. Mayer**, J.-D. Yang, A. R. Ofial, J.-P. Cheng, H. Mayr,
"Predicting Absolute Rate Constants for Huisgen Reactions of Unsaturated Iminium Ions with Diazoalkanes",
Angew. Chem. Int. Ed. **2020**, EarlyView (doi: 10.10020/anie.202003029).

Z. Li, **R. J. Mayer**, A. R. Ofial, H. Mayr,
"From Carbodiimides to Carbon Dioxide: Quantification of the Electrophilic Reactivities of Heteroallenes",
J. Am. Chem. Soc. **2020**, *142*, 8383-8402.

Contributions to Conferences

Parts of this thesis were presented at the following scientific meetings:

07/2018 24. International Conference on Physical Organic Chemistry, Faro, Portugal

Poster presentation: “From Peroxides to Hypohalites: Towards a General Understanding of the Reactivities of Anionic Oxygen Nucleophiles”

09/2018 Physical Organic Chemistry at its Best, Halle

Poster presentation: “Which Factors Control the Lewis Acidities of Diaryliodonium Ions?”

01/2019 ProcessNet-Arbeitsausschusses Kinetik und Reaktionsmechanismen, Dechema, Frankfurt

Oral presentation: “A Novel Approach for Defining Lewis Acidity of Iodine(III) Compounds towards O-, N-, and Halide-centered Lewis Bases”

03/2019 Meeting of the SFB 749, Venice, Italy

Poster presentation: “Nucleophilic Reactivity of Glutathione: Extending the Electrophilicity Scale for Michael Acceptors”

09/2019 European Symposium on Organic Reactivity, Dubrovnik, Croatia

Oral presentation: “Ambident Reactivity of Phenolate Anions Revisited: A Quantitative Approach to Phenolate Reactivities”

Table of Contents

Summary[1]

Reactivity of Oxygen and Sulfur Nucleophiles

Nucleophilic Reactivity of Bleach Reagents

The kinetics of the reactions of the hydroperoxide anion (generated from different sources), hypochlorite, hypobromite, bromite, and peroxymonosulfate with colored benzhydrylium ions (reference electrophiles) were determined in aqueous solution at 20 °C (Figure 1A-C).

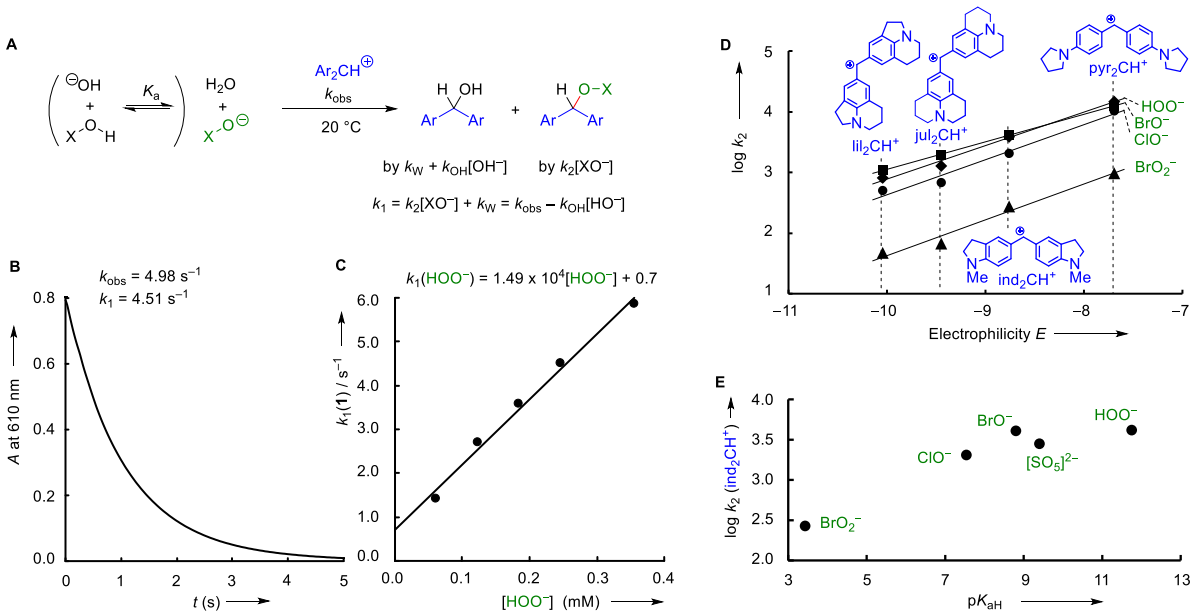

Figure 1: (A) Reaction of benzhydrylium ions with nucleophiles in alkaline, aqueous solution of bleach reagents XOH. (B) Absorbance *A* (at 610 nm) vs. time for the reaction of HOO^- (from urea-hydrogen peroxide) (c = 2.46 × 10^{-4} M) with pyr_2CH^+ (counterion: BF_4^-, c = 1.49 × 10^{-4} M) at 20 °C. (C) The slope of the linear plot of the first-order rate constant k_1 (= $k_{obs} - k_{OH}[HO^-]$) versus nucleophile concentration was used to derive the second-order rate constant k_2 for the attack of the hydroperoxide at the benzhydrylium ion pyr_2CH^+. (D) Plot of lg k_2 for the reactions of anions HOO^-, BrO^-, ClO^- and BrO_2^- with benzhydrylium ions in alkaline aqueous solution at 20 °C versus the electrophilicity parameters *E* of the benzhydrylium ions. (E) Correlation of the reactivity of electrophile ind_2CH^+ toward oxygen anions versus their basicities (pK_{aH}).

The linear free energy relationship lg $k_2 = s_N(N + E)$ was used to analyze the experimentally determined second-order rate constants to furnish the nucleophilicity parameters *N* and s_N of the oxidants (Figure 1D, Figure 2). The investigated anions have an almost identical nucleophilic reactivity toward benzhydrylium ions though their basicity differs significantly (Figure 1E). In synthesis, deprotonated hydrogen peroxide, hypochlorite/-bromite and peroxomonosulfate can, therefore, be used interchangeably as oxidants. The newly determined nucleophilicity parameters *N* enable a direct comparison of the

[1] The figures in this summary are adapted from published work. For the copyright, see the following chapters.

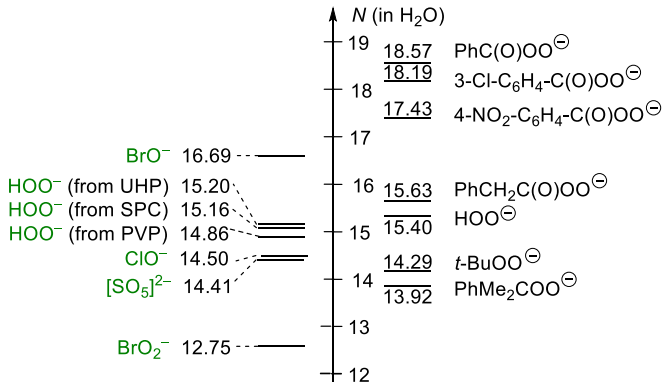

Figure 2: Comparison of the nucleophilicity parameters *N* of bleach reagents (left) with previously studied peroxide anions on the right.

reactivities of the investigated bleach reagents with those of other peroxy anions (Figure 2). Kinetic studies showed that the one-bond nucleophilicity parameters of oxidants that were determined toward the benzhydrylium reference electrophiles also hold to reliably predict the rate constants of nucleophilic Weitz-Scheffer epoxidation reactions with acceptor-substituted olefins of known electrophilicity.

Intramolecular Hydrogen-Bonding Modulates the Nucleophilic Reactivity of Ammonium-Peroxycarboxylates

Three different ammoniumperoxycarboxylic acids (APOCAs) methanesulfonates were synthesized and characterized by NMR spectroscopy and X-ray analysis (Figure 3A-B). Acidity measurements showed that APOCAs exist in aqueous solutions, depending on the pH value, either as anions, zwitterions or cations (Figure 3C). Alkaline solutions are needed to form the zwitterions or anions which are the active oxidants. Under these conditions, the APOCAs decomposed rapidly (depending on the species: $\tau_{1/2}$ = 20–100 s) by liberating hydroperoxide anions and the parent carboxylic acids (Figure 4A). For the APOCA derived from γ-aminobutyric acid, the decomposition reaction yielded γ-butyrolactam beside hydroperoxide anions (Figure 4B).

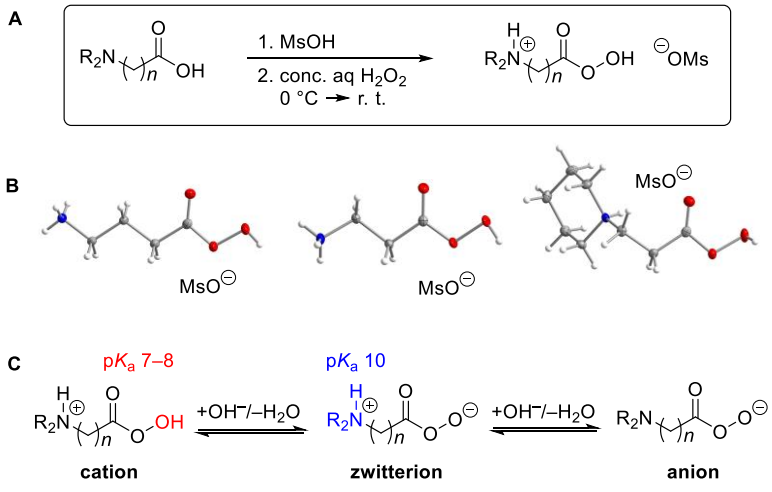

Figure 3: (A) Preparation of ammonium-peroxycarboxylic acid methanesulfonates. (B) Solid-state structures of APOCA mesylates (thermal ellipsoids are depicted at 50% probability level at *T* = 100 K, counterion MsO^- not shown). (C) Protonation equilibria of APOCAs.

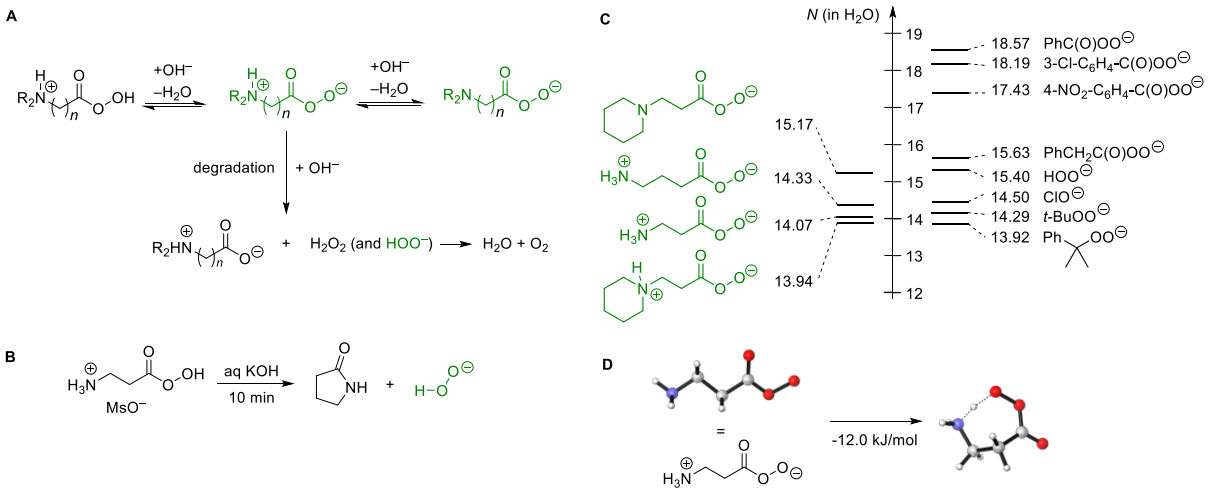

Figure 4: (A) General degradation of APOCAs in alkaline solution. (B) Decomposition of the APOCA derived from γ-aminobutyric acid to give γ-butyrolactam and hydroperoxide. (C) Comparison of nucleophilicity parameters *N* of APOCAs with those of other oxygen-centered oxidants. (D) Relative Gibbs energies (at 298 K) of the conformers of the APOCA derived from γ-aminobutyric acid at the M06-HF/6-311++G(d,p) level of theory for aqueous solution (SMD).

Kinetics of the reactions of APOCAs with benzhydrylium ions (reference electrophiles) were measured in alkaline, aqueous solutions. To overcome the rapid decomposition, APOCAs were deprotonated using the sequential mixing mode of a stopped-flow spectrometer. All reactions of anionic and zwitterionic APOCAs followed the linear-free energy relationship lg $k_2 = s_N(N + E)$ which allowed to determine their nucleophilicity parameters *N* and s_N. It was observed that the nucleophilic reactivities of the neutral peroxyammonium zwitterions are by factors 20-50 lower than those of peroxybenzoates or aliphatic peroxycarboxylates (Figure 4C).

Deprotonation of the ammonium group to give aminoperoxycarboxylate anions increased the rate of nucleophilic attack, as exemplified for the piperidino-derived APOCA. Quantum chemical calculations were used to rationalize the lower reactivity of APOCAs. These calculations showed that the formation of an intramolecular hydrogen bond between the ammonium and the peroxycarboxylate group is highly favored for ammoniumperoxycarboxylates. As a consequence, the peroxycarboxylate reactivity of zwitterionic APOCAs is attenuated (Figure 4D).

Weitz-Scheffer epoxidations of benzylidene malononitrile by APOCAs are sufficiently fast to remain unaffected by the concurrent decomposition of the oxidant. Hence, the experimentally determined rate constants for the epoxidation of this electrophile by APOCAs agreed well with the rate constants predicted by lg $k_2 = s_N(N + E)$.

Ambident Reactivity of Phenolate Anions Revisited: A Quantitative Approach to Phenolate Reactivities

Rate- and equilibrium constants for the reactions of phenolate ions with colored reference electrophiles were determined in DMSO, MeCN and DMF with the aim to characterize the ambident reactivity of phenolate ions within the framework of different linear-free energy relationships, which describe the nucleophilic and Lewis basic properties of phenolates or their nucleofugality (Figure 5).

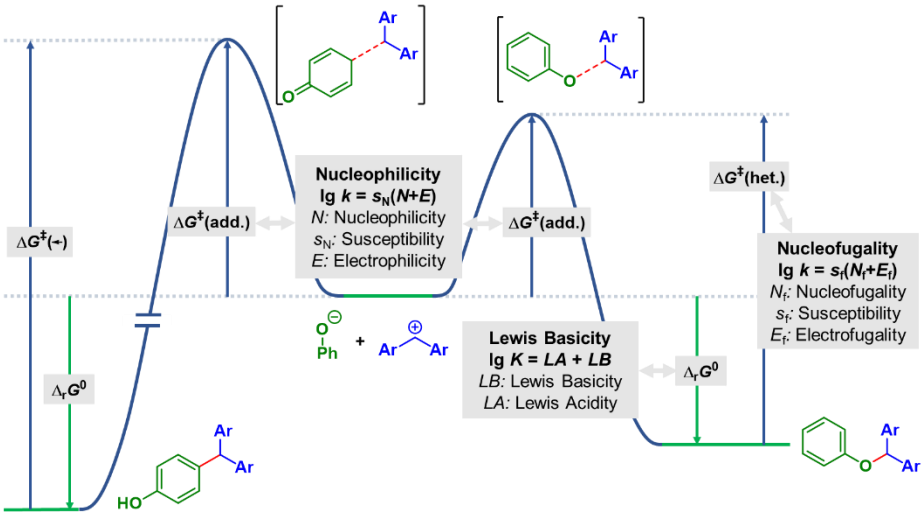

Figure 5: Qualitative Gibbs energy profile for the reaction of phenolate ions with benzhydrylium ions and the related kinetic and thermodynamic quantities within the framework of Mayr's benzhydrylium methodology.

Second-order rate constants were analyzed with the linear free energy relationship lg $k_2 = s_N(N + E)$ to give linear correlations from which 41 nucleophilicity parameters of phenolate ions in DMSO, DMF, MeCN and H_2O could be determined (Figure 6A). Based on the nucleophilicity parameters, phenolates can be compared with other nucleophiles that have been characterized previously (Figure 6B).

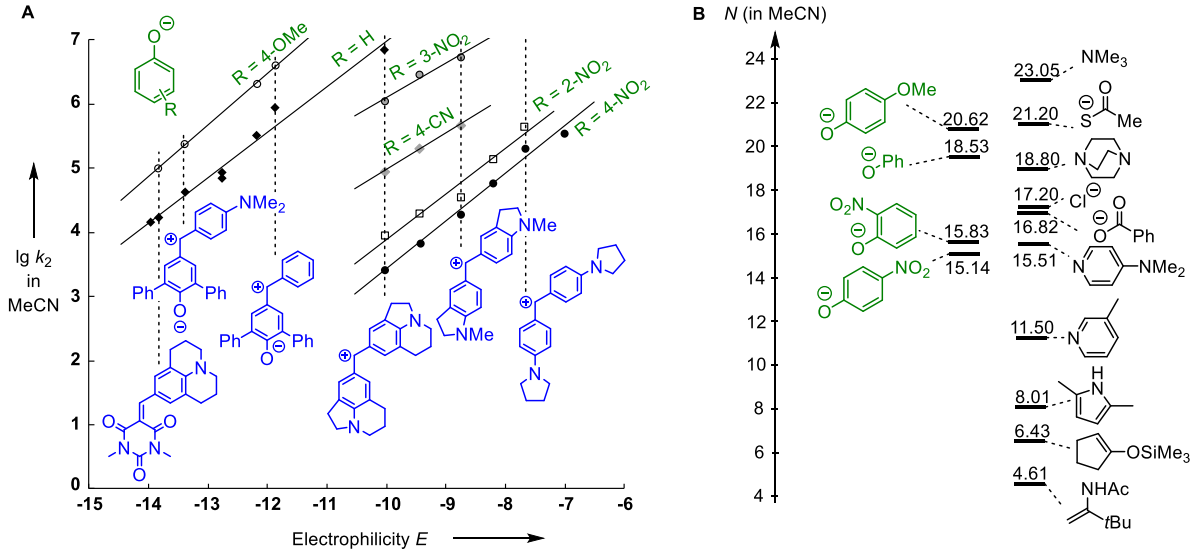

Figure 6: (A) Correlation of lg k_2 for the reactions of phenolate ions with reference electrophiles in MeCN at 20 °C with the electrophilicity parameters *E* of the latter. (B) Comparison of nucleophilicity parameters *N* of phenolates with those of other nucleophiles in acetonitrile.

Equilibrium constants for the reactions of phenolates with benzhydrylium ions of known Lewis acidity *LA* were determined by photometric titrations in MeCN (Figure 7A-C). Substitution of the equilibrium constants into the relationship lg *K* = *LA* + *LB* furnished the Lewis basicity parameters *LB* of four phenolate ions and allowed a comparison with other types of Lewis bases (Figure 7D).

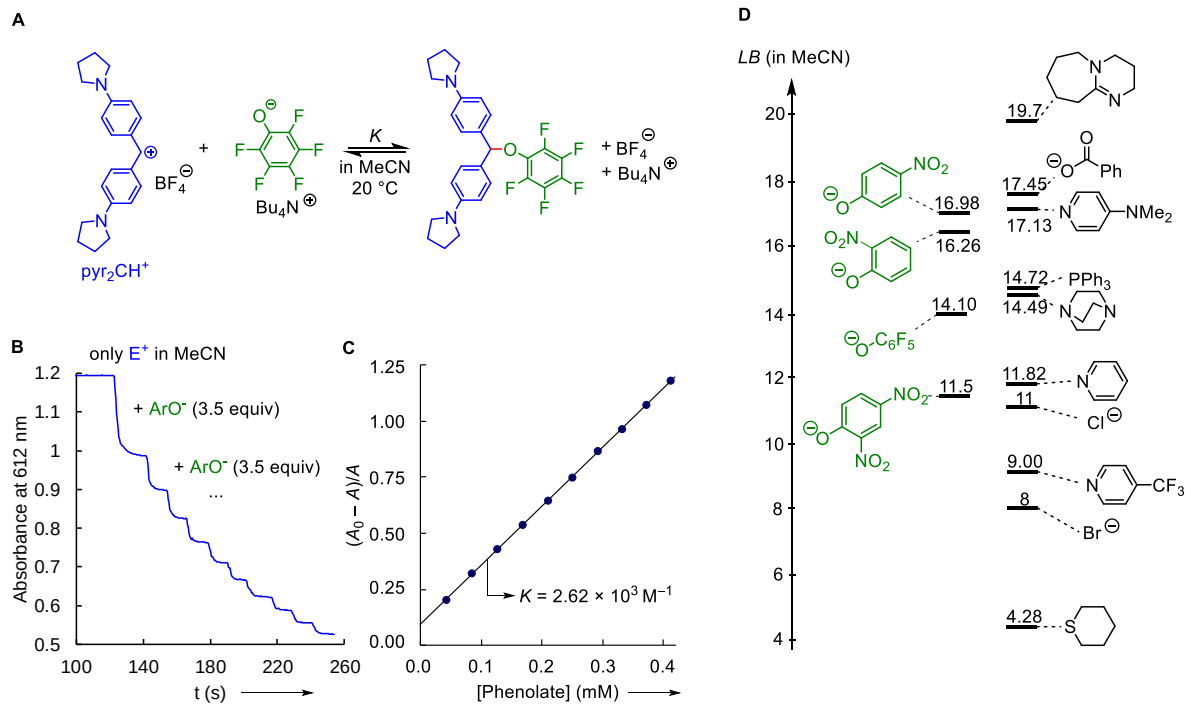

Figure 7: (A) Equilibrium reaction of pyr_2CH^+ with the pentafluorophenolate ion to furnish a Lewis adduct. (B) Absorbance *A* at 612 nm during titration of pyr_2CH^+-BF_4 by incremental addition of the perfluorinated phenolate in MeCN at 20 °C ($[pyr_2CH^+]_0 = 1.25 \times 10^{-5}$ M; values in parenthesis give the total number of equivalents of added phenolate in relation to the benzhydrylium ion). (C) Determination of the equilibrium constant *K* through the linear correlation of $(A_0^* - A)/A$ versus the concentration of free phenolate. (D) Comparison of nucleophilicity parameters *LB* of phenolates with those of other nucleophiles in acetonitrile.

It was observed that solutions of the benzhydryl ethers of 2-nitrophenolate were unstable and rearranged to triarylmethanes (Figure 8A). By following the rearrangement process of 2-nitrophenolate derived benzhydryl ethers for different benzhydrylium ions, three rate constants k_{iso} could be determined by ^{1}H NMR kinetic measurements. The isomerization rate k_{iso} is related to the rate constant of carbon attack k_{2C} by the relation $k_{iso} = k_{2C}/K$. The equilibrium constant *K* is independently accessible from the titration experiments used to characterize the Lewis basicity. As a consequence, three k_{2C} values were calculated, which were used to calculate the nucleophilicity parameter *N* and s_N of the phenolates carbon-site (Figure 8C).

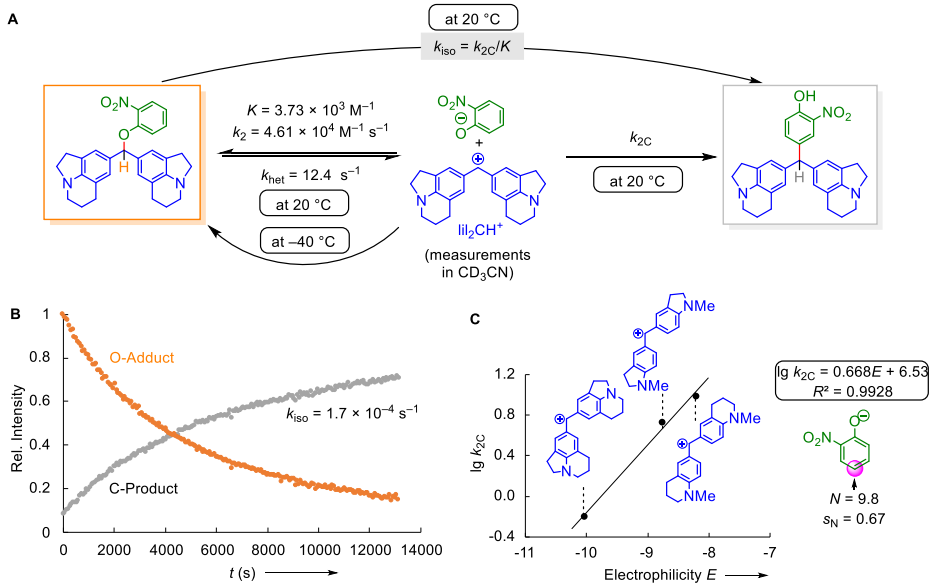

Figure 8: (A) Rearrangement of the benzhydryl ether of lil_2CH^+ and 2-nitrophenolate to the triarylmethane formed due to carbon attack. (B) ^{1}H NMR spectroscopic monitoring of the rearrangement at a concentration of the benzhydryl phenol ether of c = 2.15 × 10^{-2} M (CD_3CN, 20 °C). (C) Correlation of the second-order rate constants k_{2C} for attack of benzhydrylium ions at C-4 of 2-nitrophenolate with the corresponding electrophilicity parameters E.

Additionally, quantum-chemical calculations were performed to supplement the experimental data (Figure 9). The calculations were in good agreement with the experiments, and showed that O-attack is preferred in kinetically controlled reactions while C-attack can occur under conditions of thermodynamic control.

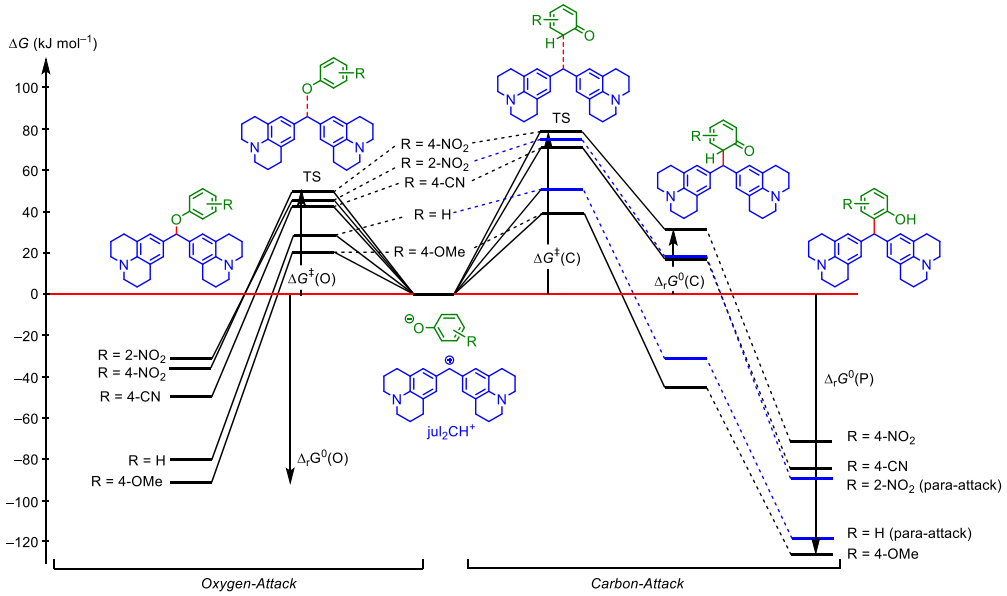

Figure 9: Gibbs energy profiles for the competing oxygen- and carbon-attack (para-attack: blue pathway) in the reaction of different ring-substituted phenolate ions with the benzhydrylium ion jul_2CH^+ calculated at the SMD(MeCN)/M06-2X/6-31+G(d,p) level of theory at 298 K.

Product distributions of the reactions of the parent phenolate ion with benzhydrylium tetrafluoroborates and benzhydryl chlorides were analyzed in order to study the selectivity of reactions that proceed under diffusion control. Oxygen attack of the phenolate ion was exclusively observed with less reactive benzhydrylium ions. More reactive carbenium ions (formed as transient intermediates in S_N1 reactions) reacted equally fast with the oxygen- and carbon site of the phenolate ion (Figure 10A). Benzhydryl chlorides of even less stabilized carbenium ions, however, reacted selectively with the oxygen-site of phenolate ions again. In these reactions, the heterolysis via an S_N1 reaction became too slow and the mechanism switched over to a non-diffusion controlled S_N2 reaction. The change in mechanism could also be verified by analyzing the product mixtures in competition reactions of phenolate and 2-nitrophenolate with benzhydryl chlorides (Figure 10B). In diffusion-controlled S_N1 reactions both phenolates react equally fast with the electrophiles, despite having different nucleophilicities. After a change to an S_N2 reactions, the product ratio again reflects the relative nucleophilicities.

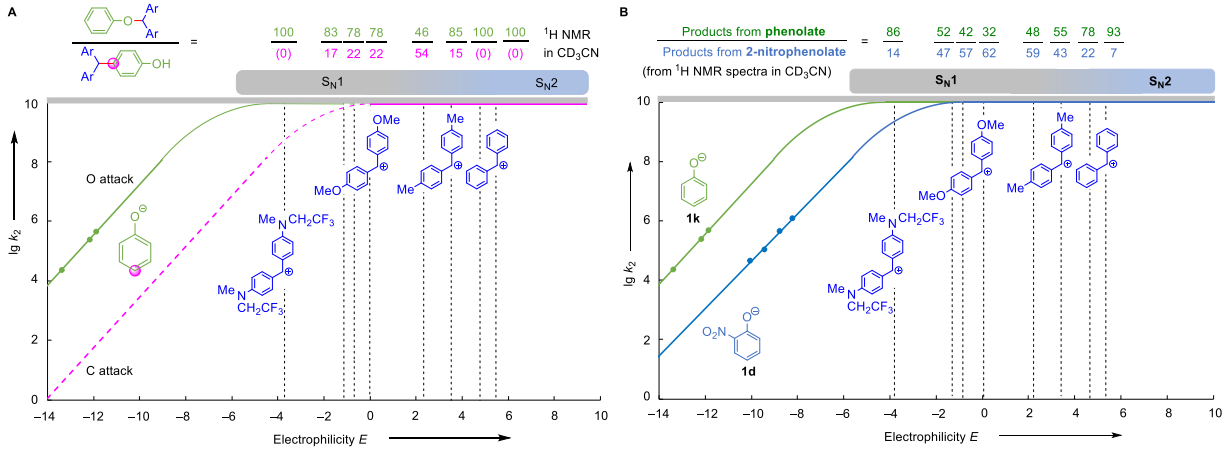

Figure 10: (A) Plot of lg k_2 (MeCN, 20 °C) for O- and C-attack of the parent phenolate ion at benzhydryl cations versus the electrophilicities *E* (rate constants for C-attack estimated from relative quantum-chemically calculated barriers for O- and C-attack). (B) Plot of lg k_2 (MeCN, 20 °C) for the attack of benzhydrylium ions at the oxygen of the unsubstituted and 2-nitro-substituted phenolate ions versus the electrophilicities *E*.

Nucleophilicity of Glutathione: A Link to Michael Acceptor Reactivities

To connect existing reactivity data for Michael acceptors from biochemical assays for glutathione (GSH) with electrophiles in Mayr's reactivity scales, the nucleophilic reactivity of glutathione was determined. Kinetics of the reactions of GSH with colored benzhydrylium ions and acceptor-substituted olefins of known electrophilicity *E* were measured in alkaline, aqueous solutions at 20 °C (Figure 11A).

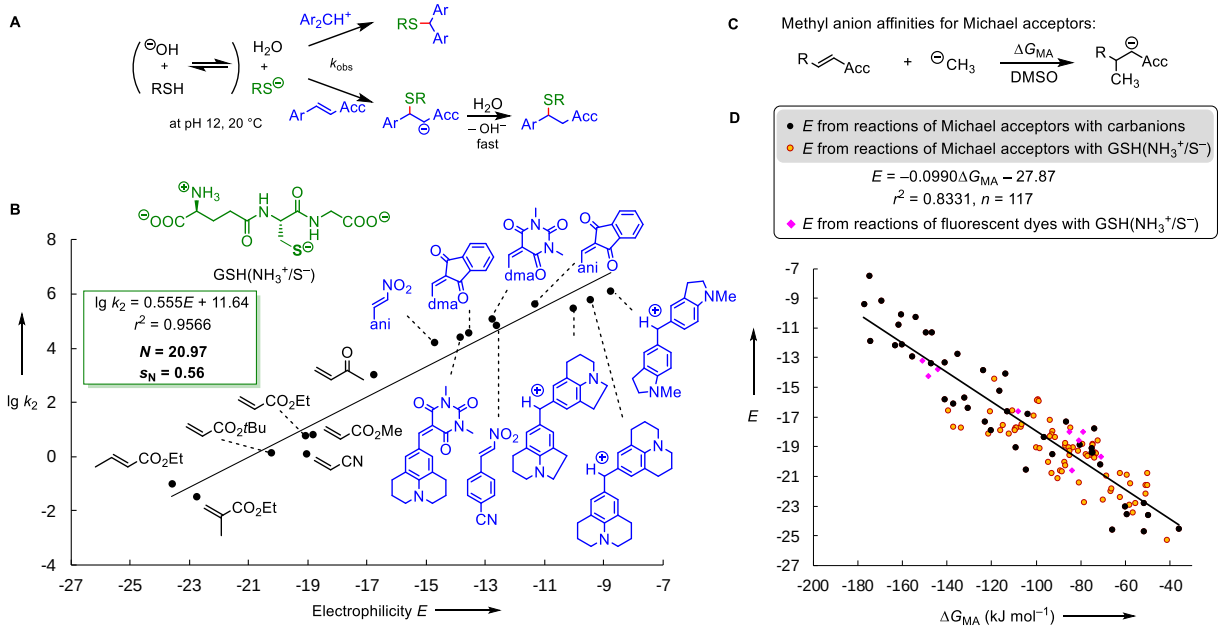

Figure 11: (A) Reactions of cationic and neutral electrophiles with thiolate ions in alkaline, aqueous solutions. (B) Determination of the nucleophilicity of GSH(NH_3^+/S^-) from the linear plot of lg k_2 for its reactions with the electrophiles versus the electrophilicity parameters E. (C) Definition of methyl anion affinities (ΔG_{MA}) of Michael acceptors. (D) Correlation between experimentally determined electrophilicities E and methyl anion affinities ΔG_{MA} in DMSO [calculated at the SMD(DMSO)/B3LYP/6-311++G(3df,2pd)//B3LYP/6-31G(d,p) level of theory] supplemented by data for fluorescent thiol probes (purple rhombs, not included when calculating the correlation line).

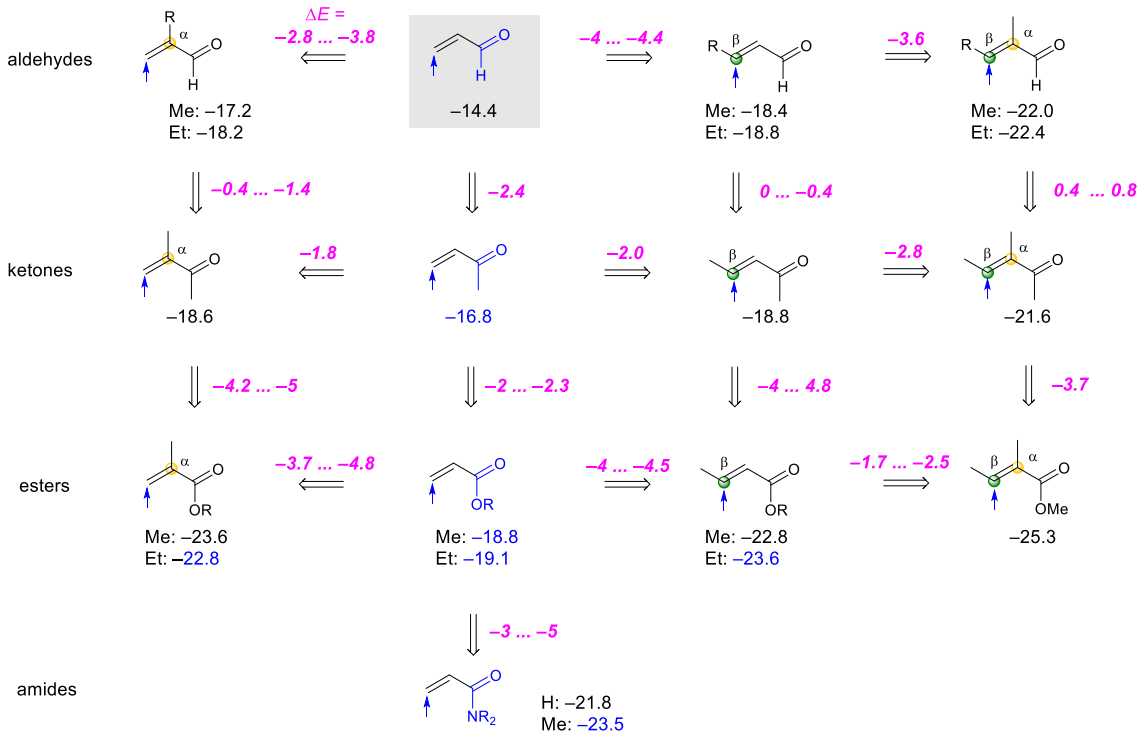

Figure 12: Structure/electrophilicity relationships for Michael acceptors based on the electrophilicities E (in blue color: electrophilicity determined in DMSO from the reactions with carbon-centered reference nucleophiles; in black color: this work, electrophilicities based on GSH reactivities).

Analysis of the rate constants for the reactions of GSH with reference electrophiles as well as with Michael acceptors of known electrophilicity *E* with the correlation equation lg $k_2 = s_N(N + E)$ allowed to determine the nucleophilicity parameters of GSH(NH_3^+/S^-) (Figure 11B). By using the inverse procedure, the nucleophilicity of GSH was applied to estimate the electrophilicity parameter *E* of 82 electron-deficient alkenes and alkynes, whose rate constants with GSH had been reported in the literature. To test the consistency of the newly determined *E* parameters, the previously established linear relationship between electrophilicity *E* and quantum-chemically calculated methyl anion affinities was applied, which showed a similar scattering (Figure 11C,D).

The knowledge of electrophilicity parameters for 34 Michal acceptors derived from GSH reactivities allowed to construct a detailed quantitative structure/electrophilicity relationships for acceptor-substituted alkenes (Figure 12).

Basicity Scales Toward Heteroatom Lewis Acids

Lewis Acidity Scale of Diaryliodonium Ions Toward Oxygen, Nitrogen, and Halogen Lewis Bases

In order to find conditions that allow to investigate the Lewis acidity of free diaryliodonium ions, conductometric studies (Figure 13A) as well as ^1H and ^{19}F diffusion ordered NMR spectroscopy (DOSY) (Figure 13B) were used. These methods revealed the effects of ion pairing of diaryliodonium salts in different organic solvents. While ion pairs of diaryliodonium triflates predominate in dichloromethane or tetrahydrofuran, acetonitrile was identified to be the ideal solvent because ion pairing was shown to be negligible in diluted solutions (< 2 mM).

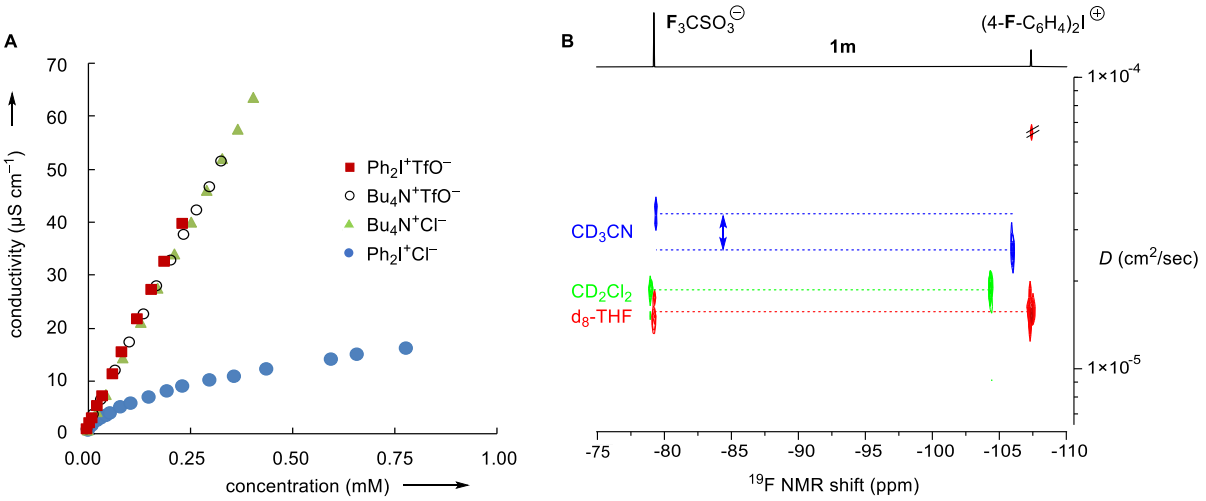

Figure 13: (A) Concentration-dependent conductivity of $Ph_2I^+TfO^-$, $Bu_4N^+TfO^-$, and $Bu_4N^+Cl^-$, and $Ph_2I^+Cl^-$ (MeCN, 20 °C). (B) ^{19}F DOSY NMR spectra (25 °C) of **1m** in CD_3CN (blue, 12 mM), CD_2Cl_2 (green, 11 mM) and THF-d_8 (red, 8 mM). The ^{19}F NMR spectrum on top refers to THF-d_8.

Equilibrium constants of the associations of diaryliodonium ions with different oxygen, nitrogen and halogen centered Lewis bases were determined by spectrophotometric titrations, isothermal titration calorimetry (Figure 14A,B), and conductometry in acetonitrile solutions at 20 °C. As diaryliodonium ions and most of the investigated Lewis bases are colorless, a new procedure for spectrophotometric titrations was developed that takes advantage of the known equilibrium constants between Lewis bases and colored benzhydrylium ions (Figure 14C,D).

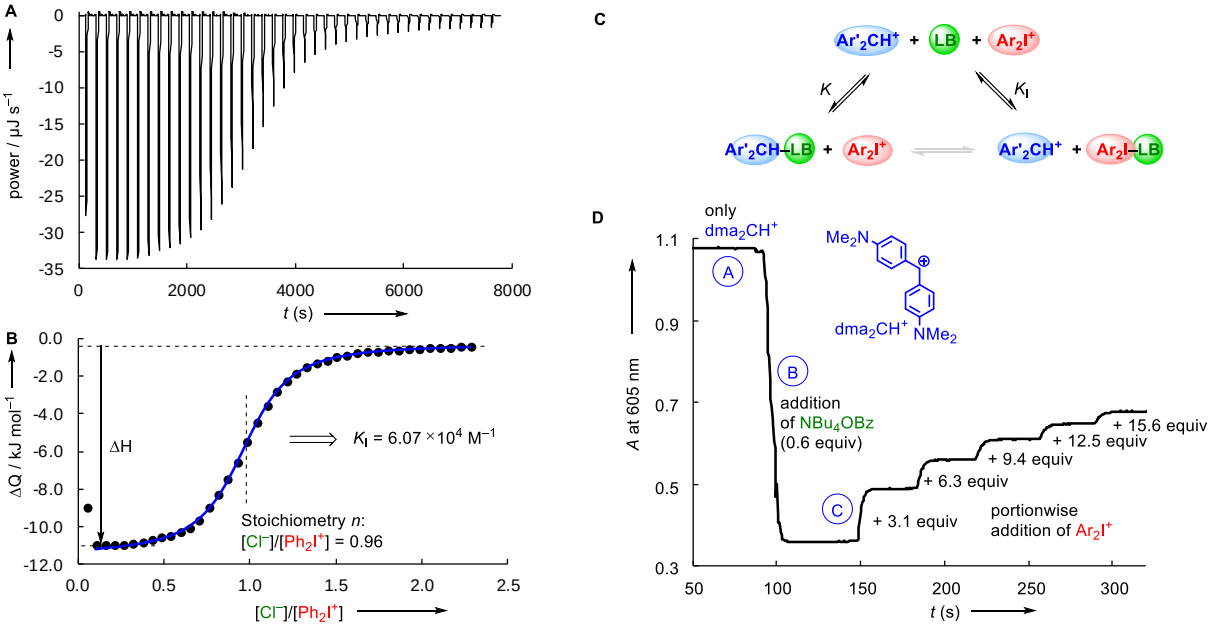

Figure 14: (A) Heat flow during the titration of $Ph_2I^+TfO^-$ (0.827 mM in MeCN) with $NBu_4^+Cl^-$ (10.0 mM in MeCN) at 20 °C (ITC trace after baseline correction). (B) Plot of the integrated heats per shot vs. the equivalents of added chloride ions (black dots). The blue line depicts the fitted titration curve (the first injection was omitted from the correlation) giving K_I for this individual experiment. (C) Competing equilibria used for the determination of equilibrium constants K_I with the help of benzhydrylium ions Ar_2CH^+ (D) Representative titration experiment with benzhydrylium ions: A solution of benzhydrylium tetrafluoroborate dma_2CH^+ (1.30×10^{-5} M, step A) was treated with $Bu_4N^+BzO^-$ (0.6 equiv), which generated a mixture of dma_2CH^+ and the colorless adduct dma_2CH^+-OBz (step B). Then a solution of bis(4-bromophenyl)iodonium triflate (1.31×10^{-2} M) was added stepwise (step C), which caused the incremental increase of the benzhydrylium ion concentration [dma_2CH^+].

The relative Lewis basicities of Lewis bases toward iodonium and benzhydrylium ions differ drastically (Figure 15). Lewis bases that have similar basicity toward benzhydrylium ions like benzoate, 4-nitrophenolate, 4-pyrrolidinopyridine or tris(4-methoxyphenyl)phosphine show a wide range of basicities toward iodonium ions. Therefore, diaryliodonium ions cannot be integrated into the linear-free energy relationship lg $K = LA + LB$ that was shown to describe the basicities toward benzhydrylium ions.

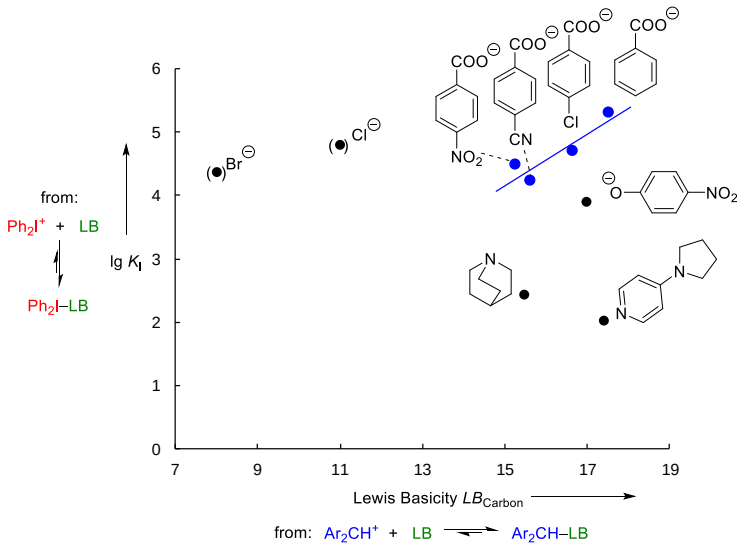

Figure 15: Plot of lg K_I for the reactions of Ph_2I^+ with various Lewis bases (MeCN, 20 °C) versus the Lewis basicity LB of the same set of Lewis bases in adduct formations with benzhydrylium ions. Blue correlation: lg K_I = 0.41LB – 2.0, R^2 = 0.832.

In order to develop a comprehensive acidity/basicity scale of diaryliodonium ions that can be used to predict the association constants with Lewis bases, equilibrium constants were subjected to a least-squares analysis with the linear free energy relationship

$$\lg K_I = s_I\, LA_I + LB_I.$$

In this analysis, Lewis bases are characterized by the iodonium-specific Lewis basicity parameters LB_I and susceptibility s_I and Lewis acids by the Lewis acidities LA_I. The acidity/basicity scale is graphically illustrated by the linear correlations in Figure 16A. This methodology allowed to compare the structure-acidity relationship for different diaryliodonium ions directly on the basis of Lewis acidities LA_I (Figure 16B).

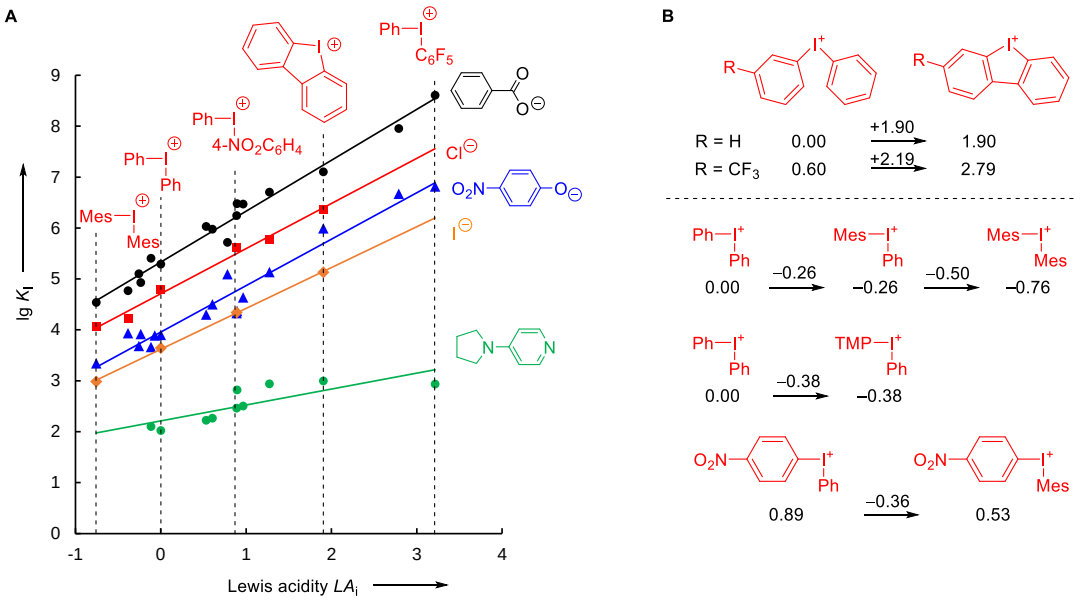

Figure 16: (A) Plot of lg K_I for the reactions of diaryliodonium ions with Lewis bases versus their newly defined Lewis acidity parameters LA_I. (B) Comparison of the Lewis Acidities LA_I of different iodonium ions. Mes: 2,4,6-trimethylphenyl, TMP: 2,4,6-trimethoxyphenyl.

Lewis Adduct Formations: Lewis Basicity Scales Toward Boranes

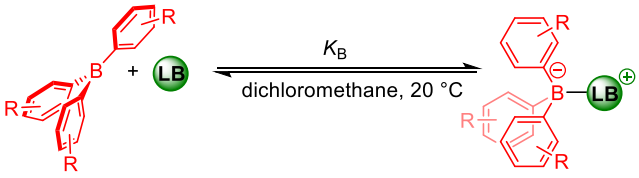

Figure 17: Equilibrium for the adduct formation between a triarylborane and a Lewis base.

Equilibrium constants for the reactions of triarylboranes with various Lewis bases were determined by NMR spectroscopic titrations and isothermal titration calorimetry in dichloromethane at 20 °C (Figure 17). In order to generate a comprehensive Lewis acidity/basicity scale that allows to predict the associations of boranes with various Lewis bases, the equilibrium constants were analyzed with a newly defined boron-specific two-parameter linear free-energy relationship which furnished the Lewis acidity LA_B and the Lewis basicity LB_B according to:

$$\lg K_I = LA_B + LB_B.$$

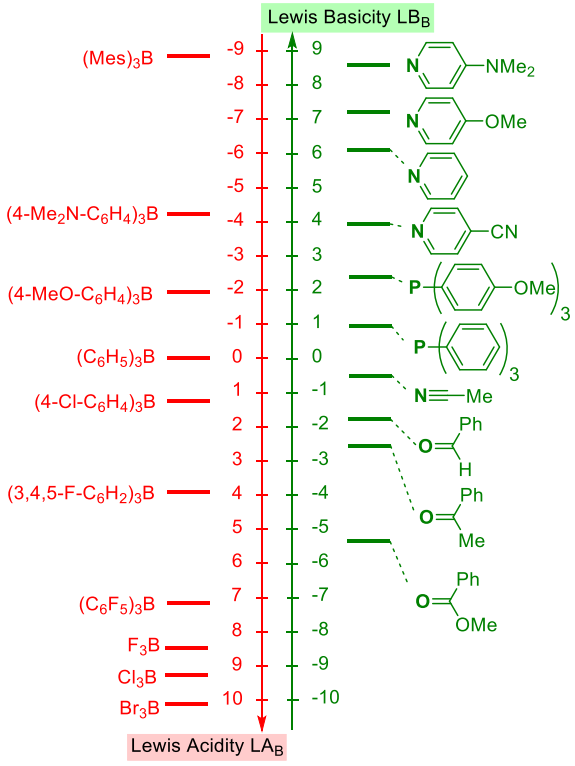

Figure 18: Experimental Lewis acidity and basicity scales for boranes and N-, O- and P-centered Lewis bases derived on the basis of lg $K_I = LA_B + LB_B$. Compounds on the same level combine with an equilibrium constant K_B = 1 M^{-1} in dichloromethane at 20 °C.

This equation allows the prediction of association constants for various combinations of boranes and Lewis bases over almost 20 orders of magnitude, ranging from highly Lewis basic pyridines to weakly basic ketones or esters (Figure 18). For para- and meta-substituted boranes, Hammett σ-parameters (Figure 19A) were found to correlate linearly with LA_B. A more general correlation of LA_B for all investigated types of boranes was found with quantum-chemically calculated fluoride ion affinities (Figure 19B).

An independent access to the Lewis basicity parameters LB_B is provided by the linear correlation with experimental BF_3 affinities, that are available for a large set of compounds in the literature (Figure 19C). For Lewis bases that lack experimental data, quantum-chemically calculated BH_3 affinities were found to correlate equally well (Figure 19D).

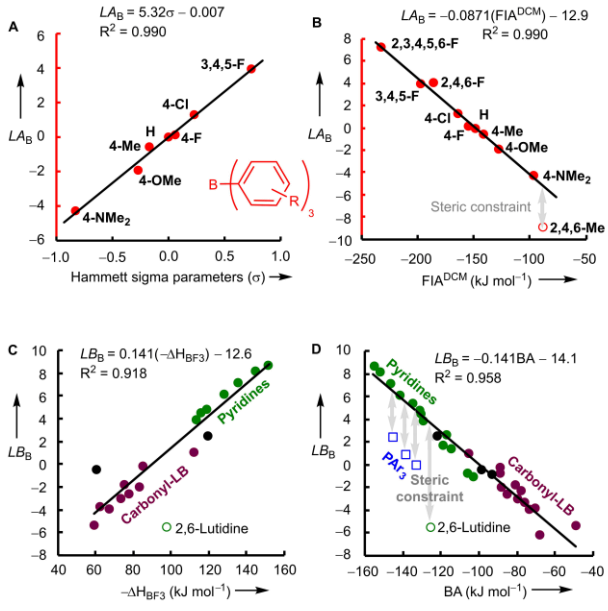

Figure 19: (A) Correlation of LA_B parameters with Hammett σ parameters. (B) Correlation of LA_B parameters with quantum-chemically calculated fluoride ion affinities in dichloromethane solution FIA^{DCM} (at the SMD(DCM)/MN15/def2-TZVP level of theory). (C) Correlation of LB_B parameters with experimental BF_3 affinities in dichloromethane ($-\Delta H_{BF3}$) from Gal.[2] (D) Correlation of LB_B parameters with quantum-chemically calculated BH_3 affinities BA (at the SMD(DCM)/MN15/def2-TZVP level of theory, referenced to the experimental $\Delta_r G$ of the reaction of triphenylborane with pyridine).

Deviations of sterically constrained Lewis acids and bases from the correlations of LA_B and LB_B with molecular descriptors (e.g. fluoride-ion affinities, borane affinities) were used to quantify the energy penalty of frustrated Lewis pairs. Additionally, the newly defined correlation equation can be used to predict the required Lewis acidity of a borane to catalyze reactions, as illustrated in Figure 20 for a Nazarov and a Diels-Alder reaction.

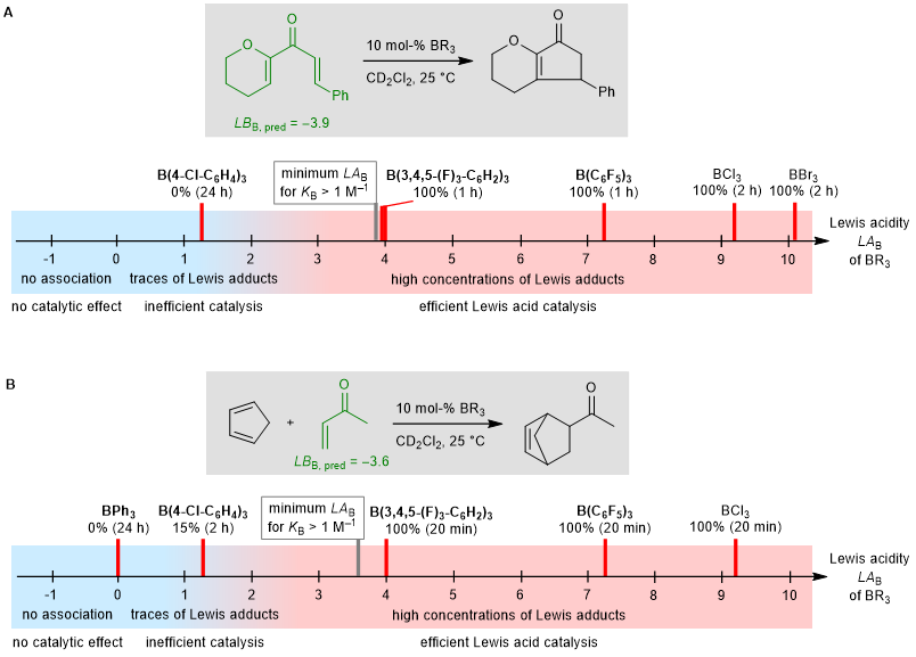

Figure 20: (A) Nazarov cyclizations catalyzed by different triarylboranes, BBr_3, and BCl_3. (B) Diels-Alder reactions of methyl vinyl ketone with cyclopentadiene catalyzed by different boranes.

[2] C. Laurence, J.-F. Gal, *Lewis Basicity and Affinity Scales: Data and Measurement*; Wiley: Chichester, UK, 2010.

Chapter 1. Introduction

1.1 Basicity and Reactivity Scales in Organic Chemistry

In the 1920-1930, the work of Brønsted, Lewis, Ingold and Hammett among others set the foundations for what is known as Physical Organic Chemistry today.[1] In 1923, Brønsted refined the previous definition of acids by Arrhenius and concluded that acids and bases are species that are able to accept or donate protons (eq. 1).[2] To quantify the strength of acids, Brønsted defined the acidity constants K_a (eq. 2-3). To date, K_a has been determined for numerous species in water but also in organic solvents.[3]

$$H^+ + \text{Base} \rightleftharpoons \text{Acid} \qquad (1) \quad \text{(Brønsted, 1923)}$$

$$\text{A-H} + H_2O \rightleftharpoons A^+ + H_3O^+ \qquad (2)$$

$$K_a = \frac{[A^+][H_3O^+]}{[\text{A-H}]} \qquad (3)$$

In the same year as Brønsted, Lewis proposed a complementary but more general definition of acidity and basicity (eq. 4).[4] According to the definition by Lewis, acids are species that accept a lone pair of electrons from a base to form a stable bond, with bases being species that furnish lone pairs. Therefore, according to the Lewis theory, the proton can be seen as the simplest Lewis acid.

$$\text{LA} + :\text{LB} \rightleftharpoons \text{LA}-\text{LB} \qquad (2) \quad \text{(Lewis, 1923)}$$

However, for the Lewis theory of acids and bases a comparable quantitative description as for the Brønsted model does not exist. While the Brønsted scale is reference toward H^+ (in water), there is an infinite number of possible Lewis acidity and basicity scales due to the infinite number of possible reference Lewis acids and bases. Different methods for the quantification of the strength of both Lewis acids and bases have therefore been proposed, which will be discussed in more detail in the subsequent sections.

While acidity and basicity describe the position of an equilibrium between an acid and a base, the time needed for a reaction to proceed is quantified by a rate constant. In 1933 Ingold proposed the terms electrophilic (electron-seeking) and nucleophilic (nucleus-seeking) to describe the kinetic propensity of reagents to form a bond.[5] Toward a reaction partner, a molecule can therefore be classified by two parameters: basicity/acidity (the thermodynamic driving force of the reaction) and nucleophilicity/electrophilicity (the reaction rate with the reaction partner).[6]

Relationships between rate and equilibrium constants initially found by Brønsted,[7] that is, correlations between rate constants and basicities/acidities, were further analyzed by Hammett[8] and ultimately led

to the formulation of eq. 5[9] and the foundation of Physical Organic Chemistry as a discipline.[10] The linear free energy relationship eq. 5, which is known as the Hammett equation, can be used to predict the rate or equilibrium constants of reactions that involve substituted arenes. The ratio of the rate or equilibrium constant for a reaction with a certain substituent (*k* or *K*) and the rate or equilibrium constant of the same reaction but with the unsubstituted arene (k_0 or K_0) corresponds to the product of a reaction-specific constant ρ and the substituent constant σ.

$$\lg \frac{K}{K_0} \quad \text{or} \quad \lg \frac{k}{k_0} = \sigma \cdot \rho \qquad (5)$$

The relationship eq. 5 proved to be so general in its ability to rationalize structure reactivity relationships, that it is still widely applied today[11] and many examples of its validity will be shown in the following chapters of this thesis.

The concept of linear-free energy relationships was subsequently applied in efforts to construct reactivity scales that allow the prediction of absolute rate constants for nucleophilic substitution reactions. The first approach to establish a nucleophilicity scale was undertaken by Swain and Scott in 1963 who took a set of rate constants determined in water at 25 °C for the addition of different nucleophiles (e.g. water, hydroxide, halides) at electrophiles (e.g. alkyl and acyl halides, epoxides) as basis.[12] They suggested that the ratio of the rate constant *k* for an electrophile/nucleophile reaction with the rate constant k_0 for the reaction of the same electrophile with water, is described by the product of a nucleophilicity constant *n* and a electrophile-specific substrate constant *s* (eq. 6).

$$\lg \frac{k}{k_0} = s \cdot n \qquad (6)$$

The reaction of nucleophiles with methyl bromide was taken as reference to defined *s* = 1. The resulting nucleophilicity and substrate constants could be used to predict rate constants for a small set of S_N2 reactions. Subsequently, there have been attempts to construct further nucleophilicity scales and extend the concept. However, in 1968 Pearson studied the rate constants for the reactions of different nucleophiles with methyl iodide and trans-$[Pt(py)_2Cl_2]$ and observed that there is little correlation of the *n* parameters derived from reactions with these two different electrophiles as would be required by eq. 6. In consequence, he concluded that "*equations in the literature for predicting nucleophilic reactivity have only a limited range of usefulness*" and "*that at present it is not possible to predict quantitatively the rates of nucleophilic displacement reactions when a number of substrates of widely varying properties are considered*".[13]

Another approach to a nucleophilicity scale was proposed by Ritchie, who used kinetic studies of the reactions of nucleophiles with a series of differently substituted tritylium and diazonium ions as reference electrophiles to derive eq. 7.[14]

$$\lg \frac{k}{k_0} = N_+ \qquad (7)$$

Like in the Swain-Scott equation (eq. 6), a ratio of the rate k for the reaction of an electrophile with a nucleophile and k_0 for the reaction of the same electrophile with water is set equal to define a nucleophilicity parameter N_+ (eq. 7). The Ritchie equation, therefore, assumes that independent of the electrophile, nucleophiles will always have a constant relative reactivity. However, it was later found that eq. 7 is not generally valid and superior correlations were observed if different types of electrophiles were correlated separately.[15,16] For example, Kane-Maguire and Sweigart used the framework of eq. 7 to derive a different set of N_{Fe} parameters which are valid for the nucleophilic additions to metal-coordinated electrophilic π-systems.[17]

So far, the most general reactivity scale that can be applied to nucleophile/electrophile combinations was developed by the Mayr group which relies on the reactions of nucleophiles with benzhydrylium ions as reference electrophiles.[18]

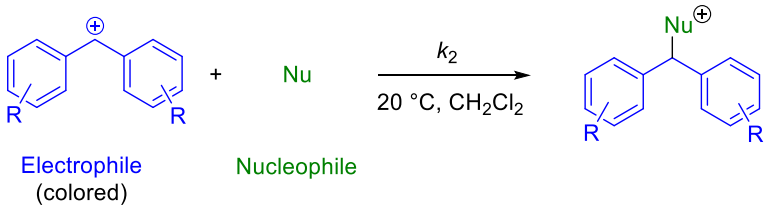

Scheme 1: Reaction of a benzhydrylium ion with a nucleophile.

Based on a series of second-order rate constants for the reactions of benzhydrylium ions with carbon-centered nucleophiles in dichloromethane at 20 °C (Scheme 1), eq. 8 was parametrized.[18a,b] As shown later, eq. 8 also holds for various other solvents and for electrophiles and nucleophiles that are not necessarily carbon centered, as long as one of the reaction partners reacts via a carbon atom.[18c-e]

$$\lg k_2\ (20\ °C) = s_N(N + E) \qquad (8)$$

In eq. 8, a second-order rate constant k_2 (at 20 °C) is related to a solvent-independent electrophilicity parameter E and two solvent-dependent nucleophilicity parameters N and susceptibility s_N. By introducing a susceptibility parameter s_N, the variable selectivity of nucleophile/electrophile reactions could be integrated. It was later shown, that eq. 8 can be connected to both the Swain-Scott and the Ritchie equations.[16,19] By extending the reference electrophiles to structurally related quinone methides, a reactivity scale of almost 40 orders of magnitude was obtained with eq. 8. So far, more

than 1200 nucleophiles and 300 electrophiles have been studied by the benzhydrylium methodology providing a broadly applicable approach to polar chemical reactivity.[18b-f]

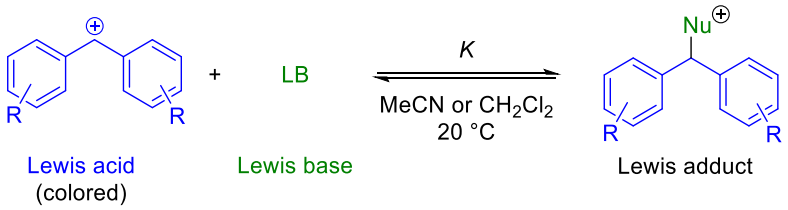

Scheme 2: Benzhydrylium ions as reference Lewis acids to determine the strength of Lewis bases.

However, the benzhydrylium ions used for the development of the reactivity scales defined by eq. 8 are not only suitable reference electrophiles for reactivity studies, but can also be used as reference Lewis acids (Scheme 2). A set of equilibrium constants determined at 20 °C in dichloromethane and acetonitrile for the reactions of differently substituted benzhydrylium ions with various oxygen, nitrogen and phosphorus centered Lewis bases served as the basis for eq. 9.[20]

$$\lg K\ (20\ °C) = LA + LB \qquad (9)$$

Eq. 9 relates equilibrium constants K in a certain solvent to the same of a Lewis acidity parameter LA and a Lewis basicity parameter LB. Based on eq. 9, the equilibrium constant K for any combination of benzhydrylium Lewis acid and base, for which LA and LB parameters are known, can be predicted.

Lastly, benzhydrylium ions can also act as leaving groups in the reverse reactions that define eq. 8. For heterolysis reactions and therefore the tendency of a compound to act as leaving group (as electrofuge or nucleofuge, see Scheme 3), a large set of experimental equilibrium constants was analyzed by the Mayr and Kronja groups according to the linear free energy relationship eq. 10.[21]

$$\lg k_{\text{heterolysis}}\ (20\ °C) = s_f(N_f + E_f) \qquad (10)$$

Eq. 10 correlates the rate constants $k_{\text{heterolysis}}$ for the heterolysis of a benzhydrylium-adduct with the solvent dependent nucleofugality N_f and the susceptibility s_f and the solvent-independent electrofugality parameter E_f.

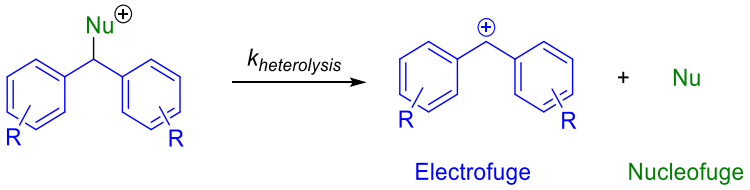

Scheme 3: Benzhydrylium ions as reference electrofuges in heterolysis reactions.

Altogether, eq. 8-10 can be used to describe the fundamental properties of reactants in polar organic pathways as well as to quantitatively predict the outcome of their reactions.[22]

1.2 Reactivity of Oxygen and Sulfur Nucleophiles

Hydrogen peroxide (H_2O_2) was discovered in the early 19th century by Louis Jacques Thénard.[23] Over the years, it became a chemical of high industrial importance with the majority of it being used for the bleaching of wood-pulp, the first step in paper production.[24] However, hydrogen peroxide also serves as reagent for the synthesis of organic peroxides like organic hydroperoxides or peroxycarboxylic acids.[25] Beside its use as aqueous solution, various solid storage forms of hydrogen peroxide, e.g. sodium percarbonate[26] or urea-hydrogen peroxide[27] are produced on a commercial scale. Due to safety concerns and possible instability of H_2O_2, persulfates[28] or hypohalites[29] are common alternatives to peroxides and were found to be equally suitable for organic synthesis as well as for bleaching purposes.

It is generally considered that the anions generated from hydrogen peroxide, organic hydroperoxides as well as hypohalites or persulfates are potent nucleophiles that can be employed for a variety of reactions. Examples of reactions that are initiated by the nucleophilic attack of a peroxide anion are the Weitz-Scheffer epoxidation of acceptor-substituted olefins[30], the Baeyer-Villiger oxidation of ketones,[31] nucleophilic hydroxylation of arenes,[32] or the Dakin oxidation of hydroxylated aryl aldehydes or aryl ketones (Scheme 4).[33] While these reactions are valuable for organic syntheses, the industrial application of peroxides to achieve bleaching of substrates relies on analogous chemical reactions, as addition of oxygen to olefins destructs the large conjugated π-systems responsible for color in biological material.[24]

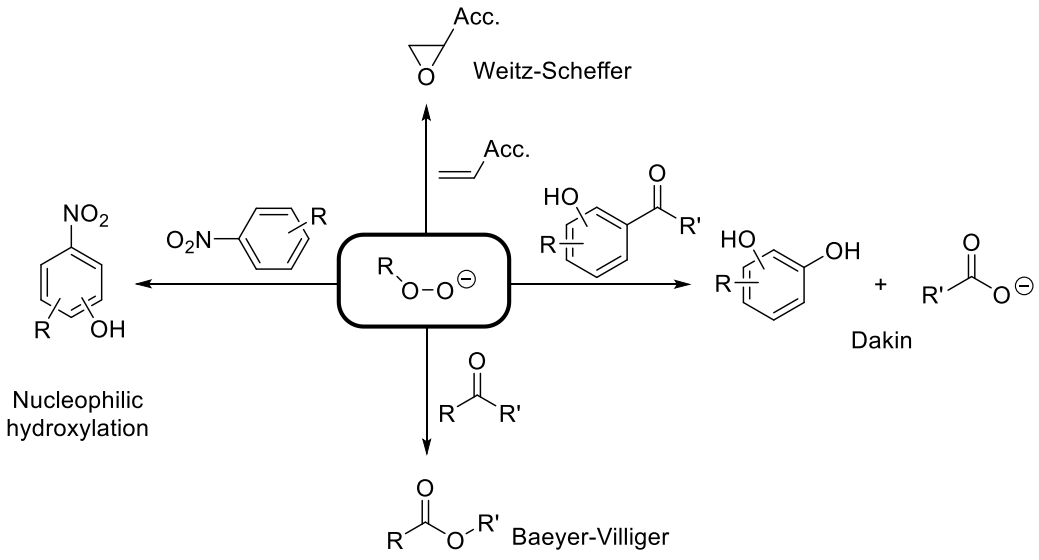

Scheme 4: Overview of the reactions of peroxide ions.

Despite the huge industrial importance, quantitative data on the reactivity of (per-)oxygen nucleophiles in aqueous solutions are scarce and mostly restricted to the anion of hydrogen peroxide: Bunton and Minkoff studied the kinetics for the epoxidation of mesityl oxide and ethylidenacetone by

hydrogen peroxide in alkaline, aqueous solution.[34] Kinetic measurements of the nucleophilic substitution of nitrophenylacetate with a series of nucleophiles which also included hydroperoxide and hypochlorite by Jencks, led to the discovery of the so-called alpha-effect.[35] Alpha-effect nucleophiles, a term that was coined by Pearson for nucleophiles bearing a heteroatom with a lone-pair in α-position to the attacking atom, were proposed to react faster than expected based on their Brønsted basicity.[36] Later studies on the alpha-effect by Dixon, which also comprised the hydroperoxide and hypochlorite ions, used the tritylium ion malachite green as reference electrophile.[37] Further reference electrophiles for the study of the nucleophilic reactivity of hydroperoxide included α-bromo-*p*-toluic acid,[38] tritylium ions,[39] aryl methanesulfonates,[40] and benzhydrylium ions.[16]

However, the reactivities of different oxygen transfer reagents were not compared so far. During my Master thesis in the Mayr/Ofial group I could show, that the nucleophilic reactivity of peroxide anions in alkaline, aqueous solution can be described by using Mayr's linear free energy relationship eq. 8 (Figure 1).[41] While the nucleophilicity parameters of the peroxide anions correctly predicted their reactivity in nucleophilic epoxidations, a surprising correlation with the basicity of the nucleophiles was observed. While increasing basicity is usually associated with increasing nucleophilicity, the opposite was found for peroxide anions: less basic peroxycarboxylate anions were found to be stronger nucleophiles than the anions of more basic hydroperoxides. This was rationalized by means of quantum-chemical calculations to originate from solvent effects with the de-solvation of the peroxide anions being a main factor.

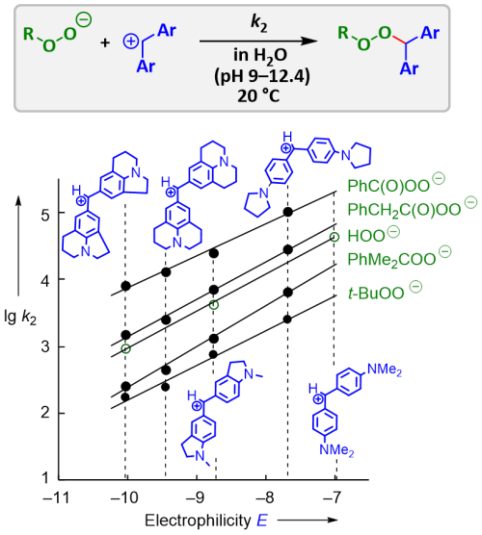

Figure 1: Plot of lg k_2 for the reactions of peroxide anions with benzhydrylium ions in alkaline aqueous solution at 20 °C versus the electrophilicity parameters *E* (with data for HOO^- from ref. 16). Figure adapted from ref. 41 (originally published in *Angewandte Chemie International Edition* and reprinted with permission from *Angew. Chem. Int. Ed.* **2017**, 13279-13282. Copyright 2017 Wiley)

However, it is unknown whether also the simpler inorganic oxygen-anions like persulfate or hypohalites show the same atypical relationship of nucleophilicity and basicity. Basicities of often used anionic oxygen transfer reagents in aqueous solution differ drastically ranging from hypochlorite (pK_{aH} = 7.53)[42] to hydroperoxide (pK_{aH} = 11.75).[43] The significantly less basic bromite anion (pK_{aH} = 3.43)[44] is

only rarely employed in chemical transformations and a quantification of its reactivity as a nucleophile was not performed to date.

Another question that arises in the context of bleach reagents is whether the reactivity of the anion of hydrogen peroxide is influenced by its origin from different formulations. While the nucleophilic reactivity of HOO^- was reported previously,[16] in commercial applications as well as in some syntheses, hydrogen peroxide is often used in the form of adducts with urea, carbonate or polymers. It is unclear, whether the presence of these coordinating additives affects the reactivity of hydroperoxide in chemical reactions. The detailed introduction and the results of the reactivity studies of bleach reagents are described in Chapter 2.

Recently, peroxyacids derived from amino acids were proposed as bleach reagents in the patent literature (Scheme 5).[45] In comparison to inorganic oxidants, it can be expected that the presence of the peroxycarboxylate moiety provides them with a higher reactivity.[41] Additionally, their high solubility in aqueous solutions and the formation of simple amino acids as side products makes ammoniumperoxycarboxylic acids (APOCAs) interesting species for both organic transformations as well as bleaching reagents. However, so far APOCAs were only shown to be active as bleaching reagents in the original patents and a comparison of their reactivity to other oxygen-transfer species therefore remained elusive.[45] Additionally, they were only characterized by melting points and elemental analysis, and no spectroscopic analysis of their constitution was performed so far. Structural characterization of APOCAs, studies of their physicochemical properties as well as their nucleophilic reactivities are discussed in Chapter 3.

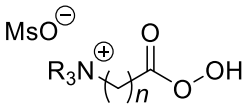

Scheme 5: Molecular formula of ammoniumperoxycarboxylic acid mesylates.

Solvation effects have been suggested to be of significant importance in modulating the reactivity of peroxide anions.[41] It is unclear whether this is a general trend for oxygen nucleophiles in aqueous solutions that also stands in aprotic solvents. Peroxide anions are known to react with a variety of organic solvents including MeCN or DMSO which hinders further studies of these nucleophiles in these solvents.[46] Therefore, phenolate ions were studied as they are oxygen-nucleophiles with a broad reactivity range: the pK_{aH} values of phenolates in water range from 0.40 for 2,4,6-trinitrophenol (picric acid)[47] to 10.2 for 4-methoxyphenol.[48] Like enolate ions, phenolate anions are ambident nucleophiles that cannot only react with electrophiles through their oxygen sites, but

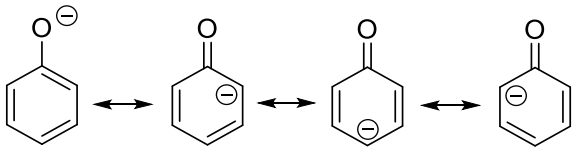

Scheme 6: Resonance structures of the phenolate ion.

also at the ortho- and para-carbon atoms as indicated by their resonance structures (Scheme 6).[49] Surprisingly, existing reactivity studies of phenolate anions with electrophiles were not able to quantitatively predict if reactions with electrophiles proceed through oxygen- or carbon attack. Traditionally, ambident reactivity has been rationalized by the principle of hard and soft acids and bases (HSAB) or the related Klopman-Salem concept of charge and orbital control.[50,51] A recent approach utilized Marcus theory and the concept of kinetic and thermodynamic control to rationalize ambident reactivity.[49] Kornblum and associates studied the S_N2 reactions of phenolate ions in different solvents and mostly found oxygen-attack to be dominating.[52] Carbon attack was only observed if the phenolate oxygen was blocked by coordination, either through hydrogen bonding in protic solvents, or through metal ions. Contradicting results were obtained by Richard and coworkers who used the azide ion diffusion clock method to determine rate constants for the reactions of phenolate in trifluoroethanol/water (1:1) mixtures.[53] In the analysis of reaction products with the 1-(4-methoxyphenyl)ethyl cation, they found comparable amounts of products originating from oxygen and carbon attack from which similar rate constants were derived (Scheme 7). However, the rate constants for the attack of both oxygen- and carbon-sites showed to be close to diffusion control, hampering the applicability to activation-controlled reactions.

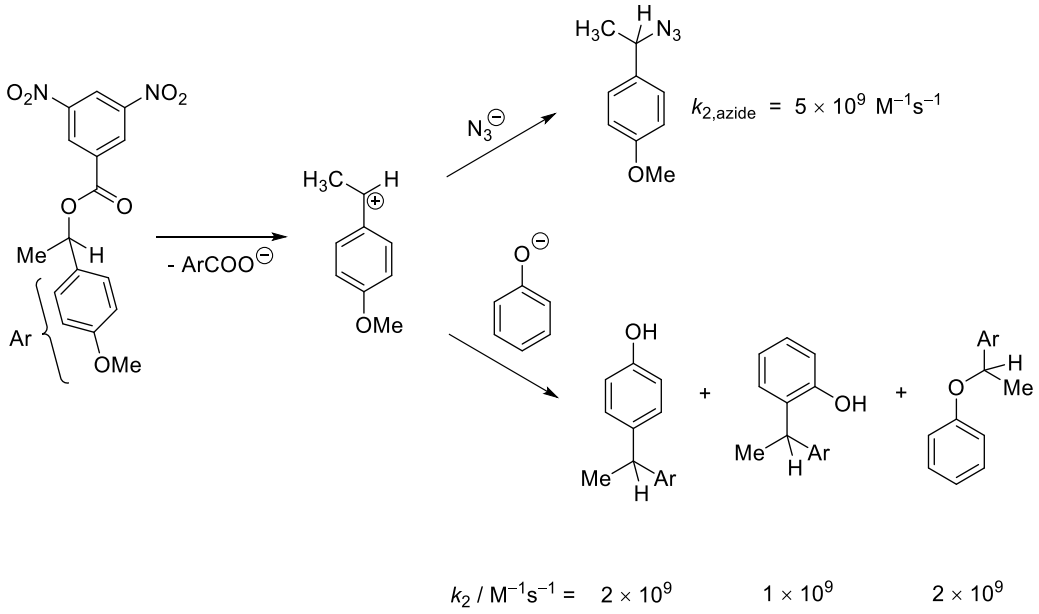

Scheme 7: Solvolysis experiments of Richard in trifluoroethanol/water (1:1) at 25 °C.[53] As the rate constants for the diffusion-controlled reactions of azide are known, experimental product ratios can be used to derive unknown rate constants.

For water as solvent, photometrically measured rate constants for the reactions of p-substituted phenolate ions with 2-aryl-4,6-dinitrobenzotriazole-1-oxides as reference electrophiles have been reported, which were analyzed according to eq. 8 and proposed to be originating from oxygen-attack at the C-7 position of the electrophiles (cf. Scheme 8 for numbering).[54] However, Buncel found that

based on NMR studies in d_6-DMSO these types of electrophiles react with potassium phenolate concurrently at their 1'-site with the phenolates' oxygen (Scheme 8, Pathway B) and at their 7-position with the phenolates' ortho- and para carbons (Scheme 8, Pathway A).[55]

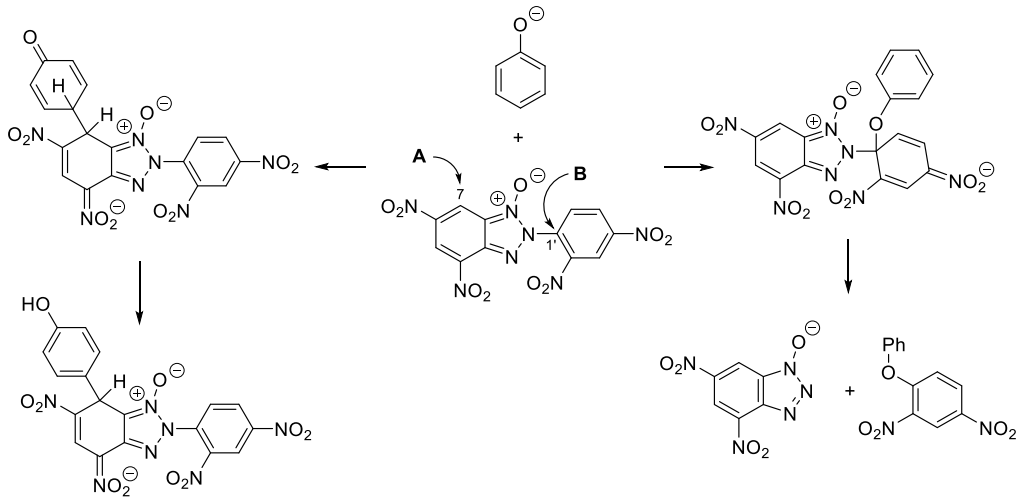

Scheme 8: Ambident reactivity of potassium phenolate with 2-*N*-(2',4'-dinitrophenyl)-4,6-dinitrobenzotriazol-1-oxide in d_6-DMSO according to NMR studies by Buncel.[55]

In order to gain insights of general validity into the reactivity of phenolate ions, it is the aim of this work to perform a detailed mechanistic study of the reactions of phenolate ions with benzhydrylium ions because the use of these electrophiles avoids problems of previous studies. While the nucleophilicity N/s_N of phenolates can be derived from kinetic measurements, the thermodynamic tendency of phenolate additions to benzhydrylium ions can be quantified by equilibrium constants according to eq. 9. In reactions where both rate and equilibrium constants are available, the rate constant for the reverse reaction can be calculated. In Chapter 4, the nucleophilic reactivity of phenolate ions is studied in detail and supplemented by an analysis of the reaction products and quantum chemical calculations.

Brønsted correlations have shown that thiolate anions are significantly stronger nucleophiles than oxygen nucleophiles of similar basicity.[56] Their high intrinsic nucleophilicity is of particular importance in biological systems where cysteine residues, which are present in proteins or peptides, form covalent bonds with a broad spectrum of electrophilic compounds. The most abundant thiol in animal cells is glutathione, a tripeptide of glutamic acid, cysteine and glycine, with intracellular concentrations in the range from 1 to 10 mM.[57] The reaction of deprotonated glutathione with electrophiles is a process of physiological importance and e.g. relevant for cell detoxification (Scheme 9).[58]

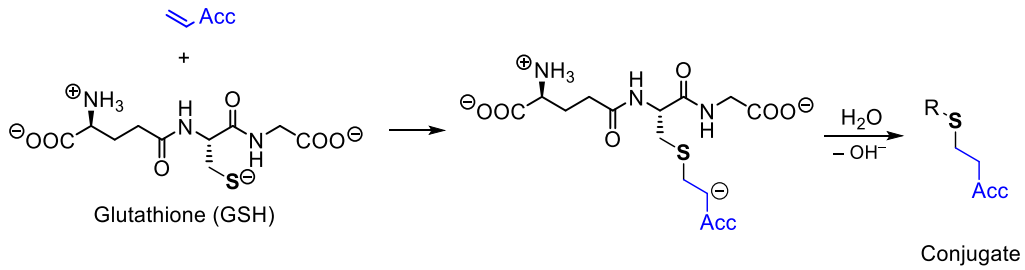

Scheme 9: Reaction of deprotonated glutathione with a Michael acceptor to a covalent conjugate.

Additionally, glutathione is frequently used as a model for the reactivity of reactive cysteine residues in proteins toward electrophilic species.[59] Therefore, methods for the determination of GSH levels in cells have been developed, which either rely on the reversible bonding of GSH to an electrophilic fluorescence probe,[60] or on kinetic assays that study the rates of the reactions of GSH with various electrophiles.[61] Kinetic studies by Esterbauer, Friedman, Schüürmann and coworkers have been performed for the reaction of hundreds of electrophiles with GSH at physiological pH value, that is pH = 7.4.[62,58] Additionally, the GSH fluorescent probes that are commonly used by biochemists, are typically characterized by the rate constant of their reactions with GSH.[60]

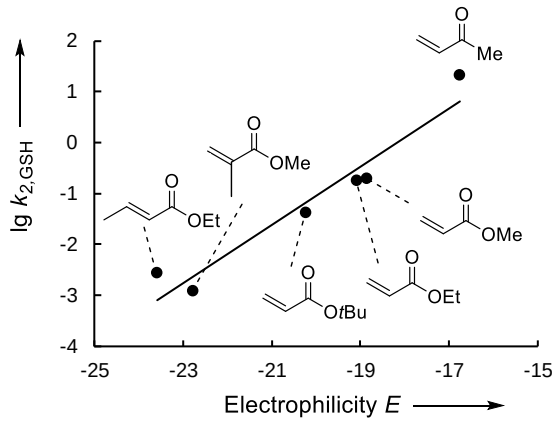

Figure 2: Correlation of the rate constants for the reaction of GSH (measured in aqueous, buffered DMSO at pH = 7.4 and 25 °C, converted from M^{-1} min^{-1} to M^{-1} s^{-1}). Adapted from ref. 63 based on data from ref. 58.

The electrophilic reactivities of Michael acceptors have recently been quantified according to eq. 8 by studying the rates of their reactions with carbanions, sulfonium and pyridinium ylides.[63] While the linear correlation of GSH-derived rate constants with electrophilicity parameters of Michael acceptors was noticed (Figure 2), no direct interconnection was performed.[63] The reason for this is the complicated acid/base behavior of GSH: A nucleophilicity parameter derived from the correlation in Figure 2 would only be valid at pH = 7.4/25 °C and not for the different conditions used in assays by other authors. Moreover, the Michael acceptors shown in Figure 2 have not yet been proven to be reliably reference electrophiles in water as their reactivity might be heavily influenced by hydrogen bonding. Another uncertainty is introduced by the biochemical assays used to derive rate constants

for the reactions of GSH with electrophiles: As these assays do not measure second-order rate constants by following the conversion of the reactants to the product but rather rely on an indicator that has to be manually added after certain time intervals, it is unknown whether these rate constants are of sufficient accuracy for general predictions. Therefore, assessment of a reliable nucleophilicity parameter of GSH makes kinetic studies with reference electrophiles at different pH values under defined reaction conditions necessary. In a next step, it can then be tested whether eq. 8 holds for both reference electrophiles and Michael acceptors and, finally, also for rate constants that have not been directly measured but obtained from biochemical assays. In Chapter 5 the results on the determination of the nucleophilicity parameters N/s_N of glutathione is discussed with the aim to establish a general connection between different reactivity scales.

1.3 Basicity Scales Toward Heteroatom Lewis Acids

The concept of Lewis acidity and basicity is of fundamental importance to chemists.[64] Different types of Lewis acids have applications both as reagents or as catalysts. Reactions of Lewis acids with Lewis bases involve the formation of a Lewis adduct. The extent of adduct formation can be quantified by an equilibrium constant. As mentioned above, a concept for the quantification of Lewis acidity and basicity is not as straightforward as for Brønsted acids/bases.

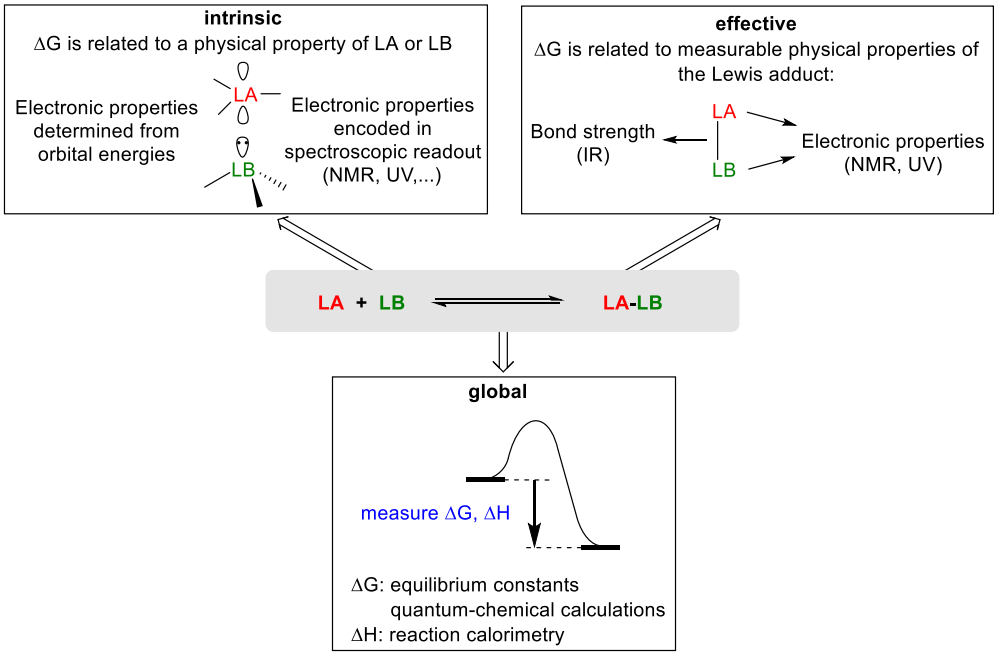

Scheme 10: Classification of scaling methods for Lewis acidity scales according to Greb,[65] generalized to also apply to Lewis basicity scales.

In a recent review, Greb classified global, effective and intrinsic methods used for the construction of Lewis acidity scales, a differentiation that can analogously be applied to Lewis basicity scales (Scheme

10).[65] Global methods characterize the adduct formation of a Lewis acid and base by the reaction Gibbs energy ΔG or in simpler setups the reaction enthalpy ΔH. These quantities are either accessible through experimental measurements e.g. by calorimetry or equilibrium measurements but also through quantum-chemical calculations. An example for a global reactivity scale relying on calorimetric measurements is the BF_3 affinity scale by Gal,[66] which ranks different Lewis bases based on their reaction enthalpy with BF_3 in dichloromethane at 25 °C, or Gutmann's SbF_5 scale for the Lewis basicity of solvents.[67] A scale which uses the Gibbs energy ΔG as observed quantity is the combined Lewis acidity/basicity scale by Mayr toward benzhydrylium ions (eq. 9).[20] Generally, Lewis acidity scales that are based on experimental equilibrium constants are rare, presumably due to difficulties associated with covering substrates of a wide reactivity range or the expensive thermochemical equipment necessary for calorimetric studies. While the above-mentioned examples show that the construction of experimentally based Lewis acidity scales is possible, most often quantum-chemical calculations are used to assess the Lewis acidity of novel compounds. Gas-phase fluoride ion affinities which can be determined by ion cyclotron resonance (ICR) spectroscopy,[68] are easily accessible by quantum-chemical calculations and found broad application in the chemical literature. Analogous "affinity scales" in both gas-phase and solution are based on the quantum-chemically calculated energetics of hydride, methyl anion or ammonia addition.[65]

The most common experimental method for the characterization of Lewis acids are effective measurements. Effective measurements study the changes in the UV, IR, or NMR spectroscopic features of a selected reference Lewis base upon the conversion from the free to the bound state.

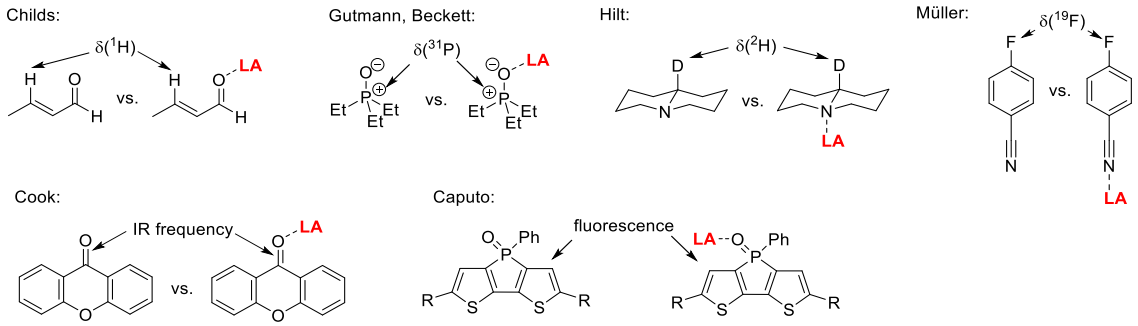

Scheme 11: Classification methods for quantifying Lewis acidity. For references, see the subsequent text.

However, the infinite number of potential reference Lewis bases gives rise to an ongoing evolvement of new methods that supplement the existing repertoire of Lewis acidity scales (some examples are shown in Scheme 11). The most popular effective methods for the characterization of Lewis acids are based on NMR spectroscopy. In the Child's method, the difference between the ^{1}H NMR shift of free *trans*-crotonaldehyde and a 1:1 complex with a Lewis acid is compared.[69] Similarly, the Gutmann-Beckett method uses the ^{31}P NMR shift of triethylphosphine oxide in its free or bound state as a

measure for the strength of a Lewis acid.[70] More recently, various new reference Lewis bases for Lewis acidity measurements have been proposed. In the method by Hilt, the ^{2}H NMR shift of a monodeuterated quinolizidine is used,[71] while Müller employed the ^{19}F nucleus of 4-fluorobenzonitrile as probe.[72] The change of the carbonyl-oxygen band in the infrared spectrum of xanthone was used by Cook,[73] while recent work by Caputo and coworkers monitored the change in the fluorescence of a thienephosphole.[74]

Lastly, intrinsic methods for the characterization of Lewis acids study the electronic structure of the Lewis acid e.g. through quantum chemically calculated LUMO energies, global electrophilicity indices or experimental properties (e.g. NMR chemical shifts) that provide information on the electronic structure of a Lewis acid. While these intrinsic methods can be used to establish a reactivity ranking for a certain class of compounds, they neglect the structural changes concurring with Lewis base binding. Therefore, they might only work within a series of structurally closely related systems.

In this thesis, it is the aim to develop Lewis acidity scales exclusively by direct measurements of equilibrium constants. Herein, two different types of Lewis acids were investigated: Diaryliodonium ions and triarylboranes. In Chapter 6 the development of a quantitative Lewis acidity for diaryliodonium ions is discussed. While some diaryliodonium ions were recently characterized by the Gutmann-Beckett method and compared to other Lewis acids,[75] only few experimental equilibrium constants with nitrogen heterocycles and 16-crown-6 were determined so far by ^{1}H NMR spectroscopy. In this work, a set of experimental equilibrium constants for the reactions of diaryliodonium ions with various O-, N-, P-, and halide Lewis bases is determined in a first step which are then analyzed to derive a global Lewis acidity scale.

In contrast to diaryliodonium ions, boranes are generally considered to be strong Lewis acids and are mostly employed as catalysts.[76] Beside catalysis due to activation of Lewis basic functional groups, the adducts of highly Lewis acidic fluorinated boranes with sterically hindered Lewis bases, so-called frustrated Lewis pairs, are potent catalysts.[77] Despite the many applications of boranes, there are only very few directly measured equilibrium constants for Lewis base/borane combinations reported in the literature.[78] Consequently, Lewis acidities determined by using the Gutmann-Beckett or Child's methods are broadly used to compare the acidities of different boranes.[79] An absolute Lewis acidity/basicity scale of boranes would therefore be of fundamental importance for the field as it enables quantitative predictions of reactions. Additionally, the availability of a Lewis acidity scale derived from equilibrium measurements would allow to test the different proposed scaling methods for their accuracy. The efforts for the development of a quantitative Lewis acidity scale for boranes are the topic of Chapter 7.

1.4 Objectives

Inorganic oxidants are generally considered to be potent nucleophiles, but only the nucleophilic reactivity of hydrogen peroxide and hypochlorite has been studied in more detail.[16,34-40] Kinetic measurements of the reactions of various inorganic oxidants with reference electrophiles (Chapter 2) should provide a precise quantification of their nucleophilic reactivities. The reactivity of oxidants should then become directly comparable with other types of peroxides based on Mayr's nucleophilicity scale.[41] This should enable the rational development of conditions e.g. for nucleophilic epoxidation reactions but also to provide further validation into the concept of the so-called α-effect.[35-37]

The compound class of ammoniumperoxycarboxylic acids (APOCAs) (Chapter 3) was so far only mentioned in the patent literature.[45] Previous studies on the nucleophilic reactivity of peroxide anions suggest that APOCAs might exhibit a high nucleophilic reactivity combined with a low acidity.[41] Thus, they might be useful compounds in synthesis. Kinetic measurements with benzhydrylium ions of known electrophilicity should allow a quantification of their nucleophilic reactivity and a definition of their synthetic scope.

To get an insight into the effects of different solvents on the rate constants of the reactions of oxygen nucleophiles with electrophiles, the nucleophilic reactivity of phenolate anions should next be investigated (Chapter 4). This should provide insights into solvation effects on the reactivity of oxygen-nucleophiles. Additionally, there are contradicting reports on the ambident reactivity of phenolates in the literature that do not allow to derive general predictions of the reactivity of phenolates with electrophiles.[52-55] The study of the products, rate and equilibrium constants of the reactions of different phenolates with various reference electrophiles together with quantum-chemical calculations should give detailed insights into the ambident reactivity of phenolate ions.

Based on the experiences gained in the study of the reactions of oxygen-nucleophile with electrophiles, the nucleophilicity of thiolate should be investigated on the example of the tripeptide glutathione (Chapter 5). Biochemical assays frequently employ rate-constants for the reactions of electrophiles with glutathione and are tabulated for numerous compounds in the literature.[58-62] However, a direct connection with Mayr's reactivity scale has not been performed yet, though a previous analysis indicates that it is possible.[63] Measurements of the rate constants of the reactions of glutathione with reference electrophiles with known electrophilicity parameters should be used to derive the nucleophilicity parameters N/s_N. Knowledge of the nucleophilicity parameters should enable to connect data from the literature with Mayr's electrophilicity scale and to derive structure-reactivity relationships for a variety of Michael acceptors.

In the second main part of this thesis, Lewis basicity scales toward heteroatom Lewis acids should be developed. Existing methods to quantify Lewis acidity often rely on the measurement of indirect spectroscopic properties of a fixed reference Lewis base in contrast to directly determined equilibrium constants. As exemplified for diaryliodonium ions (Chapter 6) and boranes (Chapter 7), methods for the determination of equilibrium constants for the associations with different O-, N-, P- and halogen Lewis bases should be developed. This should allow to derive general relationships of Lewis acidity and basicity that can be used for quantitative predictions of the association constants of Lewis adducts.

All parts of this thesis have already been published or submitted for publication. At the beginning of each chapter, the list of authors and the individual contributions are stated. Additionally, each chapter features a detailed introduction covering the relevant literature in more detail.

1.5 References

[1] H. Mayr, *Isr. J. Chem.* **2016**, *56*, 30-37.

[2] J. N. Brønsted, *Recl. Trav. Chim. Pays Bas* **1923**, *42*, 718-728.

[3] a) There are numerous summaries of acidities available in the literature. A summary of various inorganic and organic compounds was compiled by R. Williams which is accessible under: https://www.chem.wisc.edu/areas/reich/pkatable/pKa_compilation-1-Williams.pdf (accessed on 27.04.2020); b) Bordwell measured numerous acidities in DMSO: F. G. Bordwell *Acc. Chem. Res.* **1988**, *21*, 456-463; c) For a recent review covering basicities in different organic solvents see: S. Tshepelevitsh, A. Kütt, M. Lõkov, I. Kaljurand, J. Saame, A. Heering, P. G. Plieger, R. Vianello, I. Leito, *Eur. J. Org. Chem.* **2019**, 6735-6748; d) I. Leito provides an overview on various pK_a scales for organic compounds under http://tera.chem.ut.ee/~ivo/HA_UT/ (accessed on 27.04.2020); e) Internet Bond-energy Databank (pK_a and BDE)− iBonD Home Page. http://ibond.nankai.edu.cn/pka (accessed on 19.05.2020)

[4] G. N. Lewis, *Valence and the Structure of Atoms and Molecules*. New York, New York, U.S.A. **1923**: Chemical Catalog Company, pp. 142-143.

[5] C. K. Ingold, *J. Chem. Soc.* **1933**, 1120-1127.

[6] H. Mayr, A. R. Ofial, *Acc. Chem. Res.* **2016**, *49*, 952-965.

[7] J. N. Brønsted, *Chem. Rev.* **1928**, *5*, 231-338.

[8] L. P. Hammett, *Chem. Rev.* **1935**, *17*, 125-136.

[9] L. P. Hammett, *J. Am. Chem. Soc.* **1937**, *59*, 96-103.

[10] L. P. Hammett, Physical Organic Chemistry, McGraw-Hill, New York, **1940**.

[11] C. Hansch, A. Leo, D. Hoekman, Exploring QSAR – Hydrophobic, Electronic, and Steric Constants (ACS Professional Reference Book); American Chemical Society, Washington, DC, 1995.

[12] C. G. Swain, C. B. Scott, *J. Am. Chem. Soc.* **1953**, *75*, 141-147.

[13] R. G. Pearson, H. R. Sobel, J. Songstad, *J. Am. Chem. Soc.* **1968**, *90*, 319-326.

[14] a) C. D. Ritchie, *Acc. Chem. Res.* **1972**, *5*, 348–354; b) C. D. Ritchie, *J. Am. Chem. Soc.* **1975**, *97*, 1170-1179.

[15] C. D. Ritchie, *Can. J. Chem.* **1986**, *64*, 2239-2250.

[16] S. Minegishi, H. Mayr, *J. Am. Chem. Soc.* **2003**, *125*, 286-295.

[17] L. A. P. Kane-Maguire, E. D. Honig, D. A. Sweigart, *Chem. Rev.* **1984**, *84*, 525-543.

[18] a) H. Mayr, M. Patz, *Angew. Chem. Int. Ed. Engl.* **1994**, *33*, 938–957; b) H. Mayr, T. Bug, M. F. Gotta, N. Hering, B. Irrgang, B. Janker, B. Kempf, R. Loos, A. R. Ofial, G. Remennikov, H. Schimmel, *J. Am. Chem. Soc.* **2001**, *123*, 39, 9500-9512; c) H. Mayr, B. Kempf, A. R. Ofial, *Acc. Chem. Res.* **2003**, *36*, 66–77; d) H. Mayr, S. Lakhdar, B. Maji, A. R. Ofial, *Beilstein J. Org. Chem.* **2012**, *8*, 1458–1478; e) H. Mayr, A. R. Ofial, *SAR QSAR Environ. Res.* **2015**, *26*, 619–646; f) H. Mayr, *Tetrahedron* **2015**, *71*, 5095-5111.

[19] T. B. Phan, M. Breugst, H. Mayr, *Angew. Chem. Int. Ed.* **2006**, *45*, 3869-3874.

[20] H. Mayr, J. Ammer, M. Baidya, B. Maji, T. A. Nigst, A. R. Ofial, T. Singer, *J. Am. Chem. Soc.* **2015**, *137*, 2580-2599.

[21] a) B. Denegri, A. Streiter, S. Juric, A. R. Ofial, O. Kronja, H. Mayr, *Chem. Eur. J.* **2006**, *12*, 1648-1656; *Chem. Eur. J.* **2006**, *12*, 5415; b) N. Streidl, B. Denegri, O. Kronja, H. Mayr, *Acc. Chem. Res.* **2010**, *43*, 1537-1549.

[22] H. Mayr, A. R. Ofial, *Acc. Chem. Res.* **2016**, *49*, 952-965.

[23] L. J. Thénard, *Ann. Chim. Phys.* **1818**, *8*, 306–312.

[24] R. Hage, A. Lienke, *Angew. Chem. Int. Ed.* **2006**, *45*, 206 –222.

[25] a) A. Uhl, M. Bitzer, H. Wolf, D. Hermann, S. Gutewort, M. Völkl, I. Nagl, "*Peroxy Compounds, Organic*". Ullmann's Encyclopedia of Industrial Chemistry. Weinheim: Wiley-VCH, **2018**; b) G. Goor, J. Gleeneberg, S. Jacobi, J. Dadabhoy, E. Candido, "Hydrogen Peroxide". Ullmann's Encyclopedia of Industrial Chemistry. Weinheim: Wiley-VCH, **2019.**

[26] G. W. Kabalka, M. S. Reddy, Y. Chen, *e-EROS* **2016**, DOI: 10.1002/047084289X.rn00950.pub2.

[27] H. Heaney, F. Cardona, A. Goti, A. L. Frederick, *e-EROS* **2013**, DOI: 10.1002/047084289X.rh047.pub3.

[28] J. K. Crandall, Y. Shi, C. P. Burke, B. R. Buckley, *e-EROS* **2012**, DOI: 10.1002/047084289X.rp246.pub3.

[29] a) P. M. Keehn, S. O. Nwaukwa, A. A. Kulkarni, *e-EROS* **2013**, DOI: 10.1002/047084289X.rc006.pub2; b) J. M. Galvin, E. N. Jacobsen, M. Palucki, M. O. Frederick, *e-EROS* **2013**, DOI: 10.1002/047084289X.rs084.pub3.

[30] a) E. Weitz, A. Scheffer, *Chem. Ber.* **1921**, *54*, 2327-2344; b) A. Berkessel, N. Vogl in *The Chemistry of Peroxides Vol. 2* (Ed.: Z. Rappaport), Wiley, Hoboken, **2006**, Chapt 6, pp 307-596.

[31] a) M. Renz, B. Meunier, *Eur. J. Org. Chem.* **1999**, 737-750; b) I. A. Yaremenko, V. A. Vil, D. V. Demchuk, A. O. Terent'ev, *Beilstein J. Org. Chem.* **2016,** *12,* 1647–1748.

[32] For a review see: M. Makosza, *Chem. Soc. Rev.* **2010**, *39*, 2855–2868.

[33] a) H. D. Dakin, *Am. Chem. J.* **1909**, *42*, 477-498; b) M. B. Hocking, J. H. Ong, *Can. J. Chem.* **1977**, *55*, 102-110.

[34] C. A. Bunton, G. J. Minkoff, *J. Chem. Soc.* **1949**, 665-670.

[35] W. P. Jencks, J. Carriuolo, *J. Am. Chem. Soc.* **1960**, *82*, 1778-1786.

[36] J. O. Edwards, R. G. Pearson, *J. Am. Chem. Soc.* **1962**, *84*, 16-24.

[37] J. E. Dixon, T. C. Bruice, *J. Am. Chem. Soc.* **1971**, *93*, 6592-6597.

[38] I. E. Mclsaac, Jr., L. R. Subbaraman, J. Subbaraman, H. A. Mulhausen, E. J. Behrman, *J. Org. Chem.* **1972**, *37*, 1037–1041.

[39] C. D. Ritchie, M. Sawada, *J. Am. Chem. Soc.* **1977**, *99*, 3754–3761.

[40] I.-H. Um, L.-R. Im, E. Buncel, *J. Org. Chem.* **2010**, *75*, 8571–8577.

[41] R. J. Mayer, T. Tokuyasu, P. Mayer, J. Gomar, S. Sabelle, B. Mennucci, H. Mayr, A. R. Ofial, *Angew. Chem. Int. Ed.* **2017**, *56*, 13279-13282.

[42] J. W. Ingham, J. Morrison, *J. Chem. Soc.* **1933**, 1200‑1205.

[43] M. G. Evans, N. Uri, *Trans. Faraday Soc.* **1949**, *45*, 224‑230.

[44] R. C. Troy, D. W. Margerum, D. W. *Inorg. Chem.* **1991**, *30*, 3538‑3543 and refs cited therein.

[45] a) C. Venturello, C. Cavallotti, EP 0316809 A2, **1988**; b) J. R. Darwent, K. C. Francis, J. Oakes, D. W. Thornthwaite, US4904406A, **1988**; c) C. Venturello, C. Cavallotti, F. Achilli, US5117049A, **1991**; d) C. Venturello, C. Cavallotti, US5245075, **1993**; e) C. Venturello, C. Cavallotti, US5294362A, **1994**; f) J. Oakes, D. W. Thornthwaite, WO 94/21605, **1994**; g) J. Oakes, D. W. Thornthwaite, WO 97/16515, **1997.**

[46] a) G. B. Payne, P. H. Deming, P. H. Williams, *J. Org. Chem.* **1961**, *26*, 659-663; b) A. F. Choban, I. R. Yurchuk, A. S. Lyavinets, *Russ. J. Gen. Chem.* **2008**, *78*, 2071-2074.

[47] P. J. Pearce, R. J. J. Simkins, *Can. J. Chem.* **1968**, *46*, 241- 248.

[48] L. A. Cohen, W. M. Jones, *J. Am. Chem. Soc.* **1963**, *85*, 3397-3402.

[49] H. Mayr, M. Breugst, A. R. Ofial, *Angew. Chem. Int. Ed.* **2011**, *50*, 6470-6505.

[50] (a) R. G. Pearson, Hard and Soft Acids and Bases. *J. Am. Chem. Soc.* **1963**, *85*, 3533−3539. (b) R. G. Pearson, *Science* **1966**, *151*, 172−177. (c) R. G. Pearson, J. Songstad, *J. Am. Chem. Soc.* **1967**, *89*, 1827−1836. (d) R. G. Pearson, *J. Chem. Educ.* **1968**, *45*, 581. (e) R. G. Pearson, *J. Chem. Educ.* **1968**, *45*, 643− 648. (f) R. G. Pearson. Chemical Hardness; Wiley-VCH: Weinheim, Germany, 1997.

[51] (a) G. Klopman, *J. Am. Chem. Soc.* **1968**, *90*, 223− 234; (b) L. Salem, *J. Am. Chem. Soc.* **1968**, *90*, 543−552.

[52] a) N. Kornblum, A. P. Lurie, *J. Am. Chem. Soc.* **1959**, *81*, 2705-2715; b) N. Kornblum, P. J. Berrigan, W. J. Le Noble, *J. Am. Chem. Soc.* **1960**, *82*, 1257-1258; c) N. Kornblum, P. J. Berrigan, W. J. Le Noble, *J. Am. Chem. Soc.* **1963**, *85*, 1141-1147.

[53] Y. Tsuji, M. M. Toteva, H. A. Garth, J. P. Richard, *J. Am. Chem. Soc.* **2003**, *125*, 15455-15465.

[54] W. Gabsi, T. Boubaker, R. Goumont, *Int. J. Chem. Kinet.* **2014**, *46*, 711−717.

[55] E. Buncel, J. M. Dust, *Can. J. Chem.* **1988**, *66*, 1712-1719.

[56] F. G. Bordwell et al. in Nucleophilicity (J. M. Harris, S. P. Mc Manus, eds.), American Chemical Society, Washington, 1987, Chapter 9.

[57] A. Meister, *J. Biol. Chem.* **1988**, *263*, 17205–17208.

[58] A. Böhme, A. Laqua, G. Schüürmann, *Chem. Res. Toxicol.* **2016**, *29*, 952–962.

[59] L. Petri, P. Ábrányi-Balogh, P. R. Varga, T. Imre, G. M. Keserű, *Bioorg. Med. Chem.* **2020**, *28*, 115357.

[60] a) X. Jiang, J. Chen, A. Bajić, C. Zhang, X. Song, S. L. Carroll, Z.-L. Cai, M. Tang, M. Xue, N. Cheng, C. P. Schaaf, F. Li, K. R. MacKenzie, A. C. M. Ferreon, F. Xia, M. C. Wang, M. Maletić-Savatić, J. Wang, *Nat. Commun*. **2017**, *8*, 16087; b) C. Cossetti, G. Di Giovamberardino, R. Rota, A. Pastore, *Nat. Commun*. **2018**, *9*, 1588; c) K. Umezawa, M. Yoshida, M. Kamiya, T. Yamasoba, Y. Urano, *Nat. Chem*. **2017**, *9*, 279–286; d) G. Yin, T. Niu, T. Yu, Y. Gan, X. Sun, P. Yin, H. Chen, Y. Zhang, H. Li, S. Yao, *Angew. Chem. Int. Ed*. **2019**, *58*, 4557–4561.

[61] a) T. W. Schultz, J. W. Yarbrough, E. L. Johnson, *SAR QSAR Environ. Res.* **2005**, *16*, 313–322; b) J. W. Yarbrough, T. W. Schultz, *Chem. Res. Toxicol.* **2007**, *20*, 558–562.

[62] a) M. Friedman, J. F. Cavins, J. S. Wall, *J. Am. Chem. Soc*. **1965**, *87*, 3672–3682; b) H. Esterbauer, H. Zollner, N. Scholz, *Z. Naturforsch*. *C* **1975**, *30*, 466–473.

[63] D. S. Allgäuer, H. Jangra, H. Asahara, Z. Li, Q. Chen, H. Zipse, A. R. Ofial, H. Mayr, *J. Am. Chem. Soc.* **2017**, *139*, 13318-13329.

[64] a) C. Laurance, J.-F. Gal, *Lewis Basicity and Affinity Scales: Data and Measurement*; Wiley: Chichester, UK, 2010; b) E. Vedejs, S. E. Denmark, *Lewis Base Catalysis in Organic Synthesis*; Wiley-VCH: Weinheim, Germany, 2016.

[65] L. Greb, *Chem. Eur. J.* **2018**, *24*, 17881-17896.

[66] For a review of the method and an overview of BF_3 affinities see Ref. 64a, Chapter 3.

[67] For a review of the method and an overview of determined numbers see Ref. 64a, Chapter 2.

[68] J. C. Haartz, D. H. McDaniel, *J. Am. Chem. Soc.* **1973**, *95*, 8562–8565.

[69] R. F. Childs, D. L. Mulholland, A. Nixon, *Can. J. Chem* **1982***, 60,* 801–808.

[70] M. A. Beckett, G. C. Strickland, J. R. Holland, K. S. Varma, *Polymer* **1996**, *37*, 4629-4631.

[71] G. Hilt, F, Pünner, J. Möbus, V. Naseri, M. A. Bohn, *Eur. J. Org. Chem.* **2011**, 5962-5966.

[72] S. Künzler, S. Rathjen, A. Merk, M. Schmidtmann, T. Müller, *Chem. Eur. J*. **2019**, *25*, 15123-15130.

[73] D. Cook, *Can. J. Chem.* **1963**, *41*, 522-526.

[74] J. R. Gaffen, J. N. Bentley, L. C. Torres, C. Chu, T. Baumgartner, C. B. Caputo, *Chem* **2019**, *5*, 1567-1583.

[75] A. Labattut, P.-L. Tremblay, O. Moutounet, C. Y. Legault, *J. Org. Chem.* **2017**, *82*, 11891-11896.

[76] J. L. Carden, A. Dasgupta, R. L. Melen, *Chem. Soc. Rev.* **2020**, *49*, 1706-1725.

[77] D. W. Stephan, *Science* **2016**, 354, aaf7229.

[78] a) D. J. Parks, W. E. Piers, *J. Am. Chem. Soc.* **1996**, *118*, 9440-9441; b) M. M. Morgan, A. J. V. Marwitz, W. E. Piers, M. Parvez, *Organometallics* **2013**, *32*, 317-322; c) S. Geier, D. W. Stephan, *J. Am. Chem. Soc.* **2009**, *131*, 3476-3477; d) Y. Kitamoto, F. Kobayashi, T. Suzuko, Y. Miyata, H. Kita, K. Funaki, S. Oi, *Dalton Trans.* **2019**, *48*, 2118-2127.

[79] I. B. Sivaev, V. I. Bregadze, *Coord. Chem. Rev.* **2014**, *270-271*, 75-88.

Chapter 2. Nucleophilic Reactivities of Bleach Reagents

Robert J. Mayer, Armin R. Ofial, *Org. Lett.* **2018**, *20*, 2816-2820.

Author Contributions

RJM performed all experiments. The manuscript was written jointly by RJM and ARO.

Copyright

Selected supporting material for this work is provided starting with section 2.1. The complete supporting information (SI) is published online and can be accessed under https://doi.org/10.1021/acs.orglett.8b00645.

Organic LETTERS

Letter

Cite This: Org. Lett. 2018, 20, 2816−2820

pubs.acs.org/OrgLett

Nucleophilic Reactivities of Bleach Reagents

Robert J. Mayer and Armin R. Ofial*

Department Chemie, Ludwig-Maximilians-Universität München, Butenandtstraße 5−13, 81377 München, Germany

Supporting Information

ABSTRACT: The nucleophilicities of the oxidants hydroperoxide, hypochlorite, hypobromite, bromite, and peroxymonosulfate were determined by following the kinetics of their reactions with a series of benzhydrylium ions of known electrophilicity (E) in alkaline, aqueous solutions at 20 °C. The reactivities of the oxidants correlate only weakly with their basicities. Analyzing the rate constants by using the relationship $\log k_2 = s_N(N + E)$ gave the parameters N (and s_N), which were applied to predict the rates of Weitz−Scheffer epoxidations.

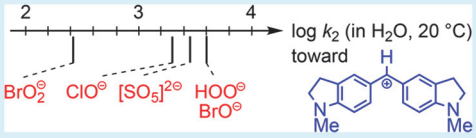

Hydrogen peroxide, hypochlorite, or persulfates are low-cost oxygen-nucleophiles and are often the oxidants of choice for industrial applications. They are used for the transfer of oxygen atoms in organic synthesis[1] and also at large scale for the bleaching of paper pulp and textiles, in disinfectants, or as ingredients in cosmetics.[2] It is generally recognized that the hydroperoxide anion, hypochlorite, or persulfate are nucleophilic species that undergo analogous reactions with organic electrophiles. Although several of these reactions had been studied kinetically[3] and reactions of bleach reagents with cationic organic food dyes are used in tutorials for introducing kinetic methods to students,[4] a direct comparison of reactivities of different oxygen-transfer reagents is not available to date.

We now set out to investigate the nucleophilic reactivity of the hydroperoxide anion (**1**, originating from H_2O_2−urea, H_2O_2−polyvinylpyrrolidone, or H_2O_2−sodium carbonate complexes), hypochlorite (**2**), hypobromite (**3**), peroxymonosulfate (**4**), and bromite (**5**) in alkaline, aqueous solution by following the kinetics of their reactions with the benzhydrylium ions **6a**−**6e** as reference electrophiles (Figure 1). The second-order rate constants k_2(20 °C) of these reactions and the known electrophilicities E of **6a**−**6e**[5] were then applied in the linear free-energy relationship (see eq 1)[6] to derive the nucleophilicity parameters N and the susceptibilities s_N of the oxidants **1**−**5**.

$$\log k_2(20°C) = s_N(N + E) \quad (1)$$

Thus, the anionic oxygen nucleophiles studied in this work can be integrated into Mayr's comprehensive nucleophilicity scale,[7] which enables the direct comparison of the nucleophiles **1**−**5** with previously investigated organic peroxide anions[8] and more than 1000 other nucleophilic species whose reactivities were investigated by the benzhydrylium method.[6c]

We observed that the decoloration of the deeply blue aqueous solution of **6a** upon treatment with an alkaline solution of hydrogen peroxide (2 equiv H_2O_2, from $\mathbf{1}_{UHP}$) was accompanied by the formation of a colorless precipitate. Concentration of a dichloromethane extract of the reaction mixture yielded colorless needles (mp 137 °C), which were analyzed by single-crystal X-ray diffraction (XRD). Instead of the expected 1:1-adduct, benzhydryl hydroperoxide **7**, the bis(benzhydryl)peroxide **8** was detected, which can be rationalized by the subsequent reaction of the initially formed benzhydryl hydroperoxide **7** with a second equivalent of **6a**. Isolating the precipitate by filtration of the aqueous reaction mixture gave **8** in a yield of 58% (see Scheme 1).

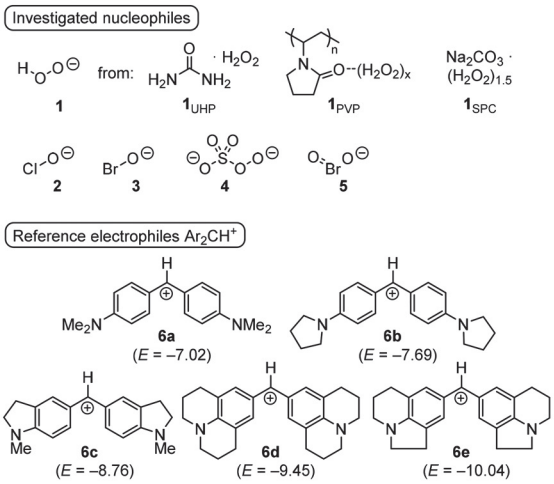

Figure 1. Nucleophiles and reference electrophiles included in this study. Electrophilicity (E) values are taken from ref 5.

As in the solid-state structure of bis(triphenylmethyl)-peroxide,[9,10] **8** has a center of inversion in its crystal structure and a C−O−O−C dihedral angle of 180°. Steric bulk around the COOC units is compensated differently in **8** and $Ph_3COOCPh_3$, however: bis(triphenylmethyl)peroxide has a "normal" O−O bond length (148.0 pm),[9,11] but elongated C−O (146.1 pm) and C−C_{ar} distances (153.3 pm). In contrast, the solid-state structure of **8** is characterized by normal C−O (140.6 pm) and C−C_{ar} bond lengths (152.5 pm), but an unusually long O−O bond (151.3 pm), which is significantly longer than the usually observed O−O bond lengths in other dialkyl peroxides (145−146 pm).[10,11] Packing effects may

Received: February 22, 2018
Published: May 9, 2018

DOI: 10.1021/acs.orglett.8b00645
Org. Lett. 2018, 20, 2816−2820

Scheme 1. Bis(benzhydryl)peroxide 8 from the Reaction of 6a with Hydrogen Peroxide in Alkaline Solution

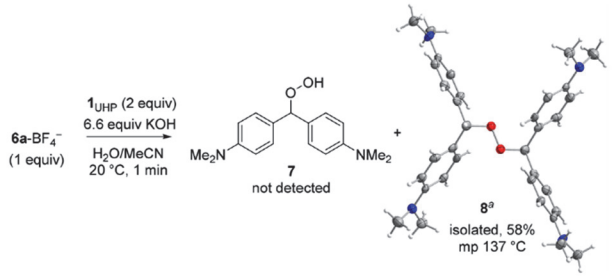

[a]Molecular structure of **8** in the crystal (thermal ellipsoids are drawn at a 50% probability level at T = 100 K).

account for these structural differences, because the solid-state structure of **8** shows motifs of intermolecular $\pi-\pi$ stacking, which are not found in the crystal structure of bis-(triphenylmethyl)peroxide [see the Supporting Information (SI)].

The kinetics of the reactions of **1**–**5** with the benzhydrylium ions **6b**–**6e** as reference electrophiles were measured in alkaline, aqueous solution by using the previously established procedure (see Figure 2).[8,12] In all kinetic experiments,

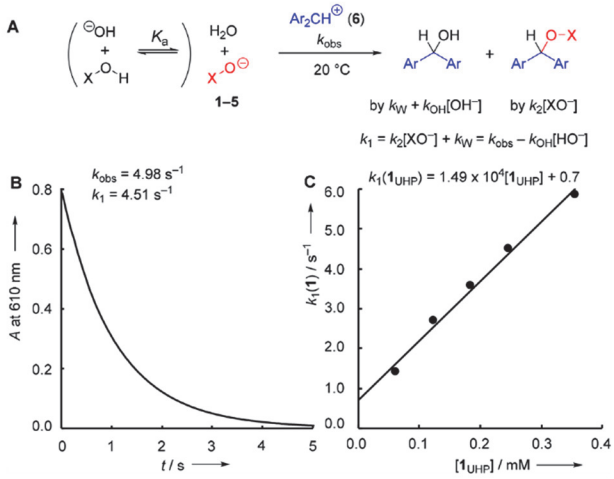

Figure 2. (A) Reaction of benzhydrylium ions **6** with nucleophiles in alkaline, aqueous solution of bleach reagents XOH. (B) Absorbance A (at 610 nm) vs time for the reaction of $\mathbf{1}_{UHP}$ (c = 2.46 × 10^{-4} M) with **6b** (c = 1.05 × 10^{-5} M) at 20 °C. (C) The slope of the linear plot of the first-order rate constant k_1 (= k_{obs} − $k_{OH}[HO^-]$) versus nucleophile concentration was used to derive the second-order rate constant k_2 for the attack of the anion **1** at the benzhydrylium ion **6b**.

acetonitrile [<0.5% (v/v)] was used as a co-solvent to solubilize the benzhydrylium tetrafluoroborates. Applying a high excess of the anions **1**–**5** over the electrophiles **6b**–**6e** caused the nucleophile concentrations to remain almost constant during the kinetic runs. As $[\mathbf{1}]_0 \gg [\mathbf{6}]_0$, electrophiles **6** were quantitatively consumed by the excess of HOO^- ions under the conditions of the kinetic experiments, and the subsequent reaction of **7** with **6** could be neglected in the kinetic analysis. We followed the progress of the reactions by time-resolved stopped-flow UV/vis photometry, which showed a mono-exponential decay of the absorption of the electrophile in all investigated reactions (Figure 2B). First-order rate constants k_{obs} (s^{-1}) were obtained from least-squares fitting of the single-exponential function $A_t = A_0 \exp(-k_{obs}t) + C$ to the decaying absorbances.

As expressed by eq 2 and Figure 2, the observed first-order rate constants k_{obs} reflect the reactions of cations **6** with water, hydroxide ions (HO^-), and the anions of the bleach reagents (XO^-).

$$k_{obs} = k_W + k_{OH}[HO^-] + k_2[XO^-] \quad (2)$$

The basicities of the investigated anions (pK_{aH} in Table 1)[13] were used to calculate the concentrations $[OH^-]$ and $[XO^-]$. Rate constants for the reactions of the cations **6a**–**6e** with water (k_W) and hydroxide ions (k_{OH}) had previously been reported.[3h] Thus, the second-order rate constants k_2 (Table 1) for the attack of the nucleophiles **1**–**5** at the benzhydrylium ions **6b**–**6e** were obtained from the slopes of the linear correlations of k_1 (= k_{obs} − $k_{OH}[HO^-]$) with the nucleophile concentrations (Figure 2C). Table 1 lists the nucleophilicity parameters for **1** (generated from different H_2O_2 formulations), along with the N and s_N values for anions **2**–**5**. The linear correlations of the second-order rate constants k_2 with the electrophilicity E of the benzhydrylium ions (Figure 3) furnished the nucleophilicity parameter N of the anions **1**–**5** as the intercept with the abscissa (equal to $-E$ at log k_2 = 0). The individual susceptibilities of the nucleophiles toward changes in the electrophiles' reactivity are reflected by the different slopes (s_N) of the log k_2 vs E correlations.

Table 1 shows that the nucleophilic reactivity of HOO^- (**1**) toward the reference electrophiles **6** is almost independent of the source of the reactant: hydrogen peroxide anions liberated from H_2O_2–urea (UHP), H_2O_2–polyvinylpyrrolidone (PVP), or sodium percarbonate (SPC) are only slightly less reactive than HOO^- generated from aqueous hydrogen peroxide, for which N = 15.40 (s_N = 0.55) was reported in ref 3h.

Bromite (BrO_2^-, **5**) is significantly less reactive than hypobromite (BrO^-, **3**). Depending on the electrophilic reaction partner, the rate constants for the reactions of **6** with **5** are lower by a factor 10–20 than the k_2 values for the reactions of **3** with the same set of electrophiles. The relative reactivities thus follow the order of basicities because BrO_2^- (pK_{aH} = 3.43) is a weaker base than BrO^- (pK_{aH} = 8.8). In contrast, the reactivities of **1**–**4** toward electrophile **6c** (Table 1) are almost identical, although their basicities (pK_{aH}) differ by 4 orders of magnitude.[14] Figure 4 is, thereby, giving another example for the fact that the Brønsted basicities cannot be used as a guideline for predicting the reactivities of nucleophiles, even when the reacting atom remains the same as in the bleach reagents XO^-.

How can the weak correlation of basicity and reactivity (r^2 = 0.4614) in the series HOO^-, ClO^-, BrO^-, $[SO_5]^{2-}$ be explained? It has recently been shown that early transition states in reactions of the anions of organic peroxides ROO^- with benzhydrylium ions put desolvation of the nucleophile into a key position for understanding the counterintuitive nucleophilicity ordering.[8] It is likely that analogous solvation effects also control the nucleophilic reactivities of anions **1**–**4** in aqueous solution.[15]

To assess the applicability of N and s_N of **1**–**5**, we next studied the kinetics of the reactions of Malachite Green (MG) with **1**, **2**, and hydroxide (see Table 2). The second-order rate constants that we determined experimentally agreed within a factor of 10 with those predicted by applying eq 1, the electrophilicity parameter for MG (E = −10.29, from ref 3h), and the nucleophile-dependent parameters N and s_N from

DOI: 10.1021/acs.orglett.8b00645
Org. Lett. 2018, 20, 2816–2820

Table 1. Basicities (pK_{aH}) and Second-Order Rate Constants k_2 for the Reactions of the Nucleophiles 1–5 with Reference Electrophiles 6a–6e in Alkaline, Aqueous Solution at 20 °C

		k_2 (M^{-1} s^{-1})				
XO^-	pK_{aH}[a]	**6e**	**6d**	**6c**	**6b**	N (s_N)
$\mathbf{1}_{UHP}$	11.75	8.18×10^2	1.28×10^3	3.89×10^3	1.49×10^4	15.20 (0.55)
$\mathbf{1}_{PVP}$	11.75	6.94×10^2	1.11×10^3	3.23×10^3	1.45×10^4	14.86 (0.58)
$\mathbf{1}_{SPC}$	11.75	6.84×10^2	1.00×10^3	2.96×10^3	1.15×10^4	15.16 (0.54)
2	7.53	5.00×10^2	6.71×10^2	2.03×10^3	1.03×10^4	14.50 (0.58)
3	8.8	1.09×10^3	1.94×10^3	4.05×10^3	1.27×10^4	16.69 (0.46)
4	9.4	5.01×10^2	6.53×10^2	2.79×10^3	1.06×10^4	14.41 (0.60)
5	3.43	4.67×10^1	6.63×10^1	2.72×10^2	9.71×10^2	12.75 (0.59)

[a]Basicities pK_{aH} are taken from ref 13.

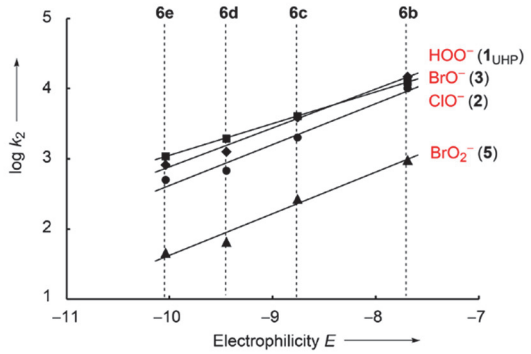

Figure 3. Plot of log k_2 (Table 1) for the reactions of anions $\mathbf{1}_{UHP}$, **2**, **3**, and **5** with electrophiles **6b–6e** in alkaline aqueous solution at 20 °C versus the electrophilicity parameters E of **6b–6e** (see the SI for individual plots for all nucleophiles).

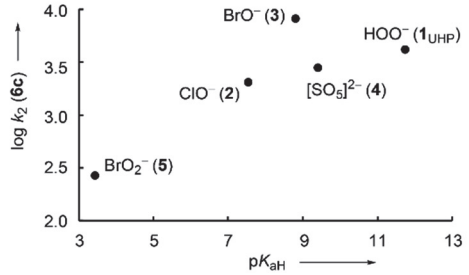

Figure 4. Correlation of the reactivities of the nucleophiles **1–5** (toward **6c**) with their basicities (pK_{aH}).

Table 2. Second-Order Rate Constants k_2 for the Reactions of MG with Nucleophiles in Aqueous Solution (at 20 °C)

	Rate Constants (M^{-1} s^{-1})		
XO^-	$k_2^{this\ work}$	k_2^{calcd} [a]	k_2^{lit}
HO^-	9.25×10^{-1}	1.25	2.18 (25 °C)[b]
HOO^- (**1**)	1.13×10^3	6.46×10^2	1.3×10^4 (30 °C)[c]
ClO^- (**2**)	2.59×10^3	2.76×10^2	5.0×10^1 (30 °C)[c]
			1.0×10^3 (23 °C)[d]

[a]Calculated based on eq 1, the electrophilicity of MG (E = −10.29, from ref 3d) and the N (and s_N) parameters in Table 1 (for **1**, **2**) and ref 3d (for OH^-). [b]Data taken from ref 16. [c]Data taken from ref 3c. [d]Data taken from ref 3d.

Table 1. The significantly lower reactivity of ClO^- (**2**) toward MG, compared to HOO^- (**1**), described by Dixon and Bruice,[3c] was not observed in our measurements, which agreed better with Ritchie's data.[3d]

Scheffer-Weitz epoxidations of arylidenemalononitriles (**9**) with various oxygen-transfer reagents had been described previously.[8,17] We used these reactions to test whether the nucleophilicity parameters N (and s_N) for **1–5** (Table 1) also hold for the reactions of **1–5** with neutral electrophiles and, therefore, determined the rate constants for the nucleophilic epoxidations of **9a–9c** (see Table 3).

Table 3. Second-Order Rate Constants k_2 for the Reactions of the Oxygen Nucleophiles 1–5 with the Neutral Electrophiles 9a–c in Alkaline, Aqueous Solution at 20 °C

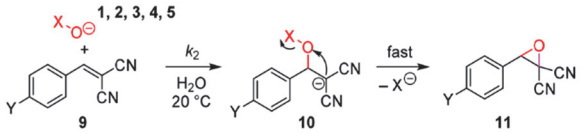

Y = H: **a**; Y = OMe: **b**; NMe_2: **c**

		Rate Constants (M^{-1} s^{-1})		
nucleophile	**9** (E)[a]	k_2^{exp}	k_2^{calcd} [b]	k_2^{exp}/k_2^{calcd}
HOO^- ($\mathbf{1}_{UHP}$)	**9a** (−9.42)	3.92×10^4	1.51×10^3	26
	9b (−10.80)	7.97×10^3	2.63×10^2	30
	9c (−13.30)	4.25×10^2	1.11×10^1	38
ClO^- (**2**)	**9a** (−9.42)	6.63×10^3	8.84×10^2	7.5
	9b (−10.80)	1.39×10^3	1.40×10^2	9.9
BrO^- (**3**)	**9a** (−9.42)	1.10×10^4	2.21×10^3	5.0
	9b (−10.80)	2.40×10^3	5.12×10^2	4.7
$[SO_5]^{2-}$ (**4**)	**9a** (−9.42)	7.99×10^3	9.86×10^2	5.4
	9b (−10.80)	1.49×10^3	1.47×10^2	10
BrO_2^- (**5**)	**9a** (−9.42)	2.91×10^1	9.35×10^1	0.31

[a]Electrophilicities E from ref 18. [b]Second-order rate constant k_2 by applying eq 1, E of **9** (this table) and N and s_N of **1–5** (from Table 1).

Table 3 shows that the predicted rate constants (k_2^{calcd}) for the epoxidations of the electron-deficient π-systems of **9** with the nucleophiles **2–5** match the experimentally obtained rate constants (k_2^{exp}) with a maximum deviation of a factor of 10, in the case of the hydroperoxide anion ($\mathbf{1}_{UHP}$) within a factor of 40. Hence, all determined rate constants for the epoxidations of **9** by **1–5** are within the usual prediction accuracy of eq 1 (that is, an error in the predicted rate constant within a factor of 10–100).[6b,c] For **2–5**, the small deviations between measured (reactions with **9a** and **9b**) and predicted rate constants (based on reactions with benzhydrylium ions **6**) suggest that analogous reaction mechanisms are operating, in which the first C–O

DOI: 10.1021/acs.orglett.8b00645
Org. Lett. 2018, 20, 2816–2820

bond formation between nucleophile and electrophile (e.g., the formation of **10**) is rate-determining.

Because of the different susceptibility of BrO^- (**3**, s_N = 0.46), the relative reactivity of **3**, if compared with other oxidants in Figure 5, will be dependent on the choice of the electrophile.

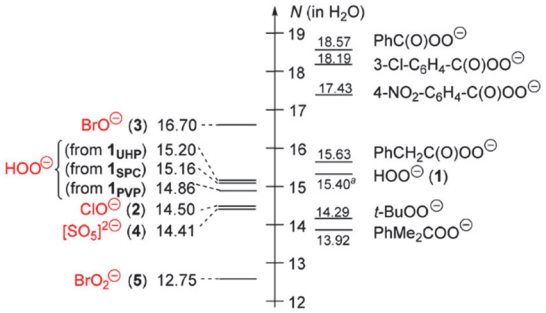

Figure 5. Comparison of nucleophilicity parameters *N* of anions **1**–**5** with those of other peroxide anions (from ref 8). [Superscript "*a*" denotes data taken from ref 3h.]

However, because of the comparable s_N values (0.54–0.60), a rough comparison of the reactivities of anions **1**, **2**, **4**, and **5** with those of other anionic oxidants can be based solely on the nucleophilicity parameter *N*. Hence, Figure 5 shows that the anions **1**, **2**, and **4** are marginally more nucleophilic than the alkyl peroxide anions and less nucleophilic than various peroxybenzoates.[8]

In conclusion, the reactivity parameters of the oxidants **1**–**5** (in H_2O) derived in this work from the rates of their reactions with benzhydrylium ions may be used for the design of oxygen-transfer reactions toward various types of C-centered electrophiles (e.g., Michael acceptors).[19] The comparable reactivities of **1**, **2**, and **4** may be of interest for practical applications: interchanging these bleach reagents will not change the resulting reactivity. Only the pH of the solution must be adjusted, since alkaline conditions are required to generate the anions **1** and **4**, while hypochlorite (**2**) is significantly deprotonated even under neutral conditions. Furthermore, the collection of reactivity data in this work and in ref 8 provides a unique foundation for a future re-evaluation of the α-effect in oxygen nucleophiles.[20]

■ ASSOCIATED CONTENT

Supporting Information

The Supporting Information is available free of charge on the ACS Publications website at DOI: 10.1021/acs.orglett.8b00645.

Synthetic procedures, analytical data, X-ray structure determinations, details of the kinetic measurements, and copies of NMR spectra (PDF)

Accession Codes

CCDC 1819620–1819621 contain the supplementary crystallographic data for this paper. These data can be obtained free of charge via www.ccdc.cam.ac.uk/data_request/cif, or by emailing data_request@ccdc.cam.ac.uk, or by contacting The Cambridge Crystallographic Data Centre, 12 Union Road, Cambridge CB2 1EZ, U.K.; fax: +44 1223 336033.

■ AUTHOR INFORMATION

Corresponding Author

*E-mail: ofial@lmu.de

ORCID

Armin R. Ofial: 0000-0002-9600-2793

Notes

The authors declare no competing financial interest.

■ ACKNOWLEDGMENTS

We thank Nathalie Hampel (LMU, preparation of **6** and **9**), Dr. Peter Mayer (LMU, X-ray crystallographic analyses of **8** and $[Ba(BrO_2)_2 \cdot (H_2O)]$), and Professor Herbert Mayr (LMU) for valuable support. The authors are grateful to Dr. Jérôme Gomar and Dr. Stéphane Sabelle (L'Oréal) for helpful discussions. Financial support by L'Oréal Research & Innovation (Aulnay sous Bois) and the Deutsche Forschungsgemeinschaft (SFB 749, project B1) is gratefully acknowledged.

■ REFERENCES

(1) (a) Muzart, J. *Synthesis* **1995**, 1325–1347. (b) McKillop, A.; Sanderson, W. R. *J. Chem. Soc., Perkin Trans. 1* **2000**, 471–476. (c) Berkessel, A.; Vogl, N. In *The Chemistry of Peroxides*, Vol. 2; Rappoport, Z., Ed.; Wiley: Hoboken, NJ, 2006; pp 307–596. (d) Hussain, H.; Green, I. R.; Ahmed, A. *Chem. Rev.* **2013**, *113*, 3329–3371. (e) Davis, R. L.; Stiller, J.; Naicker, T.; Jiang, H.; Jørgensen, K. A. *Angew. Chem., Int. Ed.* **2014**, *53*, 7406–7426.

(2) (a) Hage, R.; Lienke, A. *Angew. Chem., Int. Ed.* **2006**, *45*, 206–222. (b) Campos-Martin, J. M.; Blanco-Brieva, G.; Fierro, J. L. G. *Angew. Chem., Int. Ed.* **2006**, *45*, 6962–6984. (c) Ek, M.; Gellerstedt, G.; Henriksson, G. In *Pulping Chemistry and Technology*, Vol. 2; de Gruyter: Berlin, 2009; Chapter 10, pp 240–277. (d) Hart, P. W.; Rudie, A. W. *The Bleaching of Pulp*, 5th Edition; TAPPI Press: Norcross, GA, 2012.

(3) (a) Bunton, C. A.; Minkoff, G. J. *J. Chem. Soc.* **1949**, 665–670. (b) Edwards, J. O.; Pearson, R. G. *J. Am. Chem. Soc.* **1962**, *84*, 16–24. (c) Dixon, J. E.; Bruice, T. C. *J. Am. Chem. Soc.* **1971**, *93*, 6592–6597. (d) Ritchie, C. D.; Virtanen, P. O. I. *J. Am. Chem. Soc.* **1973**, *95*, 1882–1889. (e) Ritchie, C. D.; Sawada, M. *J. Am. Chem. Soc.* **1977**, *99*, 3754–3761. (f) Ritchie, C. D. *Can. J. Chem.* **1986**, *64*, 2239–2250. (g) Um, I.-H.; Im, L.-R.; Buncel, E. *J. Org. Chem.* **2010**, *75*, 8571–8577. (h) Minegishi, S.; Mayr, H. *J. Am. Chem. Soc.* **2003**, *125*, 286–295.

(4) (a) http://www.rsc.org/learn-chemistry/resource/download/res00000941/cmp00001333/pdf, accessed Jan. 16, 2018. (b) Henary, M. M.; Russell, A. A. *J. Chem. Educ.* **2007**, *84*, 480–482.

(5) Mayr, H.; Bug, T.; Gotta, M. F.; Hering, N.; Irrgang, B.; Janker, B.; Kempf, B.; Loos, R.; Ofial, A. R.; Remennikov, G.; Schimmel, H. *J. Am. Chem. Soc.* **2001**, *123*, 9500–9512.

(6) (a) Mayr, H.; Patz, M. *Angew. Chem., Int. Ed. Engl.* **1994**, *33*, 938–957. (b) Mayr, H.; Ofial, A. R. *SAR QSAR Environ. Res.* **2015**, *26*, 619–646. (c) Mayr, H. *Tetrahedron* **2015**, *71*, 5095–5111.

(7) A database of reactivity parameters *E*, *N*, and s_N can be accessed at http://www.cup.lmu.de/oc/mayr/DBintro.html.

(8) Mayer, R. J.; Tokuyasu, T.; Mayer, P.; Gomar, J.; Sabelle, S.; Mennucci, B.; Mayr, H.; Ofial, A. R. *Angew. Chem., Int. Ed.* **2017**, *56*, 13279–13282 and refs cited therein.

(9) Glidewell, C.; Liles, D. C.; Walton, D. J.; Sheldrick, G. M. *Acta Crystallogr., Sect. B: Struct. Crystallogr. Cryst. Chem.* **1979**, *35*, 500–502.

(10) Gougoutas, J. Z. In *The Chemistry of Functional Groups, Peroxides*; Patai, S.; Ed.; Wiley: Chichester, U.K., 1983; pp 382.

(11) Hartung, J.; Svoboda, L. In *The Chemistry of Peroxides*, Vol. 2; Rappoport, Z., Ed.; Wiley: Hoboken, NJ, 2006; Chapter 2, pp 93–144.

(12) For details on the preparation of the nucleophiles and the kinetic experiments, see the Supporting Information. Bromite ions (**5**)

DOI: 10.1021/acs.orglett.8b00645
Org. Lett. 2018, 20, 2816–2820

originated from $[Ba(BrO_2)_2 \cdot (H_2O)]$ characterized by X-ray crystallography (see Supporting Information for details).

(13) pK_{aH} for (a) HOO^- (**1**) Evans, M. G.; Uri, N. *Trans. Faraday Soc.* **1949**, *45*, 224−230. (b) ClO^- (**2**): Ingham, J. W.; Morrison, J. *J. Chem. Soc.* **1933**, 1200−1205. (c) BrO^- (**3**): Troy, R. C.; Margerum, D. W. *Inorg. Chem.* **1991**, *30*, 3538−3543 and refs cited therein. (d) $[SO_5]^{2-}$ (**4**): Fortnum, D. H.; Battaglia, C. J.; Cohen, S. R.; Edwards, J. O. *J. Am. Chem. Soc.* **1960**, *82*, 778−782. (e) BrO_2^- (**5**): de Barros Faria, R.; Epstein, I. R.; Kustin, K. *J. Phys. Chem.* **1994**, *98*, 1363−1367.

(14) The almost identical reactivities of **2**−**4** cannot be assigned to the formation of a common decomposition product given that their decomposition paths are known: (a) ClO^- (**2**): Lister, M. W. *Can. J. Chem.* **1956**, *34*, 465−478. (b) BrO^- (**3**): Beckwith, R. C.; Margerum, D. W. *Inorg. Chem.* **1997**, *36*, 3754−3760. (c) $[SO_5]^{2-}$ (**4**): Goodman, J. F.; Robson, P. *J. Chem. Soc.* **1963**, 2871−2875.

(15) Nucleophilicity parameters N (and s_N) as well as basicities pK_{aH} are solvent-dependent properties. Thus, both nucleophilicities and basicities of **1**−**5** in organic solvents will differ from those in aqueous solution investigated in this work.

(16) Ritchie, C. D.; Wright, D. J.; Huang, D.-S.; Kamego, A. A. *J. Am. Chem. Soc.* **1975**, *97*, 1163−1170.

(17) With NaOCl or $Ca(OCl)_2$: (a) Robert, A.; Jaguelin, S.; Guinamant, J. L. *Tetrahedron* **1986**, *42*, 2275−2282. (b) Foucaud, A.; Bakouetila, M. *Synthesis* **1987**, 854−856. (c) Meier, K.-R.; Linden, A.; Mloston, G.; Heimgartner, H. *Helv. Chim. Acta* **1997**, *80*, 1190−1204. (d) Gutch, P. K.; Raza, S. K.; Malhotra, R. C. *Indian J. Chem. Sect. B* **2001**, *40*, 243−247. With urea−H_2O_2: (e) Yang, F.; Zhang, X.; Li, F.; Wang, Z.; Wang, L. *Eur. J. Org. Chem.* **2016**, 1251−1254.

(18) Lemek, T.; Mayr, H. *J. Org. Chem.* **2003**, *68*, 6880−6886.

(19) Oxidations of α,β-unsaturated ketones with $KHSO_5$ (in DMF) were reported to give Baeyer−Villiger-type products: Poladura, B.; Martínez-Castaneda, Á.; Rodríguez-Solla, H.; Llavona, R.; Concellón, C.; del Amo, V. *Org. Lett.* **2013**, *15*, 2810−2813.

(20) (a) For a review, see: Buncel, E.; Um, I.-H. *Tetrahedron* **2004**, *60*, 7801−7825. (b) For a recent insightful investigation, see: Juaristi, E.; dos Passos Gomes, G.; Terent'ev, A. O.; Notario, R.; Alabugin, I. V. *J. Am. Chem. Soc.* **2017**, *139*, 10799−10813.

DOI: 10.1021/acs.orglett.8b00645
Org. Lett. 2018, 20, 2816−2820

2.1 Supporting Information - General

***CAUTION**: Pure peroxides (especially as crystalline compounds) may explode or detonate under influence of heat, shock, spark etc. Contact of peroxy compounds with reducing agents, acid media or traces of transition metals should be avoided as exothermal decomposition may occur. All reactions or handling should be carried out behind a blast shield as a precaution using open vessels while wearing appropriate safety equipment. Rotary evaporation of peroxide should be carried out carefully avoiding excessive stirring at room temperature. Generally, all handling should only be performed by experienced people trained in handling explosive compounds.*

Solvents and Reagents

Commercial reagents and dry solvents over molecular sieves as purchased from Sigma-Aldrich or Acros Organics were used without further purification. Water for reactions or kinetic experiments was used after purification by a Sartorius lab water system. Stock solutions of potassium hydroxide (KOH) and sodium thiosulfate ($Na_2S_2O_3$) were purchased from Bernd Kraft Laborchemikalien. The purity of all oxidants was determined by iodometric titration before use.

Urea-hydrogen peroxide (UHP) was obtained from Sigma-Aldrich and calcium hypochlorite (technical grade, 65%) from Acros Organics. The hydrogen peroxide-polyvinylpyrrolidone complex refers to commercially available Peroxydone™ K-30. Sodium percarbonate was prepared following the procedure by Adams[1] as fine needle-shaped crystals and the peroxide content determined iodometrically (31.8% per weight; this corresponds to a purity of 97.8%).

Solutions of hypobromite were prepared as alkaline, aqueous solutions following the procedure by Polak:[2] Bromine (0.26 mL, 5.0 mmol) was added dropwise under vigorous stirring at −4 °C to an aqueous solution of KOH (100 mL, 10 mmol). The thus prepared solution was directly used after the content of hypobromite was determined by iodometric titration. Additionally, the pH value was measured to consider the concentration of hydroxide for the kinetic experiments.

Bromite (**5**) was studied as an alkaline solution of its barium salt [$Ba(BrO_2)_2{\cdot}(H_2O)$], which was prepared according to the procedure of Noszticzius and recrystallized twice (material of before and after the second recrystallization showed identical rate constants towards electrophiles **6**).[3] As the structure of this bromite salt had not been unequivocally solved,[4] we used a single crystal X-ray structure analysis (of moderate quality) of the recrystallized salt to characterize the material and the content of crystal water prior to the subsequent kinetic measurements.

Malachite green was prepared as tetrafluoroborate salt according to the procedure by Horn.[5]

Analytics

Melting points were acquired using a Büchi Melting Point B-540 device and are not corrected.

Nuclear magnetic resonance spectra were recorded on 200 and 400 NMR spectrometers. The following abbreviations and their combinations are used in the analysis of NMR spectra: s = singlet, d = dublet, t = triplet, q = quartet, m = multiplet, br s = broad singlet. NMR signals were assigned based on information from additional 2D NMR experiments (COSY, gHSQC, gHMBC, NOESY). Internal reference was set to the residual solvent signals (δ_H = 5.32, δ_C = 54.00 for CD_2Cl_2). All ^{13}C NMR spectra were recorded under broad-band proton-decoupling.

Infrared (IR) spectra were recorded on a Perkin Elmer Spectrum BX-59343 instrument with a Smiths Detection DuraSamplIR II Diamond ATR sensor for detection in the range 4500–600 cm^{-1}. Samples were prepared as a film for liquids or neat for solids.

Raman spectra were measured with a Bruker MultiRAM FT-Raman spectrometer fitted with a liquid nitrogen cooled germanium detector and a Nd:YAG laser (λ = 1064 nm) as neat solid through a glass flask.

High resolution (HRMS) mass spectra were recorded on a Thermo Finnigan LTQ FT Ultra Fourier Transform ion cyclotron resonance mass spectrometer. For ionization electrospray ionization (ESI) was applied.

Single Crystal X-Ray Crystallography (Performed by Dr. P. Mayer)

The X-ray intensity data were measured on a Bruker D8 Venture TXS system equipped with a multilayer mirror optics monochromator and a Mo Kα rotating-anode X-ray tube (λ = 0.71073 Å) at a temperature of 100 K (**8**) or 103 K [$Ba(BrO_2)_2{\cdot}(H_2O)$]. The frames were integrated with the Bruker SAINT software package using a narrow-frame algorithm.[6] Data were corrected for absorption effects using the Multi-Scan method (SADABS for **8**, TWINABS[7] for [$Ba(BrO_2)_2{\cdot}(H_2O)$]. The structures were solved and refined using the Bruker SHELXTL Software Package.[8] The structure of [$Ba(BrO_2)_2{\cdot}(H_2O)$] was refined as a 2-component, pseudo-merohedral twin with (001) as C_2 twin axis. The hydrogen atoms in **8** were calculated in ideal geometry while those in [$Ba(BrO_2)_2{\cdot}(H_2O)$] were refined freely. The data have been deposited with the CCDC and can be obtained free of charge via https://www.ccdc.cam.ac.uk/structures/.

Kinetic measurements

The anions **1** and **4** were generated by deprotonation of HOOH and HSO_5^-, respectively, with aqueous KOH. Calcium hypochlorite [$Ca(OCl)_2$] was used as a source of hypochlorite (**2**), and the kinetic measurements were done in alkaline solution for stability reasons. For the same reason hypobromite (**3**) and bromite (**5**) were measured in alkaline solution. As the reactions of the colored benzhydrylium ions **6** (or arylidenemalononitriles **9**) with the nucleophiles **1**–**5** yielded colorless products, the kinetics of these reactions were followed by employing stopped-flow UV/Vis photometry on Applied Photophysics SX.18MV-R or Hi-Tech SF-61DX2 systems. Temperature (20.0 ± 0.2 °C) was controlled by using circulating bath cryostats.

By using a high excess of the anions **1**–**5** over the electrophiles **6** (or **9**), the peroxide concentrations remained almost constant during the kinetic runs, resulting in monoexponential decays of the electrophiles' absorptions. First-order rate constants k_{obs} (s^{-1}) were obtained by least-squares fitting the absorbances (averaged from at least four kinetic runs at each nucleophile concentration) with the single-exponential function $A_t = A_0 \exp(-k_{obs}t) + C$.

2.2 Synthesis and Characterization of Barium Bromite Monohydrate

Barium bromite was prepared following the procedure by Noszticzius on the same scale.[3] Accordingly, the crude material was dissolved in water and crystallized by slow evaporation under reduced pressure at 40 °C yielding 4.7 g of the bromite salt. The higher quality crystals that formed were separated (1 g) and recrystallized again from water by slow evaporation under reduced pressure.

About 500 mg of canary yellow, crystalline material was obtained after drying at reduced pressure which showed to be quantitatively pure by iodometric titration. This sample was analyzed by Raman spectroscopy and used to select single crystals suitable for X-ray analysis (Figure S1).

Raman (neat): 707.0 (ν_{as}), 675.2 (ν_{s}), 354.9 (δ) cm^{-1}.

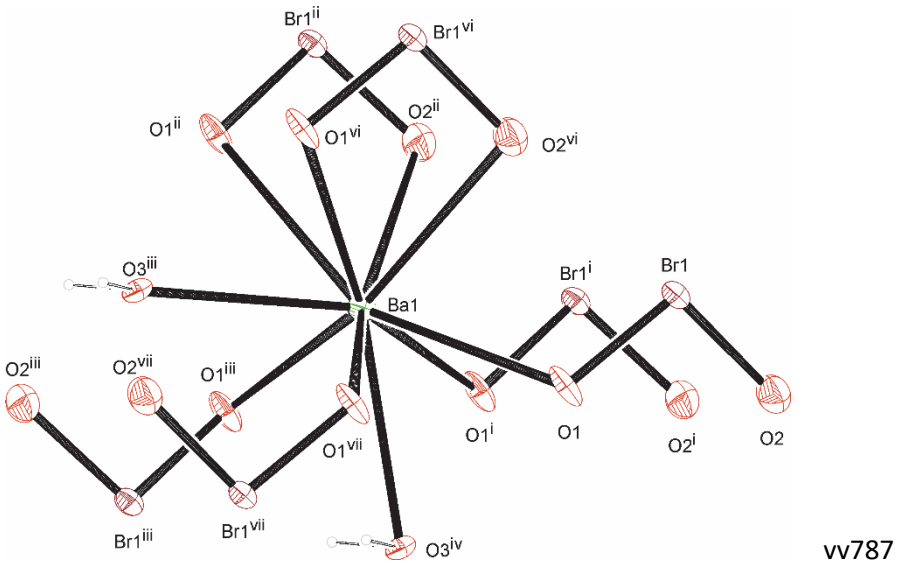

Figure S1: Single crystal X-ray structure of $[Ba(BrO_2)_2{\cdot}H_2O]$ (CCDC 1819621, thermal ellipsoids are drawn at a 50% probability level at T = 103 K).

As presumed by Noszticzius, barium bromite crystallizes as monohydrate with two formula units in the unit cell. Compared to the reported X-ray structural data of sodium bromite trihydrate $[Na(BrO_2){\cdot}(H_2O)_3]$,[9] the averaged Br−O bond distances in the barium bromite monohydrate are slightly greater (1.761 and 1.729 Å vs. 1.702 and 1.731 Å). Analogously, solid-state Raman spectra revealed lower Br−O stretching frequencies in $[Ba(BrO_2)_2{\cdot}(H_2O)]$ (707 and 675 cm^{-1}) than in $[Na(BrO_2){\cdot}(H_2O)_3]$ (728 and 680 cm^{-1}).

Table S1: Selected lengths and angles in the crystal structure of $[Ba(BrO_2)_2{\cdot}H_2O]$.

d (Br−O1)	1.729(3) Å
d (Br−O2)	1.761(3) Å
d (Ba−O1) = d (Ba−$O1^{i}$)	2.783(3) Å
d (Ba−$O1^{iii}$) = d (Ba−$O1^{vii}$)	2.837(4) Å
d (Ba-$O2^{ii}$) = d (Ba−$O2^{vi}$)	2.966(4) Å
d (Ba−$O1^{ii}$) = d (Ba−$O1^{vi}$)	2.971(4) Å
d (Ba−O_3^{iii})	2.856(3) Å
d (Ba−O_3^{iv})	2.922(4) Å
O1-Br1-O2	96.7(5)°

2.3 Product Studies

4,4',4'',4'''-(Peroxybis(methanetriyl))tetrakis(*N*,*N*-dimethylaniline) 8 – RM419

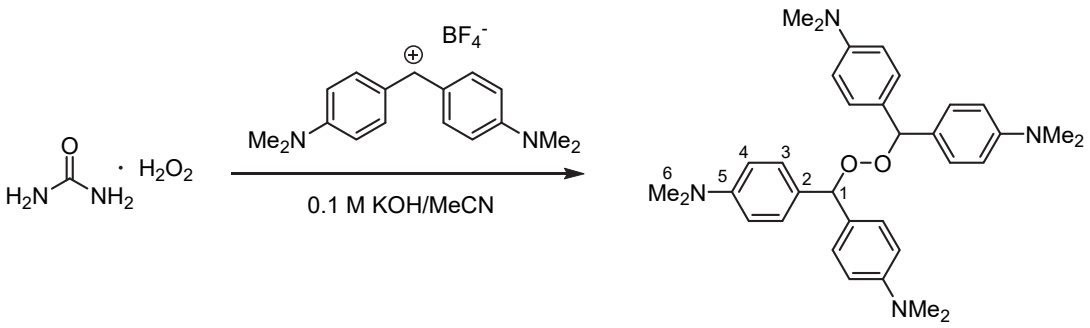

Urea-hydrogen peroxide (14.2 mg, 0.151 mmol, 2 equiv.) was dissolved in aqueous 0.1 M KOH solution (5 mL, 0.5 mmol, 6.6 equiv). Under stirring, a solution of **6a**-BF_4 (25.7 mg, 0.0755 mmol, 1 equiv.) in acetonitrile (2 mL) was added dropwise. The blue electrophile solution decolorized immediately upon being in contact with the aqueous nucleophile solution. The resulting colorless, opaque suspension was further stirred for 1 min. Then acetonitrile was removed in the vacuum (90 mbar, 40 °C water bath temperature). The colorless precipitate was separated by filtration from the remaining liquid and then dried under high vacuum (approx. 10^{-3} mbar): **8** (11.7 mg, 0.0217 mmol, yield: 58 %), colorless solid.

^{1}H NMR (400 MHz, CD_2Cl_2) δ = 7.13–7.09 (m, 8 H, 3-H), 6.68–6.64 (m, 8 H, 4-H), 5.93 (s, 2 H, 1-H), 2.91 (s, 24 H, 6-H).

^{13}C{^{1}H} NMR (101 MHz, CD_2Cl_2) δ = 150.8 (C_q, C-5), 129.1 (CH, C-3), 128.7 (C_q, C-2), 112.6 (CH, C-4), 87.4 (CH, C-1), 40.9 (CH_3, C-6).

HRMS (ESI$^+$): Calcd *m/z* for $[C_{34}H_{43}N_4O_2]^+$ [M + H$^+$]: 539.3381; Found: 539.3384.

IR (neat): 2958, 2918, 2850, 2361, 2340, 1678, 1463, 1414, 1377, 1260, 1089,1015, 864, 798, 741, 718, 708 cm^{-1}.

Mp: 137 °C (decomp.)

Single crystals of **8** were obtained by following a slightly modified procedure:

Urea-hydrogen peroxide (14.2 mg, 0.151 mmol, 2 equiv.) was dissolved in aqueous 0.1 M KOH solution (5.0 mL, 0.50 mmol, 6.6 equiv). Under stirring, a solution of **6a**-BF_4 (25.7 mg, 0.0755 mmol, 1 equiv.) in acetonitrile (2 mL) was added dropwise. The blue electrophile solution decolorized immediately upon being in contact with the aqueous nucleophile solution. The resulting colorless, opaque suspension was further stirred for 1 min. The mixture was extracted with dichloromethane (3 x 20 mL), washed with brine, dried over $MgSO_4$ and concentrated under reduced pressure. Single crystals of **8**, which were suitable for X-ray diffraction, formed as colorless needles on the inside of the flask beside an oily residue of the corresponding benzhydrol. The structure is deposited under CCDC 1819620.

Reaction of Oxygen-Centered Nucleophiles with Benzylidene Malononitriles

Arylidene malononitriles **9** are known to undergo epoxidations with several O-nucleophiles as shown in Scheme S1 (for details see references quoted in the main text).

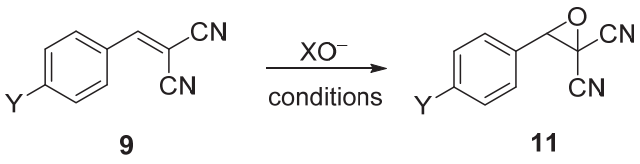

9 **11**

Scheme S1. Epoxidation of benzylidene malononitriles **9** to give epoxides **11**.

Additionaly, the epoxidation of arylidene malononitriles **9** with aqueous alkaline oxone (**4**) and with bromite (**5**) was investigated in this work: $[Ba(BrO_2)_2 \cdot H_2O]$ (3.7 mg, 0.098 mmol, 0.5 equiv) was dissolved in 0.5 mL D_2O and 0.1 mL d_3-MeCN. Then a solution of **9a** (3.0 mg, 0.019 mmol, 1 equiv) in 0.1 mL CD_3CN was added and the resulting mixture was analyzed by ^{1}H NMR spectroscopy. Analogous experiments were carried out with $Ca(OCl)_2$ (65%, 2.2 mg, 0.010 mmol, 0.5 equiv) and oxone (9.0 mg, 0.030 mmol, 1.5 equiv)/KOH (2.4 mg, 0.044 mmol, 2.3 equiv).

The ^{1}H NMR spectra for all three experiments (Figure S2) indicate that **9a** (Y = H) was quantitatively converted (as can be seen be the disappearance of the olefinic CH resonance at ca 8.1 ppm) to the epoxide **11a**, which was identified by comparison with a published ^{1}H NMR spectrum.[10]

Under analogous reaction conditions with an aqueous solution of KOBr as the epoxidation reagent, the resonance of the epoxide CH proton superimposed with the broad water signal and could not be resolved unambiguously by the available solvent-suppression methods.

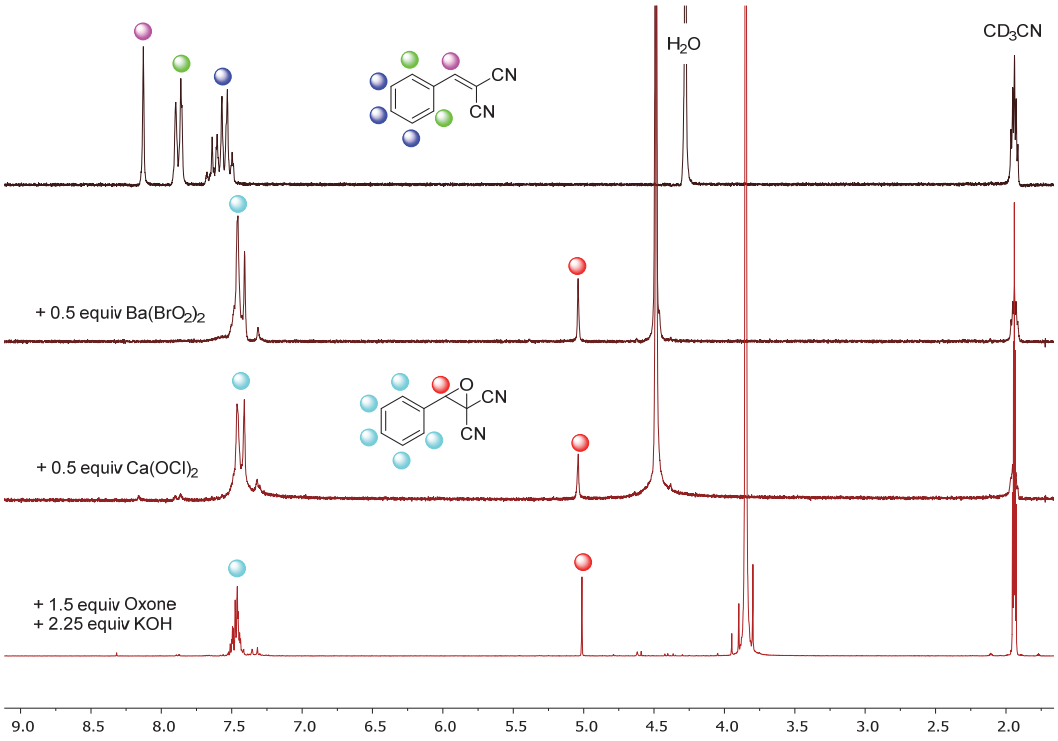

Figure S2: ^{1}H NMR spectra (200/400 MHz, CD_3CN/D_2O) of mixtures of **9a** with different oxidants. The spectrum on top shows the starting material in a mixture of 0.4/0.5 CD_3CN/D_2O for comparison. Due to the higher concentration of hydroxide in the spectrum on the bottom, the H_2O resonance is shifted in comparison to the other spectra.

2.4 Kinetic Data

Kinetics of Reactions of Bleach Reagents with Benzhydrylium Ions

Kinetics of the reactions of the hydroperoxide anion (1_{UHP}, generated from urea-hydrogen peroxide) with benzhydrylium ions 6 in water

6e + H_2O_2 in alkaline 99.6/0.4 (v/v) H_2O/CH_3CN (stopped-flow, detection at 630 nm)

$[\mathbf{6e}]_0$, mol L^{-1}	$[H_2O_2]_0$, mol L^{-1}	$[OH^-]_0$, mol L^{-1}	$[HOO^-]$, mol L^{-1}	$[OH^-]$, mol L^{-1}	k_{obs}, s^{-1}	$k_{OH}[OH^-]$, s^{-1}	$k_2[HOO^-]$, s^{-1}
1.12×10^{-5}	1.00×10^{-4}	1.00×10^{-2}	6.19×10^{-5}	9.94×10^{-3}	9.21×10^{-2}	2.15×10^{-2}	7.06×10^{-2}
1.12×10^{-5}	2.00×10^{-4}	1.00×10^{-2}	1.24×10^{-4}	9.88×10^{-3}	1.39×10^{-1}	2.14×10^{-2}	1.18×10^{-1}
1.12×10^{-5}	3.00×10^{-4}	1.00×10^{-2}	1.85×10^{-4}	9.81×10^{-3}	1.93×10^{-1}	2.12×10^{-2}	1.72×10^{-1}
1.12×10^{-5}	4.00×10^{-4}	1.00×10^{-2}	2.46×10^{-4}	9.75×10^{-3}	2.45×10^{-1}	2.11×10^{-2}	2.24×10^{-1}
1.12×10^{-5}	5.20×10^{-4}	1.00×10^{-2}	3.19×10^{-4}	9.68×10^{-3}	2.99×10^{-1}	2.09×10^{-2}	2.78×10^{-1}

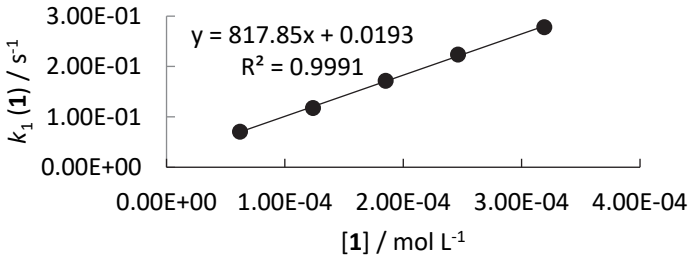

$k_2 = 8.18 \times 10^2$ M^{-1} s^{-1}
$k_{OH} = 2.16$ M^{-1} s^{-1}

6d + H_2O_2 in alkaline 99.6/0.4 (v/v) H_2O/CH_3CN (stopped-flow, detection at 640 nm)

$[\mathbf{6d}]_0$, mol L^{-1}	$[H_2O_2]_0$, mol L^{-1}	$[OH^-]_0$, mol L^{-1}	$[HOO^-]$, mol L^{-1}	$[OH^-]$, mol L^{-1}	k_{obs}, s^{-1}	$k_{OH}[OH^-]$, s^{-1}	$k_2[HOO^-]$, s^{-1}
8.65×10^{-6}	1.00×10^{-4}	1.00×10^{-2}	6.19×10^{-5}	9.94×10^{-3}	1.30×10^{-1}	3.41×10^{-2}	9.59×10^{-2}
8.65×10^{-6}	2.00×10^{-4}	1.00×10^{-2}	1.24×10^{-4}	9.88×10^{-3}	2.21×10^{-1}	3.39×10^{-2}	1.87×10^{-1}
8.65×10^{-6}	3.00×10^{-4}	1.00×10^{-2}	1.85×10^{-4}	9.81×10^{-3}	3.06×10^{-1}	3.37×10^{-2}	2.72×10^{-1}
8.65×10^{-6}	4.00×10^{-4}	1.00×10^{-2}	2.46×10^{-4}	9.75×10^{-3}	3.64×10^{-1}	3.35×10^{-2}	3.30×10^{-1}
8.65×10^{-6}	5.80×10^{-4}	1.00×10^{-2}	3.55×10^{-4}	9.64×10^{-3}	5.11×10^{-1}	3.31×10^{-2}	4.77×10^{-1}

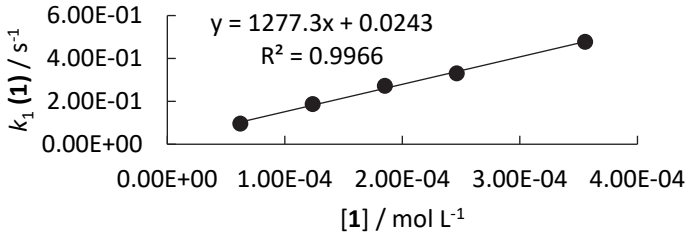

$k_2 = 1.28 \times 10^3$ M^{-1} s^{-1}
$k_{OH} = 3.44$ M^{-1} s^{-1}

6c + H_2O_2 in alkaline 99.6/0.4 (v/v) H_2O/CH_3CN (stopped-flow, detection at 615 nm)

$[\mathbf{6c}]_0$, mol L^{-1}	$[H_2O_2]_0$, mol L^{-1}	$[OH^-]_0$, mol L^{-1}	$[HOO^-]$, mol L^{-1}	$[OH^-]$, mol L^{-1}	k_{obs}, s^{-1}	$k_{OH}[OH^-]$, s^{-1}	$k_2[HOO^-]$, s^{-1}
1.30×10^{-5}	1.00×10^{-4}	1.00×10^{-2}	6.19×10^{-5}	9.94×10^{-3}	3.77×10^{-1}	1.07×10^{-1}	2.70×10^{-1}
1.30×10^{-5}	2.00×10^{-4}	1.00×10^{-2}	1.24×10^{-4}	9.88×10^{-3}	6.21×10^{-1}	1.07×10^{-1}	5.14×10^{-1}
1.30×10^{-5}	3.00×10^{-4}	1.00×10^{-2}	1.85×10^{-4}	9.81×10^{-3}	8.63×10^{-1}	1.06×10^{-1}	7.57×10^{-1}
1.30×10^{-5}	4.00×10^{-4}	1.00×10^{-2}	2.46×10^{-4}	9.75×10^{-3}	1.09	1.05×10^{-1}	9.89×10^{-1}
1.30×10^{-5}	5.20×10^{-4}	1.00×10^{-2}	3.19×10^{-4}	9.68×10^{-3}	1.37	1.04×10^{-1}	1.27

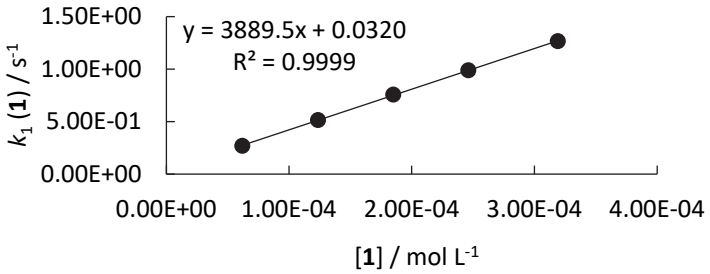

$k_2 = 3.89 \times 10^3$ M^{-1} s^{-1}
$k_{OH} = 10.8$ M^{-1} s^{-1}

6b + H_2O_2 in alkaline 99.6/0.4 (v/v) H_2O/CH_3CN (stopped-flow, detection at 610 nm)

[**6b**]$_0$, mol L^{-1}	[H_2O_2]$_0$, mol L^{-1}	[OH^-]$_0$, mol L^{-1}	[HOO^-], mol L^{-1}	[OH^-], mol L^{-1}	k_{obs}, s^{-1}	k_{OH}[OH^-], s^{-1}	k_2[HOO^-], s^{-1}
1.05×10^{-5}	1.00×10^{-4}	1.00×10^{-2}	6.19×10^{-5}	9.94×10^{-3}	1.90	4.82×10^{-1}	1.42
1.05×10^{-5}	2.00×10^{-4}	1.00×10^{-2}	1.24×10^{-4}	9.88×10^{-3}	3.17	4.79×10^{-1}	2.69
1.05×10^{-5}	3.00×10^{-4}	1.00×10^{-2}	1.85×10^{-4}	9.81×10^{-3}	4.04	4.76×10^{-1}	3.56
1.05×10^{-5}	4.00×10^{-4}	1.00×10^{-2}	2.46×10^{-4}	9.75×10^{-3}	4.98	4.73×10^{-1}	4.51
1.05×10^{-5}	5.80×10^{-4}	1.00×10^{-2}	3.55×10^{-4}	9.64×10^{-3}	6.31	4.68×10^{-1}	5.84

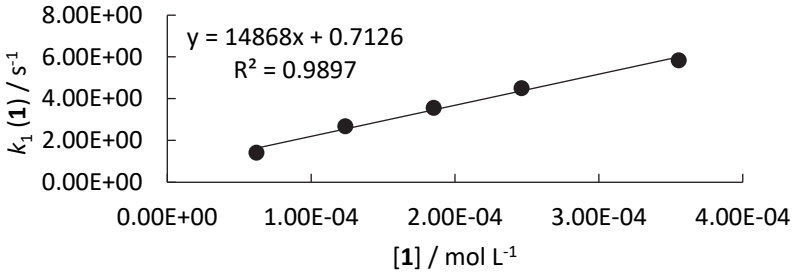

$k_2 = 1.49 \times 10^4$ M^{-1} s^{-1}
$k_{OH} = 48.5$ M^{-1} s^{-1}

Determination of N and s_N parameters for hydroperoxide ion $\mathbf{1}_{UHP}$ (generated from urea-hydrogen peroxide) in 99.6/0.4 (v/v) H_2O/CH_3CN

Reference Electrophile	Electrophilicity E	k_2 (M^{-1} s^{-1})	lg k_2
6e	–10.04	8.18×10^2	2.91
6d	–9.45	1.28×10^3	3.11
6c	–8.76	3.89×10^3	3.59
6b	–7.69	1.49×10^4	4.17

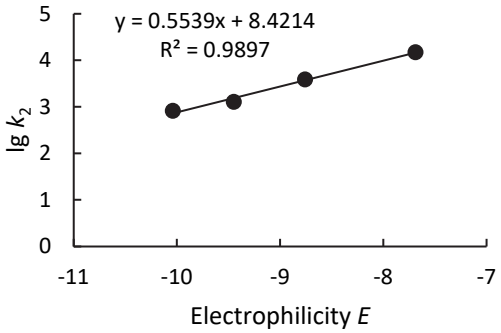

$N = 15.20$
$s_N = 0.55$

Reaction of the hydrogen peroxide ($\mathbf{1}_{PVP}$, generated from the H_2O_2-peroxydone complex, PVP) with benzhydrylium ions 6 in water

6e + H_2O_2 in alkaline 99.6/0.4 (v/v) H_2O/CH_3CN (stopped-flow, detection at 630 nm)

$[\mathbf{6e}]_0$, mol L^{-1}	$[H_2O_2]_0$, mol L^{-1}	$[OH^-]_0$, mol L^{-1}	$[HOO^-]$, mol L^{-1}	$[OH^-]$, mol L^{-1}	k_{obs}, s^{-1}	$k_{OH}[OH^-]$, s^{-1}	$k_2[HOO^-]$, s^{-1}
1.12×10^{-5}	4.00×10^{-4}	2.50×10^{-2}	3.26×10^{-4}	2.47×10^{-2}	2.79×10^{-1}	5.34×10^{-2}	2.25×10^{-1}
1.12×10^{-5}	8.00×10^{-4}	2.50×10^{-2}	6.50×10^{-4}	2.44×10^{-2}	5.08×10^{-1}	5.27×10^{-2}	4.55×10^{-1}
1.12×10^{-5}	1.20×10^{-3}	2.50×10^{-2}	9.72×10^{-4}	2.40×10^{-2}	7.32×10^{-1}	5.20×10^{-2}	6.80×10^{-1}
1.12×10^{-5}	1.60×10^{-3}	2.50×10^{-2}	1.29×10^{-3}	2.37×10^{-2}	9.44×10^{-1}	5.13×10^{-2}	8.93×10^{-1}

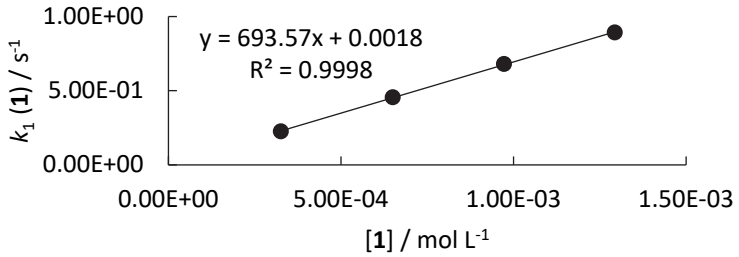

$k_2 = 6.94 \times 10^2$ M^{-1} s^{-1}
$k_{OH} = 2.16$ M^{-1} s^{-1}

6d + H_2O_2 in alkaline 99.6/0.4 (v/v) H_2O/CH_3CN (stopped-flow, detection at 640 nm)

$[\mathbf{6d}]_0$, mol L^{-1}	$[H_2O_2]_0$, mol L^{-1}	$[OH^-]_0$, mol L^{-1}	$[HOO^-]$, mol L^{-1}	$[OH^-]$, mol L^{-1}	k_{obs}, s^{-1}	$k_{OH}[OH^-]$, s^{-1}	$k_2[HOO^-]$, s^{-1}
8.65×10^{-6}	4.00×10^{-4}	2.50×10^{-2}	3.26×10^{-4}	2.47×10^{-2}	4.55×10^{-1}	8.48×10^{-2}	3.70×10^{-1}
8.65×10^{-6}	8.00×10^{-4}	2.50×10^{-2}	6.50×10^{-4}	2.44×10^{-2}	8.23×10^{-1}	8.36×10^{-2}	7.39×10^{-1}
8.65×10^{-6}	1.20×10^{-3}	2.50×10^{-2}	9.72×10^{-4}	2.40×10^{-2}	1.19	8.25×10^{-2}	1.11
8.65×10^{-6}	1.60×10^{-3}	2.50×10^{-2}	1.29×10^{-3}	2.37×10^{-2}	1.52	8.14×10^{-2}	1.44

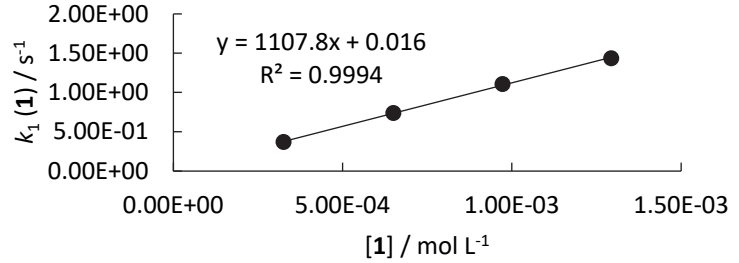

$k_2 = 1.11 \times 10^3$ M^{-1} s^{-1}
$k_{OH} = 3.44$ M^{-1} s^{-1}

6c + H_2O_2 in alkaline 99.6/0.4 (v/v) H_2O/CH_3CN (stopped-flow, detection at 615 nm)

$[\mathbf{6c}]_0$, mol L^{-1}	$[H_2O_2]_0$, mol L^{-1}	$[OH^-]_0$, mol L^{-1}	$[HOO^-]$, mol L^{-1}	$[OH^-]$, mol L^{-1}	k_{obs}, s^{-1}	$k_{OH}[OH^-]$, s^{-1}	$k_2[HOO^-]$, s^{-1}
1.30×10^{-5}	4.00×10^{-4}	2.50×10^{-2}	3.26×10^{-4}	2.47×10^{-2}	1.45	2.66×10^{-1}	1.18
1.30×10^{-5}	8.00×10^{-4}	2.50×10^{-2}	6.50×10^{-4}	2.44×10^{-2}	2.52	2.63×10^{-1}	2.26
1.30×10^{-5}	1.20×10^{-3}	2.50×10^{-2}	9.72×10^{-4}	2.40×10^{-2}	3.47	2.59×10^{-1}	3.21
1.30×10^{-5}	1.60×10^{-3}	2.50×10^{-2}	1.29×10^{-3}	2.37×10^{-2}	4.59	2.56×10^{-1}	4.33

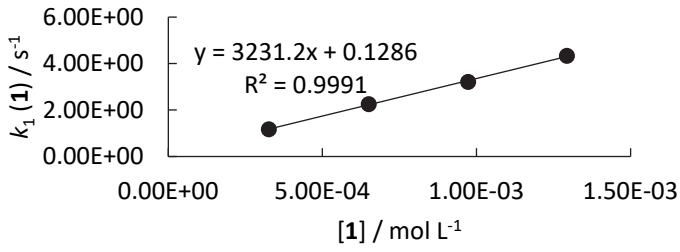

$k_2 = 3.23 \times 10^3$ M^{-1} s^{-1}
$k_{OH} = 10.8$ M^{-1} s^{-1}

6b + H_2O_2 in alkaline 99.6/0.4 (v/v) H_2O/CH_3CN (stopped-flow, detection at 610 nm)

$[\mathbf{6b}]_0$, mol L^{-1}	$[H_2O_2]_0$, mol L^{-1}	$[OH^-]_0$, mol L^{-1}	$[HOO^-]$, mol L^{-1}	$[OH^-]$, mol L^{-1}	k_{obs}, s^{-1}	$k_{OH}[OH^-]$, s^{-1}	$k_2[HOO^-]$, s^{-1}
1.05×10^{-5}	4.00×10^{-4}	2.50×10^{-2}	3.26×10^{-4}	2.47×10^{-2}	1.20×10^{1}	1.20	1.08×10^{1}
1.05×10^{-5}	8.00×10^{-4}	2.50×10^{-2}	6.50×10^{-4}	2.44×10^{-2}	1.69×10^{1}	1.18	1.58×10^{1}
1.05×10^{-5}	1.20×10^{-3}	2.50×10^{-2}	9.72×10^{-4}	2.40×10^{-2}	2.15×10^{1}	1.17	2.04×10^{1}
1.05×10^{-5}	1.60×10^{-3}	2.50×10^{-2}	1.29×10^{-3}	2.37×10^{-2}	2.60×10^{1}	1.15	2.48×10^{1}

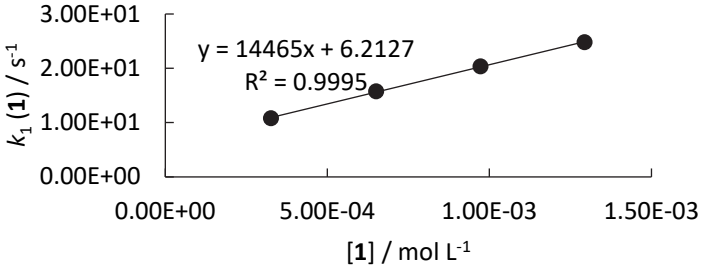

$k_2 = 1.45 \times 10^4\ M^{-1}\ s^{-1}$
$k_{OH} = 48.5\ M^{-1}\ s^{-1}$

Determination of N and s_N parameters for the hydroperoxide ion $\mathbf{1}_{PVP}$ (generated from polyvinylpyrrolidon-hydrogen peroxide) in 99.6/0.4 (v/v) H_2O/CH_3CN

Reference Electrophile	Electrophilicity E	k_2 ($M^{-1}\ s^{-1}$)	lg k_2
6e	–10.04	6.94×10^2	2.84
6d	–9.45	1.11×10^3	3.04
6c	–8.76	3.23×10^3	3.51
6b	–7.69	1.45×10^4	4.16

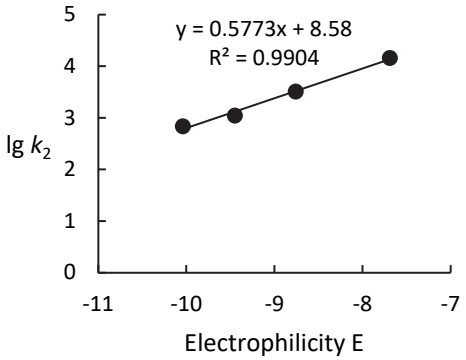

$N = 14.86$
$s_N = 0.58$

Reaction of the hydrogen peroxide ($\mathbf{1}_{SPC}$, generated from sodium percarbonate, SPC) with benzhydrylium ions 6 in water

6e + H_2O_2 in alkaline 99.6/0.4 (v/v) H_2O/CH_3CN (stopped-flow, detection at 630 nm)

$[\mathbf{6e}]_0$, mol L^{-1}	$[H_2O_2]_0$, mol L^{-1}	$[OH^-]_0$, mol L^{-1}	$[HOO^-]$, mol L^{-1}	$[OH^-]$, mol L^{-1}	k_{obs}, s^{-1}	$k_{OH}[OH^-]$, s^{-1}	$k_2[HOO^-]$, s^{-1}
2.82×10^{-5}	4.00×10^{-4}	2.50×10^{-2}	3.26×10^{-4}	2.47×10^{-2}	2.74×10^{-1}	5.34×10^{-2}	2.21×10^{-1}
2.82×10^{-5}	8.00×10^{-4}	2.50×10^{-2}	6.50×10^{-4}	2.44×10^{-2}	5.07×10^{-1}	5.27×10^{-2}	4.54×10^{-1}
2.82×10^{-5}	1.20×10^{-3}	2.50×10^{-2}	9.72×10^{-4}	2.40×10^{-2}	7.22×10^{-1}	5.20×10^{-2}	6.70×10^{-1}
2.82×10^{-5}	1.60×10^{-3}	2.50×10^{-2}	1.29×10^{-3}	2.37×10^{-2}	9.33×10^{-1}	5.13×10^{-2}	8.82×10^{-1}

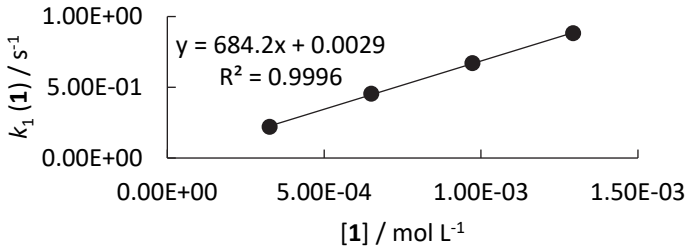

$k_2 = 6.84 \times 10^2$ M^{-1} s^{-1}
$k_{OH} = 2.16$ M^{-1} s^{-1}

6d + H_2O_2 in alkaline 99.6/0.4 (v/v) H_2O/CH_3CN (stopped-flow, detection at 640 nm)

$[\mathbf{6d}]_0$, mol L^{-1}	$[H_2O_2]_0$, mol L^{-1}	$[OH^-]_0$, mol L^{-1}	$[HOO^-]$, mol L^{-1}	$[OH^-]$, mol L^{-1}	k_{obs}, s^{-1}	$k_{OH}[OH^-]$, s^{-1}	$k_2[HOO^-]$, s^{-1}
1.86×10^{-5}	4.00×10^{-4}	2.50×10^{-2}	3.26×10^{-4}	2.47×10^{-2}	3.82×10^{-1}	8.48×10^{-2}	2.97×10^{-1}
1.86×10^{-5}	8.00×10^{-4}	2.50×10^{-2}	6.50×10^{-4}	2.44×10^{-2}	6.96×10^{-1}	8.36×10^{-2}	6.12×10^{-1}
1.86×10^{-5}	1.20×10^{-3}	2.50×10^{-2}	9.72×10^{-4}	2.40×10^{-2}	1.02	8.25×10^{-2}	9.37×10^{-1}
1.86×10^{-5}	1.60×10^{-3}	2.50×10^{-2}	1.29×10^{-3}	2.37×10^{-2}	1.34	8.14×10^{-2}	1.26

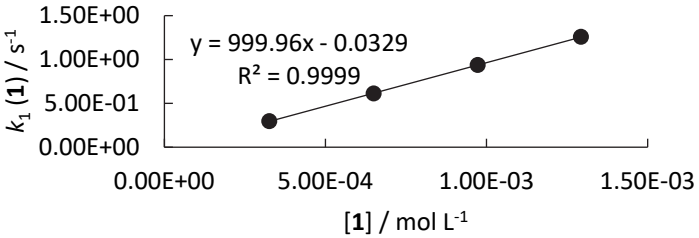

$k_2 = 1.00 \times 10^3$ M^{-1} s^{-1}
$k_{OH} = 3.44$ M^{-1} s^{-1}

6c + H_2O_2 in alkaline 99.6/0.4 (v/v) H_2O/CH_3CN (stopped-flow, detection at 615 nm)

$[\mathbf{6c}]_0$, mol L^{-1}	$[H_2O_2]_0$, mol L^{-1}	$[OH^-]_0$, mol L^{-1}	$[HOO^-]$, mol L^{-1}	$[OH^-]$, mol L^{-1}	k_{obs}, s^{-1}	$k_{OH}[OH^-]$, s^{-1}	$k_2[HOO^-]$, s^{-1}
2.55×10^{-5}	4.00×10^{-4}	2.50×10^{-2}	3.26×10^{-4}	2.47×10^{-2}	1.18	2.66×10^{-1}	9.14×10^{-1}
2.55×10^{-5}	8.00×10^{-4}	2.50×10^{-2}	6.50×10^{-4}	2.44×10^{-2}	2.17	2.63×10^{-1}	1.91
2.55×10^{-5}	1.20×10^{-3}	2.50×10^{-2}	9.72×10^{-4}	2.40×10^{-2}	3.13	2.59×10^{-1}	2.87
2.55×10^{-5}	1.60×10^{-3}	2.50×10^{-2}	1.29×10^{-3}	2.37×10^{-2}	4.03	2.56×10^{-1}	3.77

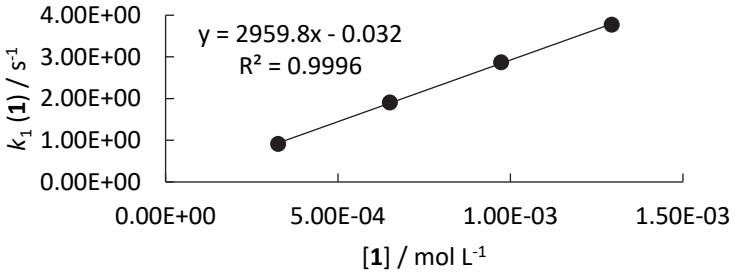

$k_2 = 2.96 \times 10^3$ M^{-1} s^{-1}
$k_{OH} = 10.8$ M^{-1} s^{-1}

6b + H_2O_2 in alkaline 99.6/0.4 (v/v) H_2O/CH_3CN (stopped-flow, detection at 610 nm)

$[\mathbf{6b}]_0$, mol L^{-1}	$[H_2O_2]_0$, mol L^{-1}	$[OH^-]_0$, mol L^{-1}	$[HOO^-]$, mol L^{-1}	$[OH^-]$, mol L^{-1}	k_{obs}, s^{-1}	$k_{OH}[OH^-]$, s^{-1}	$k_2[HOO^-]$, s^{-1}
2.18×10^{-5}	4.00×10^{-4}	2.50×10^{-2}	3.26×10^{-4}	2.47×10^{-2}	4.69	1.20	3.49
2.18×10^{-5}	8.00×10^{-4}	2.50×10^{-2}	6.50×10^{-4}	2.44×10^{-2}	8.82	1.18	7.64
2.18×10^{-5}	1.20×10^{-3}	2.50×10^{-2}	9.72×10^{-4}	2.40×10^{-2}	1.22×10^{1}	1.17	1.11×10^{1}
2.18×10^{-5}	1.60×10^{-3}	2.50×10^{-2}	1.29×10^{-3}	2.37×10^{-2}	1.59×10^{1}	1.15	1.48×10^{1}

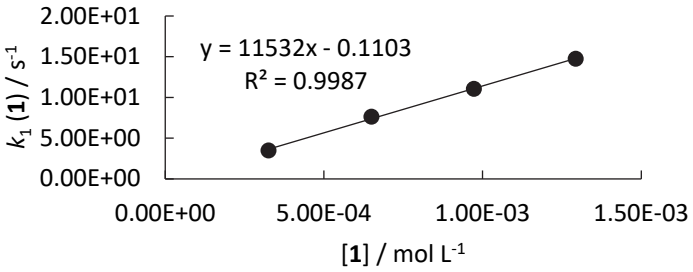

$k_2 = 1.15 \times 10^4\ M^{-1}\ s^{-1}$
$k_{OH} = 48.5\ M^{-1}\ s^{-1}$

Determination of N and s_N parameters for the hydroperoxide ion $\mathbf{1}_{SPC}$ (generated from sodium percarbonate) in 99.6/0.4 (v/v) H_2O/CH_3CN

Reference Electrophile	Electrophilicity E	k_2 ($M^{-1}\ s^{-1}$)	lg k_2
6e	–10.04	6.84×10^2	2.83
6d	–9.45	1.00×10^3	3.00
6c	–8.76	2.96×10^3	3.47
6b	–7.69	1.15×10^4	4.06

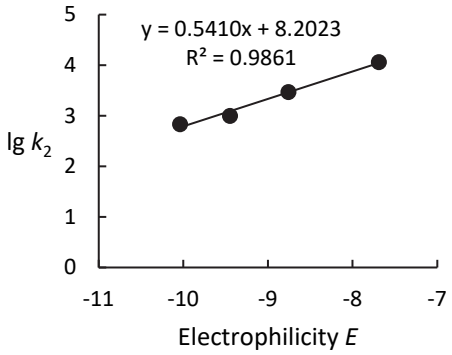

$N = 15.16$
$s_N = 0.54$

Kinetics of the reactions of the hypochlorite anion (2, from $Ca(OCl)_2$) with benzhydrylium ions 6 in water

6e + $Ca(OCl)_2$ in alkaline 99.6/0.4 (v/v) H_2O/CH_3CN (stopped-flow, detection at 630 nm)

$[\mathbf{6e}]_0$, mol L^{-1}	$[ClO^-]_0$, mol L^{-1}	$[OH^-]_0$, mol L^{-1}	k_{obs}, s^{-1}	$k_{OH}[OH^-]$, s^{-1}	$k_2[ClO^-]$, s^{-1}
1.12×10^{-5}	1.00×10^{-4}	2.50×10^{-4}	2.88×10^{-2}	5.41×10^{-4}	2.83×10^{-2}
1.12×10^{-5}	2.00×10^{-4}	2.50×10^{-4}	7.69×10^{-2}	5.41×10^{-4}	7.64×10^{-2}
1.12×10^{-5}	3.00×10^{-4}	2.50×10^{-4}	1.26×10^{-1}	5.41×10^{-4}	1.25×10^{-1}
1.12×10^{-5}	4.00×10^{-4}	2.50×10^{-4}	1.79×10^{-1}	5.41×10^{-4}	1.78×10^{-1}

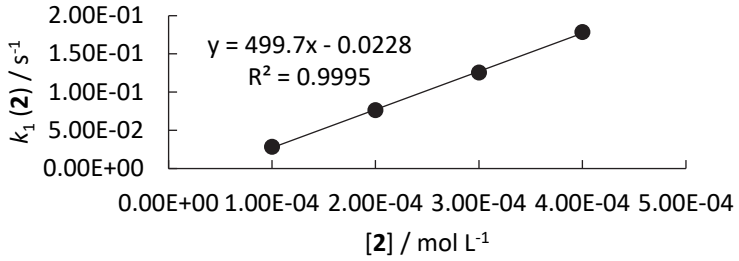

$k_2 = 5.00 \times 10^2$ M^{-1} s^{-1}
$k_{OH} = 2.16$ M^{-1} s^{-1}

6d + $Ca(OCl)_2$ in alkaline 99.6/0.4 (v/v) H_2O/CH_3CN (stopped-flow, detection at 640 nm)

$[\mathbf{6d}]_0$, mol L^{-1}	$[ClO^-]_0$, mol L^{-1}	$[OH^-]_0$, mol L^{-1}	k_{obs}, s^{-1}	$k_{OH}[OH^-]$, s^{-1}	$k_2[ClO^-]$, s^{-1}
8.65×10^{-6}	1.00×10^{-4}	2.50×10^{-4}	4.16×10^{-2}	8.59×10^{-4}	4.07×10^{-2}
8.65×10^{-6}	2.00×10^{-4}	2.50×10^{-4}	1.19×10^{-1}	8.59×10^{-4}	1.18×10^{-1}
8.65×10^{-6}	3.00×10^{-4}	2.50×10^{-4}	1.89×10^{-1}	8.59×10^{-4}	1.88×10^{-1}
8.65×10^{-6}	4.00×10^{-4}	2.50×10^{-4}	2.42×10^{-1}	8.59×10^{-4}	2.41×10^{-1}

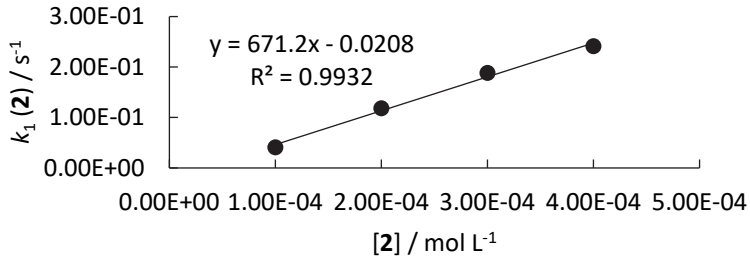

$k_2 = 6.71 \times 10^2$ M^{-1} s^{-1}
$k_{OH} = 3.44$ M^{-1} s^{-1}

6c + $Ca(OCl)_2$ in alkaline 99.6/0.4 (v/v) H_2O/CH_3CN (stopped-flow, detection at 615 nm)

$[\mathbf{6c}]_0$, mol L^{-1}	$[ClO^-]_0$, mol L^{-1}	$[OH^-]_0$, mol L^{-1}	k_{obs}, s^{-1}	$k_{OH}[OH^-]$, s^{-1}	$k_2[ClO^-]$, s^{-1}
1.30×10^{-5}	1.00×10^{-4}	2.50×10^{-4}	1.89×10^{-1}	2.70×10^{-3}	1.86×10^{-1}
1.30×10^{-5}	2.00×10^{-4}	2.50×10^{-4}	4.19×10^{-1}	2.70×10^{-3}	4.16×10^{-1}
1.30×10^{-5}	3.00×10^{-4}	2.50×10^{-4}	5.96×10^{-1}	2.70×10^{-3}	5.93×10^{-1}
1.30×10^{-5}	4.00×10^{-4}	2.50×10^{-4}	8.06×10^{-1}	2.70×10^{-3}	8.03×10^{-1}

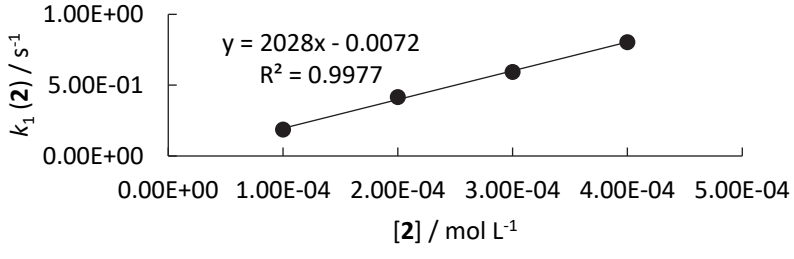

$k_2 = 2.03 \times 10^3$ M^{-1} s^{-1}
$k_{OH} = 10.8$ M^{-1} s^{-1}

6b + $Ca(OCl)_2$ in alkaline 99.6/0.4 (v/v) H_2O/CH_3CN (stopped-flow, detection at 610 nm)

$[\mathbf{6b}]_0$, mol L^{-1}	$[ClO^-]_0$, mol L^{-1}	$[OH^-]_0$, mol L^{-1}	k_{obs}, s^{-1}	$k_{OH}[OH^-]$, s^{-1}	$k_2[ClO^-]$, s^{-1}
1.05×10^{-5}	1.00×10^{-4}	2.50×10^{-4}	8.26×10^{-1}	1.21×10^{-2}	8.14×10^{-1}
1.05×10^{-5}	2.00×10^{-4}	2.50×10^{-4}	1.99	1.21×10^{-2}	1.98
1.05×10^{-5}	3.00×10^{-4}	2.50×10^{-4}	3.01	1.21×10^{-2}	3.00
1.05×10^{-5}	4.00×10^{-4}	2.50×10^{-4}	3.91	1.21×10^{-2}	3.90

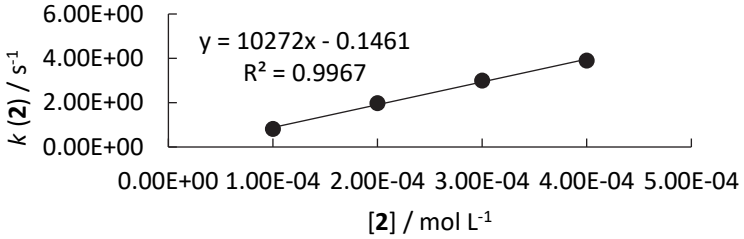

$k_2 = 1.03 \times 10^4$ M^{-1} s^{-1}
$k_{OH} = 48.5$ M^{-1} s^{-1}

Determination of N and s_N parameters for OCl^- (**2**) in 99.6/0.4 (v/v) H_2O/CH_3CN

Reference Electrophile	Electrophilicity E	k_2 (M^{-1} s^{-1})	lg k_2
6e	–10.04	5.00×10^2	2.70
6d	–9.45	6.71×10^2	2.83
6c	–8.76	2.03×10^3	3.31
6b	–7.69	1.03×10^4	4.01

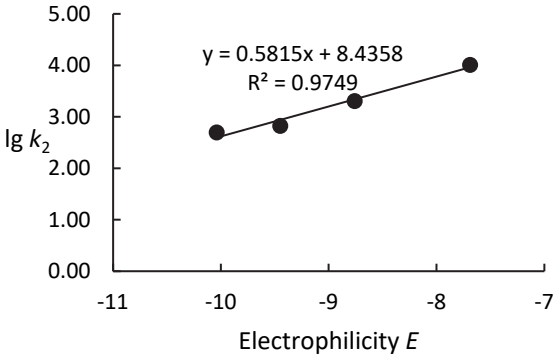

$N = 14.50$
$s_N = 0.58$

Kinetics of the reactions of the hypobromite anion (3) with benzhydrylium ions 6 in water

6e + BrO^- in alkaline 99.6/0.4 (v/v) H_2O/CH_3CN (stopped-flow, detection at 630 nm)

$[\mathbf{6e}]_0$, mol L^{-1}	$[BrO^-]_0$, mol L^{-1}	$[OH^-]_0$, mol L^{-1}	k_{obs}, s^{-1}	$k_{OH}[OH^-]$, s^{-1}	$k_2[BrO^-]$, s^{-1}
2.82×10^{-5}	8.00×10^{-4}	9.94×10^{-4}	9.23×10^{-1}	2.15×10^{-3}	9.21×10^{-1}
2.82×10^{-5}	1.00×10^{-3}	9.92×10^{-4}	1.16	2.15×10^{-3}	1.16
2.82×10^{-5}	1.20×10^{-3}	9.91×10^{-4}	1.38	2.14×10^{-3}	1.38
2.82×10^{-5}	1.40×10^{-3}	9.89×10^{-4}	1.60	2.14×10^{-3}	1.60
2.82×10^{-5}	1.60×10^{-3}	9.88×10^{-4}	1.79	2.14×10^{-3}	1.79

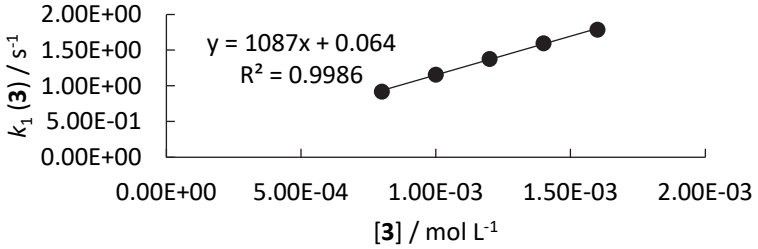

$k_2 = 1.09 \times 10^3\ M^{-1}\ s^{-1}$
$k_{OH} = 2.16\ M^{-1}\ s^{-1}$

6d + BrO^- in alkaline 99.6/0.4 (v/v) H_2O/CH_3CN (stopped-flow, detection at 640 nm)

$[\mathbf{6d}]_0$, mol L^{-1}	$[BrO^-]_0$, mol L^{-1}	$[OH^-]_0$, mol L^{-1}	k_{obs}, s^{-1}	$k_{OH}[OH^-]$, s^{-1}	$k_2[BrO^-]$, s^{-1}
1.86×10^{-5}	8.00×10^{-4}	9.94×10^{-4}	1.06	3.41×10^{-4}	1.06
1.86×10^{-5}	1.00×10^{-3}	9.92×10^{-4}	1.39	3.41×10^{-4}	1.39
1.86×10^{-5}	1.20×10^{-3}	9.91×10^{-4}	1.97	3.40×10^{-4}	1.97
1.86×10^{-5}	1.40×10^{-3}	9.89×10^{-4}	2.21	3.40×10^{-4}	2.21
1.86×10^{-5}	1.60×10^{-3}	9.88×10^{-4}	2.59	3.39×10^{-4}	2.59

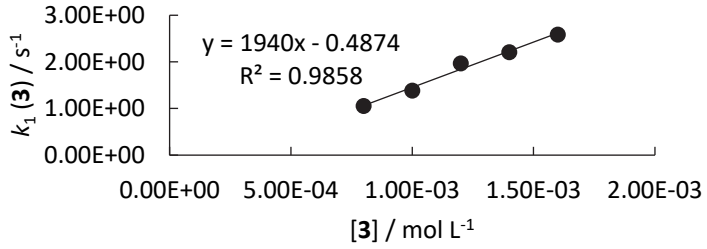

$k_2 = 1.94 \times 10^3\ M^{-1}\ s^{-1}$
$k_{OH} = 3.44\ M^{-1}\ s^{-1}$

6c + BrO^- in alkaline 99.6/0.4 (v/v) H_2O/CH_3CN (stopped-flow, detection at 615 nm)

$[\mathbf{6c}]_0$, mol L^{-1}	$[BrO^-]_0$, mol L^{-1}	$[OH^-]_0$, mol L^{-1}	k_{obs}, s^{-1}	$k_{OH}[OH^-]$, s^{-1}	$k_2[BrO^-]$, s^{-1}
2.55×10^{-5}	8.00×10^{-4}	9.94×10^{-4}	3.01	1.07×10^{-2}	3.00
2.55×10^{-5}	1.00×10^{-3}	9.92×10^{-4}	3.93	1.07×10^{-2}	3.92
2.55×10^{-5}	1.20×10^{-3}	9.91×10^{-4}	4.69	1.07×10^{-2}	4.68
2.55×10^{-5}	1.40×10^{-3}	9.89×10^{-4}	5.69	1.07×10^{-2}	5.68
2.55×10^{-5}	1.60×10^{-3}	9.88×10^{-4}	6.18	1.07×10^{-2}	6.17

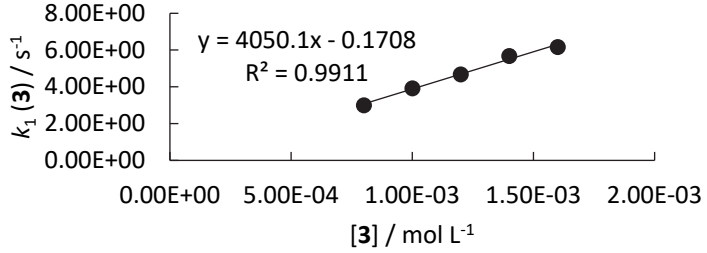

$k_2 = 4.05 \times 10^3\ M^{-1}\ s^{-1}$
$k_{OH} = 10.8\ M^{-1}\ s^{-1}$

6b + BrO^- in alkaline 99.6/0.4 (v/v) H_2O/CH_3CN (stopped-flow, detection at 610 nm)

$[\mathbf{6b}]_0$, mol L^{-1}	$[BrO^-]_0$, mol L^{-1}	$[OH^-]_0$, mol L^{-1}	k_{obs}, s^{-1}	$k_{OH}[OH^-]$, s^{-1}	$k_2[BrO^-]$, s^{-1}
2.18×10^{-5}	8.00×10^{-4}	9.94×10^{-4}	11.8	4.82×10^{-2}	11.8
2.18×10^{-5}	1.00×10^{-3}	9.92×10^{-4}	15.6	4.81×10^{-2}	15.6
2.18×10^{-5}	1.20×10^{-3}	9.91×10^{-4}	17.6	4.81×10^{-2}	17.6
2.18×10^{-5}	1.40×10^{-3}	9.89×10^{-4}	19.0	4.80×10^{-2}	19.0
2.18×10^{-5}	1.60×10^{-3}	9.88×10^{-4}	22.8	4.79×10^{-2}	22.8

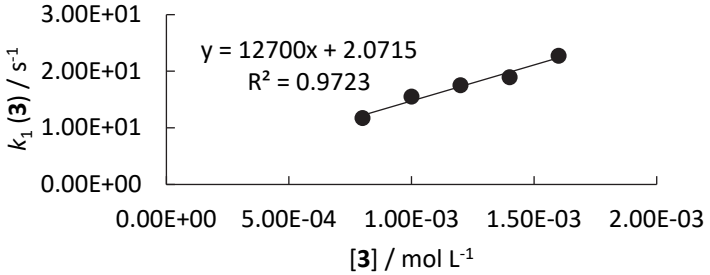

$k_2 = 1.27 \times 10^4\ M^{-1}\ s^{-1}$
$k_{OH} = 48.5\ M^{-1}\ s^{-1}$

Determination of N and s_N parameters for OBr^- (**3**) in 99.6/0.4 (v/v) H_2O/CH_3CN

Reference Electrophile	Electrophilicity E	k_2 ($M^{-1}\ s^{-1}$)	lg k_2
6e	–10.04	1.09×10^3	3.04
6d	–9.45	1.94×10^3	3.29
6c	–8.76	4.05×10^3	3.61
6b	–7.69	1.27×10^4	4.10

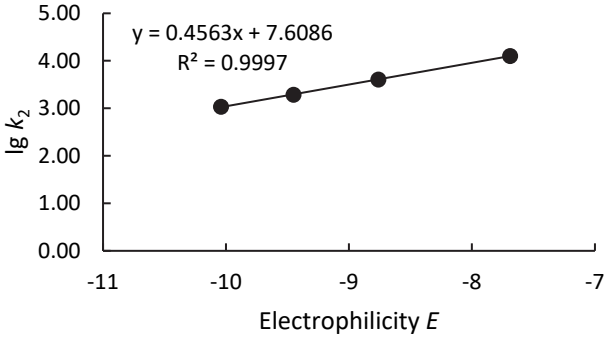

$N = 16.69$
$s_N = 0.46$

Kinetics of the reactions of the peroxymonosulfate ion (4, from Oxone®) with benzhydrylium ions 6 in water

Added hydroxide ions are consumed by 0.5 equiv. of hydrogen sulfate ions (present as part of the oxone mixture, quantitative reaction is assumed) and by the equilibrium deprotonation of HSO_5^- (equilibrium defined by the pK_a).

6e + HSO_5^- in alkaline 99.6/0.4 (v/v) H_2O/CH_3CN (stopped-flow, detection at 630 nm)

$[\mathbf{6e}]_0$, mol L^{-1}	$[HSO_5^-]_0$, mol L^{-1}	$[OH^-]_0$, mol L^{-1}	$[SO_5^{2-}]$, mol L^{-1}	$[OH^-]$, mol L^{-1}	k_{obs}, s^{-1}	$k_{OH}[OH^-]$, s^{-1}	$k_2[SO_5^{2-}]$, s^{-1}
1.12×10^{-5}	1.00×10^{-4}	1.00×10^{-3}	9.73×10^{-5}	8.53×10^{-4}	6.15×10^{-2}	1.84×10^{-3}	5.97×10^{-2}
1.12×10^{-5}	2.00×10^{-4}	1.00×10^{-3}	1.94×10^{-4}	7.06×10^{-4}	1.11×10^{-1}	1.53×10^{-3}	1.09×10^{-1}
1.12×10^{-5}	3.00×10^{-4}	1.00×10^{-3}	2.90×10^{-4}	5.60×10^{-4}	1.53×10^{-1}	1.21×10^{-3}	1.52×10^{-1}
1.12×10^{-5}	3.75×10^{-4}	1.00×10^{-3}	3.61×10^{-4}	4.52×10^{-4}	1.95×10^{-1}	9.77×10^{-4}	1.94×10^{-1}

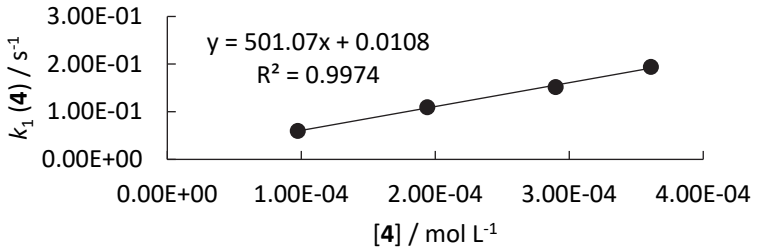

$k_2 = 5.01 \times 10^2$ M^{-1} s^{-1}
$k_{OH} = 2.16$ M^{-1} s^{-1}

6d + HSO_5^- in alkaline 99.6/0.4 (v/v) H_2O/CH_3CN (stopped-flow, detection at 640 nm)

$[\mathbf{6d}]_0$, mol L^{-1}	$[HSO_5^-]_0$, mol L^{-1}	$[OH^-]_0$, mol L^{-1}	$[SO_5^{2-}]$, mol L^{-1}	$[OH^-]$, mol L^{-1}	k_{obs}, s^{-1}	$k_{OH}[OH^-]$, s^{-1}	$k_2[SO_5^{2-}]$, s^{-1}
8.65×10^{-6}	1.00×10^{-4}	1.00×10^{-3}	9.73×10^{-5}	8.53×10^{-4}	8.82×10^{-2}	2.93×10^{-3}	8.53×10^{-2}
8.65×10^{-6}	2.00×10^{-4}	1.00×10^{-3}	1.94×10^{-4}	7.06×10^{-4}	1.49×10^{-1}	2.43×10^{-3}	1.47×10^{-1}
8.65×10^{-6}	3.00×10^{-4}	1.00×10^{-3}	2.90×10^{-4}	5.60×10^{-4}	2.04×10^{-1}	1.92×10^{-3}	2.02×10^{-1}
8.65×10^{-6}	3.75×10^{-4}	1.00×10^{-3}	3.61×10^{-4}	4.52×10^{-4}	2.63×10^{-1}	1.55×10^{-3}	2.61×10^{-1}

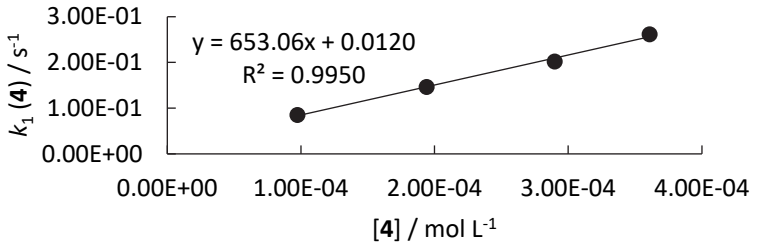

$k_2 = 6.53 \times 10^2$ M^{-1} s^{-1}
$k_{OH} = 3.44$ M^{-1} s^{-1}

6c + HSO_5^- in alkaline 99.6/0.4 (v/v) H_2O/CH_3CN (stopped-flow, detection at 615 nm)

$[\mathbf{6c}]_0$, mol L^{-1}	$[HSO_5^-]_0$, mol L^{-1}	$[OH^-]_0$, mol L^{-1}	$[SO_5^{2-}]$, mol L^{-1}	$[OH^-]$, mol L^{-1}	k_{obs}, s^{-1}	$k_{OH}[OH^-]$, s^{-1}	$k_2[SO_5^{2-}]$, s^{-1}
1.30×10^{-5}	1.00×10^{-4}	1.00×10^{-3}	9.73×10^{-5}	8.53×10^{-4}	3.77×10^{-1}	9.20×10^{-3}	3.68×10^{-1}
1.30×10^{-5}	2.00×10^{-4}	1.00×10^{-3}	1.94×10^{-4}	7.06×10^{-4}	6.52×10^{-1}	7.62×10^{-3}	6.44×10^{-1}
1.30×10^{-5}	3.00×10^{-4}	1.00×10^{-3}	2.90×10^{-4}	5.60×10^{-4}	8.66×10^{-1}	6.05×10^{-3}	8.60×10^{-1}
1.30×10^{-5}	3.75×10^{-4}	1.00×10^{-3}	3.61×10^{-4}	4.52×10^{-4}	1.13	4.87×10^{-3}	1.13

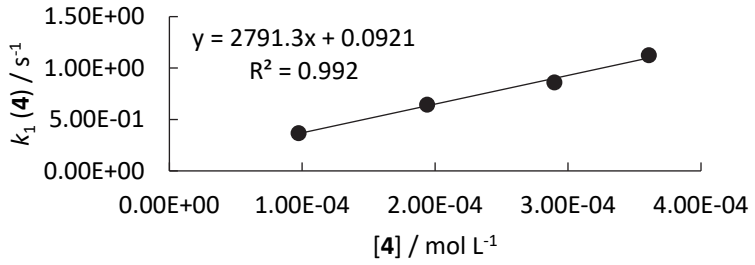

$k_2 = 2.79 \times 10^3$ M^{-1} s^{-1}
$k_{OH} = 10.8$ M^{-1} s^{-1}

6b + HSO_5^- in alkaline 99.6/0.4 (v/v) H_2O/CH_3CN (stopped-flow, detection at 610 nm)

[**6b**]$_0$, mol L^{-1}	[HSO_5^-]$_0$, mol L^{-1}	[OH^-]$_0$, mol L^{-1}	[SO_5^{2-}], mol L^{-1}	[OH^-], mol L^{-1}	k_{obs}, s^{-1}	k_{OH}[OH^-], s^{-1}	k_2[SO_5^{2-}], s^{-1}
1.05×10^{-5}	1.00×10^{-4}	1.00×10^{-3}	9.73×10^{-5}	8.53×10^{-4}	1.32	4.14×10^{-2}	1.28
1.05×10^{-5}	2.00×10^{-4}	1.00×10^{-3}	1.94×10^{-4}	7.06×10^{-4}	2.33	3.42×10^{-2}	2.30
1.05×10^{-5}	3.00×10^{-4}	1.00×10^{-3}	2.90×10^{-4}	5.60×10^{-4}	3.25	2.72×10^{-2}	3.22
1.05×10^{-5}	3.75×10^{-4}	1.00×10^{-3}	3.61×10^{-4}	4.52×10^{-4}	4.12	2.19×10^{-2}	4.10

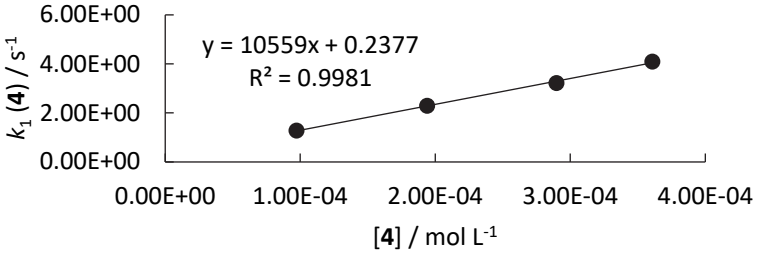

$k_2 = 1.06 \times 10^4$ M^{-1} s^{-1}
$k_{OH} = 48.5$ M^{-1} s^{-1}

Determination of N and s_N parameters for peroxymonosulfate ion (**4**) in 99.6/0.4 (v/v) H_2O/CH_3CN

Reference Electrophile	Electrophilicity E	$k_{2,1}$ (M^{-1} s^{-1})	lg $k_{2,1}$
6e	–10.04	5.01×10^2	2.70
6d	–9.45	6.53×10^2	2.82
6c	–8.76	2.79×10^3	3.45
6b	–7.69	1.06×10^4	4.02

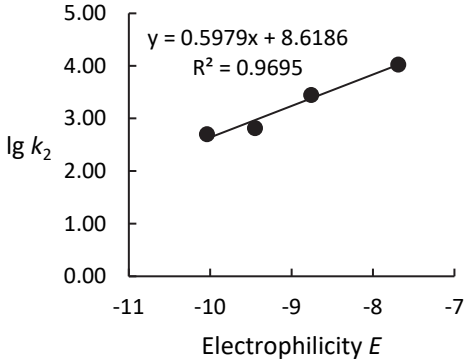

$N = 14.41$
$s_N = 0.60$

Kinetics of the reactions of the bromite ion (5) with benzhydrylium ions 6 in water

6e + BrO_2^- in alkaline 99.6/0.4 (v/v) H_2O/CH_3CN (stopped-flow, detection at 630 nm)

$[\mathbf{6e}]_0$, mol L^{-1}	$[BrO_2^-]_0$, mol L^{-1}	$[OH^-]_0$, mol L^{-1}	k_{obs}, s^{-1}	$k_{OH}[OH^-]$, s^{-1}	$k_2[BrO_2^-]$, s^{-1}
2.82×10^{-5}	8.00×10^{-4}	5.00×10^{-4}	3.87×10^{-2}	1.08×10^{-3}	3.76×10^{-2}
2.82×10^{-5}	1.00×10^{-3}	5.00×10^{-4}	4.80×10^{-2}	1.08×10^{-3}	4.69×10^{-2}
2.82×10^{-5}	1.20×10^{-3}	5.00×10^{-4}	5.78×10^{-2}	1.08×10^{-3}	5.67×10^{-2}
2.82×10^{-5}	1.40×10^{-3}	5.00×10^{-4}	6.67×10^{-2}	1.08×10^{-3}	6.56×10^{-2}
2.82×10^{-5}	1.60×10^{-3}	5.00×10^{-4}	7.60×10^{-2}	1.08×10^{-3}	7.49×10^{-2}

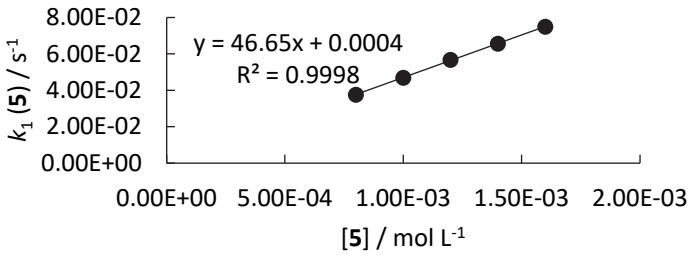

$k_2 = 4.67 \times 10^1$ M^{-1} s^{-1}
$k_{OH} = 2.16$ M^{-1} s^{-1}

6d + BrO_2^- in alkaline 99.6/0.4 (v/v) H_2O/CH_3CN (stopped-flow, detection at 640 nm)

$[\mathbf{6d}]_0$, mol L^{-1}	$[BrO_2^-]_0$, mol L^{-1}	$[OH^-]_0$, mol L^{-1}	k_{obs}, s^{-1}	$k_{OH}[OH^-]$, s^{-1}	$k_2[BrO_2^-]$, s^{-1}
1.86×10^{-5}	8.00×10^{-4}	5.00×10^{-4}	5.76×10^{-2}	1.72×10^{-3}	5.59×10^{-2}
1.86×10^{-5}	1.00×10^{-3}	5.00×10^{-4}	6.81×10^{-2}	1.72×10^{-3}	6.64×10^{-2}
1.86×10^{-5}	1.20×10^{-3}	5.00×10^{-4}	8.20×10^{-2}	1.72×10^{-3}	8.03×10^{-2}
1.86×10^{-5}	1.40×10^{-3}	5.00×10^{-4}	9.64×10^{-2}	1.72×10^{-3}	9.47×10^{-2}
1.86×10^{-5}	1.60×10^{-3}	5.00×10^{-4}	1.10×10^{-1}	1.72×10^{-3}	1.08×10^{-1}

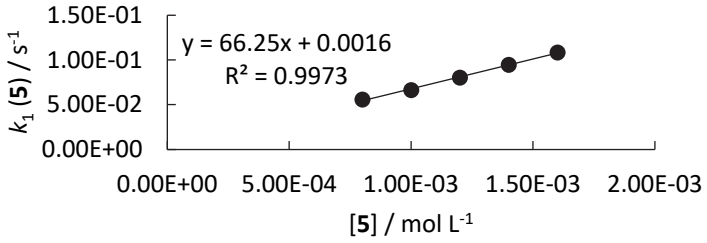

$k_2 = 6.63 \times 10^1$ M^{-1} s^{-1}
$k_{OH} = 3.44$ M^{-1} s^{-1}

6c + BrO_2^- in alkaline 99.6/0.4 (v/v) H_2O/CH_3CN (stopped-flow, detection at 615 nm)

$[\mathbf{6c}]_0$, mol L^{-1}	$[BrO_2^-]_0$, mol L^{-1}	$[OH^-]_0$, mol L^{-1}	k_{obs}, s^{-1}	$k_{OH}[OH^-]$, s^{-1}	$k_2[BrO_2^-]$, s^{-1}
2.55×10^{-5}	8.00×10^{-4}	5.00×10^{-4}	2.40×10^{-1}	5.40×10^{-3}	2.35×10^{-1}
2.55×10^{-5}	1.00×10^{-3}	5.00×10^{-4}	2.96×10^{-1}	5.40×10^{-3}	2.91×10^{-1}
2.55×10^{-5}	1.20×10^{-3}	5.00×10^{-4}	3.47×10^{-1}	5.40×10^{-3}	3.42×10^{-1}
2.55×10^{-5}	1.40×10^{-3}	5.00×10^{-4}	4.07×10^{-1}	5.40×10^{-3}	4.02×10^{-1}
2.55×10^{-5}	1.60×10^{-3}	5.00×10^{-4}	4.56×10^{-1}	5.40×10^{-3}	4.51×10^{-1}

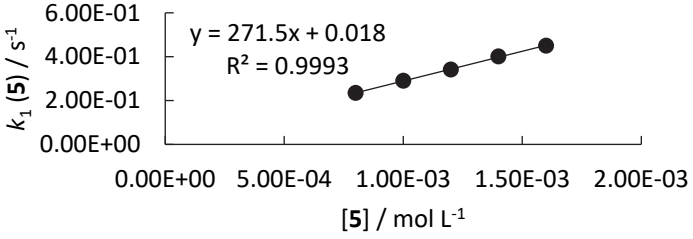

$k_2 = 2.72 \times 10^2$ M^{-1} s^{-1}
$k_{OH} = 10.8$ M^{-1} s^{-1}

6b + BrO_2^- in alkaline 99.6/0.4 (v/v) H_2O/CH_3CN (stopped-flow, detection at 610 nm)

$[\mathbf{6b}]_0$, mol L^{-1}	$[BrO_2^-]_0$, mol L^{-1}	$[OH^-]_0$, mol L^{-1}	k_{obs}, s^{-1}	$k_{OH}[OH^-]$, s^{-1}	$k_2[BrO_2^-]$, s^{-1}
2.18×10^{-5}	8.00×10^{-4}	5.00×10^{-4}	8.73×10^{-1}	2.43×10^{-2}	8.49×10^{-1}
2.18×10^{-5}	1.00×10^{-3}	5.00×10^{-4}	1.08	2.43×10^{-2}	1.06
2.18×10^{-5}	1.20×10^{-3}	5.00×10^{-4}	1.27	2.43×10^{-2}	1.25
2.18×10^{-5}	1.40×10^{-3}	5.00×10^{-4}	1.46	2.43×10^{-2}	1.44
2.18×10^{-5}	1.60×10^{-3}	5.00×10^{-4}	1.65	2.43×10^{-2}	1.63

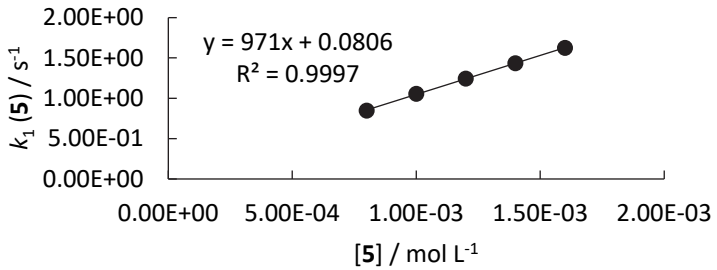

$k_2 = 9.71 \times 10^2$ M^{-1} s^{-1}
$k_{OH} = 48.5$ M^{-1} s^{-1}

Determination of N and s_N parameters for the bromite ion (**5**) in 99.6/0.4 (v/v) H_2O/CH_3CN

Reference Electrophile	Electrophilicity E	$k_{2,\mathbf{1}}$ (M^{-1} s^{-1})	lg $k_{2,\mathbf{1}}$
6e	–10.04	4.67×10^1	1.67
6d	–9.45	6.63×10^1	1.82
6c	–8.76	2.72×10^2	2.43
6b	–7.69	9.71×10^2	2.99

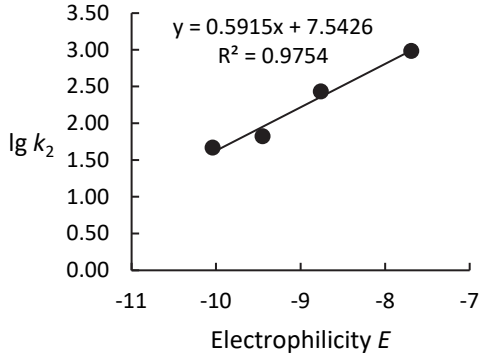

$N = 12.75$
$s_N = 0.59$

Kinetics of Reactions of Hydroxide and Bleach Reagents with Malachite Green

Malachite Green-BF_4^- + OH^- in 99.6/0.4 (v/v) H_2O/CH_3CN (stopped-flow, detection at 618 nm)

$[\mathbf{MG}]_0$, mol L^{-1}	$[OH^-]_0$, mol L^{-1}	k_{obs}, s^{-1}
1.36×10^{-5}	2.00×10^{-2}	2.63×10^{-2}
1.36×10^{-5}	3.00×10^{-2}	3.65×10^{-2}
1.36×10^{-5}	4.00×10^{-2}	4.41×10^{-2}
1.36×10^{-5}	5.00×10^{-2}	5.46×10^{-2}

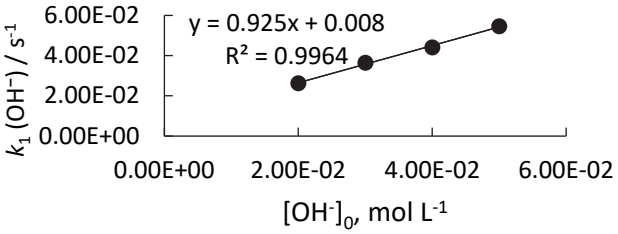

$k_{OH} = 9.25 \times 10^{-1}$ M^{-1} s^{-1}

Malachite Green-BF_4^- + H_2O_2 (from UHP) in alkaline 99.6/0.4 (v/v) H_2O/CH_3CN (stopped-flow, detection at 618 nm)

$[\mathbf{MG}]_0$, mol L^{-1}	$[H_2O_2]_0$, mol L^{-1}	$[OH^-]_0$, mol L^{-1}	$[HOO^-]$, mol L^{-1}	$[OH^-]$, mol L^{-1}	k_{obs}, s^{-1}	$k_{OH}[OH^-]$, s^{-1}	$k_2[HOO^-]$, s^{-1}
1.36×10^{-5}	4.00×10^{-4}	1.00×10^{-2}	2.54×10^{-4}	9.75×10^{-3}	3.03×10^{-1}	9.02×10^{-3}	2.94×10^{-1}
1.36×10^{-5}	8.00×10^{-4}	1.00×10^{-2}	5.02×10^{-4}	9.50×10^{-3}	5.70×10^{-1}	8.79×10^{-3}	5.61×10^{-1}
1.36×10^{-5}	1.20×10^{-3}	1.00×10^{-2}	7.46×10^{-4}	9.25×10^{-3}	8.63×10^{-1}	8.56×10^{-3}	8.54×10^{-1}
1.36×10^{-5}	1.60×10^{-3}	1.00×10^{-2}	9.85×10^{-4}	9.01×10^{-3}	1.12	8.34×10^{-3}	1.11
1.36×10^{-5}	2.00×10^{-3}	1.00×10^{-2}	1.22×10^{-3}	8.78×10^{-3}	1.39	8.12×10^{-3}	1.38

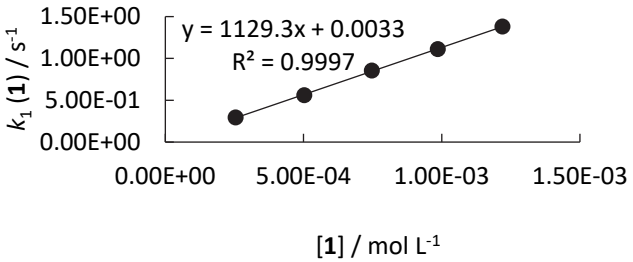

$k_2 = 1.13 \times 10^3$ M^{-1} s^{-1}
$k_{OH} = 9.25 \times 10^{-1}$ M^{-1} s^{-1}

Malachite Green-BF_4^- + $Ca(OCl)_2$ in alkaline 99.6/0.4 (v/v) H_2O/CH_3CN (stopped-flow, detection at 618 nm)

$[\mathbf{MG}]_0$, mol L^{-1}	$[ClO^-]_0$, mol L^{-1}	$[OH^-]_0$, mol L^{-1}	k_{obs}, s^{-1}	$k_{OH}[OH^-]$, s^{-1}	$k_2[ClO^-]$, s^{-1}
1.36×10^{-5}	1.00×10^{-4}	2.50×10^{-4}	2.98×10^{-1}	2.31×10^{-4}	2.98×10^{-1}
1.36×10^{-5}	2.00×10^{-4}	2.50×10^{-4}	5.74×10^{-1}	2.31×10^{-4}	5.74×10^{-1}
1.36×10^{-5}	3.00×10^{-4}	2.50×10^{-4}	8.75×10^{-1}	2.31×10^{-4}	8.75×10^{-1}
1.36×10^{-5}	4.00×10^{-4}	2.50×10^{-4}	1.08	2.31×10^{-4}	1.08
1.36×10^{-5}	5.00×10^{-4}	2.50×10^{-4}	1.34	2.31×10^{-4}	1.34

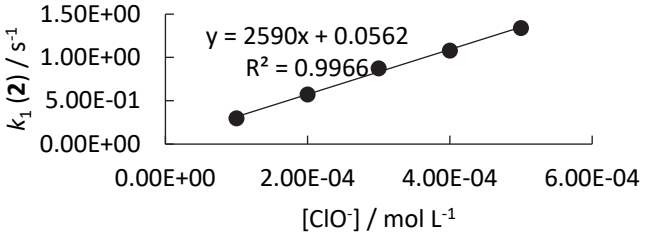

$k_2 = 2.59 \times 10^3$ M^{-1} s^{-1}
$k_{OH} = 9.25 \times 10^{-1}$ M^{-1} s^{-1}

Kinetics of Reactions of Bleach Reagents with Arylidenemalononitriles

Kinetics of the reactions of the hydroperoxide anion (1_{UHP}, generated from UHP) with arylidenemalononitriles 9 in water

9a + H_2O_2 in alkaline 99.6/0.4 (v/v) H_2O/CH_3CN (stopped-flow, detection at 316 nm)

$[\mathbf{9a}]_0$, mol L^{-1}	$[H_2O_2]_0$, mol L^{-1}	$[OH^-]_0$, mol L^{-1}	$[HOO^-]$, mol L^{-1}	$[OH^-]$, mol L^{-1}	k_{obs}, s^{-1}	$k_{OH}[OH^-]$, s^{-1}	$k_2[HOO^-]$, s^{-1}
2.53×10^{-5}	4.00×10^{-4}	2.50×10^{-2}	3.26×10^{-4}	2.47×10^{-2}	1.41×10^{1}	2.25	1.18×10^{1}
2.53×10^{-5}	8.00×10^{-4}	2.50×10^{-2}	6.50×10^{-4}	2.44×10^{-2}	2.51×10^{1}	2.22	2.29×10^{1}
2.53×10^{-5}	1.20×10^{-3}	2.50×10^{-2}	9.72×10^{-4}	2.40×10^{-2}	3.88×10^{1}	2.19	3.66×10^{1}
2.53×10^{-5}	1.60×10^{-3}	2.50×10^{-2}	1.29×10^{-3}	2.37×10^{-2}	5.14×10^{1}	2.16	4.92×10^{1}

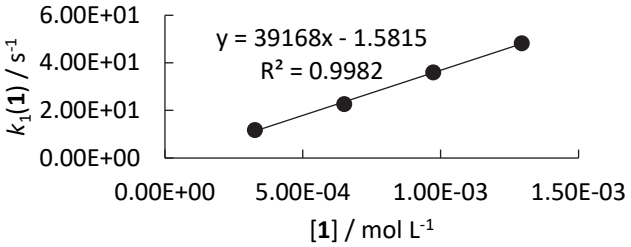

$k_2 = 3.92 \times 10^4$ M^{-1} s^{-1}
$k_{OH} = 9.13 \times 10^1$ M^{-1} s^{-1}

9b + H_2O_2 in alkaline 99.6/0.4 (v/v) H_2O/CH_3CN (stopped-flow, detection at 364 nm)

$[\mathbf{9b}]_0$, mol L^{-1}	$[H_2O_2]_0$, mol L^{-1}	$[OH^-]_0$, mol L^{-1}	$[HOO^-]$, mol L^{-1}	$[OH^-]$, mol L^{-1}	k_{obs}, s^{-1}	$k_{OH}[OH^-]$, s^{-1}	$k_2[HOO^-]$, s^{-1}
2.57×10^{-5}	4.00×10^{-4}	2.50×10^{-2}	3.26×10^{-4}	2.47×10^{-2}	3.08	6.20×10^{-1}	2.46
2.57×10^{-5}	8.00×10^{-4}	2.50×10^{-2}	6.50×10^{-4}	2.44×10^{-2}	5.45	6.12×10^{-1}	4.84
2.57×10^{-5}	1.20×10^{-3}	2.50×10^{-2}	9.72×10^{-4}	2.40×10^{-2}	8.15	6.02×10^{-1}	7.55
2.57×10^{-5}	1.60×10^{-3}	2.50×10^{-2}	1.29×10^{-3}	2.37×10^{-2}	1.07×10^{1}	5.95×10^{-1}	10.1

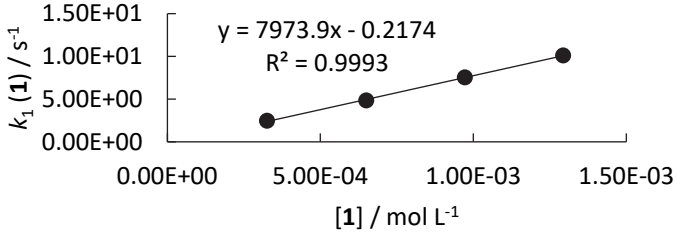

$k_2 = 7.97 \times 10^3$ M^{-1} s^{-1}
$k_{OH} = 2.51 \times 10^1$ M^{-1} s^{-1}

9c + H_2O_2 in alkaline 99.6/0.4 (v/v) H_2O/CH_3CN (stopped-flow, detection at 441 nm)

$[\mathbf{9c}]_0$, mol L^{-1}	$[H_2O_2]_0$, mol L^{-1}	$[OH^-]_0$, mol L^{-1}	$[HOO^-]$, mol L^{-1}	$[OH^-]$, mol L^{-1}	k_{obs}, s^{-1}	$k_{OH}[OH^-]$, s^{-1}	$k_2[HOO^-]$, s^{-1}
2.57×10^{-5}	4.00×10^{-4}	2.50×10^{-2}	3.26×10^{-4}	2.47×10^{-2}	1.91×10^{-1}	1.92×10^{-2}	1.72×10^{-1}
2.57×10^{-5}	8.00×10^{-4}	2.50×10^{-2}	6.50×10^{-4}	2.44×10^{-2}	3.17×10^{-1}	1.89×10^{-2}	2.98×10^{-1}
2.57×10^{-5}	1.20×10^{-3}	2.50×10^{-2}	9.72×10^{-4}	2.40×10^{-2}	4.54×10^{-1}	1.87×10^{-2}	4.35×10^{-1}
2.57×10^{-5}	1.60×10^{-3}	2.50×10^{-2}	1.29×10^{-3}	2.37×10^{-2}	6.01×10^{-1}	1.84×10^{-2}	5.83×10^{-1}

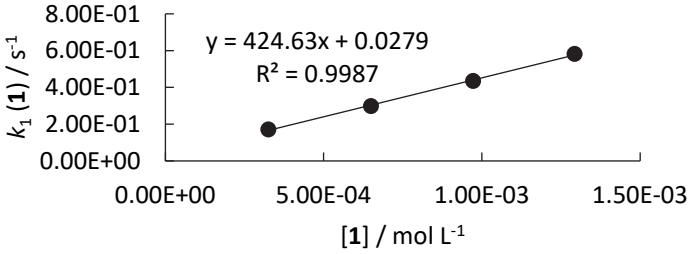

$k_2 = 4.25 \times 10^2$ M^{-1} s^{-1}
$k_{OH} = 7.77 \times 10^{-1}$ M^{-1} s^{-1}

Kinetics of the reactions of hypochlorite ion (2) with arylidenemalononitriles 9 in water

9a + $Ca(OCl)_2$ in alkaline 99.6/0.4 (v/v) H_2O/CH_3CN (stopped-flow, detection at 316 nm)

$[\mathbf{9a}]_0$, mol L^{-1}	$[ClO^-]_0$, mol L^{-1}	$[OH^-]_0$, mol L^{-1}	k_{obs}, s^{-1}	$k_{OH}[OH^-]$, s^{-1}	$k_2[ClO^-]$, s^{-1}
2.53×10^{-5}	1.00×10^{-4}	2.50×10^{-4}	6.21×10^{-1}	2.28×10^{-2}	5.98×10^{-1}
2.53×10^{-5}	2.00×10^{-4}	2.50×10^{-4}	1.27	2.28×10^{-2}	1.25
2.53×10^{-5}	3.00×10^{-4}	2.50×10^{-4}	1.96	2.28×10^{-2}	1.94
2.53×10^{-5}	4.00×10^{-4}	2.50×10^{-4}	2.60	2.28×10^{-2}	2.58

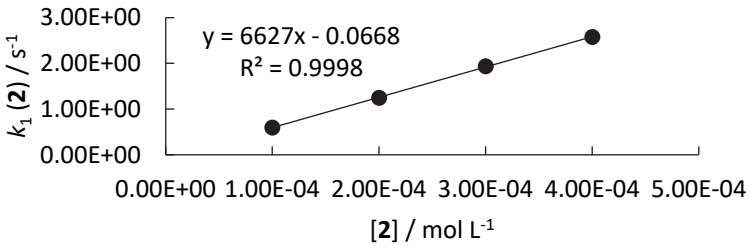

$k_2 = 6.63 \times 10^3$ м$^{-1}$ s^{-1}
$k_{OH} = 9.13 \times 10^1$ м$^{-1}$ s^{-1}

9b + $Ca(OCl)_2$ in alkaline 99.6/0.4 (v/v) H_2O/CH_3CN (stopped-flow, detection at 364 nm)

$[\mathbf{9b}]_0$, mol L^{-1}	$[ClO^-]_0$, mol L^{-1}	$[OH^-]_0$, mol L^{-1}	k_{obs}, s^{-1}	$k_{OH}[OH^-]$, s^{-1}	$k_2[ClO^-]$, s^{-1}
2.57×10^{-5}	1.00×10^{-4}	2.50×10^{-4}	1.25×10^{-1}	6.30×10^{-3}	1.19×10^{-1}
2.57×10^{-5}	2.00×10^{-4}	2.50×10^{-4}	2.60×10^{-1}	6.30×10^{-3}	2.54×10^{-1}
2.57×10^{-5}	3.00×10^{-4}	2.50×10^{-4}	3.93×10^{-1}	6.30×10^{-3}	3.87×10^{-1}
2.57×10^{-5}	4.00×10^{-4}	2.50×10^{-4}	5.44×10^{-1}	6.30×10^{-3}	5.38×10^{-1}

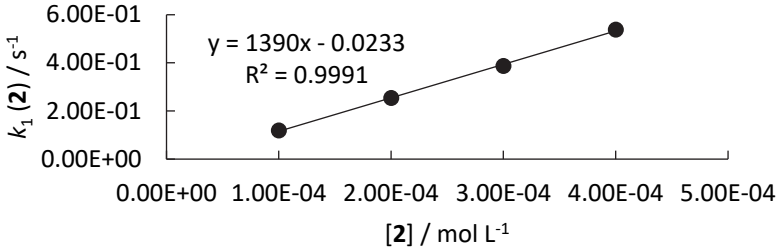

$k_2 = 1.39 \times 10^3$ м$^{-1}$ s^{-1}
$k_{OH} = 2.51 \times 10^1$ м$^{-1}$ s^{-1}

Kinetics of the reactions of hypobromite ion (3) with arylidenemalononitriles 9 in water

9a + BrO^- in alkaline 99.6/0.4 (v/v) H_2O/CH_3CN (stopped-flow, detection at 316 nm)

$[\mathbf{9a}]_0$, mol L^{-1}	$[BrO^-]_0$, mol L^{-1}	$[OH^-]_0$, mol L^{-1}	k_{obs}, s^{-1}	$k_{OH}[OH^-]$, s^{-1}	$k_2[BrO^-]$, s^{-1}
2.53×10^{-5}	8.00×10^{-4}	9.94×10^{-4}	8.83	2.50×10^{-2}	8.80
2.53×10^{-5}	1.00×10^{-3}	9.92×10^{-4}	11.0	2.50×10^{-2}	11.0
2.53×10^{-5}	1.20×10^{-3}	9.91×10^{-4}	13.1	2.50×10^{-2}	13.1
2.53×10^{-5}	1.40×10^{-3}	9.89×10^{-4}	15.7	2.49×10^{-2}	15.7
2.53×10^{-5}	1.60×10^{-3}	9.88×10^{-4}	17.5	2.49×10^{-2}	17.5

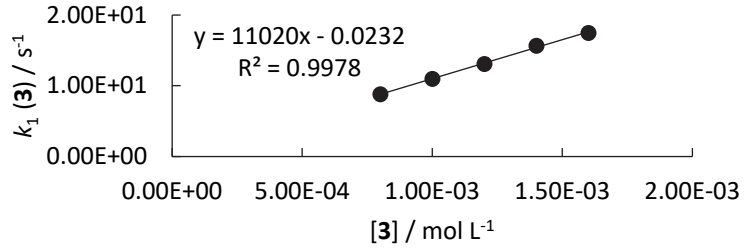

$k_2 = 1.10 \times 10^4$ м$^{-1}$ s^{-1}
$k_{OH} = 9.13 \times 10^1$ м$^{-1}$ s^{-1}

9b + BrO^- in alkaline 99.6/0.4 (v/v) H_2O/CH_3CN (stopped-flow, detection at 364 nm)

$[\mathbf{9b}]_0$, mol L^{-1}	$[BrO^-]_0$, mol L^{-1}	$[OH^-]_0$, mol L^{-1}	k_{obs}, s^{-1}	$k_{OH}[OH^-]$, s^{-1}	$k_2[BrO^-]$, s^{-1}
2.57×10^{-5}	8.00×10^{-4}	9.94×10^{-4}	1.84	9.07×10^{-3}	1.83
2.57×10^{-5}	1.00×10^{-3}	9.92×10^{-4}	2.39	9.06×10^{-3}	2.38
2.57×10^{-5}	1.20×10^{-3}	9.91×10^{-4}	2.80	9.05×10^{-3}	2.79
2.57×10^{-5}	1.40×10^{-3}	9.89×10^{-4}	3.24	9.03×10^{-3}	3.23
2.57×10^{-5}	1.60×10^{-3}	9.88×10^{-4}	3.81	9.02×10^{-3}	3.80

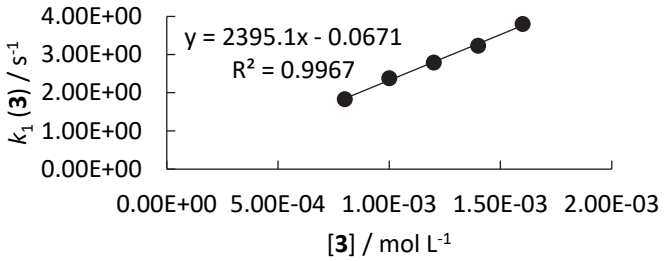

$k_2 = 2.40 \times 10^3$ M^{-1} s^{-1}
$k_{OH} = 2.51 \times 10^1$ M^{-1} s^{-1}

Kinetics of the reactions of peroxymonosulfate ion (4) with arylidenemalononitriles 9 in water

9a + HSO_5^- in alkaline 99.6/0.4 (v/v) H_2O/CH_3CN (stopped-flow, detection at 316 nm)

$[\mathbf{9a}]_0$, mol L^{-1}	$[HSO_5^-]_0$, mol L^{-1}	$[OH^-]_0$, mol L^{-1}	$[SO_5^{2-}]$, mol L^{-1}	$[OH^-]$, mol L^{-1}	k_{obs}, s^{-1}	$k_{OH}[OH^-]$, s^{-1}	$k_2[SO_5^{2-}]$, s^{-1}
2.53×10^{-5}	1.00×10^{-4}	9.50×10^{-4}	9.71×10^{-5}	8.03×10^{-4}	1.04	7.33×10^{-2}	9.67×10^{-1}
2.53×10^{-5}	2.00×10^{-4}	9.00×10^{-4}	1.93×10^{-4}	6.07×10^{-4}	2.12	5.54×10^{-2}	2.06
2.53×10^{-5}	3.00×10^{-4}	8.50×10^{-4}	2.87×10^{-4}	4.13×10^{-4}	2.71	3.77×10^{-2}	2.67
2.53×10^{-5}	4.00×10^{-4}	8.00×10^{-4}	3.78×10^{-4}	2.22×10^{-4}	3.27	2.03×10^{-2}	3.25

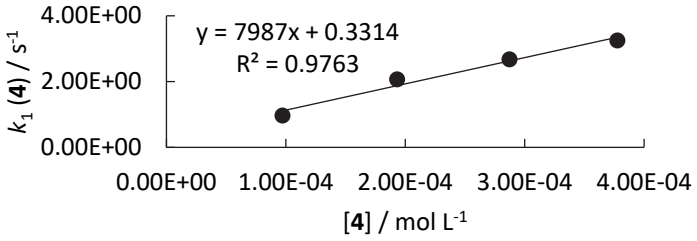

$k_2 = 7.99 \times 10^3$ M^{-1} s^{-1}
$k_{OH} = 9.13 \times 10^1$ M^{-1} s^{-1}

9b + HSO_5^- in alkaline 99.6/0.4 (v/v) H_2O/CH_3CN (stopped-flow, detection at 364 nm)

$[\mathbf{9b}]_0$, mol L^{-1}	$[HSO_5^-]_0$, mol L^{-1}	$[OH^-]_0$, mol L^{-1}	$[SO_5^{2-}]$, mol L^{-1}	$[OH^-]$, mol L^{-1}	k_{obs}, s^{-1}	$k_{OH}[OH^-]$, s^{-1}	$k_2[SO_5^{2-}]$, s^{-1}
2.57×10^{-5}	1.00×10^{-4}	9.50×10^{-4}	9.71×10^{-5}	8.03×10^{-4}	2.00×10^{-1}	2.15×10^{-2}	1.79×10^{-1}
2.57×10^{-5}	2.00×10^{-4}	9.00×10^{-4}	1.93×10^{-4}	6.07×10^{-4}	4.04×10^{-1}	1.78×10^{-2}	3.86×10^{-1}
2.57×10^{-5}	3.00×10^{-4}	8.50×10^{-4}	2.87×10^{-4}	4.13×10^{-4}	5.66×10^{-1}	1.41×10^{-2}	5.52×10^{-1}
2.57×10^{-5}	4.00×10^{-4}	8.00×10^{-4}	3.78×10^{-4}	2.22×10^{-4}	6.08×10^{-1}	1.05×10^{-2}	5.98×10^{-1}

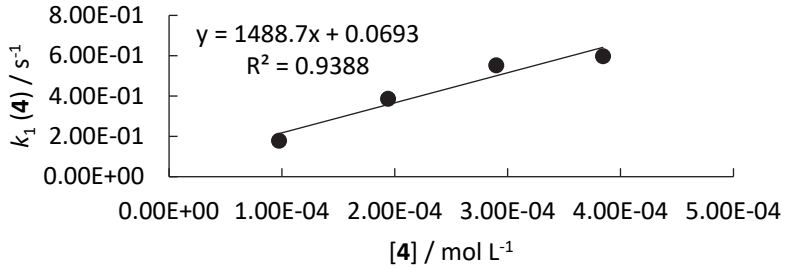

$k_2 = 1.49 \times 10^3$ M^{-1} s^{-1}
$k_{OH} = 2.51 \times 10^1$ M^{-1} s^{-1}

Kinetics of the reactions of bromite ion (5) with arylidenemalononitriles 9 in water

9a + BrO_2^- in alkaline 99.6/0.4 (v/v) H_2O/CH_3CN (stopped-flow, detection at 316 nm)

$[\mathbf{9a}]_0$, mol L^{-1}	$[BrO_2^-]_0$, mol L^{-1}	$[OH^-]_0$, mol L^{-1}	k_{obs}, s^{-1}	$k_{OH}[OH^-]$, s^{-1}	$k_2[BrO_2^-]$, s^{-1}
2.53×10^{-5}	8.00×10^{-4}	5.00×10^{-4}	9.93×10^{-2}	4.57×10^{-2}	4.83×10^{-2}
2.53×10^{-5}	1.00×10^{-3}	5.00×10^{-4}	1.02×10^{-1}	4.57×10^{-2}	5.64×10^{-2}
2.53×10^{-5}	1.20×10^{-3}	5.00×10^{-4}	1.06×10^{-1}	4.57×10^{-2}	6.04×10^{-2}
2.53×10^{-5}	1.40×10^{-3}	5.00×10^{-4}	1.10×10^{-1}	4.57×10^{-2}	6.44×10^{-2}
2.53×10^{-5}	1.60×10^{-3}	5.00×10^{-4}	1.19×10^{-1}	4.57×10^{-2}	7.34×10^{-2}

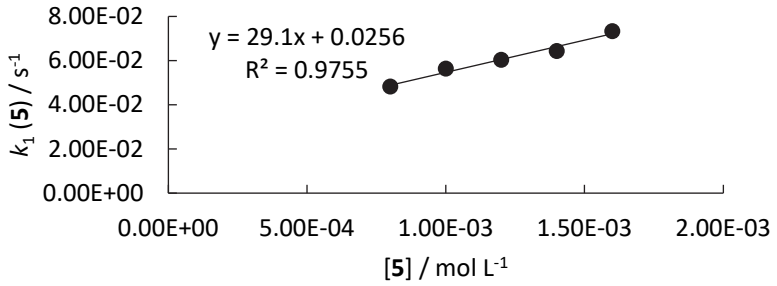

$k_2 = 2.91 \times 10^1\ M^{-1}\ s^{-1}$

$k_{OH} = 9.13 \times 10^1\ M^{-1}\ s^{-1}$

2.5 References

[1] Adams, J. M.; Pritchard, R. G. *Acta Cryst. B* **1977**, *33*, 3650–3653.

[2] Polak, H. L.; Feenstra, G.; Slagman, J. *Talanta* **1966**, *13*, 715–724.

[3] Noszticzius, Z.; Noszticzius, E.; Schelly, Z. A. *J. Phys. Chem.* **1983**, *87*, 510–524.

[4] Ropp, R. C. *Encyclopedia of the Alkaline Earth Compounds*; Elsevier: Amsterdam, 2012; pp 91–92.

[5] Horn, M.; Mayr, H. *Chem. Eur. J.* **2010**, *16*, 7469–7477.

[6] *SAINT*; Bruker AXS Inc., Madison, Wisconsin, USA: 2012.

[7] Sheldrick, G. M. *SADABS, TWINABS*; University of Göttingen, Germany: 1996.

[8] Sheldrick, G. M. *Acta Cryst. A* **2015**, *71*, 3–8.

[9] Levason, W.; Ogden, J. S.; Spicer, M. D.; Webster, M.; Young, N. A. *J. Am. Chem. Soc*. **1989**, *111*, 6210–6212.

[10] Mayer, R. J.; Tokuyasu, T.; Mayer, P.; Gomar, J.; Sabelle, S.; Mennucci, B.; Mayr, H.; Ofial, A. R. *Angew. Chem. Int. Ed*. **2017**, *56*, 13279–13282.

Chapter 3. Intramolecular Hydrogen-Bonding Modulates the Nucleophilic Reactivity of Ammonium-Peroxycarboxylates.

R. J. Mayer, A. R. Ofial, *Eur. J. Org. Chem.* **2018**, 6010-6017.

Author Contributions

RJM performed all experiments and calculations. The manuscript was written jointly by RJM and ARO.

Copyright

Selected supporting material for this work is provided starting with section 3.1. The complete supporting information (SI) is published online and can be accessed under https://doi.org/10.1002/ejoc.201801158.

ChemPubSoc Europe

DOI: 10.1002/ejoc.201801158

EurJOC European Journal of Organic Chemistry

Full Paper

Reaction Kinetics

Intramolecular Hydrogen-Bonding Modulates the Nucleophilic Reactivity of Ammonium-Peroxycarboxylates

Robert J. Mayer[a] and Armin R. Ofial*[a]

Abstract: The ammonium-peroxycarboxylic acid mesylates derived from γ-aminobutyric acid, β-alanine, and β-piperidinopropionic acid were synthesized and characterized by spectroscopic methods and X-ray crystallography. To study the nucleophilic reactivities of the corresponding ammonium- and aminoperoxycarboxylates, the kinetics of their reactions with a series of benzhydrylium ions (Ar_2CH^+) were investigated in alkaline, aqueous solutions at 20 °C. Using sequential-mixing stopped-flow UV/Vis photometry, the rates of the reactions of the short-lived nucleophiles with Ar_2CH^+ were determined and analyzed by the linear free energy relationship lg $k = s_N(N + E)$ furnishing nucleophilicity parameters (N, s_N) of the peroxycarboxylates. Quantum chemical calculations indicate that the reactivity of the zwitterionic ammonium-peroxycarboxylates is attenuated by intramolecular N–H···O hydrogen bonding.

Introduction

Recent investigations into the nucleophilic reactivity of inorganic bleach reagents and peroxide anions showed that peroxycarboxylates possess distinctly higher reactivity than the anions of alkyl hydroperoxides (ROO^-) and hydrogen peroxide (HOO^-).[1,2] In this context, some patents on the use of amino-acid derived peroxycarboxylic acids intrigued us.[3a–3g] Quaternarization of the nitrogen by alkylation or protonation along with subsequent oxidation at the carboxyl group led to solid ammonium-peroxycarboxylic acids (APOCAs, with HSO_4^- or MsO^- counterions).[3a] These APOCA salts had been characterized by elemental analysis and, in some cases, melting points. In addition, their potential application as textile bleaches was reported.[3a–3g] One would, furthermore, expect that APOCA salts could serve as stable and well water-soluble precursors of highly nucleophilic peroxycarboxylate anions.

To enhance our understanding of their reactivities, we characterized a representative set of three APOCA salts by spectroscopic methods and X-ray analysis. We then evaluated the pH-dependent reactivity of aqueous solutions of APOCA salts toward benzhydrylium ions (as reference electrophiles) by kinetic methods to define the potential of APOCAs as nucleophilic oxidants and compare their reactivities with those of related oxidants.

Results and Discussion

Characterization of Ammonium-Peroxycarboxylates. Following a literature procedure,[3a] we synthesized three APOCA mesylates **2**$^+$$MsO^-$ as depicted in Scheme 1. Dissolving γ-aminobutyric acid (**1a**, GABA), β-alanine (**1b**), and β-piperidinopropionic acid (**1c**) in methanesulfonic acid and adding an excess of concentrated (> 85 %) aqueous hydrogen peroxide[3h] generated the APOCA mesylates **2a**$^+$$MsO^-$, **2b**$^+$$MsO^-$, and **2c**$^+$$MsO^-$, respectively, which precipitated when the reaction mixture was poured on ice-cold THF.

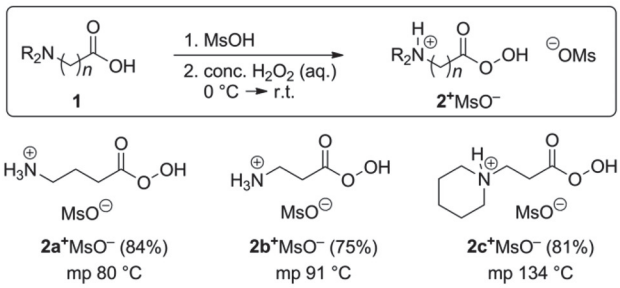

Scheme 1. Preparation of ammonium-peroxycarboxylic acid mesylates.

Beside their spectroscopic characterization (Supporting Information), **2a**$^+$$MsO^-$, **2b**$^+$$MsO^-$ and **2c**$^+$$MsO^-$ were investigated by single-crystal X-ray diffraction (Figure 1).[4] The oxygen–oxygen distances of 1.451 to 1.464 Å in **2a**$^+$, **2b**$^+$, and **2c**$^+$ are in the typical range reported for peroxycarboxylic acids.[5]

In crystals of **2a**$^+$$MsO^-$ and **2b**$^+$$MsO^-$ the C(O)–O–O–H groups adopt an almost identical conformation with C–O–O–H dihedral angles of 158.2° and 154.6°. In contrast, this dihedral angle is significantly lower in the piperidinium derivative **2c**$^+$$MsO^-$ (104.7°), probably owing to different hydrogen bonding patterns in the solid states of (**2a**–**c**)$^+$$MsO^-$. As exemplarily shown for **2a**$^+$$MsO^-$ in Figure 2, various hydrogen bonding interactions between O–H or N–H of the **2**$^+$ and the oxygen atoms of the mesylate counterions are the prevalent interactions found for all APOCA mesylates in crystalline state (Figure 2).

[a] *Department Chemie, Ludwig-Maximilians-Universität München, Butenandtstraße 5-13, 81377 München, Germany*
E-mail: ofial@lmu.de
URL: http://www.cup.uni-muenchen.de/oc/ofial/
Supporting information and ORCID(s) from the author(s) for this article are available on the WWW under https://doi.org/10.1002/ejoc.201801158.

ChemPubSoc Europe

EurJOC European Journal of Organic Chemistry
Full Paper

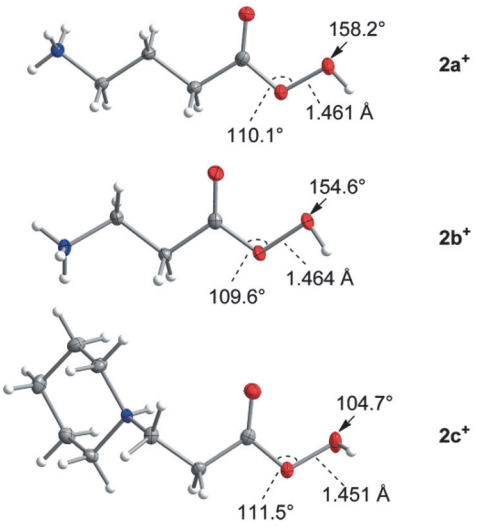

Figure 1. Solid-state structures of **2a**$^+$MsO$^-$, **2b**$^+$MsO$^-$ and **2c**$^+$MsO$^-$ (thermal ellipsoids are depicted at 50 % probability level at T = 100 K, counterion MsO$^-$ not shown).[4]

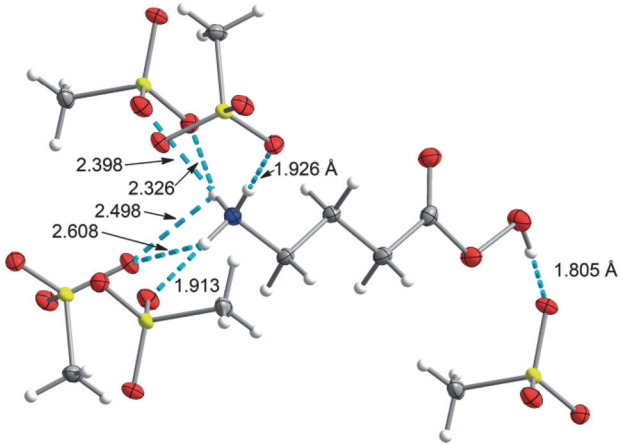

Figure 2. Hydrogen bonding in the solid-state structure of **2a**$^+$MsO$^-$ (thermal ellipsoids are depicted at 50 % probability level).

To characterize the acid/base behavior of **2**$^+$, we determined the Brønsted acidities (pK_a) of their peroxycarboxylic groups by potentiometric titration in water. The acidities of **2**$^+$ were found to be in the common range of pK_a 7–8 for aliphatic peroxyacids (see Table 1 below).[1] By assuming that the known pK_a of ammonium groups in protonated amino acids (pK_a ≈ 10) also apply for the APOCA cations **2**$^+$, it can be anticipated that amino-substituted peroxycarboxylic acids exist as cations (**2**$^+$), zwitterions (**2**), or anions (**2**$^-$) in aqueous solution (Scheme 2), depending on the pH and in analogy to the established equilibria for α-amino acids. As both, the peroxycarboxylate and the amino group, can act as the nucleophile, the reactivity of APOCA salt solutions is significantly affected by pH.

Kinetics. The nucleophilic reactivity of the amino group in aminocarboxylates derived from natural amino acids or small peptides has already been investigated.[6] Analogous N-nucleophilicities have also been determined for the deprotonated

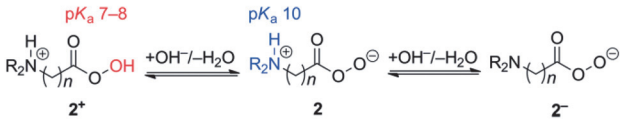

Scheme 2. Protonation equilibria of APOCAs.

forms of GABA (**1a**) and β-alanine (**1b**).[6] In this work, we set out to characterize the peroxycarboxylate groups of **2** and **2**$^-$ in alkaline, aqueous solution with the aim to compare the nucleophilic reactivities with those of other peroxide anions on the basis of Mayr's linear free energy relationship (1).[7–11]

$$\lg k_2(20\ ^\circ\mathrm{C}) = s_N(N + E) \quad (1)$$

In equation (1) the nucleophiles' reactivity is described by the solvent-dependent nucleophilicity parameter N and the nucleophile-specific susceptibility s_N. These parameters can be determined from kinetic measurements with a set of benzhydrylium ions as reference electrophiles (with known electrophilicity parameters E), employing the previously reported procedure.[1,6] As shown in Scheme 3, the kinetics were studied in alkaline, aqueous solution, in which zwitterions **2** were generated by equilibrium deprotonation of the corresponding cations **2**$^+$. The reactions of an excess of **2** with blue colored benzhydrylium ions Ar$_2$CH$^+$ **3**[12] under pseudo-first-order conditions yielded colorless reaction products, which enabled us to use stopped-flow UV/Vis photometry to monitor the reaction progress.

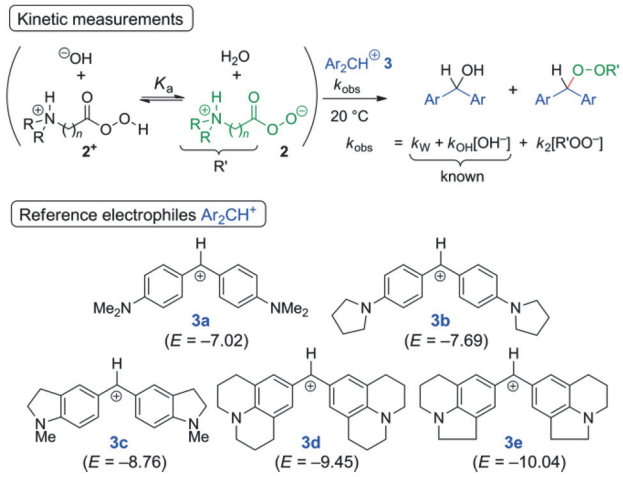

Scheme 3. Generation of nucleophilic zwitterions **2** in alkaline, aqueous solution and reactions of **2** with the benzhydrylium ions **3** (counterions: BF$_4^-$ for **3**, MsO$^-$ for **2**$^+$, electrophilicities E from ref[11]).

Initial sequential mixing experiments showed that conditions successfully used to determine the nucleophilicity of various peroxide anions[1] could not be applied without modification to study the kinetics of the reactions of **3** with the ammonium-peroxycarboxylates **2**: When we generated **2a** in a first mixing step by dissolving **2a**$^+$MsO$^-$ ([**2a**$^+$]$_0$ = 4 × 10^{-4} M) in aqueous potassium hydroxide solution ([KOH]$_0$ = 4 × 10^{-4} M), then allowed the solution to age for a defined time and, in a second mixing step, added solutions of **3**-BF$_4^-$ ([**3**]$_0$ = 1.1 × 10^{-5} M),

ChemPubSoc Europe

EurJOC European Journal of Organic Chemistry
Full Paper

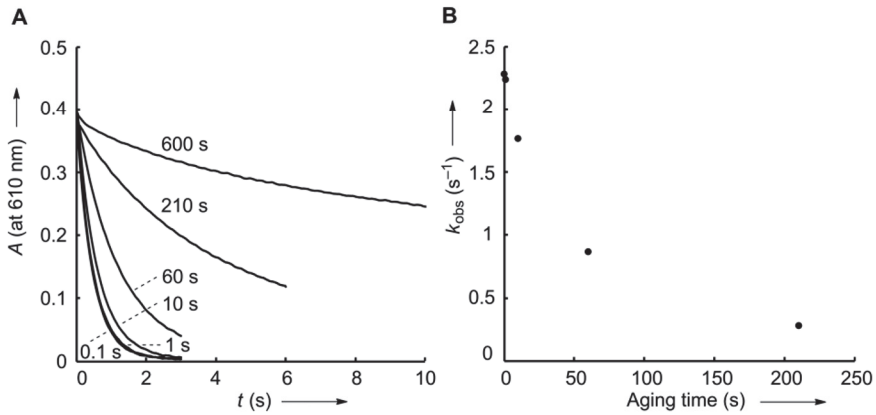

Figure 3. (A) Observed decays of benzhydryl absorbances (**3b**) for variable aging times of the nucleophile (**2a**) solutions and (B) dependence of the corresponding first-order rate constants k_{obs} on the aging times. [**2a**$^+$MsO$^-$]$_0$ = 4 × 10^{-4} M, [OH$^-$]$_0$ = 4 × 10^{-4} M, 20 °C. The slow reaction of **2a** with **3b** after 600 s aging time did not follow a mono-exponential decay.

we observed mono-exponential decays of the benzhydrylium absorbances under these pseudo-first-order conditions. However, the observed decay rates systematically decreased when the time between the first and the second mixing step, that is, the aging time of the nucleophile solution, was increased (Figure 3A). The dependence of the observed rate contants k_{obs} on the aging time indicated a first-order decomposition of the nucleophile on the seconds time scale at 20 °C ($\tau_{1/2}$ = 20–25 s, Figure 3B). The analogous variation of the aging times for reactions of reference electrophiles **3** with aqueous solutions of the nucleophilic zwitterions **2b** and **2c** (generated from **2b**$^+$MsO$^-$ and **2c**$^+$MsO$^-$, respectively) gave similar results but showed that the degradation proceeded somewhat slower ($\tau_{1/2}$ > 100 s, Supporting Information) than for **2a**.

In contrast, iodometric titration of an alkaline solution of **2a**$^+$MsO$^-$ showed that the total peroxide content of the reaction mixture decreased on the minute time-scale (Figure 4), thus, much slower than expected from the kinetic experiments shown in Figure 3.

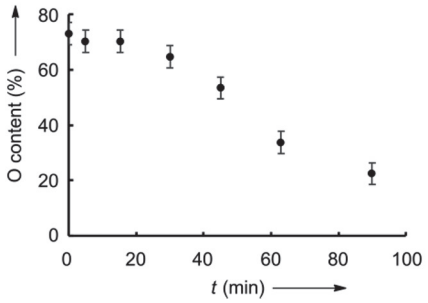

Figure 4. Peroxide content as determined by iodometric titration of an alkaline solution of **2a**$^+$MsO$^-$ (20 °C, [**2a**$^+$] = 1.4 × 10^{-3} M, [OH$^-$] = 5 × 10^{-2} M).

The NMR spectroscopic investigation of the alkaline, aqueous solutions showed that degradation of the peroxycarboxylate to the carboxylate group by attack of hydroxide ions at the carboxyl carbon is a common decomposition pathway for all investigated zwitterions **2** (Scheme 4A). This reaction path liberates hydrogen peroxide, which decomposes slowly to molecular oxygen and water.

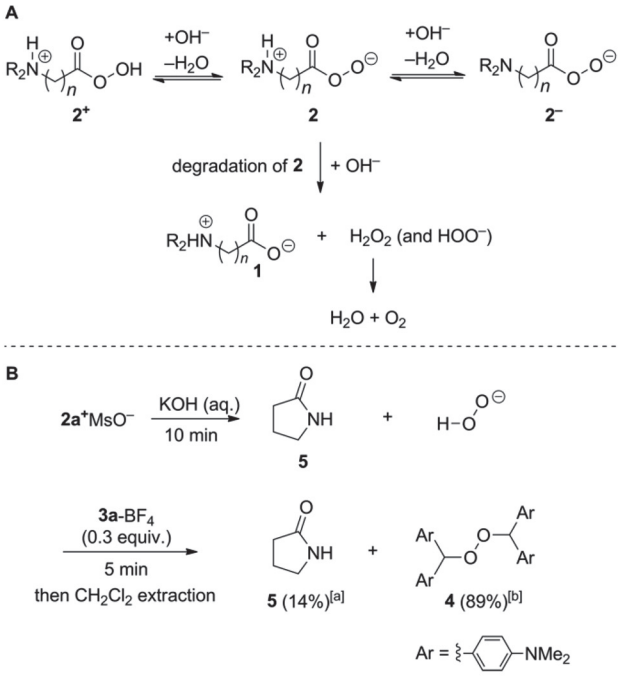

Scheme 4. (A) General degradation of **2** to **1** in alkaline solution. (B) Formation of the lactam **5** by ring closure of **2a**$^+$MsO$^-$ in alkaline solution and partial trapping of thus liberated hydrogen peroxide by **3a**. Yields were determined by using added dimethyl fumarate as integration standard. [a] The hydrophilic lactam **5** was only partially extracted by dichloromethane, which resulted in a low yield of **5** (yield refers to **2a**$^+$MsO$^-$). [b] Yield refers to **3a**-BF_4.

The peroxy version of GABA (**2a**) decomposed significantly faster than **2b** or **2c** owing to an additional option: As indicated by ^{1}H NMR spectroscopy, a mixture of the lactam **5** and the peroxide **4** was isolated after dichloromethane extraction of an aqueous, alkaline solution of **2a**$^+$MsO$^-$ that, after 10 min of aging at ambient temperature, was treated with **3a**-BF_4 (Scheme 4B). We conclude that **2a** not only degrades because of the hydroxide ion attack shown in Figure 4A but also undergoes ring closure to give γ-butyrolactam (**5**) under *alkaline* reac-

ChemPubSoc Europe

EurJOC European Journal of Organic Chemistry
Full Paper

tion conditions (pH 13). A stoichiometric amount of hydrogen peroxide anions is released in this self-condensation, which is interceptable by the known reaction with **3a**[2] to yield the bis(benzhydryl)peroxide **4**. Degradation by ring closure was not observed for **2b**, presumably because this intramolecular reaction would lead to a strained β-lactam.

To gain evidence for the oxidation of electrophiles by APOCAs, we studied the reaction of benzylidene malononitrile **6** with $\mathbf{2}^+$ under alkaline conditions (Scheme 5). When **6** was treated with an excess of $\mathbf{2a}^+MsO^-$ (2.5 equiv.), the electrophile was almost quantitatively converted into the corresponding epoxide **7**. Additionally, the formation of the corresponding GABA zwitterion **1a** and γ-butyrolactam **5** (both in comparable ratio) were observed by NMR spectroscopy. The outcome of this reaction corroborates our mechanistic outline: After quantitative generation of **2a** by deprotonation of $\mathbf{2a}^+$ under the alkaline conditions, one part of **2a** (2.5 equiv.) reacts with **6** (1 equiv.) in a nucleophilic epoxidation to furnish **7** (1 equiv.) and **1a**. The remaining 1.5 equivalents of the peroxycarboxylate **2a** decompose to hydrogen peroxide and the lactam **5**.

We, therefore, conclude that the zwitterions **2** decompose rapidly in alkaline, aqueous solution after being generated from $\mathbf{2}^+$ (as seen in Figure 3). Independent of whether decomposition of **2** is initiated by hydroxide ions that react with the peroxycarboxyl group or by amino groups that intramolecularly attack at the carboxyl carbon, H_2O_2 is released. The iodometrically determined slow decrease of the overall peroxide content for alkaline solutions of $\mathbf{2}^+$ (Figure 4), therefore, reflects the subsequent, slow decomposition of the released H_2O_2.

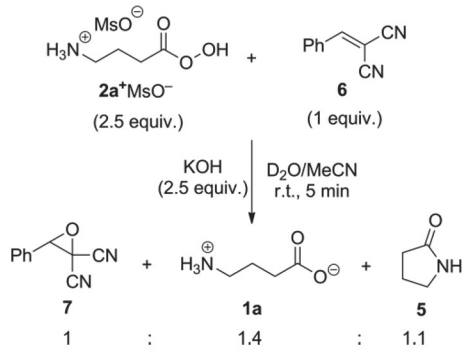

Scheme 5. Reaction of $\mathbf{2a}^+MsO^-$ with malononitrile **6** as analyzed by ^1H NMR spectroscopy.

Figure 3 defines the conditions for the determination of the nucleophilic reactivities of **2**: First, solutions of **2** have to be mixed with their electrophilic reaction partners within 1 s after generation of **2** from $\mathbf{2}^+$. Second, the half-life times of the reactions should be 10 s or less to avoid noticeable degradation of **2** during the reactions with **3**. Determining the reaction kinetics by using the sequential mixing setup of the stopped-flow spectrometer was, therefore, instrumental to access the nucleophilicities of solutions of **2**: In a first step, aqueous solutions of the base and $\mathbf{2}^+MsO^-$ were mixed and allowed to age for 1 s. Then the reaction with the reference electrophiles **3** was initiated by mixing the solution of freshly generated **2** with that of **3**.

As the degree of deprotonation of $\mathbf{2}^+$ is adjustable by the chosen hydroxide concentration, different nucleophilic species can be addressed: Treating $\mathbf{2}^+$ with an equimolar amount of base generates the ammonium-peroxycarboxylates **2**. Under these conditions, the oxygen reactivity of zwitterions **2** can be measured selectively because the more basic amino group is still protected by protonation. Alternatively, a high concentration of base generates the amino-peroxycarboxylate $\mathbf{2}^-$ as the major species. Because anions $\mathbf{2}^-$ are ambident nucleophiles that attack via either nitrogen or oxygen at Ar_2CH^+, the determination of the nucleophilicities of $\mathbf{2a}^-$ and $\mathbf{2b}^-$ was not possible unequivocally. In $\mathbf{2c}^-$, however, the nitrogen of the tertiary amine is sterically hindered and does not react with highly stabilized benzhydrylium ions, such as **3b**–**e**.[13] This enabled us to quantify the oxygen-reactivity of amino-peroxycarboxylate $\mathbf{2c}^-$ without interfering reactivity of the piperidino group.

The analysis of the observed first-order rate constants k_{obs} (s^{-1}, Figure 5A) by equation (2) was performed as reported for the anions of organic peroxides:[1,2] Brønsted acidities (pK_a) of $\mathbf{2}^+$ were employed to determine the concentrations of peroxycarboxylates and hydroxide ions, that is, [**2**] (or [$\mathbf{2}^-$]) and [OH^-]. Then, [OH^-] and the known second-order rate constants k_{OH}

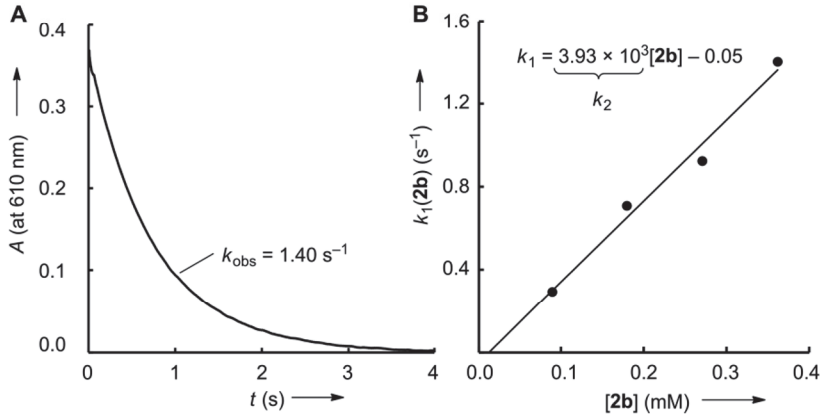

Figure 5. (A) Absorbance *A* (at 610 nm) vs. time for the reaction of **2b** (4.00×10^{-4} M) with **3b** (1.14×10^{-5} M) in aqueous solution (pH 9) at 20 °C. (B) The slope of the linear plot of the first-order rate constant k_1 (= $k_{obs} - k_{OH}[HO^-]$) vs. nucleophile concentration was used to derive the second-order rate constant k_2 for the attack of the zwitterion **2b** at the benzhydrylium ion **3b**.

ChemPubSoc Europe

EurJOC European Journal of Organic Chemistry
Full Paper

(from ref[14]) were used for the calculation of the rates of consumption of the cations **3b**–**e** by the hydroxide ions. After subtraction of the contribution by hydroxide ions ($k_{OH}[OH^-]$) from the observed first-order rate constants k_{obs}, the first-order rate constant k_1 [in Equation (3)] reflect the reaction of the electrophiles **3** with the nucleophiles with only a very minor correction for the much slower background reaction of **3** with water (k_W).

$$k_{obs} = k_W + k_{OH}[HO^-] + k_2[R'OO^-] \quad (2)$$

$$k_1 = k_2[R'OO^-] + k_W = k_{obs} - k_{OH}[HO^-] \quad (3)$$

Thereby, the second-order rate constants for the reactions of **2** (or **2**$^-$) with benzhydrylium ions **3b**–**e** can be obtained from the slope of the linear correlation of the first-order rate constant k_1 (= $k_{obs} - k_{OH}[HO^-]$) with the nucleophile concentration.

In accord with equation (3) and as exemplified in Figure 5B for the reactions of **2b** with **3b**, the first-order rate constants k_1 increased linearly with increasing concentration of the nucleophile **2b**, and the slope of these correlations corresponded to the second-order rate constant (k_2, Table 1) for the attack of **2** (or **2**$^-$) at the benzhydrylium ions **3b**–**e**.

The resulting second-order rate constants k_2 of these reactions and the known electrophilicities E of **3b**–**e**[11] were then applied in equation (1): The linear correlations of lg k_2 with the electrophilicity E allowed us to determine the nucleophilicity parameter N and the nucleophile-specific susceptibilities s_N of the peroxide species **2a**–**2c** and **2c**$^-$ (Figure 6). The reactivities of the ammonium-peroxycarboxylates **2** vary only within less than one order of magnitude. It is noteworthy that **2** react 5 to 10 times slower with **3b**–**e** than structurally related peroxycarboxylates (such as phenylperoxyacetate or ε-phthalimido-peroxyhexanoate[1]). Deprotonation of zwitterion **2c** and generation of the anionic **2c**$^-$ increased the reactivity of the RCO_3^- group by a factor of four.

The nucleophilicities of the amino groups in deprotonated GABA **1a**$^-$ and β-alanine **1b**$^-$ were reported to be N = 13.3–13.5 (s_N = 0.56–0.58).[6] Such a level of reactivity can also be anticipated for anionic **2a**$^-$ or **2b**$^-$ that carry free amino groups in a similar molecular environment. We, therefore, analyzed the contribution of *N*-attack by **2**$^-$ at benzhydrylium ions **3** under the conditions of our kinetic experiments.

First, products of *N*-attack by the γ- and β-amino-carboxylates **1a**$^-$ and **1b**$^-$ at **3a**-BF_4^- were characterized by NMR spectroscopy (Supporting Information). The typical singlets at chemical shifts of 4.61–4.64 ppm for N-C*H*Ar_2 in **8a** and **8b** (Scheme 6) were then used to analyse product mixtures obtained for reactions of equimolar amounts of **2b**$^+$MsO$^-$ and **3a**-BF_4^- at variable pH. When 1 equiv. of KOH was used to convert **2b**$^+$ to **2b**, oxygen attack of **2b** at **3a** and subsequent Criegee rearrangements gave rise to various oxidation products of **3a**, such as 4-(dimethylamino)benzaldehyde, and the benzhydrol and benzophenone derivatives of **3a**.[15] Amine **8b**, which may form through nitrogen attack of **2b** at **3a** and subsequent degradation of the peroxycarboxylic to a carboxylic acid, was not detected by ^{1}H NMR spectroscopy under these conditions. However, when 2 equiv. of KOH were used, generation of **8b** became evident from the ^{1}H NMR spectrum of the reaction mixture, and **8b** was formed in even higher yields under more alkaline conditions, that is, reactions of **2b** with **3a** in the presence of 3 equiv. of potassium hydroxide (Supporting Information).

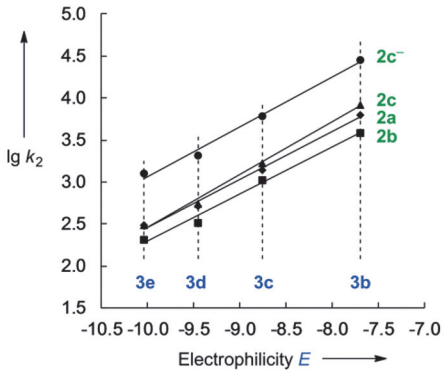

Figure 6. Correlation of lg k_2 for the reactions of nucleophiles **2a**–**c** (and **2c**$^-$) with the reference electrophiles **3b**–**e** (from Table 1) with the electrophilicity parameters E of **3**.

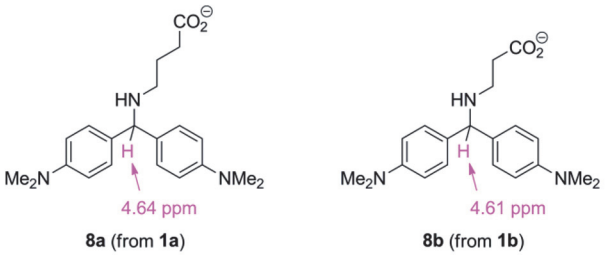

Scheme 6. Chemical shifts of the *N*-benzhydrylated amino acids **8a** and **8b** (in alkaline CD_3CN/D_2O = 4:3).

Owing to the fact that all rate constants for **2a**–**2c** collected in Table 1 were acquired by using only one equivalent of potassium hydroxide (relative to **2**$^+$MsO$^-$), we conclude that these kinetics describe exclusively the oxygen attack of the peroxycarboxylate groups of the zwitterions **2** at the cationic center of **3**. Nitrogen attack becomes only relevant at higher pH (that is, when > 1 equiv. of hydroxide ions relative to **2a**$^+$ or **2b**$^+$ are

Table 1. Basicities pK_{aH} and second-order rate constants k_2 for the oxygen attack of the ammoniumperoxycarboxylates **2** and the aminoperoxycarboxylate **2c**$^-$ at the reference electrophiles **3b**–**e** in alkaline, aqueous solution at 20 °C.

	pK_{aH}[a]	k_2 [M^{-1} s^{-1}]				N (s_N)
		3e	**3d**	**3c**	**3b**	
2a	7.77	3.10×10^2	5.20×10^2	1.39×10^3	6.33×10^3	14.33 (0.57)
2b	7.35	2.06×10^2	3.32×10^2	1.07×10^3	3.93×10^3	14.07 (0.56)
2c	7.48	3.08×10^2	5.55×10^2	1.66×10^3	8.45×10^3	13.94 (0.62)
2c$^-$	9.92[b]	1.26×10^3	2.10×10^3	6.07×10^3	2.89×10^4	15.17 (0.59)

[a] Determined by potentiometric titration. [b] Deprotonation of the piperidinium group.

ChemPubSoc Europe

EurJOC European Journal of Organic Chemistry
Full Paper

used) as the more nucleophilic 2^- then starts to compete with **2** for the electrophile **3**. As nitrogen attack of **3** by $2c^-$ is unlikely[13] (see above), the kinetics of $2c^-$ refer to oxygen attack at **3**.

Quantum Chemical Calculations. Why are the nucleophilic reactivities of the ammonium-peroxycarboxylates lower than those of common peroxybenzoates or aliphatic peroxycarboxylates? The fact that the aminoperoxycarboxylate $2c^-$ is more nucleophilic than the ammoniumperoxycarboxylate **2c** led us to investigate whether intramolecular hydrogen bonding of the peroxycarboxylate moiety with the ammonium group reduces reactivity in zwitterions **2**. To investigate the effect of intramolecular H-bonding in **2**, quantum chemical calculations with the Gaussian software were performed to evaluate the conformational space of $2a^+$–$2c^+$.[16] Conformers were optimized with the M06-HF[17]/6-311++(d,p) method taking into account aqueous solvation by the SMD version of the Polarizable Continuum Model.[18] Several methods with the 6-311++G(d,p) basis were tested (including various DFT methods, HF, MP2 and MP3; see Supporting Information for details), but only classical HF and M06-HF gave the position of the intramolecular N–H···O hydrogen bond as expected from experimental basicities.

The calculations revealed that the formation of an intramolecular hydrogen bond is highly favored in **2a**–**2c** (Figure 7), which may attenuate the rates of attack of the peroxycarboxylate groups at the carbocationic centres of the electrophiles **3**.[19]

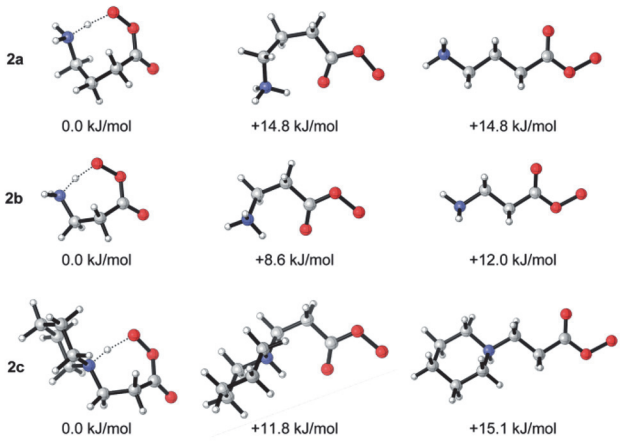

Figure 7. Relative Gibbs energies (at 298 K) of the conformers of **2a**–**2c** with the lowest Gibbs energy as calculated at the M06-HF/6-311++G(d,p) level of theory for aqueous solution (SMD).

Conclusions

Ammoniumperoxycarboxylic acid mesylates (APOCA mesylates) are easily preparable and stable peroxy compounds and, thus, a convenient source of active oxygen. At pH 8–9, ammoniumperoxycarboxylates, the corresponding zwitterions of APOCAs, can be generated, which are highly reactive epoxidation reagents. Their reactivities were characterized by Mayr's nucleophilicity parameters *N* and s_N, which allows for a direct comparison with reactivities of other peroxy anions (Figure 8) and further nucleophiles listed in Mayr's reactivity database.[10] Intramolecular N–H···O hydrogen bonding reduces the nucleophilic reactivity of β- and γ-ammonium-substituted peroxycarboxylates relative to structurally related peroxycarboxylates.

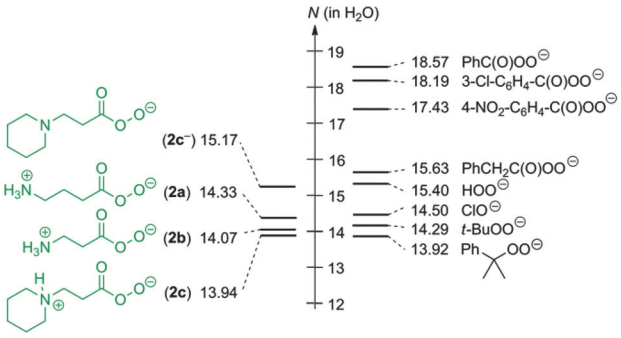

Figure 8. Comparison of nucleophilicity parameters *N* of **2** and 2^- with those of other anionic oxidants (from ref.[1,2,14]).

The application of APOCAs for oxygen transfer reactions in aqueous solution requires careful pH control, however, and is limited to very fast reactions with electrophiles because of the competing degradation to ammoniumcarboxylates and hydrogen peroxide under alkaline conditions.

A combination of the kinetic and thermodynamic data about APOCAs from this study with those for further aliphatic and aromatic peroxycarboxylic acids, hydroperoxides and related bleach reagents will provide a broad fundament for understanding structure-activity relationships, such as, for example, the so-called α-effect.[20]

Experimental Section

CAUTION: Pure peroxides may explode or detonate under influence of heat, shock, spark etc. All reactions or handling of peroxides should be carried out behind a blast shield as a precaution using open vessels while wearing appropriate safety equipment. Rotary evaporation of peroxides should be carried out carefully without excessive stirring at room temperature. Generally, all handling of peroxides should only be performed by experienced people trained in handling explosive compounds.

Analytics: Nuclear magnetic resonance spectra were recorded on 400 or 800 MHz NMR spectrometers. The following abbreviations and their combinations are used in the analysis of NMR spectra: s = singlet, d = doublet, t = triplet, q = quartet, m = multiplet, br. s = broad singlet. All ^{13}C NMR spectra were recorded under broadband proton-decoupling. NMR signals were assigned based on information from additional 2D NMR experiments (COSY, gHSQC, gHMBC, NOESY). Internal reference was set to the residual solvent signals.[21]

3-Carboperoxypropan-1-aminium Methanesulfonate ($2a^+MsO^-$): γ-Aminobutyric acid **1a** (400 mg, 3.88 mmol) was dissolved in methanesulfonic acid (2.03 mL, 31.3 mmol) with careful heating. The solution was cooled to 0 °C and H_2O_2 (0.28 mL of a 92 % aq. solution, 3 equiv.) was added dropwise. Then the reaction mixture was warmed up to room temperature. After 1 h the solution was poured into ice-cold THF (30 mL) and stirred for 30 min. The formed crystalline precipitate was collected by filtration and then washed with THF (5 mL) and diethyl ether (5 mL). Drying of the residue yielded

ChemPubSoc Europe

EurJOC European Journal of Organic Chemistry
Full Paper

2a$^+$MsO$^-$ as a colorless, crystalline solid (704 mg, 84 %); m.p. 80 °C; active oxygen content: 100 % (iodometric titration). ^{1}H NMR (400 MHz, D_2O): δ = 7.68 (br. t, $^1J_{H,N} \approx$ 40 Hz, 0.02 H, $^+NH_3$), 3.05 (t, J = 7.8 Hz, 2 H), 2.79 (s, 3 H), 2.56 (t, J = 7.3 Hz, 2 H), 2.00 (quint, J = 7.4 Hz, 2 H) ppm. ^{13}C{^{1}H} NMR (101 MHz, D_2O): δ = 173.6 (C_q), 38.43 (CH_2), 38.36 (CH_3), 27.3 (CH_2), 21.8 (CH_2) ppm. IR (ATR, neat): $\tilde{\nu}$ = 3139, 2891, 1760, 1631, 1529, 1477, 1417, 1376, 1340, 1323, 1298, 1257, 1159, 1119, 1066, 1044, 995, 974, 968, 928, 872, 781, 763, 702, 660 cm^{-1}. HRMS (FAB$^+$): m/z calcd. for [$C_4H_{10}NO_3^+$]: 120.0665, found 120.0675. Elemental Analysis: Calcd: C, 27.90; H, 6.09; N, 6.51; S, 14.90; found: C, 27.94; H, 6.15; N, 6.49; S, 14.99.

2-Carboperoxyethan-1-aminium Methanesulfonate (2b$^+$MsO$^-$): β-Alanine **1b** (200 mg, 2.24 mmol) was dissolved in methanesulfonic acid (1.01 mL, 15.6 mmol) with careful heating. The solution was cooled to 0 °C and H_2O_2 (0.13 mL of a 85 % aq. solution, 2 equiv.) was added dropwise. Then the reaction mixture was warmed up to room temperature. After 1 h the solution was poured into ice-cold THF (20 mL) and stirred for 20 min. The formed crystalline precipitate was collected by filtration, washed with THF (10 mL) and diethyl ether (10 mL). Drying of the residue yielded **2b**$^+$MsO$^-$ as colorless, crystalline solid (365 mg, 81 %). The active oxygen content of this sample was determined by iodometric titration to be 91 %. Therefore, an overall yield of 74 % of **2b**$^+$MsO$^-$ was calculated. ^{1}H NMR (400 MHz, D_2O): δ = 7.85 (br. t, $^1J_{H,N} \approx$ 42 Hz, 0.01 H, $^+NH_3$), 3.38 (t, J = 6.6 Hz, 2 H), 2.91 (t, J = 6.6 Hz, 2 H), 2.83 (s, 3 H) ppm. ^{13}C{^{1}H} NMR (101 MHz, D_2O): δ = 171.5 (C_q), 38.4 (CH_3), 34.8 (CH_2), 28.2 (CH_2) ppm.

1-(3-Hydroperoxy-3-oxopropyl)piperidin-1-ium Methanesulfonate (2c$^+$MsO$^-$): 3-(Piperidin-1-yl)propanoic acid **1c** (197 mg, 1.25 mmol) was dissolved in methanesulfonic acid (0.81 mL, 12.5 mmol). The solution was cooled to 0 °C and H_2O_2 (0.15 mL of a 85 % aq. solution, 4 equiv.) was added dropwise. Then the reaction mixture was warmed up to room temperature. After 1 h the solution was poured into ice-cold THF (20 mL) and stirred for 60 min. The formed crystalline precipitate was collected by filtration, washed with THF (10 mL) and diethyl ether (5 mL). Drying of the residue yielded **2c**$^+$MsO$^-$ as a colorless, crystalline solid (291 mg, 86 %); m.p. 134 °C (ref.:[3d] m.p. 132 °C); active oxygen content: 94 % (iodometric titration). Therefore, an overall yield of 81 % of **2c**$^+$MsO$^-$ was calculated. ^{1}H NMR (400 MHz, D_2O): δ = 8.72 (br. s, 0.06 H, $^+NH_3$), 3.53–3.50 (m, 2 H, 5-H), 3.44 (t, J = 7.1 Hz, 2 H), 2.99–2.93 (m, 4 H), 2.78 (s, 3 H), 1.96–1.87 (m, 2 H), 1.83–1.63 (m, 3 H), 1.53–1.39 (m, 1 H) ppm. ^{13}C{^{1}H} NMR (101 MHz, D_2O): δ = 170.9 (C_q), 53.4 (CH_2), 51.4 (CH_2), 38.4 (CH_3), 25.7 (CH_2), 22.6 (CH_2), 20.8 (CH_2) ppm. IR (ATR, neat): $\tilde{\nu}$ = 3021, 2961, 2775, 2721, 1773, 1480, 1451, 1349, 1208, 1139, 1122, 1087, 1066, 1037, 979, 944, 884, 845, 782, 733 cm^{-1}.

pK_a Determination: A Metrohm Titrando system (pH ± 0.001) was applied for automated titrations. Solutions of the acids in water were prepared at a constant ionic strength of I = 0.1 with a NaCl stock solution and titrated with 0.1 M KOH. The temperature during the titration was maintained constant at (20 ± 0.1) °C with a circulating bath thermostat. The titration curve was recorded automatically and the equivalence points were determined by the control software of the titration system. For every acid, the titration was repeated at least three times, the results were averaged and gathered in Table 1.

Kinetic Measurements: Kinetic measurements were performed on commercial stopped-flow UV/Vis photometry systems (Applied Photophysics SX.20). The temperature (20.0 ± 0.2 °C) was maintained constant by using circulating bath cryostats. To prevent alkaline decomposition of the peroxide solutions, the sequential-mixing setup of the instrument was employed. In a first step, equal volumes of a KOH solution and a solution of **2**$^+$MsO$^-$ were mixed. Kinetics aiming to characterize the reactivity of zwitterions **2** were carried out by mixing approx. equimolar amounts of **2**$^+$ and KOH in the first mixing step. Kinetics aiming to characterize the reactivity of the anionic **2c**$^-$ were performed by mixing **2**$^+$ [(2–5) × 10^{-4} M] with an excess of KOH (2.5 ×10^{-2} M) in the first mixing step. After 1 s ("aging time") these solutions were mixed at a second mixer with an equal volume of a solution of the electrophile **3**-BF_4. By using a high excess of the zwitterions **2** over the electrophiles **3**, the peroxide concentrations remained almost constant during the kinetic runs, resulting in mono-exponential decays of the electrophiles' absorptions. First-order rate constants k_{obs} (s^{-1}) were obtained by least-squares fitting the time-dependent absorbances with the single-exponential function $A_t = A_0 \exp(-k_{obs}t) + C$. After converting k_{obs} to k_1 by applying equation (3), the second-order rate constants for the reactions of **2** (or **2**$^-$) with benzhydrylium ions **3b**–**e** were obtained from the slope of the linear correlation of the first-order rate constants k_1 with the nucleophile concentration.

Details of the individual kinetic measurements are given in the Supporting Information.

Computational Analysis: First, all studied species were subjected to a conformational search with the OPLS3 force field[22] as implemented in the Macromodel software package[23] applying a MCMM search. The thus obtained set of conformers was subsequently optimized with the M06-HF/6-311++G(d,p) method[17] taking aqueous solvation into account by the SMD model.[18] Thermal corrections were obtained at the same level of theory from vibrational frequencies and are unscaled. Selection of an appropriate theoretical method for the structural optimization in the Gaussian software package[16] was found to be difficult as most methods are not able to correctly represent the position of the N···H···O hydrogen bond in a way that is in accord with experimental results (the amino group has the higher pK_{aH} value than the peroxycarboxylate, therefore the hydrogen should be located closer to nitrogen). Calculations in gas-phase as well as standard DFT (and MP) methods in solution (water) localize the hydrogen atom at the oxygen site. Geometries were all optimized with the 6-311++G(d,p) basis both in gas phase and aqueous solution (SMD and IEF-PCM were tested). Of the investigated methods (HF, B3LYP, B3LYP-D3, B2PLYPD, M06-2X, M06-HF, ωb97xd, MP2, MP3) only HF and M06-HF in combination with aqueous solvation were able to correctly locate the hydrogen bond.

Details of the conformational analysis and calculated geometries are given in the Supporting Information.

Acknowledgments

We thank Nathalie Hampel (LMU, preparation of **2** and **7**) and Dr. Peter Mayer (LMU, single-crystal X-ray crystallography). The authors are grateful to Professor Herbert Mayr (LMU) for continuous support, Dr Jérôme Gomar (L'Oréal) and Dr Stéphane Sabelle (L'Oréal) for helpful discussions and to Prof. Claude Y. Legault (Sherbrooke, Canada) for advice on quantum chemical calculations. Financial support by L'Oréal Research & Innovation (Aulnay sous Bois, France), the Deutsche Forschungsgemeinschaft (SFB 749, project B1), and the Fonds der Chemischen Industrie (Kekulé fellowship to RJM) is gratefully acknowledged.

Keywords: Nucleophilicity · Kinetics · Bleaching · Peroxides · Linear-free energy relationships

ChemPubSoc Europe

EurJOC European Journal of Organic Chemistry
Full Paper

[1] R. J. Mayer, T. Tokuyasu, P. Mayer, J. Gomar, S. Sabelle, B. Mennucci, H. Mayr, A. R. Ofial, *Angew. Chem. Int. Ed.* **2017**, *56*, 13279–13282; *Angew. Chem.* **2017**, *129*, 13463–13467.
[2] R. J. Mayer, A. R. Ofial, *Org. Lett.* **2018**, *20*, 2816–2820.
[3] a) C. Venturello, C. Cavallotti, EP 0316809 A2, **1988**; b) J. R. Darwent, K. C. Francis, J. Oakes, D. W. Thornthwaite, US4904406A, **1988**; c) C. Venturello, C. Cavallotti, F. Achilli, US5117049A, **1991**; d) C. Venturello, C. Cavallotti, US5245075, **1993**; e) C. Venturello, C. Cavallotti, US5294362A, **1994**; f) J. Oakes, D. W. Thornthwaite, WO 94/21605, **1994**; g) J. Oakes, D. W. Thornthwaite, WO 97/16515, **1997**; h) N.-D. H. Gamage, B. Stiasny, J. Stierstorfer, P. D. Martin, T. M. Klapötke, C. H. Winter, *Chem. Eur. J.* **2016**, *22*, 2582–2585.
[4] CCDC 1849148 (for **2a**$^{+}$MsO^{-}, uv697), 1849149 (for **2b**$^{+}$MsO^{-}, vv407), 1849150 (for **2c**$^{+}$MsO^{-}, uv132) contain the supplementary crystallographic data for this paper. These data can be obtained free of charge from The Cambridge Crystallographic Data Centre..
[5] J. Hartung, I. Svoboda in *The Chemistry of Peroxides Vol. 2* (Ed.: Z. Rappaport), Wiley, Hoboken, **2006**, Chapt 6, pp. 93–144.
[6] F. Brotzel, H. Mayr, *Org. Biomol. Chem.* **2007**, *5*, 3814–3820.
[7] H. Mayr, M. Patz, *Angew. Chem. Int. Ed. Engl.* **1994**, *33*, 938–957; *Angew. Chem.* **1994**, *106*, 990–1010.
[8] H. Mayr, A. R. Ofial, *SAR QSAR Environ. Res.* **2015**, *26*, 619–646.
[9] H. Mayr, *Tetrahedron* **2015**, *71*, 5095–5111.
[10] A database of reactivity parameters *E*, *N*, and s_N can be accessed at http://www.cup.lmu.de/oc/mayr/DBintro.html.
[11] H. Mayr, T. Bug, M. F. Gotta, N. Hering, B. Irrgang, B. Janker, B. Kempf, R. Loos, A. R. Ofial, G. Remennikov, H. Schimmel, *J. Am. Chem. Soc.* **2001**, *123*, 9500–9512.
[12] Detailed procedures for the synthesis of **3**-BF_4 are given in: R. J. Mayer, N. Hampel, P. Mayer, A. R. Ofial, H. Mayr, *Eur. J. Org. Chem.* **2018**, 10.1002/ejoc.201800835.
[13] J. Ammer, M. Baidya, S. Kobayashi, H. Mayr, *J. Phys. Org. Chem.* **2010**, *23*, 1029–1035.
[14] S. Minegishi, H. Mayr, *J. Am. Chem. Soc.* **2003**, *125*, 286–295.
[15] I. A. Yaremenko, V. A. Vil', D. D. Demchuk, A. O. Terent'ev, *Beilstein J. Org. Chem.* **2016**, *12*, 1647–1748.
[16] M. J. Frisch, G. W. Trucks, H. B. Schlegel, G. E. Scuseria, M. A. Robb, J. R. Cheeseman, G. Scalmani, V. Barone, G. A. Petersson, H. Nakatsuji, X. Li, M. Caricato, A. V. Marenich, J. Bloino, B. G. Janesko, R. Gomperts, B. Mennucci, H. P. Hratchian, J. V. Ortiz, A. F. Izmaylov, J. L. Sonnenberg, D. Williams-Young, F. Ding, F. Lipparini, F. Egidi, J. Goings, B. Peng, A. Petrone, T. Henderson, D. Ranasinghe, V. G. Zakrzewski, J. Gao, N. Rega, G. Zheng, W. Liang, M. Hada, M. Ehara, K. Toyota, R. Fukuda, J. Hasegawa, M. Ishida, T. Nakajima, Y. Honda, O. Kitao, H. Nakai, T. Vreven, K. Throssell, J. A. Montgomery, Jr., J. E. Peralta, F. Ogliaro, M. J. Bearpark, J. J. Heyd, E. N. Brothers, K. N. Kudin, V. N. Staroverov, T. A. Keith, R. Kobayashi, J. Normand, K. Raghavachari, A. P. Rendell, J. C. Burant, S. S. Iyengar, J. Tomasi, M. Cossi, J. M. Millam, M. Klene, C. Adamo, R. Cammi, J. W. Ochterski, R. L. Martin, K. Morokuma, O. Farkas, J. B. Foresman, D. J. Fox, *Gaussian 16, Revision A.03*, Gaussian, Inc., Wallingford CT, **2016**.
[17] Y. Zhao, D. G. Truhlar, *J. Phys. Chem. A* **2006**, *110*, 13126–13130.
[18] A. V. Marenich, C. J. Cramer, D. G. Truhlar, *J. Phys. Chem. B* **2009**, *113*, 6378–6396.
[19] It might be argued that also the strong electron-withdrawing effect of -$^{+}$NH$_3$ contributes through inductive effects to the reduction of the nucleophilic power of the peroxycarboxylate groups in **2**. Yet, reactivity studies on reactions of benzhydrylium ions with peroxybenzoate ions [ArC(O)OO^{-}] showed only a marginal effect on the nucleophilicities of these ions when the ring substituents were varied from *p*-NO_2 to *p*-OMe (see ref[1]). We, therefore, assume that ammonium groups in β- or γ-position along an aliphatic chain, as in **2a**–**c**, do not significantly affect the reactivity of the peroxycarboxylate group by inductive effects.
[20] Reviews: a) N. J. Fina, J. O. Edwards, *Int. J. Chem. Kinet.* **1973**, *5*, 1–26; b) E. Buncel, I.-H. Um, *Tetrahedron* **2004**, *60*, 7801–7825.
[21] G. R. Fulmer, A. J. M. Miller, N. H. Sherden, H. E. Gottlieb, A. Nudelman, B. M. Stoltz, J. E. Bercaw, K. I. Goldberg, *Organometallics* **2010**, *29*, 2176–2179.
[22] E. Harder, W. Damm, J. Maple, C. Wu, M. Reboul, J. Y. Xiang, L. Wang, D. Lupyan, M. K. Dahlgren, J. L. Knight, J. W. Kaus, D. S. Cerutti, G. Krilov, W. L. Jorgensen, R. Abel, R. A. Friesner, *J. Chem. Theory Comput.* **2016**, *12*, 281–296.
[23] *MacroModel* (Schrödinger Release 2017–1), Schrödinger, LLC, New York, NY, **2017**.

Received: July 24, 2018

3.1 Supporting Information - General

***CAUTION**: Pure peroxides (especially as crystalline compounds) may explode or detonate under influence of heat, shock, spark etc. Contact of peroxy compounds with reducing agents, acid media or traces of transition metals should be avoided as exothermal decomposition may occur. All reactions or handling should be carried out behind a blast shield as a precaution using open vessels while wearing appropriate safety equipment. Rotary evaporation of peroxide should be carried out carefully avoiding excessive stirring at room temperature. Generally, all handling should only be performed by experienced people trained in handling explosive compounds.*

Solvents and Reagents

Commercial reagents (aminocarboxylic acids, methanesulfonic acid) and dry solvents (THF) over molecular sieves as purchased from Sigma-Aldrich or Acros Organics were used without further purification. Stock solutions of potassium hydroxide (KOH) and sodium thiosulfate ($Na_2S_2O_3$, used for iodometric titrations) were purchased from Bernd Kraft Laborchemikalien.

Concentrated solutions of hydrogen peroxide (> 85%) were prepared by concentration of commercially available 50% reagent (2 mL) for 45 min on a vacuum line (0.3 mbar) under appropriate safety precautions according to the described procedure.[1] The concentration of the thus obtained solution was determined by iodometric titration.

Analytics

Melting points were acquired using a Büchi Melting Point B-540 device and are not corrected.

Nuclear magnetic resonance spectra were recorded on 400 or 800 MHz NMR spectrometers. The following abbreviations and their combinations are used in the analysis of NMR spectra: s = singlet, d = doublet, t = triplet, q = quartet, m = multiplet, br s = broad singlet. NMR signals were assigned based on information from additional 2D NMR experiments (COSY, gHSQC, gHMBC, NOESY). Internal reference was set to the residual solvent signals (δ_H = 4.79 for H_2O; δ_H = 1.940, δ_C = 1.32 for d_3-MeCN, δ_H = 7.26 for $CDCl_3$).[2] All ^{13}C NMR spectra were recorded under broad-band proton-decoupling.

Infrared (IR) spectra were recorded on a Perkin Elmer Spectrum BX-59343 instrument with a Smiths Detection DuraSamplIR II Diamond ATR sensor for detection in the range 4500–600 cm^{-1}.

High resolution (HRMS) mass spectra were recorded on a Thermo Finnigan LTQ FT Ultra Fourier Transform ion cyclotron resonance mass spectrometer or a JEOL MStation JMS 700. For ionization, electrospray ionization (ESI) or fast atom bombardment (FAB, matrix: glycerin) was applied.

Single Crystal X-Ray Crystallography (Performed by Dr. P. Mayer)

The intensity data were measured at a temperature of 100 K on a Bruker D8 Venture TXS system equipped with a multilayer mirror optics monochromator and a Mo Kα rotating-anode X-ray tube (λ = 0.71073 Å). The frames were integrated with the Bruker SAINT software package.[3] Data were corrected for absorption effects using the Multi-Scan method (SADABS).[4] The structures were solved and refined using the Bruker SHELXTL Software Package.[5] All C-bound hydrogen atoms were calculated in positions having ideal geometry riding on their parent atoms. The N- and O-bound hydrogen atoms have been refined freely for **2a**$^+$MsO$^-$ (uv697) and **2b**$^+$MsO$^-$ (vv407) while in **2c**$^+$MsO$^-$ (uv132) merely the coordinates have been refined freely [U(H) = 1.2 U(N/O)]. In **2c**$^+$MsO$^-$ (uv132) the Flack parameter (absolute structure) refined to 0.01(3). The data have been deposited with the CCDC and can be obtained free of charge via https://www.ccdc.cam.ac.uk/structures/.

Kinetic measurements

The content of active oxygen in $\mathbf{2}^{+}MsO^{-}$ was determined by iodometric titration directly before preparing the aqueous solutions of $\mathbf{2}^{+}MsO^{-}$ for the kinetic measurements and considered when calculating the initial concentrations of $\mathbf{2}^{+}$ in solution. Based on these titrations, the concentration of contaminating ammonium-carboxylic acid (that is, protonated **1**) was calculated.[6] The concentration of protonated **1** were then subtracted from the amount of hydroxide available to deprotonate $\mathbf{2}^{+}$.

Kinetic measurements were performed by employing stopped-flow UV/Vis photometry on Applied Photophysics SX.20 systems. The temperature (20.0 ± 0.2 °C) was maintained constant by using circulating bath cryostats.

To prevent alkaline decomposition of the peroxide solutions, the sequential-mixing setup of the instrument was employed. In a first step, equal volumes of a KOH solution and a solution of $\mathbf{2}^{+}MsO^{-}$ were mixed. Kinetics aiming to characterize the reactivity of zwitterions **2** were carried out by mixing equimolar amounts of $\mathbf{2}^{+}$ and KOH in the first mixing step. Kinetics aiming to characterize the reactivity of the anionic $\mathbf{2c}^{-}$ were performed by mixing $\mathbf{2}^{+}$ [(2–5) × 10^{-4} M] with an excess of KOH (2.5 ×10^{-2} M) in the first mixing step. After 1 s ('aging time') these solutions were mixed at a second mixer with an equal volume of a solution of the electrophile **3**-BF_4.

By using a high excess of the zwitterions **2** over the electrophiles **3**, the peroxide concentrations remained almost constant during the kinetic runs, resulting in mono-exponential decays of the electrophiles' absorptions. First-order rate constants k_{obs} (s^{-1}) were obtained by least-squares fitting the time-dependent absorbances with the single-exponential function $A_t = A_0 \exp(-k_{obs}t) + C$.

pK_a Determination

For the determination of pK_a values, an automated titration with a Metrohm Titrando system (pH ± 0.001) was applied. Solutions of the compounds in water were prepared at a constant ionic strength of I = 0.1 with a NaCl stock solution and titrated with 0.1 M KOH. The temperature during the titration was maintained constant at (20 ± 0.1) °C with a circulating bath thermostat. The titration curve was recorded automatically and the equivalence points were determined by the control software of the titration system. For each compound, the titration was repeated at least three times and the results were averaged (see Table 1, main text).

Computational Analysis

First, all studied species were subjected to a conformational search with the OPLS3[7] force field as implemented in the Macromodel[8] software package applying a MCMM search. The thus obtained set of conformers was subsequently optimized with the M06-HF/6-311++G(d,p) method[9] taking aqueous solvation into account by the SMD model.[10] Thermal corrections were obtained at the same level of theory from vibrational frequencies and are unscaled.

Selection of an appropriate theoretical method for the structural optimization in the Gaussian software package[11] showed to be difficult as most methods are not able to correctly represent the position of the N···H···O hydrogen bond in a way that is in line with experimental results (the amino group has the higher pK_{aH} value than the peroxycarboxylate, therefore the hydrogen should be located closer to nitrogen). Calculations in gas-phase as well as standard DFT (and MP) methods in solution (water) localize the hydrogen atom at the oxygen site. Geometries were all optimized with the 6-311++G(d,p) basis both in gas phase and aqueous solution (SMD and IEF-PCM were tested). Of the investigated methods (HF, B3LYP, B3LYP-D3, B2PLYPD, M06-2X, M06-HF, ωb97xd, MP2, MP3) only HF and M06-HF in combination with aqueous solvation were able to correctly locate the hydrogen bond.

3.2 Preparation of Ammoniumperoxycarboxylic Acids

3-Carboperoxypropan-1-aminium methanesulfonate (2a+MsO–) – RM66

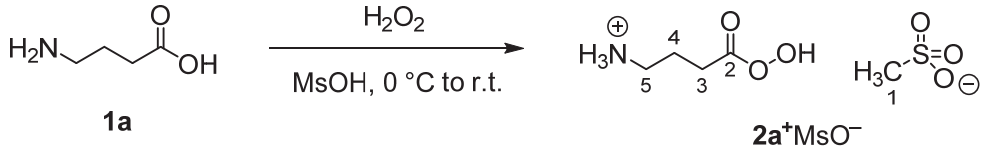

1a **2a**$^{+}$MsO^{-}

γ-Aminobutyric acid **1a** (400 mg, 3.88 mmol) was dissolved in methanesulfonic acid (2.03 mL, 31.3 mmol, 8 equiv) with careful heating. The solution was cooled to 0 °C and H_2O_2 (0.28 mL of a 92% aq. solution, 3 equiv) was added dropwise. Then the reaction mixture was allowed to warm up to room temperature. After 1 h the solution was poured into ice-cold THF (30 mL) and stirred for 30 min. The formed crystalline precipitate was collected by filtration and then washed with THF (5 mL) and diethyl ether (5 mL). Drying of the residue yielded **2a**$^{+}$MsO^{-} as a colorless, crystalline solid (704 mg, 84%); mp 80 °C (ref. 12: 44 °C); active oxygen content: 100% (iodometric titration).

^{1}H NMR (400 MHz, D_2O) δ = 7.68 (br t, $^{1}J_{H,N} \approx 40$ Hz, 0.02 H, $^{+}NH_3$), 3.05 (t, $J_{4,5}$ = 7.8 Hz, 2 H, 5-H), 2.79 (s, 3 H, 1-H), 2.56 (t, $J_{3,4}$ = 7.3 Hz, 2 H, 3-H), 2.00 (quint, J = 7.4 Hz, 2 H, 4-H).

^{13}C{^{1}H} NMR (101 MHz, D_2O) δ = 173.6 (C_q, C-2), 38.43 (CH_2, C-5), 38.36 (CH_3, C-1), 27.3 (CH_2, C-4), 21.8 (CH_2, C-3).

IR (ATR, neat): 3139, 2891, 1760, 1631, 1529, 1477, 1417, 1376, 1340, 1323, 1298, 1257, 1159, 1119, 1066, 1044, 995, 974, 968, 928, 872, 781, 763, 702, 660 cm^{-1}.

HRMS (FAB^{+}): *m/z* calcd for [$C_4H_{10}NO_3^{+}$]: 120.0665, found 120.0675.

Elemental Analysis: Calcd (%): C, 27.90; H, 6.09; N, 6.51; S, 14.90. Found (%): C, 27.94; H, 6.15; N, 6.49; S, 14.99.

2-Carboperoxyethan-1-aminium methanesulfonate (2b^{+}MsO^{-}) – RM307

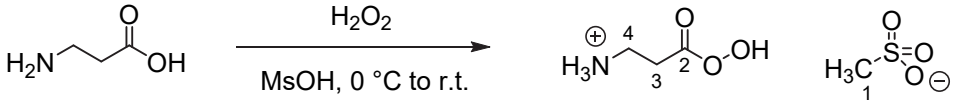

1b **2b**$^{+}$MsO^{-}

β-Alanine **1b** (200 mg, 2.24 mmol) was dissolved in methanesulfonic acid (1.01 mL, 15.6 mmol, 7 equiv) with careful heating. The solution was cooled to 0 °C and H_2O_2 (0.13 mL of a 85% aq. solution, 2 equiv) was added dropwise. Then the reaction mixture was allowed to warm up to room temperature. After 1 h the solution was poured into ice-cold THF (20 mL) and stirred for 20 min. The formed crystalline precipitate was collected by filtration, washed with THF (10 mL) and diethyl ether (10 mL). Drying of the residue yielded **2b**$^{+}$MsO^{-} as colorless, crystalline solid (365 mg, 81 %). The active oxygen content of this sample was determined by iodometric titration to be 91.0%. Therefore, an overall yield of 74% of **2b**$^{+}$MsO^{-} was calculated.

The sample for the NMR spectroscopic measurements contained about 14% of **1b**$^{+}$MsO^{-} (2-carboxyethan-1-aminium methanesulfonate). Additional resonances caused by **1b**$^{+}$MsO^{-} are marked with an asterisk (*) in the ^{13}C NMR spectrum of **2b**$^{+}$MsO^{-}.

^{1}H NMR (400 MHz, D_2O) δ = 7.85 (br t, $^{1}J_{H,N} \approx 42$ Hz, 0.01 H, $^{+}NH_3$), 3.38 (t, $J_{3,4}$ = 6.6 Hz, 2 H, 4-H), 2.91 (t, $J_{3,4}$ = 6.6 Hz, 2 H, 3-H), 2.83 (s, 3 H, 1-H).

^{13}C{^{1}H} NMR (101 MHz, D_2O) δ = 171.5 (C_q, C-2), 38.4 (CH_3, C-1), 34.8 (CH_2, C-4), 28.2 (CH_2, C-3).

LR-MS (FAB^{+}): *m/z* calcd for for [$C_3H_8NO_3^{+}$]: 106.1, found 106.1.

1-(3-Hydroperoxy-3-oxopropyl)piperidin-1-ium methanesulfonate (2c⁺MsO⁻) – RM115

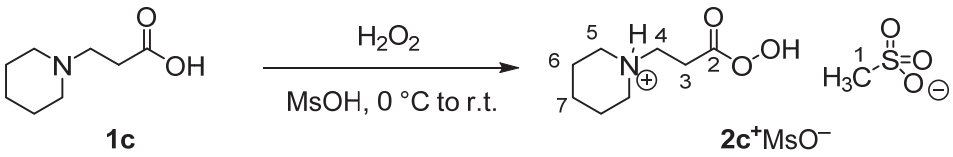

3-(Piperidin-1-yl)propanoic acid **1c** (197 mg, 1.25 mmol) was dissolved in methanesulfonic acid (0.81 mL, 12.5 mmol, 10 equiv). The solution was cooled to 0 °C and H_2O_2 (0.15 mL of a 85% aq. solution, 4 equiv) was added dropwise. Then the reaction mixture was allowed to warm up to room temperature. After 1 h the solution was poured into ice-cold THF (20 mL) and stirred for 60 min. The formed crystalline precipitate was collected by filtration, washed with THF (10 mL) and diethyl ether (5 mL). Drying of the residue yielded **2c**⁺MsO⁻ as a colorless, crystalline solid (291 mg, 86%); mp 134 °C (ref. 12: 132 °C); active oxygen content: 94% (iodometric titration). Therefore, an overall yield of 81% of **2c**⁺MsO⁻ was calculated.

^{1}H NMR (400 MHz, D_2O) δ = 8.72 (br s, 0.06 H, $^+$NH), 3.53–3.50 (m, 2 H, 5-H), 3.44 (t, $^3J_{3,4}$ = 7.1 Hz, 2 H, 4-H), 2.99–2.93 (m, 4 H, 5-H, 3-H), 2.78 (s, 3 H, 1-H), 1.96–1.87 (m, 2 H, 6-H), 1.83–1.63 (m, 3 H, 6-H, 7-H), 1.53–1.39 (m, 1 H, 7-H).

^{13}C{^{1}H} NMR (101 MHz, D_2O) δ = 170.9 (C_q, C-2), 53.4 (CH_2, C-5), 51.4 (CH_2, C-4), 38.4 (CH_3, C-1), 25.7 (CH_2, C-3), 22.6 (CH_2, C-6), 20.8 (CH_2, C-7).

IR (ATR, neat): 3021, 2961, 2775, 2721, 1773, 1480, 1451, 1349, 1208, 1139, 1122, 1087, 1066, 1037, 979, 944, 884, 845, 782, 733 cm^{-1}.

LR-MS (FAB$^+$): *m/z* calcd for [$C_8H_{16}NO_3^+$]: 174.2, found 174.2.

3.3 Product Studies

Trapping of the decomposition products of 2a⁺MsO⁻ under strong alkaline conditions with 3a - RM359 (Scheme 4)

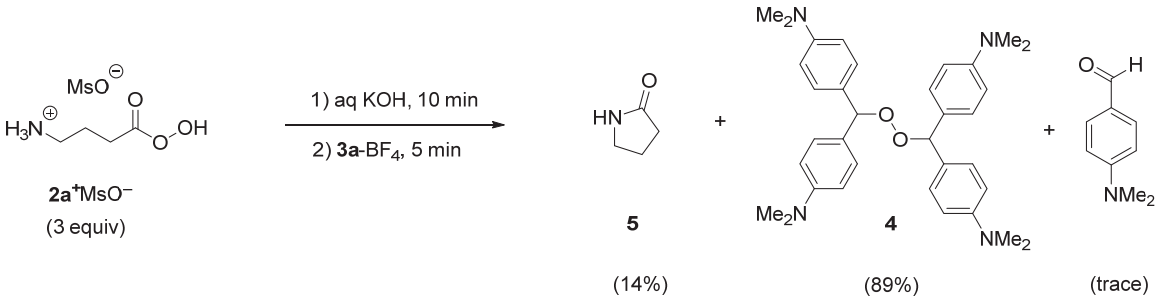

2a⁺MsO⁻ (26.9 mg, 0.125 mmol, 3 equiv) was dissolved in 10 mL KOH (0.1 M). After 10 minutes, a solution of **3a**-BF_4^- (14.2 mg, 0.0417 mmol, 1 equiv) in 2 mL MeCN was added in one portion under vigorous stirring. After another 5 min, the reaction mixture was extracted with dichloromethane (3 × 20 mL). The combined organic layers were washed with brine, dried over $MgSO_4$, filtered, and concentrated in the vacuum.

To the residue, dimethyl fumarate (11.8 mg, 0.0819 mmol) was added as NMR standard (S) and the entire material was dissolved in $CDCl_3$. Yields of products based on NMR integrals (400 MHz) were: Peroxide **4** (0.0185 mmol, 89% with respect to **3a**-BF_4), lactam **5** (0.0176 mmol, 14% with respect to **2a⁺MsO⁻**), and traces of 4-(dimethylamino)benzaldehyde.

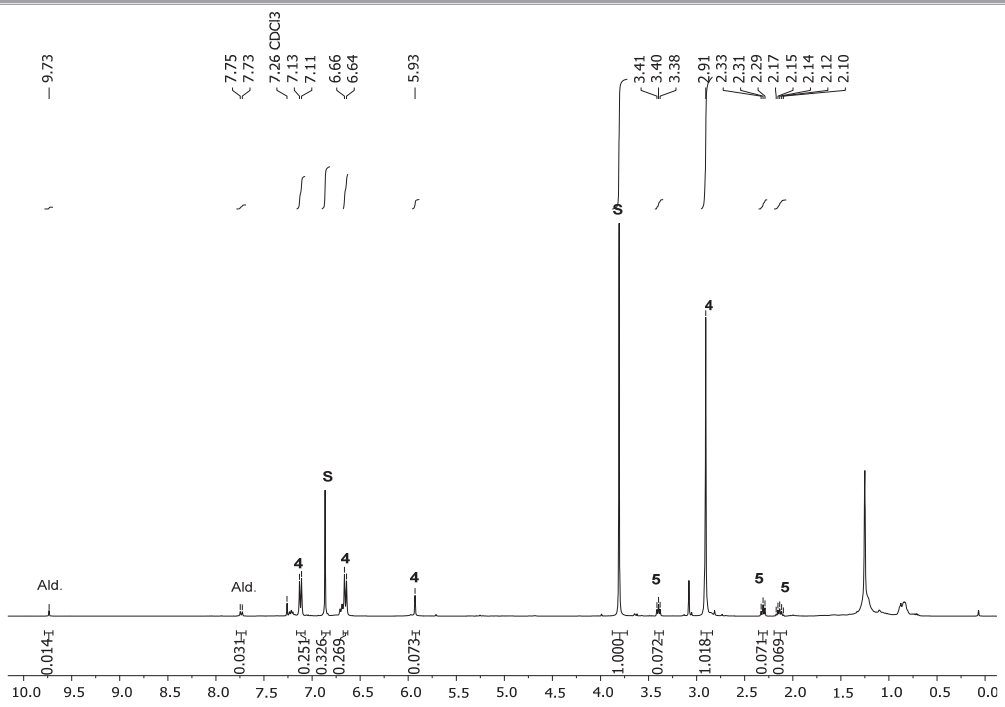

Epoxidation of 6 by 2a⁺MsO⁻ - RM202 (Scheme 5)

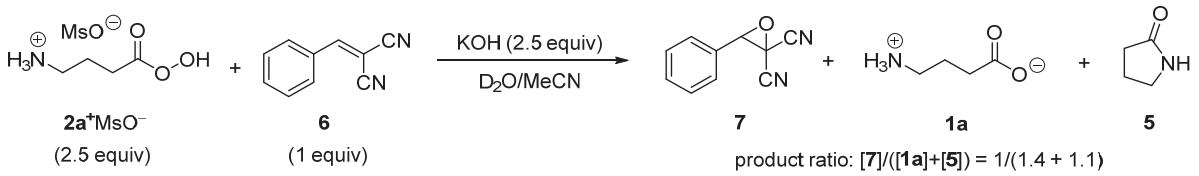

2a⁺MsO⁻ (7.6 mg, 0.035 mmol, 2.5 equiv) was dissolved in D_2O (0.5 mL) and KOH (2.5 equiv, solution in D_2O) was added. Under vigorous stirring was added a solution of **6** (2.2 mg, 0.014 mmol, 1 equiv) in d_3-MeCN (500 µL). The solution was transferred to an NMR tube and directly subjected to NMR analytics (800 MHz ^{1}H NMR spectroscopy and HSQC).

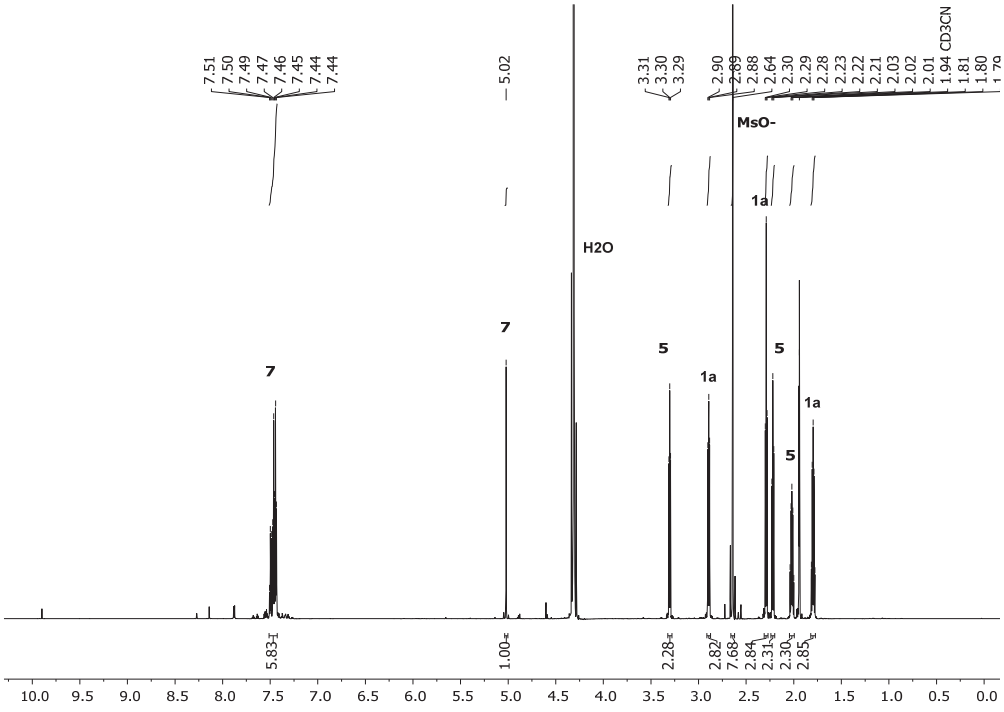

4-((Bis(4-(dimethylamino)phenyl)methyl)amino)butanoate 8a – RM317 (Scheme 6)

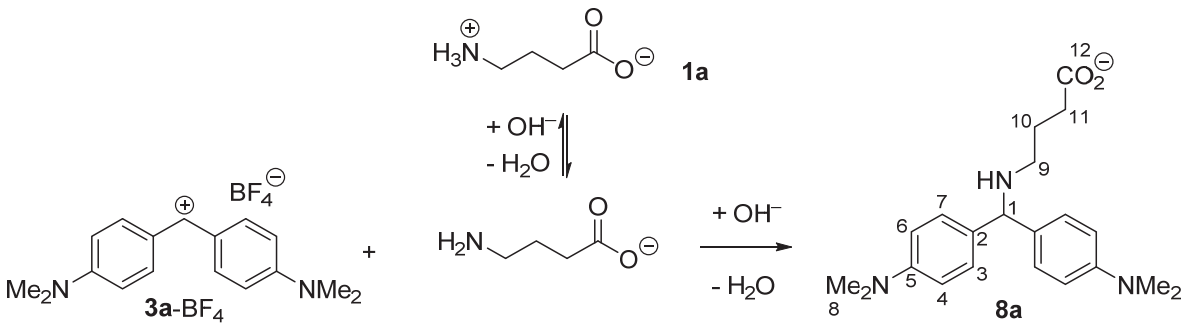

γ-Aminobutyric acid **1a** (1.5 mg, 14.5 µmol, 2 equiv) was dissolved in a solution of KOH in D_2O (0.125 M, 237 µL, 29.6 µmol, 4 equiv). Then a solution of **3a**-BF_4^- (2.5 mg, 7.4 µmol) in d_3-MeCN (250 µL) was added dropwise under stirring. The milky suspension was transferred into an NMR tube, which was then filled with d_3-MeCN to a total volume of 600 µL. By NMR spectroscopy, formation of **8a** was detected (in a mixture with remaining **1a**; resonances marked by * were assigned to remaining γ-aminobutyrate ions based on information from additional 2D NMR spectra).

^{1}H NMR (400 MHz, d_3-MeCN) δ = 7.18–7.15 (m, 4 H, 3-H and 7-H), 6.73–6.69 (m, 4 H, 4-H and6-H), 4.64 (s, 1 H, 1-H), 2.80 (s, 12 H, 8-H), 2.42 (dd, J = 7.9 Hz, J = 6.9 Hz, 2 H, 9-H), 2.02 (dd, J = 8.4 Hz, J = 6.9 Hz, 2 H, 11-H), 1.70–1.63 (m, 2 H, 10-H superimposed with resonances of **1a**).

^{13}C{^{1}H} NMR (101 MHz, d_3-MeCN) δ = 182.1 (C_q, C-12), 151.0 (C_q, C-5), 133.2 (C_q, C-2), 128.7 (CH, C-7, C-3), 114.4 (CH, C-6, C-4), 66.5 (CH, C-1), 48.5 (CH_2, C-9), 41.3 (CH_3, C-8), 36.7 (CH_2, C-11), 26.7 (CH_2, C-10).

HR-MS (ESI$^-$): m/z calcd for [$C_{21}H_{28}N_3O_2^-$]: 354.2187, found 354.2186.

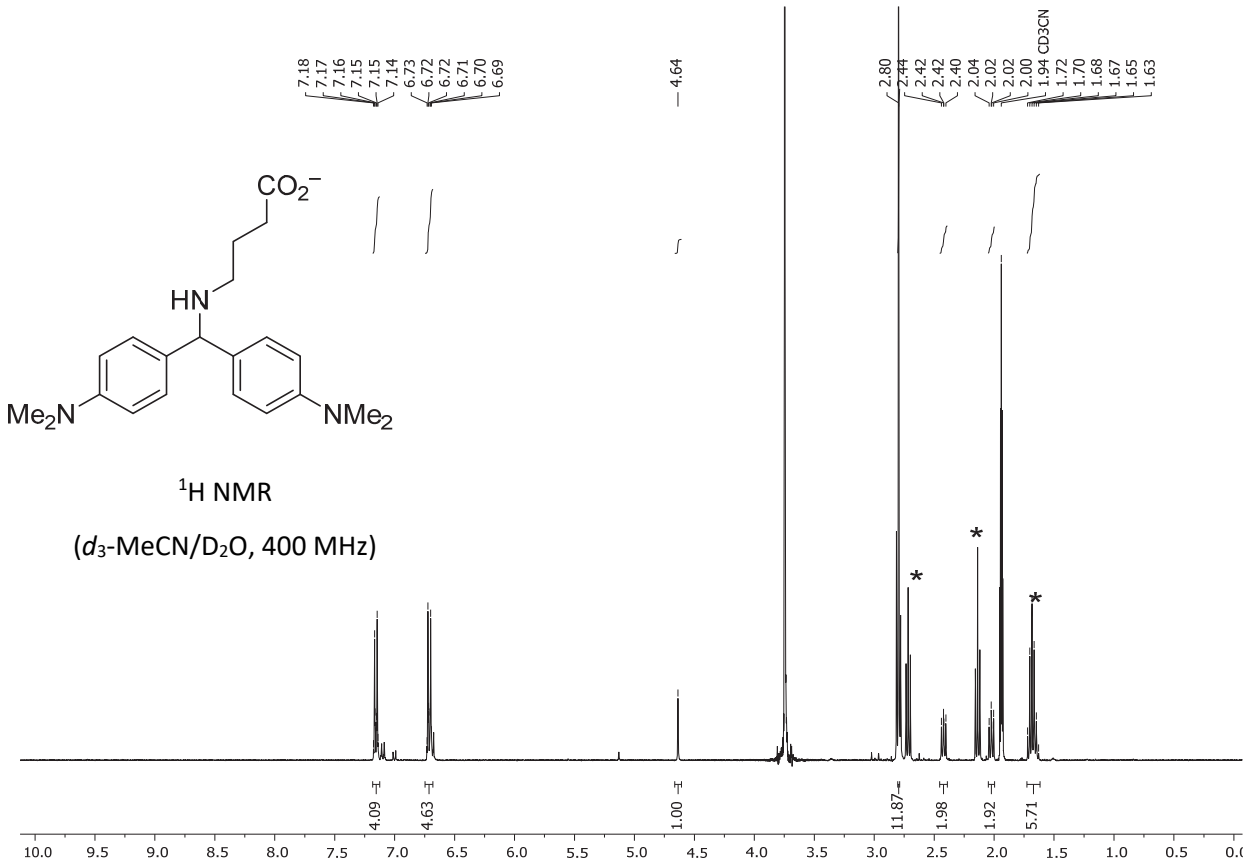

^{1}H NMR

(d_3-MeCN/D_2O, 400 MHz)

3-((Bis(4-(dimethylamino)phenyl)methyl)amino)propanoate 8b – RM318 (Scheme 6)

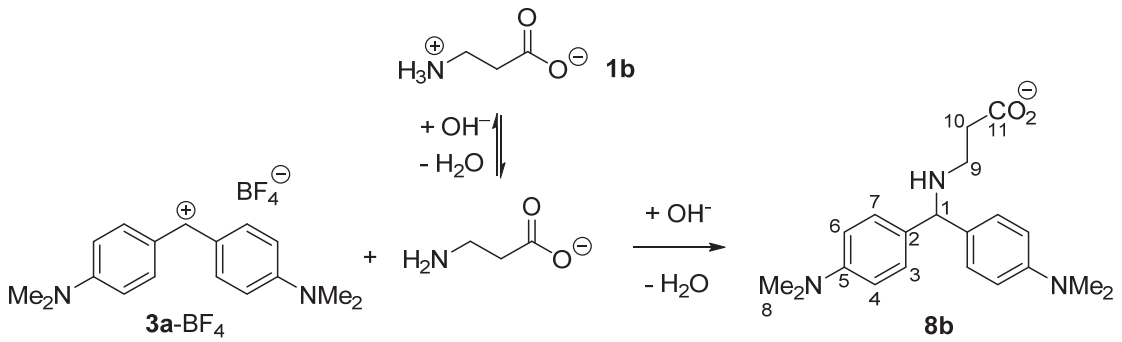

β-Alanine **1b** (1.4 mg, 16 µmol, 2.1 equiv) was dissolved in a solution of KOH in D_2O (0.125 M, 251 µL, 0.0314 mmol, 4.2 equiv). Then a solution of **3a**-BF_4^- (2.5 mg, 7.4 µmol) in d_3-MeCN (250 µL) was added dropwise under stirring. The milky suspension was transferred into a NMR tube and filled with d_3-MeCN to a total volume of 0.6 mL. By NMR spectroscopy, formation of **8b** was identified in a mixture with the excess **1b**. Resonances marked by (*) were assigned to remaining deprotonated β-alanine (based on information from additional 2D NMR spectra).

^{1}H NMR (400 MHz, d_3-MeCN) δ = 7.17–7.14 (m, 4 H, 3-H and 7-H), 6.74–6.71 (m, 4 H, 4-H and 6-H), 4.61 (s, 1 H, 1-H), 2.58 (s, 12 H, 8-H), 2.57 (t, J = 7.2 Hz, 2 H, 9-H), 2.26 (t, J = 7.2 Hz, 2 H, 10-H).

^{13}C{^{1}H} NMR (101 MHz, d_3-MeCN) δ = 180.9 (C_q, C-11), 151.0 (C_q, C-5), 134.2 (C_q, C-2), 128.7 (CH, C-7, C-3), 114.8 (CH, C-6, C-4), 66.3 (CH, C-1), 45.4 (CH_2, C-9), 41.4 (CH_3, C-8), 37.9 (CH_2, C-10).

HR-MS (ESI$^-$): m/z calcd for [$C_{20}H_{26}N_3O_2^-$]: 340.2031, found 340.2030.

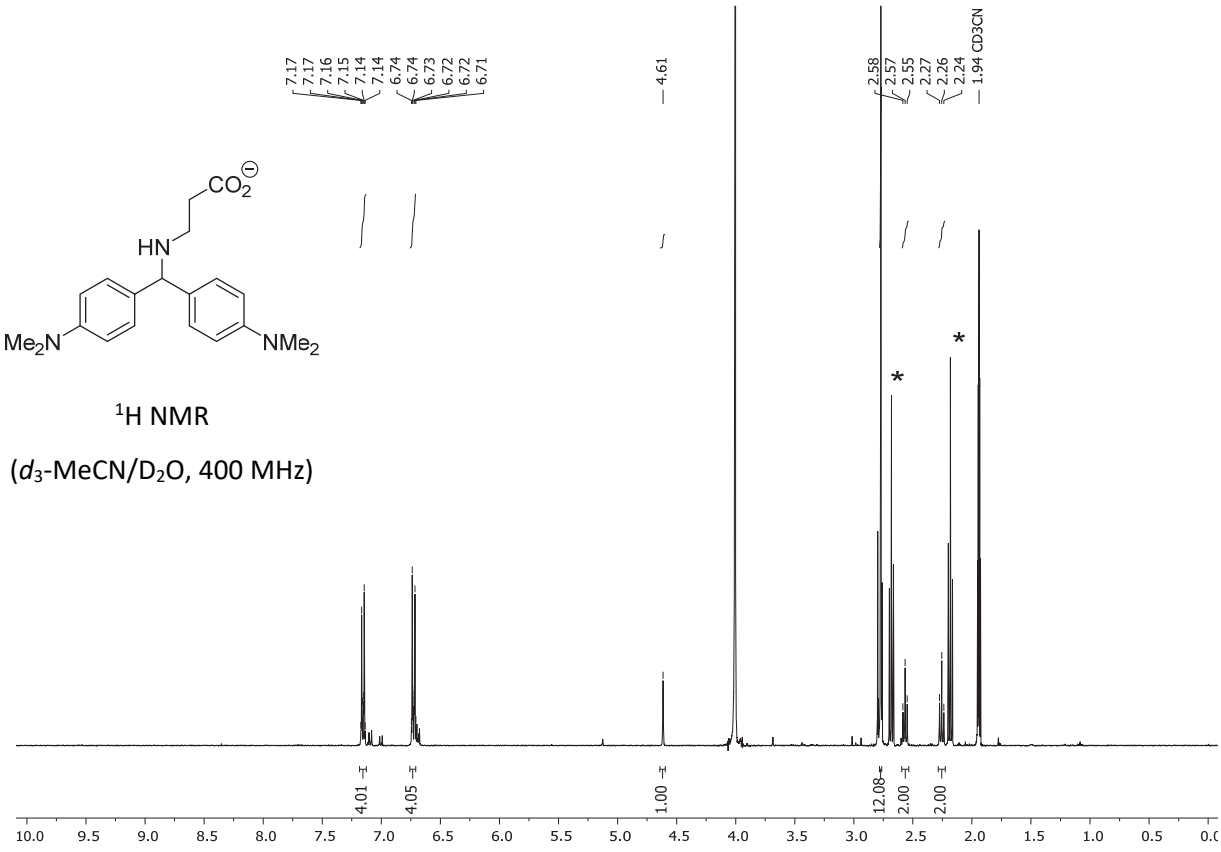

^{1}H NMR

(d_3-MeCN/D_2O, 400 MHz)

Products of the reaction of $2b^+MsO^-$ with 3a-BF_4 at different hydroxide concentrations – RM363

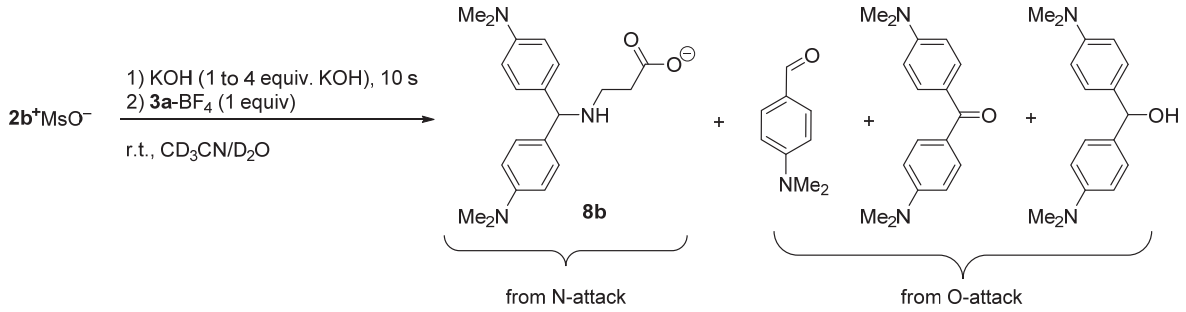

To a solution of **2b**$^+$$MsO^-$ in D_2O (1.48 mg, 7.38 µmol) was added a solution of KOH in D_2O (1 to 4 equiv). After 10 seconds, a solution of **3a**-BF_4 (2.51 mg, 7.38 µmol, 1 equiv) in d_3-MeCN was added under stirring. The mixture was transferred to an NMR tube, which was then filled with d_3-MeCN to a total volume of 600 µL and analyzed (400 MHz NMR spectrometer).

A: If relative to the **2b**$^+$ one equivalent of base was added, the benzhydryl alcohol and benzaldehyde/ketone were formed as major products (by Criegee rearrangements of the initially formed peroxide adduct).

B–**C**: When repeating the reaction of **2b**$^+$ and **3a** with increasing amounts of KOH, the secondary amine **8b** was formed in significant amount along with the aldehyde/ketone mixture, which reflects the O- and N-reactivity by **2b**$^-$.

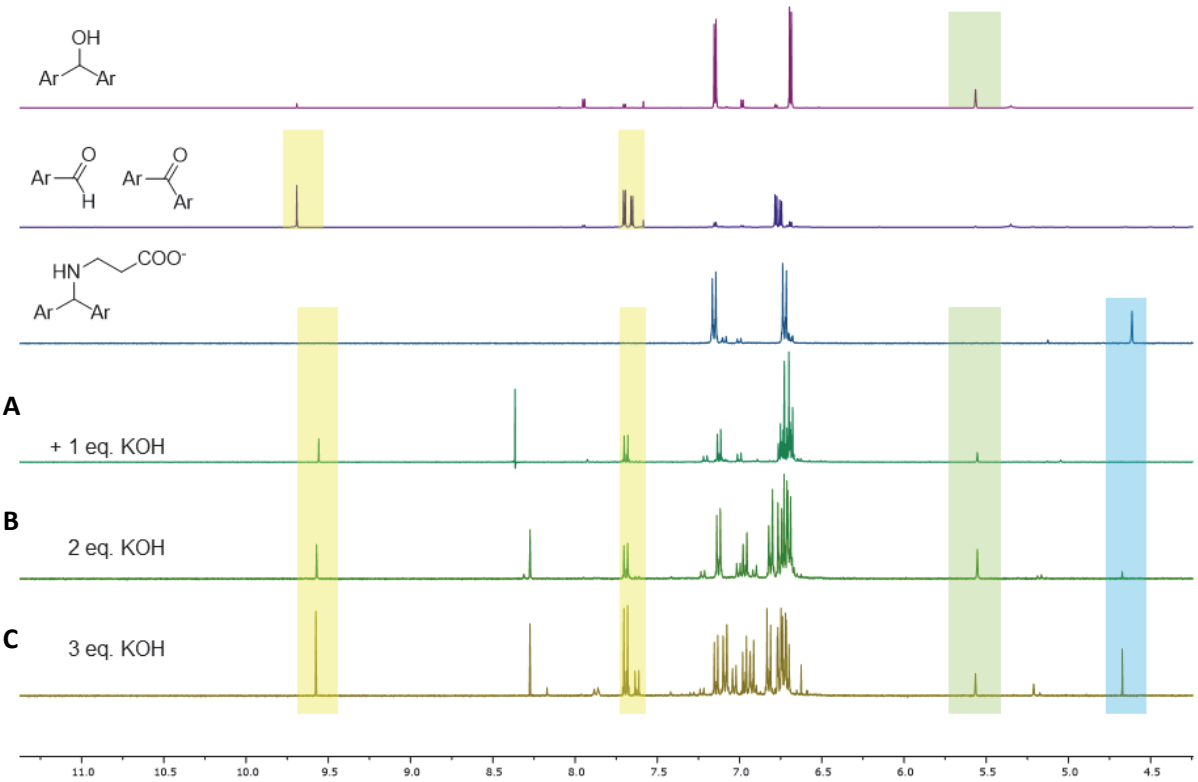

3.4 Kinetic Data

4.1 Stability of nucleophile solutions

In a sequential mixing stopped-flow instrument at 20 °C, zwitterions **2** ([**2**]$_0$ = 4 × 10^{-4} M) were generated in a first step by mixing an aqueous solution of **2**$^+$MsO$^-$ with aqueous potassium hydroxide solution ([KOH]$_0$ = 4 × 10^{-4} M). After a defined delay ('aging time'), the solution of the thus freshly generated zwitterions **2** was mixed with an aqueous solution of **3b**-BF_4^- ([**3b**]$_0$ = (1.1–1.5) × 10^{-5} M). As the nucleophilic zwitterions **2** were used in much higher concentrations than the electrophiles **3b** ([**2**] >> [**3b**]), we generally observed mono-exponential decays of the absorbance of the colored benzhydrylium ion **3b** under these pseudo-first-order conditions. However, the observed decay rates systematically slowed down when the time between the first and the second mixing step, that is, the aging time of the nucleophile solution, was increased.

The dependence of the observed rate constants k_{obs} on the aging time indicated a first-order decomposition of the nucleophile **2a** on the seconds time scale at 20°C ($\tau_{1/2}$ = 20–25 s).

The analogous variation of the aging times for reactions of the electrophiles **3b** with aqueous solutions of the nucleophilic zwitterions **2b** and **2c** (generated from **2b**$^+$MsO$^-$ and **2c**$^+$MsO$^-$, respectively) gave similar results but showed that the degradation proceeded somewhat slower ($\tau_{1/2}$ > 100 s) than for **2a**.

Influence of Aging on the Reactivity of Aqueous Solutions of Zwitterion 2a

Conditions: [**2a**$^+$]$_0$ = 4 × 10^{-4} M, [OH$^-$]$_0$ = 4 × 10^{-4} M, [**3b**] = 1.49 × 10^{-5} M

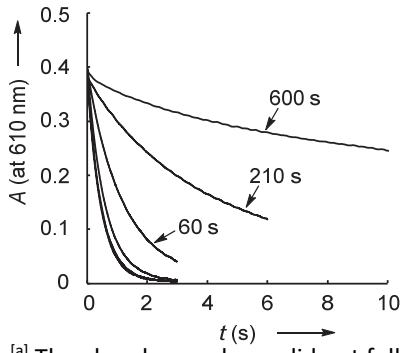

Aging time (s)	k_{obs} (s^{-1})
0.1	2.25
1	2.21
10	1.76
60	0.862
210	0.284
600	[a]

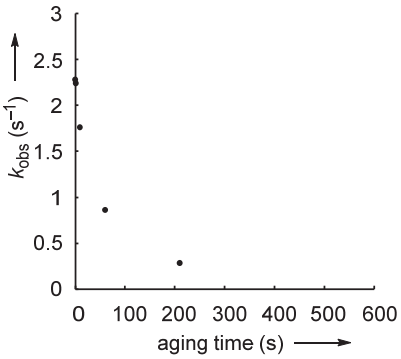

[a] The absorbance decay did not follow a mono-exponential decay function.

Influence of Aging on the Reactivity of Aqueous Solutions of Zwitterion 2b

Conditions: [**2b**$^+$]$_0$ = 4 × 10^{-4} M, [OH$^-$]$_0$ = 4 × 10^{-4} M, [**3b**] = 1.14 × 10^{-5} M

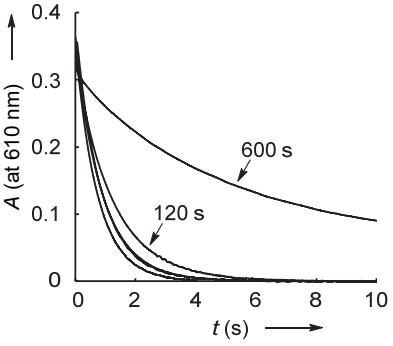

Aging time (s)	k_{obs} (s^{-1})
0.1	1.36
0.1	1.31
1	1.37
1	1.25
10	1.22
30	1.13
120	0.848
600	0.218

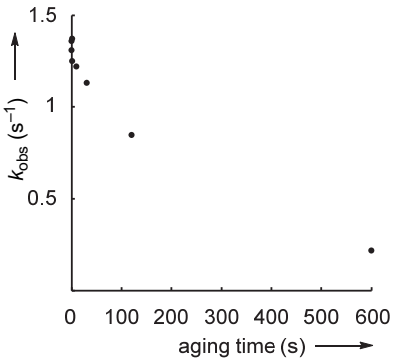

Influence of Aging on the Reactivity of Aqueous Solutions of Zwitterion 2c

Conditions: $[\mathbf{2c}^+]_0 = 4 \times 10^{-4}$ M, $[OH^-]_0 = 4 \times 10^{-4}$ M, [**3b**] = 1.49×10^{-5} M

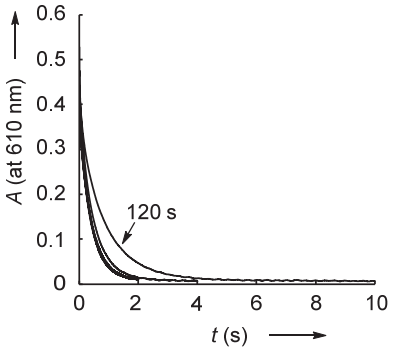

Aging time (s)	k_{obs} (s^{-1})
0.1	2.79
1	2.69
5	2.53
10	2.45
30	2.52
120	1.53

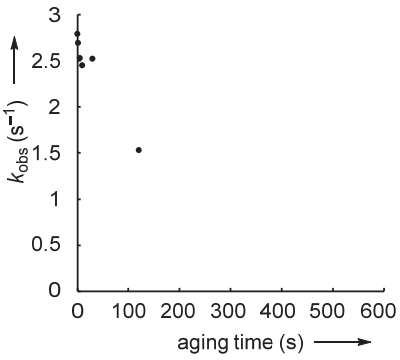

4.2 Kinetics of the reactions of 2a (generated from $2a^+MsO^-$) with benzhydrylium ions 3 in water – RM306

Active oxygen content of $\mathbf{2a}^+MsO^-$: 92.9%; pK_a($\mathbf{2a}^+$) 7.77.

$\mathbf{2a}^+MsO^-$ + **3e**-BF_4 in alkaline 99.5/0.5 (v/v) H_2O/CH_3CN (sequential mixing stopped-flow, detection at 630 nm)

$[\mathbf{3e}]_0$, mol L^{-1}	$[\mathbf{2a}^+]_0$, mol L^{-1}	$[OH^-]_0$, mol L^{-1}	[**2a**], mol L^{-1}	$[OH^-]$, mol L^{-1}	k_{obs}, s^{-1}	$k_{OH}[OH^-]$, s^{-1}	k_1, s^{-1}
1.29×10^{-5}	2.00×10^{-4}	1.85×10^{-4}	1.80×10^{-4}	5.17×10^{-6}	6.39×10^{-2}	1.12×10^{-5}	6.39×10^{-2}
1.29×10^{-5}	3.00×10^{-4}	2.77×10^{-4}	2.71×10^{-4}	5.60×10^{-6}	9.43×10^{-2}	1.21×10^{-5}	9.43×10^{-2}
1.29×10^{-5}	4.00×10^{-4}	3.69×10^{-4}	3.64×10^{-4}	5.87×10^{-6}	1.21×10^{-1}	1.27×10^{-5}	1.21×10^{-1}

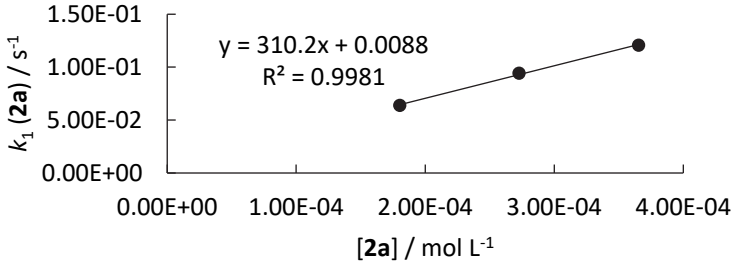

$k_2 = 3.10 \times 10^2$ M^{-1} s^{-1}
$k_{OH} = 2.16$ M^{-1} s^{-1}

$\mathbf{2a}^+MsO^-$ + **3d**-BF_4 in alkaline 99.5/0.5 (v/v) H_2O/CH_3CN (sequential mixing stopped-flow, detection at 640 nm)

$[\mathbf{3d}]_0$, mol L^{-1}	$[\mathbf{2a}^+]_0$, mol L^{-1}	$[OH^-]_0$, mol L^{-1}	[**2a**], mol L^{-1}	$[OH^-]$, mol L^{-1}	k_{obs}, s^{-1}	$k_{OH}[OH^-]$, s^{-1}	k_1, s^{-1}
1.14×10^{-5}	2.00×10^{-4}	1.85×10^{-4}	1.80×10^{-4}	5.17×10^{-6}	9.63×10^{-2}	1.78×10^{-5}	9.63×10^{-2}
1.14×10^{-5}	3.00×10^{-4}	2.77×10^{-4}	2.71×10^{-4}	5.60×10^{-6}	1.39×10^{-1}	1.92×10^{-5}	1.39×10^{-1}
1.14×10^{-5}	4.00×10^{-4}	3.69×10^{-4}	3.64×10^{-4}	5.87×10^{-6}	1.92×10^{-1}	2.02×10^{-5}	1.92×10^{-1}

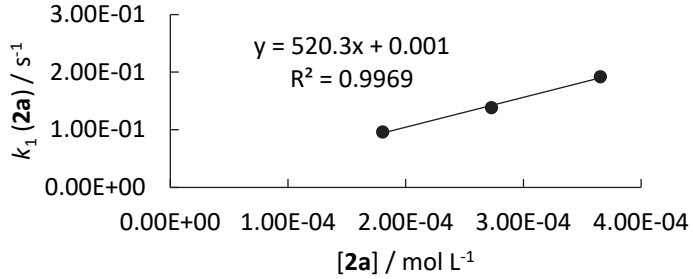

$k_2 = 5.20 \times 10^2$ M^{-1} s^{-1}
$k_{OH} = 3.44$ M^{-1} s^{-1}

2a$^+$MsO$^-$ + **3c**-BF_4 in alkaline 99.5/0.5 (v/v) H_2O/CH_3CN (sequential mixing stopped-flow, detection at 615 nm)

[**3c**]$_0$, mol L^{-1}	[**2a**$^+$]$_0$, mol L^{-1}	[OH^-]$_0$, mol L^{-1}	[**2a**], mol L^{-1}	[OH^-], mol L^{-1}	k_{obs}, s^{-1}	k_{OH}[OH^-], s^{-1}	k_1, s^{-1}
1.65×10^{-5}	2.00×10^{-4}	1.85×10^{-4}	1.80×10^{-4}	5.17×10^{-6}	2.65×10^{-1}	5.58×10^{-5}	2.65×10^{-1}
1.65×10^{-5}	3.00×10^{-4}	2.77×10^{-4}	2.71×10^{-4}	5.60×10^{-6}	3.83×10^{-1}	6.05×10^{-5}	3.83×10^{-1}
1.65×10^{-5}	4.00×10^{-4}	3.69×10^{-4}	3.64×10^{-4}	5.87×10^{-6}	5.20×10^{-1}	6.34×10^{-5}	5.20×10^{-1}

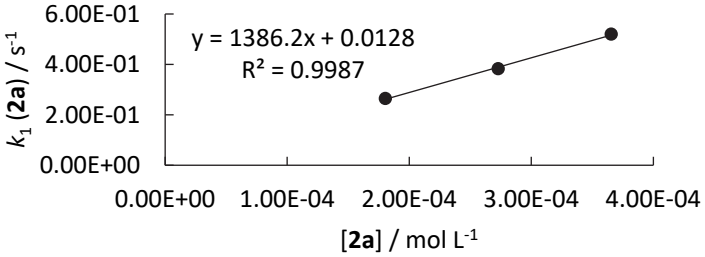

$k_2 = 1.39 \times 10^3$ M^{-1} s^{-1}
$k_{OH} = 10.8$ M^{-1} s^{-1}

2a$^+$MsO$^-$ + **3b**-BF_4 in alkaline 99.5/0.5 (v/v) H_2O/CH_3CN (sequential mixing stopped-flow, detection at 610 nm)

[**3b**]$_0$, mol L^{-1}	[**2a**$^+$]$_0$, mol L^{-1}	[OH^-]$_0$, mol L^{-1}	[**2a**], mol L^{-1}	[OH^-], mol L^{-1}	k_{obs}, s^{-1}	k_{OH}[OH^-], s^{-1}	k_1, s^{-1}
1.49×10^{-5}	1.00×10^{-4}	9.24×10^{-5}	8.80×10^{-5}	4.33×10^{-6}	4.36×10^{-1}	2.10×10^{-4}	4.36×10^{-1}
1.49×10^{-5}	2.00×10^{-4}	1.85×10^{-4}	1.80×10^{-4}	5.17×10^{-6}	9.20×10^{-1}	2.51×10^{-4}	9.20×10^{-1}
1.49×10^{-5}	3.00×10^{-4}	2.77×10^{-4}	2.71×10^{-4}	5.60×10^{-6}	1.44	2.72×10^{-4}	1.44
1.49×10^{-5}	4.00×10^{-4}	3.69×10^{-4}	3.64×10^{-4}	5.87×10^{-6}	2.20	3.85×10^{-4}	2.20

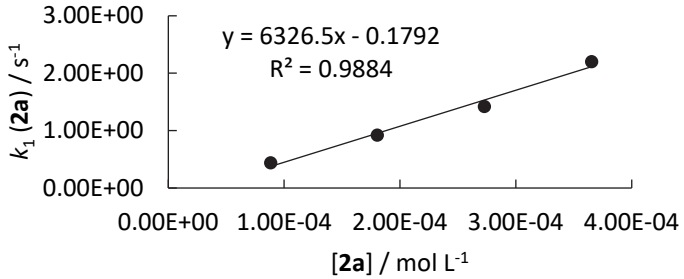

$k_2 = 6.33 \times 10^3$ M^{-1} s^{-1}
$k_{OH} = 48.5$ M^{-1} s^{-1}

Determination of N and s_N parameters for the zwitterion **2a** in 99.5/0.5 (v/v) H_2O/CH_3CN

Reference Electrophile	Electrophilicity E	k_2, M^{-1} s^{-1}	lg k_2
3e	-10.04	3.10×10^2	2.49
3d	-9.45	5.20×10^2	2.72
3c	-8.76	1.39×10^3	3.14
3b	-7.69	6.33×10^3	3.80

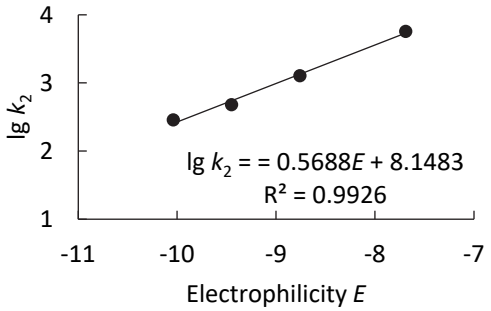

N = 14.33
s_N = 0.57

4.3 Kinetics of the reactions of 2b (generated from $2b^+MsO^-$) with benzhydrylium ions 3 in water – RM308

Active oxygen content of **2b**$^+$MsO$^-$: 91.0%; pK_a(**2b**$^+$) 7.35.

2b$^+$MsO$^-$ + **3e**-BF_4 in alkaline 99.5/0.5 (v/v) H_2O/CH_3CN (sequential mixing stopped-flow, detection at 630 nm)

[**3e**]$_0$, mol L^{-1}	[**2b**$^+$]$_0$, mol L^{-1}	[OH^-]$_0$, mol L^{-1}	[**2b**], mol L^{-1}	[OH^-], mol L^{-1}	k_{obs}, s^{-1}	k_{OH}[OH^-], s^{-1}	k_1, s^{-1}
1.29×10^{-5}	2.00×10^{-4}	1.80×10^{-4}	1.78×10^{-4}	1.85×10^{-6}	3.12×10^{-2}	3.99×10^{-6}	3.12×10^{-2}
1.29×10^{-5}	3.00×10^{-4}	2.70×10^{-4}	2.68×10^{-4}	1.90×10^{-6}	4.70×10^{-2}	4.12×10^{-6}	4.70×10^{-2}
1.29×10^{-5}	4.00×10^{-4}	3.60×10^{-4}	3.59×10^{-4}	1.93×10^{-6}	6.85×10^{-2}	4.18×10^{-6}	6.85×10^{-2}

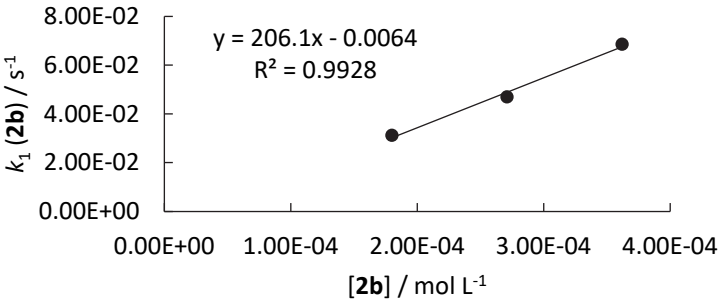

$k_2 = 2.06 \times 10^2$ M^{-1} s^{-1}
$k_{OH} = 2.16$ M^{-1} s^{-1}

2b$^+$MsO$^-$ + **3d**-BF_4 in alkaline 99.5/0.5 (v/v) H_2O/CH_3CN (sequential mixing stopped-flow, detection at 640 nm)

[**3d**]$_0$, mol L^{-1}	[**2b**$^+$]$_0$, mol L^{-1}	[OH$^-$]$_0$, mol L^{-1}	[**2b**], mol L^{-1}	[OH$^-$], mol L^{-1}	k_{obs}, s^{-1}	k_{OH}[OH$^-$], s^{-1}	k_1, s^{-1}
1.14×10^{-5}	1.00×10^{-4}	9.01×10^{-5}	8.84×10^{-5}	1.71×10^{-6}	1.97×10^{-2}	5.86×10^{-6}	1.97×10^{-2}
1.14×10^{-5}	2.00×10^{-4}	1.80×10^{-4}	1.78×10^{-4}	1.85×10^{-6}	4.34×10^{-2}	6.34×10^{-6}	4.34×10^{-2}
1.14×10^{-5}	3.00×10^{-4}	2.70×10^{-4}	2.68×10^{-4}	1.90×10^{-6}	6.84×10^{-2}	6.54×10^{-6}	6.84×10^{-2}
1.14×10^{-5}	4.00×10^{-4}	3.60×10^{-4}	3.59×10^{-4}	1.93×10^{-6}	1.11×10^{-1}	6.64×10^{-6}	1.11×10^{-1}

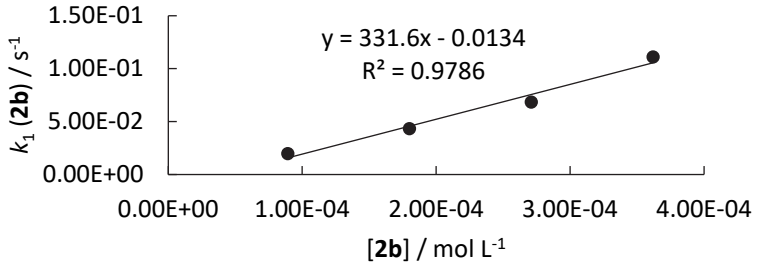

$k_2 = 3.32 \times 10^2$ M^{-1} s^{-1}
$k_{OH} = 3.44$ M^{-1} s^{-1}

2b$^+$MsO$^-$ + **3c**-BF_4 in alkaline 99.5/0.5 (v/v) H_2O/CH_3CN (sequential mixing stopped-flow, detection at 615 nm)

[**3c**]$_0$, mol L^{-1}	[**2b**$^+$]$_0$, mol L^{-1}	[OH$^-$]$_0$, mol L^{-1}	[**2b**], mol L^{-1}	[OH$^-$], mol L^{-1}	k_{obs}, s^{-1}	k_{OH}[OH$^-$], s^{-1}	k_1, s^{-1}
1.14×10^{-5}	1.00×10^{-4}	9.01×10^{-5}	8.84×10^{-5}	1.71×10^{-6}	7.46×10^{-2}	1.84×10^{-5}	7.46×10^{-2}
1.14×10^{-5}	2.00×10^{-4}	1.80×10^{-4}	1.78×10^{-4}	1.85×10^{-6}	1.67×10^{-1}	1.99×10^{-5}	1.67×10^{-1}
1.14×10^{-5}	3.00×10^{-4}	2.70×10^{-4}	2.68×10^{-4}	1.90×10^{-6}	2.27×10^{-1}	2.05×10^{-5}	2.27×10^{-1}
1.14×10^{-5}	4.00×10^{-4}	3.60×10^{-4}	3.59×10^{-4}	1.93×10^{-6}	3.76×10^{-1}	2.09×10^{-5}	3.76×10^{-1}

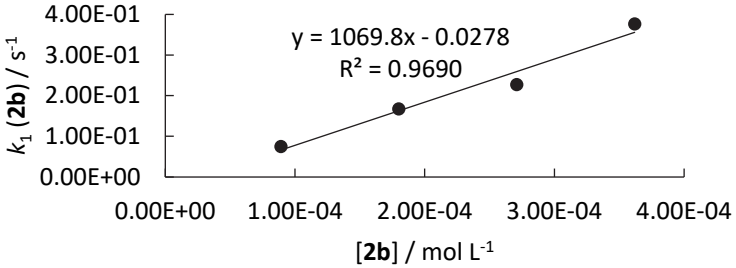

$k_2 = 1.07 \times 10^3$ M^{-1} s^{-1}
$k_{OH} = 10.8$ M^{-1} s^{-1}

2b$^+$MsO$^-$ + **3b**-BF_4 in alkaline 99.5/0.5 (v/v) H_2O/CH_3CN (sequential mixing stopped-flow, detection at 610 nm)

[**3b**]$_0$, mol L^{-1}	[**2b**$^+$]$_0$, mol L^{-1}	[OH$^-$]$_0$, mol L^{-1}	[**2b**], mol L^{-1}	[OH$^-$], mol L^{-1}	k_{obs}, s^{-1}	k_{OH}[OH$^-$], s^{-1}	k_1, s^{-1}
1.14×10^{-5}	1.00×10^{-4}	9.01×10^{-5}	8.84×10^{-5}	1.71×10^{-6}	2.91×10^{-1}	8.28×10^{-5}	2.91×10^{-1}
1.14×10^{-5}	2.00×10^{-4}	1.80×10^{-4}	1.78×10^{-4}	1.85×10^{-6}	7.07×10^{-1}	8.96×10^{-5}	7.07×10^{-1}
1.14×10^{-5}	3.00×10^{-4}	2.70×10^{-4}	2.68×10^{-4}	1.90×10^{-6}	9.23×10^{-1}	9.23×10^{-5}	9.22×10^{-1}
1.14×10^{-5}	4.00×10^{-4}	3.60×10^{-4}	3.59×10^{-4}	1.93×10^{-6}	1.40	9.38×10^{-5}	1.40

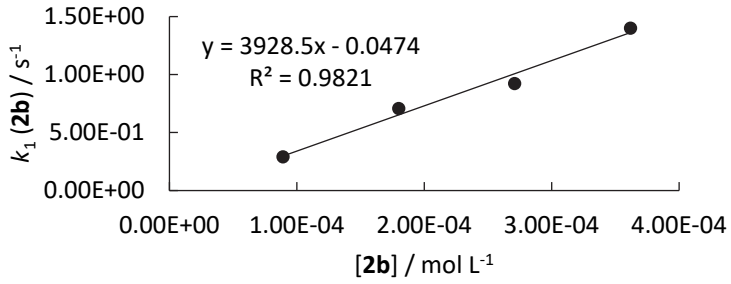

k_2 = 3.93 × 10^3 M^{-1} s^{-1}
k_{OH} = 48.5 M^{-1} s^{-1}

Determination of *N* and s_N parameters for the zwitterion **2b** in 99.5/0.5 (v/v) H_2O/CH_3CN

Reference Electrophile	Electrophilicity *E*	k_2, M^{-1} s^{-1}	lg k_2
3e	–10.04	2.06 × 10^2	2.31
3d	–9.45	3.32 × 10^2	2.52
3c	–8.76	1.07 × 10^3	3.03
3b	–7.69	3.93 × 10^3	3.59

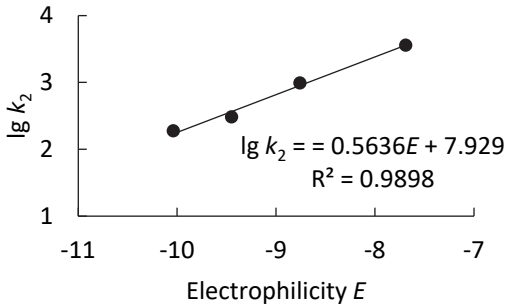

N = 14.07
s_N = 0.56

4.4 Kinetics of the reactions of 2c (generated from $2c^+MsO^-$) with benzhydrylium ions 3 in water – RM312

Active oxygen content of **2c**$^+$MsO$^-$: 93.9%; pK_a(**2c**$^+$) 7.48.

2c$^+$MsO$^-$ + **3e**-BF_4 in alkaline 99.5/0.5 (v/v) H_2O/CH_3CN (sequential mixing stopped-flow, detection at 630 nm)

[**3e**]$_0$, mol L^{-1}	[**2c**$^+$]$_0$, mol L^{-1}	[OH^-]$_0$, mol L^{-1}	[**2c**], mol L^{-1}	[OH^-], mol L^{-1}	k_{obs}, s^{-1}	k_{OH}[OH^-], s^{-1}	k_1, s^{-1}
1.29 × 10^{-5}	3.00 × 10^{-4}	2.81 × 10^{-4}	2.77 × 10^{-4}	3.62 × 10^{-6}	7.65 × 10^{-2}	7.82 × 10^{-6}	7.65 × 10^{-2}
1.29 × 10^{-5}	4.00 × 10^{-4}	3.74 × 10^{-4}	3.70 × 10^{-4}	3.76 × 10^{-6}	9.89 × 10^{-2}	8.13 × 10^{-6}	9.89 × 10^{-2}
1.29 × 10^{-5}	5.00 × 10^{-4}	4.68 × 10^{-4}	4.64 × 10^{-4}	3.85 × 10^{-6}	1.34 × 10^{-1}	8.33 × 10^{-6}	1.34 × 10^{-1}

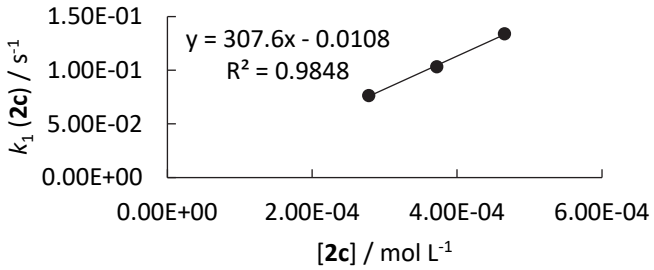

$k_2 = 3.08 \times 10^2\ M^{-1}\ s^{-1}$
$k_{OH} = 2.16\ M^{-1}\ s^{-1}$

2c$^+$MsO$^-$ + **3d**-BF_4 in alkaline 99.5/0.5 (v/v) H_2O/CH_3CN (sequential mixing stopped-flow, detection at 640 nm)

$[\mathbf{3d}]_0$, mol L^{-1}	$[\mathbf{2c}^+]_0$, mol L^{-1}	$[OH^-]_0$, mol L^{-1}	$[\mathbf{2c}]$, mol L^{-1}	$[OH^-]$, mol L^{-1}	k_{obs}, s^{-1}	$k_{OH}[OH^-]$, s^{-1}	k_1, s^{-1}
1.14×10^{-5}	2.00×10^{-4}	1.87×10^{-4}	1.84×10^{-4}	3.39×10^{-6}	7.34×10^{-2}	1.16×10^{-5}	7.34×10^{-2}
1.14×10^{-5}	3.00×10^{-4}	2.81×10^{-4}	2.77×10^{-4}	3.62×10^{-6}	1.10×10^{-1}	1.24×10^{-5}	1.10×10^{-1}
1.14×10^{-5}	4.00×10^{-4}	3.74×10^{-4}	3.70×10^{-4}	3.76×10^{-6}	1.91×10^{-1}	1.29×10^{-5}	1.91×10^{-1}
1.14×10^{-5}	5.00×10^{-4}	4.68×10^{-4}	4.64×10^{-4}	3.85×10^{-6}	2.19×10^{-1}	1.32×10^{-5}	2.19×10^{-1}

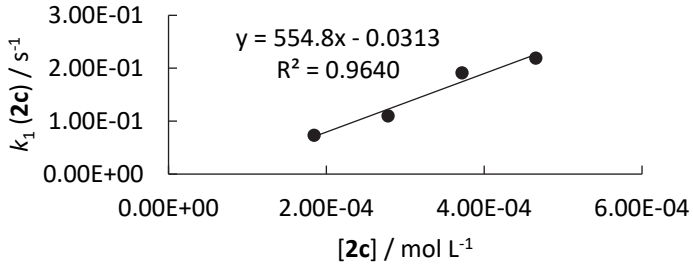

$k_2 = 5.55 \times 10^2\ M^{-1}\ s^{-1}$
$k_{OH} = 3.44\ M^{-1}\ s^{-1}$

2c$^+$MsO$^-$ + **3c**-BF_4 in alkaline 99.5/0.5 (v/v) H_2O/CH_3CN (sequential mixing stopped-flow, detection at 615 nm)

$[\mathbf{3c}]_0$, mol L^{-1}	$[\mathbf{2c}^+]_0$, mol L^{-1}	$[OH^-]_0$, mol L^{-1}	$[\mathbf{2c}]$, mol L^{-1}	$[OH^-]$, mol L^{-1}	k_{obs}, s^{-1}	$k_{OH}[OH^-]$, s^{-1}	k_1, s^{-1}
1.65×10^{-5}	2.00×10^{-4}	1.87×10^{-4}	1.84×10^{-4}	3.39×10^{-6}	1.90×10^{-1}	3.65×10^{-5}	1.96×10^{-1}
1.65×10^{-5}	3.00×10^{-4}	2.81×10^{-4}	2.77×10^{-4}	3.62×10^{-6}	3.73×10^{-1}	3.90×10^{-5}	3.73×10^{-1}
1.65×10^{-5}	4.00×10^{-4}	3.74×10^{-4}	3.70×10^{-4}	3.76×10^{-6}	5.13×10^{-1}	4.06×10^{-5}	5.13×10^{-1}
1.65×10^{-5}	5.00×10^{-4}	4.68×10^{-4}	4.64×10^{-4}	3.85×10^{-6}	6.65×10^{-1}	4.16×10^{-5}	6.65×10^{-1}

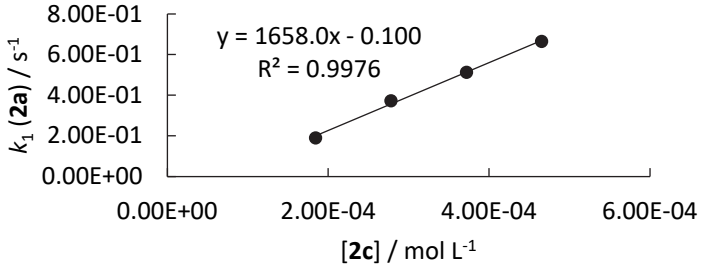

$k_2 = 1.66 \times 10^3\ M^{-1}\ s^{-1}$
$k_{OH} = 10.8\ M^{-1}\ s^{-1}$

2c$^+$MsO$^-$ + **3b**-BF_4 in alkaline 99.5/0.5 (v/v) H_2O/CH_3CN (sequential mixing stopped-flow, detection at 610 nm)

[**3b**]$_0$, mol L^{-1}	[**2c**$^+$]$_0$, mol L^{-1}	[OH$^-$]$_0$, mol L^{-1}	[**2c**], mol L^{-1}	[OH$^-$], mol L^{-1}	k_{obs}, s^{-1}	k_{OH}[OH$^-$], s^{-1}	k_1, s^{-1}
1.49×10^{-5}	2.00×10^{-4}	1.87×10^{-4}	1.84×10^{-4}	3.39×10^{-6}	1.11	1.64×10^{-4}	1.11
1.49×10^{-5}	3.00×10^{-4}	2.81×10^{-4}	2.77×10^{-4}	3.62×10^{-6}	1.82	1.76×10^{-4}	1.82
1.49×10^{-5}	4.00×10^{-4}	3.74×10^{-4}	3.70×10^{-4}	3.76×10^{-6}	2.68	1.82×10^{-4}	2.68
1.49×10^{-5}	5.00×10^{-4}	4.68×10^{-4}	4.64×10^{-4}	3.85×10^{-6}	3.45	1.87×10^{-4}	3.45

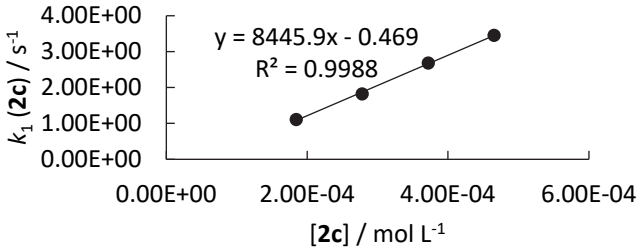

$k_2 = 8.45 \times 10^3$ M^{-1} s^{-1}
$k_{OH} = 48.5$ M^{-1} s^{-1}

Determination of N and s_N parameters for the zwitterion **2c** in 99.5/0.5 (v/v) H_2O/CH_3CN

Reference Electrophile	Electrophilicity E	k_2, M^{-1} s^{-1}	lg k_2
3e	–10.04	3.08×10^2	2.49
3d	–9.45	5.55×10^2	2.74
3c	–8.76	1.66×10^3	3.22
3b	–7.69	8.45×10^3	3.93

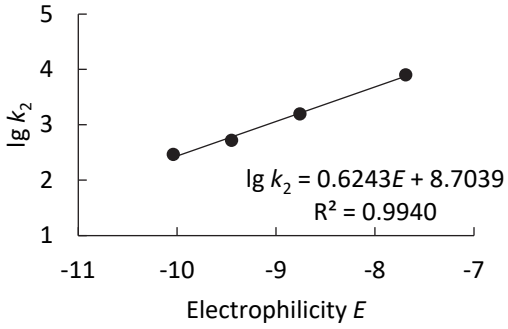

$N = 13.94$
$s_N = 0.62$

4.5 Kinetics of the reactions of 2c$^-$ (generated from 2c$^+$MsO$^-$) with benzhydrylium ions 3 in water – RM314

2c$^+$MsO$^-$ + **3e**-BF_4 in alkaline 99.5/0.5 (v/v) H_2O/CH_3CN (sequential mixing stopped-flow, detection at 630 nm)

[**3e**]$_0$, mol L^{-1}	[**2c**$^+$]$_0$, mol L^{-1}	[OH$^-$]$_0$, mol L^{-1}	[**2c**$^-$], mol L^{-1}	[OH$^-$], mol L^{-1}	k_{obs}, s^{-1}	k_{OH}[OH$^-$], s^{-1}	k_1, s^{-1}
1.29×10^{-5}	2.00×10^{-4}	2.50×10^{-2}	1.99×10^{-4}	2.46×10^{-2}	2.55×10^{-1}	5.32×10^{-2}	2.04×10^{-1}
1.29×10^{-5}	3.00×10^{-4}	2.50×10^{-2}	2.99×10^{-4}	2.44×10^{-2}	3.79×10^{-1}	5.28×10^{-2}	3.26×10^{-1}
1.29×10^{-5}	4.00×10^{-4}	2.50×10^{-2}	3.99×10^{-4}	2.42×10^{-2}	4.98×10^{-1}	5.23×10^{-2}	4.46×10^{-1}
1.29×10^{-5}	5.00×10^{-4}	2.50×10^{-2}	4.98×10^{-4}	2.40×10^{-2}	6.36×10^{-1}	5.19×10^{-2}	5.84×10^{-1}

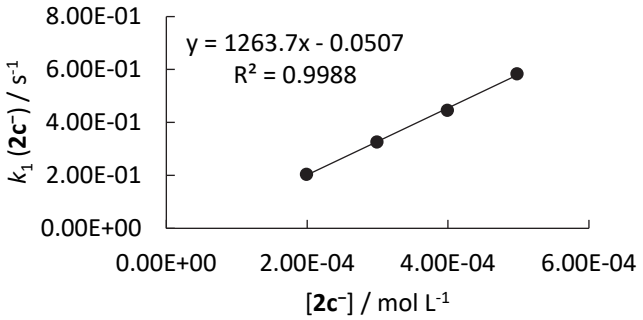

$k_2 = 1.26 \times 10^3$ M^{-1} s^{-1}
$k_{OH} = 2.16$ M^{-1} s^{-1}

2c$^+$MsO$^-$ + **3d**-BF_4 in alkaline 99.5/0.5 (v/v) H_2O/CH_3CN (sequential mixing stopped-flow, detection at 640 nm)

[**3d**]$_0$, mol L^{-1}	[**2c**$^+$]$_0$, mol L^{-1}	[OH$^-$]$_0$, mol L^{-1}	[**2c**$^-$], mol L^{-1}	[OH$^-$], mol L^{-1}	k_{obs}, s^{-1}	k_{OH}[OH$^-$], s^{-1}	k_1, s^{-1}
1.14×10^{-5}	2.00×10^{-4}	2.50×10^{-2}	1.99×10^{-4}	2.46×10^{-2}	4.25×10^{-1}	8.45×10^{-2}	3.40×10^{-1}
1.14×10^{-5}	3.00×10^{-4}	2.50×10^{-2}	2.99×10^{-4}	2.44×10^{-2}	6.54×10^{-1}	8.38×10^{-2}	5.70×10^{-1}
1.14×10^{-5}	4.00×10^{-4}	2.50×10^{-2}	3.99×10^{-4}	2.42×10^{-2}	8.92×10^{-1}	8.31×10^{-2}	8.08×10^{-1}
1.14×10^{-5}	5.00×10^{-4}	2.50×10^{-2}	4.98×10^{-4}	2.40×10^{-2}	1.04	8.24×10^{-2}	9.58×10^{-1}

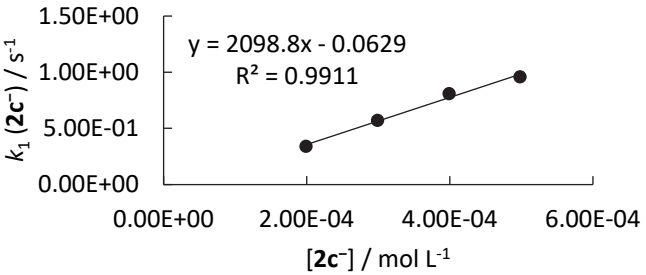

$k_2 = 2.10 \times 10^3$ M^{-1} s^{-1}
$k_{OH} = 3.44$ M^{-1} s^{-1}

2c$^+$MsO$^-$ + **3c**-BF_4 in alkaline 99.5/0.5 (v/v) H_2O/CH_3CN (sequential mixing stopped-flow, detection at 615 nm)

[**3c**]$_0$, mol L^{-1}	[**2c**$^+$]$_0$, mol L^{-1}	[OH$^-$]$_0$, mol L^{-1}	[**2c**$^-$], mol L^{-1}	[OH$^-$], mol L^{-1}	k_{obs}, s^{-1}	k_{OH}[OH$^-$], s^{-1}	k_1, s^{-1}
1.65×10^{-5}	2.00×10^{-4}	2.50×10^{-2}	1.99×10^{-4}	2.46×10^{-2}	1.30	2.65×10^{-1}	1.02
1.65×10^{-5}	3.00×10^{-4}	2.50×10^{-2}	2.99×10^{-4}	2.44×10^{-2}	1.99	2.63×10^{-1}	1.72
1.65×10^{-5}	4.00×10^{-4}	2.50×10^{-2}	3.99×10^{-4}	2.42×10^{-2}	2.51	2.61×10^{-1}	2.25
1.65×10^{-5}	5.00×10^{-4}	2.50×10^{-2}	4.98×10^{-4}	2.40×10^{-2}	3.12	2.59×10^{-1}	2.86

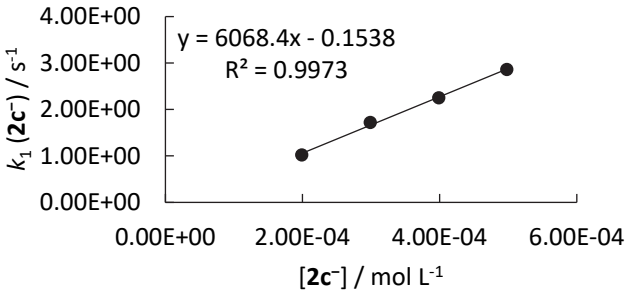

$k_2 = 6.07 \times 10^3$ M^{-1} s^{-1}
$k_{OH} = 10.8$ M^{-1} s^{-1}

2c$^+$MsO$^-$ + **3b**-BF_4 in alkaline 99.5/0.5 (v/v) H_2O/CH_3CN (sequential mixing stopped-flow, detection at 610 nm)

$[\mathbf{3b}]_0$, mol L^{-1}	$[\mathbf{2c}^+]_0$, mol L^{-1}	$[OH^-]_0$, mol L^{-1}	$[\mathbf{2c}^-]$, mol L^{-1}	$[OH^-]$, mol L^{-1}	k_{obs}, s^{-1}	$k_{OH}[OH^-]$, s^{-1}	k_1, s^{-1}
1.49×10^{-5}	2.00×10^{-4}	2.50×10^{-2}	1.99×10^{-4}	2.46×10^{-2}	7.23	1.19	6.04
1.49×10^{-5}	3.00×10^{-4}	2.50×10^{-2}	2.99×10^{-4}	2.44×10^{-2}	1.12×10^1	1.18	1.00×10^1
1.49×10^{-5}	4.00×10^{-4}	2.50×10^{-2}	3.99×10^{-4}	2.42×10^{-2}	1.34×10^1	1.17	1.22×10^1
1.49×10^{-5}	5.00×10^{-4}	2.50×10^{-2}	4.98×10^{-4}	2.40×10^{-2}	1.61×10^1	1.16	1.49×10^1

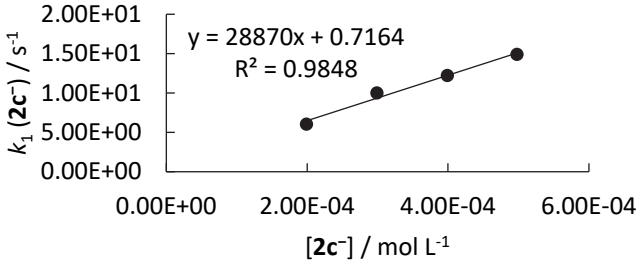

$k_2 = 2.89 \times 10^4$ M^{-1} s^{-1}
$k_{OH} = 48.5$ M^{-1} s^{-1}

Determination of N and s_N parameters for the anion **2c**$^-$ in 99.5/0.5 (v/v) H_2O/CH_3CN

Reference Electrophile	Electrophilicity E	k_2, M^{-1} s^{-1}	lg k_2
3e	–10.04	1.26×10^3	3.10
3d	–9.45	2.10×10^3	3.32
3c	–8.76	6.07×10^3	3.78
3b	–7.69	2.89×10^4	4.46

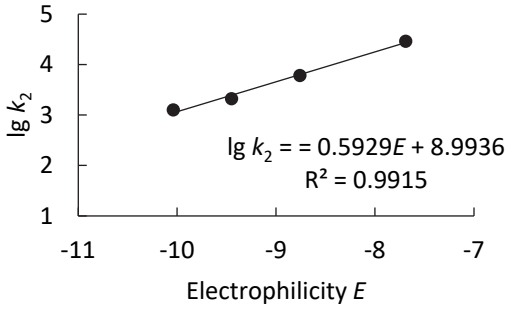

$N = 15.17$
$s_N = 0.59$

3.5 Conformational Analysis

Conformational analysis of **2a**

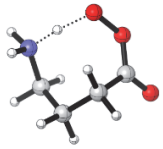

11

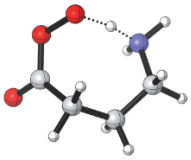

16

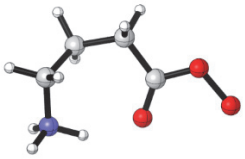

2

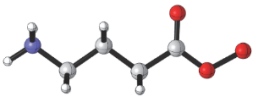

10

Number	E_{tot} [Hartree]	G_{298} [Hartree]	Relative ΔG_{298} [kJ/mol]	Contribution [%]
11	-438.202526	-438.091188	0.00	55.8288
16	-438.202169	-438.090948	0.63	43.2864
2	-438.195282	-438.085569	14.75	0.1444
10	-438.194093	-438.085538	14.83	0.1397
12	-438.194926	-438.085514	14.90	0.1362
14	-438.196915	-438.085344	15.34	0.1138
1	-438.195165	-438.085076	16.05	0.0856
13	-438.194316	-438.084364	17.92	0.0403
6	-438.195866	-438.084353	17.95	0.0398
5	-438.195866	-438.084352	17.95	0.0397
9	-438.194937	-438.084306	18.07	0.0379
15	-438.193718	-438.083949	19.01	0.0259
8	-438.193444	-438.083909	19.11	0.0248
4	-438.193779	-438.083650	19.79	0.0189
7	-438.193485	-438.083350	20.58	0.0137
3	-438.195525	-438.083184	21.01	0.0115
23	-438.191274	-438.082059	23.97	0.0035
18	-438.192253	-438.081829	24.57	0.0027
19	-438.190992	-438.081738	24.81	0.0025
21	-438.191541	-438.080956	26.86	0.0011
25	-438.190067	-438.080784	27.32	0.0009
20	-438.191159	-438.080541	27.95	0.0007
29	-438.190102	-438.079729	30.09	0.0003
22	-438.189983	-438.079559	30.53	0.0002
24	-438.191851	-438.079534	30.60	0.0002
27	-438.190429	-438.079436	30.85	0.0002
28	-438.189871	-438.078990	32.03	0.0001

Conformational analysis of **2b**

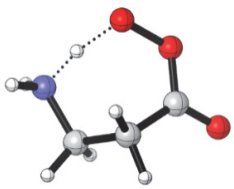

7

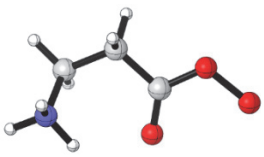

1

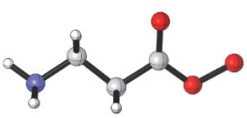

2

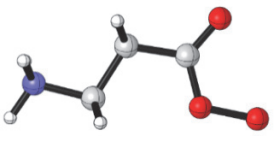

4

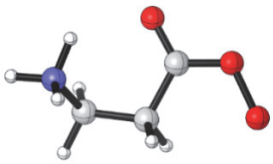

5

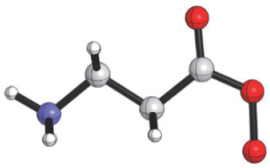

6

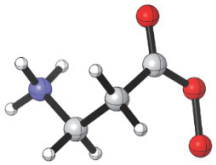

8

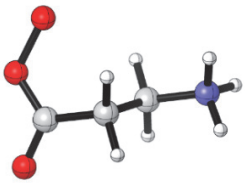

9

Number	E_{tot} [Hartree]	G_{298} [Hartree]	Relative ΔG_{298} [kJ/mol]	Contribution [%]
7	-398.887437	-398.804399	0.0	95.961
1	-398.884268	-398.801138	8.6	3.024
2	-398.881659	-398.799840	12.0	0.764
4	-398.880984	-398.798072	16.6	0.117
5	-398.881726	-398.797991	16.8	0.108
6	-398.879325	-398.796404	21.0	0.020
8	-398.878179	-398.795103	24.4	0.005
9	-398.877446	-398.794247	26.7	0.002

Conformational analysis of **2c**

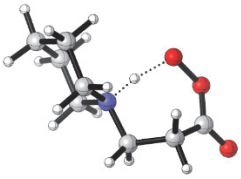

29

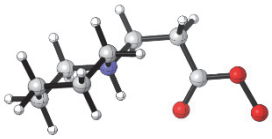

4

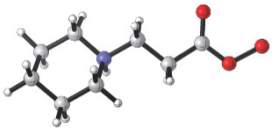

1

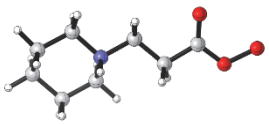

3

Number	E_{tot} [Hartree]	G_{298} [Hartree]	Relative ΔG_{298} [kJ/mol]	Contribution [%]
29	-594.242260	-594.040992	0.00	0.9827
4	-594.238955	-594.036489	11.82	0.0083
1	-594.235850	-594.035228	15.13	0.0022
3	-594.235803	-594.035046	15.61	0.0018
7	-594.237266	-594.034544	16.93	0.0011
2	-594.235007	-594.034358	17.42	0.0009
8	-594.236198	-594.034171	17.91	0.0007
12	-594.236271	-594.034150	17.96	0.0007
11	-594.236253	-594.034051	18.22	0.0006
14	-594.236370	-594.033680	19.20	0.0004
5	-594.234441	-594.032764	21.60	0.0002
10	-594.235730	-594.032588	22.06	0.0001
16	-594.234477	-594.031674	24.46	0.0001
13	-594.233414	-594.031441	25.08	0.0000
24	-594.233092	-594.031408	25.16	0.0000
6	-594.233240	-594.031321	25.39	0.0000
25	-594.233618	-594.031208	25.69	0.0000
9	-594.233162	-594.031184	25.75	0.0000
21	-594.232735	-594.031161	25.81	0.0000
19	-594.232170	-594.030778	26.82	0.0000

18	-594.233833	-594.030747	26.90	0.0000
23	-594.233959	-594.030525	27.48	0.0000
27	-594.231502	-594.030315	28.03	0.0000
17	-594.231869	-594.030207	28.32	0.0000
20	-594.231336	-594.029338	30.60	0.0000
36	-594.231364	-594.029048	31.36	0.0000
22	-594.230729	-594.028930	31.67	0.0000
34	-594.231683	-594.028859	31.86	0.0000
35	-594.229748	-594.028128	33.77	0.0000
38	-594.230055	-594.028115	33.81	0.0000
37	-594.231250	-594.027805	34.62	0.0000
32	-594.230839	-594.027664	34.99	0.0000
28	-594.229606	-594.026954	36.86	0.0000
31	-594.228063	-594.026899	37.00	0.0000
33	-594.229585	-594.026851	37.13	0.0000
26	-594.226065	-594.023983	44.66	0.0000

3.6 References

[1] N.-D. H. Gamage, B. Stiasny, J. Stierstorfer, P. D. Martin, T. M. Klapötke, C. H. Winter, *Chem. Eur. J.* **2016**, *22*, 2582–2585.

[2] G. R. Fulmer, Alexander J. M. Miller, N. H. Sherden, H. E. Gottlieb, A. Nudelman, B. M. Stoltz, J. E. Bercaw, K. I. Goldberg, *Organometallics* **2010**, *29*, 2176–2179.

[3] Bruker, *SAINT*; Bruker AXS Inc., Madison, Wisconsin, USA, **2012**.

[4] G. M. Sheldrick, *SADABS*; University of Göttingen, Germany, **1996**.

[5] G. M. Sheldrick, *Acta Cryst. A* **2015**, *71*, 3–8.

[6] Carboxylate ions formed by deprotonation of the carboxylic acids do not form covalent adducts with the benzhydrylium ions **3b**–**3e** in aqueous solutions: a) H. F. Schaller, H. Mayr, *Angew. Chem.* **2008**, *120*, 4022–4025; *Angew. Chem. Int. Ed.* **2008**, *47*, 3958–3961; b) H. F. Schaller, A. A. Tishkov, X. Feng, H. Mayr, *J. Am. Chem. Soc.* **2008**, *130*, 3012–3022.

[7] E. Harder, W. Damm, J. Maple, C. Wu, M. Reboul, J. Y. Xiang, L. Wang, D. Lupyan, M. K. Dahlgren, J. L. Knight, J. W. Kaus, D. S. Cerutti, G. Krilov, W. L. Jorgensen, R. Abel, R. A. Friesner, *J. Chem. Theory Comput.* **2016**, *12*, 281–296.

[8] *MacroModel* (Schrödinger Release 2017-1), Schrödinger, LLC, New York, NY, 2017.

[9] Y. Zhao, D. G. Truhlar, *J. Phys. Chem. A* **2006**, *110*, 13126–13130.

[10] A. V. Marenich, C. J. Cramer, D. G. Truhlar, *J. Phys. Chem. B* **2009**, *113*, 6378–6396.

[11] *Gaussian 16, Revision A.03*, M. J. Frisch, G. W. Trucks, H. B. Schlegel, G. E. Scuseria, M. A. Robb, J. R. Cheeseman, G. Scalmani, V. Barone, G. A. Petersson, H. Nakatsuji, X. Li, M. Caricato, A. V. Marenich, J. Bloino, B. G. Janesko, R. Gomperts, B. Mennucci, H. P. Hratchian, J. V. Ortiz, A. F. Izmaylov, J. L. Sonnenberg, D. Williams-Young, F. Ding, F. Lipparini, F. Egidi, J. Goings, B. Peng, A. Petrone, T. Henderson, D. Ranasinghe, V. G. Zakrzewski, J. Gao, N. Rega, G. Zheng, W. Liang, M. Hada, M. Ehara, K. Toyota, R. Fukuda, J. Hasegawa, M. Ishida, T. Nakajima, Y. Honda, O. Kitao, H. Nakai, T. Vreven, K. Throssell, J. A. Montgomery, Jr., J. E. Peralta, F. Ogliaro, M. J. Bearpark, J. J. Heyd, E. N. Brothers, K. N. Kudin, V. N. Staroverov, T. A. Keith, R. Kobayashi, J. Normand, K. Raghavachari, A. P. Rendell, J. C. Burant, S. S. Iyengar, J. Tomasi, M. Cossi, J. M. Millam, M. Klene, C. Adamo, R. Cammi, J. W. Ochterski, R. L. Martin, K. Morokuma, O. Farkas, J. B. Foresman, D. J. Fox, Gaussian, Inc., Wallingford CT, **2016**.

[12] C. Venturello, C. Cavallotti, US5245075, **1993**.

Chapter 4. Ambident Reactivity of Phenolate Anions Revisited: A Quantitative Approach to Phenolate Reactivities

R. J. Mayer, M. Breugst, N. Hampel, A. R. Ofial, H. Mayr, *J. Org. Chem.* **2019**, *84*, 8837-8858.

Author Contributions

RJM conceived the project on the basis of preliminary results obtained by MB (kinetics of electrophiles with **1c**-K, **1e**-K, **1f**-K, **1h**-K, **1k**-K in DMSO and **1c**-K, **1f**-K in MeCN; products **3cn**, **3en**, **3fn**) receiving guidance from ARO and HM. Kinetic measurements for all other species and additional kinetics with other electrophiles for the systems studied by MB as well as all equilibrium titrations were performed by RJM. Product studies and regioselectivity measurements were performed by RJM with the support from NH. Computational studies were performed by RJM. The manuscript was written jointly by RJM, ARO and HM.

Copyright

Selected supporting material for this work is provided starting with section 4.1. The complete supporting information (SI) is published online and can be accessed under https://doi.org/10.1021/acs.joc.9b01485.

JOC The Journal of Organic Chemistry
Cite This: J. Org. Chem. 2019, 84, 8837−8858
Featured Article
pubs.acs.org/joc

Ambident Reactivity of Phenolate Anions Revisited: A Quantitative Approach to Phenolate Reactivities

Robert J. Mayer, Martin Breugst,[†] Nathalie Hampel, Armin R. Ofial,* and Herbert Mayr*

Department Chemie, Ludwig-Maximilians-Universität München, Butenandtstr. 5-13, 81377 München, Germany

Supporting Information

ABSTRACT: Prompted by the observation that the regioselectivities of phenolate reactions (C versus O attack) are opposite to the predictions by the principle of hard and soft acids and bases, we performed a comprehensive experimental and computational investigation of phenolate reactivities. Rate and equilibrium constants for the reactions of various phenolate ions with benzhydrylium ions ($Aryl_2CH^+$) and structurally related quinone methides have been determined photometrically in polar aprotic solvents. Quantum chemical calculations at the SMD(MeCN)/M06-2X/6-31+G(d,p) level confirmed that O attack is generally favored under kinetically controlled conditions, whereas C attack is favored under thermodynamically controlled conditions. Exceptions are diffusion-limited reactions with strong electrophiles, which give mixtures of products arising from O and C attack, as well as reactions with metal alkoxides in nonpolar solvents, where oxygen attack is blocked by strong ion pairing. The Lewis basicity (LB) and nucleophilicity (N, s_N) parameters of phenolates determined in this work can be used to predict whether their reactions with electrophiles are kinetically or thermodynamically controlled and whether the rates are activation- or diffusion-limited. Comparison of the measured rate constants for the reactions of phenolates with carbocations with the Gibbs energies for single-electron transfer manifests that these reactions proceed via polar mechanisms.

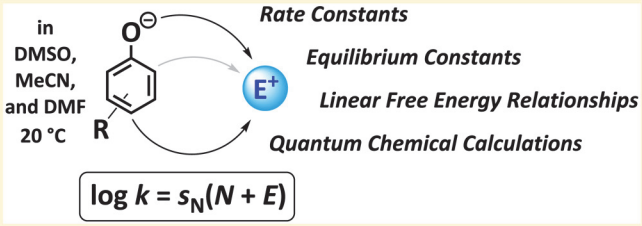

INTRODUCTION

Phenolate ions are ambident nucleophiles which may react with electrophiles either at oxygen or at carbon, as indicated by the resonance structures in Scheme 1.[1−7]

Ambident reactivity is traditionally analyzed by the principle of hard and soft acids and bases (HSAB)[8] or the related Klopman−Salem concept of charge and orbital control.[9,10] In an extensive review, we demonstrated, however, that these concepts are virtually useless in practice as the number of times they do not work is approaching the number of times that they do.[2] The most recent edition of a well-known textbook introduces the HSAB principle and concludes "Therefore, as the character of a given reaction changes from S_N1- to S_N2-like, an ambident nucleophile becomes more likely to attack with its less electronegative atom. Thus, changing from S_N1 to S_N2 conditions should favor C attack by ^-CN, N attack by NO_2^-, C attack by enolate or phenoxide ions and so on."[11]

Because we had observed just the opposite behavior, that is, that O attack at phenolates is favored when changing from S_N1 to S_N2 conditions, we now performed a systematic investigation of the Lewis basicities and nucleophilicities of phenolate ions and demonstrate that on this basis reliable predictions of their reactivities toward electrophiles are possible.

As phenolates are important reagents in organic synthesis, numerous investigations of their Brønsted basicities and nucleophilic reactivities have previously been reported.[12] The pK_a values of differently substituted phenols were used for deriving the substituent constants σ_p^- in the modified Hammett−Brown equation,[13] and substituent effects in phenolate ions served as a gauge for quantifying resonance effects.[14] Rate constants for the attack of solvolytically generated phenethyl cations at O and C sites of the parent phenolate ion in trifluoroethanol/water mixtures were determined by Richard and co-workers using the azide ion diffusion clock method.[15] Bernasconi derived "transition state imbalances" from the kinetics of the reactions of phenoxide ions with benzylidene Meldrum's acids,[16] and Denmark studied the influence of counterions on the phase-transfer-catalyzed alkylations of phenol.[17] Kornblum and associates investigated the solvent effect on the ratio of O- and C-allylation and benzylation of alkali phenolates and found exclusive O attack in most solvents, except in water and fluorinated alcohols, where O attack is retarded by hydrogen bridging with the consequence that the phenol ethers are accompanied by products of the C attack.[4c] Pliego supported this interpretation by quantum chemical calculations.[18]

Boubaker, Goumont, and co-workers determined the rate constants for the reactions of p-substituted phenolates at 2-aryl-4,6-dinitrobenzotriazole-1-oxides (electron-deficient arenes) in buffered aqueous solutions[19] and analyzed the data according to eq 1, where N and s_N are solvent-dependent

Received: June 5, 2019
Published: June 26, 2019

DOI: 10.1021/acs.joc.9b01485
J. Org. Chem. 2019, 84, 8837−8858

The Journal of Organic Chemistry Featured Article

Scheme 1. Resonance Structures of the Phenolate Ion

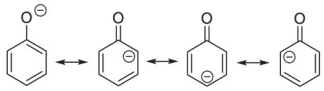

nucleophile-specific parameters and E represents an electrophilicity parameter.[20−22]

$$\log k(20\ ^{\circ}\mathrm{C}) = s_N(N + E) \quad (1)$$

Buncel and co-workers reported that the highly electrophilic 2-(2′,4′-dinitroaryl)-substituted 4,6-dinitrobenzotriazol-1-oxide reacts with phenolate ions in DMSO-d_6 solution to form C adducts accompanied by diaryl ethers, which arise from O attack.[7a]

We now report on a systematic investigation of rate and equilibrium constants of the reactions of the phenolate ions listed in Chart 1, with the reference electrophiles listed in Chart 2, in order to integrate phenolates **1** in our comprehensive Lewis basicity,[23] nucleophilicity,[20,24] and nucleofugality scales[25] and eventually combine these data for rationalizing and predicting the ambident reactivities of phenolate ions.

RESULTS

Synthesis of Phenolate Salts and Products of Their Reactions with Reference Electrophiles. Tetrabutylammonium and potassium phenolates (**1**-NBu_4 or **1**-K, Chart 1) were prepared according to modified literature procedures by treating methanolic or aqueous solutions of the phenols with either Bu_4NOH or KOH and subsequent evaporation of the solvent.[4a] All phenolate salts listed in Chart 1 were characterized by ^{1}H and ^{13}C NMR spectroscopy in DMSO-d_6.

Scheme 2 shows those reactions of phenolates **1** with the benzhydrylium ion **2a**, which exclusively yield benzhydryl aryl ethers **3** according to ^{1}H NMR spectra taken immediately after mixing equimolar amounts of these reactants in DMSO-d_6 at ambient temperature. Proton chemical shifts for the singlet of the CH−O unit in the ethers **3** are typically found in the range of 5.9 to 6.2 ppm.

When these reactions were performed on a preparative scale by adding solutions of **2a**-BF_4 (in DMSO) to stirred 0.1−0.2 M solutions of potassium phenolates **1**-K (1.1 equiv) in DMSO, fading of the blue color of **2a** generally occurred within seconds. Upon addition of aqueous ammonia, the benzhydryl phenyl ethers **3** precipitated and were isolated by filtration (Scheme 2, Method B). However, even with 2 equiv of the phenolate **1c** (p-NO_2), the blue color of **2a** did not

Chart 1. Phenolate Ions Investigated in This Study (Counterion: K^+ or NBu_4^+)

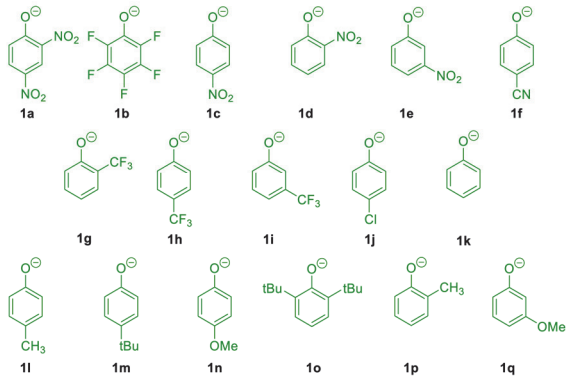

Chart 2. Reference Electrophiles 2a−m with Their Electrophilicities (E), Lewis Acidities (LA in MeCN), and Electrofugalities (E_f)[a]

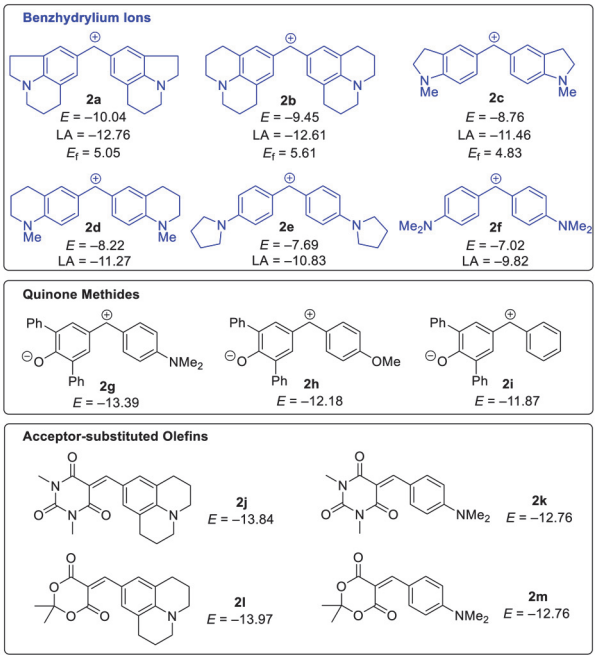

[a]Electrophilicities E for **2a−f** from ref 26, for **2g−h** from ref 27, for **2i** from ref 28, for **2j−k** from ref 29, and for **2l−m** from ref 30; Lewis acidities LA_{MeCN} from ref 31, and electrofugalities E_f from ref 25.

Scheme 2. Reaction of Phenolate Ions 1 with Benzhydrylium Ion 2a in DMSO

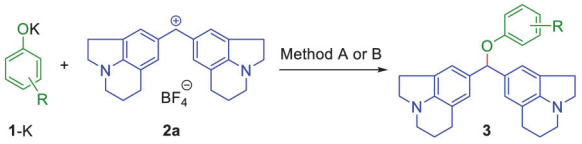

Phenolate	***Method A***[a] **1** (100 mol-%) d_6-DMSO, 20 °C	***Method B*** **1** (110–120 mol-%) DMSO, 30–60 s, 20 °C then aq NH_3 (pH 10)
1c (p-NO_2)	**3ca**[b]	[c]
1e (m-NO_2)	**3ea**	[c]
1f (p-CN)	**3fa**	[c]
1h (p-CF_3)	**3ha**[b]	**3ha** (34%)
1i (m-CF_3)	**3ia**	**3ia** (50%)
1j (p-Cl)	**3ja**	**3ja** (73%)
1k (H)	**3ka**	**3ka** (83%)
1l (p-CH_3)	**3la**	**3la** (quant.)
1m (p-*t*Bu)	**3ma**	**3ma** (74%)
1n (p-OMe)	**3na**	**3na** (quant.)
1p (o-CH_3)	**3pa**	[d]
1q (m-OMe)	**3qa**[b]	[d]

[a]According to analysis of ^{1}H NMR spectra acquired directly after mixing equimolar amounts of **1**-K and **2a**-BF_4 in DMSO-d_6. [b]**1**-NBu_4 was used instead of **1**-K. [c]Product mixture containing mostly Ar_2CHOH (hydrolysis products of **2a**). [d]Not studied.

DOI: 10.1021/acs.joc.9b01485
J. Org. Chem. 2019, 84, 8837−8858

disappear completely. The moderate yields of ethers **3ca**−**3ia** are due to their hydrolysis during aqueous workup with formation of the corresponding benzhydrols (Ar_2CHOH).

Whereas the analogous reactions of **2a** with **1d** (or **1g**) yielded the phenol ethers **3da** (or **3ga**) with small amounts of the substituted phenols **4da** (or **4ga**; ^1H NMR spectra acquired directly after mixing showed a small singlet for the central $C(sp^3)H$ at δ 5.0−5.2), the phenols **4da** (or **4ga**) were the only observable products when the DMSO solution was kept for 12 h at 20 °C (Scheme 3). Quantitative formation of the phenol ethers **3da** (or **3ga**) was observed when these reactions were carried out at −40 °C in CD_3CN. In contrast, the reaction of the 2,6-di-*tert*-butyl-substituted phenolate **1o** with **2a** led to exclusive attack at C-4 with formation of **4oa**, even when the reaction was carried out at −40 °C in DMF-d_7.[7e]

Aqueous workup of the products obtained by the reactions of **2a** with the acceptor-substituted phenolates **1c**−**1i** immediately after mixing in DMSO showed the presence of the corresponding benzhydrols (Ar_2CHOH) due to hydrolysis of the phenol ethers **3ca**−**3ia** (Method B in Schemes 2 and 3). The reason why only phenol ethers **3da** and **3ga** rearrange to the substituted phenols **4da** and **4ga**, respectively, will be discussed in the section on quantum chemical calculations.

Whereas benzhydrylium tetrafluoroborate **2a**-BF_4 did not react with the least reactive phenolates **1a** (o,p-$(NO_2)_2$) and **1b** (perfluoro), these phenolates reacted with benzhydryl bromide **2n**-Br to give benzhydryl phenyl ethers **3an** and **3bn**, respectively, like the other phenolates listed in Scheme 4. Due to the high Lewis acidity of the di(tolyl)carbenium ion **2n**, O attack is now irreversible, and all ethers **3** in Scheme 4 formed from **2n**-Br in MeCN at 20 °C could be purified by column chromatography and isolated in good yields. The higher Lewis acidity of **2n** also accounts for the fact that the phenol ethers **3dn** and **3gn** did not rearrange, unlike the structurally analogous benzhydryl ethers **3da** and **3ga** formed from the less Lewis acidic **2a** (cf Scheme 3).

Scheme 3. Reactions of Phenolates 1d,g,o with 2a in DMSO

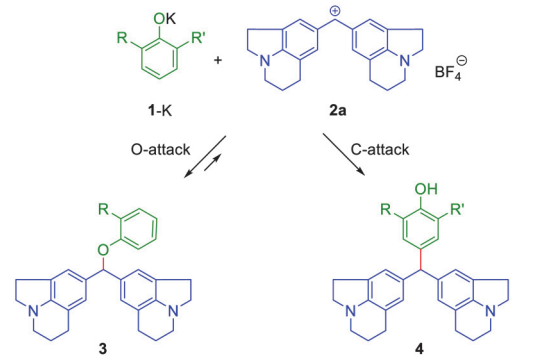

Phenolate	*Method A*[a] **1** (100 mol-%) d_6-DMSO, 20 °C	*Method B* **1** (110–120 mol-%) DMSO, 30–60 s, 20 °C then aq NH_3 (pH 10)
1d (o-NO_2)	**3da** + **4da**[b]	[c]
1g (o-CF_3)[d]	**3ga** + **4ga**[b]	[c]
1o (o,o'-(tBu)$_2$)	**4oa**	**4oa** (64%)

[a]NMR analysis directly after mixing. [b]Product ratio not constant: after 24 h, mainly **4**. [c]Product mixture contained mainly Ar_2CHOH (hydrolysis products of **2a**). [d]**1g**-NBu_4 was used.

Scheme 4. Reactions of Phenolate Salts with Bromodi(*p*-tolyl)methane 2n-Br in MeCN

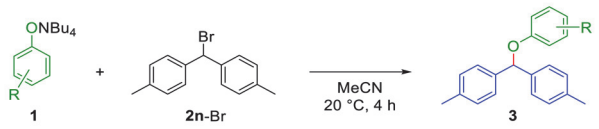

Phenolate	Product	Yield (%)
1a (o,p-$(NO_2)_2$)	**3an**	99
1b (F_5)	**3bn**	82
1c (p-NO_2)	**3cn**	80
1d (o-NO_2)	**3dn**	71
1e (m-NO_2)	**3en**	80
1f (p-CN)	**3fn**	98
1g (o-CF_3)	**3gn**	78
1n (p-OMe)[a]	**3nn**	81

[a]**1n**-K/18-crown-6 ether was used.

Thus, oxygen attack is generally the kinetically preferred reaction of phenolates. Only the combination of **2n**-Br with the sterically hindered phenolate **1o**-K (o,o'-(tBu)$_2$) gave rise to the exclusive formation of the substituted phenol **4on** (Scheme 5).[7e]

Also, in the reaction of the quinone methide **2h** with equimolar amounts of phenolate **1l** (p-Me) in DMSO-d_6, exclusive O attack was observed by NMR spectroscopy (Scheme 6).

Equilibrium Constants for the Formation of Phenol Ethers from Phenolates and Benzhydrylium Ions. In previous work, we demonstrated that equilibrium constants for the reactions of benzhydrylium ions with a variety of Lewis bases can be calculated as the sum of a Lewis acidity parameter (LA) and a Lewis basicity parameter (LB) as expressed by eq 2.[23,31]

$$\log K(20\ ^\circ C) = LA + LB \qquad (2)$$

Equilibrium constants for the formation of phenol ethers **3** from phenolates **1** and benzhydrylium ions **2** in acetonitrile were now determined by UV−vis spectrometric titrations, as illustrated in Figure 1.

Stepwise additions of solutions of the tetrabutylammonium phenolates[32] to solutions of the benzhydrylium tetrafluoroborates in acetonitrile at 20 °C led to gradual decrease of the absorbances of the benzhydrylium ions (Figure 1B). With the known molar absorption coefficients of the benzhydrylium ions[26b] and the Beer−Lambert law, the concentrations of all species were calculated according to eqs 3−5 at each step of the titration from the difference between the measured absorbance A and the absorbance A_0*, which corresponds to

Scheme 5. Reaction of 1o-K with Bromodi(*p*-tolyl)methane 2n-Br in CD_3CN (Characterized by NMR Spectroscopy)

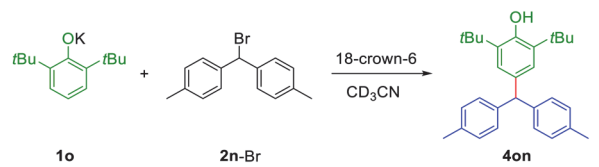

DOI: 10.1021/acs.joc.9b01485
J. Org. Chem. 2019, 84, 8837−8858

The Journal of Organic Chemistry Featured Article

Scheme 6. Reaction of Potassium Phenolate 1l-K with Quinone Methide 2h in DMSO-d_6

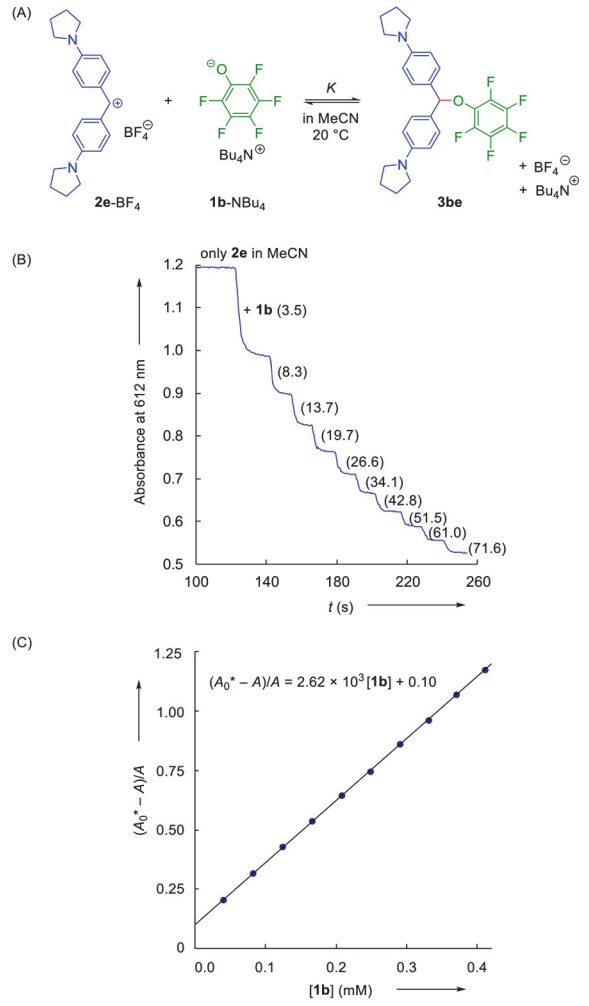

Figure 1. (A) Equilibrium reaction of benzhydrylium ion **2e** with the phenolate **1b** to furnish the Lewis adduct **3be**. (B) Titration of the benzhydrylium salt **2e**-BF_4 by incremental addition of perfluorinated phenolate **1b**-NBu_4 in MeCN at 20 °C ($[\mathbf{2e}]_0 = 1.25 \times 10^{-5}$ M; values in parentheses give the total number of equivalents of added phenolate **1b** in relation to $[\mathbf{2e}]_0$). (C) Determination of the equilibrium constant K through the linear correlation of $(A_0^* - A)/A$ with the concentration of free phenolate.

the initial absorbance A_0 corrected for the effect of dilution, that is, $A_0^* = A_0(V_0/V)$.[23]

$$\mathbf{2} + \mathbf{1} \underset{\text{MeCN}}{\overset{K}{\rightleftharpoons}} \mathbf{3} \tag{3}$$

$$K = \frac{[\mathbf{3}]}{[\mathbf{2}][\mathbf{1}]} = \frac{A_0^* - A}{A[\mathbf{1}]} \tag{4}$$

$$[\mathbf{1}] = [\mathbf{1}]_0 - [\mathbf{3}] = [\mathbf{1}]_0 - [(A_0^* - A)/\varepsilon d] \tag{5}$$

Equilibrium constants were then obtained from the linear correlation of $(A_0^* - A)/A$ with the concentration of remaining phenolate (Figure 1C). Lewis basicities LB of the phenolate ions **1** were calculated by eq 2 from the equilibrium constants (Table 1) and the reported Lewis acidities of the benzhydrylium ions in acetonitrile (LA_{MeCN}, Chart 2). The fair agreement of the individual LB values for a certain phenolate derived from the reactions with different benzhydrylium ions shows the applicability of eq 2. The smaller Lewis basicity of **1d** compared to that of **1c** must be due to steric strain between the benzhydryloxy group and the *o*-nitro group in the Lewis adducts (aryl benzhydryl ethers **3**) because **1d** ($pK_{aH} = 22.3 \pm 0.4$)[33] is a stronger Brønsted base in acetonitrile than **1c** ($pK_{aH} = 20.8 \pm 0.1$).[33]

The determination of equilibrium constants for the reactions of benzhydrylium ions with phenolates, which are more Lewis basic than **1c** (*p*-NO_2, $LB_{MeCN} = 17$), was not possible with this method because the equilibria for the reactions with all available benzhydrylium ions (Chart 2) are shifted too far to the product side.

Although this method did not allow us to derive the LB parameters of **1c** in DMSO because of the lack of suitable reference Lewis acids in DMSO, Table 1 shows that the equilibrium constant for the reaction of **1c** (*p*-NO_2) with **2a** in DMSO is 8 times smaller than K for the same reaction in acetonitrile.

Background reactions of benzhydrylium ions in DMF impeded a reliable determination of equilibrium constants for the reactions of phenolates with benzhydrylium ions in this solvent.

Kinetic Investigations: Oxygen Attack. The kinetics of the reactions of phenolates with colored electrophiles were studied by stopped-flow UV–vis photometry at 20 °C in acetonitrile, DMSO, and DMF (Figure 2A). By using the phenolates **1** in large excess over the electrophiles **2**, their concentrations remained almost constant throughout the reactions, yielding pseudo-first-order kinetics for the decay of the electrophiles' concentrations. First-order rate constants k_{obs} (s^{-1}) were obtained by least-squares fitting of the single-exponential function $A_t = A_0 \exp(-k_{obs}t) + C$ to the fading

Table 1. Equilibrium Constants K (MeCN, 20 °C) for the Reactions of the Tetrabutylammonium Phenolates 1-NBu_4 with Reference Lewis Acids 2a–f and the Resulting Lewis Basicities (LB_{MeCN}) Calculated by Equation 2

phenolate	Lewis acid	K[a] (M^{-1})	individual LB_{MeCN}	LB_{MeCN}
1a (*o*,*p*-$(NO_2)_2$)	**2f**	$(4.67 \pm 0.38) \times 10^1$	11.49	(11.5)
1b (F_5)	**2e**	$(2.42 \pm 0.14) \times 10^3$	14.21	14.10
	2f	$(1.48 \pm 0.04) \times 10^4$	13.99	
1c (*p*-NO_2)	**2a**	$(1.89 \pm 0.05) \times 10^4$	17.04	16.98
	2b	$(1.76 \pm 0.09) \times 10^4$	16.86	
	2c	$(3.86 \pm 0.11) \times 10^5$	17.05	
1d (*o*-NO_2)	**2a**	$(3.73 \pm 0.06) \times 10^3$	16.33	16.26
	2b	$(2.40 \pm 0.03) \times 10^3$	15.99	
	2c	$(9.73 \pm 0.16) \times 10^4$	16.45	
1c (*p*-NO_2)[b]	**2a**[c]	$(2.39 \pm 0.02) \times 10^3$[b]		

[a]Averaged from three independent measurements. [b]In DMSO. [c]LA of **2a** in DMSO is not known.

DOI: 10.1021/acs.joc.9b01485
J. Org. Chem. 2019, 84, 8837–8858

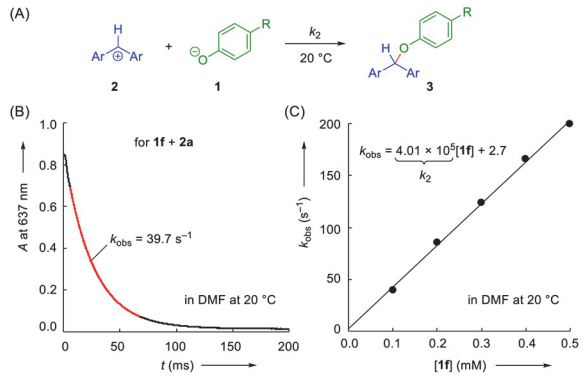

Figure 2. (A) Reactions of benzhydrylium ions **2** with phenolate ions **1**. (B) Absorbance A (at 637 nm) versus time for the reaction of **1f**-K (p-CN, c = 1.00 × 10^{-4} M) with **2a** (c = 5.89 × 10^{-6} M) at 20 °C in DMF. (C) The slope of the linear correlation of the first-order rate constants k_{obs} (s^{-1}) with the nucleophile concentrations corresponds to the second-order rate constant k_2 (DMF, 20 °C) for the attack of the anion **1f** (p-CN) at the benzhydrylium ion **2a**.

absorbances of **2** (Figure 2B). Subsequently, second-order rate constants were obtained as slopes of the plots of k_{obs} versus the concentrations of the phenolates (Figure 2C).

The second-order rate constants k_2 for the reactions of phenolate ions **1** with reference electrophiles **2** (Table 2) correlate linearly with the electrophilicity parameters E of the latter, furnishing the nucleophilicity parameters N of the phenolates **1** as the intercepts on the abscissa ($N = -E$ at log k_2 = 0, Figure 3). The slopes of these correlations (s_N) reflect the susceptibilities of the phenolates toward changes of the reactivities of the electrophiles.

The reactions of benzhydrylium ions **2** with phenolate ions **1** in water were accompanied by the reactions with hydroxide (k_{OH}) and water (k_w), and k_{obs} can be expressed by eq 6.

$$k_{obs} = k_W + k_{OH}[HO^-] + k_2[\mathbf{1}] \quad (6)$$

The concentrations of the phenolate and hydroxide ions, that is, [**1**] and [OH$^-$], respectively, were calculated from the pK_a values of phenols **1**-H. As the rate constants for the reactions of both hydroxide (k_{OH}) and water (k_W) with the benzhydrylium ions **2a–f** have previously been reported,[34] these contributions were subtracted from the observed first-order rate constants k_{obs} to furnish the phenolate reactivities k_2.

The kinetics for the reactions of reference electrophiles **2** with most phenolates in water proved to be problematic, however. When benzhydrylium ions **2a–e** were combined with acceptor-substituted phenols (**1c**, **1f**, and **1h** were tested) in alkaline aqueous solution, the measured rate constants corresponded to the reactions of the benzhydrylium ions with the hydroxide ion (HO$^-$) only. Accordingly, exclusively benzhydrols (Ar$_2$CHOH) were observed as the products.

Though benzhydryl ethers **3** were obtained by the reactions of **2a** with **1j**, **1l**, and **1n**, the reactions of **1j** (p-Cl) and **1n** (p-OMe) with benzhydrylium ions **2a–e** showed complex kinetics, and the consumption of **2** could not be fitted with a monoexponential decay function. Only for the reaction of phenolate **1l** (p-Me) with benzhydrylium ions a consistent set of kinetic data could be obtained in aqueous solution (Table 3).

The nucleophilicity parameter of **1l** (p-Me, Table 3) is approximately 3 orders of magnitude larger than that obtained by interpolation of the N values given in ref 19. This deviation may be due to the fact that the calculation of N in ref 19 was based on E parameters of electrophiles extrapolated from experimental pK_a values.

Phenolates as Leaving Groups: Nucleofugality. Whereas nucleophilicity is a measure for the rate of the reaction of a nucleophile with a reference electrophile, nucleofugality describes the solvent-dependent leaving group ability of a nucleofuge from a certain reference electrofuge.[31] In analogy to eq 1, the rates of heterolytic cleavages can be calculated by eq 7 from the solvent-dependent nucleofugality, N_f, and susceptibility parameter, s_f, of the leaving groups and the solvent-independent electrofugality parameter, E_f, of the carbenium ions.[25]

$$\log k(25\ °C) = s_f(N_f + E_f) \quad (7)$$

Kronja and co-workers recently measured the rate constants for the solvolysis of the benzhydryl ethers **3** derived from phenolates **1a** (o,p-(NO$_2$)$_2$) and **1b** (F$_5$) in aqueous solvent mixtures.[35] Heterolytic cleavage in aprotic solvents was not investigated, however. For the reactions of the p- and o-nitro-substituted phenolates **1c** (p-NO$_2$) and **1d** (o-NO$_2$) with several benzhydrylium ions **2**, both rate (k_2, Table 2) and equilibrium constants (K, Table 1) have been determined in acetonitrile. The relationship $k_{het} = k_2/K$ can, therefore, be used to calculate the rate constants for the heterolytic cleavages of the corresponding aryl benzhydryl ethers **3** in acetonitrile (Table 4).

The linear correlations between the heterolysis rates (log k_{het}) and the previously reported electrofugalities, E_f, of the benzhydrylium ions **2a–c** in Figure 4 show that eq 7 is applicable. Thus, the intercepts on the abscissa correspond to the nucleofugalities N_f ($N_f = -E_f$ for log k_{het} = 0), and the slopes equal the susceptibilities s_f for the nitrophenolates **1c,d** in acetonitrile (Table 4, right column).

Figure 5 compares the leaving group abilities of the nitrophenolate ions in acetonitrile with those of other nucleofuges. It illustrates that nitrophenolates are weaker nucleofuges in acetonitrile than DABCO and isoquinoline, better nucleofuges than N-methylimidazole (NMI) and DMAP, comparable to the benzoate ion. In other words, benzhydrylium nitrophenolates and benzhydrylium benzoates have similar S$_N$1 reactivities in acetonitrile.[25]

The finding that o-nitrophenolate (**1d**) is a better leaving group in acetonitrile than p-nitrophenolate (**1c**) is surprising at first glance because **1d** is a stronger nucleophile than **1c** (Table 2), and strong nucleophiles are commonly poor nucleofuges. Figure 6 illustrates that o-nitrophenolate (**1d**) reacts faster with **2b** than its *para*-isomer **1c**, though the reaction with the latter is more exergonic. As a consequence, the heterolytic cleavage of **3db** is also faster than the heterolysis of **3cb**.

This behavior reminds us of Bordwell's nitroalkane anomaly[37] and can be explained by Bernasconi's principle of nonperfect synchronization.[38] Steric interactions between the benzhydryloxy group and the vicinal nitro group destabilize **3db** and thus account for the lower exergonicity of the reaction of **2b** with **1d** compared to the reaction with **1c** (see discussion of Table 1). On the other hand, the reaction of the p-nitrophenolate anion **1c** proceeds over a higher intrinsic barrier because it is planar and fully resonance-stabilized.[38] Therefore, a higher degree of electronic rearrangement is needed for reaching the transition state than in the reaction of **1d**, which is less resonance-stabilized as the o-nitro group is not coplanar with the aromatic ring.

DOI: 10.1021/acs.joc.9b01485
J. Org. Chem. 2019, 84, 8837–8858

The Journal of Organic Chemistry Featured Article

Table 2. Second-Order Rate Constants k_2 (20 °C) for the Reactions of the Phenolate Anions 1 with Reference Electrophiles 2a–m in Polar Aprotic Solvents

		k_2 (M^{-1} s^{-1})		
phenolate	2	DMSO	MeCN	DMF
1b-NBu_4 (F_5)	**2e**	no reaction	–	–
	2f	too fast	–	–
1c-NBu_4 (*p*-NO_2)	**2a**	2.01×10^3	1.52×10^4	1.01×10^4
	2b	5.97×10^3	4.12×10^4	2.95×10^4
	2c	2.11×10^4	1.63×10^5	1.00×10^5
	2d	5.07×10^4	4.52×10^5	2.91×10^5
	N (s_N)	14.32 (0.77)	15.14 (0.82)	15.05 (0.80)
1c-K (*p*-NO_2)	**2a**	2.68×10^3	1.70×10^4	1.18×10^4
	2b	6.98×10^3	4.26×10^4	3.14×10^4
	2c	1.96×10^4	1.38×10^5	9.24×10^4
	2d	5.99×10^4	3.93×10^5	2.94×10^5
	2e	2.11×10^5	–	–
	2f	3.67×10^5	–	–
	N (s_N)	14.63 (0.74)	15.67 (0.75)	15.41 (0.76)
1d-NBu_4 (*o*-NO_2)	**2a**	9.10×10^3	4.61×10^4	4.39×10^4
	2b	1.99×10^4	1.07×10^5	1.09×10^5
	2c	3.62×10^4	4.41×10^5	2.88×10^5
	2d	1.41×10^5	1.24×10^6	8.73×10^5
	2e	4.59×10^5	–	–
	N (s_N)	15.48 (0.71)	15.83 (0.80)	16.65 (0.70)
1e-NBu_4 (*m*-NO_2)	**2i**	–	–	no reaction
	2a	1.11×10^6	4.51×10^6	5.03×10^6
	2b	2.94×10^6	8.09×10^6	1.05×10^7
	2c	5.53×10^6	–	–
	N (s_N)	21.29 (0.54)	25.51 (0.43)	22.41 (0.54)
1e-K (*m*-NO_2)	**2a**	1.00×10^6	4.70×10^6	–
	2b	2.41×10^6	–	–
	N (s_N)	19.31 (0.65)	–	–
1f-K (*p*-CN)	**2a**	8.97×10^4	3.85×10^5	4.01×10^5
	2b	2.09×10^5	8.53×10^5	8.04×10^5
	2c	4.80×10^5	–	3.23×10^6
	N (s_N)	18.78 (0.57)	19.58 (0.59)	17.85 (0.71)
1g-NBu_4 (*o*-CF_3)	**2a**	1.48×10^5	6.48×10^5	9.42×10^5
	2b	3.41×10^5	1.55×10^6	2.15×10^6
	2c	9.03×10^5	5.00×10^6	5.20×10^6
	N (s_N)	18.47 (0.61)	18.39 (0.69)	20.37 (0.58)
1h-NBu_4 (*p*-CF_3)	**2a**	4.13×10^5	1.48×10^6	2.15×10^6
	2b	1.22×10^6	3.04×10^6	4.40×10^6
	2c	2.69×10^6	–	–
	N (s_N)	18.98 (0.63)	21.69 (0.53)	22.05 (0.53)
1i-K (*m*-CF_3)	**2a**	2.51×10^6	5.41×10^6	6.65×10^6
	2b	5.01×10^6	–	–
	N (s_N)	22.62 (0.51)	*23.2 (0.51)*[a]	*23.4 (0.51)*[a]
1j-K (*p*-Cl)	**2j**	2.02×10^4	–	–
	2g	2.23×10^4	1.05×10^4	3.95×10^4
	2h	1.42×10^5	1.16×10^5	2.29×10^5
	2i	3.39×10^5	1.73×10^5	4.33×10^5
	2a	4.38×10^6	(1.2×10^7)[b]	1.01×10^7
	N (s_N)	20.34 (0.64)	18.32 (0.82)	19.67 (0.72)
1k-K (H)	**2l**	1.49×10^4	–	–
	2j	1.74×10^4	–	3.13×10^4
	2g	4.34×10^4	2.35×10^4	6.30×10^4
	2k	8.61×10^4	–	–
	2m	7.25×10^4	–	–
	2h	3.28×10^5	2.46×10^5	6.91×10^5
	2i	9.00×10^5	4.67×10^5	1.86×10^6
	2a	7.09×10^6	–	–
	N (s_N)	19.86 (0.71)	18.53 (0.85)	18.86 (0.89)
1l-K (*p*-CH_3)	**2l**	2.54×10^4	–	–
	2j	3.71×10^4	–	7.35×10^4
	2g	1.16×10^5	–	2.38×10^5
	2h	9.17×10^5	–	2.30×10^6
	2i	2.08×10^6	–	3.57×10^6
	N (s_N)	19.08 (0.87)	–	19.65 (0.85)
1m-K (*p*-*t*Bu)	**2j**	4.14×10^4	3.96×10^4	7.72×10^4
	2g	8.48×10^4	4.91×10^4	1.42×10^5
	2h	6.70×10^5	2.98×10^5	1.40×10^6
	2i	1.62×10^6	4.84×10^5	2.82×10^6
	N (s_N)	19.67 (0.79)	21.70 (0.58)	19.90 (0.80)
1n-K (*p*-OMe)	**2j**	1.02×10^5	4.77×10^4	6.44×10^4
	2g	2.45×10^5	1.08×10^5	3.12×10^5
	2h	2.10×10^6	7.75×10^5	2.24×10^6
	2i	4.12×10^6	1.07×10^6	3.04×10^6
	N (s_N)	20.09 (0.80)	20.62 (0.69)	19.90 (0.82)
1q-K (*m*-OMe)	**2g**	–	2.11×10^4	–
	2h	–	1.63×10^5	–
	2i	–	3.71×10^5	–
	N (s_N)	–	18.81 (0.80)	–
1o-K (*o*,*o*′-(*t*Bu)$_2$)	**2a**	3.26×10^6	–	–
	2b	7.30×10^6	–	–
	N (s_N)	21.02 (0.59)	–	–

[a] *N* estimated by using the s_N for **1i** in DMSO. [b] Not used for calculating *N* (and s_N).

Kinetic Investigations: Carbon Attack. The rate constants for carbon attack of benzhydrylium ions at **1d** (*o*-NO_2) were derived from the rates of rearrangement of the initially formed products of O attack into the thermodynamically more stable products of C attack, as illustrated for the isomerization of phenol ether **3da** into the phenol **4da** in Figure 7. For that purpose, **1d** and **2a** were combined in CD_3CN at −40 °C to give the O adduct **3da** selectively. After being warmed to 20 °C, the rate of isomerization was followed by ^1H NMR spectroscopy. Both the disappearance of the benzhydryl ether **3da** and the formation of the triarylmethane **4da** were fitted by monoexponential functions to derive the first-order rate constants k_{iso} (Figure 7).

At the concentrations used, the conversion of **1d** and **2a** to the covalent O adduct **3da** is almost quantitative, and during the isomerization of **3da** → **4da**, the concentrations of **1d** and **2a** are negligible compared to that of **3da**. Therefore, the rate of consumption of **3da** equals the rate of formation of **4da** (eq 8), and the stationary state approximation (eq 9) holds.

$$-d[\mathbf{3da}]/dt = d[\mathbf{4da}]/dt = k_{2C}[\mathbf{1d}][\mathbf{2a}] \quad (8)$$

$$\begin{aligned} d[\mathbf{1d}]/dt &= d[\mathbf{2a}]/dt \\ &= k_{het}[\mathbf{3da}] - (k_2 + k_{2C})[\mathbf{1d}][\mathbf{2a}] \\ &= 0 \end{aligned} \quad (9)$$

$$[\mathbf{1d}][\mathbf{2a}] = k_{het}[\mathbf{3da}]/(k_2 + k_{2C}) \quad (10)$$

DOI: 10.1021/acs.joc.9b01485
J. Org. Chem. 2019, 84, 8837–8858

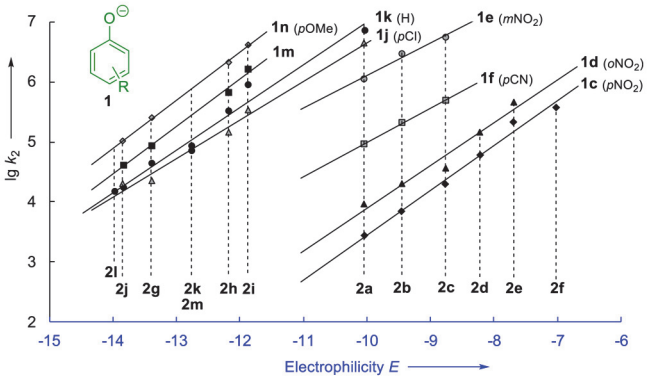

Figure 3. Correlation of log k_2 (from Table 2) for the reactions of phenolate ions **1** with reference electrophiles **2a–m** in DMSO at 20 °C with the electrophilicity parameters E of **2a–m** (see the Supporting Information for individual plots for further **1** + **2** combinations in the solvents used).

Table 3. Second-Order Rate Constants k_2 for the Reactions of the Potassium Phenolate 1l-K with Reference Electrophiles 2a–e (H_2O, 20 °C)

electrophile	k_2 (M^{-1} s^{-1})
2a	2.55×10^2
2b	3.86×10^2
2c	1.15×10^3
2e	4.54×10^3
N (s_N)	14.30 (0.55)

Table 4. Rate Constants for the Heterolytic Cleavages of Benzhydryl Aryl Ethers 3 at 20 °C in MeCN

phenolate	2	K (M^{-1})[a]	k_2 (M^{-1} s^{-1})[b]	k_{het} (s^{-1})	N_f (s_f)
1c (*p*-NO_2)	**2a**	1.89×10^4	1.52×10^4	0.804	−5.20 (0.93)
	2b	1.76×10^4	4.12×10^4	2.34	
	2c	3.86×10^5	1.63×10^5	0.422	
1d (*o*-NO_2)	**2a**	3.73×10^3	4.61×10^4	12.4	−4.23 (1.22)
	2b	2.40×10^3	1.07×10^5	44.6	
	2c	9.73×10^4	4.41×10^5	4.53	

[a]From Table 1. [b]From Table 2.

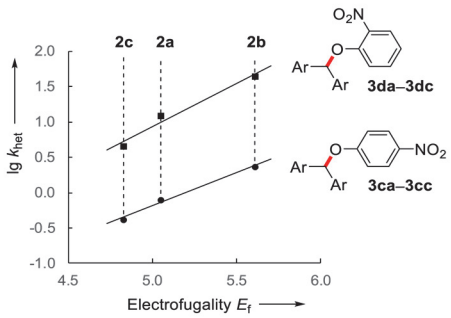

Figure 4. Correlation of log k_{het} for the heterolytic cleavage of the aryl benzhydryl ethers **3** in MeCN at 20 °C (from Table 4) with the electrofugality parameters E_f of **2a–c** (from ref 25).

Application of eq 10 in eq 8 yields eq 11.

$$d[\mathbf{4da}]/dt = k_{2C}k_{het}[\mathbf{3da}]/(k_2 + k_{2C}) \quad (11)$$

As $k_2 \gg k_{2C}$ and $k_{het}/k_2 = 1/K$, eq 11 converts to eq 12.

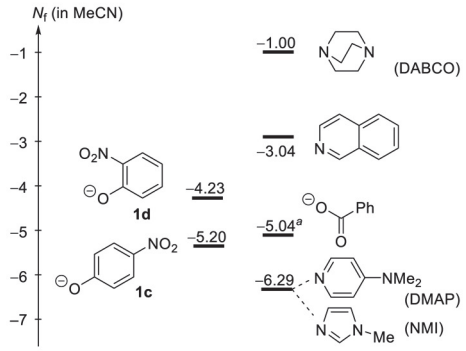

Figure 5. Comparison of the nucleofugality parameters N_f for different nucleofuges (in MeCN, 20 °C). Values from ref 25. [a]Calculated based on rate and equilibrium constants (at 25 °C) from ref 36.

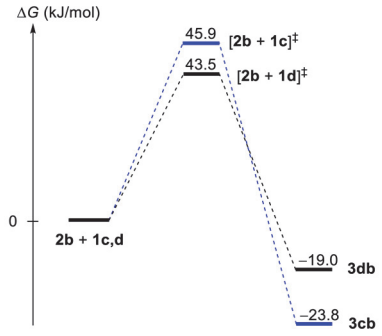

Figure 6. Gibbs energy profiles (20 °C, MeCN) for the reactions (O attack) of the tetrabutylammonium *p*- and *o*-nitrophenolates **1c** and **1d**, respectively, with benzhydrylium tetrafluoroborate **2b**-BF_4 (with data from Table 4).

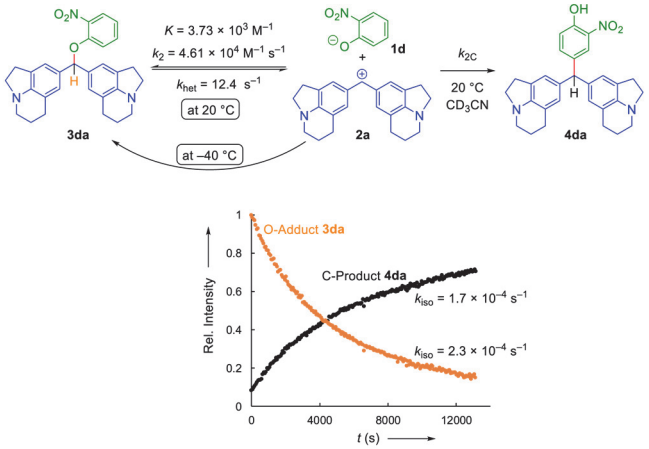

Figure 7. ^{1}H NMR spectroscopic monitoring of the rearrangement of the benzhydryl ether **3da** (c = 2.15 × 10^{-2} M) to the phenol **4da** (CD_3CN, 20 °C).

$$-d[\mathbf{3da}]/dt = d[\mathbf{4da}]/dt = (k_{2C}/K)[\mathbf{3da}] \quad (12)$$

$$k_{iso} = k_{2C}/K \quad (13)$$

According to eq 13, the observed first-order isomerization constant k_{iso} (for the formation of **4**) is independent of any concentrations, in accord with the observation that the same isomerization rate was observed when an additional 0.5 equiv of phenolate **1d** was present during the isomerization of **3da**.

DOI: 10.1021/acs.joc.9b01485
J. Org. Chem. 2019, 84, 8837–8858

In other words, as $k_2 \gg k_{2C}$, the isomerization from **3** to **4** proceeds through a fast pre-equilibrium, corresponding to a Curtin–Hammett situation, in which the observed rate constant equals the product of k_{2C} with the equilibrium constant for the formation of the reactive intermediate.

Analogous isomerization studies of the phenol ethers **3dc** and **3dd** gave rise to rate constants k_{2C} for carbon attack at **1d** by the benzhydrylium ions **2c** and **2d** (Table 5). Comparison with the corresponding rate constants in Table 2 shows that C attack at *o*-nitrophenolate (**1d**) is 10^5 times slower than O attack.

The linear correlation of the second-order rate constants for carbon attack (lg k_{2C}) for the C adduct formation from **1d** (*o*-NO_2) and the benzhydrylium ions **2a**, **2c**, and **2d** (Figure 8) shows the applicability of eq 1 and provides the reactivity parameters $N = 9.8$ and $s_N = 0.67$ for the C-4 position in **1d** (*o*-NO_2).

Low-temperature NMR studies of the reaction of **1o** (*o*,*o*′-(tBu)$_2$) with **2a** (DMF-d_7, −40 °C) showed the fast formation of triarylmethane **4oa** and did not give any indications for the intermediate formation of the phenol ether **3oa**. This observation does not allow us, however, to assign the measured rate constants for the reactions of **1o** with **2a** and **2b** to a carbon attack. Rather, we assume that the measured rate constants in Table 1 refer to O attack because they perfectly match the correlation between log k (O attack) versus basicities of the phenolates (see below). This interpretation is supported by the reported isolation of benzyl ethers when **1o** was heated with benzyl chloride with CsF/Celite as a solid base.[39] As the reaction of **1o** (*o*,*o*′-(tBu)$_2$) with **2a** is only weakly exergonic (−43 kJ mol^{-1} for the reaction of **1o** with the equally Lewis acidic benzhydrylium ion **2b**, Table S2), a fast rearrangement of the initially formed phenol ether **3oa** to the substituted phenol **4oa** appears feasible.

■ DISCUSSION

Influence of the Counterion. Neither exchange of the counterion from potassium to tetrabutylammonium in DMSO, MeCN, and DMF nor addition of 18-crown-6 affected the rate constants for the reactions of phenolates **1c** (*p*-NO_2) and **1e** (*m*-NO_2) by more than factors of 0.85–1.3 (see Table 2). Therefore, we did not pay specific attention to counterion effects. It should be noted, however, that counterion effects become important for the regioselectivities of phenolate electrophile reactions in nonpolar solvents.[1,2,4a,c,5,6]

Solvent Effects on Rate Constants. Figure 9 shows that the second-order rate constants measured in DMSO, MeCN, and DMF are linearly correlated with each other. From the different slopes, one can see that variation of the phenolate structure has the largest effect on the nucleophilicity in DMSO and the smallest on the nucleophilicity in acetonitrile. As a consequence, the ratio of k_{MeCN}/k_{DMSO} shrinks with increasing nucleophilicity of the phenolate from 7.6 for the reaction of **2a** with **1c** to 2.2 for the corresponding reaction with **1i** (Table 2). This trend continues when moving to even more nucleophilic phenolates, and Table 2 shows that donor-substituted phenolates react even slightly faster in DMSO than in acetonitrile.[40]

Whereas the rate constants in DMSO, acetonitrile, and DMF differ by less than 1 order of magnitude (Figure 10 left), the reactions in water are much slower. Though we cannot find a reference electrophile, which provides a direct comparison of the reactivities of phenolates in aprotic solvents and water, the extrapolations in Figure 10 (right) indicate that phenolates react 5–7 orders of magnitude more slowly in water than in DMSO.

General Structure–Reactivity Relationships. Brønsted basicities in DMSO, acetonitrile, and DMF have been reported

Table 5. Rate Constants k_{2C} for the Attack of Benzhydrylium Ions at C-4 of Phenolate 1d (20 °C, CD_3CN, Determined by ^{1}H NMR Spectroscopy)

electrophile	K (M^{-1})	k_{iso} (s^{-1})	k_{2C} (M^{-1} s^{-1})[a]
2a	3.73×10^3	1.7×10^{-4}	0.63
2c	9.73×10^4	5.6×10^{-5}	5.4
2d	9.77×10^{4b}	1.0×10^{-4}	9.8

[a]Calculated using eq 13. [b]Calculated from LB for **1d** (Table 1) and LA for **2d** (Chart 2) using eq 2.

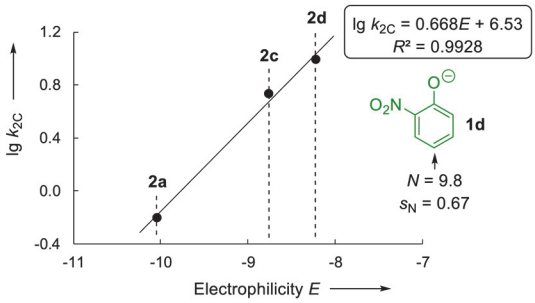

Figure 8. Correlation of the second-order rate constants k_{2C} for attack of benzhydrylium ions **2** at C-4 of **1d** with the corresponding electrophilicity parameters E.

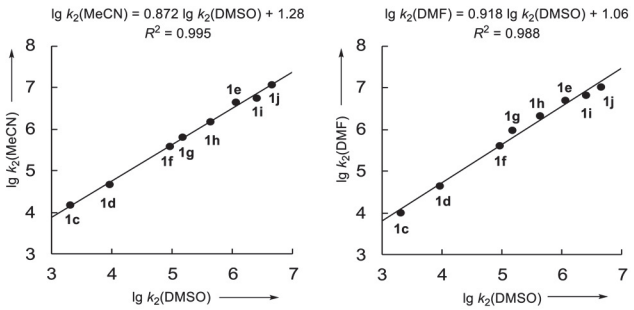

Figure 9. Correlation of log k_2 for the reactions of different phenolate ions **1** with benzhydrylium ion **2a** in acetonitrile (left) and DMF (right) with log k_2 for the corresponding reactions in DMSO.

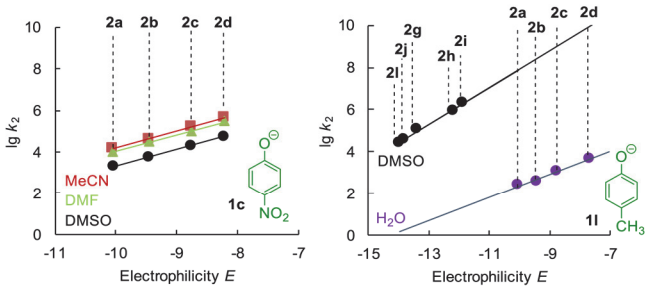

Figure 10. Comparison of log k_2 for the reactions of the phenolate ions **1c** (left) and **1l** (right) with a series of reference electrophiles **2** at 20 °C in different solvents.

DOI: 10.1021/acs.joc.9b01485
J. Org. Chem. 2019, 84, 8837–8858

The Journal of Organic Chemistry Featured Article

for the majority of phenolates studied in this work (Table 6 and Table S1).[33,41]

Figure 11A illustrates that the second-order rate constants for the reactions of phenolates with **2a** (k_2 in DMSO, from Table 2) correlate linearly with the Brønsted basicities (pK_{aH}) of the phenolates (Brønsted α = 0.50). The corresponding Brønsted correlation in DMF has a similar slope (0.52) but has a smaller slope in MeCN (0.40) (Figure S2). The significantly lower quality (R^2 = 0.795 and 0.781) of the Brønsted correlations in DMF and MeCN is in part due to the fact that fewer pK_{aH} values are available in these solvents than for DMSO.

Figure 11B shows that the second-order rate constants for the reactions of phenolates with the benzhydrylium ion **2a** in DMSO are linearly correlated with quantum chemically calculated HOMO energies of the phenolates. The second-order rate constants (log k_2) furthermore correlate linearly with Hammett substituent parameters σ_p^- or σ_m (ρ = −2.65 in DMSO, −1.66 in MeCN, and −2.36 in DMF), as illustrated in Figure S4. The different reaction constants ρ in these solvents are partially due to the fact that the substrates used in the different solvents are not identical.

Reactivity Ordering toward Other Types of Electrophiles. Due to the UV−vis absorbances of **1** at 299−502 nm (Supporting Information), the rates for the O-benzylation of acceptor-substituted phenolates with benzyl bromide could also be measured photometrically. The rate constants for the reactions of the *para*-substituted phenolates correlate linearly with the reactivities toward benzhydrylium ion **2a** (Figure 12), and the slope of this correlation (0.97) shows that variation of the phenolate ions has almost the same effect on the rates of the reactions with benzhydrylium ions as on their S_N2 reactivities toward benzyl bromide. The rate constants of the reactions of phenolate ions with *n*-butyl chloride in DMSO measured by Cripe and Bordwell[42] also follow a linear correlation (with log k_2(**2g**)) with similar slope (0.97) as depicted in Figure S5.

Analogous correlations with the reactivities toward reference electrophiles (Table 2) are shown in Figures S6−S8 for the reactions of phenolates with Ph_3SiF in DMSO[43] (slope 0.94)

Table 6. Parameters for Phenolates Used in Figure 11 for the Correlations in DMSO

phenolate	k_2 (M^{-1} s^{-1})[a]	pK_{aH}[b]	$\sigma_{p/m}$[c]	ε_{HOMO}[d]
1c (*p*-NO_2)	2.01 × 10^3	10.8	1.27	−0.10236
1d (*o*-NO_2)	9.10 × 10^3	11.0		−0.09712
1e (*m*-NO_2)	1.11 × 10^6	14.4	0.71	−0.08473
1f (*p*-CN)	8.97 × 10^4	13.2	1.00	−0.08715
1g (*o*-CF_3)	1.48 × 10^5	14.4		−0.07913
1h (*p*-CF_3)	4.13 × 10^5	15.2	0.65	−0.08235
1i (*m*-CF_3)	2.51 × 10^6	15.6	0.43	−0.07478
1j (*p*-Cl)	4.38 × 10^6	16.75	0.19	−0.06464
1k (H)	7.09 × 10^6	18.0	0	−0.05257
1l (*p*-CH_3)	7.32 × 10^7	18.9	−0.17	−0.04942
1m (*p*-*t*Bu)	4.05 × 10^7	19.05	−0.15	−0.05533
1n (*p*-OMe)	1.10 × 10^8	19.1	−0.26	−0.04541
1o (*o*,*o*′-(*t*Bu)$_2$)	3.26 × 10^6	17.3		−0.06727

[a]For the reaction with **2a** from Table 2 or calculated (**1l**−**n**) by eq 1. [b]From ref 41a; for **1d** from ref 41b, for **1g** from ref 41c. [c]Hammett substituent constants σ_p^- and σ_m from ref 13. [d]In Hartree, calculated in gas phase, at the M06-2X/6-31+G(d,p) level (this work).

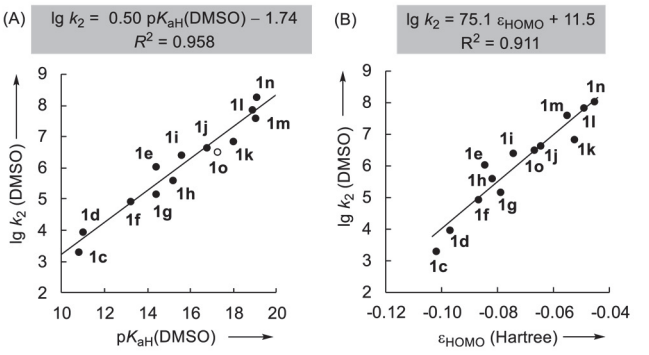

Figure 11. Correlations of the rate constants for the reactions of phenolate ions (**1**) with the benzhydrylium ion **2a** in DMSO at 20 °C (the rates for **1l**−**n** were calculated using eq 1) (A) with experimental pK_{aH} values in DMSO (from ref 41) and (B) with ε_{HOMO} (this work, gas phase, at the M06-2X/6-31+G(d,p) level) of phenolates (analogous correlations for DMF and MeCN are depicted in Figure S3).

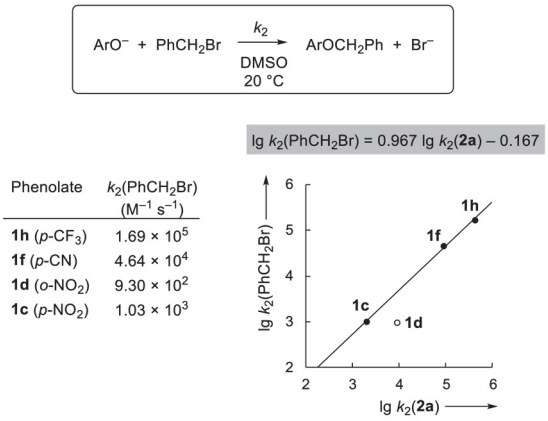

Figure 12. Correlation of the rate constants (log k_2) of the reactions of phenolates with benzyl bromide with those for the reactions with benzhydrylium ion **2a** in DMSO at 20 °C; data for **1d** (*o*-NO_2) not used for the correlation.

and acetonitrile (slope 0.41) as well as for the nucleophilic aromatic substitutions of 2,6-dimethyl-4-nitro-X-benzenes with phenolates in DMSO (for X = F, slope = 1.33; X = Cl, slope = 1.56, X = Br, slope = 1.53).[44]

Figure 12 furthermore shows that benzyl bromide reacts with similar rates with the *ortho*- and *para*-nitro-substituted phenolates **1d** and **1c**, unlike benzhydrylium ions **2**, which react faster with **1c** for the reasons discussed above (cf. Figures 4−6). Probably it is the greater steric constraint in the S_N2 transition state of the reaction of *ortho*-nitrophenolate (**1d**) with benzyl bromide, which compensates the factors that account for the higher reactivity of **1d** toward benzhydrylium ions (Figures 4 and 6).

Polar versus Electron Transfer Mechanism. In line with the correlation of the nucleophilic reactivities of the phenolates with ε_{HOMO} shown in Figure 11B, the rate constants for the reactions of phenolate anions **1** with **2a** in DMSO also correlate linearly with the one-electron oxidation potentials of **1** in DMSO determined by Bordwell[41a] and co-workers (Figure 13) and Arnett's oxidation potentials[45] in sulfolane/3-methylsulfolane 95/5 (Figure S9).

Though this correlation might be interpreted as an indication of a rate-determining single-electron transfer

DOI: 10.1021/acs.joc.9b01485
J. Org. Chem. 2019, 84, 8837−8858

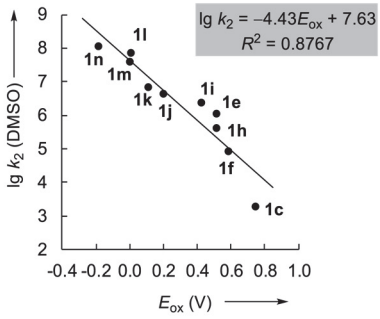

Figure 13. Correlation of the rate constants (log k_2) of the reactions of phenolates **1** with the benzhydrylium ion **2a** with the irreversible oxidation potentials E_{ox} of **1** (vs SCE[46] in DMSO, 25 °C, from ref 41a).

(SET), consideration of the energetics allows us to exclude the SET mechanism (Figure 14).

The reported one-electron oxidation potentials E_{ox} for phenolates[41a,45] and one-electron reduction potentials E°_{red} for benzhydrylium ions and quinone methides[47] allow one to calculate the Gibbs energy of electron transfer by eq 14.

$$\Delta G^{\circ}_{ET} = F(E_{ox} - E_{red}) \quad (14)$$

Figure 15 shows that the Gibbs energies ΔG°_{ET} for single-electron transfer from a series of phenolates **1** to benzhydrylium ion **2a** are much larger than the observed Gibbs activation energies $\Delta G^{\ddagger}_{obs}$ for the reactions of the phenolates with this electrophile. As $\Delta G^{\ddagger}_{ET} > \Delta G^{\circ}_{ET}$ (Figure 14), one can unequivocally rule out that the investigated reactions proceed via SET processes.

Quantum Chemical Analysis. We found a good agreement between experimental and quantum mechanically calculated activation Gibbs energies for O attack at the SMD(MeCN)/M06-2X/6-31+G(d,p)[48,49] level (Table 7), which was then applied to calculate also the reaction Gibbs energies for electrophilic C attack.

Table 7 shows the reactions of **2b** with phenolates **1** in which the calculated activation barriers for O attack agree with the directly measured values of $\Delta G^{\ddagger}(O)$ within 4 kJ mol^{-1}. Though the quantum chemically calculated reaction Gibbs energies $\Delta_r G^0(O)$ are approximately 13 kJ mol^{-1} more negative than the experimental values, their relative magnitudes appear to be correct as they accurately reproduce the unexpected observation (Figure 6) that **1c** (*p*-NO_2) is a

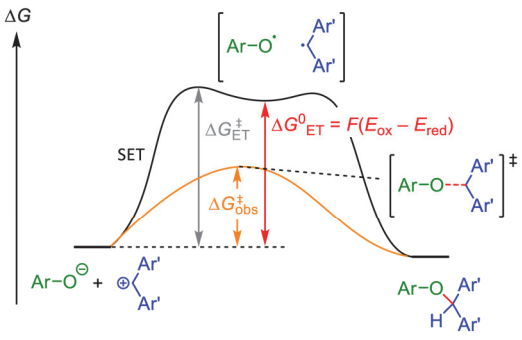

Figure 14. Energy profiles for polar and SET mechanisms for the reactions of phenolates **1** with benzhydrylium ions **2**.

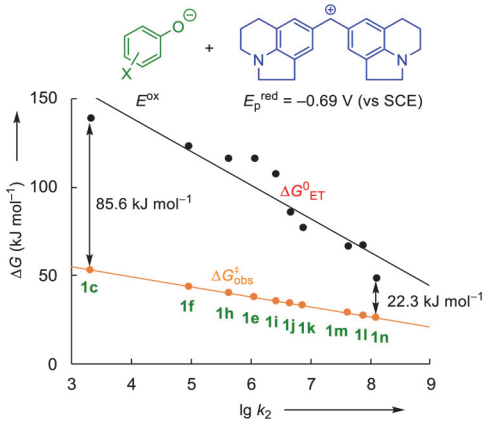

Figure 15. Comparison of the calculated Gibbs energies for electron transfer (ΔG°_{ET}) with the experimentally observed Gibbs energies of activation ($\Delta G^{\ddagger}_{obs}$) for the reactions of phenolates **1** with **2a** (E°_{ox} for **1** from ref 41a and corrected to SCE by subtracting 440 mV as outlined in ref 46; E_{red}(**2a**) = −0.69 V in DMSO, vs SCE, this work).

stronger Lewis base [$\Delta_r G^0(O)$] but a weaker nucleophile [$\Delta G^{\ddagger}(O)$] than **1d** (*o*-NO_2).

The energy profiles in Figure 16 illustrate the ambident reactivity of phenolate ions toward benzhydrylium ion **2b**. For all phenolates described in Figure 16, the activation barrier for oxygen attack is 20−30 kJ/mol lower than that for carbon attack, in line with the observation that oxygen attack was generally observed as the kinetically preferred mode of reaction.

A major reason for the smaller barrier for O attack is the fact that the phenol ethers **3** are 44−67 kJ mol^{-1} more stable than the corresponding cyclohexadienones, which are even endergonic products [$\Delta_r G^0(C)$] in reactions with acceptor-substituted phenolates (**1c**, **1d**, and **1f** in Figure 16).

In the case of **1d** and **1k**, that is, phenolates with free *para*-positions, C_{para} attack is calculated to have 3−5 kJ mol^{-1} lower barriers than C_{ortho} attack (Table 7, not shown in Figure 16 for the sake of clarity). In agreement with these calculations, the experiments described in Scheme 3 show that rearrangement of the phenol ether **3da** yields the *para*-substituted phenol **4da**.[50]

Tautomerization of the cyclohexadienones yields phenols **4**, which are 60−111 kJ mol^{-1} more stable than the corresponding cyclohexadienones. This difference is largest for the nitro-substituted compounds because of push−pull stabilization of the resulting phenols and smallest for the 3-methoxy derivative **4qb** because of conjugative stabilization of the corresponding methoxy-substituted cyclohexadienone. All phenols **4** listed in Table 7 are 33−56 kJ mol^{-1} more stable than the isomeric phenol ethers **3** and thus are the thermodynamic sinks of these reactions (see also the illustration in Figure 16).

As the tautomerizations of the cyclohexadienones to the phenols **4** are fast processes due to catalysis by traces of bases (e.g., phenolate ions), the rate-determining step for the isomerization of **3** → **4** is the attack of the benzhydrylium ion at a ring carbon of the phenolate. As discussed above in the context with Figure 7 and eqs 8−13, the activation energy for this isomerization is given by $-\Delta_r G^0(O) + \Delta G^{\ddagger}(C)$ and listed in the last column of Table 7. Interpolation of the data in Table 5 gives a rate constant for the rearrangement of **3db** of 7.15 × 10^{-4} M^{-1} s^{-1}, which corresponds to a barrier of 89.4 kJ

DOI: 10.1021/acs.joc.9b01485
J. Org. Chem. 2019, 84, 8837−8858

The Journal of Organic Chemistry Featured Article

Table 7. Quantum Chemically Calculated Reaction Gibbs Energies Δ_rG^0 and Activation Gibbs Energies $\Delta G^{\ddagger}$ for the Reaction of 2b with Different Phenolates in Acetonitrile (kJ mol^{-1}) at the SMD(MeCN)/M06-2X/6-31+G(d,p) Level of Theory

phenolates	O attack				C attack (*ortho*)			C attack (*para*)			isomerization	
	$\Delta G^{\ddagger}$(O)		Δ_rG^0(O)								$\Delta G^{\ddagger}$ (3→4)[a]	
	calcd	exptl[b]	calcd	exptl[c]	$\Delta G^{\ddagger}$(C)	Δ_rG^0(C)	Δ_rG^0(P)	$\Delta G^{\ddagger}$(C)	Δ_rG^0(C)	Δ_rG^0(P)	4_{ortho}	4_{para}
1c (*p*-NO_2)	49	46	−36	−24	78	31	−73				114	
1d (*o*-NO_2)	44	44	−33	−19	78	26	−85	73	19	−89	111	106
1f (*p*-CN)	42	38	−50	*d*	70	18	−85				120	
1k (H)	29	(28)[e]	−80	*d*	52	−28	−119	49	−32	−119	132	129
1n (*p*-OMe)	21	(29)[e]	−89	*d*	40	−45	−127				129	
1q (*m*-OMe)	27	(30)[e]	−79	*d*	*f*	*f*	*f*	37	−52	−112		116

[a] $\Delta G^{\ddagger}(\mathbf{3} \rightarrow \mathbf{4}) = \Delta G^{\ddagger}(C) - \Delta_rG^0(O)$. [b] Calculated from rate constants in Table 2 by applying the Eyring equation. [c] Calculated from the equilibrium constants *K* in Table 1. [d] Could not be determined experimentally. [e] Calculated using eq 1, *N* (and s_N) from Table 2, and *E*(**2b**) from Chart 2. [f] Not determined.

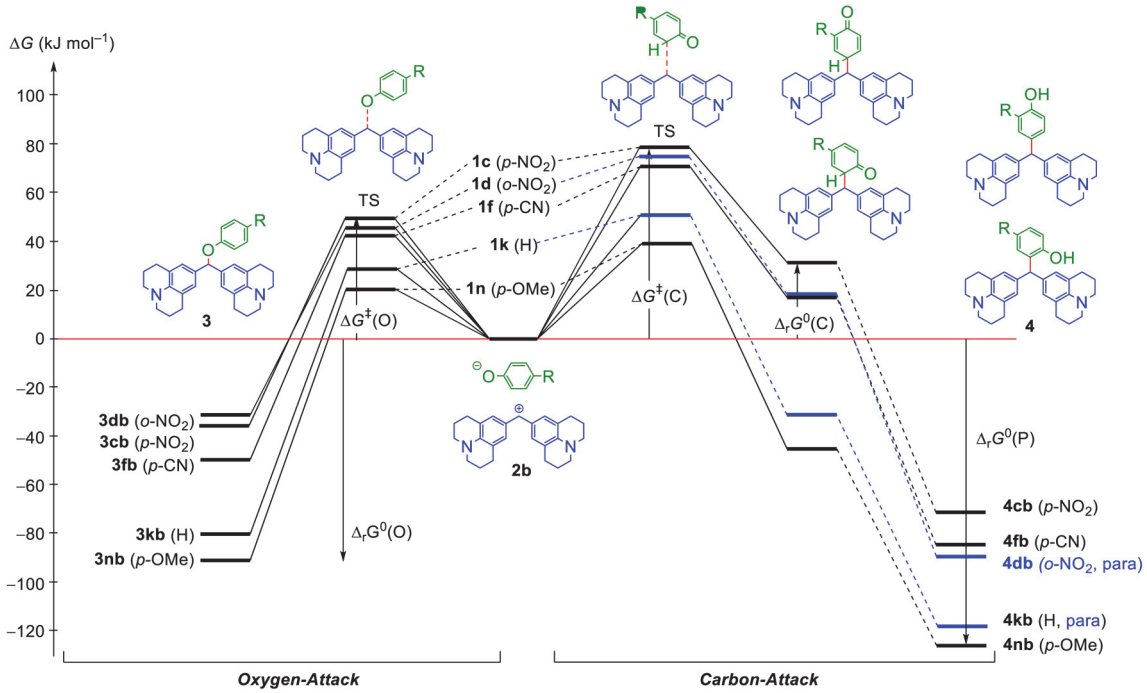

Figure 16. Energy profiles for the competing oxygen and carbon attack (*para* attack: blue pathway) in the reaction of phenolate ions with **2b** calculated at the SMD(MeCN)/M06-2X/6-31+G(d,p) level of theory at 298 K.

mol^{-1}. The quantum chemically calculated barrier (106 kJ mol^{-1}, Table 7) is 17 kJ mol^{-1} higher due to the fact that the calculated activation energies are about 3 kJ mol^{-1} greater and the calculated reaction energies are about 12−14 kJ mol^{-1} more negative than the experimental values (see left part of Table 7).

According to the right column of Table 7, the calculated isomerization barrier of phenol ether **3db** formed from 2-nitrophenol (106 kJ mol^{-1}) is the smallest of all systems investigated. For all other phenol ethers of Table 7 and Figure 16, the barrier of rearrangement is at least 8 kJ mol^{-1} greater than that of the 2-nitrophenol derivatives, which corresponds to a factor of 23 at 20 °C. As Figure 7 shows an experimental first-order rate constant of k_{iso} = 1.7 × 10^{-4} s^{-1} for the rearrangement of the 2-nitrophenol ether **3da** to the C-substitution product **4da** (that is, a half-life of about 1 h), one can derive half-lives of more than a day for the rearrangements of the other phenol ethers **3Xa** and thus rationalize why none of the phenol ethers in Scheme 2 was observed to isomerize at room temperature.

We can, therefore, conclude that thermodynamic control, that is, rearrangements of phenol ethers into substituted phenols, will not take place at room temperature during the reactions of phenolates **1** with carbenium ions that are less stabilized than systems with LA > −7.5 (exception: **1o** and related structures). For that reason, the regioselectivities reported in the following section reflect the results of kinetic control.

Regioselectivities in Kinetically Controlled Reactions of Phenolate Ions with Electrophiles. Treatment of tetrabutylammonium phenolate **1k**-NBu_4 with benzhydrylium tetrafluoroborate **2o**-BF_4 or diarylchloromethanes (**2n−u**)-Cl in acetonitrile at room temperature either gave the aryl benzhydryl ethers **3** exclusively or led to mixtures of **3** with the phenols **4**, as specified in Table 8.

One can see that the least electrophilic benzhydrylium ion of this series (**2o**) as well as the diarylchloromethanes **2t**-Cl and

DOI: 10.1021/acs.joc.9b01485
J. Org. Chem. 2019, 84, 8837−8858

The Journal of Organic Chemistry Featured Article

Table 8. Reactions of Benzhydryl Chlorides with Tetrabutylammonium Phenolates 1-NBu$_4$: Ratio of O versus C Attack (3:4, Sites of C Attack Not Differentiated) for the Reactions of Phenolates 1 with Benzhydryl Chlorides in CD_3CN and Product Mixtures from the Intermolecular Competition between Equimolar Amounts of the Phenolates 1d and 1k for Different Benzhydryl Chlorides

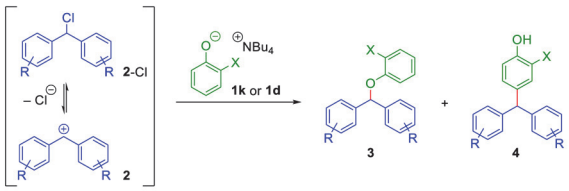

Electrophile		E(**2**)[a]	Product Ratio **3**:**4**[b] for reactions with **1k** (X = H)	Product Ratio **3**:**4**[b] for reactions with **1d** (X = NO_2)	Intermolecular competition **1k** vs. **1d**	
					Ratio[b] of **1k**- vs **1d**-derived ethers **3kX**/**3dX**	Ratio of **1k**- vs **1d**-derived products[c]
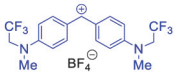	**2o**-BF_4	–3.85	100:0	100:0	86:14	86:14
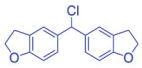	**2p**-Cl	–1.36	83:17	100:0	43:47	52:47
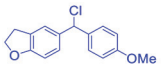	**2q**-Cl	–0.81	78:22	98:2	33:56	42:57
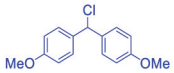	**2r**-Cl	0	78:22	94:6	25:58	32:62
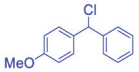	**2s**-Cl	2.11	46:54	78:22	22:46	48:59
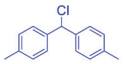	**2n**-Cl	3.63	85:15	84:16	47:36	55:43
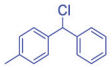	**2t**-Cl	4.43	100:0	100:0	78:22	78:22
	**2u**-Cl	5.47	100:0	100:0	93:7	93:7
	**2u**-OTs	5.47	43:57	76:24	--	--

[a]Electrophilicities E from ref 24b. [b]Analyzed by ^{1}H NMR spectroscopy. [c]Calculated from ratios of the benzhydryl ethers obtained from competing **1k** and **1d** (column 5) combined with the **3**/**4** ratios (columns 3 and 4 for reactions of **1k** and **1d**, respectively) to account for additional C attack.

2u-Cl, derived from the most electrophilic benzhydrylium ions, reacted with exclusive O attack (formation of the ethers **3**), whereas the benzhydrylium derivatives between gave mixtures arising from O and C attack. A similar behavior was found when 2-nitrophenolate (**1d**) was treated with these benzhydryl derivatives under the same conditions (Table 8).

An explanation for this behavior is given in Figure 17. The least electrophilic benzhydrylium ion **2o** reacts with diffusion control at oxygen of phenolate **1k**, whereas C attack is still considerably slower with the consequence that benzhydryl ether **3ko** is the only observable product. When more electrophilic carbenium ions are generated as intermediates of the S_N1 reactions of the benzhydryl chlorides **2**-Cl, C attack also approaches diffusion control with the consequence that O attack becomes accompanied by C attack, and one obtains mixtures of **3** and **4**. The exclusive formation of phenol ethers **3** from **1k** and **2t**-Cl or **2u**-Cl indicates that the S_N1 mechanism has become so slow that now the S_N2 mechanism is dominating, where only the more nucleophilic phenolate oxygen is reacting. As TsO^- is a 10^4–10^5-fold better nucleofuge than Cl^- in various solvents,[25] benzhydryl tosylate

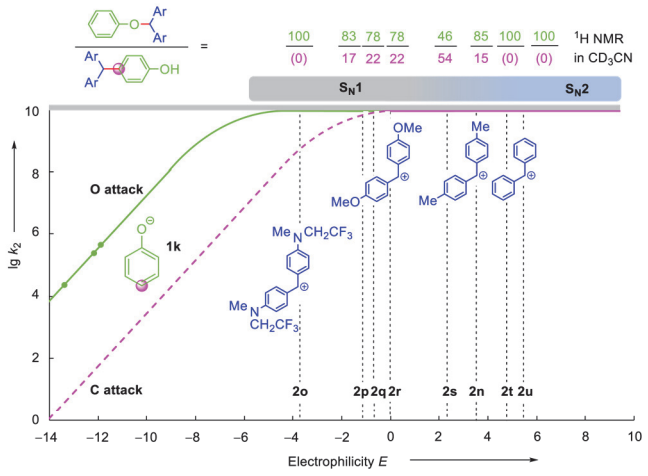

Figure 17. Plot of log k_2 (MeCN, 20 °C) for O and C attack of benzhydryl cations **2** at the parent phenolate ion **1k** versus the electrophilicities E (Table 2; rate constants for C attack calculated from relative barriers for O and C attack in Table 7).

DOI: 10.1021/acs.joc.9b01485
J. Org. Chem. 2019, 84, 8837–8858

2u-OTs again reacts through an S_N1 mechanism, and O and C attack proceed with comparable rates (last line of Table 8). Comparable amounts of phenol ethers (O attack) and substituted phenols (C attack) have previously been observed in the diffusion-limited reactions of the phenolate ion **1k** with in situ generated 1-(4-methoxyphenyl)ethyl cation in trifluoroethanol/water.[15]

To support this interpretation, we investigated the kinetics of the reactions of *o*-nitrophenolate (**1d**) with the diarylchloromethanes **2q**-Cl and **2r**-Cl under pseudo-first-order conditions, using **1d** in high excess. As depicted in Figure 18A, the pseudo-first-order rate constants were independent of the concentration of the nucleophile **1d**, in line with the operation of an S_N1 mechanism. The 7-fold faster reaction of **2q**-Cl relative to **2r**-Cl also shows that the relative reactivities reflect the relative ionization rates of these diarylchloromethanes and not the relative electrophilicities of the corresponding benzhydrylium ions.

Evidence for rate-determining ionization of the diarylchloromethanes followed by diffusion-controlled reactions of the benzhydrylium ions with the phenolates comes from Figure 18B, which shows that *o*- and *p*-nitrophenolates **1d** and **1c**, respectively, react equally fast with **2q**-Cl and **2r**-Cl, though **1d**-NBu_4 is a stronger nucleophile than **1c**-NBu_4.

Analogous kinetic experiments with the less rapidly ionizing diarylchloromethanes were hampered by the long reaction times.[51] For that reason, we employed the intermolecular selectivities k_2(**1k**)/k_2(**1d**) to investigate the change from the S_N1 to the S_N2 mechanism.

As shown in the last column of Table 8 and illustrated in Figure 19, the least electrophilic carbenium ion of this series, **2o**, reacts 7 times faster with the parent phenolate **1k** than with **1d** (*o*-NO_2) because the latter reaction is not yet diffusion-controlled. The comparable reactivities of **1k** and **1d** toward (**2n**,**p**−**s**)-Cl, which cover a reactivity range of $-1.36 < E < 3.63$ in S_N1-type reactions, indicate diffusion-controlled reactions of both phenolates toward the carbenium ions **2n**,**p**−**s** formed as intermediates of S_N1 reactions. The slightly lower reactivity of the more nucleophilic phenolate ion **1k** may be due to its tighter solvent shell, which has to be penetrated for the reaction. The significant increase of the product ratios **3kt**/**3dt** and **3ku**/**3du** in the reactions with **2t**-Cl and **2u**-Cl indicates the switchover to the S_N2 mechanism, where it can be assumed that the relative reactivities of the phenolates **1k** and **1d** are again controlled by their nucleophilicities.

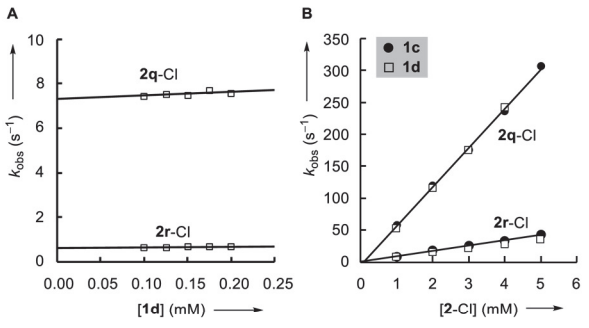

Figure 18. (A) Kinetics for the reactions of phenolate **1d** (*o*-NO_2) with the benzhydryl chlorides **2q**-Cl and **2r**-Cl in acetonitrile at 20 °C by following the disappearance of the phenolate ion **1d**. Ionic strength maintained with Bu_4NBF_4 to 0.2 mM. (B) Reactions of the phenolates **1c** (*p*-NO_2) and **1d** (*o*-NO_2) with varying concentrations of benzhydryl chlorides (MeCN, 20 °C).

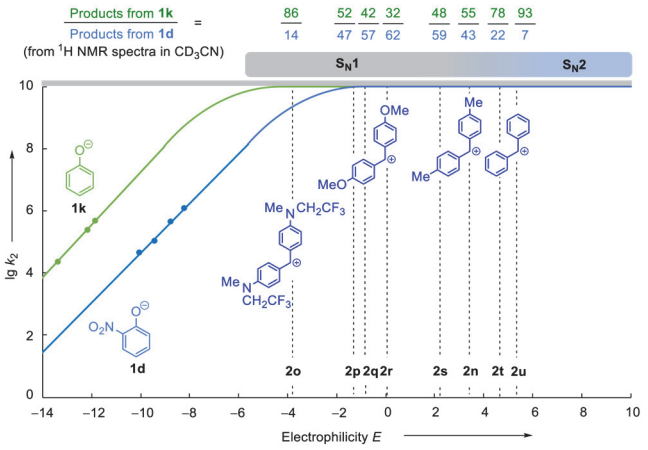

Figure 19. Plot of log k_2 (MeCN, 20 °C) for the attack of benzhydrylium ions **2** at the oxygen of phenolate ions **1k** and **1d** (Table 2) versus the electrophilicities *E* (Table 8).

■ CONCLUSION

Our product studies as well as comprehensive kinetic and equilibrium measurements agree with the early work by Kornblum,[4] who showed that allylations and benzylations of phenolates, which proceed via S_N2 mechanisms, give exclusively products of O attack in most solvents. We conclude, therefore, that the prediction of the principle of hard and soft bases, "changing from S_N1 to S_N2 conditions should favor C attack by phenolate ions"[11] is misleading.

Also the reactions of phenolate ions with benzhydrylium ions (typical S_N1-type electrophiles) in DMSO, MeCN, and DMF proceed with O attack and follow second-order kinetics. The resulting second-order rate constants correlate with Hammett's σ_p^- (and σ_m) parameters as well as with the Brønsted basicities (pK_{aH}, Figure 11A), the electrochemical oxidation potentials (E_{ox}, Figure 13), and the energies of the highest occupied molecular orbitals (ε_{HOMO}, Figure 11B). Comparison of the measured activation Gibbs energies with the Gibbs energies for electron transfer showed that all reactions investigated in DMSO proceed by polar processes and not by SET mechanisms (Figure 15).

From the linear correlation of log k_2 with the electrophilicity parameters *E* of the benzhydrylium ions (Figure 3), we derived the *N* and s_N parameters of the phenolate ions **1** in three polar aprotic solvents (DMSO, MeCN, and DMF) according to eq 1, which can be used to calculate rate constants for their reactions with more than 300 electrophiles whose *E* parameters are available in our database.[24b]

In some cases, equilibrium constants for the formation of phenol ethers **3** from phenolates **1** and benzhydrylium ions **2** could be measured (Table 1), which allowed us to determine the Lewis basicities LB (with respect to C-centered Lewis acids) of some phenolate ions and compare them with those of other classes of Lewis bases. Nucleofugalities (less precisely, leaving group abilities) of nitro-substituted phenolate ions were derived as the ratio of forward rate constant over equilibrium constants and compared with those of other nucleofuges (Figure 5).

Our observation that phenol ethers are always the exclusively formed products in kinetically controlled reactions

DOI: 10.1021/acs.joc.9b01485
J. Org. Chem. 2019, 84, 8837−8858

with weak electrophiles (Scheme 2) is in agreement with quantum chemical calculations at the SMD(MeCN)/M06-2X/6-31+G(d,p) level (Table 7 and Figure 16). These calculations show that, for all phenolates investigated, the barrier for O attack is 20−30 kJ mol^{-1} lower than the barrier for C attack, mostly due to the fact that the phenol ethers **3** are 44−67 kJ mol^{-1} more stable than the isomeric cyclohexadienones, the initial products formed by C attack.

Because the tautomerizations of the cyclohexadienones are highly exergonic to give the phenols **4**, which are 33−56 kJ mol^{-1} more stable than the phenol ethers **3**, C attack is generally preferred under conditions of thermodynamic control.

In a few cases, the rate of isomerization of the phenol ethers **3** into the phenols **4** could be measured (Table 5 and Figure 8). As the barrier for this isomerization corresponds to the sum of the negative Gibbs energy of formation of the phenol ether $[-\Delta_rG^0(O)]$ and the activation Gibbs energy of C attack $[\Delta G^{\ddagger}(C)]$, it was possible to derive an experimental value for the barrier of C attack and compare it with the computational value.

On the basis of these data, one can explain the change of regioselectivities in reactions of phenolate ions with electrophiles (Figure 17). Because the phenolate oxygen has a nucleophilicity much higher than that of the ring carbons, O attack occurs exclusively with weakly electrophilic carbocations, which may be used as stable salts or generated as intermediates of S_N1 reactions. Increasing electrophilicity (less precise, decreasing stabilization) of the intermediate carbocations of S_N1 reactions leads to a reduction of selectivity, and O and C attack proceed with similar rates when eq 1 predicts diffusion-limited reactions at both positions. Further decrease of "carbocation stability" (electrofugality) results in a change from the S_N1 to the S_N2 mechanism and increasing O attack, opposite to the HSAB predictions. Combination of rate and equilibrium constants, furthermore, allowed us to rationalize the change from kinetic to thermodynamic control, under which C attack is preferred.

■ EXPERIMENTAL SECTION

Commercial reagents and dry solvents (stored over molecular sieves) were used without further purification as purchased from Sigma-Aldrich or Acros Organics.

For thin-layer chromatography, silica gel plates with a F-254 fluorescence indicator (Merck) were used. Purification by flash column chromatography was performed using Merck silica gel 60 (0.040−0.063 mm) with freshly distilled solvents.

Melting points were acquired using a Büchi melting point B-560 device and are not corrected.

Nuclear magnetic resonance (NMR) spectra were acquired on 300 or 400 MHz spectrometers. The following abbreviations and their combinations are used when reporting NMR data: s = singlet, d = doublet, t = triplet, q = quartet, m = multiplet, br s = broad singlet. NMR signals were assigned based on information from additional 2D NMR experiments (COSY, gHSQC, gHMBC, NOESY); for the numbering of atoms in a certain molecule, see Supporting Information. Chemical shifts are given in parts per million. Internal reference was set to the residual solvent signals (for $CDCl_3$, δ_H = 7.26, δ_C = 77.16; for CD_2Cl_2, δ_H = 5.32, δ_C = 54.00; for CD_3CN, δ_H = 1.94, δ_C = 1.320; for DMSO-d_6, δ_H = 2.50, δ_C = 39.52; for DMF-d_7, δ_H = 2.92, δ_C = 39.52). The ^{13}C NMR spectra were recorded under broadband proton decoupling. ^{19}F NMR spectra (376 MHz) were recorded without decoupling and are not referenced.

Infrared (IR) spectra were acquired on a PerkinElmer Spectrum BX-59343 instrument with a Smiths Detection DuraSamplIR II Diamond ATR sensor for detection in the range of 4500−600 cm^{-1} as a film for liquids or neat for solids.

High-resolution mass spectra (HRMS) were recorded on a Finnigan MAT 90, a Finnigan MAT 95, a Thermo Finnigan LTQ FT Ultra Fourier transform ion cyclotron resonance or a Q-Exactive GC Orbitrap GC/MS. For ionization of the samples, either electron-impact ionization (EI) or electrospray ionization (ESI) was applied.

For cyclic voltammetry, the reduction potential of benzhydrylium ion **2a** was determined on a CH Instruments 630E electrochemical analyzer using a 2 mm diameter platinum working electrode, a platinum wire counter electrode, and a Ag wire pseudoreference electrode. Cyclic voltammetry measurements at a scan rate of 0.1 V/s were performed in deaerated DMSO containing 0.1 M NBu_4ClO_4 with **2a**-BF_4 (c = 3.3 × 10^{-4} M) and ferrocene (c = 3.3 × 10^{-4} M) as an internal standard. The $E_{1/2}(fc^+/fc$ in DMSO) = +0.435 V (from ref 46) was used to calibrate E_p^{red} (**2a** in DMSO) versus SCE.

Synthesis of Phenolate Salts. *General Procedure A (GPA):* Equimolar amounts of the phenol and KOH were dissolved in H_2O, if necessary with the help of heating or sonication. Subsequently, water was removed under vacuum. The product was dried with the help of careful heating under vacuum (0.1−0.01 mbar).

General Procedure B (GPB): The phenol (1.5 equiv) and KOH (1 equiv) were dissolved/suspended in H_2O. The mixture was extracted with diethyl ether (3×) to remove excess phenol. Subsequently, water was removed under vacuum. The product was dried with the help of careful heating under vacuum.

General Procedure C (GPC): To a (ca. 0.75 M) solution of the phenol in MeOH was added tetrabutylammonium hydroxide (40% solution in MeOH) dropwise. After being stirred for another minute, MeOH was removed under vacuum and the product was dried with the help of careful heating under vacuum.

Note: The phenolate salts, in particular, the **1***-K salts, are highly hygroscopic. For example, the colored salts of nitrophenolates with different counterions brighten rapidly upon contact with moisture. Drying of* **1***-K had to be done with great care as some of them are prone to sublime. For drying, the phenolate salt was placed in a round-bottom flask equipped with a big magnetic stirring bar. Under vigorous stirring, careful heating was applied by means of an oil bath or alternatively a heat gun. The drying process was complete when the initially sticky product became a fine powder.*

*Tetrabutylammonium 2,4-Dinitrophenolate (**1a**-NBu_4):* Following GPC, 2,4-dinitrophenol (506 mg, 2.75 mmol) was dissolved in MeOH (3.5 mL) with the help of heating and sonication. After being cooled to room temperature, NBu_4OH (40% solution in MeOH, 1.96 mL, 2.75 mmol) was added under stirring. Volatiles were subsequently removed, and the yellow residue was suspended in hot acetone (15 mL) and filtered to remove insoluble residues. The solution was allowed to cool to room temperature, and diethyl ether (150 mL) was added, causing the formation of a yellow precipitate, which was separated by filtration. The filtrate was washed with diethyl ether (20 mL) and dried under vacuum to yield **1a**-NBu_4 as a canary yellow solid (992 mg, 85%): mp 108−109 °C (mp 108−109 °C reported in ref 52); ^1H NMR (400 MHz, DMSO-d_6) δ = 8.59 (d, $^4J_{H3,H5}$ = 3.3 Hz, 1 H, 3-H), 7.76 (dd, $^3J_{H5,H6}$ = 9.8 Hz, $^4J_{H3,H5}$ = 3.2 Hz, 1 H, 5-H), 6.29 (d, $^3J_{H5,H6}$ = 9.8 Hz, 1 H, 6-H), 3.18−3.14 (m, 8 H, $^+NBu_4$), 1.61−1.53 (m, 8 H, $^+NBu_4$), 1.35−1.26 (m, 8 H, $^+NBu_4$), 0.93 (t, ^3J = 7.3 Hz, 12 H, $^+NBu_4$); $^{13}C\{^1H\}$ NMR (101 MHz, DMSO-d_6) δ = 170.3 (C_q, C-1), 136.1 (C_q, C-4), 127.3 (CH, C-5), 127.0 (C_q, C-2), 126.5 (CH, C-6), 125.0 (CH, C-3), 57.5 (CH_2, t, $^1J_{C,N}$ = 2.9 Hz, CH_2, C-I), 23.0 (CH_2, C-II), 19.2 (CH_2, C-III), 13.4 (CH_3, C-IV); NMR data are in agreement with those in ref 53; IR (neat) 2958, 1603, 1560, 1537, 1491, 1425, 1376, 1301, 1240, 1180, 1124, 1042, 917, 881, 829, 753, 742, 698 cm^{-1}.

*Tetrabutylammonium 2,3,4,5,6-Pentafluorophenolate (**1b**-NBu_4):* Following GPC, perfluorophenol (519 mg, 2.82 mmol) was dissolved in MeOH (3.5 mL) with the help of heating and sonication. After being cooled to room temperature, NBu_4OH was added (40% solution in MeOH, 2.01 mL, 2.82 mmol) under stirring. Volatiles were subsequently removed, and the residue was suspended in hot acetone (10 mL) and filtered to remove insoluble residues. The

DOI: 10.1021/acs.joc.9b01485
J. Org. Chem. 2019, 84, 8837−8858

The Journal of Organic Chemistry Featured Article

solution was allowed to cool to room temperature, and diethyl ether (200 mL) was added, causing the formation of a colorless precipitate which was separated by filtration. The filtrate was washed with diethyl ether (20 mL) and dried under vacuum to yield **1b**-NBu_4 as a colorless solid (930 mg, 78%): mp 99−100 °C; ^{1}H NMR (400 MHz, DMSO-d_6) δ = 3.19−3.15 (m, 8 H, $^+NBu_4$), 1.61−1.53 (m, 8 H, $^+NBu_4$), 1.35−1.26 (m, 8 H, $^+NBu_4$), 0.93 (t, ^3J = 7.3 Hz, 12 H, $^+NBu_4$); ^{19}F NMR (376 MHz, DMSO-d_6) δ = −171.25 (s, 2 F, 2-F), −171.91 (t, $^3J_{F2,F3}$ = 22.4 Hz, 2 F, 3-F), −194.67 (br s, 1 F, 4-F); ^{13}C{^{1}H} NMR (101 MHz, DMSO-d_6) δ = 57.5 (CH_2, C-I), 23.0 (CH_2, C-II), 19.2 (CH_2, C-III), 13.4 (CH_3, C-IV); the resonances of the C_6F_5 moiety could not be assigned unambiguously; IR (neat) 2962, 2875, 1641, 1589, 1503, 1488, 1474, 1243, 1226, 1108, 991, 961, 896, 882, 739, 723 cm^{-1}.

*Tetrabutylammonium 4-Nitrophenolate (**1c**-NBu_4):* Following GPC, 4-nitrophenol (4.30 g, 30.9 mmol) was dissolved in MeOH (3.5 mL) with the help of heating and sonication. After being cooled to room temperature, NBu_4OH was added (40% solution in MeOH, 20.1 mL, 28.2 mmol) under stirring. All solvents were subsequently removed, and the residue was suspended in hot acetone (100 mL) and filtered to remove insoluble residues. The solution was allowed to cool to room temperature, and diethyl ether (200 mL) was added, causing the formation of a colorless precipitate which was separated by filtration. The filtrate was washed with diethyl ether (20 mL) and dried under vacuum to yield **1c**-NBu_4 as colorless solid (11.5 g, 98%): mp 143−145 °C (mp 147−148.5 °C reported in ref 54); ^{1}H NMR (400 MHz, DMSO-d_6) δ = 7.72−7.68 (m, 2 H, 2-H), 5.89−5.85 (m, 2 H, 3-H), 3.18−3.14 (m, 8 H, $^+NBu_4$), 1.59−1.54 (m, 8 H, $^+NBu_4$), 1.33−1.28 (m, 8 H, $^+NBu_4$), 0.93 (t, ^3J = 7.3 Hz, 12 H, $^+NBu_4$); ^{13}C{^{1}H} NMR (101 MHz, DMSO-d_6) δ = 180.5 (C_q, C-1), 127.5 (CH, C-3), 127.3 (C_q, C-4), 119.4 (CH, C-2), 57.5 (CH_2, t, $^1J_{C,N}$ = 2.8 Hz, C-I), 23.0 (CH_2, C-II), 19.2 (CH_2, C-III), 13.5 (CH_3, C-IV); IR (neat) 2959, 2872, 1584, 1526, 1490, 1463, 1403, 1383, 1258, 1181, 1157, 1106, 882, 846, 831, 807, 743, 708 cm^{-1}.

*Potassium 4-Nitrophenolate (**1c**-K):* Following GPB, 4-nitrophenol (2.20 g, 15.8 mmol) and KOH (510 mg, 9.09 mmol) were combined in water (50 mL) and then stirred for 15 min. The aqueous phase was washed with diethyl ether (3 × 50 mL), and the solvents were removed under reduced pressure. The solid was carefully dried (150 °C, 1 mbar; sublimation occurs!) to obtain **1c**-K (1.50 g, 94%) as an orange solid: mp 348 °C; ^{1}H NMR (400 MHz, DMSO-d_6) δ = 7.76−7.72 (m, 2 H, 2-H), 5.96−5.91 (m, 2 H, 3-H); ^{13}C{^{1}H} NMR (101 MHz, DMSO-d_6) δ = 180.7 (C_q, C-1), 127.7 (C_q, C-4), 127.6 (CH, C-3), 119.5 (CH, C-2); NMR data are in agreement with those in ref 55; IR (neat) 1586, 1504, 1369, 1274, 1156, 1114, 1099, 979, 857, 760, 713 cm^{-1}.

*Tetrabutylammonium 2-Nitrophenolate (**1d**-NBu_4):* Following GPC, 2-nitrophenol (1.06 g, 7.62 mmol) and NBu_4OH (40% in MeOH, 5.45 mL, 7.65 mmol) were dissolved in MeOH (10 mL). The salt **1d**-NBu_4 was obtained after freeze-drying and trituration in pentane (50 mL) as an orange solid (2.54 g, 88%): mp 67−68 °C; ^{1}H NMR (400 MHz, DMSO-d_6) δ = 7.61 (dd, $^3J_{H3,H4}$ = 8.5 Hz, $^4J_{H3,H5}$ = 2.0 Hz, 1 H, 3-H), 6.89 (ddd, $^3J_{H5,H6}$ = 8.6 Hz, $^3J_{H4,H5}$ = 6.5 Hz, $^4J_{H5,H3}$ = 2.0 Hz, 1 H, 5-H), 6.33−6.30 (m, 1 H, 6-H), 5.84 (dd, $^3J_{H3,H4}$ = 8.8 Hz, $^3J_{H4,H5}$ = 6.4 Hz, 1 H, 4-H), 3.18−3.14 (m, 8 H, $^+NBu_4$), 1.60−1.52 (m, 8 H, $^+NBu_4$), 1.31 (sext, ^3J = 7.4 Hz, 8 H, $^+NBu_4$), 0.93 (t, ^3J = 7.3 Hz, 12 H, $^+NBu_4$); ^{13}C{^{1}H} NMR (101 MHz, DMSO-d_6) δ = 168.3 (C_q, C-1), 135.8 (C_q, C-2), 133.1 (CH, C-5), 128.0 (CH, C-6), 126.6 (CH, C-3), 106.6 (CH, C-4), 57.5 (CH_2, C-I), 23.0 (CH_2, C-II), 19.2 (CH_2, C-III), 13.5 (CH_3, C-IV); the resonance of C-2 was not detected; IR (neat) 2956, 2873, 1604, 1542, 1508, 1491, 1467, 1321, 1226, 1203, 1128, 1117, 1061, 1011, 881, 871, 835, 741, 700 cm^{-1}.

*Potassium 2-Nitrophenolate (**1d**-K):* Following GPA, **1d**-K was prepared from 2-nitrophenol (646 mg, 4.64 mmol) and KOH (174 mg, 3.10 mmol) with water as solvent (50 mL) as a bright red solid (353 mg, 64%): mp 292−293 °C (sample changed color to black at >286 °C); ^{1}H NMR (400 MHz, DMSO-d_6) δ = 7.64 (dd, $^3J_{H3,H4}$ = 8.6 Hz, $^4J_{H3,H5}$ = 2.0 Hz, 1 H, 3-H), 6.91 (ddd, $^3J_{H5,H6}$ = 8.7 Hz, $^3J_{H4,H5}$ = 6.4 Hz, $^4J_{H5,H3}$ = 2.1 Hz, 1 H, 5-H), 6.32 (dd, $^3J_{H5,H6}$ = 8.8 Hz, $^4J_{H6,H4}$ = 1.4 Hz, 1 H, 6-H), 5.85 (ddd, $^3J_{H3,H4}$ = 8.6 Hz, $^3J_{H4,H5}$ = 6.4 Hz, $^4J_{H4,H6}$ = 1.4 Hz, 1 H, 4-H); ^{13}C{^{1}H} NMR (101 MHz, DMSO-d_6) δ = 169.2 (C_q, C-1), 135.6 (C_q, C-2), 133.4 (CH, C-5), 128.5 (CH, C-6), 126.7 (CH, C-3), 106.7 (CH, C-4); IR (neat) 1614, 1540, 1511, 1399, 1328, 1240, 1211, 1169, 1146, 1073, 1017, 877, 747, 703 cm^{-1}.

*Tetrabutylammonium 3-Nitrophenolate (**1e**-NBu_4):* Following GPC, **1e**-NBu_4 was prepared from 3-nitrophenol (500 mg, 3.59 mmol) and NBu_4OH (40% in MeOH, 2.92 mL, 3.59 mmol). From a mixture of acetone (7 mL) and diethyl ether (90 mL), **1e**-NBu_4 precipitated as a deeply red solid (1.29 g, 94%): mp 101 °C; ^{1}H NMR (400 MHz, DMSO-d_6) δ = 6.81 (t, $^3J_{H5,H4}$ = $^3J_{H5,H6}$ = 8.0 Hz, 1 H, 5-H), 6.61−6.59 (m, 1 H, 4-H), 6.57−6.54 (m, 1 H, 2-H), 6.35−6.29 (m, 1 H, 6-H), 3.18−3.14 (m, 8 H, $^+NBu_4$), 1.60−1.53 (m, 8 H, $^+NBu_4$), 1.31 (sext, ^3J = 7.4 Hz, 8 H, $^+NBu_4$), 0.93 (t, ^3J = 7.3 Hz, 12 H, $^+NBu_4$); ^{13}C{^{1}H} NMR (101 MHz, DMSO-d_6) δ = 172.8 (C_q, C-1), 149.7 (C_q, C-3), 128.3 (CH, C-5), 126.9 (CH, C-6), 111.2 (CH, C-4), 99.4 (CH, C-2), 57.5 (CH_2, C-I), 23.0 (CH_2, C-II), 19.2 (CH_2, C-III), 13.5 (CH_3, C-IV); IR (neat) 2958, 1589, 1496, 1329, 1308, 1285, 984, 877, 851, 816, 735, 674 cm^{-1}.

*Potassium 3-Nitrophenolate (**1e**-K):* 3-Nitrophenol (2.20 g, 15.8 mmol) and KOH (540 mg, 9.62 mmol) were combined in water (30 mL) and stirred for 15 min. The aqueous phase was washed with diethyl ether (3 × 50 mL), and the solvent was removed under reduced pressure. The solid residue was dried carefully (140 °C, 1 mbar) to obtain **1e**-K (1.50 g, 88%) as a red solid: mp 248−251 °C (sample changed color to black at >240 °C); ^{1}H NMR (400 MHz, DMSO-d_6) δ = 6.84 (dd, $^3J_{H5,H6}$ = 8.3 Hz, $^3J_{H4,H5}$ = 7.8 Hz, 1 H, 5-H), 6.69 (t, $^4J_{H2,H4}$ = $^4J_{H2,H6}$ = 2.5 Hz, 1 H, 2-H), 6.61 (ddd, $^3J_{H4,H5}$ = 7.9 Hz, $^4J_{H2,H4}$ = 2.5 Hz, $^4J_{H4,H6}$ = 1.0 Hz, 1 H, 4-H), 6.39 (ddd, $^3J_{H5,H6}$ = 8.3 Hz, $^4J_{H2,H6}$ = 2.6 Hz, $^4J_{H4,H6}$ = 0.9 Hz, 1 H, 6-H); ^{13}C{^{1}H} NMR (101 MHz, DMSO-d_6) δ = 172.8 (C_q, C-1), 149.7 (C_q, C-3), 128.4 (CH, C-5), 127.0 (CH, C-6), 111.5 (CH, C-4), 100.0 (CH, C-2); IR (neat) 1595, 1503, 1468, 1434, 1345, 1322, 1281, 1247, 1155, 1078, 986, 863, 819, 779, 736, 675 cm^{-1}.

*Potassium 4-Cyanophenolate (**1f**-K):* Following GPB, 4-cyanophenol (2.3 g, 19 mmol) and KOH (0.74 mg, 13 mmol) were combined in water (30 mL) and stirred for 15 min. The aqueous phase was washed with diethyl ether (3 × 50 mL), and the solvent was removed under reduced pressure. The solid residue was dried carefully (150 °C, 1 mbar) to obtain **1f**-K (1.96 g, 96%) as a colorless solid: mp 303−307 °C; ^{1}H NMR (400 MHz, DMSO-d_6) δ = 7.02−6.97 (m, 2 H, 2-H), 6.02−5.97 (m, 2 H, 3-H); ^{13}C{^{1}H} NMR (101 MHz, DMSO-d_6) δ = 176.4 (C_q, C-1), 133.1 (CH, C-3), 123.9 (C_q, C-4), 120.3 (CH, C-2), 84.0 (C_q, 4-CN); IR (neat) 2191, 1575, 1499, 1346, 1209, 1156, 1100, 994, 836, 708 cm^{-1}.

*Tetrabutylammonium 2-(Trifluoromethyl)phenolate (**1g**-NBu_4):* Following GPC, 2-(trifluoromethyl)phenol (413 mg, 2.55 mmol) and NBu_4OH (40% in MeOH, 1.82 mL, 2.55 mmol) were dissolved in MeOH (4.1 mL). The salt **1g**-NBu_4 was obtained after freeze-drying as a colorless solid (752 mg, 73%): mp 71−74 °C; ^{1}H NMR (400 MHz, DMSO-d_6) δ = 6.91 (dd, $^3J_{H3,H4}$ = 7.7 Hz, $^4J_{H3,F}$ = 2.1 Hz, 1 H, 3-H), 6.81−6.76 (m, 1 H, 5-H), 6.01 (dd, $^3J_{H6,H5}$ = 8.6 Hz, $^4J_{H6,H4}$ = 1.2 Hz, 1 H, 6-H), 5.72−5.67 (m, 1 H, 4-H), 3.18−3.14 (m, 8 H, $^+NBu_4$), 1.61−1.53 (m, 8 H, $^+NBu_4$), 1.31 (sext, ^3J = 7.3 Hz, 8 H, $^+NBu_4$), 0.93 (t, ^3J = 7.3 Hz, 12 H, $^+NBu_4$); ^{13}C{^{1}H} NMR (101 MHz, DMSO-d_6) δ = 171.1 (C_q, q, $^3J_{C1,F}$ = 1.4 Hz, C-1), 131.8 (CH, C-5), 127.4 (C_q, q, ^1J = 271.3 Hz, 2-CF_3), 125.9 (CH, q, $^3J_{C3,F}$ = 5.4 Hz, C-3), 122.4 (CH, q, $^4J_{C6,F}$ = 1.3 Hz, C-6), 102.9 (CH, C-4), 57.5 (CH_2, t, $^1J_{C,N}$ = 2.8 Hz, C-I), 23.0 (CH_2, C-II), 19.2 (CH_2, C-III), 13.5 (CH_3, C-IV); the resonance of C-2 was not detected; ^{19}F NMR (376 MHz, DMSO-d_6) δ = −59.9 (2-CF_3); IR (neat) 2960, 2874, 1596, 1531, 1484, 1458, 1357, 1322, 1284, 1198, 1146, 1079, 1030, 1016, 891, 876, 851, 754, 731 cm^{-1}.

*Tetrabutylammonium 4-(Trifluoromethyl)phenolate (**1h**-NBu_4):* Following GPC, 4-(trifluoromethyl)phenol (662 mg, 4.08 mmol) and NBu_4OH (40% in MeOH, 2.90 mL, 4.07 mmol) were used to prepare **1h**-NBu_4, which was obtained after freeze-drying from benzene (20

DOI: 10.1021/acs.joc.9b01485
J. Org. Chem. 2019, 84, 8837−8858

mL) as a pale yellow solid (1.35 g, 82%): mp 50−52 °C; ^{1}H NMR (400 MHz, DMSO-d_6) δ = 7.03−7.00 (m, 2 H, 3-H), 6.16 (s, 2 H, 2-H), 3.18−3.14 (m, 8 H, $^+$NBu$_4$), 1.61−1.53 (m, 8 H, $^+$NBu$_4$), 1.31 (sext, ^3J = 7.4 Hz, 8 H, $^+$NBu$_4$), 0.93 (t, ^3J = 7.3 Hz, 12 H, $^+$NBu$_4$); ^{13}C{^{1}H} NMR (101 MHz, DMSO-d_6) δ = 126.0 (CH, q, ^4J = 3.6 Hz, C-3), 117.9 (CH, C-2), 57.5 (CH$_2$, t, $^1J_{CN}$ = 2.8 Hz, C-I), 23.0 (CH$_2$, C-II), 19.2 (CH$_2$, C-III), 13.4 (CH$_2$, C-IV); resonances for C-1, C-4, and 4-CF$_3$ were not detected; ^{19}F NMR (376 MHz, DMSO-d_6) δ = −56.8 (4-CF$_3$); IR (neat) 2960, 1591, 1514, 1344, 1308, 1165, 1137, 1090, 1051, 885, 845, 742 cm^{-1}.

*Potassium 3-(Trifluoromethyl)phenolate (**1i**-K):*[56] 3-(Trifluoromethyl)phenol (1.15 g, 7.11 mmol) was added to KOtBu (798 mg, 7.11 mmol) in a flame-dried Schlenk flask under nitrogen with stirring. The suspension solidified within 30 s. THF (2 mL) was added, and stirring continued for 15 min. All volatiles were removed under vacuum to obtain **1i**-K as a colorless solid containing residual amounts of coordinated THF (1.46 g, 93% purity, 95%): ^{1}H NMR (400 MHz, DMSO-d_6) δ = 6.82−6.78 (m, 1 H, 5-H), 6.22−6.13 (m, 2 H, 2-H and 4-H), 6.01 (d, $^3J_{H5,H6}$ = 7.4 Hz, 1 H, 6-H); ^{13}C{^{1}H} NMR (101 MHz, DMSO-d_6) δ = 172.0 (C$_q$, C-1), 129.4 (C$_q$, q, $^2J_{C3,F}$ = 29.0 Hz, C-3), 128.9 (CH, C-5), 125.8 (C$_q$, q, ^1J = 272.4 Hz, 3-CF$_3$), 122.6 (CH, C-4), 114.4 (q, $^3J_{C2,F}$ = 3.3 Hz, C-2), 101.1 (CH, C-6); ^{19}F NMR (376 MHz, DMSO-d_6) δ = −60.8 (3-CF$_3$); IR (neat) 1592, 1573, 1479, 1430, 1335, 1310, 1277, 1242, 1154, 1110, 1085, 1054, 984, 899, 875, 856, 784, 747, 703, 655 cm^{-1}.

*Potassium 4-Chlorophenolate (**1j**-K):* Following GPA, **1j**-K was prepared from 4-chlorophenol (1.61 g, 12.5 mmol) and KOH (700 mg, 12.5 mmol) with water as solvent (20 mL) as a colorless solid (1.73 g, 10.4 mmol, 83%): mp 127−135 °C; ^{1}H NMR (400 MHz, DMSO-d_6) δ = 6.68−6.64 (m, 2 H, 3-H), 6.05−6.03 (m, 2 H, 2-H); ^{13}C{^{1}H} NMR (101 MHz, DMSO-d_6) δ = 169.6 (C$_q$, C-1), 128.1 (CH, C-3), 119.5 (CH, C-2), 109.4 (C$_q$, C-4); IR (neat) 1578, 1478, 1295, 1238, 1165, 1098, 1082, 824, 699 cm^{-1}.

*Potassium Phenolate (**1k**-K).* Following GPA, phenol (1.68 g, 17.8 mmol) and KOH (1.00 g, 17.8 mmol) were combined in water (20 mL) and stirred for 15 min. The solvent was removed under reduced pressure, and the resulting solid was dried carefully (140 °C, 1 mbar) to obtain **1k**-K (2.30 g, 98%) as a colorless solid: mp 292−294 °C (sample changed color to black at >282 °C) (mp 285−289 °C reported in ref 57); ^{1}H NMR (400 MHz, DMSO-d_6) δ = 6.71−6.67 (m, 2 H, 3-H), 6.07−6.03 (m, 2 H, 2-H), 5.84−5.79 (m, 1 H, 4-H); ^{13}C{^{1}H} NMR (101 MHz, DMSO-d_6) δ = 172.5 (C$_q$, C-1), 128.7 (CH, C-3), 119.1 (CH, C-2), 106.0 (CH, C-4); IR (neat) 1583, 1474, 1303, 1161, 1065, 979, 873, 821, 791, 782, 761, 711, 699 cm^{-1}. NMR data are in agreement with those in ref 58.

*Tetrabutylammonium Phenolate (**1k**-NBu$_4$):* Following GPC, phenol (1.13 g, 12.0 mmol) and NBu$_4$OH (40% in MeOH, 8.56 mL, 12.0 mmol) were used to prepare **1k**-NBu$_4$, which was obtained after freeze-drying from benzene (20 mL) as a colorless solid (3.63 g, 90%): ^{1}H NMR (400 MHz, DMSO-d_6) δ = 6.71−6.67 (m, 2 H, 3-H), 6.06 (d, $^3J_{H2,H3}$ = 7.6 Hz, 2 H, 2-H), 5.86 (t, $^3J_{H3,H4}$ = 6.7 Hz, 1 H, 4-H), 3.18−3.14 (m, 8 H, $^+$NBu$_4$ superimposed with traces of MeOH), 1.60−1.52 (m, 8 H, $^+$NBu$_4$), 1.30 (sext, ^3J = 7.4 Hz, 8 H, $^+$NBu$_4$), 0.93 (t, ^3J = 7.3 Hz, 12 H, $^+$NBu$_4$); ^{13}C{^{1}H} NMR (101 MHz, DMSO-d_6) δ = 171.0 (C$_q$, C-1), 128.5 (CH, C-3), 118.5 (CH, C-2), 106.9 (CH, C-4), 57.5 (CH$_2$, C-I), 23.1 (CH$_2$, C-II), 19.2 (CH$_2$, C-III), 13.5 (CH$_2$, C-IV); IR (neat) 2959, 2874, 1581, 1486, 1471, 1382, 1321, 1156, 1054, 978, 880, 822, 757, 738, 698 cm^{-1}.

*Potassium 4-Methylphenolate (**1l**-K):* Following GPA, 4-methylphenol (1.54 g, 14.2 mmol) and KOH (800 mg, 14.3 mmol) were combined in water (20 mL) and stirred for 15 min. The solvent was removed under reduced pressure, and the resulting solid was dried carefully (60 °C, 1 mbar) to obtain **1l**-K (1.95 g, 94%) as a colorless solid: mp 270−271 °C (sample changed color black at >234 °C); ^{1}H NMR (400 MHz, DMSO-d_6) δ = 6.53−6.50 (m, 2 H, 3-H), 6.00−5.96 (m, 2 H, 2-H), 2.02 (s, 3 H, 4-CH$_3$); ^{13}C{^{1}H} NMR (101 MHz, DMSO-d_6) δ = 170.2 (C$_q$, C-1), 129.4 (CH, C-3), 118.5 (CH, C-2), 113.1 (C$_q$, C-4), 20.4 (CH$_3$, 4-CH$_3$); IR (neat) 1602, 1541, 1500, 1465, 1324, 1310, 1236, 1168, 1105, 995, 840, 829, 751 cm^{-1}.

*Potassium 4-tert-Butylphenolate (**1m**-K):* Following GPA, **1m**-K was prepared from 4-*tert*-butylphenol (2.65 g, 17.6 mmol) and KOH (990 mg, 17.6 mmol) with water as solvent (20 mL) as a colorless solid (2.49 g, 13.2 mmol, 75%): mp >350 °C (sample changed color to dark brown at >300 °C); ^{1}H NMR (400 MHz, DMSO-d_6) δ = 6.77−6.73 (m, 2 H, 3-H), 6.06−6.04 (m, 2 H, 2-H), 1.15 (s, 9 H, 6-H); ^{13}C{^{1}H} NMR (101 MHz, DMSO-d_6) δ = 168.0 (br, C$_q$, C-1), 129.0 (br, C$_q$, C-4), 125.1 (CH, C-3), 117.4 (CH, C-2), 33.0 (C$_q$, C-5), 32.0 (CH$_3$, C-6); IR (neat) 2956, 1598, 1493, 1283, 1265, 1180, 832, 670 cm^{-1}.

*Potassium 4-Methoxyphenolate (**1n**-K):* 4-Methoxyphenol (1.50 g, 12.1 mmol, 1 equiv) and KOH (678 mg, 12.1 mmol) were combined in water (20 mL) and stirred for 15 min. The solvent was removed under reduced pressure, and the resulting solid was dried carefully (140 °C, 6 × 10^{-3} mbar) to obtain **1n**-K (1.37 g, 70%) as a colorless solid: mp 148−158 °C; ^{1}H NMR (400 MHz, DMSO-d_6) δ = 6.37−6.33 (m, 2 H, 3-H), 5.89−5.87 (m, 2 H, 2-H), 3.49 (s, 3 H, 4-OMe); ^{13}C{^{1}H} NMR (101 MHz, DMSO-d_6) δ = 167.4 (C$_q$, C-1), 143.6 (C$_q$, C-4), 117.5 (CH, C-2), 115.5 (CH, C-3), 56.4 (CH$_3$, 4-OMe); IR (neat) 1597, 1489, 1440, 1309, 1246, 1216, 1177, 1095, 1034, 989, 826, 742 cm^{-1}.

*Potassium 2,6-Di-tert-butylphenolate (**1o**-K):* 2,6-Di-*tert*-butylphenol (2.00 g, 9.69 mmol) and KO*t*Bu (1.00 g, 8.91 mmol) were combined in dry ethanol (20 mL) and stirred for 15 min. The solvent was removed under reduced pressure, and the solid residue was washed with dry diethyl ether (4 × 40 mL) to obtain **1o**-K (2.00 g, 92%) as a lime green solid: mp >350 °C; ^{1}H NMR (400 MHz, DMSO-d_6) δ = 6.58 (d, $^3J_{H3,H4}$ = 7.4 Hz, 2 H, 3-H), 5.56 (t, $^3J_{H3,H4}$ = 7.3 Hz, 1 H, 4-H), 1.32 (s, 18 H, 6-H); ^{13}C{^{1}H} NMR (101 MHz, DMSO-d_6) δ = 171.5 (C$_q$, C-1), 135.6 (C$_q$, C-2), 123.0 (CH, C-3), 102.6 (CH, C-4), 35.2 (C$_q$, C-5), 30.5 (CH$_3$, C-6); IR (neat) 2951, 1572, 1410, 1373, 1353, 1298, 1275, 1253, 1198, 1094, 879, 855, 811, 755 cm^{-1}. NMR data are in agreement with those in ref 59.

*Potassium 2-Methylphenolate (**1p**-K):* Following GPA, 2-methylphenol (1.47 g, 13.5 mmol) and KOH (750 mg, 13.4 mmol) were combined in water (5 mL) and stirred for 5 min. The solvent was removed under reduced pressure, and the solid residue was carefully dried to obtain **1p**-K (1.47 g, 75%) as a colorless solid: mp 198−202 °C (sample changed color to black at >180 °C); ^{1}H NMR (400 MHz, DMSO-d_6) δ = 6.64−6.61 (m, 1 H), 6.56−6.51 (m, 1 H), 5.94−5.91 (m, 1 H), 5.72−5.67 (m, 1 H), 1.86 (s, 3 H, 2-CH$_3$); ^{13}C{^{1}H} NMR (101 MHz, DMSO-d_6) δ = 171.1 (C$_q$, C-1), 128.7 (CH, C-3), 126.4 (CH, C-5), 125.3 (C$_q$, C-2), 117.0 (CH, C-6), 105.0 (CH, C-4), 18.4 (CH$_3$, 2-CH$_3$); IR (neat) 1582, 1471, 1429, 1293, 1106, 1039, 858, 761, 722 cm^{-1}.

*Potassium 3-Methoxyphenolate (**1q**-K):* Following GPA, 3-methoxyphenol (1.58 g, 12.7 mmol) and KOH (708 mg, 12.6 mmol) were combined in water (5 mL) and stirred for 5 min. The solvent was removed under reduced pressure, and the solid residue was carefully dried to obtain **1q**-K (2.03 g, 99%) as a colorless solid: mp 97−110 °C; ^{1}H NMR (400 MHz, DMSO-d_6) δ = 6.60 (t, $^3J_{H5,H4}$ = $^3J_{H6,H5}$ = 8.0 Hz, 1 H, 5-H), 5.77 (d, $^3J_{H5,H4}$ = 8.5 Hz, 1 H, 4-H), 5.73 (s, 1 H, 2-H), 5.57 (d, $^3J_{H6,H5}$ = 7.9 Hz, 1 H, 6-H), 3.53 (s, 3 H, 3-OMe); ^{13}C{^{1}H} NMR (101 MHz, DMSO-d_6) δ = 171.2 (C$_q$, C-1), 160.8 (C$_q$, C-3), 128.4 (CH, C-5), 111.7 (CH, C-6), 102.9 (CH, C-2), 94.7 (CH, C-4), 53.9 (CH$_3$, 3-OMe); IR (neat) 1590, 1553, 1474, 1441, 1335, 1300, 1260, 1201, 1167, 1152, 1141, 1043, 1026, 983, 944, 921, 841, 780, 769, 752, 702, 692 cm^{-1}.

UV−vis Spectra of Phenolates in DMSO. Photometric measurements were carried out using a J&M TIDAS diode array spectrophotometer controlled by TIDASDAQ3 (v3) software and connected to a Hellma 661.502-QX quartz Suprasil immersion probe (light path d = 5 mm) via fiber-optic cables and standard SMA connectors. To a volume of DMSO (typically 20 to 25 mL) was portionwise added a DMSO solution of the phenolate (typically 10−20 mg of the phenolate salt in 10 mL DMSO) by means of a microliter syringe. Molar absorption coefficients were then determined by linear regression of the linear correlation of absorbance (at the absorption maximum) with the concentration of the phenolate.

DOI: 10.1021/acs.joc.9b01485
J. Org. Chem. 2019, 84, 8837−8858

Reactions of 2a with Phenolate Anions. *NMR Analysis of Product Mixtures without Workup (Scheme 2, Method A):* Under an atmosphere of dry argon, equimolar amounts of **2a**-BF_4 and the potassium or tetrabutylammonium phenolate **1**-K/NBu_4 were dissolved in equal volumes of anhydrous DMSO-d_6 (from sealed ampule, 0.75 mL). Both solutions were mixed by pipetting, then transferred into an NMR tube, sealed, and submitted to ^{1}H NMR (and HSQC) spectroscopic analysis. Products from O and C attack of **2a** at the ambident phenolates **1** were differentiated based on the NMR chemical shifts of the benzhydrylic CH (for details, see the Supporting Information).

*Reactions of **2a** with Phenolate Ions **1d** at −40 °C:* Under a dry nitrogen atmosphere in a flame-dried flask, **1d**-NBu_4 (7.6 mg, 0.020 mmol) was dissolved in CD_3CN (0.5 mL). After being cooled to −40 °C, a solution of **2a**-BF_4 (8.3 mg, 0.020 mmol) in CD_3CN (0.25 mL + 0.25 mL to rinse) was added under stirring. The blue solution was transferred into a precooled NMR tube (−78 °C) and kept at this temperature. The NMR tube with the frozen sample was placed in the precooled NMR spectrometer and warmed to −40 °C. After spectra acquisition at −40 °C, the sample was allowed to warm to ambient temperature (ca. 25 °C). After standing overnight at ambient temperature, the sample was analyzed again by NMR techniques. At −40 °C, **3da** was detected (oxygen attack of **1d** at **2a**). At room temperature, **3da** rearranged to **4da**, the product of carbon attack.

*Reactions of **2a** with Phenolate Ions **1o** at −40 °C:* Under a dry nitrogen atmosphere in a flame-dried flask, **1o**-K (5.5 mg, 0.023 mmol) was dissolved in DMF-d_7 (0.4 mL). After being cooled to −40 °C, a solution of **2a**-BF_4 (9.4 mg, 0.023 mmol, 1 equiv) in DMF-d_7 (0.35 mL) was added under stirring. The blue solution was transferred into a precooled NMR tube (−78 °C) and kept at this temperature. The NMR tube with the frozen sample was placed in the precooled NMR spectrometer and warmed to −40 °C. The proton resonance at δ 5.25 ppm (δ_C 56.6 ppm) indicated the exclusive formation of **4oa**, formed via the C attack of phenolate **1o** at **2a**.

General Procedure D (GPD; Scheme 2, Method B): To a deeply blue solution of **2a**-BF_4 in DMSO was added a solution of the phenolate salt (1.1 to 2 equiv) in DMSO, which caused decolorization within 1 min. Subsequently, aqueous ammonia (pH 10, 50 mL) was added to precipitate the benzhydryl ether as a voluminous, blue material, which was isolated by filtration, washed with aqueous ammonia and dried under vacuum to furnish colorless aryl benzhydryl ethers **3**.

When **2a**-BF_4 reacted with weakly Lewis basic phenolates (**1c**-NBu_4, **1e**-K, **1f**-K) according to GPD, analysis of the crude product mixture showed the predominant formation of benzhydrol **2a**-OH. No further attempts were made to isolate phenyl ethers **3** from these mixtures.

*8,8′-((4-(Trifluoromethyl)phenoxy)methylene)bis(1,2,5,6-tetrahydro-4H-pyrrolo[3,2,1-ij]quinoline) (**3ha**):* According to GPD, from **2a**-BF_4 (26.8 mg, 0.0644 mmol) and **1h**-K (18.4 mg, 0.0919 mmol) in DMSO (3 mL), a pale blue solid was obtained (10.8 mg, 34%): ^{1}H NMR (400 MHz, CD_2Cl_2) δ = 7.49−7.44 (m, 2 H, 15-H), 7.03−7.01 (m, 2 H, 14-H), 6.93 (s, 2 H, 3-H), 6.82 (s, 2 H, 7-H), 6.01 (s, 1 H, 1-H), 3.25−3.21 (m, 4 H, 9-H), 2.96−2.94 (m, 4 H, 10-H), 2.88−2.81 (m, 4 H, 8-H), 2.68−2.59 (m, 4 H, 12-H), 2.09−1.99 (m, 4 H, 11-H); ^{13}C{^{1}H} NMR (101 MHz, CD_2Cl_2) δ = 161.7 (C_q, C-13), 150.4 (C_q, C-5), 132.0 (C_q, C-2), 129.6 (C_q, C-4), 127.1 (CH, q, $^3J_{C,F}$ = 3.8 Hz, C-15), 125.4 (CH, C-7), 125.2 (C_q, q, $^1J_{C,F}$ = 273 Hz, 16-CF_3), 122.6 (C_q, q, $^2J_{C,F}$ = 32.6 Hz, C-16), 120.9 (CH, C-3), 119.6 (C_q, C-6), 116.5 (CH, C-14), 83.5 (CH, C-1), 55.7 (CH_2, C-9), 47.7 (CH_2, C-10), 29.2 (CH_2, C-8), 24.5 (CH_2, C-12), 23.7 (CH_2, C-11); ^{19}F NMR (377 MHz, CD_2Cl_2) δ = −61.7 (CF_3); HRMS (EI$^+$) calcd m/z for [$C_{30}H_{29}F_3N_2O^{\bullet+}$] [$M^{\bullet+}$] 490.2226; found 490.2213; IR (neat) 2938, 2806, 1612, 1515, 1493, 1466, 1435, 1323, 1281, 1246, 1176, 1157, 1109, 1067, 1002, 881, 834, 734 cm^{-1}.

*8,8′-((3-(Trifluoromethyl)phenoxy)methylene)bis(1,2,5,6-tetrahydro-4H-pyrrolo[3,2,1-ij]quinoline) (**3ia**):* According to GPD, from **2a**-BF_4 (19.4 mg, 0.0466 mmol) and **1i**-K (14.0 mg, 0.0699 mmol) in DMSO (5 mL), a grayish solid was obtained (11.5 mg, 50%): mp 70−72 °C; ^{1}H NMR (400 MHz, CD_2Cl_2) δ = 7.36−7.30 (m, 1 H, 18-H), 7.23−7.22 (m, 1 H, 14-H), 7.14−7.10 (m, 2 H, 16-H and 17-H), 6.94 (s, 2 H, 3-H), 6.83 (s, 2 H, 7-H), 6.00 (s, 1 H, 1-H), 3.25−3.21 (m, 4 H, 9-H), 2.99−2.94 (m, 4 H, 10-H), 2.87−2.81 (m, 4 H, 8-H), 2.67−2.61 (m, 4 H, 12-H), 2.09−1.99 (m, 4 H, 11-H); ^{13}C{^{1}H} NMR (101 MHz, CD_2Cl_2) δ = 159.2 (C_q, C-13), 150.3 (C_q, C-5), 132.1 (C_q, C-2), 130.4 (CH, C-18), 129.6 (C_q, C-4), 125.8 (C_q, q, $^2J_{C,F}$ = 52.3 Hz, C-15), 125.4 (CH, C-7), 122.3 (C_q, q, $^2J_{C,F}$ = 204 Hz, 15-CF_3), 120.9 (CH, C-3), 119.6 (C_q, C-6), 119.4 (br, CH, C-17), 117.4 (CH, q, $^3J_{C,F}$ = 3.9 Hz, C-16), 114.0 (CH, q, $^3J_{C,F}$ = 3.9 Hz, C-14), 83.6 (CH, C-1), 55.7 (CH_2, C-9), 47.7 (CH_2, C-10), 29.2 (CH_2, C-8), 24.5 (CH_2, C-12), 23.7 (CH_2, C-11); ^{19}F NMR (377 MHz, CD_2Cl_2) δ = −63.0 (CF_3).

*8,8′-((4-Chlorophenoxy)methylene)bis(1,2,5,6-tetrahydro-4H-pyrrolo[3,2,1-ij]quinoline) (**3ja**):* According to GPD, from **2a**-BF_4 (25.7 mg, 0.0617 mmol) and **1j**-K (11.3 mg, 0.0678 mmol) in DMSO (5 mL), a grayish solid was obtained (20.6 mg, 73%): ^{1}H NMR (400 MHz, CD_2Cl_2) δ = 7.19−7.13 (m, 2 H, 14-H), 6.91 (s, 2 H, 3-H), 6.90−6.85 (m, 2 H, 15-H), 6.81 (s, 2 H, 7-H), 5.91 (s, 1 H, 1-H), 3.25−3.21 (m, 4 H, 9-H), 2.96−2.93 (m, 4 H, 10-H), 2.88−2.79 (m, 4 H, 8-H), 2.65−2.58 (m, 4 H, 12-H), 2.10−1.97 (m, 4 H, 11-H); ^{13}C{^{1}H} NMR (101 MHz, CD_2Cl_2) δ = 157.7 (C_q, C-13), 150.3 (C_q, C-5), 132.3 (C_q, C-2), 129.54 (CH, C-15), 129.51 (C_q, C-4), 125.5 (C_q, C-16), 125.4 (CH, C-7), 120.9 (CH, C-3), 119.6 (C_q, C-6), 117.9 (CH, C-14), 83.5 (CH, C-1), 55.7 (CH_2, C-9), 47.8 (CH_2, C-10), 29.2 (CH_2, C-8), 24.5 (CH_2, C-12), 23.7 (CH_2, C-11).

*8,8′-(Phenoxymethylene)bis(1,2,5,6-tetrahydro-4H-pyrrolo-[3,2,1-ij]quinoline) (**3ka**):* According to GPD, from **2a**-BF_4 (36.1 mg, 0.0866 mmol) and **1k**-K (12.6 mg, 0.0953 mmol) in DMSO (5 mL), a grayish solid was obtained (30.2 mg, 83%): mp 75 °C; ^{1}H NMR (400 MHz, CD_2Cl_2) δ = 7.23−7.19 (m, 2 H, 15-H), 6.95−6.93 (m, 4 H, 3-H and 14-H), 6.89−6.85 (m, 1 H, 16-H), 6.84 (s, 2 H, 7-H), 5.96 (s, 1 H, 1-H), 3.25−3.21 (m, 4 H, 9-H), 2.98−2.92 (m, 4 H, 10-H), 2.87−2.83 (m, 4 H, 8-H), 2.66−2.62 (m, 4 H, 12-H), 2.08−2.00 (m, 4 H, 11-H); ^{13}C{^{1}H} NMR (101 MHz, CD_2Cl_2) δ = 159.1 (C_q, C-13), 150.2 (C_q, C-5), 132.9 (C_q, C-2), 129.7 (CH, C-15), 129.5 (C_q, C-4), 125.3 (CH, C-7), 121.0 (CH, C-3), 120.8 (CH, C-16), 119.6 (C_q, C-6), 116.5 (CH, C-14), 82.9 (CH, C-1), 55.7 (CH_2, C-9), 47.8 (CH_2, C-10), 29.3 (CH_2, C-8), 24.5 (CH_2, C-12), 23.8 (CH_2, C-11); HRMS (ESI$^+$) calcd m/z for [$C_{29}H_{31}N_2O^+$] [M + H$^+$] 423.2431; found 423.2428; IR (neat) 2912, 2803, 1596, 1491, 1467, 1435, 1329, 1280, 1224, 1190, 1173, 1145, 1124, 1028, 1007, 880, 842, 751, 735, 691 cm^{-1}.

*8,8′-((p-Tolyloxy)methylene)bis(1,2,5,6-tetrahydro-4H-pyrrolo-[3,2,1-ij]quinoline) (**3la**):* According to GPD, from **2a**-BF_4 (28.2 mg, 0.0672 mmol) and **1l**-K (10.9 mg, 0.0745 mmol) in DMSO (5 mL), a grayish solid was obtained (33.3 mg). The sample contained residual amounts of water: ^{1}H NMR (400 MHz, CD_2Cl_2) δ = 7.01−6.99 (m, 2 H, 15-H), 6.93 (s, 2 H, 3-H), 6.83−6.81 (m, 4 H, 14-H and 7-H), 5.91 (s, 1 H, 1-H), 3.24−3.20 (m, 4 H, 9-H), 2.95−2.92 (m, 4 H, 10-H), 2.84−2.82 (m, 4 H, 8-H), 2.65−2.61 (m, 4 H, 12-H), 2.23 (s, 3 H, 16-CH_3), 2.07−2.01 (m, 4 H, 11-H); ^{13}C{^{1}H} NMR (101 MHz, CD_2Cl_2) δ = 156.9 (C_q, C-13), 150.1 (C_q, C-5), 133.1 (C_q, C-2), 130.2 (CH, C-15), 129.4 (C_q, C-4), 125.3 (CH, C-7), 120.9 (CH, C-3), 119.5 (C_q, C-6), 116.3 (CH, C-14), 83.0 (CH, C-1), 55.7 (CH_2, C-9), 47.8 (CH_2, C-10), 29.3 (CH_2, C-8), 24.5 (CH_2, C-12), 23.8 (CH_2, C-11), 20.7 (CH_3, 16-CH_3); the resonance for C-16 was not detected; HRMS (ESI$^+$) calcd m/z for [$C_{30}H_{33}N_2O^+$] [M + H$^+$] 437.2587; found 437.2584; IR (neat) 2922, 2801, 1609, 1507, 1492, 1467, 1434, 1329, 1280, 1226, 1189, 1174, 1145, 1124, 1037, 1011, 983, 881, 814, 782, 734 cm^{-1}.

*8,8′-((4-(tert-Butyl)phenoxy)methylene)bis(1,2,5,6-tetrahydro-4H-pyrrolo[3,2,1-ij]quinoline) (**3ma**):* According to GPD, from **2a**-BF_4 (27.3 mg, 0.0656 mmol) and **1m**-K (13.6 mg, 0.0722 mmol) in DMSO (5 mL), a grayish solid was obtained (23.3 mg, 0.0487 mmol, 74%): mp 85 °C; ^{1}H NMR (400 MHz, CD_2Cl_2) δ = 7.26−7.20 (m, 2 H, 15-H), 6.94 (s, 2 H, 3-H), 6.89−6.84 (m, 2 H, 14-H), 6.83 (s, 2 H, 7-H), 5.93 (s, 1 H, 1-H), 3.24−3.20 (m, 4 H, 9-H), 2.97−2.92 (m, 4 H, 10-H), 2.86−2.82 (m, 4 H, 8-H), 2.66−2.61 (m, 4 H, 12-H), 2.08−2.00 (m, 4 H, 11-H), 1.26 (s, 9 H, 18-H); ^{13}C{^{1}H} NMR (101 MHz, CD_2Cl_2) δ = 156.8 (C_q, C-13), 150.1 (C_q, C-5), 143.5 (C_q, C-

DOI: 10.1021/acs.joc.9b01485
J. Org. Chem. 2019, 84, 8837−8858

16), 133.1 (C_q, C-2), 129.5 (C_q, C-4), 126.6 (CH, C-15), 125.3 (CH, C-7), 121.0 (CH, C-3), 119.6 (C_q, C-6), 115.9 (CH, C-14), 82.9 (CH, C-1), 55.8 (CH_2, C-9), 47.8 (CH_2, C-10), 34.4 (C_q, C-17), 31.8 (CH_3, C-18), 29.3 (CH_2, C-8), 24.5 (CH_2, C-12), 23.8 (CH_2, C-11); HRMS (EI^+) calcd m/z for $[C_{33}H_{38}N_2O^{\bullet+}]$ 478.2979; found 478.2971; IR (neat) 2947, 2801, 1609, 1510, 1493, 1464, 1436, 1329, 1274, 1236, 1181, 1145, 1124, 1011, 880, 825, 736 cm^{-1}.

*8,8′-((4-Methoxyphenoxy)methylene)bis(1,2,5,6-tetrahydro-4H-pyrrolo[3,2,1-ij]quinoline) (**3na**):* According to GPD, from **2a**-BF_4 (24.4 mg, 0.0586 mmol) and **1n**-K (11.3 mg, 0.0696 mmol) in DMSO (5 mL), a grayish solid was obtained (37.0 mg). The sample contained residual amounts of water: ^1H NMR (400 MHz, CD_2Cl_2) δ = 6.92 (s, 2 H, 3-H), 6.88−6.83 (m, 2 H, 14-H), 6.81 (s, 2 H, 7-H), 6.77−6.73 (m, 2 H, 15-H), 5.85 (s, 1 H, 1-H), 3.71 (s, 3 H, 16-OMe), 3.23−3.20 (m, 4 H, 9-H), 2.95−2.92 (m, 4 H, 10-H), 2.85−2.81 (m, 4 H, 8-H), 2.66−2.59 (m, 4 H, 12-H), 2.09−1.99 (m, 4 H, 11-H); $^{13}C\{^1H\}$ NMR (101 MHz, CD_2Cl_2) δ = 154.1 (C_q, C-16), 153.1 (C_q, C-13), 150.1 (C_q, C-5), 133.1 (C_q, C-2), 129.4 (C_q, C-4), 125.3 (CH, C-7), 120.9 (CH, C-3), 119.5 (C_q, C-6), 117.4 (CH, C-14), 114.8 (CH, C-15), 83.6 (CH, C-1), 56.1 (CH_3, 16-OMe), 55.7 (CH_2, C-9), 47.8 (CH_2, C-10), 29.2 (CH_2, C-8), 24.5 (CH_2, C-12), 23.7 (CH_2, C-11); HRMS (EI^+) calcd m/z for $[C_{30}H_{33}N_2O_2^+]$ [M + H^+] 453.2537; found 453.2536.

*4-(Bis(1,2,5,6-tetrahydro-4H-pyrrolo[3,2,1-ij]quinolin-8-yl)-methyl)-2,6-di-tert-butylphenol (**4oa**):* According to GPD, from **2a**-BF_4 (27.6 mg, 0.0663 mmol) and **1o**-K (24.3 mg, 0.0994 mmol) in DMSO (2 mL), a grayish solid was obtained (31.0 mg). The precipitated material contained residual phenol **1o**-H (26%), and **4oa** was obtained in a yield of 64% (22.8 mg, 0.0426 mmol). The ^1H NMR spectrum (in CD_2Cl_2) agreed with that detected for the crude reaction mixture of **2a** + **1o**-K in DMSO-d_6 (see the Supporting Information) but comprised additional resonances for **1o**-H: HRMS (ESI^+) calcd m/z for $[C_{37}H_{47}N_2O^+]$ [M + H^+] 535.3683; found 535.3680.

Reactions of 2n-Br with Phenolate Anions in Acetonitrile. *4,4′-((2,4-Dinitrophenoxy)methylene)bis(methylbenzene) (**3an**):* **1a**-NBu_4 (138 mg, 0.325 mmol) and **2n**-Br (50 mg, 0.182 mmol) were dissolved in MeCN (10 mL) and stirred for 4 h at room temperature to yield a yellow solution. After removal of the solvent, the crude product was purified by flash column chromatography (SiO_2, 20% pentane in ethyl acetate, R_f = 0.88) to yield **3an** as a colorless oil (68.8 mg, 99%): ^1H NMR (400 MHz, $CDCl_3$) δ = 8.72 (d, J = 2.8 Hz, 1 H, 11-H), 8.25 (dd, J = 9.3 Hz, J = 2.8 Hz, 1 H, 9-H), 7.36−7.34 (m, 4 H, 3-H), 7.20−7.16 (m, 5 H, 4-H and 8-H), 6.43 (s, 1 H, 1-H), 2.32 (s, 6 H, 6-H); $^{13}C\{^1H\}$ NMR (101 MHz, $CDCl_3$) δ = 155.7 (C_q, C-7), 140.1 (C_q, C-10), 139.7 (C_q, C-12), 138.6 (C_q, C-5), 136.2 (C_q, C-2), 129.9 (CH, C-4), 128.8 (CH, C-9), 126.4 (CH, C-3), 121.9 (CH, C-11), 116.4 (CH, C-8), 84.2 (CH, C-1), 21.3 (CH_3, C-6); IR (neat) 3093, 3025, 2921, 1603, 1522, 1484, 1418, 1340, 1273, 1178, 1121, 1066, 998, 974, 907, 833, 819, 804, 773, 763, 742, 724 cm^{-1}.

*4,4′-((Perfluorophenoxy)methylene)bis(methylbenzene) (**3bn**):* **1b**-NBu_4 (138 mg, 0.325 mmol) and **2n**-Br (50 mg, 0.182 mmol) were dissolved in MeCN (10 mL) and stirred for 4 h at room temperature. After removal of the solvent, the crude product was filtered through silica (SiO_2, 1% pentane in ethyl acetate, R_f = 1) to yield **3bn** as a colorless oil (56.6 mg, 82%): ^1H NMR (400 MHz, $CDCl_3$) δ = 7.32−7.30 (m, 4 H, 3-H), 7.16−7.15 (m, 4 H, 4-H), 6.34 (s, 1 H, 1-H), 2.34 (s, 3 H, 6-H); $^{13}C\{^1H\}$ NMR (101 MHz, $CDCl_3$) δ = 138.4 (C_q, C-5), 136.8 (C_q, C-2), 129.3 (CH, C-4), 127.2 (CH, C-3), 87.2 (CH, C-1), 21.3 (CH_3, C-6); the resonances of the perfluorophenyl ring could not be clearly assigned; ^{19}F NMR (377 MHz, $CDCl_3$) δ = −154.15 to −154.24 (m, 2 F, 8-F), −163.00 to −163.13 (m, 1 F, 10-F), −163.57 to −163.72 (m, 2 F, 9-F); HRMS (EI^+) calcd m/z for $[C_{21}H_{14}F_5O^{\bullet+}]$ 377.0959; found 377.0971; IR (neat) 3026, 3923, 1508, 1465, 1302, 1181, 1152, 1018, 992, 950, 923, 806, 786, 774, 806, 786, 762 cm^{-1}.

*4,4′-((4-Nitrophenoxy)methylene)bis(methylbenzene) (**3cn**):* **1c**-NBu_4 (235 mg, 0.618 mmol) and **2n**-Br (95.0 mg, 0.345 mmol) were dissolved in MeCN (ca. 20 mL) and stirred for 4 h. After removal of the solvent, the crude product was purified by chromatography (SiO_2, 20% pentane in ethyl acetate, R_f = 0.71) to obtain **3cn** (92.4 mg, 80%): ^1H NMR (300 MHz, $CDCl_3$) δ = 8.17−8.10 (m, 2 H, 8-H), 7.33−7.29 (m, 4 H, 3-H), 7.21−7.18 (m, 4 H, 4-H), 7.04−7.01 (m, 2 H, 9-H), 6.29 (s, 1 H, 1-H), 2.36 (s, 6 H, 6-H); $^{13}C\{^1H\}$ NMR (75.5 MHz, $CDCl_3$) δ = 163.3 (C_q, C-7), 141.6 (C_q, C-10), 138.1 (C_q, C-5), 137.2 (C_q, C-2), 129.6 (CH, C-4), 126.8 (CH, C-3), 125.9 (CH, C-9), 116.1 (CH, C-8), 82.4 (CH, C-1), 21.2 (CH_3, C-6); HRMS (EI^+) calcd m/z for $[C_{21}H_{19}NO_3^{\bullet+}]$ 333.1359; found 333.1366.

*4,4′-((2-Nitrophenoxy)methylene)bis(methylbenzene) (**3dn**):* In a flame-dried flask under nitrogen were dissolved **1d**-NBu_4 (124 mg, 0.325 mmol) and **2n**-Br (50 mg, 0.182 mmol) in MeCN (10 mL) and stirred for 4 h at room temperature to yield a yellow solution. After removal of the solvent, the crude product was purified by flash column chromatography (SiO_2, 1−10% pentane in ethyl acetate, R_f = 0.68) to yield **3dn** as a pale yellow oil (42.8 mg, 71%): ^1H NMR (400 MHz, $CDCl_3$) δ = 7.82 (dd, J = 8.1 Hz, J = 1.7 Hz, 1 H, 11-H), 7.40−7.38 (m, 4 H, 3-H), 7.36−7.33 (m, 1 H, 9-H), 7.17−7.14 (m, 4 H, 4-H), 7.06 (dd, J = 8.6 Hz, J = 1.2 Hz, 1 H, 8-H), 6.97−6.93 (m, 1 H, 10-H), 6.33 (s, 1 H, 1-H), 2.32 (s, 6 H, 6-H); $^{13}C\{^1H\}$ NMR (101 MHz, $CDCl_3$) δ = 151.2 (C_q, C-7), 140.7 (C_q, C-12), 137.9 (C_q, C-5), 137.6 (C_q, C-2), 133.8 (CH, C-9), 129.6 (CH, C-4), 126.5 (CH, C-3), 125.6 (CH, C-11), 120.4 (CH, C-10), 116.4 (CH, C-8), 82.7 (CH, C-1), 21.2 (CH_3, C-6); HRMS (EI^+) calcd m/z for $[C_{21}H_{19}NO_3^{\bullet+}]$ 333.1359; found 333.1371; IR (neat) 3024, 2912, 1604, 1582, 1519, 1482, 1451, 1248, 1304, 1274, 1248, 1178, 1164, 1089, 1043, 1007, 861, 829, 805, 763, 742, 667 cm^{-1}.

*4,4′-((3-Nitrophenoxy)methylene)bis(methylbenzene) (**3en**):* **1e**-NBu_4 (124 mg, 0.325 mmol) and **2n**-Br (50 mg, 0.182 mmol) were dissolved in MeCN (10 mL) and stirred for 4 h at room temperature to yield a yellow solution. After removal of the solvent, the crude product was purified by flash column chromatography (SiO_2, 5% pentane in ethyl acetate, R_f = 0.92) to yield **3en** as a yellow oil (48.7 mg, 80%): ^1H NMR (599 MHz, $CDCl_3$) δ = 7.80 (app t, J = 2.3 Hz, 1 H, 12-H), 7.77 (ddd, J = 8.0 Hz, J = 2.2 Hz, J = 0.9 Hz, 1 H, 10-H), 7.36 (app t, J = 8.2 Hz, 1 H, 9-H), 7.31−7.30 (m, 4 H, 3-H), 7.28 (ddd, J = 8.3 Hz, J = 2.5 Hz, J = 1.0 Hz, 1 H, 8-H), 7.18−7.16 (m, 4 H, 4-H), 6.25 (s, 1 H, 1-H), 2.34 (s, 6 H, 6-H); $^{13}C\{^1H\}$ NMR (151 MHz, $CDCl_3$) δ = 158.7 (C_q, C-7), 149.2 (C_q, C-11), 138.0 (C_q, C-5), 137.4 (C_q, C-2), 130.0 (CH, C-9), 129.6 (CH, C-4), 126.9 (CH, C-3), 122.8 (CH, C-8), 116.0 (CH, C-10), 111.0 (CH, C-12), 82.3 (CH, C-1), 21.3 (CH_3, C-6); HRMS (EI^+) calcd m/z for $[C_{21}H_{19}NO_3^{\bullet+}]$ 333.1359; found 333.1351; IR (neat) 3022, 2931, 1618, 1580, 1524, 1477, 1450, 1247, 1318, 1283, 1234, 1177, 1013, 822, 804, 763, 736, 671 cm^{-1}.

*4-(Di-p-tolylmethoxy)benzonitrile (**3fn**):* **1f**-NBu_4 (292 mg, 0.810 mmol) and **2n**-Br (106 mg, 0.385 mmol) were dissolved in MeCN (ca. 20 mL) and stirred for 4 h. After removal of the solvent, the crude product was purified by chromatography (SiO_2, 20% pentane in ethyl acetate, R_f = 0.53) to obtain **3fn** (118 mg, 98%) as a yellowish oil: ^1H NMR (300 MHz, $CDCl_3$) δ = 7.54−7.49 (m, 2 H, 9-H), 7.32−7.28 (m, 4 H, 3-H), 7.20−7.15 (m, 4 H, 4-H), 7.05−6.99 (m, 2 H, 8-H), 6.24 (s, 1 H, 1-H), 2.36 (s, 6 H, 6-H); $^{13}C\{^1H\}$ NMR (75.5 MHz, $CDCl_3$) δ = 161.5 (C_q, C-7), 138.0 (C_q, C-5), 137.4 (C_q, C-2), 133.9 (CH, C-9), 129.6 (CH, C-4), 126.8 (CH, C-3), 119.3 (C_q, 10-CN), 116.8 (CH, C-8), 104.1 (C_q, C-10), 82.0 (CH, C-1), 21.2 (CH_3, C-6); HRMS (EI^+) calcd m/z for $[C_{22}H_{19}NO^{\bullet+}]$ 313.1461; found 313.1460.

*4,4′-((2-(Trifluoromethyl)phenoxy)methylene)bis-(methylbenzene) (**3gn**):* **1g**-NBu_4 (131 mg, 0.325 mmol) and **2n**-Br (50 mg, 0.182 mmol) were dissolved in MeCN (10 mL) and stirred for 4 h at room temperature to yield a pale yellow solution. After removal of the solvent, the crude product was purified by flash column chromatography (SiO_2, 5% pentane in ethyl acetate, R_f = 0.87) to yield **3gn** as a pale yellow oil (50.9 mg, 78%): ^1H NMR (400 MHz, $CDCl_3$) δ = 7.58 (dd, J = 7.7 Hz, J = 1.7 Hz, 1 H, 11-H), 7.36−7.34 (m, 4 H, 3-H), 7.32−7.30 (m, 1 H, 9-H), 7.15−7.13 (m, 4 H, 4-H), 6.96−6.91 (m, 2 H, 8-H and 10-H), 6.28 (s, 1 H, 1-H), 2.31 (s, 6 H, 6-H); $^{13}C\{^1H\}$ NMR (101 MHz, $CDCl_3$) δ = 155.7 (C_q, q, $J_{C,F}$ = 1.8 Hz, C-7), 138.2 (C_q, C-2), 137.6 (C_q, C-5), 133.1 (CH, C-9), 129.5

DOI: 10.1021/acs.joc.9b01485
J. Org. Chem. 2019, 84, 8837−8858

(CH, C-4), 127.3 (CH, q, $J_{C,F}$ = 5.2 Hz, C-11), 126.5 (CH, C-3), 124.0 (C_q, q, $J_{C,F}$ = 275 Hz, 12-CF_3), 120.0 (CH, C-10), 119.5 (C_q, q, $J_{C,F}$ = 30.7 Hz, C-12), 114.4 (CH, C-8), 81.4 (CH, C-1), 21.3 (CH_3, C-6); HRMS (EI$^+$) calcd m/z for [$C_{22}H_{19}F_3O^{\bullet+}$] 356.1383; found 356.1386; IR (neat) 3023, 2921, 2853, 1607, 1590, 1511, 1490, 1459, 1319, 1272, 1246, 1177, 1160, 1128, 1114, 1055, 1036, 1014, 942, 840, 804, 763, 751 cm^{-1}.

*4,4′-((4-Methoxyphenoxy)methylene)bis(methylbenzene) (**3nn**):* **1n**-K (50.0 mg, 0.309 mmol) and 18-crown-6 ether (81.5 mg, 0.308 mmol) were dissolved in MeCN (3.0 mL). To the resulting pale green solution was added a solution of **2n**-Br (84.8 mg, 0.308 mmol) in MeCN (1.5 mL), causing a color change to orange. After being stirred for 2 h at room temperature, the solvent was removed and the crude reaction product purified by flash column chromatography (SiO_2, 5% ethyl acetate in pentane, R_f = 0.91) to yield **3nn** as a yellow oil (79.1 mg, 81%): ^{1}H NMR (400 MHz, $CDCl_3$) δ = 7.30−7.28 (m, 4 H, 3-H), 7.16−7.13 (m, 4 H, 4-H), 6.90−6.86 (m, 2 H, 8-H), 6.78−6.74 (m, 2 H, 9-H), 6.06 (s, 1 H, 1-H), 3.73 (s, 3 H, 10-OMe), 2.33 (s, 6 H, 6-H); ^{13}C{^{1}H} NMR (101 MHz, $CDCl_3$) δ = 154.0 (C_q, C-10), 152.5 (C_q, C-7), 138.9 (C_q, C-2), 137.4 (C_q, C-5), 129.3 (CH, C-4), 127.0 (CH, C-3), 117.3 (CH, C-8), 114.6 (CH, C-9), 82.4 (CH, C-1), 55.8 (CH_3, 10-OMe), 21.3 (CH_3, C-6); HRMS (EI$^+$) calcd m/z for [$C_{22}H_{22}O_2^{\bullet+}$] 318.1614; found 318.1614; IR (neat) 3000, 2920, 2831, 1503, 1462, 1440, 1289, 1222, 1176, 1107, 1037, 1017, 906, 821, 806, 778, 765, 729 cm^{-1}.

*2,6-Di-tert-butyl-4-(di-p-tolylmethyl)phenol (**4on**):* Under dry argon atmosphere, a mixture of **1o**-K (9.06 mg, 0.37 mmol) and 18-crown-6 ether (9.80 mg, 0.37 mmol) in CD_3CN (0.5 mL) was added to a solution of **2n**-Br (10.2 mg, 0.037 mmol) in CD_3CN (0.25 mL). The resulting mixture was then transferred into an NMR tube, sealed, and submitted to ^{1}H NMR (and HSQC) spectroscopic analysis. The following resonances were assigned to **4on**: ^{1}H NMR (400 MHz, CD_3CN) δ = 7.10−7.08 (m, 4 H, 3-H), 7.01−6.99 (m, 4 H, 4-H), 6.97 (s, 2 H, 8-H), 5.40 (s, 1H, OH), 5.37 (s, 1 H, 1-H), 2.28 (s, 6 H, 6-H), 1.32 (s, 18 H, 12-H); ^{13}C{^{1}H} NMR (CD_3CN, from ^{1}H,^{13}C HSQC) δ = 130.05 (CH, C-4), 130.04 (CH, C-3), 56.8 (CH, C-1), 30.7 (CH_3, C-12), 20.9 (CH_3, C-6).

Reaction of Quinone Methide 2h with 1l-K. Under an atmosphere of dry argon, equimolar amounts of **1l**-K (4.0 mg, 0.027 mmol) and **2h** (9.8 mg, 0.027 mmol) were mixed in anhydrous DMSO-d_6 (total amount = 0.75 mL). The resulting green solution was analyzed by NMR spectroscopy.

Equilibrium Constants for Reactions of Phenolate Ions with Benzhydrylium Ions. The determination of equilibrium constants (at 20 °C) was carried out using a J&M TIDAS diode array spectrophotometer controlled by TIDASDAQ3 (v3) software and connected to a Hellma 661.502-QX quartz Suprasil immersion probe (light path d = 5 mm) via fiber-optic cables and standard SMA connectors. To a volume of acetonitrile (typically 20 to 25 mL) was first added a solution of the reference Lewis acid **2**-BF_4 to achieve an initial absorbance of ca. A = 1. Subsequently, a MeCN solution of the tetrabutylammonium phenolate **1**-NBu_4 was added portionwise by means of a microliter syringe.

Kinetic Measurements (Stopped-Flow Photometry). The kinetics of the reactions of phenolates (**1**) with colored electrophiles (**2**) were studied by stopped-flow UV−vis photometry (Applied Photophysics SX.20 systems) at 20 °C in acetonitrile, DMSO, and DMF. Solutions were prepared by using dry solvents that were kept under a dry nitrogen atmosphere. By using the phenolates **1** in large excess over the electrophiles **2**, their concentrations remained almost constant throughout the reactions, yielding pseudo-first-order kinetics for the decay of the electrophiles' concentrations. In some of the kinetic measurements with potassium phenolates **1**-K, 18-crown-6 ether was added to assess ion pairing effects for **1**-K solutions.

First-order rate constants k_{obs} (s^{-1}) were obtained by least-squares fitting of the single-exponential function $A_t = A_0 \exp(-k_{obs}t) + C$ to the fading absorbances of **2**. Subsequently, second-order rate constants k_2 (M^{-1} s^{-1}) were obtained as slopes of the plots of k_{obs} versus the concentrations of the phenolates **1**. See the Supporting Information for details of the individual kinetic measurements and graphs of the k_{obs} versus [**1**] correlations.

The second-order rate constants k_2 for the reactions of phenolate ions **1** with reference electrophiles **2** correlate linearly with the electrophilicity parameters E of the latter, furnishing the nucleophilicity parameters N of the phenolates **1** as the intercepts on the abscissa. The slopes of these correlations (s_N) reflect the susceptibilities of the phenolates toward changes of the reactivities of the electrophiles.

The kinetics of the reactions of phenolates with benzyl bromide in DMSO (20 °C) were measured by stopped-flow photometry following the decay of the phenolates' absorption. Benzyl bromide was used in excess to achieve pseudo-first-order conditions.

Stopped-flow techniques were also applied for following the kinetics of the reactions of benzhydryl chlorides **2r**-Cl and **2q**-Cl with varying concentrations of **1d**-NBu_4 in acetonitrile solution. Tetrabutylammonium tetrafluoroborate was added to achieve a constant ionic strength I = 2.00 × 10^{-4} M for the different reaction mixtures at 20 °C. The influence of the electrophile concentration on rates of the reactions of phenolates with benzhydryl chlorides was investigated by following the kinetics of reactions of phenolates **1c**-NBu_4 and **1d**-NBu_4 (at constant concentration) with an excess of the benzhydryl chlorides **2r**-Cl and **2q**-Cl, respectively, in acetonitrile at 20 °C.

NMR Kinetics of the 3 → 4 Isomerization. In a flame-dried flask under nitrogen, **1d**-NBu_4 (8.2 mg, 0.022 mmol) was dissolved in CD_3CN (0.5 mL) and cooled to −40 °C. Under stirring, a solution of **2a**-BF_4 (9.0 mg, 0.022 mmol) in 0.5 mL of CD_3CN was added to the cooled **1d**-NBu_4 solution and stirred for another minute. The reaction mixture was transferred into a cooled NMR tube (−78 °C), kept under nitrogen, sealed, and stored at −78 °C. The thus-prepared sample was then placed into an NMR spectrometer (at 20 °C). The progress of the isomerization reaction from **3da** to **4da** was followed by acquisition of ^{1}H NMR spectra (400 MHz, 16 scans) every 66.1 s. Whereas the increase of the product of C4 attack (**4da**) followed a monoexponential function, the decrease of the integral over the resonance of benzhydryl ethers (**3da**) did not always follow a monoexponential decease. The rearrangement of **3da** did not give the product of C-4 attack (**4da**) exclusively, however. As indicated by further resonances in the range from 5.0 to 5.5 ppm (Supporting Information), minor amounts of further C attack products formed, which were not evaluated in the kinetic analysis. By following this procedure, a first-order rate constant, k_{iso} = 1.7 × 10^{-4} s^{-1} (from the increase of **4da**), was determined (Figure 7).

Analogous results were obtained when the mixing was performed at ambient temperature followed by immediate cooling to stop the reaction progress:

(a) In an argon-filled glovebox, a solution of **2a**-BF_4 (9.8 mg, 0.024 mmol) in 0.5 mL CD_3CN was added to a solution of **1d**-NBu_4 (1 equiv, 9.0 mg, 0.024 mmol) in CD_3CN (0.5 mL). The resulting reaction mixture was transferred to an NMR tube, sealed, and immediately chilled to −78 °C. The sample was then placed into an NMR spectrometer (at 20 °C), and the isomerization was traced by evaluating the increasing integral over the resonance for the product of C-4 attack (**4da**): k_{iso} = 1.6 × 10^{-4} s^{-1}.

(b) As described above in (a) using **1d**-NBu_4 (1.5 equiv, 13.4 mg, 0.035 mmol) and **2a**-BF_4 (9.8 mg, 0.024 mmol) in 1.0 mL CD_3CN: k_{iso} = 1.7 × 10^{-4} s^{-1}.

(c) As described above in (a) using equimolar amounts of **1d**-NBu_4 (11.3 mg, 0.030 mmol) and **2c**-BF_4 (10.8 mg, 0.030 mmol) in 1.0 mL CD_3CN: k_{iso} = 5.6 × 10^{-5} s^{-1}.

(d) As described above in (a) using equimolar amounts of **1d**-NBu_4 (10.5 mg, 0.0276 mmol) and **2d**-BF_4 (10.8 mg, 0.0276 mmol) in 1.0 mL CD_3CN: k_{iso} = 1.0 × 10^{-4} s^{-1}.

Regioselectivities of Kinetically Controlled Reactions.

(a) *Intramolecular competition*: In an argon-filled glovebox, a solution of **1**-NBu_4 in 0.75 mL of anhydrous CD_3CN (distilled over CaH_2 and stored over molecular sieves) was added to an

DOI: 10.1021/acs.joc.9b01485
J. Org. Chem. 2019, 84, 8837−8858

equimolar amount of the solid benzhydryl chlorides **2**(**n**−**u**)-Cl or the benzhydryl tosylate **2u**-OTs.[60] The resulting solution was mixed, then transferred into an NMR tube, sealed, and submitted to analysis (^{1}H NMR, ^{1}H,^{13}C-HSQC).

The ratio of benzhydrylation of phenolates at O and C sites was assigned based on integration of the resonances of the benzhydrylic CH as outlined in the section on NMR kinetics. Typically, various C-alkylation products were observed, which resulted from reactions at competing aromatic positions but also possible multiple alkylations. The **3**/**4** ratios were determined without differentiating between the different carbon attack products (as exemplified for the reaction **1k**-NBu_4 + **2p**-Cl; see the Supporting Information). In a few cases, minor amounts of hydrolysis products of the benzhydrylium ion were formed (e.g., benzhydrol **2**-OH). Formation of **2**-OH does not affect the evaluation of the **3**/**4** ratio, however.

(b) *Intermolecular competition*: In an argon-filled glovebox, a solution of equimolar amounts of the tetrabutylammonium phenolates **1d**-NBu_4 and **1k**-NBu_4 in 0.75 mL of anhydrous CD_3CN (distilled over CaH_2 and stored over molecular sieves) was added to 0.5 equiv of the solid electrophile **2**(**p**−**u**)-Cl (or **2o**-BF_4) and mixed. The resulting solution was transferred into an NMR tube, sealed, and submitted to analysis (^{1}H NMR, ^{1}H,^{13}C-HSQC). To also reflect contributions by the C attack at phenolates, the product ratio of aryl benzhydryl ethers **3kX**/**3dX** was corrected with the results of the intramolecular competition experiments (see above).

The results of the intra- and intermolecular competition experiments are gathered in Table 8. Further details are given in the Supporting Information.

Computational Investigations. All systems were subjected to a conformational search with the OPLS3[61] force field as implemented in MacroModel[62] with the MCMM method in gas phase. Next, all conformers were preoptimized with the semiempirical RM1[63] method as included in the NDDO package in Maestro. Redundant conformers were eliminated, and the 10 energetically lowest lying species were optimized at the M06-2X/6-31+g(d,p) level of theory considering solvation by the SMD model for acetonitrile.[48] Thermal corrections at 298 K were obtained at the same level of theory from vibrational frequencies and are unscaled. Transition states were validated by the presence of one imaginary frequency and IRC calculations. A free energy correction of +7.91 kJ mol^{-1} was applied to all free energies to consider the conversion from gas phase (1 atm) to liquid phase (1 M). All quantum chemical calculations were performed with the Gaussian 16 A.03 set of codes.[64]

■ ASSOCIATED CONTENT

Supporting Information

The Supporting Information is available free of charge on the ACS Publications website at DOI: 10.1021/acs.joc.9b01485.

Structure−reactivity relationships; NMR and UV−vis spectra of potassium or tetrabutylammonium phenolates **1**-K/NBu_4; cyclic voltammetry for **2a**; NMR analysis of product distributions for reactions of **1**-K/NBu_4 with **2a**-BF_4; NMR spectra of all characterized products **3** and **4**; details of the determination of equilibrium constants; intra- and intermolecular competition studies; details on the regioselectivity studies; kinetic studies on the S_N1/S_N2 reactivity; details of the computational analysis (PDF)

Coordinates of optimized structures (ZIP)

■ AUTHOR INFORMATION

Corresponding Authors

*E-mail: ofial@lmu.de.

*E-mail: herbert.mayr@cup.uni-muenchen.de.

ORCID

Martin Breugst: 0000-0003-0950-8858

Armin R. Ofial: 0000-0002-9600-2793

Herbert Mayr: 0000-0003-0768-5199

Present Address

†Department of Chemistry, Organic Chemistry, University of Cologne, Greinstrasse 4, 50939 Cologne, Germany.

Notes

The authors declare no competing financial interest.

■ ACKNOWLEDGMENTS

Dedicated to Professor Hans-Ulrich Reißig on the occasion of his 70th birthday. We thank Dr. Artem I. Leonov for helpful discussions, and the Leibniz Supercomputing Center (LRZ) for providing computational resources. Financial support by the Deutsche Forschungsgemeinschaft (SFB 749, project B1) and the Fonds der Chemischen Industrie (Kekulé fellowship to R.J.M.) is gratefully acknowledged.

■ REFERENCES

(1) Gompper, R. Relations between Structure and Reactivity of Ambifunctional Nucleophilic Compounds. *Angew. Chem., Int. Ed. Engl.* **1964**, *3*, 560−570.

(2) Mayr, H.; Breugst, M.; Ofial, A. R. A Farewell to the HSAB Treatment of Ambident Reactivity. *Angew. Chem., Int. Ed.* **2011**, *50*, 6470−6505 and references on the ambident reactivity of phenolates cited therein .

(3) Breslow, R.; Groves, K.; Mayer, M. U. Antihydrophobic Cosolvent Effects for Alkylation Reactions in Water Solution, Particularly Oxygen versus Carbon Alkylations of Phenoxide Ions. *J. Am. Chem. Soc.* **2002**, *124*, 3622−3635.

(4) (a) Kornblum, N.; Lurie, A. P. Heterogeneity as a Factor in the Alkylation of Ambident Anions: Phenoxide Ions. *J. Am. Chem. Soc.* **1959**, *81*, 2705−2715. (b) Kornblum, N.; Berrigan, P. J.; Le Noble, W. J. Chemical Effects Arising From Selective Solvation: Selective Solvation as a Factor in the Alkylation of Ambident Anions. *J. Am. Chem. Soc.* **1960**, *82*, 1257−1258. (c) Kornblum, N.; Berrigan, P. J.; Le Noble, W. J. Solvation as a Factor in the Alkylation of Ambident Anions: The Importance of the Hydrogen Bonding Capacity of the Solvent. *J. Am. Chem. Soc.* **1963**, *85*, 1141−1147. (d) Fang, Y.-r.; Lai, Z.-g.; Westaway, K. C. Isotope effects in nucleophilic substitution reactions X. The effect of changing the nucleophilic atom on ion-pairing in an S_N2 reaction. *Can. J. Chem.* **1998**, *76*, 758−764.

(5) Kremers, F.; Roth, F.; Tietze, E.; Claisen, L. Über C-Alkylierung (Kernalkylierung) von Phenolen. *Justus Liebigs Ann. Chem.* **1925**, *442*, 210−245.

(6) Curtin, D. Y.; Crawford, R. J.; Wilhelm, M. Factors Controlling Position of Alkylation of Alkali Metal Salts of Phenols, Benzyl and Allyl Halides. Curtin D. Y. *J. Am. Chem. Soc.* **1958**, *80*, 1391−1397.

(7) (a) Buncel, E.; Dust, J. M. Ambident reactivity in the reaction of phenoxide ion with 2-*N*-(2′,4′-dinitrophenyl)- and 2-*N*-(4′-nitrophenyl)-4,6-dinitrobenzotriazole 1-oxides, new superelectrophiles. *Can. J. Chem.* **1988**, *66*, 1712−1719. (b) Buncel, E.; Dust, J. M.; Jonczyk, A.; Manderville, R. A.; Onyido, I. Ambident nucleophilic reactivity. 9. Regioselectivity in the reaction of ambident phenoxide ion and methoxide and hydroxide ions with 2,4,6-trinitroanisole. Kinetic and thermodynamic control. *J. Am. Chem. Soc.* **1992**, *114*, 5610−5619. (c) Buncel, E.; Manderville, R. A. Ambident reactivity of aryloxide ions towards 1,3,5-trinitrobenzene, low-temperature characterization of the elusive oxygen-bonded σ-complexes by ^{1}H and ^{13}C NMR spectroscopy. *J. Phys. Org. Chem.* **1993**, *6*, 71−82. (d) Manderville, R. A.; Dust, J. M.; Buncel, E. Reaction pathways for ambident aryloxide O- and C-nucleophiles in S_NAr displacement versus Meisenheimer complex formation with picryl halides. Stereoelectronic effects on regioselectivity. *J. Phys. Org. Chem.* **1996**, *9*, 515−528. (e) Dust, J. M.; Manderville, R. A. Carbon versus oxygen nucleophilic

DOI: 10.1021/acs.joc.9b01485
J. Org. Chem. 2019, 84, 8837−8858

selectivity in the reaction of the aryloxide ions, 2,6- and 3,5-di-tert-butylphenoxide, with the 2-[(nitro)$_x$aryl]-4,6-dinitrobenzotriazole 1-oxide series of super-electrophiles. Stereoelectronic factors on C-7 Meisenheimer complex formation versus C-1' S_NAr displacement. *Can. J. Chem.* **1998**, *76*, 662−671.
(8) (a) Pearson, R. G. Hard and Soft Acids and Bases. *J. Am. Chem. Soc.* **1963**, *85*, 3533−3539. (b) Pearson, R. G. Acids and Bases. *Science* **1966**, *151*, 172−177. (c) Pearson, R. G.; Songstad, J. Application of the Principle of Hard and Soft Acids and Bases to Organic Chemistry. *J. Am. Chem. Soc.* **1967**, *89*, 1827−1836. (d) Pearson, R. G. Hard and soft acids and bases, HSAB, part 1: Fundamental principles. *J. Chem. Educ.* **1968**, *45*, 581. (e) Pearson, R. G. Hard and soft acids and bases, HSAB, part II: Underlying theories. *J. Chem. Educ.* **1968**, *45*, 643−648. (f) Pearson, R. G. *Chemical Hardness*; Wiley-VCH: Weinheim, Germany, 1997.
(9) (a) Klopman, G. Chemical reactivity and the concept of charge- and frontier-controlled reactions. *J. Am. Chem. Soc.* **1968**, *90*, 223−234. (b) Salem, L. Intermolecular orbital theory of the interaction between conjugated systems. I. General theory. *J. Am. Chem. Soc.* **1968**, *90*, 543−552.
(10) Fleming, I. *Molecular Orbitals and Organic Chemical Reactions*; Wiley: Chichester, UK, 2009.
(11) Smith, M. B. *March's Advanced Organic Chemistry*, 7th ed.; Wiley: Hoboken, NJ, 2013; p 449.
(12) (a) Nguyen, M. T.; Kryachko, E. S.; Vanquickenborne, L. G. General and theoretical aspects of phenols. In *The Chemistry of Phenols*; Rappoport, Z., Ed.; Wiley: Chichester, UK, 2003; Chapter 1, Vol. 2, pp 1−198. (b) Yamaguchi, M. Synthetic uses of phenols. In *The Chemistry of Phenols*; Rappoport, Z., Ed.; Wiley: Chichester, UK, 2003; Chapter 10, Vol. 2, pp 661−712. (c) Reddy, V. P.; Prakash, G. K. S. Electrophilic reactions of phenols. In *The Chemistry of Phenols*; Rappoport, Z., Ed.; Wiley: Chichester, UK, 2003; Chapter 10, Vol. 2, pp 605−660.
(13) Hansch, C.; Leo, A.; Taft, R. W. A survey of Hammett substituent constants and resonance and field parameters. *Chem. Rev.* **1991**, *91*, 165−195.
(14) Williams, A. *Free Energy Relationships in Organic and Bio-Organic Chemistry*; The Royal Society of Chemistry: Cambridge, UK, 2003.
(15) Tsuji, Y.; Toteva, M. M.; Garth, H. W.; Richard, J. P. Kinetic and Thermodynamic Barriers to Carbon and Oxygen Alkylation of Phenol and Phenoxide Ion by the 1-(4-Methoxyphenyl)ethyl Carbocation. *J. Am. Chem. Soc.* **2003**, *125*, 15455−15465.
(16) Bernasconi, C. F.; Leonarduzzi, G. D. Nucleophilic addition to olefins. 6. Structure-reactivity relationships in the reactions of substituted benzylidene Meldrum's acids with water, hydroxide ion, and aryloxide ions. *J. Am. Chem. Soc.* **1982**, *104*, 5133−5142.
(17) Denmark, S. E.; Weintraub, R. C.; Gould, N. D. Effects of Charge Separation, Effective Concentration, and Aggregate Formation on the Phase Transfer Catalyzed Alkylation of Phenol. *J. Am. Chem. Soc.* **2012**, *134*, 13415−13429.
(18) (a) Nogueira, I. C.; Pliego, J. R., Jr Theoretical study of the mechanism and regioselectivity of the alkylation reaction of the phenoxide ion in polar protic and aprotic solvents. *Comput. Theor. Chem.* **2018**, *1138*, 117−122. (b) Nogueira, I. C.; Pliego, J. R., Jr Counter-ion and solvent effects in the C- and O-alkylation of the phenoxide ion with allyl chloride. *J. Phys. Org. Chem.* **2019**, *32*, e3947.
(19) Gabsi, W.; Boubaker, T.; Goumont, R. Nucleophilicities of Para-Substituted Phenoxide Ions in Water and Correlation Analysis. *Int. J. Chem. Kinet.* **2014**, *46*, 711−717.
(20) Mayr, H.; Bug, T.; Gotta, M. F.; Hering, N.; Irrgang, B.; Janker, B.; Kempf, B.; Loos, R.; Ofial, A. R.; Remennikov, G.; Schimmel, H. Reference Scales for the Characterization of Cationic Electrophiles and Neutral Nucleophiles. *J. Am. Chem. Soc.* **2001**, *123*, 9500−9512.
(21) Recently, Boubaker used the nucleophilicity parameters for ArO^- to assess the electrophilicity of 4-nitrobenzofurazan; see ref 22.
(22) Ben Salah, S.; Boubaker, T.; Goumont, R. Kinetics and mechanism of phenoxide anions addition to 4-nitrobenzofurazan in aqueous solution. *Can. J. Chem.* **2017**, *95*, 723−728.
(23) Mayr, H.; Ammer, J.; Baidya, M.; Maji, B.; Nigst, T. A.; Ofial, A. R.; Singer, T. Scales of Lewis Basicities toward C-centered Lewis Acids (Carbocations). *J. Am. Chem. Soc.* **2015**, *137*, 2580−2599.
(24) (a) Mayr, H.; Patz, M. Scales of Nucleophilicity and Electrophilicity: A System for Ordering Polar Organic and Organometallic Reactions. *Angew. Chem., Int. Ed. Engl.* **1994**, *33*, 938−957. (b) For a listing of reactivity parameters *N*, s_N, and *E*, see http://www.cup.uni-muenchen.de/oc/mayr/DBintro.html.
(25) Streidl, N.; Denegri, B.; Kronja, O.; Mayr, H. A Practical Guide for Estimating Rates of Heterolysis Reactions. *Acc. Chem. Res.* **2010**, *43*, 1537−1549.
(26) (a) Mayr, H.; Kempf, B.; Ofial, A. R. π-Nucleophilicity in Carbon-Carbon Bond-Forming Reactions. *Acc. Chem. Res.* **2003**, *36*, 66−77. (b) Mayer, R. J.; Hampel, N.; Mayer, P.; Ofial, A. R.; Mayr, H. Synthesis, Structure and Properties of Amino-Substituted Benzhydrylium Ions - a Link Between Ordinary Carbocations and Neutral Electrophiles. *Eur. J. Org. Chem.* **2019**, 412−421.
(27) Lucius, R.; Loos, R.; Mayr, H. Kinetic Studies of Carbocation-Carbanion Combinations: Key to a General Concept of Polar Organic Reactivity. *Angew. Chem., Int. Ed.* **2002**, *41*, 91−95.
(28) Richter, D.; Hampel, N.; Singer, T.; Ofial, A. R.; Mayr, H. Synthesis and Characterization of Novel Quinone Methides: Reference Electrophiles for the Construction of Nucleophilicity Scales. *Eur. J. Org. Chem.* **2009**, 3203−3211.
(29) Seeliger, F.; Berger, S. T. A.; Remennikov, G. Y.; Polborn, K.; Mayr, H. Electrophilicity of 5-Benzylidene-1,3-dimethyl-barbituric and -thiobarbituric Acids. *J. Org. Chem.* **2007**, *72*, 9170−9180.
(30) Kaumanns, O.; Mayr, H. Electrophilicity Parameters of 5-Benzylidene-2,2-dimethyl-[1,3]dioxane-4,6-diones (Benzylidene Meldrum's Acids). *J. Org. Chem.* **2008**, *73*, 2738−2745.
(31) Mayr, H.; Ofial, A. R. Philicities, Fugalities, and Equilibrium Constants. *Acc. Chem. Res.* **2016**, *49*, 952−965.
(32) Equilibrium measurements with tetrabutylammonium phenolates were better reproducible than those with potassium phenolates.
(33) (a) Chantooni, M. K., Jr.; Kolthoff, I. M. Comparison of Substituent Effects on Dissociation and Conjugation of Phenols with Those of Carboxylic Acids in Acetonitrile, *N,N*-Dimethylformamide, and Dimethyl Sulfoxide. *J. Phys. Chem.* **1976**, *80*, 1306−1310. (b) Kütt, A.; Leito, I.; Kaljurand, I.; Sooväli, L.; Vlasov, V. M.; Yagupolskii, L. M.; Koppel, I. A. A Comprehensive Self-Consistent Spectrophotometric Acidity Scale of Neutral Brønsted Acids in Acetonitrile. *J. Org. Chem.* **2006**, *71*, 2829−2838.
(34) Minegishi, S.; Mayr, H. How Constant are Ritchie's "Constant Selectivity Relationships"? − A General Reactivity Scale for n-, π-, and σ-Nucleophiles. *J. Am. Chem. Soc.* **2003**, *125*, 286−295.
(35) (a) Matić, M.; Denegri, B.; Kronja, O. Solvolytic Reactivity of 2,4-Dinitrophenolates. *Eur. J. Org. Chem.* **2010**, 6019−6024. (b) Matić, M.; Bebek, N.; Denegri, B.; Kronja, O. Nucleofugality of Pentafluorophenolate in Various Solvents: Solvolytic Behavior of Phenolates. *Croat. Chem. Acta* **2016**, *89*, 355−362. (c) Denegri, B.; Matić, M.; Kronja, O. Impact of Electronic Effects on the Nucleofugality of Leaving Groups. *Synthesis* **2017**, *49*, 3422−3432.
(36) Schaller, H. F.; Tishkov, A. A.; Feng, X.; Mayr, H. Direct Observation of the Ionization Step in Solvolysis Reactions: Electrophilicity versus Electrofugality of Carbocations. *J. Am. Chem. Soc.* **2008**, *130*, 3012−3022.
(37) Bordwell, F. G.; Boyle, W. J., Jr.; Hautala, J. A.; Yee, K. C. Brønsted Coefficients Larger Than 1 and Less than 0 for Proton Removal from Carbon Acids. *J. Am. Chem. Soc.* **1969**, *91*, 4002−4003.
(38) (a) Bernasconi, C. F. The principle of nonperfect synchronization: recent developments. *Adv. Phys. Org. Chem.* **2010**, *44*, 223−324. (b) Bernasconi, C. F. Nucleophilic addition to olefins. Kinetics and mechanism. *Tetrahedron* **1989**, *45*, 4017−4090. (c) Bernasconi, C. F. Intrinsic Barriers of Reactions and the Principle of Nonperfect Synchronization. *Acc. Chem. Res.* **1987**, *20*, 301−308. (d) Bernasconi, C. F. The Principle of Non-perfect Synchronization. *Adv. Phys. Org. Chem.* **1992**, *27*, 119−238.
(39) Shad, S. T. A.; Khan, K. M.; Heinrich, A. M.; Choudhary, M. I.; Voelter, W. An efficient approach towards syntheses of ethers and

DOI: 10.1021/acs.joc.9b01485
J. Org. Chem. 2019, 84, 8837−8858

esters using CsF−Celite as a solid base. *Tetrahedron Lett.* **2002**, *43*, 8603−8606.
(40) As more nucleophilic phenolate ions cannot be studied with respect to **2a**, this crossing of relative reactivities cannot be shown in Figure 9.
(41) (a) Bordwell, F. G.; Cheng, J.-P. Substituent effects on the stabilities of phenoxyl radicals and the acidities of phenoxyl radical cations. *J. Am. Chem. Soc.* **1991**, *113*, 1736−1743. (b) Kolthoff, I. M.; Chantooni, M. K., Jr.; Bhowmik, S. Dissociation Constants of Uncharged and Monovalent Cation Acids in Dimethyl Sulfoxide. *J. Am. Chem. Soc.* **1968**, *90*, 23−28. (c) Kütt, A.; Movchun, V.; Rodima, T.; Dansauer, T.; Rusanov, E. B.; Leito, I.; Kaljurand, I.; Koppel, J.; Pihl, V.; Koppel, I.; Ovsjannikov, G.; Toom, L.; Mishima, M.; Medebielle, M.; Lork, E.; Röschenthaler, G.-V.; Koppel, I. A.; Kolomeitsev, A. A. Pentakis(trifluoromethyl)phenyl, a Sterically Crowded and Electron-withdrawing Group: Synthesis and Acidity of Pentakis(trifluoromethyl)benzene, -toluene, -phenol, and -aniline. *J. Org. Chem.* **2008**, *73*, 2607−2620.
(42) (a) Cripe, T. A. Nucleophilicity and Basicity. Ph.D. Dissertation, Nothwestern University, Evanston, IL, 1986. (b) Bordwell, F. G.; Cripe, T. A.; Hughes, D. L. Nucleophilicity, Basicity, and the Brønsted Equation. In *Nucleophilicity*; Harris, J. M., McManus, S. P., Eds.; American Chemical Society: Washington, DC, 1987; Chapter 9, pp 137−153.
(43) Ellington, J. C.; Arnett, E. M. Kinetics and Thermodynamics of Phenolate Silylation and Alkylation. *J. Am. Chem. Soc.* **1988**, *110*, 7778−7785.
(44) Bartoli, G.; Ciminale, F.; Todesco, P. E. Electronic and Steric Effects in Nucleophilic Aromatic Substitution. Reaction by Phenoxides as Nucleophiles in Dimethyl Sulfoxide. *J. Org. Chem.* **1975**, *40*, 872−874.
(45) Arnett, E. M.; Amarnath, K.; Harvey, N. G.; Venimadhavan, S. Heterolysis and Homolysis Energies for Some Carbon-Oxygen Bonds. *J. Am. Chem. Soc.* **1990**, *112*, 7346−7353.
(46) (a) Bordwell and co-workers measured the oxidation potentials of phenolate ions with the Fc^+/Fc couple as internal standard, for which they reported a value of 875 mV (vs Ag/AgI, from ref 41a). We converted these data to E_{ox} vs SCE by re-referencing to the Fc^+/Fc potential of 435 mV in DMSO reported in ref 46b, that is, we subtracted 440 mV from Bordwell's E_{ox}. (b) Aranzaes, J. R.; Daniel, M.-C.; Astruc, D. Metallocenes as references for the determination of redox potentials by cyclic voltammetry − Permethylated iron and cobalt sandwich complexes, inhibition by polyamine dendrimers, and the role of hydroxy-containing ferrocenes. *Can. J. Chem.* **2006**, *84*, 288−299.
(47) Ofial, A. R.; Ohkubo, K.; Fukuzumi, S.; Lucius, R.; Mayr, H. Role of Electron Transfer Processes in Reactions of Diarylcarbenium Ions and Related Quinone Methides with Nucleophiles. *J. Am. Chem. Soc.* **2003**, *125*, 10906−10912.
(48) (a) Zhao, Y.; Truhlar, D. G. The M06 suite of density functionals for main group thermochemistry, thermochemical kinetics, noncovalent interactions, excited states, and transition elements: two new functionals and systematic testing of four M06-class functionals and 12 other functionals. *Theor. Chem. Acc.* **2008**, *120*, 215−241. (b) Marenich, A. V.; Cramer, C. J.; Truhlar, D. G. Universal Solvation Model Based on Solute Electron Density and on a Continuum Model of the Solvent Defined by the Bulk Dielectric Constant and Atomic Surface Tensions. *J. Phys. Chem. B* **2009**, *113*, 6378−6396.
(49) In order to directly compare experimental with calculated Gibbs energies in solution, a free energy change of + 7.91 kJ/mol was applied to all free energies for their conversion from gas phase (1 atm) to liquid phase (1 M).
(50) Scheme 3 shows a similar behavior of the phenolate **1g** (*o*-CF_3), which also possesses a free *para*-position. Low concentrations of byproducts (<5%) were observed in the ^{1}H NMR spectra of crude **4da** and **4ga** but could not be assigned unequivocally to products from *ortho* attack at the corresponding phenolates.
(51) For example, the reaction of **2u**-Cl with **1d**-NBu_4 reached only 37% conversion after 3 days at ambient temperature (further examples are given in the Supporting Information).
(52) Flora, H. B., II; Gilkerson, W. R. Association of triethanolamine and related ligands with alkali metal ions and ion pairs in tetrahydrofuran at 25 °C. *J. Phys. Chem.* **1976**, *80*, 679−685.
(53) S, S.; Min, J. K.; Seong, J. E.; Na, S. J.; Lee, B. Y. A Highly Active and Recyclable Catalytic System for CO_2/Propylene Oxide Copolymerization. *Angew. Chem., Int. Ed.* **2008**, *47*, 7306−7309.
(54) Binder, D. A.; Kreevoy, M. M. Interaction of Li+ with Phenoxide Ions in Acetonitrile. *J. Phys. Chem.* **1994**, *98*, 10008−10016.
(55) Khalfina, I. A.; Beregovaya, I. V.; Vlasov, V. M. Structure of Potassium Carbonate Complexes with Phenols and Thiophenols in Aproyic Dipolar Solvents. *Russ. J. Org. Chem.* **2003**, *39*, 1104−1115.
(56) Shi, A.; Nguyen, T. A.; Battina, S. K.; Rana, S.; Takemoto, D. J.; Chiang, P. K.; Hua, D. H. Synthesis and anti-breast cancer activities of substituted quinolones. *Bioorg. Med. Chem. Lett.* **2008**, *18*, 3364−3368.
(57) Rodrigue, A.; Bovenkamp, J. W.; Lacroix, B. V.; Bannard, R. A. B.; Buchanan, G. W. Complexes of 18-crown-6 macrocyclic ethers obtained from ethereal solvents. Complexes of potassium and sodium salts with host:guest ratios of 1:2 and 1:3. *Can. J. Chem.* **1986**, *64*, 808−815.
(58) Ibrahim, N.; Vilhelmsen, M. H.; Pernpointner, M.; Rominger, F.; Hashmi, A. S. K. Gold Phenolate Complexes: Synthesis, Structure, and Reactivity. *Organometallics* **2013**, *32*, 2576−2583.
(59) Manderville, R. A.; Buncel, E. An Unexpected Ring Protonation in Meisenheimer Complex Formation. *J. Org. Chem.* **1997**, *62*, 7614−7620.
(60) (a) Denegri, B.; Streiter, A.; Jurić, S.; Ofial, A. R.; Kronja, O.; Mayr, H. Kinetics of the Solvolyses of Benzhydryl Derivatives: Basis for the Construction of a Comprehensive Nucleofugality Scale. *Chem. - Eur. J.* **2006**, *12*, 1648−1656; *Chem. - Eur. J.* **2006**, *12*, 5415. (b) The tosylate **2u**-OTs was prepared from **2u**-Cl and AgOTs in Et_2O. After filtration from the precipitated silver salts, the filtrate was concentrated carefully until precipitation started. The remaining solvent was removed by using a Pasteur pipet, and the solid residue was dried in vacuum at −78 °C. Dry **2u**-OTs was highly unstable and turned reddish at room temperature within seconds. Therefore, care was taken to ensure that **2u**-OTs was handled at as low temperatures as possible.
(61) Harder, E.; Damm, W.; Maple, J.; Wu, C.; Reboul, M.; Xiang, J. Y.; Wang, L.; Lupyan, D.; Dahlgren, M. K.; Knight, J. L.; Kaus, J. W.; Cerutti, D.S.; Krilov, G.; Jorgensen, W. L.; Abel, R.; Friesner, R. A. OPLS3: A Force Field Providing Broad Coverage of Drug-like Small Molecules and Proteins. *J. Chem. Theory Comput.* **2016**, *12*, 281−296.
(62) *Schrödinger Release 2019-1*; MacroModel, Schrödinger, LLC: New York, 2019.
(63) Rocha, G. B.; Freire, R. O.; Simas, A. M.; Stewart, J. J. P. RM1: A reparameterization of AM1 for H, C, N, O, P, S, F, Cl, Br, and I. *J. Comput. Chem.* **2006**, *27*, 1101−1111.
(64) Frisch, M. J.; Trucks, G. W.; Schlegel, H. B.; Scuseria, G. E.; Robb, M. A.; Cheeseman, J. R.; Scalmani, G.; Barone, V.; Petersson, G. A.; Nakatsuji, H.; Li, X.; Caricato, M.; Marenich, A. V.; Bloino, J.; Janesko, B. G.; Gomperts, R.; Mennucci, B.; Hratchian, H. P.; Ortiz, J. V.; Izmaylov, A. F.; Sonnenberg, J. L.; Williams-Young, D.; Ding, F.; Lipparini, F.; Egidi, F.; Goings, J.; Peng, B.; Petrone, A.; Henderson, T.; Ranasinghe, D.; Zakrzewski, V. G.; Gao, J.; Rega, N.; Zheng, G.; Liang, W.; Hada, M.; Ehara, M.; Toyota, K.; Fukuda, R.; Hasegawa, J.; Ishida, M.; Nakajima, T.; Honda, Y.; Kitao, O.; Nakai, H.; Vreven, T.; Throssell, K.; Montgomery, J. A., Jr.; Peralta, J. E.; Ogliaro, F.; Bearpark, M. J.; Heyd, J. J.; Brothers, E. N.; Kudin, K. N.; Staroverov, V. N.; Keith, T. A.; Kobayashi, R.; Normand, J.; Raghavachari, K.; Rendell, A. P.; Burant, J. C.; Iyengar, S. S.; Tomasi, J.; Cossi, M.; Millam, J. M.; Klene, M.; Adamo, C.; Cammi, R.; Ochterski, J. W.; Martin, R. L.; Morokuma, K.; Farkas, O.; Foresman, J. B.; Fox, D. J. *Gaussian 16*, revision A.03; Gaussian, Inc.: Wallingford, CT, 2016.

DOI: 10.1021/acs.joc.9b01485
J. Org. Chem. 2019, 84, 8837−8858

4.1 Additional Figures and Correlations

Table S1: Physicochemical Properties of Phenolates Used for the Correlations Below

Phenolate	pK_{aH}(DMSO)	pK_{aH}(MeCN)	pK_{aH}(DMF)	$\sigma_{p/m}$[a]	ε_{HOMO}[b]
1c (*p*-NO_2)	10.8[c]	20.7[f]	11.84[f]	1.27	−0.10236
1d (*o*-NO_2)	11.0[d]	22[f]	12.14[f]	-	−0.09712
1e (*m*-NO_2)	14.4[c]	23.85[f]	13.85[f]	0.71	−0.08473
1f (*p*-CN)	13.2[c]	22.77[f]	13.3[i]	1.00	−0.08715
1g (*o*-CF_3)	14.4[e]	24.88[e]	-	-	−0.07913
1h (*p*-CF_3)	15.2[c]	25.54[e]	-	0.65	−0.08235
1i (*m*-CF_3)	15.6[c]	24.9[f]	15.7[j]	0.43	−0.07478
1j (*p*-Cl)	16.75[c]	25.44[f]	14.5[f]	0.19	−0.06464
1k (H)	18.0[c]	26.6[f]	18.4[f]	0	−0.05257
1l (*p*-CH_3)	18.9[c]	27.45[f]	18.6[i]	−0.17	−0.04942
1m (*p*-*t*Bu)	19.05[c]	27.48[g]		−0.15	−0.05533
1n (*p*-OMe)	19.1[c]	28.14[f]	19.1[i]	−0.26	−0.04541
1o (*o,o'*-(*t*Bu)$_2$)	17.3[c]	(27.6)[h]	-	-	−0.06727
1q (*m*-OMe)	-	-	-	0.12	-

[a] From ref. 1. [b] In Hartree, calculated in gas phase at the M06-2X/6-31+G(d,p) level of theory (for details, see the computational part in this Supporting Information). [c] From ref. 2. [d] From ref. 3. [e] From ref. 4. [f] from ref. 5. [g] from ref. 6. [h] pK_{aH} estimated from the linear correlation of pK_{aH}(MeCN) vs. pK_{aH}(DMSO) in Figure S1. [i] From ref. 7. [j] From ref. 8.

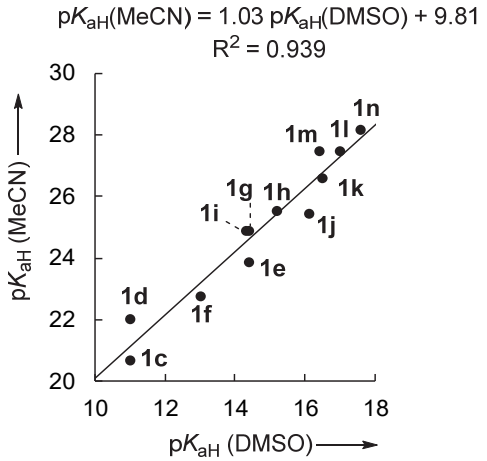

Figure S1: Correlation of pK_{aH} of phenolates in MeCN with those in DMSO.

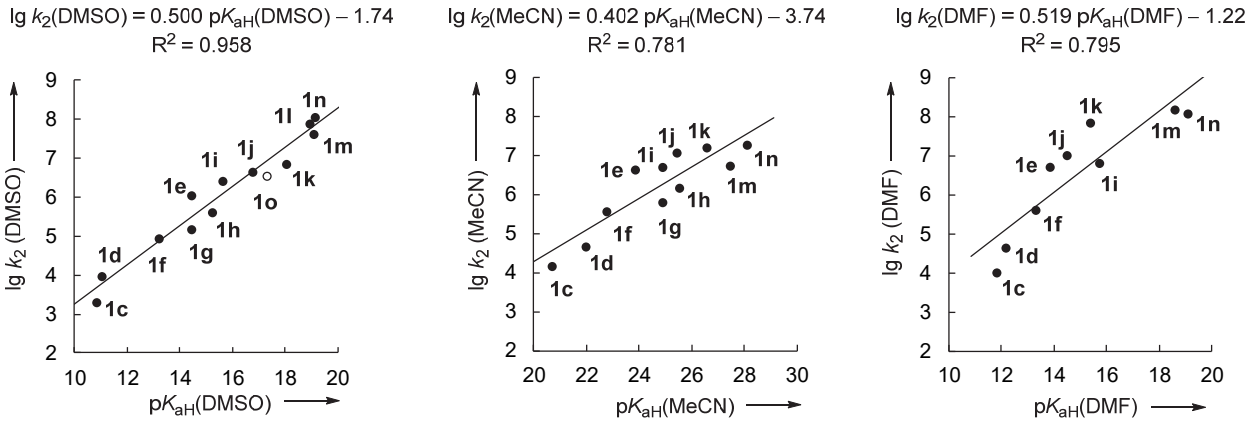

Figure S2: Brønsted correlations of the rate constants for the reactions of phenolate ions with benzhydrylium ion **2a** (the rates for **1l**–**n** were calculated using equation 1) with experimental pK_{aH} values of **1** in DMSO, MeCN, and DMF (left to right).

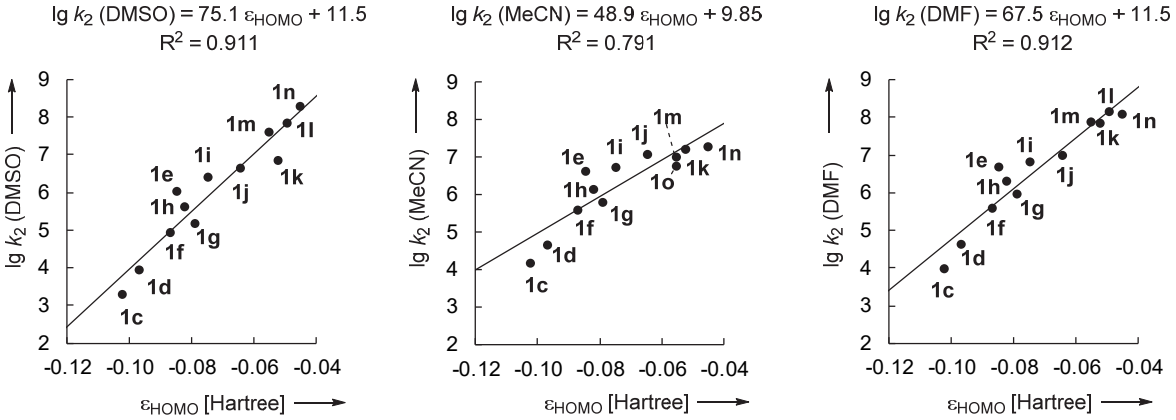

Figure S3: Linear correlation of lg k_2(**2a**) vs ε_{HOMO} of phenolates **1** (gas phase, M06-2X/6-31+G(d,p)).

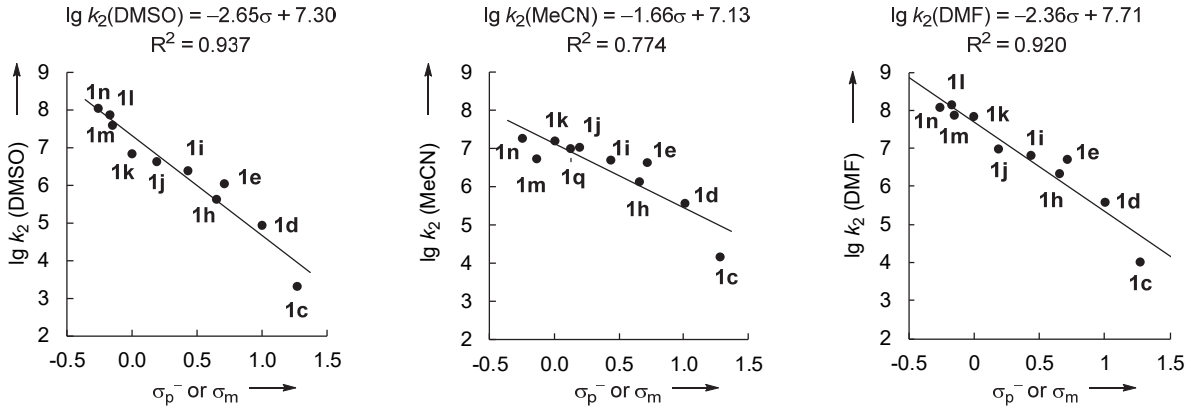

Figure S4: Correlation of the rate constants (lg k_2) for the reactions of phenolates **1** and the benzhydrylium ion **2a** with Hammett substituent constants σ_p^- (or σ_m) in DMSO, MeCN and DMF.

4.2 Correlation of Phenolate Reactivities with Literature Data

The following section gives an overview on previously reported experimental rate constants for the reactions of phenoxide ions with electrophiles in S_N2 and S_NAr reactions in aprotic solvents, which were correlated with rate constants determined in this work using benzhydrylium ions or quinone methides as reference electrophiles.

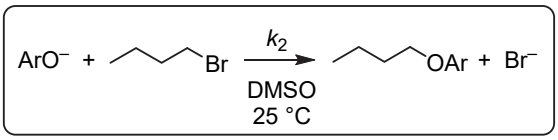

lg k_2(*n*BuBr) = 0.967 lg k_2(**2g**) – 7.00

Phenolate	k_2(*n*-BuBr) (M^{-1} s^{-1})
1j (*p*-Cl)	1.23×10^{-3}
1k (H)	4.19×10^{-3}
1n (*p*-OMe)	1.45×10^{-2}

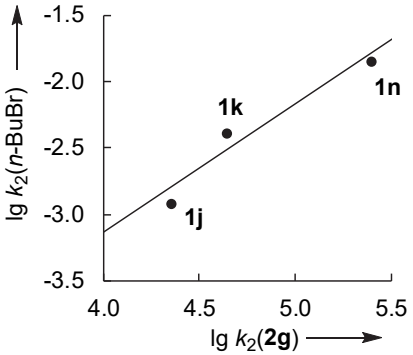

Figure S5: Correlation of rate constants for the reactions of phenolates **1** with n-BuCl (DMSO, 25 °C) from Cripe and Bordwell[9] against their reactivities towards **2g** (DMSO, 20 °C).

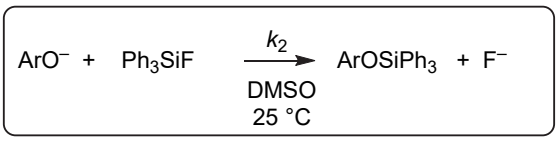

lg k_2(Ph_3SiF) = 0.94 lg k_2(**2a**) – 3.59

Phenolate	k_2(Ph_3SiF) (M^{-1} s^{-1})
1c (*p*-NO_2)	2.21×10^{-1}
1f (*p*-CN)	7.58
1h (*p*-CF_3)	3.23×10^{2}
1j (*p*-Cl)	6.61×10^{2}
1m (*p*-tBu)	1.28×10^{3}

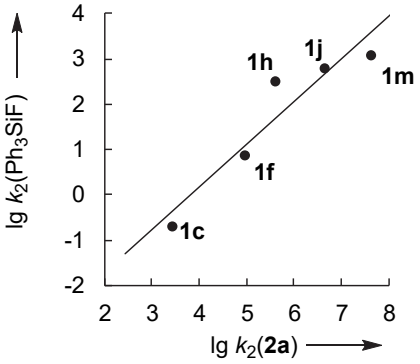

Figure S6: Correlation of rate constants for the reactions of potassium phenolates **1**-K with Ph_3SiF (DMSO, 25 °C) from Arnett and coworkers[10] against their reactivities towards **2a** (DMSO, 20 °C).

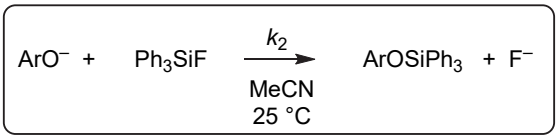

lg k_2(Ph$_3$SiF) = 0.41 lg k_2(**2a**) – 2.00

Phenolate	k_2(Ph$_3$SiF) (M^{-1} s^{-1})
1c (*p*-NO_2)	7.16×10^{-1}
1f (*p*-CN)	1.16
1h (*p*-CF_3)	2.91
1j (*p*-Cl)	1.06×10^{1}

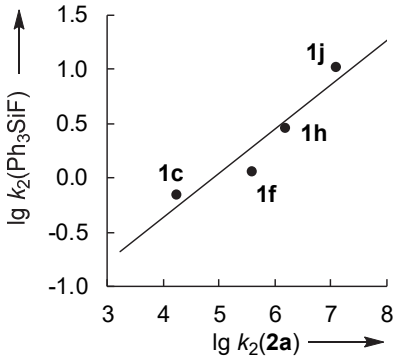

Figure S7: Correlation of rate constants for the reactions of potassium phenolates **1**-K with Ph_3SiF (MeCN, 25 °C) from Arnett and coworkers[10] against their reactivities towards **2a** (MeCN, 20 °C).

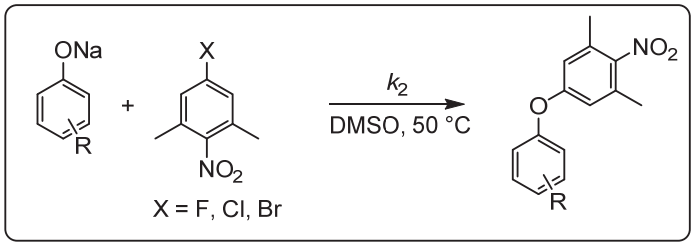

Phenolate	k_2(X = F) (M^{-1} s^{-1})	k_2(X = Cl) (M^{-1} s^{-1})	k_2(X = Br) (M^{-1} s^{-1})
1j (*p*-Cl)	1.20×10^{-1}	4.40×10^{-4}	6.70×10^{-4}
1k (H)	4.90×10^{-1}	2.10×10^{-3}	4.00×10^{-3}
1l (*p*-Me)	1.45	8.20×10^{-3}	1.20×10^{-2}

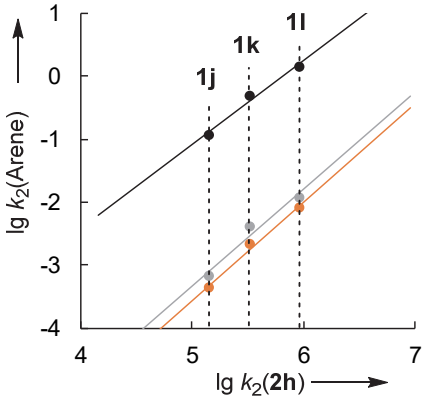

lg k_2(X = F) = 1.33 lg k_2(**2h**) – 7.70

lg k_2(X = Br) = 1.53 lg k_2(**2h**) – 11.0

lg k_2(X = Cl) = 1.56 lg k_2(**2h**) – 11.4

Figure S8: Correlations of rate constants for the reactions of sodium phenolates **1**-Na with 2,6-dimethyl-4-nitro-1-halobenzenes (DMSO, 50 °C) from Bartoli and coworkers[11] against their reactivities towards **2h** (DMSO, 20 °C).

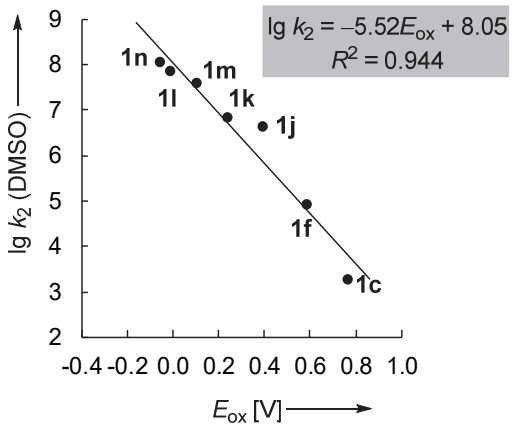

Figure S9: Correlation of the rate constants (lg k_2) of the reactions of phenolates **1** with the benzhydrylium ion **2a** with the reversible oxidation potentials E_{ox} [vs SCE in sulfolane/3-methylsulfolane (5%), 25 °C] from Arnett.[12] The values were converted from the SHE to the SCE by subtraction of 244 mV.

4.3 Lewis Basicity of Phenolates (in MeCN)

As outlined in the main text, we studied the reactions of phenolates **1** with the electrophile **2b** at the M06-2X/6-31+G(d,p) level in combination with the SMD continuum solvation model for acetonitrile. Reaction Gibbs energies for the carbon-oxygen bond forming reactions are collected in Table S2. Figure S10 shows a correlation of $\Delta_rG^0_{calcd}$ (from Table S2) with the pK_{aH} of the phenolates in MeCN. The $\Delta_rG^0_{calcd}$ in acetonitrile also correlate linearly with σ_p and σ_m of substituents at the phenolates (Figure S11).

Table S2: Quantum chemically calculated Gibbs energies Δ_rG^0 (kJ mol^{-1}) for the reaction of **2b** with different phenolates (O-attack) in MeCN.

Nu	pK_{aH}(MeCN)	$\Delta_rG^0_{exptl}$[a]	$\Delta_rG^0_{calcd}$
1a	16.66	(+5.9)	+4.3
1b	20.11	−8.0	−21.8
1c	20.7	−22.7	−35.7
1d	22	−18.1	−32.8
1e	23.85		−58.8
1f	22.77		−49.7
1g	24.88		−52.2
1h	25.54		−57.8
1i	24.9		−59.0
1j	25.44		−72.7
1k	26.6		−80.2
1l	27.45		−88.4
1m	27.48		−86.2
1n	28.14		−89.2
1o	(27.6)[b]		−42.8

[a] Calculated from $\Delta_rG^0 = -RT\ln K$ with experimental equilibrium constants (Table 1) or equilibrium constants calculated using equation 2 based on the Lewis basicities LB in Table 1 and Lewis acidities LA from Chart 2. [b] pK_{aH} estimated from the linear correlation of pK_{aH}(MeCN) vs. pK_{aH}(DMSO) in Figure S1.

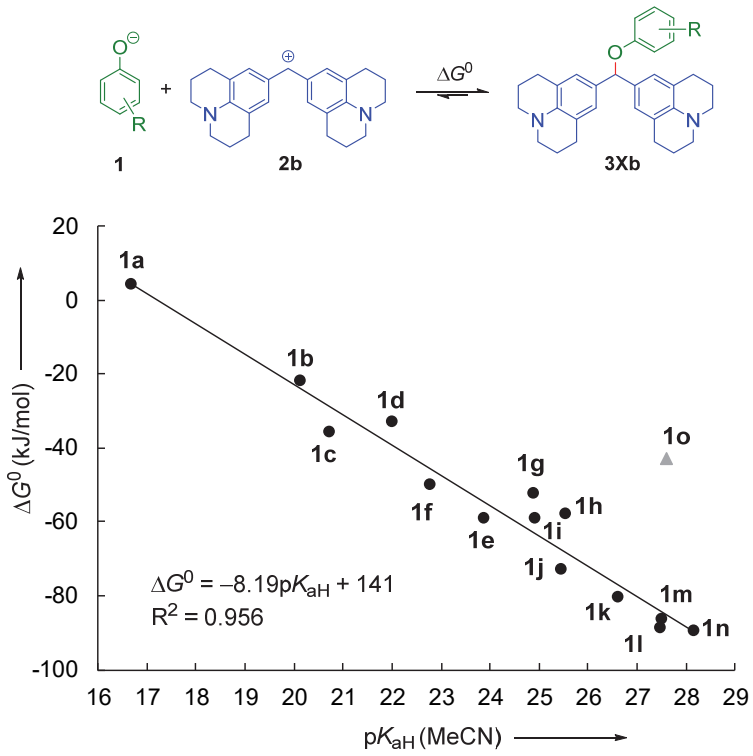

Figure S10: Correlation of quantum chemically determined Gibbs energies for the reactions of phenolates (O-attack) with **2b** with the Brønsted basicities (pK_{aH}) of the phenolates in acetonitrile (see Table S1, for **1a** and **1b** see ref. 13). The point for **1o** was not used for calculating the correlation (pK_{aH} for **1o** was estimated from the linear correlation of pK_{aH}(MeCN) vs. pK_{aH}(DMSO) in Figure S1).

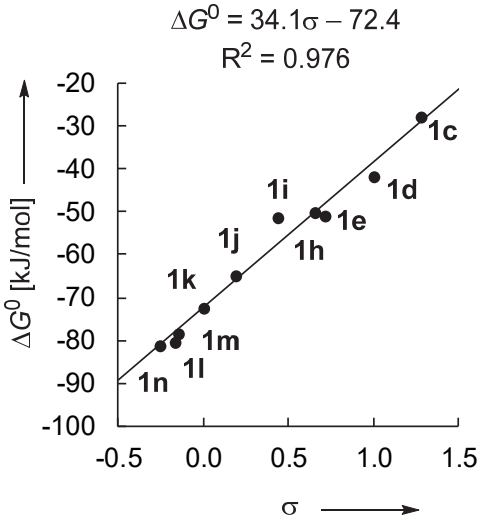

Figure S11: Correlation quantum-chemically calculated Gibbs energies $\Delta_r G^0$ for the reaction of **2b** with different phenolates in acetonitrile with Hammett σ_p^- and σ_m constants for the substituents at the phenolates.

4.4 Electrochemical Characterization of 2a

Cyclic voltammetry measurements were performed in deaerated DMSO containing 0.1 M NBu_4ClO_4 with **2a**-BF_4 (c = 3.3 × 10^{-4} M) and ferrocene (c = 3.3 × 10^{-4} M) as an internal standard.

The $E_{1/2}(fc^+/fc$ in DMSO) = +0.435 V (from ref. 14) was used to calibrate E_p^{red} (**2a** in DMSO) vs SCE.

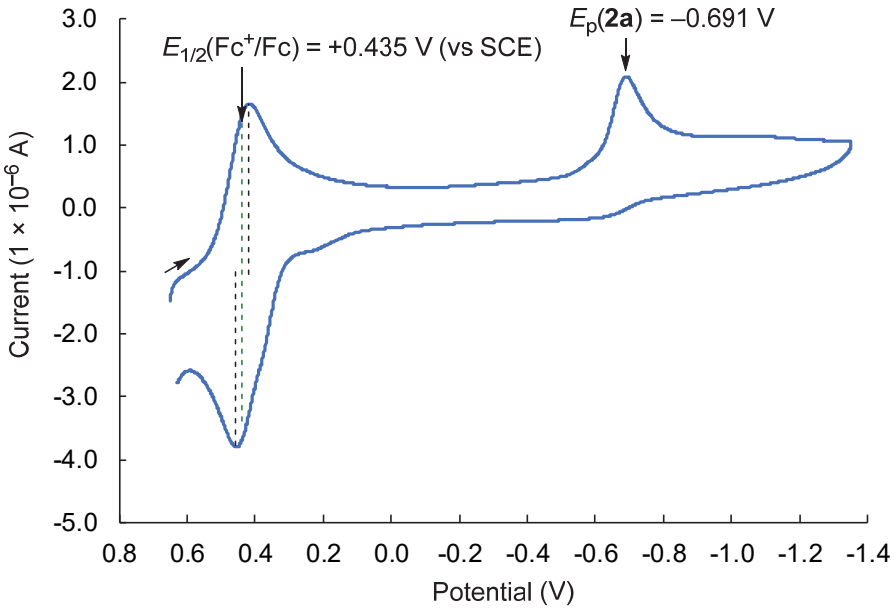

4.5 UV/Vis Spectra of Phenolates in DMSO

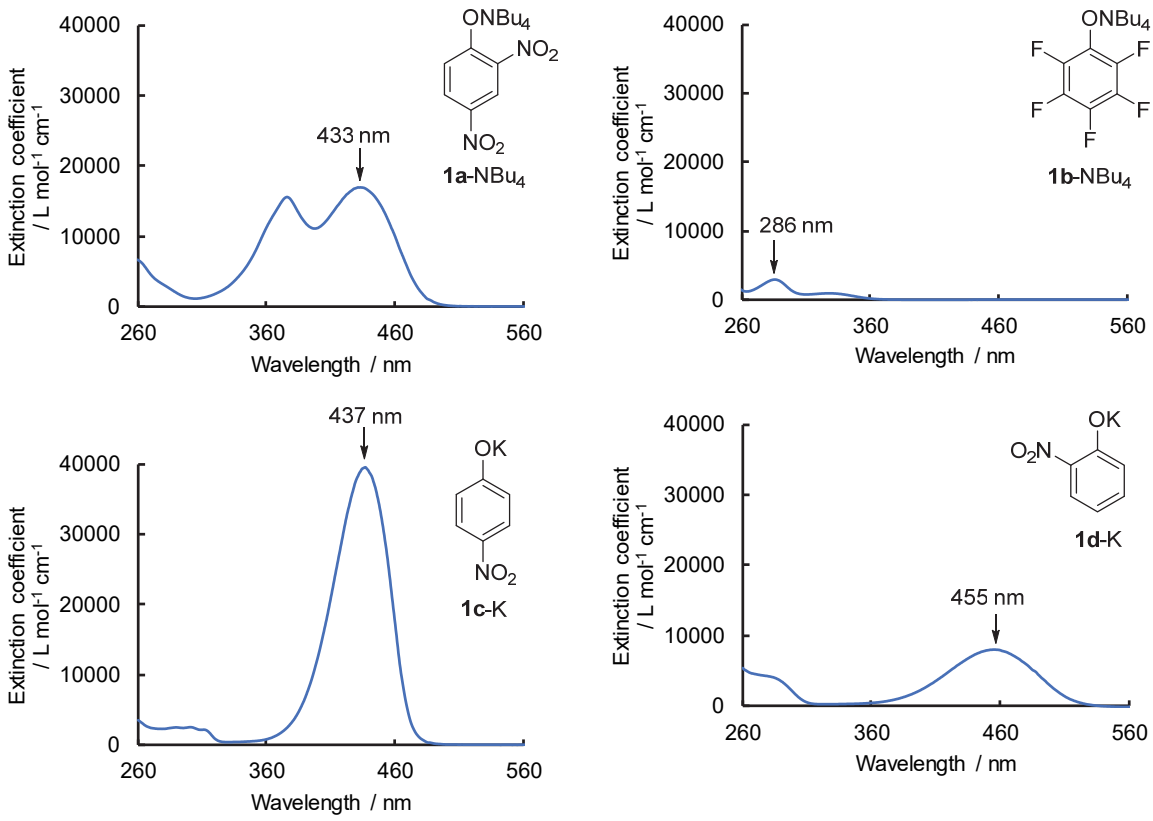

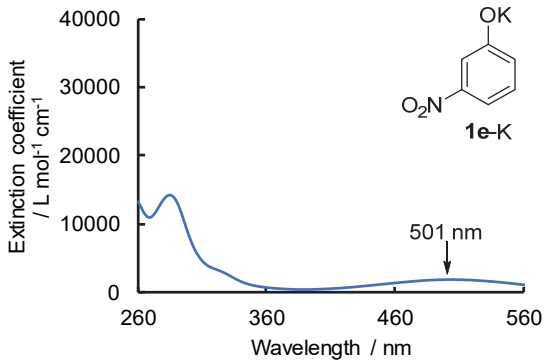
Extinction coefficient / L mol-1 cm-1
40000
30000
20000
10000
0
260
360
460
560
Wavelength / nm
OK
O2N
1e-K
501 nm

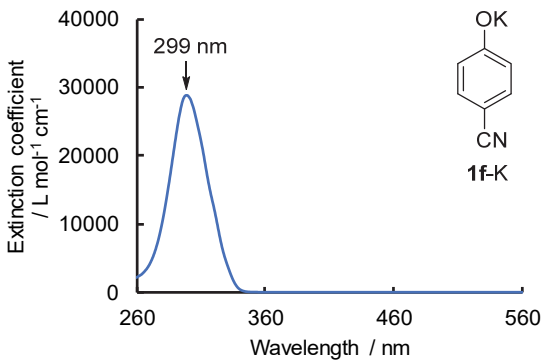
Extinction coefficient / L mol-1 cm-1
40000
30000
20000
10000
0
260
360
460
560
Wavelength / nm
299 nm
OK
CN
1f-K

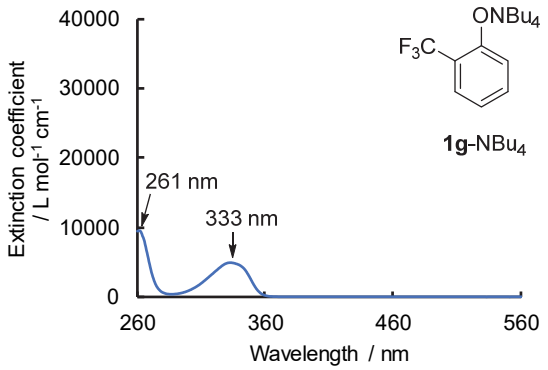
Extinction coefficient / L mol-1 cm-1
40000
30000
20000
10000
0
260
360
460
560
Wavelength / nm
ONBu4
F3C
1g-NBu4
261 nm
333 nm

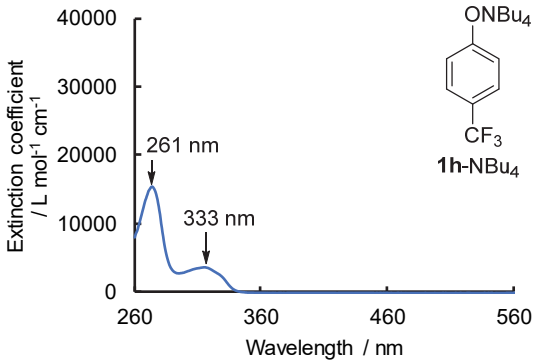
Extinction coefficient / L mol-1 cm-1
40000
30000
20000
10000
0
260
360
460
560
Wavelength / nm
ONBu4
CF3
1h-NBu4
261 nm
333 nm

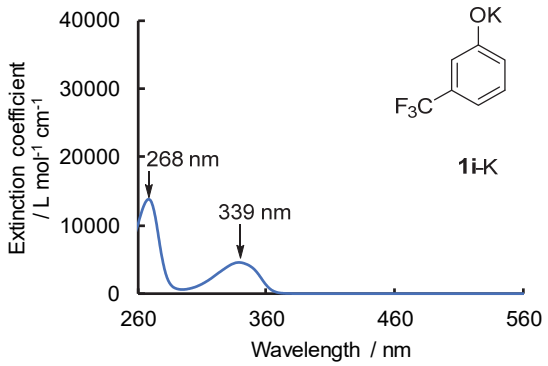
Extinction coefficient / L mol-1 cm-1
40000
30000
20000
10000
0
260
360
460
560
Wavelength / nm
OK
F3C
1i-K
268 nm
339 nm

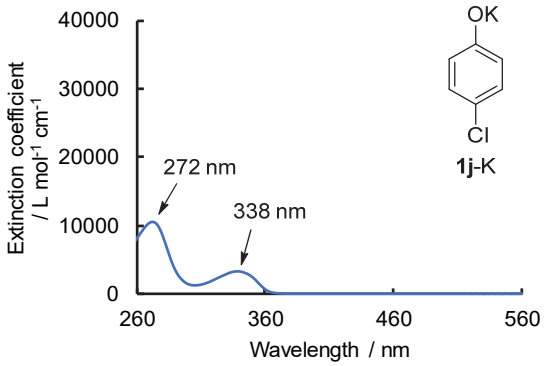
Extinction coefficient / L mol-1 cm-1
40000
30000
20000
10000
0
260
360
460
560
Wavelength / nm
OK
Cl
1j-K
272 nm
338 nm

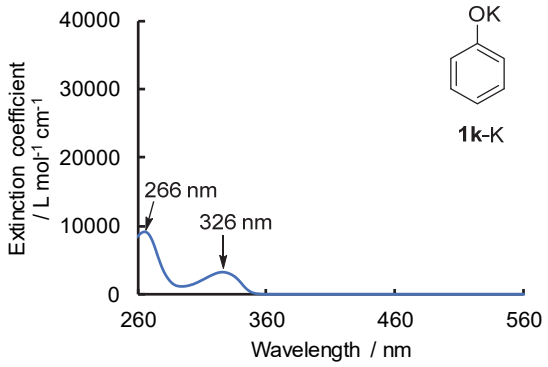
Extinction coefficient / L mol-1 cm-1
40000
30000
20000
10000
0
260
360
460
560
Wavelength / nm
OK
1k-K
266 nm
326 nm

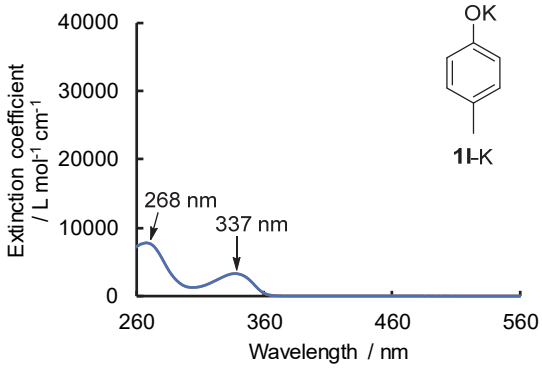
Extinction coefficient / L mol-1 cm-1
40000
30000
20000
10000
0
260
360
460
560
Wavelength / nm
OK
1l-K
268 nm
337 nm

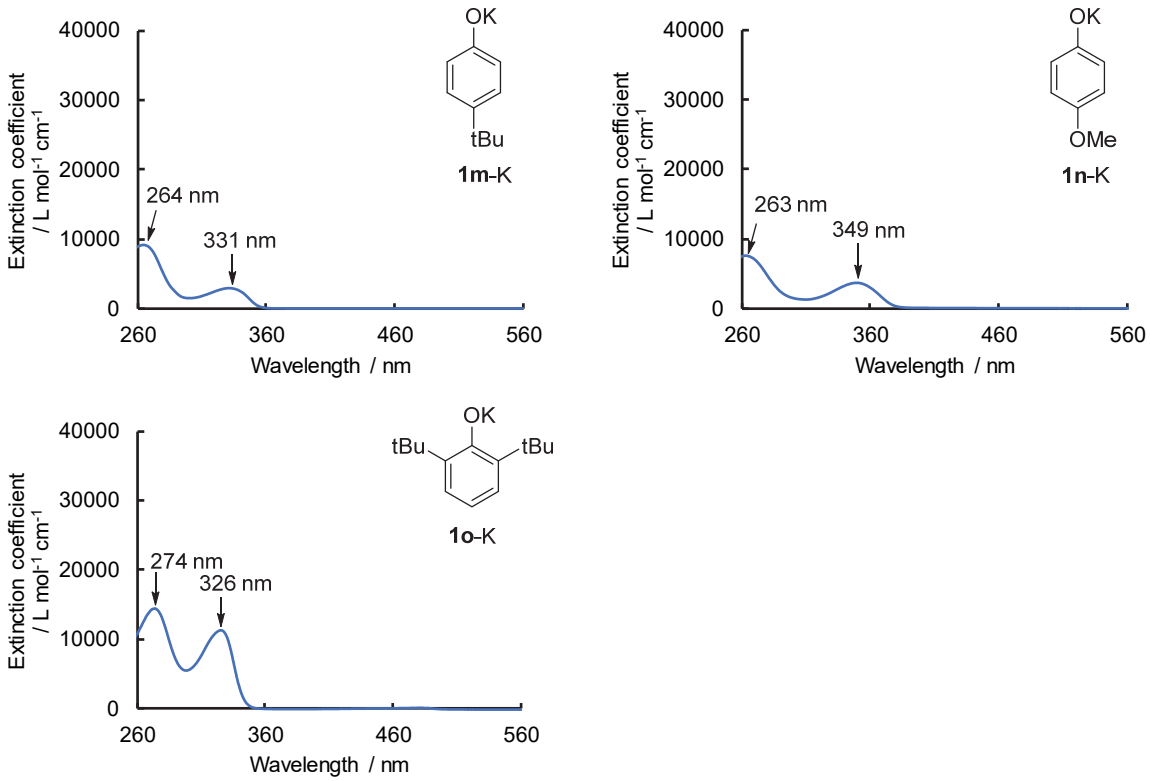

4.6 Product Studies

NMR Experiments – Reactions of 2a with Phenolate Ions

Under an atmosphere of dry argon, equimolar amounts of **2a**-BF_4 and the potassium or tetrabutylammonium phenolate **1**-K/NBu_4 (for details see the table below), were dissolved in equal volumes of anhydrous d_6-DMSO (from sealed ampule, 0.75 mL). Both solutions were mixed by pipetting and then transferred into an NMR tube, sealed, and submitted to ^{1}H NMR (and HSQC) spectroscopic analysis.

Reaction	**1**-K/NBu_4	**2a**-BF_4	NMR method
1a-NBu_4 + **2a** (RNH71)	10.2 mg, 0.024 mmol	10.0 mg, 0.024 mmol	^{1}H & HSQC
1b-NBu_4 + **2a** (RNH72)	10.2 mg, 0.024 mmol	10.0 mg, 0.024 mmol	^{1}H
1c-NBu_4 + **2a** (RM721)	8.1 mg, 0.023 mmol	9.4 mg, 0.023 mmol	^{1}H
1d-K + **2a** (RM759)	4.6 mg, 0.026 mmol	10.7 mg, 0.026 mmol	^{1}H & HSQC
1e-K + **2a** (RM759)	4.2 mg, 0.024 mmol	9.9 mg, 0.024 mmol	^{1}H
1f-K + **2a** (RM759)	3.9 mg, 0.025 mmol	10.2 mg, 0.025 mmol	^{1}H & HSQC
1g-NBu_4 + **2a** (RM762)	9.4 mg, 0.023 mmol	9.7 mg, 0.023 mmol	^{1}H
1h-NBu_4 + **2a** (RM762)	9.8 mg, 0.024 mmol	10.1 mg, 0.024 mmol	^{1}H
1i-K + **2a** (RM762)	5.1 mg, 0.026 mmol	10.6 mg, 0.026 mmol	^{1}H
1j-K + **2a** (RNH76)	4.0 mg, 0.024 mmol	10.0 mg, 0.024 mmol	^{1}H
1k-K + **2a** (RM758)	3.9 mg, 0.030 mmol	12.3 mg, 0.030 mmol	^{1}H
1l-K + **2a** (RM759)	3.5 mg, 0.024 mmol	10.0 mg, 0.024 mmol	^{1}H & HSQC
1m-K + **2a** (RNH75)	8.9 mg, 0.024 mmol	10.0 mg, 0.024 mmol	^{1}H
1n-K + **2a** (RM762)	4.5 mg, 0.027 mmol	11.4 mg, 0.027 mmol	^{1}H
1o-K + **2a** (RM750)	7.4 mg, 0.030 mmol	12.6 mg, 0.030 mmol	^{1}H, ^{13}C, and HSQC
1p-K + **2a** (RM765)	6.4 mg, 0.044 mmol	18.2 mg, 0.044 mmol	^{1}H
1q-K + **2a** (RM762)	3.9 mg, 0.024 mmol	10.0 mg, 0.024 mmol	^{1}H

Products from O- and C-attack of **2a** at the ambident phenolates **1** were differentiated based on the NMR chemical shifts of the benzhydrylic CH:

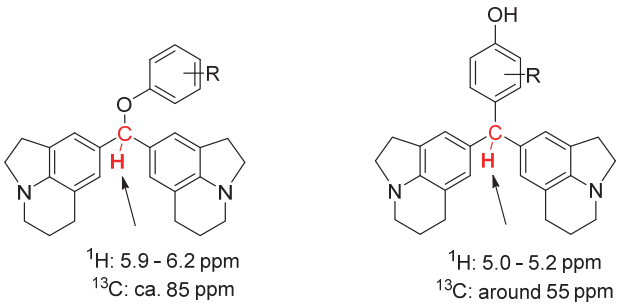

As these experiments primarily aimed to characterize oxygen- vs carbon-attack, the main focus was the spectral range from 4 to 9 ppm. The aliphatic regions were densely crowded with resonances due to overlap of the CH_2 groups of **2a** and the CH_2 and CH_3 groups of the tetrabutylammonium ions.

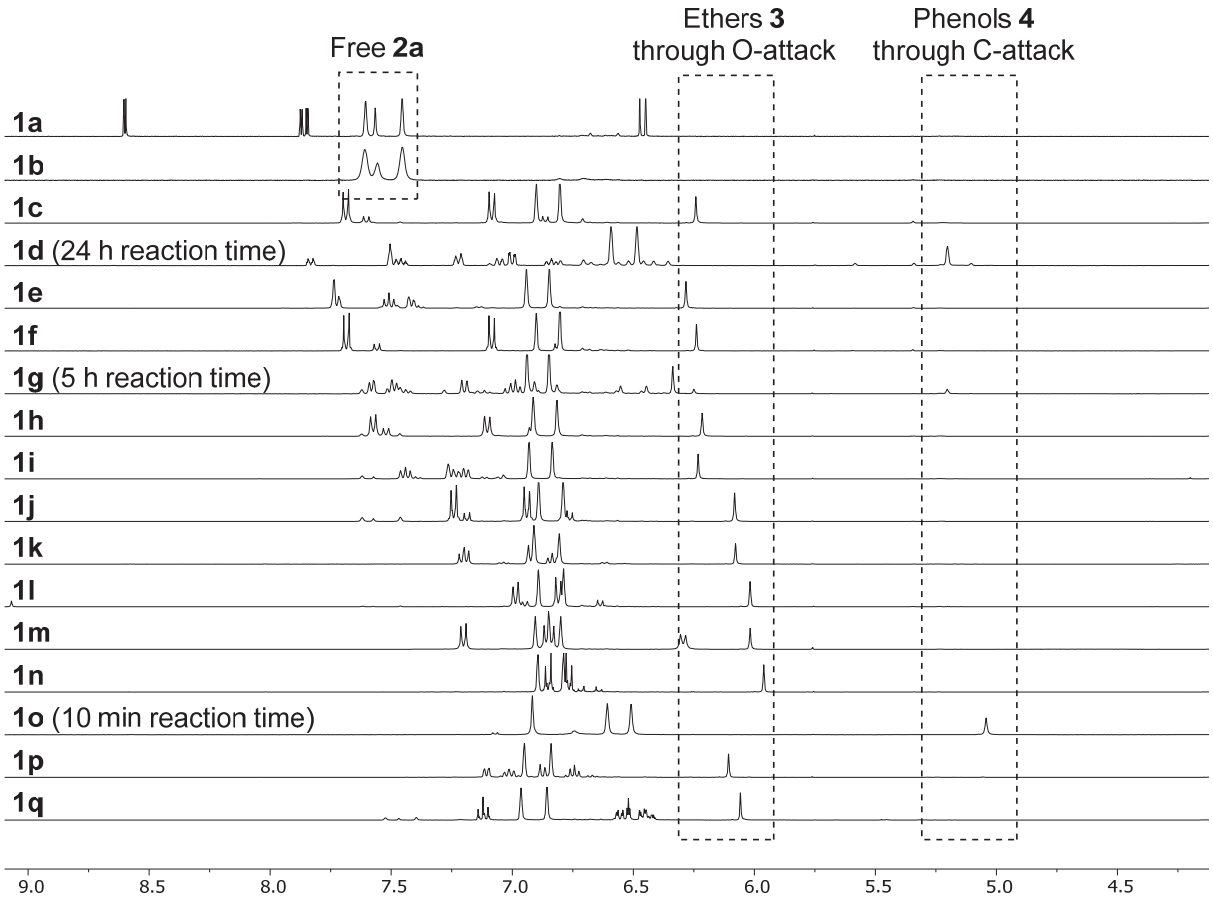

(^{1}H NMR, 400 MHz, d_6-DMSO)

Reactions of 2a with Phenolate Ions 1d and 1o at –40°C

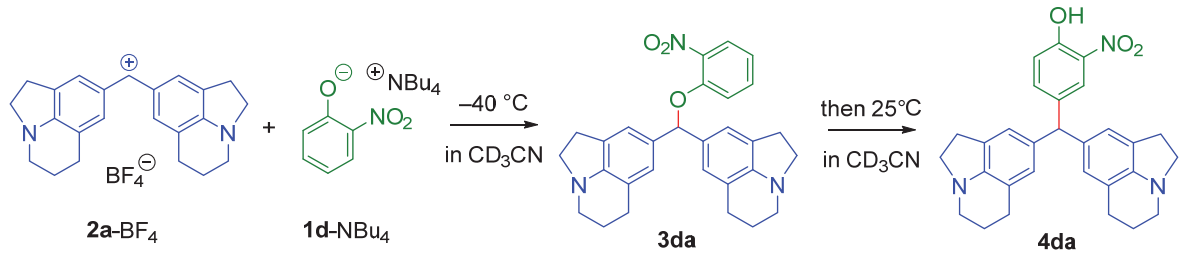

(RM772)

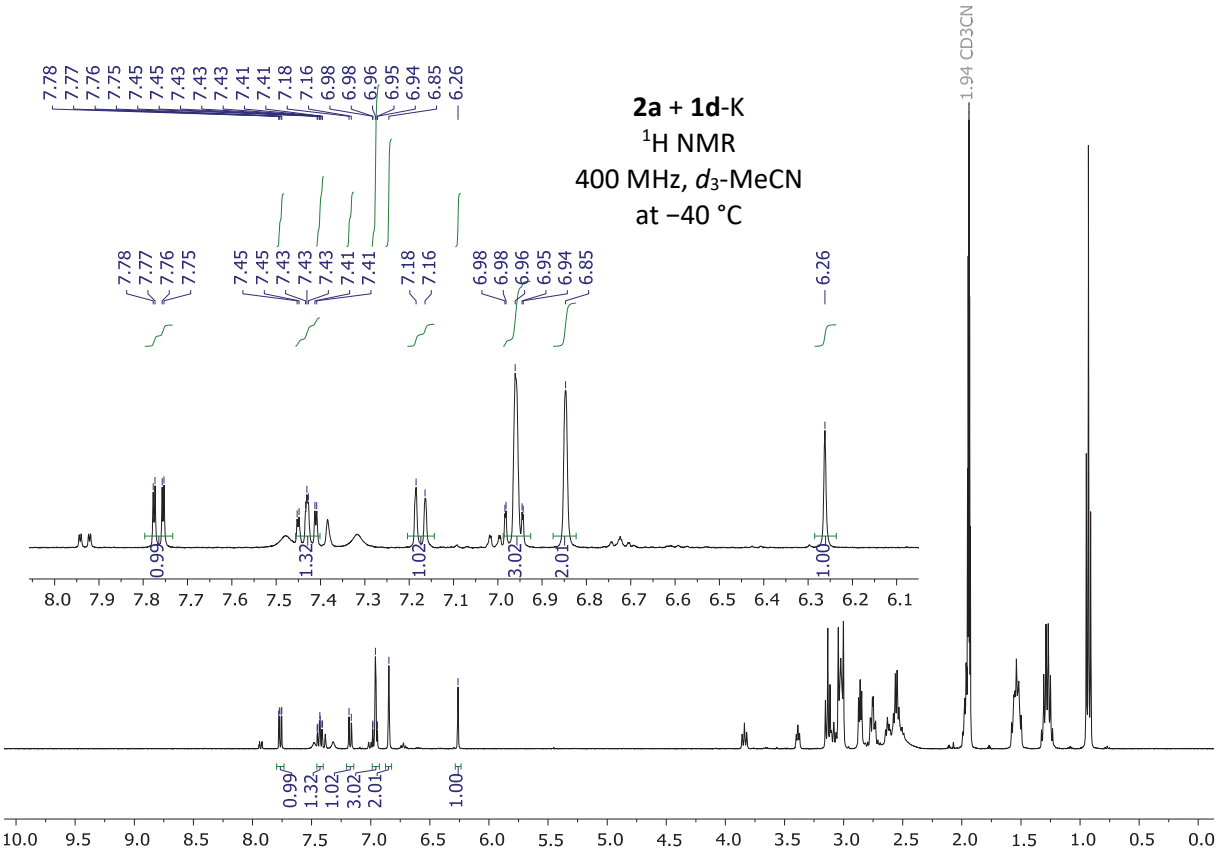

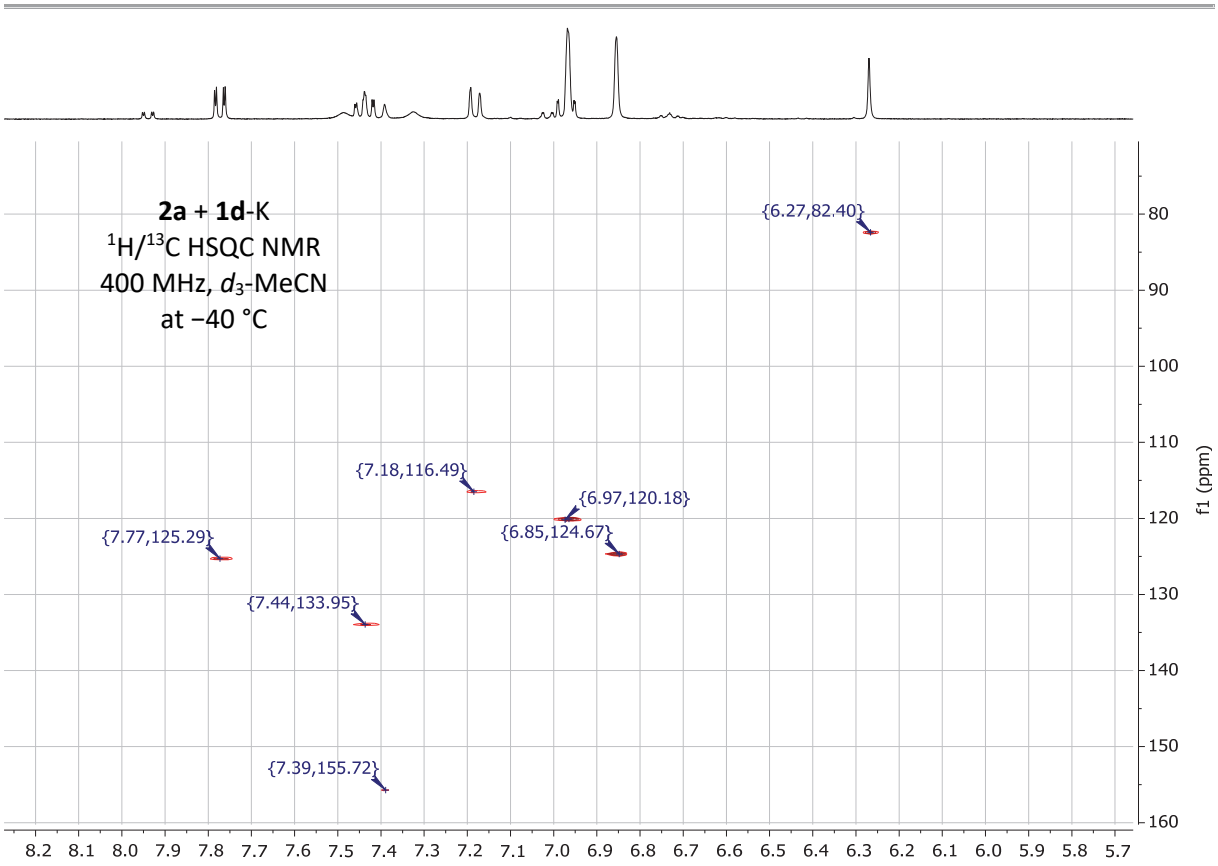
2a + 1d-K
1H/13C HSQC NMR
400 MHz, d3-MeCN
at −40 °C
{6.27,82.40}
{7.18,116.49}
{6.97,120.18}
{6.85,124.67}
{7.77,125.29}
{7.44,133.95}
{7.39,155.72}
f1 (ppm)

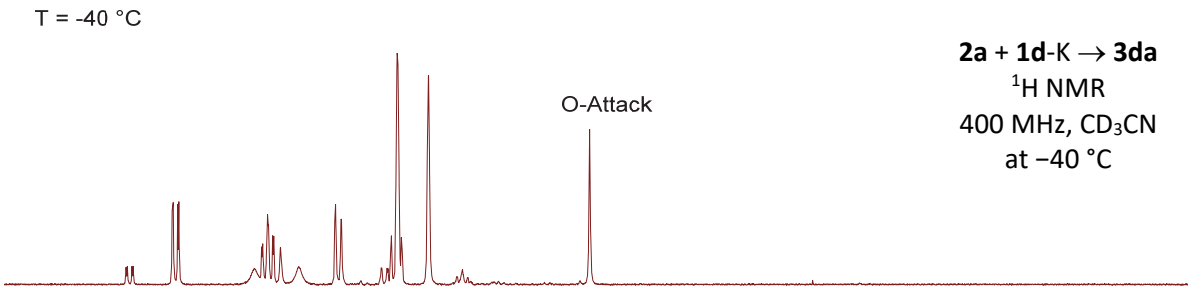
T = -40 °C
O-Attack
2a + 1d-K → 3da
1H NMR
400 MHz, CD3CN
at −40 °C

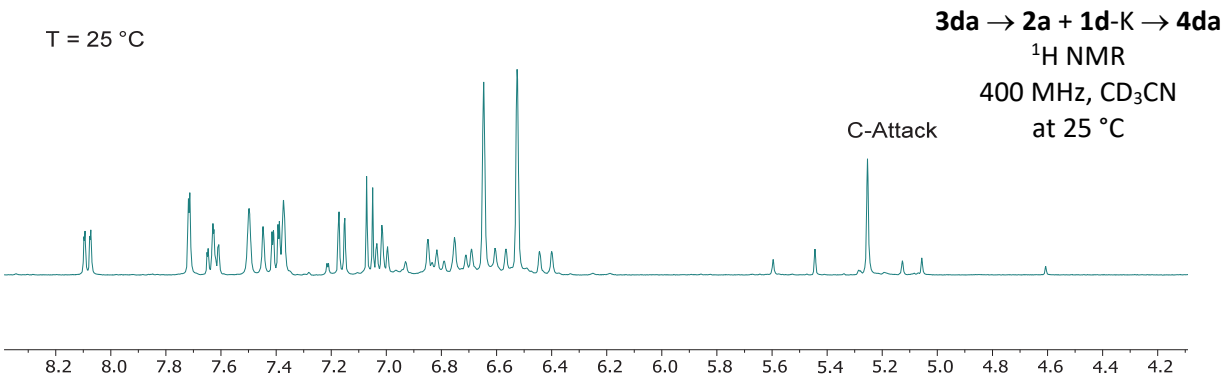
T = 25 °C
C-Attack
3da → 2a + 1d-K → 4da
1H NMR
400 MHz, CD3CN
at 25 °C

4.7 Equilibrium Constants for Reactions of Phenolate Ions with Benzhydrylium Ions (Table 1)

In this chapter A_0* corresponds to the initial absorbance A_0 corrected for the effect of dilution, that is, $A_0^* = A_0(V_0/V)$.

Reaction of 1a-NBu_4 with 2f-BF_4 (in MeCN, 20 °C, RM677)

Step	V_{LB} / mL	$V_{tot,LB}$ / mL	V_{tot} / mL	A	[**2f**]	$A_0^* - A_{eq}$	[**1a**]$_0$	[**1a**]$_0$ / [**2f**]$_0$	[**1a**]$_{eq}$	$(A_0^* - A_{eq})/A_{eq}$
0	0	0	24.15	0.911	1.10E-05					
1	0.10	0.10	24.25	0.895	1.08E-05	0.012	5.96E-05	5.4	5.94E-05	0.014
2	0.20	0.30	24.45	0.883	1.06E-05	0.017	1.77E-04	16.4	1.77E-04	0.019
3	0.20	0.50	24.65	0.869	1.05E-05	0.024	2.93E-04	27.5	2.93E-04	0.027
4	0.20	0.70	24.85	0.858	1.03E-05	0.027	4.07E-04	38.9	4.07E-04	0.032
5	0.30	1.00	25.15	0.841	1.01E-05	0.034	5.75E-04	55.6	5.74E-04	0.040

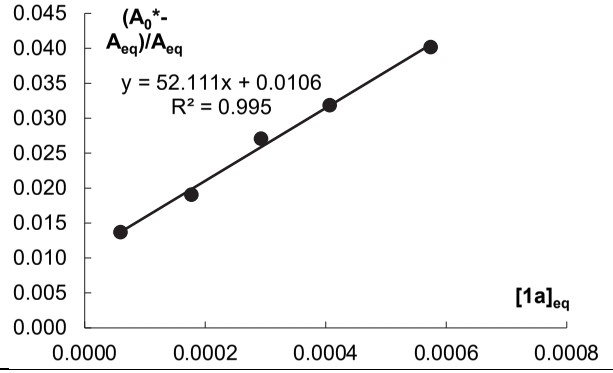

Step	V_{LB} / mL	$V_{tot,LB}$ / mL	V_{tot} / mL	A	[**2f**]	$A_0^* - A_{eq}$	[**1a**]$_0$	[**1a**]$_0$ / [**2f**]$_0$	[**1a**]$_{eq}$	$(A_0^* - A_{eq})/A_{eq}$
0	0	0	24.15	0.936	1.13E-05					
1	0.20	0.20	24.35	0.919	1.11E-05	0.009	1.19E-04	10.5	1.19E-04	0.010
2	0.20	0.40	24.55	0.907	1.09E-05	0.014	2.35E-04	21.3	2.35E-04	0.015
3	0.20	0.60	24.75	0.895	1.08E-05	0.018	3.50E-04	32.1	3.50E-04	0.020
4	0.20	0.80	24.95	0.884	1.07E-05	0.022	4.63E-04	43.0	4.63E-04	0.025
5	0.20	1.00	25.15	0.872	1.05E-05	0.027	5.75E-04	53.9	5.74E-04	0.031

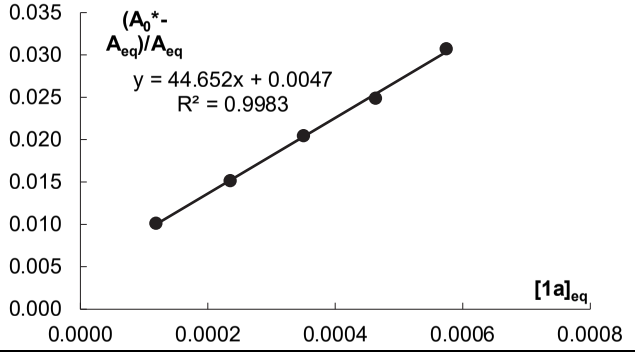

Step	V_{LB} / mL	$V_{tot,LB}$ / mL	V_{tot} / mL	A	[**2f**]	$A_0^* - A_{eq}$	[**1a**]$_0$	[**1a**]$_0$ / [**2f**]$_0$	[**1a**]$_{eq}$	$(A_0^* - A_{eq})/A_{eq}$
0	0	0	24.15	1.010	1.22E-05					
1	0.20	0.20	24.35	0.992	1.20E-05	0.010	1.19E-04	9.8	1.19E-04	0.010
2	0.20	0.40	24.55	0.979	1.18E-05	0.015	2.35E-04	19.7	2.35E-04	0.015
3	0.20	0.60	24.75	0.966	1.16E-05	0.020	3.50E-04	29.7	3.50E-04	0.020
4	0.20	0.80	24.95	0.954	1.15E-05	0.024	4.63E-04	39.8	4.63E-04	0.025
5	0.20	1.00	25.15	0.942	1.14E-05	0.028	5.75E-04	50.0	5.74E-04	0.030

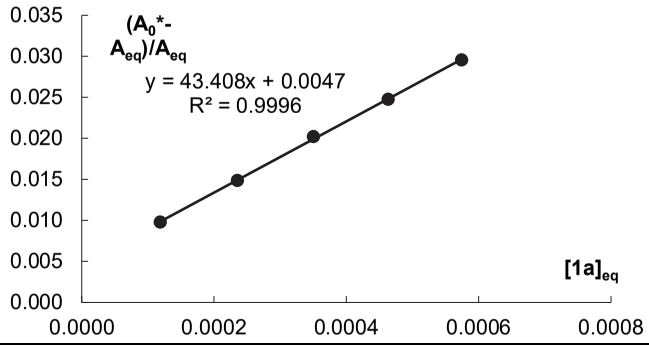

$K_{average} = (4.67 \pm 0.38) \times 10^1\ M^{-1}$

Reaction of 1b-NBu_4 with 2e-BF_4 (in MeCN, 20 °C, RM672)

Step	V_{LB} / mL	$V_{tot,LB}$ / mL	V_{tot} / mL	A	[**2e**]	$A_0^* - A_{eq}$	[**1b**]$_0$	[**1b**]$_0$ / [**2e**]$_0$	[**1b**]$_{eq}$	$(A_0^* - A_{eq})/A_{eq}$
0	0	0	24.15	1.194	1.25E-05					
1	0.10	0.10	24.25	0.988	1.04E-05	0.201	4.33E-05	3.5	4.12E-05	0.204
2	0.10	0.20	24.35	0.899	9.44E-06	0.285	8.63E-05	8.3	8.33E-05	0.317
3	0.10	0.30	24.45	0.826	8.67E-06	0.353	1.29E-04	13.7	1.25E-04	0.428
4	0.10	0.40	24.55	0.764	8.02E-06	0.411	1.71E-04	19.7	1.67E-04	0.537
5	0.10	0.50	24.65	0.711	7.46E-06	0.459	2.13E-04	26.6	2.08E-04	0.645
6	0.10	0.60	24.75	0.667	7.00E-06	0.498	2.55E-04	34.1	2.49E-04	0.747
7	0.10	0.70	24.85	0.623	6.54E-06	0.537	2.96E-04	42.3	2.90E-04	0.863
8	0.10	0.80	24.95	0.589	6.18E-06	0.567	3.37E-04	51.5	3.31E-04	0.962
8	0.10	0.90	25.05	0.556	5.84E-06	0.595	3.77E-04	61.0	3.71E-04	1.070
8	0.10	1.00	25.15	0.527	5.53E-06	0.620	4.18E-04	71.6	4.11E-04	1.176

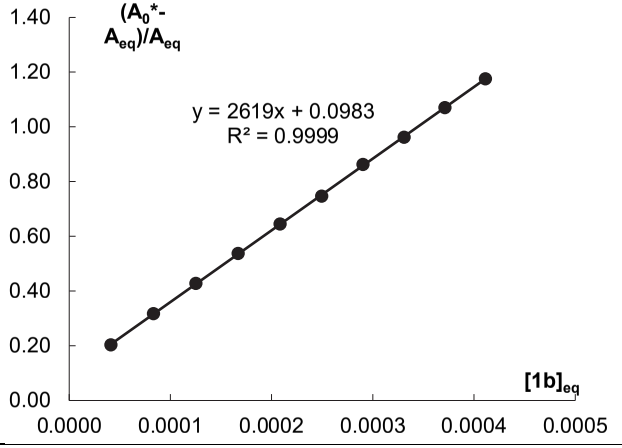

Step	V_{LB} / mL	$V_{tot,LB}$ / mL	V_{tot} / mL	A	[**2e**]	$A_0^* - A_{eq}$	[**1b**]$_0$	[**1b**]$_0$ / [**2e**]$_0$	[**1b**]$_{eq}$	$(A_0^* - A_{eq})/A_{eq}$
0	0	0	24.14	1.081	1.13E-05					
1	0.10	0.10	24.24	0.961	1.01E-05	0.116	4.33E-05	3.8	4.21E-05	0.120
2	0.10	0.20	24.34	0.877	9.21E-06	0.195	8.63E-05	8.6	8.43E-05	0.222
3	0.10	0.30	24.44	0.807	8.47E-06	0.261	1.29E-04	14.0	1.26E-04	0.323
4	0.10	0.40	24.54	0.748	7.85E-06	0.315	1.71E-04	20.2	1.68E-04	0.422
5	0.10	0.50	24.64	0.700	7.35E-06	0.359	2.13E-04	27.2	2.09E-04	0.513
6	0.10	0.60	24.74	0.655	6.87E-06	0.400	2.55E-04	34.7	2.51E-04	0.610
7	0.10	0.70	24.84	0.615	6.46E-06	0.436	2.96E-04	43.1	2.91E-04	0.708
8	0.10	0.80	24.94	0.582	6.11E-06	0.464	3.37E-04	52.2	3.32E-04	0.798
9	0.10	0.90	25.04	0.552	5.79E-06	0.490	3.78E-04	61.8	3.72E-04	0.888
10	0.10	1.00	25.14	0.525	5.51E-06	0.513	4.18E-04	72.1	4.12E-04	0.977

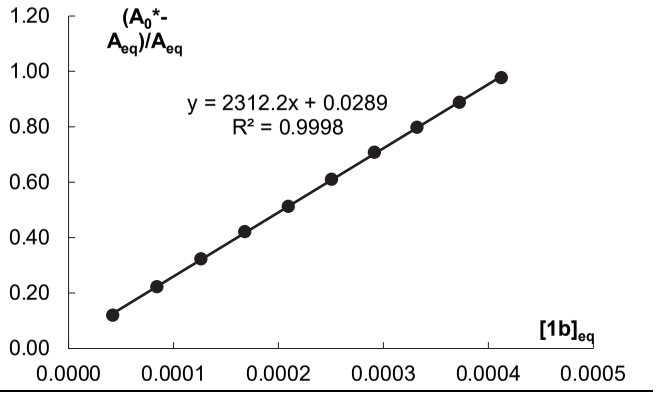

Step	V_{LB} / mL	$V_{tot,LB}$ / mL	V_{tot} / mL	A	[**2e**]	$A_0^* - A_{eq}$	[**1b**]$_0$	[**1b**]$_0$ / [**2e**]$_0$	[**1b**]$_{eq}$	$(A_0^* - A_{eq})/A_{eq}$
0	0	0	24.14	1.145	1.20E-05					
1	0.10	0.10	24.24	1.022	1.07E-05	0.118	4.33E-05	3.6	4.21E-05	0.116
2	0.10	0.20	24.34	0.932	9.78E-06	0.204	8.63E-05	8.0	8.42E-05	0.218
3	0.10	0.30	24.44	0.859	9.02E-06	0.272	1.29E-04	13.2	1.26E-04	0.317
4	0.10	0.40	24.54	0.796	8.35E-06	0.330	1.71E-04	19.0	1.68E-04	0.415
5	0.10	0.50	24.64	0.743	7.80E-06	0.379	2.13E-04	25.5	2.09E-04	0.510
6	0.10	0.60	24.74	0.696	7.31E-06	0.421	2.55E-04	32.7	2.50E-04	0.605
7	0.10	0.70	24.84	0.654	6.86E-06	0.459	2.96E-04	40.5	2.91E-04	0.701
8	0.10	0.80	24.94	0.618	6.49E-06	0.490	3.37E-04	49.1	3.32E-04	0.793
9	0.10	0.90	25.04	0.585	6.14E-06	0.519	3.78E-04	58.2	3.72E-04	0.887
10	0.10	1.00	25.14	0.556	5.84E-06	0.543	4.18E-04	68.0	4.12E-04	0.977

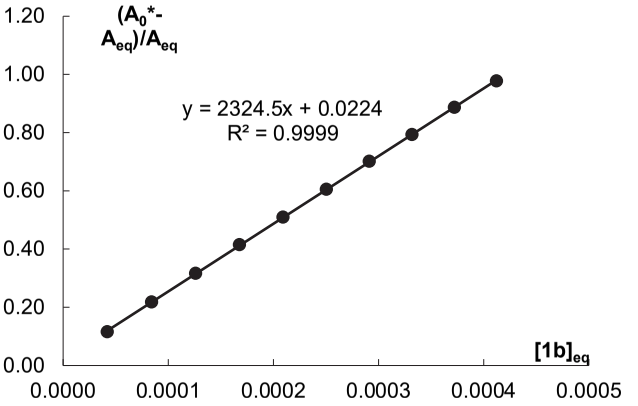

$K_{average} = (2.42 \pm 0.14) \times 10^3\ M^{-1}$

Reaction of 1b-NBu_4 with 2f-BF_4 (in MeCN, 20 °C, RM656)

Step	V_{LB} / mL	$V_{tot,LB}$ / mL	V_{tot} / mL	A	[**2f**]	$A_0^* - A_{eq}$	[**1b**]$_0$	[**1b**]$_0$ / [**2f**]$_0$	[**1b**]$_{eq}$	$(A_0^* - A_{eq})/A_{eq}$
0	0	0	24.20	1.142	1.38E-05					
1	0.05	0.05	24.25	0.900	1.08E-05	0.240	1.95E-05	1.4	1.66E-05	0.266
2	0.05	0.10	24.30	0.747	9.00E-06	0.390	3.89E-05	3.6	3.42E-05	0.522
3	0.05	0.15	24.35	0.633	7.63E-06	0.502	5.82E-05	6.5	5.21E-05	0.793
4	0.05	0.20	24.40	0.548	6.60E-06	0.585	7.74E-05	10.2	7.04E-05	1.067
5	0.05	0.25	24.45	0.481	5.80E-06	0.649	9.66E-05	14.6	8.88E-05	1.350
6	0.05	0.30	24.50	0.429	5.17E-06	0.699	1.16E-04	20.0	1.07E-04	1.629
7	0.05	0.35	24.55	0.386	4.65E-06	0.740	1.35E-04	26.1	1.26E-04	1.916
8	0.05	0.40	24.60	0.349	4.21E-06	0.774	1.54E-04	33.0	1.44E-04	2.219
9	0.05	0.45	24.65	0.321	3.87E-06	0.800	1.72E-04	41.0	1.63E-04	2.493
10	0.04	0.49	24.69	0.301	3.63E-06	0.818	1.87E-04	48.5	1.78E-04	2.719

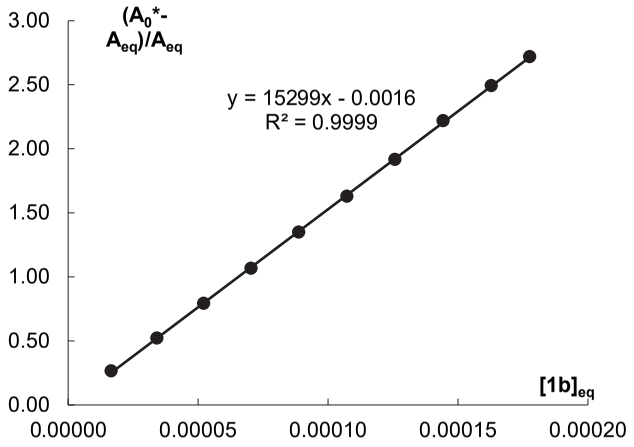

Step	V_{LB} / mL	$V_{tot,LB}$ / mL	V_{tot} / mL	A	[**2f**]	$A_0^* - A_{eq}$	[**1b**]$_0$	[**1b**]$_0$ / [**2f**]$_0$	[**1b**]$_{eq}$	$(A_0^* - A_{eq})/A_{eq}$
0	0	0	24.20	1.149	1.38E-05					
1	0.05	0.05	24.25	0.923	1.11E-05	0.224	1.95E-05	1.4	1.68E-05	0.242
2	0.05	0.10	24.30	0.762	9.18E-06	0.382	3.89E-05	3.5	3.43E-05	0.502
3	0.05	0.15	24.35	0.656	7.91E-06	0.486	5.82E-05	6.3	5.23E-05	0.741
4	0.05	0.20	24.40	0.575	6.93E-06	0.565	7.74E-05	9.8	7.06E-05	0.982
5	0.05	0.25	24.45	0.502	6.05E-06	0.635	9.66E-05	13.9	8.89E-05	1.265
6	0.05	0.30	24.50	0.443	5.34E-06	0.692	1.16E-04	19.1	1.07E-04	1.562
7	0.05	0.35	24.55	0.402	4.84E-06	0.731	1.35E-04	25.2	1.26E-04	1.817
8	0.05	0.40	24.60	0.365	4.40E-06	0.765	1.54E-04	31.7	1.44E-04	2.097
9	0.05	0.45	24.65	0.336	4.05E-06	0.792	1.72E-04	39.2	1.63E-04	2.357
10	0.04	0.49	24.69	0.314	3.78E-06	0.812	1.87E-04	46.3	1.78E-04	2.587

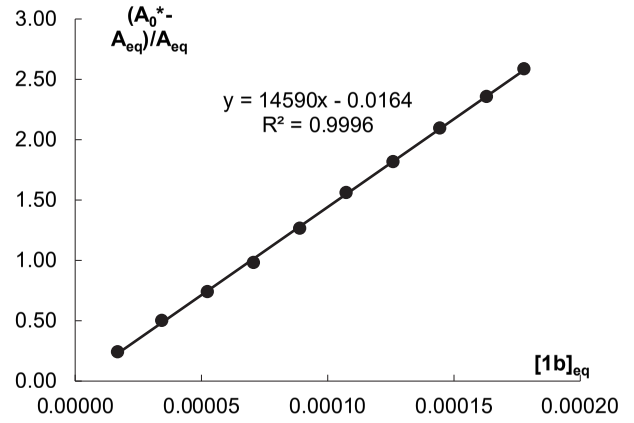

Step	V_{LB} / mL	$V_{tot,LB}$ / mL	V_{tot} / mL	A	[**2f**]	$A_0^* - A_{eq}$	[**1b**]$_0$	[**1b**]$_0$ / [**2f**]$_0$	[**1b**]$_{eq}$	$(A_0^* - A_{eq})/A_{eq}$
0	0	0	24.20	1.150	1.39E-05					
1	0.05	0.05	24.25	0.932	1.12E-05	0.216	1.95E-05	1.4	1.69E-05	0.231
2	0.05	0.10	24.30	0.761	9.17E-06	0.384	3.89E-05	3.5	3.42E-05	0.505
3	0.05	0.15	24.35	0.655	7.89E-06	0.488	5.82E-05	6.3	5.23E-05	0.745
4	0.05	0.20	24.40	0.570	6.87E-06	0.571	7.74E-05	9.8	7.06E-05	1.001
5	0.05	0.25	24.45	0.500	6.03E-06	0.638	9.66E-05	14.1	8.89E-05	1.276
6	0.05	0.30	24.50	0.447	5.39E-06	0.689	1.16E-04	19.2	1.07E-04	1.541
7	0.05	0.35	24.55	0.402	4.84E-06	0.732	1.35E-04	25.0	1.26E-04	1.820
8	0.05	0.40	24.60	0.368	4.43E-06	0.763	1.54E-04	31.7	1.44E-04	2.074
9	0.05	0.45	24.65	0.338	4.07E-06	0.791	1.72E-04	38.9	1.63E-04	2.340
10	0.04	0.49	24.69	0.315	3.80E-06	0.812	1.87E-04	46.0	1.78E-04	2.578

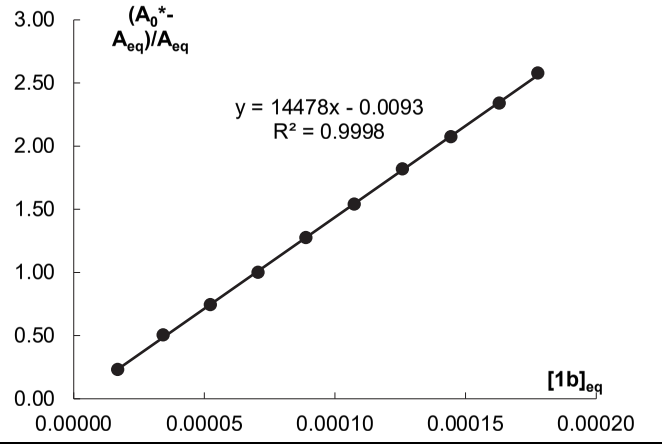

$K_{average} = (1.48 \pm 0.04) \times 10^4\ M^{-1}$

Reaction of 1c-NBu_4 with 2a-BF_4 (in MeCN, 20 °C, RM644)

Step	V_{LB} / mL	$V_{tot,LB}$ / mL	V_{tot} / mL	A	[**2a**]	$A_0^* - A_{eq}$	[**1c**]$_0$	[**1c**]$_0$ / [**2a**]$_0$	[**1c**]$_{eq}$	$(A_0^* - A_{eq})/A_{eq}$
0	0	0	24.72	0.963	1.33E-05					
1	0.05	0.05	24.77	0.765	1.06E-05	0.196	1.78E-05	1.3	1.51E-05	0.256
2	0.05	0.10	24.82	0.630	8.72E-06	0.329	3.55E-05	3.3	3.09E-05	0.522
3	0.05	0.15	24.87	0.528	7.31E-06	0.429	5.31E-05	6.1	4.71E-05	0.813
4	0.05	0.20	24.92	0.447	6.19E-06	0.508	7.06E-05	9.7	6.36E-05	1.137
5	0.05	0.25	24.97	0.388	5.37E-06	0.565	8.81E-05	14.2	8.03E-05	1.457
6	0.05	0.30	25.02	0.340	4.70E-06	0.611	1.06E-04	19.7	9.71E-05	1.798
7	0.10	0.40	25.12	0.278	3.85E-06	0.670	1.40E-04	29.8	1.31E-04	2.409
8	0.11	0.51	25.23	0.228	3.15E-06	0.716	1.78E-04	46.2	1.68E-04	3.138

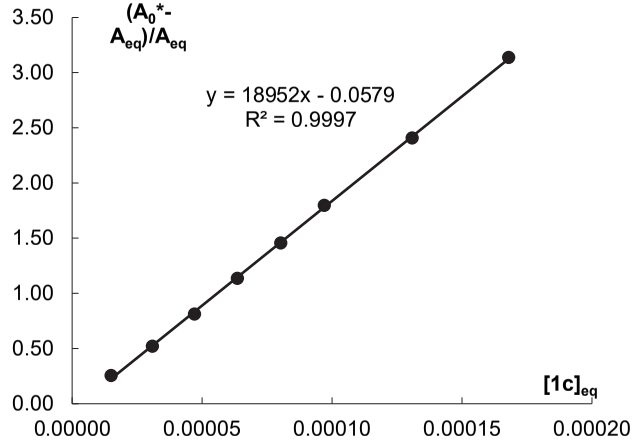

Step	V_{LB} / mL	$V_{tot,LB}$ / mL	V_{tot} / mL	A	[**2a**]	$A_0^* - A_{eq}$	[**1c**]$_0$	[**1c**]$_0$ / [**2a**]$_0$	[**1c**]$_{eq}$	$(A_0^* - A_{eq})/A_{eq}$

0	0	0		24.61	1.030	1.43E-05				
1	0.05	0.05		24.66	0.819	1.13E-05	0.209	1.78E-05	1.3	1.50E-05	0.255
2	0.05	0.10		24.71	0.678	9.38E-06	0.348	3.56E-05	3.1	3.08E-05	0.513
3	0.05	0.15		24.76	0.566	7.83E-06	0.458	5.33E-05	5.7	4.70E-05	0.809
4	0.05	0.20		24.81	0.486	6.72E-06	0.536	7.10E-05	9.1	6.35E-05	1.102
5	0.05	0.25		24.86	0.424	5.87E-06	0.596	8.85E-05	13.2	8.03E-05	1.405
6	0.05	0.30		24.91	0.372	5.15E-06	0.646	1.06E-04	18.1	9.71E-05	1.735
7	0.10	0.40		25.01	0.302	4.18E-06	0.712	1.41E-04	27.4	1.31E-04	2.356
8	0.11	0.51		25.12	0.250	3.46E-06	0.759	1.79E-04	42.8	1.68E-04	3.036

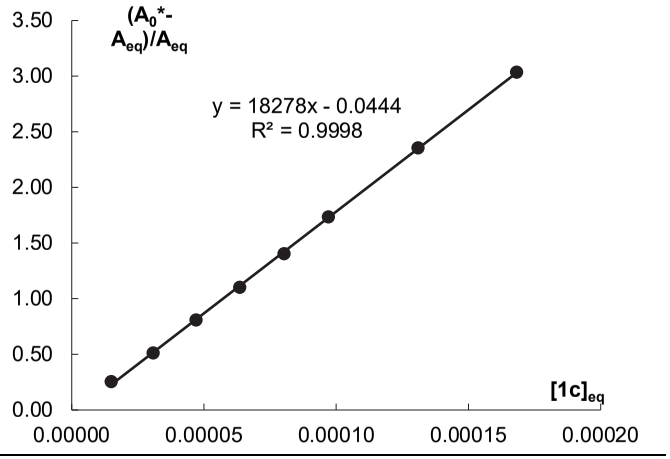

Step	V_{LB} / mL	$V_{tot,LB}$ / mL	V_{tot} / mL	A	[**2a**]	$A_0^* - A_{eq}$	[**1c**]$_0$	[**1c**]$_0$ / [**2a**]$_0$	[**1c**]$_{eq}$	$(A_0^* - A_{eq})/A_{eq}$
0	0	0	24.34	0.962	1.33E-05					
1	0.05	0.05	24.39	0.766	1.06E-05	0.194	1.84E-05	1.4	1.57E-05	0.253
2	0.05	0.10	24.44	0.622	8.61E-06	0.336	3.67E-05	3.5	3.20E-05	0.540
3	0.05	0.15	24.49	0.518	7.17E-06	0.438	5.49E-05	6.4	4.88E-05	0.846
4	0.05	0.20	24.54	0.438	6.06E-06	0.516	7.30E-05	10.2	6.59E-05	1.178
5	0.05	0.25	24.59	0.378	5.23E-06	0.574	9.11E-05	15.0	8.31E-05	1.519
6	0.05	0.30	24.64	0.332	4.59E-06	0.618	1.09E-04	20.9	1.01E-04	1.862
7	0.10	0.40	24.74	0.266	3.68E-06	0.680	1.45E-04	31.5	1.35E-04	2.558
8	0.10	0.50	24.84	0.222	3.07E-06	0.721	1.80E-04	49.0	1.70E-04	3.246

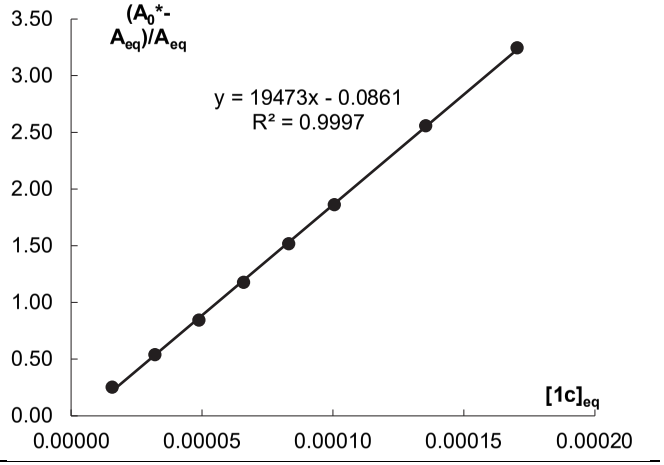

$K_{average} = (1.89 \pm 0.05) \times 10^4\ M^{-1}$

Reaction of 1c-NBu_4 with 2b-BF_4 (in MeCN, 20 °C, RM644)

Step	V_{LB} / mL	$V_{tot,LB}$ / mL	V_{tot} / mL	A	[**2b**]	$A_0^* - A_{eq}$	[**1c**]$_0$	[**1c**]$_0$ / [**2b**]$_0$	[**1c**]$_{eq}$	$(A_0^* - A_{eq})/A_{eq}$
0	0	0	24.75	0.985	1.08E-05					
1	0.05	0.05	24.80	0.800	8.79E-06	0.183	1.81E-05	1.7	1.60E-05	0.229
2	0.05	0.10	24.85	0.664	7.30E-06	0.317	3.60E-05	4.1	3.26E-05	0.477
3	0.05	0.15	24.90	0.564	6.20E-06	0.415	5.40E-05	7.4	4.94E-05	0.736
4	0.05	0.20	24.95	0.484	5.32E-06	0.493	7.18E-05	11.6	6.64E-05	1.019
5	0.05	0.25	25.00	0.418	4.59E-06	0.557	8.96E-05	16.8	8.35E-05	1.333
6	0.05	0.30	25.05	0.368	4.04E-06	0.605	1.07E-04	23.4	1.01E-04	1.645
7	0.10	0.40	25.15	0.300	3.30E-06	0.669	1.42E-04	35.2	1.35E-04	2.231
8	0.11	0.51	25.26	0.248	2.73E-06	0.717	1.81E-04	54.9	1.73E-04	2.892

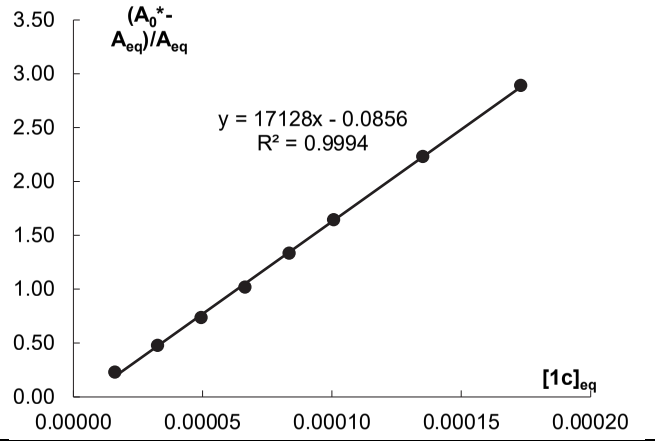

Step	V_{LB} / mL	$V_{tot,LB}$ / mL	V_{tot} / mL	A	[**2b**]	$A_0^* - A_{eq}$	[**1c**]$_0$	[**1c**]$_0$ / [**2b**]$_0$	[**1c**]$_{eq}$	$(A_0^* - A_{eq})/A_{eq}$
0	0	0	25.01	1.010	1.11E-05					
1	0.05	0.05	25.06	0.840	9.23E-06	0.168	1.68E-05	1.5	1.49E-05	0.200
2	0.05	0.10	25.11	0.715	7.86E-06	0.291	3.35E-05	3.6	3.03E-05	0.407
3	0.05	0.15	25.16	0.610	6.70E-06	0.394	5.01E-05	6.4	4.58E-05	0.646
4	0.05	0.20	25.21	0.524	5.76E-06	0.478	6.67E-05	9.9	6.15E-05	0.912
5	0.05	0.25	25.26	0.458	5.03E-06	0.542	8.32E-05	14.4	7.73E-05	1.183
6	0.05	0.30	25.31	0.402	4.42E-06	0.596	9.97E-05	19.8	9.31E-05	1.483
7	0.10	0.40	25.41	0.328	3.60E-06	0.666	1.32E-04	30.0	1.25E-04	2.031
8	0.11	0.51	25.52	0.274	3.01E-06	0.716	1.68E-04	46.6	1.60E-04	2.612

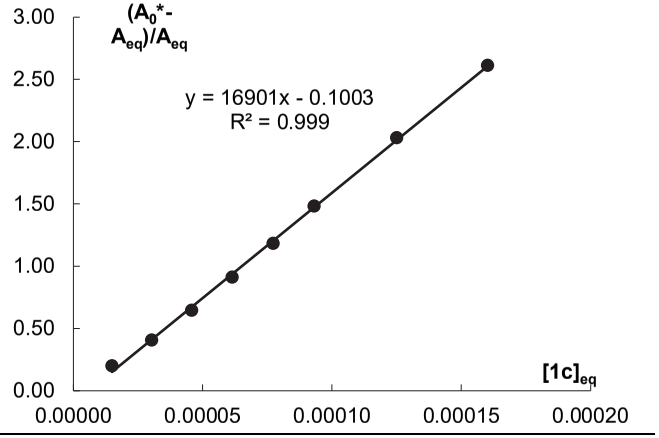

Step	V_{LB} / mL	$V_{tot,LB}$ / mL	V_{tot} / mL	A	[**2b**]	$A_0^* - A_{eq}$	[**1c**]$_0$	[**1c**]$_0$ / [**2b**]$_0$	[**1c**]$_{eq}$	$(A_0^* - A_{eq})/A_{eq}$
0	0	0	25.52	0.968	1.06E-05					
1	0.05	0.05	25.57	0.790	8.68E-06	0.176	1.64E-05	1.5	1.45E-05	0.223
2	0.05	0.10	25.62	0.660	7.25E-06	0.304	3.28E-05	3.8	2.95E-05	0.461
3	0.05	0.15	25.67	0.560	6.15E-06	0.402	4.91E-05	6.8	4.47E-05	0.718
4	0.05	0.20	25.72	0.480	5.28E-06	0.480	6.54E-05	10.6	6.01E-05	1.001
5	0.05	0.25	25.77	0.410	4.51E-06	0.549	8.16E-05	15.5	7.55E-05	1.338
6	0.05	0.30	25.82	0.360	3.96E-06	0.597	9.77E-05	21.7	9.11E-05	1.658

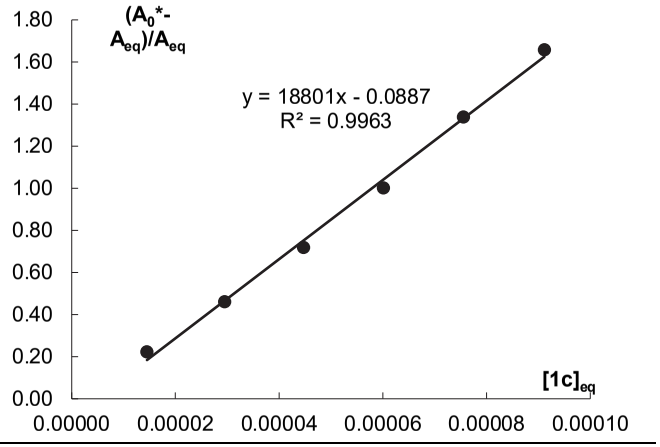

$K_{average} = (1.76 \pm 0.09) \times 10^4\ M^{-1}$

Reaction of 1c-NBu_4 with 2c-BF_4 (in MeCN, 20 °C, RM644)

Step	V_{LB} / mL	$V_{tot,LB}$ / mL	V_{tot} / mL	A	[**2c**]	$A_0^* - A_{eq}$	[**1c**]$_0$	[**1c**]$_0$ / [**2c**]$_0$	[**1c**]$_{eq}$	$(A_0^* - A_{eq})/A_{eq}$
0	0	0	24.70	0.970	1.41E-05					
1	0.01	0.01	24.71	0.800	1.16E-05	0.170	3.63E-06	0.3	1.17E-06	0.212
2	0.01	0.02	24.72	0.635	9.20E-06	0.334	7.25E-06	0.6	2.41E-06	0.526
3	0.01	0.03	24.73	0.482	6.98E-06	0.487	1.09E-05	1.2	3.81E-06	1.010
4	0.01	0.04	24.74	0.361	5.23E-06	0.607	1.45E-05	2.1	5.68E-06	1.683
5	0.01	0.05	24.75	0.265	3.84E-06	0.703	1.81E-05	3.5	7.91E-06	2.653
6	0.01	0.06	24.76	0.203	2.94E-06	0.765	2.17E-05	5.7	1.06E-05	3.767
7	0.01	0.07	24.77	0.160	2.32E-06	0.807	2.53E-05	8.6	1.36E-05	5.045
8	0.01	0.08	24.78	0.131	1.90E-06	0.836	2.89E-05	12.5	1.68E-05	6.381

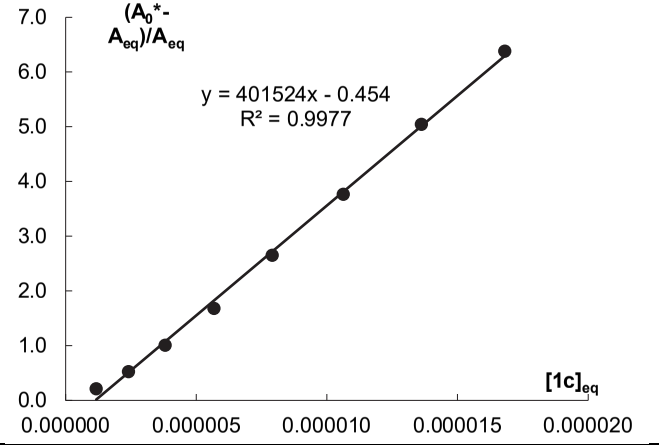

Step	V_{LB} / mL	$V_{tot,LB}$ / mL	V_{tot} / mL	A	[**2c**]	$A_0^* - A_{eq}$	[**1c**]$_0$	[**1c**]$_0$ / [**2c**]$_0$	[**1c**]$_{eq}$	$(A_0^* - A_{eq})/A_{eq}$
0	0	0	24.70	0.990	1.43E-05					
1	0.01	0.01	24.71	0.859	1.24E-05	0.131	3.17E-06	0.2	1.28E-06	0.152
2	0.01	0.02	24.72	0.707	1.02E-05	0.282	6.33E-06	0.5	2.24E-06	0.399
3	0.01	0.03	24.73	0.572	8.29E-06	0.417	9.50E-06	0.9	3.46E-06	0.729
4	0.01	0.04	24.74	0.450	6.52E-06	0.538	1.27E-05	1.5	4.86E-06	1.196
5	0.01	0.05	24.75	0.335	4.86E-06	0.653	1.58E-05	2.4	6.36E-06	1.947
6	0.01	0.06	24.76	0.274	3.97E-06	0.714	1.90E-05	3.9	8.63E-06	2.604
7	0.01	0.07	24.77	0.216	3.13E-06	0.771	2.21E-05	5.6	1.09E-05	3.570
8	0.01	0.08	24.78	0.175	2.54E-06	0.812	2.53E-05	8.1	1.35E-05	4.639
9	0.01	0.09	24.79	0.146	2.12E-06	0.840	2.84E-05	11.2	1.62E-05	5.756

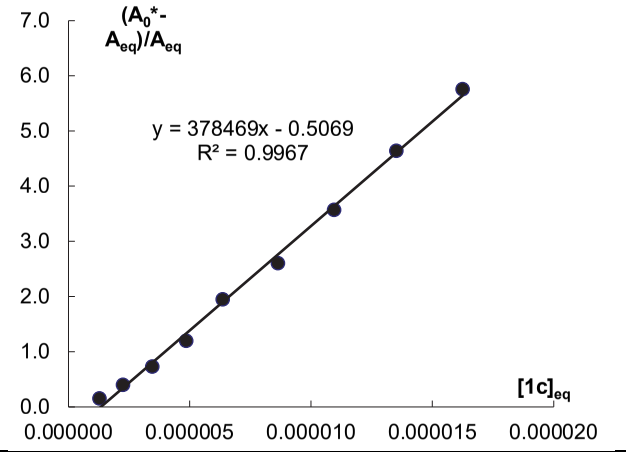

Step	V_{LB} / mL	$V_{tot,LB}$ / mL	V_{tot} / mL	A	[**2c**]	$A_0^* - A_{eq}$	[**1c**]$_0$	[**1c**]$_0$ / [**2c**]$_0$	[**1c**]$_{eq}$	$(A_0^* - A_{eq})/A_{eq}$
0	0	0	24.83	1.030	1.49E-05					
1	0.01	0.01	24.84	0.878	1.27E-05	0.152	3.15E-06	0.2	9.56E-07	0.173
2	0.01	0.02	24.85	0.735	1.06E-05	0.294	6.30E-06	0.5	2.04E-06	0.400
3	0.01	0.03	24.86	0.599	8.68E-06	0.430	9.45E-06	0.9	3.22E-06	0.717
4	0.01	0.04	24.87	0.467	6.77E-06	0.561	1.26E-05	1.5	4.46E-06	1.202
5	0.01	0.05	24.88	0.366	5.30E-06	0.662	1.57E-05	2.3	6.14E-06	1.809
6	0.01	0.06	24.89	0.285	4.13E-06	0.743	1.89E-05	3.6	8.11E-06	2.605
7	0.01	0.07	24.90	0.227	3.29E-06	0.800	2.20E-05	5.3	1.04E-05	3.525
8	0.01	0.08	24.91	0.186	2.69E-06	0.841	2.51E-05	7.6	1.30E-05	4.520
9	0.01	0.09	24.92	0.155	2.25E-06	0.871	2.83E-05	10.5	1.57E-05	5.621

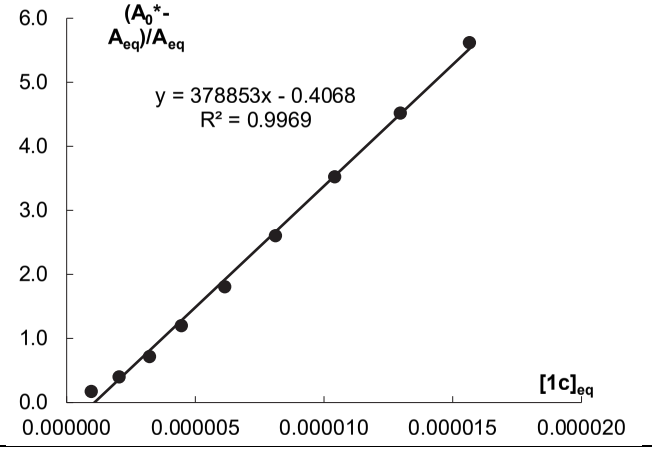

$K_{average} = (3.86 \pm 0.11) \times 10^5\ M^{-1}$

Reaction of 1d-NBu_4 with 2a-BF_4 (in MeCN, 20 °C, RM671)

Step	V_{LB} / mL	$V_{tot,LB}$ / mL	V_{tot} / mL	A	[**2a**]	$A_0^* - A_{eq}$	[**1d**]$_0$	[**1d**]$_0$ / [**2a**]$_0$	[**1d**]$_{eq}$	$(A_0^* - A_{eq})/A_{eq}$
0	0	0	24.00	1.015	1.40E-05		0.000E+00			
1	0.025	0.03	24.03	0.945	1.31E-05	0.069	1.52E-05	1.1	1.43E-05	0.073
2	0.025	0.05	24.05	0.893	1.24E-05	0.120	3.04E-05	2.3	2.88E-05	0.134
3	0.025	0.08	24.08	0.845	1.17E-05	0.167	4.56E-05	3.7	4.33E-05	0.197
4	0.025	0.10	24.10	0.810	1.12E-05	0.201	6.07E-05	5.2	5.80E-05	0.248
5	0.025	0.13	24.13	0.772	1.07E-05	0.238	7.58E-05	6.8	7.25E-05	0.308
6	0.025	0.15	24.15	0.738	1.02E-05	0.271	9.09E-05	8.5	8.72E-05	0.367
7	0.025	0.18	24.18	0.711	9.84E-06	0.297	1.06E-04	10.4	1.02E-04	0.417
8	0.025	0.20	24.20	0.683	9.45E-06	0.324	1.21E-04	12.3	1.16E-04	0.474
9	0.025	0.23	24.23	0.658	9.10E-06	0.348	1.36E-04	14.4	1.31E-04	0.528
10	0.025	0.25	24.25	0.639	8.84E-06	0.366	1.51E-04	16.6	1.46E-04	0.572

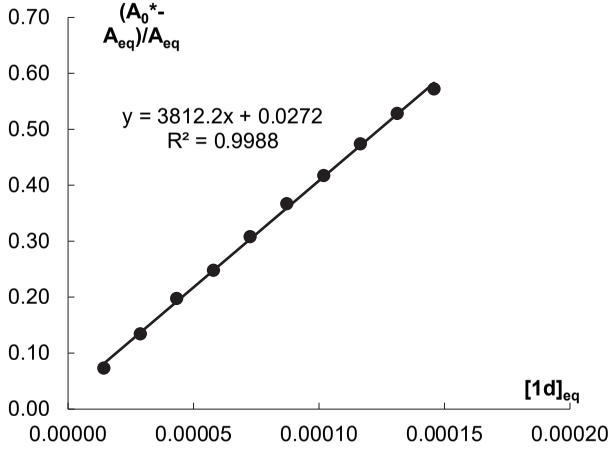

Step	V_{LB} / mL	$V_{tot,LB}$ / mL	V_{tot} / mL	A	[**2a**]	$A_0^* - A_{eq}$	[**1d**]$_0$	[**1d**]$_0$ / [**2a**]$_0$	[**1d**]$_{eq}$	$(A_0^* - A_{eq})/A_{eq}$
0	0	0	24.00	1.038	1.44E-05		0.000E+00			
1	0.050	0.05	24.05	0.915	1.27E-05	0.121	3.04E-05	2.1	2.88E-05	0.132
2	0.050	0.10	24.10	0.829	1.15E-05	0.205	6.07E-05	4.8	5.79E-05	0.247
3	0.050	0.15	24.15	0.759	1.05E-05	0.273	9.09E-05	7.9	8.71E-05	0.359
4	0.050	0.20	24.20	0.700	9.69E-06	0.329	1.21E-04	11.5	1.16E-04	0.471
5	0.050	0.25	24.25	0.651	9.01E-06	0.376	1.51E-04	15.6	1.46E-04	0.578
6	0.050	0.30	24.30	0.607	8.40E-06	0.418	1.81E-04	20.1	1.75E-04	0.689
7	0.050	0.35	24.35	0.571	7.90E-06	0.452	2.10E-04	25.0	2.04E-04	0.792
8	0.050	0.40	24.40	0.538	7.44E-06	0.483	2.40E-04	30.4	2.33E-04	0.898
9	0.050	0.45	24.45	0.509	7.04E-06	0.510	2.69E-04	36.2	2.62E-04	1.002
10	0.050	0.50	24.50	0.483	6.68E-06	0.534	2.99E-04	42.4	2.91E-04	1.105

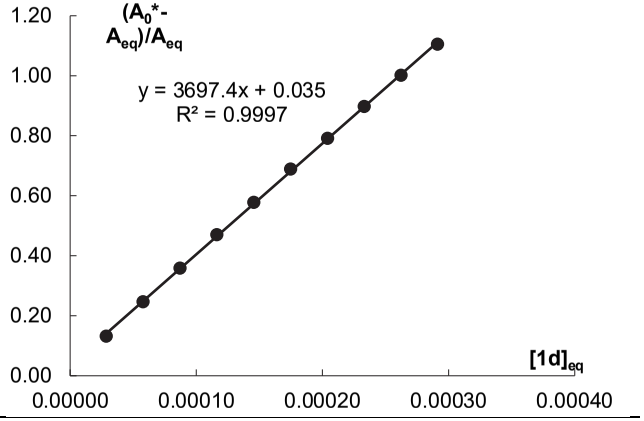

Step	V_{LB} / mL	$V_{tot,LB}$ / mL	V_{tot} / mL	A	[**2a**]	$A_0^* - A_{eq}$	[**1d**]$_0$	[**1d**]$_0$ / [**2a**]$_0$	[**1d**]$_{eq}$	$(A_0^* - A_{eq})/A_{eq}$
0	0	0	24.00	1.047	1.45E-05		0.000E+00			
1	0.050	0.05	24.05	0.931	1.29E-05	0.114	3.04E-05	2.1	2.89E-05	0.122
2	0.050	0.10	24.10	0.841	1.16E-05	0.202	6.07E-05	4.7	5.79E-05	0.240
3	0.050	0.15	24.15	0.769	1.06E-05	0.271	9.09E-05	7.8	8.71E-05	0.353
4	0.050	0.20	24.20	0.713	9.87E-06	0.325	1.21E-04	11.4	1.16E-04	0.456
5	0.050	0.25	24.25	0.663	9.17E-06	0.373	1.51E-04	15.3	1.46E-04	0.563
6	0.050	0.30	24.30	0.617	8.54E-06	0.417	1.81E-04	19.7	1.75E-04	0.676
7	0.050	0.35	24.35	0.582	8.05E-06	0.450	2.10E-04	24.6	2.04E-04	0.773
8	0.050	0.40	24.40	0.547	7.57E-06	0.483	2.40E-04	29.8	2.33E-04	0.883
9	0.050	0.45	24.45	0.517	7.15E-06	0.511	2.69E-04	35.6	2.62E-04	0.988
10	0.050	0.50	24.50	0.490	6.78E-06	0.536	2.99E-04	41.8	2.91E-04	1.093

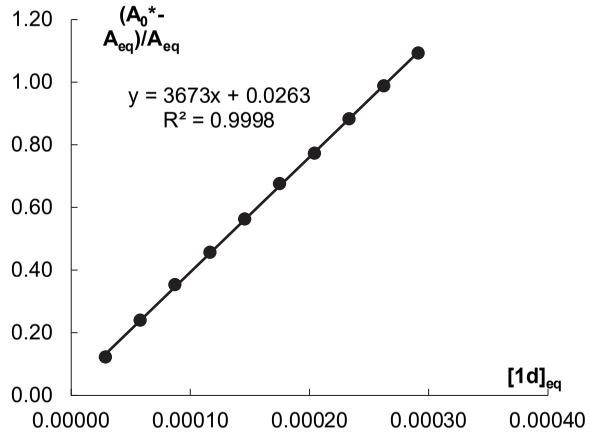

$K_{average} = (3.73 \pm 0.06) \times 10^3\ M^{-1}$

Reaction of 1d-NBu_4 with 2b-BF_4 (in MeCN, 20 °C, RM671)

Step	V_{LB} / mL	$V_{tot,LB}$ / mL	V_{tot} / mL	A	[**2b**]	$A_0^* - A_{eq}$	[**1d**]$_0$	[**1d**]$_0$ / [**2b**]$_0$	[**1d**]$_{eq}$	$(A_0^* - A_{eq})/A_{eq}$
0	0	0	24.00	1.087	1.19E-05		0.000E+00			
1	0.050	0.05	24.05	1.022	1.12E-05	0.063	3.04E-05	2.5	2.97E-05	0.061
2	0.050	0.10	24.10	0.961	1.06E-05	0.121	6.07E-05	5.4	5.94E-05	0.126
3	0.050	0.15	24.15	0.903	9.92E-06	0.177	9.09E-05	8.6	8.90E-05	0.196
4	0.050	0.20	24.20	0.853	9.38E-06	0.225	1.21E-04	12.2	1.18E-04	0.264
5	0.050	0.25	24.25	0.807	8.87E-06	0.269	1.51E-04	16.1	1.48E-04	0.333
6	0.050	0.30	24.30	0.764	8.40E-06	0.310	1.81E-04	20.4	1.77E-04	0.405
7	0.050	0.35	24.35	0.726	7.98E-06	0.345	2.10E-04	25.1	2.07E-04	0.476
8	0.050	0.40	24.40	0.694	7.63E-06	0.375	2.40E-04	30.1	2.36E-04	0.541
9	0.050	0.45	24.45	0.658	7.23E-06	0.409	2.69E-04	35.3	2.65E-04	0.622
10	0.050	0.50	24.50	0.630	6.92E-06	0.435	2.99E-04	41.3	2.94E-04	0.690

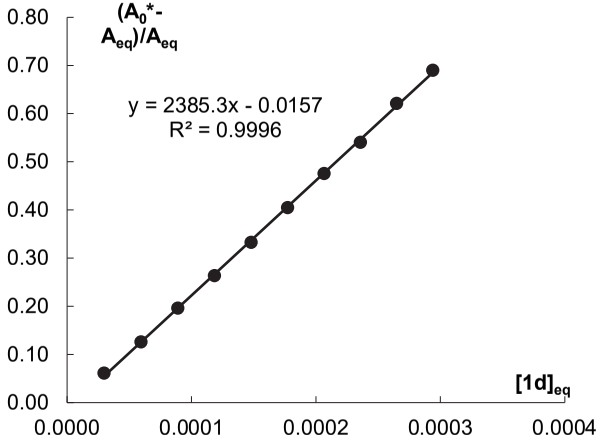

Step	V_{LB} / mL	$V_{tot,LB}$ / mL	V_{tot} / mL	A	[**2b**]	$A_0^* - A_{eq}$	[**1d**]$_0$	[**1d**]$_0$ / [**2b**]$_0$	[**1d**]$_{eq}$	$(A_0^* - A_{eq})/A_{eq}$
0	0	0	24.00	1.088	1.20E-05		0.000E+00			
1	0.050	0.05	24.05	1.018	1.12E-05	0.068	3.04E-05	2.5	2.97E-05	0.067
2	0.050	0.10	24.10	0.957	1.05E-05	0.126	6.07E-05	5.4	5.93E-05	0.132
3	0.050	0.15	24.15	0.900	9.89E-06	0.181	9.09E-05	8.6	8.89E-05	0.201
4	0.050	0.20	24.20	0.850	9.34E-06	0.229	1.21E-04	12.2	1.18E-04	0.269
5	0.050	0.25	24.25	0.804	8.84E-06	0.273	1.51E-04	16.2	1.48E-04	0.339
6	0.050	0.30	24.30	0.765	8.41E-06	0.310	1.81E-04	20.4	1.77E-04	0.405
7	0.050	0.35	24.35	0.727	7.99E-06	0.345	2.10E-04	25.0	2.07E-04	0.475
8	0.050	0.40	24.40	0.692	7.61E-06	0.378	2.40E-04	30.0	2.36E-04	0.546
9	0.050	0.45	24.45	0.660	7.25E-06	0.408	2.69E-04	35.4	2.65E-04	0.618
10	0.050	0.50	24.50	0.629	6.91E-06	0.437	2.99E-04	41.2	2.94E-04	0.694

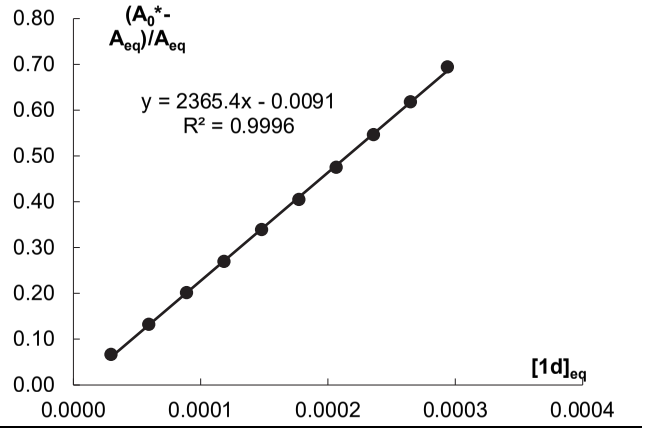

Step	V_{LB} / mL	$V_{tot,LB}$ / mL	V_{tot} / mL	A	[**2b**]	$A_0^* - A_{eq}$	[**1d**]$_0$	[**1d**]$_0$ / [**2b**]$_0$	[**1d**]$_{eq}$	$(A_0^* - A_{eq})/A_{eq}$
0	0	0	24.00	1.132	1.24E-05		0.000E+00			
1	0.050	0.05	24.05	1.063	1.17E-05	0.067	3.04E-05	2.4	2.97E-05	0.063
2	0.050	0.10	24.10	1.004	1.10E-05	0.123	6.07E-05	5.2	5.94E-05	0.123
3	0.050	0.15	24.15	0.994	1.09E-05	0.131	9.09E-05	8.2	8.95E-05	0.132
4	0.050	0.20	24.20	0.889	9.77E-06	0.234	1.21E-04	11.1	1.18E-04	0.263
5	0.050	0.25	24.25	0.843	9.27E-06	0.277	1.51E-04	15.4	1.48E-04	0.329
6	0.050	0.30	24.30	0.796	8.75E-06	0.322	1.81E-04	19.5	1.77E-04	0.405
7	0.050	0.35	24.35	0.756	8.31E-06	0.360	2.10E-04	24.0	2.06E-04	0.476
8	0.050	0.40	24.40	0.721	7.92E-06	0.392	2.40E-04	28.9	2.36E-04	0.544
9	0.050	0.45	24.45	0.687	7.55E-06	0.424	2.69E-04	34.0	2.65E-04	0.617
10	0.050	0.50	24.50	0.657	7.22E-06	0.452	2.99E-04	39.6	2.94E-04	0.688

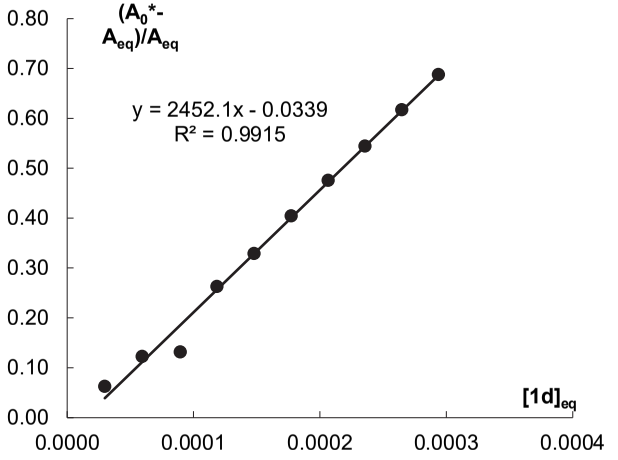

$K_{average} = (2.40 \pm 0.03) \times 10^3\ M^{-1}$

Reaction of 1d-NBu_4 with 2c-BF_4 (in MeCN, 20 °C, RM671)

Step	V_{LB} / mL	$V_{tot,LB}$ / mL	V_{tot} / mL	A	[**2c**]	$A_0^* - A_{eq}$	[**1d**]$_0$	[**1d**]$_0$ / [**2c**]$_0$	[**1d**]$_{eq}$	$(A_0^* - A_{eq})/A_{eq}$
0	0	0	24.00	1.118	1.62E-05		0.000E+00			
1	0.025	0.03	24.03	0.664	9.62E-06	0.453	1.52E-05	0.9	8.67E-06	0.682
2	0.025	0.05	24.05	0.401	5.81E-06	0.715	3.04E-05	3.2	2.01E-05	1.782
3	0.025	0.08	24.08	0.271	3.93E-06	0.844	4.56E-05	7.8	3.34E-05	3.113
4	0.025	0.10	24.10	0.202	2.93E-06	0.911	6.07E-05	15.5	4.75E-05	4.512
5	0.025	0.13	24.13	0.163	2.36E-06	0.949	7.58E-05	25.9	6.21E-05	5.823
6	0.025	0.15	24.15	0.134	1.94E-06	0.977	9.09E-05	38.5	7.68E-05	7.291

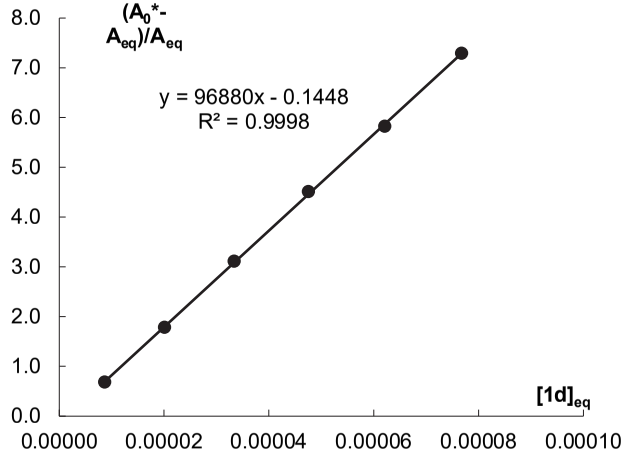

Step	V_{LB} / mL	$V_{tot,LB}$ / mL	V_{tot} / mL	A	[**2c**]	$A_0^* - A_{eq}$	[**1d**]$_0$	[**1d**]$_0$ / [**2c**]$_0$	[**1d**]$_{eq}$	$(A_0^* - A_{eq})/A_{eq}$
0	0	0	24.00	1.115	1.62E-05		0.000E+00			
1	0.025	0.03	24.03	0.648	9.39E-06	0.466	1.52E-05	0.9	8.48E-06	0.719
2	0.025	0.05	24.05	0.392	5.68E-06	0.721	3.04E-05	3.2	2.00E-05	1.838
3	0.025	0.08	24.08	0.269	3.90E-06	0.843	4.56E-05	8.0	3.34E-05	3.132
4	0.025	0.10	24.10	0.202	2.93E-06	0.908	6.07E-05	15.6	4.76E-05	4.497
5	0.025	0.13	24.13	0.160	2.32E-06	0.949	7.58E-05	25.9	6.21E-05	5.933
6	0.025	0.15	24.15	0.135	1.96E-06	0.973	9.09E-05	39.2	7.68E-05	7.208

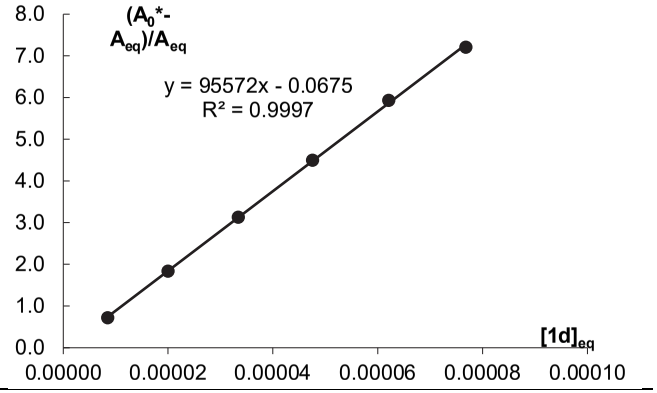

Step	V_{LB} / mL	$V_{tot,LB}$ / mL	V_{tot} / mL	A	[**2c**]	$A_0^* - A_{eq}$	[**1d**]$_0$	[**1d**]$_0$ / [**2c**]$_0$	[**1d**]$_{eq}$	$(A_0^* - A_{eq})/A_{eq}$
0	0	0	24.00	1.136	1.65E-05		0.000E+00			
1	0.025	0.03	24.03	0.679	9.84E-06	0.456	1.52E-05	0.9	8.63E-06	0.671
2	0.025	0.05	24.05	0.401	5.81E-06	0.733	3.04E-05	3.1	1.98E-05	1.827
3	0.025	0.08	24.08	0.271	3.93E-06	0.861	4.56E-05	7.8	3.31E-05	3.179
4	0.025	0.10	24.10	0.205	2.97E-06	0.926	6.07E-05	15.5	4.73E-05	4.518
5	0.025	0.13	24.13	0.161	2.33E-06	0.969	7.58E-05	25.5	6.18E-05	6.019
6	0.025	0.15	24.15	0.134	1.94E-06	0.995	9.09E-05	39.0	7.65E-05	7.425

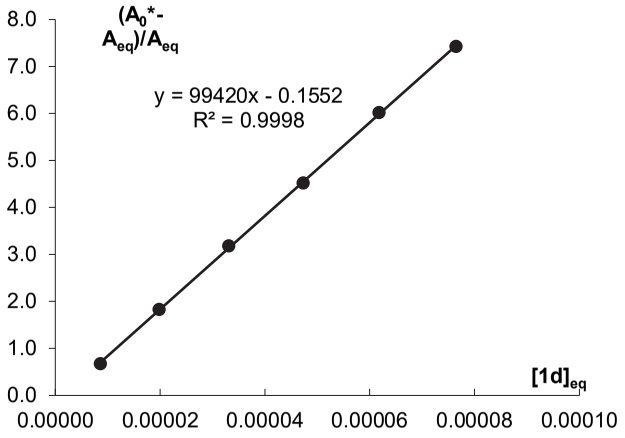

$K_{average} = (9.73 \pm 0.16) \times 10^4\ M^{-1}$

Reaction of 1c-NBu_4 with 2a-BF_4 (in DMSO, 20 °C, RM719)

Step	V_{LB} / mL	$V_{tot,LB}$ / mL	V_{tot} / mL	A	[**2a**]	$A_0^* - A_{eq}$	[**1c**]$_0$	[**1c**]$_0$ / [**2c**]$_0$	[**1c**]$_{eq}$	$(A_0^* - A_{eq})/A_{eq}$
0	0	0	24.09	1.063	1.69E-05		0.000E+00			
1	0.025	0.03	24.12	0.988	1.57E-05	0.074	2.88E-05	1.7	2.76E-05	0.075
2	0.025	0.05	24.14	0.963	1.53E-05	0.098	5.75E-05	3.7	5.60E-05	0.102
3	0.025	0.08	24.17	0.887	1.41E-05	0.173	8.62E-05	5.6	8.35E-05	0.195
4	0.025	0.10	24.19	0.837	1.33E-05	0.222	1.15E-04	8.1	1.11E-04	0.265
5	0.025	0.13	24.22	0.794	1.26E-05	0.264	1.43E-04	10.8	1.39E-04	0.332
6	0.025	0.15	24.24	0.757	1.20E-05	0.299	1.72E-04	13.6	1.67E-04	0.396
7	0.025	0.18	24.27	0.723	1.15E-05	0.332	2.00E-04	16.7	1.95E-04	0.460
8	0.025	0.20	24.29	0.689	1.09E-05	0.365	2.29E-04	19.9	2.23E-04	0.530

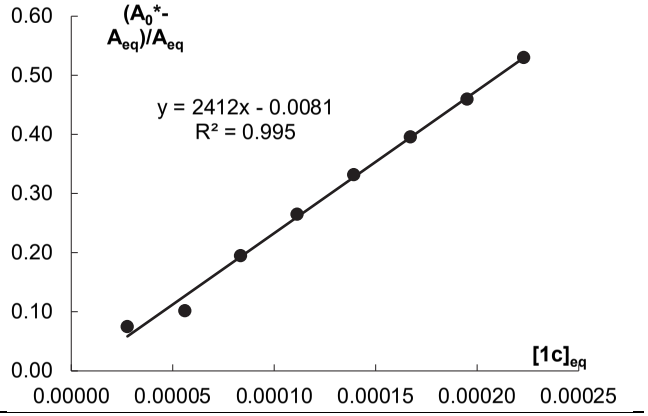

Step	V_{LB} / mL	$V_{tot,LB}$ / mL	V_{tot} / mL	A	[**2a**]	$A_0^* - A_{eq}$	[**1c**]$_0$	[**1c**]$_0$ / [**2c**]$_0$	[**1c**]$_{eq}$	$(A_0^* - A_{eq})/A_{eq}$
0	0	0	24.09	1.077	1.71E-05		0.000E+00			
1	0.025	0.03	24.12	1.000	1.59E-05	0.076	2.88E-05	1.7	2.76E-05	0.076
2	0.025	0.05	24.14	0.942	1.50E-05	0.133	5.75E-05	3.6	5.54E-05	0.141
3	0.025	0.08	24.17	0.887	1.41E-05	0.187	8.62E-05	5.8	8.32E-05	0.210
4	0.025	0.10	24.19	0.843	1.34E-05	0.230	1.15E-04	8.1	1.11E-04	0.272
5	0.025	0.13	24.22	0.799	1.27E-05	0.272	1.43E-04	10.7	1.39E-04	0.341
6	0.025	0.15	24.24	0.760	1.21E-05	0.310	1.72E-04	13.5	1.67E-04	0.408
7	0.025	0.18	24.27	0.727	1.15E-05	0.342	2.00E-04	16.6	1.95E-04	0.471
8	0.025	0.20	24.29	0.694	1.10E-05	0.374	2.29E-04	19.8	2.23E-04	0.539

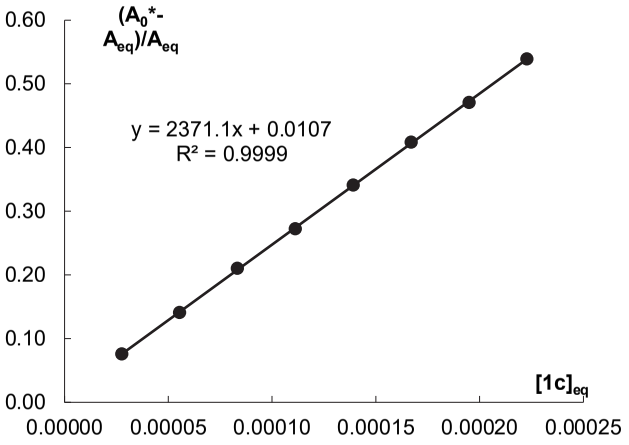

Step	V_{LB} / mL	$V_{tot,LB}$ / mL	V_{tot} / mL	A	[**2a**]	$A_0^* - A_{eq}$	[**1c**]$_0$	[**1c**]$_0$ / [**2c**]$_0$	[**1c**]$_{eq}$	$(A_0^* - A_{eq})/A_{eq}$
0	0	0	24.09	1.080	1.72E-05		0.000E+00			
1	0.025	0.03	24.12	1.002	1.59E-05	0.077	2.88E-05	1.7	2.76E-05	0.077
2	0.025	0.05	24.14	0.940	1.49E-05	0.138	5.75E-05	3.6	5.53E-05	0.147
3	0.025	0.08	24.17	0.889	1.41E-05	0.188	8.62E-05	5.8	8.32E-05	0.211
4	0.025	0.10	24.19	0.842	1.34E-05	0.234	1.15E-04	8.1	1.11E-04	0.277
5	0.025	0.13	24.22	0.800	1.27E-05	0.274	1.43E-04	10.7	1.39E-04	0.343
6	0.025	0.15	24.24	0.761	1.21E-05	0.312	1.72E-04	13.5	1.67E-04	0.410
7	0.025	0.18	24.27	0.726	1.15E-05	0.346	2.00E-04	16.6	1.95E-04	0.477
8	0.025	0.20	24.29	0.693	1.10E-05	0.378	2.29E-04	19.8	2.23E-04	0.546

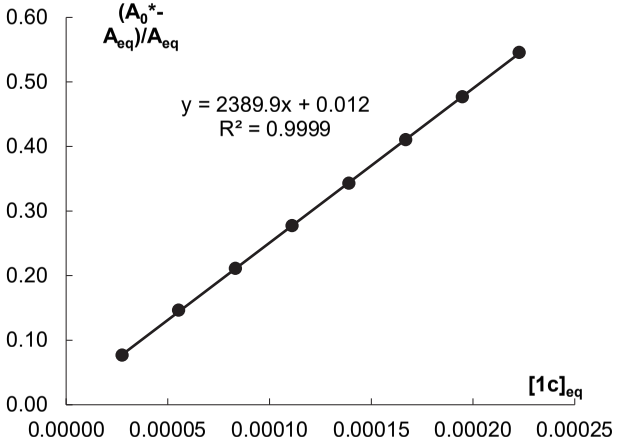

$K_{average} = (2.39 \pm 0.02) \times 10^3\ M^{-1}$

4.8 Kinetics of Reactions of Phenolates in DMSO

Tetrabutylammonium 4-Nitrophenolate

1c-**NBu$_4$** + **2a** in DMSO (stopped-flow, detection at 640 nm)

[**2a**]$_0$, mol L^{-1}	[**1c**]$_0$, mol L^{-1}	k_{obs}, s^{-1}
9.21×10^{-6}	1.00×10^{-4}	1.45
9.21×10^{-6}	2.00×10^{-4}	1.56
9.21×10^{-6}	3.00×10^{-4}	1.76
9.21×10^{-6}	4.00×10^{-4}	2.03
9.21×10^{-6}	5.00×10^{-4}	2.22

$k_2 = 2.01 \times 10^3$ M^{-1} s^{-1}

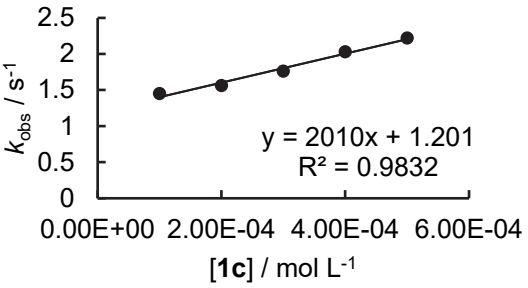

1c-**NBu$_4$** + **2b** in DMSO (stopped-flow, detection at 644 nm)

[**2b**]$_0$, mol L^{-1}	[**1c**]$_0$, mol L^{-1}	k_{obs}, s^{-1}
7.15×10^{-6}	1.00×10^{-4}	5.57
7.15×10^{-6}	2.00×10^{-4}	6.45
7.15×10^{-6}	3.00×10^{-4}	7.00
7.15×10^{-6}	4.00×10^{-4}	7.44
7.15×10^{-6}	5.00×10^{-4}	8.06

$k_2 = 5.97 \times 10^3$ M^{-1} s^{-1}

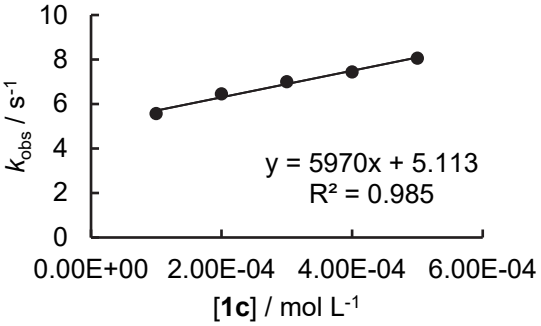

1c-**NBu$_4$** + **2c** in DMSO (stopped-flow, detection at 625 nm)

[**2c**]$_0$, mol L^{-1}	[**1c**]$_0$, mol L^{-1}	k_{obs}, s^{-1}
7.15×10^{-6}	1.00×10^{-4}	2.90
7.15×10^{-6}	2.00×10^{-4}	5.16
7.15×10^{-6}	3.00×10^{-4}	6.97
7.15×10^{-6}	4.00×10^{-4}	9.22
7.15×10^{-6}	5.00×10^{-4}	11.4

$k_2 = 2.11 \times 10^4$ M^{-1} s^{-1}

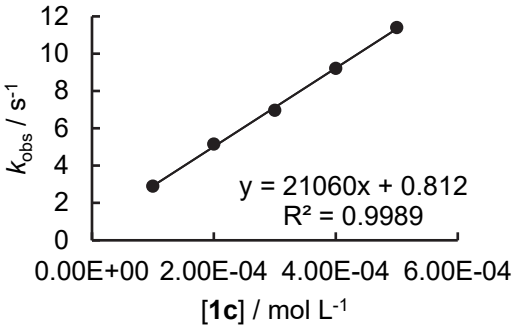

1c-**NBu$_4$** + **2d** in DMSO (stopped-flow, detection at 629 nm)

[**2d**]$_0$, mol L^{-1}	[**1c**]$_0$, mol L^{-1}	k_{obs}, s^{-1}
7.15×10^{-6}	1.00×10^{-4}	6.94
7.15×10^{-6}	2.00×10^{-4}	12.6
7.15×10^{-6}	3.00×10^{-4}	17.9
7.15×10^{-6}	4.00×10^{-4}	23.8
7.15×10^{-6}	5.00×10^{-4}	26.7

$k_2 = 5.07 \times 10^4$ M^{-1} s^{-1}

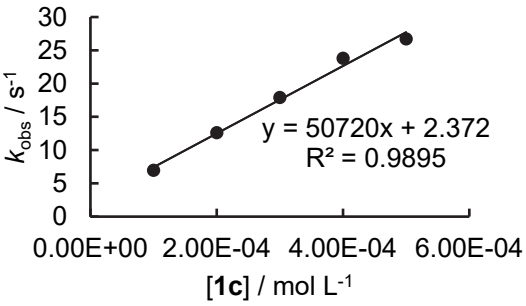

Determination of N and s_N parameters for **1c**-NBu_4 in DMSO.

Reference Electrophile	Electrophilicity E	k_2 (M^{-1} s^{-1})	lg k_2
2a	–10.04	2.01×10^3	3.30
2b	–9.45	5.97×10^3	3.78
2c	–8.76	2.11×10^4	4.32
2d	–8.22	5.07×10^4	4.71

$N = 14.32$

$s_N = 0.77$

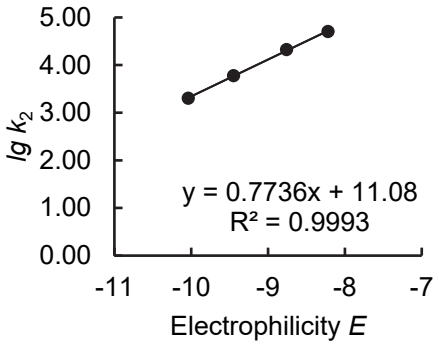

Potassium 4-Nitrophenolate

1c-**K** + **2a** in DMSO (stopped-flow, detection at 630 nm)

$[\mathbf{2a}]_0$, mol L^{-1}	$[\mathbf{1c}]_0$, mol L^{-1}	[18-c-6], mol L^{-1}	k_{obs}, s^{-1}
1.03×10^{-5}	2.26×10^{-4}		2.18
1.03×10^{-5}	4.51×10^{-4}	8.40×10^{-4}	2.80
1.03×10^{-5}	6.77×10^{-4}		3.39
1.03×10^{-5}	9.02×10^{-4}	1.68×10^{-3}	4.03
1.03×10^{-5}	1.13×10^{-3}		4.59

$k_2 = 2.68 \times 10^3$ M^{-1} s^{-1}

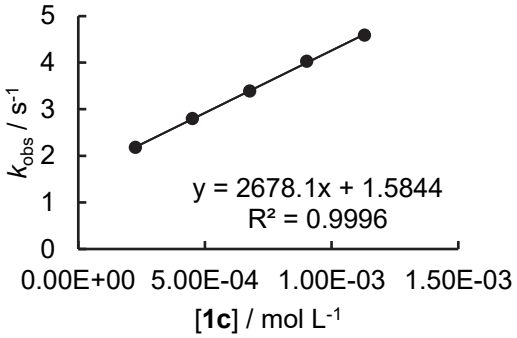

1c-**K** + **2b** in DMSO (stopped-flow, detection at 635 nm)

$[\mathbf{2b}]_0$, mol L^{-1}	$[\mathbf{1c}]_0$, mol L^{-1}	[18-c-6], mol L^{-1}	k_{obs}, s^{-1}
1.01×10^{-5}	1.63×10^{-4}		6.18
1.01×10^{-5}	3.25×10^{-4}	6.87×10^{-4}	7.24
1.01×10^{-5}	4.88×10^{-4}		8.54
1.01×10^{-5}	6.51×10^{-4}	1.37×10^{-3}	9.57
1.01×10^{-5}	8.14×10^{-4}		10.7

$k_2 = 6.98 \times 10^3$ M^{-1} s^{-1}

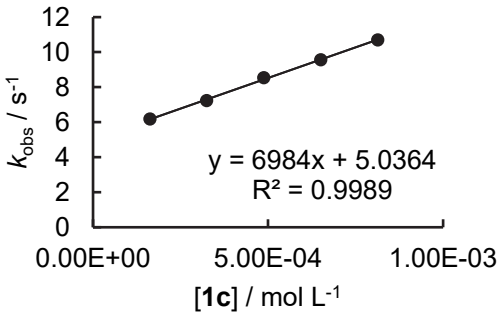

1c-**K** + **2c** in DMSO (stopped-flow, detection at 630 nm)

$[\mathbf{2c}]_0$, mol L^{-1}	$[\mathbf{1c}]_0$, mol L^{-1}	[18-c-6], mol L^{-1}	k_{obs}, s^{-1}
9.61×10^{-6}	2.26×10^{-4}		5.84
9.61×10^{-6}	4.51×10^{-4}	8.40×10^{-4}	10.4
9.61×10^{-6}	6.77×10^{-4}		14.9
9.61×10^{-6}	9.02×10^{-4}	1.68×10^{-3}	19.6
9.61×10^{-6}	1.13×10^{-3}		23.4

$k_2 = 1.96 \times 10^4$ M^{-1} s^{-1}

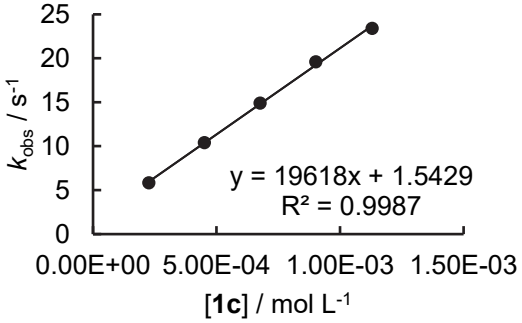

1c-**K** + **2d** in DMSO (stopped-flow, detection at 618 nm)

$[\mathbf{2d}]_0$, mol L^{-1}	$[\mathbf{1c}]_0$, mol L^{-1}	[18-c-6], mol L^{-1}	k_{obs}, s^{-1}
9.18×10^{-6}	1.49×10^{-4}		13.1
9.18×10^{-6}	2.98×10^{-4}	6.23×10^{-4}	22.8
9.18×10^{-6}	4.48×10^{-4}		31.6
9.18×10^{-6}	5.97×10^{-4}	1.25×10^{-3}	41.2
9.18×10^{-6}	7.46×10^{-4}		48.6

$k_2 = 5.99 \times 10^4$ M^{-1} s^{-1}

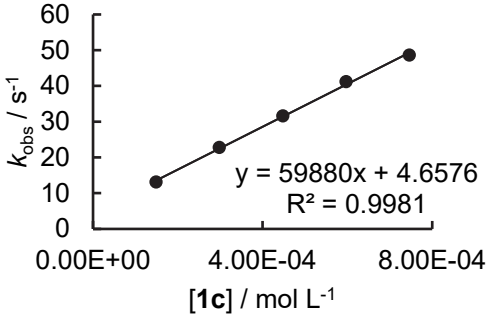

1c-**K** + **2e** in DMSO (stopped-flow, detection at 620 nm)

$[\mathbf{2e}]_0$, mol L^{-1}	$[\mathbf{1c}]_0$, mol L^{-1}	[18-c-6], mol L^{-1}	k_{obs}, s^{-1}
1.02×10^{-5}	1.63×10^{-4}		44.2
1.02×10^{-5}	3.25×10^{-4}	6.87×10^{-4}	86.6
1.02×10^{-5}	4.88×10^{-4}		117
1.02×10^{-5}	6.51×10^{-4}	1.37×10^{-3}	154
1.02×10^{-5}	8.14×10^{-4}		182

$k_2 = 2.11 \times 10^5$ M^{-1} s^{-1}

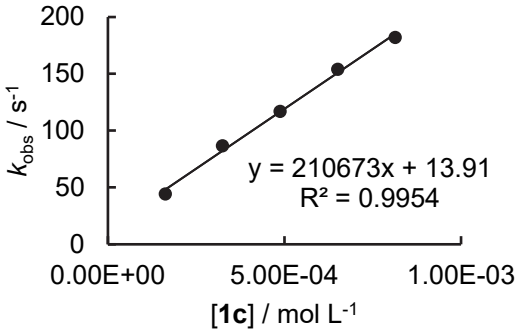

1c-**K** + **2f** in DMSO (stopped-flow, detection at 613 nm)

$[\mathbf{2f}]_0$, mol L^{-1}	$[\mathbf{1c}]_0$, mol L^{-1}	[18-c-6], mol L^{-1}	k_{obs}, s^{-1}
9.88×10^{-6}	1.49×10^{-4}		83.5
9.88×10^{-6}	2.98×10^{-4}	6.23×10^{-4}	148
9.88×10^{-6}	4.48×10^{-4}		204
9.88×10^{-6}	5.97×10^{-4}	1.25×10^{-3}	257
9.88×10^{-6}	7.46×10^{-4}		303

$k_2 = 3.67 \times 10^5$ M^{-1} s^{-1}

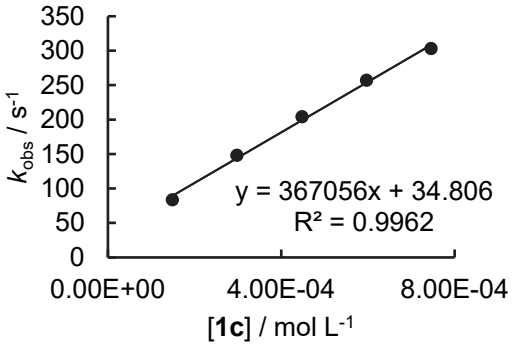

Determination of N and s_N parameters for **1c**-K in DMSO.

Reference Electrophile	Electrophilicity E	k_2 (M^{-1} s^{-1})	lg k_2
2a	−10.04	2.68×10^3	3.43
2b	−9.45	6.98×10^3	3.84
2c	−8.76	1.96×10^4	4.29
2d	−8.22	5.99×10^4	4.78
2e	−7.69	2.11×10^5	5.32
2f	−7.02	3.67×10^5	5.56

$N = 14.63$

$s_N = 0.74$

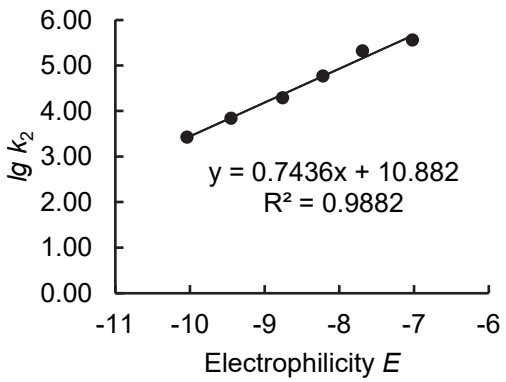

Tetrabutylammonium 2-Nitrophenolate

1d-NBu_4 + **2a** in DMSO (stopped-flow, detection at 640 nm)

$[\mathbf{2a}]_0$, mol L^{-1}	$[\mathbf{1d}]_0$, mol L^{-1}	k_{obs}, s^{-1}
6.48×10^{-6}	1.00×10^{-4}	12.8
6.48×10^{-6}	2.00×10^{-4}	14.1
6.48×10^{-6}	3.00×10^{-4}	14.9
6.48×10^{-6}	4.00×10^{-4}	15.8
6.48×10^{-6}	5.00×10^{-4}	16.5

$k_2 = 9.10 \times 10^3$ M^{-1} s^{-1}

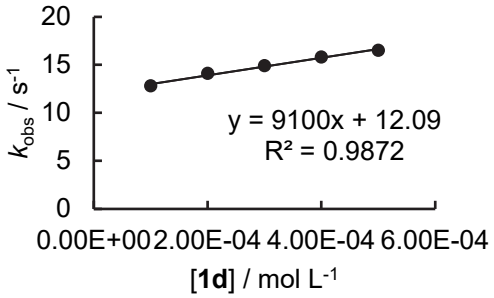

1d-NBu_4 + **2b** in DMSO (stopped-flow, detection at 644 nm)

$[\mathbf{2b}]_0$, mol L^{-1}	$[\mathbf{1d}]_0$, mol L^{-1}	k_{obs}, s^{-1}
5.83×10^{-6}	1.00×10^{-4}	46.3
5.83×10^{-6}	3.00×10^{-4}	50.6
5.83×10^{-6}	4.00×10^{-4}	52.2

$k_2 = 1.99 \times 10^4$ M^{-1} s^{-1}

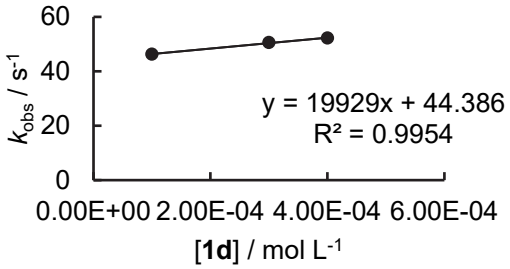

1d-NBu_4 + **2c** in DMSO (stopped-flow, detection at 625 nm)

$[\mathbf{2c}]_0$, mol L^{-1}	$[\mathbf{1d}]_0$, mol L^{-1}	k_{obs}, s^{-1}
9.86×10^{-6}	1.00×10^{-4}	9.88
9.86×10^{-6}	2.00×10^{-4}	13.3
9.86×10^{-6}	3.00×10^{-4}	16.3
9.86×10^{-6}	4.00×10^{-4}	20.3
9.86×10^{-6}	5.00×10^{-4}	24.5

$k_2 = 3.62 \times 10^4$ M^{-1} s^{-1}

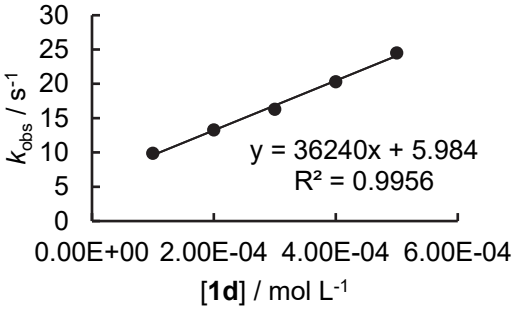

1d-NBu_4 + **2d** in DMSO (stopped-flow, detection at 629 nm)

$[\mathbf{2d}]_0$, mol L^{-1}	$[\mathbf{1d}]_0$, mol L^{-1}	k_{obs}, s^{-1}
8.79×10^{-6}	1.00×10^{-4}	21.5
8.79×10^{-6}	2.00×10^{-4}	35.5
8.79×10^{-6}	3.00×10^{-4}	53.3
8.79×10^{-6}	4.00×10^{-4}	67.3
8.79×10^{-6}	5.00×10^{-4}	76.1

$k_2 = 1.41 \times 10^5$ M^{-1} s^{-1}

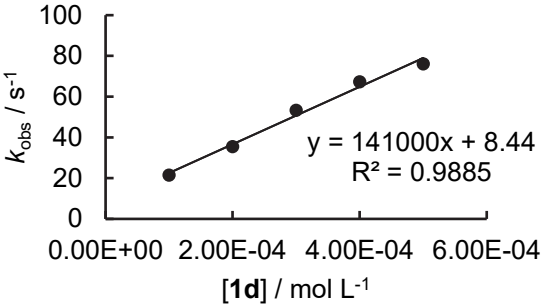

1d-**NBu$_4$** + **2e** in DMSO (stopped-flow, detection at 622 nm)

[**2e**]$_0$, mol L^{-1}	[**1d**]$_0$, mol L^{-1}	k_{obs}, s^{-1}
4.84×10^{-6}	1.00×10^{-4}	55.7
4.84×10^{-6}	2.00×10^{-4}	101
4.84×10^{-6}	3.00×10^{-4}	145
4.84×10^{-6}	4.00×10^{-4}	191
4.84×10^{-6}	5.00×10^{-4}	240

$k_2 = 4.59 \times 10^5$ M^{-1} s^{-1}

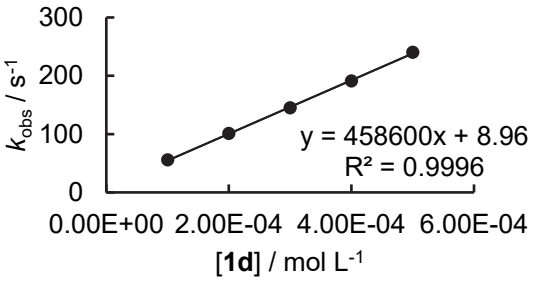

Determination of *N* and s_N parameters for **1d**-NBu$_4$ in DMSO.

Reference Electrophile	Electrophilicity *E*	k_2 (M^{-1} s^{-1})	lg k_2
2a	−10.04	9.10×10^3	3.96
2b	−9.45	1.99×10^4	4.30
2c	−8.76	3.62×10^4	4.56
2d	−8.22	1.41×10^5	5.15
2e	−7.69	4.59×10^5	5.66

N = 15.48

s_N = 0.71

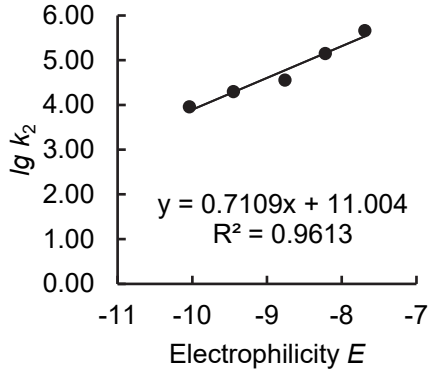

Tetrabutylammonium 3-Nitrophenolate

1e-**NBu$_4$** + **2a** in DMSO (stopped-flow, detection at 640 nm)

[**2a**]$_0$, mol L^{-1}	[**1e**]$_0$, mol L^{-1}	k_{obs}, s^{-1}
1.76×10^{-5}	1.00×10^{-4}	82.2
1.76×10^{-5}	2.00×10^{-4}	202
1.76×10^{-5}	4.00×10^{-4}	407
1.76×10^{-5}	5.00×10^{-4}	533

$k_2 = 1.11 \times 10^6$ M^{-1} s^{-1}

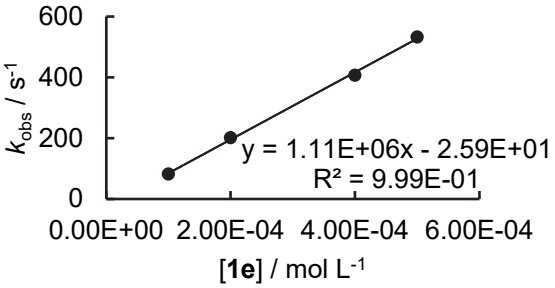

1e-**NBu$_4$** + **2b** in DMSO (stopped-flow, detection at 644 nm)

[**2b**]$_0$, mol L^{-1}	[**1e**]$_0$, mol L^{-1}	k_{obs}, s^{-1}
1.65×10^{-5}	1.00×10^{-4}	103
1.65×10^{-5}	2.00×10^{-4}	386
1.65×10^{-5}	3.00×10^{-4}	734
1.65×10^{-5}	4.00×10^{-4}	967

$k_2 = 2.94 \times 10^6$ M^{-1} s^{-1}

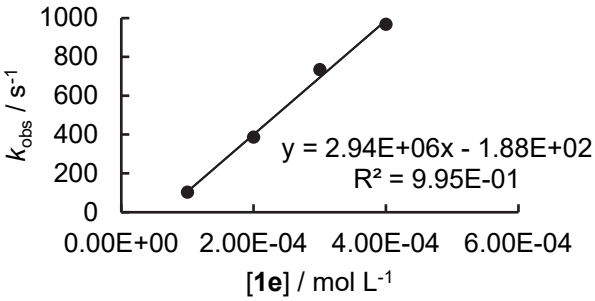

1e-**NBu$_4$** + **2c** in DMSO (stopped-flow, detection at 625 nm)

[**2c**]$_0$, mol L^{-1}	[**1e**]$_0$, mol L^{-1}	k_{obs}, s^{-1}
1.11×10^{-5}	1.00×10^{-4}	404
1.11×10^{-5}	2.00×10^{-4}	970
1.11×10^{-5}	3.00×10^{-4}	1.51×10^{3}

$k_2 = 5.53 \times 10^6$ M^{-1} s^{-1}

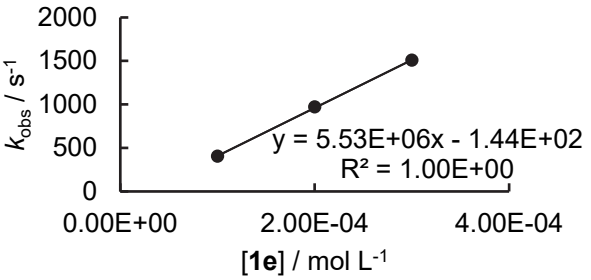

Determination of *N* and s_N parameters for **1e**-NBu$_4$ in DMSO.

Reference Electrophile	Electrophilicity *E*	k_2 (M^{-1} s^{-1})	lg k_2
2a	−10.04	1.11×10^6	6.05
2b	−9.45	2.94×10^6	6.47
2c	−8.76	5.53×10^6	6.74

N = 21.29

s_N = 0.54

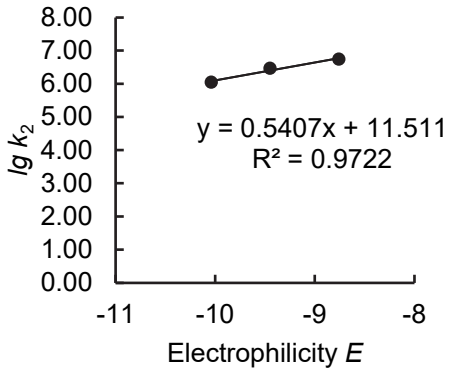

Potassium 3-Nitrophenolate

1e-**K**+ **2a** in DMSO (stopped-flow, detection at 630 nm)

[**2a**]$_0$, mol L^{-1}	[**1e**]$_0$, mol L^{-1}	[18-c-6], mol L^{-1}	k_{obs}, s^{-1}
7.50×10^{-6}	5.81×10^{-5}		61.5
7.50×10^{-6}	1.16×10^{-4}	1.50×10^{-4}	129
7.50×10^{-6}	1.74×10^{-4}		186
7.50×10^{-6}	2.33×10^{-4}	3.00×10^{-4}	240
7.50×10^{-6}	2.91×10^{-4}		298

$k_2 = 1.00 \times 10^6$ M^{-1} s^{-1}

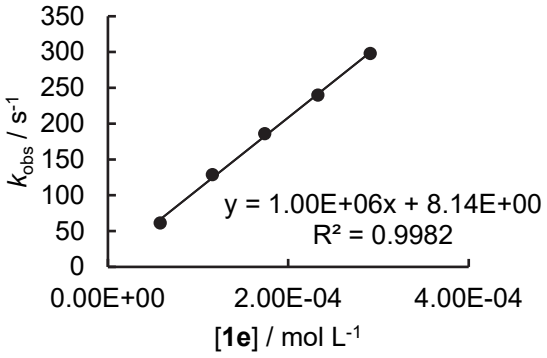

1e-**K**+ **2b** in DMSO (stopped-flow, detection at 635 nm)

[**2b**]$_0$, mol L^{-1}	[**1e**]$_0$, mol L^{-1}	[18-c-6], mol L^{-1}	k_{obs}, s^{-1}
5.58×10^{-6}	5.81×10^{-5}		152
5.58×10^{-6}	8.72×10^{-5}	1.20×10^{-4}	232
5.58×10^{-6}	1.16×10^{-4}		299
5.58×10^{-6}	1.45×10^{-4}	1.50×10^{-4}	367
5.58×10^{-6}	1.74×10^{-4}		433

$k_2 = 2.41 \times 10^6$ M^{-1} s^{-1}

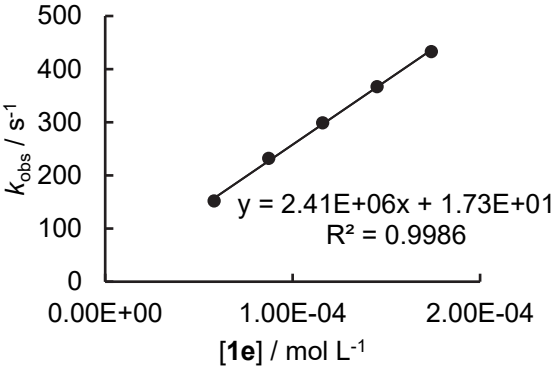

Determination of N and s_N parameters for **1e**-K in DMSO.

Reference Electrophile	Electrophilicity E	k_2 (M^{-1} s^{-1})	lg k_2
2a	−10.04	1.00×10^6	6.00
2b	−9.45	2.41×10^6	6.38

N = 19.31

s_N = 0.65

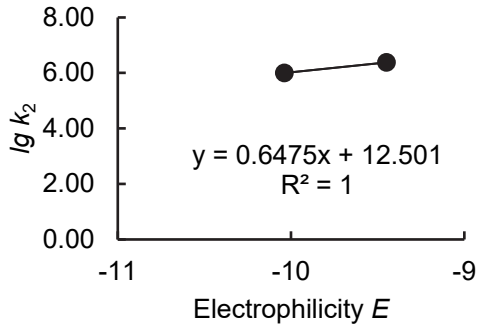

Potassium 4-Cyanophenolate

1f-**K**+ **2a** in DMSO (stopped-flow, detection at 630 nm)

$[\mathbf{2a}]_0$, mol L^{-1}	$[\mathbf{1f}]_0$, mol L^{-1}	$[Crown]_0$, mol L^{-1}	k_{obs}, s^{-1}
9.42×10^{-6}	8.36×10^{-5}		7.41
9.42×10^{-6}	1.67×10^{-4}	2.27×10^{-4}	15.4
9.42×10^{-6}	2.51×10^{-4}		23.1
9.42×10^{-6}	3.35×10^{-4}	4.54×10^{-4}	29.3
9.42×10^{-6}	4.18×10^{-4}		38.0

$k_2 = 8.97 \times 10^4$ M^{-1} s^{-1}

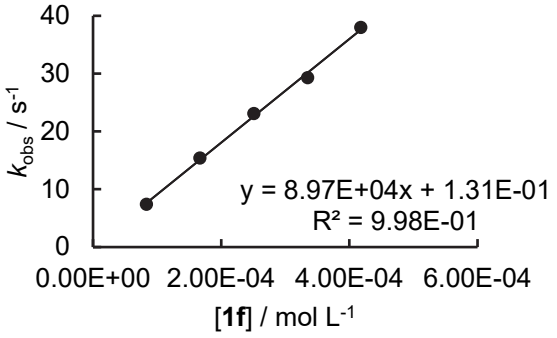

1f-**K**+ **2b** in DMSO (stopped-flow, detection at 635 nm)

$[\mathbf{2b}]_0$, mol L^{-1}	$[\mathbf{1f}]_0$, mol L^{-1}	$[Crown]_0$, mol L^{-1}	k_{obs}, s^{-1}
8.10×10^{-6}	1.01×10^{-4}		29.9
8.10×10^{-6}	2.02×10^{-4}	2.79×10^{-4}	52.6
8.10×10^{-6}	3.02×10^{-4}		73.5
8.10×10^{-6}	4.08×10^{-4}	5.58×10^{-4}	93.7
8.10×10^{-6}	5.04×10^{-4}		115

$k_2 = 2.09 \times 10^5$ M^{-1} s^{-1}

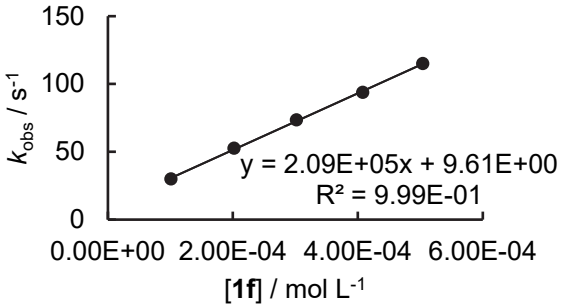

1f-**K**+ **2c** in DMSO (stopped-flow, detection at 627 nm)

$[\mathbf{2c}]_0$, mol L^{-1}	$[\mathbf{1f}]_0$, mol L^{-1}	$[Crown]_0$, mol L^{-1}	k_{obs}, s^{-1}
8.57×10^{-6}	8.36×10^{-5}		42.4
8.57×10^{-6}	1.67×10^{-4}	2.27×10^{-4}	86.5
8.57×10^{-6}	2.51×10^{-4}		129
8.57×10^{-6}	3.35×10^{-4}	4.54×10^{-4}	161
8.57×10^{-6}	4.18×10^{-4}		206

$k_2 = 4.80 \times 10^5$ M^{-1} s^{-1}

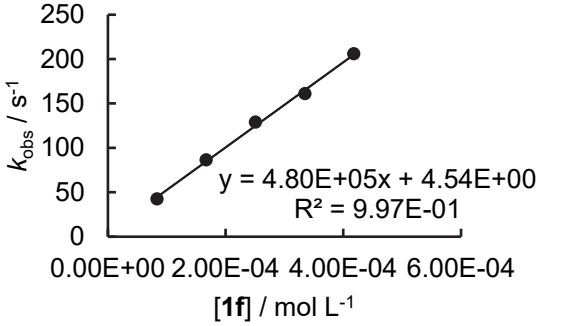

Determination of N and s_N parameters for **1f**-K in DMSO.

Reference Electrophile	Electrophilicity E	k_2 (M^{-1} s^{-1})	lg k_2
2a	−10.04	8.97×10^4	4.95
2b	−9.45	2.09×10^5	5.32
2c	−8.76	4.80×10^5	5.68

$N = 18.78$

$s_N = 0.57$

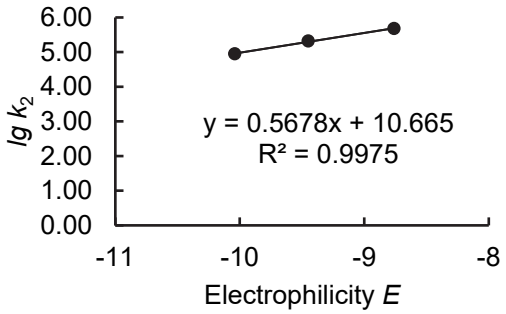

Tetrabutylammonium 2-(Trifluoromethyl)phenolate

1g-NBu_4 + **2a** in DMSO (stopped-flow, detection at 640 nm)

$[\mathbf{2a}]_0$, mol L^{-1}	$[\mathbf{1g}]_0$, mol L^{-1}	k_{obs}, s^{-1}
2.07×10^{-5}	1.00×10^{-4}	11.8
2.07×10^{-5}	2.00×10^{-4}	25.4
2.07×10^{-5}	3.00×10^{-4}	39.5
2.07×10^{-5}	4.00×10^{-4}	54.0
2.07×10^{-5}	5.00×10^{-4}	71.3

$k_2 = 1.48 \times 10^5$ M^{-1} s^{-1}

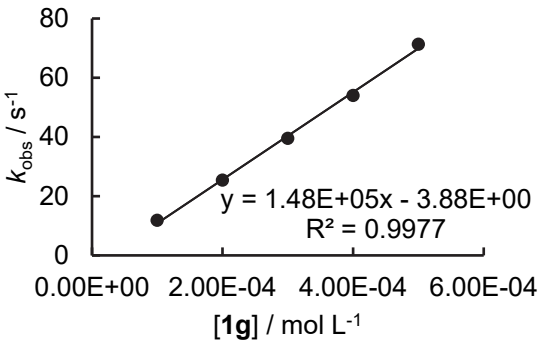

1g-NBu_4 + **2b** in DMSO (stopped-flow, detection at 644 nm)

$[\mathbf{2b}]_0$, mol L^{-1}	$[\mathbf{1g}]_0$, mol L^{-1}	k_{obs}, s^{-1}
1.59×10^{-5}	1.00×10^{-4}	24.4
1.59×10^{-5}	2.00×10^{-4}	57.4
1.59×10^{-5}	3.00×10^{-4}	87.4
1.59×10^{-5}	4.00×10^{-4}	125
1.59×10^{-5}	5.00×10^{-4}	161

$k_2 = 3.41 \times 10^5$ M^{-1} s^{-1}

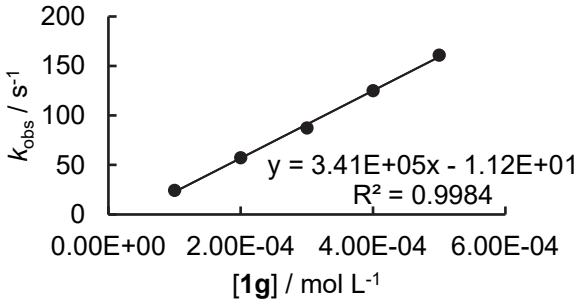

1g-NBu_4 + **2c** in DMSO (stopped-flow, detection at 625 nm)

$[\mathbf{2c}]_0$, mol L^{-1}	$[\mathbf{1g}]_0$, mol L^{-1}	k_{obs}, s^{-1}
1.38×10^{-5}	1.00×10^{-4}	80.5
1.38×10^{-5}	2.00×10^{-4}	165
1.38×10^{-5}	3.00×10^{-4}	238
1.38×10^{-5}	4.00×10^{-4}	335
1.38×10^{-5}	5.00×10^{-4}	447

$k_2 = 9.03 \times 10^5$ M^{-1} s^{-1}

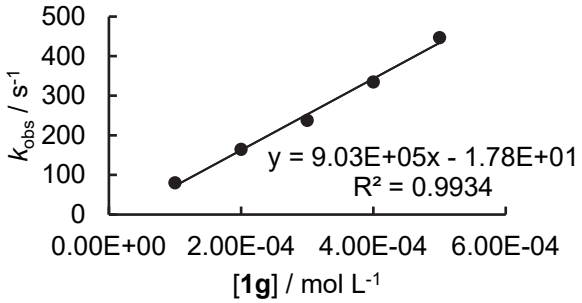

Determination of N and s_N parameters for **1g**-NBu_4 in DMSO.

Reference Electrophile	Electrophilicity E	k_2 (M^{-1} s^{-1})	lg k_2
2a	−10.04	1.48×10^5	5.17
2b	−9.45	3.41×10^5	5.53
2c	−8.76	9.03×10^5	5.96
	N = 18.47		
	s_N = 0.61		

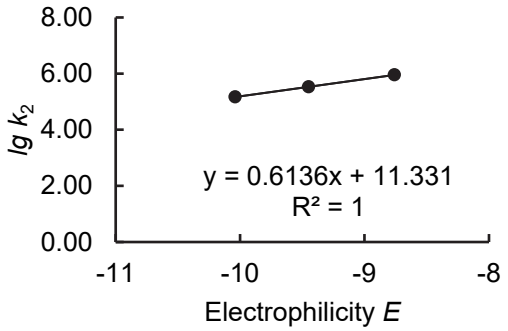

Tetrabutylammonium 4-(Trifluoromethyl)phenolate

1h-**NBu$_4$** + **2a** in DMSO (stopped-flow, detection at 640 nm)

[**2a**]$_0$, mol L^{-1}	[**1h**]$_0$, mol L^{-1}	k_{obs}, s^{-1}
1.11×10^{-5}	1.00×10^{-4}	46.1
1.11×10^{-5}	2.00×10^{-4}	66.7
1.11×10^{-5}	3.00×10^{-4}	114
1.11×10^{-5}	4.00×10^{-4}	140
1.11×10^{-5}	5.00×10^{-4}	216

$k_2 = 4.13 \times 10^5$ M^{-1} s^{-1}

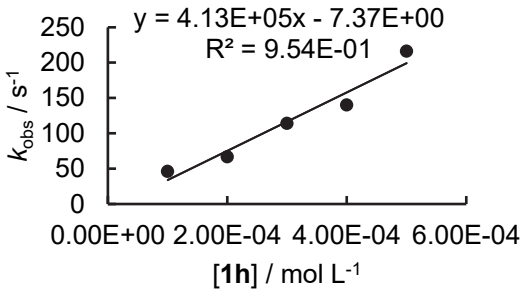

1h-**NBu$_4$** + **2b** in DMSO (stopped-flow, detection at 644 nm)

[**2b**]$_0$, mol L^{-1}	[**1h**]$_0$, mol L^{-1}	k_{obs}, s^{-1}
7.28×10^{-6}	1.00×10^{-4}	110
7.28×10^{-6}	2.00×10^{-4}	202
7.28×10^{-6}	3.00×10^{-4}	330
7.28×10^{-6}	4.00×10^{-4}	460
7.28×10^{-6}	5.00×10^{-4}	592

$k_2 = 1.22 \times 10^6$ M^{-1} s^{-1}

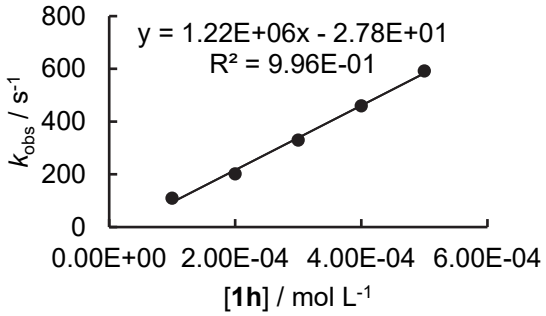

1h-**NBu$_4$** + **2c** in DMSO (stopped-flow, detection at 625 nm)

[**2c**]$_0$, mol L^{-1}	[**1h**]$_0$, mol L^{-1}	k_{obs}, s^{-1}
1.22×10^{-5}	1.00×10^{-4}	203
1.22×10^{-5}	2.00×10^{-4}	396
1.22×10^{-5}	3.00×10^{-4}	731
1.22×10^{-5}	4.00×10^{-4}	1.01×10^3
1.22×10^{-5}	5.00×10^{-4}	1.24×10^3

$k_2 = 2.69 \times 10^6$ M^{-1} s^{-1}

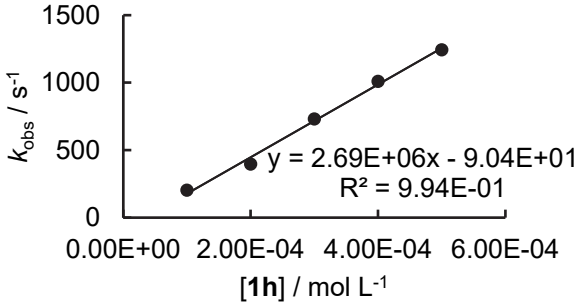

Determination of N and s_N parameters for **1h**-NBu_4 in DMSO.

Reference Electrophile	Electrophilicity E	k_2 (M^{-1} s^{-1})	lg k_2
2a	−10.04	4.13×10^5	5.62
2b	−9.45	1.22×10^6	6.09
2c	−8.76	2.69×10^6	6.43

N = 18.98
s_N = 0.63

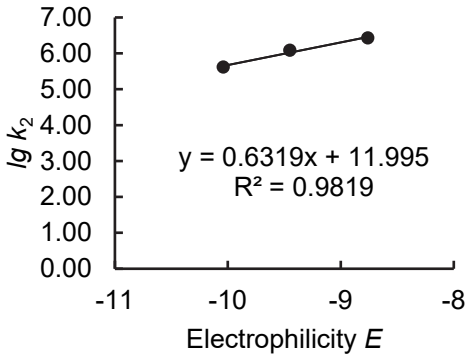

Potassium 3-(Trifluoromethyl)phenolate

1i-**K**+ **2a** in DMSO (stopped-flow, detection at 640 nm)

$[\mathbf{2a}]_0$, mol L^{-1}	$[\mathbf{1i}]_0$, mol L^{-1}	k_{obs}, s^{-1}
1.09×10^{-5}	1.00×10^{-4}	203
1.09×10^{-5}	2.00×10^{-4}	477
1.09×10^{-5}	3.00×10^{-4}	716
1.09×10^{-5}	4.00×10^{-4}	977
1.09×10^{-5}	5.00×10^{-4}	1.21×10^3

$k_2 = 2.51 \times 10^6$ M^{-1} s^{-1}

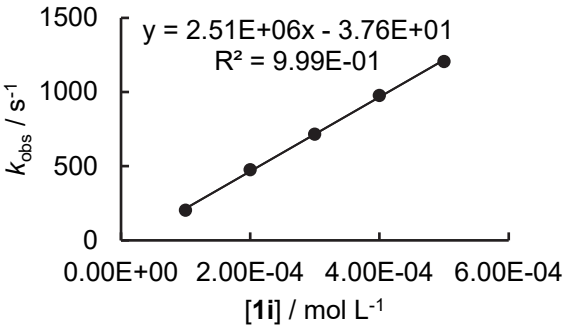

1i-**K**+ **2b** in DMSO (stopped-flow, detection at 644 nm)

$[\mathbf{2b}]_0$, mol L^{-1}	$[\mathbf{1i}]_0$, mol L^{-1}	k_{obs}, s^{-1}
1.38×10^{-5}	1.00×10^{-4}	215
1.38×10^{-5}	2.00×10^{-4}	875
1.38×10^{-5}	3.00×10^{-4}	1.31×10^3
1.38×10^{-5}	4.00×10^{-4}	1.74×10^3

$k_2 = 5.01 \times 10^6$ M^{-1} s^{-1}

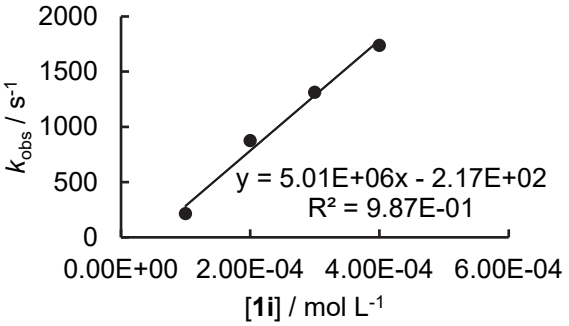

Determination of N and s_N parameters for **1i**-K in DMSO.

Reference Electrophile	Electrophilicity E	k_2 (M^{-1} s^{-1})	lg k_2
2a	−10.04	2.51×10^6	6.40
2b	−9.45	5.01×10^6	6.70

N = 22.62
s_N = 0.51

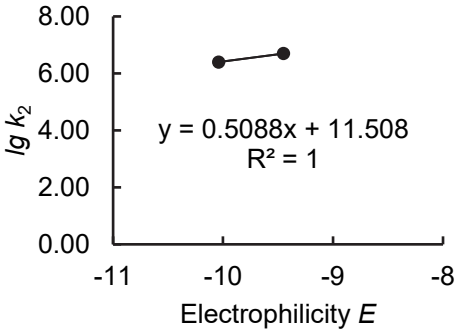

Potassium 4-Chlorophenolate

1j-**K**+ **2j** in DMSO (stopped-flow, detection at 500 nm)

$[\mathbf{2j}]_0$, mol L^{-1}	$[\mathbf{1j}]_0$, mol L^{-1}	k_{obs}, s^{-1}
1.52×10^{-5}	4.00×10^{-4}	48.9
1.52×10^{-5}	5.00×10^{-4}	52.0
1.52×10^{-5}	7.00×10^{-4}	56.4
1.52×10^{-5}	9.00×10^{-4}	59.1

$k_2 = 2.02 \times 10^4$ M^{-1} s^{-1}

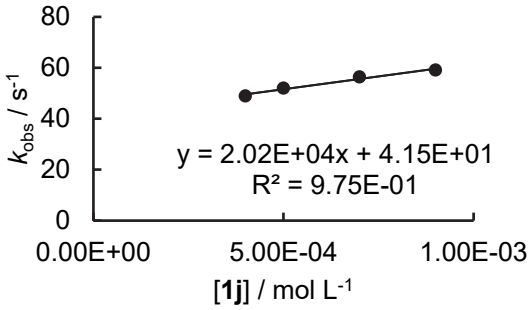

1j-**K**+ **2g** in DMSO (stopped-flow, detection at 533 nm)

$[\mathbf{2g}]_0$, mol L^{-1}	$[\mathbf{1j}]_0$, mol L^{-1}	k_{obs}, s^{-1}
6.44×10^{-6}	4.00×10^{-4}	50.5
6.44×10^{-6}	5.00×10^{-4}	54.6
6.44×10^{-6}	7.00×10^{-4}	59.4
6.44×10^{-6}	9.00×10^{-4}	61.9

$k_2 = 2.23 \times 10^4$ M^{-1} s^{-1}

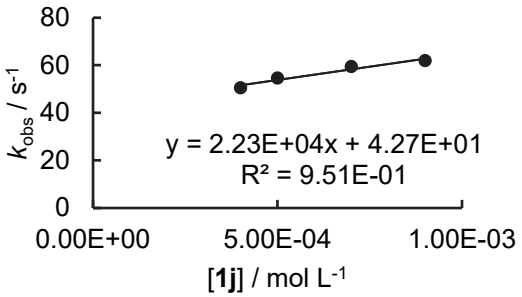

1j-**K**+ **2h** in DMSO (stopped-flow, detection at 422 nm)

$[\mathbf{2h}]_0$, mol L^{-1}	$[\mathbf{1j}]_0$, mol L^{-1}	k_{obs}, s^{-1}
1.32×10^{-5}	1.00×10^{-4}	25.8
1.32×10^{-5}	2.00×10^{-4}	40.5
1.32×10^{-5}	3.00×10^{-4}	52.7
1.32×10^{-5}	4.00×10^{-4}	69.6
1.32×10^{-5}	5.00×10^{-4}	82.0

$k_2 = 1.42 \times 10^5$ M^{-1} s^{-1}

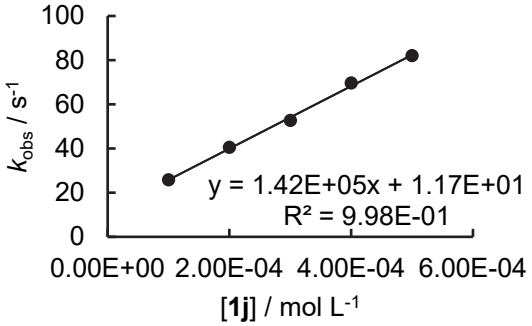

1j-**K**+ **2i** in DMSO (stopped-flow, detection at 384 nm)

$[\mathbf{2i}]_0$, mol L^{-1}	$[\mathbf{1j}]_0$, mol L^{-1}	k_{obs}, s^{-1}
3.73×10^{-5}	1.00×10^{-4}	35.6
3.73×10^{-5}	2.00×10^{-4}	68.3
3.73×10^{-5}	3.00×10^{-4}	98.5
3.73×10^{-5}	4.00×10^{-4}	136
3.73×10^{-5}	5.00×10^{-4}	171

$k_2 = 3.39 \times 10^5$ M^{-1} s^{-1}

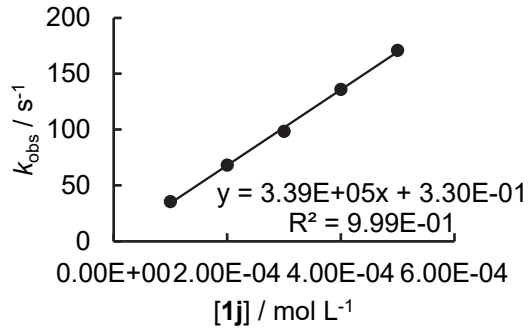

1j-**K**+ **2a** in DMSO (stopped-flow, detection at 640 nm)

[**2a**]$_0$, mol L^{-1}	[**1j**]$_0$, mol L^{-1}	k_{obs}, s^{-1}
1.33×10^{-5}	5.00×10^{-5}	122
1.33×10^{-5}	1.00×10^{-4}	275
1.33×10^{-5}	2.00×10^{-4}	770
1.33×10^{-5}	3.00×10^{-4}	1.19×10^{3}
1.33×10^{-5}	4.00×10^{-4}	1.63×10^{3}

$k_2 = 4.38 \times 10^6$ M^{-1} s^{-1}

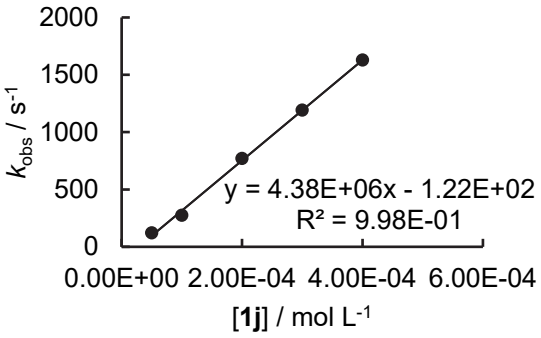

Determination of N and s_N parameters for **1j**-K in DMSO.

Reference Electrophile	Electrophilicity E	k_2 (M^{-1} s^{-1})	lg k_2
2j	–13.84	2.02×10^4	4.31
2g	–13.39	2.23×10^4	4.35
2h	–12.18	1.42×10^5	5.15
2i	–11.87	3.39×10^5	5.53
2a	–10.04	4.38×10^6	6.64

$N = 20.34$

$s_N = 0.64$

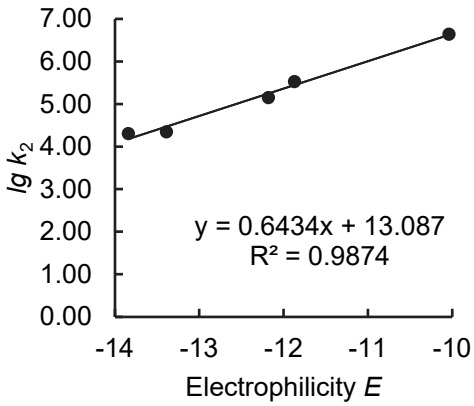

Potassium Phenolate

1k-**K**+ **2l** in DMSO (stopped-flow, detection at 487 nm)

[**2l**]$_0$, mol L^{-1}	[**1k**]$_0$, mol L^{-1}	[18-c-6], mol L^{-1}	k_{obs}, s^{-1}
2.05×10^{-5}	3.09×10^{-4}		13.5
2.05×10^{-5}	6.17×10^{-4}	8.50×10^{-4}	18.6
2.05×10^{-5}	9.26×10^{-4}		22.7
2.05×10^{-5}	1.23×10^{-3}	1.70×10^{-3}	27.6
2.05×10^{-5}	1.54×10^{-3}		31.9

$k_2 = 1.49 \times 10^4$ M^{-1} s^{-1}

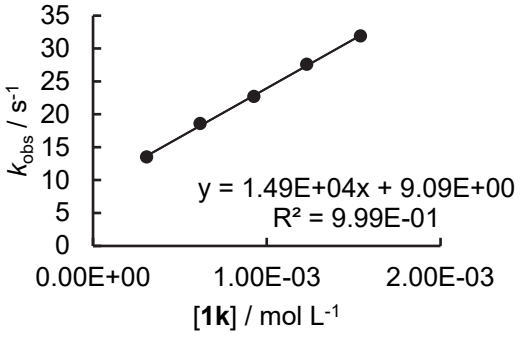

1k-**K**+ **2j** in DMSO (stopped-flow, detection at 487 nm)

[**2j**]$_0$, mol L^{-1}	[**1k**]$_0$, mol L^{-1}	[18-c-6], mol L^{-1}	k_{obs}, s^{-1}
1.38×10^{-5}	2.97×10^{-4}		9.42
1.38×10^{-5}	5.95×10^{-4}	8.50×10^{-4}	15.8
1.38×10^{-5}	8.92×10^{-4}		20.7
1.38×10^{-5}	1.19×10^{-3}	1.70×10^{-3}	26.0
1.38×10^{-5}	1.49×10^{-3}		30.3

$k_2 = 1.74 \times 10^4$ M^{-1} s^{-1}

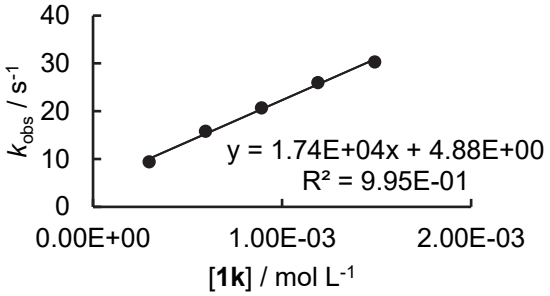

1k-**K**+ **2g** in DMSO (stopped-flow, detection at 533 nm)

$[\mathbf{2g}]_0$, mol L^{-1}	$[\mathbf{1k}]_0$, mol L^{-1}	[18-c-6], mol L^{-1}	k_{obs}, s^{-1}
1.35×10^{-5}	3.73×10^{-4}		19.7
1.35×10^{-5}	7.46×10^{-4}	8.50×10^{-4}	36.5
1.35×10^{-5}	1.12×10^{-3}		51.5
1.35×10^{-5}	1.49×10^{-3}	1.70×10^{-3}	69.1
1.35×10^{-5}	1.86×10^{-3}		84.1

$k_2 = 4.34 \times 10^4$ M^{-1} s^{-1}

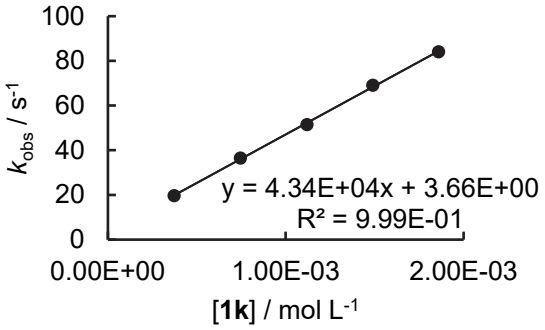

1k-**K**+ **2k** in DMSO (stopped-flow, detection at 487 nm)

$[\mathbf{2k}]_0$, mol L^{-1}	$[\mathbf{1k}]_0$, mol L^{-1}	[18-c-6], mol L^{-1}	k_{obs}, s^{-1}
1.95×10^{-5}	2.97×10^{-4}		25.6
1.95×10^{-5}	5.95×10^{-4}	8.50×10^{-4}	50.9
1.95×10^{-5}	8.92×10^{-4}		77.8
1.95×10^{-5}	1.19×10^{-3}	1.70×10^{-3}	102

$k_2 = 8.61 \times 10^4$ M^{-1} s^{-1}

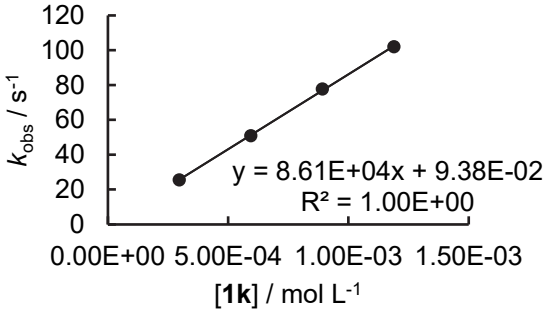

1k-**K**+ **2m** in DMSO (stopped-flow, detection at 460 nm)

$[\mathbf{2m}]_0$, mol L^{-1}	$[\mathbf{1k}]_0$, mol L^{-1}	[18-c-6], mol L^{-1}	k_{obs}, s^{-1}
1.78×10^{-5}	3.09×10^{-4}		30.8
1.78×10^{-5}	6.17×10^{-4}	8.50×10^{-4}	56.7
1.78×10^{-5}	9.26×10^{-4}		75.8
1.78×10^{-5}	1.23×10^{-3}	1.70×10^{-3}	99.1
1.78×10^{-5}	1.54×10^{-3}		121

$k_2 = 7.25 \times 10^4$ M^{-1} s^{-1}

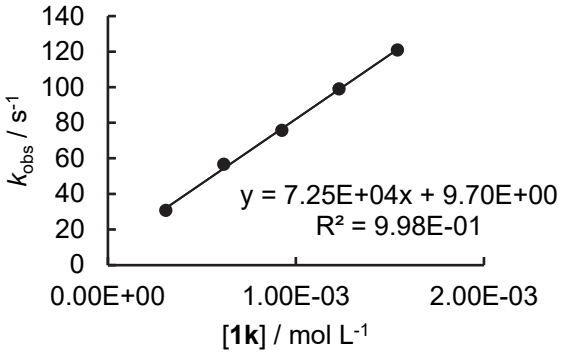

1k-**K**+ **2h** in DMSO (stopped-flow, detection at 422 nm)

$[\mathbf{2h}]_0$, mol L^{-1}	$[\mathbf{1k}]_0$, mol L^{-1}	[18-c-6], mol L^{-1}	k_{obs}, s^{-1}
1.84×10^{-5}	2.14×10^{-4}		71.0
1.84×10^{-5}	4.28×10^{-4}	6.38×10^{-4}	152
1.84×10^{-5}	6.42×10^{-4}		219
1.84×10^{-5}	8.56×10^{-4}	1.28×10^{-3}	283
1.84×10^{-5}	1.07×10^{-3}		356

$k_2 = 3.28 \times 10^5$ M^{-1} s^{-1}

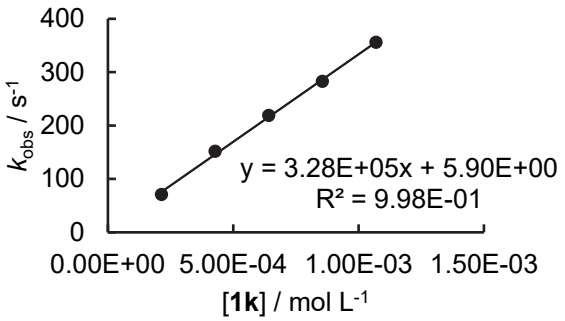

1k-**K**+ **2i** in DMSO (stopped-flow, detection at 384 nm)

$[\mathbf{2i}]_0$, mol L^{-1}	$[\mathbf{1k}]_0$, mol L^{-1}	k_{obs}, s^{-1}
3.16×10^{-5}	1.00×10^{-4}	70.5
3.16×10^{-5}	2.00×10^{-4}	134
3.16×10^{-5}	3.00×10^{-4}	227
3.16×10^{-5}	4.00×10^{-4}	327
3.16×10^{-5}	5.00×10^{-4}	424

$k_2 = 9.00 \times 10^5$ M^{-1} s^{-1}

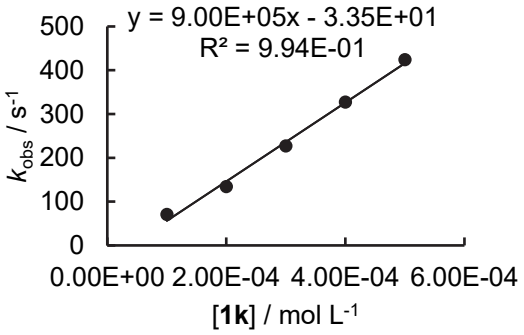

1k-**K**+ **2a** in DMSO (stopped-flow, detection at 640 nm)

$[\mathbf{2a}]_0$, mol L^{-1}	$[\mathbf{1k}]_0$, mol L^{-1}	k_{obs}, s^{-1}
1.02×10^{-5}	1.00×10^{-4}	285
1.02×10^{-5}	2.00×10^{-4}	1.01×10^3
1.02×10^{-5}	3.00×10^{-4}	1.70×10^3
1.02×10^{-5}	4.00×10^{-4}	2.42×10^3

$k_2 = 7.09 \times 10^6$ M^{-1} s^{-1}

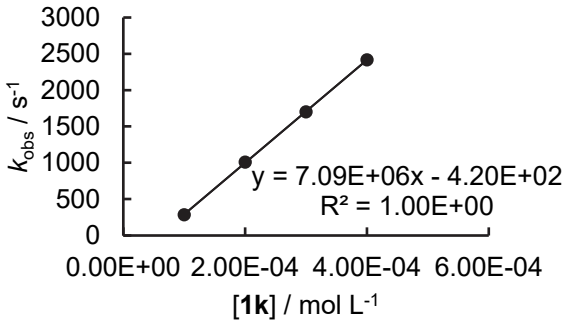

Determination of N and s_N parameters for **1k**-K in DMSO.

Reference Electrophile	Electrophilicity E	k_2 (M^{-1} s^{-1})	lg k_2
2l	–13.97	1.49×10^4	4.17
2j	–13.84	1.74×10^4	4.24
2g	–13.39	4.34×10^4	4.64
2k	–12.76	8.61×10^4	4.94
2m	–12.76	7.25×10^4	4.86
2h	–12.18	3.28×10^5	5.52
2i	–11.87	9.00×10^5	5.95
2a	–10.04	7.09×10^6	6.85

$N = 19.86$

$s_N = 0.71$

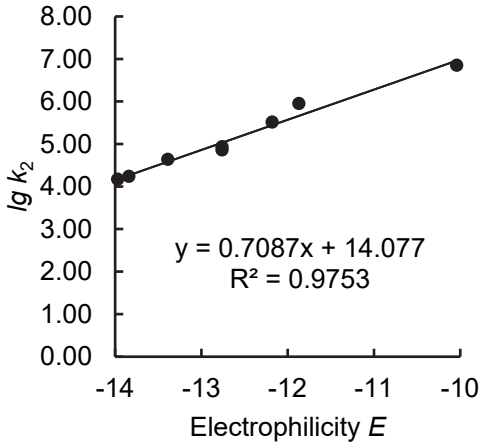

Potassium 4-Methylphenolate

1l-**K**+ **2l** in DMSO (stopped-flow, detection at 487 nm)

$[\mathbf{2l}]_0$, mol L^{-1}	$[\mathbf{1l}]_0$, mol L^{-1}	[18-c-6], mol L^{-1}	k_{obs}, s^{-1}
2.84×10^{-5}	3.42×10^{-4}		11.8
2.84×10^{-5}	6.84×10^{-4}	7.94×10^{-4}	21.0
2.84×10^{-5}	1.03×10^{-3}		29.0
2.84×10^{-5}	1.37×10^{-3}	1.59×10^{-3}	38.1
2.84×10^{-5}	1.71×10^{-3}		46.7

$k_2 = 2.54 \times 10^4$ M^{-1} s^{-1}

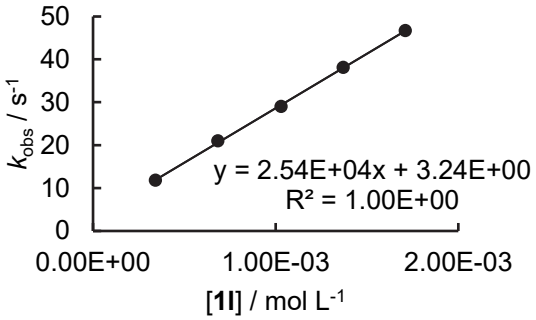

1l-**K**+ **2j** in DMSO (stopped-flow, detection at 487 nm)

$[\mathbf{2j}]_0$, mol L^{-1}	$[\mathbf{1l}]_0$, mol L^{-1}	[18-c-6], mol L^{-1}	k_{obs}, s^{-1}
2.77×10^{-5}	3.42×10^{-4}		15.2
2.77×10^{-5}	6.84×10^{-4}	7.94×10^{-4}	29.1
2.77×10^{-5}	1.03×10^{-3}		42.7
2.77×10^{-5}	1.37×10^{-3}	1.59×10^{-3}	55.9
2.77×10^{-5}	1.71×10^{-3}		65.3

$k_2 = 3.71 \times 10^4$ M^{-1} s^{-1}

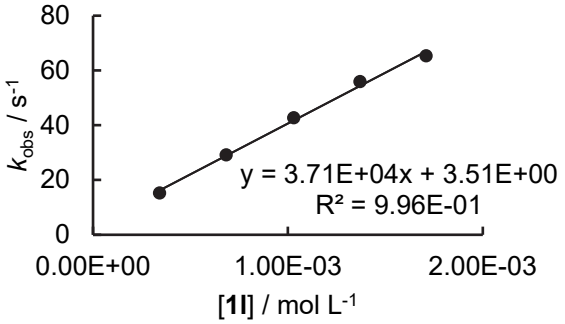

1l-**K**+ **2g** in DMSO (stopped-flow, detection at 533 nm)

$[\mathbf{2g}]_0$, mol L^{-1}	$[\mathbf{1l}]_0$, mol L^{-1}	[18-c-6], mol L^{-1}	k_{obs}, s^{-1}
2.43×10^{-5}	1.93×10^{-4}		25.4
2.43×10^{-5}	3.86×10^{-4}	5.96×10^{-4}	45.5
2.43×10^{-5}	5.79×10^{-4}		68.5
2.43×10^{-5}	7.72×10^{-4}	1.19×10^{-3}	94.3
2.43×10^{-5}	9.64×10^{-4}		113

$k_2 = 1.16 \times 10^5$ M^{-1} s^{-1}

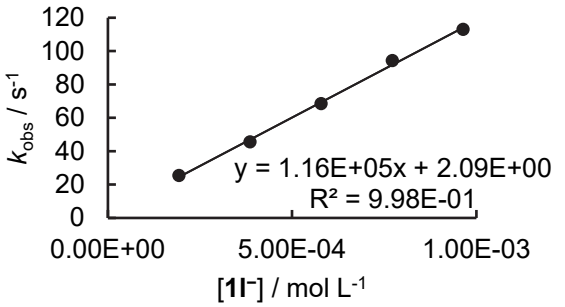

1l-**K**+ **2h** in DMSO (stopped-flow, detection at 422 nm)

$[\mathbf{2h}]_0$, mol L^{-1}	$[\mathbf{1l}]_0$, mol L^{-1}	k_{obs}, s^{-1}
3.54×10^{-5}	1.00×10^{-4}	46.4
3.54×10^{-5}	2.00×10^{-4}	126
3.54×10^{-5}	3.00×10^{-4}	212
3.54×10^{-5}	4.00×10^{-4}	306
3.54×10^{-5}	5.00×10^{-4}	415

$k_2 = 9.17 \times 10^5$ M^{-1} s^{-1}

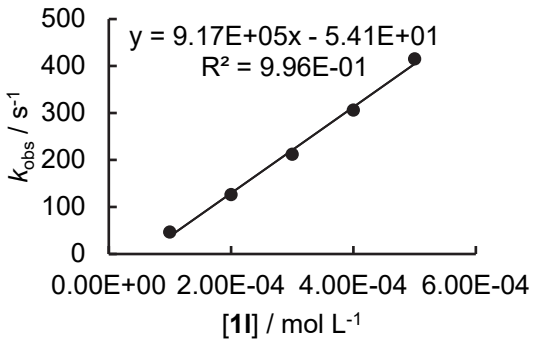

1l-**K**+ **2i** in DMSO (stopped-flow, detection at 384 nm)

$[\mathbf{2i}]_0$, mol L^{-1}	$[\mathbf{1l}]_0$, mol L^{-1}	k_{obs}, s^{-1}
4.37×10^{-5}	1.00×10^{-4}	123
4.37×10^{-5}	2.00×10^{-4}	315
4.37×10^{-5}	3.00×10^{-4}	552
4.37×10^{-5}	4.00×10^{-4}	747
4.37×10^{-5}	5.00×10^{-4}	949

$k_2 = 2.08 \times 10^6$ M^{-1} s^{-1}

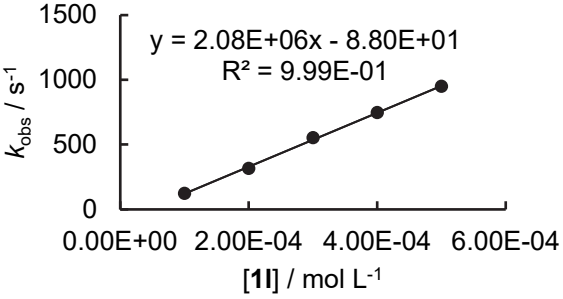

Determination of N and s_N parameters for **1l**-K in DMSO.

Reference Electrophile	Electrophilicity E	k_2 (M^{-1} s^{-1})	lg k_2
2l	–13.97	2.54×10^4	4.40
2j	–13.84	3.71×10^4	4.57
2g	–13.39	1.16×10^5	5.06
2h	–12.18	9.17×10^5	5.96
2i	–11.87	2.08×10^6	6.32

N = 19.08

s_N = 0.87

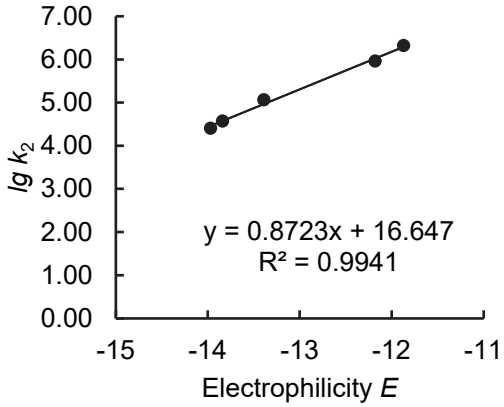

Potassium 4-*tert*-Butylphenolate

1m-**K**+ **2j** in DMSO (stopped-flow, detection at 500 nm)

[**2j**]$_0$, mol L^{-1}	[**1m**]$_0$, mol L^{-1}	k_{obs}, s^{-1}
1.99×10^{-5}	1.00×10^{-4}	6.10
1.99×10^{-5}	2.00×10^{-4}	10.0
1.99×10^{-5}	3.00×10^{-4}	13.8
1.99×10^{-5}	4.00×10^{-4}	18.6
1.99×10^{-5}	5.00×10^{-4}	22.5

$k_2 = 4.14 \times 10^4$ M^{-1} s^{-1}

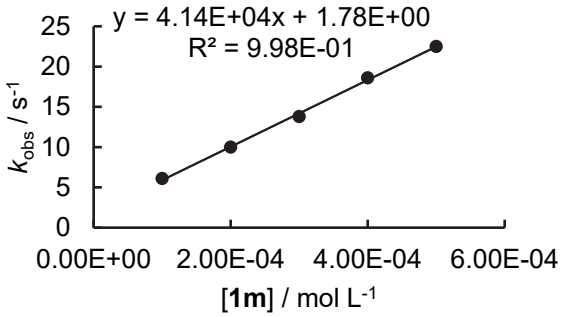

1m-**K**+ **2g** in DMSO (stopped-flow, detection at 533 nm)

[**2g**]$_0$, mol L^{-1}	[**1m**]$_0$, mol L^{-1}	k_{obs}, s^{-1}
6.72×10^{-6}	1.00×10^{-4}	7.43
6.72×10^{-6}	2.00×10^{-4}	14.5
6.72×10^{-6}	3.00×10^{-4}	25.3
6.72×10^{-6}	4.00×10^{-4}	32.2
6.72×10^{-6}	5.00×10^{-4}	41.0

$k_2 = 8.48 \times 10^4$ M^{-1} s^{-1}

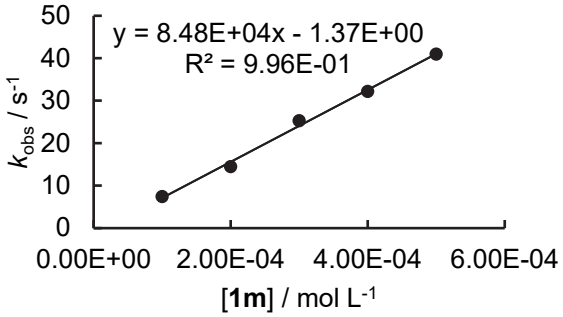

1m-**K**+ **2h** in DMSO (stopped-flow, detection at 422 nm)

[**2h**]$_0$, mol L^{-1}	[**1m**]$_0$, mol L^{-1}	k_{obs}, s^{-1}
3.38×10^{-5}	1.00×10^{-4}	50.1
3.38×10^{-5}	2.00×10^{-4}	116
3.38×10^{-5}	3.00×10^{-4}	208
3.38×10^{-5}	4.00×10^{-4}	256
3.38×10^{-5}	5.00×10^{-4}	315

$k_2 = 6.70 \times 10^5$ M^{-1} s^{-1}

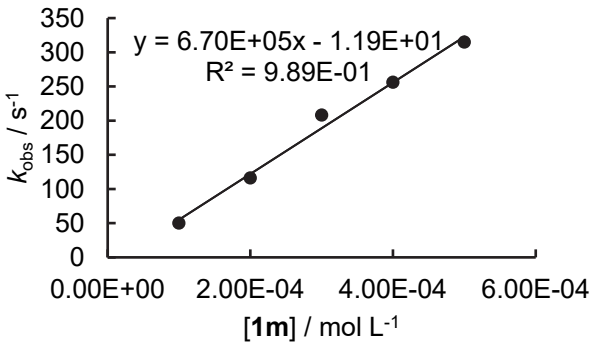

1m-**K**+ **2i** in DMSO (stopped-flow, detection at 384 nm)

$[\mathbf{2i}]_0$, mol L^{-1}	$[\mathbf{1m}]_0$, mol L^{-1}	k_{obs}, s^{-1}
3.01×10^{-5}	1.00×10^{-4}	120
3.01×10^{-5}	2.00×10^{-4}	217
3.01×10^{-5}	3.00×10^{-4}	377
3.01×10^{-5}	4.00×10^{-4}	549
3.01×10^{-5}	5.00×10^{-4}	762

$k_2 = 1.62 \times 10^6$ M^{-1} s^{-1}

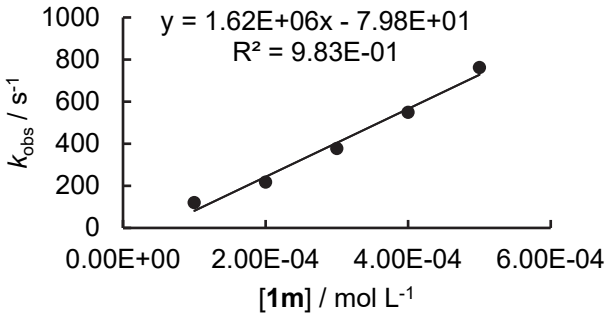

Determination of N and s_N parameters for **1m**-K in DMSO.

Reference Electrophile	Electrophilicity E	k_2 (M^{-1} s^{-1})	lg k_2
2j	–13.84	4.14×10^4	4.62
2g	–13.39	8.48×10^4	4.93
2h	–12.18	6.70×10^5	5.83
2i	–11.87	1.62×10^6	6.21

$N = 19.67$

$s_N = 0.79$

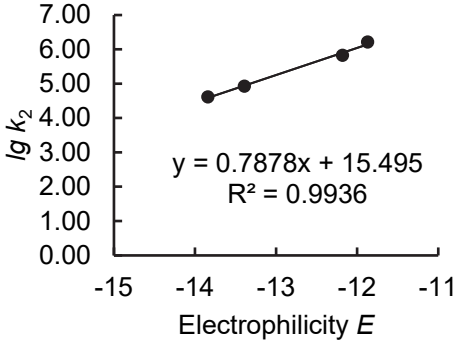

Potassium 4-Methoxyphenolate

1n-**K**+ **2j** in DMSO (stopped-flow, detection at 500 nm)

$[\mathbf{2j}]_0$, mol L^{-1}	$[\mathbf{1n}]_0$, mol L^{-1}	k_{obs}, s^{-1}
	2.00×10^{-4}	21.3
	3.00×10^{-4}	32.1
	4.00×10^{-4}	41.8
	5.00×10^{-4}	51.9
	6.00×10^{-4}	62.6

$k_2 = 1.02 \times 10^5$ M^{-1} s^{-1}

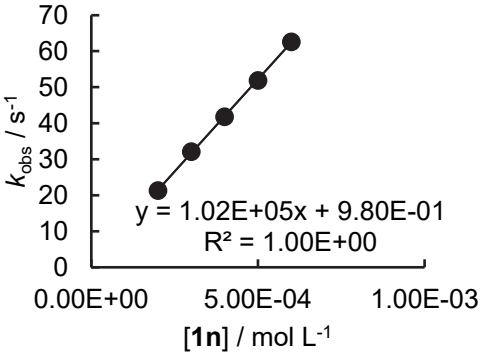

1n-**K**+ **2g** in DMSO (stopped-flow, detection at 533 nm)

$[\mathbf{2g}]_0$, mol L^{-1}	$[\mathbf{1n}]_0$, mol L^{-1}	k_{obs}, s^{-1}
	3.00×10^{-4}	66.3
	4.00×10^{-4}	90.9
	5.00×10^{-4}	115
	6.00×10^{-4}	140

$k_2 = 2.45 \times 10^5$ M^{-1} s^{-1}

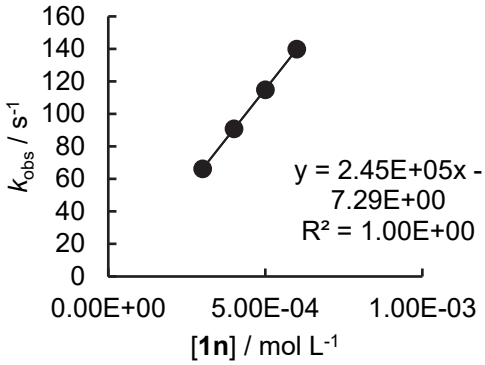

1n-**K**+ **2h** in DMSO (stopped-flow, detection at 422 nm)

$[\mathbf{2h}]_0$, mol L^{-1}	$[\mathbf{1n}]_0$, mol L^{-1}	k_{obs}, s^{-1}
	2.00×10^{-4}	306
	2.50×10^{-4}	393
	3.00×10^{-4}	513
	3.50×10^{-4}	633
	4.00×10^{-4}	711

$k_2 = 2.10 \times 10^6$ M^{-1} s^{-1}

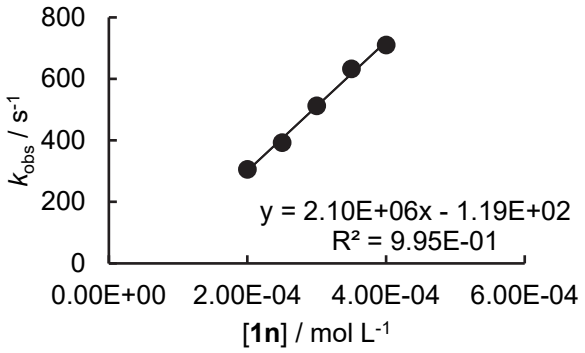

1n-**K**+ **2i** in DMSO (stopped-flow, detection at 384 nm)

$[\mathbf{2i}]_0$, mol L^{-1}	$[\mathbf{1n}]_0$, mol L^{-1}	k_{obs}, s^{-1}
	2.00×10^{-4}	703
	2.50×10^{-4}	892
	3.00×10^{-4}	1.07×10^3
	3.50×10^{-4}	1.33×10^3

$k_2 = 4.12 \times 10^6$ M^{-1} s^{-1}

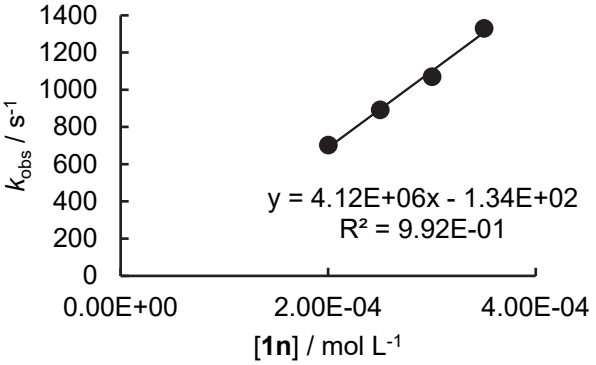

Determination of N and s_N parameters for **1n**-K in DMSO.

Reference Electrophile	Electrophilicity E	k_2 (M^{-1} s^{-1})	lg k_2
2j	–13.84	1.02×10^5	5.01
2g	–13.39	2.45×10^5	5.39
2h	–12.18	2.10×10^6	6.32
2i	–11.87	4.12×10^6	6.61

$N = 20.09$

$s_N = 0.80$

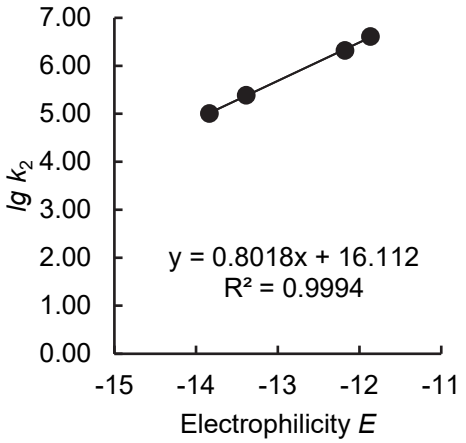

Potassium 2,6-Ditertbutylphenolate

1o-**K**+ **2a** in DMSO (stopped-flow, detection at 513 nm)

$[\mathbf{2a}]_0$, mol L^{-1}	$[\mathbf{1o}]_0$, mol L^{-1}	k_{obs}, s^{-1}
2.38×10^{-5}	1.00×10^{-4}	137
2.38×10^{-5}	2.00×10^{-4}	457
2.38×10^{-5}	3.00×10^{-4}	824
2.38×10^{-5}	4.00×10^{-4}	1130
2.38×10^{-5}	5.00×10^{-4}	1430

$k_2 = 3.26 \times 10^6$ M^{-1} s^{-1}

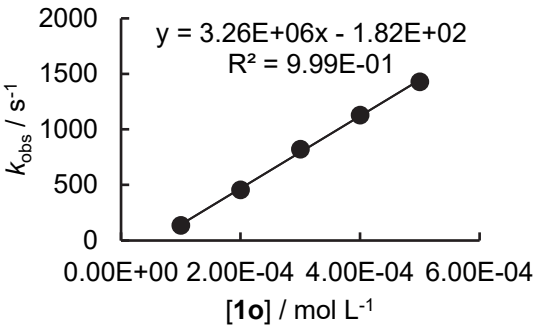

1o-**K**+ **2h** in DMSO (stopped-flow, detection at 412 nm)

$[\mathbf{2h}]_0$, mol L^{-1}	$[\mathbf{1o}]_0$, mol L^{-1}	k_{obs}, s^{-1}
1.97×10^{-5}	1.00×10^{-4}	375
1.97×10^{-5}	2.00×10^{-4}	827
1.97×10^{-5}	3.00×10^{-4}	1160
1.97×10^{-5}	4.00×10^{-4}	1480

$k_2 = 7.30 \times 10^6$ M^{-1} s^{-1}

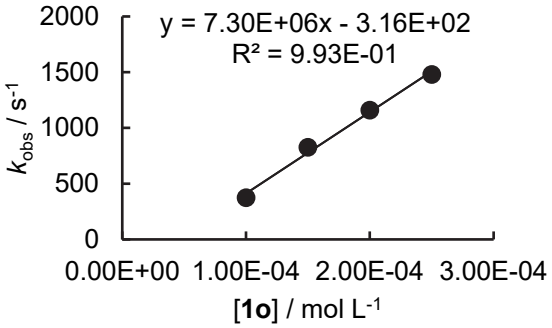

Determination of N and s_N parameters for **1o**-K in DMSO.

Reference Electrophile	Electrophilicity E	k_2 (M^{-1} s^{-1})	lg k_2
2a	−10.04	3.26×10^6	6.51
2b	−9.45	7.30×10^6	6.86

$N = 21.02$

$s_N = 0.59$

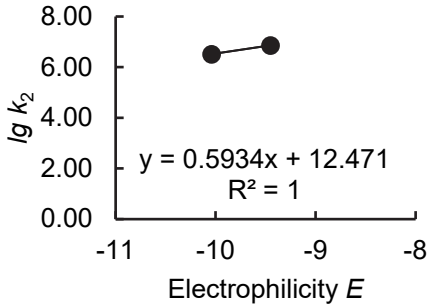

4.9 Kinetics of Reactions of Phenolates in MeCN

Tetrabutylammonium 4-Nitrophenolate

1c-**NBu$_4$** + **2a** in MeCN (stopped-flow, detection at 632 nm)

[**2a**]$_0$, mol L^{-1}	[**1c**]$_0$, mol L^{-1}	k_{obs}, s^{-1}
6.09×10^{-6}	1.00×10^{-4}	2.89
6.09×10^{-6}	2.00×10^{-4}	4.48
6.09×10^{-6}	3.00×10^{-4}	5.41
6.09×10^{-6}	4.00×10^{-4}	7.31
6.09×10^{-6}	5.00×10^{-4}	9.05

$k_2 = 1.52 \times 10^4$ M^{-1} s^{-1}

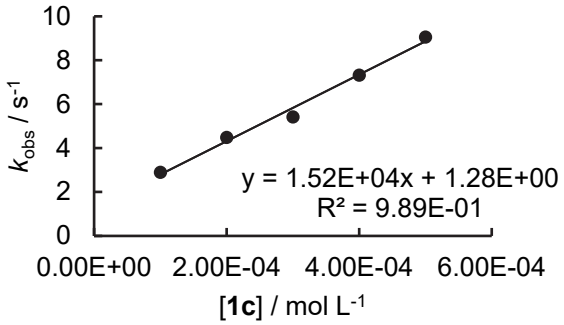

1c-**NBu$_4$** + **2b** in MeCN (stopped-flow, detection at 635 nm)

[**2b**]$_0$, mol L^{-1}	[**1c**]$_0$, mol L^{-1}	k_{obs}, s^{-1}
3.65×10^{-6}	1.00×10^{-4}	9.02
3.65×10^{-6}	2.00×10^{-4}	13.0
3.65×10^{-6}	3.00×10^{-4}	16.9
3.65×10^{-6}	4.00×10^{-4}	21.2
3.65×10^{-6}	5.00×10^{-4}	25.5

$k_2 = 4.12 \times 10^4$ M^{-1} s^{-1}

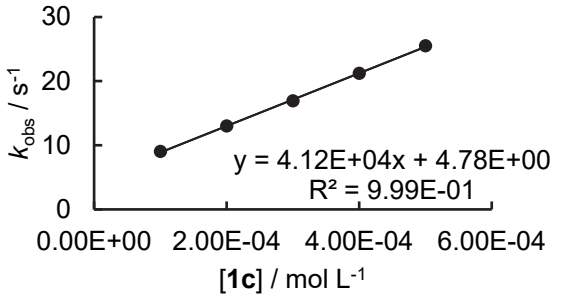

1c-**NBu$_4$** + **2c** in MeCN (stopped-flow, detection at 616 nm)

[**2c**]$_0$, mol L^{-1}	[**1c**]$_0$, mol L^{-1}	k_{obs}, s^{-1}
6.32×10^{-6}	1.00×10^{-4}	16.8
6.32×10^{-6}	2.00×10^{-4}	32.5
6.32×10^{-6}	3.00×10^{-4}	49.2
6.32×10^{-6}	4.00×10^{-4}	64.9
6.32×10^{-6}	5.00×10^{-4}	82.0

$k_2 = 1.63 \times 10^5$ M^{-1} s^{-1}

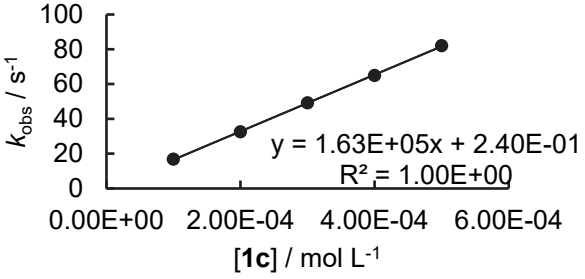

1c-**NBu$_4$** + **2d** in MeCN (stopped-flow, detection at 620 nm)

[**2d**]$_0$, mol L^{-1}	[**1c**]$_0$, mol L^{-1}	k_{obs}, s^{-1}
5.62×10^{-6}	1.00×10^{-4}	43.4
5.62×10^{-6}	2.00×10^{-4}	86.0
5.62×10^{-6}	3.00×10^{-4}	134
5.62×10^{-6}	4.00×10^{-4}	177
5.62×10^{-6}	5.00×10^{-4}	224

$k_2 = 4.52 \times 10^5$ M^{-1} s^{-1}

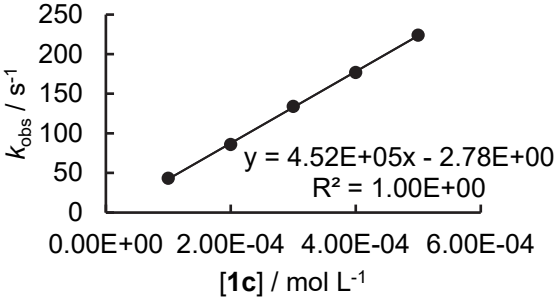

Determination of N and s_N parameters for **1c**-NBu_4 in MeCN.

Reference Electrophile	Electrophilicity E	k_2 (M^{-1} s^{-1})	lg k_2
2a	−10.04	1.52×10^4	4.18
2b	−9.45	4.12×10^4	4.61
2c	−8.76	1.63×10^5	5.21
2d	−8.22	4.52×10^5	5.66

$N = 15.14$

$s_N = 0.82$

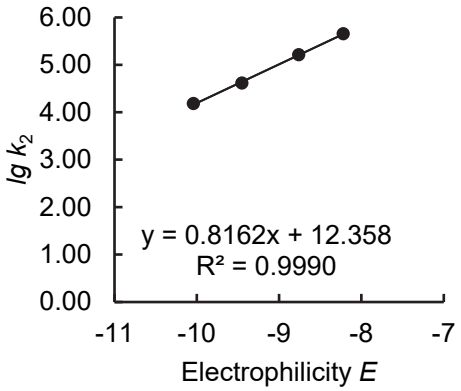

Potassium 4-Nitrophenolate

1c-**K**+ **2a** in MeCN (stopped-flow, detection at 630 nm)

$[\mathbf{2a}]_0$, mol L^{-1}	$[\mathbf{1c}]_0$, mol L^{-1}	$[Crown]_0$, mol L^{-1}	k_{obs}, s^{-1}
8.46×10^{-6}	2.06×10^{-4}	3.23×10^{-4}	5.89
8.46×10^{-6}	4.12×10^{-4}	6.47×10^{-4}	9.52
8.46×10^{-6}	6.18×10^{-4}	9.70×10^{-4}	13.0
8.46×10^{-6}	8.24×10^{-4}	1.29×10^{-3}	16.7
8.46×10^{-6}	1.03×10^{-3}	1.62×10^{-3}	19.8

$k_2 = 1.70 \times 10^4$ M^{-1} s^{-1}

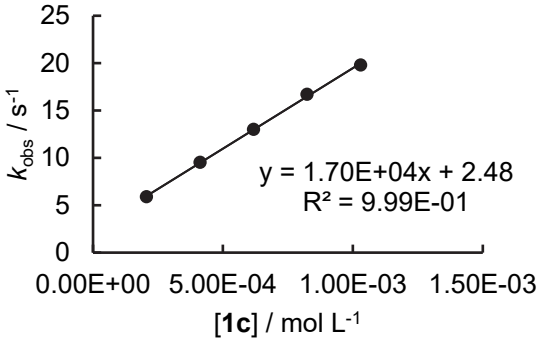

1c-**K**+ **2b** in MeCN (stopped-flow, detection at 635 nm)

$[\mathbf{2b}]_0$, mol L^{-1}	$[\mathbf{1c}]_0$, mol L^{-1}	$[Crown]_0$, mol L^{-1}	k_{obs}, s^{-1}
8.24×10^{-6}	1.03×10^{-4}	1.33×10^{-4}	11.0
8.24×10^{-6}	2.07×10^{-4}	2.66×10^{-4}	16.0
8.24×10^{-6}	3.10×10^{-4}	3.99×10^{-4}	20.2
8.24×10^{-6}	4.13×10^{-4}	5.32×10^{-4}	24.6
8.24×10^{-6}	5.16×10^{-4}	6.65×10^{-4}	28.7

$k_2 = 4.26 \times 10^4$ M^{-1} s^{-1}

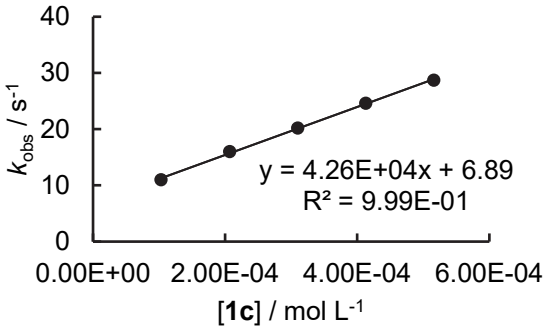

1c-**K**+ **2c** in MeCN (stopped-flow, detection at 627 nm)

$[\mathbf{2c}]_0$, mol L^{-1}	$[\mathbf{1c}]_0$, mol L^{-1}	$[Crown]_0$, mol L^{-1}	k_{obs}, s^{-1}
9.39×10^{-6}	2.06×10^{-4}	3.23×10^{-4}	39.0
9.39×10^{-6}	4.12×10^{-4}	6.47×10^{-4}	69.7
9.39×10^{-6}	6.18×10^{-4}	9.70×10^{-4}	97.6
9.39×10^{-6}	8.24×10^{-4}	1.29×10^{-3}	128
9.39×10^{-6}	1.03×10^{-3}	1.62×10^{-3}	152

$k_2 = 1.38 \times 10^5$ M^{-1} s^{-1}

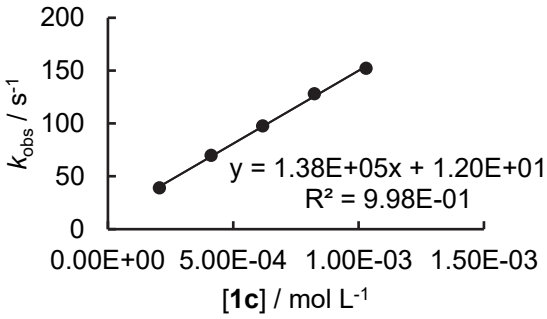

1c-**K**+ **2d** in MeCN (stopped-flow, detection at 618 nm)

$[\mathbf{2d}]_0$, mol L^{-1}	$[\mathbf{1c}]_0$, mol L^{-1}	$[\text{Crown}]_0$, mol L^{-1}	k_{obs}, s^{-1}
7.95×10^{-6}	1.03×10^{-4}	1.33×10^{-4}	57.9
7.95×10^{-6}	2.07×10^{-4}	2.66×10^{-4}	103
7.95×10^{-6}	3.10×10^{-4}	3.99×10^{-4}	143
7.95×10^{-6}	4.13×10^{-4}	5.32×10^{-4}	180
7.95×10^{-6}	5.16×10^{-4}	6.65×10^{-4}	222

$k_2 = 3.93 \times 10^5$ M^{-1} s^{-1}

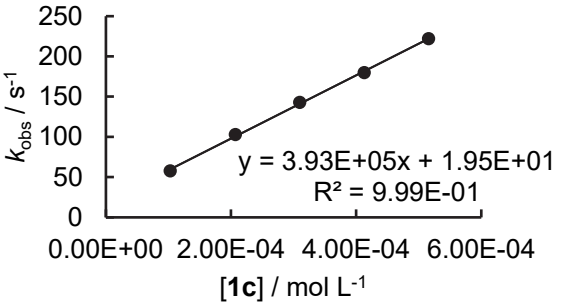

Determination of N and s_N parameters for **1c**-K in MeCN.

Reference Electrophile	Electrophilicity E	k_2 (M^{-1} s^{-1})	lg k_2
2a	−10.04	1.70×10^4	4.23
2b	−9.45	4.26×10^4	4.63
2c	−8.76	1.38×10^5	5.14
2d	−8.22	3.93×10^5	5.59

$N = 15.67$

$s_N = 0.75$

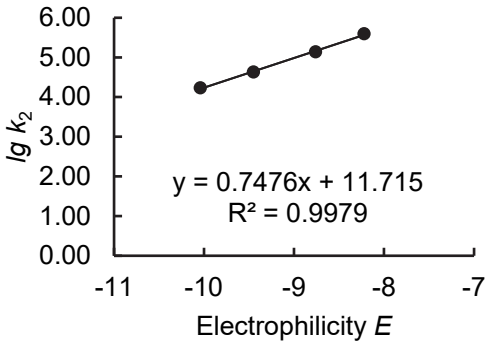

Tetrabutylammonium 2-Nitrophenolate

1d-**NBu$_4$** + **2a** in MeCN (stopped-flow, detection at 632 nm)

$[\mathbf{2a}]_0$, mol L^{-1}	$[\mathbf{1d}]_0$, mol L^{-1}	k_{obs}, s^{-1}
6.26×10^{-6}	1.00×10^{-4}	23.4
6.26×10^{-6}	2.00×10^{-4}	28.1
6.26×10^{-6}	3.00×10^{-4}	32.9
6.26×10^{-6}	4.00×10^{-4}	37.0
6.26×10^{-6}	5.00×10^{-4}	42.0

$k_2 = 4.61 \times 10^4$ M^{-1} s^{-1}

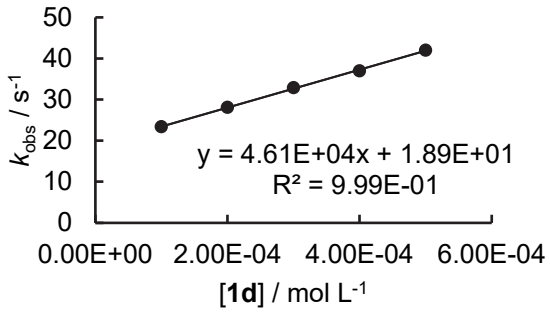

1d-**NBu$_4$** + **2b** in MeCN (stopped-flow, detection at 635 nm)

$[\mathbf{2b}]_0$, mol L^{-1}	$[\mathbf{1d}]_0$, mol L^{-1}	k_{obs}, s^{-1}
5.00×10^{-6}	1.00×10^{-4}	71.7
5.00×10^{-6}	2.00×10^{-4}	81.5
5.00×10^{-6}	3.00×10^{-4}	90.5
5.00×10^{-6}	4.00×10^{-4}	104
5.00×10^{-6}	5.00×10^{-4}	114

$k_2 = 1.07 \times 10^5$ M^{-1} s^{-1}

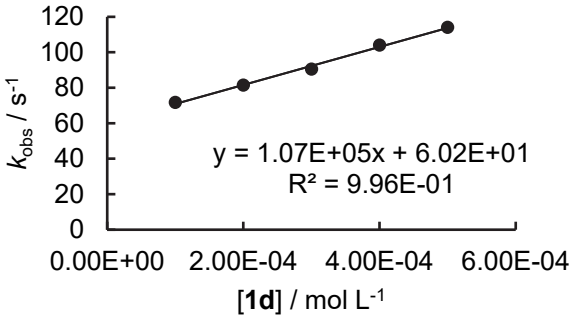

1d-**NBu$_4$** + **2c** in MeCN (stopped-flow, detection at 616 nm)

[**2c**]$_0$, mol L^{-1}	[**1d**]$_0$, mol L^{-1}	k_{obs}, s^{-1}
5.14×10^{-6}	1.00×10^{-4}	54.4
5.14×10^{-6}	2.00×10^{-4}	98.2
5.14×10^{-6}	3.00×10^{-4}	147
5.14×10^{-6}	4.00×10^{-4}	186
5.14×10^{-6}	5.00×10^{-4}	231

$k_2 = 4.41 \times 10^5$ M^{-1} s^{-1}

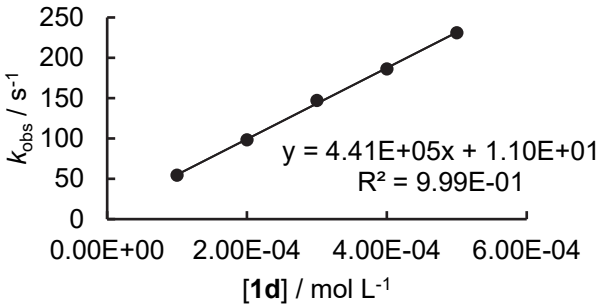

1d-**NBu$_4$** + **2d** in MeCN (stopped-flow, detection at 620 nm)

[**2d**]$_0$, mol L^{-1}	[**1d**]$_0$, mol L^{-1}	k_{obs}, s^{-1}
7.46×10^{-6}	1.00×10^{-4}	116
7.46×10^{-6}	2.00×10^{-4}	227
7.46×10^{-6}	3.00×10^{-4}	347
7.46×10^{-6}	4.00×10^{-4}	470
7.46×10^{-6}	5.00×10^{-4}	613

$k_2 = 1.24 \times 10^6$ M^{-1} s^{-1}

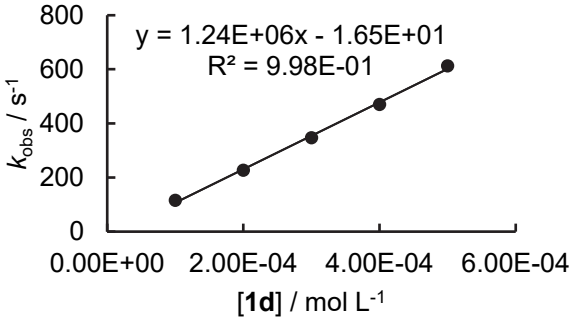

Determination of *N* and s_N parameters for **1d**-NBu$_4$ in MeCN.

Reference Electrophile	Electrophilicity *E*	k_2 (M^{-1} s^{-1})	lg k_2
2a	−10.04	4.61×10^4	4.66
2b	−9.45	1.07×10^5	5.03
2c	−8.76	4.41×10^5	5.64
2d	−8.22	1.24×10^6	6.09

N = 15.83

s_N = 0.80

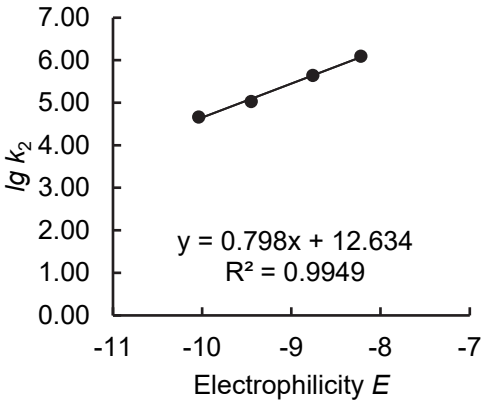

Tetrabutylammonium 3-Nitrophenolate

1e-**NBu$_4$** + **2a** in MeCN (stopped-flow, detection at 632 nm)

[**2a**]$_0$, mol L^{-1}	[**1e**]$_0$, mol L^{-1}	k_{obs}, s^{-1}
1.02×10^{-5}	1.00×10^{-4}	421
1.02×10^{-5}	2.00×10^{-4}	932
1.02×10^{-5}	3.00×10^{-4}	1.31×10^3
1.02×10^{-5}	4.00×10^{-4}	1.76×10^3
1.02×10^{-5}	5.00×10^{-4}	2.26×10^3

$k_2 = 4.51 \times 10^6$ M^{-1} s^{-1}

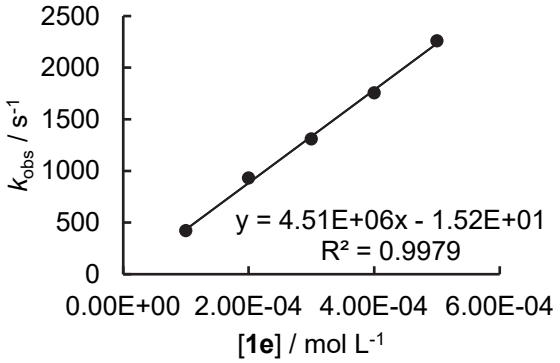

1e-NBu_4 + **2b** in MeCN (stopped-flow, detection at 635 nm)

$[\mathbf{2b}]_0$, mol L^{-1}	$[\mathbf{1e}]_0$, mol L^{-1}	k_{obs}, s^{-1}
6.70×10^{-6}	1.00×10^{-4}	873
6.70×10^{-6}	2.00×10^{-4}	1.78×10^{3}
6.70×10^{-6}	3.00×10^{-4}	2.49×10^{3}

$k_2 = 8.09 \times 10^6$ M^{-1} s^{-1}

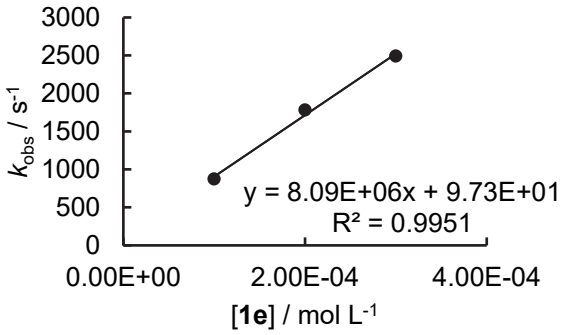

Determination of N and s_N parameters for **1e**-NBu_4 in MeCN.

Reference Electrophile	Electrophilicity E	k_2 (M^{-1} s^{-1})	lg k_2
2a	−10.04	4.50×10^6	6.65
2b	−9.45	8.09×10^6	6.91

$N = 25.51$

$s_N = 0.43$

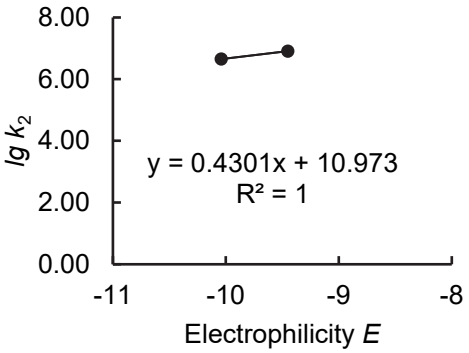

Potassium 3-Nitrophenolate

1e-**K**+ **2a** in MeCN (stopped-flow, detection at 632 nm)

$[\mathbf{2a}]_0$, mol L^{-1}	$[\mathbf{1e}]_0$, mol L^{-1}	k_{obs}, s^{-1}
6.50×10^{-6}	1.00×10^{-4}	374
6.50×10^{-6}	2.00×10^{-4}	923
6.50×10^{-6}	3.00×10^{-4}	1.35×10^{3}
6.50×10^{-6}	4.00×10^{-4}	1.80×10^{3}

$k_2 = 4.70 \times 10^6$ M^{-1} s^{-1}

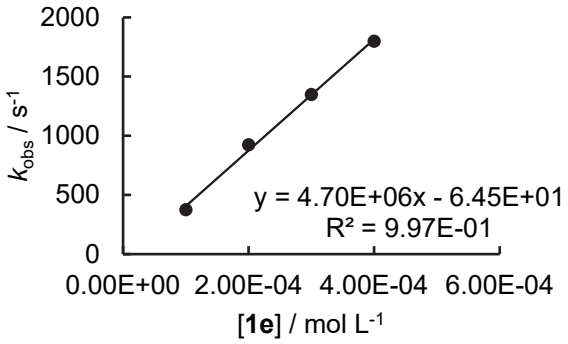

Potassium 4-Cyanophenolate

1f-**K**+ **2a** in MeCN (stopped-flow, detection at 630 nm)

$[\mathbf{2a}]_0$, mol L^{-1}	$[\mathbf{1f}]_0$, mol L^{-1}	$[Crown]_0$, mol L^{-1}	k_{obs}, s^{-1}
8.07×10^{-6}	8.08×10^{-5}	1.02×10^{-4}	28.8
8.07×10^{-6}	1.62×10^{-4}	2.03×10^{-4}	62.5
8.07×10^{-6}	2.42×10^{-4}	3.05×10^{-4}	97.0
8.07×10^{-6}	3.23×10^{-4}	4.06×10^{-4}	125
8.07×10^{-6}	4.04×10^{-4}	5.08×10^{-4}	153

$k_2 = 3.85 \times 10^5$ M^{-1} s^{-1}

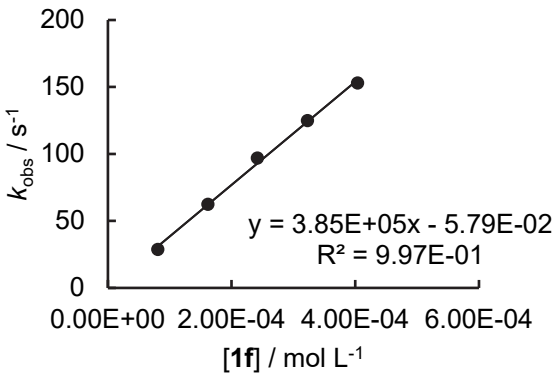

1f-K+ **2b** in MeCN (stopped-flow, detection at 635 nm)

$[\mathbf{2b}]_0$, mol L^{-1}	$[\mathbf{1f}]_0$, mol L^{-1}	$[Crown]_0$, mol L^{-1}	k_{obs}, s^{-1}
6.75×10^{-6}	8.08×10^{-5}	1.02×10^{-4}	65.6
6.75×10^{-6}	1.62×10^{-4}	2.03×10^{-4}	139
6.75×10^{-6}	2.42×10^{-4}	3.05×10^{-4}	213
6.75×10^{-6}	3.23×10^{-4}	4.06×10^{-4}	279
6.75×10^{-6}	4.04×10^{-4}	5.08×10^{-4}	340

$k_2 = 8.53 \times 10^5$ M^{-1} s^{-1}

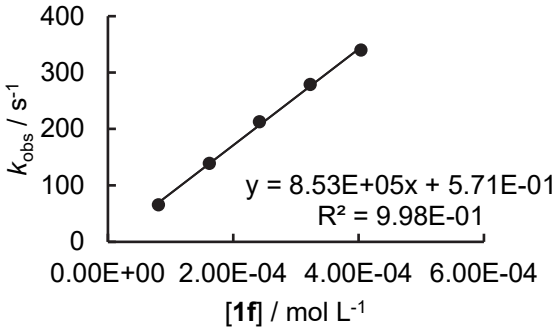

Determination of N and s_N parameters for **1f**-K in MeCN.

Reference Electrophile	Electrophilicity E	k_2 (M^{-1} s^{-1})	lg k_2
2a	−10.04	3.85×10^5	5.59
2b	−9.45	8.53×10^5	5.93

$N = 19.58$

$s_N = 0.59$

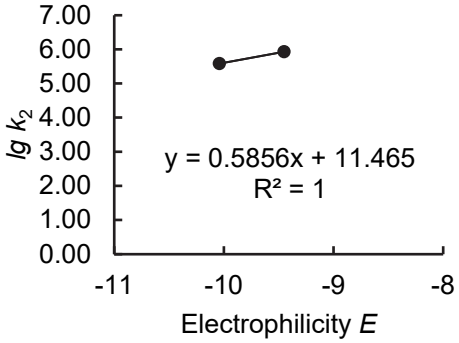

Tetrabutylammonium 2-(Trifluoromethyl)phenolate

1g-**NBu$_4$** + **2a** in MeCN (stopped-flow, detection at 632 nm)

$[\mathbf{2a}]_0$, mol L^{-1}	$[\mathbf{1g}]_0$, mol L^{-1}	k_{obs}, s^{-1}
1.45×10^{-5}	1.00×10^{-4}	52.0
1.45×10^{-5}	2.00×10^{-4}	125
1.45×10^{-5}	3.00×10^{-4}	190
1.45×10^{-5}	4.00×10^{-4}	257
1.45×10^{-5}	5.00×10^{-4}	310

$k_2 = 6.48 \times 10^5$ M^{-1} s^{-1}

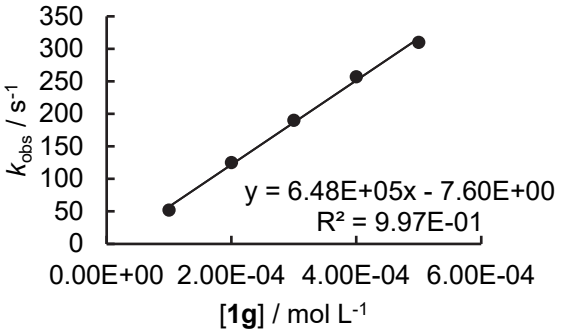

1g-**NBu$_4$** + **2b** in MeCN (stopped-flow, detection at 635 nm)

$[\mathbf{2b}]_0$, mol L^{-1}	$[\mathbf{1g}]_0$, mol L^{-1}	k_{obs}, s^{-1}
1.15×10^{-5}	1.00×10^{-4}	107
1.15×10^{-5}	2.00×10^{-4}	239
1.15×10^{-5}	3.00×10^{-4}	375
1.15×10^{-5}	4.00×10^{-4}	570
1.15×10^{-5}	5.00×10^{-4}	718

$k_2 = 1.55 \times 10^6$ M^{-1} s^{-1}

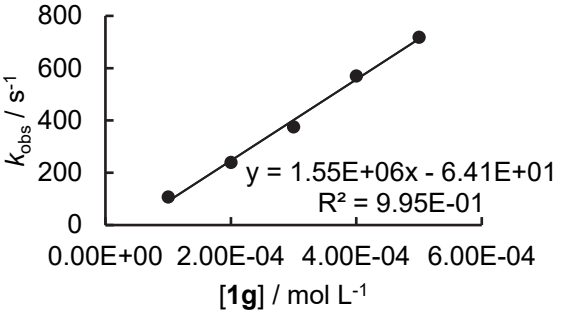

1g-**NBu$_4$** + **2c** in MeCN (stopped-flow, detection at 616 nm)

[**2c**]$_0$, mol L^{-1}	[**1g**]$_0$, mol L^{-1}	k_{obs}, s^{-1}
1.35×10^{-5}	1.00×10^{-4}	347
1.35×10^{-5}	2.00×10^{-4}	999
1.35×10^{-5}	3.00×10^{-4}	1.49×10^{3}
1.35×10^{-5}	4.00×10^{-4}	1.85×10^{3}

$k_2 = 5.00 \times 10^6$ M^{-1} s^{-1}

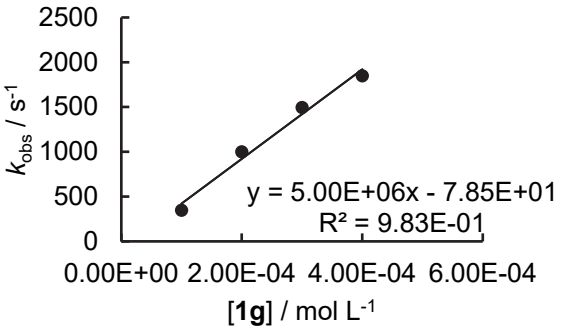

Determination of N and s_N parameters for **1g**-NBu$_4$ in MeCN.

Reference Electrophile	Electrophilicity E	k_2 (M^{-1} s^{-1})	lg k_2
2a	−10.04	6.48×10^5	5.81
2b	−9.45	1.55×10^6	6.19
2c	−8.76	5.00×10^6	6.70

$N = 18.39$

$s_N = 0.69$

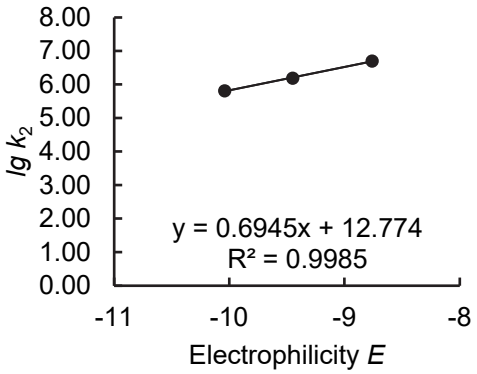

Tetrabutylammonium 4-(Trifluoromethyl)phenolate

1h-**NBu$_4$** + **2a** in MeCN (stopped-flow, detection at 632 nm)

[**2a**]$_0$, mol L^{-1}	[**1h**]$_0$, mol L^{-1}	k_{obs}, s^{-1}
9.31×10^{-6}	1.00×10^{-4}	93.9
9.31×10^{-6}	2.00×10^{-4}	232
9.31×10^{-6}	3.00×10^{-4}	381
9.31×10^{-6}	4.00×10^{-4}	529
9.31×10^{-6}	5.00×10^{-4}	684

$k_2 = 1.48 \times 10^6$ M^{-1} s^{-1}

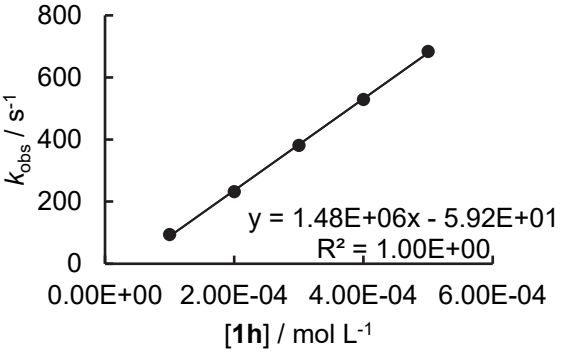

1h-**NBu$_4$** + **2b** in MeCN (stopped-flow, detection at 635 nm)

[**2b**]$_0$, mol L^{-1}	[**1h**]$_0$, mol L^{-1}	k_{obs}, s^{-1}
6.96×10^{-6}	1.00×10^{-4}	197
6.96×10^{-6}	2.00×10^{-4}	523
6.96×10^{-6}	3.00×10^{-4}	839
6.96×10^{-6}	4.00×10^{-4}	1.10×10^{3}
6.96×10^{-6}	5.00×10^{-4}	1.43×10^{3}

$k_2 = 3.04 \times 10^6$ M^{-1} s^{-1}

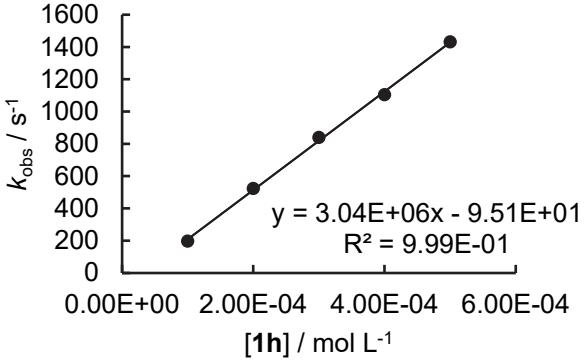

Determination of N and s_N parameters for **1h**-NBu_4 in MeCN.

Reference Electrophile	Electrophilicity E	k_2 (M^{-1} s^{-1})	lg k_2
2a	−10.04	1.48×10^6	6.17
2b	−9.45	3.04×10^6	6.48

N = 21.69

s_N = 0.53

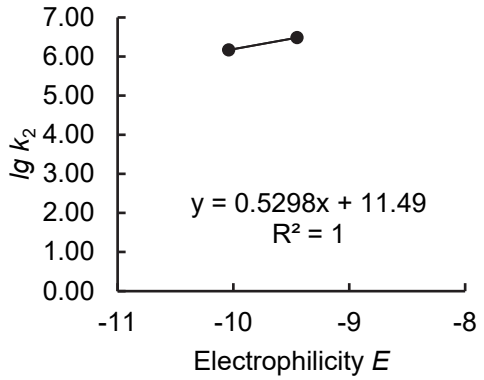

Potassium 3-(Trifluoromethyl)phenolate

1i-**K**+ **2a** in MeCN (stopped-flow, detection at 632 nm)

[**2a**]$_0$, mol L^{-1}	[**1i**]$_0$, mol L^{-1}	k_{obs}, s^{-1}
4.86×10^{-6}	1.00×10^{-4}	492
4.86×10^{-6}	2.00×10^{-4}	1.16×10^3
4.86×10^{-6}	3.00×10^{-4}	1.75×10^3
4.86×10^{-6}	4.00×10^{-4}	2.20×10^3
4.86×10^{-6}	5.00×10^{-4}	2.68×10^3

$k_2 = 5.41 \times 10^6$ M^{-1} s^{-1}

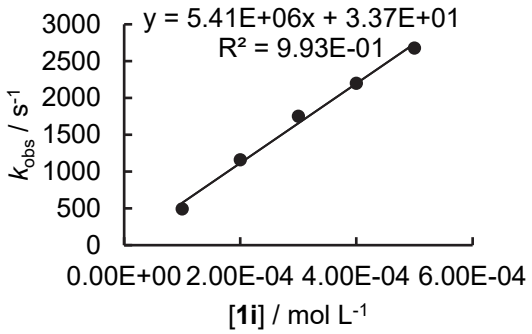

Potassium 4-Chlorophenolate

1j-**K**+ **2g** in MeCN (stopped-flow, detection at 513 nm)

[**2g**]$_0$, mol L^{-1}	[**1l**]$_0$, mol L^{-1}	k_{obs}, s^{-1}
3.43×10^{-5}	3.00×10^{-4}	37.7
3.43×10^{-5}	4.00×10^{-4}	39.8
3.43×10^{-5}	5.00×10^{-4}	39.8
3.43×10^{-5}	6.00×10^{-4}	41.2

$k_2 = 1.05 \times 10^4$ M^{-1} s^{-1}

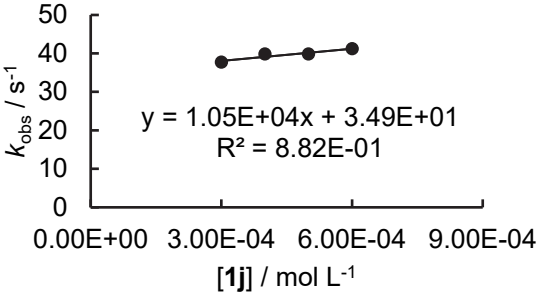

1j-**K**+ **2h** in MeCN (stopped-flow, detection at 412 nm)

[**2h**]$_0$, mol L^{-1}	[**1l**]$_0$, mol L^{-1}	k_{obs}, s^{-1}
2.91×10^{-5}	1.00×10^{-4}	14.0
2.91×10^{-5}	2.00×10^{-4}	22.8
2.91×10^{-5}	3.00×10^{-4}	36.3
2.91×10^{-5}	4.00×10^{-4}	48.0
2.91×10^{-5}	5.00×10^{-4}	59.4

$k_2 = 1.16 \times 10^5$ M^{-1} s^{-1}

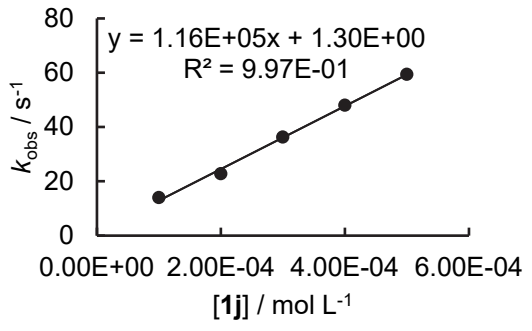

1j-**K**+ **2i** in MeCN (stopped-flow, detection at 375 nm)

$[\mathbf{2i}]_0$, mol L^{-1}	$[\mathbf{1l}]_0$, mol L^{-1}	k_{obs}, s^{-1}
5.49×10^{-5}	1.00×10^{-4}	12.9
5.49×10^{-5}	2.00×10^{-4}	30.6
5.49×10^{-5}	3.00×10^{-4}	46.6
5.49×10^{-5}	4.00×10^{-4}	64.7
5.49×10^{-5}	5.00×10^{-4}	82.2

$k_2 = 1.73 \times 10^5$ M^{-1} s^{-1}

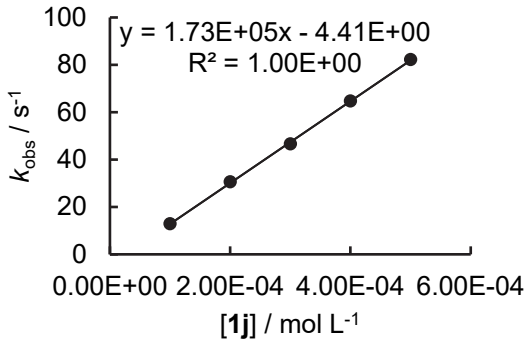

1j-**K**+ **2a** in MeCN (stopped-flow, detection at 632 nm)

$[\mathbf{2a}]_0$, mol L^{-1}	$[\mathbf{1l}]_0$, mol L^{-1}	k_{obs}, s^{-1}
1.87×10^{-5}	2.00×10^{-4}	1.03×10^3
1.87×10^{-5}	2.50×10^{-4}	1.65×10^3
1.87×10^{-5}	3.00×10^{-4}	2.21×10^3

$k_2 = 1.18 \times 10^7$ M^{-1} s^{-1}

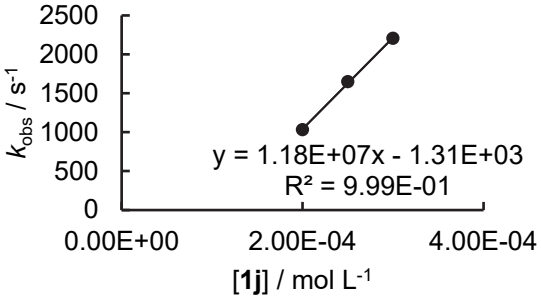

Determination of N and s_N parameters for **1j**-K in MeCN.

Reference Electrophile	Electrophilicity E	k_2 (M^{-1} s^{-1})	lg k_2
2g	–13.39	1.05×10^4	4.02
2h	–12.18	1.16×10^5	5.06
2i	–11.87	1.73×10^5	5.24
2a	–10.04	(1.18×10^7)	(7.07)[a]

[a] Not used for calculating N and s_N.

$N = 18.32$
$s_N = 0.82$

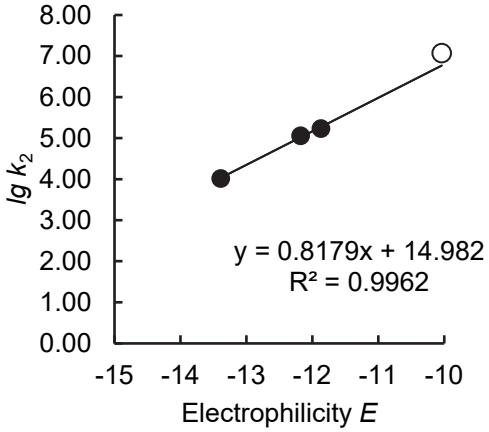

Potassium Phenolate

1k-**K**+ **2g** in MeCN (stopped-flow, detection at 513 nm)

$[\mathbf{2g}]_0$, mol L^{-1}	$[\mathbf{1l}]_0$, mol L^{-1}	k_{obs}, s^{-1}
3.38×10^{-5}	1.00×10^{-4}	2.03
3.38×10^{-5}	2.00×10^{-4}	4.84
3.38×10^{-5}	3.00×10^{-4}	7.50
3.38×10^{-5}	4.00×10^{-4}	8.97

$k_2 = 2.35 \times 10^4$ M^{-1} s^{-1}

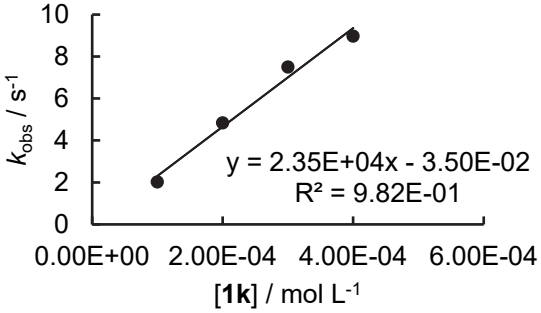

1k-**K**+ **2h** in MeCN (stopped-flow, detection at 412 nm)

$[\mathbf{2h}]_0$, mol L^{-1}	$[\mathbf{1l}]_0$, mol L^{-1}	k_{obs}, s^{-1}
2.51×10^{-5}	1.00×10^{-4}	7.53
2.51×10^{-5}	2.00×10^{-4}	25.9
2.51×10^{-5}	3.00×10^{-4}	54.2
2.51×10^{-5}	4.00×10^{-4}	73.4
2.51×10^{-5}	5.00×10^{-4}	107

$k_2 = 2.46 \times 10^5$ M^{-1} s^{-1}

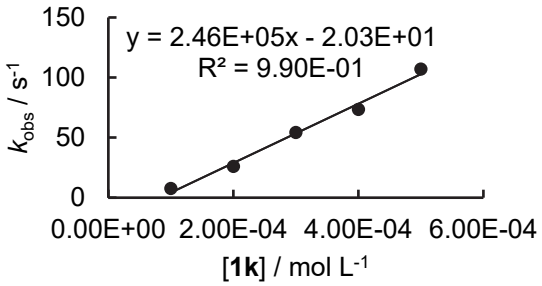

1k-**K**+ **2i** in MeCN (stopped-flow, detection at 375 nm)

$[\mathbf{2i}]_0$, mol L^{-1}	$[\mathbf{1l}]_0$, mol L^{-1}	k_{obs}, s^{-1}
5.63×10^{-5}	2.00×10^{-4}	39.5
5.63×10^{-5}	3.00×10^{-4}	76.0
5.63×10^{-5}	4.00×10^{-4}	118
5.63×10^{-5}	5.00×10^{-4}	181

$k_2 = 4.67 \times 10^5$ M^{-1} s^{-1}

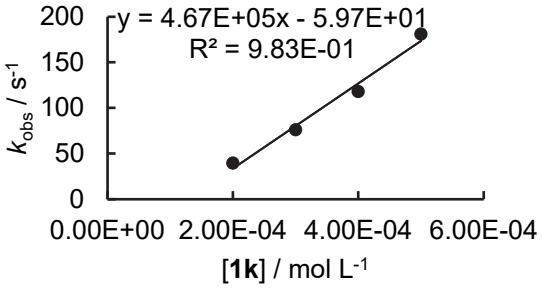

Determination of N and s_N parameters for **1k**-K in MeCN.

Reference Electrophile	Electrophilicity E	k_2 (M^{-1} s^{-1})	lg k_2
2g	–13.39	2.35×10^4	4.37
2h	–12.18	2.46×10^5	5.39
2i	–11.87	4.67×10^5	5.67

$N = 18.53$

$s_N = 0.85$

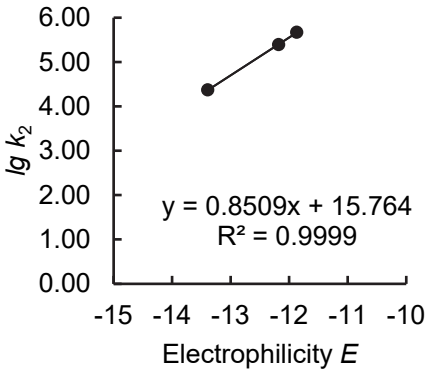

Potassium 4-*tert*-Butylphenolate

1m-**K**+ **2j** in MeCN (stopped-flow, detection at 486 nm)

$[\mathbf{2j}]_0$, mol L^{-1}	$[\mathbf{1m}]_0$, mol L^{-1}	k_{obs}, s^{-1}
1.29×10^{-5}	1.00×10^{-4}	4.16
1.29×10^{-5}	2.00×10^{-4}	9.03
1.29×10^{-5}	3.00×10^{-4}	11.9
1.29×10^{-5}	4.00×10^{-4}	16.9
1.29×10^{-5}	5.00×10^{-4}	20.0

$k_2 = 3.96 \times 10^4$ M^{-1} s^{-1}

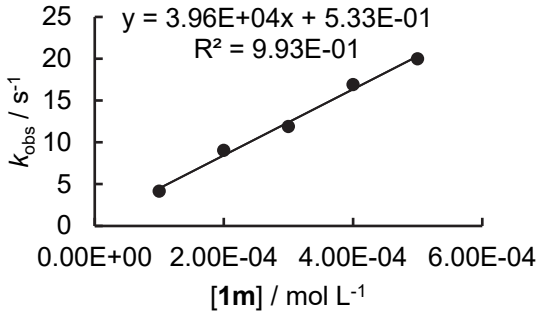

1m-**K**+ **2g** in MeCN (stopped-flow, detection at 513 nm)

$[\mathbf{2g}]_0$, mol L^{-1}	$[\mathbf{1m}]_0$, mol L^{-1}	k_{obs}, s^{-1}
2.67×10^{-5}	1.00×10^{-4}	2.43
2.67×10^{-5}	2.00×10^{-4}	5.63
2.67×10^{-5}	3.00×10^{-4}	10.4
2.67×10^{-5}	4.00×10^{-4}	17.6
2.67×10^{-5}	5.00×10^{-4}	21.0

$k_2 = 4.91 \times 10^4$ M^{-1} s^{-1}

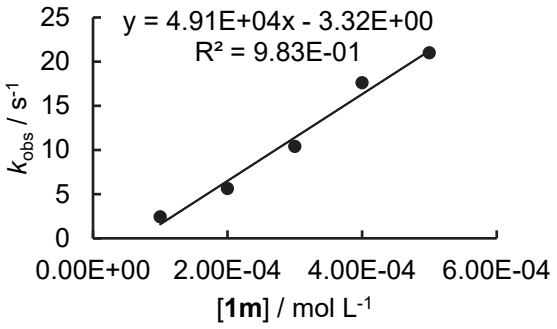

1m-**K**+ **2h** in MeCN (stopped-flow, detection at 412 nm)

$[\mathbf{2h}]_0$, mol L^{-1}	$[\mathbf{1m}]_0$, mol L^{-1}	k_{obs}, s^{-1}
1.82×10^{-5}	1.00×10^{-4}	10.0
1.82×10^{-5}	2.00×10^{-4}	37.5
1.82×10^{-5}	3.00×10^{-4}	64.2
1.82×10^{-5}	5.00×10^{-4}	129

$k_2 = 2.98 \times 10^5$ M^{-1} s^{-1}

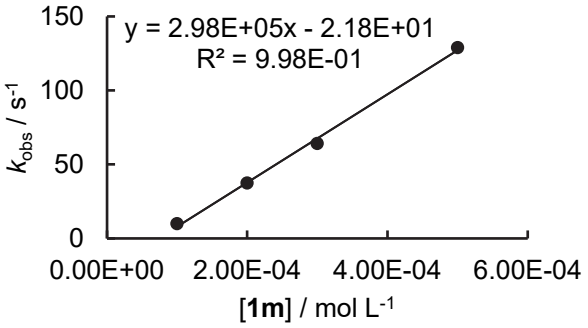

1m-**K**+ **2i** in MeCN (stopped-flow, detection at 375 nm)

$[\mathbf{2i}]_0$, mol L^{-1}	$[\mathbf{1m}]_0$, mol L^{-1}	k_{obs}, s^{-1}
4.48×10^{-5}	2.00×10^{-4}	33.8
4.48×10^{-5}	3.00×10^{-4}	79.6
4.48×10^{-5}	4.00×10^{-4}	122
4.48×10^{-5}	5.00×10^{-4}	181

$k_2 = 4.84 \times 10^5$ M^{-1} s^{-1}

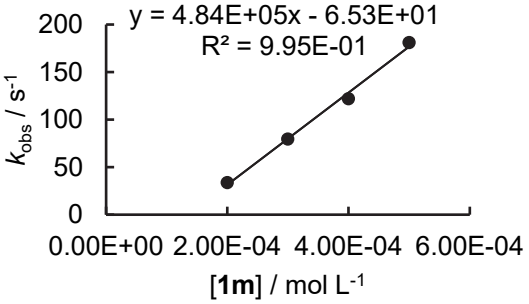

Determination of N and s_N parameters for **1m**-K in MeCN.

Reference Electrophile	Electrophilicity E	k_2 (M^{-1} s^{-1})	lg k_2
2j	–13.84	3.96×10^4	4.60
2g	–13.39	4.91×10^4	4.69
2h	–12.18	2.98×10^5	5.47
2i	–11.87	4.84×10^5	5.68

$N = 21.70$

$s_N = 0.58$

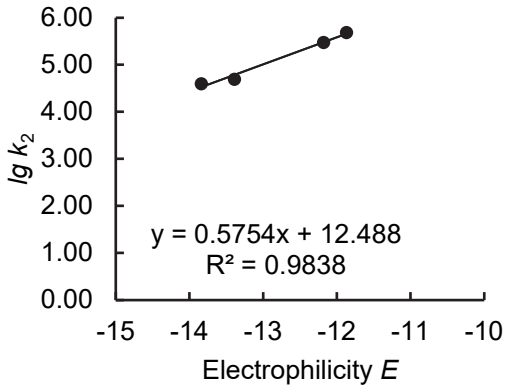

Potassium 4-Methoxyphenolate

1n-K+ **2j** in MeCN (stopped-flow, detection at 486 nm)

$[\mathbf{2j}]_0$, mol L^{-1}	$[\mathbf{1n}]_0$, mol L^{-1}	k_{obs}, s^{-1}
1.42×10^{-5}	1.00×10^{-4}	4.68
1.42×10^{-5}	2.00×10^{-4}	10.1
1.42×10^{-5}	3.00×10^{-4}	14.8
1.42×10^{-5}	4.00×10^{-4}	19.0
1.42×10^{-5}	5.00×10^{-4}	24.1

$k_2 = 4.77 \times 10^4$ M^{-1} s^{-1}

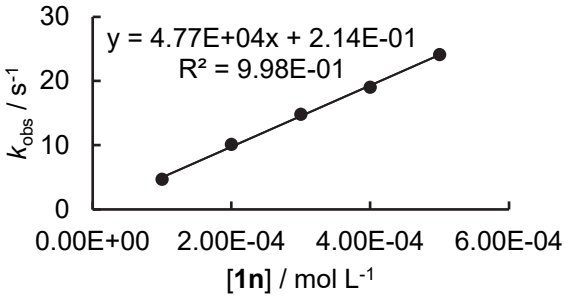

1n-K+ **2g** in MeCN (stopped-flow, detection at 513 nm)

$[\mathbf{2g}]_0$, mol L^{-1}	$[\mathbf{1n}]_0$, mol L^{-1}	k_{obs}, s^{-1}
3.29×10^{-5}	2.00×10^{-4}	4.78
3.29×10^{-5}	3.00×10^{-4}	19.1
3.29×10^{-5}	4.00×10^{-4}	25.4
3.29×10^{-5}	5.00×10^{-4}	38.7

$k_2 = 1.08 \times 10^5$ M^{-1} s^{-1}

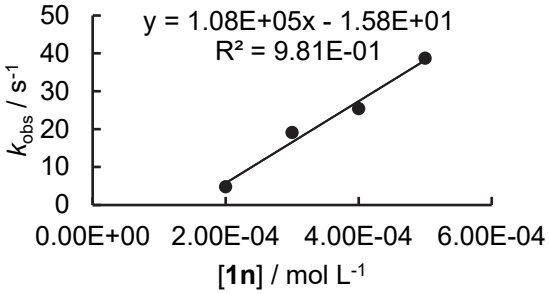

1n-K+ **2h** in MeCN (stopped-flow, detection at 412 nm)

$[\mathbf{2h}]_0$, mol L^{-1}	$[\mathbf{1n}]_0$, mol L^{-1}	k_{obs}, s^{-1}
1.70×10^{-5}	2.00×10^{-4}	40.2
1.70×10^{-5}	3.00×10^{-4}	105
1.70×10^{-5}	4.00×10^{-4}	176
1.70×10^{-5}	5.00×10^{-4}	275

$k_2 = 7.75 \times 10^5$ M^{-1} s^{-1}

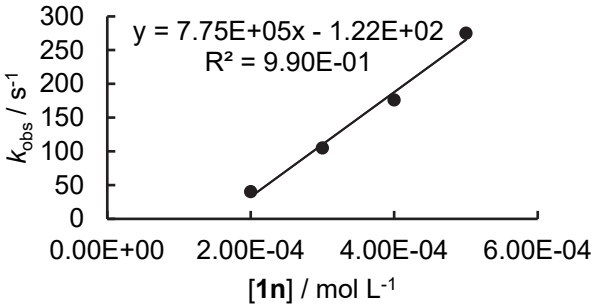

1n-K+ **2i** in MeCN (stopped-flow, detection at 375 nm)

$[\mathbf{2i}]_0$, mol L^{-1}	$[\mathbf{1n}]_0$, mol L^{-1}	k_{obs}, s^{-1}
4.60×10^{-5}	2.00×10^{-4}	88.5
4.60×10^{-5}	3.00×10^{-4}	182
4.60×10^{-5}	4.00×10^{-4}	326
4.60×10^{-5}	5.00×10^{-4}	398

$k_2 = 1.07 \times 10^6$ M^{-1} s^{-1}

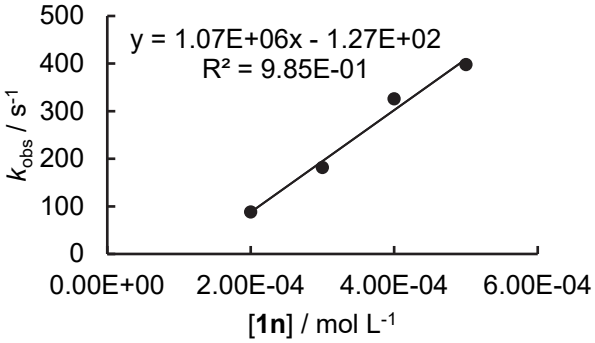

Determination of N and s_N parameters for **1n**-K in MeCN.

Reference Electrophile	Electrophilicity E	k_2 (M^{-1} s^{-1})	lg k_2
2j	–13.84	4.77×10^4	4.68
2g	–13.39	1.08×10^5	5.03
2h	–12.18	7.75×10^5	5.89
2i	–11.87	1.07×10^6	6.29

$N = 20.62$

$s_N = 0.69$

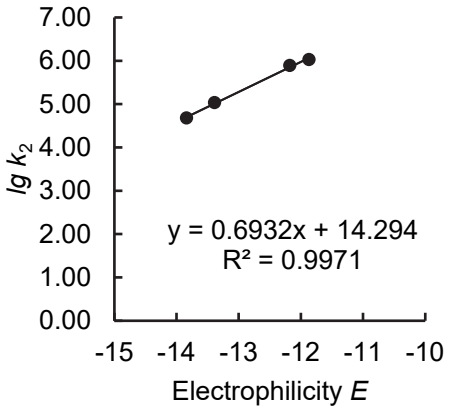

Potassium 3-Methoxyphenolate

1q-**K**+ **2g** in MeCN (stopped-flow, detection at 513 nm)

$[\mathbf{2g}]_0$, mol L^{-1}	$[\mathbf{1q}]_0$, mol L^{-1}	k_{obs}, s^{-1}
7.13×10^{-5}	1.00×10^{-4}	5.51
7.13×10^{-5}	2.00×10^{-4}	9.19
7.13×10^{-5}	3.00×10^{-4}	9.30
7.13×10^{-5}	4.00×10^{-4}	12.7
7.13×10^{-5}	5.00×10^{-4}	14.3

$k_2 = 2.11 \times 10^4$ M^{-1} s^{-1}

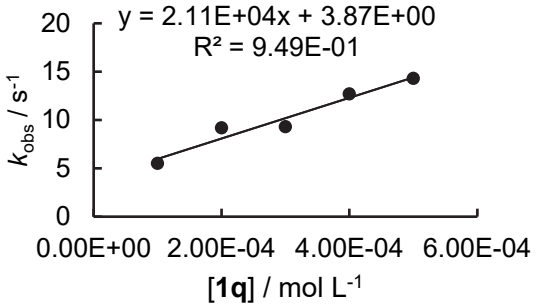

1q-**K**+ **2h** in MeCN (stopped-flow, detection at 412 nm)

$[\mathbf{2h}]_0$, mol L^{-1}	$[\mathbf{1q}]_0$, mol L^{-1}	k_{obs}, s^{-1}
4.26×10^{-5}	1.00×10^{-4}	9.34
4.26×10^{-5}	2.00×10^{-4}	26.0
4.26×10^{-5}	3.00×10^{-4}	38.6
4.26×10^{-5}	4.00×10^{-4}	60.9
4.26×10^{-5}	5.00×10^{-4}	73.5

$k_2 = 1.63 \times 10^5$ M^{-1} s^{-1}

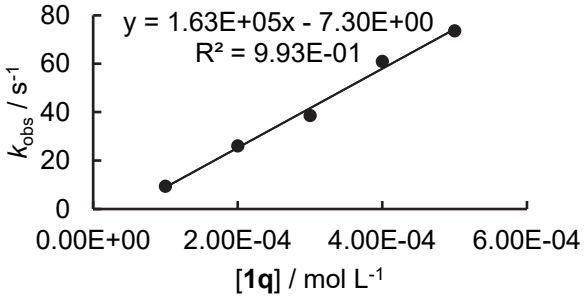

1q-**K**+ **2i** in MeCN (stopped-flow, detection at 375 nm)

$[\mathbf{2i}]_0$, mol L^{-1}	$[\mathbf{1q}]_0$, mol L^{-1}	k_{obs}, s^{-1}
2.74×10^{-5}	1.00×10^{-4}	14.9
2.74×10^{-5}	2.00×10^{-4}	47.3
2.74×10^{-5}	3.00×10^{-4}	67.3
2.74×10^{-5}	4.00×10^{-4}	128
2.74×10^{-5}	5.00×10^{-4}	160

$k_2 = 3.71 \times 10^5$ M^{-1} s^{-1}

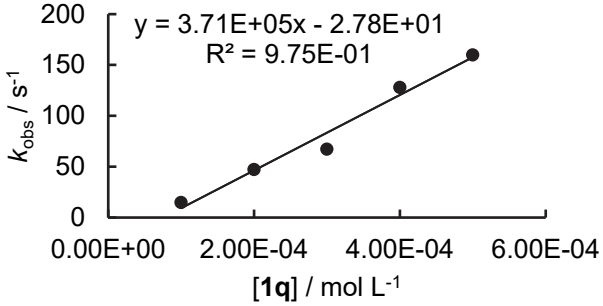

Determination of N and s_N parameters for **1q**-K in MeCN.

Reference Electrophile	Electrophilicity E	k_2 (M^{-1} s^{-1})	lg k_2
2g	–13.39	2.11×10^4	4.32
2h	–12.18	1.63×10^5	5.21
2i	–11.87	3.71×10^5	5.57

N = 18.81

s_N = 0.80

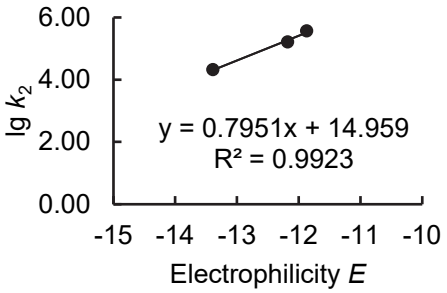

4.10 Kinetics of Reactions of Phenolates in DMF

Tetrabutylammonium 4-Nitrophenolate

1c-**NBu$_4$** + **2a** in DMF (stopped-flow, detection at 637 nm)

$[\mathbf{2a}]_0$, mol L^{-1}	$[\mathbf{1c}]_0$, mol L^{-1}	k_{obs}, s^{-1}
1.38×10^{-5}	1.00×10^{-4}	2.54
1.38×10^{-5}	2.00×10^{-4}	3.50
1.38×10^{-5}	3.00×10^{-4}	4.45
1.38×10^{-5}	4.00×10^{-4}	5.43
1.38×10^{-5}	5.00×10^{-4}	6.63

$k_2 = 1.01 \times 10^4$ M^{-1} s^{-1}

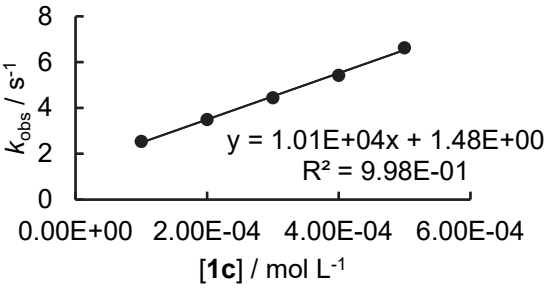

1c-**NBu$_4$** + **2b** in DMF (stopped-flow, detection at 640 nm)

$[\mathbf{2b}]_0$, mol L^{-1}	$[\mathbf{1c}]_0$, mol L^{-1}	k_{obs}, s^{-1}
7.69×10^{-6}	1.00×10^{-4}	7.48
7.69×10^{-6}	2.00×10^{-4}	10.7
7.69×10^{-6}	3.00×10^{-4}	13.4
7.69×10^{-6}	4.00×10^{-4}	16.4
7.69×10^{-6}	5.00×10^{-4}	19.4

$k_2 = 2.95 \times 10^4$ M^{-1} s^{-1}

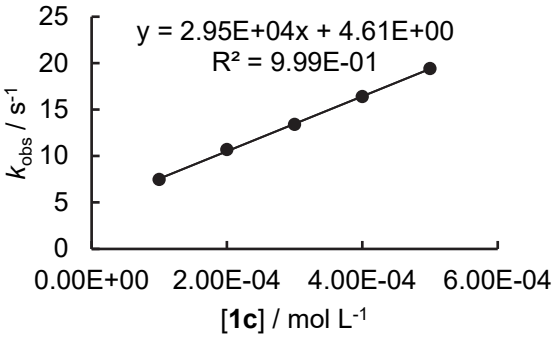

1c-**NBu$_4$** + **2c** in DMF (stopped-flow, detection at 622 nm)

$[\mathbf{2c}]_0$, mol L^{-1}	$[\mathbf{1c}]_0$, mol L^{-1}	k_{obs}, s^{-1}
6.95×10^{-6}	1.00×10^{-4}	15.0
6.95×10^{-6}	2.00×10^{-4}	27.0
6.95×10^{-6}	3.00×10^{-4}	36.4
6.95×10^{-6}	4.00×10^{-4}	45.7
6.95×10^{-6}	5.00×10^{-4}	55.7

$k_2 = 1.00 \times 10^5$ M^{-1} s^{-1}

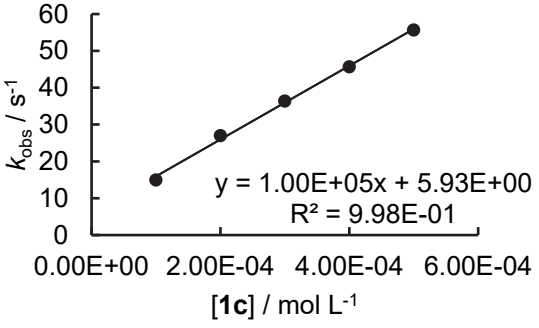

1c-**NBu$_4$** + **2d** in DMF (stopped-flow, detection at 626 nm)

[**2d**]$_0$, mol L^{-1}	[**1c**]$_0$, mol L^{-1}	k_{obs}, s^{-1}
8.60×10^{-6}	1.00×10^{-4}	38.2
8.60×10^{-6}	2.00×10^{-4}	72.6
8.60×10^{-6}	3.00×10^{-4}	98.2
8.60×10^{-6}	4.00×10^{-4}	126
8.60×10^{-6}	5.00×10^{-4}	157

$k_2 = 2.91 \times 10^5$ M^{-1} s^{-1}

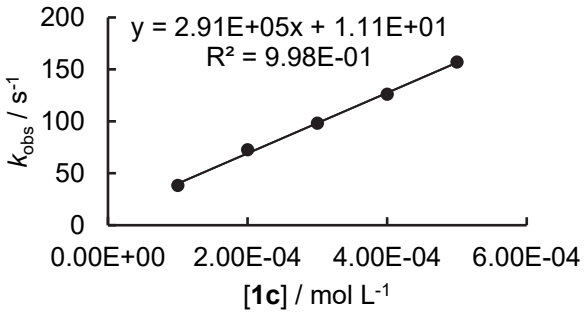

Determination of *N* and s_N parameters for **1c**-NBu$_4$ in DMF.

Reference Electrophile	Electrophilicity *E*	k_2 (M^{-1} s^{-1})	lg k_2
2a	−10.04	1.01×10^4	4.00
2b	−9.45	2.95×10^4	4.47
2c	−8.76	1.00×10^5	5.00
2d	−8.22	2.91×10^5	5.46

N = 15.05

s_N = 0.80

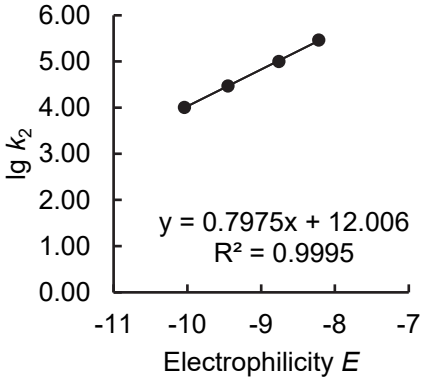

Potassium 4-Nitrophenolate

1c-**K** + **2a** in DMF (stopped-flow, detection at 637 nm)

[**2a**]$_0$, mol L^{-1}	[**1c**]$_0$, mol L^{-1}	k_{obs}, s^{-1}
9.48×10^{-6}	1.00×10^{-4}	2.05
9.48×10^{-6}	2.00×10^{-4}	3.36
9.48×10^{-6}	3.00×10^{-4}	4.36
9.48×10^{-6}	4.00×10^{-4}	5.65
9.48×10^{-6}	5.00×10^{-4}	6.78

$k_2 = 1.18 \times 10^4$ M^{-1} s^{-1}

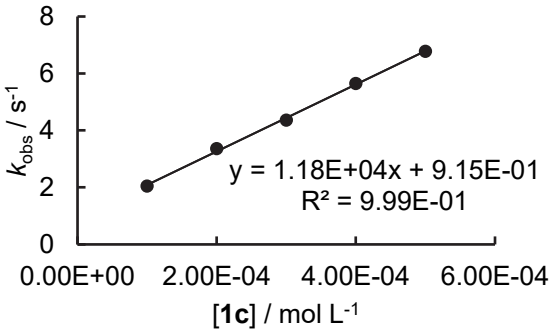

1c-**K** + **2b** in DMF (stopped-flow, detection at 640 nm)

[**2b**]$_0$, mol L^{-1}	[**1c**]$_0$, mol L^{-1}	k_{obs}, s^{-1}
7.25×10^{-6}	1.00×10^{-4}	5.91
7.25×10^{-6}	2.00×10^{-4}	9.08
7.25×10^{-6}	3.00×10^{-4}	12.6
7.25×10^{-6}	4.00×10^{-4}	15.1
7.25×10^{-6}	5.00×10^{-4}	18.6

$k_2 = 3.14 \times 10^4$ M^{-1} s^{-1}

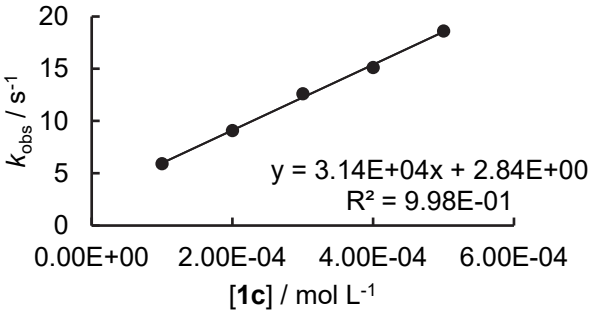

1c-**K** + **2c** in DMF (stopped-flow, detection at 622 nm)

$[\mathbf{2c}]_0$, mol L^{-1}	$[\mathbf{1c}]_0$, mol L^{-1}	k_{obs}, s^{-1}
8.26×10^{-6}	1.00×10^{-4}	12.5
8.26×10^{-6}	2.00×10^{-4}	23.3
8.26×10^{-6}	3.00×10^{-4}	32.0
8.26×10^{-6}	4.00×10^{-4}	41.1
8.26×10^{-6}	5.00×10^{-4}	49.8

$k_2 = 9.24 \times 10^4$ M^{-1} s^{-1}

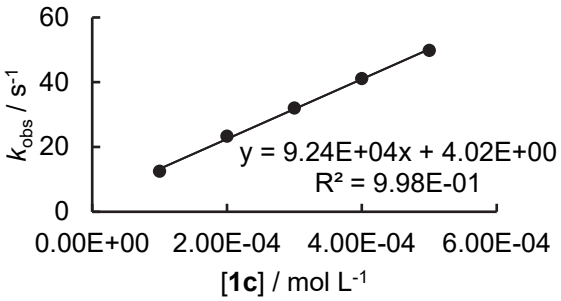

1c-**K** + **2d** in DMF (stopped-flow, detection at 626 nm)

$[\mathbf{2d}]_0$, mol L^{-1}	$[\mathbf{1c}]_0$, mol L^{-1}	k_{obs}, s^{-1}
6.47×10^{-6}	1.00×10^{-4}	37.0
6.47×10^{-6}	2.00×10^{-4}	68.6
6.47×10^{-6}	3.00×10^{-4}	96.8
6.47×10^{-6}	4.00×10^{-4}	127
6.47×10^{-6}	5.00×10^{-4}	155

$k_2 = 2.94 \times 10^5$ M^{-1} s^{-1}

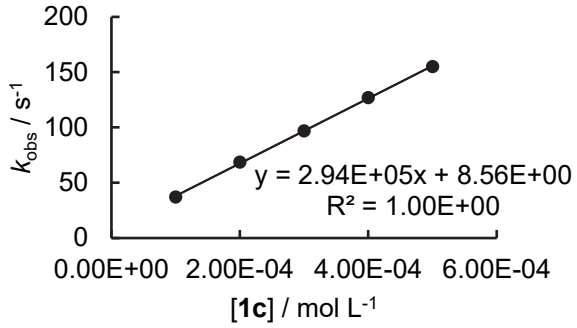

Determination of N and s_N parameters for **1c**-K in DMF.

Reference Electrophile	Electrophilicity E	k_2 (M^{-1} s^{-1})	lg k_2
2a	−10.04	1.18×10^4	4.07
2b	−9.45	3.14×10^4	4.50
2c	−8.76	9.24×10^4	4.97
2d	−8.22	2.94×10^5	5.47

$N = 15.41$

$s_N = 0.76$

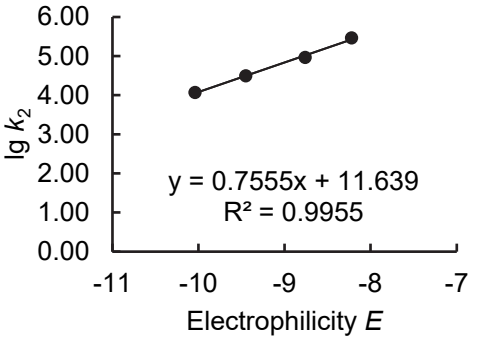

Tetrabutylammonium 2-Nitrophenolate

1d-**NBu$_4$** + **2a** in DMF (stopped-flow, detection at 637 nm)

$[\mathbf{2a}]_0$, mol L^{-1}	$[\mathbf{1d}]_0$, mol L^{-1}	k_{obs}, s^{-1}
1.25×10^{-5}	1.00×10^{-4}	12.2
1.25×10^{-5}	2.00×10^{-4}	17.4
1.25×10^{-5}	3.00×10^{-4}	21.6
1.25×10^{-5}	4.00×10^{-4}	25.7
1.25×10^{-5}	5.00×10^{-4}	30.0

$k_2 = 4.39 \times 10^4$ M^{-1} s^{-1}

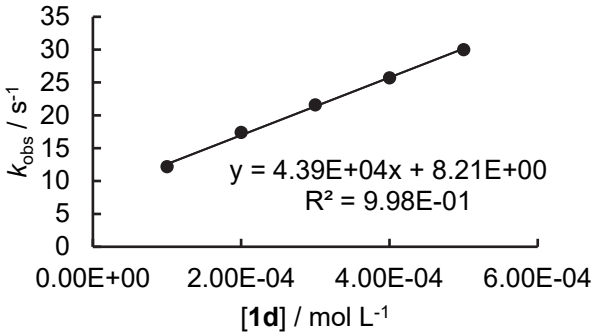

1d-NBu_4 + **2b** in DMF (stopped-flow, detection at 640 nm)

$[\mathbf{2b}]_0$, mol L^{-1}	$[\mathbf{1d}]_0$, mol L^{-1}	k_{obs}, s^{-1}
9.99×10^{-6}	1.00×10^{-4}	33.7
9.99×10^{-6}	2.00×10^{-4}	47.4
9.99×10^{-6}	3.00×10^{-4}	57.3
9.99×10^{-6}	4.00×10^{-4}	68.1
9.99×10^{-6}	5.00×10^{-4}	77.7

$k_2 = 1.09 \times 10^5$ M^{-1} s^{-1}

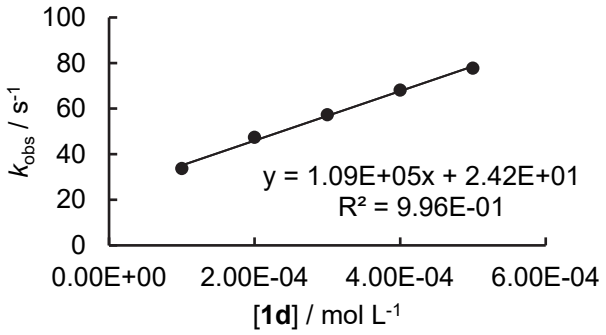

1d-NBu_4 + **2c** in DMF (stopped-flow, detection at 622 nm)

$[\mathbf{2c}]_0$, mol L^{-1}	$[\mathbf{1d}]_0$, mol L^{-1}	k_{obs}, s^{-1}
1.03×10^{-5}	1.00×10^{-4}	38.7
1.03×10^{-5}	2.00×10^{-4}	73.4
1.03×10^{-5}	3.00×10^{-4}	101
1.03×10^{-5}	4.00×10^{-4}	125
1.03×10^{-5}	5.00×10^{-4}	157

$k_2 = 2.88 \times 10^5$ M^{-1} s^{-1}

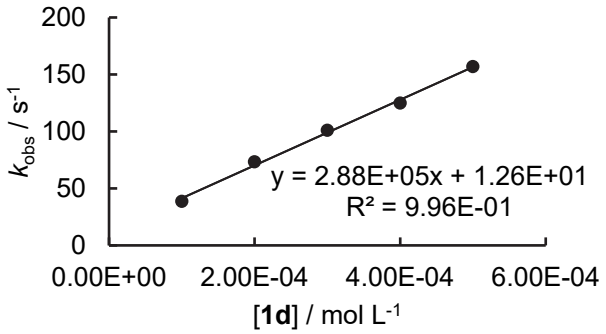

1d-NBu_4 + **2d** in DMF (stopped-flow, detection at 626 nm)

$[\mathbf{2d}]_0$, mol L^{-1}	$[\mathbf{1d}]_0$, mol L^{-1}	k_{obs}, s^{-1}
1.49×10^{-5}	1.00×10^{-4}	94.8
1.49×10^{-5}	2.00×10^{-4}	190
1.49×10^{-5}	3.00×10^{-4}	270
1.49×10^{-5}	4.00×10^{-4}	355
1.49×10^{-5}	5.00×10^{-4}	449

$k_2 = 8.73 \times 10^5$ M^{-1} s^{-1}

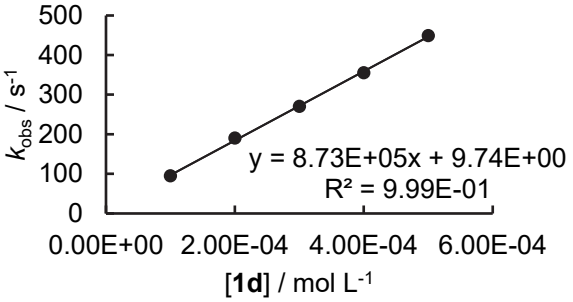

Determination of N and s_N parameters for **1d**-NBu_4 in DMF.

Reference Electrophile	Electrophilicity E	k_2 (M^{-1} s^{-1})	lg k_2
2a	−10.04	4.39×10^4	4.64
2b	−9.45	1.09×10^5	5.04
2c	−8.76	2.88×10^5	5.46
2d	−8.22	8.73×10^5	5.94

$N = 16.65$

$s_N = 0.70$

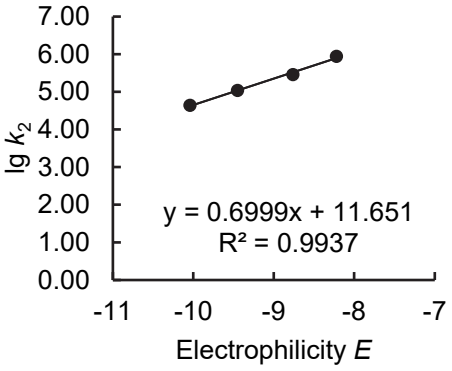

Tetrabutylammonium 3-Nitrophenolate

1e-**NBu$_4$** + **2a** in DMF (stopped-flow, detection at 637 nm)

[**2a**]$_0$, mol L^{-1}	[**1e**]$_0$, mol L^{-1}	k_{obs}, s^{-1}
1.02×10^{-5}	1.00×10^{-4}	538
1.02×10^{-5}	2.00×10^{-4}	1.13×10^{3}
1.02×10^{-5}	3.00×10^{-4}	1.59×10^{3}
1.02×10^{-5}	4.00×10^{-4}	2.06×10^{3}

$k_2 = 5.03 \times 10^{6}$ M^{-1} s^{-1}

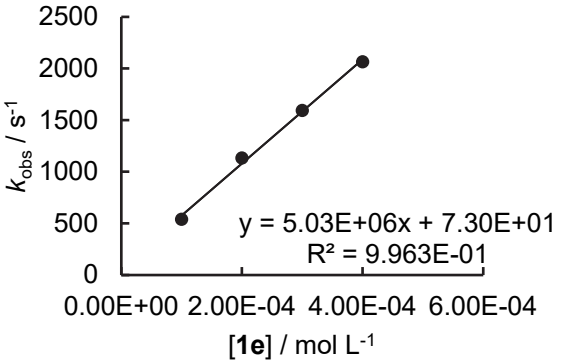

1e-**NBu$_4$** + **2b** in DMF (stopped-flow, detection at 640 nm)

[**2b**]$_0$, mol L^{-1}	[**1e**]$_0$, mol L^{-1}	k_{obs}, s^{-1}
6.70×10^{-6}	1.00×10^{-4}	999
6.70×10^{-6}	1.50×10^{-4}	1.54×10^{3}
6.70×10^{-6}	2.00×10^{-4}	2.05×10^{3}

$k_2 = 1.05 \times 10^{7}$ M^{-1} s^{-1}

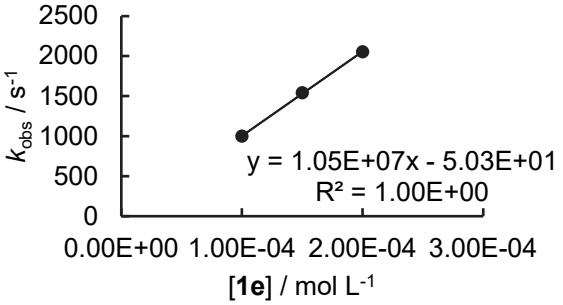

Determination of N and s_N parameters for **1e**-NBu$_4$ in DMF.

Reference Electrophile	Electrophilicity E	k_2 (M^{-1} s^{-1})	lg k_2
2a	−10.04	5.03×10^{6}	6.70
2b	−9.45	1.05×10^{7}	7.02

$N = 22.41$

$s_N = 0.54$

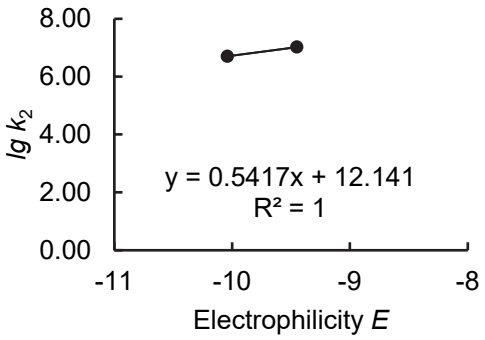

Potassium 4-Cyanophenolate

1f-**K** + **2a** in DMF (stopped-flow, detection at 637 nm)

[**2a**]$_0$, mol L^{-1}	[**1f**]$_0$, mol L^{-1}	k_{obs}, s^{-1}
5.89×10^{-6}	1.00×10^{-4}	39.7
5.89×10^{-6}	2.00×10^{-4}	85.5
5.89×10^{-6}	3.00×10^{-4}	124
5.89×10^{-6}	4.00×10^{-4}	166
5.89×10^{-6}	5.00×10^{-4}	200

$k_2 = 4.01 \times 10^{5}$ M^{-1} s^{-1}

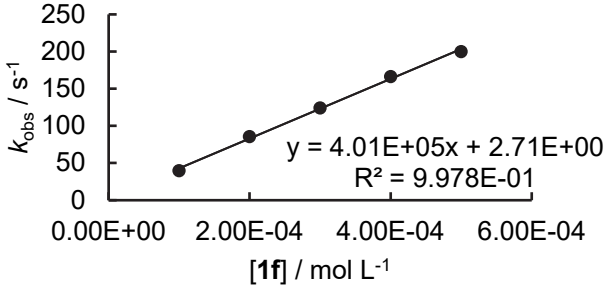

1f-**K** + **2b** in DMF (stopped-flow, detection at 640 nm)

$[\mathbf{2b}]_0$, mol L^{-1}	$[\mathbf{1f}]_0$, mol L^{-1}	k_{obs}, s^{-1}
1.43×10^{-5}	1.00×10^{-4}	79.6
1.43×10^{-5}	2.00×10^{-4}	191
1.43×10^{-5}	3.00×10^{-4}	255
1.43×10^{-5}	4.00×10^{-4}	322
1.43×10^{-5}	5.00×10^{-4}	416

$k_2 = 8.04 \times 10^5$ M^{-1} s^{-1}

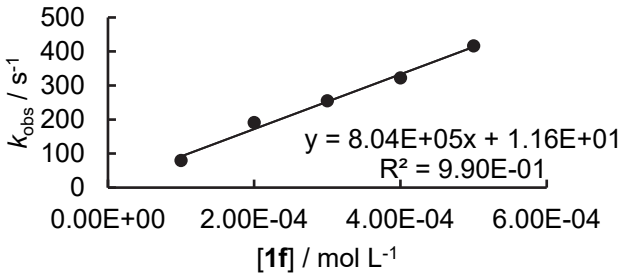

1f-**K** + **2c** in DMF (stopped-flow, detection at 622 nm)

$[\mathbf{2c}]_0$, mol L^{-1}	$[\mathbf{1f}]_0$, mol L^{-1}	k_{obs}, s^{-1}
1.88×10^{-5}	1.00×10^{-4}	182
1.88×10^{-5}	2.00×10^{-4}	416
1.88×10^{-5}	3.00×10^{-4}	774
1.88×10^{-5}	4.00×10^{-4}	1.14×10^3

$k_2 = 3.23 \times 10^6$ M^{-1} s^{-1}

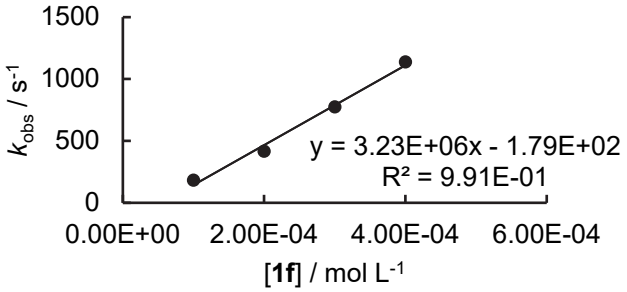

Determination of N and s_N parameters for **1f**-K in DMF.

Reference Electrophile	Electrophilicity E	k_2 (M^{-1} s^{-1})	lg k_2
2a	−10.04	4.01×10^5	5.60
2b	−9.45	8.04×10^5	5.91
2c	−8.76	3.23×10^6	6.51

$N = 17.85$

$s_N = 0.71$

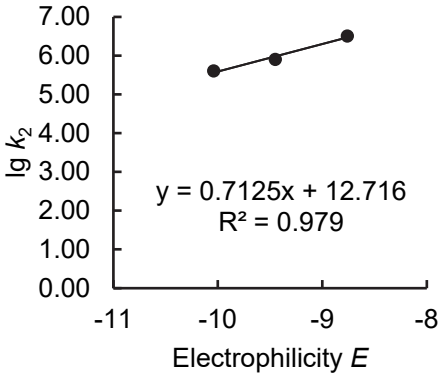

Tetrabutylammonium 2-(Trifluoromethyl)phenolate

1g-**NBu$_4$** + **2a** in DMF (stopped-flow, detection at 637 nm)

$[\mathbf{2a}]_0$, mol L^{-1}	$[\mathbf{1g}]_0$, mol L^{-1}	k_{obs}, s^{-1}
1.45×10^{-5}	1.00×10^{-4}	79.8
1.45×10^{-5}	2.00×10^{-4}	176
1.45×10^{-5}	3.00×10^{-4}	263
1.45×10^{-5}	4.00×10^{-4}	350
1.45×10^{-5}	5.00×10^{-4}	464

$k_2 = 9.42 \times 10^5$ M^{-1} s^{-1}

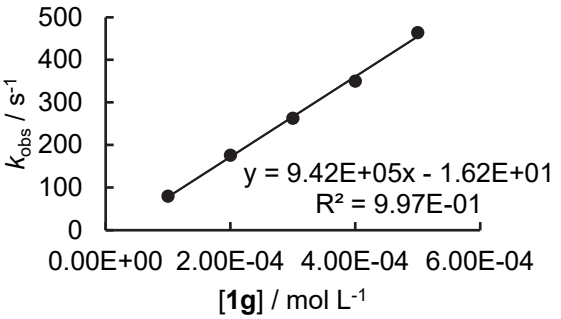

1g-**NBu$_4$** + **2b** in DMF (stopped-flow, detection at 640 nm)

[**2b**]$_0$, mol L^{-1}	[**1g**]$_0$, mol L^{-1}	k_{obs}, s^{-1}
1.15×10^{-5}	1.00×10^{-4}	149
1.15×10^{-5}	2.00×10^{-4}	373
1.15×10^{-5}	3.00×10^{-4}	573
1.15×10^{-5}	4.00×10^{-4}	823
1.15×10^{-5}	5.00×10^{-4}	999

$k_2 = 2.15 \times 10^6$ M^{-1} s^{-1}

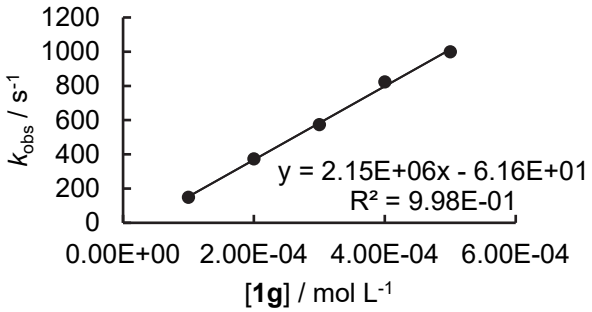

1g-**NBu$_4$** + **2c** in DMF (stopped-flow, detection at 622 nm)

[**2c**]$_0$, mol L^{-1}	[**1g**]$_0$, mol L^{-1}	k_{obs}, s^{-1}
1.35×10^{-5}	1.00×10^{-4}	469
1.35×10^{-5}	2.00×10^{-4}	1.05×10^3
1.35×10^{-5}	4.00×10^{-4}	2.04×10^3

$k_2 = 5.20 \times 10^6$ M^{-1} s^{-1}

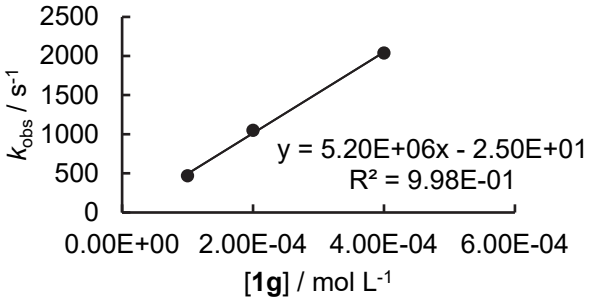

Determination of N and s_N parameters for **1g**-NBu$_4$ in DMF.

Reference Electrophile	Electrophilicity E	k_2 (M^{-1} s^{-1})	lg k_2
2a	−10.04	9.42×10^5	5.97
2b	−9.45	2.15×10^6	6.33
2c	−8.76	5.20×10^6	6.72

$N = 20.37$

$s_N = 0.58$

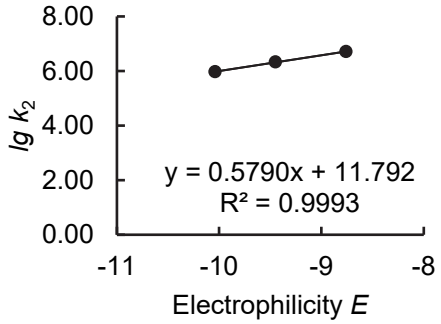

Tetrabutylammonium 4-(Trifluoromethyl)phenolate

1h-**NBu$_4$** + **2a** in DMF (stopped-flow, detection at 637 nm)

[**2a**]$_0$, mol L^{-1}	[**1h**]$_0$, mol L^{-1}	k_{obs}, s^{-1}
9.31×10^{-6}	1.00×10^{-4}	163
9.31×10^{-6}	3.00×10^{-4}	554
9.31×10^{-6}	4.00×10^{-4}	807
9.31×10^{-6}	5.00×10^{-4}	1.02×10^3

$k_2 = 2.15 \times 10^6$ M^{-1} s^{-1}

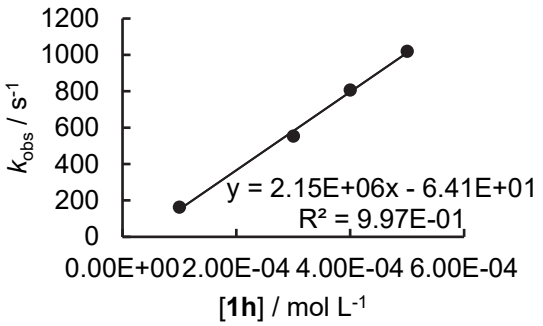

1h-NBu_4 + **2b** in DMF (stopped-flow, detection at 640 nm)

$[\mathbf{2b}]_0$, mol L^{-1}	$[\mathbf{1h}]_0$, mol L^{-1}	k_{obs}, s^{-1}
6.96×10^{-6}	1.00×10^{-4}	350
6.96×10^{-6}	2.00×10^{-4}	880
6.96×10^{-6}	3.00×10^{-4}	1.32×10^{3}
6.96×10^{-6}	4.00×10^{-4}	1.67×10^{3}

$k_2 = 4.40 \times 10^6$ M^{-1} s^{-1}

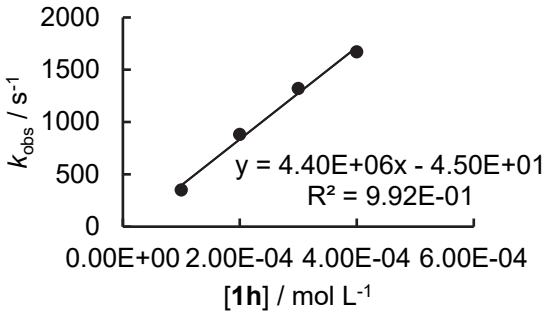

Determination of N and s_N parameters for **1h**-NBu_4 in DMF.

Reference Electrophile	Electrophilicity E	k_2 (M^{-1} s^{-1})	lg k_2
2a	–10.04	2.15×10^6	6.33
2b	–9.45	4.40×10^6	6.64

$N = 22.05$

$s_N = 0.53$

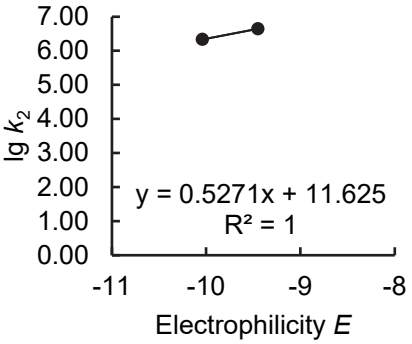

Potassium 3-(Trifluoromethyl)phenolate

1i-**K** + **2a** in DMF (stopped-flow, detection at 637 nm)

$[\mathbf{2a}]_0$, mol L^{-1}	$[\mathbf{1i}]_0$, mol L^{-1}	k_{obs}, s^{-1}
4.86×10^{-6}	1.00×10^{-4}	549
4.86×10^{-6}	2.00×10^{-4}	1.23×10^{3}
4.86×10^{-6}	3.00×10^{-4}	1.91×10^{3}
4.86×10^{-6}	4.00×10^{-4}	2.54×10^{3}

$k_2 = 6.65 \times 10^6$ M^{-1} s^{-1}

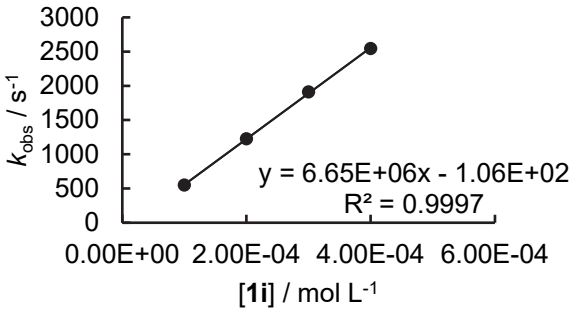

Potassium 4-Chlorophenolate

1j-**K** + **2g** in DMF (stopped-flow, detection at 522 nm)

$[\mathbf{2g}]_0$, mol L^{-1}	$[\mathbf{1j}]_0$, mol L^{-1}	k_{obs}, s^{-1}
2.03×10^{-5}	4.00×10^{-4}	65.3
2.03×10^{-5}	5.00×10^{-4}	74.3
2.03×10^{-5}	7.00×10^{-4}	78.7
2.03×10^{-5}	9.00×10^{-4}	86.9

$k_2 = 3.95 \times 10^4$ M^{-1} s^{-1}

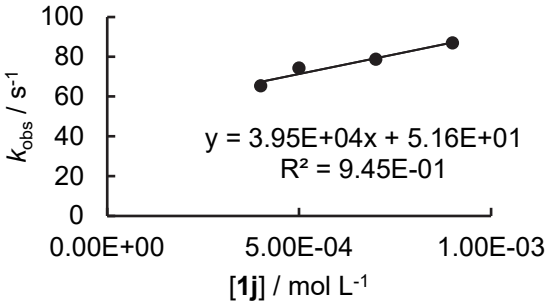

1j-**K** + **2h** in DMF (stopped-flow, detection at 419 nm)

$[\mathbf{2h}]_0$, mol L^{-1}	$[\mathbf{1j}]_0$, mol L^{-1}	k_{obs}, s^{-1}
1.89×10^{-5}	1.00×10^{-4}	33.5
1.89×10^{-5}	2.00×10^{-4}	57.2
1.89×10^{-5}	3.00×10^{-4}	81.3
1.89×10^{-5}	4.00×10^{-4}	107
1.89×10^{-5}	5.00×10^{-4}	123

$k_2 = 2.29 \times 10^5$ M^{-1} s^{-1}

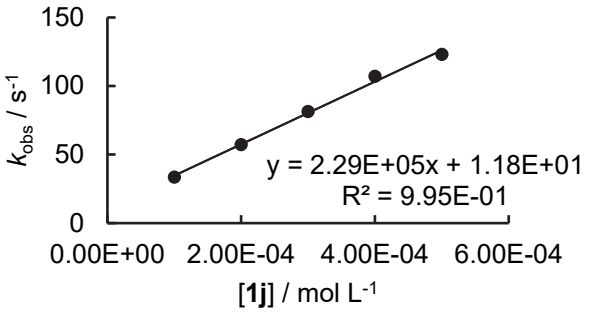

1j-**K** + **2i** in DMF (stopped-flow, detection at 382 nm)

$[\mathbf{2i}]_0$, mol L^{-1}	$[\mathbf{1j}]_0$, mol L^{-1}	k_{obs}, s^{-1}
6.25×10^{-5}	1.00×10^{-4}	39.7
6.25×10^{-5}	2.00×10^{-4}	73.6
6.25×10^{-5}	3.00×10^{-4}	116
6.25×10^{-5}	4.00×10^{-4}	170

$k_2 = 4.33 \times 10^5$ M^{-1} s^{-1}

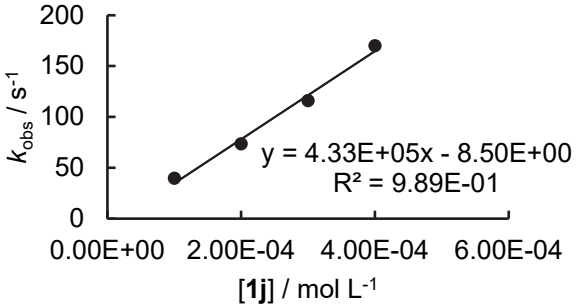

1j-**K** + **2a** in DMF (stopped-flow, detection at 637 nm)

$[\mathbf{2a}]_0$, mol L^{-1}	$[\mathbf{1j}]_0$, mol L^{-1}	k_{obs}, s^{-1}
1.34×10^{-5}	2.00×10^{-4}	1.76×10^3
1.34×10^{-5}	2.50×10^{-4}	2.25×10^3
1.34×10^{-5}	3.00×10^{-4}	2.77×10^3

$k_2 = 1.01 \times 10^7$ M^{-1} s^{-1}

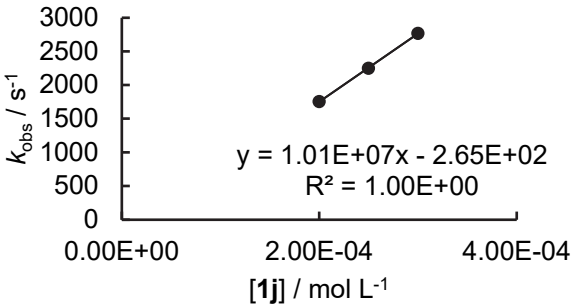

Determination of N and s_N parameters for **1j**-K in DMF.

Reference Electrophile	Electrophilicity E	k_2 (M^{-1} s^{-1})	lg k_2
2g	–13.39	3.95×10^4	4.60
2h	–12.18	2.29×10^5	5.36
2i	–11.87	4.33×10^5	5.64
2a	–10.04	1.01×10^7	7.02

$N = 19.67$

$s_N = 0.72$

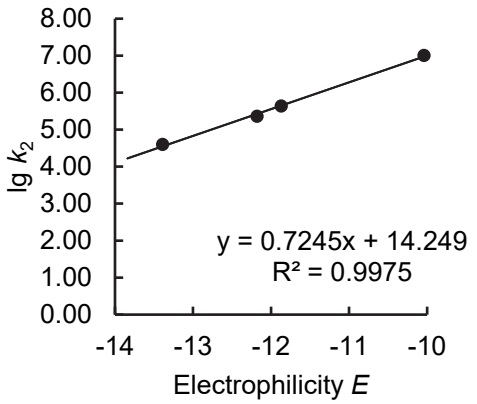

Potassium Phenolate

1k-**K** + **2j** in DMF (stopped-flow, detection at 490 nm)

[**2j**]$_0$, mol L^{-1}	[**1k**]$_0$, mol L^{-1}	k_{obs}, s^{-1}
1.26×10^{-5}	1.00×10^{-4}	6.68
1.26×10^{-5}	2.00×10^{-4}	9.20
1.26×10^{-5}	3.00×10^{-4}	12.1
1.26×10^{-5}	4.00×10^{-4}	15.9
1.26×10^{-5}	5.00×10^{-4}	19.0

$k_2 = 3.13 \times 10^4$ M^{-1} s^{-1}

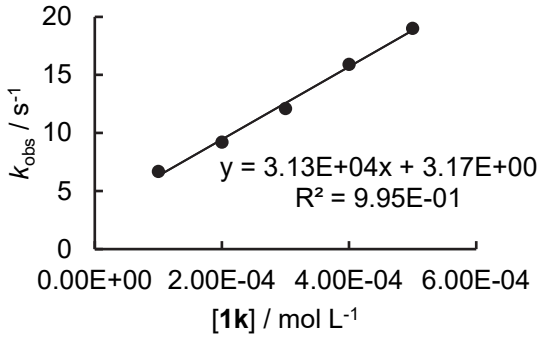

1k-**K** + **2g** in DMF (stopped-flow, detection at 522 nm)

[**2g**]$_0$, mol L^{-1}	[**1k**]$_0$, mol L^{-1}	k_{obs}, s^{-1}
2.53×10^{-5}	1.00×10^{-4}	8.03
2.53×10^{-5}	2.00×10^{-4}	14.2
2.53×10^{-5}	3.00×10^{-4}	19.5
2.53×10^{-5}	5.00×10^{-4}	33.3

$k_2 = 6.30 \times 10^4$ M^{-1} s^{-1}

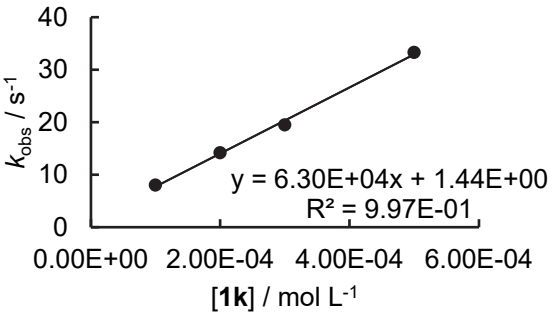

1k-**K** + **2h** in DMF (stopped-flow, detection at 419 nm)

[**2h**]$_0$, mol L^{-1}	[**1k**]$_0$, mol L^{-1}	k_{obs}, s^{-1}
2.00×10^{-5}	1.00×10^{-4}	35.1
2.00×10^{-5}	2.00×10^{-4}	105
2.00×10^{-5}	3.00×10^{-4}	175
2.00×10^{-5}	4.00×10^{-4}	242

$k_2 = 6.91 \times 10^5$ M^{-1} s^{-1}

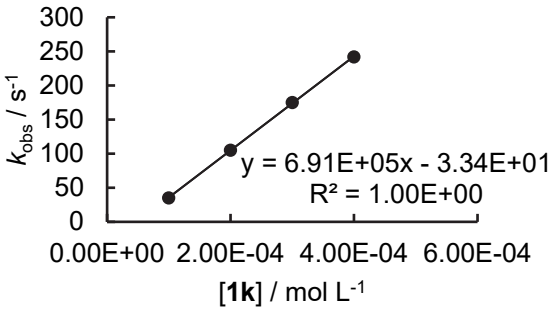

1k-**K** + **2i** in DMF (stopped-flow, detection at 382 nm)

[**2i**]$_0$, mol L^{-1}	[**1k**]$_0$, mol L^{-1}	k_{obs}, s^{-1}
6.12×10^{-5}	2.00×10^{-4}	165
6.12×10^{-5}	3.00×10^{-4}	344
6.12×10^{-5}	4.00×10^{-4}	540
6.12×10^{-5}	5.00×10^{-4}	720

$k_2 = 1.86 \times 10^6$ M^{-1} s^{-1}

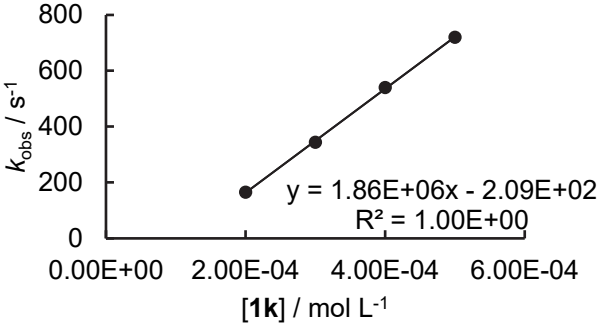

Determination of N and s_N parameters for **1k**-K in DMF.

Reference Electrophile	Electrophilicity E	k_2 (M^{-1} s^{-1})	lg k_2
2j	-13.84	3.13×10^4	4.50
2g	-13.39	6.30×10^4	4.80
2h	-12.18	6.91×10^5	5.84
2i	-11.87	1.86×10^6	6.27

$N = 18.86$

$s_N = 0.89$

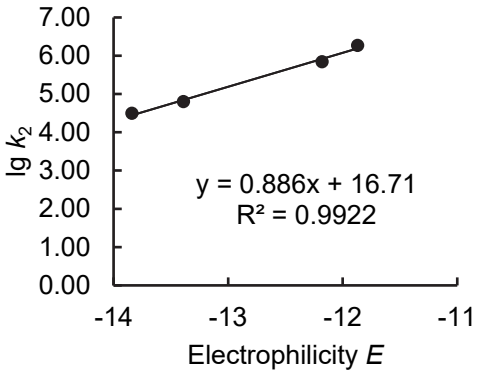

Potassium 4-Methylphenolate

1l-K + **2j** in DMF (stopped-flow, detection at 490 nm)

$[\mathbf{2j}]_0$, mol L^{-1}	$[\mathbf{1l}]_0$, mol L^{-1}	k_{obs}, s^{-1}
7.40×10^{-6}	2.00×10^{-4}	5.73
7.40×10^{-6}	4.00×10^{-4}	20.0
7.40×10^{-6}	5.00×10^{-4}	27.9

$k_2 = 7.35 \times 10^4$ M^{-1} s^{-1}

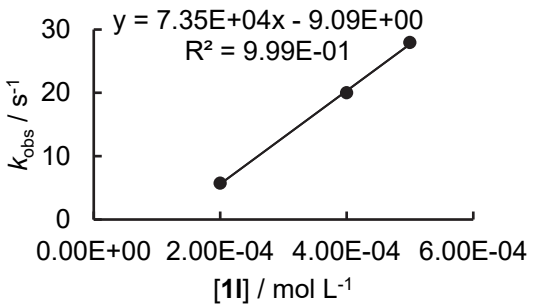

1l-K + **2g** in DMF (stopped-flow, detection at 522 nm)

$[\mathbf{2g}]_0$, mol L^{-1}	$[\mathbf{1l}]_0$, mol L^{-1}	k_{obs}, s^{-1}
3.08×10^{-5}	2.00×10^{-4}	22.7
3.08×10^{-5}	3.00×10^{-4}	43.6
3.08×10^{-5}	4.00×10^{-4}	70.5
3.08×10^{-5}	5.00×10^{-4}	92.9

$k_2 = 2.38 \times 10^5$ M^{-1} s^{-1}

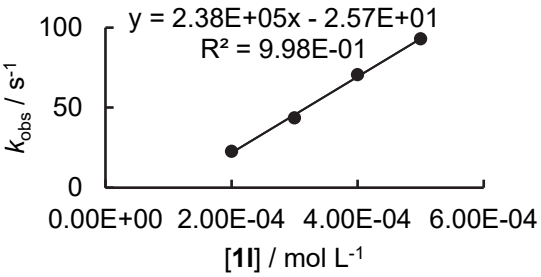

1l-K + **2h** in DMF (stopped-flow, detection at 419 nm)

$[\mathbf{2h}]_0$, mol L^{-1}	$[\mathbf{1l}]_0$, mol L^{-1}	k_{obs}, s^{-1}
3.28×10^{-5}	2.00×10^{-4}	183
3.28×10^{-5}	3.00×10^{-4}	397
3.28×10^{-5}	4.00×10^{-4}	629
3.28×10^{-5}	5.00×10^{-4}	873

$k_2 = 2.30 \times 10^6$ M^{-1} s^{-1}

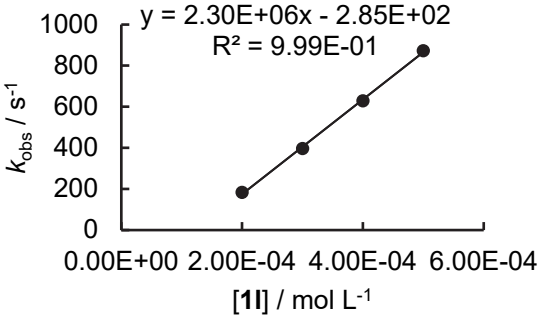

1l-**K** + **2i** in DMF (stopped-flow, detection at 382 nm)

$[\mathbf{2i}]_0$, mol L^{-1}	$[\mathbf{1l}]_0$, mol L^{-1}	k_{obs}, s^{-1}
2.99×10^{-5}	1.00×10^{-4}	126
2.99×10^{-5}	2.00×10^{-4}	390
2.99×10^{-5}	3.00×10^{-4}	779
2.99×10^{-5}	4.00×10^{-4}	1.17×10^{3}
2.99×10^{-5}	5.00×10^{-4}	1.52×10^{3}

$k_2 = 3.57 \times 10^6$ M^{-1} s^{-1}

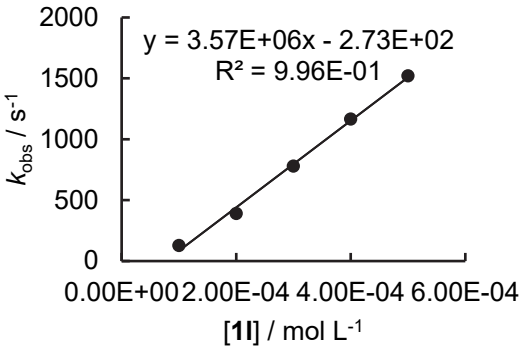

Determination of N and s_N parameters for **1l**-K in DMF.

Reference Electrophile	Electrophilicity E	k_2 (M^{-1} s^{-1})	lg k_2
2j	–13.84	7.35×10^4	4.87
2g	–13.39	2.38×10^5	5.38
2h	–12.18	2.30×10^6	6.36
2i	–11.87	3.57×10^6	6.55

$N = 19.65$

$s_N = 0.85$

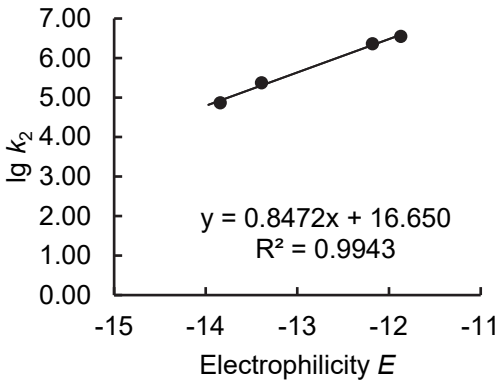

Potassium 4-*tert*-Butylphenolate

1m-**K** + **2j** in DMF (stopped-flow, detection at 490 nm)

$[\mathbf{2j}]_0$, mol L^{-1}	$[\mathbf{1m}]_0$, mol L^{-1}	k_{obs}, s^{-1}
1.19×10^{-5}	1.00×10^{-4}	6.10
1.19×10^{-5}	2.00×10^{-4}	11.7
1.19×10^{-5}	3.00×10^{-4}	18.6
1.19×10^{-5}	4.00×10^{-4}	29.9
1.19×10^{-5}	5.00×10^{-4}	35.6

$k_2 = 7.72 \times 10^4$ M^{-1} s^{-1}

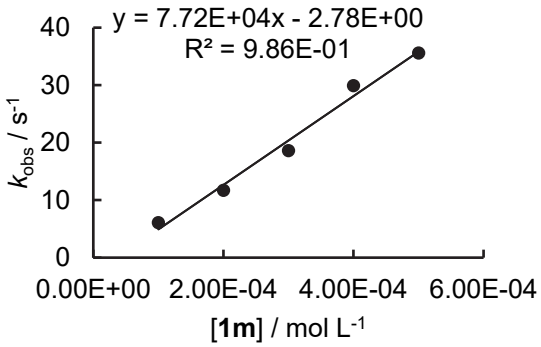

1m-**K** + **2g** in DMF (stopped-flow, detection at 522 nm)

$[\mathbf{2g}]_0$, mol L^{-1}	$[\mathbf{1m}]_0$, mol L^{-1}	k_{obs}, s^{-1}
1.90×10^{-5}	1.00×10^{-4}	9.51
1.90×10^{-5}	2.00×10^{-4}	23.1
1.90×10^{-5}	3.00×10^{-4}	36.4
1.90×10^{-5}	4.00×10^{-4}	54.4
1.90×10^{-5}	5.00×10^{-4}	65.0

$k_2 = 1.42 \times 10^5$ M^{-1} s^{-1}

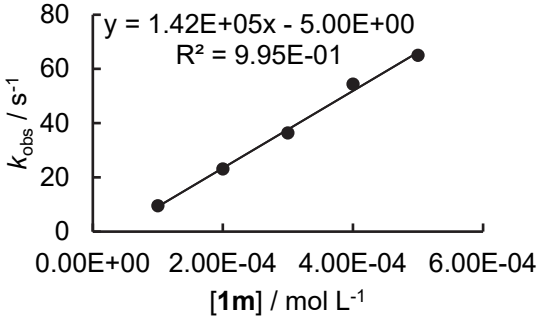

1m-**K** + **2h** in DMF (stopped-flow, detection at 419 nm)

$[\mathbf{2h}]_0$, mol L^{-1}	$[\mathbf{1m}]_0$, mol L^{-1}	k_{obs}, s^{-1}
1.43×10^{-5}	2.00×10^{-4}	93.6
1.43×10^{-5}	3.00×10^{-4}	204
1.43×10^{-5}	4.00×10^{-4}	354
1.43×10^{-5}	5.00×10^{-4}	509

$k_2 = 1.40 \times 10^6$ M^{-1} s^{-1}

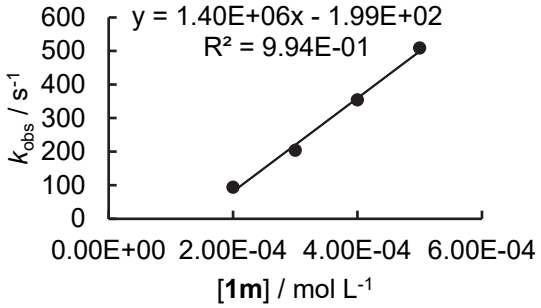

1m-**K** + **2i** in DMF (stopped-flow, detection at 382 nm)

$[\mathbf{2i}]_0$, mol L^{-1}	$[\mathbf{1m}]_0$, mol L^{-1}	k_{obs}, s^{-1}
3.11×10^{-5}	2.00×10^{-4}	203
3.11×10^{-5}	3.00×10^{-4}	412
3.11×10^{-5}	4.00×10^{-4}	750
3.11×10^{-5}	5.00×10^{-4}	1.03×10^3

$k_2 = 2.82 \times 10^6$ M^{-1} s^{-1}

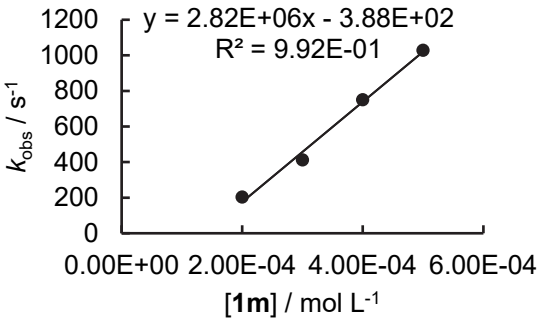

Determination of N and s_N parameters for **1m**-K in DMF.

Reference Electrophile	Electrophilicity E	k_2 (M^{-1} s^{-1})	lg k_2
2j	–13.84	7.72×10^4	4.89
2g	–13.39	1.42×10^5	5.15
2h	–12.18	1.40×10^6	6.15
2i	–11.87	2.82×10^6	6.45

$N = 19.90$

$s_N = 0.80$

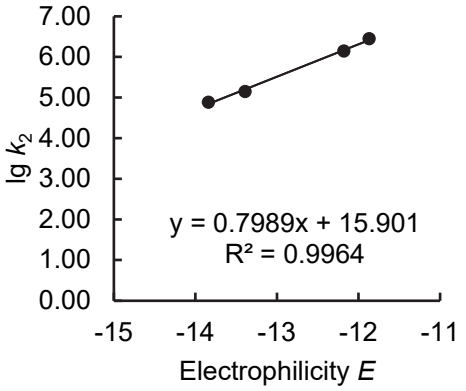

Potassium 4-Methoxyphenolate

1n-**K** + **2j** in DMF (stopped-flow, detection at 490 nm)

$[\mathbf{2j}]_0$, mol L^{-1}	$[\mathbf{1n}]_0$, mol L^{-1}	k_{obs}, s^{-1}
1.45×10^{-5}	1.00×10^{-4}	5.35
1.45×10^{-5}	2.00×10^{-4}	10.4
1.45×10^{-5}	4.00×10^{-4}	24.4

$k_2 = 6.44 \times 10^4$ M^{-1} s^{-1}

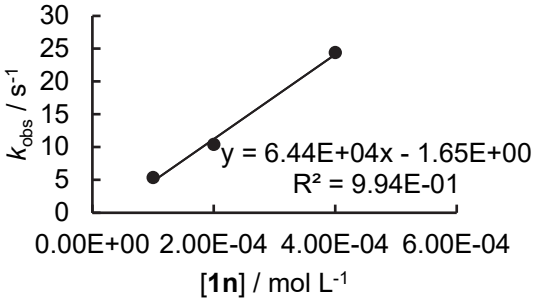

1n-**K** + **2g** in DMF (stopped-flow, detection at 522 nm)

$[\mathbf{2g}]_0$, mol L^{-1}	$[\mathbf{1n}]_0$, mol L^{-1}	k_{obs}, s^{-1}
2.97×10^{-5}	1.00×10^{-4}	11.7
2.97×10^{-5}	2.00×10^{-4}	39.2
2.97×10^{-5}	3.00×10^{-4}	67.8
2.97×10^{-5}	4.00×10^{-4}	106

$k_2 = 3.12 \times 10^5$ M^{-1} s^{-1}

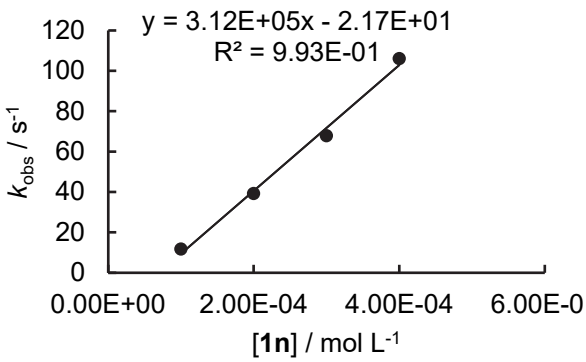

1n-**K** + **2h** in DMF (stopped-flow, detection at 419 nm)

$[\mathbf{2h}]_0$, mol L^{-1}	$[\mathbf{1n}]_0$, mol L^{-1}	k_{obs}, s^{-1}
5.49×10^{-5}	2.00×10^{-4}	179
5.49×10^{-5}	3.00×10^{-4}	390
5.49×10^{-5}	4.00×10^{-4}	587
5.49×10^{-5}	5.00×10^{-4}	860

$k_2 = 2.24 \times 10^6$ M^{-1} s^{-1}

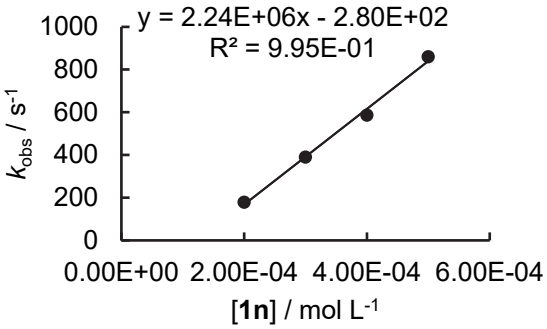

1n-**K** + **2i** in DMF (stopped-flow, detection at 382 nm)

$[\mathbf{2i}]_0$, mol L^{-1}	$[\mathbf{1n}]_0$, mol L^{-1}	k_{obs}, s^{-1}
2.54×10^{-5}	2.00×10^{-4}	203
2.54×10^{-5}	3.00×10^{-4}	496
2.54×10^{-5}	4.00×10^{-4}	846
2.54×10^{-5}	5.00×10^{-4}	1.10×10^3

$k_2 = 3.04 \times 10^6$ M^{-1} s^{-1}

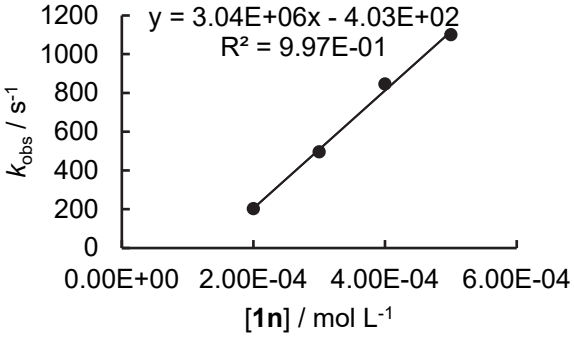

Determination of N and s_N parameters for **1n**-K in DMF.

Reference Electrophile	Electrophilicity E	k_2 (M^{-1} s^{-1})	lg k_2
2j	–13.84	6.44×10^4	4.81
2g	–13.39	3.12×10^5	5.49
2h	–12.18	2.24×10^6	6.35
2i	–11.87	3.04×10^6	6.48

$N = 19.90$

$s_N = 0.82$

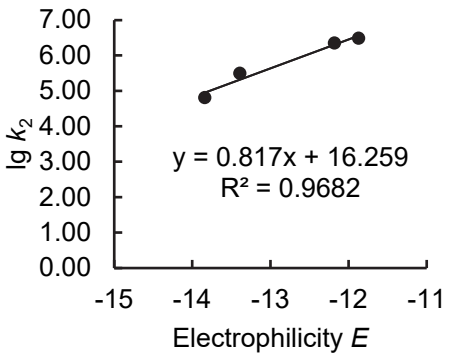

4.11 Kinetics of Reactions of Phenolates in Water

4-Methylphenol / KOH in water

pK_a 10.28 (from ref. 15) of 4-methylphenol used for the analysis.

2a + **1l** in alkaline 99.5/0.5 (v/v) H_2O/CH_3CN (stopped-flow, detection at 630 nm)

[**2a**]$_0$, mol L^{-1}	[**1l**-H]$_0$, mol L^{-1}	[OH$^-$]$_0$, mol L^{-1}	[**1l**], mol L^{-1}	[OH$^-$], mol L^{-1}	k_{obs}, s^{-1}	k_{OH}[OH$^-$], s^{-1}	k_2[**1l**], s^{-1}
9.32×10^{-6}	2.00×10^{-4}	1.00×10^{-2}	1.96×10^{-4}	9.80×10^{-3}	6.91×10^{-2}	2.12×10^{-2}	4.79×10^{-2}
9.32×10^{-6}	4.00×10^{-4}	1.00×10^{-2}	3.92×10^{-4}	9.60×10^{-3}	1.20×10^{-1}	2.08×10^{-2}	9.92×10^{-2}
9.32×10^{-6}	6.00×10^{-4}	1.00×10^{-2}	5.88×10^{-4}	9.40×10^{-3}	1.68×10^{-1}	2.03×10^{-2}	1.48×10^{-1}
9.32×10^{-6}	8.00×10^{-4}	1.00×10^{-2}	7.84×10^{-4}	9.20×10^{-3}	1.99×10^{-1}	1.99×10^{-2}	1.79×10^{-1}
9.32×10^{-6}	1.00×10^{-3}	1.00×10^{-2}	9.79×10^{-4}	9.00×10^{-3}	2.77×10^{-1}	1.95×10^{-2}	2.58×10^{-1}

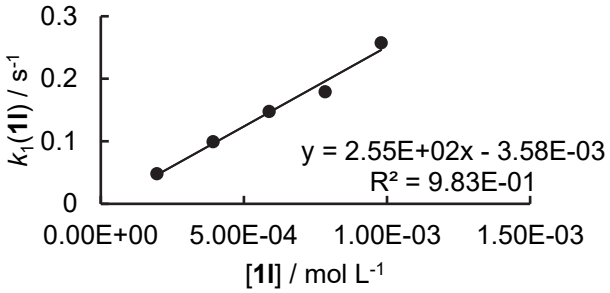

$k_2 = 2.55 \times 10^2$ M^{-1} s^{-1}

$k_{OH} = 2.16$ M^{-1} s^{-1}

2b + **1l** in alkaline 99.5/0.5 (v/v) H_2O/CH_3CN (stopped-flow, detection at 634 nm)

[**2b**]$_0$, mol L^{-1}	[**1l**-H]$_0$, mol L^{-1}	[OH$^-$]$_0$, mol L^{-1}	[**1l**], mol L^{-1}	[OH$^-$], mol L^{-1}	k_{obs}, s^{-1}	k_{OH}[OH$^-$], s^{-1}	k_2[**1l**], s^{-1}
6.76×10^{-6}	2.00×10^{-4}	1.00×10^{-2}	1.96×10^{-4}	9.80×10^{-3}	7.20×10^{-2}	3.37×10^{-2}	3.83×10^{-2}
6.76×10^{-6}	4.00×10^{-4}	1.00×10^{-2}	3.92×10^{-4}	9.60×10^{-3}	1.59×10^{-1}	3.30×10^{-2}	1.26×10^{-1}
6.76×10^{-6}	6.00×10^{-4}	1.00×10^{-2}	5.88×10^{-4}	9.40×10^{-3}	2.25×10^{-1}	3.23×10^{-2}	1.93×10^{-1}
6.76×10^{-6}	8.00×10^{-4}	1.00×10^{-2}	7.84×10^{-4}	9.20×10^{-3}	2.83×10^{-1}	3.17×10^{-2}	2.51×10^{-1}
6.76×10^{-6}	1.00×10^{-3}	1.00×10^{-2}	9.79×10^{-4}	9.00×10^{-3}	3.85×10^{-1}	3.10×10^{-2}	3.54×10^{-1}

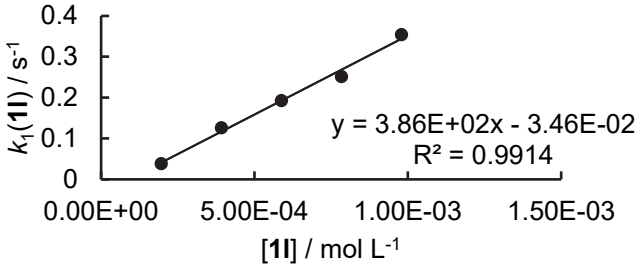

$k_2 = 3.86 \times 10^2$ M^{-1} s^{-1}

$k_{OH} = 3.44$ M^{-1} s^{-1}

2c + **1l** in alkaline 99.5/0.5 (v/v) H_2O/CH_3CN (stopped-flow, detection at 614 nm)

$[\mathbf{2c}]_0$, mol L^{-1}	$[\mathbf{1l}\text{-H}]_0$, mol L^{-1}	$[OH^-]_0$, mol L^{-1}	$[\mathbf{1l}]$, mol L^{-1}	$[OH^-]$, mol L^{-1}	k_{obs}, s^{-1}	$k_{OH}[OH^-]$, s^{-1}	$k_2[\mathbf{1l}]$, s^{-1}
8.21×10^{-6}	2.00×10^{-4}	1.00×10^{-2}	1.96×10^{-4}	9.80×10^{-3}	2.99×10^{-1}	1.06×10^{-1}	1.93×10^{-1}
8.21×10^{-6}	4.00×10^{-4}	1.00×10^{-2}	3.92×10^{-4}	9.60×10^{-3}	5.23×10^{-1}	1.04×10^{-1}	4.19×10^{-1}
8.21×10^{-6}	6.00×10^{-4}	1.00×10^{-2}	5.88×10^{-4}	9.40×10^{-3}	7.70×10^{-1}	1.02×10^{-1}	6.68×10^{-1}
8.21×10^{-6}	8.00×10^{-4}	1.00×10^{-2}	7.84×10^{-4}	9.20×10^{-3}	9.82×10^{-1}	9.94×10^{-2}	8.83×10^{-1}
8.21×10^{-6}	1.00×10^{-3}	1.00×10^{-2}	9.79×10^{-4}	9.00×10^{-3}	1.19	9.73×10^{-2}	1.09E+00

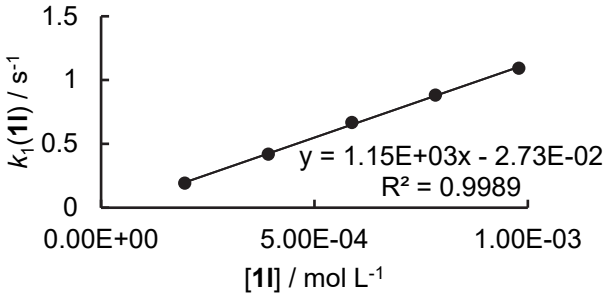

$k_2 = 1.15 \times 10^3$ M^{-1} s^{-1}

$k_{OH} = 10.8$ M^{-1} s^{-1}

2e + **1l** in alkaline 99.5/0.5 (v/v) H_2O/CH_3CN (stopped-flow, detection at 610 nm)

$[\mathbf{2e}]_0$, mol L^{-1}	$[\mathbf{1l}\text{-H}]_0$, mol L^{-1}	$[OH^-]_0$, mol L^{-1}	$[\mathbf{1l}]$, mol L^{-1}	$[OH^-]$, mol L^{-1}	k_{obs}, s^{-1}	$k_{OH}[OH^-]$, s^{-1}	$k_2[\mathbf{1l}]$, s^{-1}
6.44×10^{-6}	2.00×10^{-4}	1.00×10^{-2}	1.96×10^{-4}	9.80×10^{-3}	9.99×10^{-1}	4.76×10^{-1}	5.23×10^{-1}
6.44×10^{-6}	4.00×10^{-4}	1.00×10^{-2}	3.92×10^{-4}	9.60×10^{-3}	1.80	4.66×10^{-1}	1.33
6.44×10^{-6}	6.00×10^{-4}	1.00×10^{-2}	5.88×10^{-4}	9.40×10^{-3}	2.54	4.57×10^{-1}	2.08
6.44×10^{-6}	8.00×10^{-4}	1.00×10^{-2}	7.84×10^{-4}	9.20×10^{-3}	3.58	4.47×10^{-1}	3.13
6.44×10^{-6}	1.00×10^{-3}	1.00×10^{-2}	9.79×10^{-4}	9.00×10^{-3}	4.51	4.38×10^{-1}	4.07

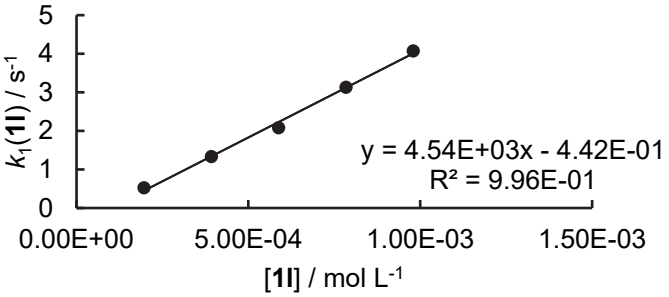

$k_2 = 4.54 \times 10^3$ M^{-1} s^{-1}

$k_{OH} = 58.5$ M^{-1} s^{-1}

Determination of N and s_N parameters for **1l**-K in water.

Reference Electrophile	Electrophilicity E	k_2 (M^{-1} s^{-1})	lg k_2
2a	−10.04	2.55×10^2	2.41
2b	−9.45	3.86×10^2	2.59
2c	−8.76	1.15×10^3	3.06
2e	−7.69	4.54×10^3	3.66

N = 14.30

s_N = 0.55

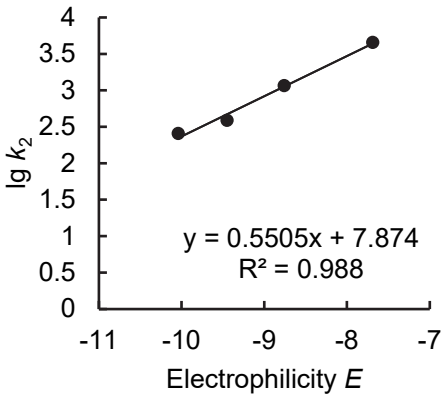

4.12 NMR Kinetics (Figure 7)

2a-BF_4 + 1d-NBu_4

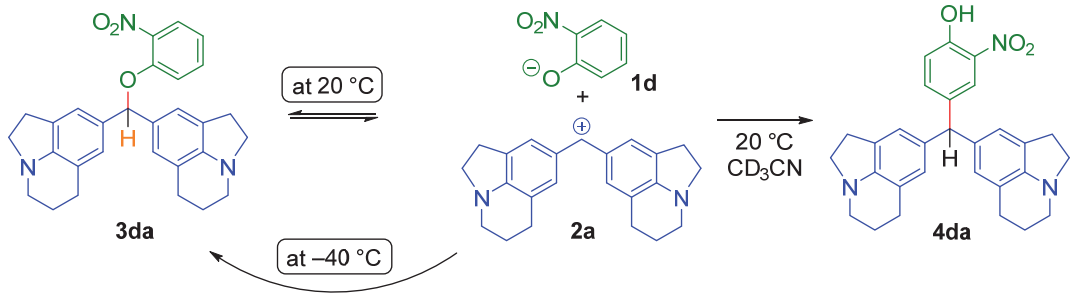

(RM774)

Isomerization from **3da** to **4da** at 20 °C was monitored by ^{1}H NMR spectroscopy. The product of C-4 attack (**4da**) was not formed exclusively. Further resonances in the range from δ = 5.0 to 5.5 ppm indicate the formation of minor amounts of further C-attack products.

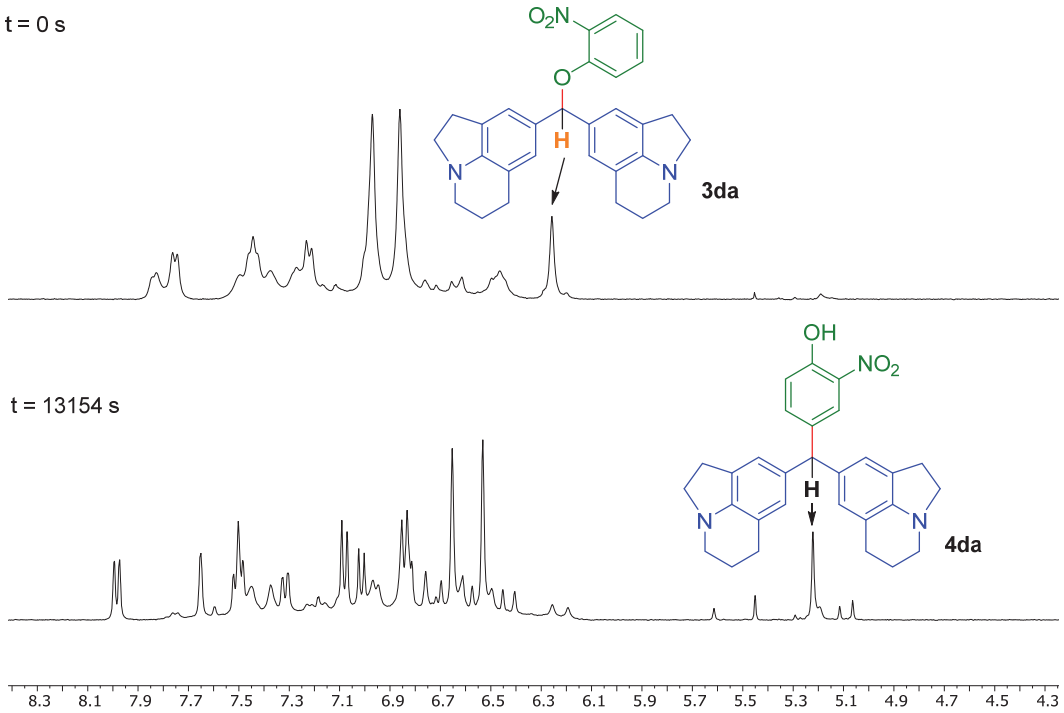

4.13 Kinetics of the Reactions of Phenolates with Benzyl Bromide in DMSO (Figure 12)

1c-NBu_4 + benzyl bromide in DMSO (stopped-flow, detection at 437 nm)

$[\mathbf{1c}]_0$, mol L^{-1}	$[BnBr]_0$, mol L^{-1}	k_{obs}, s^{-1}
2.93×10^{-5}	1.00×10^{-3}	2.06
2.93×10^{-5}	2.00×10^{-3}	3.24
2.93×10^{-5}	3.00×10^{-3}	4.55
2.93×10^{-5}	4.00×10^{-3}	5.35
2.93×10^{-5}	5.00×10^{-3}	6.14

$k_2 = 1.03 \times 10^3$ M^{-1} s^{-1}

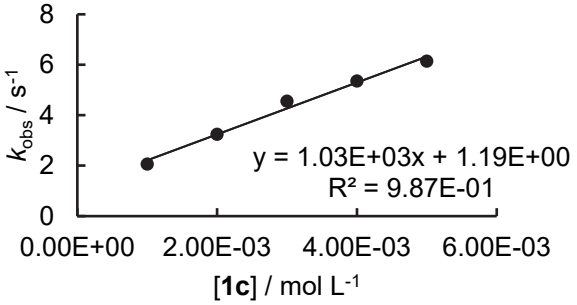

1d-NBu_4 + benzyl bromide in DMSO (stopped-flow, detection at 455 nm)

$[\mathbf{1d}]_0$, mol L^{-1}	$[BnBr]_0$, mol L^{-1}	k_{obs}, s^{-1}
5.89×10^{-5}	1.00×10^{-3}	2.20
5.89×10^{-5}	2.00×10^{-3}	3.37
5.89×10^{-5}	3.00×10^{-3}	4.51
5.89×10^{-5}	4.00×10^{-3}	5.13
5.89×10^{-5}	5.00×10^{-3}	5.97

$k_2 = 9.30 \times 10^2$ M^{-1} s^{-1}

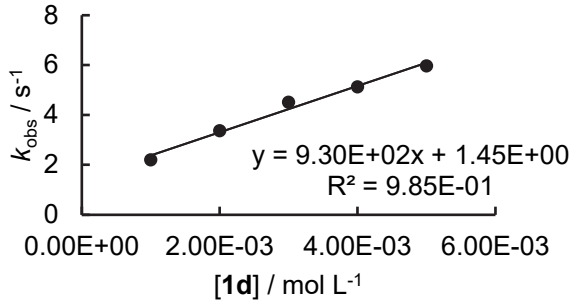

1f-K + benzyl bromide in DMSO (stopped-flow, detection at 299 nm)

$[\mathbf{1d}]_0$, mol L^{-1}	$[BnBr]_0$, mol L^{-1}	k_{obs}, s^{-1}
3.75×10^{-5}	1.00×10^{-3}	41.9
3.75×10^{-5}	2.00×10^{-3}	88.9
3.75×10^{-5}	3.00×10^{-3}	139
3.75×10^{-5}	4.00×10^{-3}	181
3.75×10^{-5}	5.00×10^{-3}	228

$k_2 = 4.64 \times 10^4$ M^{-1} s^{-1}

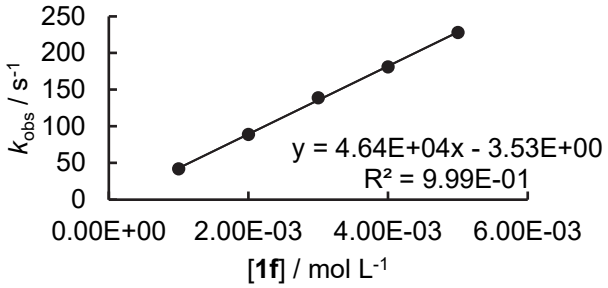

1h-K + **BnBr** in DMSO (stopped-flow, detection at 315 nm)

$[\mathbf{1d}]_0$, mol L^{-1}	$[BnBr]_0$, mol L^{-1}	k_{obs}, s^{-1}
9.94×10^{-5}	2.00×10^{-3}	355
9.94×10^{-5}	3.00×10^{-3}	566
9.94×10^{-5}	4.00×10^{-3}	744
9.94×10^{-5}	5.00×10^{-3}	859

$k_2 = 1.69 \times 10^5$ M^{-1} s^{-1}

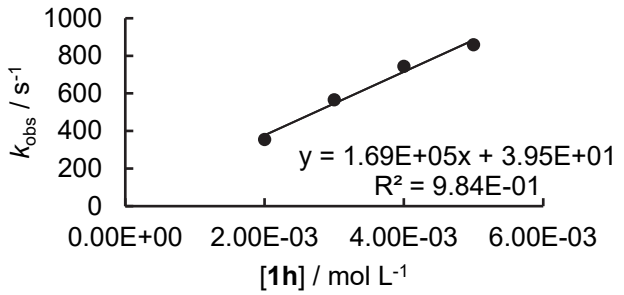

4.14 Regioselectivities in Kinetically Controlled Reactions of Phenolate Ions with Electrophiles (Table 8)

Intramolecular Competition Experiments

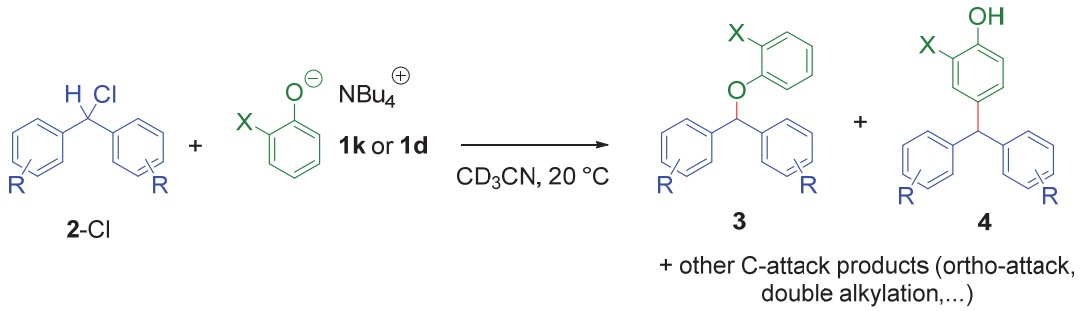

In an argon-filled glovebox, a solution of the tetrabutylammonium phenolate **1**-NBu_4 in 0.75 mL of anhydrous CD_3CN (distilled over CaH_2 and stored over molecular sieves) was added to an equimolar amount of the solid electrophile **2**-Cl (or **2u**-OTs). The resulting solution was mixed and then transferred into an NMR tube, sealed, and submitted to analysis (^{1}H NMR, ^{1}H,^{13}C-HSQC).

Reaction	Phenolate	Electrophile	**3**:**4**
1k-NBu_4 + **2o**-BF_4 (RNH241)	7.0 mg, 0.021 mmol	10.0 mg, 0.021 mmol	100:0
1k-NBu_4 + **2p**-Cl (RNH208)	12.1 mg, 0.036 mmol	10.3 mg, 0.036 mmol	83:17
1k-NBu_4 + **2q**-Cl (RNH222)	12.9 mg, 0.039 mmol	10.6 mg, 0.039 mmol	78:22
1k-NBu_4 + **2r**-Cl (RNH225)	13.5 mg, 0.040 mmol	10.6 mg, 0.040 mmol	78:22
1k-NBu_4 + **2s**-Cl (RNH215)	16.6 mg, 0.049 mmol	11.5 mg, 0.049 mmol	46:54
1k-NBu_4 + **2n**-Cl (RM924-1)	17.5 mg, 0.052 mmol	12.0 mg, 0.052 mmol	85:15 (89% conv)[a]
1k-NBu_4 + **2t**-Cl (RNH236)	15.5 mg, 0.046 mmol	10.0 mg, 0.046 mmol	100:0 (80% conv)[b]
1k-NBu_4 + **2u**-Cl (RM925-1)	18.2 mg, 0.054 mmol	11.0 mg, 0.054 mmol	100:0 (86% conv)[a]
1k-NBu_4 + **2u**-OTs (RNH218)	9.3 mg, 0.028 mmol	8.3 mg, 0.025 mmol	43:57
1d-NBu_4 + **2o**-BF_4 (RNH242)	8.0 mg, 0.021 mmol	10.0 mg, 0.021 mmol	100:0
1d-NBu_4 + **2p**-Cl (RNH197)	13.5 mg, 0.036 mmol	10.2 mg, 0.036 mmol	100:0
1d-NBu_4 + **2q**-Cl (RNH223)	14.7 mg, 0.039 mmol	10.6 mg, 0.039 mmol	98:2
1d-NBu_4 + **2r**-Cl (RNH193)	14.5 mg, 0.038 mmol	10.0 mg, 0.038 mmol	94:6
1d-NBu_4 + **2s**-Cl (RNH216)	16.7 mg, 0.044 mmol	10.2 mg, 0.044 mmol	78:22
1d-NBu_4 + **2n**-Cl (RM924-2)	20.6 mg, 0.054 mmol	12.5 mg, 0.054 mmol	84:16 (89% conv)[a]
1d-NBu_4 + **2t**-Cl (RNH237)	18.1 mg, 0.048 mmol	10.3 mg, 0.048 mmol	100:0 (80% conv)[b]
1d-NBu_4 + **2u**-Cl (RM925-2)	22.9 mg, 0.060 mmol	12.2 mg, 0.060 mmol	100:0 (37% conv)[a]
1d-NBu_4 + **2u**-OTs (RNH219)	12.0 mg, 0.032 mmol	10.0 mg, 0.030 mmol	76:24

[a] After 3 d at ambient temperature. [b] After 2 d at ambient temperature.

A representative example (reaction of **1k**-NBu_4 + **2p**-Cl) is depicted below:

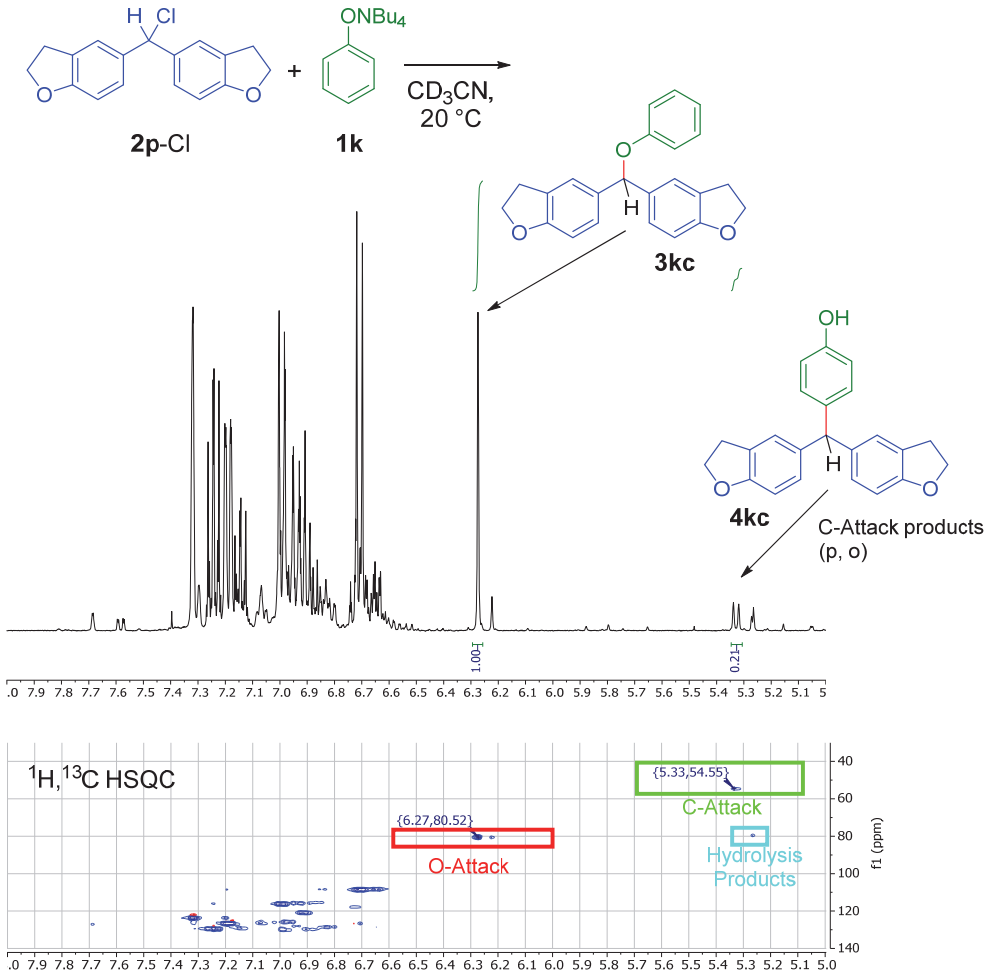

Intermolecular Competition Experiments

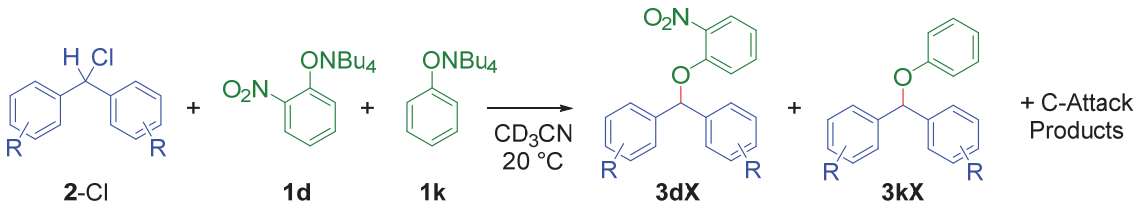

In an argon-filled glovebox, a solution of equimolar amounts of the tetrabutylammonium phenolates **1d**-NBu_4 and **1k**-NBu_4 in 0.75 mL of anhydrous CD_3CN (distilled over CaH_2 and stored over molecular sieves) was added to 0.5 equivs of the solid electrophile **2**(**p–u**)-Cl (or **2o**-BF_4) and mixed. The resulting solution was transferred into an NMR tube, sealed and submitted to analysis (^1H NMR, $^1H,^{13}C$-HSQC).

Reaction	Electrophile **2**	Phenolate **1k**	Phenolate **1d**	**3kX**: **3dX**: CA[a]
1k-NBu_4 + **1d**-NBu_4 + **2o**-BF_4 (RNH241)	10.0 mg, 0.021 mmol	7.0 mg, 0.021 mmol	8.0 mg, 0.021 mmol	86:14:0
1k-NBu_4 + **1d**-NBu_4 + **2p**-Cl (RM930-4)	10.5 mg, 0.037 mmol	12.3 mg, 0.037 mmol	13.9 mg, 0.037 mmol	43:47:10
1k-NBu_4 + **1d**-NBu_4 + **2q**-Cl (RNH282)	10.7 mg, 0.039 mmol	13.1 mg, 0.039 mmol	14.8 mg, 0.039 mmol	33:56:11
1k-NBu_4 + **1d**-NBu_4 + **2r**-Cl (RM930-3)	10.8 mg, 0.041 mmol	13.8 mg, 0.041 mmol	15.6 mg, 0.041 mmol	25:58:17
1k-NBu_4 + **1d**-NBu_4 + **2s**-Cl (RNH234)	10.8 mg, 0.046 mmol	15.6 mg, 0.046 mmol	17.7 mg, 0.046 mmol	22:46:32
1k-NBu_4 + **1d**-NBu_4 + **2n**-Cl (RM930-2)	11.4 mg, 0.049 mmol	16.6 mg, 0.049 mmol	18.8 mg, 0.049 mmol	47:36:17
1k-NBu_4 + **1d**-NBu_4 + **2t**-Cl (RNH235)	11.4 mg, 0.053 mmol	17.7 mg, 0.053 mmol	20.0 mg, 0.053 mmol	78:22:0
1k-NBu_4 + **1d**-NBu_4 + **2u**-Cl (RM930-1)	10.0 mg, 0.049 mmol	16.6 mg, 0.049 mmol	18.8 mg, 0.049 mmol	93:7:0

[a] Integral ratios (CA: different products from C-attack at phenolates were summarized in the integration).

The benzhydryl ethers originating from the different phenolates were assigned based on the previous experiments, in which we studied the products of the reactions of benzhydryl chlorides with **1d** and **1k** separately.

To also reflect contributions by the C-attack at phenolates, the product ratio of aryl benzhydryl ethers **3kX/3dX** was corrected with the results of the intramolecular competition experiment.

For example, for the reaction of **2n**-Cl with **1k**-NBu_4 and **1d**-NBu_4 a ratio of the aryl benzhydryl ethers **3kn/3dn** of 47:36 was detected along with some further products of C-attack. With the information from the intramolecular competition experiments that **1k**-NBu_4 reacts with **2n**-Cl to give an O/C ratio of 85:15 (or analogously for **1d**-NBu_4 with **2n**-Cl: 84:16) it becomes possible to calculate the ratio of **1k**- vs **1d**-derived products.

$$\frac{Products\ originating\ from\ \mathbf{1k}}{Products\ originating\ from\ \mathbf{1d}} = \frac{47 + 47 * \frac{15}{85}}{36 + 36 * \frac{16}{84}} = \frac{55}{43}$$

In theory the fractions of **1k**- vs **1d**-derived products should add up to 100 %. Deviations from this result are attributed to experimental inaccuracies of the integration of the ^1H NMR spectra of the crude reaction mixtures.

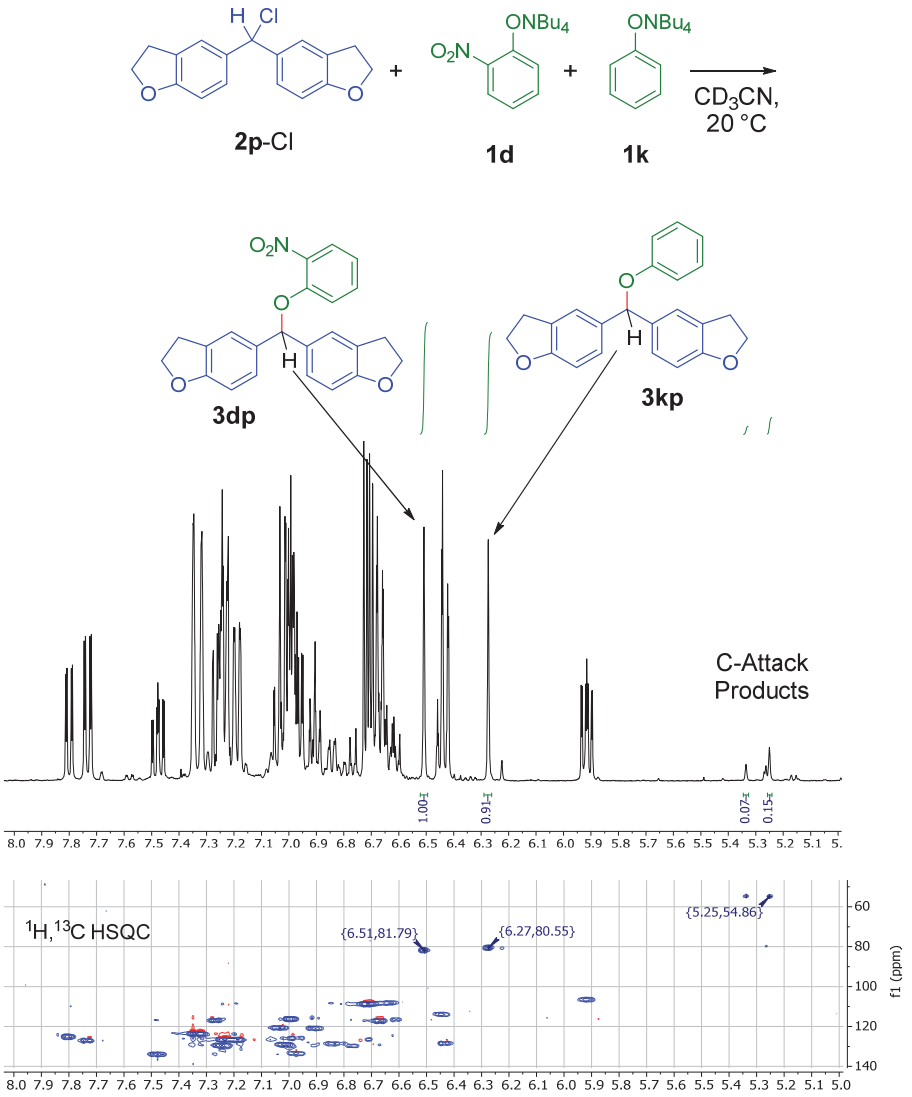
H Cl
ONBu4
O2N
ONBu4
CD3CN,
20 °C
2p-Cl
1d
1k
O2N
3dp
3kp
C-Attack
Products
1.00
0.91
0.07
0.15
8.0 7.9 7.8 7.7 7.6 7.5 7.4 7.3 7.2 7.1 7.0 6.9 6.8 6.7 6.6 6.5 6.4 6.3 6.2 6.1 6.0 5.9 5.8 5.7 5.6 5.5 5.4 5.3 5.2 5.1 5.
1H,13C HSQC
{6.51,81.79}
{6.27,80.55}
{5.25,54.86}
60
80
100
120
140
f1 (ppm)
8.0 7.9 7.8 7.7 7.6 7.5 7.4 7.3 7.2 7.1 7.0 6.9 6.8 6.7 6.6 6.5 6.4 6.3 6.2 6.1 6.0 5.9 5.8 5.7 5.6 5.5 5.4 5.3 5.2 5.1 5.0

4.15 S_N1 vs S_N2 – Kinetics (Figure 18)

Measurements with the Nucleophile in Excess

Tetrabutylammonium tetrafluoroborate was added to achieve a constant ionic strength $I = 2.00 \times 10^{-4}$ M for the different reaction mixtures at 20 °C.

1d-NBu_4 + NBu_4BF_4 + **2r**-Cl in MeCN (stopped-flow, detection at 448 nm, RM927)

[**1d**]$_0$, mol L^{-1}	[NBu_4BF_4]$_0$, mol L^{-1}	[**2r**-Cl]$_0$, mol L^{-1}	k_{obs}, s^{-1}
1.00×10^{-4}	1.00×10^{-4}	2.50×10^{-5}	0.657
1.25×10^{-4}	0.75×10^{-4}	2.50×10^{-5}	0.656
1.50×10^{-4}	0.50×10^{-4}	2.50×10^{-5}	0.669
1.75×10^{-4}	0.25×10^{-4}	2.50×10^{-5}	0.678
2.00×10^{-4}	--	2.50×10^{-5}	0.679

1d-NBu_4 + NBu_4BF_4 + **2q**-Cl in MeCN (stopped-flow, detection at 448 nm, RM927)

[**1d**]$_0$, mol L^{-1}	[NBu_4BF_4]$_0$, mol L^{-1}	[**2q**-Cl]$_0$, mol L^{-1}	k_{obs}, s^{-1}
1.00×10^{-4}	1.00×10^{-4}	2.50×10^{-5}	7.43
1.25×10^{-4}	0.75×10^{-4}	2.50×10^{-5}	7.52
1.50×10^{-4}	0.50×10^{-4}	2.50×10^{-5}	7.47
1.75×10^{-4}	0.25×10^{-4}	2.50×10^{-5}	7.70
2.00×10^{-4}	--	2.50×10^{-5}	7.54

Measurements with the Electrophile in Excess

The kinetics for reactions of phenolates (at constant concentration) with an excess of the benzhydryl chlorides was measured in acetonitrile at 20 °C.

1c-NBu_4 + **2r**-Cl or **2q**-Cl in MeCN (stopped-flow, detection at 448 nm, RM929)

[**1c**]$_0$, mol L^{-1}	[**2r**-Cl]$_0$, mol L^{-1}	k_{obs}, s^{-1}	[**2q**-Cl]$_0$, mol L^{-1}	k_{obs}, s^{-1}
1.05×10^{-4}	1.00×10^{-3}	8.56	1.00×10^{-3}	58.1
1.05×10^{-4}	2.00×10^{-3}	17.8	2.00×10^{-3}	119
1.05×10^{-4}	3.00×10^{-3}	25.6	3.00×10^{-3}	175
1.05×10^{-4}	4.00×10^{-3}	33.3	4.00×10^{-3}	236
1.05×10^{-4}	5.00×10^{-3}	42.7	5.00×10^{-3}	307

1d-NBu_4 + **2r**-Cl or **2q**-Cl in MeCN (stopped-flow, detection at 448 nm, RM926)

[**1d**]$_0$, mol L^{-1}	[**2r**-Cl]$_0$, mol L^{-1}	k_{obs}, s^{-1}	[**2q**-Cl]$_0$, mol L^{-1}	k_{obs}, s^{-1}
1.05×10^{-4}	1.00×10^{-3}	7.52	1.00×10^{-3}	52.4
1.05×10^{-4}	2.00×10^{-3}	14.5	2.00×10^{-3}	115
1.05×10^{-4}	3.00×10^{-3}	21.0	3.00×10^{-3}	174
1.05×10^{-4}	4.00×10^{-3}	27.8	4.00×10^{-3}	241
1.05×10^{-4}	5.00×10^{-3}	34.6		

4.16 Computational Investigations

Benzhydrylium ion 2b

Electronic and Gibbs energies for the phenolate anions **2b** at the SMD(MeCN)/M06-2X/6-31+G(d,p) level. Conformers were taken from ref. 16.

2b			
File	E_{tot}	G_{298}	Contribution
REDO_jul_oa_2	-1079.125582	-1078.680906	0.0155
REDO_jul_oa_3	-1079.125426	-1078.681727	0.0371
REDO_jul_oa_4	-1079.125254	-1078.681266	0.0228
REDO_jul_oa_5	-1079.126529	-1078.683049	0.1508
REDO_jul_oa_6	-1079.126479	-1078.682766	0.1117
REDO_jul_oa_9	-1079.126318	-1078.682355	0.0723
REDO_jul_oa_10	-1079.126399	-1078.682728	0.1073
REDO_jul_oa_13	-1079.127402	-1078.683350	0.2074
REDO_jul_oa_14	-1079.127349	-1078.682676	0.1015
REDO_jul_oa_16	-1079.127458	-1078.683182	0.1736
Boltzmann weighted		-1078.682857	

Phenolates 1

Electronic and Gibbs energies for the phenolate anions **1** at the SMD(MeCN)/M06-2X/6-31+G(d,p) level.

Compound	File	E_{tot}	G_{298}
1a (2,4-NO_2)	dinitro_phenolat_2	-715.776966	-715.716442
1b (F_5)	pfp_sm_1	-802.909288	-802.892677
1c (4-NO_2)	pnp_m06_631_smd	-511.337467	-511.275328
1d (2-NO_2)	o_no2_phenolat_1	-511.328373	-511.266407
1e (3-NO_2)	m_no2_phenolat_1	-511.324836	-511.263555
1f (4-CN)	p_cn_sm_1	-399.114856	-399.055497
1g (2-CF_3)	o_cf3_phenolat_1	-643.845138	-643.782465
1h (4-CF_3)	p_cf3_sm_1	-643.844641	-643.783658
1i (3-CF_3)	m_cf3_phenolat_1	-643.840680	-643.781454
1j (4-Cl)	p_cl_sm_1	-766.451880	-766.400584
1k (H)	h_sm_1	-306.879010	-306.815943
1l (4-CH_3)	p_me_phenolat_1	-346.175193	-346.087781
1m (4-tBu)	p_tbu_phenolat_1	-464.065627	-463.896407
1n (4-MeO)	p_meo_phenolat_1	-421.356541	-421.264359
1o (2,6-tBu)	tbu2_sm	-621.247684	-620.970789
1q (3-MeO)	mmeo_phenolate	-421.364553	-421.271953

Electronic and Gibbs energies for the phenolate anions **1** at the M06-2X/6-31+G(d,p) level in gas-phase (used for HOMO energies).

Compound	File	E_{tot}	G_{298}
1c (4-NO_2)	REDO_REDO_pnp_m06_631_smd	-511.261764	-511.199223
1d (2-NO_2)	REDO_REDO_o_no2_phenolat_1	-511.245983	-511.184798
1e (3-NO_2)	REDO_REDO_m_no2_phenolat_1	-511.245930	-511.184382
1f (4-CN)	REDO_REDO_p_cn_phenolate	-399.034950	-398.975692
1g (2-CF_3)	REDO_REDO_o_cf3_phenolat_1	-643.762205	-643.699715
1h (4-CF_3)	REDO_REDO_p_cf3_sm_1	-643.765654	-643.704392
1i (3-CF_3)	REDO_REDO_m_cf3_phenolat_1	-643.760252	-643.699153
1j (4-Cl)	REDO_REDO_p_cl_sm_1	-766.366537	-766.315551
1k (H)	REDO_REDO_h_sm_1	-306.787432	-306.724756
1l (4-CH_3)	REDO_REDO_p_me_phenolat_1	-346.083401	-345.994990

1m (4-tBu)	REDO_REDO_p_tbu_phenolat_1	-463.974941	-463.805958
1n (4-MeO)	REDO_REDO_p_meo_phenolat_1	-421.263807	-421.172340
1o (2,6-tBu)	REDO_tbu2_sm_gas	-621.170746	-620.893144
1q (3-MeO)	REDO_REDO_mmeo_phenolate	-421.272878	-421.180593

Oxygen Attack Products 3Xb

Electronic and Gibbs energies for the oxygen-attack products **3Xb** at the SMD(MeCN)/M06-2X/6-31+G(d,p) level.

3ab (2,4-NO_2)	E_{tot}	G_{298}	Contribution
REDO_dinitro_jul_o1	-1794.920637	-1794.391160	0.0037
REDO_dinitro_jul_o2	-1794.920902	-1794.393940	0.0712
REDO_dinitro_jul_o3	-1794.920867	-1794.393785	0.0604
REDO_dinitro_jul_o4	-1794.920703	-1794.394572	0.1390
REDO_dinitro_jul_o5	-1794.921607	-1794.394779	0.1732
REDO_dinitro_jul_o21	-1794.921570	-1794.394613	0.1452
REDO_dinitro_jul_o22	-1794.921607	-1794.394876	0.1920
REDO_dinitro_jul_o23	-1794.921557	-1794.394974	0.2129
REDO_dinitro_jul_o24	-1794.916836	-1794.390276	0.0015
REDO_dinitro_jul_o25	-1794.916889	-1794.389783	0.0009
Boltzmann weighted		-1794.394642	

3bb (F_5)	E_{tot}	G_{298}	Contribution
pfp_jul_sm_1_3	-1882.063220	-1881.581265	0.1780
pfp_jul_sm_2	-1882.063163	-1881.580573	0.0855
pfp_jul_sm_3	-1882.063140	-1881.581101	0.1497
pfp_jul_sm_4	-1882.063184	-1881.580950	0.1275
pfp_jul_sm_5	-1882.061944	-1881.580936	0.1257
pfp_jul_sm_6	-1882.060696	-1881.579807	0.0380
pfp_jul_sm_7	-1882.061965	-1881.580859	0.1158
pfp_jul_sm_8	-1882.061897	-1881.580757	0.1039
pfp_jul_sm_9	-1882.060721	-1881.579777	0.0368
pfp_jul_sm_10	-1882.060772	-1881.579832	0.0390
Boltzmann weighted		-1881.580834	

3cb (4-NO_2)	E_{tot}	G_{298}	Contribution
REDO_p_no2_jul_sm_1	-1590.490642	-1589.961494	0.0001
REDO_p_no2_jul_sm_2	-1590.496474	-1589.969259	0.2586
REDO_p_no2_jul_sm_3	-1590.490523	-1589.961219	0.0001
REDO_p_no2_jul_sm_4	-1590.496422	-1589.968655	0.1363
REDO_p_no2_jul_sm_5	-1590.490624	-1589.961382	0.0001
REDO_p_no2_jul_sm_6	-1590.496568	-1589.968790	0.1572
REDO_p_no2_jul_sm_7	-1590.496552	-1589.968457	0.1104
REDO_p_no2_jul_sm_8	-1590.496497	-1589.968610	0.1299
REDO_p_no2_jul_sm_9	-1590.496520	-1589.968558	0.1229
REDO_p_no2_jul_sm_10	-1590.496509	-1589.968204	0.0845
Boltzmann weighted		-1589.968753	

3db (2-NO_2)	E_{tot}	G_{298}	Contribution
REDO_o_no2_jul1	-1590.481040	-1589.951487	0.0002
REDO_o_no2_jul2	-1590.480936	-1589.951727	0.0002
REDO_o_no2_jul3	-1590.480892	-1589.951535	0.0002
REDO_o_no2_jul4	-1590.487235	-1589.958987	0.4434
REDO_o_no2_jul5	-1590.480984	-1589.951313	0.0001

REDO_o_no2_jul6	-1590.480759	-1589.951774	0.0002
REDO_o_no2_jul7	-1590.480826	-1589.951920	0.0002
REDO_o_no2_jul8	-1590.487210	-1589.958439	0.2480
REDO_o_no2_jul9	-1590.479650	-1589.951557	0.0002
REDO_o_no2_jul10	-1590.487235	-1589.958641	0.3073
Boltzmann weighted		-1589.958735	

3eb (3-NO_2)	E_{tot}	G_{298}	Contribution
REDO_m_no2_jul_sm_conf1	-1590.488616	-1589.959291	0.0003
REDO_m_no2_jul_sm_conf2	-1590.488586	-1589.959139	0.0002
REDO_m_no2_jul_sm_conf3	-1590.493602	-1589.965495	0.1838
REDO_m_no2_jul_sm_conf4	-1590.488570	-1589.959245	0.0002
REDO_m_no2_jul_sm_conf5	-1590.493620	-1589.965713	0.2316
REDO_m_no2_jul_sm_conf6	-1590.488522	-1589.959452	0.0003
REDO_m_no2_jul_sm_conf7	-1590.493638	-1589.965960	0.3009
REDO_m_no2_jul_sm_conf8	-1590.487529	-1589.958479	0.0001
REDO_m_no2_jul_sm_conf9_2	-1590.493629	-1589.965900	0.2824
REDO_m_no2_jul_sm_conf10	-1590.487458	-1589.959083	0.0002
Boltzmann weighted		-1589.965791	

3fb (4-CN)	E_{tot}	G_{298}	Contribution
REDO_p_cn_jul_sm_1	-1478.279196	-1477.753761	0.0904
REDO_p_cn_jul_sm_2	-1478.273170	-1477.746304	0.0000
REDO_p_cn_jul_sm_3	-1478.279174	-1477.753654	0.0807
REDO_p_cn_jul_sm_4	-1478.279167	-1477.754729	0.2524
REDO_p_cn_jul_sm_5	-1478.273103	-1477.746187	0.0000
REDO_p_cn_jul_sm_6	-1478.279188	-1477.754197	0.1436
REDO_p_cn_jul_sm_7	-1478.273141	-1477.746217	0.0000
REDO_p_cn_jul_sm_8	-1478.279144	-1477.754226	0.1481
REDO_p_cn_jul_sm_9	-1478.279176	-1477.754391	0.1763
REDO_p_cn_jul_sm_10	-1478.279162	-1477.753933	0.1084
Boltzmann weighted		-1477.754257	

3gb (2-CF_3)	E_{tot}	G_{298}	Contribution
REDO_o_cf3_jul1	-1723.005452	-1722.475641	0.0003
REDO_o_cf3_jul2	-1723.005565	-1722.476004	0.0005
REDO_o_cf3_jul3	-1723.005511	-1722.475630	0.0003
REDO_o_cf3_jul4	-1723.011444	-1722.482471	0.4616
REDO_o_cf3_jul5	-1723.005419	-1722.475530	0.0003
REDO_o_cf3_jul6	-1723.011466	-1722.481999	0.2800
REDO_o_cf3_jul7	-1723.011491	-1722.481913	0.2555
REDO_o_cf3_jul8	-1723.003663	-1722.476842	0.0012
REDO_o_cf3_jul9	-1723.004155	-1722.475256	0.0002
REDO_o_cf3_jul10	-1723.003597	-1722.474731	0.0001
Boltzmann weighted		-1722.482177	

3hb (4-CF_3)	E_{tot}	G_{298}	Contribution
p_cf3_jul_sm_1	-1723.007229	-1722.477519	0.0000
p_cf3_jul_sm_2	-1723.007279	-1722.477416	0.0000
p_cf3_jul_sm_3	-1723.013112	-1722.485168	0.1457
p_cf3_jul_sm_4	-1723.007270	-1722.478197	0.0001
p_cf3_jul_sm_5	-1723.013181	-1722.484693	0.0881
p_cf3_jul_sm_6	-1723.007193	-1722.477328	0.0000
p_cf3_jul_sm_7	-1723.013226	-1722.486217	0.4434

p_cf3_jul_sm_8	-1723.013070	-1722.484286	0.0572
p_cf3_jul_sm_9	-1723.013233	-1722.485316	0.1706
p_cf3_jul_sm_10	-1723.013221	-1722.484763	0.0948
Boltzmann weighted		-1722.485526	

3ib (3-CF_3)	E_{tot}	G_{298}	Contribution
REDO_m_cf3_jul_sm_conf1	-1723.006621	-1722.478583	0.0014
REDO_m_cf3_jul_sm_conf2	-1723.006648	-1722.477668	0.0005
REDO_m_cf3_jul_sm_conf3	-1723.005854	-1722.476621	0.0002
REDO_m_cf3_jul_sm_conf4	-1723.005922	-1722.476977	0.0003
REDO_m_cf3_jul_sm_conf5_4	-1723.011853	-1722.484163	0.5253
REDO_m_cf3_jul_sm_conf6_2	-1723.005778	-1722.476517	0.0002
REDO_m_cf3_jul_sm_conf7	-1723.011493	-1722.483462	0.2498
REDO_m_cf3_jul_sm_conf8_2	-1723.006672	-1722.477680	0.0005
REDO_m_cf3_jul_sm_conf9	-1723.011518	-1722.483348	0.2214
REDO_m_cf3_jul_sm_conf10	-1723.006612	-1722.477312	0.0004
Boltzmann weighted		-1722.483786	

3jb (4-Cl)	E_{tot}	G_{298}	Contribution
p_cl_jul_sm_1	-1845.625434	-1845.108056	0.1371
p_cl_jul_sm_2	-1845.619675	-1845.100896	0.0001
p_cl_jul_sm_3	-1845.619556	-1845.101002	0.0001
p_cl_jul_sm_4	-1845.625437	-1845.108438	0.2055
p_cl_jul_sm_5	-1845.625456	-1845.108147	0.1509
p_cl_jul_sm_6	-1845.625419	-1845.107741	0.0982
p_cl_jul_sm_7	-1845.625426	-1845.108094	0.1428
p_cl_jul_sm_8	-1845.625475	-1845.107740	0.0980
p_cl_jul_sm_9	-1845.619680	-1845.100855	0.0001
p_cl_jul_sm_10	-1845.625386	-1845.108244	0.1673
Boltzmann weighted		-1845.108121	

3kb (4-H)	E_{tot}	G_{298}	Contribution
h_jul_sm_1	-1386.049861	-1385.519767	0.0001
h_jul_sm_2	-1386.055712	-1385.526245	0.1358
h_jul_sm_3	-1386.055724	-1385.526742	0.2298
h_jul_sm_4	-1386.055706	-1385.526325	0.1478
h_jul_sm_5	-1386.055688	-1385.526081	0.1141
h_jul_sm_6	-1386.055720	-1385.526068	0.1125
h_jul_sm_7	-1386.055746	-1385.525946	0.0989
h_jul_sm_8	-1386.055740	-1385.526405	0.1608
h_jul_sm_9	-1386.049696	-1385.519854	0.0002
h_jul_sm_10	-1386.049832	-1385.519595	0.0001
Boltzmann weighted		-1385.526326	

3lb (4-CH_3)	E_{tot}	G_{298}	Contribution
REDO_p_me_jul_sm_1	-1425.354321	-1424.799766	0.0383
REDO_p_me_jul_sm_2	-1425.354323	-1424.801616	0.2726
REDO_p_me_jul_sm_3	-1425.348534	-1424.793095	0.0000
REDO_p_me_jul_sm_4_2	-1425.354345	-1424.799862	0.0424
REDO_p_me_jul_sm_5	-1425.354338	-1424.801633	0.2774
REDO_p_me_jul_sm_6	-1425.354371	-1424.799885	0.0435
REDO_p_me_jul_sm_7_2	-1425.354366	-1424.801560	0.2569
REDO_p_me_jul_sm_8	-1425.348335	-1424.793184	0.0000
REDO_p_me_jul_sm_9	-1425.348444	-1424.793236	0.0000

REDO_p_me_jul_sm_10	-1425.354390	-1424.800317	0.0688
Boltzmann weighted		-1424.801296	

3mb (4-tBu)	E_{tot}	G_{298}	Contribution
REDO_p_tbu_jul_sm_conf1	-1543.244403	-1542.608850	0.1014
REDO_p_tbu_jul_sm_conf2	-1543.238731	-1542.601647	0.0000
REDO_p_tbu_jul_sm_conf3	-1543.244506	-1542.609293	0.1622
REDO_p_tbu_jul_sm_conf4	-1543.238648	-1542.602150	0.0001
REDO_p_tbu_jul_sm_conf5	-1543.244547	-1542.609307	0.1647
REDO_p_tbu_jul_sm_conf6	-1543.244329	-1542.609234	0.1524
REDO_p_tbu_jul_sm_conf7	-1543.244357	-1542.608978	0.1161
REDO_p_tbu_jul_sm_conf8	-1543.244427	-1542.608608	0.0784
REDO_p_tbu_jul_sm_conf9	-1543.244618	-1542.608491	0.0693
REDO_p_tbu_jul_sm_conf10	-1543.244601	-1542.609252	0.1553
Boltzmann weighted		-1542.609088	

3nb (4-MeO)	E_{tot}	G_{298}	Contribution
REDO_p_meo_jul_sm_1	-1500.536136	-1499.978058	0.1325
REDO_p_meo_jul_sm_2	-1500.536142	-1499.978171	0.1493
REDO_p_meo_jul_sm_3	-1500.537768	-1499.978470	0.2050
REDO_p_meo_jul_sm_4	-1500.535692	-1499.977442	0.0689
REDO_p_meo_jul_sm_5	-1500.536178	-1499.978252	0.1627
REDO_p_meo_jul_sm_6	-1500.532053	-1499.971929	0.0002
REDO_p_meo_jul_sm_7	-1500.531925	-1499.972975	0.0006
REDO_p_meo_jul_sm_8	-1500.536152	-1499.978044	0.1305
REDO_p_meo_jul_sm_9	-1500.535630	-1499.978176	0.1501
REDO_p_meo_jul_sm_10	-1500.532068	-1499.972045	0.0002
Boltzmann weighted		-1499.978159	

3ob (2,6-tBu)	E_{tot}	G_{298}	Contribution
REDO_tbu2_oa_1	-1700.414389	-1699.667036	0.1240
REDO_tbu2_oa_2	-1700.414362	-1699.667011	0.1208
REDO_tbu2_oa_3	-1700.414287	-1699.666669	0.0841
REDO_tbu2_oa_4	-1700.412340	-1699.666994	0.1186
REDO_tbu2_oa_5	-1700.412856	-1699.666753	0.0919
REDO_tbu2_oa_6	-1700.412297	-1699.665460	0.0233
REDO_tbu2_oa_7	-1700.412275	-1699.666761	0.0927
REDO_tbu2_oa_8	-1700.414312	-1699.666534	0.0729
REDO_tbu2_oa_9	-1700.412899	-1699.666596	0.0778
REDO_tbu2_oa_10	-1700.412237	-1699.667457	0.1938
Boltzmann weighted		-1699.666920	

3qb (3-MeO)	E_{tot}	G_{298}	Contribution
REDO_mmeo_oa_1	-1500.540672	-1499.982135	0.2143
REDO_mmeo_oa_2	-1500.540705	-1499.981269	0.0856
REDO_mmeo_oa_3	-1500.540736	-1499.981871	0.1621
REDO_mmeo_oa_4	-1500.535521	-1499.975789	0.0003
REDO_mmeo_oa_5	-1500.540715	-1499.981524	0.1122
REDO_mmeo_oa_6	-1500.540711	-1499.981239	0.0829
REDO_mmeo_oa_7	-1500.540705	-1499.982041	0.1940
REDO_mmeo_oa_8	-1500.534642	-1499.975383	0.0002
REDO_mmeo_oa_9	-1500.540712	-1499.981780	0.1472
REDO_mmeo_oa_10	-1500.535440	-1499.977285	0.0013
Boltzmann weighted		-1499.981796	

Carbon Attack Products 4Xb

Electronic and Gibbs energies for the carbon-attack products **4Xb** at the SMD(MeCN)/M06-2X/6-31+G(d,p) level.

4cb (4-NO_2, dienone), ortho-attack	E_{tot}	G_{298}	Contribution
REDO_pno2_qi_1	-1590.471543	-1589.943517	0.1439
REDO_pno2_qi_2	-1590.471622	-1589.943482	0.1387
REDO_pno2_qi_3	-1590.471698	-1589.943271	0.1108
REDO_pno2_qi_4	-1590.471654	-1589.943022	0.0852
REDO_pno2_qi_5	-1590.469920	-1589.942699	0.0604
REDO_pno2_qi_6	-1590.469819	-1589.943288	0.1129
REDO_pno2_qi_7	-1590.469955	-1589.943032	0.0860
REDO_pno2_qi_8	-1590.469785	-1589.941004	0.0100
REDO_pno2_qi_9	-1590.469866	-1589.942830	0.0695
REDO_pno2_qi_10	-1590.469716	-1589.943741	0.1825
Boltzmann weighted		-1589.943294	

4cb (4-NO_2), ortho-attack	E_{tot}	G_{298}	Contribution
REDO_pno2_ca_1	-1590.511558	-1589.983374	0.2497
REDO_pno2_ca_2	-1590.511517	-1589.981041	0.0211
REDO_pno2_ca_3	-1590.511521	-1589.982610	0.1111
REDO_pno2_ca_4	-1590.511469	-1589.983403	0.2575
REDO_pno2_ca_5	-1590.510015	-1589.982164	0.0692
REDO_pno2_ca_6	-1590.510029	-1589.982582	0.1078
REDO_pno2_ca_7	-1590.510065	-1589.981869	0.0507
REDO_pno2_ca_8	-1590.510111	-1589.980663	0.0141
REDO_pno2_ca_9	-1590.509734	-1589.982505	0.0994
REDO_pno2_ca_10	-1590.510153	-1589.980962	0.0194
Boltzmann weighted		-1589.982831	

4db (2-NO_2, dienone), ortho-attack	E_{tot}	G_{298}	Contribution
REDO_ono2_o_qi_1_2	-1590.465619	-1589.936224	0.1137
REDO_ono2_o_qi_2	-1590.465637	-1589.936625	0.1738
REDO_ono2_o_qi_3	-1590.464790	-1589.935309	0.0431
REDO_ono2_o_qi_4	-1590.465670	-1589.936334	0.1277
REDO_ono2_o_qi_5	-1590.464697	-1589.934792	0.0249
REDO_ono2_o_qi_6	-1590.464773	-1589.935298	0.0426
REDO_ono2_o_qi_7	-1590.465625	-1589.936497	0.1518
REDO_ono2_o_qi_8	-1590.464683	-1589.934649	0.0214
REDO_ono2_o_qi_9	-1590.462956	-1589.935161	0.0368
REDO_ono2_o_qi_10	-1590.465005	-1589.937020	0.2641
Boltzmann weighted		-1589.936372	

4db (2-NO_2), ortho-attack	E_{tot}	G_{298}	Contribution
REDO_ono2_o_ca_1	-1590.507962	-1589.978782	0.1256
REDO_ono2_o_ca_2	-1590.507949	-1589.978472	0.0904
REDO_ono2_o_ca_3	-1590.507922	-1589.978624	0.1062
REDO_ono2_o_ca_4	-1590.507893	-1589.978702	0.1153
REDO_ono2_o_ca_5	-1590.506032	-1589.979210	0.1977
REDO_ono2_o_ca_6	-1590.506016	-1589.978713	0.1167
REDO_ono2_o_ca_7	-1590.505922	-1589.978337	0.0783

REDO_ono2_o_ca_8	-1590.506005	-1589.978270	0.0729
REDO_ono2_o_ca_9	-1590.505914	-1589.976339	0.0094
REDO_ono2_o_ca_10	-1590.505952	-1589.978441	0.0875
Boltzmann weighted		-1589.978680	

4db (2-NO_2, dienone), para-attack	E_{tot}	G_{298}	Contribution
REDO_ono2_p_qi_1	-1590.466729	-1589.939231	0.1101
REDO_ono2_p_qi_2	-1590.466989	-1589.939141	0.1001
REDO_ono2_p_qi_3	-1590.466701	-1589.939290	0.1172
REDO_ono2_p_qi_4	-1590.466701	-1589.938988	0.0851
REDO_ono2_p_qi_5	-1590.466808	-1589.938634	0.0584
REDO_ono2_p_qi_6	-1590.466958	-1589.939681	0.1774
REDO_ono2_p_qi_7	-1590.466811	-1589.938545	0.0532
REDO_ono2_p_qi_8	-1590.466809	-1589.938367	0.0441
REDO_ono2_p_qi_9	-1590.466839	-1589.939212	0.1079
REDO_ono2_p_qi_10	-1590.466965	-1589.939500	0.1464
Boltzmann weighted		-1589.939216	

4db (2-NO_2), para-attack	E_{tot}	G_{298}	Contribution
REDO_ono2_p_ca_1	-1590.506797	-1589.979175	0.0725
REDO_ono2_p_ca_2	-1590.507641	-1589.978977	0.0588
REDO_ono2_p_ca_3	-1590.506757	-1589.979060	0.0642
REDO_ono2_p_ca_4	-1590.506740	-1589.981141	0.5826
REDO_ono2_p_ca_5	-1590.507648	-1589.978909	0.0547
REDO_ono2_p_ca_6	-1590.506774	-1589.978326	0.0294
REDO_ono2_p_ca_7	-1590.507668	-1589.978980	0.0590
REDO_ono2_p_ca_8	-1590.507630	-1589.978980	0.0589
REDO_ono2_p_ca_9	-1590.504871	-1589.977384	0.0109
REDO_ono2_p_ca_10_2	-1590.504835	-1589.977223	0.0092
Boltzmann weighted		-1589.980202	

4fb (4-CN, dienone), ortho-attack	E_{tot}	G_{298}	Contribution
REDO_pcn_jul_qi_1	-1478.254432	-1477.728361	0.0982
REDO_pcn_jul_qi_2	-1478.254501	-1477.728643	0.1325
REDO_pcn_jul_qi_3	-1478.254487	-1477.728379	0.1001
REDO_pcn_jul_qi_4	-1478.254511	-1477.728764	0.1507
REDO_pcn_jul_qi_5	-1478.252659	-1477.727814	0.0550
REDO_pcn_jul_qi_6	-1478.252701	-1477.728018	0.0683
REDO_pcn_jul_qi_7	-1478.252594	-1477.728912	0.1762
REDO_pcn_jul_qi_8	-1478.252577	-1477.728518	0.1160
REDO_pcn_jul_qi_9	-1478.252556	-1477.728280	0.0901
REDO_pcn_jul_qi_10	-1478.252635	-1477.726442	0.0129
Boltzmann weighted		-1477.728491	

4kb (4-CN), ortho-attack	E_{tot}	G_{298}	Contribution
REDO_pcn_jul_ca_1	-1478.293886	-1477.767690	0.1231
REDO_pcn_jul_ca_2	-1478.293852	-1477.767720	0.1270
REDO_pcn_jul_ca_3	-1478.293879	-1477.767983	0.1679
REDO_pcn_jul_ca_4	-1478.293856	-1477.767780	0.1354
REDO_pcn_jul_ca_5	-1478.292340	-1477.767416	0.0920
REDO_pcn_jul_ca_6	-1478.292031	-1477.766006	0.0206
REDO_pcn_jul_ca_7	-1478.292375	-1477.766991	0.0586

REDO_pcn_jul_ca_8	-1478.292079	-1477.767344	0.0852
REDO_pcn_jul_ca_9	-1478.292047	-1477.767462	0.0967
REDO_pcn_jul_ca_10	-1478.292315	-1477.767430	0.0934
Boltzmann weighted		-1477.767579	

4kb (4-H, dienone), ortho-attack	E_{tot}	G_{298}	Contribution
REDO_h_o_qi_1	-1386.034286	-1385.504943	0.0385
REDO_h_o_qi_2	-1386.034318	-1385.505373	0.0606
REDO_h_o_qi_3	-1386.034282	-1385.504825	0.0339
REDO_h_o_qi_4	-1386.034312	-1385.505073	0.0441
REDO_h_o_qi_5	-1386.034972	-1385.506699	0.2474
REDO_h_o_qi_6	-1386.034980	-1385.506285	0.1595
REDO_h_o_qi_7	-1386.034944	-1385.507072	0.3672
REDO_h_o_qi_8	-1386.032336	-1385.504422	0.0221
REDO_h_o_qi_9	-1386.032349	-1385.504377	0.0211
REDO_h_o_qi_10	-1386.032367	-1385.503106	0.0055
Boltzmann weighted		-1385.506368	

4kb (4-H), ortho-attack	E_{tot}	G_{298}	Contribution
REDO_h_o_ca_1	-1386.070244	-1385.540174	0.0612
REDO_h_o_ca_2	-1386.070219	-1385.541044	0.1540
REDO_h_o_ca_3	-1386.070208	-1385.541610	0.2805
REDO_h_o_ca_4	-1386.070214	-1385.541202	0.1821
REDO_h_o_ca_5	-1386.070194	-1385.540881	0.1295
REDO_h_o_ca_6	-1386.069298	-1385.539797	0.0411
REDO_h_o_ca_7	-1386.068295	-1385.537996	0.0061
REDO_h_o_ca_8	-1386.069317	-1385.538540	0.0108
REDO_h_o_ca_9	-1386.068276	-1385.540031	0.0526
REDO_h_o_ca_10	-1386.068527	-1385.540451	0.0821
Boltzmann weighted		-1385.540958	

4kb (4-H, dienone), para-attack	E_{tot}	G_{298}	Contribution
REDO_h_p_qi_1	-1386.037484	-1385.508189	0.1415
REDO_h_p_qi_2	-1386.037555	-1385.508256	0.1520
REDO_h_p_qi_3	-1386.037483	-1385.508368	0.1712
REDO_h_p_qi_4	-1386.037543	-1385.508266	0.1536
REDO_h_p_qi_5_2	-1386.035618	-1385.507470	0.0661
REDO_h_p_qi_6	-1386.035598	-1385.507842	0.0980
REDO_h_p_qi_7	-1386.035620	-1385.507841	0.0979
REDO_h_p_qi_8	-1386.035572	-1385.506090	0.0153
REDO_h_p_qi_9	-1386.035623	-1385.507273	0.0536
REDO_h_p_qi_10	-1386.035606	-1385.507225	0.0509
Boltzmann weighted		-1385.507996	

4kb (4-H), para-attack	E_{tot}	G_{298}	Contribution
REDO_h_p_ca_1	-1386.068403	-1385.540385	0.0765
REDO_h_p_ca_2	-1386.068366	-1385.540406	0.0782
REDO_h_p_ca_3	-1386.068396	-1385.538081	0.0066
REDO_h_p_ca_4	-1386.068405	-1385.541664	0.2967
REDO_h_p_ca_5	-1386.068347	-1385.540853	0.1256
REDO_h_p_ca_6	-1386.068343	-1385.540930	0.1364
REDO_h_p_ca_7	-1386.068372	-1385.541292	0.2001

REDO_h_p_ca_8	-1386.068379	-1385.537490	0.0036
REDO_h_p_ca_9	-1386.066316	-1385.539696	0.0368
REDO_h_p_ca_10	-1386.066333	-1385.539759	0.0394
Boltzmann weighted		-1385.541005	

4nb (4-MeO), ortho-attack	E_{tot}	G_{298}	Contribution
REDO_pmeo_qi_1	-1500.520784	-1499.960908	0.1001
REDO_pmeo_qi_2	-1500.520838	-1499.961107	0.1235
REDO_pmeo_qi_3	-1500.520810	-1499.960746	0.0842
REDO_pmeo_qi_4	-1500.520828	-1499.961039	0.1150
REDO_pmeo_qi_5	-1500.518935	-1499.960564	0.0694
REDO_pmeo_qi_6	-1500.515039	-1499.955143	0.0002
REDO_pmeo_qi_7	-1500.520666	-1499.961590	0.2062
REDO_pmeo_qi_8	-1500.520603	-1499.961709	0.2338
REDO_pmeo_qi_9	-1500.518826	-1499.960534	0.0673
REDO_pmeo_qi_10	-1500.515041	-1499.955242	0.0002
Boltzmann weighted		-1499.961210	

4nb (4-MeO, dienone), ortho-attack	E_{tot}	G_{298}	Contribution
REDO_pmeo_ca_1	-1500.552367	-1499.992816	0.1327
REDO_pmeo_ca_2	-1500.552376	-1499.992859	0.1388
REDO_pmeo_ca_3	-1500.552371	-1499.992796	0.1299
REDO_pmeo_ca_4	-1500.552363	-1499.992759	0.1248
REDO_pmeo_ca_5	-1500.552333	-1499.992423	0.0875
REDO_pmeo_ca_6	-1500.552328	-1499.992169	0.0668
REDO_pmeo_ca_7	-1500.552313	-1499.992515	0.0964
REDO_pmeo_ca_8	-1500.550750	-1499.992200	0.0690
REDO_pmeo_ca_9	-1500.550696	-1499.992377	0.0832
REDO_pmeo_ca_10	-1500.550444	-1499.992226	0.0710
Boltzmann weighted		-1499.992585	

4qb (3-MeO, dienone), para-attack	E_{tot}	G_{298}	Contribution
REDO_mmeo_p_qi_1	-1500.532149	-1499.971978	0.2475
REDO_mmeo_p_qi_2	-1500.532174	-1499.971190	0.1073
REDO_mmeo_p_qi_3	-1500.532219	-1499.971699	0.1841
REDO_mmeo_p_qi_4	-1500.532085	-1499.971859	0.2181
REDO_mmeo_p_qi_5	-1500.529555	-1499.970311	0.0422
REDO_mmeo_p_qi_6	-1500.529570	-1499.970380	0.0455
REDO_mmeo_p_qi_7	-1500.529582	-1499.970093	0.0335
REDO_mmeo_p_qi_8	-1500.529586	-1499.970260	0.0400
REDO_mmeo_p_qi_9	-1500.529544	-1499.970544	0.0541
REDO_mmeo_p_qi_10	-1500.529555	-1499.969910	0.0276
Boltzmann weighted		-1499.971407	

4qb (3-MeO), para-attack	E_{tot}	G_{298}	Contribution
REDO_mmeo_p_ca_1	-1500.553498	-1499.994087	0.0748
REDO_mmeo_p_ca_2	-1500.553482	-1499.994306	0.0944
REDO_mmeo_p_ca_3	-1500.553510	-1499.994504	0.1164
REDO_mmeo_p_ca_4	-1500.553506	-1499.994192	0.0836
REDO_mmeo_p_ca_5	-1500.553875	-1499.994763	0.1532

REDO_mmeo_p_ca_6	-1500.553862	-1499.994553	0.1227
REDO_mmeo_p_ca_7	-1500.553477	-1499.994305	0.0943
REDO_mmeo_p_ca_8	-1500.553903	-1499.994241	0.0881
REDO_mmeo_p_ca_9	-1500.553485	-1499.993899	0.0613
REDO_mmeo_p_ca_10	-1500.553862	-1499.994460	0.1111
Boltzmann weighted		-1499.994390	

Summary of Quantum-Chemical Calculations (Table 7)

Summary of calculated Gibbs energies for the reactions of phenolates **1** with the benzhydrylium ion **2b** at the SMD(MeCN)/M06-2X/6-31+G(d,p) level of theory

		G_{298} [Hartree]		[kJ/mol]
2b	weighted	-1078.682857		
1a	dinitro_phenolat_2	-715.716442		
3ab	weighted	-1794.394642	Δ_rG^0(O) =	4.3
1b	pfp_sm_1	-802.892677		
3bb	weighted	-1881.580834	Δ_rG^0(O) =	-21.8
1c	pnp_m06_631_smd	-511.275328		
	REDO_p_no2_jul_sm_2_ts1	-1589.936566	$\Delta G^{\ddagger}$(O) =	48.8
3cb	weighted	-1589.968753	Δ_rG^0(O) =	-35.7
	REDO_pno2_qi_10_ts1	-1589.925475	$\Delta G^{\ddagger}$(C) =	78.0
CHD	weighted	-1589.943294	Δ_rG^0(C) =	31.2
4cb	weighted	-1589.982831	Δ_rG^0(P) =	-72.6
1d	o_no2_phenolat_1	-511.266407		
	o_no2_jul4_ts1	-1589.929446	$\Delta G^{\ddagger}$(O) =	44.1
3db	weighted	-1589.958735	Δ_rG^0(O) =	-32.8
	REDO_ono2_o_qi_2_ts1f	-1589.916726	$\Delta G^{\ddagger}(C_{ortho})$ =	77.5
CHD	weighted	-1589.936372	$\Delta_rG^0(C_{ortho})$ =	25.9
4db$_{ortho}$	weighted	-1589.978680	$\Delta_rG^0(P_{ortho})$ =	-85.1
	REDO_ono2_p_qi_6_ts1	-1589.912886		
	REDO_ono2_p_qi_6_ts2	-1589.918394	$\Delta G^{\ddagger}(C_{para})$ =	73.1
CHD	weighted	-1589.939216	$\Delta_rG^0(C_{para})$ =	18.5
4db$_{para}$	weighted	-1589.980202	$\Delta_rG^0(P_{para})$ =	-89.1
1e	m_no2_phenolat_1	-511.263555		
3eb	REDO_m_no2_jul_sm_conf10	-1589.965791	Δ_rG^0(O) =	-58.8
1f	p_cn_sm_1	-399.055497		
	p_cn_jul_sm_ts1_2	-1477.719450	$\Delta G^{\ddagger}$(O) =	41.7
3fb	weighted	-1477.754257	Δ_rG^0(O) =	-49.7
	REDO_pcn_jul_qi_7_ts1	-1477.708679	$\Delta G^{\ddagger}$(C) =	70.0
CHD	weighted	-1477.728491	Δ_rG^0(C) =	18.0
4fb	weighted	-1477.767579	Δ_rG^0(P) =	-84.6
1g	o_cf3_phenolat_1	-643.782465		
3gb	weighted	-1722.482177	Δ_rG^0(O) =	-52.2
1h	p_cf3_sm_1	-643.783658		
3hb	weighted	-1722.485526	Δ_rG^0(O) =	-57.8
1i	m_cf3_phenolat_1	-643.781454		

3ib	weighted	-1722.483786	Δ_rG^0(O) =	-59.0
1j	p_cl_sm_1	-766.400584		
3jb	weighted	-1845.108121	Δ_rG^0(O) =	-72.7
1k	h_sm_1	-306.815943		
	h_jul_sm_3_ts1	-1385.484948	$\Delta G^‡$(O) =	28.5
3kb	weighted	-1385.526326	Δ_rG^0(O) =	-80.2
	REDO_h_o_qi_8_ts1	-1385.475996	$\Delta G^‡$(C_{ortho}) =	52.0
CHD	weighted	-1385.506368	Δ_rG^0(C_{ortho}) =	-27.8
4kb$_{ortho}$	weighted	-1385.540958	Δ_rG^0(P_{ortho}) =	-118.6
	REDO_h_p_qi_3_ts1	-1385.471398		
	REDO_h_p_qi_3_ts2_2	-1385.477075	$\Delta G^‡$(C_{para}) =	49.1
CHD	weighted	-1385.507996	Δ_rG^0(C_{para}) =	-32.1
4kb$_{para}$	weighted	-1385.541005	Δ_rG^0(P_{para}) =	-118.7
1l	p_me_phenolat_1	-346.087781		
3lb	weighted	-1424.801296	Δ_rG^0(O) =	-88.4
1m	p_tbu_phenolat_1	-463.896407		
3mb	weighted	-1542.609088	Δ_rG^0(O) =	-86.2
1n	p_meo_phenolat_1	-421.264359		
	REDO_p_meo_jul_sm_3_ts1	-1499.936263	$\Delta G^‡$(O) =	20.8
3nb	weighted	-1499.978159	Δ_rG^0(O) =	-89.2
	REDO_pmeo_qi_8_ts1	-1499.929120	$\Delta G^‡$(C) =	39.6
CHD	weighted	-1499.961210	Δ_rG^0(C) =	-44.7
4nb	weighted	-1499.992585	Δ_rG^0(P) =	-127.0
1o	tbu2_sm	-620.970789		
3ob	REDO_tbu2_oa_10	-1699.666920	Δ_rG^0(O) =	-42.8
1q	mmeo_phenolate	-421.271953		
	REDO_mmeo_oa_1_ts1	-1499.941504	$\Delta G^‡$(O) =	27.0
3qb	weighted	-1499.981796	Δ_rG^0(O) =	-78.8
	REDO_mmeo_p_qi_1_ts1	-1499.937854	$\Delta G^‡$(C) =	36.6
CHD	weighted	-1499.971407	Δ_rG^0(C) =	-51.5
4qb$_{para}$	weighted	-1499.994390	Δ_rG^0(P) =	-111.8

4.17 References

[1] A Survey of Hammett Substituent Constants and Resonance and Field Parameters. Hansch, C.; Leo, A.; Taft, R. W. *Chem. Rev.* **1991**, *91*, 165–195.

[2] Substituent Effects on the Stabilities of Phenoxyl Radicals and the Acidities of Phenoxyl Radical Cations. Bordwell F. G.; Cheng, J.-P. *J. Am. Chem. Soc.* **1991**, *113*, 1736–1743.

[3] Dissociation Constants of Uncharged and Monovalent Cation Acids in Dimethyl Sulfoxide. Kolthoff, I. M.; Chantooni Jr., M. K.; Bhowmik, S. *J. Am. Chem. Soc.* **1968**, *90*, 23–28.

[4] Pentakis(trifluoromethyl)phenyl, a Sterically Crowded and Electron-withdrawing Group: Synthesis and Acidity of Pentakis(trifluoromethyl)benzene, -toluene, -phenol, and -aniline. Kütt, A.; Movchun, V.; Rodima, T.; Dansauer, T.; Rusanov, E. B.; Leito, I.; Kaljurand, I.; Koppel, J.; Pihl, V.; Koppel, I.; Ovsjannikov, G.; Toom, L.; Mishima, M.; Medebielle, M.; Lork, E.; Röschenthaler, G.-V.; Koppel, I. A.; Kolomeitsev, A. A. *J. Org. Chem.* **2008**, *73*, 2607–2620.

[5] Scope and limitations of a ^{1}H NMR method for the prediction of substituted phenols pK_a values in water, CH_3CN, DMF, DMSO and *i*-PrOH. Penhoat, M. *Tetrahedron Lett.* **2013**, *54*, 2571–2574.

[6] Ortho Effect of the Alkylthio Group. Dissociation Constants of 4-tert-Butyl-2-(alkylthio)phenols in Acetonitrile. Voronkov, M. G.; Kashik, T. V.; Ponomareva, S. M.; Kuliev, F. A.; Farzaliev, V. M. *J. Gen. Chem. USSR (Engl. Transl.)* **1979**, *49*, 1813–1817; *Zh. Obshch. Khim*. **1979**, *49*, 2063–2068.

[7] Enthalpy–Entropy Correlations in Reactions of Aryl Benzoates with Potassium Aryloxides in Dimethylformamide. Khalfina, I. A.; Vlasov, V. M. *Int. J. Chem. Kin.* **2013**, *45*, 266–282.

[8] Electrochemical Determination of the pK_a of Weak Acids in *N*,*N*-Dimethylformamide. Maran, F.; Celadon, D.; Severin, M. G.; Vianello, E. *J. Am. Chem. Soc.* **1991**, *113*, 9320–9329

[9] Nucleophilicity and Basicity. Cripe, T. A. Ph. D. Dissertation, Nothwestern University, Evanston, Illinois, 1986.

[10] Kinetics and Thermodynamics of Phenolate Silylation and Alkylation. Ellington, J. C.; Arnett, E. M. *J. Am. Chem. Soc.* **1988**, *110*, 7778–7785.

[11] Electronic and Steric Effects in Nucleophilic Aromatic Substitution. Reaction by Phenoxides as Nucleophiles in Dimethyl Sulfoxide. Bartoli, G.; Ciminale, F.; Todesco, P. E. *J. Org. Chem.* **1975**, *40*, 872–874.

[12] Heterolysis and Homolysis Energies for Some Carbon-Oxygen Bonds. Arnett, E. M.; Amarnath, K.; Harvey, N. G.; Venimadhavan, S. *J. Am. Chem. Soc.* **1990**, *112*, 7346–7353.

[13] A Comprehensive Self-Consistent Spectrophotometric Acidity Scale of Neutral Brønsted Acids in Acetonitrile. Kütt, A.; Leito, I.; Kaljurand, I.; Sooväli, L.; Vlasov, V. M.; Yagupolskii, L. M.; Koppel, I. A. *J. Org. Chem.*, **2006**, *71*, 2829–2838.

[14] Metallocenes as references for the determination of redox potentials by cyclic voltammetry - Permethylated iron and cobalt sandwich complexes, inhibition by polyamine dendrimers, and the role of hydroxy-containing ferrocenes. Aranzaes, J. R.; Daniel, M.-C.; Astruc, D. *Can. J. Chem.* **2006**, *84*, 288–299.

[15] One-Electron Redox Potentials of Phenols in Aqueous Solution. Li, C.; Hoffman, M. Z. *J. Phys. Chem. B* **1999**, *103*, 6653–6656.

[16] Synthesis, Structure and Properties of Amino-Substituted Benzhydrylium Ions - a Link Between Ordinary Carbocations and Neutral Electrophiles. Mayer, R. J.; Hampel, N.; Mayer, P.; Ofial, A. R.; Mayr, H. *Eur. J. Org. Chem.* **2019**, 412–421.

Chapter 5. Nucleophilicity of Glutathione: A Link to Michael Acceptor Reactivities

R. J. Mayer, A. R. Ofial, *Angew. Chem. Int. Ed.* **2019**, *58*, 17704-17708; *Angew. Chem.* **2019**, *131*, 17868-17872.

Author Contributions

RJM performed all experiments and calculations. The manuscript was written jointly by RJM and ARO.

Copyright

Selected supporting material for this work is provided starting with section 5.1. The complete supporting information (SI) is published online and can be accessed under https://doi.org/10.1002/anie.201909803.

GDCh Communications Angewandte International Edition Chemie

Electrophilicity

International Edition: DOI: 10.1002/anie.201909803
German Edition: DOI: 10.1002/ange.201909803

Nucleophilicity of Glutathione: A Link to Michael Acceptor Reactivities

*Robert J. Mayer and Armin R. Ofial**

Abstract: *Deprotonated glutathione is among the most potent biological nucleophiles and plays an important physiological role in cellular detoxification by forming covalent conjugates with Michael acceptors. The electrophilicity E of various Michael acceptors was characterized recently according to the Patz–Mayr relation $\lg k_2 = s_N(N+E)$. We now determined the nucleophilic reactivity (N, s_N) of glutathione (GSH) in aqueous solution at 20 °C to connect published GSH reactivities (k_{GSH}) with Mayr's electrophilicity scale (E). In this way, electrophilicities E of more than 70 Michael acceptors could be estimated, which can now be used to systematically predict novel reactions with the multitude of nucleophiles whose nucleophilicity parameters N/s_N are known.*

Michael acceptors are often used and versatile electrophiles in organic synthesis. Their capability to form conjugates with peptides bearing nucleophilic groups, such as the thiol of the tripeptide glutathione (GSH), supplies them with a broad spectrum of bioactivity. To assess the toxicity of xenobiotic Michael acceptors[1,2] as well as to estimate their potential as biological tools[3–5] or covalent drugs,[2,6] the kinetics of non-enzymatic GSH thiol–Michael additions have been broadly investigated under physiological conditions.[2,6l,7–9] The corresponding second-order rate constants, k_{GSH}, provide the experimental basis for structure–activity relationships that comprise, for example, α,β-unsaturated aldehydes, ketones, and esters.[2,6g]

The kinetics of Michael additions of carbon-centered reference nucleophiles were extensively studied by Mayr and co-workers, who used Equation (1) to establish an ordering system for the electrophilic reactivity of structurally diverse Michael acceptors.[10] Equation (1) is a linear free energy relationship that calculates solvent-independent electrophilicity parameters E from experimentally determined second-order rate constants k_2 for the reactions of electrophiles with nucleophiles of known nucleophilic reactivities N and susceptibilities s_N (in a certain solvent).[11]

$$\lg k_2(20\,^{\circ}\mathrm{C}) = s_N(N+E) \quad (1)$$

Kamiya, Urano, and co-workers recently demonstrated that Mayr's electrophilicities E provide a useful guide for the rational design of real-time dynamic GSH fluorescent probes.[4a] We therefore set out to interconnect electrophilicity rankings for Michael acceptors originating from rate constants of their reactions with GSH[2d,7–9] with those relying on Mayr electrophilicities E.[10,12] To achieve the contact between both reactivity scales we determined the Mayr nucleophilicity of GSH in aqueous solution from the kinetics of its reactions with the reference electrophiles **E1**–**E17** (Figure 1). As a consequence, the mutual interconversion of known electrophilic reactivities $\lg k_{GSH}$ and E becomes possible.

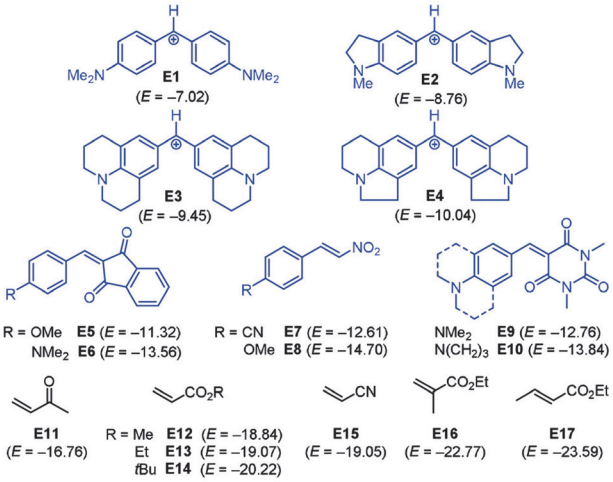

Figure 1. Reference electrophiles **E1**–**E17** used in this study (counter-ion for benzhydrylium ions **E1**–**E4**: BF_4^-; electrophilicities E from Refs. [10, 11b, 12]).

Dropwise addition of a deeply blue acetonitrile solution of the electrophile **E1**[13] to a neutral, aqueous solution of GSH led to fading of the blue color within seconds because of the rapid formation of the colorless S-benzhydrylated adduct **GS-E1**·HBF_4 (Scheme 1).

Thiolate attack at the cationic center of **E1** also occurred, though significantly faster, when **E1** was added to an alkaline, aqueous solution of GSH to yield **GS-E1**. Competing attack of the γ-glutamyl NH_2 group of GSH at **E1** was not detected (see the Supporting Information), in agreement with the rate ratio of $>100{:}1$ for the S^-/NH_2 attack of GSH at acrylonitrile (pH 8.1, 30 °C) determined by Friedman and co-workers.[7a,14] Accordingly, the analogous reaction of **E1** with *N*-acetylcys-

[*] R. J. Mayer, Dr. A. R. Ofial
Department Chemie
Ludwig-Maximilians-Universität München
Butenandtstraße 5–13, 81377 München (Germany)
E-mail: ofial@lmu.de

Supporting information and the ORCID identification number(s) for the author(s) of this article can be found under: https://doi.org/10.1002/anie.201909803.

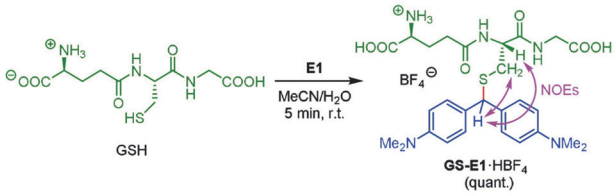

Scheme 1. Adduct formation between GSH and the benzhydrylium tetrafluoroborate **E1** in neutral, aqueous solution. NOESY experiments indicated a benzhydrylated Cys moiety in **GS-E1**.

teine (AcCys), which is devoid of a reactive NH_2 group, gave rise to S-benzhydrylated AcCys (see the Supporting Information).

Owing to the similar acidities of the thiol and the ammonium group of GSH(NH_3^+/SH), they are deprotonated simultaneously in the pH range 7 to 12, producing two reactive thiolate species, that is, GSH(NH_3^+/S^-) and GSH(NH_2/S^-). Depending on the pH value, variable fractions of the individual thiolates are present in the aqueous solutions, and microscopic ionization constants are needed to describe the acid–base equilibria[7a,15] (see the Supporting Information).

The rates of GSH adduct formation with reference electrophiles **E2–E10** were investigated at pH 12 in aqueous solution (20 °C). At this pH, the thiol groups of GSH[15a–c] and AcCys,[15d] respectively, are almost quantitatively (> 99 %) deprotonated to the corresponding thiolates RS^- [that is, GSH(NH_2/S^-) from GSH]. The thiolates RS^- add directly to the cationic reference electrophiles **E2–E4** or undergo conjugate additions to the neutral Michael acceptors **E5–E10** (Scheme 2).

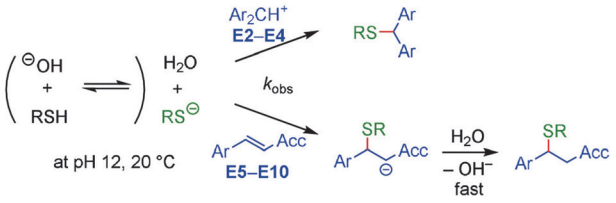

Scheme 2. Reactions of cationic and neutral electrophiles **E** with thiolate ions generated from GSH or AcCys in alkaline, aqueous solutions.

The kinetics of the covalent bond formation between the deprotonated GSH (or AcCys) and the electrophiles **E** were monitored by following the decay of the UV/Vis absorbance of the colored cationic or neutral electrophiles by using the stopped-flow technique (see the Supporting Information). With thiolate ions at at least tenfold higher concentrations than their electrophilic reaction partners (pseudo-first-order conditions), we observed rapid mono-exponential decays of the electrophile concentrations. First-order rate constants k_{obs} (s^{-1}) were obtained by least-squares fitting of the single-exponential function $A_t = A_0 e^{-k_{obs}t} + C$ to the time-dependent absorbance (Figure 2a).

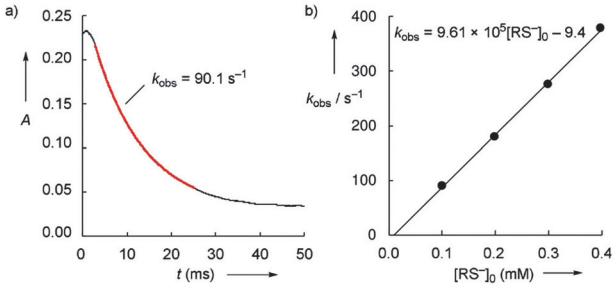

Figure 2. a) Decay of the absorbance *A* (at 383 nm) in the reaction of GSH ($c = 1.00 \times 10^{-4}$ M) with **E5** ($c = 1.03 \times 10^{-5}$ M) at 20 °C (aqueous solution, pH 12). The fitted mono-exponential function is depicted in red. b) The slope of the linear correlation of the first-order rate constant k_{obs} with the initial concentration of the GSH thiolate $[RS^-]_0$ was used to derive the second-order rate constant k_2 for the attack of the GSH thiolate at the Michael acceptor **E5**.

Table 1 lists the second-order rate constants k_2 ($M^{-1}s^{-1}$) for the attack of thiolate ions generated from GSH and AcCys, respectively, at the reference electrophiles **E2–E10**, which (according to $k_{obs} = k_2[RS^-]_0$) were obtained as the slopes of the linear correlations of k_{obs} with the thiolate concentrations

Table 1: Second-order rate constants k_2 for the reactions of **E2–E10** with thiolates generated from glutathione (GSH), *N*-acetylcysteine (AcCys), and cysteine (Cys) by deprotonation at pH 12 in aqueous solution at 20 °C.

Electrophile	k_2 ($M^{-1}s^{-1}$)		
	GSH	AcCys	Cys[a]
E2	2.70×10^6	1.47×10^6	1.29×10^6
E3	1.37×10^6	5.57×10^5	6.41×10^5
E4	6.60×10^5	3.47×10^5	3.79×10^5
E5	9.61×10^5	5.21×10^5	–
E6	7.60×10^4	–	–
E7	1.46×10^5	–	–
E8	3.62×10^4	3.14×10^4	–
E9	2.58×10^5	1.96×10^5	–
E10	5.31×10^4	4.12×10^4	–

[a] With k_2 from Ref. [16].

(as exemplified for the reaction of GSH with **E5** in Figure 2b and for all other combinations in the Supporting Information). Table 1 also comprises rate constants for the reactions of cysteine with benzhydrylium ions **E2–E4**, which were determined by Brotzel and Mayr.[16] For each of the electrophiles **E2–E10**, the reactivities towards GSH and the less functionalized AcCys (or Cys) agree within a factor of 2.5. We conclude from this comparison that exclusively the thiolate reactivity of GSH(NH_2/S^-) was detected in our kinetic measurements.

Kinetic assays used to investigate GSH reactivity towards electrophilic targets, such as Michael acceptors, are performed in buffered solutions at physiological pH, that is, usually at pH 7.4. In the range pH 7 to 8, only GSH(NH_3^+/S^-) is formed as a reactive thiolate. Although weakly populated (1–10 % of $[GSH]_0$),[15a–c] this fraction *F* of nucleophilic thiolate ions accounts for the observed GSH reactivity

towards electrophiles under physiological conditions. Equation (2) allows one to convert the second-order rate constants k_{GSH} into second-order rate constants k_2 for the corresponding GSH(NH_3^+/S^-) thiolate reactions.

$$k_2\,(M^{-1}\,s^{-1}) = k_{GSH}/F \qquad (2)$$

Reported pH-dependent second-order rate constants k_{GSH}[2d,7] for the reactions of GSH with the Michael acceptors **E11–E17**, whose Mayr electrophilicities E are known, are compiled in Table 2 along with the second-order rate constants k_2 for the corresponding thiolate reactivity [from Eq. (2)].

Table 2: Second-order rate constants k_{GSH} as reported for the reactions of GSH with electrophiles **E11–E17** at a certain pH value in aqueous, buffered solutions and second-order rate constants k_2 [calculated by using Eq. (2)] for the reactions of the GSH(NH_3^+/S^-) thiolate.

Electrophile	E[a]	k_{GSH} ($M^{-1}\,s^{-1}$)	k_2 ($M^{-1}\,s^{-1}$)
E11	−16.76	3.19×10^{1} (pH 7.4)[b]	1.14×10^{3}
E12	−18.84	1.90×10^{-1} (pH 7.4)[c]	6.79
E13	−19.07	1.77×10^{-1} (pH 7.4)[c]	6.31
E14	−20.22	4.17×10^{-2} (pH 7.4)[c]	1.49
E15	−19.05	1.73×10^{-1} (pH 8.1)[d]	1.36
E16	−22.77	9.67×10^{-4} (pH 7.4)[c]	3.45×10^{-2}
E17	−23.59	3.10×10^{-3} (pH 7.4)[c]	1.11×10^{-1}

[a] Mayr electrophilicities E from Ref. [10]. [b] At 20 °C, from Ref. [7b]; $F=0.0280$. [c] At 25 °C, from Ref. [2d]; $F=0.0280$. [d] At 30 °C, from Ref. [7a]; $F=0.127$.

As shown in Table 1, the relative electrophilic reactivities E of **E2–E10** also hold for their reactions towards the GSH(NH_2/S^-) thiolate in aqueous solution. Friedman showed that protonation at the remote γ-glutamyl NH_2 group in GSH reduces the thiolate reactivity by a factor of 2[7a] (see the Supporting Information for evidence that this factor is also appropriate in our studies). By applying Friedman's factor to convert the k_2 values from Table 1, a linear correlation over 15 orders of magnitude of electrophilic reactivity results from the combined set of second-order rate constants for reactions of the thiolate GSH(NH_3^+/S^-) with **E2–E17** when correlated with their E descriptors (Figure 3).[17] The slope of the linear correlation in Figure 3 corresponds to s_N (=0.56) for the thiolate GSH(NH_3^+/S^-) in water, and from the intercept with the abscissa, a nucleophilicity of $N=20.97$ is obtained.

Conversely, the thus determined GSH nucleophilicity (N, s_N) allows one to estimate the electrophilicity for Michael acceptors whose reactivity had thus far only been investigated in kinetic GSH assays.[2d,7–9] After converting the reported rate constants k_{GSH} into k_2 [Eq. (2)], Equation (1) was used to assess E for various enones, ynones, enals, ynals, and further α,β-unsaturated carbonyl compounds **M1–M73** (see Table S4 in the Supporting Information). For example, applying $k_{GSH}=8.12\,M^{-1}\,s^{-1}$ (pH 7.4, 25 °C, from Ref. [2d]) for 2-octynal (**M28**) in Equation (2) yields $k_2=290\,M^{-1}\,s^{-1}$. After inserting k_2 into Equation (1), the electrophilic reactivity of 2-octynal is rated with $E=-16.5$. Analogously, electrophilicities E of another

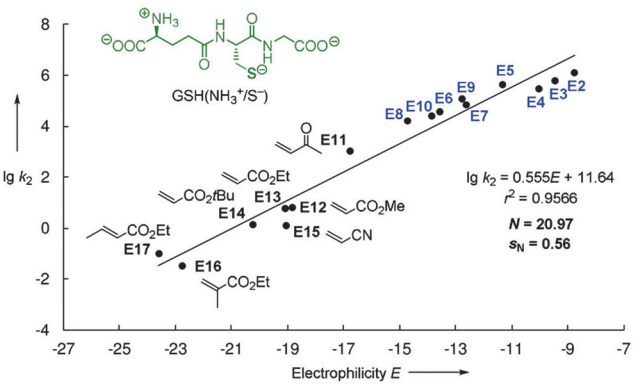

Figure 3. Determination of the nucleophilicity of GSH(NH_3^+/S^-) from the linear plot of lg k_2 for its reactions with the electrophiles **E2–E17** (with 0.5 k_2 from Table 1 and k_2 from Table 2) versus the electrophilicity parameters E.

72 Michael acceptors within the range of $-14.4 \le E \le -25.3$ were estimated.[18] Available rate constants furthermore create opportunities to integrate the recently developed dynamic GSH fluorescent probes **M74–M82** into Mayr's electrophilicity scale (Scheme 3).[3a,4b,19]

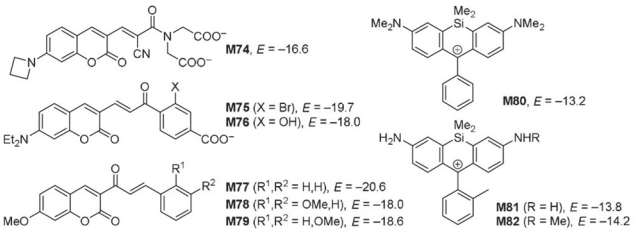

Scheme 3. Estimated electrophilicities E of the GSH fluorescent probes **M74–M82** (see Table S7 in the Supporting Information for details).

It was proposed that quantum-chemically calculated methyl anion affinities ΔG_{MA} (Figure 4a) could be used to predict trends in the electrophilic reactivities E of Michael acceptors.[10] The E vs. ΔG_{MA} correlation for the Michael acceptors with E derived from reactions with carbon-centered nucleophiles was reported to be linear ($r^2=0.8857$, $n=44$, black dots in Figure 4b).[10] The E parameters estimated in this work solely from a single rate constant in kinetic GSH assays cannot be expected to be as accurate as classical electrophilicities E,[18] which are based on evaluating a set of kinetics for C–C bond-forming reactions with carbon-centered reference nucleophiles.[10] To assess the general consistency, however, we included calculated ΔG_{MA} values for the Michael acceptors **M1–M73** with GSH-derived electrophilicities E (orange dots) in Figure 4b. Although the correlation coefficient decreases to $r^2=0.8331$ ($n=117$), the scattering range of the E vs. ΔG_{MA} correlation does not widen significantly when GSH-based E values are included. Purple rhombs in Figure 4b show additional entries for **M74–M82**. Their positions indicate that the E vs. ΔG_{MA} correlation for prototypical Michael acceptors also holds for roughly esti-

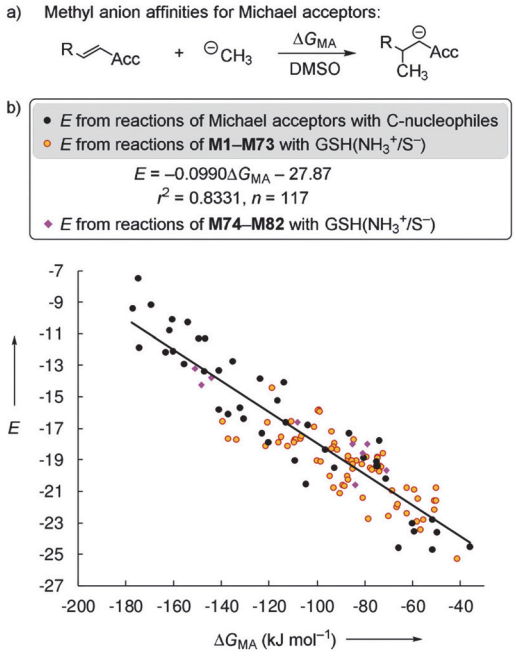

Figure 4. a) Definition of the methyl anion affinities (ΔG_{MA}) of Michael acceptors. b) Correlation between experimentally determined electrophilicities E and methyl anion affinities ΔG_{MA} in DMSO [calculated at the SMD(DMSO)/B3LYP/6-311++G(3df,2pd)//B3LYP/6-31G(d,p) level of theory, see Supporting Information for details] supplemented by data for the fluorescent probes **M74–M82** (not included when calculating the correlation line).

mating the reactivity of the structurally more sophisticated fluorescent probes **M74–M82**.

Within a reactivity range that currently covers 40 orders of magnitude, using Equation (1) usually allows chemists to calculate second-order rate constants within a precision of factor <100 for reactions at 20 °C, in which exactly one new C–X or C–C σ-bond is formed.[20] Table S6 collects 80 experimental second-order rate constants k_2^{exp} for the reactions of Michael acceptors with structurally diverse N-, O-, or S-centered nucleophiles in different solvents at temperatures between 19 and 30 °C. The comparison with second-order rate constants k_2^{eq1} (20 °C) calculated by using Equation (1) and the reactivity parameters E, N, and s_N shows that $k_2^{exp}/k_2^{eq1} < 100$ is fulfilled for 71 (of 80) Michael additions (Table S6). This analysis confirms that the GSH-derived E values for Michael acceptors can also be used to predict reaction rates for Michael additions of other classes of nucleophiles.[21] Rates of Corey–Chaykovsky cyclopropanations,[22] stepwise Huisgen reactions,[10] Weitz–Scheffer epoxidations,[23] cyanoethylations,[24] or simple 1,4-additions of Michael acceptors with amines, alkoxide ions, and thiolates[24] can thus be assessed by using Equation (1) and the available reactivity parameters E, N, and s_N.[12]

In conclusion, the nucleophilic reactivity for the thiolate $GSH(NH_3^+/S^-)$ in water ($N=20.97$; $s_N=0.56$) has been established. If $k_2=10^{-3}\,M^{-1}\,s^{-1}$ is considered as a minimum rate constant for practical reactions at 20 °C,[11c] $GSH(NH_3^+/S^-)$ can be expected to react successfully with electrophiles of $E>-26$. This limiting E value may give orientation for the future development of so-called "warheads" in covalently inhibiting drugs.[2,6] The applicability of Mayr reactivity parameters for the rational design of dynamic real-time GSH-selective fluorescent probes has already been shown.[4a] The conversion of GSH reactivities ($\lg k_{GSH}$) into Mayr E values (Tables S4 and S7), as proposed in this work, enables the prediction of relevant second-order rate constants for competing nucleophilic sites, which is a frequent challenge in the development of thiol-selective probe molecules.[3,4] Furthermore, the GSH-based estimated electrophilicities of >70 Michael acceptors provide new insight into general structure–reactivity relationships (Figure S4).[6g] The estimated Mayr E parameters considerably enrich the structural diversity in the chemist's toolkit for the systematic prediction of thus far unexplored 1,4-additions of Michael acceptors to a wide range of C-, N-, P-, O-, and S-centered nucleophiles for which N and s_N are known[12] (Figure S5).

Acknowledgements

We thank Professor Herbert Mayr for helpful discussions and Nathalie Hampel for the synthesis of **E1–E7**. This work was funded by the Deutsche Forschungsgemeinschaft (DFG), project number 410831260. Support by the Fonds der Chemischen Industrie (Kekulé fellowship to R.J.M.) is gratefully acknowledged.

Conflict of interest

The authors declare no conflict of interest.

Keywords: electrophilicity · kinetics · Michael addition · nucleophilicity · thiols

How to cite: *Angew. Chem. Int. Ed.* **2019**, *58*, 17704–17708
Angew. Chem. **2019**, *131*, 17868–17872

[1] R. M. LoPachin, T. Gavin, *Free Radical Res.* **2016**, *50*, 195–202.
[2] a) T. W. Schultz, J. W. Yarbrough, E. L. Johnson, *SAR QSAR Environ. Res.* **2005**, *16*, 313–322; b) J. W. Yarbrough, T. W. Schultz, *Chem. Res. Toxicol.* **2007**, *20*, 558–562; c) A. Böhme, D. Thaens, A. Paschke, G. Schüürmann, *Chem. Res. Toxicol.* **2009**, *22*, 742–750; d) A. Böhme, A. Laqua, G. Schüürmann, *Chem. Res. Toxicol.* **2016**, *29*, 952–962.
[3] a) X. Jiang, J. Chen, A. Bajić, C. Zhang, X. Song, S. L. Carroll, Z.-L. Cai, M. Tang, M. Xue, N. Cheng, C. P. Schaaf, F. Li, K. R. MacKenzie, A. C. M. Ferreon, F. Xia, M. C. Wang, M. Maletić-Savatić, J. Wang, *Nat. Commun.* **2017**, *8*, 16087; b) C. Cossetti, G. Di Giovamberardino, R. Rota, A. Pastore, *Nat. Commun.* **2018**, *9*, 1588.
[4] a) K. Umezawa, M. Yoshida, M. Kamiya, T. Yamasoba, Y. Urano, *Nat. Chem.* **2017**, *9*, 279–286; b) G. Yin, T. Niu, T. Yu, Y. Gan, X. Sun, P. Yin, H. Chen, Y. Zhang, H. Li, S. Yao, *Angew. Chem. Int. Ed.* **2019**, *58*, 4557–4561; *Angew. Chem.* **2019**, *131*, 4605–4609.
[5] a) X. Chen, Y. Zhou, X. Peng, J. Yoon, *Chem. Soc. Rev.* **2010**, *39*, 2120–2135; b) S. Lee, J. Li, X. Zhou, J. Yin, J. Yoon, *Coord. Chem. Rev.* **2018**, *366*, 29–68.

[6] a) S. Amslinger, *ChemMedChem* **2010**, *5*, 351 – 356; b) I. M. Serafimova, M. A. Pufall, S. Krishnan, K. Duda, M. S. Cohen, R. L. Maglathlin, J. M. McFarland, R. M. Miller, M. Frödin, J. Taunton, *Nat. Chem. Biol.* **2012**, *8*, 471 – 476; c) N. J. Pace, E. Weerapana, *ACS Chem. Biol.* **2013**, *8*, 283 – 296; d) S. Krishnan, R. M. Miller, B. Tian, R. D. Mullins, M. P. Jacobson, J. Taunton, *J. Am. Chem. Soc.* **2014**, *136*, 12624 – 12630; e) E. H. Krenske, R. C. Petter, K. N. Houk, *J. Org. Chem.* **2016**, *81*, 11726 – 11733; f) R. Lonsdale, J. Burgess, N. Colclough, N. L. Davies, E. M. Lenz, A. L. Orton, R. A. Ward, *J. Chem. Inf. Model.* **2017**, *57*, 3124 – 3137; g) P. A. Jackson, J. C. Widen, D. A. Harki, K. M. Brummond, *J. Med. Chem.* **2017**, *60*, 839 – 885; h) J. M. Strelow, *SLAS Discov.* **2017**, *22*, 3 – 20; i) Z. Zhao, P. E. Bourne, *Drug Discovery Today* **2018**, *23*, 727 – 735; j) R. Lonsdale, R. A. Ward, *Chem. Soc. Rev.* **2018**, *47*, 3816 – 3830; k) A. Keeley, P. Ábrányi-Balogh, G. M. Keserü, *MedChemComm* **2019**, *10*, 263 – 267; l) for the kinetics of GSH binding to a series of acrylamides at 37 °C, see: V. J. Cee, L. P. Volak, Y. Chen, M. D. Bartberger, C. Tegley, T. Arvedson, J. McCarter, A. S. Tasker, C. Fotsch, *J. Med. Chem.* **2015**, *58*, 9171 – 9178.

[7] a) M. Friedman, J. F. Cavins, J. S. Wall, *J. Am. Chem. Soc.* **1965**, *87*, 3672 – 3682; b) H. Esterbauer, H. Zollner, N. Scholz, *Z. Naturforsch. C* **1975**, *30*, 466 – 473.

[8] a) G. Eisenbrand, J. Schuhmacher, P. Gölzer, *Chem. Res. Toxicol.* **1995**, *8*, 40 – 46; b) K. Chan, R. Poon, P. J. O'Brien, *J. Appl. Toxicol.* **2008**, *28*, 1027 – 1039.

[9] J. A. H. Schwöbel, D. Wondrousch, Y. K. Koleva, J. C. Madden, M. T. D. Cronin, G. Schüürmann, *Chem. Res. Toxicol.* **2010**, *23*, 1576 – 1585.

[10] D. S. Allgäuer, H. Jangra, H. Asahara, Z. Li, Q. Chen, H. Zipse, A. R. Ofial, H. Mayr, *J. Am. Chem. Soc.* **2017**, *139*, 13318 – 13329.

[11] a) H. Mayr, M. Patz, *Angew. Chem. Int. Ed. Engl.* **1994**, *33*, 938 – 957; *Angew. Chem.* **1994**, *106*, 990 – 1010; b) H. Mayr, T. Bug, M. F. Gotta, N. Hering, B. Irrgang, B. Janker, B. Kempf, R. Loos, A. R. Ofial, G. Remennikov, H. Schimmel, *J. Am. Chem. Soc.* **2001**, *123*, 9500 – 9512; c) H. Mayr, A. R. Ofial, *SAR QSAR Environ. Res.* **2015**, *26*, 619 – 646.

[12] A free database of reactivity parameters *E*, *N*, and s_N can be accessed at: http://www.cup.lmu.de/oc/mayr/DBintro.html.

[13] R. J. Mayer, N. Hampel, P. Mayer, A. R. Ofial, H. Mayr, *Eur. J. Org. Chem.* **2019**, 412 – 421.

[14] a) J. A. H. Schwöbel, Y. K. Koleva, S. J. Enoch, F. Bajot, M. Hewitt, J. C. Madden, D. W. Roberts, T. W. Schultz, M. T. D. Cronin, *Chem. Rev.* **2011**, *111*, 2562 – 2596; b) for the detection of the thermodynamically preferred, terminal glutamyl N-bound 1:1 adducts of GSH and hexenones by MS techniques after 24 h reaction time, see: C. Slawik, C. Rickmeyer, M. Brehm, A. Böhme, G. Schüürmann, *Environ. Sci. Technol.* **2017**, *51*, 4018 – 4026.

[15] a) D. L. Rabenstein, *J. Am. Chem. Soc.* **1973**, *95*, 2797 – 2803; b) A. Mirzahosseini, M. Somlyay, B. Noszál, *Chem. Phys. Lett.* **2015**, *622*, 50 – 56; c) the pH-dependent thiolate concentrations for GSH(NH_3^+/S^-) and GSH(NH_2/S^-) were calculated by using the GSH ionization scheme of Rabenstein (Ref. [15a]) and the corresponding microscopic ionization constants from Ref. [15b] (see the Supporting Information for details); d) for the SH acidity of AcCys (pK_a 9.62), see: A. Meißner, P. Gockel, H. Vahrenkamp, *Chem. Ber.* **1994**, *127*, 1235 – 1241.

[16] F. Brotzel, H. Mayr, *Org. Biomol. Chem.* **2007**, *5*, 3814 – 3820.

[17] Second-order rate constants determined at different temperatures (from 20 to 30 °C) were used indiscriminately to construct Figure 3.

[18] We estimate that *E*(**M1**–**M73**) may be assessed with a precision of ± 2 units in *E* if only rate constants from kinetic GSH assays are available.

[19] a) X. Jiang, Y. Yu, J. Chen, M. Zhao, H. Chen, X. Song, A. J. Matzuk, S. L. Carroll, X. Tan, A. Sizovs, N. Cheng, M. C. Wang, J. Wang, *ACS Chem. Biol.* **2015**, *10*, 864 – 874; b) J. Chen, X. Jiang, S. L. Carroll, J. Huang, J. Wang, *Org. Lett.* **2015**, *17*, 5978 – 5981; c) O. García-Beltrán, C. González, E. G. Pérez, B. K. Cassels, J. G. Santos, D. Millán, N. Mena, P. Pavez, M. E. Aliaga, *J. Phys. Org. Chem.* **2012**, *25*, 946 – 952.

[20] H. Mayr, *Angew. Chem. Int. Ed.* **2011**, *50*, 3612 – 3618; *Angew. Chem.* **2011**, *123*, 3692 – 3698.

[21] Only for methyl crotonate (**M61**), the ratio k_2^{exp}/k_2^{eq1} slightly exceeds a factor of 100 for five of six available k_2^{exp} values at 30 °C, which may in part be due to the 10 K difference in the reference temperatures for k_2^{exp} and k_2^{eq1}.

[22] R. Appel, N. Hartmann, H. Mayr, *J. Am. Chem. Soc.* **2010**, *132*, 17894 – 17900.

[23] a) R. J. Mayer, T. Tokuyasu, P. Mayer, J. Gomar, S. Sabelle, B. Mennucci, H. Mayr, A. R. Ofial, *Angew. Chem. Int. Ed.* **2017**, *56*, 13279 – 13282; *Angew. Chem.* **2017**, *129*, 13463 – 13467; b) R. J. Mayer, A. R. Ofial, *Org. Lett.* **2018**, *20*, 2816 – 2820; c) R. J. Mayer, A. R. Ofial, *Eur. J. Org. Chem.* **2018**, 6010 – 6017.

[24] For references, see Table S6 in the Supporting Information.

Manuscript received: August 2, 2019
Accepted manuscript online: September 27, 2019
Version of record online: October 31, 2019

5.1 Supporting Information - General

Reagents

Glutathione (GSH) and acetyl cysteine (AcCys) were purchased from Sigma-Aldrich. Stock solutions of potassium hydroxide (KOH) were purchased from Bernd Kraft Laborchemikalien.

Analytics

Melting points were acquired using a Büchi Melting Point B-560 device and are not corrected.

Nuclear magnetic resonance spectra were recorded on 400 MHz NMR spectrometers. The following abbreviations and their combinations are used in the analysis of NMR spectra: s = singlet, d = doublet, t = triplet, q = quartet, m = multiplet, br s = broad singlet. NMR signals were assigned based on information from additional 2D NMR experiments (COSY, gHSQC, gHMBC, NOESY). Internal reference was set to the residual solvent signals (δ_H = 4.79 for D_2O). The ^{13}C NMR spectra were recorded under broad-band proton-decoupling.

Infrared (IR) spectra were recorded on a Perkin Elmer Spectrum BX-59343 instrument with a Smiths Detection DuraSamplIR II Diamond ATR sensor for detection in the range 4500–600 cm^{-1}.

High resolution (HRMS) mass spectra were recorded on a Thermo Finnigan LTQ FT Ultra Fourier Transform ion cyclotron resonance mass spectrometer. For ionization of the samples, electrospray ionization (ESI) was applied.

Kinetic measurements

Kinetics of reactions in alkaline, aqueous solution (degassed and prepared under an atmosphere of N_2) were followed by employing stopped-flow UV/Vis photometry on Applied Photophysics SX20 systems. The temperature (20.0 ± 0.2 °C) was controlled by using circulating bath cryostats. Acetonitrile was used as a co-solvent (0.5 or 11 vol-%) to solubilize the electrophiles.

5.2 Product Analysis

GS-E1·HBF_4 (RM551)

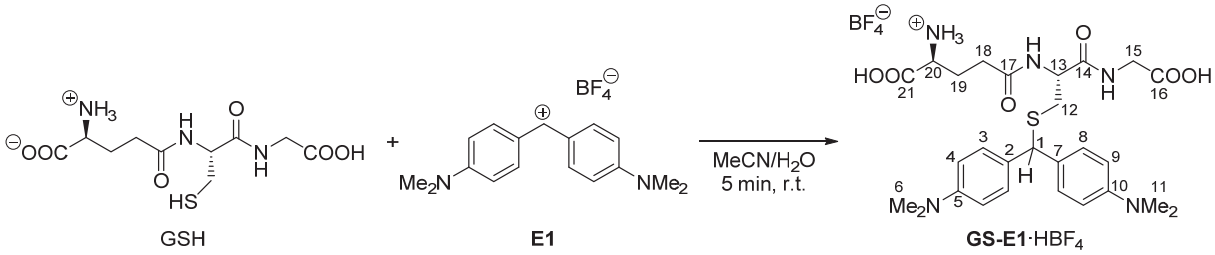

GSH E1 **GS-E1**·HBF_4

Glutathione (GSH, 35.2 mg, 0.115 mmol) was dissolved in water (5 mL). Under stirring, a solution of **E1**-BF_4 (39.0 mg, 0.115 mmol) in acetonitrile (2 mL) was added dropwise. The resulting pale greenish suspension was stirred for another 2 min. Then all solvents were removed in the vacuum. The residual highly viscous green oil slowly solidified to yield a pale green solid: **GS-E1**·HBF_4 (74.2 mg, yield: quant.).

^1H NMR (400 MHz, D_2O): δ = 7.68–7.64 (m, 4 H, 3-H and 8-H), 7.55–7.51 (m, 4 H, 4-H and 9-H), 5.48 (s, 1 H, 1-H), 4.42 (dd, J = 8.7 Hz, J = 5.1 Hz, 1 H, 13-H), 3.84–3.81 (m, 2 H, 15-H), 3.79 (t, J = 6.4 Hz, 1 H, 20-H), 3.234 (s, 6 H, 6-H or 11-H), 3.230 (s, 6 H, 6-H or 11-H), 3.04 (dd, ^2J = 14.3 Hz, ^3J = 5.1, 1 H, 12-H^a), 2.86 (dd, ^2J = 14.2 Hz, ^3J = 8.8 Hz, 1 H, 12-H^b), 2.55–2.51 (m, 2 H, 18-H), 2.20–2.14 (m, 2 H, 19-H).

$^{13}C\{^1H\}$ NMR (101 MHz, D_2O): δ = 174.9 (C_q, C-16), 174.5 (C_q, C-17), 173.7 (C_q, C-21), 171.7 (C_q, C-14), 142.2 (C_q, C-5 and C-10), 141.6 (C-2), 141.3 (C-7), 130.0 (CH, C-3 and C-8), 120.3 (CH, C-4 and C-9), 53.9 (CH, C-20), 52.7 (CH, C-13), 52.0 (CH, C-1), 45.70 (CH_3, C-6 or C-11), 45.66 (CH_3, C-6 or C-11), 42.5 (CH_2, C-15), 33.5 (CH_2, C-12), 31.4 (CH_2, C-18), 26.2 (CH_2, C-19).

HRMS (ESI$^+$): Calcd *m/z* for $[C_{27}H_{38}N_5O_6S]^+$ [M + H$^+$]: 560.2537; Found: 560.2548.

IR (ATR, neat): 2934, 2509, 1726, 1609, 1518, 1448, 1410, 1351, 1228, 1054, 806, 764 cm^{-1}.

mp 140–145 °C (the sample turned bright blue at 80 °C and then dark blue at 120 °C; the exact melting point could therefore not be determined).

AcCys-E1·HBF_4 (RNH45)

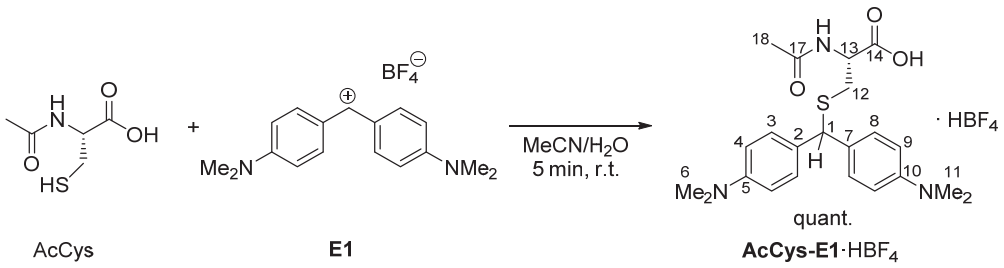

To a stirred solution of *N*-acetylcysteine (18.7 mg, 0.115 mmol) in water (5 mL) was added dropwise a solution of **E1**-BF_4 (39.0 mg, 0.115 mmol) in acetonitrile (2 mL). The resulting pale blue solution was stirred for another 2 min. Then all solvents were removed in the vacuum. The residual highly viscous green oil slowly solidified to yield a pale blue solid: **AcCys-E1**·HBF_4 (57.5 mg, 0.0114 mmol, yield: 99%).

^{1}H NMR (400 MHz, D_2O) δ = 7.71–7.66 (m, 4 H, 3-H and 8-H), 7.58–7.54 (m, 4 H, 4-H and 9-H), 5.52 (s, 1 H, 1-H), 4.30 (dd, ^3J = 8.1 Hz, ^3J = 4.5 Hz, 1 H, 13-H), 3.26 (s, 12 H, 6-H and 11-H), 2.99 (dd, ^2J = 14.0 Hz, ^3J = 4.5 Hz, 1 H, 12-H^a), 2.86 (dd, ^2J = 14.0 Hz, ^3J = 8.1 Hz, 1 H, 12-H^b), 2.03 (s, 3 H, 18-H).

^{13}C{^{1}H} NMR (101 MHz, D_2O) δ = 175.8 (C_q, C-14), 173.4 (C_q, C-17), 142.1 (C_q), 141.9 (C_q), 141.83 (C_q), 141.81 (C_q), 130.09 (CH, C-3 or C-8), 130.07 (CH, C-3 or C-8), 120.44 (CH, C-4 or C-9), 120.39 (CH, C-4 or C-9), 53.7 (CH, C-13), 51.8 (CH, C-1), 45.88 (CH_3, C-6 or C-11), 45.86 (CH_3, C-6 or C-11), 34.0 (CH_2, C-12), 21.8 (CH_3, C-18).

HRMS (ESI$^-$): Calcd *m/z* for $[C_{22}H_{28}N_3O_3S]^-$: 414.1857; Found: 414.1864.

IR (ATR, neat): 2470, 1727, 1608, 1517, 1374, 1185, 1052, 900, 805, 763 cm^{-1}.

mp 55–65 °C (the sample turned green-black when heated to > 50 °C).

5.3 GSH Microscopic Protonation Constants

If multiple acidic sites in a molecule dissociate simultaneously at a certain pH value, macroscopic protonation constants are hybrid and do not accurately describe the degree of ionization at the molecular level. Instead, microscopic ionizations constants are required for polyvalent acids to calculate the precise distribution of protonated and deprotonated species at a certain pH.[1]

Details of the acid-base chemistry of glutathione (GSH) have previously been analyzed by Friedman and co-workers,[2] Rabenstein,[3] and more recently by Noszál and co-workers.[4]

We used the GSH ionization scheme by Rabenstein, which involves the seven species **A** to **H** that are interconnected by eight microscopic dissociation constants (Scheme S1).[3] In the pH range from 7 to 12, the species **D** to **H** and the dissociation constants K_{DF}, K_{DG}, K_{FH}, and K_{GH} are relevant.

Scheme S1: Protonation scheme for GSH and the related microscopic protonation constants according to Rabenstein.[3]

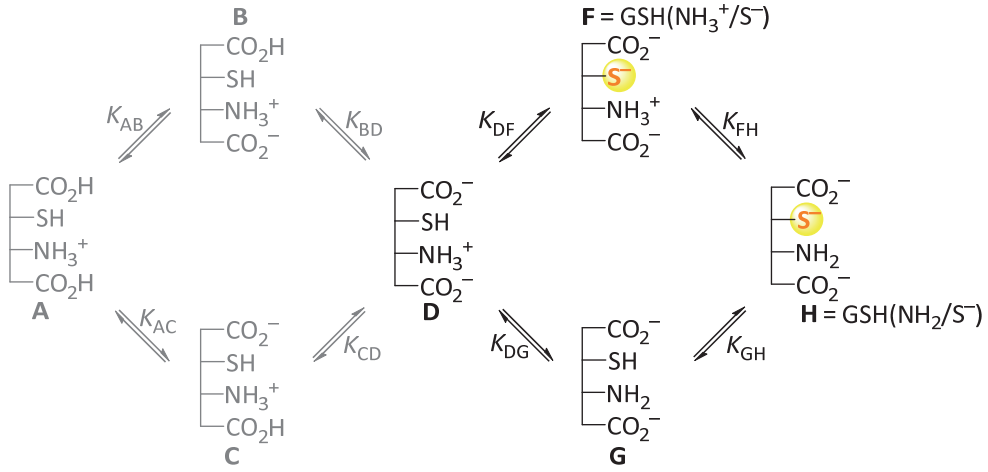

$$K_{AB} = \frac{[H^+][\mathbf{B}]}{[\mathbf{A}]} \qquad K_{BD} = \frac{[H^+][\mathbf{D}]}{[\mathbf{B}]} \qquad K_{DF} = \frac{[H^+][\mathbf{F}]}{[\mathbf{D}]} \qquad K_{FH} = \frac{[H^+][\mathbf{H}]}{[\mathbf{F}]}$$

$$K_{AC} = \frac{[H^+][\mathbf{C}]}{[\mathbf{A}]} \qquad K_{CD} = \frac{[H^+][\mathbf{D}]}{[\mathbf{C}]} \qquad K_{DG} = \frac{[H^+][\mathbf{G}]}{[\mathbf{D}]} \qquad K_{GH} = \frac{[H^+][\mathbf{H}]}{[\mathbf{G}]}$$

At a certain pH, the fraction F_i of each species i present in the equilibrium can be calculated from the microscopic dissociation constants as exemplified for species **F** [= GSH(NH_3^+/S^-)] in equation S1 and for species **H** [= GSH(NH_2/S^-)] in equation S2.

$$\text{for GSH}(NH_3^+/S^-): \quad F_{\mathbf{F}} = \frac{[\mathbf{F}]}{[\mathbf{D}] + [\mathbf{F}] + [\mathbf{G}] + [\mathbf{H}]} = \frac{K_{DF}/K_{DG}}{[H^+]/K_{DG} + K_{DF}/K_{DG} + 1 + K_{GH}/[H^+]} \qquad \text{(S1)}$$

$$\text{for GSH}(NH_2/S^-): \quad F_{\mathbf{H}} = \frac{[\mathbf{H}]}{[\mathbf{D}] + [\mathbf{F}] + [\mathbf{G}] + [\mathbf{H}]} = \frac{K_{GH}/[H^+]}{[H^+]/K_{DG} + K_{DF}/K_{DG} + 1 + K_{GH}/[H^+]} \qquad \text{(S2)}$$

Analogously, the total fraction of reactive nucleophilic species, for example, for GSH species with a free thiolate group (F_{S^-}) or GSH species with a free amino group (F_{NH2}) can be calculated by equations S3 and S4, respectively.

$$F_{S^-} = F_{\mathbf{F}} + F_{\mathbf{H}} = \frac{[\mathbf{F}] + [\mathbf{H}]}{[\mathbf{D}] + [\mathbf{F}] + [\mathbf{G}] + [\mathbf{H}]} = \frac{K_{DF}/K_{DG} + K_{GH}/[H^+]}{[H^+]/K_{DG} + K_{DF}/K_{DG} + 1 + K_{GH}/[H^+]} \quad \text{(S3)}$$

$$F_{NH2} = F_{\mathbf{G}} + F_{\mathbf{H}} = \frac{[\mathbf{G}] + [\mathbf{H}]}{[\mathbf{D}] + [\mathbf{F}] + [\mathbf{G}] + [\mathbf{H}]} = \frac{1 + K_{GH}/[H^+]}{[H^+]/K_{DG} + K_{DF}/K_{DG} + 1 + K_{GH}/[H^+]} \quad \text{(S4)}$$

Microscopic protonation constants for GSH have been determined by ^{1}H NMR spectroscopic titration experiments.[3,4] In this work, we used the microscopic protonation constants by Noszál and co-workers (Table S1) who followed the changes of ^{1}H NMR chemical shifts in the GSH protonation equilibria by using a 600 MHz NMR spectrometer.[4]

Table S1: Microscopic protonation constants for the equilibria between GSH species **D**, **F**, **G**, and **H** (in H_2O/D_2O 95:5 (v/v), at 25 °C and 0.15 mol L^{-1} ionic strength, from ref. 4)

pK_{DF}	8.94 ± 0.02
pK_{DG}	9.17 ± 0.02
pK_{FH}	9.49 ± 0.01
pK_{GH}	9.26 ± 0.01

By applying the microscopic protonation constants from Table S1 in equations S1–S3, one can calculate the pH-dependent distribution of reactive GSH species in aqueous solution. As depicted in Figure S1, at pH < 8 nucleophilic GSH reactivity is mostly caused by species **F** [= GSH(NH_3^+/S^-)]. Thiolate **F** is also the only relevant species for nucleophilic reactions of GSH under physiological conditions (pH 7.4). At pH > 11, the GSH species **H** [= GSH(NH_2/S^-)] predominates.

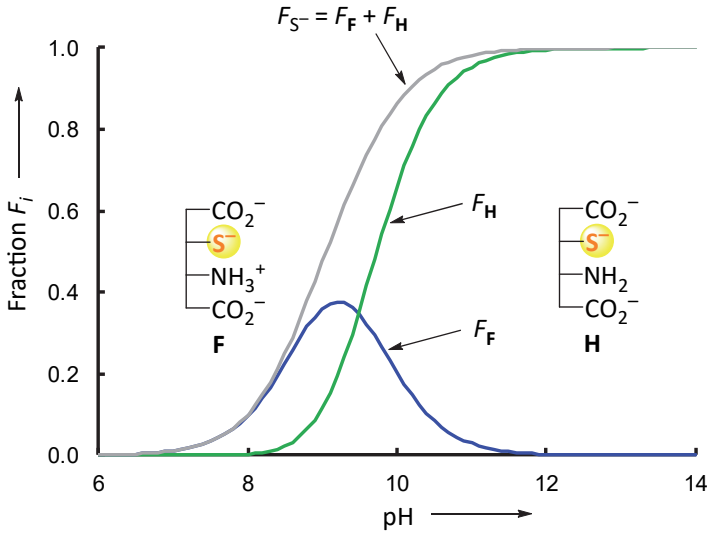

Figure S1: Distribution of GSH species **F** and **H** with a reactive thiolate group as a function of pH.

5.4 Relative Reactivity of GSH(NH_3^+/S^-) and GSH(NH_2/S^-)

Friedman showed that protonation at the remote γ-glutamyl NH_2 group (that is, **F** → **H**) reduced the GSH thiolate reactivity toward acrylonitrile by a factor of 2.[2]

To assess whether this reactivity difference between both reactive GSH thiolate species **F** [that is, GSH(NH_3^+/S^-)] and **H** [that is, GSH(NH_2/S^-)] also holds for our series of experiments, we studied the pH-dependent reactivity of GSH with the benzhydrylium ion **E4**.

Stock solutions of GSH, Na_3PO_4, $Na_2H_2PO_4$ and NaH_2PO_4 were mixed in variable ratios to achieve a certain pH in the reaction chamber of the stopped-flow instrument. The reactions between the electrophile **E4** and the nucleophilic GSH species were then monitored by following the mono-exponential decay of the UV-Vis absorbance of the colored **E4** by using the stopped-flow technique. Experimental conditions and observed first-order rate constants k_{obs} are gathered in Table S2.

Concentrations of the reactive GSH species **F** and **H** at different pH were calculated from the relationships [**F**] = F_F[GSG]$_0$ and [**H**] = F_H[GSH]$_0$. Partial second-order rate constants k_F^{calcd} and k_H^{calcd} for the nucleophilic GSH species **F** and **H** were then determined by equations S5 and S6, respectively.

$$k_F^{calcd} = 0.5k_2[GSH]_0F_F \qquad (S5)$$

$$k_H^{calcd} = k_2[GSH]_0F_H \qquad (S6)$$

The second-order rate constant k_2(20 °C) for the reaction of **E4** with **H** [that is, GSH(NH_2/S^-)] at pH 12 was determined experimentally in this work (k_2 = 6.60 × 10^5 M^{-1} s^{-1}, see below). The factor 0.5 in equation S5 considers the relative reactivity of **F** and **H** towards electrophiles reported by Friedman.[2] In this way, the overall rate constant $k_{S^-}^{calcd}$ for the reaction of GSH with **E4** at a certain pH was obtained as the sum of both partial rate constants (equation S7).

$$k_{S^-}^{calcd} = k_F^{calcd} + k_H^{calcd} \qquad (S7)$$

Table S2: Dependency of the first-order rate constants for reactions of GSH ([GSH]$_0$ = 1.00 × 10^{-4} M) and **E4** ([**E4**]$_0$ = 5.45 × 10^{-6} M) on the pH of the aqueous solution (20 °C).

pH[a]	k_{obs} (s^{-1})	lg k_{obs}	F_F	k_F^{calcd} (s^{-1})	F_H	k_H^{calcd} (s^{-1})	lg $k_{S^-}^{calcd}$
11.93	5.66 × 10^1	**1.75**	3.61 × 10^{-3}	1.19 × 10^{-1}	9.94 × 10^{-1}	65.6 × 10^1	**1.82**
11.67	4.80 × 10^1	**1.68**	6.54 × 10^{-3}	2.16 × 10^{-1}	9.90 × 10^{-1}	65.3 × 10^1	**1.82**
11.41	5.43 × 10^1	**1.73**	1.18 × 10^{-2}	3.89 × 10^{-1}	9.81 × 10^{-1}	6.48 × 10^1	**1.81**
10.85	5.39 × 10^1	**1.74**	4.08 × 10^{-2}	1.35	9.35 × 10^{-1}	6.17 × 10^1	**1.80**
10.40	5.37 × 10^1	**1.73**	1.03 × 10^{-1}	3.38	8.34 × 10^{-1}	5.50 × 10^1	**1.77**
9.81	4.37 × 10^1	**1.64**	2.62 × 10^{-1}	8.65	5.48 × 10^{-1}	3.62 × 10^1	**1.65**
9.56	3.93 × 10^1	**1.59**	3.33 × 10^{-1}	1.10 × 10^1	3.91 × 10^{-1}	2.58 × 10^1	**1.57**
9.23	2.67 × 10^1	**1.43**	3.77 × 10^{-1}	1.24 × 10^1	2.07 × 10^{-1}	1.37 × 10^1	**1.42**
8.64	1.79 × 10^1	**1.25**	2.68 × 10^{-1}	8.86	3.79 × 10^{-2}	2.50	**1.06**
8.56	8.92	**0.95**	2.44 × 10^{-1}	8.04	2.86 × 10^{-2}	1.89	**1.00**
8.45	1.25 × 10^1	**1.10**	2.10 × 10^{-1}	6.92	1.91 × 10^{-2}	1.26	**0.91**
8.01	2.45	**0.39**	9.87 × 10^{-2}	3.26	3.27 × 10^{-3}	2.16 × 10^{-1}	**0.54**
7.17	1.03	**0.01**	1.65 × 10^{-2}	5.46 × 10^{-1}	7.91 × 10^{-5}	5.22 × 10^{-3}	**–0.26**
6.89	2.92 × 10^{-1}	**–0.53**	8.79 × 10^{-3}	2.90 × 10^{-1}	2.21 × 10^{-5}	1.46 × 10^{-3}	**–0.54**
6.12	6.87 × 10^{-2}	**–1.16**	1.51 × 10^{-3}	4.98 × 10^{-2}	6.44 × 10^{-7}	4.25 × 10^{-5}	**–1.30**
4.90	4.92 × 10^{-3}	**–2.31**	9.12 × 10^{-5}	3.01 × 10^{-3}	2.34 × 10^{-9}	1.55 × 10^{-7}	**–2.52**

[a] An aliquot of each GSH/phosphate buffer solution was mixed with water in a 1:1 ratio (as in the reaction chamber of the stopped-flow spectrometer) and the pH value was determined.

Figures S2 compares the observed pH-dependent reactivity of GSH towards electrophile **E4** (lg k_{obs}) with the predicted behavior for the thiolate species of GSH (lg $k_{S^-}^{calcd}$). The fact that the experimental data points (black dots, from column 3 in Table S2) are located in close vicinity to the predicted rate constants lg $k_{S^-}^{calcd}$ (dashed grey line, from last column in Table S2) demonstrates that GSH reactivity in aqueous solutions is clearly dominated by the reactivity of the two thiolate species **F** and **H** in the pH range from 4 to 13.

Analogous calculations showed that the free amino groups in the GSH species **G** and **H** (dashed red line for lg k_{NH2}^{calcd} in Figure S2) can be expected to contribute only to a negligible extent (<0.1%) to the

kinetics of the GSH reactions with the electrophile **E4**. Also, background reactions of **E4** with hydroxide ions or water (lg k_{OH}^{calcd}) do not play a significant role at pH > 4.

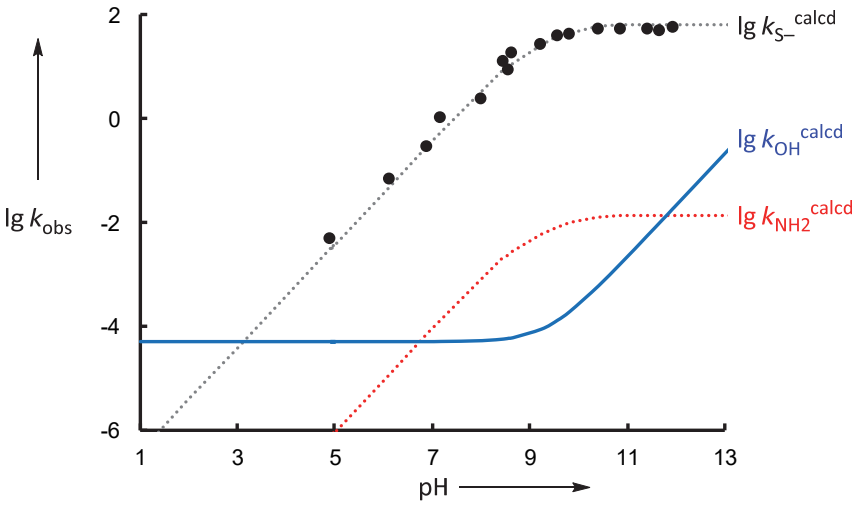

Figure S2: Observed first-order rate constants lg k_{obs} (20 °C) for the reaction of GSH with **E4** (dashed grey line: lg k_{S-}^{calcd} from Table S2; dashed red line: lg k_{NH2}^{calcd} calculated from $k_{NH2} = k_2 F_{NH2}$ by using k_2 = 140 M^{-1} s^{-1} for the reaction of glutamate with **E4**, from ref. 5b and F_{NH2} as defined in equation S4; blue line: background reaction of **E4** with hydroxide ions and/or water).

Furthermore, the excellent agreement between lg k_{obs} and lg k_{S-}^{calcd} in Figure S2 corroborates that the relative reactivity of the GSH thiolate species **F** and **H** towards electrophiles is generally described by $k_F = 0.5k_H$, as initially found by Friedman and co-workers for the reaction of GSH with acrylonitrile.[2] As a consequence, we have used the relation $k_F = 0.5k_H$ for converting our rate constants of GSH/electrophile reactions at pH 12 (where the reactive GSH species **H** prevails) to the more commonly used rate constants of GSH/electrophile reactions at physiological pH 7.4 (where the reactive GSH species **F** predominates).

In Table 2 (main text), we applied equation S8 to convert reported second-order rate constants k_{GSH} into second-order rate constants $k_2(GS^-)$ for the relevant thiolate reactivity of GSH.

$$k_2(GS^-) = k_{GSH}/(F_F + 2F_H) = k_{GSH}/F \qquad (S8)$$

The Friedman factor ($k_H = 2k_F$) was applied to reflect the different reactivity of the thiolate species **F** and **H** in the overall fraction F of nucleophilic thiolate ions, that is, $F = F_F + 2F_H$. The fractions of GSH thiolates present at pH 7.2, 7.4, 8.0, and 8.1, previously used to determine k_{GSH} (see Table S4 below) are listed in Table S3.

Table S3: Partial fractions F_F and F_H and overall fraction F (= $F_F + 2F_H$) of reactive GSH thiolate species in aqueous solution at different pH.

pH	F_F	F_H	F
7.2	0.0177	9.07×10^{-5}	0.0179
7.4	0.0276	2.24×10^{-4}	0.0280
8.0	0.0968	3.13×10^{-3}	0.103
8.1	0.117	4.77×10^{-3}	0.127

5.5 Kinetics

The aqueous solution of GSH were mixed with an equal volume of an aqueous KOH (0.04 M). Then, the obtained solution (with $[OH^-]$ = 0.02 M) was used to fill one of the reservoir syringes of the stopped-flow spectrometer. After mixing with the electrophile solution, a hydroxide concentration of $[OH^-]_0$ = 0.01 M (pH 12) was achieved in the observation cell of the stopped-flow spectrometer.

We assumed quantitative deprotonation of the Gly-COOH, the glutamyl-NH_3^+, and the cysteine-SH groups in GSH at pH 12, which consumes 3 equivs of hydroxide ions. Under the conditions of the kinetic experiments (pH 12) >99.5% of GSH was deprotonated to the thiolate **H** [that is, GSH(NH_2/S^-)]. Likewise, we assumed quantitative deprotonation of the COOH group in AcCys at pH 12, which consumes 1 equiv of hydroxide ions. The remaining OH^- concentration was then used to calculate the concentration of the thiolate $AcCys^-$ in the reaction mixture from pK_a(AcCys) 9.62[6] according to the method described in ref. 5. Under the conditions of the kinetic experiments (that is, at pH 12) >99% of the supplied AcCys was deprotonated to the thiolate $AcCys^-$.

By using a high excess of the nucleophilic thiolates RS^- (GS^- or $AcCys^-$) over the electrophiles **E**, the concentrations of RS^- remained almost constant during the kinetic runs, resulting in mono-exponential decays of the electrophiles' absorptions. First-order rate constants k_{obs} (s^{-1}) were obtained by least-squares fitting the single-exponential function $A_t = A_0 \exp(-k_{obs}t) + C$ to the time-dependent absorbances (averaged from typically four to eight kinetic runs at each nucleophile concentration).

The contribution of competing nucleophiles (H_2O and HO^-) to the consumption of the electrophiles during their reactions with RS^- was found to be negligible (<1% in total, cf Figure S2), which allowed us to directly plot the observed first-order rate constants k_{obs} vs $[RS^-]$ to derive the second-order rate constant k_2 (M^{-1} s^{-1}) from the slopes of the resulting linear correlations.

Kinetics of GSH with cationic and neutral reference electrophiles

E2 + GSH in alkaline 99.5/0.5 (v/v) H_2O/CH_3CN (stopped-flow, detection at 614 nm)

$[\mathbf{E2}]_0$, mol L^{-1}	$[GSH]_0$, mol L^{-1}	$[OH^-]_0$, mol L^{-1}	$[GS^-]$, mol L^{-1}	$[OH^-]$, mol L^{-1}	k_{obs}, s^{-1}
4.38×10^{-6}	1.00×10^{-4}	1.00×10^{-2}	1.00×10^{-4}	9.70×10^{-3}	2.47×10^{2}
4.38×10^{-6}	2.00×10^{-4}	1.00×10^{-2}	2.00×10^{-4}	9.40×10^{-3}	5.04×10^{2}
4.38×10^{-6}	3.00×10^{-4}	1.00×10^{-2}	3.00×10^{-4}	9.10×10^{-3}	8.83×10^{2}
4.38×10^{-6}	4.00×10^{-4}	1.00×10^{-2}	4.00×10^{-4}	8.80×10^{-3}	1.02×10^{3}

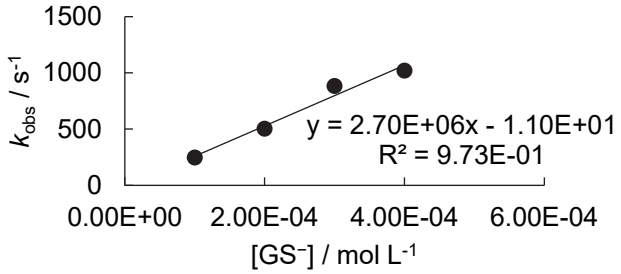

$k_2 = 2.70 \times 10^6$ M^{-1} s^{-1}

E3 + GSH in alkaline 99.5/0.5 (v/v) H_2O/CH_3CN (stopped-flow, detection at 634 nm)

$[\mathbf{E3}]_0$, mol L^{-1}	$[GSH]_0$, mol L^{-1}	$[OH^-]_0$, mol L^{-1}	$[GS^-]$, mol L^{-1}	$[OH^-]$, mol L^{-1}	k_{obs}, s^{-1}
2.32×10^{-6}	1.00×10^{-4}	1.00×10^{-2}	1.00×10^{-4}	9.70×10^{-3}	8.41×10^{1}
2.32×10^{-6}	2.00×10^{-4}	1.00×10^{-2}	2.00×10^{-4}	9.40×10^{-3}	2.07×10^{2}
2.32×10^{-6}	3.00×10^{-4}	1.00×10^{-2}	3.00×10^{-4}	9.10×10^{-3}	3.27×10^{2}
2.32×10^{-6}	4.00×10^{-4}	1.00×10^{-2}	4.00×10^{-4}	8.80×10^{-3}	5.00×10^{2}

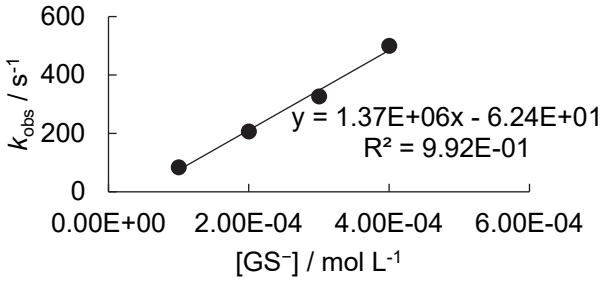

$k_2 = 1.37 \times 10^6$ M^{-1} s^{-1}

E4 + GSH in alkaline 99.5/0.5 (v/v) H_2O/CH_3CN (stopped-flow, detection at 630 nm)

$[\mathbf{E4}]_0$, mol L^{-1}	$[GSH]_0$, mol L^{-1}	$[OH^-]_0$, mol L^{-1}	$[GS^-]$, mol L^{-1}	$[OH^-]$, mol L^{-1}	k_{obs}, s^{-1}
5.45×10^{-6}	1.00×10^{-4}	1.00×10^{-2}	1.00×10^{-4}	9.70×10^{-3}	6.69×10^{1}
5.45×10^{-6}	2.00×10^{-4}	1.00×10^{-2}	2.00×10^{-4}	9.40×10^{-3}	1.43×10^{2}
5.45×10^{-6}	3.00×10^{-4}	1.00×10^{-2}	3.00×10^{-4}	9.10×10^{-3}	2.06×10^{2}
5.45×10^{-6}	4.00×10^{-4}	1.00×10^{-2}	4.00×10^{-4}	8.80×10^{-3}	2.66×10^{2}

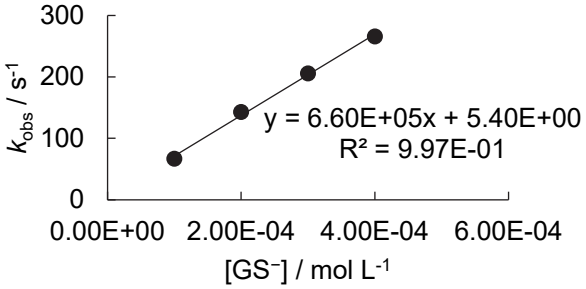

$k_2 = 6.60 \times 10^5$ M^{-1} s^{-1}

E5 + GSH in alkaline 89/11 (v/v) H_2O/CH_3CN (stopped-flow, detection at 396 nm)

$[\mathbf{E5}]_0$, mol L^{-1}	$[GSH]_0$, mol L^{-1}	$[OH^-]_0$, mol L^{-1}	$[GS^-]$, mol L^{-1}	$[OH^-]$, mol L^{-1}	k_{obs}, s^{-1}
1.03×10^{-5}	1.00×10^{-4}	1.00×10^{-2}	1.00×10^{-4}	9.70×10^{-3}	9.01×10^{1}
1.03×10^{-5}	2.00×10^{-4}	1.00×10^{-2}	2.00×10^{-4}	9.40×10^{-3}	1.79×10^{2}
1.03×10^{-5}	3.00×10^{-4}	1.00×10^{-2}	3.00×10^{-4}	9.10×10^{-3}	2.76×10^{2}
1.03×10^{-5}	4.00×10^{-4}	1.00×10^{-2}	4.00×10^{-4}	8.80×10^{-3}	3.78×10^{2}

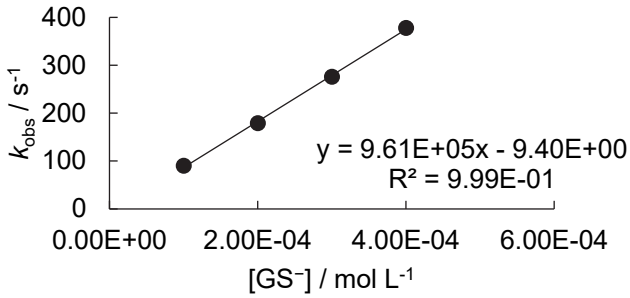

$k_2 = 9.61 \times 10^5$ M^{-1} s^{-1}

E6 + GSH in alkaline 89/11 (v/v) H_2O/CH_3CN (stopped-flow, detection at 504 nm)

$[\mathbf{E6}]_0$, mol L^{-1}	$[GSH]_0$, mol L^{-1}	$[OH^-]_0$, mol L^{-1}	$[GS^-]$, mol L^{-1}	$[OH^-]$, mol L^{-1}	k_{obs}, s^{-1}
1.21×10^{-5}	1.00×10^{-4}	1.00×10^{-2}	1.00×10^{-4}	9.70×10^{-3}	1.14×10^{1}
1.21×10^{-5}	2.00×10^{-4}	1.00×10^{-2}	2.00×10^{-4}	9.40×10^{-3}	1.83×10^{1}
1.21×10^{-5}	3.00×10^{-4}	1.00×10^{-2}	3.00×10^{-4}	9.10×10^{-3}	2.62×10^{1}
1.21×10^{-5}	4.00×10^{-4}	1.00×10^{-2}	4.00×10^{-4}	8.80×10^{-3}	3.41×10^{1}

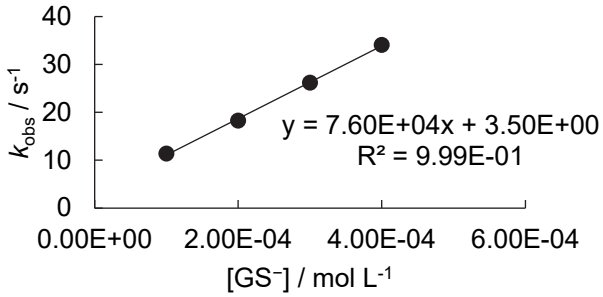

$k_2 = 7.60 \times 10^4$ M^{-1} s^{-1}

E7 + GSH in alkaline 99.5/0.5 (v/v) H_2O/CH_3CN (stopped-flow, detection at 310 nm)

$[\mathbf{E7}]_0$, mol L^{-1}	$[GSH]_0$, mol L^{-1}	$[OH^-]_0$, mol L^{-1}	$[GS^-]$, mol L^{-1}	$[OH^-]$, mol L^{-1}	k_{obs}, s^{-1}
1.90×10^{-5}	1.00×10^{-4}	1.00×10^{-2}	1.00×10^{-4}	9.70×10^{-3}	1.50×10^{1}
1.90×10^{-5}	2.00×10^{-4}	1.00×10^{-2}	2.00×10^{-4}	9.40×10^{-3}	3.01×10^{1}
1.90×10^{-5}	3.00×10^{-4}	1.00×10^{-2}	3.00×10^{-4}	9.10×10^{-3}	4.65×10^{1}
1.90×10^{-5}	4.00×10^{-4}	1.00×10^{-2}	4.00×10^{-4}	8.80×10^{-3}	5.81×10^{1}

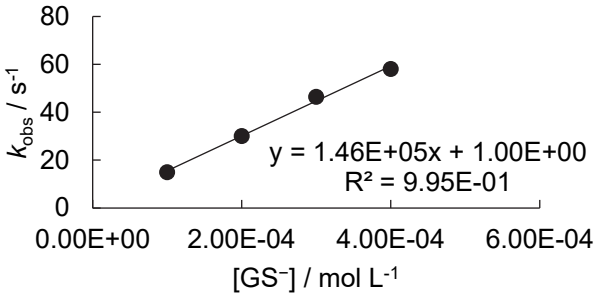

$k_2 = 1.46 \times 10^5$ M^{-1} s^{-1}

E8 + GSH in alkaline 99.5/0.5 (v/v) H_2O/CH_3CN (stopped-flow, detection at 362 nm)

$[\mathbf{E8}]_0$, mol L^{-1}	$[GSH]_0$, mol L^{-1}	$[OH^-]_0$, mol L^{-1}	$[GS^-]$, mol L^{-1}	$[OH^-]$, mol L^{-1}	k_{obs}, s^{-1}
1.96×10^{-5}	1.00×10^{-4}	1.00×10^{-2}	1.00×10^{-4}	9.70×10^{-3}	3.40
1.96×10^{-5}	2.00×10^{-4}	1.00×10^{-2}	2.00×10^{-4}	9.40×10^{-3}	6.83
1.96×10^{-5}	3.00×10^{-4}	1.00×10^{-2}	3.00×10^{-4}	9.10×10^{-3}	1.06×10^{1}
1.96×10^{-5}	4.00×10^{-4}	1.00×10^{-2}	4.00×10^{-4}	8.80×10^{-3}	1.42×10^{1}

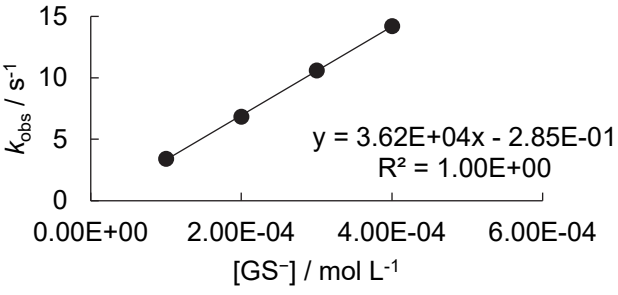

$k_2 = 3.62 \times 10^4$ M^{-1} s^{-1}

E9 + GSH in alkaline 89/11 (v/v) H_2O/CH_3CN (stopped-flow, detection at 487 nm)

$[\mathbf{E9}]_0$, mol L^{-1}	$[GSH]_0$, mol L^{-1}	$[OH^-]_0$, mol L^{-1}	$[GS^-]$, mol L^{-1}	$[OH^-]$, mol L^{-1}	k_{obs}, s^{-1}
3.27×10^{-5}	1.00×10^{-4}	1.00×10^{-2}	1.00×10^{-4}	9.70×10^{-3}	2.42×10^{1}
3.27×10^{-5}	2.00×10^{-4}	1.00×10^{-2}	2.00×10^{-4}	9.40×10^{-3}	5.16×10^{1}
3.27×10^{-5}	3.00×10^{-4}	1.00×10^{-2}	3.00×10^{-4}	9.10×10^{-3}	7.65×10^{1}
3.27×10^{-5}	4.00×10^{-4}	1.00×10^{-2}	4.00×10^{-4}	8.80×10^{-3}	1.02×10^{2}

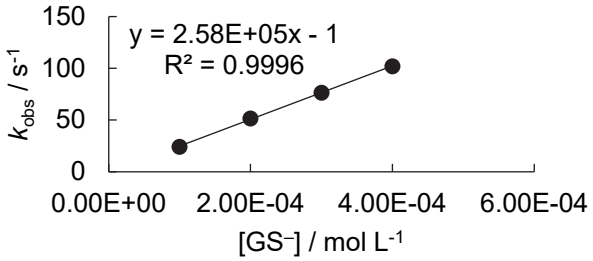

$k_2 = 2.58 \times 10^5$ M^{-1} s^{-1}

E10 + GSH in alkaline 89/11 (v/v) H_2O/CH_3CN (stopped-flow, detection at 512 nm)

$[\mathbf{E10}]_0$, mol L^{-1}	$[GSH]_0$, mol L^{-1}	$[OH^-]_0$, mol L^{-1}	$[GS^-]$, mol L^{-1}	$[OH^-]$, mol L^{-1}	k_{obs}, s^{-1}
3.36×10^{-5}	1.00×10^{-4}	1.00×10^{-2}	1.00×10^{-4}	9.70×10^{-3}	5.19
3.36×10^{-5}	2.00×10^{-4}	1.00×10^{-2}	2.00×10^{-4}	9.40×10^{-3}	1.09×10^{1}
3.36×10^{-5}	3.00×10^{-4}	1.00×10^{-2}	3.00×10^{-4}	9.10×10^{-3}	1.64×10^{1}
3.36×10^{-5}	4.00×10^{-4}	1.00×10^{-2}	4.00×10^{-4}	8.80×10^{-3}	2.20×10^{1}
3.36×10^{-5}	5.00×10^{-4}	1.00×10^{-2}	5.00×10^{-4}	8.50×10^{-3}	2.62×10^{1}

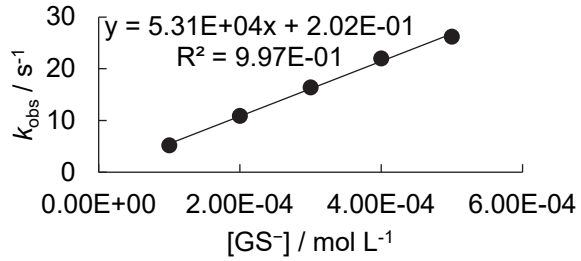

$k_2 = 5.31 \times 10^4$ M^{-1} s^{-1}

Kinetics of AcCys with cationic and neutral reference electrophiles

E2 + AcCys in alkaline 99.5/0.5 (v/v) H_2O/CH_3CN (stopped-flow, detection at 614 nm)

$[\mathbf{E2}]_0$, mol L^{-1}	$[AcCys]_0$, mol L^{-1}	$[OH^-]_0$, mol L^{-1}	$[AcCys^-]$, mol L^{-1}	$[OH^-]$, mol L^{-1}	k_{obs}, s^{-1}
3.06×10^{-6}	1.00×10^{-4}	1.00×10^{-2}	9.96×10^{-5}	9.80×10^{-3}	1.18×10^{2}
3.06×10^{-6}	2.00×10^{-4}	1.00×10^{-2}	1.99×10^{-4}	9.60×10^{-3}	2.58×10^{2}
3.06×10^{-6}	3.00×10^{-4}	1.00×10^{-2}	2.99×10^{-4}	9.40×10^{-3}	4.16×10^{2}
3.06×10^{-6}	4.00×10^{-4}	1.00×10^{-2}	3.98×10^{-4}	9.20×10^{-3}	5.64×10^{2}
3.06×10^{-6}	5.00×10^{-4}	1.00×10^{-2}	4.98×10^{-4}	9.00×10^{-3}	6.97×10^{2}

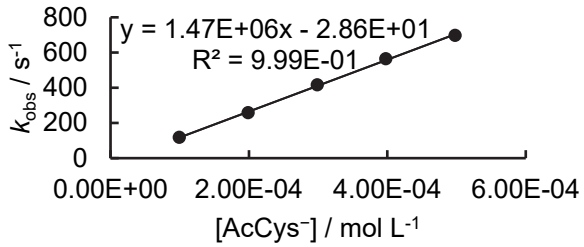

$k_2 = 1.47 \times 10^6$ M^{-1} s^{-1}

E3 + AcCys in alkaline 99.5/0.5 (v/v) H_2O/CH_3CN (stopped-flow, detection at 634 nm)

$[\mathbf{E3}]_0$, mol L^{-1}	$[AcCys]_0$, mol L^{-1}	$[OH^-]_0$, mol L^{-1}	$[AcCys^-]$, mol L^{-1}	$[OH^-]$, mol L^{-1}	k_{obs}, s^{-1}
2.88×10^{-6}	1.00×10^{-4}	1.00×10^{-2}	9.96×10^{-5}	9.80×10^{-3}	4.62×10^{1}
2.88×10^{-6}	2.00×10^{-4}	1.00×10^{-2}	1.99×10^{-4}	9.60×10^{-3}	9.28×10^{1}
2.88×10^{-6}	3.00×10^{-4}	1.00×10^{-2}	2.99×10^{-4}	9.40×10^{-3}	1.54×10^{2}
2.88×10^{-6}	4.00×10^{-4}	1.00×10^{-2}	3.98×10^{-4}	9.20×10^{-3}	2.04×10^{2}
2.88×10^{-6}	5.00×10^{-4}	1.00×10^{-2}	4.98×10^{-4}	9.00×10^{-3}	2.68×10^{2}

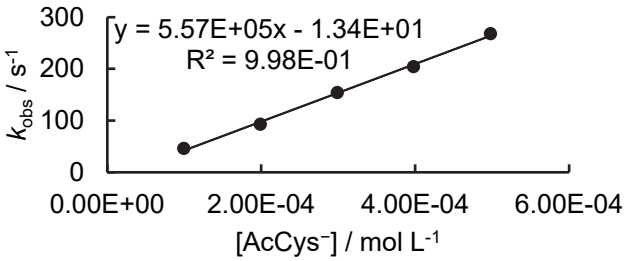

$k_2 = 5.57 \times 10^5$ M^{-1} s^{-1}

E4 + AcCys in alkaline 99.5/0.5 (v/v) H_2O/CH_3CN (stopped-flow, detection at 630 nm)

$[\mathbf{E4}]_0$, mol L^{-1}	$[AcCys]_0$, mol L^{-1}	$[OH^-]_0$, mol L^{-1}	$[AcCys^-]$, mol L^{-1}	$[OH^-]$, mol L^{-1}	k_{obs}, s^{-1}
3.24×10^{-6}	1.00×10^{-4}	1.00×10^{-2}	9.96×10^{-5}	9.80×10^{-3}	3.31×10^{1}
3.24×10^{-6}	2.00×10^{-4}	1.00×10^{-2}	1.99×10^{-4}	9.60×10^{-3}	6.50×10^{1}
3.24×10^{-6}	3.00×10^{-4}	1.00×10^{-2}	2.99×10^{-4}	9.40×10^{-3}	1.02×10^{2}
3.24×10^{-6}	4.00×10^{-4}	1.00×10^{-2}	3.98×10^{-4}	9.20×10^{-3}	1.37×10^{2}
3.24×10^{-6}	5.00×10^{-4}	1.00×10^{-2}	4.98×10^{-4}	9.00×10^{-3}	1.70×10^{2}

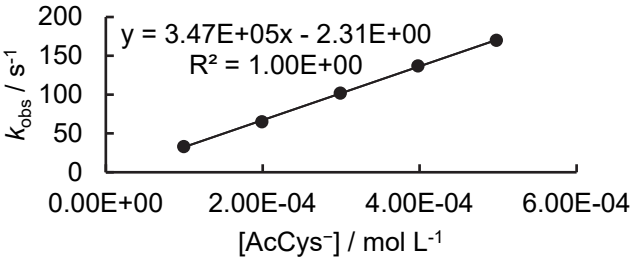

$k_2 = 3.47 \times 10^5$ M^{-1} s^{-1}

E5 + AcCys in alkaline 89/11 (v/v) H_2O/CH_3CN (stopped-flow, detection at 396 nm)

$[\mathbf{E5}]_0$, mol L^{-1}	$[AcCys]_0$, mol L^{-1}	$[OH^-]_0$, mol L^{-1}	$[AcCys^-]$, mol L^{-1}	$[OH^-]$, mol L^{-1}	k_{obs}, s^{-1}
3.09×10^{-5}	1.00×10^{-4}	1.00×10^{-2}	9.96×10^{-5}	9.80×10^{-3}	5.32×10^{1}
3.09×10^{-5}	2.00×10^{-4}	1.00×10^{-2}	1.99×10^{-4}	9.60×10^{-3}	1.08×10^{2}
3.09×10^{-5}	3.00×10^{-4}	1.00×10^{-2}	2.99×10^{-4}	9.40×10^{-3}	1.55×10^{2}
3.09×10^{-5}	4.00×10^{-4}	1.00×10^{-2}	3.98×10^{-4}	9.20×10^{-3}	2.13×10^{2}
3.09×10^{-5}	5.00×10^{-4}	1.00×10^{-2}	4.98×10^{-4}	9.00×10^{-3}	2.60×10^{2}

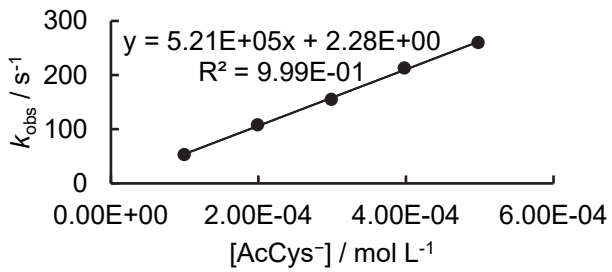

$k_2 = 5.21 \times 10^5$ M^{-1} s^{-1}

E8 + AcCys in alkaline 99.5/0.5 (v/v) H_2O/CH_3CN (stopped-flow, detection at 362 nm)

$[\mathbf{E8}]_0$, mol L^{-1}	$[AcCys]_0$, mol L^{-1}	$[OH^-]_0$, mol L^{-1}	$[AcCys^-]$, mol L^{-1}	$[OH^-]$, mol L^{-1}	k_{obs}, s^{-1}
4.30×10^{-5}	1.00×10^{-4}	1.00×10^{-2}	9.96×10^{-5}	9.80×10^{-3}	2.60
4.30×10^{-5}	2.00×10^{-4}	1.00×10^{-2}	1.99×10^{-4}	9.60×10^{-3}	5.93
4.30×10^{-5}	3.00×10^{-4}	1.00×10^{-2}	2.99×10^{-4}	9.40×10^{-3}	8.88
4.30×10^{-5}	4.00×10^{-4}	1.00×10^{-2}	3.98×10^{-4}	9.20×10^{-3}	1.22×10^{1}
4.30×10^{-5}	5.00×10^{-4}	1.00×10^{-2}	4.98×10^{-4}	9.00×10^{-3}	1.51×10^{1}

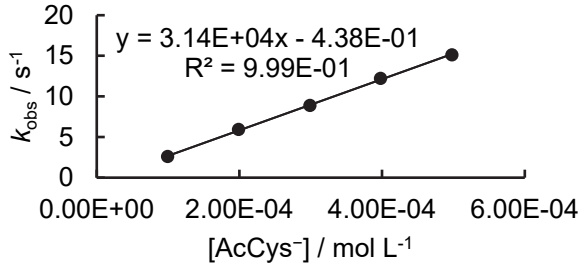

$k_2 = 3.14 \times 10^4$ M^{-1} s^{-1}

E9 + AcCys in alkaline 89/11 (v/v) H_2O/CH_3CN (stopped-flow, detection at 487 nm)

$[\mathbf{E9}]_0$, mol L^{-1}	$[AcCys]_0$, mol L^{-1}	$[OH^-]_0$, mol L^{-1}	$[AcCys^-]$, mol L^{-1}	$[OH^-]$, mol L^{-1}	k_{obs}, s^{-1}
3.27×10^{-5}	1.00×10^{-4}	1.00×10^{-2}	9.96×10^{-5}	9.80×10^{-3}	2.00×10^{1}
3.27×10^{-5}	2.00×10^{-4}	1.00×10^{-2}	1.99×10^{-4}	9.60×10^{-3}	4.03×10^{1}
3.27×10^{-5}	3.00×10^{-4}	1.00×10^{-2}	2.99×10^{-4}	9.40×10^{-3}	5.96×10^{1}
3.27×10^{-5}	4.00×10^{-4}	1.00×10^{-2}	3.98×10^{-4}	9.20×10^{-3}	7.94×10^{1}
3.27×10^{-5}	5.00×10^{-4}	1.00×10^{-2}	4.98×10^{-4}	9.00×10^{-3}	9.80×10^{1}

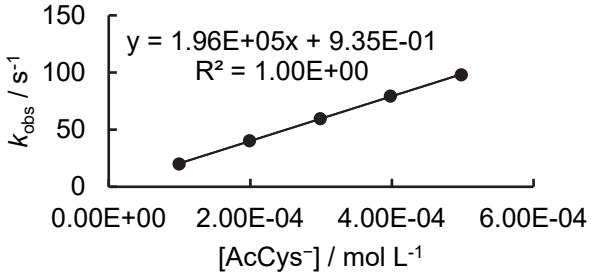

$k_2 = 1.96 \times 10^5$ M^{-1} s^{-1}

E10 + AcCys in alkaline 89/11 (v/v) H_2O/CH_3CN (stopped-flow, detection at 512 nm)

$[\mathbf{E10}]_0$, mol L^{-1}	$[AcCys]_0$, mol L^{-1}	$[OH^-]_0$, mol L^{-1}	$[AcCys^-]$, mol L^{-1}	$[OH^-]$, mol L^{-1}	k_{obs}, s^{-1}
3.36×10^{-5}	1.00×10^{-4}	1.00×10^{-2}	9.96×10^{-5}	9.80×10^{-3}	4.35
3.36×10^{-5}	2.00×10^{-4}	1.00×10^{-2}	1.99×10^{-4}	9.60×10^{-3}	8.85×10^{0}
3.36×10^{-5}	3.00×10^{-4}	1.00×10^{-2}	2.99×10^{-4}	9.40×10^{-3}	1.28×10^{1}
3.36×10^{-5}	4.00×10^{-4}	1.00×10^{-2}	3.98×10^{-4}	9.20×10^{-3}	1.70×10^{1}
3.36×10^{-5}	5.00×10^{-4}	1.00×10^{-2}	4.98×10^{-4}	9.00×10^{-3}	2.08×10^{1}

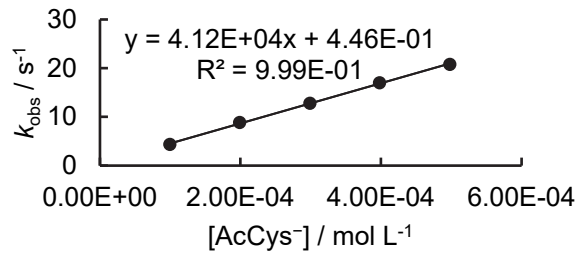

$k_2 = 4.12 \times 10^4$ M^{-1} s^{-1}

5.6 Electrophilicity of Michael Acceptors towards GSH in Kinetic Assays

Table S4: Rate constants for reactions of Michael acceptors with GSH from kinetic assays.

Label	Michael acceptor	k_{GSH} (M^{-1} s^{-1})	pH (*T*)	$k_2(GS^-)$[a] (M^{-1} s^{-1})	Estimated *E*[b]	ΔG_{MA}[c] (kJ mol^{-1})
	α,β-unsaturated aldehydes					
M1	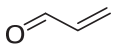 acrolein	1.21×10^2 1.20×10^2 7.28	7.4 (20 °C)[d] 7.2 (25 °C)[e] 8.0 (25 °C)[f]	4.32×10^3	–14.4	–119.0
M2	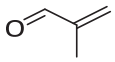 methacrolein	3.38	7.4 (25 °C)[g]	121	–17.2	–94.2
M3	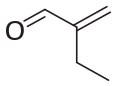 2-ethyl acrolein	9.90×10^{-1}	7.4 (25 °C)[g]	35.4	–18.2	–93.2
M4	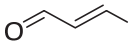 cinnamaldehyde	9.15×10^{-2}	7.4 (25 °C)[g]	3.27	–20.0	–94.9
M5	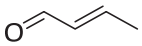 crotonaldehyde	7.85×10^{-1} 7.2×10^{-1} 2.67	7.4 (20 °C)[d] 7.2 (25 °C)[e] 8.0 (25 °C)[f]	28.0	–18.4	–91.6
M6	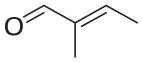 trans-2-methyl-2-butenal	7.90×10^{-3}	7.4 (25 °C)[g]	2.82×10^{-1}	–22.0	–66.8
M7	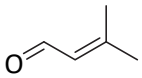 3-methyl-2-butenal	2.85×10^{-2}	7.4 (25 °C)[g]	1.02	–21.0	–68.8
M8	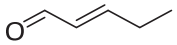 2-pentenal	4.71×10^{-1} 4.72×10^{-1} 1.5	7.4 (20 °C)[d] 7.4 (25 °C)[g] 8.0 (25 °C)[f]	16.8	–18.8	–87.3
M9	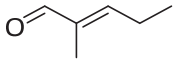 trans-2-methyl-2-pentenal	4.57×10^{-3}	7.4 (25 °C)[g]	1.63×10^{-1}	–22.4	–62.5
M10	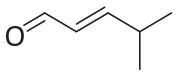 4-methyl-2-pentenal	1.77×10^{-1}	7.4 (25 °C)[g]	6.31	–19.5	–78.0
M11	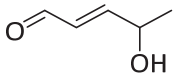 4-hydroxy-2-pentenal	2.19	7.4 (20 °C)[d]	78.2	–17.6	–115.2
M12	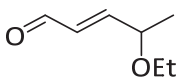 4-ethoxy-2-pentenal	1.83	7.4 (20 °C)[d]	65.4	–17.7	–85.0
M13	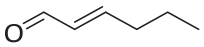 2-hexenal	3.30×10^{-1} 4.18×10^{-1} 3.40×10^{-1} 9.0×10^{-1}	7.4 (20 °C)[d] 7.4 (25 °C)[g] 7.2 (25 °C)[e] 8.0 (25 °C)[f]	11.8	–19.0	–85.7

M14	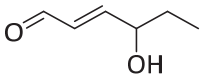 4-hydroxy-2-hexenal	1.56	7.4 (20 °C)[d]	55.7	–17.8	–109.7
M15	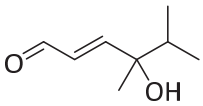 (E)-4-hydroxy-4,5-dimethylhex-2-enal	3.57×10^{-2}	7.4 (20 °C)[d]	1.28	–20.8	–93.4
M16	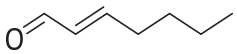 2-heptenal	9.3×10^{-1}	8.0 (25 °C)[f]	9.0	–19.2	–85.2
M17	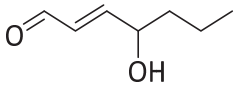 4-hydroxy-2-heptenal	1.83	7.4 (20 °C)[d]	65.4	–17.7	–109.4
M18	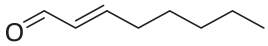 trans-2-octenal	3.00×10^{-1} 2.8×10^{-1} 7.2×10^{-1}	7.4 (25 °C)[g] 7.2 (25 °C)[e] 8.0 (25 °C)[f]	10.7	–19.1	–85.1
M19	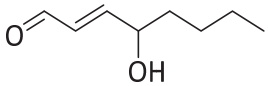 4-hydroxy-2-octenal	1.74	7.4 (20 °C)[d]	62.1	–17.7	–109.0
M20	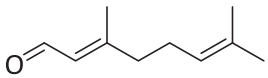 citral	3.23×10^{-2} 3.3×10^{-2}	7.4 (20 °C)[d] 8.0 (25 °C)[f]	1.15	–20.9	–59.5
M21	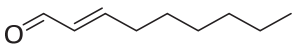 trans-2-nonenal	2.52×10^{-1} 6.5×10^{-1}	7.4 (25 °C)[g] 8.0 (25 °C)[f]	8.99	–19.3	–81.5
M22	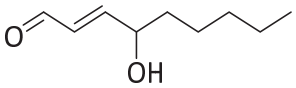 4-hydroxy-2-nonenal	1.09	7.4 (20 °C)[d]	38.9	–18.1	–112.3
M23	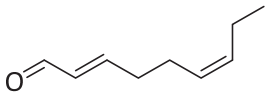 trans-2-cis-6-nonadienal	3.80×10^{-1} 5.7×10^{-1} 1.1	7.4 (25 °C)[g] 7.2 (25 °C)[e] 8.0 (25 °C)[f]	13.6	–18.9	–87.3
M24	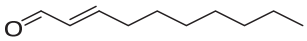 trans-2-decenal	1.68×10^{-1}	7.4 (25 °C)[g]	6.01	–19.6	–85.1
M25	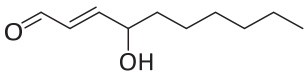 4-hydroxy-2-decenal	1.96	7.4 (20 °C)[d]	70.0	–17.6	–107.1
M26	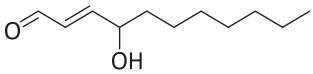 4-hydroxy-2-undecenal	1.47	7.4 (20 °C)[d]	52.5	–17.9	–109.7
M27	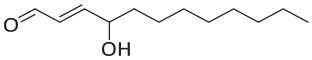 4-hydroxy-2-dodecenal	2.44	7.4 (20 °C)[d]	87.1	–17.5	–106.8
M28	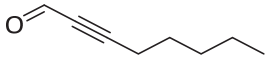 2-octynal	8.12	7.4 (25 °C)[g]	290	–16.5	–111.0

M29	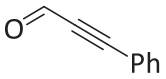 phenyl propiolaldehyde	7.43	7.4 (25 °C)[g]	265	–16.6	–121.0
	α,β-unsaturated ketones					
E11	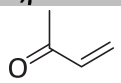 methyl vinylketone	3.19×10^{1}	7.4 (20 °C)[d]	1.14×10^{3}	–16.8[h]	–104.2[h]
M30	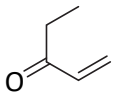 1-penten-3-one	2.10×10^{1}	7.4 (25 °C)[g]	751	–15.8	–99.3
M31	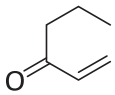 1-hexen-3-one	1.96×10^{1}	7.4 (25 °C)[g]	698	–15.8	–99.7
M32	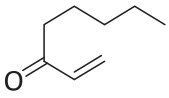 1-octen-3-one	1.79×10^{1}	7.4 (25 °C)[g]	639	–15.9	–99.0
M33	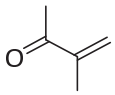 3-methyl-3-buten-2-one	6.00×10^{-1}	7.4 (20 °C)[d]	21.4	–18.6	–72.6
M34	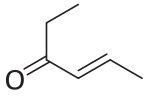 4-hexen-3-one	4.03×10^{-1}	7.4 (25 °C)[g]	14.4	–18.9	–74.9
M35	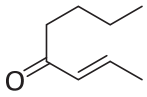 2-octen-4-one	4.35×10^{-1}	7.4 (25 °C)[g]	15.5	–18.8	–74.8
M36	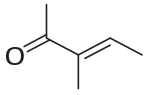 3-methyl-3-penten-2-one	1.30×10^{-2}	7.4 (25 °C)[g]	4.64×10^{-1}	–21.6	–51.0
M37	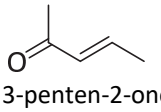 3-penten-2-one	4.45×10^{-1}	7.4 (25 °C)[g]	15.9	–18.8	–79.5
M38	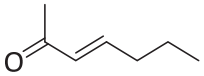 3-hepten-2-one	2.08×10^{-1}	7.4 (25 °C)[g]	7.44	–19.4	–73.7
M39	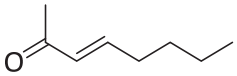 3-octen-2-one	1.90×10^{-1}	7.4 (25 °C)[g]	6.79	–19.5	–73.5
M40	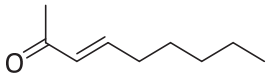 3-nonen-2-one	1.80×10^{-1}	7.4 (25 °C)[g]	6.43	–19.5	–75.4
M41	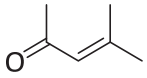 mesityl oxide	2.30×10^{-3} 3.47×10^{-3}	7.4 (20 °C)[d] 7.4 (25 °C)[g]	8.21×10^{-2}	–22.9	–58.6
M42	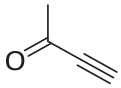 3-butyn-2-one	7.62	7.4 (25 °C)[i]	272	–16.6	–139.5

M43	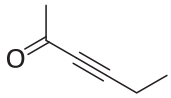 3-hexyn-2-one	1.33	7.4 (25 °C)[g]	47.6	–17.9	–92.9
M44	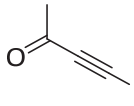 4-phenyl-3-butyn-2-one	5.03	7.4 (25 °C)[i]	180	–16.9	–101.5
	α,β-unsaturated esters					
M45	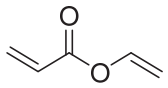 vinyl acrylate	1.49	7.4 (25 °C)[i]	53.1	–17.9	–116.4
M46	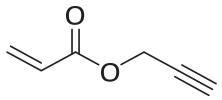 propargyl acrylate	8.57×10^{-1}	7.4 (25 °C)[g]	30.6	–18.3	–94.2
M47	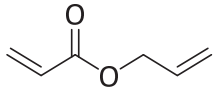 allyl acrylate	3.27×10^{-1}	7.4 (25 °C)[g]	11.7	–19.0	–83.6
M48	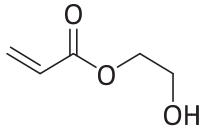 2-hydroxyethyl acrylate	3.32×10^{-1}	7.4 (25 °C)[g]	11.8	–19.0	–100.3
M49	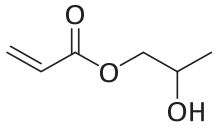 2-hydroxypropyl acrylate	3.00×10^{-1}	7.4 (25 °C)[g]	10.7	–19.1	–98.6
E12	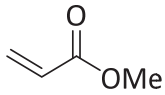 methyl acrylate	1.90×10^{-1}	7.4 (25 °C)[g]	6.79	–18.8[h]	–80.7[h]
E13	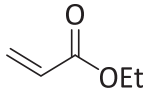 ethyl acrylate	1.77×10^{-1}	7.4 (25 °C)[g]	6.31	–19.1[h]	–75.1[h]
M50	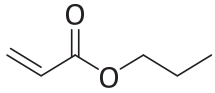 n-propyl acrylate	1.70×10^{-1}	7.4 (25 °C)[g]	6.07	–19.6	–75.1
M51	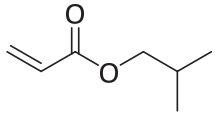 iso-butyl acrylate	1.57×10^{-1}	7.4 (25 °C)[g]	5.60	–19.6	–77.3
M52	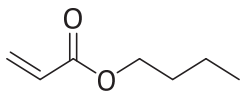 n-butyl acrylate	1.42×10^{-1}	7.4 (25 °C)[g]	5.08	–19.7	–74.3
M53	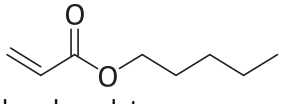 hexyl acrylate	1.32×10^{-1}	7.4 (25 °C)[i]	4.73	–19.8	–74.1

E14	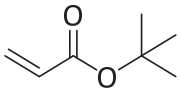 tert-butyl acrylate	4.17×10^{-2}	7.4 (25 °C)[g]	1.49	–20.2[h]	–71.6[h]
M54	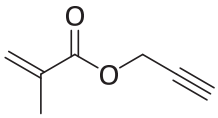 propargyl methacrylate	3.67×10^{-3}	7.4 (25 °C)[g]	1.31×10^{-1}	–22.6	–70.4
M55	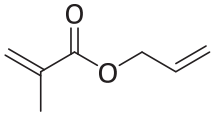 allyl methacrylate	1.52×10^{-2}	7.4 (25 °C)[i]	5.43×10^{-1}	–21.4	–58.2
M56	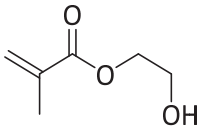 2-hydroxyethyl methacrylate	2.90×10^{-3}	7.4 (25 °C)[i]	1.03×10^{-1}	–22.7	–78.8
M57	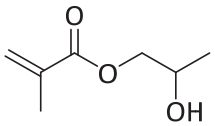 2-hydroxypropyl methacrylate	1.56×10^{-2}	7.4 (25 °C)[i]	5.56×10^{-1}	–21.4	–81.2
M58	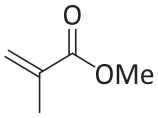 methyl methacrylate	1.20×10^{-3}	7.4 (25 °C)[g]	4.29×10^{-2}	–23.4	–57.0
E16	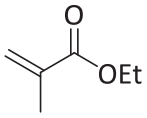 ethyl methacrylate	9.67×10^{-4}	7.4 (25 °C)[g]	3.45×10^{-2}	–22.8[h]	–51.9[h]
M59	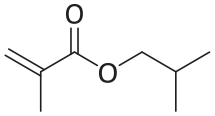 isobutyl methacrylate	6.05×10^{-3}	7.4 (25 °C)[i]	2.16×10^{-1}	–22.2	–51.0
M60	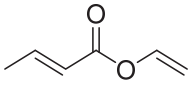 vinyl crotonate	2.30×10^{-2}	7.4 (25 °C)[i]	8.22×10^{-1}	–21.1	–90.7
M61	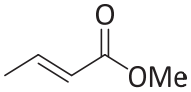 methyl crotonate	2.73×10^{-3}	7.4 (25 °C)[g]	9.76×10^{-2}	–22.8	–55.8
E17	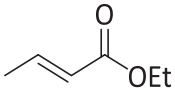 ethyl crotonate	3.10×10^{-3} 2.68×10^{-3}	7.4 (20 °C)[d] 7.4 (25 °C)[g]	1.11×10^{-1}	–23.6[h]	–49.8[h]
M62	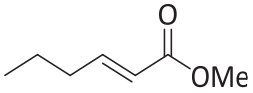 methyl trans-2-hexenoate	3.63×10^{-2}	7.4 (25 °C)[g]	1.30	–20.8	–50.5

M63	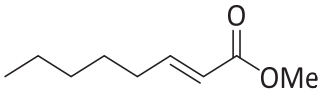 methyl trans-2-octenoate	1.31×10^{-2}	7.4 (25 °C)[g]	4.67×10^{-1}	–21.6	–50.2
M64	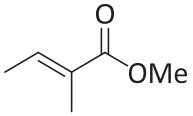 methyl tiglate	1.17×10^{-4}	7.4 (25 °C)[g]	4.17×10^{-3}	–25.3	–41.4
M65	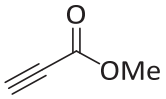 methyl propiolate	1.95	7.4 (25 °C)[g]	69.6	–17.6	–137.3
M66	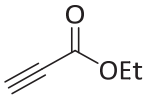 ethyl propiolate	1.75	7.4 (25 °C)[g]	62.5	–17.7	–133.9
M67	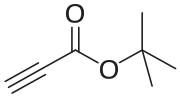 tert-butyl propiolate	1.04	7.4 (25 °C)[g]	37.3	–18.1	–121.7
M68	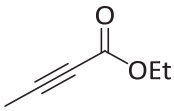 ethyl 2-butynoate	4.03×10^{-2}	7.4 (25 °C)[g]	1.44	–20.7	–88.8
M69	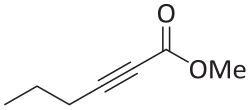 methyl 2-hexynoate	9.50×10^{-2}	7.4 (25 °C)[g]	3.39	–20.0	–87.4
M70	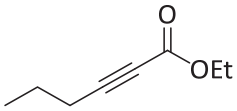 ethyl hex-2-ynoate	6.95×10^{-2}	7.4 (25 °C)[i]	2.48	–20.3	–87.3
M71	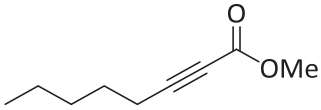 methyl 2-octynoate	4.60×10^{-2}	7.4 (25 °C)[g]	1.64	–20.6	–89.6
	further Michael acceptors					
M72	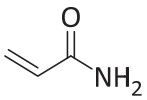 acrylamide	9.27×10^{-3}	7.4 (25 °C)[g]	3.31×10^{-1}	–21.8	–66.5
E15	 acrylonitrile	1.73×10^{-1}	8.1 (30 °C)[j]	1.36	–19.1[h]	–109.4[h]
M73	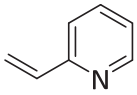 2-vinylpyridine	3.48×10^{-2}	7.4 (25 °C)[i]	1.24	–20.8	–62.8

[a] Calculated by using Equation 2 (main text). [b] Calculated by using equation 1 (main text), lg $k_2(GS^-)$, and the reactivity parameters for GS^- (N = 20.97, s_N = 0.55[5]). [c] For details of the quantum-chemical calculation of methyl anion affinities ΔG_{MA} see Table S5. [d] From ref. 7a. [e] From ref. 7b. [f] From ref. 7c. [g] From ref. 8. [h] From ref. 10c. [i] From ref. 9. [j] From ref. 2.

5.7 Quantum-Chemically Calculated Methyl Anion Affinities (ΔG_{MA}) of Michael Acceptors

Gas phase methyl anion affinities ΔG_{MA} were calculated as described in ref. 10 as negative Gibbs free energies at 298.15 K for the reactions of Michael acceptors (from Table S4) with the methyl anion:

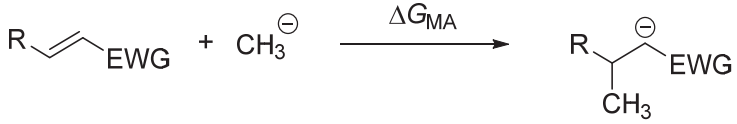

All structures were subjected to a conformational search employing the OPLS-3[11] force field in gas phase with the MCMM method as implemented in Macromodel 2019-1.[12] The 10 conformers with the lowest OPLS-3 energy for every system were subsequently optimized at the B3LYP/6-31G(d,p)[13–15] level in gas phase. For the optimized structures, single-point gas-phase energies with the B3LYP/6-311++G(3df,2pd)[13–16] method and single-point solvation energies at the B3LYP/6-31G(d,p) level employing the SMD model for DMSO[17] were calculated. Final Gibbs free energies were obtained by combining the single point energies at the B3LYP/6-311++G(3df,2pd) with the thermochemical corrections at the B3LYP/6-31G(d,p) level and single point solvation energies at the B3LYP/6-31G(d,p) level. Methyl anion affinities were then determined for every electrophile by calculating the reaction energy for the lowest lying conformer. The quantum-mechanical calculations were performed with Gaussian 16, Rev. A.03.[18]

Table S5: Quantum-mechanically calculated methyl anion affinities ΔG_{MA} for the 1,4-addition to Michael acceptors [in kJ mol^{-1}, calculated at the SMD(DMSO)/B3LYP/6-311++G(3df,2pd)//B3LYP/6-31G(d,p) level of theory]

Michael acceptor	Filename	E_{tot} (B3LYP/6-31G(d,p)	G_{298}	$E_{tot, solv.}$ (SMD(DMSO)/B3LYP/6-31G(d,p)// B3LYP/6-31G(d,p))	$E_{tot, high.}$ (B3LYP/6-311++G(3df,2pd)// B3LYP/6-31G(d,p))	ΔG	ΔG_{solv}	G_{298} (SMD(DMSO)/ B3LYP/6-311++G(3df,2pd)// B3LYP/6-31G(d,p))
	Methyl anion	-39.796028	-39.787379	-39.921582	-39.856638	0.008649	-0.125554	-39.973543
M1	REDO_i1_1	-191.918015	-191.882803	-191.924399	-191.988117	0.035212	-0.006383	-191.959289
	REDO_i1_me_1	-231.853632	-231.784191	-231.943587	-231.957660	0.069441	-0.089955	-231.978175
	ΔG_{MA} [kJ/mol]							-119.0
M2	REDO_c3_1	-231.242222	-231.181138	-231.247954	-231.322077	0.061084	-0.005733	-231.266726
	REDO_c3_me_1	-271.175466	-271.079880	-271.260892	-271.286296	0.095586	-0.085426	-271.276136
	ΔG_{MA} [kJ/mol]							-94.2
M3	REDO_c4_2	-270.558038	-270.470110	-270.564109	-270.648129	0.087928	-0.006072	-270.566273
	REDO_c4_me_1	-310.492882	-310.371014	-310.576525	-310.613557	0.121868	-0.083643	-310.575331
	ΔG_{MA} [kJ/mol]							-93.2
M4	REDO_d5_2	-422.980777	-422.871238	-422.992696	-423.116060	0.109539	-0.011919	-423.018440
	REDO_d5_me_1	-462.922634	-462.778142	-463.006667	-463.088570	0.144492	-0.084033	-463.028111
	ΔG_{MA} [kJ/mol]							-94.9
M5	REDO_i2_1	-231.242908	-231.181824	-231.250957	-231.323428	0.061084	-0.008048	-231.270392
	REDO_i2_me_1	-271.172711	-271.077290	-271.260402	-271.286556	0.095421	-0.087691	-271.278826
	ΔG_{MA} [kJ/mol]							-91.6
M6	REDO_d8_1	-270.564682	-270.478248	-270.571891	-270.654736	0.086434	-0.007209	-270.575511
	REDO_d8_me_1	-310.492232	-310.370375	-310.576055	-310.612538	0.121857	-0.083823	-310.574504
	ΔG_{MA} [kJ/mol]							-66.8
M7	REDO_d7_1	-270.562109	-270.475089	-270.570839	-270.652713	0.087020	-0.008730	-270.574423
	REDO_d7_me_1	-310.492110	-310.368810	-310.575659	-310.613938	0.123300	-0.083549	-310.574187

	ΔG_{MA} [kJ/mol]							-68.8
M8	REDO_c5_2	-270.559083	-270.471641	-270.567542	-270.650239	0.087442	-0.008459	-270.571256
	REDO_c5_me_1	-310.488659	-310.366958	-310.575798	-310.612606	0.121701	-0.087139	-310.578044
	ΔG_{MA} [kJ/mol]							-87.3
M9	REDO_d9_1	-309.880666	-309.767875	-309.888274	-309.981348	0.112791	-0.007608	-309.876165
	REDO_d9_me_2	-349.810641	-349.662218	-349.892601	-349.939981	0.148423	-0.081959	-349.873517
	ΔG_{MA} [kJ/mol]							-62.5
M10	REDO_d1_2	-309.876274	-309.762585	-309.884656	-309.977986	0.113689	-0.008382	-309.872678
	REDO_d1_me_3	-349.806352	-349.658561	-349.890765	-349.939297	0.147791	-0.084413	-349.875919
	ΔG_{MA} [kJ/mol]							-78.0
M11	REDO_j1_5	-345.769903	-345.679573	-345.782967	-345.895474	0.090330	-0.013064	-345.818208
	REDO_j1_me_1	-385.728671	-385.601316	-385.810742	-385.880908	0.127355	-0.082071	-385.835624
	ΔG_{MA} [kJ/mol]							-115.2
M12	REDO_k2_2	-424.399116	-424.257026	-424.409095	-424.542253	0.142090	-0.009980	-424.410143
	REDO_k2_me_6	-464.336063	-464.159079	-464.419347	-464.509774	0.176984	-0.083284	-464.416075
	ΔG_{MA} [kJ/mol]							-85.0
M13	REDO_c6_5	-309.875846	-309.762144	-309.884757	-309.977593	0.113702	-0.008912	-309.872803
	REDO_c6_me_1	-349.808250	-349.660388	-349.893620	-349.941483	0.147862	-0.085370	-349.878991
	ΔG_{MA} [kJ/mol]							-85.7
M14	REDO_j2_1	-385.086609	-384.969895	-385.099891	-385.222268	0.116714	-0.013282	-385.118836
	REDO_j2_me_5	-425.046221	-424.892369	-425.126745	-425.207475	0.153852	-0.080524	-425.134147
	ΔG_{MA} [kJ/mol]							-109.7
M15	REDO_k1_1	-463.721092	-463.551338	-463.733724	-463.875862	0.169754	-0.012631	-463.718740
	REDO_k1_me_4	-503.678261	-503.471030	-503.754772	-503.858591	0.207231	-0.076512	-503.727871
	ΔG_{MA} [kJ/mol]							-93.4
M16	REDO_heptenal_sm_6	-349.192414	-349.052486	-349.201785	-349.304745	0.139928	-0.009372	-349.174188

	REDO_heptenal_z_me1	-389.125072	-388.951038	-389.210507	-389.268765	0.174034	-0.085435	-389.180167
	ΔG_{MA} [kJ/mol]							-85.2
M17	REDO_j3_2	-424.403103	-424.260133	-424.416793	-424.549299	0.142970	-0.013690	-424.420018
	REDO_j3_me_5	-464.363255	-464.183259	-464.443591	-464.534889	0.179996	-0.080336	-464.435229
	ΔG_{MA} [kJ/mol]							-109.4
M18	REDO_c8_6	-388.508941	-388.342793	-388.518748	-388.631841	0.166148	-0.009807	-388.475500
	REDO_c8_me_1	-428.441839	-428.241638	-428.527426	-428.596065	0.200201	-0.085586	-428.481451
	ΔG_{MA} [kJ/mol]							-85.1
M19	REDO_j4_1	-463.719708	-463.550470	-463.733819	-463.876493	0.169238	-0.014111	-463.721366
	REDO_j4_me_8	-503.680033	-503.473806	-503.760513	-503.862170	0.206227	-0.080480	-503.736423
	ΔG_{MA} [kJ/mol]							-109.0
M20	REDO_i5_5	-465.912235	-465.718285	-465.923361	-466.057924	0.193950	-0.011126	-465.875099
	REDO_i5_me_3	-505.847732	-505.616551	-505.927987	-506.022214	0.231181	-0.080255	-505.871287
	ΔG_{MA} [kJ/mol]							-59.5
M21	REDO_c9_6	-427.825467	-427.633000	-427.835713	-427.958932	0.192467	-0.010246	-427.776711
	REDO_c9_me_3	-467.756998	-467.530912	-467.842703	-467.921660	0.226086	-0.085705	-467.781280
	ΔG_{MA} [kJ/mol]							-81.5
M22	REDO_j5_1	-503.034905	-502.839469	-503.049570	-503.202112	0.195436	-0.014665	-503.021341
	REDO_j5_me_8	-542.996725	-542.764285	-543.077451	-543.189391	0.232440	-0.080725	-543.037676
	ΔG_{MA} [kJ/mol]							-112.3
M23	REDO_c7_9	-426.589054	-426.420075	-426.600138	-426.725468	0.168979	-0.011083	-426.567572
	REDO_c7_me_6	-466.521497	-466.318566	-466.608479	-466.690333	0.202931	-0.086982	-466.574385
	ΔG_{MA} [kJ/mol]							-87.3
M24	REDO_d2_3	-467.141984	-466.923270	-467.152666	-467.286009	0.218714	-0.010682	-467.077977
	REDO_d2_me_1	-507.075054	-506.822461	-507.161207	-507.250380	0.252593	-0.086153	-507.083940
	ΔG_{MA} [kJ/mol]							-85.1

M25	REDO_j6_2	-542.351407	-542.130080	-542.365984	-542.529800	0.221327	-0.014578	-542.323051
	REDO_j6_me_1	-582.311861	-582.052922	-582.393036	-582.515167	0.258939	-0.081175	-582.337403
	ΔG_{MA} [kJ/mol]							-107.1
M26	REDO_j7_2	-581.670815	-581.422442	-581.685464	-581.858547	0.248373	-0.014649	-581.624823
	REDO_j7_me_3	-621.629888	-621.344964	-621.711313	-621.843637	0.284924	-0.081425	-621.640138
	ΔG_{MA} [kJ/mol]							-109.7
M27	REDO_j8_2	-620.986526	-620.712325	-621.001121	-621.185797	0.274201	-0.014595	-620.926191
	REDO_j8_me_2	-660.950233	-660.638070	-661.030356	-661.172447	0.312163	-0.080123	-660.940407
	ΔG_{MA} [kJ/mol]							-106.8
M28	REDO_c1_10	-387.247611	-387.106584	-387.257439	-387.372770	0.141027	-0.009828	-387.241571
	REDO_c1_me_3	-427.188505	-427.012085	-427.276907	-427.345391	0.176420	-0.088402	-427.257373
	ΔG_{MA} [kJ/mol]							-111.0
M29	REDO_c2_2	-421.726202	-421.641391	-421.737083	-421.864057	0.084811	-0.010882	-421.790128
	REDO_c2_me_1_geo	-461.680011	-461.559559	-461.763700	-461.846506	0.120452	-0.083689	-461.809743
	ΔG_{MA} [kJ/mol]							-121.0
M30	REDO_a1_1	-270.561057	-270.473673	-270.568330	-270.651156	0.087384	-0.007273	-270.571045
	REDO_a1_me_2	-310.497782	-310.375663	-310.583127	-310.619165	0.122119	-0.085345	-310.582391
	ΔG_{MA} [kJ/mol]							-99.3
M31	REDO_a2_1	-309.877494	-309.763885	-309.885157	-309.977992	0.113609	-0.007663	-309.872046
	REDO_a2_me_1	-349.815492	-349.667236	-349.900267	-349.947029	0.148256	-0.084775	-349.883547
	ΔG_{MA} [kJ/mol]							-99.7
M32	REDO_a3_1	-349.194018	-349.054189	-349.202152	-349.305099	0.139829	-0.008134	-349.173404
	REDO_a3_me_1	-389.132468	-388.958031	-389.217107	-389.274442	0.174437	-0.084639	-389.184644
	ΔG_{MA} [kJ/mol]							-99.0
M33	REDO_k4_1	-270.566698	-270.479635	-270.573222	-270.656490	0.087063	-0.006524	-270.575951
	REDO_k4_me_2	-310.493668	-310.373137	-310.577268	-310.614084	0.120531	-0.083599	-310.577152
	ΔG_{MA} [kJ/mol]							-72.6

M34	REDO_a8_1	-309.886761	-309.773701	-309.894743	-309.986154	0.113060	-0.007983	-309.881077
	REDO_a8_me_1	-349.816660	-349.668600	-349.899881	-349.947975	0.148060	-0.083220	-349.883136
	ΔG_{MA} [kJ/mol]							-74.9
M35	REDO_a6_1	-388.519660	-388.354156	-388.528523	-388.640032	0.165504	-0.008862	-388.483390
	REDO_a6_me_1	-428.451287	-428.250883	-428.533907	-428.603226	0.200404	-0.082620	-428.485441
	ΔG_{MA} [kJ/mol]							-74.8
M36	REDO_b3_1	-309.887652	-309.774991	-309.895490	-309.987539	0.112661	-0.007838	-309.882716
	REDO_b3_me_1	-349.810485	-349.664179	-349.892164	-349.940304	0.146306	-0.081679	-349.875677
	ΔG_{MA} [kJ/mol]							-51.0
M37	REDO_a5_2	-270.567929	-270.481160	-270.576801	-270.658667	0.086769	-0.008871	-270.580770
	REDO_a5_me_1	-310.497079	-310.375772	-310.582637	-310.620354	0.121307	-0.085558	-310.584604
	ΔG_{MA} [kJ/mol]							-79.5
M38	REDO_a9_9	-349.200855	-349.061497	-349.210606	-349.312785	0.139358	-0.009751	-349.183178
	REDO_a9_me_1	-389.132472	-388.958878	-389.215618	-389.275222	0.173594	-0.083147	-389.184775
	ΔG_{MA} [kJ/mol]							-73.7
M39	REDO_b1_10	-388.517412	-388.351807	-388.527629	-388.639923	0.165605	-0.010217	-388.484535
	REDO_b1_me_1	-428.449287	-428.249591	-428.532540	-428.602508	0.199696	-0.083253	-428.486065
	ΔG_{MA} [kJ/mol]							-73.5
M40	REDO_b2_10	-427.835075	-427.643448	-427.844884	-427.966892	0.191627	-0.009810	-427.785075
	REDO_b2_me_1	-467.766057	-467.540292	-467.849347	-467.929818	0.225765	-0.083290	-467.787343
	ΔG_{MA} [kJ/mol]							-75.4
M41	REDO_b4_1	-309.889482	-309.777238	-309.896846	-309.988608	0.112244	-0.007364	-309.883728
	REDO_b4_me_1	-349.816162	-349.666903	-349.897634	-349.947366	0.149259	-0.081471	-349.879579
	ΔG_{MA} [kJ/mol]							-58.6
M42	REDO_s38_1	-229.979031	-229.942369	-229.986544	-230.062459	0.036662	-0.007514	-230.033311
	REDO_s38_me_1	-269.925383	-269.853863	-270.015191	-270.041716	0.071520	-0.089808	-270.060004

	ΔG_{MA} [kJ/mol]							-139.5
M43	REDO_a4_1	-269.310353	-269.249924	-269.319851	-269.403699	0.060429	-0.009498	-269.352768
	REDO_a4_me_1	-309.246005	-309.148475	-309.334159	-309.371062	0.097530	-0.088154	-309.361686
	ΔG_{MA} [kJ/mol]							-92.9
M44	REDO_s40_1	-461.055363	-460.945369	-461.067571	-461.203712	0.109994	-0.012208	-461.105926
	REDO_s40_me_1_geo	-501.004588	-500.858374	-501.088023	-501.180896	0.146214	-0.083436	-501.118118
	ΔG_{MA} [kJ/mol]							-101.5
M45	REDO_s25_1	-344.559792	-344.491526	-344.564092	-344.682385	0.068266	-0.004300	-344.618420
	REDO_s25_me_2	-384.507671	-384.405545	-384.586318	-384.659793	0.102126	-0.078646	-384.636313
	ΔG_{MA} [kJ/mol]							-116.4
M46	REDO_e4_1	-382.611097	-382.540714	-382.618557	-382.748691	0.070383	-0.007460	-382.685769
	REDO_e4_me_1	-422.550945	-422.447162	-422.632856	-422.717045	0.103783	-0.081911	-422.695174
	ΔG_{MA} [kJ/mol]							-94.2
M47	REDO_e6_3	-383.873145	-383.779175	-383.879726	-384.007423	0.093970	-0.006581	-383.920034
	REDO_e6_me_5	-423.808625	-423.681165	-423.890388	-423.971102	0.127460	-0.081763	-423.925405
	ΔG_{MA} [kJ/mol]							-83.6
M48	REDO_e5_5	-421.006849	-420.912312	-421.016937	-421.161743	0.094537	-0.010088	-421.077294
	REDO_e5_me_1	-460.959985	-460.830140	-461.039119	-461.139742	0.129845	-0.079135	-461.089031
	ΔG_{MA} [kJ/mol]							-100.3
M49	REDO_e7_9	-460.329314	-460.208734	-460.339281	-460.494273	0.120580	-0.009966	-460.383659
	REDO_e7_me_1	-500.282433	-500.126524	-500.361094	-500.472012	0.155909	-0.078661	-500.394764
	ΔG_{MA} [kJ/mol]							-98.6
M50	REDO_f1_4	-385.114737	-384.997384	-385.121528	-385.245495	0.117353	-0.006791	-385.134933
	REDO_f1_me_3	-425.046330	-424.895343	-425.129172	-425.205218	0.150987	-0.082842	-425.137073
	ΔG_{MA} [kJ/mol]							-75.1
M51	REDO_f2_1	-385.119670	-385.001940	-385.125603	-385.249716	0.117730	-0.005933	-385.137919

	REDO_f2me_1	-425.050950	-424.900204	-425.133080	-425.209506	0.150746	-0.082129	-425.140889
	ΔG_{MA} [kJ/mol]							-77.3
M52	REDO_f3_5	-424.431136	-424.287561	-424.438385	-424.572486	0.143575	-0.007249	-424.436160
	REDO_f3_me_3	-464.363013	-464.185753	-464.445904	-464.532388	0.177260	-0.082891	-464.438019
	ΔG_{MA} [kJ/mol]							-74.3
M53	REDO_s64_10	-503.064217	-502.868172	-503.072358	-503.226701	0.196045	-0.008140	-503.038796
	REDO_s64_me_3	-542.996417	-542.766784	-543.079781	-543.186837	0.229633	-0.083364	-543.040568
	ΔG_{MA} [kJ/mol]							-74.1
M54	REDO_g2_1	-421.932781	-421.836619	-421.939734	-422.080027	0.096162	-0.006953	-421.990818
	REDO_g2_me_2	-461.868901	-461.739398	-461.946956	-462.042630	0.129503	-0.078055	-461.991182
	ΔG_{MA} [kJ/mol]							-70.4
M55	REDO_s62_2	-423.194194	-423.075700	-423.200225	-423.337971	0.118494	-0.006031	-423.225508
	REDO_s62_me_2	-463.126791	-462.973723	-463.203977	-463.297092	0.153068	-0.077185	-463.221209
	ΔG_{MA} [kJ/mol]							-58.2
M56	REDO_s37_6	-460.328261	-460.207879	-460.338018	-460.492747	0.120382	-0.009757	-460.382123
	REDO_s37_me_1	-500.278211	-500.122503	-500.353902	-500.465704	0.155708	-0.075690	-500.385687
	ΔG_{MA} [kJ/mol]							-78.8
M57	REDO_s51_5	-499.650642	-499.503808	-499.659726	-499.824702	0.146834	-0.009084	-499.686953
	REDO_s51_me_1	-539.600643	-539.418866	-539.675892	-539.797965	0.181777	-0.075249	-539.691438
	ΔG_{MA} [kJ/mol]							-81.2
M58	REDO_g5_1	-345.798024	-345.707217	-345.802809	-345.917744	0.090807	-0.004785	-345.831722
	REDO_g5_me_2	-385.723908	-385.601028	-385.802900	-385.870870	0.122880	-0.078992	-385.826982
	ΔG_{MA} [kJ/mol]							-57.0
M59	REDO_s61_10	-463.753656	-463.584181	-463.759741	-463.904147	0.169475	-0.006085	-463.740757
	REDO_s61_me_8	-503.683880	-503.480710	-503.760830	-503.859937	0.203170	-0.076950	-503.733717
	ΔG_{MA} [kJ/mol]							-51.0

M60	REDO_s35_1	-383.884854	-383.790704	-383.890649	-384.017526	0.094150	-0.005794	-383.929170
	REDO_s35_me_1	-423.826011	-423.697914	-423.903119	-423.988231	0.128097	-0.077108	-423.937242
	ΔG_{MA} [kJ/mol]							-90.7
M61	REDO_g3_1	-345.801220	-345.710301	-345.807848	-345.921379	0.090919	-0.006628	-345.837089
	REDO_g3_me_1	-385.724244	-385.601022	-385.805589	-385.873751	0.123222	-0.081346	-385.831874
	ΔG_{MA} [kJ/mol]							-55.8
M62	REDO_f8_5	-424.434122	-424.290559	-424.441684	-424.575444	0.143563	-0.007562	-424.439443
	REDO_f8_me_1	-464.359591	-464.183742	-464.438973	-464.528681	0.175849	-0.079382	-464.432214
	ΔG_{MA} [kJ/mol]							-50.5
M63	REDO_f9_6	-503.067191	-502.871141	-503.075660	-503.229650	0.196050	-0.008468	-503.042068
	REDO_f9_me_1	-542.993147	-542.764966	-543.072783	-543.183266	0.228181	-0.079636	-543.034721
	ΔG_{MA} [kJ/mol]							-50.2
M64	REDO_g7_2	-385.119375	-385.003005	-385.125372	-385.248982	0.116370	-0.005997	-385.138609
	REDO_g7_me_1	-425.040635	-424.894278	-425.117847	-425.197066	0.146357	-0.077212	-425.127922
	ΔG_{MA} [kJ/mol]							-41.4
M65	REDO_e1_1	-305.206873	-305.165722	-305.213310	-305.320452	0.041151	-0.006436	-305.285737
	REDO_e1_me_1	-345.152337	-345.077868	-345.241631	-345.296744	0.074469	-0.089294	-345.311570
	ΔG_{MA} [kJ/mol]							-137.3
M66	REDO_e2_2	-344.528890	-344.461676	-344.536280	-344.652701	0.067214	-0.007390	-344.592877
	REDO_e2_me_1	-384.474398	-384.374038	-384.563758	-384.628411	0.100360	-0.089360	-384.617411
	ΔG_{MA} [kJ/mol]							-133.9
M67	REDO_e3_1	-423.166769	-423.046397	-423.173448	-423.309934	0.120372	-0.006679	-423.196241
	REDO_e3_me_3	-463.113635	-462.959444	-463.198988	-463.284991	0.154191	-0.085353	-463.216153
	ΔG_{MA} [kJ/mol]							-121.7
M68	REDO_f7_1	-344.538437	-344.474223	-344.547013	-344.661982	0.064214	-0.008577	-344.606345
	REDO_f7_me_1	-384.472952	-384.372716	-384.560795	-384.626113	0.100236	-0.087844	-384.613721
	ΔG_{MA} [kJ/mol]							-88.8

M69	REDO_f4_7	-423.171856	-423.053801	-423.181180	-423.316533	0.118055	-0.009325	-423.207803
	REDO_f4_me_2_geo	-463.106414	-462.954081	-463.193210	-463.280169	0.152333	-0.086796	-463.214631
	ΔG_{MA} [kJ/mol]							-87.4
M70	REDO_s44_3	-462.493614	-462.348919	-462.503764	-462.648212	0.144695	-0.010150	-462.513667
	REDO_s44_me_2_geo2	-502.428423	-502.250172	-502.515311	-502.611814	0.178251	-0.086888	-502.520451
	ΔG_{MA} [kJ/mol]							-87.3
M71	REDO_f5_8	-501.804833	-501.633796	-501.814833	-501.970453	0.171037	-0.010000	-501.809416
	REDO_f5_me_8	-541.739889	-541.535104	-541.827089	-541.934658	0.204785	-0.087199	-541.817073
	ΔG_{MA} [kJ/mol]							-89.6
M72	REDO_g1_1	-247.303114	-247.252383	-247.314463	-247.395434	0.050731	-0.011349	-247.356052
	REDO_g1_me_1	-287.222902	-287.137727	-287.314249	-287.348744	0.085175	-0.091347	-287.354916
	ΔG_{MA} [kJ/mol]							-66.5
M73	REDO_s29_1	-325.698761	-325.607659	-325.705499	-325.798965	0.091102	-0.006738	-325.714601
	REDO_s29_me_1	-365.620293	-365.496916	-365.706127	-365.749589	0.123377	-0.085834	-365.712046
	ΔG_{MA} [kJ/mol]							-62.8

5.8 Applications

Example 1: Prediction of rate constants for the reactions of Michael acceptors with nucleophiles

The GSH-derived Mayr electrophilicity parameters *E* (Table S4) can be applied in equation 1 to predict second-order rate constants for the reactions of the Michael acceptors **M1**–**M73** with further types of nucleophiles, whose nucleophilicity parameters *N* and s_N have been determined.

While *N* and s_N for nucleophiles are solvent-dependent, the same electrophilicity parameter *E* for a certain Michael acceptor can be used in different solvents. Within a total reactivity range of 40 orders of magnitude, using equation 1 usually allows to calculate second-order rate constants within a precision of factor <100 for reactions at 20 °C, in which exactly one new C-X or C-C σ-bond is formed.[19] Significant deviations of more than a factor of 1000 may indicate the operation of a different mechanism, the influence of specific solvation on the energetics of the observed reaction or further effects that alter the energy profile of a reaction.

Table S6 compares the second-order rate constants $k_2^{eq\ 1}$ (M^{-1} s^{-1}) calculated by equation 1 for reactions at 20 °C with reported experimental second-order rate constants k_2^{exp} (M^{-1} s^{-1}) for the reactions of Michael acceptors with diverse nitrogen-, oxygen-, or sulfur-centered nucleophiles in different solvents at the given temperature.

For example, a second-order rate constant k_2^{exp} = 4.3 M^{-1} s^{-1} has been experimentally determined by Heo and Bunting for the reaction of acrolein (**M1**) with the pyridone anion in aqueous solution at 25 °C (Table S6, entry 1).[20] Using equation 1, the

electrophilicity *E* = –14.4 of acrolein (**M1**) from Table S4, and the

nucleophile-specific reactivity parameters of the 4-pyridone anion (in H_2O):

N = 14.76, s_N = 0.48 (from Mayr's reactivity database[21]) we calculate

lg $k_2^{eq\ 1}$ = $s_N(N + E)$ = 0.17, which corresponds to $k_2^{eq\ 1}$ = 1.5 M^{-1} s^{-1} (at 20 °C).

The comparison with second-order rate constants $k_2^{eq\ 1}$ (20 °C) calculated by using equation 1 and the Mayr reactivity parameters *E*, *N*, and s_N shows that $k_2^{exp}/k_2^{eq\ 1} < 100$ is fulfilled for 71 Michael additions (Table S6). In the reaction of hydrazine (in water) with the butynone **M42** (Table S6, entry 28) a lowering of the activation barrier may be due to the simultaneous C–N and C–H bond formation in the transition state of, as proposed by Um and coworkers.[28] Only for methyl crotonate (**M61**) the ratio $k_2^{exp}/k_2^{eq\ 1}$ is in the range of 130 to 600 for 5 of 6 available k_2^{exp} at 30 °C (Table S6, entries 48–53). The slight exceeding of the precision criterion of $k_2^{exp}/k_2^{eq\ 1} < 100$ may in part be due to the 10 K difference in the reference temperatures for k_2^{exp} and $k_2^{eq\ 1}$ but we refrain from a further interpretation of this deviation. The analysis in Table S6 proves that the GSH-derived *E* for Michael acceptors can, in general, be used to predict reaction rates for Michael additions of other classes of nucleophiles.

Table S6: Experimental (k_2^{exp}) and calculated second-order rate constants ($k_2^{eq\,1}$) for the 1,4-additions of various N-, O- and S-centered nucleophiles to Michael acceptors **M1**, **M2**, **M5**, **E11**, **M30**, **M33**, **M42**, **E12**, **M58**, **M61**, **M66**, **M72**, and **E15**.

Entry	Electrophile	E[a]	Nucleophile (Solvent)	N (s_N)[b]	k_2^{exp} (M^{-1} s^{-1})	T (°C)	Reference	$k_2^{eq\,1}$ (M^{-1} s^{-1})	$k_2^{exp}/k_2^{eq\,1}$
1	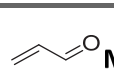 **M1**	–14.4	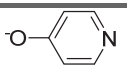 (in H_2O)	14.76 (0.48)	**4.3**	25	20	**1.49**	2.9
2	**M1**	–14.4	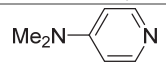 (in H_2O)	13.19 (0.56)	**2.39**	25	20	**0.21**	11
3	**M1**	–14.4	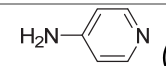 (in H_2O)	12.19 (0.66)	**1.65**	25	20	**3.48×10^{-2}**	47
4	**M1**	–14.4	morpholine (in MeOH)	15.40 (0.64)	**1.28**	30	22	**4.37**	0.29
5	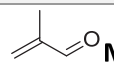 **M2**	–17.2	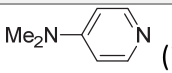 (in H_2O)	13.19 (0.56)	**1.8×10^{-2}**	25	20	**5.68×10^{-3}**	3.2
6	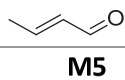 **M5**	–18.4	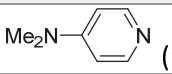 (in H_2O)	13.19 (0.56)	**8×10^{-3}**	25	20	**1.21×10^{-3}**	6.6
7	**M5**	–18.4	^-O_2C-CH_2-S^- (in H_2O)	22.62 (0.43)	**15**	25	23	**65.3**	0.23
8	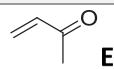 **E11**	–16.8	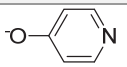 (in H_2O)	14.76 (0.48)	**0.96**	25	20	**0.105**	9.2
9	**E11**	–16.8	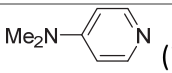 (in H_2O)	13.19 (0.56)	**0.55**	25	20	**9.51×10^{-3}**	58
10	**E11**	–16.8	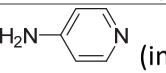 (in H_2O)	12.19 (0.66)	**0.42**	25	20	**9.07×10^{-4}**	4.6×10^2
11	**E11**	–16.8	morpholine (in MeOH)	15.40 (0.64)	**1.20**	30	22	**0.127**	9.4
12	**E11**	–16.8	Gly^- (in H_2O)	13.51 (0.58)	**0.400**	30	24	**1.24×10^{-2}**	32
13	**E11**	–16.8	Ala^- (in H_2O)	13.01 (0.58)	**0.228**	30	24	**6.34×10^{-3}**	36
14	**E11**	–16.8	MeO^- (in MeOH)	15.78 (0.56)	**0.378**	19	25	**0.268**	1.4
15	**E11**	–16.8	EtO^- (in EtOH)	15.78 (0.65)	**1.56**	19	25	**0.217**	7.2
16	**E11**	–16.8	$iPrO^-$ (in iPrOH)	17.03 (0.63)	**3.15**	19	25	**1.40**	2.3

17	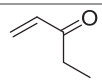 **M30**	–15.8	MeO^- (in MeOH)	15.78 (0.56)	**0.235**	24	26	**0.975**	0.24
18	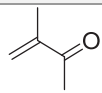 **M33**	–18.6	MeO^- (in MeOH)	15.78 (0.56)	**8.0×10^{-3}** [c]	24	26	**2.64×10^{-2}**	0.30
19	**M33**	–18.6	$iPrO^-$ (in iPrOH)	17.03 (0.63)	**2.6×10^{-2}** [c]	24	26	**0.103**	0.25
20	 **M42**	–16.6	aniline (in H_2O)	12.99 (0.73)	**0.375**	25	27	**2.32×10^{-3}**	1.6×10^2
21	**M42**	–16.6	*p*-anisidine (in H_2O)	14.28 (0.68)	**1.34**	25	27	**2.64×10^{-2}**	51
22	**M42**	–16.6	$EtGly^-$ (in H_2O)	12.08 (0.60)	**0.147**	25	28	**1.94×10^{-3}**	76
23	**M42**	–16.6	ethanolamine (in H_2O)	12.61 (0.58)	**0.336**	25	28	**4.85×10^{-3}**	69
24	**M42**	–16.6	$GlyGly^-$ (in H_2O)	12.91 (0.59)	**0.160**	25	28	**6.65×10^{-3}**	24
25	**M42**	–16.6	Gly^- (in H_2O)	13.51 (0.58)	**0.594**	25	28	**1.61×10^{-2}**	37
26	**M42**	–16.6	ethylamine (in H_2O)	12.87 (0.58)	**0.670**	25	28	**6.86×10^{-3}**	98
27	**M42**	–16.6	benzylamine (in H_2O)	13.44 (0.55)	**0.454**	25	28	**1.83×10^{-2}**	25
28	**M42**	–16.6	hydrazine (in H_2O)	13.46 (0.57)	**3.66**	25	28	**1.62×10^{-2}**	2.3×10^2 [d]
29	**M42**	–16.6	piperidine (in H_2O)	18.13 (0.44)	**4.12**	25	29	**4.71**	0.87
30	**M42**	–16.6	morpholine (in H_2O)	15.62 (0.54)	**10.9**	25	29	**0.296**	37
31	**M42**	–16.6	piperazine (in H_2O)	17.22 (0.50)	**13.3**	25	29	**2.04**	6.5
32	**M42**	–16.6	piperidine (in MeCN)	17.35 (0.68)	**5.62**	25	29	**3.24**	1.7
33	**M42**	–16.6	morpholine (in MeCN)	15.65 (0.74)	**0.520**	25	29	**0.198**	2.6
34	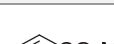 **E12**	–18.8	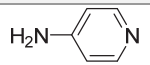 (in H_2O)	12.19 (0.66)	**1.46×10^{-2}**	25	20	**7.22×10^{-4}**	20
35	**E12**	–18.8	morpholine (in MeOH)	15.40 (0.64)	**1.04×10^{-2}**	30	22	**6.67×10^{-3}**	1.6
36	**E12**	–18.8	$GlyGly^-$ (in H_2O)	12.91 (0.59)	**4.6×10^{-3}**	30	24	**3.35×10^{-4}**	14
37	**E12**	–18.8	Gly^- (in H_2O)	13.51 (0.58)	**1.82×10^{-2}**	30	24	**8.55×10^{-4}**	21
38	**E12**	–18.8	β-Ala^- (in H_2O)	13.26 (0.58)	**2.84×10^{-2}**	30	24	**6.12×10^{-4}**	46
39	**E12**	–18.8	Phe^- (in H_2O)	14.12 (0.53)	**6.40×10^{-3}**	30	24	**3.31×10^{-3}**	1.9
40	**E12**	–18.8	Met^- (in H_2O	13.16 (0.58)	**6.90×10^{-3}**	30	24	**5.36×10^{-4}**	13

41	**E12**	–18.8	Ala^- (in H_2O)	13.01 (0.58)	**1.11×10^{-2}**	30	24	**4.38×10^{-4}**	25
42	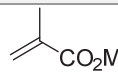 **M58**	–23.4	$GlyGly^-$ (in H_2O)	12.91 (0.59)	**1.35×10^{-5}**	30	24	**6.47×10^{-7}**	21
43	**M58**	–23.4	Gly^- (in H_2O)	13.51 (0.58)	**5.80×10^{-5}**	30	24	**1.84×10^{-6}**	32
44	**M58**	–23.4	β-Ala^- (in H_2O	13.26 (0.58)	**1.37×10^{-4}**	30	24	**1.31×10^{-6}**	1.0×10^2
45	**M58**	–23.4	Phe^- (in H_2O)	14.12 (0.53)	**2.48×10^{-5}**	30	24	**1.21×10^{-5}**	2.1
46	**M58**	–23.4	Met^- (in H_2O	13.16 (0.58)	**2.93×10^{-5}**	30	24	**1.15×10^{-6}**	26
47	**M58**	–23.4	Ala^- (in H_2O)	13.01 (0.58)	**3.64×10^{-5}**	30	24	**9.41×10^{-7}**	39
48	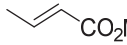 **M61**	–22.8	$GlyGly^-$ (in H_2O)	12.91 (0.59)	**2.20×10^{-4}**	30	24	**1.46×10^{-6}**	1.5×10^2
49	**M61**	–22.8	Gly^- (in H_2O)	13.51 (0.58)	**1.20×10^{-3}**	30	24	**4.09×10^{-6}**	2.9×10^2
50	**M61**	–22.8	β-Ala^- (in H_2O)	13.26 (0.58)	**1.76×10^{-3}**	30	24	**2.93×10^{-6}**	6.0×10^2
51	**M61**	–22.8	Phe^- (in H_2O)	14.12 (0.53)	**3.31×10^{-4}**	30	24	**2.51×10^{-5}**	13
52	**M61**	–22.8	Met^- (in H_2O	13.16 (0.58)	**3.36×10^{-4}**	30	24	**2.56×10^{-6}**	1.3×10^2
53	**M61**	–22.8	Ala^- (in H_2O)	13.01 (0.58)	**5.85×10^{-4}**	30	24	**2.10×10^{-6}**	2.8×10^2
54	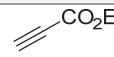 **M66**	–17.7	piperidine (in H_2O)	18.13 (0.44)	**1.24**	25	30	**1.55**	0.80
55	**M66**	–17.7	morpholine (in H_2O)	15.62 (0.54)	**0.245**	25	30	**7.53×10^{-2}**	3.3
56	**M66**	–17.7	piperazine (in H_2O)	17.22 (0.50)	**0.935**	25	30	**0.575**	1.6
57	**M66**	–17.7	piperidine (in MeCN)	17.35 (0.68)	**0.902**	25	30	**0.578**	1.6
58	**M66**	–17.7	morpholine (in MeCN)	15.65 (0.74)	**7.48×10^{-2}**	25	30	**3.04×10^{-2}**	2.5
59	 **M72**	–21.8	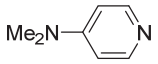 (in H_2O)	13.19 (0.56)	**6.1×10^{-4}**	25	20	**1.51×10^{-5}**	41
60	**M72**	–21.8	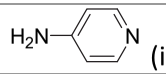 (in H_2O)	12.19 (0.66)	**5.3×10^{-4}**	25	20	**4.54×10^{-7}**	1.2×10^3
61	**M72**	–21.8	morpholine (in MeOH)	15.40 (0.64)	**3.57×10^{-4}**	30	22	**8.02×10^{-5}**	0.65
62	**M72**	–21.8	pyrrolidine (in MeOH)	15.97 (0.63)	**8.27×10^{-3}**	30	22	**2.12×10^{-4}**	1.6
63	**M72**	–21.8	$GlyGly^-$ (in H_2O)	12.91 (0.59)	**2.0×10^{-4}**	30	24	**5.69×10^{-6}**	35
64	**M72**	–21.8	Gly^- (in H_2O)	13.51 (0.58)	**6.3×10^{-4}**	30	24	**1.56×10^{-5}**	41

65	**M72**	–21.8	Phe^- (in H_2O)	14.12 (0.53)	**2.2×10^{-4}**	30	24	**8.50×10^{-5}**	2.6
66	**M72**	–21.8	Ala^- (in H_2O)	13.01 (0.58)	**3.5×10^{-4}**	30	24	**7.98×10^{-6}**	44
67	**M72**	–21.8	$iPrO^-$ (in iPrOH)	17.03 (0.63)	**3.2×10^{-4}**	24	26	**9.88×10^{-4}**	0.30
68	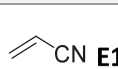 **E15**	–19.1	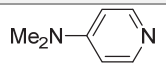 (in H_2O)	13.19 (0.56)	**4.03×10^{-3}**	25	20	**4.90×10^{-4}**	8.2
69	**E15**	–19.1	morpholine (in MeOH)	15.40 (0.64)	**5.68×10^{-3}**	30	22	**4.29×10^{-3}**	1.3
70	**E15**	–19.1	$GlyGly^-$ (in H_2O)	12.91 (0.59)	**1.37×10^{-3}**	30	24	**2.23×10^{-4}**	6.2
71	**E15**	–19.1	Gly^- (in H_2O)	13.51 (0.58)	**5.00×10^{-3}**	30	24	**5.73×10^{-4}**	8.7
72	**E15**	–19.1	β-Ala^- (in H_2O)	13.26 (0.58)	**8.92×10^{-3}**	30	24	**4.10×10^{-4}**	22
73	**E15**	–19.1	Phe^- (in H_2O)	14.12 (0.53)	**1.76×10^{-3}**	30	24	**2.29×10^{-3}**	0.77
74	**E15**	–19.1	Met^- (in H_2O	13.16 (0.58)	**1.76×10^{-3}**	30	24	**3.59×10^{-4}**	4.9
75	**E15**	–19.1	Ala^- (in H_2O)	13.01 (0.58)	**3.53×10^{-3}**	30	24	**2.94×10^{-4}**	12
76	**E15**	–19.1	MeO^- (in MeOH)	15.78 (0.56)	**5.80×10^{-3}**	20	31	**1.38×10^{-2}**	0.42
77	**E15**	–19.1	MeO^- (in MeOH)	15.78 (0.56)	**1.22×10^{-2}**	24	26	**1.38×10^{-2}**	0.88
78	**E15**	–19.1	EtO^- (in EtOH)	15.78 (0.65)	**5.25×10^{-2}**	20	31	**6.95×10^{-3}**	7.6
79	**E15**	–19.1	$nPrO^-$ (in nPrOH)	16.03 (0.70)	**9.58×10^{-2}**	20	31	**7.10×10^{-3}**	14
80	**E15**	–19.1	$iPrO^-$ (in iPrOH)	17.03 (0.63)	**0.287**	20	31	**4.96×10^{-2}**	5.8

[a] From Table S4. [b] From ref. 21. [c] Second-order rate constants during the initial phase of the reactions. [d] Concerted C–N and C–H bond formation in the transition state was proposed in ref. 28.

Example 2: Estimating the electrophilicity of fluorescent thiol probes

Rate constants with GSH are an often used measure for the reactivity of fluorescent electrophilic thiol probes. Electrophilicity parameters *E* for these fluorescence probes can be derived from the available rate constants k_{GSH}. Once the electrophilicity parameter *E* of a fluorescent thiol probe is known, rate constants of their reactions with further competing nucleophilic sites in peptides can be estimated by using equation 1.

For example, Jiang et al. introduced the GSH probe 'RealThiol' for quantitative real-time imaging of glutathione in living cells. For the reaction of RealThiol with GSH the authors measured a second-order rate constant k_{GSH} = 7.5 M^{-1} s^{-1} (pH 7.4, 37 °C).[32] Applying k_{GSH} in equation 2 (with *F* = 0.0280) gives a second-order rate constant $k_2 = 2.7 \times 10^2$ M^{-1} s^{-1}. With equation 1 and the nucleophilicity parameter of GSH(NH_3^+/S^-), that is *N* = 20.97 (s_N = 0.56), an approximate electrophilicity of *E* = –16.6 can be calculated for RealThiol (Table S7, entry 1). Further examples for estimated electrophilicity parameters *E* for fluorescent thiol probes are collected in Table S7.

Though in lack of the nucleophilicity parameters for GSH, Kamyia and Urano used Mayr electrophilicity parameters *E* for a rational design strategy to develop highly reactive fluorescence probes.[33] ThiolQuant Green (TQ Green)[34] was reported to undergo relatively slow reactions with GSH (see Table S7, entry 2). Kamiya, Urano and coworkers then estimated the electrophilicity *E* of TQ Green based on a comparison with the structurally analogous chalcone fragment whose *E* is available in Mayr's database (*E* = –19).[21] They concluded, that in order to achieve the required higher reactivity of the GSH probe for real-time dynamic quantification of GSH in living cells, a carbocationic fragment in the GSH probe would be more suitable. The nucleophilicity of GSH (*N* = 20.97, s_N = 0.56), determined in this work, can now be used to estimate the electrophilicities *E* of the fluorescent probes developed by Urano and Kamiya (Table S7, entries 7–9), which may help to further improve the performance of these fluorescent probes in real-time dynamic GSH monitoring in living cells.

Table S7: Rate constants k_{GSH}^{exp} (at pH 7.4) for reactions of fluorescence probes **M74–M82** with GSH, estimated electrophilicities *E* of the probes, and their quantum-chemically calculated methyl anion affinities ΔG_{MA}.

Entry	Probe	k_{GSH}^{exp} (M^{-1} s^{-1})	*T*	Reference	$k_2(GS^-)$ (M^{-1} s^{-1})	Estimated *E*[a]	ΔG_{MA}[b] (kJ mol^{-1})
1	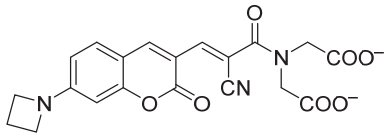 **M74** (RealThiol)	7.5	37 °C	32	2.7×10^2	–16.6	–108.4
2	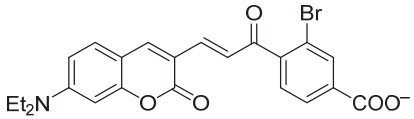 **M75** (TQ Green)	0.15	–[c]	34	5.4	–19.7	–70.9
3	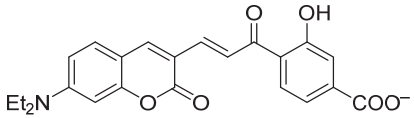 **M76**	1.29	–[c]	35	46.1	–18.0	–85.2
4	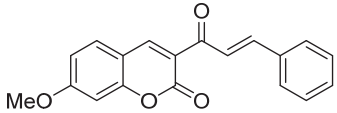 **M77**	--	30 °C	36	1.56[d]	–20.6	–83.9
5	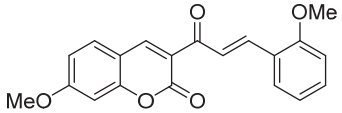 **M78**	--	30 °C	36	44.4[d]	–18.0	–79.3
6	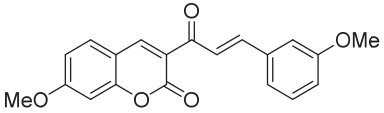 **M79**	--	30 °C	36	19.9[d]	–18.6	–81.1

7	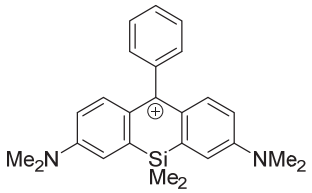 **M80** (Ph SiR650)	560	– [c]	33	2.00×10^4	–13.2	–148.4
8	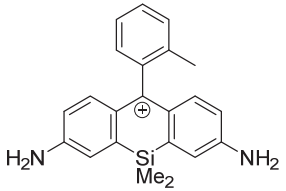 **M81** (2'Me SiR600)	272	– [c]	33	9.71×10^3	–13.8	–151.2
9	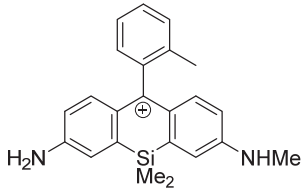 **M82** (2'Me-SiR610)	153	– [c]	33	5.46×10^3	–14.2	–144.4

[a] Calculated by using equation 1 (main text), lg $k_2(GS^-)$, and the reactivity parameters for GS^- (N = 20.97, s_N = 0.55[5]). [b] For details of the quantum-chemical calculation of methyl anion affinities ΔG_{MA} see Table S8. [c] Temperature not reported. [d] As reported in ref. 36.

Quantum-chemically calculated methyl anion affinities (ΔG_{MA}) of fluorescent thiol probes

The methyl anion affinities ΔG_{MA} for **M74**–**M82** listed in column 8 of Table S7 were calculated by following the same procedure as described on page S32. Figure S3 shows the linear correlation of electrophilicities *E* with ΔG_{MA} for 117 Michael acceptors (black dots: from ref. 10c, orange dots: this work). Purple rhombs (◆) show the additional *E* vs ΔG_{MA} data for the 9 fluorescence probes **M74**–**M82** from Table S7.

Figure S3 demonstrates that the correlation between quantum chemically calculated methyl anion affinities ΔG_{MA} and the electrophilicities *E* of prototypical Michael acceptors is also applicable for roughly estimating the reactivity of the structurally more sophisticated fluorescence probes **M74**–**M82**.

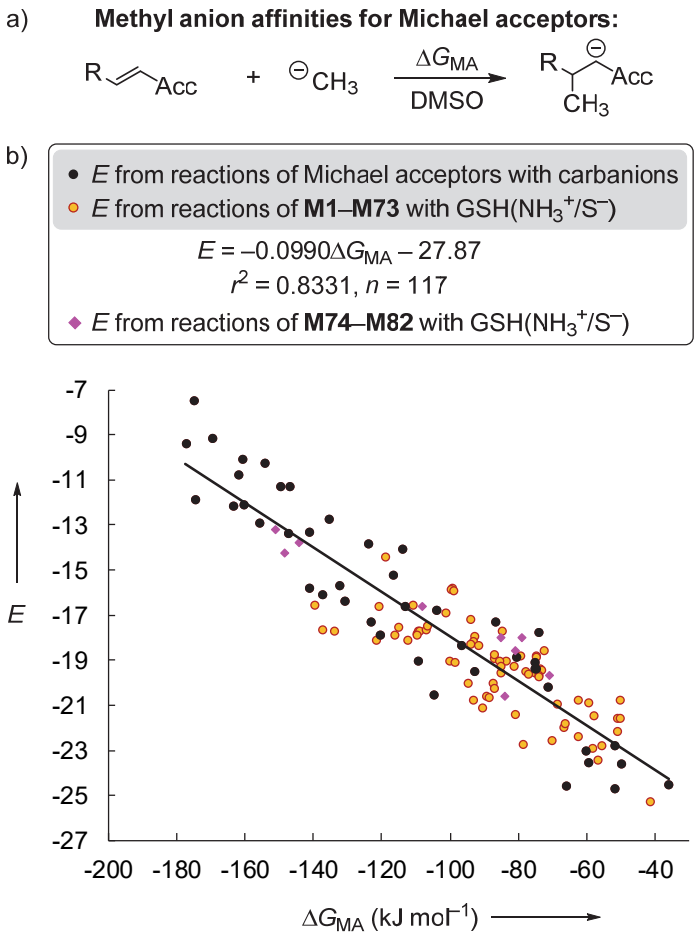

Figure S3: Correlation of experimentally determined Michael acceptor electrophilicities *E* and methyl anion affinities ΔG_{MA} in DMSO [calculated at the SMD(DMSO)/B3LYP/6-311++G(3df,2pd)//B3LYP/6-31G(d,p) level of theory, ref. 10c and this work] supplemented by data for the fluorescent thiol probes **M74**–**M82** (purple rhombs ◆, with data from Table S7, not included when calculating the correlation line; details of the quantum-chemical calculations for **M74**–**M82** are given in Table S8).

Table S8: Quantum-mechanically calculated methyl anion affinities ΔG_{MA} for Michael acceptors **M74**–**M82** [in kJ mol^{-1}, calculated at the SMD(DMSO)/B3LYP/6-311++G(3df,2pd)//B3LYP/6-31G(d,p) level of theory]

Michael acceptor	Filename	E_{tot} (B3LYP/6-31G(d,p)	G_{298}	$E_{tot, solv.}$ (SMD(DMSO)/B3LYP/6-31G(d,p)// B3LYP/6-31G(d,p))	$E_{tot, high.}$ (B3LYP/6-311++G(3df,2pd)// B3LYP/6-31G(d,p))	ΔG	ΔG_{solv}	G_{298} (SMD(DMSO)/ B3LYP/6-311++G(3df,2pd)// B3LYP/6-31G(d,p))
	Methyl anion	-39.796028	-39.787379	-39.921582	-39.856638	0.008649	-0.125554	-39.973543
M74	REDO_rt_sm_4	-1461.991496	-1461.726753	-1462.242350	-1462.528398	0.264743	-0.250854	-1462.514509
	REDO_rt_me_e_10	-1501.767394	-1501.464592	-1502.265339	-1502.334190	0.302802	-0.497945	-1502.529333
	ΔG_{MA} [kJ/mol]							-108.4
M75	REDO_tq_green_3	-3890.559432	-3890.249532	-3890.661877	-3893.442293	0.309900	-0.102446	-3893.234839
	REDO_tq_green_me_z_6	-3930.424837	-3930.081397	-3930.666410	-3933.337252	0.343440	-0.241572	-3933.235385
	ΔGMA [kJ/mol]							-70.9
M76	REDO_tq_oh_4	-1394.693066	-1394.368129	-1394.798509	-1395.165252	0.324937	-0.105443	-1394.945758
	REDO_tq_oh_me_z_1	-1434.562243	-1434.201384	-1434.808150	-1435.066722	0.360859	-0.245907	-1434.951770
	ΔG_{MA} [kJ/mol]							-85.2
M77	REDO_og1_1	-1033.361672	-1033.127333	-1033.383033	-1033.690881	0.234339	-0.021361	-1033.477902
	REDO_og1_me_6	-1073.309088	-1073.041347	-1073.392650	-1073.667583	0.267741	-0.083562	-1073.483404
	ΔG_{MA} [kJ/mol]							-83.9
M78	REDO_og5_2	-1147.885858	-1147.622673	-1147.908687	-1148.255234	0.263185	-0.022829	-1148.014878
	REDO_og5_me_6	-1187.830709	-1187.532938	-1187.917590	-1188.229515	0.297771	-0.086881	-1188.018625
	ΔGMA [kJ/mol]							-79.3
M79	REDO_og3_1	-1147.887399	-1147.623893	-1147.909568	-1148.257465	0.263506	-0.022169	-1148.016127
	REDO_og3_me_4	-1187.836132	-1187.539153	-1187.918804	-1188.234850	0.296979	-0.082673	-1188.020543
	ΔG_{MA} [kJ/mol]							-81.1
M80	REDO_sir650_1	-1369.005284	-1368.586678	-1369.069411	-1369.337823	0.418606	-0.064127	-1368.983344

	REDO_sir650_me_2	-1409.102782	-1408.645544	-1409.118965	-1409.454462	0.457238	-0.016183	-1409.013407
	ΔGMA [kJ/mol]							-148.4
M81	REDO_sir600_1	-1251.087586	-1250.746939	-1251.160216	-1251.392682	0.340647	-0.072630	-1251.124664
	REDO_sir600_me_1	-1291.189851	-1290.810080	-1291.209840	-1291.515573	0.379771	-0.019988	-1291.155791
	ΔGMA [kJ/mol]							-151.2
M82	REDO_sir610_2	-1290.399281	-1290.032363	-1290.469631	-1290.713713	0.366918	-0.070350	-1290.417145
	REDO_sir610_me_2	-1330.498349	-1330.092475	-1330.517105	-1330.832799	0.405874	-0.018757	-1330.445682
	ΔGMA [kJ/mol]							-144.4

Example 3: Quantitative structure/reactivity relationships for α,β-unsaturated carbonyl compounds

With the Mayr electrophilicities *E* for a broad set of α,β-unsaturated carbonyl compounds at hand (from this work), we analyzed the impact of substituents on their electrophilic reactivity in 1,4-additions. The differences in *E* between typical classes of Michael acceptors might be used as increments (expressed as Δ*E*) together with equation 1 to rationalize or estimate the reactivity of Michael acceptors of unknown *E*.

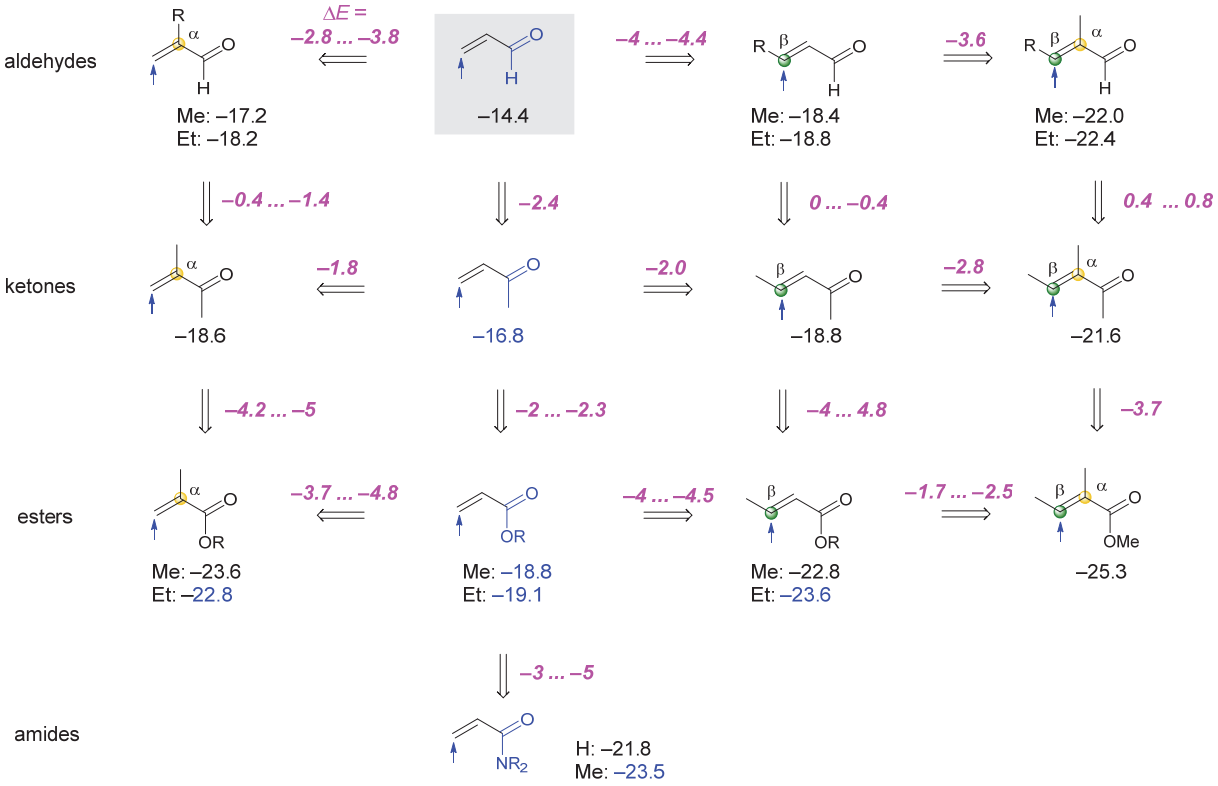

Figure S4: Structure/electrophilicity relationships for Michael acceptors based on the electrophilicities *E* (in blue color: from ref. 10c; in black color: this work).

Generally, introduction of alkyl substituents in the α-position reduces the electrophilic reactivity of the Michael acceptor on average by 3 to 4 *E* units. Analogously, alkyl substituents in the β-position reduce reactivity by 2.0 to 4.5 *E* units. While the reactivity of α,β-unsaturated aldehydes and the corresponding ketones is in a comparable range (going from an aldehyde to a structurally related ketone generally slightly reduces the reactivity, but the effects are rather small), esters are significantly less reactive by on average of 3 to 5 *E* units than the corresponding ketones. Swapping a ketone for an amide reduces the electrophilicity significantly (Δ*E* = –5 to –8).

Example 4: Rational prediction of Michael additions

According to the Patz-Mayr equation (equation 1, main text), electrophilicity *E* is defined as a solvent-independent parameter.[37a] Therefore, the electrophilicity parameters *E* of Michael acceptors determined in this study can be combined with any known solvent-dependent nucleophilicity parameter *N* (and s_N) of potential reaction partners[21] to predict second-order rate constants for their 1,4-addition reactions.[37b]

Will I get a product within reasonable reaction time? In the majority of the possible electrophile-nucleophile combinations the answer to this most important question for synthetic chemists can be given by calculating the sum lg k_2(20 °C) = $E + N$. If $E + N > -3$, the reaction should be feasible at 20 °C when applying typical reactant concentrations of 0.1 M.

In Figure S5 Michael acceptors and nucleophiles are arranged in a way that $E + N = -3$ for reaction partners on the same horizontal level. Michael acceptors can be expected to react at ambient temperature with nucleophiles on the same level in Figure S5. When equimolar concentrations of 0.1 M are used for the electrophile-nucleophile mixture and s_N is in the typical range (0.5 to 0.8 for nucleophiles with $N > 11$ that undergo Michael additions), a half-reaction time between 1 and 3 hours is expected for a certain Michael acceptor when reacting with nucleophilic reaction partners located at the same horizontal level in Figure S5. A certain Michael acceptor will also react at ambient temperature with those nucleophiles, which are positioned below itself in Figure S5, but only sluggish or not at all with those above its own position. Slower reactions may become feasible under harsher reaction conditions, for example, upon heating or increasing the concentrations of reactants up to neat. This is only a crude approximation, however, and considering the susceptibility parameter s_N in equation 1 is advised for borderline cases.

Please note that the Patz-Mayr equation (equation 1) only analyzes the *kinetic* feasibility for the formation of a σ-bond. Sufficiently *favorable thermodynamics* is another condition for the success of an intended Michael addition. Nevertheless, Figure S5 summarizes well-known synthetically employed reactions of Michael acceptors with nucleophiles. For example, rates of Corey-Chaykovsky cyclopropanations,[38] stepwise 1,3-dipolar cycloadditions (Huisgen reactions),[10c] Weitz-Scheffer epoxidations,[39] cyanoethylations[20,22,24,26,31] or simple Michael adduct formations (1,4-addition) of Michael acceptors with amines, alkoxide ions, and thiolates[20-31] can be predicted by using equation 1 and the available Mayr reactivity parameters *E*, *N* and s_N.[21] The precision of these predictions can be assessed from the $k_2^{exp}/k_2^{eq\ 1}$ ratios, which compare reported experimental rate constants k_2^{exp} with rate constants $k_2^{eq\ 1}$ predicted by equation 1 (see Table S6 above).

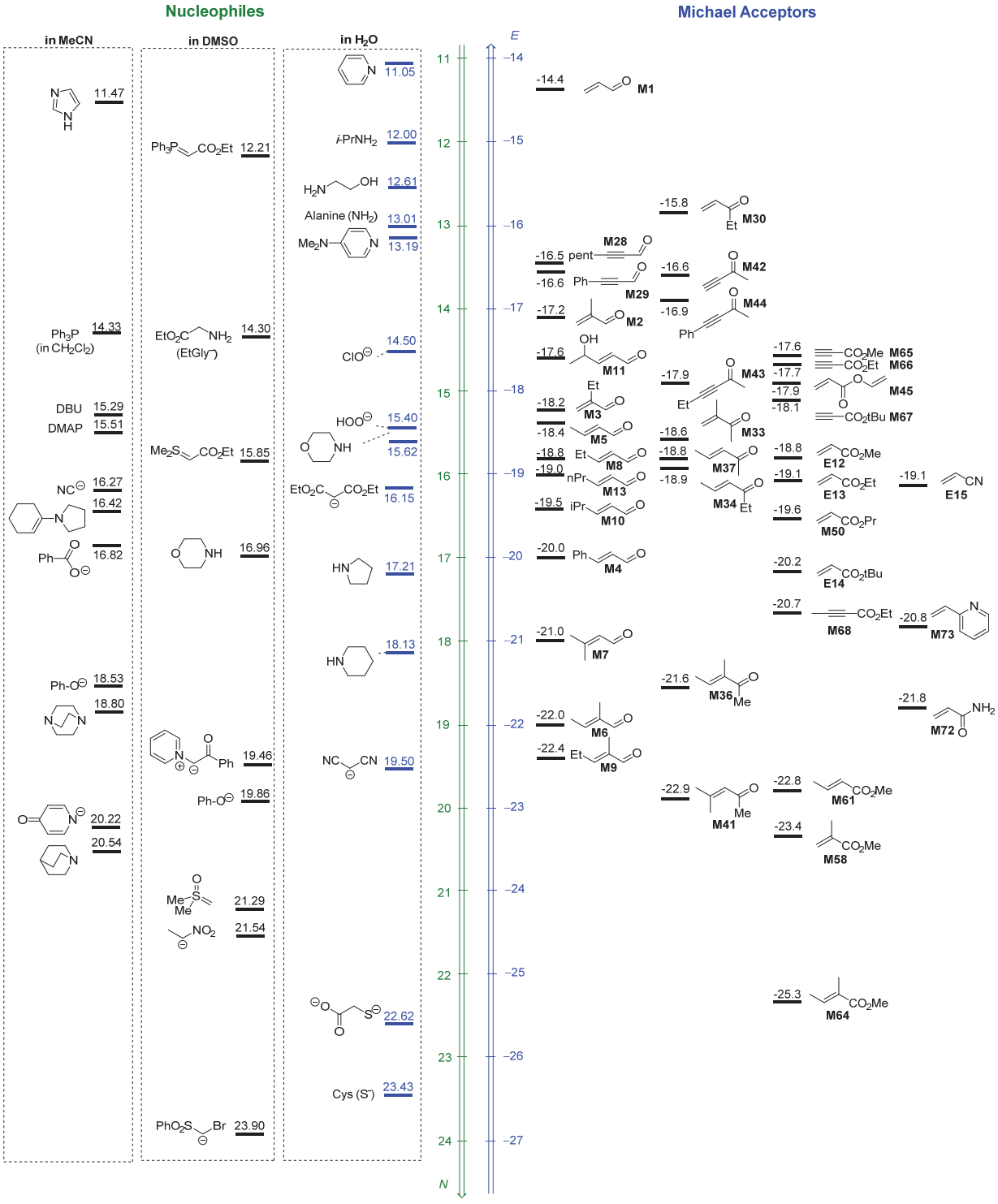

Figure S5: Nucleophilicity (*N*) and electrophilicity (*E*) scales arranged in a way that a certain Michael acceptor will react with those nucleophiles, which are positioned below its own level ($N + E > -3$). Nucleophile-specific parameters *N* were taken from ref. 21, electrophilicity parameters *E* for Michael acceptors were taken from Table S4.

5.9 References

[1] J. T. Edsall, J. Wyman, *Biophysical Chemistry*, Academic Press, New York, 1958.

[2] M. Friedman, J. F. Cavins, J. S. Wall, *J. Am. Chem. Soc.* **1965**, *87*, 3672–3682.

[3] D. L. Rabenstein, *J. Am. Chem. Soc.* **1973**, *95*, 2797–2803.

[4] A. Mirzahosseini, M. Somlyay, B. Noszál, *Chem. Phys. Lett.* **2015**, *622*, 50–56.

[5] a) T. Bug, H. Mayr, *J. Am. Chem. Soc.* **2003**, *125*, 12980–12986. b) F. Brotzel, H. Mayr, *Org. Biomol. Chem.* **2007**, *5*, 3814–3820.

[6] A. Meißner, P. Gockel, H. Vahrenkamp, *Chem. Ber.* **1994**, *127*, 1235–1241.

[7] a) H. Esterbauer, H. Zollner, N. Scholz, *Z. Naturforsch*. *C* **1975**, *30*, 466–473. b) G. Eisenbrand, J. Schuhmacher, P. Gölzer, *Chem. Res. Toxicol*. **1995**, *8*, 40–46. c) K. Chan, R. Poon, P. J. O'Brien, *J. Appl. Toxicol*. **2008**, *28*, 1027–1039.

[8] A. Böhme, A. Laqua, G. Schüürmann, *Chem. Res. Toxicol.* **2016**, *29*, 952–962.

[9] J. A. H. Schwöbel, D. Wondrousch, Y. K. Koleva, J. C. Madden, M. T. D. Cronin, G. Schüürmann, *Chem. Res. Toxicol*. **2010**, *23*, 1576–1585.

[10] a) H. Mayr, J. Ammer, M. Baidya, B. Maji, T. A. Nigst, A. R. Ofial, T. Singer, *J. Am. Chem. Soc.* **2015**, *137*, 2580–2599; b) P. A. Byrne, S. Kobayashi, E.-U. Würthwein, J. Ammer, H. Mayr, *J. Am. Chem. Soc.* **2017**, *139*, 1499–1511; c) D. S. Allgäuer, H. Jangra, H. Asahara, Z. Li, Q. Chen, H. Zipse, A. R. Ofial, H. Mayr, *J. Am. Chem. Soc.* **2017**, *139*, 13318–13329.

[11] E. Harder, W. Damm, J. Maple, C. Wu, M. Reboul, J. Y. Xiang, L. Wang, D. Lupyan, M. K. Dahlgren, J. L. Knight, J. W. Kaus, D. S. Cerutti, G. Krilov, W. L. Jorgensen, R. Abel, R. A. Friesner, *J. Chem. Theory Comput.* **2016**, *12*, 281–296.

[12] *MacroModel* (Schrödinger Release 2019-1), Schrödinger, LLC, New York, NY, 2019.

[13] A. D. Becke, *J. Chem. Phys.* **1993**, *98*, 5648–5652.

[14] R. Ditchfield, W. J. Hehre, J. A. Pople, *J. Chem. Phys.* **1971**, *54*, 724–728.

[15] R. Krishnan, J. S. Binkley, R. Seeger, J. A. Pople, *J. Chem. Phys.* **1980**, *72*, 650–654.

[16] T. Clark, J. Chandrasekhar, G. W. Spitznagel, P. v. R. Schleyer, *J. Comput. Chem.* **1983**, *4*, 294–301.

[17] A. V. Marenich, C. J. Cramer, D. G. Truhlar, *J. Phys. Chem. B.* **2009**, *113*, 6378–6396.

[18] *Gaussian 16, Revision A.03*, M. J. Frisch, G. W. Trucks, H. B. Schlegel, G. E. Scuseria, M. A. Robb, J. R. Cheeseman, G. Scalmani, V. Barone, G. A. Petersson, H. Nakatsuji, X. Li, M. Caricato, A. V. Marenich, J. Bloino, B. G. Janesko, R. Gomperts, B. Mennucci, H. P. Hratchian, J. V. Ortiz, A. F. Izmaylov, J. L. Sonnenberg, D. Williams-Young, F. Ding, F. Lipparini, F. Egidi, J. Goings, B. Peng, A. Petrone, T. Henderson, D. Ranasinghe, V. G. Zakrzewski, J. Gao, N. Rega, G. Zheng, W. Liang, M. Hada, M. Ehara, K. Toyota, R. Fukuda, J. Hasegawa, M. Ishida, T. Nakajima, Y. Honda, O. Kitao, H. Nakai, T. Vreven, K. Throssell, J. A. Montgomery, Jr., J. E. Peralta, F. Ogliaro, M. J. Bearpark, J. J. Heyd, E. N. Brothers, K. N. Kudin, V. N. Staroverov, T. A. Keith, R. Kobayashi, J. Normand, K. Raghavachari, A. P. Rendell, J. C. Burant, S. S. Iyengar, J. Tomasi, M. Cossi, J. M. Millam, M. Klene, C. Adamo, R. Cammi, J. W. Ochterski, R. L. Martin, K. Morokuma, O. Farkas, J. B. Foresman, and D. J. Fox, Gaussian, Inc., Wallingford CT, 2016.

[19] H. Mayr, *Angew. Chem.* **2011**, *123*, 3692–3698; *Angew. Chem. Int. Ed.* **2011**, *50*, 3612–3618.

[20] C. K. M. Heo, J. W. Bunting, *J. Org. Chem.* **1992**, *57*, 3570–3578.

[21] A free database of reactivity parameters *E*, *N*, and s_N can be accessed at: www.cup.lmu.de/oc/mayr/DBintro.html.

[22] H. Shenhav, Z. Rappoport, S. Patai, *J. Chem. Soc. B* **1970**, 469–476.

[23] H. Esterbauer, *Monatsh. Chem.* **1970**, *101*, 782–810.

[24] M. Friedman, J. S. Wall, *J. Org. Chem.* **1966**, *31*, 2888–2894.

[25] N. Ferry, F. J. McQuillin, *J. Chem. Soc.* **1962**, 103–113.

[26] R. N. Ring, G. C. Tesoro, D. R. Moore, *J. Org. Chem.* **1967**, *32*, 1091–1094.

[27] I.-H. Um, E.-J. Lee, J.-S. Min, *Tetrahedron* **2001**, *57*, 9585–9589.

[28] I.-H. Um, J.-S. Lee, S.-M. Yuk, *J. Org. Chem*. **1998**, *63*, 9152–9153.

[29] I.-H. Um, J.-S. Lee, S.-M. Yuk, *Bull. Korean Chem. Soc*. **1998**, *19*, 776–779.

[30] S.-I Kim, H.-W. Baek, I.-H. Um, *Bull. Korean Chem. Soc*. **2009**, *30*, 2909–2912.

[31] B.-A. Feit, A. Zilkha, *J. Org. Chem.* **1963**, *28*, 406–410.
[32] X. Jiang, J. Chen, A. Bajić, C. Zhang, X. Song, S. L. Carroll, Z.-L. Cai, M. Tang, M. Xue, N. Cheng, C. P. Schaaf, F. Li, K. R. MacKenzie, A. C. M. Ferreon, F. Xia, M. C. Wang, M. Maletić-Savatić, J. Wang, *Nat. Commun*. **2017**, *8*, 16087.
[33] K. Umezawa, M. Yoshida, M. Kamiya, T. Yamasoba, Y. Urano, *Nat. Chem*. **2017**, *9*, 279–286.
[34] X. Jiang, Y. Yu, J. Chen, M. Zhao, H. Chen, X. Song, A. J. Matzuk, S. L. Carroll, X. Tan, A. Sizovs, N. Cheng, M. C. Wang, J. Wang, *ACS Chem. Biol.* **2015**, *10*, 864–874.
[35] J. Chen, X. Jiang, S. L. Carroll, J. Huang, J. Wang, *Org. Lett*. **2015**, *17*, 5978–5981.
[36] O. García-Beltrán, C. González, E. G. Pérez, B. K. Cassels, J. G. Santos, D. Millán, N. Mena, P. Pavez, M. E. Aliaga, *J. Phys. Org. Chem*. **2012**, *25*, 946–952.
[37] a) H. Mayr, M. Patz, *Angew. Chem.* **1994**, *106*, 990-1010; *Angew. Chem. Int. Ed. Engl.* **1994**, *33*, 938–957. b) H. Mayr, A. R. Ofial, *Pure Appl. Chem.* **2017**, *89*, 729-744.
[38] R. Appel, N. Hartmann, H. Mayr, *J. Am. Chem. Soc.* **2010**, *132*, 17894–17900.
[39] a) R. J. Mayer, T. Tokuyasu, P. Mayer, J. Gomar, S. Sabelle, B. Mennucci, H. Mayr, A. R. Ofial, *Angew. Chem.* **2017**, *129*, 13463–13467; *Angew. Chem. Int. Ed.* **2017**, *56*, 13279–13282. b) R. J. Mayer, A. R. Ofial, *Org. Lett.* **2018**, *20*, 2816–2820. c) R. J. Mayer, A. R. Ofial, *Eur. J. Org. Chem.* **2018**, 6010–6017.

Chapter 6. Lewis Acidity Scale of Diaryliodonium Ions toward Oxygen, Nitrogen, and Halogen Lewis Bases

R. J. Mayer, A. R. Ofial, H. Mayr, C. Y. Legault, *J. Am. Chem. Soc.* **2020**, *142*, 5221-5233

Author Contributions

RJM and CYL conceived the project receiving input from ARO and HM. RJM performed and analyzed the conductivity measurements, determination of Lewis basicities with benzhydrylium ions, BIMT experiments (**1d**+**3a**, **1e**+**3a**, **2a**+**3a** were performed by CYL), ITC titrations and kinetic studies. CYL performed spectrophotometric titration experiments (PT method, **1g**+**3e**, **1l**+**3e**, **1k**+**3e**, **1n**+**3e** were performed by RJM) and analyzed all experiments done with the PT method. The manuscript was written jointly by RJM, CYL, ARO and HM.

Copyright

Selected supporting material for this work is provided starting with section 6.1. The complete supporting information (SI) is published online and can be accessed under https://doi.org/10.1021/jacs.9b12998.

JACS
JOURNAL OF THE AMERICAN CHEMICAL SOCIETY
pubs.acs.org/JACS
Article

Lewis Acidity Scale of Diaryliodonium Ions toward Oxygen, Nitrogen, and Halogen Lewis Bases

Robert J. Mayer,* Armin R. Ofial, Herbert Mayr, and Claude Y. Legault*

Cite This: J. Am. Chem. Soc. 2020, 142, 5221−5233
Read Online
ACCESS | Metrics & More | Article Recommendations | Supporting Information

ABSTRACT: Equilibrium constants for the associations of 17 diaryliodonium salts $Ar_2I^+X^-$ with 11 different Lewis bases (halide ions, carboxylates, *p*-nitrophenolate, amines, and tris(*p*-anisyl)-phosphine) have been investigated by titrations followed by photometric or conductometric methods as well as by isothermal titration calorimetry (ITC) in acetonitrile at 20 °C. The resulting set of equilibrium constants K_I covers 6 orders of magnitude and can be expressed by the linear free-energy relationship lg K_I = s_I LA_I + LB_I, which characterizes iodonium ions by the Lewis acidity parameter LA_I, as well as the iodonium-specific affinities of Lewis bases by the Lewis basicity parameter LB_I and the susceptibility s_I. Least squares minimization with the definition LA_I = 0 for Ph_2I^+ and s_I = 1.00 for the benzoate ion provides Lewis acidities LA_I for 17 iodonium ions and Lewis basicities LB_I and s_I for 10 Lewis bases. The lack of a general correlation between the Lewis basicities LB_I (with respect to Ar_2I^+) and LB (with respect to Ar_2CH^+) indicates that different factors control the thermodynamics of Lewis adduct formation for iodonium ions and carbenium ions. Analysis of temperature-dependent equilibrium measurements as well as ITC experiments reveal a large entropic contribution to the observed Gibbs reaction energies for the Lewis adduct formations from iodonium ions and Lewis bases originating from solvation effects. The kinetics of the benzoate transfer from the bis(4-dimethylamino)-substituted benzhydryl benzoate Ar_2CH−OBz to the phenyl(perfluorophenyl)iodonium ion was found to follow a first-order rate law. The first-order rate constant k_{obs} was not affected by the concentration of $Ph(C_6F_5)I^+$ indicating that the benzoate release from Ar_2CH−OBz proceeds via an unassisted S_N1-type mechanism followed by interception of the released benzoate ions by $Ph(C_6F_5)I^+$ ions.

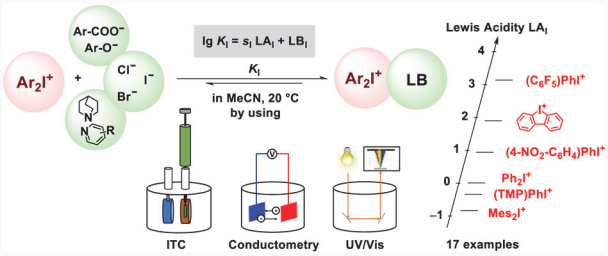

INTRODUCTION

Diaryliodonium ions **1** (Scheme 1) are frequently employed reagents for organic transformations.[1] In particular, they are useful for arylations, in which their ability to transfer an aryl-group to oxygen, nitrogen, sulfur, halide, or carbon nucleophiles, either with or without metal catalysis, gives them a broad synthetic scope.[2] Since the preassociation of the nucleophile to the iodonium center is essential for the reaction to proceed,[3] the reactivity of diaryliodonium ions is largely influenced by their Lewis acidity.

Scheme 1. Structures of Diaryliodonium (1) and Iodolium Ions (2)

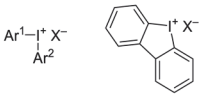

1 2

More recently, applications exploiting the Lewis acidity of iodonium ions as catalysts have also emerged. Liu, Han, and co-workers employed diaryliodonium salts as Lewis acidic catalysts for Mannich reactions,[4] and the Huber group reported the application of dibenzo[*b*,*d*]iodolium salts (**2**)[5] for catalyzing Diels−Alder reactions.[6] Toste and co-workers reported on the stereoselective C−H functionalization of cyclic ethers with Lewis adducts of diaryliodonium salts with chiral phosphates as key intermediates.[7]

Reports on the quantification of the Lewis acidities of diaryliodonium ions are scarce. In 2003, Ochiai and co-workers determined the binding constants of a small set of diaryl-iodonium salts with 18-crown-6 by ^{1}H NMR spectroscopy.[8] In 2006, the same group reported on the binding constants of nitrogen heteroarenes with $Ph_2I^+BF_4^-$.[9] Okuyama studied analogous reactions of cyclohexenyl phenyl iodonium ions with bromide, and in this context also determined equilibrium constants for the bromide addition.[10] Recently, the Gutmann−Beckett method[11] was used to derive the relative Lewis acidities of a small set of diaryliodonium salts from ^{31}P NMR chemical shift differences between triethylphosphine oxide and

Received: December 7, 2019
Published: March 3, 2020

https://dx.doi.org/10.1021/jacs.9b12998
J. Am. Chem. Soc. 2020, 142, 5221−5233

the corresponding Lewis adducts.[12] This experimental Lewis acidity scale was then combined with quantum chemical calculations to extrapolate Lewis acidities of further iodine(III) species.

Previously, Mayr and co-workers studied the equilibria for the reactions of benzhydrylium ions with various C-, N-, O-, P-, and S-centered Lewis bases in dichloromethane and acetonitrile at 20 °C (eq 1).

$$Ar_2CH^+ + LB^v \underset{}{\overset{K}{\rightleftharpoons}} Ar_2CH{-}LB^{v+1} \quad (1)$$

in MeCN or CH_2Cl_2, 20 °C

The obtained equilibrium constants were correlated by eq 2:[13]

$$\lg K = LA + LB \quad (2)$$

in which LA corresponds to a Lewis base independent Lewis acidity parameter [LA = 0 for $(4\text{-}MeOC_6H_4)_2CH^+$] and LB is a Lewis base parameter, which is assumed to generally hold for reactions of Lewis bases with benzhydrylium ions.

We now report on the construction of a quantitative Lewis acidity scale[14] for diaryliodonium and iodolium ions by measuring equilibrium constants K_I for their association with Lewis bases:

$$Ar_2I^+ + LB^v \underset{}{\overset{K_I}{\rightleftharpoons}} Ar_2I{-}LB^{v+1} \quad (3)$$

in MeCN, 20 °C

Chart 1 lists the 17 Lewis acidic diaryliodonium (**1a–n**) and dibenzo[*b*,*d*]iodolium ions (**2a–c**) covered in this work. Chart 2 gathers the structures of the 11 anionic and neutral entities that were selected as reference Lewis bases.

Chart 1. Diaryliodonium and Iodolium Ions Investigated in This Study

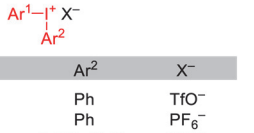

$Ar^1(Ar^2)I^+X^-$	Ar^1	Ar^2	X^-
1a	Ph	Ph	TfO^-
1b	Ph	Ph	PF_6^-
1c	Ph	3-CF_3-C_6H_4	TfO^-
1d	Ph	3,5-$(CF_3)_2$-C_6H_3	PF_6^-
1e	Ph	C_6F_5	PF_6^-
1f	Ph	4-NO_2-C_6H_4	TfO^-
1g	Ph	Mes	TfO^-
1h	Mes	4-NO_2-C_6H_4	TfO^-
1i	Mes	Mes	TfO^-
1j	4-CH_3-C_6H_4	4-CH_3-C_6H_4	TfO^-
1k	4-t-Bu-C_6H_4	4-t-Bu-C_6H_4	TfO^-
1l	4-Br-C_6H_4	4-Br-C_6H_4	TfO^-
1m	4-F-C_6H_4	4-F-C_6H_4	TfO^-
1n	2,4,6-$(MeO)_3$-C_6H_2	Ph	PF_6^-

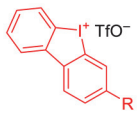

2a (R = H)
2b (R = CF_3)

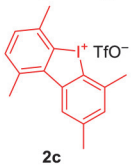

2c

Chart 2. Reference Lewis Bases Used

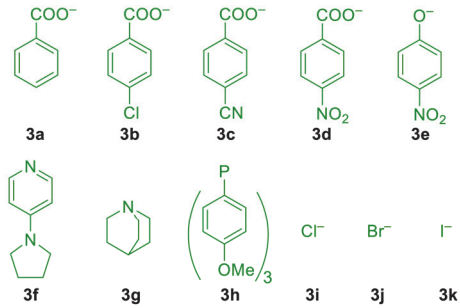

3a **3b** **3c** **3d** **3e** **3f** **3g** **3h** **3i** **3j** **3k**

RESULTS AND DISCUSSION

Structure of Iodonium Base Adducts. Solid-state (X-ray) structures[15] of the adducts of the diphenyliodonium ion Ph_2I^+ (**1a**) with chloride,[16] bromide,[16] iodide,[16] different pyridines,[9] 18-crown-6,[8] and DABCO[17] have been reported in the literature. The Lewis adducts of **1a** with benzoate and *p*-nitrophenolates (**4a** and **4b**), were prepared in this work by anion metathesis reactions (Scheme 2),[18] which were driven by the low solubility of potassium chloride in acetonitrile. Sonication of a suspension of $Ph_2I^+Cl^-$ and potassium benzoate (**3a**-K) or potassium 4-nitrophenolate (**3e**-K) in acetonitrile led to precipitation of KCl and afforded acetonitrile solutions of adducts **4a** and **4b**.

Scheme 2. Adducts of 1a with Benzoate Ion 3a and Phenolate Ion 3e

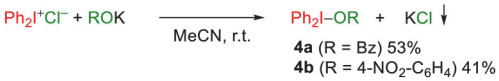

The Lewis adducts **4a** and **4b** crystallized upon partial evaporation of the solvent. The iodonium benzoate **4a** was isolated in 53% yield. Crystals of **4a** suitable for X-ray crystallography were then obtained by diffusion of diethyl ether into a concentrated acetonitrile solution of **4a**. Iodonium *p*-nitrophenolate **4b** (isolated in 41% yield) was crystallized from a concentrated acetonitrile solution.

In the solid-state structures of both adducts (Figure 1), iodine adopts a square-planar coordination sphere with Ph–I–Ph angles close to 90°. In **4a** (benzoate adduct) this coordination at iodine is achieved by formation of 2:2 adducts where iodonium ions are linked by two benzoate ions in an eight-membered ring. Analogous 2:2 adducts can be found in the solid-state structure of the acetate salt of **1n**.[19] In crystals of **4b**, strands are formed with the 4-nitrophenolate oxygen acting as a μ_2-bridging ligand.[20] Both isolated adducts **4a** and **4b** are stable at room temperature but undergo reductive elimination to the corresponding ester/ether at higher temperatures, as previously reported by Olofsson.[21]

Determination of Equilibrium Constants. Equilibrium constants for the formation of Lewis adducts from iodonium species **1** (or **2**) and Lewis bases **3** were determined by different methods: conductometry, isothermal titration calorimetry, UV/vis spectrometry, and NMR spectroscopic titration.

Conductivity Measurements. Previous crystal structure analyses[8,9,16,17,19] as well as the results in this work (Figure 1) illustrate the high tendency of the Lewis adducts of iodonium ions to fill the coordination sphere of the iodine center by formation of dimers or oligomers (Scheme 3). On the basis of dimeric adducts found in the gas-phase in LC-MS experiments and quantum-chemical calculations, Lee and co-workers postulated that diaryliodonium chlorides also form 2:2 adducts in solution.[22]

To deepen our insight into the association equilibria of iodonium salts, we used conductometry to study the degree of dissociation of ammonium and iodonium salts in up to 1 mM acetonitrile solutions.[23] Figure 2 shows that the conductivities of $Ph_2I^+TfO^-$ (**1a**), $Bu_4N^+Cl^-$, and $Bu_4N^+TfO^-$ solutions increase linearly with the salt concentrations in MeCN, indicating almost complete dissociation of these salts and

https://dx.doi.org/10.1021/jacs.9b12998
J. Am. Chem. Soc. 2020, 142, 5221–5233

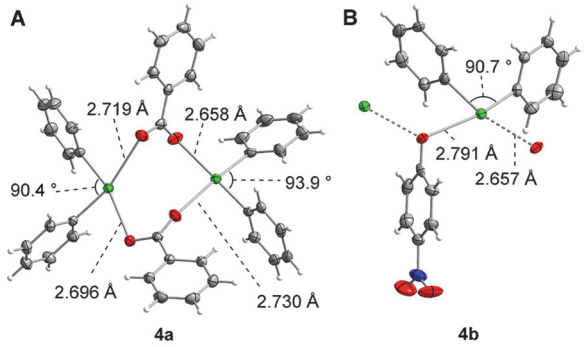

Figure 1. X-ray structures of (A) diphenyliodonium benzoate **4a** (CCDC 1960557) and (B) diphenyliodonium 4-nitrophenolate **4b** (CCDC 1960556) at 173 and 143 K, respectively. Thermal ellipsoids of **4a** and **4b** are depicted at a 50% probability level. For **4b**, the closest neighboring O and I atoms are shown (connected via dashed lines). For **4b**, the repetitive unit of the adduct strands is depicted with the closest neighboring O and I atoms connected via dashed lines. CCDC 1960556 and 1960557 contain the supplementary crystallographic data for this paper. These data can be obtained free of charge from The Cambridge Crystallographic Data Centre via https://www.ccdc.cam.ac.uk/structures/.

Scheme 3. Possible Association Equilibria of Ph_2I^+ Ions with Chloride Ions

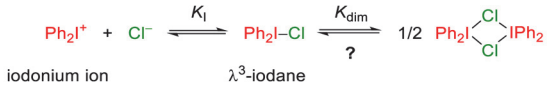

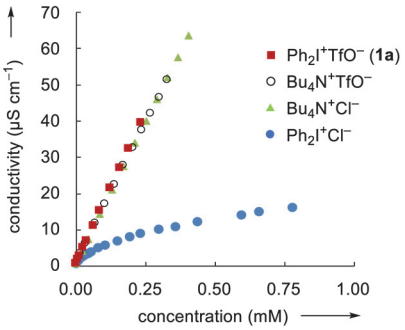

Figure 2. Concentration-dependent conductivity of $Ph_2I^+TfO^-$ (**1a**), $Bu_4N^+TfO^-$, and $Bu_4N^+Cl^-$, and $Ph_2I^+Cl^-$ (MeCN, 20 °C).

comparable molar conductivities of the involved ions in highly diluted solution.[24]

At higher concentrations of $Ph_2I^+TfO^-$ **1a**, the conductivity increase loses its linear correlation with salt concentration due to the formation of ion pairs (Figure S1). If compared to the other ionic species in Figure 2, then the much lower conductivities of the $Ph_2I^+Cl^-$ solutions in acetonitrile imply that even at low concentration this salt is only partially dissociated into free Ph_2I^+ and Cl^- ions.[25]

From the measured conductivities of solutions of $Ph_2I^+Cl^-$ and the specific conductivities of the fully dissociated salts (Figure 2) at high dilution (Kohlrausch's law), one can calculate the concentration of the free ions $[Ph_2I^+]$ (= $[Cl^-]$) in Ph_2ICl solutions in acetonitrile.

Assuming that Ph_2ICl exists as a monomer (λ^3-iodane) in acetonitrile solution and not as a dimer or oligomer (i.e., K_{dim} of Scheme 3 is negligibly small), the association constant K_I is given by eq 4. The concentration of free ions can be calculated when eq 4 is converted into eq 6 by using eq 5.

$$K_I = \frac{[Ph_2I–Cl]}{[Ph_2I^+][Cl^-]} \quad (4)$$

$$[Ph_2I–Cl] = [Ph_2I–Cl]_0 - [Cl^-] \quad (5)$$

$$[Ph_2I^+] = [Cl^-] = \frac{-1 \pm \sqrt{1 + 4K_I[Ph_2I–Cl]_0}}{2K_I} \quad (6)$$

Fitting of $[Ph_2I^+]$ calculated by eq 6 to the experimental $[Ph_2I^+]$ (blue dots in Figure 3) yields an excellent agreement of

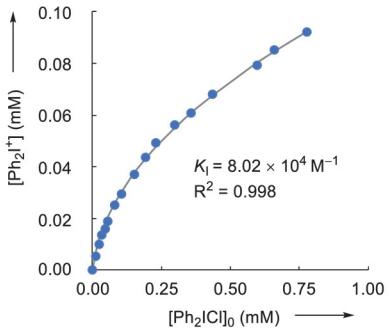

Figure 3. Concentration of free Ph_2I^+ ions in a solution of $Ph_2I^+Cl^-$ and fit (black line) of the experimental data with eq 6 (MeCN, 20 °C).

experimental and calculated ion concentrations for K_I = (8.02 ± 0.10) × 10^4 M^{-1} (black line in Figure 3). It is thus shown that a 1:1 association model is sufficient to describe the behavior of Ph_2ICl in acetonitrile solution. Furthermore, diffusion NMR experiments (DOSY) of the diphenyliodonium ion in the presence of different counterions (Cl^-, TfO^-) (see the Figure S3 for further details) indicated that the formation of higher aggregates (dimers or oligomers) of Ph_2ICl is insignificant under our experimental conditions (<1 mM solutions).

Isothermal Titration Calorimetry (ITC). In a microcalorimeter, small amounts of Lewis base (typically 40 × 6 μL portions of a 10 mM solution) were added to a solution of the iodonium salt (1.8 mL, 1 mM) at 20 °C, which gave rise to heat evolution within the sample cell (Figure 4A). Integration gives the heat evolution per injection. A plot of the heats of reaction for the individual injections versus the molar ratio of Lewis base over the iodonium ion yields a binding isotherm (Figure 4B), which was analyzed with a 1:1 binding model using the Affinimeter software package to afford the equilibrium constant K_I and the enthalpy of the binding reaction $\Delta_r H$.[26] The inflection point of the titration curve provides experimental evidence for the 1:1 stoichiometry of the interaction of Lewis bases and iodonium ions (shown for all combinations in the Supporting Information).

Solvent Effects on Equilibrium Constants. NMR titrations were previously used to compare association constants of $Ph_2I^+PF_6^-$ (**1b**) with triethylphosphine oxide in acetonitrile and dichloromethane at 25 °C, which showed that $K_I(CH_2Cl_2)/K_I(MeCN)$ = 3.8.[12]

Our ITC studies on the association of **1a** with benzoate (**3a**) showed effects in the same order of magnitude when comparing acetonitrile with the less polar solvents dichloromethane [$K_I(CH_2Cl_2)/K_I(MeCN)$ = 8.2] and THF

https://dx.doi.org/10.1021/jacs.9b12998
J. Am. Chem. Soc. 2020, 142, 5221−5233

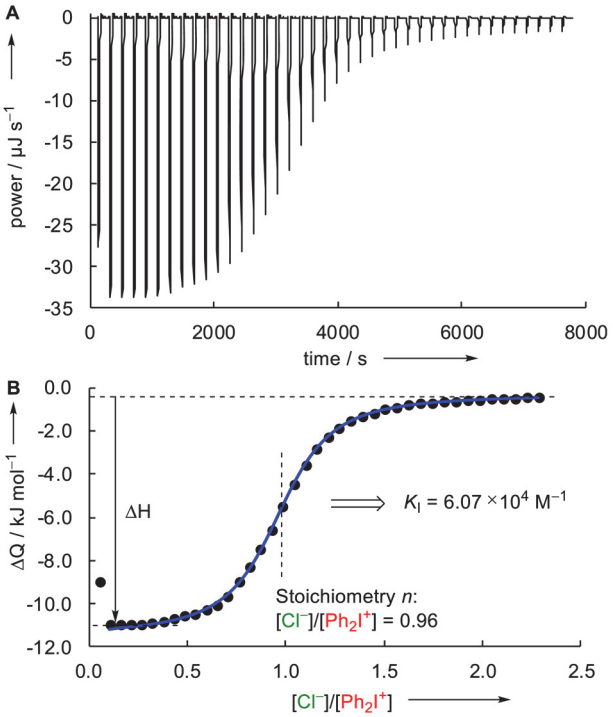

Figure 4. (A) Heat flow during the titration of $Ph_2I^+TfO^-$ (**1a**, 0.827 mM in MeCN) with $NBu_4^+Cl^-$ (10.0 mM in MeCN) at 20 °C (ITC trace after baseline correction). (B) Plot of the integrated heats per shot vs the equivalents of added chloride ions (black dots). The blue line depicts the fitted titration curve (the first injection was omitted from the correlation) giving K_I for this individual experiment.

$[K_I(THF)/K_I(MeCN) = 20]$ (Table 1). The three equilibrium constants (log K_I) for the Lewis adduct formation **1a** + **3a** correlate linearly with Reichardt's E_T^N values (r^2 = 0.9867).[27]

Table 1. Equilibrium Constants for the Lewis Adduct Formation between $Ph_2I^+TfO^-$ (1a) and Tetrabutylammonium Benzoate (3a) in Different Solvents[a]

solvent	K_I (M^{-1})
MeCN	$(1.76 \pm 0.16) \times 10^5$
CH_2Cl_2	$(1.45 \pm 0.44) \times 10^6$
THF	$(3.58 \pm 0.16) \times 10^6$

[a]ITC method, 20 °C.

We demonstrated above (Figure 2) that $Ph_2I^+TfO^-$ (**1a**) is mostly dissociated in diluted acetonitrile solutions at <1 mM and association of less than 5−15% is observed at concentrations <2 mM (Figures S1 and S2). A different situation is, however, observed in dichloromethane and THF. In these less polar solvents, conductivity studies show that $Ph_2I^+TfO^-$ (**1a**) exists mainly as ion pairs (Figure S5)[28] whose precise nature remains to be clarified. Additional evidence for the influence of organic solvents on the extent of dissociation of diaryliodonium triflates was obtained by ^{19}F DOSY NMR spectroscopy of iodonium salt **1m** (Figure 5). In acetonitrile, separate diffusion of the cation and the anion is detected. The identical diffusion rates for both ions of **1m**, however, provide additional evidence for the presence of adducts (ion pairs) in dichloromethane and THF. We have, therefore, focused our further investigations on equilibria in acetonitrile solutions.

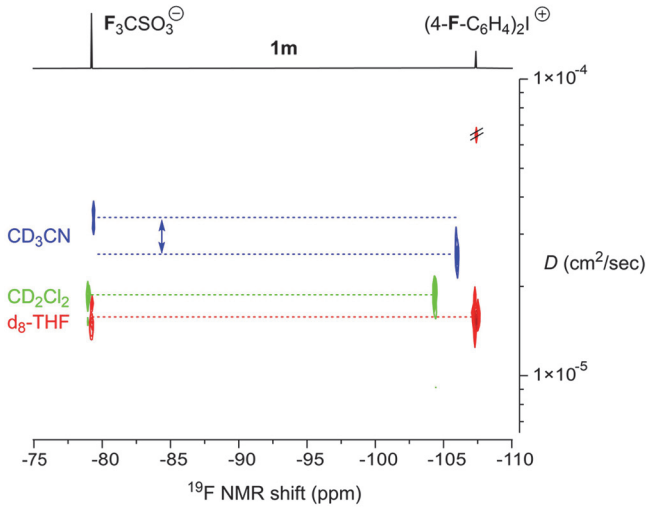

Figure 5. ^{19}F DOSY NMR spectra (25 °C) of **1m** in CD_3CN (blue, 12 mM), CD_2Cl_2 (green, 11 mM), and THF-d_8 (red, 8 mM). The ^{19}F NMR spectrum on top refers to THF-d_8.

Photometric Titrations (PT). K_I (eq 3) for the association of the colored Lewis base *p*-nitrophenolate (**3e**) with diaryliodonium ions can be determined by direct spectrophotometric titration (Scheme 4). Stepwise addition of a $Ph_2I^+TfO^-$ (**1a**) solution in acetonitrile to a solution of **3e** (λ_{max} = 430 nm) in the same solvent led to a hypsochromic shift (Figure 6A) of the absorption maximum, which we assigned to the formation of the phenolate-iodonium complex.

Due to the overlap of the absorption bands of **3e** and those of corresponding iodonium adduct **4b**, we determined the molar fraction of phenolate χ_{LB} from A^λ at every step of the titration (eq 12 in Scheme 4). As exemplified in Figure 6C, the equilibrium constant K_I was then obtained according to eq 8 (Scheme 4) from the slope of the linear correlation of the [**4b**]/[**3e**] ratio (eq 9, Scheme 4) with the concentration of [**1a**] (eq 11, Scheme 4). As full saturation cannot be achieved experimentally for some species, we used the value of A^λ_{ad} in the fitting process as a free variable to achieve an intercept of the correlation in eq 8 (Scheme 4) that equals 0.

The PT method is reliable for the determination of equilibrium constants $K < 10^6$ M^{-1}. Photometric titration of p-nitrophenolate (**3e**) allowed to determine equilibrium constants K_I for the association of **3e** with most of the iodonium (**1**) ions investigated in this work (Supporting Information).

Benzhydrylium-Indicator Method of Titration (BIMT). The direct determination of the equilibrium constants by the methods discussed so far are limited by physicochemical properties of the Lewis base (charge, color), or the range, in which reliable equilibrium constants can be obtained. We were, therefore, seeking a more general method for the determination of K_I.

Given the known reversibility of the reactions of many Lewis bases with benzhydrylium ions (Ar'_2CH^+) in acetonitrile, we chose colored benzhydrylium ions **B1** and **B2**[29] as indicators to establish equilibrium constants K_I of diaryliodonium-Lewis base reactions (Chart 3).

The BIMT relies on the thermodynamic relation illustrated in Figure 7A. In analogy to the PT method and as shown in Figure 7C, equilibrium constants K_I are obtained from the slope of the linear correlation of the $[Ar_2I{-}LB^+]/[LB]$ ratio

https://dx.doi.org/10.1021/jacs.9b12998
J. Am. Chem. Soc. 2020, 142, 5221−5233

Journal of the American Chemical Society pubs.acs.org/JACS Article

Scheme 4. Determination of the Equilibrium Constants K_I by Photometric Methods: Direct Titration with Colored Lewis Bases (PT Method) and Benzhydrylium-Indicator Method of Titration (BIMT)

$$Ar_2I^+ + LB \underset{}{\overset{K_I}{\rightleftharpoons}} Ar_2I^+–LB \; ; \quad \text{with } K_I = \frac{[Ar_2I^+–LB]}{[Ar_2I^+][LB]} \qquad (7)$$

$$[Ar_2I^+–LB]/[LB] = K_I[Ar_2I^+] \qquad (8)$$

PT Method

The consumption of the colored Lewis base LB by incremental addition of Ar_2I^+ is monitored directly by photometry

$$[Ar_2I^+–LB]/[LB] = (1 - \chi_{LB})/\chi_{LB} \qquad (9)$$

$$\text{Since } [Ar_2I^+] = [Ar_2I^+]_0 - [Ar_2I^+–LB] \qquad (10)$$

$$[Ar_2I^+] = [Ar_2I^+]_0 - (1 - \chi_{LB})[LB]_0 \qquad (11)$$

where

χ_{LB}: molar fraction of free LB

$$\chi_{LB} = \frac{[LB]}{[Ar_2I^+–LB] + [LB]} = \frac{A^\lambda - A^\lambda_{ad}(V_0/V)}{(A_0^\lambda - A^\lambda_{ad})(V_0/V)} \qquad (12)$$

A_0^λ: initial absorbance of the LB solution at a given wavelength λ

A^λ_{ad}: absorbance of the Lewis adduct Ar_2I^+–LB at wavelength λ

A^λ: absorbance at wavelength λ at different stages of the titration

$A^\lambda = \chi_{LB}A_0^\lambda(V_0/V) + (1 - \chi_{LB})A^\lambda_{ad}(V_0/V)$

V_0: volume of the initial LB solution (before addition of Ar_2I^+)

V : volume of the reaction mixture at different stages of the titration

BIMT Method

The formation of the colored benzhydrylium ions (Ar'_2CH^+, indicators) is followed during the incremental addition of Ar_2I^+ to solutions of Ar'_2CH–LB^+ adducts

$$[Ar_2I^+\text{-}LB] = [LB]_0 - [Ar'_2CH^+\text{-}LB] - [LB] \qquad (13)$$

$$[LB] = \frac{[Ar'_2CH^+–LB]}{[Ar'_2CH^+]K} \qquad (14)$$

$$[Ar_2I^+] = [Ar_2I^+]_0 - [Ar_2I^+–LB^+] \qquad (15)$$

with

$$[Ar'_2CH^+] = A/(\varepsilon\, d) \qquad (16)$$

$$[Ar'_2CH^+–LB] = [A_0(V_0/V) - A]/(\varepsilon\, d) \qquad (17)$$

and

K: equilibrium constant as defined in equation 1

A_0: absorbance of the initial Ar'_2CH^+ solution (before addition of LB)

A: absorbance of Ar'_2CH^+ during the titration

V_0: volume of the initial Ar'_2CH^+ solution (before addition of LB)

V : volume of the reaction mixture at different stages of the titration

ε: molar absorption coefficient of Ar'_2CH^+ (from ref 29)

d: optical path length (in cm) of the UV-vis cell

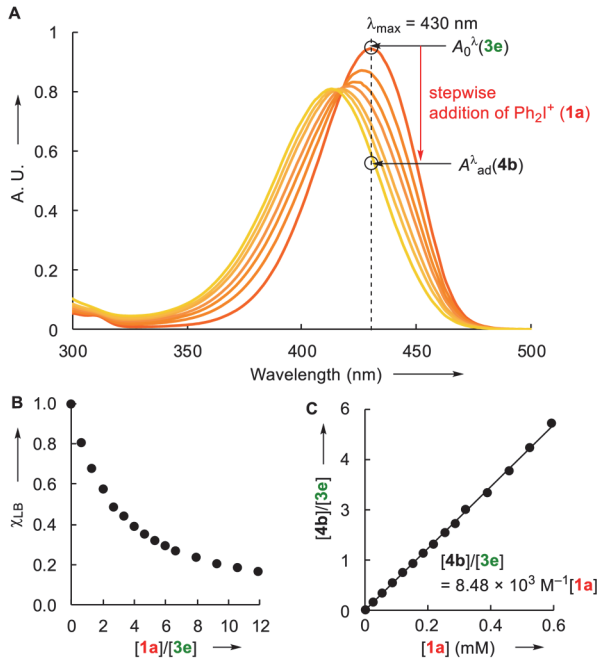

Figure 6. (A) Hypsochromic shift during the titration of **1a** with **3e** (in MeCN at 20 °C: NBu_4^+). (B) Plot of the molar fraction χ_{LB} vs [**1a**]/[**3e**] and (C) determination of the equilibrium constant K_I from the slope of a linear plot of [**4b**]/[**3e**] vs [**1a**].

Chart 3. Benzhydrylium Ions Used as Indicators for the BIMT

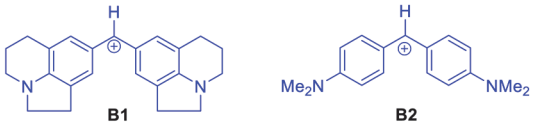

λ_{max} = 632 nm
LA_{MeCN} = –12.76

λ_{max} = 605 nm
LA_{MeCN} = –9.82

with [Ar_2I^+] (eq 8, Scheme 4). However, applying BIMT requires additional knowledge of the equilibrium constants K (eq 1) for the reactions of the Lewis bases with benzhydrylium ions. Alternatively, K can be calculated from Lewis acidity and Lewis basicity parameters LA and LB, respectively, by applying eq 2. Chart 3 lists the known Lewis acidity parameters LA for **B1** and **B2**,[13] and Table 2 contains LB parameters for the relevant charged and neutral Lewis bases (in acetonitrile).

Figure 7B illustrates how the titration of the benzhydrylium ion **B2** with BzO^- (**3a**) and iodonium ion **1l** can be monitored by UV/vis spectrometry. A solution of blue benzhydrylium salt **B2**-BF_4 (stage A in Figure 7B) is first treated with $Bu_4N^+BzO^-$ to convert approximately 50–70% of **B2** into covalent, colorless benzhydryl benzoate **B2**-OBz (step B in Figure 7B). Iodonium ion **1l** (with the noncoordinating TfO^- counterion) was then added to the solution (step C in Figure 7B). The reaction of the free Lewis base (BzO^-) with the iodonium ion disturbs the benzhydrylium-Lewis base equilibrium (K in Figure 7A) and leads to regeneration of colored benzhydrylium ion **B2** from the reservoir of covalent **B2**-OBz.

The most striking feature of BIMT is that it is capable of characterizing equilibrium constants involving a broad range of colorless Lewis acids: Equilibrium constants K_I from 10^2 to 10^8 M^{-1} can be determined, which is a significantly wider range than with the PT method. By changing the reference benzhydrylium ion (i.e., variation of K), this range can even be extended. However, the equilibrium constant for the

https://dx.doi.org/10.1021/jacs.9b12998
J. Am. Chem. Soc. 2020, 142, 5221–5233

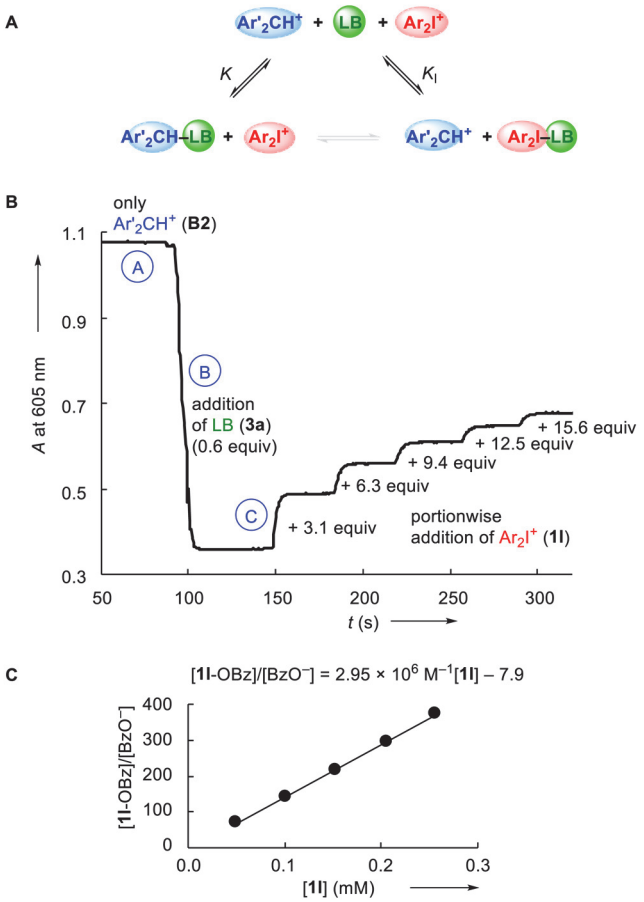

Figure 7. (A) Competing equilibria used for the determination of equilibrium constants K_I. (B) Representative BIMT experiment: A solution of benzhydrylium tetrafluoroborate **B2** (1.30×10^{-5} M, stage A) was treated with $Bu_4N^+BzO^-$ (0.6 equiv), which generated a mixture of **B2** and the adduct **B2**-OBz (step B). Then a solution of **1l** (6.53 mM, counterion: TfO^-) was added stepwise (step C), which caused the incremental increase of the benzhydrylium ion concentration [**B2**]. (C) Evaluation of K_I according to eq 8 (Scheme 4) from the slope of the linear correlation of [**1l**-OBz]/[BzO^-] vs [**1l**].

Table 2. Lewis Basicities LB[a]

Lewis base	LB (in MeCN)	ref
3a	17.54	this work[b]
3b	16.66	this work[b]
3c	15.64	this work[b]
3d	15.28	this work[b]
3e	16.98	30
3f	17.39	13
3g	15.48	13
3h	17.26	13
3i	≈11	13
3j	≈8	13
3k	not known	

[a]As defined in eq 2. [b]LB was determined by following the method described in ref 13. For details, see the Supporting Information.

reaction of the benzhydrylium ion with the Lewis base K (eq 1) needs to be known with sufficient precision. As a consequence, BIMT was inapplicable for determining K_I of halide anions **3i–k**: The binding constants K for the reaction of benzhydrylium ions with Cl^- (**3i**) and Br^- (**3j**) have a high uncertainty, and K remains to be determined for I^- (**3k**).[13]

Comparison of Methods. To validate the consistency of equilibrium constants K_I derived by different methods, we compared K_I for the reactions of diphenyliodonium triflate (**1a**) with the Lewis bases benzoate (**3a**), *p*-nitrophenolate (**3e**), 4-(pyrrolidino)pyridine (**3f**), and chloride (**3i**). As shown in Table 3, the agreement between K_I from BIMT, ITC, and PT methods is usually within the precision of the measurements. Depending on the Lewis base/acid combination, the biggest deviations are found for BIMT applications: While the errors are small when the equilibrium constant K for the interactions of the Lewis base with the benzhydrylium ions was directly measured, higher deviations (of factors up to 3) have to be tolerated when K was extrapolated by eq 2 using averaged LA and LB parameters because errors in K (eq 1) propagate into K_I (eq 14 in Scheme 4).

Table 3. Equilibrium Constants K_I for the Adduct Formation of Ph_2I^+ (1a) with Lewis Bases 3a, 3e, 3f, and 3i Determined by Four Different Methods[a]

Ph_2I^+ (**1a**) + LB	method	K_I (M^{-1})
1a + **3a**	BIMT	$(1.97 \pm 0.10) \times 10^5$
	ITC	$(1.76 \pm 0.16) \times 10^5$
1a + **3e**	BIMT	$(1.66 \pm 0.56) \times 10^4$
	PT	$(8.02 \pm 0.33) \times 10^3$
	ITC	$(7.24 \pm 0.26) \times 10^3$
1a + **3f**	BIMT	$(1.06 \pm 0.05) \times 10^2$
	NMR	$(3.34 \pm 0.26) \times 10^1$[b]
1a + Cl^- (**3i**)	conduct.	$(8.02 \pm 0.10) \times 10^4$
	ITC	$(6.29 \pm 0.42) \times 10^4$

[a]MeCN, 20 °C. [b]In CD_3CN.

The equilibrium constants for the reaction of $NBu_4^+Cl^-$ with $Ph_2I^+OTf^-$ (**1a**) in acetonitrile determined by ITC agree well with K_I derived from the conductivity experiments (Figure 3), which supports the assumed association model, that is, the formation of a 1:1 Lewis acid–base adduct in solution. However, differences in the total ion concentrations may explain the 22% difference of K_I for the **1a** + **3i** adduct formation derived from conductometric titrations and ITC. Solutions for conductometric measurements only contain Ph_2I^+ and Cl^- ions. In contrast, applying ITC requires the presence of additional counterions, that is, TfO^- (for **1a**) and Bu_4N^+ (for **3i**), which may cause a change in the degree of ion pairing that is seen in a slightly lower driving force for Lewis adduct formation.

A similar trend is also found when comparing K_I for **1a** + **3f** obtained by applying the BIMT method with K_I for the same reaction from NMR titrations (Table 3).[31] The equilibrium constant K_I under the conditions of the NMR spectroscopic titration, which is by a factor of 3 lower than K_I from BIMT measurements, may indicate a higher degree of ion pairing (cf. ref 23 and Figures S1 and S2) owing to the more than 5-fold higher total ion concentrations in NMR experiments than in photometric or ITC experiments.

Table 4 lists all equilibrium constants K_I for reactions of Lewis bases with iodonium (**1**) and iodolium ions (**2**) in acetonitrile (at 20 °C) that were determined in this work. Almost identical equilibrium constants K_I were measured for the adduct formation of phenolate ion **3e** with the diphenyliodonium triflate (**1a**) and the diphenyliodonium

https://dx.doi.org/10.1021/jacs.9b12998
J. Am. Chem. Soc. 2020, 142, 5221–5233

Table 4. Equilibrium Constants K_I (M^{-1}) for the Reactions of Diaryliodonium Ions 1 and 2 with Lewis Bases 5[a]

Lewis acid	LA_I	Lewis base	LB_I	s_I	K_I^{exptl} [b]	method	K_I^{calcd} [c]	K_I^{calcd}/K_I^{exptl}
1a	0.00	3a	5.33	1.00	$(1.97 \pm 0.10) \times 10^5$	BIMT[d]	2.13×10^5	1.1
1a	0.00	3b	4.78	0.94	$(4.95 \pm 0.45) \times 10^4$	BIMT[d]	5.98×10^4	1.2
1a	0.00	3c	4.28	0.92	$(1.68 \pm 0.09) \times 10^4$	BIMT[d]	1.91×10^4	1.1
1a	0.00	3d	4.52	0.88	$(2.94 \pm 0.06) \times 10^4$	BIMT[d]	3.30×10^4	1.1
1a	0.00	3e	3.96	0.91	$(8.02 \pm 0.33) \times 10^3$	PT	9.02×10^3	1.1
1a	0.00	3f	2.21	0.31	$(1.06 \pm 0.05) \times 10^2$	BIMT[e]	1.62×10^2	1.5
1a	0.00	3g	2.25	0.85	$(2.66 \pm 0.23) \times 10^2$	BIMT[d]	1.78×10^2	0.67
1a	0.00	3i	4.71	0.89	$(6.29 \pm 0.42) \times 10^4$	ITC	5.12×10^4	0.81
1a	0.00	3j	4.29	0.84	$(2.32 \pm 0.06) \times 10^4$	ITC	1.94×10^4	0.84
1a	0.00	3k	3.62	0.80	$(4.39 \pm 0.44) \times 10^3$	ITC	4.14×10^3	0.94
1b	−0.07	3e	3.96	0.91	$(7.78 \pm 0.65) \times 10^3$	PT	–	–
1c	0.60	3a	5.33	1.00	$(9.52 \pm 0.10) \times 10^5$	BIMT[d]	8.58×10^5	0.90
1c	0.60	3e	3.96	0.91	$(3.18 \pm 0.12) \times 10^4$	PT	3.21×10^4	1.0
1c	0.60	3f	2.21	0.31	$(1.85 \pm 0.15) \times 10^2$	BIMT[e]	2.51×10^2	1.4
1d	1.27	3a	5.33	1.00	$(5.10 \pm 0.09) \times 10^6$	BIMT[d]	3.99×10^6	0.78
1d	1.27	3e	3.96	0.91	$(1.37 \pm 0.08) \times 10^5$	PT	1.31×10^5	0.95
1d	1.27	3f	2.21	0.31	$(8.71 \pm 0.35) \times 10^2$	BIMT[e]	4.07×10^2	0.47
1d	1.27	3g	2.25	0.85	$(1.32 \pm 0.02) \times 10^3$	BIMT[d]	2.12×10^3	1.6
1d	1.27	3i	4.71	0.89	$(5.95 \pm 0.14) \times 10^5$	ITC	6.85×10^5	1.2
1e	3.21	3a	5.33	1.00	$(4.07 \pm 0.11) \times 10^8$	BIMT[d]	3.50×10^8	0.86
1e	3.21	3e	3.96	0.91	$(6.57 \pm 0.58) \times 10^6$	BIMT[d]	7.72×10^6	1.2
1e	3.21	3f	2.21	0.31	$(8.68 \pm 0.86) \times 10^2$	BIMT[e]	1.65×10^3	1.9
1e	3.21	3g	2.25	0.85	$(1.18 \pm 0.11) \times 10^5$	BIMT[d]	9.36×10^4	0.79
1f	0.89	3a	5.33	1.00	$(1.76 \pm 0.03) \times 10^6$	BIMT[d]	1.65×10^6	0.94
1f	0.89	3b	4.78	0.94	$(5.83 \pm 1.08) \times 10^5$	BIMT[d]	4.09×10^5	0.70
1f	0.89	3c	4.28	0.92	$(1.59 \pm 0.09) \times 10^5$	BIMT[d]	1.25×10^5	0.79
1f	0.89	3d	4.52	0.88	$(2.48 \pm 0.06) \times 10^5$	BIMT[d]	1.99×10^5	0.80
1f	0.89	3e	3.96	0.91	$(2.14 \pm 0.28) \times 10^4$	PT	5.83×10^4	2.7
1f	0.89	3f	2.21	0.31	$(2.92 \pm 0.20) \times 10^2$	BIMT[e]	3.08×10^2	1.1
1f	0.89	3g	2.25	0.85	$(8.58 \pm 0.14) \times 10^2$	BIMT[d]	1.00×10^3	1.2
1f	0.89	3i	4.71	0.89	$(4.23 \pm 0.19) \times 10^5$	ITC	3.13×10^5	0.74
1f	0.89	3j	4.29	0.84	$(1.03 \pm 0.05) \times 10^5$	ITC	1.07×10^5	1.0
1f	0.89	3k	3.62	0.80	$(2.21 \pm 0.07) \times 10^4$	ITC	2.14×10^4	0.97
1g	−0.26	3a	5.33	1.00	$(1.27 \pm 0.02) \times 10^5$	BIMT[d]	1.18×10^5	0.93
1g	−0.26	3e	3.96	0.91	$(4.85 \pm 0.14) \times 10^3$	PT	5.26×10^3	1.1
1h	0.53	3a	5.33	1.00	$(1.08 \pm 0.03) \times 10^6$	BIMT[d]	7.26×10^5	0.67
1h	0.53	3e	3.96	0.91	$(2.01 \pm 0.13) \times 10^4$	PT	2.76×10^4	1.4
1h	0.53	3f	2.21	0.31	$(1.68 \pm 0.17) \times 10^2$	BIMT[e]	2.38×10^2	1.4
1i	−0.76	3a	5.33	1.00	$(3.47 \pm 0.05) \times 10^4$	BIMT[d]	3.74×10^4	1.1
1i	−0.76	3e	3.96	0.91	$(2.20 \pm 0.48) \times 10^3$	PT	1.84×10^3	0.84
1i	−0.76	3i	4.71	0.89	$(1.16 \pm 0.06) \times 10^4$	ITC	1.10×10^4	0.94
1i	−0.76	3j	4.29	0.84	$(4.04 \pm 0.22) \times 10^3$	ITC	4.52×10^3	1.1
1i	−0.76	3k	3.62	0.80	$(9.71 \pm 2.12) \times 10^2$	ITC	1.02×10^3	1.1
1j	−0.11	3a	5.33	1.00	$(2.55 \pm 0.34) \times 10^5$	BIMT[d]	1.64×10^5	0.64
1j	−0.11	3e	3.96	0.91	$(4.62 \pm 0.11) \times 10^3$	PT	7.09×10^3	1.5
1j	−0.11	3f	2.21	0.31	$(1.27 \pm 0.05) \times 10^2$	BIMT[e]	1.50×10^2	1.2
1k	−0.24	3a	5.33	1.00	$(8.53 \pm 0.77) \times 10^4$	BIMT[d]	1.24×10^5	1.5
1k	−0.24	3e	3.96	0.91	$(8.28 \pm 0.05) \times 10^3$	PT	5.50×10^3	0.66
1l	0.96	3a	5.33	1.00	$(2.97 \pm 0.02) \times 10^6$	BIMT[d]	1.96×10^6	0.66
1l	0.96	3e	3.96	0.91	$(4.36 \pm 0.07) \times 10^4$	PT	6.82×10^4	1.6
1l	0.96	3f	2.21	0.31	$(3.19 \pm 0.17) \times 10^2$	BIMT[e]	3.26×10^2	1.0
1m	0.89	3a	5.33	1.00	$(3.03 \pm 0.12) \times 10^6$	BIMT[d]	1.67×10^6	0.55
1m	0.89	3e	3.96	0.91	$(2.35 \pm 0.03) \times 10^4$	PT	5.88×10^4	2.5
1m	0.89	3f	2.21	0.31	$(6.62 \pm 0.09) \times 10^2$	BIMT[e]	3.09×10^2	0.47
1n	−0.38	3a	5.33	1.00	$(5.92 \pm 0.98) \times 10^4$	BIMT[d]	8.81×10^4	1.5
1n	−0.38	3e	3.96	0.91	$(8.60 \pm 1.14) \times 10^3$	PT	4.03×10^3	0.47
1n	−0.38	3i	4.71	0.89	$(1.68 \pm 0.03) \times 10^4$	ITC	2.34×10^4	1.4
2a	1.90	3a	5.33	1.00	$(1.27 \pm 0.05) \times 10^7$	BIMT[d]	1.71×10^7	1.4
2a	1.90	3b	4.78	0.94	$(3.12 \pm 0.28) \times 10^6$	BIMT[d]	3.68×10^6	1.2
2a	1.90	3c	4.28	0.92	$(9.69 \pm 0.74) \times 10^5$	BIMT[d]	1.08×10^6	1.1
2a	1.90	3d	4.52	0.88	$(1.41 \pm 0.09) \times 10^6$	BIMT[d]	1.56×10^6	1.1

https://dx.doi.org/10.1021/jacs.9b12998
J. Am. Chem. Soc. 2020, 142, 5221−5233

Table 4. continued

Lewis acid	LA_I	Lewis base	LB_I	s_I	K_I^{exptl} [b]	method	K_I^{calcd} [c]	K_I^{calcd}/K_I^{exptl}
2a	1.90	**3e**	3.96	0.91	$(9.87 \pm 0.38) \times 10^5$	BIMT[d]	4.92×10^5	0.50
2a	1.90	**3f**	2.21	0.31	$(1.00 \pm 0.91) \times 10^3$	BIMT[d]	6.42×10^2	0.64
2a	1.90	**3g**	2.25	0.85	$(9.89 \pm 0.80) \times 10^2$[d,f]	BIMT[d]	7.28×10^3	7.4
2a	1.90	**3i**	4.71	0.89	$(2.27 \pm 0.14) \times 10^6$	ITC	2.48×10^6	1.1
2a	1.90	**3j**	4.29	0.84	$(7.43 \pm 0.05) \times 10^5$	ITC	7.61×10^5	1.0
2a	1.90	**3k**	3.62	0.80	$(1.35 \pm 0.10) \times 10^5$	ITC	1.40×10^5	1.0
2b	2.79	**3a**	5.33	1.00	$(9.08 \pm 0.16) \times 10^7$[g]	BIMT[d]	1.31×10^8	1.4
2b	2.79	**3e**	3.96	0.91	$(4.72 \pm 0.08) \times 10^6$[g]	BIMT[d]	3.15×10^6	0.67
2c	0.78	**3a**	5.33	1.00	$(5.23 \pm 0.33) \times 10^5$[e]	BIMT[d]	1.29×10^6	2.5
2c	0.78	**3e**	3.96	0.91	$(1.25 \pm 0.06) \times 10^5$[e]	BIMT[d]	4.65×10^4	0.37

[a]Determined in acetonitrile at 20 °C and compared with the equilibrium constants derived by applying eq 18. [b]Averaged from at least three measurements. [c]Calculated by applying LA_I, LB_I, and s_I in eq 18. [d]With **B2** as competition partner. [e]With **B1** as competition partner. [f]Not used for the least-squares minimization. [g]Measurements of lower quality.

hexafluorophosphate (**1b**) indicating the marginal counterion effect of these noncoordinating anions. Interactions of iodonium ions with tris(*p*-anisyl)phosphine (**3h**) are so weak that K_I could not even be determined for the most Lewis acidic iodonium ion **1e**.[32]

Correlation Analysis of the Equilibrium Constants K_I. As shown in Figure 8, in general, the ordering of the Lewis

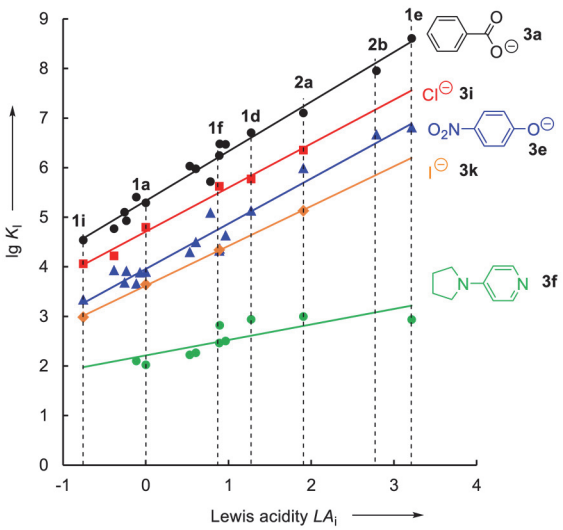

Figure 8. Plot of lg K_I for the reactions of diaryliodonium ions **1** (and **2**) with Lewis bases **3** versus their Lewis acidity parameters LA_I (all individual correlations are shown in Figure S6).

acidities of iodonium ions is the same with respect to different Lewis bases, but the relative Lewis basicities slightly depend on the nature of the iodonium ion. The equilibrium constants can be expressed by the linear-free energy relationship (eq 18), where the Lewis acidities of the diaryliodonium (and iodolium) ions are characterized by the parameter LA_I and the Lewis basicities are characterized by the parameter LB_I and the Lewis base specific susceptibilities by s_I.

$$\lg K_I = s_I \cdot LA_I + LB_I \tag{18}$$

These parameters were determined by least-squares minimization of Δ^2 (eq 19) from 70 equilibrium constants K_I (Table 4) with the definitions $LA_I(Ph_2I^+) = 0.00$ and $s_I(BzO^-) = 1.00$.

$$\Delta^2 = \sum (\lg K_I^{exptl} - \lg K_I^{calcd})^2 = \sum (\lg K_I^{exptl} - (s_I LA_I + LB_I))^2 \tag{19}$$

The resulting iodonium-specific Lewis basicity parameters LB_I (and s_I) for **3** as well as the Lewis acidities LA_I of iodonium ions **1** and **2** are listed in the left columns of Table 4. The columns on the right show that the equilibrium constants K_I^{calcd} calculated by eq 18 from s_I, LA_I, and LB_I (obtained by least-squares minimization of Δ^2, eq 19) deviate from the individual experimental K_I^{exptl} by less than a factor of 3 (exception: **2a** + **3g**). The quality of the linear correlations is illustrated by Figure 8, which also indicates the different slopes s_I of the correlations. To assess the overall quality of our correlation, Figure S7 shows the plot of calculated lg K_I^{calcd} versus experimental lg K_I^{exptl} values, giving an excellent linear correlation ($R^2 = 0.987$).

The experimental equilibrium constant K_I for the adduct formation between quinuclidine (**3g**) and iodolium ion **2a** is 7.5 times smaller than K_I^{calcd}. This observation might be caused by repulsive interactions between the sterically demanding quinuclidine (**3g**) in combination with the rigid structure of iodolium ion **2a** which enforces binding within its plane.

Structure–Reactivity Relationships of Iodonium Ions. The Lewis acidity parameters for iodonium ions LA_I, which correspond to averaged lg K_I values, can now be used to elucidate the impact of steric and electronic effects on the observed Lewis acidities (Scheme 5). The Lewis acidities LA_I of dibenzo[*b*,*d*]iodolium ions **2** are about 2 orders of magnitude greater than those of the analogously substituted diaryliodonium ions **1** (Scheme 5A).

Comparison of **1a** with **1g** and of **1f** with **1h** (Scheme 5B) shows that replacement of phenyl by mesityl reduces the Lewis acidity only slightly. The equilibrium constants K_I for iodonium ions bearing one mesityl moiety are by a factor of 2 smaller than for those that carry a phenyl group instead. Exchanging one phenyl group in Ph_2I^+ by a 2,4,6-trimethoxyphenyl (TMP) group (**1a** vs **1n**) reduces the Lewis acidity by 0.38 LA_I units. The large atomic radius of iodine (140 pm) and the fact that the plane of the aryl groups is perpendicular to the C–I–C plane may explain the observation that the steric bulk of the mesityl or the TMP group has only a small effect on the Lewis acidity. This rationalization is also in line with the solid-state structures of the Lewis adducts in Figure 1, which illustrate that the two aryl groups adopt a conformation perpendicular to the C–I–C plane and that the distance between iodine and the

https://dx.doi.org/10.1021/jacs.9b12998
J. Am. Chem. Soc. 2020, 142, 5221–5233

Scheme 5. Comparison of the Lewis Acidities LA_I of Different Iodonium Ions

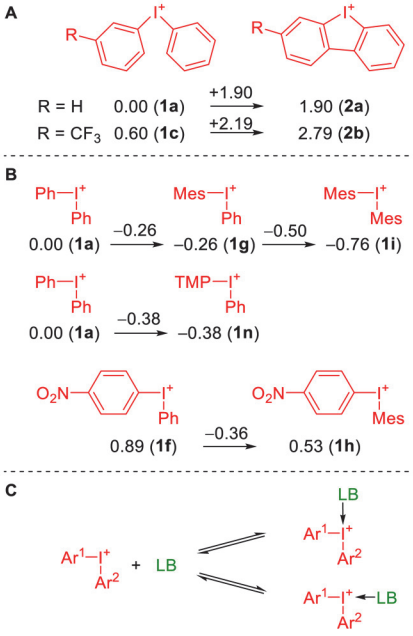

coordinating oxygen atom in the Lewis base is kept relatively long.

Why does the exchange of phenyl by mesityl have a larger effect on LA_I ($\Delta LA_I = -0.51$) when **1g** and **1i** are compared? According to calculations,[12] the Lewis base preferentially binds trans to the most electron-deficient aryl group when the T-shaped adduct is formed (Scheme 5C). Since only in the comparison of **1g**/**1i** the aryl group is exchanged, which will be located trans to the Lewis base in the adduct, the change from phenyl to mesityl has the strongest impact. Nevertheless, even in this case, the equilibrium constant K_I is reduced only by a factor of 3.

Reaction Enthalpies of Lewis Adduct Formation. The ITC measurements yield not only the equilibrium constant K_I for a certain Lewis adduct formation but also the related enthalpy of reaction (Δ_rH) the combination of which yields the entropy of reaction (Δ_rS) (Table 5).

For examining the consistency of the thermodynamic data obtained from ITC measurements at 20 °C, we additionally determined temperature-dependent equilibrium constants K_I by ITC, PT, and BIMT.[33] The temperature-dependent K_I values were then analyzed according to the van 't Hoff equation to calculate Δ_rH and Δ_rS.

For all studied systems, there is a fair agreement between directly measured enthalpies (by ITC) with those based on a van 't Hoff analysis (K_I from ITC, PT and BIMT). However, van 't Hoff derived enthalpies Δ_rH are systematically by 2−5 kJ mol^{-1} less negative than the directly measured heats of reaction (Δ_rH). From the entries in Table 5, it is evident that there is a significant entropic contribution to the interactions of Ph_2I^+ with Lewis bases. The positive entropy Δ_rS for reactions of **1a** with anions can be rationalized by the higher ordering of the solvent molecules around the ionic reactants. Adduct formation reduces the electron density at the atoms of both reaction centers resulting in less positive Δ_rS for the highly delocalized 4-nitrophenolate (**3e**): The importance of stabilization by the solvation shell, and thus the entropic component, is reduced compared to the benzoate ion (**3a**) with the more localized negative charge.

In reactions of **1a** with neutral Lewis base **3g** the opposite entropic effect is observed: Δ_rS is now negative, causing a reduction of the exergonicity for the formation of the corresponding Lewis adduct. Notably, the reaction enthalpy of association for **3g** is by more than 30 kJ/mol more negative than for the association with **3a** though the latter has a higher affinity towards iodonium ions (Δ_rG).

The strong entropic effect is furthermore illustrated in a comparison of the reactions of various iodonium ions with the same Lewis base (e.g., chloride (**3i**)), which shows that the increase of the binding constants is mostly due to an increase of entropy, while the reaction enthalpy is almost constant (Table 6).

Kinetics of the Iodonium-Induced Ionization of Benzhydryl Benzoates. Rate constants for ionizations of covalent benzhydryl benzoate **B2**-OBz in the presence of variable amounts of the Lewis acidic iodonium ion **1e** in acetonitrile were determined using stopped-flow UV/vis photometry by monitoring the increasing absorption of the reaction mixture caused by the released benzhydrylium ion **B2**.

As depicted in Scheme 6, the heterolysis of **B2**-OBz may proceed through two mechanistic pathways: (A) The iodonium ion attacks at the benzhydryl benzoate to yield complex **C**, which may be an intermediate or a transition state on the way to the final products. In pathway (B), the heterolytic cleavage of the benzhydryl benzoate occurs without assistance by the iodonium ion, and the iodonium ion Ar_2I^+ just traps the benzoate ion generated in an S_N1 process.

Table 5. Thermodynamics of the Lewis Adduct Formation between $Ph_2I^+TfO^-$ (1a) and Lewis Bases 3[a]

entry	Lewis base	method	Δ_rG (kJ mol^{-1})	Δ_rH (kJ mol^{-1})	$T\Delta_rS$ (kJ mol^{-1})	Δ_rS (J mol^{-1} K^{-1})
1	BzO^- (**3a**)	ITC (20 °C)	−29.4 ± 0.2	−18.1 ± 0.5	11.4 ± 0.3	38.9 ± 1.2
2	BzO^- (**3a**)	ITC (20 to 50 °C)[b]		−13.2 ± 1.6	16.3 ± 1.6	55.6 ± 5.3
3	*p*-nitrophenolate (**3e**)	ITC (20 °C)	−21.9 ± 0.3	−16.9 ± 0.4	5.0 ± 0.4	17.2 ± 1.4
4	*p*-nitrophenolate (**3e**)	ITC (20 to 40 °C)[b]		−14.3 ± 2.0	7.5 ± 1.9	25.5 ± 6.5
5[c]	*p*-nitrophenolate (**3e**)	PT (10 to 40 °C)[b]	−21.9 ± 0.1	−14.0 ± 0.6	7.9 ± 0.6	26.9 ± 2.2
6	quinuclidine (**3g**)	BIMT (−10 to 20 °C)[b]	−13.6 ± 0.2	−50.6 ± 3.5	−37.2 ± 3.8	−127 ± 13
7	Cl^- (**3i**)	ITC (20 °C)	−26.9 ± 0.1	−11.2 ± 0.3	15.7 ± 0.2	53.6 ± 0.4
8	Cl^- (**3i**)	ITC (20 to 50 °C)[b]		−9.7 ± 0.8	17.1 ± 0.8	58.3 ± 2.6
9	Br^- (**3j**)	ITC (20 °C)	−24.5 ± 0.1	−10.8 ± 0.1	13.7 ± 0.1	56.6 ± 0.5
10	I^- (**3k**)	ITC (20 °C)	−20.4 ± 0.2	−9.8 ± 0.3	10.6 ± 0.5	36.2 ± 1.8

[a]In MeCN, 20 °C. [b]Equilibrium constants K_I were determined at variable temperatures and used in a van 't Hoff plot to determine Δ_rH and Δ_rS (see the Supporting Information). [c]$Ph_2I^+PF_6^-$ (**1b**) was used.

https://dx.doi.org/10.1021/jacs.9b12998
J. Am. Chem. Soc. 2020, 142, 5221−5233

Journal of the American Chemical Society pubs.acs.org/JACS Article

Table 6. Thermodynamics of the Lewis Adduct Formation between Chloride Ion 3i and Iodonium Salts 1a, 1d, 1f, 1i, and 2a[a]

iodonium salt	K_I (M^{-1})	Δ_rG (kJ mol^{-1})	Δ_rH (kJ mol^{-1})	$T\Delta_rS$ (kJ mol^{-1})	Δ_rS (J mol^{-1} K^{-1})
1i	$(1.16 \pm 0.06) \times 10^4$	−22.8 ± 0.1	−10.2 ± 0.2	12.6 ± 0.3	43.1 ± 1.1
1a	$(6.29 \pm 0.42) \times 10^4$	−26.9 ± 0.1	−11.2 ± 0.3	15.7 ± 0.2	53.6 ± 0.4
1f	$(4.23 \pm 0.19) \times 10^5$	−31.6 ± 0.1	−12.2 ± 0.1	19.4 ± 0.1	66.2 ± 0.4
1d	$(5.95 \pm 0.14) \times 10^5$	−32.4 ± 0.1	−10.5 ± 0.1	21.9 ± 0.1	74.6 ± 0.3
2a	$(2.27 \pm 0.14) \times 10^6$	−35.7 ± 0.1	−13.5 ± 0.2	22.2 ± 0.1	75.8 ± 0.5

[a]ITC method, MeCN, 20 °C.

Scheme 6. Pathways for the Benzoate Transfer from a Benzhydrylium Benzoate to an Iodonium Ion

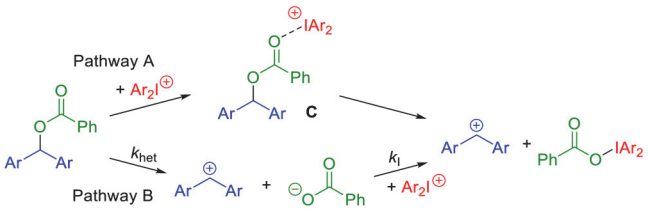

When the formation of benzhydrylium ion **B2** from **B2**-OBz (in the presence of 30% **B2**) was monitored photometrically with different concentrations of added $Ph(C_6F_5)I^+PF_6^-$ (**1e**), first-order kinetics were observed. The observed first-order rate constants k_{obs} were independent of the concentration of the added iodonium ion (**1e**, Figure 9). From this observation, one

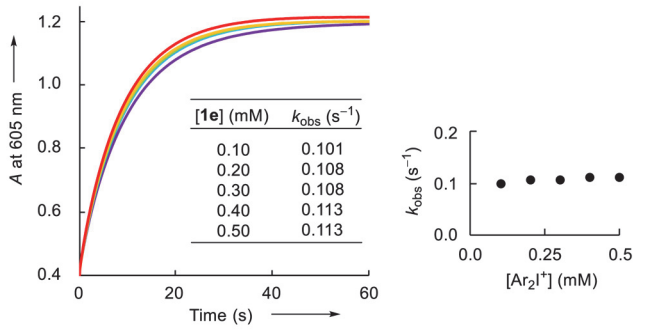

Figure 9. Time-dependent absorbance A (at 605 nm) for the reaction of **B2**-OBz ($\approx 6 \times 10^{-6}$ M) with different concentrations of the iodonium ion **1e** (0.1 to 0.5 mM) in acetonitrile at 20 °C.

can already conclude that the iodonium ions **1e** are not involved in the rate-determining step. Benzoate ions are generated by unassisted heterolytic cleavage of **B2**-OBz (path B in Scheme 6), and iodonium ion **1e** just serves as a trap for the released benzoate ions.

This conclusion is further corroborated by the similarity of the measured k_{obs} (0.11 s^{-1}, Figure 8) and the rate constant for the unassisted heterolysis k_{het} (0.12 s^{-1}) derived in Scheme 7.

Scheme 7. Estimating the Ionization Constant k_{het} of B2-OBz in Acetonitrile from Reactivity and Lewis Acidity/Basicity Parameters

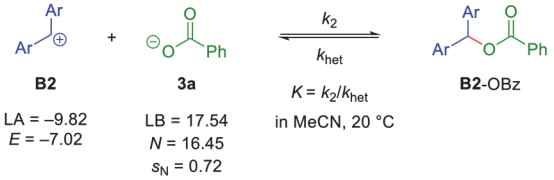

The rate constant k_{het}(20 °C) for the unassisted heterolysis of the covalent **B2**-OBz in acetonitrile can independently be estimated from the ratio $k_{het} = k_2/K$ according to Scheme 7.

The equilibrium constant for the reaction of benzhydrylium ion **B2** with **3a** in acetonitrile can be calculated to be $K = 5.2 \times 10^7$ M^{-1} by eq 2, from the Lewis acidity LA = −9.82 of **B2** and the Lewis basicity LB = 17.54 of BzO^- (**3a**). The second-order rate constant $k_2 = 6.2 \times 10^6$ M^{-1} s^{-1} for the reaction of **B2** (E = −7.02) with **3a** (N = 16.45, s_N = 0.72)[34] in acetonitrile can be calculated by using the Mayr−Patz equation (eq 20).[35]

$$\lg k_2(20°C) = s_N(N + E) \quad (20)$$

The ratio $k_2/K = 0.12$ s^{-1} equals the unassisted heterolysis rate constant k_{het}. Obviously, the presence of Lewis acidic iodonium ions **1e** at a submillimolar concentration does not significantly increase the rate of the heterolytic cleavage of the $Ar_2CH-OCOPh$ bond in **B2**-OBz.

In line with this interpretation, Huber found almost identical rates for the solvolysis reaction of Ph_2CH-Cl in wet acetonitrile with both iodolium ions **2a** and **2b**[6] even though their Lewis acidity differs by 1 order of magnitude according to our measurements.

Comparison of Lewis Basicities toward Iodine- and Carbon-Centered Lewis Acids. The blue correlation line in Figure 10 shows that the equilibrium constants K_I for the reactions of *p*-substituted benzoate ions **3a−d** with diphenyliodonium ion **1a** correlate linearly with the Lewis basicities LB (toward benzhydrylium ions) of these anions. The slope of this correlation (0.41) implies that variation of the substituents affects the equilibrium constants toward iodonium ions by 41% of the effect on the equilibrium constants of reactions with

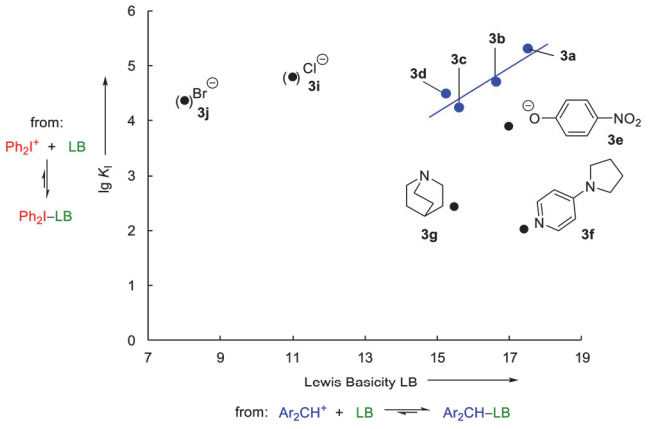

Figure 10. Plot of lg K_I for the reactions of Ph_2I^+ (**1a**) with various Lewis bases (MeCN, 20 °C) versus the Lewis basicity LB of the same set of Lewis bases in adduct formations with benzhydrylium ions (with data from Table 2). Blue correlation: lg K_I = 0.41LB − 2.0, R^2 = 0.832.

https://dx.doi.org/10.1021/jacs.9b12998
J. Am. Chem. Soc. 2020, 142, 5221−5233

benzhydrylium ions. The weak interaction between iodonium ions and these Lewis bases, which can be derived from this small slope (e.g., for benzoates), is in line with the observation that also the UV/vis spectrum of *p*-nitrophenolate is only slightly changed during association with an iodonium ion (Figure 6A).

The scatter of the other entries in Figure 10 shows that Lewis basicity toward iodonium ions is controlled by other factors than basicity toward carbon centers. While benzoate (**3a**), 4-nitrophenolate (**3e**), and 4-pyrrolidinopyridine (**3f**) have comparable Lewis basicities toward benzhydrylium ions, their ability to form Lewis adducts with Ph_2I^+ (**1a**) differs by more than 3 orders of magnitude. The equilibrium constant K_I for the reaction of Ph_2I^+ (**1a**) with tris(4-methoxyphenyl)-phosphine (**3h**) was so small that we were not able to determine it though its LB toward Ar_2CH^+ (17.26) is comparable to that of **3a**, **3e**, and **3f**. In contrast, bromide (**3j**) and chloride ions (**3i**) have K_I toward Ph_2I^+ similar to those of benzoate and *p*-nitrophenolate, while their Lewis basicities toward benzhydrylium ions differ by almost 9 orders of magnitude.

CONCLUSION

In previous work, it has been demonstrated that the equilibrium constants for the reactions of Lewis bases with benzhydrylium ions can be described by the sum of a base-independent Lewis acidity parameter LA and an acid-independent Lewis basicity parameter LB (eq 2), that is, the relative strengths of different Lewis bases are the same toward benzhydrylium ions of low and high Lewis acidity. The situation is more complex for the formation of Lewis adducts from iodonium ions and Lewis bases.

In organic solvents, diaryliodonium triflates and hexafluorphosphates can form ion pairs to a certain extent. While ion-pairing is negligible in diluted acetonitrile solution (<2 mM, Figures S1 and S2), in dichloromethane and THF it is already significant in the submillimolar concentration range (Figure S5).

Using conductometric and photometric titration (PT), ITC, and titrations using colored benzhydrylium ions **B1** and **B2** as indicators (BIMT), equilibrium constants for the coordination of iodonium ions with Lewis bases (halide, benzoate, and phenolate ions, as well as amines) have been determined in acetonitrile at 20 °C.

By subjecting these 70 equilibrium constants K_I to a least-squares minimization on the basis of eq 18, Lewis acidity parameters LA_I for different types of diaryliodonium ions have been obtained which apply for associations with all types of Lewis bases (Figure 8). Figure 11 shows that the acidities of the diaryliodonium ions increase with increasing electron-accepting abilities of the substituents and cover 4 orders of magnitude from the weakest Lewis acid, the dimesityliodonium ion (**1i**), to the strongest one, phenyl(pentafluorophenyl)-iodonium ion (**1e**). Cyclic iodonium ions **2a–c** have a considerably higher Lewis acidity than their acyclic analogs. The Lewis acidity scale for diaryliodonium ions derived in this work is in line with the relative acidities determined by the Gutmann–Beckett method.[12] While NMR experiments, which are usually carried out at higher concentrations, give the same ranking of Lewis acidities, the absolute values of K_I can be expected to be somewhat lower than the K_I determined in this study due to the effects of ion pairing.

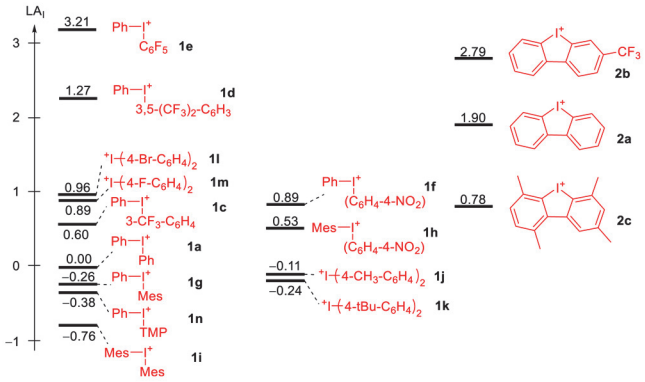

Figure 11. Lewis acidities LA_I of iodonium ions in acetonitrile.

Only for structurally closely related Lewis bases (*p*-substituted benzoates) do the Lewis basicities toward iodonium ions correlate with the Lewis basicities toward carbenium ions. In contrast, the relative Lewis basicities of halide anions, O-, N-, and P-centered Lewis bases, toward iodonium ions differ dramatically from their relative Lewis basicities toward benzhydrylium ions (Figure 10).

Kinetic investigations of the iodonium-ion-promoted ionization of benzhydryl benzoate **B2**-OBz showed that not even the most Lewis acidic iodonium ion in this work **1e** accelerated the ionization of **B2**-OBz. Iodonium ion rather quenches the benzoate ions generated by unassisted ionization of **B2**-OBz and thus increases the degree of ionization of the benzhydrylium benzoate (Le Chatelier principle).

ASSOCIATED CONTENT

Supporting Information

The Supporting Information is available free of charge at https://pubs.acs.org/doi/10.1021/jacs.9b12998.

Synthetic procedures, details of the determination of equilibrium constants K and K_I, details of kinetic measurements (PDF)

Crystallographic data for **4a** and **4b** (CIF, CIF)

AUTHOR INFORMATION

Corresponding Authors

Robert J. Mayer − *Department Chemie, Ludwig-Maximilians-Universität München, 81377 München, Germany;* orcid.org/0000-0002-9864-7042; Email: robert.mayer@cup.uni-muenchen.de

Claude Y. Legault − *University of Sherbrooke, Department of Chemistry, Centre in Green Chemistry and Catalysis, Sherbrooke, Québec J1K 2R1, Canada;* orcid.org/0000-0002-0730-0263; Email: claude.legault@usherbrooke.ca

Authors

Armin R. Ofial − *Department Chemie, Ludwig-Maximilians-Universität München, 81377 München, Germany;* orcid.org/0000-0002-9600-2793

Herbert Mayr − *Department Chemie, Ludwig-Maximilians-Universität München, 81377 München, Germany;* orcid.org/0000-0003-0768-5199

Complete contact information is available at: https://pubs.acs.org/10.1021/jacs.9b12998

https://dx.doi.org/10.1021/jacs.9b12998
J. Am. Chem. Soc. 2020, 142, 5221−5233

Author Contributions

The manuscript was written through contributions of all authors. All authors have given approval to the final version of the manuscript.

Notes

The authors declare no competing financial interest.

■ ACKNOWLEDGMENTS

We thank Prof. Stefan Huber and Flemming Heinen (Ruhr-Universität Bochum, Germany) for providing samples of the iodolium salts **2a–c** and for helpful discussions. We thank Nathalie Hampel (LMU München) for the experimental support and Dr. Peter Mayer (LMU München) for single crystal X-ray structure determinations. This work was supported by the National Science and Engineering Research Council (NSERC) of Canada, the Canada Foundation for Innovation (CFI), the Fonds de Recherche du Québec – Nature et Technologies (FRQNT), and the Université de Sherbrooke. R.J.M. thanks the Fonds der Chemischen Industrie for a Kekulé fellowship. The authors want to thank one anonymous referee for alerting us of the significance of ion pairing in the context of this work.

■ REFERENCES

(1) (a) Merritt, E. A.; Olofsson, B. Diaryliodonium salts: A Journey from Obscurity to Fame. *Angew. Chem., Int. Ed.* **2009**, *48*, 9052–9070. (b) Wang, M.; Chen, S.; Jiang, X. Atom-Economical Applications of Diaryliodonium Salts. *Chem. - Asian J.* **2018**, *13*, 2195–2207.

(2) (a) Olofsson, B.; Wirth, T. Arylation with Diaryliodonium Salts. *Top. Curr. Chem.* **2015**, *373*, 135–166. (b) Aradi, K.; Tóth, B. L.; Tolnai, G. L.; Novák, Z. Diaryliodonium Salts in Organic Syntheses: A Useful Compound Class for Novel Arylation Strategies. *Synlett* **2016**, *27*, 1456–1485. (c) Stuart, D. R. Aryl Transfer Selectivity in Metal-Free Reactions of Unsymmetrical Diaryliodonium Salts. *Chem. - Eur. J.* **2017**, *23*, 15852–15863. (d) Villo, P.; Olofsson, B. Arylations Promoted by Hypervalent Iodine Reagents. In *The Chemistry of Hypervalent Halogen Compounds (PATAI'S Chemistry of Functional Groups)*; Olofsson, B., Marek, I., Rappoport, Z., Eds.; Wiley: Chichester, U.K., 2019; Chapter 11, pp 461–522.

(3) Intermediates of arylation reactions of iodonium ions, which correspond to Lewis adducts of diaryliodonium salts with Lewis bases, have been characterized by X-ray crystallography and NMR spectroscopy: (a) Ozanne-Beaudenon, A.; Quideau, S. Regioselective Hypervalent-Iodine(III)-Mediated Dearomatizing Phenylation of Phenols through Direct Ligand Coupling. *Angew. Chem., Int. Ed.* **2005**, *44*, 7065–7069. (b) Lucchetti, N.; Scalone, M.; Fantasia, S.; Muñiz, K. Sterically Congested 2,6-Disubstituted Anilines from Direct C–N Bond Formation at an Iodine(III) Center. *Angew. Chem., Int. Ed.* **2016**, *55*, 13335–13339. (c) Dohi, T.; Koseki, D.; Sumida, K.; Okada, K.; Mizuno, S.; Kato, A.; Morimoto, K.; Kita, Y. Metal-Free *O*-Arylation of Carboxylic Acid by Active Diaryliodonium(III) Intermediates Generated *in situ* from Iodosoarenes. *Adv. Synth. Catal.* **2017**, *359*, 3503–3508. (d) Kervefors, G.; Becker, A.; Dey, C.; Olofsson, B. Metal-free formal synthesis of phenoxazine. *Beilstein J. Org. Chem.* **2018**, *14*, 1491–1497.

(4) Zhang, Y.; Han, J.; Liu, Z.-J. Diaryliodonium salts as efficient Lewis acid catalysts for direct three component Mannich reactions. *RSC Adv.* **2015**, *5*, 25485–25488.

(5) (a) For an overview on cyclic diaryliodonium species see Grushin, V. V. Cyclic diaryliodonium ions: old mysteries solved and new applications envisaged. *Chem. Soc. Rev.* **2000**, *29*, 315–324. (b) Postnikov, P. S.; Guselnikova, O. A.; Yusubov, M. S.; Yoshimura, A.; Nemykin, V. N.; Zhdankin, V. V. Preparation and X-ray Structural Study of Dibenziodolium Derivatives. *J. Org. Chem.* **2015**, *80*, 5783–5788. (c) Beringer, F. M.; Ganis, P.; Avitabile, G.; Jaffe, H. Synthesis, Structure, and Reactions of a Benziodolium Cation. *J. Org. Chem.* **1972**, *37*, 879–886.

(6) Heinen, F.; Engelage, E.; Dreger, A.; Weiss, R.; Huber, S. M. Iodine(III) derivatives as halogen bonding organocatalysts. *Angew. Chem., Int. Ed.* **2018**, *57*, 3830–3833.

(7) Ye, B.; Zhao, J.; Zhao, K.; McKenna, J. M.; Toste, F. D. Chiral Diaryliodonium Phosphate Enables Light Driven Diastereoselective α-C(sp^3)–H Acetalization. *J. Am. Chem. Soc.* **2018**, *140*, 8350–8356.

(8) Ochiai, M.; Suefuji, T.; Miyamoto, K.; Tada, N.; Goto, S.; Shiro, M.; Sakamoto, S.; Yamaguchi, K. Secondary Hypervalent I(III)···O Interactions: Synthesis and Structure of Hypervalent Complexes of Diphenyl-λ^3-iodanes with 18-Crown-6. *J. Am. Chem. Soc.* **2003**, *125*, 769–773.

(9) Suefuji, T.; Shiro, M.; Yamaguchi, K.; Ochiai, M. Complexation of Diphenyl(tetrafluoroborato)-λ^3-iodane with Pyridines. *Heterocycles* **2006**, *67*, 391–397.

(10) Okuyama, T.; Imamura, S.; Fujita, M. Reactions of Cyclohexenyl Iodonium Tetrafluoroborate with Bromide Ion: Retardation Due to the Formation of λ^3-Bromoiodane. *J. Org. Chem.* **2006**, *71*, 1609–1613.

(11) Beckett, M. A.; Strickland, G. C.; Holland, J. R.; Sukumar Varma, K. A convenient n.m.r. method for the measurement of Lewis acidity at boron centres: correlation of reaction rates of Lewis acid initiated epoxide polymerizations with Lewis acidity. *Polymer* **1996**, *37*, 4629–4631.

(12) Labattut, A.; Tremblay, P.-L.; Moutounet, O.; Legault, C. Y. Experimental and Theoretical Quantification of the Lewis Acidity of Iodine(III) Species. *J. Org. Chem.* **2017**, *82*, 11891–11896.

(13) (a) Mayr, H.; Ammer, J.; Baidya, M.; Maji, B.; Nigst, T. A.; Ofial, A. R.; Singer, T. Scales of Lewis Basicities toward C-Centered Lewis Acids (Carbocations). *J. Am. Chem. Soc.* **2015**, *137*, 2580–2599. (b) Mayr, H.; Ofial, A. R. Philicities, Fugalities, and Equilibrium Constants. *Acc. Chem. Res.* **2016**, *49*, 952–965. (c) Timofeeva, D. S.; Mayer, R. J.; Mayer, P.; Ofial, A. R.; Mayr, H. Which Factors Control the Nucleophilic Reactivities of Enamines? *Chem. - Eur. J.* **2018**, *24*, 5901–5910.

(14) (a) For an overview on Lewis Basicity and Acidity scales, see Laurence, C.; Gal, J.-F. *Lewis Basicity and Affinity Scales: Data and Measurement*; Wiley: Chichester, UK, 2010. (b) For an application of reactivity scales to dynamic covalent chemistry, see Zhou, Y.; Li, L.; Ye, H.; Zhang, L.; You, L. Quantitative Reactivity Scales for Dynamic Covalent and Systems Chemistry. *J. Am. Chem. Soc.* **2016**, *138*, 381–389.

(15) Justik, M. W. Structural chemistry of hypervalent iodine compounds. In *The Chemistry of Hypervalent Halogen Compounds (PATAI'S Chemistry of Functional Groups)*; Olofsson, B., Marek, I., Rappoport, Z., Eds.; Wiley: Chichester, U.K., 2019; Chapter 2, pp 31–118.

(16) Alcock, N. W.; Countryman, R. M. Secondary bonding. Part 1. Crystal and molecular structures of $(C_6H_5)_2$ IX (X = Cl, Br, or I). *J. Chem. Soc., Dalton Trans.* **1977**, 217–219.

(17) Bugaenko, D. I.; Yurovskaya, M. A.; Karchava, A. V. *N*-Arylation of DABCO with Diaryliodonium Salts: General Synthesis of *N*-Aryl-DABCO Salts as Precursors for 1,4-Disubstituted Piperazines. *Org. Lett.* **2018**, *20*, 6389–6393.

(18) Gallagher, R. T.; Seidl, T. L.; Bader, J.; Orella, C.; Vickery, T.; Stuart, D. R. Anion Metathesis of Diaryliodonium Tosylate Salts with a Solid-Phase Column Constructed from Readily Available Laboratory Consumables. *Org. Process Res. Dev.* **2019**, *23*, 1269–1274.

(19) China, H.; Koseki, D.; Samura, K.; Kikushima, K.; In, Y.; Dohi, T. Dataset on synthesis and crystallographic structure of phenyl-(TMP)iodonium(III) acetate. *Data in Brief* **2019**, *25*, 104063.

(20) Analogous oligomers exist in the solid-state structures of diphenyliodonium halides (chloride, bromide, and iodide); see ref 15.

(21) (a) Jalalian, N.; Ishikawa, E. E.; Silva, L. F., Jr.; Olofsson, B. Room Temperature, Metal-Free Synthesis of Diaryl Ethers with Use of Diaryliodonium Salts. *Org. Lett.* **2011**, *13*, 1552–1555. (b) Jalalian, N.; Petersen, T. B.; Olofsson, B. Metal-Free Arylation of Oxygen

https://dx.doi.org/10.1021/jacs.9b12998
J. Am. Chem. Soc. 2020, 142, 5221–5233

Nucleophiles with Diaryliodonium Salts. *Chem. - Eur. J.* **2012**, *18*, 14140−14149.
(22) (a) Lee, Y.-S.; Hodošček, M.; Chun, J.-H.; Pike, V. W. Conformational Structure and Energetics of 2-Methylphenyl(2′-methoxyphenyl)iodonium Chloride: Evidence for Solution Clusters. *Chem. - Eur. J.* **2010**, *16*, 10418−10423. (b) Lee, Y.-S.; Chun, J.-H.; Hodošček, M.; Pike, V. W. Crystal Structures of Diaryliodonium Fluorides and Their Implications for Fluorination Mechanisms. *Chem. - Eur. J.* **2017**, *23*, 4353−4363.
(23) Kline, E. R.; Kraus, C. A. Properties of Electrolytic Solutions. XXVI. The Conductance of Some Onium Type Salts in Ethylene Chloride at 25 °. *J. Am. Chem. Soc.* **1947**, *69*, 814−816.
(24) It is known that tetrabutylammonium salts associate in organic solvents at higher concentrations: LeSuer, R. J.; Buttolph, C.; Geiger, W. E. Comparison of the Conductivity Properties of the Tetrabutylammonium Salt of Tetrakis(pentafluorophenyl)borate Anion with Those of Traditional Supporting Electrolyte Anions in Nonaqueous Solvents. *Anal. Chem.* **2004**, *76*, 6395−6401.
(25) The nature of $Ph_2I^+Cl^-$ as tight ion pairs in acetonitrile was also derived from photolysis experiments: Hacker, N. P.; Leff, D. V.; Dektar, J. L. The Photochemistry of Diphenyliodonium Halides: Evidence for Reactions from Solvent-Separated and Tight Ion pairs. *J. Org. Chem.* **1991**, *56*, 2280−2282.
(26) Piñeiro, A.; Muñoz, E.; Sabín, J.; Costas, M.; Bastos, M.; Velázquez-Campoy, A.; Garrido, P. F.; Dumas, P.; Ennifar, E.; García-Río, L.; Rial, J.; Pérez, D.; Fraga, P.; Rodríguez, A.; Cotelo, C. AFFINImeter: A software to analyze molecular recognition processes from experimental data. *Anal. Biochem.* **2019**, *577*, 117−134.
(27) Reichardt, C., Welton, T. *Solvents and Solvent Effects in Organic Chemistry*, 4th ed.; Wiley-VCH: Weinheim, 2011; pp 425−508.
(28) For ion pair dissociation constants for the hexafluorophosphate of **1k** and the tetrafluoroborate of **1j** in MeCN and dichloromethane, see Ledwith, A.; Al-Kass, S.; Sherrington, D. C.; Bonner, P. Ion pair dissociation equilibria for iodonium and sulphonium salts useful in photoinitiated cationic polymerization. *Polymer* **1981**, *22*, 143−145.
(29) Mayer, R. J.; Hampel, N.; Mayer, P.; Ofial, A. R.; Mayr, H. Synthesis, Structure and Properties of Amino-Substituted Benzhydrylium Ions - a Link Between Ordinary Carbocations and Neutral Electrophiles. *Eur. J. Org. Chem.* **2019**, *2019*, 412−421.
(30) Mayer, R. J.; Breugst, M.; Hampel, N.; Ofial, A. R.; Mayr, H. Ambident Reactivity of Phenolate Anions Revisited: A Quantitative Approach to Phenolate Reactivities. *J. Org. Chem.* **2019**, *84*, 8837−8858.
(31) NMR titrations were performed as described in the Supporting Information and analyzed according to Thordarson, P. Binding Constants and Their Measurement. In *Supramolecular Chemistry*; Gale, P. A., Steed, J. W., Ed.; Wiley: Chichester, U.K., 2012; Vol. 2, pp 461−522.
(32) (a) We were not able to measure the equilibrium constants for the association of phosphine **3h** with diaryliodonium ions. However, EDA complexes between triphenylphosphine and iodonium ion **1g** have been reported: Bugaenko, D. I.; Volkov, A. A.; Livantsov, M. V.; Yurovskaya, M. A.; Karchava, A. V. Catalyst-Free Arylation of Tertiary Phosphines with Diaryliodonium Salts Enabled by Visible Light. *Chem. - Eur. J.* **2019**, *25*, 12502−12506. (b) Lewis adduct formation between Ph_2I^+ (**1a**) and $P(OEt)_3$ in acetonitrile was undetectable by spectroscopic methods (UV/vis, ^1H and ^{31}P NMR) and quantum-chemically calculated to be endergonic (in CH_2Cl_2, iefpcm solvent model): Lecroq, W.; Bazille, P.; Morlet-Savary, F.; Breugst, M.; Lalevee, J.; Gaumont, A.-C.; Lakhdar, S. Visible-Light-Mediated Metal-Free Synthesis of Aryl Phosphonates: Synthetic and Mechanistic Investigations. *Org. Lett.* **2018**, *20*, 4164−4167.
(33) As required for the analysis of the BIMT experiments, the temperature-dependent equilibrium constants K (eq 1) for the reactions of **B2** with quinuclidine were determined. See the Supporting Information for details.
(34) As determined in this work at 20 °C (Supporting Information). For nucleophilicity parameters N and s_N of **3a** (in MeCN) determined at 25 °C: Schaller, H. F.; Tishkov, A. A.; Feng, X.; Mayr, H. Direct Observation of the Ionization Step in Solvolysis Reactions: Electrophilicity versus Electrofugality of Carbocations. *J. Am. Chem. Soc.* **2008**, *130*, 3012−3022.
(35) Mayr, H.; Bug, T.; Gotta, M. F.; Hering, N.; Irrgang, B.; Janker, B.; Kempf, B.; Loos, R.; Ofial, A. R.; Remennikov, G.; Schimmel, H. Reference Scales for the Characterization of Cationic Electrophiles and Neutral Nucleophiles. *J. Am. Chem. Soc.* **2001**, *123*, 9500−9512.

https://dx.doi.org/10.1021/jacs.9b12998
J. Am. Chem. Soc. 2020, 142, 5221−5233

6.1 Additional Figures and Correlations

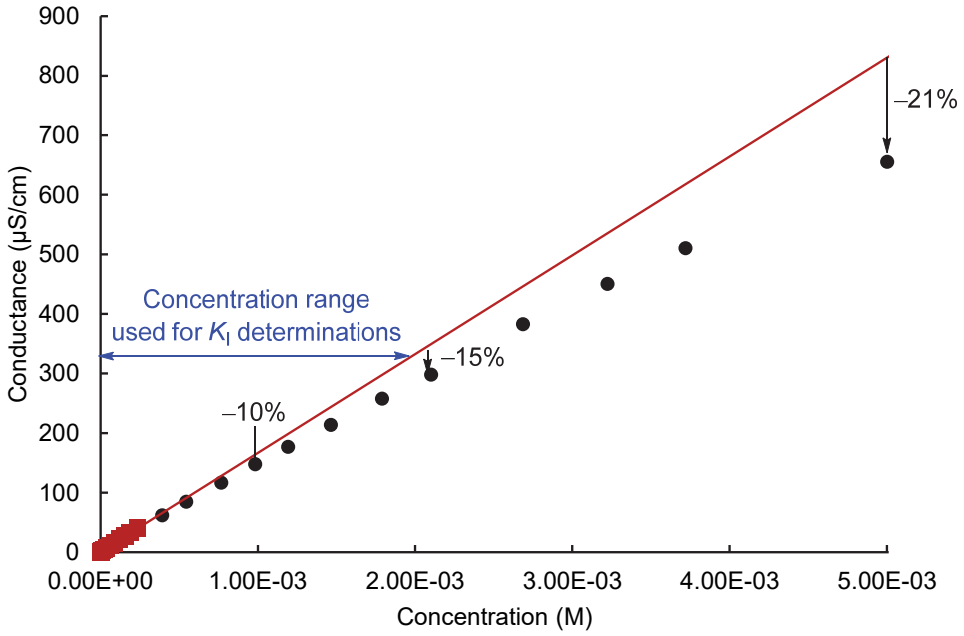

Figure S1: Comparison of experimental conductivity of Ph_2IOTf in MeCN at 20 °C with the predicted conductivity from measurements performed at low concentration (< 0.25 mM).

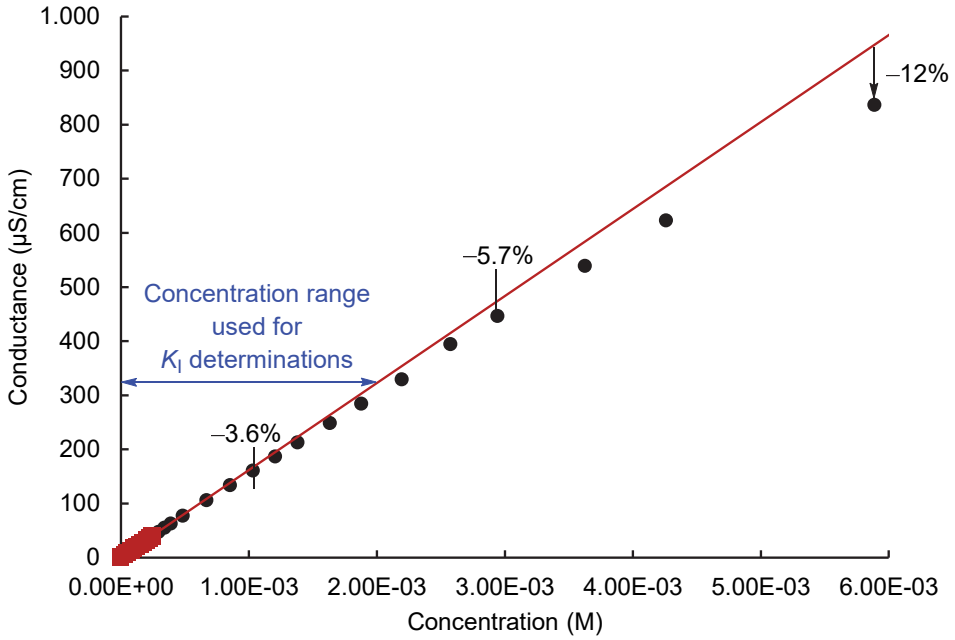

Figure S2: Comparison of experimental conductivity of Ph_2IPF_6 in MeCN at 20 °C with the predicted conductivity from measurements performed at low concentration (< 0.25 mM).

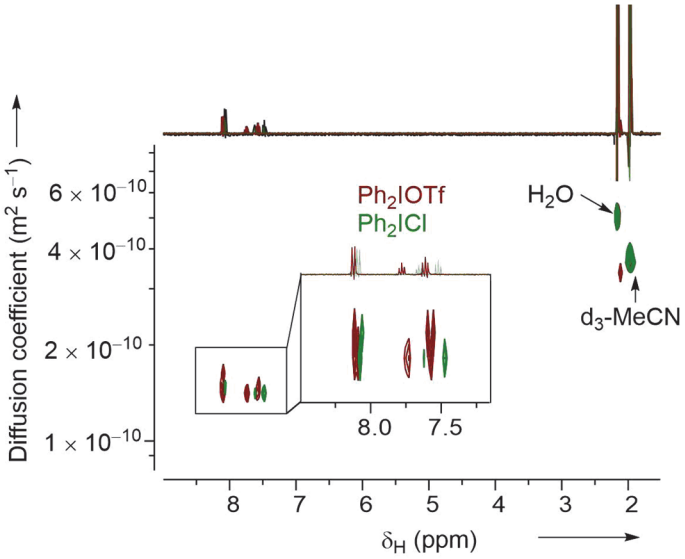

Figure S3: Overlay of ^{1}H DOSY measurements of 1.4 mM solutions of Ph_2IOTf (red) and Ph_2ICl (green) in CD_3CN.

To additionally characterize Ph_2ICl we investigated the diffusion coefficient for the diphenyliodonium ion in the presence of different counterions by ^{1}H DOSY NMR spectroscopy. As shown in conductivity measurements, diphenyliodonium triflate (**1a**) dissociates quantitatively under the typical conditions of our experiments (Figure 2), which allows to determine the diffusion coefficient of the free Ph_2I^+ ion. For coordinating counterions, e.g. chloride, either the fully dissociated species (only present to a minor extent according to our equilibrium constants), the monomeric adduct Ph_2ICl, or the corresponding dimer $(Ph_2ICl)_2$ should be observable depending on the concentration. As shown in Figure S3, 1.4 mM solutions of both $Ph_2I^+TfO^-$ and Ph_2ICl (CD_3CN, 20 °C) have almost identical diffusion coefficients. Hence, we conclude that the formation of higher aggregates (dimers or oligomers) of Ph_2ICl is insignificant under our experimental conditions (<1 mM solutions).

These DOSY measurements do not provide information on the nature of the association of the diaryliodonium ions in solution. The similarity of the diffusion coefficients of $Ph_2I^+TfO^-$ and Ph_2ICl might be rationalized by the insignificant impact of the chloride ion on the size of the diffusing species as illustrated in Figure S4.

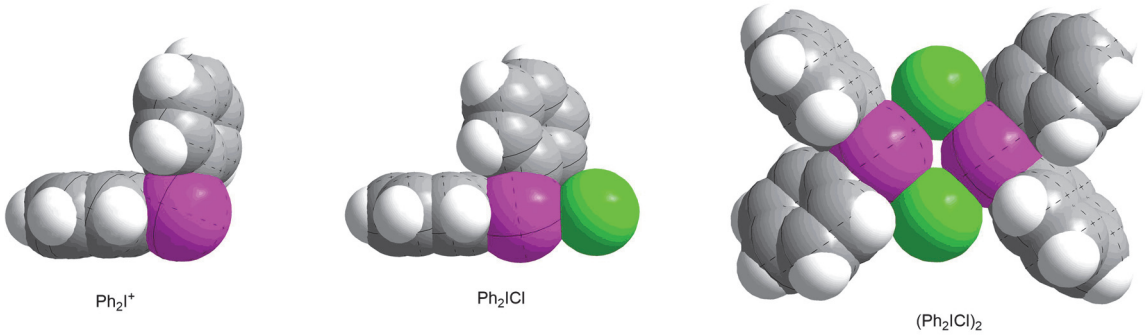

Figure S4: Molecular structures with van der Waals radii of Ph_2I^+ (based on the x-ray structure of Ph_2IOTf, ref. 1) and Ph_2ICl as monomer and dimer (ref. 2).

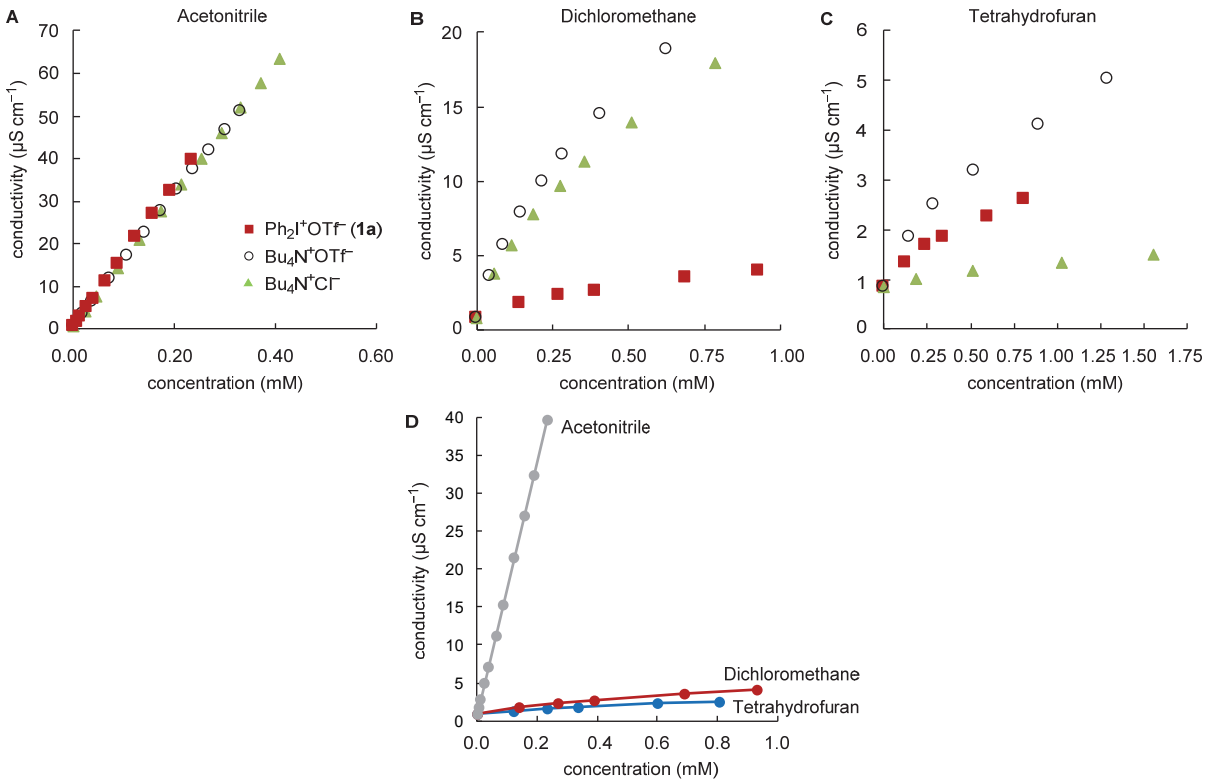

Figure S5: Conductivity (at 20 °C) of solutions of Ph_2IOTf (**1a**), NBu_4OTf and NBu_4Cl in (A) acetonitrile, (B) dichloromethane, and (C) tetrahydrofuran as well as (D) of Ph_2IOTf (**1a**) in different solvents.

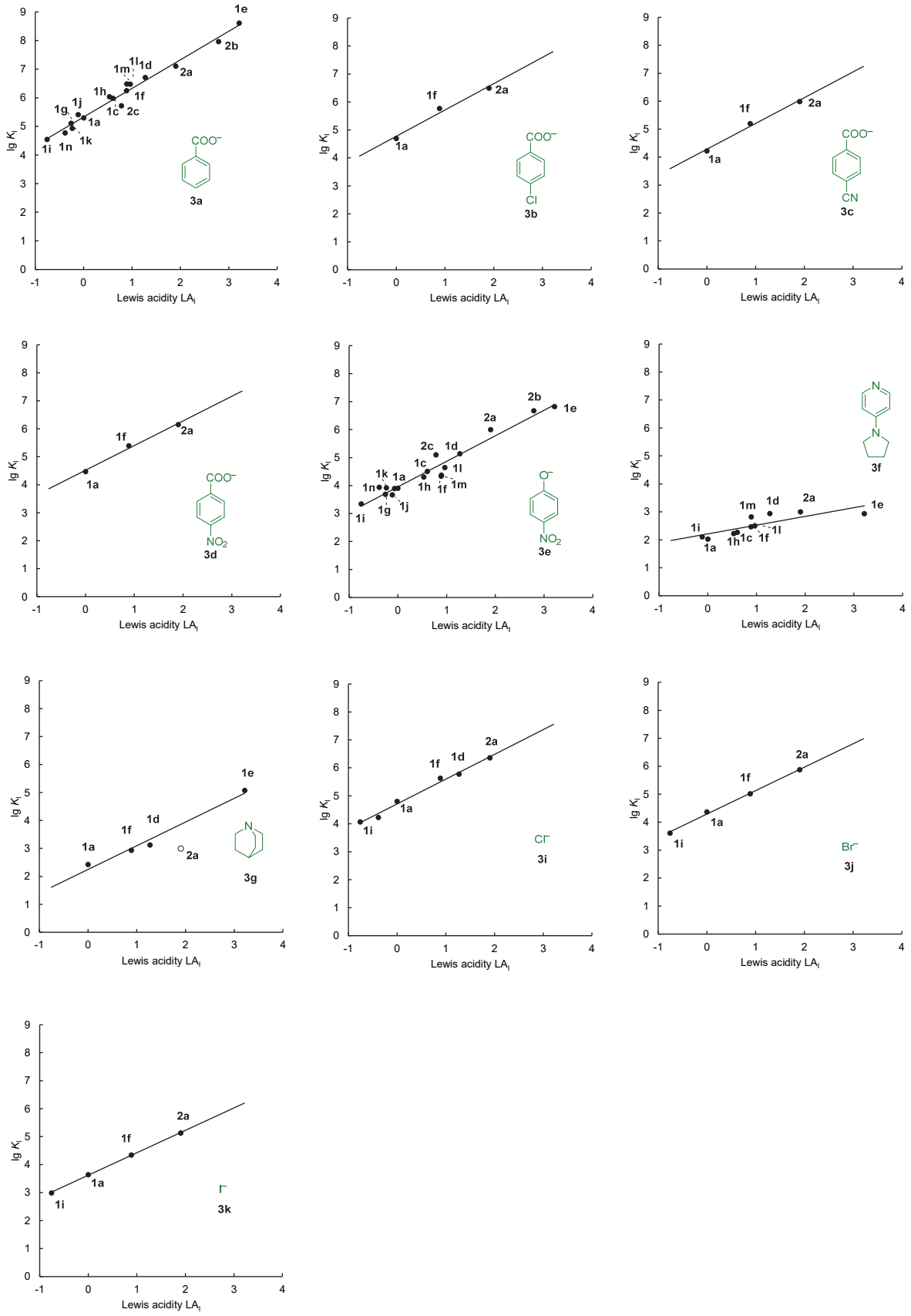

Figure S6: Correlations of equilibrium constants K_I for the Lewis adduct formation between Lewis bases and diaryliodonium ions with the Lewis acidities LA_I of the diaryliodonium ions (MeCN, 20 °C).

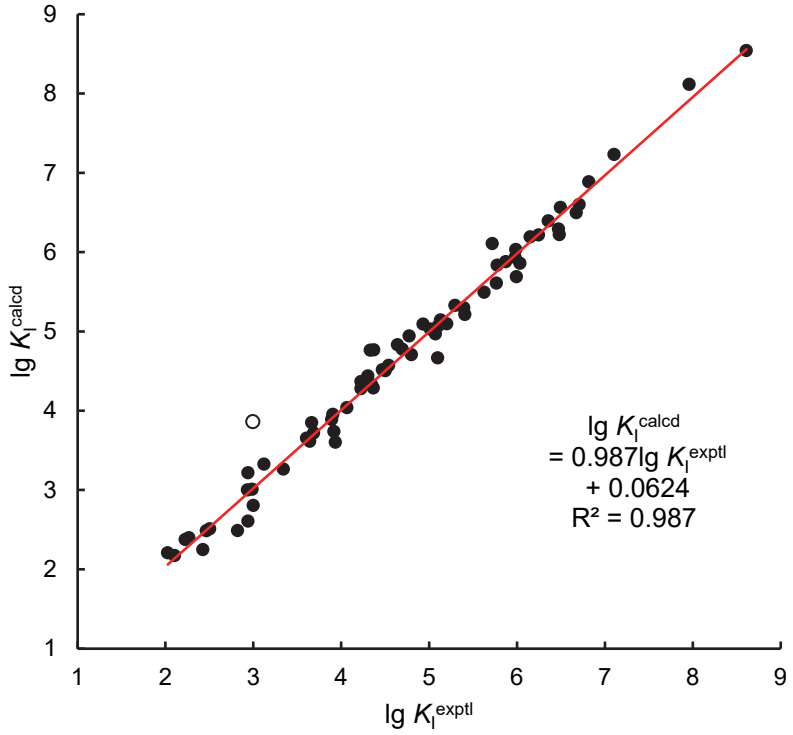

Figure S7: Plot of calculated lg K_I^{calcd} versus experimental lg K_I^{exptl} with the equilibrium constants K_I from Table 3 (main text). The open circle was not used for the least-squares minimization.

6.2 Supporting Information - General

Solvents, Reagents, and Analytics

Diaryliodonium ions **1a**-**c**, **1f**, and **1h**-**m** were purchased (Sigma-Aldrich or TCI Chemicals). Iodonium ions **1d** and **1e** were prepared according to the previously described procedure.[3] Iodonium ion **1g** was prepared according to the procedure outlined below. Samples of iodolium triflates **2a**-**c** were provided by Prof. Stefan Huber (Ruhr-Universität Bochum, Germany). Benzhydrylium tetrafluoroborates were synthesized according to previously reported procedures.[4]

Melting points were acquired using Büchi Melting Point M-560 devices and are not corrected.

Nuclear magnetic resonance (NMR) spectra were acquired on 400 MHz spectrometers. The following abbreviations and their combinations were used in the analysis of NMR spectra: s = singlet, d = doublet, t = triplet, q = quartet, m = multiplet, br s = broad singlet. NMR signals were assigned based on information from additional 2D NMR experiments (COSY, gHSQC, gHMBC, NOESY). Chemical shifts are given in ppm. Internal reference was set to the residual solvent signals (for CD_3CN: δ_H = 1.94, δ_C = 1.320; for d_6-DMSO: δ_H = 2.50, δ_C = 39.52).[5] The ^{13}C NMR spectra (101 MHz) were recorded under broad-band proton-decoupling.

^1H NMR DOSY measurements were performed on 400 MHz Bruker NMR spectrometer by using the stebpgp1s19 pulse sequence with variation of the gradient strength from 5 to 95% in 32 steps with 16 scans per increment. Spectra were analyzed with Mestrenova and 2d-transformed after phase and baseline correction with the "Peak Fit" method.

Conductivity measurements were carried out at 20 °C by using a WTW LF530 conductimeter with a Pt electrode LTA 1/NS in acetonitrile. The conductometric setup was calibrated with aqueous KCl solutions (0.007 M, 0.0145 M and 0.0375 M; commercial conductivity standard solutions purchased from Alfa Aesar) referring to the conductivity of 1273 µS/cm for an 0.01 M solution of aq KCl at 20 °C.[6] Temperature (20.0 ± 0.1 °C) was controlled by using circulating bath cryostats.

Infrared (IR) spectra were acquired on a Perkin Elmer Spectrum BX-59343 instrument with a Smiths Detection DuraSamplIR II Diamond ATR sensor for detection in the range 4500–600 cm^{-1} as a film for liquids or neat for solids.

High resolution (HRMS) mass spectra were recorded on a Thermo Finnigan LTQ FT Ultra Fourier Transform ion cyclotron resonance mass spectrometer. For ionization of the samples, electrospray ionization (ESI) was applied.

Single Crystal X-Ray Crystallography (Performed by Dr. P. Mayer)

The data of **4a** were collected at a temperature of 173 K on a Bruker D8 Quest IµS diffractometer while those of **4b** were collected at 143 K on an Oxford Diffraction Xcalibur3 diffractometer. Mo Kα radiation monochromated by multilayer mirror optics (**4a**) or a graphite crystal (**4b**) was applied in both experiments. The frames for **4a** were integrated with the Bruker SAINT software package[7] using a narrow-frame algorithm. Data were corrected for absorption effects using the Multi-Scan method of SADABS.[8] The structure was solved and refined using the Bruker SHELXTL Software Package.[9] For **4b** the CrysAlis PRO software package[10] was applied for data processing including absorption correction. The structure of **4b** was solved by direct methods with SIR97[11] and refined with SHELXL.[12] In both structures, the hydrogen atoms were calculated in ideal geometry riding on their parent atoms.

Depicted crystal structures in this Supporting Information were drawn with ellipsoids at the 50% probability level (ORTEP[13]).

Crystallographic data have been deposited with the Cambridge Crystallographic Data Centre (CCDC 1960556 (**4b**), 1960557 (**4a**)). These supplementary crystallographic data can be obtained free of charge from The Cambridge Crystallographic Data Centre via https://www.ccdc.cam.ac.uk/structures/.

Photometric Measurements

The UV/Vis titration experiments (BIMT or PT method) were performed using a J&M TIDAS diode array spectrophotometer controlled by TIDASDAQ3 (v3) software and connected to a Hellma 661.502-QX quartz Suprasil immersion probe (light path d = 5 mm) via fiber optic cables and standard SMA connectors in a flame-dried flask under an atmosphere of dry nitrogen. Temperature (20.0 ± 0.1 °C) was controlled by using circulating bath cryostats.

The temperature dependent density of acetonitrile had been shown to follow a linear correlation.[14] The density of acetonitrile at various temperatures was then calculated based on the thus obtained correlation line.

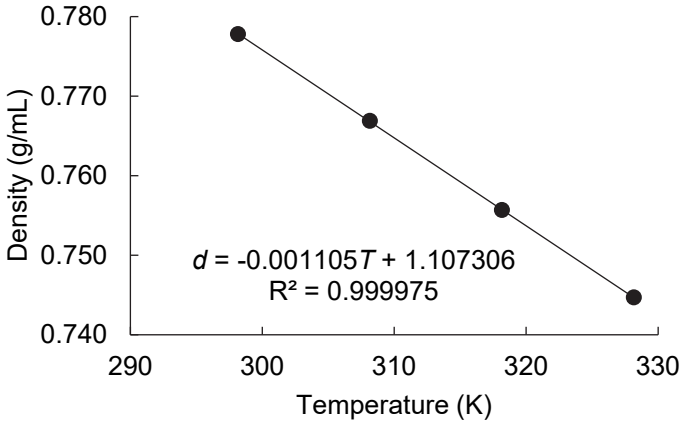

In this work, the following density values were used for calculating concentrations in acetonitrile solutions:

T (°C)	T (K)	Density (g/mL)
−10	263.15	0.8165
0	273.15	0.8055
10	283.15	0.7944
20	293.15	0.7834
30	303.15	0.7723
40	313.15	0.7613

For BIMT experiments, the initial Lewis base concentration, $[LB]_0$, was calculated from the known molar absorption coefficient ε of the benzhydrylium ions Ar_2CH^+ (from ref. 4) and the absorbance difference upon addition of the Lewis base to a benzhydrylium ion solution. The equilibrium for the Lewis adduct formation between a benzhydrylium ion and a Lewis base is described by the equilibrium constant K in eq S1.[15]

$$[LB] + [Ar_2CH^+] \underset{}{\overset{K}{\rightleftharpoons}} [Ar_2CH{-}LB] \qquad (S1)$$

The equilibrium constant K is defined in eq S2 and can be related to the absorbance of the benzhydrylium ion, A, and the concentration of the free Lewis base in equilibrium, [LB].

$$K = \frac{[Ar_2CH{-}LB]}{[Ar_2CH^+]\,[LB]} = \frac{A_0(V_0/V) - A}{A\ [LB]} \qquad (S2)$$

According to eq S3 the concentration of the free Lewis base in equilibrium, [LB], is related to the initial concentration of the Lewis base, $[LB]_0$, and the concentration of the Lewis adduct, which can be calculated from the measured absorbance of the solution by applying eq S4.

$$[LB] = [LB]_0 - [Ar_2CH\text{–}LB] = [LB]_0 - \frac{A_0(V_0/V) - A}{\varepsilon\, d} \qquad (S3)$$

with $[Ar_2CH\text{-}LB] = [A_0(V_0/V) - A]/(\varepsilon\, d)$ (S4)

Rearrangement of eq S2 to eq S5, subsequent combination with eq S3 and solving for $[LB]_0$ gives eq S6:

$$[LB] = \frac{A_0(V_0/V) - A}{A\ K} \qquad (S5)$$

$$[LB]_0 = [A_0(V_0/V) - A]\left(\frac{1}{A\ K} + \frac{1}{\varepsilon\, d}\right) \qquad (S6)$$

Determination of Lewis Basicities LB Towards Benzhydrylium Ions

We determined the Lewis basicity of benzoates **3a**-**d** towards benzhydrylium ions (C-centered reference Lewis acids) in acetonitrile at 20 °C by following the previously published photometric procedure.[15] With the known molar absorption coefficients of the benzhydrylium ions,[4] the Beer-Lambert law and by applying the eqs S1, S2, and S3, the concentrations of all species were calculated for each step of the titration. In addition, the equilibrium constants for **3g** + **B2** at variable temperature were determined.

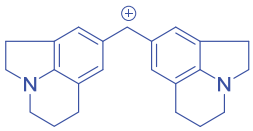

B1

LA = –12.76

ε = 1.45 × 10^5 M^{-1} cm^{-1}

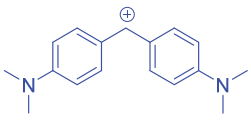

B2

LA = –9.82

ε = 1.66 × 10^5 M^{-1} cm^{-1}

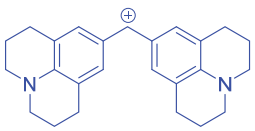

B3

LA = –12.61

ε = 1.82 × 10^5 M^{-1} cm^{-1}

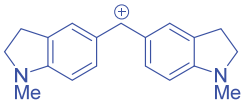

B4

LA = –11.46

ε = 1.38 × 10^5 M^{-1} cm^{-1}

To a volume of MeCN (typically 24 mL) was first added a solution of the benzhydrylium tetrafluoroborate to achieve an absorbance of ca 1.0 A.U. Subsequently, a MeCN solution of the tetrabutylammonium benzoate (for **3a**-**d**) or quinuclidine (**3g**), respectively, was added portionwise by means of a microliter syringe.

Isothermal Titration Calorimetry (ITC)

The ITC measurements were performed on a Microcal VP-ITC instrument with solutions maintained under an atmosphere of dry nitrogen. The reference cell was filled with acetonitrile (HPLC grade, stored under dry nitrogen) and the sample cell was filled with a solution of the iodonium species in the same solvent. The syringe was filled with a solution of the Lewis base in acetonitrile, which was then gradually injected (6 µL/injection, 40 steps, 120 s spacing between injections) into the sample cell. The ITC raw data were processed and analyzed with the AFFINImeter ITC software (v.2.1710) assuming a 1:1 interaction model.[16]

Determination of the Nucleophilicity Parameters *N* and s_N for the Benzoate Ion

We determined the nucleophilicity of the parent benzoate ion **3a** in acetonitrile at 20 °C by using a set of four benzhydrylium ions as reference electrophiles and following the procedure in ref. 17.

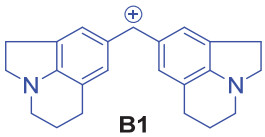

B1
E = –10.04

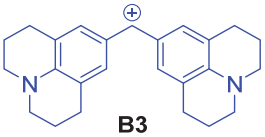

B3
E = –9.45

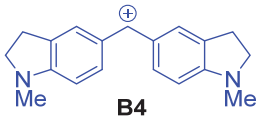

B4
E = –8.76

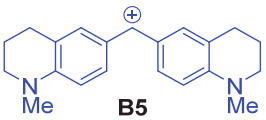

B5
E = –8.22

The kinetics of the reactions of the benzoate ion **3a** with colored benzhyrdrylium ions (**B**) were studied by stopped-flow UV/Vis photometry (Applied Photophysics SX.20 systems) in acetonitrile at (20.0 ± 0.1) °C. Solutions were prepared by using dry solvents that were kept under a dry nitrogen atmosphere. By using **3a** in large excess over the electrophiles **B**, its concentrations remained almost constant throughout the reactions yielding pseudo-first order kinetics for the decay of the electrophiles' concentrations.

First-order rate constants k_{obs} (s^{-1}) were obtained by least-squares fitting of the single-exponential function $A_t = A_0 \exp(-k_{obs}t) + C$ to the fading absorbances of **B**. Subsequently, second-order rate constants k_2 (M^{-1} s^{-1}) were obtained as slopes of the plots of k_{obs} vs. the concentrations of benzoate (**3a**).

The second-order rate constants k_2 for the reactions of benzoate (**3a**) with the reference electrophiles **B** correlated linearly with their electrophilicity parameters E furnishing the nucleophilicity parameters N of the benzoate (**3a**) as the intercept on the abscissa according to the Patz-Mayr equation $\lg k_2 = s_N (N + E)$.[18] The slope of the linear correlation equals to the nucleophile-dependent susceptibility parameter s_N.

NMR Titrations

NMR titration experiments was performed in an argon filled glovebox by preparing a series of solutions in anhydrous CD_3CN in NMR tubes. ^{1}H NMR measurements were then performed on a 400 MHz NMR spectrometer at 20 °C. The resulting dependency of the chemical shift difference Δδ (in ppm) of the resonance of the Lewis acid vs. the concentration of the excess component was then analyzed according the equation below[19] by non-linear fitting with Origin.

$$\Delta\delta = \frac{\Delta\delta_{max}}{[\boldsymbol{LA}]}\left(\frac{1}{2}\left\{\left([\boldsymbol{LA}] + [\boldsymbol{LB}] + \frac{1}{K_I}\right) - \sqrt{\left([\boldsymbol{LA}] + [\boldsymbol{LB}] + \frac{1}{K_I}\right)^2 + 4[\boldsymbol{LA}][\boldsymbol{LB}]}\right\}\right)$$

6.3 Synthesis

Mesityl(phenyl)iodonium triflate (1g-OTf, RNH114)

Synthesis according to the modified procedure in ref. 20.

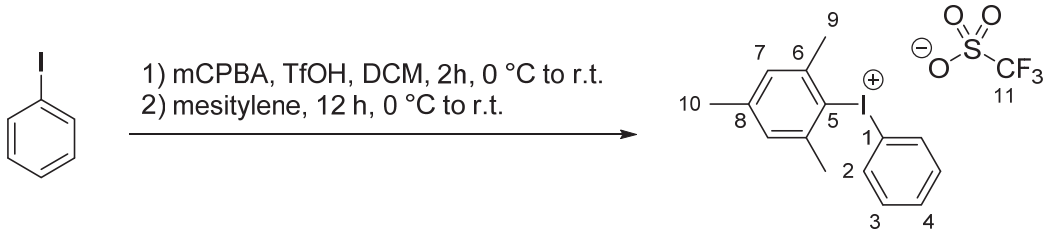

In a flame-dried Schlenk flask under nitrogen a solution of mCPBA (pre-dried under high-vacuum for 1 h, 1.42 g, 8.23 mmol) in dichloromethane (15 mL) was prepared. After cooling to 0 °C iodobenzene (0.55 mL, 4.9 mmol) was added. Subsequent dropwise addition of triflic acid (0.72 mL, 8.0 mmol) gave a yellow suspension, which was stirred for 2 h at room temperature. The mixture was cooled to 0 °C, mesitylene (0.75 mL, 5.4 mmol) was added dropwise, and the resulting yellow suspension was allowed to warm up to room temperature. After stirring for 12 h, a suspension with a beige precipitate was obtained. All solvents were removed under reduced pressure and the residue was triturated with diethyl ether (40 mL) and dried under high vacuum.

To remove residual amounts of benzoate salts, the crude product was dissolved in dichloromethane (250 mL) and washed with water (2 × 50 mL). The dichloromethane solution was concentrated to dryness and again triturated in diethyl ether (40 mL). Filtration and drying for 1 h at 100 °C gave the product as colorless solid (1.97 g, 85%).

^{1}H NMR (400 MHz, CD_3CN) δ = 7.87–7.83 (m, 2 H, 2-H), 7.68–7.64 (m, 1 H, 4-H), 7.52–7.47 (m, 2 H, 3-H), 7.23–7.22 (m, 2 H, 7-H), 2.60 (s, 6 H, 9-H), 2.35 (s, 3 H, 10-H).

^{13}C{^{1}H} NMR (101 MHz, CD_3CN) δ = 146.0 (C_q, C-8), 143.6 (C_q, C-6), 135.3 (CH, C-2), 133.6 (CH, C-4), 133.5 (CH, C-3), 131.4 (CH, C-7), 122.1 (q, $^{1}J_{C,F}$ = 320.8 Hz, C-11), 121.4 (C_q, C-1), 112.8 (C_q, C-5), 27.2 (CH_3, C-9), 21.1 (CH_3, C-10).

NMR data agree with those reported in ref. 20.

(2,4,6-Trimethoxyphenyl)(phenyl)iodonium hexafluorophosphate (1n-PF_6, RM1219)

The iodonium tosylate **1n**-OTs was prepared according to a procedure by Stuart and coworkers[21] combined with a modified procedure for the counterion exchange.[3]

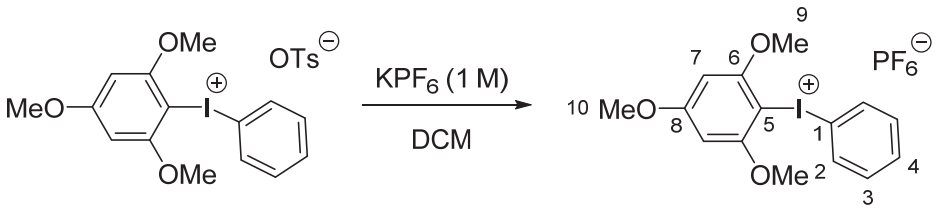

A solution of iodonium tosylate **1n**-OTs (760 mg, 1.40 mmol) in dichloromethane (100 mL) was placed in a separatory funnel. Then a 1 M aq KPF_6 solution (10 mL) was added. After vigorous shaking, the aqueous phase was removed. Addition of the KPF_6 solution and phase separation were repeated for another three times. After the fourth cycle, the organic phase was dried over Na_2SO_4 and concentrated under reduced pressure to give a colorless solid. The residue was triturated with diethyl ether (20 mL), filtered, and dried under vacuum to give the product as colorless solid (500 mg, 69%).

Mp.: 132 °C (decomp.)

HRMS (ESI$^+$): Calcd *m/z* for [$C_{15}H_{16}IO_3^+$] [M^+]: 371.0139; Found: 371.0143.

HRMS (ESI$^-$): Calcd *m/z* for [PF_6^-] [M^-]: 144.9647; Found: 144.9647.

^{1}H NMR (400 MHz, DMSO-d_6) δ = 7.93–7.90 (m, 2 H, 2-H), 7.63–7.59 (m, 1 H, 4-H), 7.49–7.44 (m, 2 H, 3-H), 6.47 (s, 2 H, 7-H), 3.94 (s, 6 H, 9-H), 3.87 (s, 3 H, 10-H).

^{13}C{^{1}H} NMR (101 MHz, DMSO) δ = 166.2 (C_q, C-8), 159.4 (C_q, C-6), 134.3 (CH, C-2), 131.6 (CH, C-3, C-4), 116.1 (C_q, C-1), 92.1 (CH, C-7), 87.0 (C_q, C-5), 57.3 (CH_3, C-9), 56.1 (CH_3, C-10).

^{31}P NMR (162 MHz, DMSO-d_6) δ = −144.2 (hept, J_{PF} = 711.2 Hz).

^{19}F NMR (377 MHz, DMSO-d_6) δ = −70.1 (d, J_{PF} = 711.3 Hz).

IR: 1579, 1471, 1415, 1349, 1233, 1210, 1164, 1117, 1068, 989, 827, 747, 682 cm^{-1}.

Diphenyliodonium benzoate (4a, RNH320)

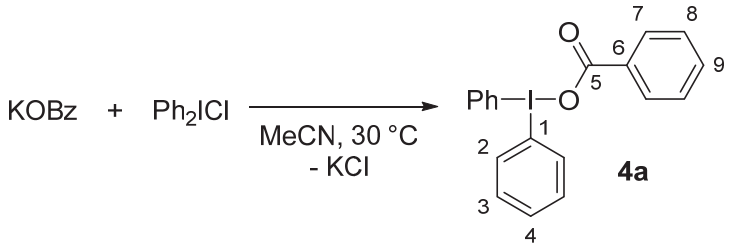

Diphenyliodonium chloride (60.5 mg, 0.191 mmol) and potassium benzoate (30.6 mg, 0.191 mmol) were placed in a flame-dried 25 mL Schlenk flask under nitrogen. Acetonitrile (dry, 10 mL) was added and the resulting suspension sonicated for 10 min at 40 °C. After cooling to room temperature, the mixture was filtered and concentrated under reduced pressure to give **4a** as a colorless, crystalline solid (41.2 mg, 53%).

Diffusion of diethyl ether into an acetonitrile solution of **4a** yielded crystals suitable for single-crystal x-ray diffraction.

Mp.: 165-178 °C (turns bright brown at 155 °C)

HRMS (ESI$^+$): Calcd *m/z* for [$C_{12}H_{10}I^+$] [M^+]: 280.9822; Found: 280.9821.

HRMS (ESI$^-$): Calcd *m/z* for [$C_7H_5O_2^-$] [M^-]: 121.0295; Found: 121.0295.

^{1}H NMR (400 MHz, CD_3CN) δ = 8.07–8.04 (m, 4 H, 2-H), 7.77–7.74 (m, 2 H, 7-H), 7.57–7.53 (m, 2 H, 4-H), 7.44–7.39 (m, 4 H, 3-H), 7.36–7.31 (m, 1 H, 9-H), 7.28–7.23 (m, 2 H, 8-H).

^{13}C{^{1}H} NMR (101 MHz, CD_3CN) δ = 172.1 (C_q, C-5), 138.9 (C_q, C-6), 135.7 (CH, C-2), 132.2 (CH, C-3), 132.1 (CH, C-4), 130.6 (CH, C-9), 130.0 (CH, C-7), 128.4 (CH, C-8), 121.4 (C_q, C-1).

IR: 3048, 1593, 1566, 1543, 1471, 1439, 1362, 1268, 1176, 1159, 1064, 990, 829, 759, 739, 720, 680, 669 cm^{-1}.

Diphenyliodonium Benzoate (alternative procedure, RM862)

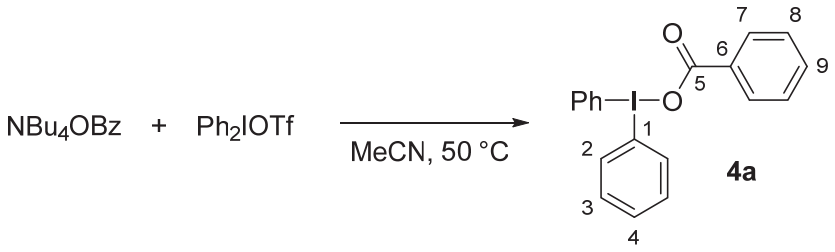

A mixture of tetrabutylammonium benzoate (69.4 mg, 0.191 mmol) and diphenyliodonium triflate (82.1 mg, 0.191 mmol) was suspended in dry acetonitrile (1 mL) under gentle heating. After 30 seconds, the clear solution was placed in a sonication bath causing the crystallization of the diphenyliodonium benzoate within seconds. The resulting suspension was placed in a freezer for 30 min at –25 °C. Next, the supernatant acetonitrile was removed with a Pasteur pipette. The colorless solid residue was washed with dry diethyl ether (4 ×). After drying, **4a** was obtained as a colorless solid (53.8 mg, 70%).

Mp.: 165-178 °C.

HRMS (ESI$^+$): Calcd *m/z* for [$C_{12}H_{10}I^+$] [M^+]: 280.9822; Found: 280.9821.

^{1}H NMR (400 MHz, CD_3CN) δ = 8.07–8.06 (m, 4 H, 2-H), 7.78–7.76 (m, 2 H, 7-H), 7.57–7.53 (m, 2 H, 4-H), 7.44–7.39 (m, 4 H, 3-H), 7.35–7.30 (m, 1 H, 9-H), 7.28–7.24 (m, 2 H, 8-H).

^{13}C{^{1}H} NMR (101 MHz, CD_3CN) δ = 172.2 (C_q, C-5), 139.4 (C_q, C-6), 135.7 (CH, C-2), 132.1 (CH, C-3), 132.1 (CH, C-4), 130.4 (CH, C-9), 130.0 (CH, C-7), 128.4 (CH, C-8), 121.5 (C_q, C-1).

IR: 3051, 1592, 1565, 1533, 1470, 1440, 1360, 1267, 1177, 1153, 1065, 990, 827, 760, 736, 720, 688, 682, 668 cm^{-1}.

Diphenyliodonium 4-nitrophenolate (RNH18)

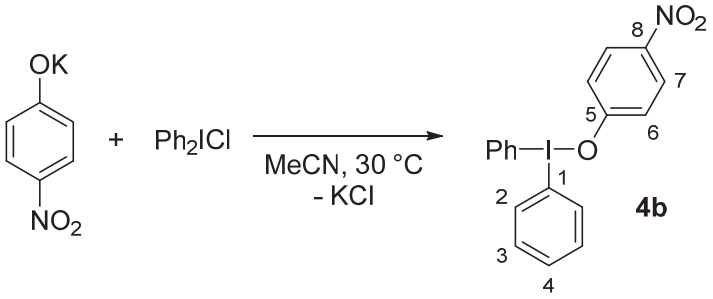

Diphenyliodonium chloride (107.2 mg, 0.339 mmol) and potassium 4-nitrophenolate (60.0 mg, 0.339 mmol) were placed in a flame-dried 50 mL Schlenk flask under nitrogen. Acetonitrile (extra-dry, 20 mL) was added and the resulting initially orange suspension sonicated for 10 minutes at 30 °C. Over that time, the suspension changed its color to yellow. The suspension was stirred for another 2 min at room temperature and then the solids were allowed to settle. The mixture was filtered through a syringe filter (0.45 µL) and concentrated under reduced pressure to 2 mL causing the formation of a precipitate. The solution was concentrated carefully to a volume of 0.5 mL and placed in a freezer for 10 min. Remaining solvents were removed and the solid residue dried under vacuum to give **4b** as a deep-yellow, crystalline solid (58.6 mg, 41%).

Mp.: 122-123 °C.

^{1}H NMR (400 MHz, d_6-DMSO) δ = 8.23–8.20 (m, 4 H, 2-H), 7.74–7.70 (m, 2 H, 6-H), 7.65–7.61 (m, 2 H, 4-H), 7.52–7.48 (m, 4 H, 3-H), 5.95–5.91 (m, 2 H, 7-H).

$^{13}C\{^{1}H\}$ NMR (101 MHz, d_6-DMSO) δ = 179.8 (C_q, C-5), 135.0 (CH, C-2), 131.7 (CH, C-4), 131.6 (CH, C-3), 128.2 (C_q, C-8), 127.4 (CH, C-6), 119.2 (CH, C-7), 117.7 (C_q, C-1).

HRMS (ESI^+): Calcd *m/z* for $[C_{12}H_{10}I^+]$ $[M^+]$: 280.9822; Found: 280.9821.

IR: 3053, 1576, 1562, 1490, 1470, 1440, 1456, 1440, 1344, 1275, 1268, 1158, 1103, 994, 989, 982, 854, 730, 707, 679 cm^{-1}.

Dissolving the crude material in acetonitrile and allowing the material to crystallize in the freezer at –35 °C yielded yellow needles suitable for single-crystal X-ray diffraction.

6.4 Conductometric Measurements

Concentration dependent conductivity of NBu_4Cl in MeCN at 20 °C (RM967).

[NBu_4Cl] / M	Conductance (µS/cm)
0.00	8.40×10^{-1}
2.22×10^{-5}	4.20
4.42×10^{-5}	7.56
8.75×10^{-5}	1.44×10^{1}
1.30×10^{-4}	2.12×10^{1}
1.72×10^{-4}	2.76×10^{1}
2.12×10^{-4}	3.39×10^{1}
2.53×10^{-4}	4.00×10^{1}
2.92×10^{-4}	4.60×10^{1}
3.30×10^{-4}	5.21×10^{1}
3.68×10^{-4}	5.76×10^{1}
4.06×10^{-4}	6.35×10^{1}

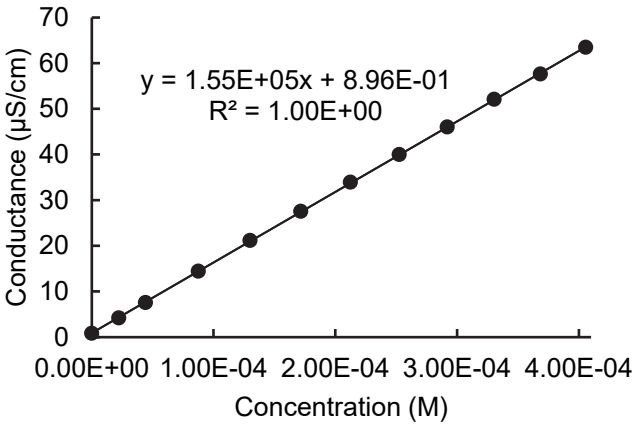

Concentration dependent conductivity of NBu_4OTf in MeCN at 20 °C (RM967).

[NBu_4OTf] / M	Conductance (µS/cm)
0.00	8.40×10^{-1}
1.80×10^{-5}	3.53
3.59×10^{-5}	6.38
7.11×10^{-5}	1.18×10^{1}
1.06×10^{-4}	1.71×10^{1}
1.40×10^{-4}	2.25×10^{1}
1.73×10^{-4}	2.77×10^{1}
2.05×10^{-4}	3.26×10^{1}
2.37×10^{-4}	3.75×10^{1}
2.69×10^{-4}	4.20×10^{1}
3.00×10^{-4}	4.65×10^{1}
3.30×10^{-4}	5.12×10^{1}

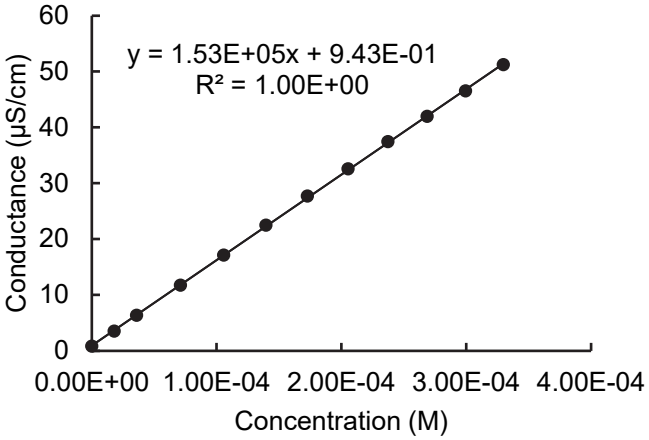

Concentration dependent conductivity of Ph_2IOTf in MeCN at 20 °C (RM967).

[Ph_2IOTf] / M	Conductance (µS/cm)
0.00	8.40×10^{-1}
6.43×10^{-6}	1.85
1.28×10^{-5}	2.86
2.55×10^{-5}	5.04
3.81×10^{-5}	7.06
6.29×10^{-5}	1.13×10^{1}
8.73×10^{-5}	1.53×10^{1}
1.23×10^{-4}	2.15×10^{1}
1.57×10^{-4}	2.70×10^{1}
1.91×10^{-4}	3.23×10^{1}
2.35×10^{-4}	3.96×10^{1}

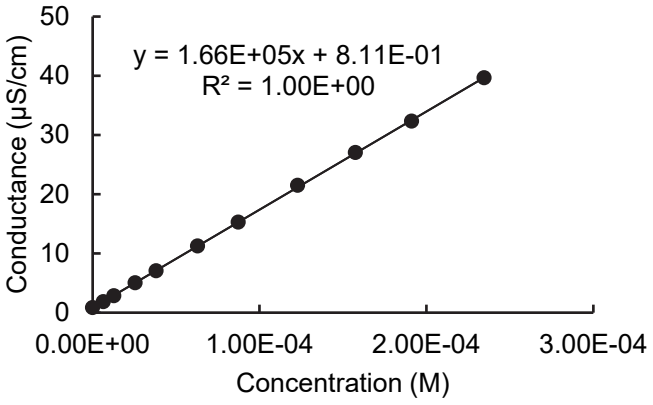

Concentration dependent conductivity of Ph_2ICl in MeCN at 20 °C (RM967).

[Ph_2ICl] / M	Conductance (µS/cm)
0.00	8.40×10^{-1}
1.14×10^{-5}	1.76
2.26×10^{-5}	2.52
3.36×10^{-5}	3.11
4.43×10^{-5}	3.53
5.49×10^{-5}	4.03
8.04×10^{-5}	5.04
1.05×10^{-4}	5.80
1.50×10^{-4}	7.06
1.92×10^{-4}	8.15
2.31×10^{-4}	9.07
2.99×10^{-4}	1.02×10^{1}
3.58×10^{-4}	1.10×10^{1}
4.36×10^{-4}	1.23×10^{1}
5.95×10^{-4}	1.41×10^{1}
6.58×10^{-4}	1.51×10^{1}
7.78×10^{-4}	1.63×10^{1}

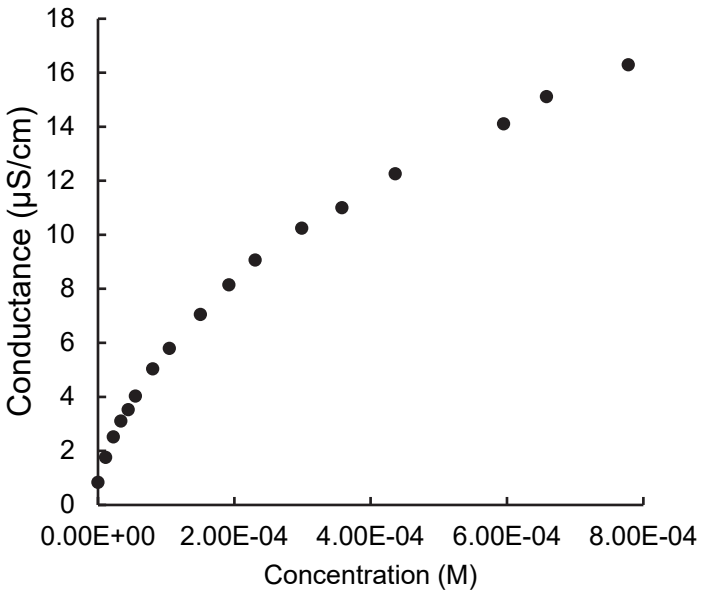

The specific molar conductivity for hypothetically completely dissociated $Ph_2I^+Cl^-$ can be calculated according to

$$C(Ph_2ICl) = C(Ph_2IOTf) + C(NBu_4Cl) - C(NBu_4OTf) = 1.674 \times 10^5\ \mu S\ cm^{-1}\ M^{-1}$$

This value for $C(Ph_2ICl)$ was then used to calculate the concentration of dissociated $Ph_2I^+Cl^-$ from the experimentally measured conductivity for a certain concentration $[Ph_2ICl]_0$ (Figures 2 and 3, main text).

Effects of ion pairing for Ph_2IOTf (**1a**) were investigated by additional measurements of the concentration dependent conductivity at higher concentrations.

Concentration dependent conductivity of Ph_2IOTf in MeCN at 20 °C (RM1244).

[Ph_2IOTf] / M	Conductance (µS/cm)
0.00	8.40×10^{-1}
8.02×10^{-5}	1.34×10^{1}
1.60×10^{-4}	2.62×10^{1}
2.38×10^{-4}	3.81×10^{1}
3.93×10^{-4}	6.18×10^{1}
5.45×10^{-4}	8.45×10^{1}
7.67×10^{-4}	1.17×10^{2}
9.84×10^{-4}	1.48×10^{2}
1.19×10^{-3}	1.77×10^{2}
1.47×10^{-3}	2.14×10^{2}
1.79×10^{-3}	2.58×10^{2}
2.10×10^{-3}	2.98×10^{2}
2.69×10^{-3}	3.83×10^{2}
3.22×10^{-3}	4.50×10^{2}
3.72×10^{-3}	5.11×10^{2}
5.00×10^{-3}	6.55×10^{2}

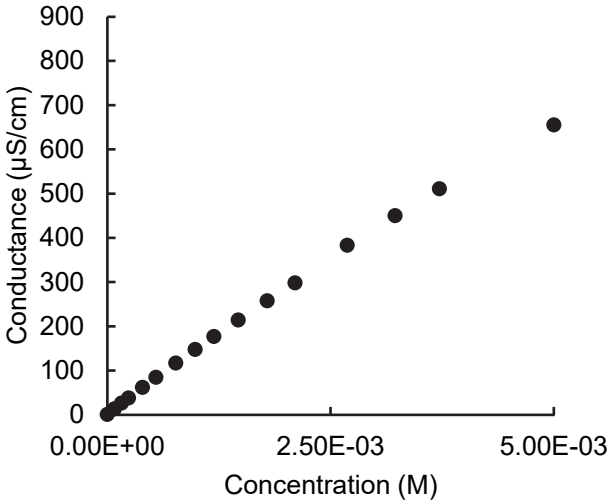

By using the linear relation of conductivity and concentration determined at low concentration (< 0.25 mM), the concentration of free Ph_2I^+ ions for a given concentration of Ph_2IOTf can be extrapolated. In analogy to the analysis for the behavior of $Ph_2I^+Cl^-$ in acetonitrile solution (main text, equations 4-6), an association constant of K = 71.2 ± 2.4 M^{-1} is estimated for the ion pair formation from Ph_2I^+ and TfO^-.

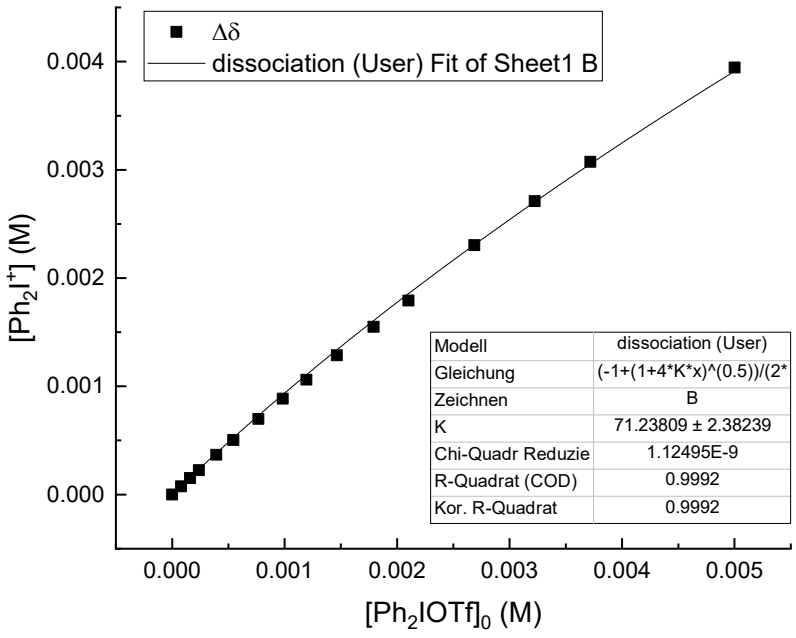

Concentration dependent conductivity of Ph_2IPF_6 in MeCN at 20 °C (RM1245).

[Ph_2IOTf] / M	Conductance (µS/cm)
0.00	8.40×10^{-1}
2.46×10^{-5}	4.87
4.92×10^{-5}	9.07
7.37×10^{-5}	1.29×10^{1}
9.82×10^{-5}	1.71×10^{1}
1.23×10^{-4}	2.10×10^{1}
1.47×10^{-4}	2.49×10^{1}
1.71×10^{-4}	2.86×10^{1}
1.95×10^{-4}	3.26×10^{1}
2.20×10^{-4}	3.63×10^{1}
2.44×10^{-4}	4.00×10^{1}
2.92×10^{-4}	4.77×10^{1}
3.39×10^{-4}	5.54×10^{1}
3.87×10^{-4}	6.28×10^{1}
4.81×10^{-4}	7.76×10^{1}
6.67×10^{-4}	1.06×10^{2}
8.50×10^{-4}	1.34×10^{2}
1.03×10^{-3}	1.61×10^{2}
1.20×10^{-3}	1.87×10^{2}
1.38×10^{-3}	2.13×10^{2}
1.63×10^{-3}	2.49×10^{2}
1.88×10^{-3}	2.84×10^{2}
2.19×10^{-3}	3.30×10^{2}
2.57×10^{-3}	3.95×10^{2}
2.94×10^{-3}	4.47×10^{2}
3.63×10^{-3}	5.39×10^{2}
4.26×10^{-3}	6.23×10^{2}
5.89×10^{-3}	8.37×10^{2}

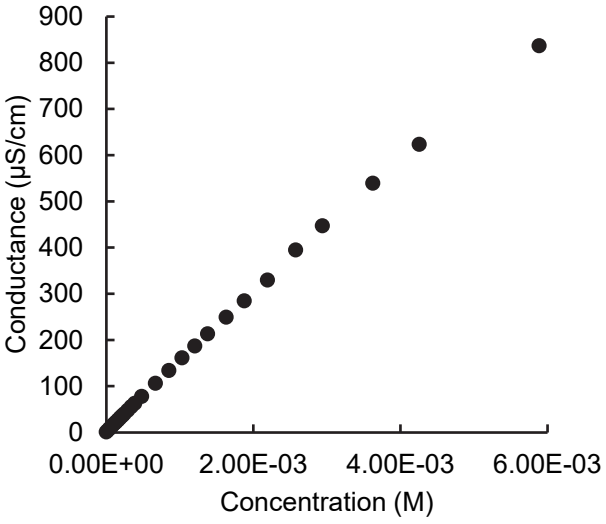

By using the linear relation of conductivity and concentration determined at low concentration (< 0.25 mM), the concentration of free Ph_2I^+ ions for a given concentration of Ph_2I PF_6 can be extrapolated. In analogy to the analysis for the behavior of $Ph_2I^+Cl^-$ in acetonitrile solution (main text, equations 4-6), an association constant of $K = 25.6 \pm 0.5\ M^{-1}$ is estimated for the ion pair formation from Ph_2I^+ and PF_6^- .

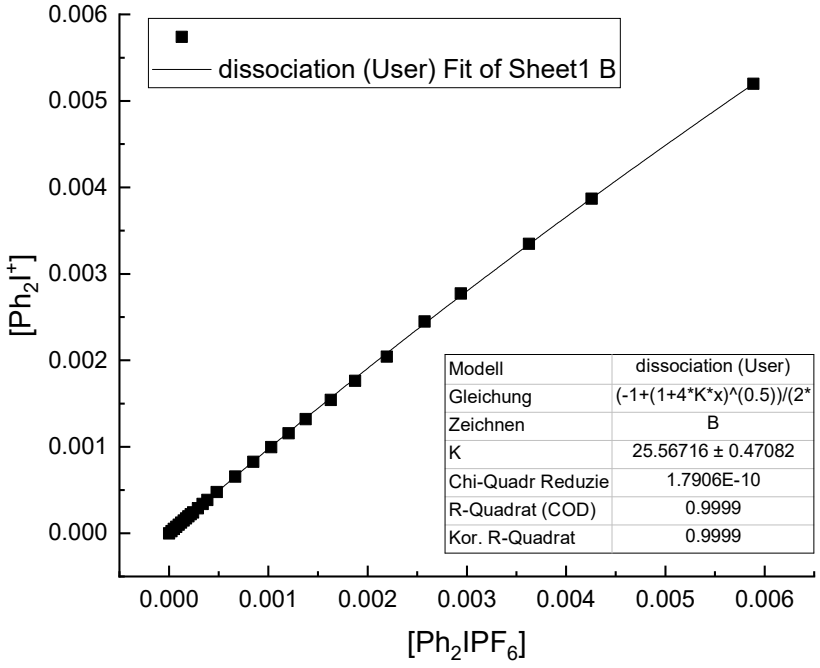

Concentration dependent conductivity of NBu_4Cl in DCM at 20 °C (RM1235).

[NBu_4Cl] / M	Conductance (µS/cm)
0.00	8.40×10^{-1}
5.82×10^{5}	3.86
1.15×10^{-4}	5.71
1.88×10^{-5}	7.81
2.75×10^{-4}	9.74
3.58×10^{-4}	1.13×10^{1}
5.14×10^{-4}	1.39×10^{1}
7.88×10^{-4}	1.80×10^{1}

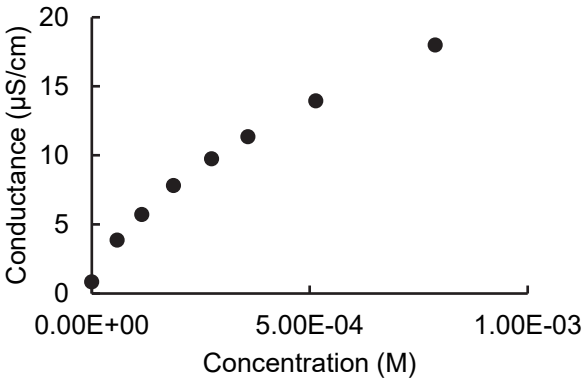

Concentration dependent conductivity of NBu_4OTf in DCM at 20 °C (RM1235).

[NBu_4OTf] / M	Conductance (µS/cm)
0.00	8.40×10^{-1}
4.62×10^{-5}	3.61
9.12×10^{-5}	5.71
1.49×10^{-4}	7.90
2.18×10^{-4}	1.00×10^{1}
2.85×10^{-4}	1.18×10^{1}
4.08×10^{-4}	1.45×10^{1}
6.26×10^{-4}	1.89×10^{1}

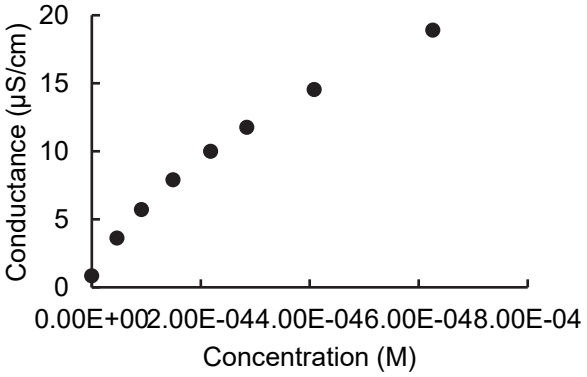

Concentration dependent conductivity of Ph_2IOTf in DCM at 20 °C (RM1233).

[Ph_2IOTf] / M	Conductance (µS/cm)
0.00	8.40×10^{-1}
1.43×10^{-4}	1.85
2.72×10^{-4}	2.35
3.91×10^{-4}	2.69
6.91×10^{-4}	3.53
9.30×10^{-4}	4.03

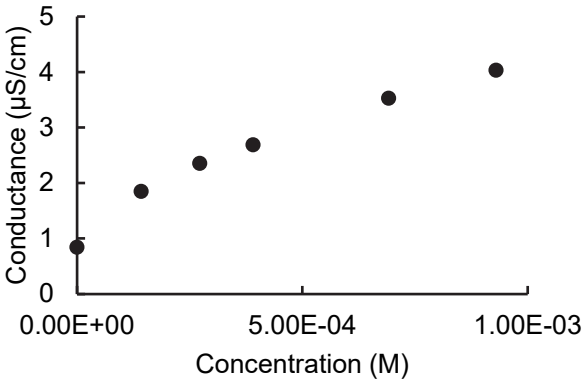

Concentration dependent conductivity of NBu_4Cl in THF at 20 °C (RM1235).

[NBu_4Cl] / M	Conductance (µS/cm)
0.00	8.40×10^{-1}
1.88×10^{-4}	1.01
5.14×10^{-4}	1.18
1.02×10^{-3}	1.34
1.55×10^{-3}	1.51

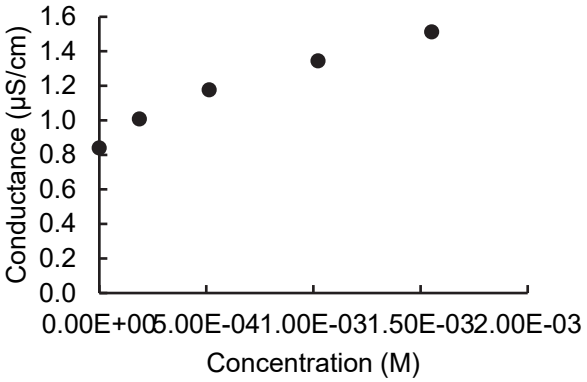

Concentration dependent conductivity of NBu_4OTf in THF at 20 °C (RM1235).

[NBu_4OTf] / M	Conductance (µS/cm)
0.00	8.40×10^{-1}
1.49×10^{-4}	1.85
2.85×10^{-4}	2.52
5.22×10^{-4}	3.19
8.94×10^{-4}	4.12
1.29×10^{-3}	5.04

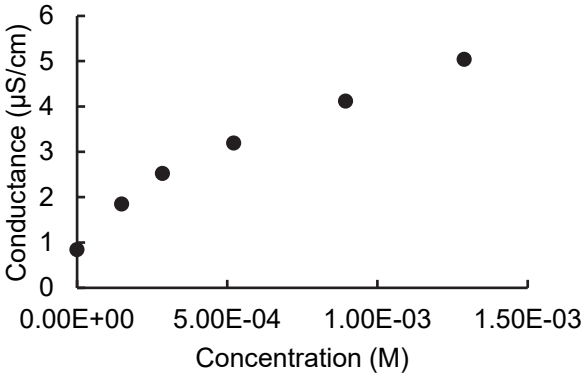

Concentration dependent conductivity of Ph_2IOTf in THF at 20 °C (RM1233).

[Ph_2IOTf] / M	Conductance (µS/cm)
0.00	8.40×10^{-1}
1.24×10^{-4}	1.34
2.36×10^{-4}	1.68
3.39×10^{-4}	1.85
5.99×10^{-4}	2.27
8.06×10^{-4}	2.60

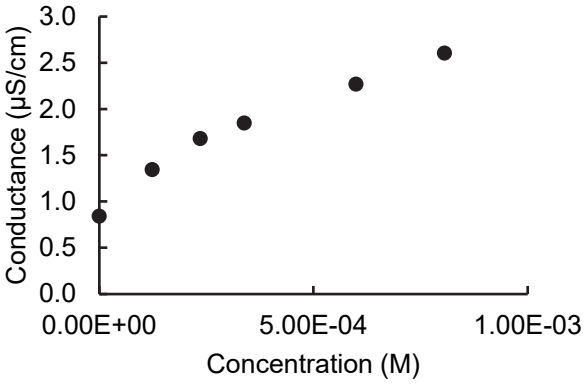

6.5 Determination of Lewis Basicities LB Towards Benzhydrylium Ions

Equilibrium Constants and Lewis Basicity Parameters LB Determined in This Work (Acetonitrile)

Lewis Base	*T* (°C)	Lewis Acid (LA)	*K* (M^{-1})	LB	$LB_{averaged}$
3a	20.0	**B1** (−12.76)	$(7.56 \pm 0.30) \times 10^4$	17.64	
3a	20.0	**B3** (−12.61)	$(4.42 \pm 0.05) \times 10^4$	17.26	17.54 ± 0.21
3a	20.0	**B4** (−11.46)	$(1.91 \pm 0.03) \times 10^6$	17.74	
3b	20.0	**B1** (−12.76)	$(1.03 \pm 0.03) \times 10^4$	16.77	
3b	20.0	**B3** (−12.61)	$(5.47 \pm 0.29) \times 10^3$	16.35	16.66 ± 0.22
3b	20.0	**B4** (−11.46)	$(2.46 \pm 0.21) \times 10^5$	16.85	
3c	20.0	**B1** (−12.76)	$(9.02 \pm 0.46) \times 10^2$	15.72	
3c	20.0	**B3** (−12.61)	$(5.65 \pm 0.16) \times 10^2$	15.36	15.64 ± 0.17
3c	20.0	**B4** (−11.46)	$(2.35 \pm 0.09) \times 10^4$	15.83	
3d	20.0	**B1** (−12.76)	$(3.96 \pm 0.23) \times 10^2$	15.36	
3d	20.0	**B3** (−12.61)	$(2.79 \pm 0.13) \times 10^2$	15.06	15.28 ± 0.20
3d	20.0	**B4** (−11.46)	$(9.28 \pm 0.39) \times 10^3$	15.43	
3g	10.0	**B2** (−9.82)	$(8.92 \pm 0.44) \times 10^5$	-	
3g	20.0	**B2** (−9.82)	$(3.55 \pm 0.20) \times 10^5$	-	
3g	30.0	**B2** (−9.82)	$(1.44 \pm 0.02) \times 10^5$	-	
3g	40.0	**B2** (−9.82)	$(6.20 \pm 0.15) \times 10^4$	-	

Van't Hoff analysis for the reaction of B2 with quinuclidine (3g):

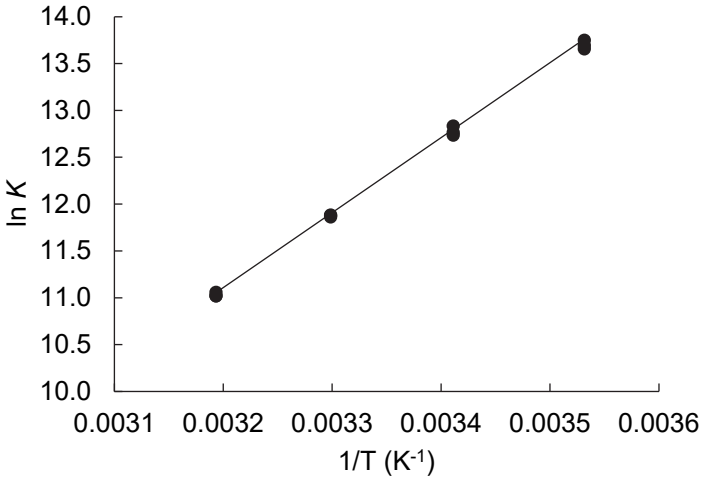

ln K = (7.89 ± 0.08) × 10^3 1/T − (14.2 ± 0.3),

R^2 = 0.999

ΔH = (−65.6 ± 0.7) kJ mol^{-1}

ΔS = (−118 ± 3) J mol^{-1} K^{-1}

Extrapolated equilibrium constants K (in MeCN) for the reactions of quinuclidine (**3g**) with **B2** (LA = –9.82) at different temperatures:

T (°C)	K (M^{-1})
−10	7.15×10^6
0	2.39×10^6

B1 + 3a (in MeCN, 20 °C, RM986), *c*(LB stock) = 4.79×10^{-3} M

Step	*V*(LB) (mL)	V_{tot} (LB) (mL)	*V* (mL)	*A*	$[Ar_2CH^+]$ (M)	$A_0(V_0/V) - A$	$[LB]_0$ (M)	$[LB]_0/[Ar_2CH^+]_0$	[LB] (M)	$(A_0(V_0/V)-A)/A$
0	0	0	24.12	1.032	1.43×10^{-5}		0.000			
1	0.100	0.10	24.22	0.544	7.53×10^{-6}	0.484	1.98×10^{-5}	1.4	1.31×10^{-5}	0.889
2	0.100	0.20	24.32	0.323	4.47×10^{-6}	0.701	3.94×10^{-5}	5.2	2.97×10^{-5}	2.169
3	0.100	0.30	24.42	0.227	3.14×10^{-6}	0.792	5.88×10^{-5}	13.2	4.78×10^{-5}	3.490
4	0.100	0.40	24.52	0.172	2.38×10^{-6}	0.843	7.81×10^{-5}	24.9	6.64×10^{-5}	4.902
5	0.100	0.50	24.62	0.140	1.94×10^{-6}	0.871	9.72×10^{-5}	40.8	8.51×10^{-5}	6.222

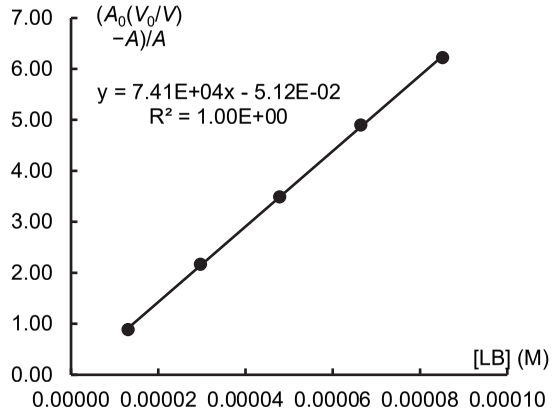

Step	*V*(LB) (mL)	V_{tot} (LB) (mL)	*V* (mL)	*A*	$[Ar_2CH^+]$ (M)	$A_0(V_0/V) - A$	$[LB]_0$ (M)	$[LB]_0/[Ar_2CH^+]_0$	[LB] (M)	$(A_0(V_0/V)-A)/A$
0	0	0	24.12	1.068	1.48×10^{-5}		0.000			
1	0.100	0.10	24.22	0.557	7.71×10^{-6}	0.507	1.98×10^{-5}	1.3	1.27×10^{-5}	0.909
2	0.100	0.20	24.32	0.333	4.61×10^{-6}	0.726	3.94×10^{-5}	5.1	2.93×10^{-5}	2.181
3	0.100	0.30	24.42	0.232	3.21×10^{-6}	0.823	5.88×10^{-5}	12.8	4.74×10^{-5}	3.547
4	0.100	0.40	24.52	0.181	2.50×10^{-6}	0.870	7.81×10^{-5}	24.3	6.60×10^{-5}	4.820
5	0.100	0.50	24.62	0.146	2.01×10^{-6}	0.901	9.72×10^{-5}	38.9	8.47×10^{-5}	6.191

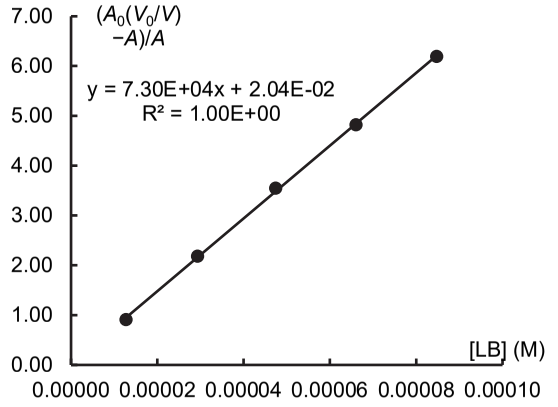

Step	V(LB) (mL)	V_{tot} (LB) (mL)	V (mL)	A	[Ar_2CH^+] (M)	$A_0(V_0/V) - A$	[LB]$_0$ (M)	[LB]$_0$/[Ar_2CH^+]$_0$	[LB] (M)	$(A_0(V_0/V)-A)/A$
0	0	0	24.12	1.054	1.46×10^{-5}		0.000			
1	0.100	0.10	24.22	0.539	7.46×10^{-6}	0.511	1.98×10^{-5}	1.4	1.27×10^{-5}	0.947
2	0.100	0.20	24.32	0.321	4.44×10^{-6}	0.724	3.94×10^{-5}	5.3	2.93×10^{-5}	2.256
3	0.100	0.30	24.42	0.221	3.05×10^{-6}	0.821	5.88×10^{-5}	13.2	4.74×10^{-5}	3.721
4	0.100	0.40	24.52	0.167	2.31×10^{-6}	0.870	7.81×10^{-5}	25.6	6.60×10^{-5}	5.208
5	0.100	0.50	24.62	0.135	1.86×10^{-6}	0.898	9.72×10^{-5}	42.1	8.48×10^{-5}	6.677

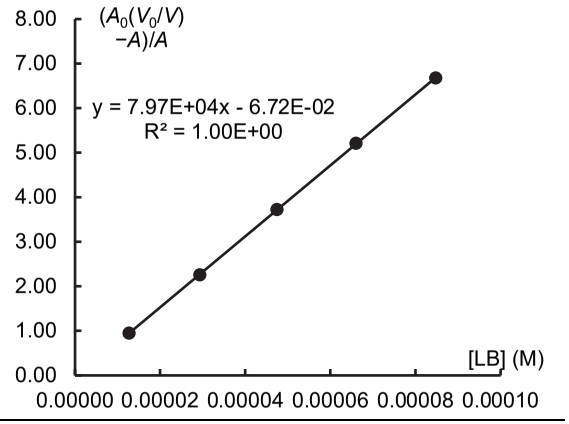

B3 + 3a (in MeCN, 20 °C, RM986), c(LB stock) = 4.79×10^{-3} M

Step	V(LB) (mL)	V_{tot} (LB) (mL)	V (mL)	A	[Ar_2CH^+] (M)	$A_0(V_0/V) - A$	[LB]$_0$ (M)	[LB]$_0$/[Ar_2CH^+]$_0$	[LB] (M)	$(A_0(V_0/V)-A)/A$
0	0	0	24.19	1.095	1.20×10^{-5}		0.000			
1	0.100	0.10	24.29	0.749	8.23×10^{-6}	0.341	1.97×10^{-5}	1.6	1.59×10^{-5}	0.456
2	0.100	0.20	24.39	0.512	5.63×10^{-6}	0.574	3.92×10^{-5}	4.8	3.29×10^{-5}	1.121
3	0.100	0.30	24.49	0.373	4.10×10^{-6}	0.709	5.86×10^{-5}	10.4	5.08×10^{-5}	1.900
4	0.100	0.40	24.59	0.288	3.16×10^{-6}	0.790	7.78×10^{-5}	19.0	6.92×10^{-5}	2.747
5	0.100	0.50	24.69	0.233	2.56×10^{-6}	0.840	9.69×10^{-5}	30.7	8.77×10^{-5}	3.604

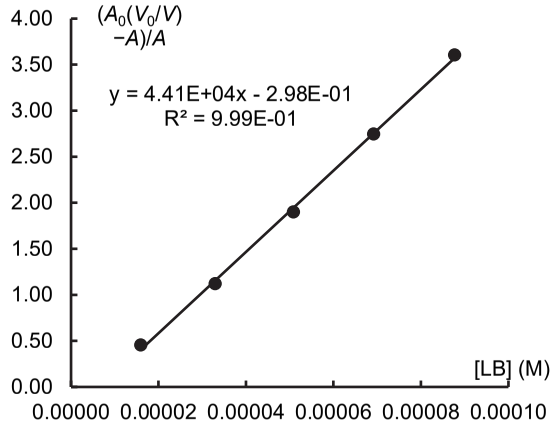

Step	V(LB) (mL)	V_{tot} (LB) (mL)	V (mL)	A	[Ar_2CH^+] (M)	$A_0(V_0/V) - A$	[LB]$_0$ (M)	[LB]$_0$/[Ar_2CH^+]$_0$	[LB] (M)	$(A_0(V_0/V)-A)/A$
0	0	0	24.19	1.092	1.20×10^{-5}		0.000			
1	0.100	0.10	24.29	0.736	8.09×10^{-6}	0.352	1.97×10^{-5}	1.6	1.58×10^{-5}	0.478
2	0.100	0.20	24.39	0.509	5.59×10^{-6}	0.574	3.92×10^{-5}	4.9	3.29×10^{-5}	1.128
3	0.100	0.30	24.49	0.371	4.07×10^{-6}	0.708	5.86×10^{-5}	10.5	5.08×10^{-5}	1.911
4	0.100	0.40	24.59	0.287	3.15×10^{-6}	0.787	7.78×10^{-5}	19.1	6.92×10^{-5}	2.743
5	0.100	0.50	24.69	0.233	2.56×10^{-6}	0.837	9.69×10^{-5}	30.7	8.77×10^{-5}	3.602

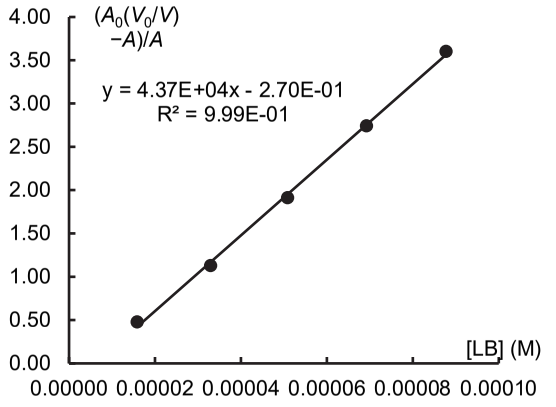

Step	V(LB) (mL)	V_{tot} (LB) (mL)	V (mL)	A	[Ar_2CH^+] (M)	$A_0(V_0/V) - A$	[LB]$_0$ (M)	[LB]$_0$/[Ar_2CH^+]$_0$	[LB] (M)	$(A_0(V_0/V)-A)/A$
0	0	0	24.19	1.093	1.20×10^{-5}		0.000			
1	0.100	0.10	24.29	0.729	8.01×10^{-6}	0.360	1.97×10^{-5}	1.6	1.58×10^{-5}	0.493
2	0.100	0.20	24.39	0.501	5.51×10^{-6}	0.583	3.92×10^{-5}	4.9	3.28×10^{-5}	1.164
3	0.100	0.30	24.49	0.365	4.01×10^{-6}	0.715	5.86×10^{-5}	10.6	5.08×10^{-5}	1.958
4	0.100	0.40	24.59	0.282	3.10×10^{-6}	0.793	7.78×10^{-5}	19.4	6.91×10^{-5}	2.813
5	0.100	0.50	24.69	0.228	2.51×10^{-6}	0.843	9.69×10^{-5}	31.3	8.77×10^{-5}	3.697

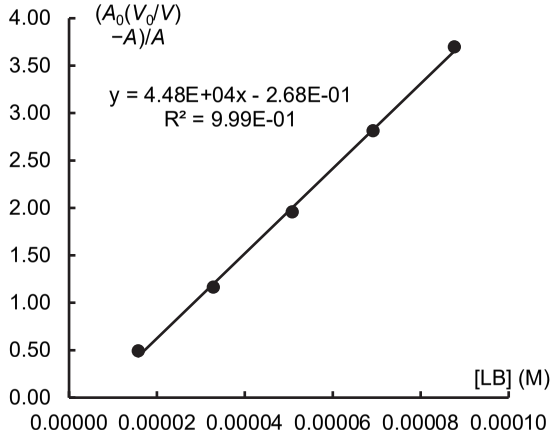

B4 + 3a (in MeCN, 20 °C, RM986), *c*(LB stock) = 4.79×10^{-3} M

Step	*V*(LB) (mL)	V_{tot} (LB) (mL)	*V* (mL)	*A*	$[Ar_2CH^+]$ (M)	$A_0(V_0/V) - A$	$[LB]_0$ (M)	$[LB]_0/[Ar_2CH^+]_0$	[LB] (M)	$(A_0(V_0/V)-A)/A$
0	0	0	24.14	1.047	1.52×10^{-5}		0.000			
1	0.025	0.03	24.17	0.831	1.20×10^{-5}	0.215	4.95×10^{-6}	0.3	1.84×10^{-6}	0.259
2	0.025	0.05	24.19	0.518	7.51×10^{-6}	0.527	9.89×10^{-6}	0.8	2.26×10^{-6}	1.017
3	0.025	0.08	24.22	0.248	3.59×10^{-6}	0.796	1.48×10^{-5}	2.0	3.29×10^{-6}	3.209
4	0.025	0.10	24.24	0.106	1.54×10^{-6}	0.937	1.97×10^{-5}	5.5	6.17×10^{-6}	8.837
5	0.025	0.13	24.27	0.059	8.55×10^{-7}	0.983	2.47×10^{-5}	16.1	1.04×10^{-5}	16.654
6	0.025	0.15	24.29	0.040	5.72×10^{-7}	1.001	2.96×10^{-5}	34.6	1.51×10^{-5}	25.343

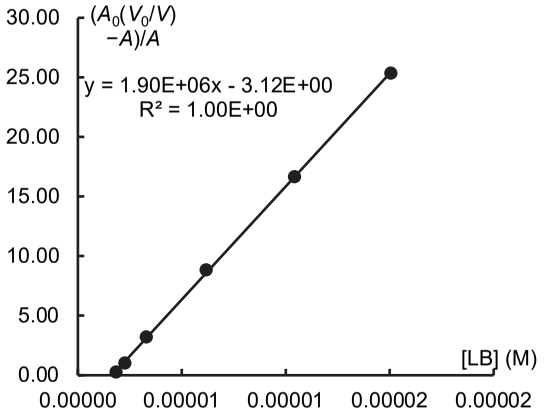

Step	*V*(LB) (mL)	V_{tot} (LB) (mL)	*V* (mL)	*A*	$[Ar_2CH^+]$ (M)	$A_0(V_0/V) - A$	$[LB]_0$ (M)	$[LB]_0/[Ar_2CH^+]_0$	[LB] (M)	$(A_0(V_0/V)-A)/A$
0	0	0	24.14	1.017	1.47×10^{-5}		0.000			
1	0.025	0.03	24.17	0.784	1.14×10^{-5}	0.232	4.95×10^{-6}	0.3	1.59×10^{-6}	0.296
2	0.025	0.05	24.19	0.481	6.97×10^{-6}	0.534	9.89×10^{-6}	0.9	2.16×10^{-6}	1.110
3	0.025	0.08	24.22	0.224	3.25×10^{-6}	0.790	1.48×10^{-5}	2.1	3.38×10^{-6}	3.526
4	0.025	0.10	24.24	0.095	1.38×10^{-6}	0.918	1.97×10^{-5}	6.1	6.45×10^{-6}	9.661
5	0.025	0.13	24.27	0.053	7.68×10^{-7}	0.959	2.47×10^{-5}	17.9	1.08×10^{-5}	18.090
6	0.025	0.15	24.29	0.036	5.22×10^{-7}	0.975	2.96×10^{-5}	38.5	1.54×10^{-5}	27.076

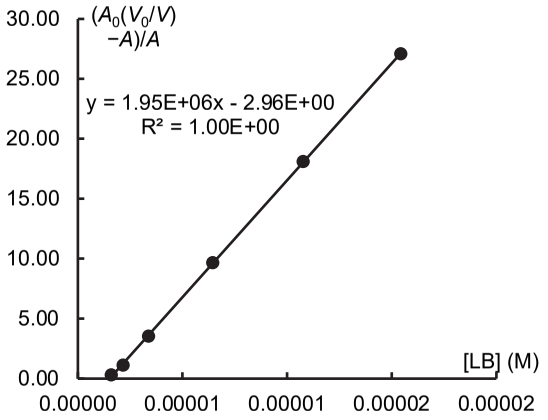

Step	V(LB) (mL)	V_{tot} (LB) (mL)	V (mL)	A	[Ar_2CH^+] (M)	$A_0(V_0/V) - A$	$[LB]_0$ (M)	$[LB]_0/[Ar_2CH^+]_0$	[LB] (M)	$(A_0(V_0/V)-A)/A$
0	0	0	24.14	1.056	1.53×10^{-5}		0.000			
1	0.025	0.03	24.17	0.830	1.20×10^{-5}	0.225	4.95×10^{-6}	0.3	1.69×10^{-6}	0.271
2	0.025	0.05	24.19	0.535	7.75×10^{-6}	0.519	9.89×10^{-6}	0.8	2.37×10^{-6}	0.970
3	0.025	0.08	24.22	0.258	3.74×10^{-6}	0.795	1.48×10^{-5}	1.9	3.31×10^{-6}	3.080
4	0.025	0.10	24.24	0.119	1.72×10^{-6}	0.933	1.97×10^{-5}	5.3	6.23×10^{-6}	7.837
5	0.025	0.13	24.27	0.061	8.84×10^{-7}	0.990	2.47×10^{-5}	14.3	1.03×10^{-5}	16.222
6	0.025	0.15	24.29	0.041	5.87×10^{-7}	1.009	2.96×10^{-5}	33.4	1.49×10^{-5}	24.913

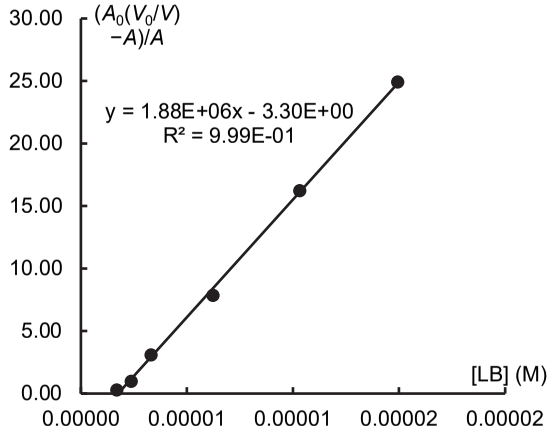

B1 + 3b (in MeCN, 20 °C, RM818), c(LB stock) = 8.69×10^{-3} M

Step	V(LB) (mL)	V_{tot} (LB) (mL)	V (mL)	A	[Ar_2CH^+] (M)	$A_0(V_0/V) - A$	$[LB]_0$ (M)	$[LB]_0/[Ar_2CH^+]_0$	[LB] (M)	$(A_0(V_0/V)-A)/A$
0	0	0	24.10	0.910	1.26×10^{-5}		0.000			
1	0.100	0.10	24.20	0.626	8.66×10^{-6}	0.280	3.59×10^{-5}	2.9	3.20×10^{-5}	0.448
2	0.100	0.20	24.30	0.493	6.82×10^{-6}	0.410	7.15×10^{-5}	8.3	6.59×10^{-5}	0.831
3	0.100	0.30	24.40	0.410	5.67×10^{-6}	0.489	1.07×10^{-4}	15.7	1.00×10^{-4}	1.192
4	0.100	0.40	24.50	0.352	4.87×10^{-6}	0.543	1.42×10^{-4}	25.0	1.34×10^{-4}	1.543
5	0.100	0.50	24.60	0.311	4.30×10^{-6}	0.581	1.77×10^{-4}	36.3	1.69×10^{-4}	1.871

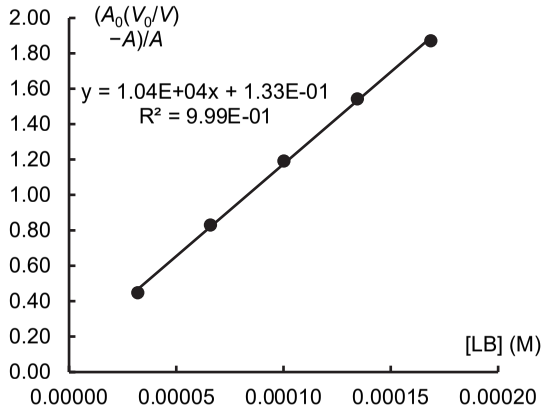

Step	V(LB) (mL)	V_{tot} (LB) (mL)	V (mL)	A	[Ar_2CH^+] (M)	$A_0(V_0/V) - A$	$[LB]_0$ (M)	$[LB]_0/[Ar_2CH^+]_0$	[LB] (M)	$(A_0(V_0/V)-A)/A$
0	0	0	24.10	0.982	1.36×10^{-5}		0.000			
1	0.100	0.10	24.20	0.682	9.44×10^{-6}	0.296	3.59×10^{-5}	2.6	3.18×10^{-5}	0.434
2	0.100	0.20	24.30	0.533	7.37×10^{-6}	0.441	7.15×10^{-5}	7.6	6.54×10^{-5}	0.827
3	0.100	0.30	24.40	0.441	6.10×10^{-6}	0.529	1.07×10^{-4}	14.5	9.96×10^{-5}	1.199
4	0.100	0.40	24.50	0.382	5.29×10^{-6}	0.584	1.42×10^{-4}	23.3	1.34×10^{-4}	1.529
5	0.100	0.50	24.60	0.334	4.62×10^{-6}	0.628	1.77×10^{-4}	33.4	1.68×10^{-4}	1.880

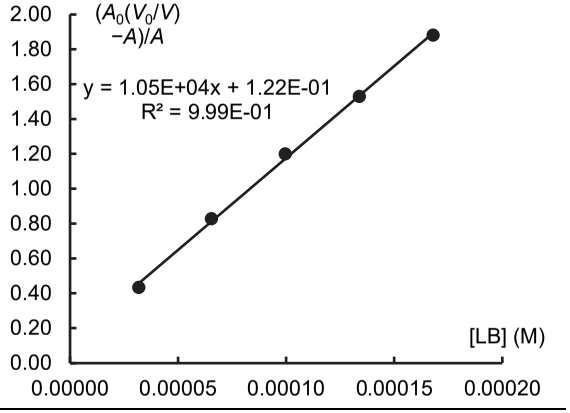

Step	V(LB) (mL)	V_{tot} (LB) (mL)	V (mL)	A	[Ar_2CH^+] (M)	$A_0(V_0/V) - A$	$[LB]_0$ (M)	$[LB]_0/[Ar_2CH^+]_0$	[LB] (M)	$(A_0(V_0/V)-A)/A$
0	0	0	24.10	0.965	1.34×10^{-5}		0.000			
1	0.100	0.10	24.20	0.672	9.30×10^{-6}	0.289	3.59×10^{-5}	2.7	3.19×10^{-5}	0.430
2	0.100	0.20	24.30	0.532	7.36×10^{-6}	0.425	7.15×10^{-5}	7.7	6.57×10^{-5}	0.799
3	0.100	0.30	24.40	0.444	6.14×10^{-6}	0.509	1.07×10^{-4}	14.5	9.98×10^{-5}	1.147
4	0.100	0.40	24.50	0.385	5.33×10^{-6}	0.564	1.42×10^{-4}	23.1	1.34×10^{-4}	1.466
5	0.100	0.50	24.60	0.339	4.68×10^{-6}	0.607	1.77×10^{-4}	33.2	1.68×10^{-4}	1.793

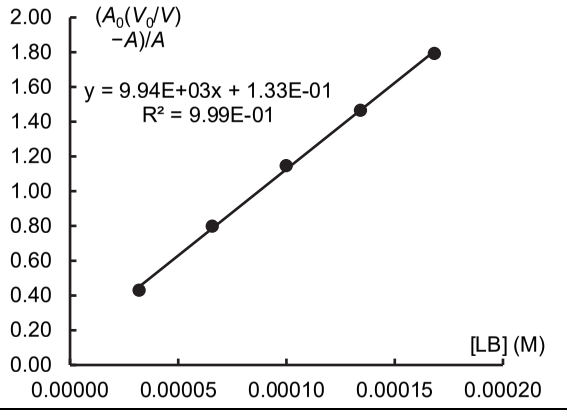

B3 + 3b (in MeCN, 20 °C, RM818), *c*(LB stock) = 8.69 × 10^{-3} M

Step	*V*(LB) (mL)	V_{tot} (LB) (mL)	*V* (mL)	*A*	[Ar_2CH^+] (M)	$A_0(V_0/V) - A$	$[LB]_0$ (M)	$[LB]_0/[Ar_2CH^+]_0$	[LB] (M)	$(A_0(V_0/V)-A)/A$
0	0	0	24.20	1.047	1.15×10^{-5}		0.000			
1	0.100	0.10	24.30	0.852	9.36×10^{-6}	0.191	3.58×10^{-5}	3.1	3.37×10^{-5}	0.224
2	0.100	0.20	24.40	0.731	8.03×10^{-6}	0.307	7.13×10^{-5}	7.6	6.79×10^{-5}	0.421
3	0.100	0.30	24.50	0.635	6.98×10^{-6}	0.399	1.06×10^{-4}	13.2	1.02×10^{-4}	0.629
4	0.100	0.40	24.60	0.563	6.19×10^{-6}	0.467	1.41×10^{-4}	20.3	1.36×10^{-4}	0.829
5	0.100	0.50	24.70	0.507	5.57×10^{-6}	0.519	1.76×10^{-4}	28.4	1.70×10^{-4}	1.023

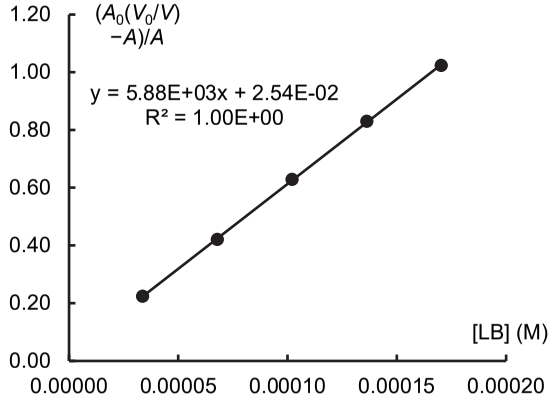

Step	*V*(LB) (mL)	V_{tot} (LB) (mL)	*V* (mL)	*A*	[Ar_2CH^+] (M)	$A_0(V_0/V) - A$	$[LB]_0$ (M)	$[LB]_0/[Ar_2CH^+]_0$	[LB] (M)	$(A_0(V_0/V)-A)/A$
0	0	0	24.20	1.057	1.16×10^{-5}		0.000			
1	0.100	0.10	24.30	0.904	9.94×10^{-6}	0.149	3.58×10^{-5}	3.1	3.41×10^{-5}	0.164
2	0.100	0.20	24.40	0.786	8.64×10^{-6}	0.262	7.13×10^{-5}	7.2	6.84×10^{-5}	0.334
3	0.100	0.30	24.50	0.687	7.55×10^{-6}	0.357	1.06×10^{-4}	12.3	1.03×10^{-4}	0.520
4	0.100	0.40	24.60	0.611	6.72×10^{-6}	0.429	1.41×10^{-4}	18.7	1.37×10^{-4}	0.702
5	0.100	0.50	24.70	0.551	6.06×10^{-6}	0.485	1.76×10^{-4}	26.2	1.71×10^{-4}	0.879

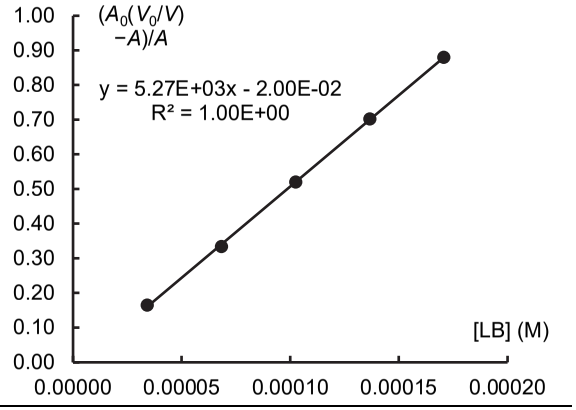

Step	V(LB) (mL)	V_{tot} (LB) (mL)	V (mL)	A	[Ar_2CH^+] (M)	$A_0(V_0/V) - A$	$[LB]_0$ (M)	$[LB]_0/[Ar_2CH^+]_0$	[LB] (M)	$(A_0(V_0/V)-A)/A$
0	0	0	24.20	1.092	1.20×10^{-5}		0.000			
1	0.100	0.10	24.30	0.934	1.03×10^{-5}	0.154	3.58×10^{-5}	3.0	3.41×10^{-5}	0.164
2	0.100	0.20	24.40	0.811	8.91×10^{-6}	0.272	7.13×10^{-5}	6.9	6.83×10^{-5}	0.335
3	0.100	0.30	24.50	0.711	7.81×10^{-6}	0.368	1.06×10^{-4}	11.9	1.02×10^{-4}	0.517
4	0.100	0.40	24.60	0.631	6.94×10^{-6}	0.443	1.41×10^{-4}	18.1	1.36×10^{-4}	0.702
5	0.100	0.50	24.70	0.570	6.26×10^{-6}	0.500	1.76×10^{-4}	25.4	1.70×10^{-4}	0.879

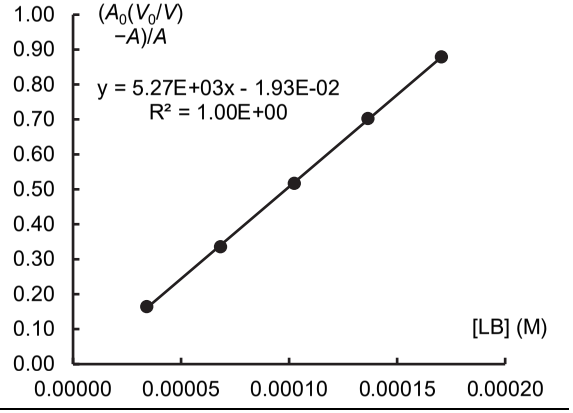

B4 + 3b (in MeCN, 20 °C, RM818), c(LB stock) = 8.69×10^{-3} M

Step	V(LB) (mL)	V_{tot} (LB) (mL)	V (mL)	A	[Ar_2CH^+] (M)	$A_0(V_0/V) - A$	$[LB]_0$ (M)	$[LB]_0/[Ar_2CH^+]_0$	[LB] (M)	$(A_0(V_0/V)-A)/A$
0	0	0	24.15	0.916	1.33×10^{-5}		0.000			
1	0.050	0.05	24.20	0.405	5.87×10^{-6}	0.509	1.80×10^{-5}	1.4	1.06×10^{-5}	1.257
2	0.025	0.08	24.23	0.241	3.49×10^{-6}	0.672	2.69×10^{-5}	4.6	1.72×10^{-5}	2.789
3	0.025	0.10	24.25	0.167	2.42×10^{-6}	0.745	3.58×10^{-5}	10.3	2.50×10^{-5}	4.462
4	0.025	0.13	24.28	0.124	1.80×10^{-6}	0.787	4.48×10^{-5}	18.5	3.34×10^{-5}	6.349
5	0.025	0.15	24.30	0.099	1.43×10^{-6}	0.811	5.37×10^{-5}	29.9	4.19×10^{-5}	8.195

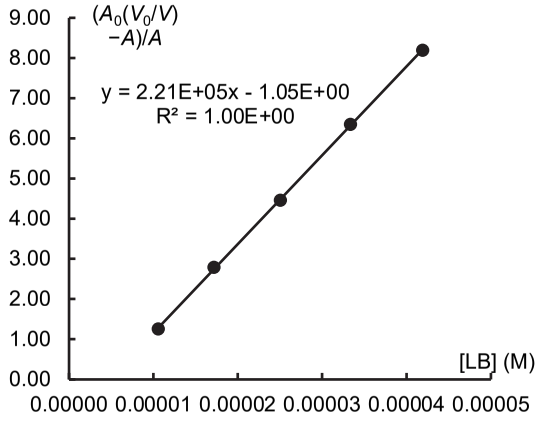

Step	V(LB) (mL)	V_{tot} (LB) (mL)	V (mL)	A	[Ar_2CH^+] (M)	$A_0(V_0/V) - A$	[LB]$_0$ (M)	[LB]$_0$/[Ar_2CH^+]$_0$	[LB] (M)	$(A_0(V_0/V)-A)/A$
0	0	0	24.15	0.896	1.30×10^{-5}		0.000			
1	0.050	0.05	24.20	0.414	6.00×10^{-6}	0.480	1.80×10^{-5}	1.4	1.10×10^{-5}	1.160
2	0.025	0.08	24.23	0.239	3.46×10^{-6}	0.654	2.69×10^{-5}	4.5	1.74×10^{-5}	2.737
3	0.025	0.10	24.25	0.154	2.23×10^{-6}	0.738	3.58×10^{-5}	10.4	2.51×10^{-5}	4.794
4	0.025	0.13	24.28	0.109	1.58×10^{-6}	0.782	4.48×10^{-5}	20.1	3.34×10^{-5}	7.178
5	0.025	0.15	24.30	0.085	1.23×10^{-6}	0.805	5.37×10^{-5}	34.0	4.20×10^{-5}	9.476

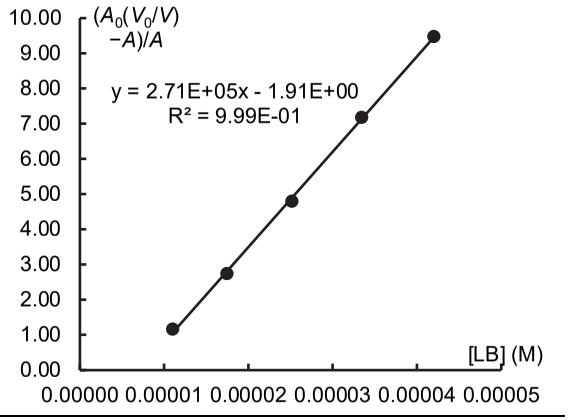

Step	V(LB) (mL)	V_{tot} (LB) (mL)	V (mL)	A	[Ar_2CH^+] (M)	$A_0(V_0/V) - A$	[LB]$_0$ (M)	[LB]$_0$/[Ar_2CH^+]$_0$	[LB] (M)	$(A_0(V_0/V)-A)/A$
0	0	0	24.15	0.927	1.34×10^{-5}		0.000			
1	0.050	0.05	24.20	0.430	6.23×10^{-6}	0.495	1.80×10^{-5}	1.3	1.08×10^{-5}	1.151
2	0.025	0.08	24.23	0.256	3.71×10^{-6}	0.668	2.69×10^{-5}	4.3	1.72×10^{-5}	2.610
3	0.025	0.10	24.25	0.169	2.45×10^{-6}	0.754	3.58×10^{-5}	9.7	2.49×10^{-5}	4.463
4	0.025	0.13	24.28	0.121	1.75×10^{-6}	0.801	4.48×10^{-5}	18.3	3.32×10^{-5}	6.622
5	0.025	0.15	24.30	0.096	1.38×10^{-6}	0.826	5.37×10^{-5}	30.6	4.17×10^{-5}	8.647

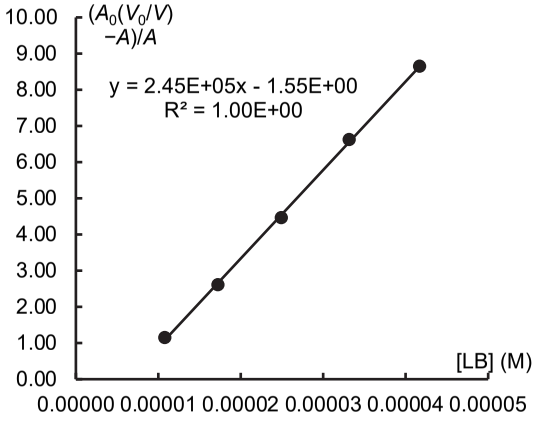

B1 + 3c (in MeCN, 20 °C, RM811), *c*(LB stock) = 1.08×10^{-2} M

Step	*V*(LB) (mL)	V_{tot} (LB) (mL)	*V* (mL)	*A*	$[Ar_2CH^+]$ (M)	$A_0(V_0/V) - A$	$[LB]_0$ (M)	$[LB]_0/[Ar_2CH^+]_0$	[LB] (M)	$(A_0(V_0/V)-A)/A$
0	0	0	24.10	0.969	1.34×10^{-5}		0.000			
1	0.100	0.10	24.20	0.911	1.26×10^{-5}	0.054	4.46×10^{-5}	3.3	4.38×10^{-5}	0.059
2	0.100	0.20	24.30	0.871	1.21×10^{-5}	0.090	8.88×10^{-5}	7.0	8.75×10^{-5}	0.103
3	0.100	0.30	24.40	0.836	1.16×10^{-5}	0.121	1.33×10^{-4}	11.0	1.31×10^{-4}	0.145
4	0.100	0.40	24.50	0.807	1.12×10^{-5}	0.146	1.76×10^{-4}	15.2	1.74×10^{-4}	0.181
5	0.100	0.50	24.60	0.779	1.08×10^{-5}	0.170	2.19×10^{-4}	19.6	2.17×10^{-4}	0.219
6	0.100	0.60	24.70	0.754	1.04×10^{-5}	0.191	2.62×10^{-4}	24.3	2.59×10^{-4}	0.254
7	0.200	0.80	24.90	0.711	9.84×10^{-6}	0.227	3.47×10^{-4}	33.2	3.43×10^{-4}	0.319
8	0.200	1.00	25.10	0.673	9.31×10^{-6}	0.257	4.30×10^{-4}	43.7	4.26×10^{-4}	0.382

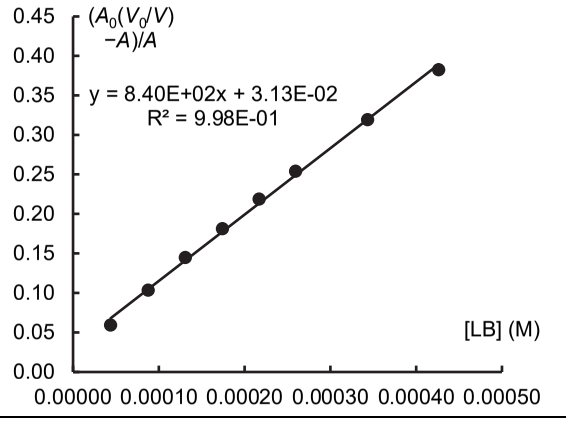

Step	*V*(LB) (mL)	V_{tot} (LB) (mL)	*V* (mL)	*A*	$[Ar_2CH^+]$ (M)	$A_0(V_0/V) - A$	$[LB]_0$ (M)	$[LB]_0/[Ar_2CH^+]_0$	[LB] (M)	$(A_0(V_0/V)-A)/A$
0	0	0	24.10	0.938	1.30×10^{-5}		0.000			
1	0.200	0.20	24.30	0.828	1.15×10^{-5}	0.102	8.88×10^{-5}	6.8	8.74×10^{-5}	0.124
2	0.200	0.40	24.50	0.761	1.05×10^{-5}	0.162	1.76×10^{-4}	15.4	1.74×10^{-4}	0.212
3	0.200	0.60	24.70	0.707	9.78×10^{-6}	0.208	2.62×10^{-4}	24.9	2.59×10^{-4}	0.295
4	0.200	0.80	24.90	0.664	9.19×10^{-6}	0.244	3.47×10^{-4}	35.4	3.43×10^{-4}	0.367
5	0.200	1.00	25.10	0.628	8.69×10^{-6}	0.273	4.30×10^{-4}	46.8	4.26×10^{-4}	0.434

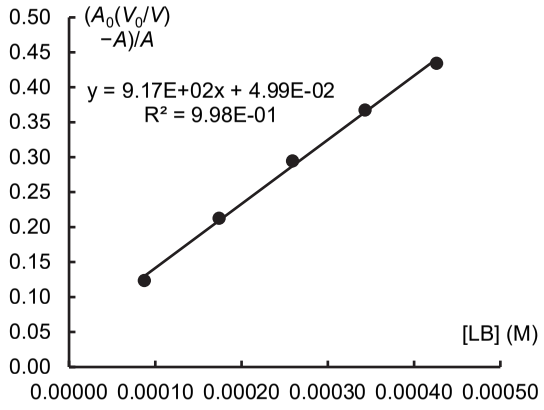

Step	V(LB) (mL)	V_{tot} (LB) (mL)	V (mL)	A	[Ar_2CH^+] (M)	$A_0(V_0/V) - A$	[LB]$_0$ (M)	[LB]$_0$/[Ar_2CH^+]$_0$	[LB] (M)	$(A_0(V_0/V)-A)/A$
0	0	0	24.10	0.943	1.30×10^{-5}		0.000			
1	0.200	0.20	24.30	0.828	1.15×10^{-5}	0.107	8.88×10^{-5}	6.8	8.73×10^{-5}	0.130
2	0.200	0.40	24.50	0.759	1.05×10^{-5}	0.169	1.76×10^{-4}	15.4	1.74×10^{-4}	0.223
3	0.200	0.60	24.70	0.705	9.75×10^{-6}	0.215	2.62×10^{-4}	25.0	2.59×10^{-4}	0.305
4	0.200	0.80	24.90	0.661	9.15×10^{-6}	0.252	3.47×10^{-4}	35.5	3.43×10^{-4}	0.381
5	0.200	1.00	25.10	0.624	8.63×10^{-6}	0.282	4.30×10^{-4}	47.0	4.26×10^{-4}	0.452

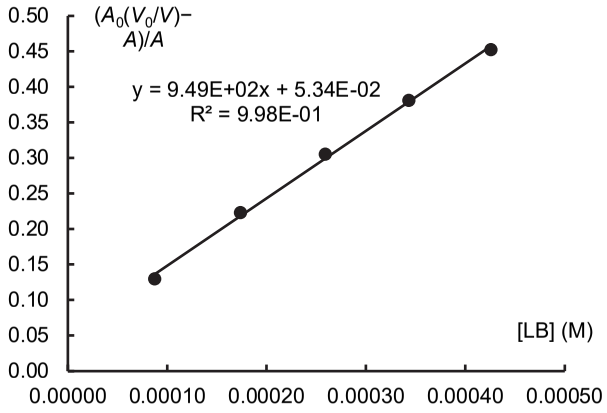

B3 + 3c (in MeCN, 20 °C, RM811), c(LB stock) = 1.08×10^{-2} M

Step	V(LB) (mL)	V_{tot} (LB) (mL)	V (mL)	A	[Ar_2CH^+] (M)	$A_0(V_0/V) - A$	[LB]$_0$ (M)	[LB]$_0$/[Ar_2CH^+]$_0$	[LB] (M)	$(A_0(V_0/V)-A)/A$
0	0	0	24.14	1.080	1.19×10^{-5}		0.000			
1	0.200	0.20	24.34	1.003	1.10×10^{-5}	0.068	8.86×10^{-5}	7.5	8.79×10^{-5}	0.068
2	0.200	0.40	24.54	0.949	1.04×10^{-5}	0.113	1.76×10^{-4}	15.9	1.75×10^{-4}	0.119
3	0.200	0.60	24.74	0.904	9.94×10^{-6}	0.150	2.62×10^{-4}	25.1	2.60×10^{-4}	0.166
4	0.200	0.80	24.94	0.864	9.50×10^{-6}	0.181	3.46×10^{-4}	34.8	3.44×10^{-4}	0.210
5	0.200	1.00	25.14	0.828	9.10×10^{-6}	0.209	4.29×10^{-4}	45.2	4.27×10^{-4}	0.252

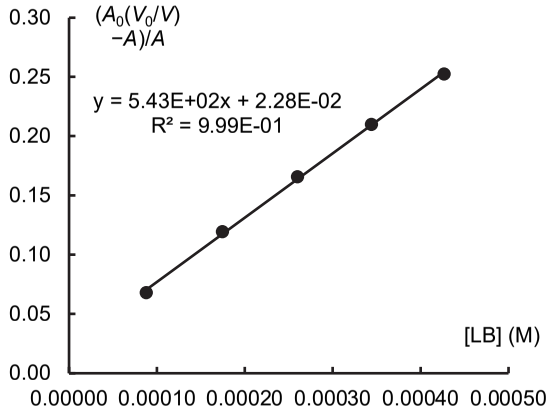

Step	V(LB) (mL)	V_{tot} (LB) (mL)	V (mL)	A	[Ar_2CH^+] (M)	$A_0(V_0/V) - A$	[LB]$_0$ (M)	[LB]$_0$/[Ar_2CH^+]$_0$	[LB] (M)	$(A_0(V_0/V)-A)/A$
0	0	0	24.14	1.067	1.17×10^{-5}		0.000			
1	0.200	0.20	24.34	0.987	1.08×10^{-5}	0.071	8.86×10^{-5}	7.6	8.78×10^{-5}	0.072
2	0.200	0.40	24.54	0.931	1.02×10^{-5}	0.119	1.76×10^{-4}	16.2	1.74×10^{-4}	0.127
3	0.200	0.60	24.74	0.884	9.72×10^{-6}	0.157	2.62×10^{-4}	25.6	2.60×10^{-4}	0.178
4	0.200	0.80	24.94	0.844	9.28×10^{-6}	0.189	3.46×10^{-4}	35.6	3.44×10^{-4}	0.224
5	0.200	1.00	25.14	0.808	8.88×10^{-6}	0.217	4.29×10^{-4}	46.2	4.27×10^{-4}	0.268

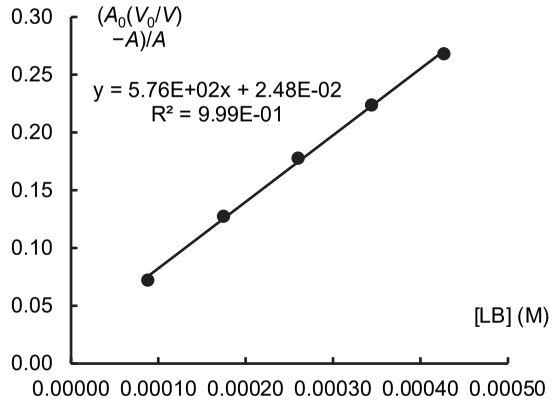

Step	V(LB) (mL)	V_{tot} (LB) (mL)	V (mL)	A	[Ar_2CH^+] (M)	$A_0(V_0/V) - A$	[LB]$_0$ (M)	[LB]$_0$/[Ar_2CH^+]$_0$	[LB] (M)	$(A_0(V_0/V)-A)/A$
0	0	0	24.14	1.111	1.22×10^{-5}		0.000			
1	0.200	0.20	24.34	1.029	1.13×10^{-5}	0.073	8.86×10^{-5}	7.3	8.78×10^{-5}	0.071
2	0.200	0.40	24.54	0.971	1.07×10^{-5}	0.122	1.76×10^{-4}	15.5	1.74×10^{-4}	0.126
3	0.200	0.60	24.74	0.922	1.01×10^{-5}	0.162	2.62×10^{-4}	24.5	2.60×10^{-4}	0.176
4	0.200	0.80	24.94	0.880	9.67×10^{-6}	0.195	3.46×10^{-4}	34.1	3.44×10^{-4}	0.222
5	0.200	1.00	25.14	0.842	9.25×10^{-6}	0.225	4.29×10^{-4}	44.4	4.27×10^{-4}	0.267

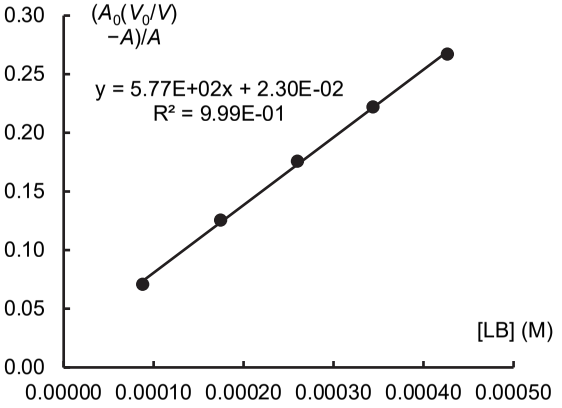

B4 + 3c (in MeCN, 20 °C, RM811), *c*(LB stock) = 1.08×10^{-2} M

Step	*V*(LB) (mL)	V_{tot} (LB) (mL)	*V* (mL)	*A*	$[Ar_2CH^+]$ (M)	$A_0(V_0/V) - A$	$[LB]_0$ (M)	$[LB]_0/[Ar_2CH^+]_0$	[LB] (M)	$(A_0(V_0/V)-A)/A$
0	0	0	24.11	0.922	1.34×10^{-5}		0.000			
1	0.050	0.05	24.16	0.608	8.81×10^{-6}	0.312	2.23×10^{-5}	1.7	1.78×10^{-5}	0.513
2	0.050	0.10	24.21	0.456	6.61×10^{-6}	0.462	4.45×10^{-5}	5.1	3.79×10^{-5}	1.014
3	0.050	0.15	24.26	0.362	5.24×10^{-6}	0.554	6.67×10^{-5}	10.1	5.87×10^{-5}	1.531
4	0.050	0.20	24.31	0.301	4.36×10^{-6}	0.613	8.87×10^{-5}	16.9	7.98×10^{-5}	2.038
5	0.050	0.25	24.36	0.258	3.74×10^{-6}	0.655	1.11×10^{-4}	25.4	1.01×10^{-4}	2.537

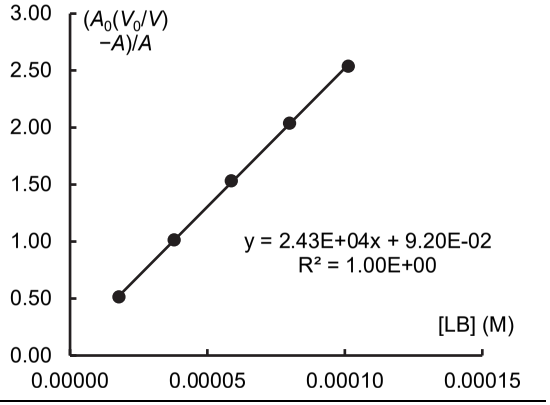

Step	*V*(LB) (mL)	V_{tot} (LB) (mL)	*V* (mL)	*A*	$[Ar_2CH^+]$ (M)	$A_0(V_0/V) - A$	$[LB]_0$ (M)	$[LB]_0/[Ar_2CH^+]_0$	[LB] (M)	$(A_0(V_0/V)-A)/A$
0	0	0	24.11	0.958	1.39×10^{-5}		0.000			
1	0.050	0.05	24.16	0.655	9.49×10^{-6}	0.301	2.23×10^{-5}	1.6	1.80×10^{-5}	0.460
2	0.050	0.10	24.21	0.496	7.19×10^{-6}	0.458	4.45×10^{-5}	4.7	3.79×10^{-5}	0.923
3	0.050	0.15	24.26	0.399	5.78×10^{-6}	0.553	6.67×10^{-5}	9.3	5.87×10^{-5}	1.386
4	0.050	0.20	24.31	0.333	4.82×10^{-6}	0.617	8.87×10^{-5}	15.3	7.98×10^{-5}	1.853
5	0.050	0.25	24.36	0.286	4.14×10^{-6}	0.662	1.11×10^{-4}	22.9	1.01×10^{-4}	2.315

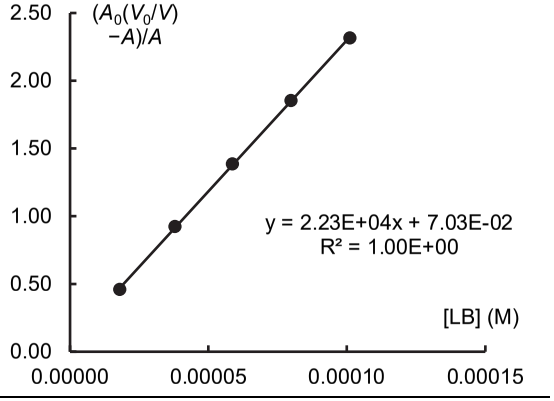

Step	V(LB) (mL)	V_{tot} (LB) (mL)	V (mL)	A	[Ar_2CH^+] (M)	$A_0(V_0/V) - A$	$[LB]_0$ (M)	$[LB]_0/[Ar_2CH^+]_0$	[LB] (M)	$(A_0(V_0/V)-A)/A$
0	0	0	24.11	0.936	1.36×10^{-5}		0.000			
1	0.050	0.05	24.16	0.624	9.04×10^{-6}	0.310	2.23×10^{-5}	1.6	1.78×10^{-5}	0.497
2	0.050	0.10	24.21	0.465	6.74×10^{-6}	0.467	4.45×10^{-5}	4.9	3.78×10^{-5}	1.005
3	0.050	0.15	24.26	0.374	5.42×10^{-6}	0.556	6.67×10^{-5}	9.9	5.86×10^{-5}	1.487
4	0.050	0.20	24.31	0.310	4.49×10^{-6}	0.618	8.87×10^{-5}	16.4	7.98×10^{-5}	1.995
5	0.050	0.25	24.36	0.265	3.84×10^{-6}	0.661	1.11×10^{-4}	24.6	1.01×10^{-4}	2.496

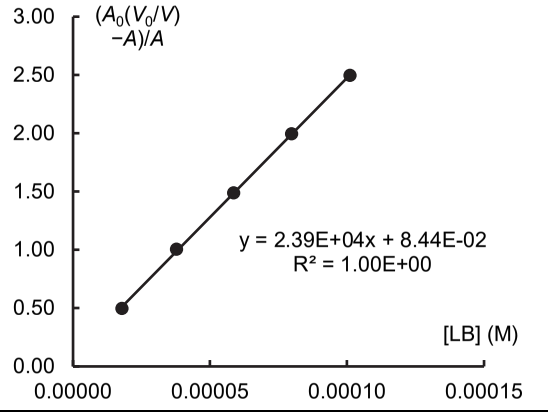

B1 + 3d (in MeCN, 20 °C, RM816), c(LB stock) = 1.01×10^{-2} M

Step	V(LB) (mL)	V_{tot} (LB) (mL)	V (mL)	A	[Ar_2CH^+] (M)	$A_0(V_0/V) - A$	$[LB]_0$ (M)	$[LB]_0/[Ar_2CH^+]_0$	[LB] (M)	$(A_0(V_0/V)-A)/A$
0	0	0	24.09	1.043	1.44×10^{-5}		0.000			
1	0.200	0.20	24.29	0.981	1.36×10^{-5}	0.053	8.28×10^{-5}	5.7	8.21×10^{-5}	0.054
2	0.200	0.40	24.49	0.939	1.30×10^{-5}	0.087	1.64×10^{-4}	12.1	1.63×10^{-4}	0.093
3	0.200	0.60	24.69	0.904	1.25×10^{-5}	0.114	2.44×10^{-4}	18.8	2.43×10^{-4}	0.126
4	0.200	0.80	24.89	0.873	1.21×10^{-5}	0.136	3.23×10^{-4}	25.8	3.21×10^{-4}	0.156
5	0.200	1.00	25.09	0.844	1.17×10^{-5}	0.157	4.01×10^{-4}	33.2	3.99×10^{-4}	0.187

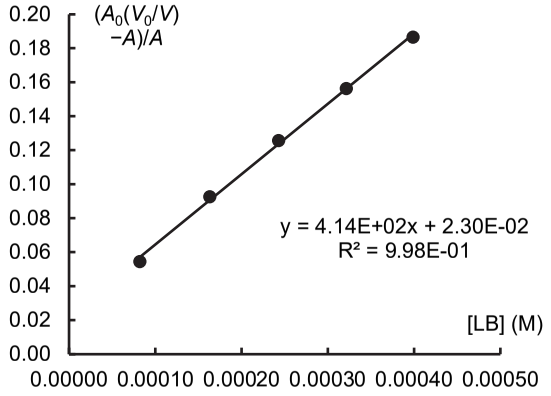

Step	V(LB) (mL)	V_{tot} (LB) (mL)	V (mL)	A	[Ar_2CH^+] (M)	$A_0(V_0/V) - A$	[LB]$_0$ (M)	[LB]$_0$/[Ar_2CH^+]$_0$	[LB] (M)	$(A_0(V_0/V)-A)/A$
0	0	0	24.09	1.082	1.50×10^{-5}		0.000			
1	0.200	0.20	24.29	1.015	1.40×10^{-5}	0.058	8.28×10^{-5}	5.5	8.20×10^{-5}	0.057
2	0.200	0.40	24.49	0.973	1.35×10^{-5}	0.091	1.64×10^{-4}	11.7	1.63×10^{-4}	0.094
3	0.200	0.60	24.69	0.936	1.30×10^{-5}	0.120	2.44×10^{-4}	18.2	2.43×10^{-4}	0.128
4	0.200	0.80	24.89	0.903	1.25×10^{-5}	0.144	3.23×10^{-4}	25.0	3.21×10^{-4}	0.160
5	0.200	1.00	25.09	0.876	1.21×10^{-5}	0.163	4.01×10^{-4}	32.1	3.99×10^{-4}	0.186

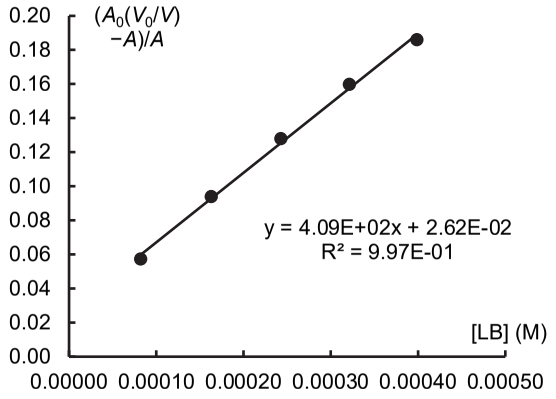

Step	V(LB) (mL)	V_{tot} (LB) (mL)	V (mL)	A	[Ar_2CH^+] (M)	$A_0(V_0/V) - A$	[LB]$_0$ (M)	[LB]$_0$/[Ar_2CH^+]$_0$	[LB] (M)	$(A_0(V_0/V)-A)/A$
0	0	0	24.09	1.025	1.42×10^{-5}		0.000			
1	0.200	0.20	24.29	0.977	1.35×10^{-5}	0.040	8.28×10^{-5}	5.8	8.23×10^{-5}	0.040
2	0.200	0.40	24.49	0.940	1.30×10^{-5}	0.068	1.64×10^{-4}	12.2	1.63×10^{-4}	0.073
3	0.200	0.60	24.69	0.909	1.26×10^{-5}	0.091	2.44×10^{-4}	18.8	2.43×10^{-4}	0.100
4	0.200	0.80	24.89	0.879	1.22×10^{-5}	0.113	3.23×10^{-4}	25.7	3.22×10^{-4}	0.129
5	0.200	1.00	25.09	0.851	1.18×10^{-5}	0.133	4.01×10^{-4}	33.0	3.99×10^{-4}	0.156

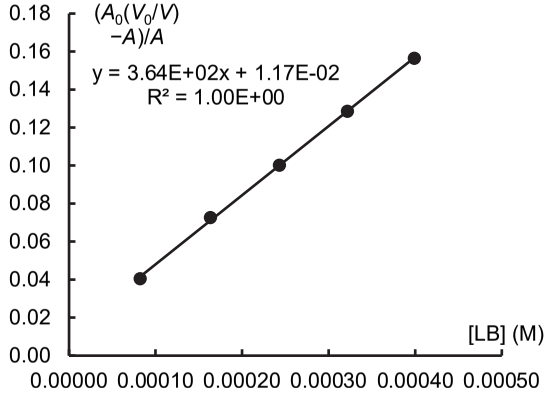

B3 + 3d (in MeCN, 20 °C, RM816), *c*(LB stock) = 1.01×10^{-2} M

Step	*V*(LB) (mL)	V_{tot} (LB) (mL)	*V* (mL)	*A*	$[Ar_2CH^+]$ (M)	$A_0(V_0/V) - A$	$[LB]_0$ (M)	$[LB]_0/[Ar_2CH^+]_0$	[LB] (M)	$(A_0(V_0/V)-A)/A$
0	0	0	24.13	1.000	1.10×10^{-5}		0.000			
1	0.200	0.20	24.33	0.962	1.06×10^{-5}	0.030	8.27×10^{-5}	7.5	8.24×10^{-5}	0.031
2	0.200	0.40	24.53	0.934	1.03×10^{-5}	0.050	1.64×10^{-4}	15.5	1.63×10^{-4}	0.053
3	0.200	0.60	24.73	0.909	9.99×10^{-6}	0.067	2.44×10^{-4}	23.8	2.43×10^{-4}	0.073
4	0.200	0.80	24.93	0.885	9.73×10^{-6}	0.083	3.23×10^{-4}	32.3	3.22×10^{-4}	0.094
5	0.200	1.00	25.13	0.862	9.47×10^{-6}	0.098	4.00×10^{-4}	41.2	3.99×10^{-4}	0.114

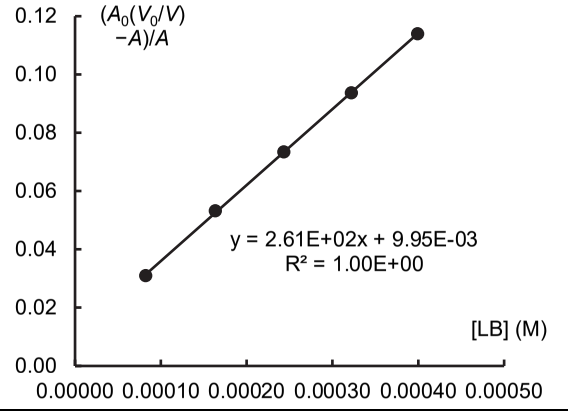

Step	*V*(LB) (mL)	V_{tot} (LB) (mL)	*V* (mL)	*A*	$[Ar_2CH^+]$ (M)	$A_0(V_0/V) - A$	$[LB]_0$ (M)	$[LB]_0/[Ar_2CH^+]_0$	[LB] (M)	$(A_0(V_0/V)-A)/A$
0	0	0	24.13	1.002	1.10×10^{-5}		0.000			
1	0.200	0.20	24.33	0.959	1.05×10^{-5}	0.035	8.27×10^{-5}	7.5	8.23×10^{-5}	0.036
2	0.200	0.40	24.53	0.928	1.02×10^{-5}	0.058	1.64×10^{-4}	15.6	1.63×10^{-4}	0.062
3	0.200	0.60	24.73	0.901	9.90×10^{-6}	0.077	2.44×10^{-4}	23.9	2.43×10^{-4}	0.085
4	0.200	0.80	24.93	0.876	9.63×10^{-6}	0.094	3.23×10^{-4}	32.6	3.22×10^{-4}	0.107
5	0.200	1.00	25.13	0.852	9.36×10^{-6}	0.110	4.00×10^{-4}	41.6	3.99×10^{-4}	0.129

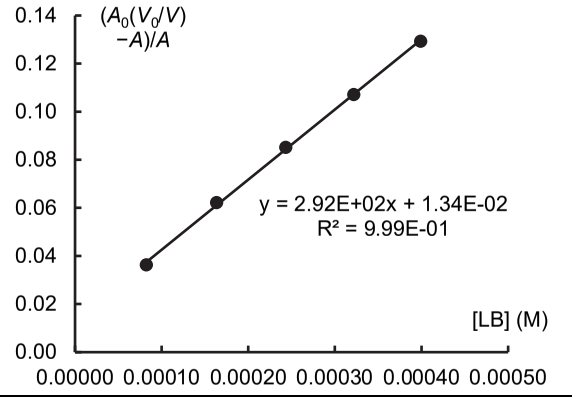

Step	V(LB) (mL)	V_{tot} (LB) (mL)	V (mL)	A	[Ar_2CH^+] (M)	$A_0(V_0/V) - A$	[LB]$_0$ (M)	[LB]$_0$/[Ar_2CH^+]$_0$	[LB] (M)	$(A_0(V_0/V)-A)/A$
0	0	0	24.13	0.985	1.08×10^{-5}		0.000			
1	0.200	0.20	24.33	0.944	1.04×10^{-5}	0.033	8.27×10^{-5}	7.6	8.23×10^{-5}	0.035
2	0.200	0.40	24.53	0.915	1.01×10^{-5}	0.054	1.64×10^{-4}	15.8	1.63×10^{-4}	0.059
3	0.200	0.60	24.73	0.889	9.77×10^{-6}	0.072	2.44×10^{-4}	24.3	2.43×10^{-4}	0.081
4	0.200	0.80	24.93	0.864	9.50×10^{-6}	0.089	3.23×10^{-4}	33.0	3.22×10^{-4}	0.103
5	0.200	1.00	25.13	0.841	9.24×10^{-6}	0.105	4.00×10^{-4}	42.2	3.99×10^{-4}	0.125

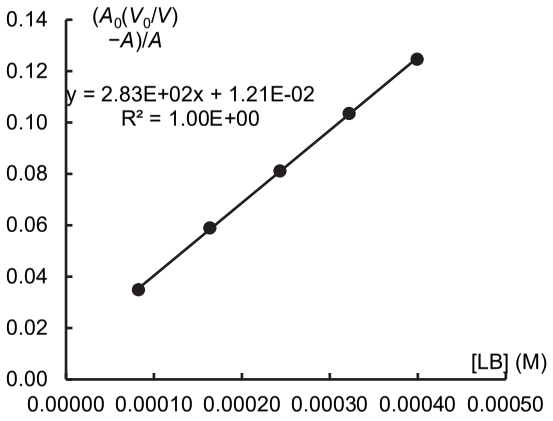

B4 + 3d (in MeCN, 20 °C, RM816), c(LB stock) = 1.01×10^{-2} M

Step	V(LB) (mL)	V_{tot} (LB) (mL)	V (mL)	A	[Ar_2CH^+] (M)	$A_0(V_0/V) - A$	[LB]$_0$ (M)	[LB]$_0$/[Ar_2CH^+]$_0$	[LB] (M)	$(A_0(V_0/V)-A)/A$
0	0	0	24.15	1.032	1.50×10^{-5}		0.000			
1	0.050	0.05	24.20	0.880	1.28×10^{-5}	0.150	2.08×10^{-5}	1.4	1.86×10^{-5}	0.170
2	0.050	0.10	24.25	0.765	1.11×10^{-5}	0.263	4.15×10^{-5}	3.3	3.77×10^{-5}	0.343
3	0.050	0.15	24.30	0.676	9.79×10^{-6}	0.350	6.21×10^{-5}	5.6	5.70×10^{-5}	0.517
4	0.050	0.20	24.35	0.607	8.79×10^{-6}	0.417	8.26×10^{-5}	8.4	7.66×10^{-5}	0.686
5	0.050	0.25	24.40	0.550	7.97×10^{-6}	0.471	1.03×10^{-4}	11.7	9.62×10^{-5}	0.857

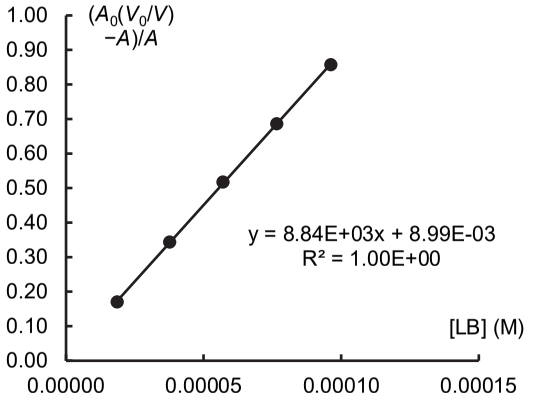

Step	V(LB) (mL)	V_{tot} (LB) (mL)	V (mL)	A	[Ar_2CH^+] (M)	$A_0(V_0/V) - A$	[LB]$_0$ (M)	[LB]$_0$/[Ar_2CH^+]$_0$	[LB] (M)	$(A_0(V_0/V)-A)/A$
0	0	0	24.15	1.030	1.49×10^{-5}		0.000			
1	0.050	0.05	24.20	0.877	1.27×10^{-5}	0.151	2.08×10^{-5}	1.4	1.86×10^{-5}	0.172
2	0.050	0.10	24.25	0.751	1.09×10^{-5}	0.275	4.15×10^{-5}	3.3	3.75×10^{-5}	0.366
3	0.050	0.15	24.30	0.658	9.53×10^{-6}	0.366	6.21×10^{-5}	5.7	5.68×10^{-5}	0.556
4	0.050	0.20	24.35	0.587	8.50×10^{-6}	0.435	8.26×10^{-5}	8.7	7.63×10^{-5}	0.740
5	0.050	0.25	24.40	0.528	7.65×10^{-6}	0.491	1.03×10^{-4}	12.1	9.59×10^{-5}	0.931

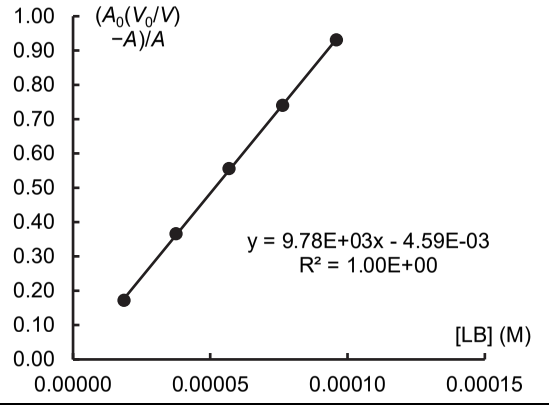

Step	V(LB) (mL)	V_{tot} (LB) (mL)	V (mL)	A	[Ar_2CH^+] (M)	$A_0(V_0/V) - A$	[LB]$_0$ (M)	[LB]$_0$/[Ar_2CH^+]$_0$	[LB] (M)	$(A_0(V_0/V)-A)/A$
0	0	0	24.15	1.041	1.51×10^{-5}		0.000			
1	0.050	0.05	24.20	0.895	1.30×10^{-5}	0.144	2.08×10^{-5}	1.4	1.87×10^{-5}	0.161
2	0.050	0.10	24.25	0.770	1.12×10^{-5}	0.267	4.15×10^{-5}	3.2	3.76×10^{-5}	0.346
3	0.050	0.15	24.30	0.679	9.84×10^{-6}	0.356	6.21×10^{-5}	5.6	5.69×10^{-5}	0.524
4	0.050	0.20	24.35	0.607	8.79×10^{-6}	0.425	8.26×10^{-5}	8.4	7.65×10^{-5}	0.701
5	0.050	0.25	24.40	0.549	7.95×10^{-6}	0.481	1.03×10^{-4}	11.7	9.61×10^{-5}	0.877

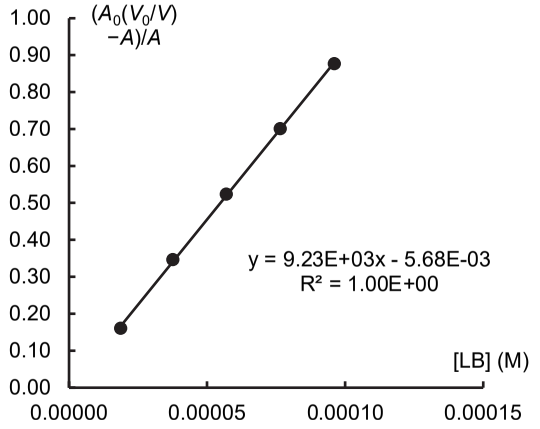

B2 + 3g (in MeCN, 10 °C, RM1034), *c*(LB stock) = 1.15×10^{-2} M

Step	*V* (LB) (mL)	V_{tot} (LB) (mL)	*V* (mL)	V_{corr} (mL)	*A*	$[Ar_2CH^+]$ (M)	$A_0(V_0/V) - A$	$[LB]_0$ (M)	$[LB]_0/[Ar_2CH^+]_0$	[LB] (M)	$(A_0(V_0/V)-A)/A$
0	0	0	24.15	23.82	1.041	1.25×10^{-5}		0.000			
1	0.020	0.02	24.17	23.83	0.456	5.49×10^{-6}	0.584	9.66×10^{-6}	0.8	2.62×10^{-6}	1.281
2	0.020	0.04	24.19	23.85	0.139	1.67×10^{-6}	0.900	1.93×10^{-5}	3.5	8.46×10^{-6}	6.477
3	0.020	0.06	24.21	23.87	0.067	8.07×10^{-7}	0.971	2.89×10^{-5}	17.3	1.72×10^{-5}	14.500
4	0.020	0.08	24.23	23.89	0.042	5.06×10^{-7}	0.996	3.85×10^{-5}	47.8	2.66×10^{-5}	23.705

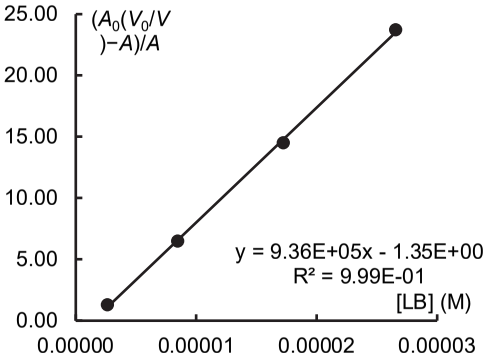

Step	*V* (LB) (mL)	V_{tot} (LB) (mL)	*V* (mL)	V_{corr} (mL)	*A*	$[Ar_2CH^+]$ (M)	$A_0(V_0/V) - A$	$[LB]_0$ (M)	$[LB]_0/[Ar_2CH^+]_0$	[LB] (M)	$(A_0(V_0/V)-A)/A$
0	0	0	24.15	23.82	1.051	1.27×10^{-5}		0.000			
1	0.020	0.02	24.17	23.83	0.411	4.95×10^{-6}	0.639	9.66×10^{-6}	0.8	1.96×10^{-6}	1.555
2	0.020	0.04	24.19	23.85	0.125	1.51×10^{-6}	0.924	1.93×10^{-5}	3.9	8.17×10^{-6}	7.395
3	0.020	0.06	24.21	23.87	0.065	7.83×10^{-7}	0.983	2.89×10^{-5}	19.2	1.71×10^{-5}	15.130
4	0.020	0.08	24.23	23.89	0.043	5.18×10^{-7}	1.005	3.85×10^{-5}	49.2	2.64×10^{-5}	23.363

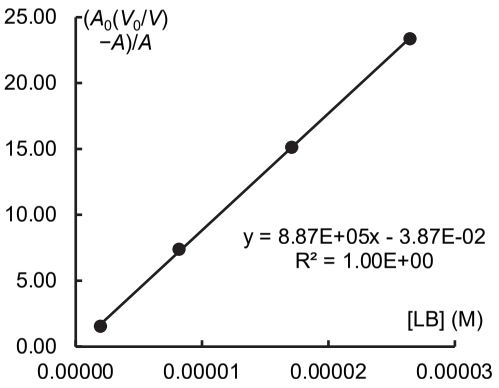

Step	V(LB) (mL)	V_{tot} (LB) (mL)	V (mL)	V_{corr} (mL)	A	$[Ar_2CH^+]$ (M)	$A_0(V_0/V) - A$	$[LB]_0$ (M)	$[LB]_0/[Ar_2CH^+]_0$	[LB] (M)	$(A_0(V_0/V)-A)/A$
0	0	0	24.15	23.82	1.039	1.25×10^{-5}		0.000			
1	0.020	0.02	24.17	23.83	0.532	6.41×10^{-6}	0.506	9.66×10^{-6}	0.8	3.56×10^{-6}	0.952
2	0.020	0.04	24.19	23.85	0.165	1.99×10^{-6}	0.872	1.93×10^{-5}	3.0	8.80×10^{-6}	5.287
3	0.020	0.06	24.21	23.87	0.075	9.04×10^{-7}	0.961	2.89×10^{-5}	14.6	1.74×10^{-5}	12.820
4	0.020	0.08	24.23	23.89	0.048	5.78×10^{-7}	0.988	3.85×10^{-5}	42.7	2.66×10^{-5}	20.576

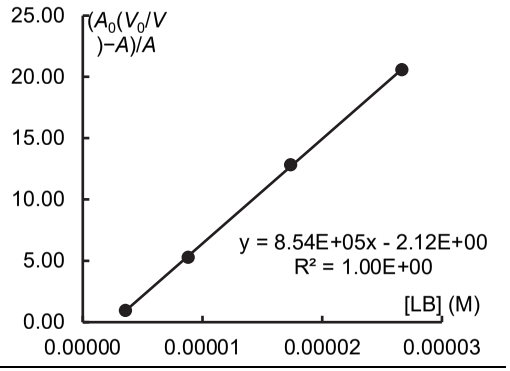

B2 + 3g (in MeCN, 20 °C, RM995), c(LB stock) = 1.28×10^{-2} M

Step	V(LB) (mL)	V_{tot} (LB) (mL)	V (mL)	A	$[Ar_2CH^+]$ (M)	$A_0(V_0/V) - A$	$[LB]_0$ (M)	$[LB]_0/[Ar_2CH^+]_0$	[LB] (M)	$(A_0(V_0/V)-A)/A$
0	0	0	24.09	1.106	1.33×10^{-5}		0.000			
1	0.020	0.02	24.11	0.525	6.33×10^{-6}	0.580	1.06×10^{-5}	0.8	3.61×10^{-6}	1.105
2	0.020	0.04	24.13	0.234	2.82×10^{-6}	0.870	2.12×10^{-5}	3.3	1.07×10^{-5}	3.719
3	0.020	0.06	24.15	0.135	1.63×10^{-6}	0.968	3.17×10^{-5}	11.3	2.01×10^{-5}	7.172
4	0.020	0.08	24.17	0.093	1.12×10^{-6}	1.009	4.23×10^{-5}	26.0	3.01×10^{-5}	10.853
5	0.020	0.10	24.19	0.069	8.31×10^{-7}	1.032	5.28×10^{-5}	47.1	4.04×10^{-5}	14.963

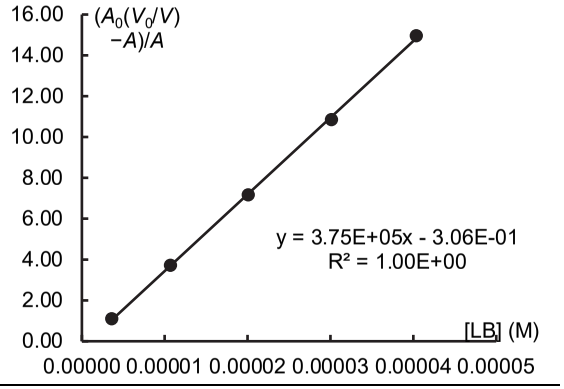

Step	V(LB) (mL)	V_{tot} (LB) (mL)	V (mL)	A	[Ar_2CH^+] (M)	$A_0(V_0/V) - A$	[LB]$_0$ (M)	[LB]$_0$/[Ar_2CH^+]$_0$	[LB] (M)	$(A_0(V_0/V)-A)/A$
0	0	0	24.09	1.204	1.45×10^{-5}		0.000			
1	0.020	0.02	24.11	0.597	7.19×10^{-6}	0.606	1.06×10^{-5}	0.7	3.29×10^{-6}	1.015
2	0.020	0.04	24.13	0.277	3.34×10^{-6}	0.925	2.12×10^{-5}	2.9	1.00×10^{-5}	3.339
3	0.020	0.06	24.15	0.158	1.90×10^{-6}	1.043	3.17×10^{-5}	9.5	1.92×10^{-5}	6.601
4	0.020	0.08	24.17	0.109	1.31×10^{-6}	1.091	4.23×10^{-5}	22.2	2.91×10^{-5}	10.009
5	0.020	0.10	24.19	0.082	9.88×10^{-7}	1.117	5.28×10^{-5}	40.2	3.93×10^{-5}	13.622

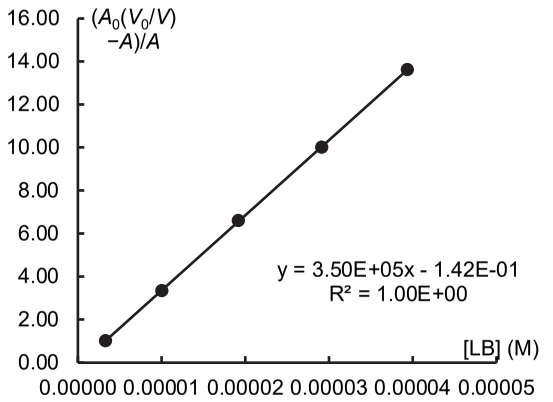

Step	V(LB) (mL)	V_{tot} (LB) (mL)	V (mL)	A	[Ar_2CH^+] (M)	$A_0(V_0/V) - A$	[LB]$_0$ (M)	[LB]$_0$/[Ar_2CH^+]$_0$	[LB] (M)	$(A_0(V_0/V)-A)/A$
0	0	0	24.09	1.221	1.47×10^{-5}		0.000			
1	0.020	0.02	24.11	0.622	7.49×10^{-6}	0.598	1.06×10^{-5}	0.7	3.39×10^{-6}	0.961
2	0.020	0.04	24.13	0.285	3.43×10^{-6}	0.934	2.12×10^{-5}	2.8	9.92×10^{-6}	3.277
3	0.020	0.06	24.15	0.166	2.00×10^{-6}	1.052	3.17×10^{-5}	9.2	1.91×10^{-5}	6.337
4	0.020	0.08	24.17	0.113	1.36×10^{-6}	1.104	4.23×10^{-5}	21.1	2.90×10^{-5}	9.770
5	0.020	0.10	24.19	0.086	1.04×10^{-6}	1.130	5.28×10^{-5}	38.8	3.92×10^{-5}	13.139

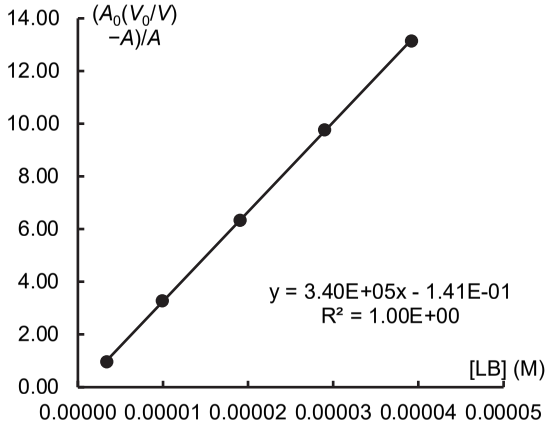

B2 + 3g (in MeCN, 30 °C, RM1034), *c*(LB stock) = 1.15×10^{-2} M

Step	*V* (LB) (mL)	V_{tot} (LB) (mL)	*V* (mL)	V_{corr} (mL)	*A*	$[Ar_2CH^+]$ (M)	$A_0(V_0/V) - A$	$[LB]_0$ (M)	$[LB]_0/[Ar_2CH^+]_0$	[LB] (M)	$(A_0(V_0/V)-A)/A$
0	0	0	24.15	24.50	0.988	1.19×10^{-5}		0.000			
1	0.020	0.02	24.17	24.52	0.602	7.25×10^{-6}	0.385	9.39×10^{-6}	0.8	4.75×10^{-6}	0.640
2	0.020	0.04	24.19	24.54	0.379	4.57×10^{-6}	0.607	1.88×10^{-5}	2.6	1.14×10^{-5}	1.603
3	0.020	0.06	24.21	24.56	0.263	3.17×10^{-6}	0.723	2.81×10^{-5}	6.2	1.94×10^{-5}	2.747
4	0.020	0.08	24.23	24.58	0.197	2.37×10^{-6}	0.788	3.75×10^{-5}	11.8	2.80×10^{-5}	3.999
5	0.020	0.10	24.25	24.60	0.157	1.89×10^{-6}	0.827	4.68×10^{-5}	19.7	3.68×10^{-5}	5.267

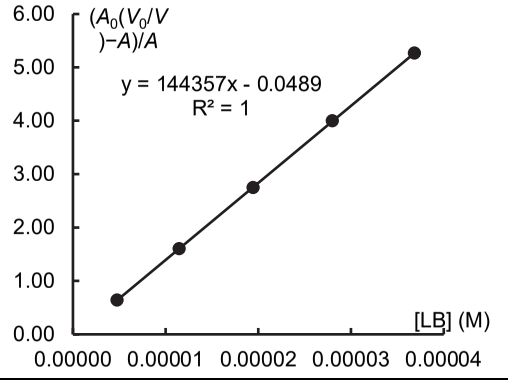

Step	*V* (LB) (mL)	V_{tot} (LB) (mL)	*V* (mL)	V_{corr} (mL)	*A*	$[Ar_2CH^+]$ (M)	$A_0(V_0/V) - A$	$[LB]_0$ (M)	$[LB]_0/[Ar_2CH^+]_0$	[LB] (M)	$(A_0(V_0/V)-A)/A$
0	0	0	24.15	24.50	0.988	1.19×10^{-5}		0.000			
1	0.020	0.02	24.17	24.52	0.602	7.25×10^{-6}	0.385	9.39×10^{-6}	0.8	4.75×10^{-6}	0.640
2	0.020	0.04	24.19	24.54	0.378	4.55×10^{-6}	0.608	1.88×10^{-5}	2.6	1.14×10^{-5}	1.609
3	0.020	0.06	24.21	24.56	0.263	3.17×10^{-6}	0.723	2.81×10^{-5}	6.2	1.94×10^{-5}	2.747
4	0.020	0.08	24.23	24.58	0.195	2.35×10^{-6}	0.790	3.75×10^{-5}	11.8	2.80×10^{-5}	4.050
5	0.020	0.10	24.25	24.60	0.157	1.89×10^{-6}	0.827	4.68×10^{-5}	19.9	3.68×10^{-5}	5.267

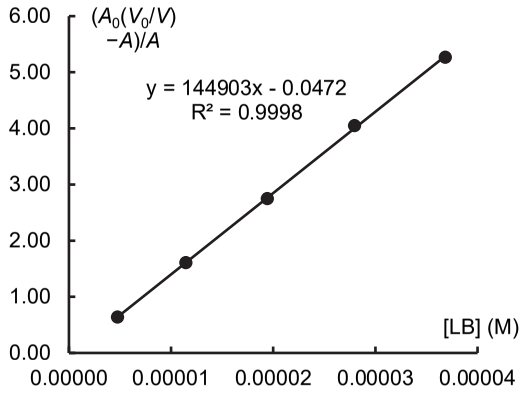

Step	V (LB) (mL)	V_{tot} (LB) (mL)	V (mL)	V_{corr} (mL)	A	$[Ar_2CH^+]$ (M)	$A_0(V_0/V) - A$	$[LB]_0$ (M)	$[LB]_0/[Ar_2CH^+]_0$	[LB] (M)	$(A_0(V_0/V)-A)/A$
0	0	0	24.15	24.50	1.002	1.21×10^{-5}		0.000			
1	0.020	0.02	24.17	24.52	0.623	7.51×10^{-6}	0.378	9.39×10^{-6}	0.8	4.84×10^{-6}	0.607
2	0.020	0.04	24.19	24.54	0.393	4.73×10^{-6}	0.607	1.88×10^{-5}	2.5	1.15×10^{-5}	1.545
3	0.020	0.06	24.21	24.56	0.272	3.28×10^{-6}	0.728	2.81×10^{-5}	5.9	1.94×10^{-5}	2.675
4	0.020	0.08	24.23	24.58	0.203	2.45×10^{-6}	0.796	3.75×10^{-5}	11.4	2.79×10^{-5}	3.920
5	0.020	0.10	24.25	24.60	0.163	1.96×10^{-6}	0.835	4.68×10^{-5}	19.1	3.67×10^{-5}	5.122

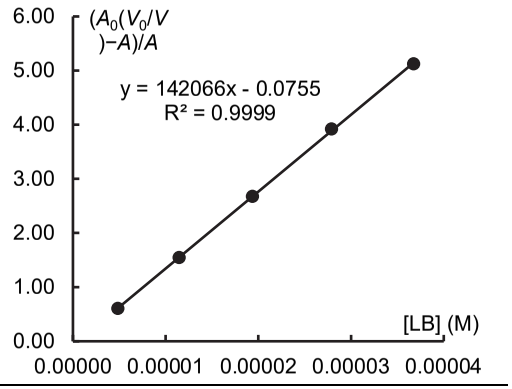

B2 + 3g (in MeCN, 40 °C, RM1034), c(LB stock) = 1.15×10^{-2} M

Step	V (LB) (mL)	V_{tot} (LB) (mL)	V (mL)	V_{corr} (mL)	A	$[Ar_2CH^+]$ (M)	$A_0(V_0/V) - A$	$[LB]_0$ (M)	$[LB]_0/[Ar_2CH^+]_0$	[LB] (M)	$(A_0(V_0/V)-A)/A$
0	0	0	24.15	24.85	0.942	1.13×10^{-5}		0.000			
1	0.020	0.02	24.17	24.87	0.686	8.27×10^{-6}	0.255	9.26×10^{-6}	0.8	6.18×10^{-6}	0.372
2	0.020	0.04	24.19	24.89	0.515	6.20×10^{-6}	0.425	1.85×10^{-5}	2.2	1.34×10^{-5}	0.826
3	0.020	0.06	24.21	24.91	0.404	4.87×10^{-6}	0.536	2.77×10^{-5}	4.5	2.13×10^{-5}	1.326
4	0.020	0.08	24.23	24.93	0.328	3.95×10^{-6}	0.611	3.69×10^{-5}	7.6	2.96×10^{-5}	1.862
5	0.020	0.10	24.25	24.95	0.276	3.33×10^{-6}	0.662	4.61×10^{-5}	11.7	3.82×10^{-5}	2.399

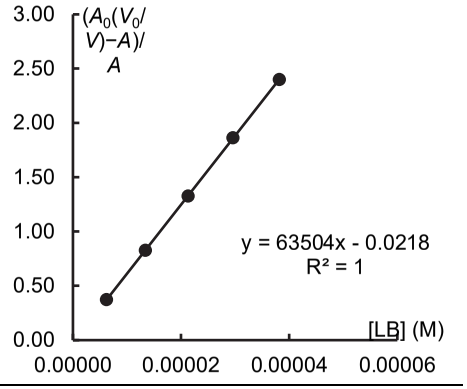

Step	V (LB) (mL)	V_{tot} (LB) (mL)	V (mL)	V_{corr} (mL)	A	$[Ar_2CH^+]$ (M)	$A_0(V_0/V) - A$	$[LB]_0$ (M)	$[LB]_0/[Ar_2CH^+]_0$	[LB] (M)	$(A_0(V_0/V)-A)/A$
0	0	0	24.15	24.85	0.968	1.17×10^{-5}		0.000			
1	0.020	0.02	24.17	24.87	0.699	8.42×10^{-6}	0.268	9.26×10^{-6}	0.8	6.03×10^{-6}	0.384
2	0.020	0.04	24.19	24.89	0.528	6.36×10^{-6}	0.438	1.85×10^{-5}	2.2	1.32×10^{-5}	0.830
3	0.020	0.06	24.21	24.91	0.417	5.02×10^{-6}	0.549	2.77×10^{-5}	4.4	2.11×10^{-5}	1.316
4	0.020	0.08	24.23	24.93	0.344	4.14×10^{-6}	0.621	3.69×10^{-5}	7.4	2.95×10^{-5}	1.805
5	0.020	0.10	24.25	24.95	0.288	3.47×10^{-6}	0.676	4.61×10^{-5}	11.1	3.80×10^{-5}	2.347

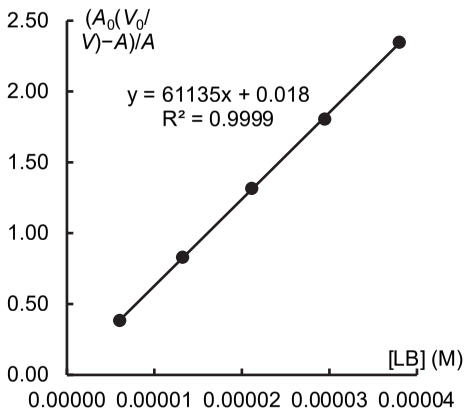

Step	V (LB) (mL)	V_{tot} (LB) (mL)	V (mL)	V_{corr} (mL)	A	$[Ar_2CH^+]$ (M)	$A_0(V_0/V) - A$	$[LB]_0$ (M)	$[LB]_0/[Ar_2CH^+]_0$	[LB] (M)	$(A_0(V_0/V)-A)/A$
0	0	0	24.15	24.85	0.983	1.18×10^{-5}		0.000			
1	0.020	0.02	24.17	24.87	0.715	8.61×10^{-6}	0.267	9.26×10^{-6}	0.8	6.04×10^{-6}	0.374
2	0.020	0.04	24.19	24.89	0.546	6.58×10^{-6}	0.435	1.85×10^{-5}	2.1	1.33×10^{-5}	0.797
3	0.020	0.06	24.21	24.91	0.430	5.18×10^{-6}	0.551	2.77×10^{-5}	4.2	2.11×10^{-5}	1.280
4	0.020	0.08	24.23	24.93	0.350	4.22×10^{-6}	0.630	3.69×10^{-5}	7.1	2.94×10^{-5}	1.799
5	0.020	0.10	24.25	24.95	0.295	3.55×10^{-6}	0.684	4.61×10^{-5}	10.9	3.79×10^{-5}	2.318

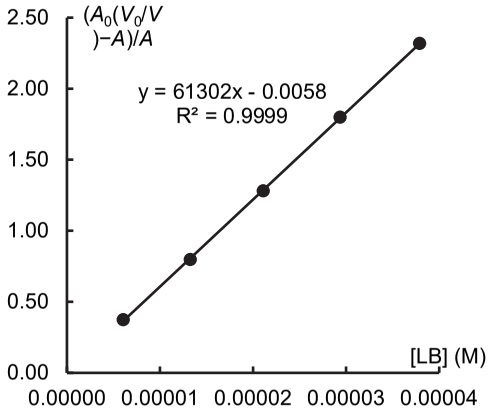

6.6 Benzhydrylium-Indicator Method of Titration (BIMT)

All BIMT measurements were performed in acetonitrile.

Summary – Equilibrium Constants from BIMT Experiments (in MeCN)

Lewis Acid	Lewis Base	T (°C)	Titration	K_I (M^{-1})
1a	**3a**	20.0	RM690-1	1.96×10^5
1a	**3a**	20.0	RM690-2	2.10×10^5
1a	**3a**	20.0	RM690-3	1.91×10^5
1a	**3a**	20.0	RM690-4	1.92×10^5
			Average	$(1.97 \pm 0.10) \times 10^5$
1c	**3a**	20.0	RM695-1	9.63×10^5
1c	**3a**	20.0	RM695-2	9.47×10^5
1c	**3a**	20.0	RM695-3	9.47×10^5
			Average	$(9.52 \pm 0.10) \times 10^5$
1d	**3a**	20.0	CYL054-1	5.00×10^6
1d	**3a**	20.0	CYL054-2	5.14×10^6
1d	**3a**	20.0	CYL054-3	5.15×10^6
			Average	$(5.10 \pm 0.09) \times 10^6$
1e	**3a**	20.0	CYL053-1	3.96×10^8
1e	**3a**	20.0	CYL053-2	4.16×10^8
1e	**3a**	20.0	CYL053-3	4.10×10^8
			Average	$(4.07 \pm 0.11) \times 10^8$
1f	**3a**	20.0	RM693-1	1.79×10^6
1f	**3a**	20.0	RM693-2	1.73×10^6
1f	**3a**	20.0	RM693-3	1.76×10^6
			Average	$(1.76 \pm 0.03) \times 10^6$
1g	**3a**	20.0	RM858-1	1.28×10^5
1g	**3a**	20.0	RM858-2	1.28×10^5
1g	**3a**	20.0	RM858-3	1.26×10^5
			Average	$(1.27 \pm 0.02) \times 10^5$
1h	**3a**	20.0	RM694-1	1.09×10^6
1h	**3a**	20.0	RM694-2	1.06×10^6
1h	**3a**	20.0	RM694-3	1.10×10^6
			Average	$(1.08 \pm 0.03) \times 10^6$
1i	**3a**	20.0	RM827-1	3.30×10^4
1i	**3a**	20.0	RM827-2	3.13×10^4
1i	**3a**	20.0	RM827-3	3.98×10^4
			Average	$(3.47 \pm 0.05) \times 10^4$
1j	**3a**	20.0	RM689-1	2.19×10^5
1j	**3a**	20.0	RM689-2	2.86×10^5
1j	**3a**	20.0	RM689-3	2.59×10^5
			Average	$(2.55 \pm 0.34) \times 10^5$
1k	**3a**	20.0	RM828-2	7.65×10^4

1k	**3a**	20.0	RM828-3	8.91×10^4
1k	**3a**	20.0	RM828-4	9.03×10^4
			Average	$(8.53 \pm 0.77) \times 10^4$
1l	**3a**	20.0	RM692-1	2.95×10^6
1l	**3a**	20.0	RM692-2	2.98×10^6
1l	**3a**	20.0	RM692-3	2.98×10^6
			Average	$(2.97 \pm 0.02) \times 10^6$
1m	**3a**	20.0	RM691-1	3.03×10^6
1m	**3a**	20.0	RM691-2	2.92×10^6
1m	**3a**	20.0	RM691-3	3.15×10^6
			Average	$(3.03 \pm 0.12) \times 10^6$
1n	**3a**	20.0	RM1225-1	4.91×10^4
1n	**3a**	20.0	RM1225-2	6.86×10^4
1n	**3a**	20.0	RM1225-3	6.00×10^4
			Average	$(5.92 \pm 0.98) \times 10^4$
2a	**3a**	20.0	CYL055-1	1.22×10^7
2a	**3a**	20.0	CYL055-2	1.30×10^7
2a	**3a**	20.0	CYL055-3	1.30×10^7
			Average	$(1.27 \pm 0.05) \times 10^7$
2b	**3a**	20.0	RM696-3	9.03×10^7
2b	**3a**	20.0	RM696-4	8.96×10^7
2b	**3a**	20.0	RM696-5	9.26×10^7
			Average	$(9.08 \pm 0.16) \times 10^7$
2c	**3a**	20.0	RM697-2	5.39×10^5
2c	**3a**	20.0	RM697-3	4.86×10^5
2c	**3a**	20.0	RM697-4	5.45×10^5
			Average	$(5.23 \pm 0.33) \times 10^5$
1a	**3b**	20.0	RM821-1	5.23×10^4
1a	**3b**	20.0	RM821-2	5.19×10^4
1a	**3b**	20.0	RM821-3	4.44×10^4
			Average	$(4.95 \pm 0.45) \times 10^4$
1f	**3b**	20.0	RM822-1	7.01×10^5
1f	**3b**	20.0	RM822-2	5.60×10^5
1f	**3b**	20.0	RM822-3	4.89×10^5
			Average	$(5.83 \pm 1.08) \times 10^5$
2a	**3b**	20.0	RM823-1	2.81×10^6
2a	**3b**	20.0	RM823-2	3.21×10^6
2a	**3b**	20.0	RM823-5	3.35×10^6
			Average	$(3.12 \pm 0.28) \times 10^6$
1a	**3c**	20.0	RM812-1	1.58×10^4
1a	**3c**	20.0	RM812-2	1.75×10^4
1a	**3c**	20.0	RM812-4	1.70×10^4
			Average	$(1.68 \pm 0.09) \times 10^4$

1f	**3c**	20.0	RM813-1	1.63×10^5
1f	**3c**	20.0	RM813-2	1.65×10^5
1f	**3c**	20.0	RM813-3	1.49×10^5
			Average	$(1.59 \pm 0.09) \times 10^5$
2a	**3c**	20.0	RM814-1	8.87×10^5
2a	**3c**	20.0	RM814-2	9.91×10^5
2a	**3c**	20.0	RM814-3	1.03×10^6
			Average	$(9.69 \pm 0.74) \times 10^5$
1a	**3d**	20.0	RM700-2	3.00×10^4
1a	**3d**	20.0	RM700-3	2.90×10^4
1a	**3d**	20.0	RM700-4	2.91×10^4
			Average	$(2.94 \pm 0.06) \times 10^4$
1f	**3d**	20.0	RM701-1	2.42×10^5
1f	**3d**	20.0	RM701-2	2.51×10^5
1f	**3d**	20.0	RM701-3	2.52×10^5
			Average	$(2.48 \pm 0.06) \times 10^5$
2a	**3d**	20.0	RM1040-1	1.36×10^6
2a	**3d**	20.0	RM1040-2	1.51×10^6
2a	**3d**	20.0	RM1040-3	1.36×10^6
			Average	$(1.41 \pm 0.09) \times 10^6$
1a	**3e**	20.0	RM830-1	1.09×10^4
1a	**3e**	20.0	RM830-2	1.70×10^4
1a	**3e**	20.0	RM830-3	2.19×10^4
			Average	$(1.66 \pm 0.56) \times 10^4$
1e	**3e**	20.0	RM803-1	5.92×10^6
1e	**3e**	20.0	RM803-3	6.79×10^6
1e	**3e**	20.0	RM803-4	7.00×10^6
			Average	$(6.57 \pm 0.58) \times 10^6$
2a	**3e**	20.0	RM947-2	9.62×10^5
2a	**3e**	20.0	RM947-3	1.03×10^6
2a	**3e**	20.0	RM947-4	9.68×10^5
			Average	$(9.87 \pm 0.38) \times 10^5$
2b	**3e**	20.0	RM835-1	4.80×10^6
2b	**3e**	20.0	RM835-2	4.73×10^6
2b	**3e**	20.0	RM835-3	4.64×10^6
			Average	$(4.72 \pm 0.08) \times 10^6$
2c	**3e**	20.0	RM836-1	1.32×10^5
2c	**3e**	20.0	RM836-2	1.22×10^5
2c	**3e**	20.0	RM836-3	1.22×10^5
			Average	$(1.25 \pm 0.06) \times 10^5$
1a	**3f**	20.0	RM790-2	1.08×10^2
1a	**3f**	20.0	RM790-3	1.08×10^2

1a	**3f**	20.0	RM790-5	1.01×10^2
			Average	$(1.06 \pm 0.05) \times 10^2$
1c	**3f**	20.0	RM796-1	2.02×10^2
1c	**3f**	20.0	RM796-2	1.72×10^2
1c	**3f**	20.0	RM796-3	1.81×10^2
			Average	$(1.85 \pm 0.15) \times 10^2$
1d	**3f**	20.0	RM795-2	8.86×10^2
1d	**3f**	20.0	RM795-3	8.96×10^2
1d	**3f**	20.0	RM795-4	8.31×10^2
			Average	$(8.71 \pm 0.35) \times 10^2$
1e	**3f**	20.0	RM794-1	9.16×10^3
1e	**3f**	20.0	RM794-2	7.67×10^3
1e	**3f**	20.0	RM794-3	9.19×10^3
			Average	$(8.68 \pm 0.86) \times 10^2$
1f	**3f**	20.0	RM792-1	3.10×10^2
1f	**3f**	20.0	RM792-2	2.71×10^2
1f	**3f**	20.0	RM792-3	2.94×10^2
			Average	$(2.92 \pm 0.20) \times 10^2$
1h	**3f**	20.0	RM797-1	1.87×10^2
1h	**3f**	20.0	RM797-2	1.61×10^2
1h	**3f**	20.0	RM797-3	1.56×10^2
			Average	$(1.68 \pm 0.17) \times 10^2$
1j	**3f**	20.0	RM800-1	1.32×10^2
1j	**3f**	20.0	RM800-2	1.24×10^2
1j	**3f**	20.0	RM800-3	1.25×10^2
			Average	$(1.27 \pm 0.05) \times 10^2$
1l	**3f**	20.0	RM798-1	3.00×10^2
1l	**3f**	20.0	RM798-2	3.24×10^2
1l	**3f**	20.0	RM798-3	3.32×10^2
			Average	$(3.19 \pm 0.17) \times 10^2$
1m	**3f**	20.0	RM799-1	6.73×10^2
1m	**3f**	20.0	RM799-2	6.57×10^2
1m	**3f**	20.0	RM799-3	6.57×10^2
			Average	$(6.62 \pm 0.09) \times 10^2$
2a	**3f**	20.0	RM793-1	9.07×10^2
2a	**3f**	20.0	RM793-2	1.11×10^3
2a	**3f**	20.0	RM793-3	1.00×10^3
			Average	$(1.00 \pm 0.91) \times 10^3$
1a	**3g**	−10.0	RM1041-M10-1	2.40×10^3
1a	**3g**	−10.0	RM1041-M10-2	2.55×10^3
1a	**3g**	−10.0	RM1041-M10-3	2.86×10^3
			Average	$(2.60 \pm 0.24) \times 10^3$

1a	**3g**	0.0	RM1041-0-1	1.87×10^3
1a	**3g**	0.0	RM1041-0-2	1.01×10^3
1a	**3g**	0.0	RM1041-0-4	9.63×10^2
			Average	$(1.28 \pm 0.52) \times 10^3$
1a	**3g**	10.0	RM1035-10-1	4.19×10^2
1a	**3g**	10.0	RM1035-10-2	4.54×10^2
1a	**3g**	10.0	RM1035-10-3	4.27×10^2
			Average	$(4.33 \pm 0.19) \times 10^2$
1a	**3g**	20.0	RM1035-20-1	2.89×10^2
1a	**3g**	20.0	RM1035-20-2	2.63×10^2
1a	**3g**	20.0	RM1035-20-3	2.45×10^2
			Average	$(2.66 \pm 0.23) \times 10^2$
1d	**3g**	20.0	RM1038-1	1.33×10^3
1d	**3g**	20.0	RM1038-2	1.33×10^3
1d	**3g**	20.0	RM1038-3	1.30×10^3
			Average	$(1.32 \pm 0.02) \times 10^3$
1e	**3g**	20.0	RM1042-1	1.14×10^5
1e	**3g**	20.0	RM1042-2	1.10×10^5
1e	**3g**	20.0	RM1042-3	1.30×10^5
			Average	$(1.18 \pm 0.11) \times 10^5$
1f	**3g**	20.0	RM1036-1	8.49×10^2
1f	**3g**	20.0	RM1036-2	8.52×10^2
1f	**3g**	20.0	RM1036-3	8.74×10^2
			Average	$(8.58 \pm 0.14) \times 10^2$
2a	**3g**	20.0	RM1037-1	9.32×10^2
2a	**3g**	20.0	RM1037-2	9.55×10^2
2a	**3g**	20.0	RM1037-3	1.08×10^3
			Average	$(9.89 \pm 0.80) \times 10^2$

Van't Hoff Analysis for the Reaction of 1a with 3g

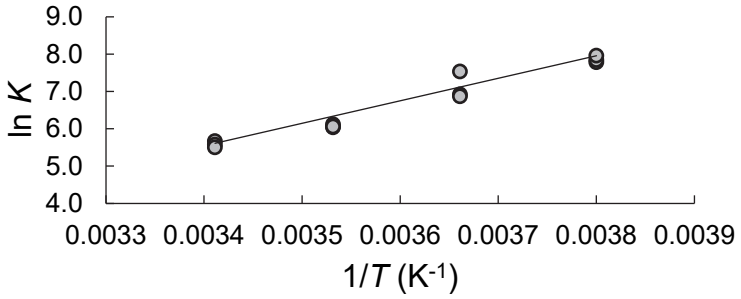

$\ln K_I = (6.09 \pm 0.42) \times 10^3\ 1/T - (15.3 \pm 1.5)$, $R^2 = 0.956$

$\Delta H = (-50.6 \pm 3.5)$ kJ mol^{-1}

$\Delta S = (-127 \pm 13)$ J mol^{-1} K^{-1}

1a + 3a (20 °C) - RM690

BIMT experiment (MeCN, 20 °C) for the benzoate ion **3a** with **1a** (stock solution: 23.1 mM) competing against the benzhydrylium ion **B2** (605 nm, ε = 1.66 × 10^5 M^{-1} cm^{-1}, K = 5.25 × 10^7 M^{-1} from LA and LB).

RM690-1

Titration						
Entry	$V_{tot,\,LB}$ (mL)	V (mL)	A	$[Ar_2CH^+]$ (M)	$A_0*(V_0/V)$-A	$[LB]_0$ (M)
1	–	24.08	**1.032**	1.24×10^{-5}		
2	0.03	24.11	**0.475**	5.72×10^{-6}	0.556	6.72×10^{-6}

Cross-Titration											
Entry	$V_{tot,\,Ar2I+}$ (mL)	V (mL)	A	$[Ar_2CH^+]$ (M)	$[LB]_0(V_0/V)$ (M)	$[Ar_2I^+]_{0,i}$ (M)	$[Ar_2I^+]_0$/ $[LB]_0(V_0/V)$	$(A_0*(V_0/V)$-$A)/A$	[LB] (M)	$[Ar_2I$-LB] (M)	$[Ar_2I^+]$ (M)	$[Ar_2I$-LB]/ [LB]
1	0.10	24.21	0.504	6.07×10^{-6}	6.69×10^{-6}	9.54×10^{-5}	14.3	1.04	1.98×10^{-8}	3.75×10^{-7}	9.51×10^{-5}	1.90×10^{1}
2	0.20	24.31	0.526	6.34×10^{-6}	6.66×10^{-6}	1.90×10^{-4}	28.5	0.94	1.80×10^{-8}	6.66×10^{-7}	1.89×10^{-4}	3.70×10^{1}
3	0.30	24.41	0.545	6.56×10^{-6}	6.64×10^{-6}	2.84×10^{-4}	42.8	0.87	1.66×10^{-8}	9.14×10^{-7}	2.83×10^{-4}	5.52×10^{1}
4	0.40	24.51	0.561	6.76×10^{-6}	6.61×10^{-6}	3.77×10^{-4}	57.1	0.81	1.54×10^{-8}	1.14×10^{-6}	3.76×10^{-4}	7.39×10^{1}
5	0.50	24.61	0.575	6.93×10^{-6}	6.58×10^{-6}	4.69×10^{-4}	71.3	0.76	1.44×10^{-8}	1.33×10^{-6}	4.68×10^{-4}	9.22×10^{1}

RM690-2

Titration						
Entry	$V_{tot,\,LB}$ (mL)	V (mL)	A	$[Ar_2CH^+]$ (M)	$A_0*(V_0/V)$-A	$[LB]_0$ (M)
1	–	24.08	**1.040**	1.25×10^{-5}		
2	0.03	24.11	**0.513**	6.18×10^{-6}	0.526	6.35×10^{-6}

Entry	$V_{tot,\,Ar2I+}$ (mL)	V (mL)	A	$[Ar_2CH^+]$ (M)	$[LB]_0(V_0/V)$ (M)	$[Ar_2I^+]_{0,i}$ (M)	$[Ar_2I^+]_0$/ $[LB]_0(V_0/V)$	$(A_0*(V_0/V)$-$A)/A$	[LB] (M)	$[Ar_2I$-LB] (M)	$[Ar_2I^+]$ (M)	$[Ar_2I$-LB]/ [LB]
1	0.10	24.21	0.543	6.54×10^{-6}	6.33×10^{-6}	9.54×10^{-5}	15.1	0.91	1.73×10^{-8}	3.83×10^{-7}	9.51×10^{-5}	2.22×10^{1}
2	0.20	24.31	0.565	6.81×10^{-6}	6.30×10^{-6}	1.90×10^{-4}	30.2	0.82	1.57×10^{-8}	6.81×10^{-7}	1.89×10^{-4}	4.34×10^{1}
3	0.30	24.41	0.581	7.00×10^{-6}	6.28×10^{-6}	2.84×10^{-4}	45.3	0.77	1.46×10^{-8}	9.00×10^{-7}	2.83×10^{-4}	6.17×10^{1}
4	0.40	24.51	0.597	7.19×10^{-6}	6.25×10^{-6}	3.77×10^{-4}	60.3	0.71	1.36×10^{-8}	1.12×10^{-6}	3.76×10^{-4}	8.25×10^{1}
5	0.50	24.61	0.609	7.34×10^{-6}	6.22×10^{-6}	4.69×10^{-4}	75.4	0.67	1.28×10^{-8}	1.29×10^{-6}	4.68×10^{-4}	1.01×10^{2}

RM690-3

Titration						
Entry	$V_{tot,\,LB}$ (mL)	V (mL)	A	$[Ar_2CH^+]$ (M)	$A_0*(V_0/V)$-A	$[LB]_0$ (M)
1	–	24.08	**1.038**	1.25×10^{-5}		
2	0.04	24.12	**0.314**	3.78×10^{-6}	0.722	8.75×10^{-6}

Entry	$V_{tot,\,Ar2I+}$ (mL)	V (mL)	A	$[Ar_2CH^+]$ (M)	$[LB]_0(V_0/V)$ (M)	$[Ar_2I^+]_{0,i}$ (M)	$[Ar_2I^+]_0/[LB]_0(V_0/V)$	$(A_0*(V_0/V)-A)/A$	[LB] (M)	[Ar$_2$I-LB] (M)	$[Ar_2I^+]$ (M)	[Ar$_2$I-LB]/[LB]
1	0.10	24.22	0.365	4.40×10^{-6}	8.71×10^{-6}	9.54×10^{-5}	11.0	1.83	3.48×10^{-8}	6.39×10^{-7}	9.48×10^{-5}	1.83×10^{1}
2	0.20	24.32	0.400	4.82×10^{-6}	8.67×10^{-6}	1.90×10^{-4}	21.9	1.57	2.99×10^{-8}	1.08×10^{-6}	1.89×10^{-4}	3.61×10^{1}
3	0.30	24.42	0.428	5.15×10^{-6}	8.64×10^{-6}	2.84×10^{-4}	32.9	1.39	2.66×10^{-8}	1.43×10^{-6}	2.82×10^{-4}	5.39×10^{1}
4	0.40	24.52	0.452	5.45×10^{-6}	8.60×10^{-6}	3.77×10^{-4}	43.8	1.26	2.39×10^{-8}	1.74×10^{-6}	3.75×10^{-4}	7.29×10^{1}
5	0.50	24.62	0.470	5.66×10^{-6}	8.57×10^{-6}	4.69×10^{-4}	54.8	1.16	2.21×10^{-8}	1.97×10^{-6}	4.67×10^{-4}	8.90×10^{1}

RM690-4

Titration						
Entry	$V_{tot,\,LB}$ (mL)	V (mL)	A	$[Ar_2CH^+]$ (M)	$A_0*(V_0/V)$-A	$[LB]_0$ (M)
1	–	24.08	**1.046**	1.26×10^{-5}		
2	0.04	24.12	**0.330**	3.97×10^{-6}	0.715	8.65×10^{-6}

Entry	$V_{tot,\,Ar2I+}$ (mL)	V (mL)	A	$[Ar_2CH^+]$ (M)	$[LB]_0(V_0/V)$ (M)	$[Ar_2I^+]_{0,i}$ (M)	$[Ar_2I^+]_0/[LB]_0(V_0/V)$	$(A_0*(V_0/V)-A)/A$	[LB] (M)	[Ar$_2$I-LB] (M)	$[Ar_2I^+]$ (M)	[Ar$_2$I-LB]/[LB]
1	0.10	24.22	0.384	4.63×10^{-6}	8.62×10^{-6}	9.54×10^{-5}	11.1	1.71	3.25×10^{-8}	6.82×10^{-7}	9.47×10^{-5}	2.09×10^{1}
2	0.20	24.32	0.412	4.96×10^{-6}	8.58×10^{-6}	1.90×10^{-4}	22.1	1.51	2.88×10^{-8}	1.04×10^{-6}	1.89×10^{-4}	3.60×10^{1}
3	0.30	24.42	0.439	5.29×10^{-6}	8.55×10^{-6}	2.84×10^{-4}	33.2	1.35	2.57×10^{-8}	1.38×10^{-6}	2.82×10^{-4}	5.38×10^{1}
4	0.40	24.52	0.464	5.59×10^{-6}	8.51×10^{-6}	3.77×10^{-4}	44.3	1.21	2.31×10^{-8}	1.70×10^{-6}	3.75×10^{-4}	7.36×10^{1}
5	0.50	24.62	0.483	5.82×10^{-6}	8.48×10^{-6}	4.69×10^{-4}	55.4	1.12	2.13×10^{-8}	1.95×10^{-6}	4.67×10^{-4}	9.15×10^{1}

1c + 3a (20 °C) - RM695

BIMT experiment (MeCN, 20 °C) for the benzoate ion **3a** with **1c** (stock solution: 11.0 mM) competing against the benzhydrylium ion **B2** (605 nm, ε = 1.66 × 10^5 M^{-1} cm^{-1}, K = 5.25 × 10^7 M^{-1} from LA and LB).

RM695-1

Titration						
Entry	$V_{tot,\,LB}$ (mL)	V (mL)	A	$[Ar_2CH^+]$ (M)	$A_0*(V_0/V)$-A	$[LB]_0$ (M)
1	–	24.10	**1.070**	1.29×10^{-5}		
2	0.04	24.14	**0.323**	3.89×10^{-6}	0.745	9.02×10^{-6}

Entry	$V_{tot,\,Ar2I+}$ (mL)	V (mL)	A	$[Ar_2CH^+]$ (M)	$[LB]_0(V_0/V)$ (M)	$[Ar_2I^+]_{0,i}$ (M)	$[Ar_2I^+]_0$/ $[LB]_0(V_0/V)$	$(A_0*(V_0/V)$-A)/A	[LB] (M)	$[Ar_2I$-LB] (M)	$[Ar_2I^+]$ (M)	$[Ar_2I$-LB]/ [LB]
1	0.10	24.24	0.423	5.10×10^{-6}	8.99×10^{-6}	4.52×10^{-5}	5.0	1.51	2.89×10^{-8}	1.24×10^{-6}	4.40×10^{-5}	4.28×10^{1}
2	0.20	24.34	0.482	5.81×10^{-6}	8.95×10^{-6}	9.01×10^{-5}	10.1	1.20	2.28×10^{-8}	1.97×10^{-6}	8.81×10^{-5}	8.62×10^{1}
3	0.30	24.44	0.522	6.29×10^{-6}	8.91×10^{-6}	1.35×10^{-4}	15.1	1.02	1.95×10^{-8}	2.47×10^{-6}	1.32×10^{-4}	1.27×10^{2}
4	0.40	24.54	0.555	6.69×10^{-6}	8.88×10^{-6}	1.79×10^{-4}	20.1	0.89	1.70×10^{-8}	2.88×10^{-6}	1.76×10^{-4}	1.69×10^{2}
5	0.50	24.64	0.582	7.01×10^{-6}	8.84×10^{-6}	2.22×10^{-4}	25.2	0.80	1.52×10^{-8}	3.23×10^{-6}	2.19×10^{-4}	2.12×10^{2}

RM695-2

Titration						
Entry	$V_{tot,\,LB}$ (mL)	V (mL)	A	$[Ar_2CH^+]$ (M)	$A_0*(V_0/V)$-A	$[LB]_0$ (M)
1	–	24.10	**1.079**	1.30×10^{-5}		
2	0.04	24.14	**0.348**	4.19×10^{-6}	0.729	8.83×10^{-6}

Entry	$V_{tot,\,Ar2I+}$ (mL)	V (mL)	A	$[Ar_2CH^+]$ (M)	$[LB]_0(V_0/V)$ (M)	$[Ar_2I^+]_{0,i}$ (M)	$[Ar_2I^+]_0$/ $[LB]_0(V_0/V)$	$(A_0*(V_0/V)$-A)/A	[LB] (M)	$[Ar_2I$-LB] (M)	$[Ar_2I^+]$ (M)	$[Ar_2I$-LB]/ [LB]
1	0.10	24.24	0.445	5.36×10^{-6}	8.79×10^{-6}	4.52×10^{-5}	5.1	1.41	2.69×10^{-8}	1.20×10^{-6}	4.40×10^{-5}	4.46×10^{1}
2	0.20	24.34	0.501	6.04×10^{-6}	8.75×10^{-6}	9.01×10^{-5}	10.3	1.13	2.16×10^{-8}	1.90×10^{-6}	8.82×10^{-5}	8.79×10^{1}
3	0.30	24.44	0.540	6.51×10^{-6}	8.72×10^{-6}	1.35×10^{-4}	15.4	0.97	1.85×10^{-8}	2.39×10^{-6}	1.32×10^{-4}	1.29×10^{2}
4	0.40	24.54	0.571	6.88×10^{-6}	8.68×10^{-6}	1.79×10^{-4}	20.6	0.86	1.63×10^{-8}	2.78×10^{-6}	1.76×10^{-4}	1.70×10^{2}
5	0.50	24.64	0.596	7.18×10^{-6}	8.65×10^{-6}	2.22×10^{-4}	25.7	0.77	1.47×10^{-8}	3.10×10^{-6}	2.19×10^{-4}	2.11×10^{2}

RM695-3

Titration						
Entry	$V_{tot,\,LB}$ (mL)	V (mL)	A	$[Ar_2CH^+]$ (M)	$A_0*(V_0/V)$-A	$[LB]_0$ (M)
1	–	24.10	**1.076**	1.30×10^{-5}		
2	0.04	24.14	**0.313**	3.77×10^{-6}	0.761	9.22×10^{-6}

Entry	$V_{tot,\,Ar2I+}$ (mL)	V (mL)	A	$[Ar_2CH^+]$ (M)	$[LB]_0(V_0/V)$ (M)	$[Ar_2I^+]_{0,i}$ (M)	$[Ar_2I^+]_0/[LB]_0(V_0/V)$	$(A_0*(V_0/V)-A)/A$	[LB] (M)	$[Ar_2I$-LB] (M)	$[Ar_2I^+]$ (M)	$[Ar_2I$-LB]/[LB]
1	0.10	24.24	0.418	5.04×10^{-6}	9.18×10^{-6}	4.52×10^{-5}	4.9	1.56	2.97×10^{-8}	1.30×10^{-6}	4.39×10^{-5}	4.37×10^{1}
2	0.20	24.34	0.478	5.76×10^{-6}	9.14×10^{-6}	9.01×10^{-5}	9.9	1.23	2.34×10^{-8}	2.04×10^{-6}	8.80×10^{-5}	8.72×10^{1}
3	0.30	24.44	0.520	6.26×10^{-6}	9.10×10^{-6}	1.35×10^{-4}	14.8	1.04	1.99×10^{-8}	2.56×10^{-6}	1.32×10^{-4}	1.29×10^{2}
4	0.40	24.54	0.552	6.65×10^{-6}	9.07×10^{-6}	1.79×10^{-4}	19.7	0.91	1.74×10^{-8}	2.97×10^{-6}	1.76×10^{-4}	1.70×10^{2}
5	0.50	24.64	0.577	6.95×10^{-6}	9.03×10^{-6}	2.22×10^{-4}	24.6	0.82	1.57×10^{-8}	3.29×10^{-6}	2.19×10^{-4}	2.09×10^{2}

1d + 3a (20 °C) - CYL054

BIMT experiment (MeCN, 20 °C) for the benzoate ion **3a** with **1d** (stock solution: 18.7 mM) competing against the benzhydrylium ion **B2** (605 nm, ε = 1.66×10^5 M^{-1} cm^{-1}, K = 5.25×10^7 M^{-1} from LA and LB).

CYL054-1

Titration						
Entry	$V_{tot,\,LB}$ (mL)	V (mL)	A	$[Ar_2CH^+]$ (M)	$A_0*(V_0/V)$-A	$[LB]_0$ (M)
1	–	23.55	**1.064**	1.28×10^{-5}		
2	0.03	23.58	**0.204**	2.46×10^{-6}	0.859	1.04×10^{-5}

Entry	$V_{tot,\,Ar2I+}$ (mL)	V (mL)	A	$[Ar_2CH^+]$ (M)	$[LB]_0(V_0/V)$ (M)	$[Ar_2I^+]_{0,i}$ (M)	$[Ar_2I^+]_0/[LB]_0(V_0/V)$	$(A_0*(V_0/V)-A)/A$	[LB] (M)	$[Ar_2I$-LB] (M)	$[Ar_2I^+]$ (M)	$[Ar_2I$-LB]/[LB]
1	0.01	23.59	0.343	4.13×10^{-6}	1.04×10^{-5}	7.92×10^{-6}	0.8	2.10	4.00×10^{-8}	1.72×10^{-6}	6.20×10^{-6}	4.29×10^{1}
2	0.02	23.60	0.406	4.89×10^{-6}	1.04×10^{-5}	1.58×10^{-5}	1.5	1.62	3.08×10^{-8}	2.49×10^{-6}	1.33×10^{-5}	8.08×10^{1}
3	0.04	23.62	0.490	5.90×10^{-6}	1.04×10^{-5}	3.16×10^{-5}	3.0	1.16	2.22×10^{-8}	3.51×10^{-6}	2.81×10^{-5}	1.58×10^{2}
4	0.06	23.64	0.551	6.64×10^{-6}	1.04×10^{-5}	4.74×10^{-5}	4.6	0.92	1.76×10^{-8}	4.25×10^{-6}	4.32×10^{-5}	2.41×10^{2}
5	0.10	23.68	0.628	7.57×10^{-6}	1.04×10^{-5}	7.89×10^{-5}	7.6	0.68	1.31×10^{-8}	5.19×10^{-6}	7.37×10^{-5}	3.97×10^{2}
6	0.15	23.73	0.692	8.34×10^{-6}	1.04×10^{-5}	1.18×10^{-4}	11.4	0.53	1.00×10^{-8}	5.96×10^{-6}	1.12×10^{-4}	5.95×10^{2}
7	0.20	23.78	0.734	8.84×10^{-6}	1.03×10^{-5}	1.57×10^{-4}	15.2	0.44	8.30×10^{-9}	6.48×10^{-6}	1.51×10^{-4}	7.80×10^{2}
8	0.30	23.88	0.790	9.52×10^{-6}	1.03×10^{-5}	2.35×10^{-4}	22.8	0.33	6.25×10^{-9}	7.16×10^{-6}	2.28×10^{-4}	1.15×10^{3}

CYL054-2

Titration						
Entry	$V_{tot,\,LB}$ (mL)	V (mL)	A	$[Ar_2CH^+]$ (M)	$A_0*(V_0/V)$-A	$[LB]_0$ (M)
1	–	23.55	**1.064**	1.28×10^{-5}		
2	0.03	23.58	**0.200**	2.41×10^{-6}	0.863	1.05×10^{-5}

Entry	$V_{tot,\,Ar2I+}$ (mL)	V (mL)	A	$[Ar_2CH^+]$ (M)	$[LB]_0(V_0/V)$ (M)	$[Ar_2I^+]_{0,i}$ (M)	$[Ar_2I^+]_0/[LB]_0(V_0/V)$	$(A_0*(V_0/V)\text{-}A)/A$	[LB] (M)	$[Ar_2I\text{-}LB]$ (M)	$[Ar_2I^+]$ (M)	$[Ar_2I\text{-}LB]/[LB]$
1	0.02	23.60	0.384	4.63×10^{-6}	1.05×10^{-5}	1.58×10^{-5}	1.5	1.76	3.36×10^{-8}	2.27×10^{-6}	1.36×10^{-5}	6.74×10^{1}
2	0.04	23.62	0.482	5.81×10^{-6}	1.05×10^{-5}	3.16×10^{-5}	3.0	1.20	2.29×10^{-8}	3.46×10^{-6}	2.82×10^{-5}	1.51×10^{2}
3	0.06	23.64	0.545	6.57×10^{-6}	1.04×10^{-5}	4.74×10^{-5}	4.5	0.94	1.80×10^{-8}	4.23×10^{-6}	4.32×10^{-5}	2.35×10^{2}
4	0.10	23.68	0.626	7.54×10^{-6}	1.04×10^{-5}	7.89×10^{-5}	7.6	0.69	1.32×10^{-8}	5.21×10^{-6}	7.37×10^{-5}	3.96×10^{2}
5	0.15	23.73	0.690	8.31×10^{-6}	1.04×10^{-5}	1.18×10^{-4}	11.3	0.53	1.01×10^{-8}	5.99×10^{-6}	1.12×10^{-4}	5.93×10^{2}
6	0.20	23.78	0.735	8.86×10^{-6}	1.04×10^{-5}	1.57×10^{-4}	15.1	0.43	8.26×10^{-9}	6.54×10^{-6}	1.51×10^{-4}	7.91×10^{2}
7	0.30	23.88	0.792	9.54×10^{-6}	1.03×10^{-5}	2.35×10^{-4}	22.7	0.32	6.19×10^{-9}	7.24×10^{-6}	2.27×10^{-4}	1.17×10^{3}

CYL054-3

Titration						
Entry	$V_{tot,\,LB}$ (mL)	V (mL)	A	$[Ar_2CH^+]$ (M)	$A_0*(V_0/V)$-A	$[LB]_0$ (M)
1	–	23.55	**1.045**	1.26×10^{-5}		
2	0.03	23.58	**0.191**	2.30×10^{-6}	0.853	1.04×10^{-5}

Entry	$V_{tot,\,Ar2I+}$ (mL)	V (mL)	A	$[Ar_2CH^+]$ (M)	$[LB]_0(V_0/V)$ (M)	$[Ar_2I^+]_{0,i}$ (M)	$[Ar_2I^+]_0/[LB]_0(V_0/V)$	$(A_0*(V_0/V)\text{-}A)/A$	[LB] (M)	$[Ar_2I\text{-}LB]$ (M)	$[Ar_2I^+]$ (M)	$[Ar_2I\text{-}LB]/[LB]$
1	0.02	23.60	0.391	4.71×10^{-6}	1.03×10^{-5}	1.58×10^{-5}	1.5	1.67	3.18×10^{-8}	2.46×10^{-6}	1.34×10^{-5}	7.76×10^{1}
2	0.04	23.62	0.478	5.76×10^{-6}	1.03×10^{-5}	3.16×10^{-5}	3.1	1.18	2.25×10^{-8}	3.52×10^{-6}	2.81×10^{-5}	1.57×10^{2}
3	0.06	23.64	0.535	6.45×10^{-6}	1.03×10^{-5}	4.74×10^{-5}	4.6	0.95	1.80×10^{-8}	4.22×10^{-6}	4.32×10^{-5}	2.34×10^{2}
4	0.10	23.68	0.616	7.42×10^{-6}	1.03×10^{-5}	7.89×10^{-5}	7.6	0.69	1.31×10^{-8}	5.20×10^{-6}	7.37×10^{-5}	3.97×10^{2}
5	0.15	23.73	0.680	8.19×10^{-6}	1.03×10^{-5}	1.18×10^{-4}	11.5	0.53	1.00×10^{-8}	5.98×10^{-6}	1.12×10^{-4}	5.98×10^{2}
6	0.20	23.78	0.724	8.72×10^{-6}	1.03×10^{-5}	1.57×10^{-4}	15.3	0.43	8.18×10^{-9}	6.52×10^{-6}	1.51×10^{-4}	7.97×10^{2}
7	0.30	23.88	0.780	9.40×10^{-6}	1.02×10^{-5}	2.35×10^{-4}	22.9	0.32	6.12×10^{-9}	7.20×10^{-6}	2.28×10^{-4}	1.18×10^{3}

1e + 3a (20 °C) - CYL053

BIMT experiment (MeCN, 20 °C) for the benzoate ion **3a** with **1e** (stock solution: 13.2 mM) competing against the benzhydrylium ion **B2** (605 nm, ε = 1.66 × 10^5 M^{-1} cm^{-1}, K = 5.25 × 10^7 M^{-1} from LA and LB).

CYL053-1

Titration						
Entry	$V_{tot,\,LB}$ (mL)	V (mL)	A	$[Ar_2CH^+]$ (M)	$A_0*(V_0/V)$-A	$[LB]_0$ (M)
1	–	23.55	**1.067**	1.29×10^{-5}		
2	0.025	23.58	**0.363**	4.37×10^{-6}	0.703	8.51×10^{-6}

Entry	$V_{tot,\,Ar2I+}$ (mL)	V (mL)	A	$[Ar_2CH^+]$ (M)	$[LB]_0(V_0/V)$ (M)	$[Ar_2I^+]_{0,i}$ (M)	$[Ar_2I^+]_0$/ $[LB]_0(V_0/V)$	$(A_0*(V_0/V)$-A)/A	[LB] (M)	$[Ar_2I$-LB] (M)	$[Ar_2I^+]$ (M)	$[Ar_2I$-LB]/ [LB]
1	0.02	23.60	0.766	9.23×10^{-6}	8.50×10^{-6}	1.12×10^{-5}	1.3	0.39	7.44×10^{-9}	4.89×10^{-6}	6.28×10^{-6}	6.57×10^{2}
2	0.03	23.61	0.921	1.11×10^{-5}	8.49×10^{-6}	1.67×10^{-5}	2.0	0.16	2.97×10^{-9}	6.76×10^{-6}	9.99×10^{-6}	2.28×10^{3}
3	0.04	23.62	0.977	1.18×10^{-5}	8.49×10^{-6}	2.23×10^{-5}	2.6	0.09	1.70×10^{-9}	7.44×10^{-6}	1.49×10^{-5}	4.38×10^{3}
4	0.05	23.63	0.998	1.20×10^{-5}	8.49×10^{-6}	2.79×10^{-5}	3.3	0.07	1.25×10^{-9}	7.70×10^{-6}	2.02×10^{-5}	6.14×10^{3}

CYL053-2

Titration						
Entry	$V_{tot,\,LB}$ (mL)	V (mL)	A	$[Ar_2CH^+]$ (M)	$A_0*(V_0/V)$-A	$[LB]_0$ (M)
1	–	23.55	**1.035**	1.25×10^{-5}		
2	0.030	23.58	**0.196**	2.36×10^{-6}	0.838	1.02×10^{-5}

Entry	$V_{tot,\,Ar2I+}$ (mL)	V (mL)	A	$[Ar_2CH^+]$ (M)	$[LB]_0(V_0/V)$ (M)	$[Ar_2I^+]_{0,i}$ (M)	$[Ar_2I^+]_0$/ $[LB]_0(V_0/V)$	$(A_0*(V_0/V)$-A)/A	[LB] (M)	$[Ar_2I$-LB] (M)	$[Ar_2I^+]$ (M)	$[Ar_2I$-LB]/ [LB]
1	0.02	23.60	0.627	7.55×10^{-6}	1.02×10^{-5}	1.12×10^{-5}	1.1	0.65	1.23×10^{-8}	5.26×10^{-6}	5.90×10^{-6}	4.27×10^{2}
2	0.03	23.61	0.824	9.93×10^{-6}	1.02×10^{-5}	1.67×10^{-5}	1.6	0.25	4.82×10^{-9}	7.65×10^{-6}	9.10×10^{-6}	1.59×10^{3}
3	0.04	23.62	0.914	1.10×10^{-5}	1.02×10^{-5}	2.23×10^{-5}	2.2	0.13	2.46×10^{-9}	8.73×10^{-6}	1.36×10^{-5}	3.55×10^{3}
4	0.05	23.63	0.956	1.15×10^{-5}	1.02×10^{-5}	2.79×10^{-5}	2.7	0.08	1.50×10^{-9}	9.24×10^{-6}	1.86×10^{-5}	6.14×10^{3}
5	0.06	23.64	0.969	1.17×10^{-5}	1.01×10^{-5}	3.34×10^{-5}	3.3	0.06	1.22×10^{-9}	9.40×10^{-6}	2.40×10^{-5}	7.70×10^{3}

CYL053-3

Titration						
Entry	$V_{tot,\,LB}$ (mL)	V (mL)	A	$[Ar_2CH^+]$ (M)	$A_0*(V_0/V)-A$	$[LB]_0$ (M)
1	–	23.55	**1.044**	1.26×10^{-5}		
2	0.03	23.58	**0.196**	2.36×10^{-6}	0.847	1.03×10^{-5}

Entry	$V_{tot,\,Ar2I+}$ (mL)	V (mL)	A	$[Ar_2CH^+]$ (M)	$[LB]_0(V_0/V)$ (M)	$[Ar_2I^+]_{0,i}$ (M)	$[Ar_2I^+]_0/[LB]_0(V_0/V)$	$(A_0*(V_0/V)-A)/A$	[LB] (M)	$[Ar_2I$-LB] (M)	$[Ar_2I^+]$ (M)	$[Ar_2I$-LB]/[LB]
1	0.02	23.60	0.641	7.72×10^{-6}	1.03×10^{-5}	1.12×10^{-5}	1.1	0.63	1.19×10^{-8}	5.43×10^{-6}	5.73×10^{-6}	4.56×10^{2}
2	0.03	23.61	0.821	9.89×10^{-6}	1.03×10^{-5}	1.67×10^{-5}	1.6	0.27	5.11×10^{-9}	7.61×10^{-6}	9.13×10^{-6}	1.49×10^{3}
3	0.04	23.62	0.924	1.11×10^{-5}	1.03×10^{-5}	2.23×10^{-5}	2.2	0.13	2.41×10^{-9}	8.85×10^{-6}	1.35×10^{-5}	3.67×10^{3}
4	0.05	23.63	0.963	1.16×10^{-5}	1.03×10^{-5}	2.79×10^{-5}	2.7	0.08	1.53×10^{-9}	9.33×10^{-6}	1.86×10^{-5}	6.08×10^{3}
5	0.06	23.64	0.976	1.18×10^{-5}	1.03×10^{-5}	3.34×10^{-5}	3.3	0.07	1.25×10^{-9}	9.48×10^{-6}	2.40×10^{-5}	7.59×10^{3}

1f + 3a (20 °C) - RM693

BIMT experiment (MeCN, 20 °C) for the benzoate ion **3a** with **1f** (stock solution: 16.9 mM) competing against the benzhydrylium ion **B2** (605 nm, ε = 1.66×10^5 M^{-1} cm^{-1}, K = 5.25×10^7 M^{-1} from LA and LB).

RM693-1

Titration						
Entry	$V_{tot,\,LB}$ (mL)	V (mL)	A	$[Ar_2CH^+]$ (M)	$A_0*(V_0/V)-A$	$[LB]_0$ (M)
1	–	24.10	**1.046**	1.26×10^{-5}		
2	0.05	24.15	**0.074**	8.92×10^{-7}	0.970	1.19×10^{-5}

Entry	$V_{tot,\,Ar2I+}$ (mL)	V (mL)	A	$[Ar_2CH^+]$ (M)	$[LB]_0(V_0/V)$ (M)	$[Ar_2I^+]_{0,i}$ (M)	$[Ar_2I^+]_0/[LB]_0(V_0/V)$	$(A_0*(V_0/V)-A)/A$	[LB] (M)	$[Ar_2I$-LB] (M)	$[Ar_2I^+]$ (M)	$[Ar_2I$-LB]/[LB]
1	0.10	24.25	0.389	4.69×10^{-6}	1.19×10^{-5}	6.98×10^{-5}	5.9	1.67	3.19×10^{-8}	4.02×10^{-6}	6.58×10^{-5}	1.26×10^{2}
2	0.20	24.35	0.493	5.94×10^{-6}	1.18×10^{-5}	1.39×10^{-4}	11.7	1.10	2.10×10^{-8}	5.28×10^{-6}	1.34×10^{-4}	2.52×10^{2}
3	0.30	24.45	0.558	6.72×10^{-6}	1.18×10^{-5}	2.08×10^{-4}	17.6	0.85	1.62×10^{-8}	6.07×10^{-6}	2.02×10^{-4}	3.76×10^{2}
4	0.40	24.55	0.603	7.27×10^{-6}	1.17×10^{-5}	2.76×10^{-4}	23.5	0.70	1.34×10^{-8}	6.62×10^{-6}	2.69×10^{-4}	4.94×10^{2}
5	0.50	24.65	0.637	7.67×10^{-6}	1.17×10^{-5}	3.43×10^{-4}	29.4	0.61	1.15×10^{-8}	7.03×10^{-6}	3.36×10^{-4}	6.10×10^{2}

RM693-2

Titration						
Entry	$V_{tot,\,LB}$ (mL)	V (mL)	A	$[Ar_2CH^+]$ (M)	$A_0*(V_0/V)$-A	$[LB]_0$ (M)
1	–	24.10	**1.055**	1.27×10^{-5}		
2	0.04	24.14	**0.280**	3.37×10^{-6}	0.773	9.37×10^{-6}

Entry	$V_{tot,\,Ar2I+}$ (mL)	V (mL)	A	$[Ar_2CH^+]$ (M)	$[LB]_0(V_0/V)$ (M)	$[Ar_2I^+]_{0,i}$ (M)	$[Ar_2I^+]_0/[LB]_0(V_0/V)$	$(A_0*(V_0/V)-A)/A$	[LB] (M)	$[Ar_2I$-LB] (M)	$[Ar_2I^+]$ (M)	$[Ar_2I$-LB]/[LB]
1	0.10	24.24	0.501	6.04×10^{-6}	9.33×10^{-6}	6.98×10^{-5}	7.5	1.09	2.08×10^{-8}	2.71×10^{-6}	6.71×10^{-5}	1.30×10^{2}
2	0.20	24.34	0.587	7.07×10^{-6}	9.29×10^{-6}	1.39×10^{-4}	15.0	0.78	1.49×10^{-8}	3.76×10^{-6}	1.35×10^{-4}	2.53×10^{2}
3	0.30	24.44	0.641	7.72×10^{-6}	9.25×10^{-6}	2.08×10^{-4}	22.4	0.62	1.19×10^{-8}	4.43×10^{-6}	2.03×10^{-4}	3.73×10^{2}
4	0.40	24.54	0.679	8.18×10^{-6}	9.22×10^{-6}	2.76×10^{-4}	29.9	0.53	1.00×10^{-8}	4.90×10^{-6}	2.71×10^{-4}	4.89×10^{2}
5	0.50	24.64	0.707	8.51×10^{-6}	9.18×10^{-6}	3.43×10^{-4}	37.4	0.46	8.78×10^{-9}	5.25×10^{-6}	3.38×10^{-4}	5.98×10^{2}

RM693-3

Titration						
Entry	$V_{tot,\,LB}$ (mL)	V (mL)	A	$[Ar_2CH^+]$ (M)	$A_0*(V_0/V)$-A	$[LB]_0$ (M)
1	–	24.10	**1.066**	1.28×10^{-5}		
2	0.04	24.14	**0.285**	3.43×10^{-6}	0.779	9.44×10^{-6}

Entry	$V_{tot,\,Ar2I+}$ (mL)	V (mL)	A	$[Ar_2CH^+]$ (M)	$[LB]_0(V_0/V)$ (M)	$[Ar_2I^+]_{0,i}$ (M)	$[Ar_2I^+]_0/[LB]_0(V_0/V)$	$(A_0*(V_0/V)-A)/A$	[LB] (M)	$[Ar_2I$-LB] (M)	$[Ar_2I^+]$ (M)	$[Ar_2I$-LB]/[LB]
1	0.10	24.24	0.501	6.04×10^{-6}	9.40×10^{-6}	6.98×10^{-5}	7.4	1.12	2.13×10^{-8}	2.65×10^{-6}	6.72×10^{-5}	1.25×10^{2}
2	0.20	24.34	0.590	7.11×10^{-6}	9.36×10^{-6}	1.39×10^{-4}	14.8	0.79	1.50×10^{-8}	3.74×10^{-6}	1.35×10^{-4}	2.49×10^{2}
3	0.30	24.44	0.646	7.78×10^{-6}	9.32×10^{-6}	2.08×10^{-4}	22.3	0.63	1.20×10^{-8}	4.43×10^{-6}	2.03×10^{-4}	3.71×10^{2}
4	0.40	24.54	0.685	8.25×10^{-6}	9.29×10^{-6}	2.76×10^{-4}	29.7	0.53	1.01×10^{-8}	4.92×10^{-6}	2.71×10^{-4}	4.88×10^{2}
5	0.50	24.64	0.714	8.60×10^{-6}	9.25×10^{-6}	3.43×10^{-4}	37.1	0.46	8.77×10^{-9}	5.28×10^{-6}	3.38×10^{-4}	6.02×10^{2}

1g + 3a (20 °C) - RM858

BIMT experiment (MeCN, 20 °C) for the benzoate ion **3a** with **1g** (stock solution: 23.5 mM) competing against the benzhydrylium ion **B2** (605 nm, ε = 1.66 × 10^5 M^{-1} cm^{-1}, K = 5.25 × 10^7 M^{-1} from LA and LB).

RM858-1

Titration						
Entry	$V_{tot,\,LB}$ (mL)	V (mL)	A	$[Ar_2CH^+]$ (M)	$A_0*(V_0/V)$-A	$[LB]_0$ (M)
1	–	24.10	**1.073**	1.29×10^{-5}		
2	0.05	24.15	**0.465**	5.60×10^{-6}	0.606	7.32×10^{-6}

Entry	$V_{tot,\,Ar2I+}$ (mL)	V (mL)	A	$[Ar_2CH^+]$ (M)	$[LB]_0(V_0/V)$ (M)	$[Ar_2I^+]_{0,i}$ (M)	$[Ar_2I^+]_0$/ $[LB]_0(V_0/V)$	$(A_0*(V_0/V)$-A)/A	[LB] (M)	$[Ar_2I$-LB] (M)	$[Ar_2I^+]$ (M)	$[Ar_2I$-LB]/ [LB]
1	0.20	24.35	0.504	6.07×10^{-6}	7.26×10^{-6}	1.93×10^{-4}	26.5	1.11	2.11×10^{-8}	5.19×10^{-7}	1.92×10^{-4}	2.46×10^{1}
2	0.40	24.55	0.531	6.40×10^{-6}	7.20×10^{-6}	3.82×10^{-4}	53.1	0.98	1.87×10^{-8}	8.92×10^{-7}	3.81×10^{-4}	4.76×10^{1}
3	0.60	24.75	0.553	6.66×10^{-6}	7.15×10^{-6}	5.69×10^{-4}	79.6	0.89	1.69×10^{-8}	1.20×10^{-6}	5.68×10^{-4}	7.10×10^{1}
4	0.80	24.95	0.572	6.89×10^{-6}	7.09×10^{-6}	7.52×10^{-4}	106.1	0.81	1.55×10^{-8}	1.48×10^{-6}	7.51×10^{-4}	9.55×10^{1}
5	1.00	25.15	0.587	7.07×10^{-6}	7.03×10^{-6}	9.33×10^{-4}	132.7	0.75	1.43×10^{-8}	1.70×10^{-6}	9.31×10^{-4}	1.19×10^{2}

RM858-2

Titration						
Entry	$V_{tot,\,LB}$ (mL)	V (mL)	A	$[Ar_2CH^+]$ (M)	$A_0*(V_0/V)$-A	$[LB]_0$ (M)
1	–	24.10	**1.049**	1.26×10^{-5}		
2	0.05	24.15	**0.413**	4.98×10^{-6}	0.634	7.67×10^{-6}

Entry	$V_{tot,\,Ar2I+}$ (mL)	V (mL)	A	$[Ar_2CH^+]$ (M)	$[LB]_0(V_0/V)$ (M)	$[Ar_2I^+]_{0,i}$ (M)	$[Ar_2I^+]_0$/ $[LB]_0(V_0/V)$	$(A_0*(V_0/V)$-A)/A	[LB] (M)	$[Ar_2I$-LB] (M)	$[Ar_2I^+]$ (M)	$[Ar_2I$-LB]/ [LB]
1	0.20	24.35	0.457	5.51×10^{-6}	7.60×10^{-6}	1.93×10^{-4}	25.3	1.27	2.42×10^{-8}	5.76×10^{-7}	1.92×10^{-4}	2.38×10^{1}
2	0.40	24.55	0.488	5.88×10^{-6}	7.54×10^{-6}	3.82×10^{-4}	50.7	1.11	2.12×10^{-8}	9.92×10^{-7}	3.81×10^{-4}	4.69×10^{1}
3	0.60	24.75	0.513	6.18×10^{-6}	7.48×10^{-6}	5.69×10^{-4}	76.0	0.99	1.89×10^{-8}	1.34×10^{-6}	5.67×10^{-4}	7.07×10^{1}
4	0.80	24.95	0.533	6.42×10^{-6}	7.42×10^{-6}	7.52×10^{-4}	101.4	0.90	1.72×10^{-8}	1.62×10^{-6}	7.51×10^{-4}	9.41×10^{1}
5	1.00	25.15	0.550	6.63×10^{-6}	7.36×10^{-6}	9.33×10^{-4}	126.7	0.83	1.58×10^{-8}	1.86×10^{-6}	9.31×10^{-4}	1.18×10^{2}

RM858-3

Titration						
Entry	$V_{tot,\,LB}$ (mL)	V (mL)	A	$[Ar_2CH^+]$ (M)	$A_0*(V_0/V)$-A	$[LB]_0$ (M)
1	–	24.10	**1.045**	1.26×10^{-5}		
2	0.05	24.15	**0.400**	4.82×10^{-6}	0.643	7.78×10^{-6}

Entry	$V_{tot,\,Ar2I+}$ (mL)	V (mL)	A	$[Ar_2CH^+]$ (M)	$[LB]_0(V_0/V)$ (M)	$[Ar_2I^+]_{0,i}$ (M)	$[Ar_2I^+]_0/[LB]_0(V_0/V)$	$(A_0*(V_0/V)\text{-}A)/A$	[LB] (M)	$[Ar_2I\text{-}LB]$ (M)	$[Ar_2I^+]$ (M)	$[Ar_2I\text{-}LB]/[LB]$
1	0.20	24.35	0.445	5.36×10^{-6}	7.71×10^{-6}	1.93×10^{-4}	25.0	1.32	2.52×10^{-8}	5.87×10^{-7}	1.92×10^{-4}	2.33×10^{1}
2	0.40	24.55	0.477	5.75×10^{-6}	7.65×10^{-6}	3.82×10^{-4}	50.0	1.15	2.19×10^{-8}	1.01×10^{-6}	3.81×10^{-4}	4.63×10^{1}
3	0.60	24.75	0.502	6.05×10^{-6}	7.59×10^{-6}	5.69×10^{-4}	75.0	1.03	1.96×10^{-8}	1.36×10^{-6}	5.67×10^{-4}	6.93×10^{1}
4	0.80	24.95	0.523	6.30×10^{-6}	7.53×10^{-6}	7.52×10^{-4}	100.0	0.93	1.77×10^{-8}	1.65×10^{-6}	7.51×10^{-4}	9.30×10^{1}
5	1.00	25.15	0.540	6.51×10^{-6}	7.47×10^{-6}	9.33×10^{-4}	124.9	0.85	1.63×10^{-8}	1.89×10^{-6}	9.31×10^{-4}	1.16×10^{2}

1h + 3a (20 °C) - RM694

BIMT experiment (MeCN, 20 °C) for the benzoate ion **3a** with **1h** (stock solution: 11.2 mM) competing against the benzhydrylium ion **B2** (605 nm, ε = 1.66×10^5 M^{-1} cm^{-1}, K = 5.25×10^7 M^{-1} from LA and LB).

RM694-1

Titration						
Entry	$V_{tot,\,LB}$ (mL)	V (mL)	A	$[Ar_2CH^+]$ (M)	$A_0*(V_0/V)$-A	$[LB]_0$ (M)
1	–	24.10	**1.061**	1.28×10^{-5}		
2	0.04	24.14	**0.277**	3.34×10^{-6}	0.782	9.48×10^{-6}

Entry	$V_{tot,\,Ar2I+}$ (mL)	V (mL)	A	$[Ar_2CH^+]$ (M)	$[LB]_0(V_0/V)$ (M)	$[Ar_2I^+]_{0,i}$ (M)	$[Ar_2I^+]_0/[LB]_0(V_0/V)$	$(A_0*(V_0/V)\text{-}A)/A$	[LB] (M)	$[Ar_2I\text{-}LB]$ (M)	$[Ar_2I^+]$ (M)	$[Ar_2I\text{-}LB]/[LB]$
1	0.10	24.24	0.406	4.89×10^{-6}	9.44×10^{-6}	4.63×10^{-5}	4.9	1.60	3.05×10^{-8}	1.59×10^{-6}	4.47×10^{-5}	5.19×10^{1}
2	0.20	24.34	0.472	5.69×10^{-6}	9.40×10^{-6}	9.21×10^{-5}	9.8	1.23	2.34×10^{-8}	2.41×10^{-6}	8.97×10^{-5}	1.03×10^{2}
3	0.30	24.44	0.518	6.24×10^{-6}	9.36×10^{-6}	1.38×10^{-4}	14.7	1.02	1.94×10^{-8}	2.98×10^{-6}	1.35×10^{-4}	1.53×10^{2}
4	0.40	24.54	0.552	6.65×10^{-6}	9.32×10^{-6}	1.83×10^{-4}	19.6	0.89	1.69×10^{-8}	3.40×10^{-6}	1.79×10^{-4}	2.01×10^{2}
5	0.50	24.64	0.579	6.98×10^{-6}	9.29×10^{-6}	2.28×10^{-4}	24.5	0.79	1.51×10^{-8}	3.74×10^{-6}	2.24×10^{-4}	2.48×10^{2}

RM694-2

Titration						
Entry	$V_{tot,\,LB}$ (mL)	V (mL)	A	$[Ar_2CH^+]$ (M)	$A_0*(V_0/V)$-A	$[LB]_0$ (M)
1	–	24.10	**1.067**	1.29×10^{-5}		
2	0.04	24.14	**0.281**	3.39×10^{-6}	0.784	9.50×10^{-6}

Entry	$V_{tot,\,Ar2I+}$ (mL)	V (mL)	A	$[Ar_2CH^+]$ (M)	$[LB]_0(V_0/V)$ (M)	$[Ar_2I^+]_{0,i}$ (M)	$[Ar_2I^+]_0/[LB]_0(V_0/V)$	$(A_0*(V_0/V)-A)/A$	[LB] (M)	$[Ar_2I$-LB] (M)	$[Ar_2I^+]$ (M)	$[Ar_2I$-LB]/[LB]
1	0.10	24.24	0.411	4.95×10^{-6}	9.46×10^{-6}	4.63×10^{-5}	4.9	1.58	3.01×10^{-8}	1.60×10^{-6}	4.47×10^{-5}	5.32×10^{1}
2	0.20	24.34	0.475	5.72×10^{-6}	9.42×10^{-6}	9.21×10^{-5}	9.8	1.22	2.33×10^{-8}	2.39×10^{-6}	8.97×10^{-5}	1.03×10^{2}
3	0.30	24.44	0.520	6.27×10^{-6}	9.39×10^{-6}	1.38×10^{-4}	14.7	1.02	1.95×10^{-8}	2.95×10^{-6}	1.35×10^{-4}	1.51×10^{2}
4	0.40	24.54	0.553	6.66×10^{-6}	9.35×10^{-6}	1.83×10^{-4}	19.6	0.89	1.71×10^{-8}	3.37×10^{-6}	1.79×10^{-4}	1.97×10^{2}
5	0.50	24.64	0.580	6.99×10^{-6}	9.31×10^{-6}	2.28×10^{-4}	24.4	0.80	1.52×10^{-8}	3.71×10^{-6}	2.24×10^{-4}	2.43×10^{2}

RM694-3

Titration						
Entry	$V_{tot,\,LB}$ (mL)	V (mL)	A	$[Ar_2CH^+]$ (M)	$A_0*(V_0/V)$-A	$[LB]_0$ (M)
1	–	24.10	**1.078**	1.30×10^{-5}		
2	0.04	24.14	**0.309**	3.72×10^{-6}	0.767	9.29×10^{-6}

Entry	$V_{tot,\,Ar2I+}$ (mL)	V (mL)	A	$[Ar_2CH^+]$ (M)	$[LB]_0(V_0/V)$ (M)	$[Ar_2I^+]_{0,i}$ (M)	$[Ar_2I^+]_0/[LB]_0(V_0/V)$	$(A_0*(V_0/V)-A)/A$	[LB] (M)	$[Ar_2I$-LB] (M)	$[Ar_2I^+]$ (M)	$[Ar_2I$-LB]/[LB]
1	0.10	24.24	0.429	5.17×10^{-6}	9.25×10^{-6}	4.63×10^{-5}	5.0	1.50	2.85×10^{-8}	1.48×10^{-6}	4.48×10^{-5}	5.18×10^{1}
2	0.20	24.34	0.493	5.94×10^{-6}	9.21×10^{-6}	9.21×10^{-5}	10.0	1.17	2.22×10^{-8}	2.27×10^{-6}	8.99×10^{-5}	1.02×10^{2}
3	0.30	24.44	0.538	6.48×10^{-6}	9.18×10^{-6}	1.38×10^{-4}	15.0	0.98	1.86×10^{-8}	2.83×10^{-6}	1.35×10^{-4}	1.52×10^{2}
4	0.40	24.54	0.572	6.89×10^{-6}	9.14×10^{-6}	1.83×10^{-4}	20.0	0.85	1.62×10^{-8}	3.26×10^{-6}	1.80×10^{-4}	2.01×10^{2}
5	0.50	24.64	0.599	7.22×10^{-6}	9.10×10^{-6}	2.28×10^{-4}	25.0	0.76	1.45×10^{-8}	3.60×10^{-6}	2.24×10^{-4}	2.49×10^{2}

1i + 3a (20 °C) - RM827

BIMT experiment (MeCN, 20 °C) for the benzoate ion **3a** with **1i** (stock solution: 24.7 mM) competing against the benzhydrylium ion **B2** (605 nm, ε = 1.66 × 10^5 M^{-1} cm^{-1}, K = 5.25 × 10^7 M^{-1} from LA and LB).

RM827-1

Titration						
Entry	$V_{tot,\,LB}$ (mL)	V (mL)	A	$[Ar_2CH^+]$ (M)	$A_0*(V_0/V)$-A	$[LB]_0$ (M)
1	–	24.09	**1.003**	1.21×10^{-5}		
2	0.04	24.13	**0.454**	5.47×10^{-6}	0.547	6.62×10^{-6}

Entry	$V_{tot,\,Ar2I+}$ (mL)	V (mL)	A	$[Ar_2CH^+]$ (M)	$[LB]_0(V_0/V)$ (M)	$[Ar_2I^+]_{0,i}$ (M)	$[Ar_2I^+]_0$/ $[LB]_0(V_0/V)$	$(A_0*(V_0/V)-A)/A$	[LB] (M)	$[Ar_2I$-LB] (M)	$[Ar_2I^+]$ (M)	$[Ar_2I$-LB]/ [LB]
1	0.20	24.33	0.465	5.60×10^{-6}	6.56×10^{-6}	2.03×10^{-4}	31.0	1.14	2.16×10^{-8}	1.79×10^{-7}	2.03×10^{-4}	8.25
2	0.40	24.53	0.472	5.69×10^{-6}	6.51×10^{-6}	4.03×10^{-4}	62.0	1.09	2.07×10^{-8}	3.08×10^{-7}	4.03×10^{-4}	1.49×10^{1}
3	0.60	24.73	0.477	5.75×10^{-6}	6.46×10^{-6}	6.00×10^{-4}	92.9	1.05	2.00×10^{-8}	4.12×10^{-7}	6.00×10^{-4}	2.06×10^{1}
4	0.80	24.93	0.483	5.82×10^{-6}	6.41×10^{-6}	7.94×10^{-4}	123.9	1.01	1.92×10^{-8}	5.28×10^{-7}	7.93×10^{-4}	2.75×10^{1}
5	1.00	25.13	0.488	5.88×10^{-6}	6.35×10^{-6}	9.84×10^{-4}	154.9	0.97	1.85×10^{-8}	6.31×10^{-7}	9.83×10^{-4}	3.41×10^{1}

RM827-2

Titration						
Entry	$V_{tot,\,LB}$ (mL)	V (mL)	A	$[Ar_2CH^+]$ (M)	$A_0*(V_0/V)$-A	$[LB]_0$ (M)
1	–	24.09	**1.026**	1.24×10^{-5}		
2	0.04	24.13	**0.398**	4.80×10^{-6}	0.626	7.58×10^{-6}

Entry	$V_{tot,\,Ar2I+}$ (mL)	V (mL)	A	$[Ar_2CH^+]$ (M)	$[LB]_0(V_0/V)$ (M)	$[Ar_2I^+]_{0,i}$ (M)	$[Ar_2I^+]_0$/ $[LB]_0(V_0/V)$	$(A_0*(V_0/V)-A)/A$	[LB] (M)	$[Ar_2I$-LB] (M)	$[Ar_2I^+]$ (M)	$[Ar_2I$-LB]/ [LB]
1	0.20	24.33	0.411	4.95×10^{-6}	7.51×10^{-6}	2.03×10^{-4}	27.1	1.47	2.80×10^{-8}	1.98×10^{-7}	2.03×10^{-4}	7.05
2	0.40	24.53	0.419	5.05×10^{-6}	7.45×10^{-6}	4.03×10^{-4}	54.1	1.40	2.68×10^{-8}	3.34×10^{-7}	4.03×10^{-4}	1.25×10^{1}
3	0.60	24.73	0.428	5.16×10^{-6}	7.39×10^{-6}	6.00×10^{-4}	81.2	1.34	2.54×10^{-8}	4.82×10^{-7}	6.00×10^{-4}	1.89×10^{1}
4	0.80	24.93	0.435	5.24×10^{-6}	7.33×10^{-6}	7.94×10^{-4}	108.2	1.28	2.44×10^{-8}	6.04×10^{-7}	7.93×10^{-4}	2.48×10^{1}
5	1.00	25.13	0.443	5.33×10^{-6}	7.27×10^{-6}	9.84×10^{-4}	135.3	1.22	2.33×10^{-8}	7.32×10^{-7}	9.83×10^{-4}	3.14×10^{1}

RM827-3

Titration						
Entry	$V_{tot,\,LB}$ (mL)	V (mL)	A	$[Ar_2CH^+]$ (M)	$A_0*(V_0/V)$-A	$[LB]_0$ (M)
1	–	24.09	**1.038**	1.25×10^{-5}		
2	0.04	24.13	**0.464**	5.59×10^{-6}	0.572	6.92×10^{-6}

Entry	$V_{tot,\,Ar2I+}$ (mL)	V (mL)	A	$[Ar_2CH^+]$ (M)	$[LB]_0(V_0/V)$ (M)	$[Ar_2I^+]_{0,i}$ (M)	$[Ar_2I^+]_0/[LB]_0(V_0/V)$	$(A_0*(V_0/V)-A)/A$	[LB] (M)	$[Ar_2I$-LB] (M)	$[Ar_2I^+]$ (M)	$[Ar_2I$-LB]/[LB]
1	0.20	24.33	0.477	5.75×10^{-6}	6.86×10^{-6}	2.03×10^{-4}	29.6	1.15	2.20×10^{-8}	2.04×10^{-7}	2.03×10^{-4}	9.27
2	0.40	24.53	0.486	5.86×10^{-6}	6.81×10^{-6}	4.03×10^{-4}	59.3	1.10	2.09×10^{-8}	3.58×10^{-7}	4.03×10^{-4}	1.71×10^{1}
3	0.60	24.73	0.494	5.95×10^{-6}	6.75×10^{-6}	6.00×10^{-4}	88.9	1.05	1.99×10^{-8}	5.00×10^{-7}	6.00×10^{-4}	2.51×10^{1}
4	0.80	24.93	0.501	6.04×10^{-6}	6.70×10^{-6}	7.94×10^{-4}	118.5	1.00	1.91×10^{-8}	6.29×10^{-7}	7.93×10^{-4}	3.29×10^{1}
5	1.00	25.13	0.507	6.10×10^{-6}	6.64×10^{-6}	9.84×10^{-4}	148.1	0.96	1.84×10^{-8}	7.39×10^{-7}	9.83×10^{-4}	4.02×10^{1}

1j + 3a (20 °C) - RM689

BIMT experiment (MeCN, 20 °C) for the benzoate ion **3a** with **1j** (stock solution: 22.5 mM) competing against the benzhydrylium ion **B2** (605 nm, ε = 1.66×10^5 M^{-1} cm^{-1}, K = 5.25×10^7 M^{-1} from LA and LB).

RM689-1

Titration						
Entry	$V_{tot,\,LB}$ (mL)	V (mL)	A	$[Ar_2CH^+]$ (M)	$A_0*(V_0/V)$-A	$[LB]_0$ (M)
1	–	24.10	**1.363**	1.64×10^{-5}		
2	0.05	24.15	**0.486**	5.86×10^{-6}	0.874	1.06×10^{-5}

Entry	$V_{tot,\,Ar2I+}$ (mL)	V (mL)	A	$[Ar_2CH^+]$ (M)	$[LB]_0(V_0/V)$ (M)	$[Ar_2I^+]_{0,i}$ (M)	$[Ar_2I^+]_0/[LB]_0(V_0/V)$	$(A_0*(V_0/V)-A)/A$	[LB] (M)	$[Ar_2I$-LB] (M)	$[Ar_2I^+]$ (M)	$[Ar_2I$-LB]/[LB]
1	0.03	24.18	**0.500**	6.02×10^{-6}	1.06×10^{-5}	2.33×10^{-5}	2.2	1.72	3.27×10^{-8}	1.76×10^{-7}	2.31×10^{-5}	5.39
2	0.10	24.25	**0.530**	6.39×10^{-6}	1.05×10^{-5}	9.29×10^{-5}	8.8	1.56	2.96×10^{-8}	5.59×10^{-7}	9.23×10^{-5}	1.88×10^{1}
3	0.20	24.35	**0.563**	6.78×10^{-6}	1.05×10^{-5}	1.85×10^{-4}	17.7	1.40	2.66×10^{-8}	9.83×10^{-7}	1.84×10^{-4}	3.70×10^{1}
4	0.30	24.45	**0.596**	7.18×10^{-6}	1.04×10^{-5}	2.76×10^{-4}	26.5	1.25	2.39×10^{-8}	1.41×10^{-6}	2.75×10^{-4}	5.89×10^{1}
5	0.44	24.59	**0.631**	7.60×10^{-6}	1.04×10^{-5}	4.03×10^{-4}	38.8	1.12	2.13×10^{-8}	1.86×10^{-6}	4.01×10^{-4}	8.76×10^{1}

BIMT experiment (MeCN, 20 °C) for the benzoate ion **3a** with **1j** (stock solution: 27.5 mM) competing against the benzhydrylium ion **B2** (605 nm, ε = 1.66 × 10^5 M^{-1} cm^{-1}, K = 5.25 × 10^7 M^{-1} from LA and LB).

RM689-2

Titration						
Entry	$V_{tot,\,LB}$ (mL)	V (mL)	A	$[Ar_2CH^+]$ (M)	$A_0*(V_0/V)$-A	$[LB]_0$ (M)
1	–	24.10	**1.094**	1.32×10^{-5}		
2	0.03	24.13	**0.582**	7.01×10^{-6}	0.511	6.17×10^{-6}

Entry	$V_{tot,\,Ar2I+}$ (mL)	V (mL)	A	$[Ar_2CH^+]$ (M)	$[LB]_0(V_0/V)$ (M)	$[Ar_2I^+]_{0,i}$ (M)	$[Ar_2I^+]_0/[LB]_0(V_0/V)$	$(A_0*(V_0/V)\text{-}A)/A$	[LB] (M)	$[Ar_2I\text{-}LB]$ (M)	$[Ar_2I^+]$ (M)	$[Ar_2I\text{-}LB]/[LB]$
1	0.10	24.23	**0.615**	7.41×10^{-6}	6.14×10^{-6}	1.13×10^{-4}	18.5	0.77	1.47×10^{-8}	4.29×10^{-7}	1.13×10^{-4}	2.92×10^{1}
2	0.20	24.33	**0.641**	7.72×10^{-6}	6.12×10^{-6}	2.26×10^{-4}	36.9	0.69	1.32×10^{-8}	7.72×10^{-7}	2.25×10^{-4}	5.87×10^{1}
3	0.30	24.43	**0.664**	8.00×10^{-6}	6.09×10^{-6}	3.37×10^{-4}	55.4	0.63	1.19×10^{-8}	1.08×10^{-6}	3.36×10^{-4}	9.05×10^{1}
4	0.40	24.53	**0.683**	8.23×10^{-6}	6.07×10^{-6}	4.48×10^{-4}	73.8	0.57	1.09×10^{-8}	1.34×10^{-6}	4.47×10^{-4}	1.22×10^{2}
5	0.50	24.63	**0.700**	8.43×10^{-6}	6.04×10^{-6}	5.58×10^{-4}	92.3	0.53	1.01×10^{-8}	1.57×10^{-6}	5.56×10^{-4}	1.56×10^{2}

BIMT experiment (MeCN, 20 °C) for the benzoate ion **3a** with **1j** (stock solution: 27.5 mM) competing against the benzhydrylium ion **B2** (605 nm, ε = 1.66 × 10^5 M^{-1} cm^{-1}, K = 5.25 × 10^7 M^{-1} from LA and LB).

RM689-3

Titration						
Entry	$V_{tot,\,LB}$ (mL)	V (mL)	A	$[Ar_2CH^+]$ (M)	$A_0*(V_0/V)$-A	$[LB]_0$ (M)
1	–	24.10	**1.006**	1.21×10^{-5}		
2	0.03	24.13	**0.478**	5.76×10^{-6}	0.527	6.37×10^{-6}

Entry	$V_{tot,\,Ar2I+}$ (mL)	V (mL)	A	$[Ar_2CH^+]$ (M)	$[LB]_0(V_0/V)$ (M)	$[Ar_2I^+]_{0,i}$ (M)	$[Ar_2I^+]_0/[LB]_0(V_0/V)$	$(A_0*(V_0/V)\text{-}A)/A$	[LB] (M)	$[Ar_2I\text{-}LB]$ (M)	$[Ar_2I^+]$ (M)	$[Ar_2I\text{-}LB]/[LB]$
1	0.10	24.23	**0.515**	6.20×10^{-6}	6.34×10^{-6}	1.13×10^{-4}	17.9	0.94	1.80×10^{-8}	4.73×10^{-7}	1.13×10^{-4}	2.63×10^{1}
2	0.20	24.33	**0.544**	6.55×10^{-6}	6.31×10^{-6}	2.26×10^{-4}	35.8	0.83	1.58×10^{-8}	8.48×10^{-7}	2.25×10^{-4}	5.35×10^{1}
3	0.30	24.43	**0.567**	6.83×10^{-6}	6.29×10^{-6}	3.38×10^{-4}	53.7	0.75	1.43×10^{-8}	1.15×10^{-6}	3.36×10^{-4}	8.04×10^{1}
4	0.40	24.53	**0.588**	7.08×10^{-6}	6.26×10^{-6}	4.48×10^{-4}	71.6	0.68	1.30×10^{-8}	1.43×10^{-6}	4.47×10^{-4}	1.10×10^{2}
5	0.50	24.63	**0.607**	7.31×10^{-6}	6.24×10^{-6}	5.58×10^{-4}	89.5	0.62	1.18×10^{-8}	1.68×10^{-6}	5.56×10^{-4}	1.42×10^{2}

1k + 3a (20 °C) - RM828

BIMT experiment (MeCN, 20 °C) for the benzoate ion **3a** with **1k** (stock solution: 17.3 mM) competing against the benzhydrylium ion **B2** (605 nm, ε = 1.66 × 10^5 M^{-1} cm^{-1}, K = 5.25 × 10^7 M^{-1} from LA and LB).

RM828-2

Titration						
Entry	$V_{tot,\,LB}$ (mL)	V (mL)	A	$[Ar_2CH^+]$ (M)	$A_0*(V_0/V)$-A	$[LB]_0$ (M)
1	–	24.09	**1.034**	1.25×10^{-5}		
2	0.04	24.13	**0.359**	4.33×10^{-6}	0.673	8.15×10^{-6}

Entry	$V_{tot,\,Ar2I+}$ (mL)	V (mL)	A	$[Ar_2CH^+]$ (M)	$[LB]_0(V_0/V)$ (M)	$[Ar_2I^+]_{0,i}$ (M)	$[Ar_2I^+]_0$/ $[LB]_0(V_0/V)$	$(A_0*(V_0/V)-A)/A$	[LB] (M)	$[Ar_2I$-LB] (M)	$[Ar_2I^+]$ (M)	$[Ar_2I$-LB]/ [LB]
1	0.20	24.33	0.395	4.76×10^{-6}	8.08×10^{-6}	1.42×10^{-4}	17.6	1.59	3.03×10^{-8}	4.74×10^{-7}	1.42×10^{-4}	1.56×10^{1}
2	0.40	24.53	0.416	5.01×10^{-6}	8.01×10^{-6}	2.82×10^{-4}	35.2	1.44	2.75×10^{-8}	7.65×10^{-7}	2.81×10^{-4}	2.79×10^{1}
3	0.60	24.73	0.431	5.19×10^{-6}	7.95×10^{-6}	4.20×10^{-4}	52.8	1.34	2.55×10^{-8}	9.82×10^{-7}	4.19×10^{-4}	3.85×10^{1}
4	0.80	24.93	0.443	5.34×10^{-6}	7.89×10^{-6}	5.55×10^{-4}	70.4	1.26	2.39×10^{-8}	1.16×10^{-6}	5.54×10^{-4}	4.86×10^{1}
5	1.00	25.13	0.452	5.45×10^{-6}	7.82×10^{-6}	6.88×10^{-4}	88.0	1.19	2.27×10^{-8}	1.30×10^{-6}	6.87×10^{-4}	5.74×10^{1}

RM828-3

Titration						
Entry	$V_{tot,\,LB}$ (mL)	V (mL)	A	$[Ar_2CH^+]$ (M)	$A_0*(V_0/V)$-A	$[LB]_0$ (M)
1	–	24.09	**1.071**	1.29×10^{-5}		
2	0.04	24.13	**0.446**	5.37×10^{-6}	0.623	7.54×10^{-6}

Entry	$V_{tot,\,Ar2I+}$ (mL)	V (mL)	A	$[Ar_2CH^+]$ (M)	$[LB]_0(V_0/V)$ (M)	$[Ar_2I^+]_{0,i}$ (M)	$[Ar_2I^+]_0$/ $[LB]_0(V_0/V)$	$(A_0*(V_0/V)-A)/A$	[LB] (M)	$[Ar_2I$-LB] (M)	$[Ar_2I^+]$ (M)	$[Ar_2I$-LB]/ [LB]
1	0.20	24.33	0.473	5.70×10^{-6}	7.47×10^{-6}	1.42×10^{-4}	19.0	1.24	2.37×10^{-8}	3.72×10^{-7}	1.42×10^{-4}	1.57×10^{1}
2	0.40	24.53	0.490	5.90×10^{-6}	7.41×10^{-6}	2.82×10^{-4}	38.0	1.15	2.18×10^{-8}	6.22×10^{-7}	2.81×10^{-4}	2.85×10^{1}
3	0.60	24.73	0.504	6.07×10^{-6}	7.35×10^{-6}	4.20×10^{-4}	57.1	1.07	2.04×10^{-8}	8.35×10^{-7}	4.19×10^{-4}	4.09×10^{1}
4	0.80	24.93	0.515	6.20×10^{-6}	7.29×10^{-6}	5.55×10^{-4}	76.1	1.01	1.92×10^{-8}	1.01×10^{-6}	5.54×10^{-4}	5.25×10^{1}
5	1.00	25.13	0.525	6.33×10^{-6}	7.24×10^{-6}	6.88×10^{-4}	95.1	0.96	1.82×10^{-8}	1.17×10^{-6}	6.87×10^{-4}	6.44×10^{1}

RM828-4

Titration						
Entry	$V_{tot,\,LB}$ (mL)	V (mL)	A	$[Ar_2CH^+]$ (M)	$A_0*(V_0/V)-A$	$[LB]_0$ (M)
1	–	24.09	**1.052**	1.27×10^{-5}		
2	0.04	24.13	**0.419**	5.05×10^{-6}	0.631	7.63×10^{-6}

Entry	$V_{tot,\,Ar2I+}$ (mL)	V (mL)	A	$[Ar_2CH^+]$ (M)	$[LB]_0(V_0/V)$ (M)	$[Ar_2I^+]_{0,i}$ (M)	$[Ar_2I^+]_0/[LB]_0(V_0/V)$	$(A_0*(V_0/V)-A)/A$	[LB] (M)	$[Ar_2I$-LB] (M)	$[Ar_2I^+]$ (M)	$[Ar_2I$-LB]/[LB]
1	0.20	24.33	0.451	5.43×10^{-6}	7.57×10^{-6}	1.42×10^{-4}	18.8	1.31	2.50×10^{-8}	4.31×10^{-7}	1.42×10^{-4}	1.73×10^{1}
2	0.40	24.53	0.470	5.66×10^{-6}	7.51×10^{-6}	2.82×10^{-4}	37.6	1.20	2.28×10^{-8}	7.02×10^{-7}	2.81×10^{-4}	3.08×10^{1}
3	0.60	24.73	0.484	5.83×10^{-6}	7.45×10^{-6}	4.20×10^{-4}	56.3	1.12	2.13×10^{-8}	9.12×10^{-7}	4.19×10^{-4}	4.29×10^{1}
4	0.80	24.93	0.495	5.96×10^{-6}	7.39×10^{-6}	5.55×10^{-4}	75.1	1.06	2.01×10^{-8}	1.08×10^{-6}	5.54×10^{-4}	5.37×10^{1}
5	1.00	25.13	0.507	6.11×10^{-6}	7.33×10^{-6}	6.88×10^{-4}	93.9	0.99	1.88×10^{-8}	1.27×10^{-6}	6.87×10^{-4}	6.74×10^{1}

1l + 3a (20 °C) - RM692

BIMT experiment (MeCN, 20 °C) for the benzoate ion **3a** with **1l** (stock solution: 6.53 mM) competing against the benzhydrylium ion **B2** (605 nm, ε = 1.66×10^5 M^{-1} cm^{-1}, K = 5.25×10^7 M^{-1} from LA and LB).

RM692-1

Titration						
Entry	$V_{tot,\,LB}$ (mL)	V (mL)	A	$[Ar_2CH^+]$ (M)	$A_0*(V_0/V)-A$	$[LB]_0$ (M)
1	–	24.08	**1.078**	1.30×10^{-5}		
2	0.04	24.12	**0.361**	4.35×10^{-6}	0.715	8.65×10^{-6}

Entry	$V_{tot,\,Ar2I+}$ (mL)	V (mL)	A	$[Ar_2CH^+]$ (M)	$[LB]_0(V_0/V)$ (M)	$[Ar_2I^+]_{0,i}$ (M)	$[Ar_2I^+]_0/[LB]_0(V_0/V)$	$(A_0*(V_0/V)-A)/A$	[LB] (M)	$[Ar_2I$-LB] (M)	$[Ar_2I^+]$ (M)	$[Ar_2I$-LB]/[LB]
1	0.10	24.22	0.489	5.89×10^{-6}	8.62×10^{-6}	2.70×10^{-5}	3.1	1.19	2.27×10^{-8}	1.58×10^{-6}	2.54×10^{-5}	6.94×10^{1}
2	0.20	24.32	0.560	6.75×10^{-6}	8.58×10^{-6}	5.37×10^{-5}	6.3	0.91	1.73×10^{-8}	2.45×10^{-6}	5.13×10^{-5}	1.42×10^{2}
3	0.30	24.42	0.611	7.36×10^{-6}	8.55×10^{-6}	8.02×10^{-5}	9.4	0.74	1.41×10^{-8}	3.08×10^{-6}	7.72×10^{-5}	2.18×10^{2}
4	0.40	24.52	0.648	7.81×10^{-6}	8.51×10^{-6}	1.07×10^{-4}	12.5	0.63	1.21×10^{-8}	3.55×10^{-6}	1.03×10^{-4}	2.94×10^{2}
5	0.50	24.62	0.679	8.18×10^{-6}	8.48×10^{-6}	1.33×10^{-4}	15.6	0.55	1.05×10^{-8}	3.95×10^{-6}	1.29×10^{-4}	3.75×10^{2}

RM692-2

Titration						
Entry	$V_{tot,\,LB}$ (mL)	V (mL)	A	$[Ar_2CH^+]$ (M)	$A_0*(V_0/V)$-A	$[LB]_0$ (M)
1	–	24.08	**1.055**	1.27×10^{-5}		
2	0.04	24.12	**0.329**	3.96×10^{-6}	0.724	8.77×10^{-6}

Entry	$V_{tot,\,Ar2I+}$ (mL)	V (mL)	A	$[Ar_2CH^+]$ (M)	$[LB]_0(V_0/V)$ (M)	$[Ar_2I^+]_{0,i}$ (M)	$[Ar_2I^+]_0/[LB]_0(V_0/V)$	$(A_0*(V_0/V)\text{-}A)/A$	[LB] (M)	$[Ar_2I$-LB] (M)	$[Ar_2I^+]$ (M)	$[Ar_2I$-LB]/[LB]
1	0.10	24.22	0.465	5.60×10^{-6}	8.73×10^{-6}	2.70×10^{-5}	3.1	1.26	2.39×10^{-8}	1.67×10^{-6}	2.53×10^{-5}	6.99×10^{1}
2	0.20	24.32	0.537	6.47×10^{-6}	8.70×10^{-6}	5.37×10^{-5}	6.2	0.95	1.80×10^{-8}	2.56×10^{-6}	5.11×10^{-5}	1.42×10^{2}
3	0.30	24.42	0.589	7.10×10^{-6}	8.66×10^{-6}	8.02×10^{-5}	9.3	0.77	1.46×10^{-8}	3.21×10^{-6}	7.70×10^{-5}	2.20×10^{2}
4	0.40	24.52	0.628	7.57×10^{-6}	8.62×10^{-6}	1.07×10^{-4}	12.4	0.65	1.24×10^{-8}	3.70×10^{-6}	1.03×10^{-4}	2.99×10^{2}
5	0.50	24.62	0.658	7.93×10^{-6}	8.59×10^{-6}	1.33×10^{-4}	15.4	0.57	1.08×10^{-8}	4.07×10^{-6}	1.29×10^{-4}	3.76×10^{2}

RM692-3

Titration						
Entry	$V_{tot,\,LB}$ (mL)	V (mL)	A	$[Ar_2CH^+]$ (M)	$A_0*(V_0/V)$-A	$[LB]_0$ (M)
1	–	24.08	**1.073**	1.29×10^{-5}		
2	0.04	24.12	**0.404**	4.87×10^{-6}	0.667	8.07×10^{-6}

Entry	$V_{tot,\,Ar2I+}$ (mL)	V (mL)	A	$[Ar_2CH^+]$ (M)	$[LB]_0(V_0/V)$ (M)	$[Ar_2I^+]_{0,i}$ (M)	$[Ar_2I^+]_0/[LB]_0(V_0/V)$	$(A_0*(V_0/V)\text{-}A)/A$	[LB] (M)	$[Ar_2I$-LB] (M)	$[Ar_2I^+]$ (M)	$[Ar_2I$-LB]/[LB]
1	0.10	24.22	0.522	6.29×10^{-6}	8.04×10^{-6}	2.70×10^{-5}	3.4	1.04	1.99×10^{-8}	1.45×10^{-6}	2.55×10^{-5}	7.31×10^{1}
2	0.20	24.32	0.588	7.08×10^{-6}	8.00×10^{-6}	5.37×10^{-5}	6.7	0.81	1.54×10^{-8}	2.27×10^{-6}	5.14×10^{-5}	1.48×10^{2}
3	0.30	24.42	0.634	7.64×10^{-6}	7.97×10^{-6}	8.02×10^{-5}	10.1	0.67	1.27×10^{-8}	2.85×10^{-6}	7.74×10^{-5}	2.24×10^{2}
4	0.40	24.52	0.670	8.07×10^{-6}	7.94×10^{-6}	1.07×10^{-4}	13.4	0.57	1.09×10^{-8}	3.30×10^{-6}	1.03×10^{-4}	3.03×10^{2}
5	0.50	24.62	0.698	8.41×10^{-6}	7.91×10^{-6}	1.33×10^{-4}	16.8	0.50	9.59×10^{-9}	3.66×10^{-6}	1.29×10^{-4}	3.82×10^{2}

1m + 3a (20 °C) - RM691

BIMT experiment (MeCN, 20 °C) for the benzoate ion **3a** with **1m** (stock solution: 9.35 mM) competing against the benzhydrylium ion **B2** (605 nm, ε = 1.66 × 10^5 M^{-1} cm^{-1}, K = 5.25 × 10^7 M^{-1} from LA and LB).

RM691-1

Titration						
Entry	$V_{tot,\,LB}$ (mL)	V (mL)	A	$[Ar_2CH^+]$ (M)	$A_0*(V_0/V)$-A	$[LB]_0$ (M)
1	–	24.08	**1.080**	1.30×10^{-5}		
2	0.04	24.12	**0.346**	4.17×10^{-6}	0.732	8.86×10^{-6}

Entry	$V_{tot,\,Ar2I+}$ (mL)	V (mL)	A	$[Ar_2CH^+]$ (M)	$[LB]_0(V_0/V)$ (M)	$[Ar_2I^+]_{0,i}$ (M)	$[Ar_2I^+]_0$/ $[LB]_0(V_0/V)$	$(A_0*(V_0/V)-A)/A$	[LB] (M)	$[Ar_2I$-LB] (M)	$[Ar_2I^+]$ (M)	$[Ar_2I$-LB]/ [LB]
1	0.10	24.22	0.481	5.80×10^{-6}	8.83×10^{-6}	3.86×10^{-5}	4.4	1.23	2.35×10^{-8}	1.66×10^{-6}	3.70×10^{-5}	7.07×10^{1}
2	0.20	24.32	0.566	6.82×10^{-6}	8.79×10^{-6}	7.69×10^{-5}	8.8	0.89	1.69×10^{-8}	2.71×10^{-6}	7.42×10^{-5}	1.60×10^{2}
3	0.30	24.42	0.630	7.59×10^{-6}	8.75×10^{-6}	1.15×10^{-4}	13.1	0.69	1.32×10^{-8}	3.50×10^{-6}	1.11×10^{-4}	2.66×10^{2}
4	0.40	24.52	0.679	8.18×10^{-6}	8.72×10^{-6}	1.53×10^{-4}	17.5	0.56	1.07×10^{-8}	4.11×10^{-6}	1.48×10^{-4}	3.84×10^{2}
5	0.50	24.62	0.721	8.68×10^{-6}	8.68×10^{-6}	1.90×10^{-4}	21.9	0.47	8.88×10^{-9}	4.63×10^{-6}	1.85×10^{-4}	5.21×10^{2}

RM691-2

Titration						
Entry	$V_{tot,\,LB}$ (mL)	V (mL)	A	$[Ar_2CH^+]$ (M)	$A_0*(V_0/V)$-A	$[LB]_0$ (M)
1	–	24.08	**0.965**	1.16×10^{-5}		
2	0.04	24.12	**0.237**	2.86×10^{-6}	0.726	8.81×10^{-6}

Entry	$V_{tot,\,Ar2I+}$ (mL)	V (mL)	A	$[Ar_2CH^+]$ (M)	$[LB]_0(V_0/V)$ (M)	$[Ar_2I^+]_{0,i}$ (M)	$[Ar_2I^+]_0$/ $[LB]_0(V_0/V)$	$(A_0*(V_0/V)-A)/A$	[LB] (M)	$[Ar_2I$-LB] (M)	$[Ar_2I^+]$ (M)	$[Ar_2I$-LB]/ [LB]
1	0.10	24.22	0.391	4.71×10^{-6}	8.77×10^{-6}	3.86×10^{-5}	4.4	1.45	2.77×10^{-8}	1.90×10^{-6}	3.67×10^{-5}	6.85×10^{1}
2	0.20	24.32	0.476	5.73×10^{-6}	8.74×10^{-6}	7.69×10^{-5}	8.8	1.01	1.92×10^{-8}	2.94×10^{-6}	7.40×10^{-5}	1.53×10^{2}
3	0.30	24.42	0.537	6.47×10^{-6}	8.70×10^{-6}	1.15×10^{-4}	13.2	0.77	1.47×10^{-8}	3.69×10^{-6}	1.11×10^{-4}	2.51×10^{2}
4	0.40	24.52	0.588	7.08×10^{-6}	8.67×10^{-6}	1.53×10^{-4}	17.6	0.61	1.17×10^{-8}	4.32×10^{-6}	1.48×10^{-4}	3.71×10^{2}
5	0.50	24.62	0.628	7.57×10^{-6}	8.63×10^{-6}	1.90×10^{-4}	22.0	0.50	9.58×10^{-9}	4.82×10^{-6}	1.85×10^{-4}	5.03×10^{2}

RM691-3

Titration						
Entry	$V_{tot,\,LB}$ (mL)	V (mL)	A	$[Ar_2CH^+]$ (M)	$A_0*(V_0/V)$-A	$[LB]_0$ (M)
1	–	24.08	**1.112**	1.34×10^{-5}		
2	0.04	24.12	**0.388**	4.67×10^{-6}	0.722	8.74×10^{-6}

Entry	$V_{tot,\,Ar2I+}$ (mL)	V (mL)	A	$[Ar_2CH^+]$ (M)	$[LB]_0(V_0/V)$ (M)	$[Ar_2I^+]_{0,i}$ (M)	$[Ar_2I^+]_0/[LB]_0(V_0/V)$	$(A_0*(V_0/V)\text{-}A)/A$	[LB] (M)	$[Ar_2I\text{-}LB]$ (M)	$[Ar_2I^+]$ (M)	$[Ar_2I\text{-}LB]/[LB]$
1	0.10	24.22	0.515	6.20×10^{-6}	8.70×10^{-6}	3.86×10^{-5}	4.4	1.15	2.19×10^{-8}	1.56×10^{-6}	3.71×10^{-5}	7.15×10^{1}
2	0.20	24.32	0.597	7.19×10^{-6}	8.66×10^{-6}	7.69×10^{-5}	8.9	0.84	1.61×10^{-8}	2.58×10^{-6}	7.43×10^{-5}	1.60×10^{2}
3	0.30	24.42	0.661	7.96×10^{-6}	8.63×10^{-6}	1.15×10^{-4}	13.3	0.66	1.26×10^{-8}	3.37×10^{-6}	1.12×10^{-4}	2.68×10^{2}
4	0.40	24.52	0.713	8.59×10^{-6}	8.59×10^{-6}	1.53×10^{-4}	17.8	0.53	1.01×10^{-8}	4.02×10^{-6}	1.49×10^{-4}	3.97×10^{2}
5	0.50	24.62	0.754	9.08×10^{-6}	8.56×10^{-6}	1.90×10^{-4}	22.2	0.44	8.43×10^{-9}	4.53×10^{-6}	1.85×10^{-4}	5.37×10^{2}

1n + 3a (20 °C) – RM1225

BIMT experiment (MeCN, 20 °C) for the benzoate ion **3a** with **1n** (stock solution: 23.7 mM) competing against the benzhydrylium ion **B2** (605 nm, ε = 1.66×10^5 M^{-1} cm^{-1}, $K = 5.25 \times 10^7$ M^{-1} from LA and LB).

RM1225-1

Titration						
Entry	$V_{tot,\,LB}$ (mL)	V (mL)	A	$[Ar_2CH^+]$ (M)	$A_0*(V_0/V)$-A	$[LB]_0$ (M)
1	–	24.11	1.040	1.25×10^{-5}		
2	0.10	24.21	0.207	2.49×10^{-6}	0.829	1.01×10^{-5}

Entry	$V_{tot,\,Ar2I+}$ (mL)	V (mL)	A	$[Ar_2CH^+]$ (M)	$[LB]_0(V_0/V)$ (M)	$[Ar_2I^+]_{0,i}$ (M)	$[Ar_2I^+]_0/[LB]_0(V_0/V)$	$(A_0*(V_0/V)\text{-}A)/A$	[LB] (M)	$[Ar_2I\text{-}LB]$ (M)	$[Ar_2I^+]$ (M)	$[Ar_2I\text{-}LB]/[LB]$
1	0.20	24.41	0.253	3.05×10^{-6}	9.98×10^{-6}	1.95×10^{-4}	19.5	3.06	5.83×10^{-8}	5.92×10^{-7}	1.94×10^{-4}	1.02×10^{1}
2	0.40	24.61	0.282	3.40×10^{-6}	9.90×10^{-6}	3.86×10^{-4}	39.0	2.61	4.98×10^{-8}	9.69×10^{-7}	3.85×10^{-4}	1.95×10^{1}
3	0.60	24.81	0.304	3.66×10^{-6}	9.82×10^{-6}	5.74×10^{-4}	58.5	2.32	4.43×10^{-8}	1.26×10^{-6}	5.73×10^{-4}	2.84×10^{1}
4	0.80	25.01	0.323	3.89×10^{-6}	9.74×10^{-6}	7.60×10^{-4}	78.0	2.10	4.01×10^{-8}	1.51×10^{-6}	7.58×10^{-4}	3.77×10^{1}
5	1.00	25.21	0.339	4.08×10^{-6}	9.66×10^{-6}	9.42×10^{-4}	97.5	1.93	3.69×10^{-8}	1.73×10^{-6}	9.40×10^{-4}	4.68×10^{1}

RM1225-2

Titration						
Entry	$V_{tot,\,LB}$ (mL)	V (mL)	A	$[Ar_2CH^+]$ (M)	$A_0*(V_0/V)$-A	$[LB]_0$ (M)
1	–	24.11	1.102	1.33×10^{-5}		
2	0.10	24.21	0.298	3.59×10^{-6}	0.799	9.68×10^{-6}

Entry	$V_{tot,\,Ar2I+}$ (mL)	V (mL)	A	$[Ar_2CH^+]$ (M)	$[LB]_0(V_0/V)$ (M)	$[Ar_2I^+]_{0,i}$ (M)	$[Ar_2I^+]_0/[LB]_0(V_0/V)$	$(A_0*(V_0/V)\text{-}A)/A$	[LB] (M)	$[Ar_2I\text{-}LB]$ (M)	$[Ar_2I^+]$ (M)	$[Ar_2I\text{-}LB]/[LB]$
1	0.20	24.41	0.340	4.10×10^{-6}	9.60×10^{-6}	1.95×10^{-4}	20.3	2.20	4.19×10^{-8}	5.44×10^{-7}	1.94×10^{-4}	1.30×10^{1}
2	0.40	24.61	0.370	4.46×10^{-6}	9.53×10^{-6}	3.86×10^{-4}	40.5	1.92	3.65×10^{-8}	9.40×10^{-7}	3.85×10^{-4}	2.57×10^{1}
3	0.60	24.81	0.394	4.75×10^{-6}	9.45×10^{-6}	5.74×10^{-4}	60.8	1.72	3.27×10^{-8}	1.26×10^{-6}	5.73×10^{-4}	3.85×10^{1}
4	0.80	25.01	0.414	4.99×10^{-6}	9.37×10^{-6}	7.60×10^{-4}	81.0	1.57	2.98×10^{-8}	1.53×10^{-6}	7.58×10^{-4}	5.13×10^{1}
5	1.00	25.21	0.431	5.19×10^{-6}	9.30×10^{-6}	9.42×10^{-4}	101.3	1.45	2.75×10^{-8}	1.77×10^{-6}	9.40×10^{-4}	6.41×10^{1}

RM1225-3

Titration						
Entry	$V_{tot,\,LB}$ (mL)	V (mL)	A	$[Ar_2CH^+]$ (M)	$A_0*(V_0/V)$-A	$[LB]_0$ (M)
1	–	24.11	**1.059**	1.28×10^{-5}		
2	0.10	24.21	**0.103**	1.24×10^{-6}	0.952	1.16×10^{-5}

Entry	$V_{tot,\,Ar2I+}$ (mL)	V (mL)	A	$[Ar_2CH^+]$ (M)	$[LB]_0(V_0/V)$ (M)	$[Ar_2I^+]_{0,i}$ (M)	$[Ar_2I^+]_0/[LB]_0(V_0/V)$	$(A_0*(V_0/V)\text{-}A)/A$	[LB] (M)	$[Ar_2I\text{-}LB]$ (M)	$[Ar_2I^+]$ (M)	$[Ar_2I\text{-}LB]/[LB]$
1	0.20	24.41	0.177	2.13×10^{-6}	1.15×10^{-5}	1.95×10^{-4}	16.9	4.91	9.35×10^{-8}	9.83×10^{-7}	1.94×10^{-4}	1.05×10^{1}
2	0.40	24.61	0.218	2.63×10^{-6}	1.15×10^{-5}	3.86×10^{-4}	33.7	3.76	7.16×10^{-8}	1.51×10^{-6}	3.84×10^{-4}	2.10×10^{1}
3	0.60	24.81	0.250	3.01×10^{-6}	1.14×10^{-5}	5.74×10^{-4}	50.6	3.12	5.94×10^{-8}	1.91×10^{-6}	5.72×10^{-4}	3.22×10^{1}
4	0.80	25.01	0.276	3.33×10^{-6}	1.13×10^{-5}	7.60×10^{-4}	67.4	2.70	5.14×10^{-8}	2.24×10^{-6}	7.57×10^{-4}	4.36×10^{1}
5	1.00	25.21	0.298	3.59×10^{-6}	1.12×10^{-5}	9.42×10^{-4}	84.3	2.40	4.57×10^{-8}	2.52×10^{-6}	9.40×10^{-4}	5.52×10^{1}

2a + 3a (20 °C) - CYL055

BIMT experiment (MeCN, 20 °C) for the benzoate ion **3a** with **2a** (stock solution: 41.1 mM) competing against the benzhydrylium ion **B2** (605 nm, ε = 1.66 × 10^5 M^{-1} cm^{-1}, K = 5.25 × 10^7 M^{-1} from LA and LB).

CYL055-1

Titration						
Entry	$V_{tot,\,LB}$ (mL)	V (mL)	A	$[Ar_2CH^+]$ (M)	$A_0*(V_0/V)$-A	$[LB]_0$ (M)
1	–	23.55	**1.069**	1.29×10^{-5}		
2	0.03	23.58	**0.205**	2.47×10^{-6}	0.863	1.05×10^{-5}

Entry	$V_{tot,\,Ar2I+}$ (mL)	V (mL)	A	$[Ar_2CH^+]$ (M)	$[LB]_0(V_0/V)$ (M)	$[Ar_2I^+]_{0,i}$ (M)	$[Ar_2I^+]_0$/ $[LB]_0(V_0/V)$	$(A_0*(V_0/V)-A)/A$	[LB] (M)	[Ar_2I-LB] (M)	$[Ar_2I^+]$ (M)	[Ar_2I-LB]/ [LB]
1	0.02	23.60	0.645	7.77×10^{-6}	1.05×10^{-5}	3.48×10^{-5}	3.3	0.65	1.25×10^{-8}	5.37×10^{-6}	2.95×10^{-5}	4.31×10^{2}
2	0.03	23.61	0.710	8.55×10^{-6}	1.05×10^{-5}	5.22×10^{-5}	5.0	0.50	9.56×10^{-9}	6.16×10^{-6}	4.61×10^{-5}	6.44×10^{2}
3	0.04	23.62	0.756	9.11×10^{-6}	1.05×10^{-5}	6.96×10^{-5}	6.7	0.41	7.81×10^{-9}	6.71×10^{-6}	6.29×10^{-5}	8.60×10^{2}
4	0.05	23.63	0.790	9.52×10^{-6}	1.05×10^{-5}	8.70×10^{-5}	8.3	0.35	6.64×10^{-9}	7.13×10^{-6}	7.98×10^{-5}	1.07×10^{3}
5	0.10	23.68	0.884	1.07×10^{-5}	1.04×10^{-5}	1.74×10^{-4}	16.6	0.20	3.86×10^{-9}	8.27×10^{-6}	1.65×10^{-4}	2.14×10^{3}
6	0.15	23.73	0.927	1.12×10^{-5}	1.04×10^{-5}	2.60×10^{-4}	25.0	0.14	2.75×10^{-9}	8.79×10^{-6}	2.51×10^{-4}	3.19×10^{3}
7	0.25	23.83	0.966	1.16×10^{-5}	1.04×10^{-5}	4.31×10^{-4}	41.6	0.09	1.78×10^{-9}	9.27×10^{-6}	4.22×10^{-4}	5.20×10^{3}

CYL055-2

Titration						
Entry	$V_{tot,\,LB}$ (mL)	V (mL)	A	$[Ar_2CH^+]$ (M)	$A_0*(V_0/V)$-A	$[LB]_0$ (M)
1	–	23.55	**1.065**	1.28×10^{-5}		
2	0.03	23.58	**0.179**	2.16×10^{-6}	0.885	1.08×10^{-5}

Entry	$V_{tot,\,Ar2I+}$ (mL)	V (mL)	A	$[Ar_2CH^+]$ (M)	$[LB]_0(V_0/V)$ (M)	$[Ar_2I^+]_{0,i}$ (M)	$[Ar_2I^+]_0$/ $[LB]_0(V_0/V)$	$(A_0*(V_0/V)-A)/A$	[LB] (M)	[Ar_2I-LB] (M)	$[Ar_2I^+]$ (M)	[Ar_2I-LB]/ [LB]
1	0.01	23.59	0.521	6.28×10^{-6}	1.07×10^{-5}	1.74×10^{-5}	1.6	1.04	1.98×10^{-8}	4.20×10^{-6}	1.32×10^{-5}	2.12×10^{2}
2	0.02	23.60	0.637	7.67×10^{-6}	1.07×10^{-5}	3.48×10^{-5}	3.2	0.67	1.27×10^{-8}	5.60×10^{-6}	2.92×10^{-5}	4.40×10^{2}
3	0.03	23.61	0.719	8.66×10^{-6}	1.07×10^{-5}	5.22×10^{-5}	4.9	0.48	9.10×10^{-9}	6.59×10^{-6}	4.56×10^{-5}	7.25×10^{2}
4	0.05	23.63	0.788	9.49×10^{-6}	1.07×10^{-5}	8.70×10^{-5}	8.1	0.35	6.61×10^{-9}	7.43×10^{-6}	7.95×10^{-5}	1.12×10^{3}
5	0.10	23.68	0.882	1.06×10^{-5}	1.07×10^{-5}	1.74×10^{-4}	16.2	0.20	3.83×10^{-9}	8.57×10^{-6}	1.65×10^{-4}	2.24×10^{3}
6	0.15	23.73	0.926	1.12×10^{-5}	1.07×10^{-5}	2.60×10^{-4}	24.3	0.14	2.69×10^{-9}	9.10×10^{-6}	2.51×10^{-4}	3.38×10^{3}
7	0.25	23.83	0.965	1.16×10^{-5}	1.06×10^{-5}	4.31×10^{-4}	40.5	0.09	1.73×10^{-9}	9.58×10^{-6}	4.22×10^{-4}	5.55×10^{3}

CYL055-3

Titration						
Entry	$V_{tot,\,LB}$ (mL)	V (mL)	A	$[Ar_2CH^+]$ (M)	$A_0*(V_0/V)$-A	$[LB]_0$ (M)
1	–	23.55	**1.060**	1.28×10^{-5}		
2	0.03	23.58	**0.184**	2.22×10^{-6}	0.875	1.06×10^{-5}

Entry	$V_{tot,\,Ar2I+}$ (mL)	V (mL)	A	$[Ar_2CH^+]$ (M)	$[LB]_0(V_0/V)$ (M)	$[Ar_2I^+]_{0,i}$ (M)	$[Ar_2I^+]_0/[LB]_0(V_0/V)$	$(A_0*(V_0/V)\text{-}A)/A$	[LB] (M)	$[Ar_2I\text{-}LB]$ (M)	$[Ar_2I^+]$ (M)	$[Ar_2I\text{-}LB]/[LB]$
1	0.01	23.59	0.503	6.06×10^{-6}	1.06×10^{-5}	1.74×10^{-5}	1.6	1.10	2.10×10^{-8}	3.91×10^{-6}	1.35×10^{-5}	1.86×10^{2}
2	0.02	23.60	0.627	7.55×10^{-6}	1.06×10^{-5}	3.48×10^{-5}	3.3	0.69	1.31×10^{-8}	5.42×10^{-6}	2.94×10^{-5}	4.14×10^{2}
3	0.03	23.61	0.695	8.37×10^{-6}	1.06×10^{-5}	5.22×10^{-5}	4.9	0.52	9.93×10^{-9}	6.24×10^{-6}	4.60×10^{-5}	6.28×10^{2}
4	0.05	23.63	0.780	9.40×10^{-6}	1.06×10^{-5}	8.70×10^{-5}	8.2	0.35	6.75×10^{-9}	7.27×10^{-6}	7.97×10^{-5}	1.08×10^{3}
5	0.10	23.68	0.878	1.06×10^{-5}	1.06×10^{-5}	1.74×10^{-4}	16.4	0.20	3.82×10^{-9}	8.46×10^{-6}	1.65×10^{-4}	2.21×10^{3}
6	0.15	23.73	0.921	1.11×10^{-5}	1.06×10^{-5}	2.60×10^{-4}	24.6	0.14	2.71×10^{-9}	8.98×10^{-6}	2.51×10^{-4}	3.31×10^{3}
7	0.20	23.78	0.945	1.14×10^{-5}	1.05×10^{-5}	3.46×10^{-4}	32.8	0.11	2.11×10^{-9}	9.28×10^{-6}	3.36×10^{-4}	4.39×10^{3}

2b + 3a (20 °C) - RM696

BIMT experiment (MeCN, 20 °C) for the benzoate ion **3a** with **2b** (stock solution: 8.51 mM) competing against the benzhydrylium ion **B2** (605 nm, ε = 1.66×10^5 M^{-1} cm^{-1}, $K = 5.25 \times 10^7$ M^{-1} from LA and LB).

RM696-3

Titration						
Entry	$V_{tot,\,LB}$ (mL)	V (mL)	A	$[Ar_2CH^+]$ (M)	$A_0*(V_0/V)$-A	$[LB]_0$ (M)
1	–	24.10	**1.066**	1.28×10^{-5}		
2	0.04	24.14	**0.474**	5.71×10^{-6}	0.590	7.13×10^{-6}

Entry	$V_{tot,\,Ar2I+}$ (mL)	V (mL)	A	$[Ar_2CH^+]$ (M)	$[LB]_0(V_0/V)$ (M)	$[Ar_2I^+]_{0,i}$ (M)	$[Ar_2I^+]_0/[LB]_0(V_0/V)$	$(A_0*(V_0/V)\text{-}A)/A$	[LB] (M)	$[Ar_2I\text{-}LB]$ (M)	$[Ar_2I^+]$ (M)	$[Ar_2I\text{-}LB]/[LB]$
1	0.01	24.15	0.611	7.36×10^{-6}	7.13×10^{-6}	3.52×10^{-6}	0.5	0.74	1.41×10^{-8}	1.66×10^{-6}	1.86×10^{-6}	1.18×10^{2}
2	0.02	24.16	0.716	8.63×10^{-6}	7.13×10^{-6}	7.04×10^{-6}	1.0	0.49	9.24×10^{-9}	2.93×10^{-6}	4.11×10^{-6}	3.17×10^{2}
3	0.03	24.17	0.789	9.51×10^{-6}	7.13×10^{-6}	1.06×10^{-5}	1.5	0.35	6.62×10^{-9}	3.82×10^{-6}	6.74×10^{-6}	5.77×10^{2}
4	0.04	24.18	0.836	1.01×10^{-5}	7.12×10^{-6}	1.41×10^{-5}	2.0	0.27	5.16×10^{-9}	4.39×10^{-6}	9.68×10^{-6}	8.50×10^{2}
5	0.05	24.19	0.868	1.05×10^{-5}	7.12×10^{-6}	1.76×10^{-5}	2.5	0.22	4.26×10^{-9}	4.78×10^{-6}	1.28×10^{-5}	1.12×10^{3}
6	0.07	24.21	0.911	1.10×10^{-5}	7.11×10^{-6}	2.46×10^{-5}	3.5	0.16	3.14×10^{-9}	5.30×10^{-6}	1.93×10^{-5}	1.69×10^{3}

RM696-4

Titration						
Entry	$V_{tot,\,LB}$ (mL)	V (mL)	A	$[Ar_2CH^+]$ (M)	$A_0*(V_0/V)$-A	$[LB]_0$ (M)
1	–	24.10	**1.076**	1.30×10^{-5}		
2	0.04	24.14	**0.333**	4.01×10^{-6}	0.741	8.97×10^{-6}

Entry	$V_{tot,\,Ar2I+}$ (mL)	V (mL)	A	$[Ar_2CH^+]$ (M)	$[LB]_0(V_0/V)$ (M)	$[Ar_2I^+]_{0,i}$ (M)	$[Ar_2I^+]_0/[LB]_0(V_0/V)$	$(A_0*(V_0/V)\text{-}A)/A$	[LB] (M)	$[Ar_2I\text{-}LB]$ (M)	$[Ar_2I^+]$ (M)	$[Ar_2I\text{-}LB]/[LB]$
1	0.01	24.15	0.505	6.08×10^{-6}	8.97×10^{-6}	3.52×10^{-6}	0.4	1.13	2.15×10^{-8}	2.09×10^{-6}	1.43×10^{-6}	9.76×10^{1}
2	0.02	24.16	0.639	7.70×10^{-6}	8.97×10^{-6}	7.04×10^{-6}	0.8	0.68	1.30×10^{-8}	3.72×10^{-6}	3.32×10^{-6}	2.87×10^{2}
3	0.03	24.17	0.725	8.73×10^{-6}	8.96×10^{-6}	1.06×10^{-5}	1.2	0.48	9.14×10^{-9}	4.76×10^{-6}	5.80×10^{-6}	5.21×10^{2}
4	0.04	24.18	0.786	9.47×10^{-6}	8.96×10^{-6}	1.41×10^{-5}	1.6	0.36	6.94×10^{-9}	5.50×10^{-6}	8.57×10^{-6}	7.92×10^{2}
5	0.05	24.19	0.826	9.95×10^{-6}	8.95×10^{-6}	1.76×10^{-5}	2.0	0.30	5.67×10^{-9}	5.98×10^{-6}	1.16×10^{-5}	1.05×10^{3}
6	0.07	24.21	0.878	1.06×10^{-5}	8.95×10^{-6}	2.46×10^{-5}	2.7	0.22	4.19×10^{-9}	6.62×10^{-6}	1.80×10^{-5}	1.58×10^{3}

RM696-5

Titration						
Entry	$V_{tot,\,LB}$ (mL)	V (mL)	A	$[Ar_2CH^+]$ (M)	$A_0*(V_0/V)$-A	$[LB]_0$ (M)
1	–	24.10	**1.073**	1.29×10^{-5}		
2	0.04	24.14	**0.300**	3.61×10^{-6}	0.771	9.34×10^{-6}

Entry	$V_{tot,\,Ar2I+}$ (mL)	V (mL)	A	$[Ar_2CH^+]$ (M)	$[LB]_0(V_0/V)$ (M)	$[Ar_2I^+]_{0,i}$ (M)	$[Ar_2I^+]_0/[LB]_0(V_0/V)$	$(A_0*(V_0/V)\text{-}A)/A$	[LB] (M)	$[Ar_2I\text{-}LB]$ (M)	$[Ar_2I^+]$ (M)	$[Ar_2I\text{-}LB]/[LB]$
1	0.01	24.15	0.495	5.96×10^{-6}	9.34×10^{-6}	3.52×10^{-6}	0.4	1.16	2.22×10^{-8}	2.38×10^{-6}	1.14×10^{-6}	1.07×10^{2}
2	0.02	24.16	0.628	7.57×10^{-6}	9.33×10^{-6}	7.04×10^{-6}	0.8	0.70	1.34×10^{-8}	3.99×10^{-6}	3.05×10^{-6}	2.97×10^{2}
3	0.03	24.17	0.715	8.61×10^{-6}	9.33×10^{-6}	1.06×10^{-5}	1.1	0.50	9.46×10^{-9}	5.04×10^{-6}	5.51×10^{-6}	5.33×10^{2}
4	0.04	24.18	0.776	9.35×10^{-6}	9.33×10^{-6}	1.41×10^{-5}	1.5	0.38	7.21×10^{-9}	5.78×10^{-6}	8.29×10^{-6}	8.03×10^{2}
5	0.05	24.19	0.820	9.88×10^{-6}	9.32×10^{-6}	1.76×10^{-5}	1.9	0.30	5.79×10^{-9}	6.32×10^{-6}	1.13×10^{-5}	1.09×10^{3}
6	0.07	24.21	0.873	1.05×10^{-5}	9.31×10^{-6}	2.46×10^{-5}	2.6	0.22	4.27×10^{-9}	6.95×10^{-6}	1.76×10^{-5}	1.63×10^{3}

2c + 3a (20 °C) - RM697

BIMT experiment (MeCN, 20 °C) for the benzoate ion **3a** with **2b** (stock solution: 8.30 mM) competing against the benzhydrylium ion **B2** (605 nm, ε = 1.66 × 10^5 M^{-1} cm^{-1}, K = 5.25 × 10^7 M^{-1} from LA and LB).

RM697-2

Titration						
Entry	$V_{tot,\,LB}$ (mL)	V (mL)	A	$[Ar_2CH^+]$ (M)	$A_0*(V_0/V)$-A	$[LB]_0$ (M)
1	–	24.10	**1.080**	1.30×10^{-5}		
2	0.04	24.14	**0.343**	4.13×10^{-6}	0.735	8.90×10^{-6}

Entry	$V_{tot,\,Ar2I+}$ (mL)	V (mL)	A	$[Ar_2CH^+]$ (M)	$[LB]_0(V_0/V)$ (M)	$[Ar_2I^+]_{0,i}$ (M)	$[Ar_2I^+]_0$/ $[LB]_0(V_0/V)$	$(A_0*(V_0/V)-A)/A$	[LB] (M)	[Ar$_2$I-LB] (M)	$[Ar_2I^+]$ (M)	[Ar$_2$I-LB]/ [LB]
1	0.20	24.34	0.389	4.69×10^{-6}	8.83×10^{-6}	6.82×10^{-5}	7.7	1.75	3.33×10^{-8}	5.95×10^{-7}	6.76×10^{-5}	1.79×10^{1}
2	0.40	24.54	0.432	5.20×10^{-6}	8.75×10^{-6}	1.35×10^{-4}	15.5	1.46	2.77×10^{-8}	1.15×10^{-6}	1.34×10^{-4}	4.16×10^{1}
3	0.60	24.74	0.473	5.70×10^{-6}	8.68×10^{-6}	2.01×10^{-4}	23.2	1.22	2.33×10^{-8}	1.68×10^{-6}	2.00×10^{-4}	7.21×10^{1}
4	0.80	24.94	0.513	6.18×10^{-6}	8.61×10^{-6}	2.66×10^{-4}	30.9	1.03	1.97×10^{-8}	2.20×10^{-6}	2.64×10^{-4}	1.12×10^{2}
5	1.00	25.14	0.549	6.61×10^{-6}	8.54×10^{-6}	3.30×10^{-4}	38.6	0.89	1.69×10^{-8}	2.67×10^{-6}	3.28×10^{-4}	1.58×10^{2}

RM697-3

Titration						
Entry	$V_{tot,\,LB}$ (mL)	V (mL)	A	$[Ar_2CH^+]$ (M)	$A_0*(V_0/V)$-A	$[LB]_0$ (M)
1	–	24.10	**1.059**	1.28×10^{-5}		
2	0.04	24.14	**0.296**	3.57×10^{-6}	0.761	9.22×10^{-6}

Entry	$V_{tot,\,Ar2I+}$ (mL)	V (mL)	A	$[Ar_2CH^+]$ (M)	$[LB]_0(V_0/V)$ (M)	$[Ar_2I^+]_{0,i}$ (M)	$[Ar_2I^+]_0$/ $[LB]_0(V_0/V)$	$(A_0*(V_0/V)-A)/A$	[LB] (M)	[Ar$_2$I-LB] (M)	$[Ar_2I^+]$ (M)	[Ar$_2$I-LB]/ [LB]
1	0.20	24.34	0.347	4.18×10^{-6}	9.14×10^{-6}	6.82×10^{-5}	7.5	2.02	3.85×10^{-8}	6.54×10^{-7}	6.76×10^{-5}	1.70×10^{1}
2	0.40	24.54	0.390	4.70×10^{-6}	9.07×10^{-6}	1.35×10^{-4}	14.9	1.67	3.18×10^{-8}	1.21×10^{-6}	1.34×10^{-4}	3.80×10^{1}
3	0.60	24.74	0.432	5.20×10^{-6}	9.00×10^{-6}	2.01×10^{-4}	22.4	1.39	2.64×10^{-8}	1.75×10^{-6}	2.00×10^{-4}	6.60×10^{1}
4	0.80	24.94	0.472	5.69×10^{-6}	8.92×10^{-6}	2.66×10^{-4}	29.8	1.17	2.23×10^{-8}	2.26×10^{-6}	2.64×10^{-4}	1.02×10^{2}
5	1.00	25.14	0.508	6.12×10^{-6}	8.85×10^{-6}	3.30×10^{-4}	37.3	1.00	1.90×10^{-8}	2.72×10^{-6}	3.27×10^{-4}	1.43×10^{2}

RM697-4

Titration						
Entry	$V_{tot,\,LB}$ (mL)	V (mL)	A	$[Ar_2CH^+]$ (M)	$A_0*(V_0/V)$-A	$[LB]_0$ (M)
1	–	24.10	**1.079**	1.30×10^{-5}		
2	0.04	24.14	**0.307**	3.70×10^{-6}	0.770	9.33×10^{-6}

Entry	$V_{tot,\,Ar2I+}$ (mL)	V (mL)	A	$[Ar_2CH^+]$ (M)	$[LB]_0(V_0/V)$ (M)	$[Ar_2I^+]_{0,i}$ (M)	$[Ar_2I^+]_0/[LB]_0(V_0/V)$	$(A_0*(V_0/V)-A)/A$	[LB] (M)	$[Ar_2I$-LB] (M)	$[Ar_2I^+]$ (M)	$[Ar_2I$-LB]/[LB]
1	0.20	24.34	0.360	4.34×10^{-6}	9.25×10^{-6}	6.82×10^{-5}	7.4	1.97	3.75×10^{-8}	6.79×10^{-7}	6.75×10^{-5}	1.81×10^{1}
2	0.40	24.54	0.406	4.89×10^{-6}	9.18×10^{-6}	1.35×10^{-4}	14.7	1.61	3.07×10^{-8}	1.27×10^{-6}	1.34×10^{-4}	4.14×10^{1}
3	0.60	24.74	0.452	5.45×10^{-6}	9.10×10^{-6}	2.01×10^{-4}	22.1	1.33	2.53×10^{-8}	1.86×10^{-6}	1.99×10^{-4}	7.36×10^{1}
4	0.80	24.94	0.492	5.93×10^{-6}	9.03×10^{-6}	2.66×10^{-4}	29.5	1.12	2.13×10^{-8}	2.37×10^{-6}	2.64×10^{-4}	1.11×10^{2}
5	1.00	25.14	0.532	6.41×10^{-6}	8.96×10^{-6}	3.30×10^{-4}	36.9	0.94	1.80×10^{-8}	2.89×10^{-6}	3.27×10^{-4}	1.60×10^{2}

1a + 3b (20 °C) - RM821

BIMT experiment (MeCN, 20 °C) for the benzoate ion **3b** with **1a** (stock solution: 21.8 mM) competing against the benzhydrylium ion **B2** (605 nm, ε = 1.66×10^5 M^{-1} cm^{-1}, K = 6.92×10^6 M^{-1} from LA and LB).

RM821-1

Titration						
Entry	$V_{tot,\,LB}$ (mL)	V (mL)	A	$[Ar_2CH^+]$ (M)	$A_0*(V_0/V)$-A	$[LB]_0$ (M)
1	–	24.08	**1.030**	1.24×10^{-5}		
2	0.03	24.11	**0.430**	5.18×10^{-6}	0.599	7.41×10^{-6}

Entry	$V_{tot,\,Ar2I+}$ (mL)	V (mL)	A	$[Ar_2CH^+]$ (M)	$[LB]_0(V_0/V)$ (M)	$[Ar_2I^+]_{0,i}$ (M)	$[Ar_2I^+]_0/[LB]_0(V_0/V)$	$(A_0*(V_0/V)-A)/A$	[LB] (M)	$[Ar_2I$-LB] (M)	$[Ar_2I^+]$ (M)	$[Ar_2I$-LB]/[LB]
1	0.10	24.21	0.497	5.99×10^{-6}	7.38×10^{-6}	8.99×10^{-5}	12.2	1.06	1.53×10^{-7}	8.76×10^{-7}	8.90×10^{-5}	5.71
2	0.20	24.31	0.537	6.47×10^{-6}	7.35×10^{-6}	1.79×10^{-4}	24.3	0.90	1.30×10^{-7}	1.40×10^{-6}	1.78×10^{-4}	1.08×10^{1}
3	0.30	24.41	0.566	6.82×10^{-6}	7.32×10^{-6}	2.67×10^{-4}	36.5	0.80	1.15×10^{-7}	1.79×10^{-6}	2.66×10^{-4}	1.55×10^{1}
4	0.40	24.51	0.588	7.08×10^{-6}	7.29×10^{-6}	3.55×10^{-4}	48.7	0.72	1.04×10^{-7}	2.08×10^{-6}	3.53×10^{-4}	2.00×10^{1}
5	0.50	24.61	0.605	7.29×10^{-6}	7.26×10^{-6}	4.42×10^{-4}	60.9	0.67	9.62×10^{-8}	2.31×10^{-6}	4.40×10^{-4}	2.41×10^{1}

RM821-2

Titration						
Entry	$V_{tot,\,LB}$ (mL)	V (mL)	A	$[Ar_2CH^+]$ (M)	$A_0*(V_0/V)$-A	$[LB]_0$ (M)
1	–	24.08	**1.032**	1.24×10^{-5}		
2	0.03	24.11	**0.430**	5.18×10^{-6}	0.601	7.44×10^{-6}

Entry	$V_{tot,\,Ar2I+}$ (mL)	V (mL)	A	$[Ar_2CH^+]$ (M)	$[LB]_0(V_0/V)$ (M)	$[Ar_2I^+]_{0,i}$ (M)	$[Ar_2I^+]_0/[LB]_0(V_0/V)$	$(A_0*(V_0/V)-A)/A$	[LB] (M)	$[Ar_2I$-LB] (M)	$[Ar_2I^+]$ (M)	$[Ar_2I$-LB]/[LB]
1	0.10	24.21	0.501	6.04×10^{-6}	7.41×10^{-6}	8.99×10^{-5}	12.1	1.05	1.52×10^{-7}	9.26×10^{-7}	8.89×10^{-5}	6.11
2	0.20	24.31	0.540	6.51×10^{-6}	7.38×10^{-6}	1.79×10^{-4}	24.3	0.89	1.29×10^{-7}	1.44×10^{-6}	1.78×10^{-4}	1.11×10^{1}
3	0.30	24.41	0.568	6.84×10^{-6}	7.35×10^{-6}	2.67×10^{-4}	36.4	0.79	1.15×10^{-7}	1.81×10^{-6}	2.66×10^{-4}	1.58×10^{1}
4	0.40	24.51	0.589	7.10×10^{-6}	7.32×10^{-6}	3.55×10^{-4}	48.5	0.72	1.04×10^{-7}	2.09×10^{-6}	3.53×10^{-4}	2.01×10^{1}
5	0.50	24.61	0.607	7.31×10^{-6}	7.29×10^{-6}	4.42×10^{-4}	60.7	0.66	9.59×10^{-8}	2.34×10^{-6}	4.40×10^{-4}	2.44×10^{1}

RM821-3

Titration						
Entry	$V_{tot,\,LB}$ (mL)	V (mL)	A	$[Ar_2CH^+]$ (M)	$A_0*(V_0/V)$-A	$[LB]_0$ (M)
1	–	24.08	**1.047**	1.26×10^{-5}		
2	0.03	24.11	**0.481**	5.80×10^{-6}	0.565	6.97×10^{-6}

Entry	$V_{tot,\,Ar2I+}$ (mL)	V (mL)	A	$[Ar_2CH^+]$ (M)	$[LB]_0(V_0/V)$ (M)	$[Ar_2I^+]_{0,i}$ (M)	$[Ar_2I^+]_0/[LB]_0(V_0/V)$	$(A_0*(V_0/V)-A)/A$	[LB] (M)	$[Ar_2I$-LB] (M)	$[Ar_2I^+]$ (M)	$[Ar_2I$-LB]/[LB]
1	0.10	24.21	0.538	6.48×10^{-6}	6.94×10^{-6}	8.99×10^{-5}	12.9	0.94	1.35×10^{-7}	7.44×10^{-7}	8.91×10^{-5}	5.50
2	0.20	24.31	0.570	6.87×10^{-6}	6.92×10^{-6}	1.79×10^{-4}	25.9	0.82	1.18×10^{-7}	1.17×10^{-6}	1.78×10^{-4}	9.88
3	0.30	24.41	0.594	7.16×10^{-6}	6.89×10^{-6}	2.67×10^{-4}	38.8	0.74	1.07×10^{-7}	1.49×10^{-6}	2.66×10^{-4}	1.40×10^{1}
4	0.40	24.51	0.612	7.37×10^{-6}	6.86×10^{-6}	3.55×10^{-4}	51.8	0.68	9.84×10^{-8}	1.74×10^{-6}	3.53×10^{-4}	1.77×10^{1}
5	0.50	24.61	0.626	7.54×10^{-6}	6.83×10^{-6}	4.42×10^{-4}	64.7	0.64	9.20×10^{-8}	1.94×10^{-6}	4.40×10^{-4}	2.11×10^{1}

1f + 3b (20 °C) - RM822

BIMT experiment (MeCN, 20 °C) for the benzoate ion **3b** with **1f** (stock solution: 7.28 mM) competing against the benzhydrylium ion **B2** (605 nm, ε = 1.66 × 10^5 M^{-1} cm^{-1}, K = 6.92 × 10^6 M^{-1} from LA and LB).

RM822-1

Titration						
Entry	$V_{tot,\,LB}$ (mL)	V (mL)	A	$[Ar_2CH^+]$ (M)	$A_0*(V_0/V)$-A	$[LB]_0$ (M)
1	–	24.08	**1.027**	1.24×10^{-5}		
2	0.03	24.11	**0.398**	4.80×10^{-6}	0.628	7.79×10^{-6}

Entry	$V_{tot,\,Ar2I+}$ (mL)	V (mL)	A	$[Ar_2CH^+]$ (M)	$[LB]_0(V_0/V)$ (M)	$[Ar_2I^+]_{0,i}$ (M)	$[Ar_2I^+]_0$/ $[LB]_0(V_0/V)$	$(A_0*(V_0/V)$-A)/A	[LB] (M)	$[Ar_2I$-LB] (M)	$[Ar_2I^+]$ (M)	$[Ar_2I$-LB]/ [LB]
1	0.03	24.14	0.458	5.52×10^{-6}	7.78×10^{-6}	7.54×10^{-6}	1.0	1.24	1.79×10^{-7}	7.77×10^{-7}	6.77×10^{-6}	4.34
2	0.05	24.16	0.504	6.07×10^{-6}	7.77×10^{-6}	1.51×10^{-5}	1.9	1.03	1.49×10^{-7}	1.37×10^{-6}	1.37×10^{-5}	9.16
3	0.08	24.19	0.540	6.51×10^{-6}	7.77×10^{-6}	2.26×10^{-5}	2.9	0.89	1.29×10^{-7}	1.82×10^{-6}	2.08×10^{-5}	1.41×10^{1}
4	0.10	24.21	0.569	6.86×10^{-6}	7.76×10^{-6}	3.01×10^{-5}	3.9	0.80	1.15×10^{-7}	2.19×10^{-6}	2.79×10^{-5}	1.91×10^{1}
5	0.13	24.24	0.594	7.16×10^{-6}	7.75×10^{-6}	3.76×10^{-5}	4.8	0.72	1.04×10^{-7}	2.51×10^{-6}	3.50×10^{-5}	2.42×10^{1}

RM822-2

Titration						
Entry	$V_{tot,\,LB}$ (mL)	V (mL)	A	$[Ar_2CH^+]$ (M)	$A_0*(V_0/V)$-A	$[LB]_0$ (M)
1	–	24.08	**1.039**	1.25×10^{-5}		
2	0.03	24.11	**0.448**	5.40×10^{-6}	0.590	7.30×10^{-6}

Entry	$V_{tot,\,Ar2I+}$ (mL)	V (mL)	A	$[Ar_2CH^+]$ (M)	$[LB]_0(V_0/V)$ (M)	$[Ar_2I^+]_{0,i}$ (M)	$[Ar_2I^+]_0$/ $[LB]_0(V_0/V)$	$(A_0*(V_0/V)$-A)/A	[LB] (M)	$[Ar_2I$-LB] (M)	$[Ar_2I^+]$ (M)	$[Ar_2I$-LB]/ [LB]
1	0.03	24.14	0.499	6.01×10^{-6}	7.29×10^{-6}	7.54×10^{-6}	1.0	1.08	1.56×10^{-7}	6.54×10^{-7}	6.89×10^{-6}	4.20
2	0.05	24.16	0.536	6.46×10^{-6}	7.28×10^{-6}	1.51×10^{-5}	2.1	0.93	1.35×10^{-7}	1.13×10^{-6}	1.39×10^{-5}	8.36
3	0.08	24.19	0.565	6.81×10^{-6}	7.27×10^{-6}	2.26×10^{-5}	3.1	0.83	1.20×10^{-7}	1.50×10^{-6}	2.11×10^{-5}	1.25×10^{1}
4	0.10	24.21	0.588	7.08×10^{-6}	7.27×10^{-6}	3.01×10^{-5}	4.1	0.76	1.09×10^{-7}	1.79×10^{-6}	2.83×10^{-5}	1.63×10^{1}
5	0.13	24.24	0.608	7.33×10^{-6}	7.26×10^{-6}	3.76×10^{-5}	5.2	0.70	1.01×10^{-7}	2.04×10^{-6}	3.55×10^{-5}	2.03×10^{1}

RM822-3

Titration						
Entry	$V_{tot,\,LB}$ (mL)	V (mL)	A	$[Ar_2CH^+]$ (M)	$A_0*(V_0/V)$-A	$[LB]_0$ (M)
1	–	24.08	**1.033**	1.24×10^{-5}		
2	0.03	24.11	**0.429**	5.17×10^{-6}	0.603	7.46×10^{-6}

Entry	$V_{tot,\,Ar2I+}$ (mL)	V (mL)	A	$[Ar_2CH^+]$ (M)	$[LB]_0(V_0/V)$ (M)	$[Ar_2I^+]_{0,i}$ (M)	$[Ar_2I^+]_0/[LB]_0(V_0/V)$	$(A_0*(V_0/V)-A)/A$	[LB] (M)	$[Ar_2I$-LB] (M)	$[Ar_2I^+]$ (M)	$[Ar_2I$-LB]/[LB]
1	0.03	24.14	0.482	5.81×10^{-6}	7.46×10^{-6}	7.54×10^{-6}	1.0	1.14	1.65×10^{-7}	6.82×10^{-7}	6.86×10^{-6}	4.15
2	0.05	24.16	0.516	6.22×10^{-6}	7.45×10^{-6}	1.51×10^{-5}	2.0	1.00	1.44×10^{-7}	1.12×10^{-6}	1.40×10^{-5}	7.77
3	0.08	24.19	0.544	6.55×10^{-6}	7.44×10^{-6}	2.26×10^{-5}	3.0	0.89	1.29×10^{-7}	1.48×10^{-6}	2.11×10^{-5}	1.15×10^{1}
4	0.10	24.21	0.566	6.82×10^{-6}	7.43×10^{-6}	3.01×10^{-5}	4.0	0.82	1.18×10^{-7}	1.76×10^{-6}	2.83×10^{-5}	1.49×10^{1}
5	0.13	24.24	0.584	7.04×10^{-6}	7.43×10^{-6}	3.76×10^{-5}	5.1	0.76	1.09×10^{-7}	1.99×10^{-6}	3.56×10^{-5}	1.81×10^{1}

2a + 3b (20 °C) - RM823

BIMT experiment (MeCN, 20 °C) for the benzoate ion **3b** with **2a** (stock solution: 11.0 mM) competing against the benzhydrylium ion **B2** (605 nm, ε = 1.66×10^5 M^{-1} cm^{-1}, K = 6.92×10^6 M^{-1} from LA and LB).

RM823-1

Titration						
Entry	$V_{tot,\,LB}$ (mL)	V (mL)	A	$[Ar_2CH^+]$ (M)	$A_0*(V_0/V)$-A	$[LB]_0$ (M)
1	–	24.08	**1.042**	1.26×10^{-5}		
2	0.03	24.11	**0.464**	5.59×10^{-6}	0.577	7.13×10^{-6}

Entry	$V_{tot,\,Ar2I+}$ (mL)	V (mL)	A	$[Ar_2CH^+]$ (M)	$[LB]_0(V_0/V)$ (M)	$[Ar_2I^+]_{0,i}$ (M)	$[Ar_2I^+]_0/[LB]_0(V_0/V)$	$(A_0*(V_0/V)-A)/A$	[LB] (M)	$[Ar_2I$-LB] (M)	$[Ar_2I^+]$ (M)	$[Ar_2I$-LB]/[LB]
1	0.01	24.12	0.566	6.82×10^{-6}	7.12×10^{-6}	4.56×10^{-6}	0.6	0.84	1.21×10^{-7}	1.29×10^{-6}	3.27×10^{-6}	1.06×10^{1}
2	0.02	24.13	0.633	7.63×10^{-6}	7.12×10^{-6}	9.11×10^{-6}	1.3	0.64	9.29×10^{-8}	2.13×10^{-6}	6.98×10^{-6}	2.29×10^{1}
3	0.03	24.14	0.676	8.14×10^{-6}	7.12×10^{-6}	1.37×10^{-5}	1.9	0.54	7.77×10^{-8}	2.66×10^{-6}	1.10×10^{-5}	3.43×10^{1}
4	0.04	24.15	0.709	8.54×10^{-6}	7.12×10^{-6}	1.82×10^{-5}	2.6	0.47	6.73×10^{-8}	3.07×10^{-6}	1.51×10^{-5}	4.57×10^{1}
5	0.05	24.16	0.733	8.83×10^{-6}	7.11×10^{-6}	2.27×10^{-5}	3.2	0.42	6.03×10^{-8}	3.37×10^{-6}	1.94×10^{-5}	5.60×10^{1}

RM823-2

Titration						
Entry	$V_{tot,\,LB}$ (mL)	V (mL)	A	$[Ar_2CH^+]$ (M)	$A_0*(V_0/V)$-A	$[LB]_0$ (M)
1	–	24.08	**1.028**	1.24×10^{-5}		
2	0.03	24.11	**0.438**	5.28×10^{-6}	0.589	7.29×10^{-6}

Entry	$V_{tot,\,Ar2I+}$ (mL)	V (mL)	A	$[Ar_2CH^+]$ (M)	$[LB]_0(V_0/V)$ (M)	$[Ar_2I^+]_{0,i}$ (M)	$[Ar_2I^+]_0/[LB]_0(V_0/V)$	$(A_0*(V_0/V)-A)/A$	[LB] (M)	$[Ar_2I$-LB] (M)	$[Ar_2I^+]$ (M)	$[Ar_2I$-LB]/[LB]
1	0.01	24.12	0.543	6.54×10^{-6}	7.28×10^{-6}	4.56×10^{-6}	0.6	0.89	1.29×10^{-7}	1.33×10^{-6}	3.22×10^{-6}	1.04×10^{1}
2	0.02	24.13	0.618	7.45×10^{-6}	7.28×10^{-6}	9.11×10^{-6}	1.3	0.66	9.54×10^{-8}	2.27×10^{-6}	6.84×10^{-6}	2.38×10^{1}
3	0.03	24.14	0.666	8.02×10^{-6}	7.28×10^{-6}	1.37×10^{-5}	1.9	0.54	7.80×10^{-8}	2.87×10^{-6}	1.08×10^{-5}	3.68×10^{1}
4	0.04	24.15	0.702	8.46×10^{-6}	7.28×10^{-6}	1.82×10^{-5}	2.5	0.46	6.65×10^{-8}	3.32×10^{-6}	1.49×10^{-5}	4.99×10^{1}
5	0.05	24.16	0.727	8.76×10^{-6}	7.27×10^{-6}	2.27×10^{-5}	3.1	0.41	5.92×10^{-8}	3.63×10^{-6}	1.91×10^{-5}	6.13×10^{1}

RM823-5

Titration						
Entry	$V_{tot,\,LB}$ (mL)	V (mL)	A	$[Ar_2CH^+]$ (M)	$A_0*(V_0/V)$-A	$[LB]_0$ (M)
1	–	24.08	**1.039**	1.25×10^{-5}		
2	0.03	24.11	**0.446**	5.37×10^{-6}	0.592	7.32×10^{-6}

Entry	$V_{tot,\,Ar2I+}$ (mL)	V (mL)	A	$[Ar_2CH^+]$ (M)	$[LB]_0(V_0/V)$ (M)	$[Ar_2I^+]_{0,i}$ (M)	$[Ar_2I^+]_0/[LB]_0(V_0/V)$	$(A_0*(V_0/V)-A)/A$	[LB] (M)	$[Ar_2I$-LB] (M)	$[Ar_2I^+]$ (M)	$[Ar_2I$-LB]/[LB]
1	0.01	24.12	0.557	6.70×10^{-6}	7.32×10^{-6}	4.56×10^{-6}	0.6	0.6	1.25×10^{-7}	1.40×10^{-6}	3.16×10^{-6}	1.12×10^{1}
2	0.02	24.13	0.630	7.59×10^{-6}	7.31×10^{-6}	9.11×10^{-6}	1.2	1.2	9.33×10^{-8}	2.32×10^{-6}	6.79×10^{-6}	2.48×10^{1}
3	0.03	24.14	0.679	8.18×10^{-6}	7.31×10^{-6}	1.37×10^{-5}	1.9	1.9	7.61×10^{-8}	2.93×10^{-6}	1.07×10^{-5}	3.85×10^{1}
4	0.04	24.15	0.715	8.61×10^{-6}	7.31×10^{-6}	1.82×10^{-5}	2.5	2.5	6.49×10^{-8}	3.38×10^{-6}	1.48×10^{-5}	5.20×10^{1}
5	0.05	24.16	0.741	8.93×10^{-6}	7.31×10^{-6}	2.27×10^{-5}	3.1	3.1	5.75×10^{-8}	3.70×10^{-6}	1.90×10^{-5}	6.44×10^{1}

1a + 3c (20 °C) - RM812

BIMT experiment (MeCN, 20 °C) for the benzoate ion **3c** with **1a** (stock solution: 28.2 mM) competing against the benzhydrylium ion **B2** (605 nm, ε = 1.66 × 10^5 M^{-1} cm^{-1}, K = 6.61 × 10^5 M^{-1} from LA and LB).

RM812-1

Titration						
Entry	$V_{tot,\,LB}$ (mL)	V (mL)	A	[Ar_2CH^+] (M)	A_0*(V_0/V)-A	[LB]$_0$ (M)
1	–	24.10	**0.991**	1.19 × 10^{-5}		
2	0.04	24.14	**0.446**	5.37 × 10^{-6}	0.543	8.39 × 10^{-6}

Entry	$V_{tot,\,Ar2I+}$ (mL)	V (mL)	A	[Ar_2CH^+] (M)	[LB]$_0$(V_0/V) (M)	[Ar_2I^+]$_{0,i}$ (M)	[Ar_2I^+]$_0$/ [LB]$_0$(V_0/V)	(A_0*(V_0/V)-A)/A	[LB] (M)	[Ar_2I-LB] (M)	[Ar_2I^+] (M)	[Ar_2I-LB]/ [LB]
1	0.05	24.19	0.533	6.42 × 10^{-6}	8.37 × 10^{-6}	5.82 × 10^{-5}	7.0	0.85	1.29 × 10^{-6}	1.61 × 10^{-6}	5.66 × 10^{-5}	1.25
2	0.10	24.24	0.582	7.01 × 10^{-6}	8.36 × 10^{-6}	1.16 × 10^{-4}	13.9	0.69	1.05 × 10^{-6}	2.45 × 10^{-6}	1.14 × 10^{-4}	2.33
3	0.15	24.29	0.614	7.40 × 10^{-6}	8.34 × 10^{-6}	1.74 × 10^{-4}	20.9	0.60	9.10 × 10^{-7}	2.98 × 10^{-6}	1.71 × 10^{-4}	3.27
4	0.20	24.34	0.637	7.67 × 10^{-6}	8.32 × 10^{-6}	2.32 × 10^{-4}	27.8	0.54	8.18 × 10^{-7}	3.36 × 10^{-6}	2.28 × 10^{-4}	4.10
5	0.25	24.39	0.655	7.89 × 10^{-6}	8.30 × 10^{-6}	2.89 × 10^{-4}	34.8	0.49	7.49 × 10^{-7}	3.65 × 10^{-6}	2.85 × 10^{-4}	4.87

RM812-2

Titration						
Entry	$V_{tot,\,LB}$ (mL)	V (mL)	A	[Ar_2CH^+] (M)	A_0*(V_0/V)-A	[LB]$_0$ (M)
1	–	24.10	**0.983**	1.18 × 10^{-5}		
2	0.04	24.14	**0.431**	5.19 × 10^{-6}	0.550	8.56 × 10^{-6}

Entry	$V_{tot,\,Ar2I+}$ (mL)	V (mL)	A	[Ar_2CH^+] (M)	[LB]$_0$(V_0/V) (M)	[Ar_2I^+]$_{0,i}$ (M)	[Ar_2I^+]$_0$/ [LB]$_0$(V_0/V)	(A_0*(V_0/V)-A)/A	[LB] (M)	[Ar_2I-LB] (M)	[Ar_2I^+] (M)	[Ar_2I-LB]/ [LB]
1	0.05	24.19	0.534	6.43 × 10^{-6}	8.55 × 10^{-6}	5.82 × 10^{-5}	6.8	0.83	1.26 × 10^{-6}	1.92 × 10^{-6}	5.63 × 10^{-5}	1.52
2	0.10	24.24	0.584	7.04 × 10^{-6}	8.53 × 10^{-6}	1.16 × 10^{-4}	13.6	0.67	1.02 × 10^{-6}	2.77 × 10^{-6}	1.13 × 10^{-4}	2.72
3	0.15	24.29	0.616	7.42 × 10^{-6}	8.51 × 10^{-6}	1.74 × 10^{-4}	20.4	0.58	8.83 × 10^{-7}	3.30 × 10^{-6}	1.71 × 10^{-4}	3.74
4	0.20	24.34	0.640	7.71 × 10^{-6}	8.49 × 10^{-6}	2.32 × 10^{-4}	27.3	0.52	7.88 × 10^{-7}	3.69 × 10^{-6}	2.28 × 10^{-4}	4.68
5	0.25	24.39	0.658	7.93 × 10^{-6}	8.48 × 10^{-6}	2.89 × 10^{-4}	34.1	0.48	7.21 × 10^{-7}	3.98 × 10^{-6}	2.85 × 10^{-4}	5.52

RM812-4

Titration						
Entry	$V_{tot,\,LB}$ (mL)	V (mL)	A	$[Ar_2CH^+]$ (M)	$A_0*(V_0/V)$-A	$[LB]_0$ (M)
1	–	24.10	**0.955**	1.15×10^{-5}		
2	0.04	24.14	**0.425**	5.12×10^{-6}	0.528	8.25×10^{-6}

Entry	$V_{tot,\,Ar2I+}$ (mL)	V (mL)	A	$[Ar_2CH^+]$ (M)	$[LB]_0(V_0/V)$ (M)	$[Ar_2I^+]_{0,i}$ (M)	$[Ar_2I^+]_0/[LB]_0(V_0/V)$	$(A_0*(V_0/V)-A)/A$	[LB] (M)	$[Ar_2I$-LB] (M)	$[Ar_2I^+]$ (M)	$[Ar_2I$-LB]/[LB]
1	0.05	24.19	0.523	6.30×10^{-6}	8.23×10^{-6}	5.82×10^{-5}	7.1	0.82	1.24×10^{-6}	1.83×10^{-6}	5.64×10^{-5}	1.48
2	0.10	24.24	0.570	6.87×10^{-6}	8.21×10^{-6}	1.16×10^{-4}	14.1	0.67	1.01×10^{-6}	2.63×10^{-6}	1.14×10^{-4}	2.61
3	0.15	24.29	0.601	7.24×10^{-6}	8.20×10^{-6}	1.74×10^{-4}	21.2	0.58	8.73×10^{-7}	3.15×10^{-6}	1.71×10^{-4}	3.61
4	0.20	24.34	0.624	7.52×10^{-6}	8.18×10^{-6}	2.32×10^{-4}	28.3	0.52	7.80×10^{-7}	3.53×10^{-6}	2.28×10^{-4}	4.52
5	0.25	24.39	0.642	7.73×10^{-6}	8.16×10^{-6}	2.89×10^{-4}	35.4	0.47	7.11×10^{-7}	3.82×10^{-6}	2.85×10^{-4}	5.37

1f + 3c (20 °C) - RM813

BIMT experiment (MeCN, 20 °C) for the benzoate ion **3c** with **1f** (stock solution: 9.27 mM) competing against the benzhydrylium ion **B2** (605 nm, ε = 1.66×10^5 M^{-1} cm^{-1}, K = 6.61×10^5 M^{-1} from LA and LB).

RM813-1

Titration						
Entry	$V_{tot,\,LB}$ (mL)	V (mL)	A	$[Ar_2CH^+]$ (M)	$A_0*(V_0/V)$-A	$[LB]_0$ (M)
1	–	24.10	**0.957**	1.15×10^{-5}		
2	0.04	24.14	**0.385**	4.64×10^{-6}	0.570	9.11×10^{-6}

Entry	$V_{tot,\,Ar2I+}$ (mL)	V (mL)	A	$[Ar_2CH^+]$ (M)	$[LB]_0(V_0/V)$ (M)	$[Ar_2I^+]_{0,i}$ (M)	$[Ar_2I^+]_0/[LB]_0(V_0/V)$	$(A_0*(V_0/V)-A)/A$	[LB] (M)	$[Ar_2I$-LB] (M)	$[Ar_2I^+]$ (M)	$[Ar_2I$-LB]/[LB]
1	0.02	24.16	0.484	5.83×10^{-6}	9.11×10^{-6}	7.67×10^{-6}	0.8	0.97	1.47×10^{-6}	1.97×10^{-6}	5.71×10^{-6}	1.34
2	0.04	24.18	0.542	6.53×10^{-6}	9.10×10^{-6}	1.53×10^{-5}	1.7	0.76	1.15×10^{-6}	2.99×10^{-6}	1.23×10^{-5}	2.60
3	0.06	24.20	0.582	7.01×10^{-6}	9.09×10^{-6}	2.30×10^{-5}	2.5	0.64	9.65×10^{-7}	3.66×10^{-6}	1.93×10^{-5}	3.79
4	0.08	24.22	0.611	7.36×10^{-6}	9.08×10^{-6}	3.06×10^{-5}	3.4	0.56	8.45×10^{-7}	4.13×10^{-6}	2.65×10^{-5}	4.88
5	0.10	24.24	0.634	7.64×10^{-6}	9.08×10^{-6}	3.82×10^{-5}	4.2	0.50	7.58×10^{-7}	4.49×10^{-6}	3.37×10^{-5}	5.93

RM813-2

Titration						
Entry	$V_{tot,\,LB}$ (mL)	V (mL)	A	$[Ar_2CH^+]$ (M)	$A_0*(V_0/V)$-A	$[LB]_0$ (M)
1	–	24.10	**0.949**	1.14×10^{-5}		
2	0.04	24.14	**0.370**	4.46×10^{-6}	0.577	9.32×10^{-6}

Entry	$V_{tot,\,Ar2I+}$ (mL)	V (mL)	A	$[Ar_2CH^+]$ (M)	$[LB]_0(V_0/V)$ (M)	$[Ar_2I^+]_{0,i}$ (M)	$[Ar_2I^+]_0/[LB]_0(V_0/V)$	$(A_0*(V_0/V)-A)/A$	[LB] (M)	$[Ar_2I$-LB] (M)	$[Ar_2I^+]$ (M)	$[Ar_2I$-LB]/[LB]
1	0.02	24.16	0.472	5.69×10^{-6}	9.31×10^{-6}	7.67×10^{-6}	0.8	1.01	1.52×10^{-6}	2.07×10^{-6}	5.60×10^{-6}	1.36
2	0.04	24.18	0.529	6.37×10^{-6}	9.30×10^{-6}	1.53×10^{-5}	1.6	0.79	1.19×10^{-6}	3.09×10^{-6}	1.22×10^{-5}	2.59
3	0.06	24.20	0.569	6.86×10^{-6}	9.30×10^{-6}	2.30×10^{-5}	2.5	0.66	1.00×10^{-6}	3.76×10^{-6}	1.92×10^{-5}	3.76
4	0.08	24.22	0.598	7.20×10^{-6}	9.29×10^{-6}	3.06×10^{-5}	3.3	0.58	8.76×10^{-7}	4.24×10^{-6}	2.64×10^{-5}	4.84
5	0.10	24.24	0.624	7.52×10^{-6}	9.28×10^{-6}	3.82×10^{-5}	4.1	0.51	7.75×10^{-7}	4.66×10^{-6}	3.36×10^{-5}	6.01

RM813-3

Titration						
Entry	$V_{tot,\,LB}$ (mL)	V (mL)	A	$[Ar_2CH^+]$ (M)	$A_0*(V_0/V)$-A	$[LB]_0$ (M)
1	–	24.10	**0.983**	1.18×10^{-5}		
2	0.04	24.14	**0.424**	5.11×10^{-6}	0.557	8.70×10^{-6}

Entry	$V_{tot,\,Ar2I+}$ (mL)	V (mL)	A	$[Ar_2CH^+]$ (M)	$[LB]_0(V_0/V)$ (M)	$[Ar_2I^+]_{0,i}$ (M)	$[Ar_2I^+]_0/[LB]_0(V_0/V)$	$(A_0*(V_0/V)-A)/A$	[LB] (M)	$[Ar_2I$-LB] (M)	$[Ar_2I^+]$ (M)	$[Ar_2I$-LB]/[LB]
1	0.02	24.16	0.517	6.23×10^{-6}	8.70×10^{-6}	7.67×10^{-6}	0.9	0.90	1.36×10^{-6}	1.76×10^{-6}	5.92×10^{-6}	1.29
2	0.04	24.18	0.571	6.88×10^{-6}	8.69×10^{-6}	1.53×10^{-5}	1.8	0.72	1.08×10^{-6}	2.68×10^{-6}	1.27×10^{-5}	2.48
3	0.06	24.20	0.608	7.33×10^{-6}	8.68×10^{-6}	2.30×10^{-5}	2.6	0.61	9.23×10^{-7}	3.29×10^{-6}	1.97×10^{-5}	3.56
4	0.08	24.22	0.635	7.65×10^{-6}	8.68×10^{-6}	3.06×10^{-5}	3.5	0.54	8.18×10^{-7}	3.72×10^{-6}	2.69×10^{-5}	4.55
5	0.10	24.24	0.657	7.92×10^{-6}	8.67×10^{-6}	3.82×10^{-5}	4.4	0.49	7.38×10^{-7}	4.07×10^{-6}	3.42×10^{-5}	5.52

2a + 3c (20 °C) - RM814

BIMT experiment (MeCN, 20 °C) for the benzoate ion **3c** with **2a** (stock solution: 6.43 mM) competing against the benzhydrylium ion **B2** (605 nm, ε = 1.66 × 10^5 M^{-1} cm^{-1}, K = 6.61 × 10^5 M^{-1} from LA and LB).

RM814-1

Titration						
Entry	$V_{tot,\,LB}$ (mL)	V (mL)	A	$[Ar_2CH^+]$ (M)	$A_0*(V_0/V)$-A	$[LB]_0$ (M)
1	–	24.10	**0.984**	1.19×10^{-5}		
2	0.04	24.14	**0.425**	5.12×10^{-6}	0.557	8.70×10^{-6}

Entry	$V_{tot,\,Ar2I+}$ (mL)	V (mL)	A	$[Ar_2CH^+]$ (M)	$[LB]_0(V_0/V)$ (M)	$[Ar_2I^+]_{0,i}$ (M)	$[Ar_2I^+]_0$/ $[LB]_0(V_0/V)$	$(A_0*(V_0/V)$-A)/A	[LB] (M)	$[Ar_2I$-LB] (M)	$[Ar_2I^+]$ (M)	$[Ar_2I$-LB]/ [LB]
1	0.01	24.15	0.507	6.11×10^{-6}	8.70×10^{-6}	2.66×10^{-6}	0.3	0.94	1.42×10^{-6}	1.56×10^{-6}	1.11×10^{-6}	1.10
2	0.02	24.16	0.577	6.95×10^{-6}	8.69×10^{-6}	5.33×10^{-6}	0.6	0.70	1.06×10^{-6}	2.76×10^{-6}	2.57×10^{-6}	2.60
3	0.03	24.17	0.630	7.59×10^{-6}	8.69×10^{-6}	7.99×10^{-6}	0.9	0.56	8.44×10^{-7}	3.62×10^{-6}	4.37×10^{-6}	4.29
4	0.04	24.18	0.670	8.07×10^{-6}	8.69×10^{-6}	1.06×10^{-5}	1.2	0.46	7.02×10^{-7}	4.24×10^{-6}	6.40×10^{-6}	6.04
5	0.05	24.19	0.700	8.43×10^{-6}	8.68×10^{-6}	1.33×10^{-5}	1.5	0.40	6.06×10^{-7}	4.70×10^{-6}	8.60×10^{-6}	7.75

RM814-2

Titration						
Entry	$V_{tot,\,LB}$ (mL)	V (mL)	A	$[Ar_2CH^+]$ (M)	$A_0*(V_0/V)$-A	$[LB]_0$ (M)
1	–	24.10	**0.962**	1.16×10^{-5}		
2	0.04	24.14	**0.388**	4.67×10^{-6}	0.572	9.13×10^{-6}

Entry	$V_{tot,\,Ar2I+}$ (mL)	V (mL)	A	$[Ar_2CH^+]$ (M)	$[LB]_0(V_0/V)$ (M)	$[Ar_2I^+]_{0,i}$ (M)	$[Ar_2I^+]_0$/ $[LB]_0(V_0/V)$	$(A_0*(V_0/V)$-A)/A	[LB] (M)	$[Ar_2I$-LB] (M)	$[Ar_2I^+]$ (M)	$[Ar_2I$-LB]/ [LB]
1	0.01	24.15	0.477	5.75×10^{-6}	9.13×10^{-6}	2.66×10^{-6}	0.3	1.01	1.53×10^{-6}	1.77×10^{-6}	8.91×10^{-7}	1.16
2	0.02	24.16	0.554	6.67×10^{-6}	9.12×10^{-6}	5.33×10^{-6}	0.6	0.73	1.11×10^{-6}	3.13×10^{-6}	2.20×10^{-6}	2.82
3	0.03	24.17	0.612	7.37×10^{-6}	9.12×10^{-6}	7.99×10^{-6}	0.9	0.57	8.59×10^{-7}	4.08×10^{-6}	3.91×10^{-6}	4.75
4	0.04	24.18	0.653	7.87×10^{-6}	9.11×10^{-6}	1.06×10^{-5}	1.2	0.47	7.09×10^{-7}	4.72×10^{-6}	5.92×10^{-6}	6.66
5	0.05	24.19	0.681	8.20×10^{-6}	9.11×10^{-6}	1.33×10^{-5}	1.5	0.41	6.17×10^{-7}	5.15×10^{-6}	8.15×10^{-6}	8.35

RM814-3

Titration						
Entry	$V_{tot,\,LB}$ (mL)	V (mL)	A	$[Ar_2CH^+]$ (M)	$A_0*(V_0/V)$-A	$[LB]_0$ (M)
1	–	24.10	**0.960**	1.16×10^{-5}		
2	0.04	24.14	**0.395**	4.76×10^{-6}	0.563	8.95×10^{-6}

Entry	$V_{tot,\,Ar2I+}$ (mL)	V (mL)	A	$[Ar_2CH^+]$ (M)	$[LB]_0(V_0/V)$ (M)	$[Ar_2I^+]_{0,i}$ (M)	$[Ar_2I^+]_0/[LB]_0(V_0/V)$	$(A_0*(V_0/V)-A)/A$	[LB] (M)	$[Ar_2I$-LB] (M)	$[Ar_2I^+]$ (M)	$[Ar_2I$-LB]/[LB]
1	0.01	24.15	0.494	5.95×10^{-6}	8.94×10^{-6}	2.66×10^{-6}	0.3	0.94	1.42×10^{-6}	1.93×10^{-6}	7.33×10^{-7}	1.36
2	0.02	24.16	0.570	6.87×10^{-6}	8.94×10^{-6}	5.33×10^{-6}	0.6	0.68	1.03×10^{-6}	3.24×10^{-6}	2.09×10^{-6}	3.15
3	0.03	24.17	0.625	7.53×10^{-6}	8.94×10^{-6}	7.99×10^{-6}	0.9	0.53	8.05×10^{-7}	4.13×10^{-6}	3.86×10^{-6}	5.13
4	0.04	24.18	0.665	8.01×10^{-6}	8.93×10^{-6}	1.06×10^{-5}	1.2	0.44	6.64×10^{-7}	4.75×10^{-6}	5.89×10^{-6}	7.15
5	0.05	24.19	0.693	8.35×10^{-6}	8.93×10^{-6}	1.33×10^{-5}	1.5	0.38	5.75×10^{-7}	5.18×10^{-6}	8.12×10^{-6}	9.00

1a + 3d (20 °C) - RM700

BIMT experiment (MeCN, 20 °C) for the benzoate ion **3d** with **1a** (stock solution: 33.8 mM) competing against the benzhydrylium ion **B2** (605 nm, ε = 1.66×10^5 M^{-1} cm^{-1}, K = 2.88×10^5 M^{-1} from LA and LB).

RM700-2

Titration						
Entry	$V_{tot,\,LB}$ (mL)	V (mL)	A	$[Ar_2CH^+]$ (M)	$A_0*(V_0/V)$-A	$[LB]_0$ (M)
1	–	24.08	**1.040**	1.25×10^{-5}		
2	0.05	24.13	**0.357**	4.30×10^{-6}	0.681	1.48×10^{-5}

Entry	$V_{tot,\,Ar2I+}$ (mL)	V (mL)	A	$[Ar_2CH^+]$ (M)	$[LB]_0(V_0/V)$ (M)	$[Ar_2I^+]_{0,i}$ (M)	$[Ar_2I^+]_0/[LB]_0(V_0/V)$	$(A_0*(V_0/V)-A)/A$	[LB] (M)	$[Ar_2I$-LB] (M)	$[Ar_2I^+]$ (M)	$[Ar_2I$-LB]/[LB]
1	0.05	24.18	0.571	6.88×10^{-6}	1.48×10^{-5}	6.99×10^{-5}	4.7	0.81	2.82×10^{-6}	6.36×10^{-6}	6.35×10^{-5}	2.26
2	0.10	24.23	0.675	8.13×10^{-6}	1.48×10^{-5}	1.39×10^{-4}	9.5	0.53	1.84×10^{-6}	8.59×10^{-6}	1.31×10^{-4}	4.67
3	0.15	24.28	0.729	8.78×10^{-6}	1.47×10^{-5}	2.09×10^{-4}	14.2	0.41	1.44×10^{-6}	9.64×10^{-6}	1.99×10^{-4}	6.70
4	0.20	24.33	0.766	9.23×10^{-6}	1.47×10^{-5}	2.78×10^{-4}	18.9	0.34	1.19×10^{-6}	1.03×10^{-5}	2.68×10^{-4}	8.67
5	0.25	24.38	0.792	9.54×10^{-6}	1.47×10^{-5}	3.47×10^{-4}	23.6	0.30	1.03×10^{-6}	1.08×10^{-5}	3.36×10^{-4}	1.05×10^{1}

RM700-3

Titration						
Entry	$V_{tot,\,LB}$ (mL)	V (mL)	A	$[Ar_2CH^+]$ (M)	$A_0*(V_0/V)$-A	$[LB]_0$ (M)
1	–	24.08	**1.021**	1.23×10^{-5}		
2	0.05	24.13	**0.358**	4.31×10^{-6}	0.661	1.44×10^{-5}

Entry	$V_{tot,\,Ar2I+}$ (mL)	V (mL)	A	$[Ar_2CH^+]$ (M)	$[LB]_0(V_0/V)$ (M)	$[Ar_2I^+]_{0,i}$ (M)	$[Ar_2I^+]_0/[LB]_0(V_0/V)$	$(A_0*(V_0/V)-A)/A$	[LB] (M)	$[Ar_2I$-LB] (M)	$[Ar_2I^+]$ (M)	$[Ar_2I$-LB]/[LB]
1	0.05	24.18	0.572	6.89×10^{-6}	1.43×10^{-5}	6.99×10^{-5}	4.9	0.78	2.70×10^{-6}	6.28×10^{-6}	6.36×10^{-5}	2.33
2	0.10	24.23	0.666	8.02×10^{-6}	1.43×10^{-5}	1.39×10^{-4}	9.8	0.52	1.82×10^{-6}	8.29×10^{-6}	1.31×10^{-4}	4.57
3	0.15	24.28	0.720	8.67×10^{-6}	1.43×10^{-5}	2.09×10^{-4}	14.6	0.41	1.41×10^{-6}	9.34×10^{-6}	1.99×10^{-4}	6.63
4	0.20	24.33	0.756	9.11×10^{-6}	1.42×10^{-5}	2.78×10^{-4}	19.5	0.34	1.17×10^{-6}	1.00×10^{-5}	2.68×10^{-4}	8.58
5	0.25	24.38	0.779	9.39×10^{-6}	1.42×10^{-5}	3.47×10^{-4}	24.4	0.29	1.02×10^{-6}	1.04×10^{-5}	3.36×10^{-4}	1.02×10^{1}

RM700-4

Titration						
Entry	$V_{tot,\,LB}$ (mL)	V (mL)	A	$[Ar_2CH^+]$ (M)	$A_0*(V_0/V)$-A	$[LB]_0$ (M)
1	–	24.08	**1.030**	1.24×10^{-5}		
2	0.05	24.13	**0.364**	4.39×10^{-6}	0.664	1.43×10^{-5}

Entry	$V_{tot,\,Ar2I+}$ (mL)	V (mL)	A	$[Ar_2CH^+]$ (M)	$[LB]_0(V_0/V)$ (M)	$[Ar_2I^+]_{0,i}$ (M)	$[Ar_2I^+]_0/[LB]_0(V_0/V)$	$(A_0*(V_0/V)-A)/A$	[LB] (M)	$[Ar_2I$-LB] (M)	$[Ar_2I^+]$ (M)	$[Ar_2I$-LB]/[LB]
1	0.05	24.18	0.578	6.96×10^{-6}	1.43×10^{-5}	6.99×10^{-5}	4.9	0.77	2.69×10^{-6}	6.21×10^{-6}	6.37×10^{-5}	2.31
2	0.10	24.23	0.674	8.12×10^{-6}	1.43×10^{-5}	1.39×10^{-4}	9.8	0.52	1.80×10^{-6}	8.25×10^{-6}	1.31×10^{-4}	4.59
3	0.15	24.28	0.725	8.73×10^{-6}	1.42×10^{-5}	2.09×10^{-4}	14.7	0.41	1.42×10^{-6}	9.24×10^{-6}	2.00×10^{-4}	6.52
4	0.20	24.33	0.761	9.17×10^{-6}	1.42×10^{-5}	2.78×10^{-4}	19.6	0.34	1.18×10^{-6}	9.91×10^{-6}	2.68×10^{-4}	8.42
5	0.25	24.38	0.788	9.49×10^{-6}	1.42×10^{-5}	3.47×10^{-4}	24.5	0.29	1.01×10^{-6}	1.04×10^{-5}	3.36×10^{-4}	1.03×10^{1}

1f + 3d (20 °C) - RM701

BIMT experiment (MeCN, 20 °C) for the benzoate ion **3d** with **1f** (stock solution: 13.6 mM) competing against the benzhydrylium ion **B2** (605 nm, ε = 1.66 × 10^5 M^{-1} cm^{-1}, K = 2.88 × 10^5 M^{-1} from LA and LB).

RM701-1

Titration						
Entry	$V_{tot,\,LB}$ (mL)	V (mL)	A	$[Ar_2CH^+]$ (M)	$A_0*(V_0/V)$-A	$[LB]_0$ (M)
1	–	24.08	**1.042**	1.26×10^{-5}		
2	0.05	24.13	**0.367**	4.42×10^{-6}	0.673	1.45×10^{-5}

Entry	$V_{tot,\,Ar2I+}$ (mL)	V (mL)	A	$[Ar_2CH^+]$ (M)	$[LB]_0(V_0/V)$ (M)	$[Ar_2I^+]_{0,i}$ (M)	$[Ar_2I^+]_0$/ $[LB]_0(V_0/V)$	$(A_0*(V_0/V)-A)/A$	[LB] (M)	$[Ar_2I$-LB] (M)	$[Ar_2I^+]$ (M)	$[Ar_2I$-LB]/ [LB]
1	0.025	24.16	0.593	7.14×10^{-6}	1.44×10^{-5}	1.40×10^{-5}	1.0	0.75	2.61×10^{-6}	6.47×10^{-6}	7.56×10^{-6}	2.48
2	0.050	24.18	0.712	8.58×10^{-6}	1.44×10^{-5}	2.80×10^{-5}	1.9	0.46	1.59×10^{-6}	8.92×10^{-6}	1.91×10^{-5}	5.63
3	0.075	24.21	0.780	9.39×10^{-6}	1.44×10^{-5}	4.20×10^{-5}	2.9	0.33	1.14×10^{-6}	1.02×10^{-5}	3.18×10^{-5}	8.90
4	0.100	24.23	0.820	9.88×10^{-6}	1.44×10^{-5}	5.59×10^{-5}	3.9	0.26	9.11×10^{-7}	1.09×10^{-5}	4.50×10^{-5}	1.20×10^{1}
5	0.125	24.26	0.847	1.02×10^{-5}	1.44×10^{-5}	6.98×10^{-5}	4.9	0.22	7.67×10^{-7}	1.14×10^{-5}	5.85×10^{-5}	1.48×10^{1}

RM701-2

Titration						
Entry	$V_{tot,\,LB}$ (mL)	V (mL)	A	$[Ar_2CH^+]$ (M)	$A_0*(V_0/V)$-A	$[LB]_0$ (M)
1	–	24.08	**1.025**	1.23×10^{-5}		
2	0.05	24.13	**0.353**	4.25×10^{-6}	0.670	1.47×10^{-5}

Entry	$V_{tot,\,Ar2I+}$ (mL)	V (mL)	A	$[Ar_2CH^+]$ (M)	$[LB]_0(V_0/V)$ (M)	$[Ar_2I^+]_{0,i}$ (M)	$[Ar_2I^+]_0$/ $[LB]_0(V_0/V)$	$(A_0*(V_0/V)-A)/A$	[LB] (M)	$[Ar_2I$-LB] (M)	$[Ar_2I^+]$ (M)	$[Ar_2I$-LB]/ [LB]
1	0.025	24.16	0.577	6.95×10^{-6}	1.46×10^{-5}	1.40×10^{-5}	1.0	0.77	2.67×10^{-6}	6.60×10^{-6}	7.42×10^{-6}	2.47
2	0.050	24.18	0.698	8.41×10^{-6}	1.46×10^{-5}	2.80×10^{-5}	1.9	0.46	1.60×10^{-6}	9.13×10^{-6}	1.89×10^{-5}	5.69
3	0.075	24.21	0.766	9.23×10^{-6}	1.46×10^{-5}	4.20×10^{-5}	2.9	0.33	1.15×10^{-6}	1.04×10^{-5}	3.16×10^{-5}	9.06
4	0.100	24.23	0.807	9.72×10^{-6}	1.46×10^{-5}	5.59×10^{-5}	3.8	0.26	9.09×10^{-7}	1.11×10^{-5}	4.48×10^{-5}	1.22×10^{1}
5	0.125	24.26	0.834	1.00×10^{-5}	1.46×10^{-5}	6.98×10^{-5}	4.8	0.22	7.63×10^{-7}	1.16×10^{-5}	5.82×10^{-5}	1.52×10^{1}

RM701-3

Titration						
Entry	$V_{tot,\,LB}$ (mL)	V (mL)	A	$[Ar_2CH^+]$ (M)	$A_0*(V_0/V)$-A	$[LB]_0$ (M)
1	–	24.08	**1.040**	1.25×10^{-5}		
2	0.05	24.13	**0.364**	4.39×10^{-6}	0.674	1.45×10^{-5}

Entry	$V_{tot,\,Ar2I+}$ (mL)	V (mL)	A	$[Ar_2CH^+]$ (M)	$[LB]_0(V_0/V)$ (M)	$[Ar_2I^+]_{0,i}$ (M)	$[Ar_2I^+]_0/[LB]_0(V_0/V)$	$(A_0*(V_0/V)-A)/A$	[LB] (M)	$[Ar_2I$-LB] (M)	$[Ar_2I^+]$ (M)	$[Ar_2I$-LB]/[LB]
1	0.025	24.16	0.607	7.31×10^{-6}	1.45×10^{-5}	1.40×10^{-5}	1.0	0.71	2.45×10^{-6}	6.89×10^{-6}	7.14×10^{-6}	2.81
2	0.050	24.18	0.723	8.71×10^{-6}	1.45×10^{-5}	2.80×10^{-5}	1.9	0.43	1.50×10^{-6}	9.24×10^{-6}	1.88×10^{-5}	6.16
3	0.075	24.21	0.789	9.51×10^{-6}	1.45×10^{-5}	4.20×10^{-5}	2.9	0.31	1.08×10^{-6}	1.05×10^{-5}	3.15×10^{-5}	9.68
4	0.100	24.23	0.826	9.95×10^{-6}	1.45×10^{-5}	5.59×10^{-5}	3.9	0.25	8.71×10^{-7}	1.11×10^{-5}	4.48×10^{-5}	1.27×10^{1}
5	0.125	24.26	0.852	1.03×10^{-5}	1.45×10^{-5}	6.98×10^{-5}	4.8	0.21	7.35×10^{-7}	1.16×10^{-5}	5.83×10^{-5}	1.57×10^{1}

2a + 3d (20 °C) - RM1040

BIMT experiment (MeCN, 20 °C) for the benzoate ion **3d** with **2a** (stock solution: 13.8 mM) competing against the benzhydrylium ion **B2** (605 nm, ε = 1.66×10^5 M^{-1} cm^{-1}, K = 2.88×10^5 M^{-1} from LA and LB).

RM1040-1

Titration						
Entry	$V_{tot,\,LB}$ (mL)	V (mL)	A	$[Ar_2CH^+]$ (M)	$A_0*(V_0/V)$-A	$[LB]_0$ (M)
1	–	24.15	**1.043**	1.26×10^{-5}		
2	0.04	24.19	**0.475**	5.72×10^{-6}	0.566	1.10×10^{-5}

Entry	$V_{tot,\,Ar2I+}$ (mL)	V (mL)	A	$[Ar_2CH^+]$ (M)	$[LB]_0(V_0/V)$ (M)	$[Ar_2I^+]_{0,i}$ (M)	$[Ar_2I^+]_0/[LB]_0(V_0/V)$	$(A_0*(V_0/V)-A)/A$	[LB] (M)	$[Ar_2I$-LB] (M)	$[Ar_2I^+]$ (M)	$[Ar_2I$-LB]/[LB]
1	0.01	24.20	0.669	8.06×10^{-6}	1.10×10^{-5}	5.69×10^{-6}	0.5	0.56	1.93×10^{-6}	4.54×10^{-6}	1.15×10^{-6}	2.36
2	0.02	24.21	0.812	9.78×10^{-6}	1.09×10^{-5}	1.14×10^{-5}	1.0	0.28	9.75×10^{-7}	7.22×10^{-6}	4.16×10^{-6}	7.40
3	0.03	24.22	0.886	1.07×10^{-5}	1.09×10^{-5}	1.71×10^{-5}	1.6	0.17	6.03×10^{-7}	8.48×10^{-6}	8.58×10^{-6}	1.41×10^{1}
4	0.04	24.23	0.922	1.11×10^{-5}	1.09×10^{-5}	2.27×10^{-5}	2.1	0.13	4.42×10^{-7}	9.08×10^{-6}	1.37×10^{-5}	2.05×10^{1}
5	0.05	24.24	0.943	1.14×10^{-5}	1.09×10^{-5}	2.84×10^{-5}	2.6	0.10	3.53×10^{-7}	9.42×10^{-6}	1.90×10^{-5}	2.67×10^{1}

RM1040-2

Titration						
Entry	$V_{tot,\,LB}$ (mL)	V (mL)	A	$[Ar_2CH^+]$ (M)	$A_0*(V_0/V)$-A	$[LB]_0$ (M)
1	–	24.15	**1.025**	1.23×10^{-5}		
2	0.04	24.19	**0.472**	5.69×10^{-6}	0.551	1.07×10^{-5}

Entry	$V_{tot,\,Ar2I+}$ (mL)	V (mL)	A	$[Ar_2CH^+]$ (M)	$[LB]_0(V_0/V)$ (M)	$[Ar_2I^+]_{0,i}$ (M)	$[Ar_2I^+]_0/[LB]_0(V_0/V)$	$(A_0*(V_0/V)\text{-}A)/A$	[LB] (M)	$[Ar_2I$-LB] (M)	$[Ar_2I^+]$ (M)	$[Ar_2I$-LB]/[LB]
1	0.01	24.20	0.679	8.18×10^{-6}	1.07×10^{-5}	5.69×10^{-6}	0.5	0.51	1.76×10^{-6}	4.79×10^{-6}	9.05×10^{-7}	2.73
2	0.02	24.21	0.809	9.75×10^{-6}	1.07×10^{-5}	1.14×10^{-5}	1.1	0.26	9.15×10^{-7}	7.20×10^{-6}	4.19×10^{-6}	7.87
3	0.03	24.22	0.878	1.06×10^{-5}	1.07×10^{-5}	1.71×10^{-5}	1.6	0.16	5.69×10^{-7}	8.37×10^{-6}	8.69×10^{-6}	1.47×10^{1}
4	0.04	24.23	0.916	1.10×10^{-5}	1.07×10^{-5}	2.27×10^{-5}	2.1	0.12	4.00×10^{-7}	9.00×10^{-6}	1.37×10^{-5}	2.25×10^{1}
5	0.05	24.24	0.937	1.13×10^{-5}	1.07×10^{-5}	2.84×10^{-5}	2.7	0.09	3.12×10^{-7}	9.34×10^{-6}	1.91×10^{-5}	3.00×10^{1}

RM1040-3

Titration						
Entry	$V_{tot,\,LB}$ (mL)	V (mL)	A	$[Ar_2CH^+]$ (M)	$A_0*(V_0/V)$-A	$[LB]_0$ (M)
1	–	24.15	**1.027**	1.24×10^{-5}		
2	0.04	24.19	**0.490**	5.90×10^{-6}	0.535	1.02×10^{-5}

Entry	$V_{tot,\,Ar2I+}$ (mL)	V (mL)	A	$[Ar_2CH^+]$ (M)	$[LB]_0(V_0/V)$ (M)	$[Ar_2I^+]_{0,i}$ (M)	$[Ar_2I^+]_0/[LB]_0(V_0/V)$	$(A_0*(V_0/V)\text{-}A)/A$	[LB] (M)	$[Ar_2I$-LB] (M)	$[Ar_2I^+]$ (M)	$[Ar_2I$-LB]/[LB]
1	0.01	24.20	0.697	8.40×10^{-6}	1.02×10^{-5}	5.69×10^{-6}	0.6	0.47	1.63×10^{-6}	4.65×10^{-6}	1.04×10^{-6}	2.85
2	0.02	24.21	0.824	9.93×10^{-6}	1.02×10^{-5}	1.14×10^{-5}	1.1	0.24	8.44×10^{-7}	6.97×10^{-6}	4.41×10^{-6}	8.26
3	0.03	24.22	0.886	1.07×10^{-5}	1.02×10^{-5}	1.71×10^{-5}	1.7	0.16	5.40×10^{-7}	8.02×10^{-6}	9.05×10^{-6}	1.48×10^{1}
4	0.04	24.23	0.918	1.11×10^{-5}	1.02×10^{-5}	2.27×10^{-5}	2.2	0.12	3.99×10^{-7}	8.55×10^{-6}	1.42×10^{-5}	2.14×10^{1}
5	0.05	24.24	0.938	1.13×10^{-5}	1.02×10^{-5}	2.84×10^{-5}	2.8	0.09	3.15×10^{-7}	8.87×10^{-6}	1.95×10^{-5}	2.82×10^{1}

1a + 3e (20 °C) - RM830

BIMT experiment (MeCN, 20 °C) for the *p*-nitrophenolate ion (**3e**) with **1a** (stock solution: 41.4 mM) competing against the benzhydrylium ion **B2** (605 nm, ε = 1.66×10^5 M^{-1} cm^{-1}, $K = 1.45 \times 10^7$ M^{-1} from LA and LB).

RM830-1

Titration						
Entry	$V_{tot,\,LB}$ (mL)	V (mL)	A	$[Ar_2CH^+]$ (M)	$A_0*(V_0/V)$-A	$[LB]_0$ (M)
1	–	24.09	**1.052**	1.27×10^{-5}		
2	0.03	24.12	**0.097**	1.17×10^{-6}	0.954	1.22×10^{-5}

Entry	$V_{tot,\,Ar2I+}$ (mL)	V (mL)	A	$[Ar_2CH^+]$ (M)	$[LB]_0(V_0/V)$ (M)	$[Ar_2I^+]_{0,i}$ (M)	$[Ar_2I^+]_0/[LB]_0(V_0/V)$	$(A_0*(V_0/V)\text{-}A)/A$	[LB] (M)	[Ar$_2$I-LB] (M)	$[Ar_2I^+]$ (M)	[Ar$_2$I-LB]/[LB]
1	0.10	24.22	0.144	1.73×10^{-6}	1.21×10^{-5}	1.71×10^{-4}	14.1	6.27	4.34×10^{-7}	8.15×10^{-7}	1.70×10^{-4}	1.88
2	0.20	24.32	0.172	2.07×10^{-6}	1.21×10^{-5}	3.40×10^{-4}	28.2	5.06	3.50×10^{-7}	1.24×10^{-6}	3.39×10^{-4}	3.54
3	0.30	24.42	0.197	2.37×10^{-6}	1.20×10^{-5}	5.08×10^{-4}	42.3	4.27	2.95×10^{-7}	1.60×10^{-6}	5.07×10^{-4}	5.40
4	0.40	24.52	0.217	2.61×10^{-6}	1.20×10^{-5}	6.75×10^{-4}	56.4	3.76	2.60×10^{-7}	1.87×10^{-6}	6.73×10^{-4}	7.20
5	0.50	24.62	0.236	2.84×10^{-6}	1.19×10^{-5}	8.40×10^{-4}	70.5	3.36	2.33×10^{-7}	2.13×10^{-6}	8.38×10^{-4}	9.17

RM830-2

Titration						
Entry	$V_{tot,\,LB}$ (mL)	V (mL)	A	$[Ar_2CH^+]$ (M)	$A_0*(V_0/V)$-A	$[LB]_0$ (M)
1	–	24.09	**1.054**	1.27×10^{-5}		
2	0.02	24.11	**0.420**	5.06×10^{-6}	0.633	7.73×10^{-6}

Entry	$V_{tot,\,Ar2I+}$ (mL)	V (mL)	A	$[Ar_2CH^+]$ (M)	$[LB]_0(V_0/V)$ (M)	$[Ar_2I^+]_{0,i}$ (M)	$[Ar_2I^+]_0/[LB]_0(V_0/V)$	$(A_0*(V_0/V)\text{-}A)/A$	[LB] (M)	[Ar$_2$I-LB] (M)	$[Ar_2I^+]$ (M)	[Ar$_2$I-LB]/[LB]
1	0.10	24.21	0.446	5.37×10^{-6}	7.70×10^{-6}	1.71×10^{-4}	22.2	1.35	9.35×10^{-8}	3.45×10^{-7}	1.71×10^{-4}	3.68
2	0.20	24.31	0.461	5.55×10^{-6}	7.67×10^{-6}	3.40×10^{-4}	44.4	1.27	8.76×10^{-8}	5.51×10^{-7}	3.40×10^{-4}	6.30
3	0.30	24.41	0.475	5.72×10^{-6}	7.64×10^{-6}	5.09×10^{-4}	66.6	1.19	8.23×10^{-8}	7.46×10^{-7}	5.08×10^{-4}	9.06
4	0.40	24.51	0.488	5.88×10^{-6}	7.61×10^{-6}	6.75×10^{-4}	88.8	1.12	7.77×10^{-8}	9.27×10^{-7}	6.74×10^{-4}	1.19×10^{1}
5	0.50	24.61	0.501	6.04×10^{-6}	7.58×10^{-6}	8.41×10^{-4}	111.0	1.06	7.33×10^{-8}	1.11×10^{-6}	8.40×10^{-4}	1.51×10^{1}

RM830-3

Titration						
Entry	$V_{tot,\,LB}$ (mL)	V (mL)	A	$[Ar_2CH^+]$ (M)	$A_0*(V_0/V)$-A	$[LB]_0$ (M)
1	–	24.09	**1.006**	1.21×10^{-5}		
2	0.02	24.11	**0.479**	5.77×10^{-6}	0.526	6.42×10^{-6}

Entry	$V_{tot,\,Ar2I+}$ (mL)	V (mL)	A	$[Ar_2CH^+]$ (M)	$[LB]_0(V_0/V)$ (M)	$[Ar_2I^+]_{0,i}$ (M)	$[Ar_2I^+]_0/[LB]_0(V_0/V)$	$(A_0*(V_0/V)\text{-}A)/A$	[LB] (M)	$[Ar_2I\text{-}LB]$ (M)	$[Ar_2I^+]$ (M)	$[Ar_2I\text{-}LB]/[LB]$
1	0.10	24.21	0.515	6.20×10^{-6}	6.39×10^{-6}	1.71×10^{-4}	26.8	0.94	6.53×10^{-8}	4.68×10^{-7}	1.70×10^{-4}	7.17
2	0.20	24.31	0.532	6.41×10^{-6}	6.36×10^{-6}	3.40×10^{-4}	53.5	0.87	6.05×10^{-8}	7.01×10^{-7}	3.40×10^{-4}	1.16×10^{1}
3	0.30	24.41	0.544	6.55×10^{-6}	6.34×10^{-6}	5.09×10^{-4}	80.3	0.83	5.71×10^{-8}	8.72×10^{-7}	5.08×10^{-4}	1.53×10^{1}
4	0.40	24.51	0.554	6.67×10^{-6}	6.31×10^{-6}	6.75×10^{-4}	107.0	0.78	5.43×10^{-8}	1.02×10^{-6}	6.74×10^{-4}	1.88×10^{1}
5	0.50	24.61	0.562	6.77×10^{-6}	6.28×10^{-6}	8.41×10^{-4}	133.8	0.75	5.20×10^{-8}	1.14×10^{-6}	8.40×10^{-4}	2.19×10^{1}

1e + 3e (20 °C) - RM803

BIMT experiment (MeCN, 20 °C) for the *p*-nitrophenolate ion (**3e**) with **1e** (stock solution: 10.2 mM) competing against the benzhydrylium ion **B2** (605 nm, ε = 1.66×10^5 M^{-1} cm^{-1}, $K = 1.45 \times 10^7$ M^{-1} from LA and LB).

RM803-1

Titration						
Entry	$V_{tot,\,LB}$ (mL)	V (mL)	A	$[Ar_2CH^+]$ (M)	$A_0*(V_0/V)$-A	$[LB]_0$ (M)
1	–	24.10	**0.954**	1.15×10^{-5}		
2	0.025	24.13	**0.201**	2.42×10^{-6}	0.752	9.32×10^{-6}

Entry	$V_{tot,\,Ar2I+}$ (mL)	V (mL)	A	$[Ar_2CH^+]$ (M)	$[LB]_0(V_0/V)$ (M)	$[Ar_2I^+]_{0,i}$ (M)	$[Ar_2I^+]_0/[LB]_0(V_0/V)$	$(A_0*(V_0/V)\text{-}A)/A$	[LB] (M)	$[Ar_2I\text{-}LB]$ (M)	$[Ar_2I^+]$ (M)	$[Ar_2I\text{-}LB]/[LB]$
1	0.01	24.14	0.308	3.71×10^{-6}	9.32×10^{-6}	4.22×10^{-6}	0.5	2.09	1.45×10^{-7}	1.40×10^{-6}	2.82×10^{-6}	9.70
2	0.02	24.15	0.412	4.96×10^{-6}	9.31×10^{-6}	8.44×10^{-6}	0.9	1.31	9.07×10^{-8}	2.71×10^{-6}	5.73×10^{-6}	2.99×10^{1}
3	0.03	24.16	0.484	5.83×10^{-6}	9.31×10^{-6}	1.27×10^{-5}	1.4	0.97	6.69×10^{-8}	3.60×10^{-6}	9.06×10^{-6}	5.39×10^{1}
4	0.04	24.17	0.526	6.34×10^{-6}	9.30×10^{-6}	1.69×10^{-5}	1.8	0.81	5.60×10^{-8}	4.12×10^{-6}	1.28×10^{-5}	7.37×10^{1}
5	0.05	24.18	0.555	6.69×10^{-6}	9.30×10^{-6}	2.11×10^{-5}	2.3	0.71	4.94×10^{-8}	4.48×10^{-6}	1.66×10^{-5}	9.07×10^{1}

RM803-3

Titration						
Entry	$V_{tot,\,LB}$ (mL)	V (mL)	A	$[Ar_2CH^+]$ (M)	$A_0*(V_0/V)$-A	$[LB]_0$ (M)
1	–	24.10	**0.959**	1.16×10^{-5}		
2	0.025	24.13	**0.206**	2.48×10^{-6}	0.752	9.31×10^{-6}

Entry	$V_{tot,\,Ar2I+}$ (mL)	V (mL)	A	$[Ar_2CH^+]$ (M)	$[LB]_0(V_0/V)$ (M)	$[Ar_2I^+]_{0,i}$ (M)	$[Ar_2I^+]_0/[LB]_0(V_0/V)$	$(A_0*(V_0/V)-A)/A$	[LB] (M)	$[Ar_2I$-LB] (M)	$[Ar_2I^+]$ (M)	$[Ar_2I$-LB]/[LB]
1	0.01	24.14	0.319	3.84×10^{-6}	9.31×10^{-6}	4.22×10^{-6}	0.5	2.00	1.38×10^{-7}	1.48×10^{-6}	2.75×10^{-6}	1.07×10^{1}
2	0.02	24.15	0.428	5.16×10^{-6}	9.31×10^{-6}	8.44×10^{-6}	0.9	1.24	8.55×10^{-8}	2.84×10^{-6}	5.60×10^{-6}	3.32×10^{1}
3	0.03	24.16	0.502	6.05×10^{-6}	9.30×10^{-6}	1.27×10^{-5}	1.4	0.91	6.27×10^{-8}	3.76×10^{-6}	8.90×10^{-6}	6.00×10^{1}
4	0.04	24.17	0.548	6.60×10^{-6}	9.30×10^{-6}	1.69×10^{-5}	1.8	0.75	5.16×10^{-8}	4.33×10^{-6}	1.25×10^{-5}	8.39×10^{1}
5	0.05	24.18	0.576	6.94×10^{-6}	9.29×10^{-6}	2.11×10^{-5}	2.3	0.66	4.56×10^{-8}	4.67×10^{-6}	1.64×10^{-5}	1.02×10^{2}

RM803-4

Titration						
Entry	$V_{tot,\,LB}$ (mL)	V (mL)	A	$[Ar_2CH^+]$ (M)	$A_0*(V_0/V)$-A	$[LB]_0$ (M)
1	–	24.10	**0.975**	1.17×10^{-5}		
2	0.025	24.13	**0.256**	3.08×10^{-6}	0.718	8.84×10^{-6}

Entry	$V_{tot,\,Ar2I+}$ (mL)	V (mL)	A	$[Ar_2CH^+]$ (M)	$[LB]_0(V_0/V)$ (M)	$[Ar_2I^+]_{0,i}$ (M)	$[Ar_2I^+]_0/[LB]_0(V_0/V)$	$(A_0*(V_0/V)-A)/A$	[LB] (M)	$[Ar_2I$-LB] (M)	$[Ar_2I^+]$ (M)	$[Ar_2I$-LB]/[LB]
1	0.01	24.14	0.366	4.41×10^{-6}	8.84×10^{-6}	4.22×10^{-6}	0.5	1.66	1.15×10^{-7}	1.41×10^{-6}	2.82×10^{-6}	1.22×10^{1}
2	0.02	24.15	0.471	5.67×10^{-6}	8.84×10^{-6}	8.44×10^{-6}	1.0	1.07	7.38×10^{-8}	2.71×10^{-6}	5.73×10^{-6}	3.68×10^{1}
3	0.03	24.16	0.541	6.52×10^{-6}	8.83×10^{-6}	1.27×10^{-5}	1.4	0.80	5.52×10^{-8}	3.58×10^{-6}	9.08×10^{-6}	6.48×10^{1}
4	0.04	24.17	0.583	7.02×10^{-6}	8.83×10^{-6}	1.69×10^{-5}	1.9	0.67	4.62×10^{-8}	4.09×10^{-6}	1.28×10^{-5}	8.86×10^{1}
5	0.05	24.18	0.611	7.36×10^{-6}	8.83×10^{-6}	2.11×10^{-5}	2.4	0.59	4.09×10^{-8}	4.44×10^{-6}	1.66×10^{-5}	1.09×10^{2}

2a + 3e (20 °C) - RM947

BIMT experiment (MeCN, 20 °C) for the *p*-nitrophenolate ion (**3e**) with **2a** (stock solution: 7.01 mM) competing against the benzhydrylium ion **B2** (605 nm, ε = 1.66×10^5 M^{-1} cm^{-1}, $K = 1.45 \times 10^7$ M^{-1} from LA and LB).

RM947-2

Titration						
Entry	$V_{tot,\,LB}$ (mL)	V (mL)	A	$[Ar_2CH^+]$ (M)	$A_0*(V_0/V)$-A	$[LB]_0$ (M)
1	–	24.12	**1.029**	1.24×10^{-5}		
2	0.08	24.20	**0.311**	3.75×10^{-6}	0.715	8.77×10^{-6}

Entry	$V_{tot,\,Ar2I+}$ (mL)	V (mL)	A	$[Ar_2CH^+]$ (M)	$[LB]_0(V_0/V)$ (M)	$[Ar_2I^+]_{0,i}$ (M)	$[Ar_2I^+]_0$/ $[LB]_0(V_0/V)$	$(A_0*(V_0/V)\text{-}A)/A$	[LB] (M)	$[Ar_2I\text{-}LB]$ (M)	$[Ar_2I^+]$ (M)	$[Ar_2I\text{-}LB]$/ [LB]
1	0.025	24.23	0.377	4.54×10^{-6}	8.76×10^{-6}	7.23×10^{-6}	0.8	1.70	1.18×10^{-7}	8.64×10^{-7}	6.37×10^{-6}	7.33
2	0.050	24.25	0.423	5.10×10^{-6}	8.75×10^{-6}	1.44×10^{-5}	1.7	1.42	9.82×10^{-8}	1.42×10^{-6}	1.30×10^{-5}	1.44×10^{1}
3	0.075	24.28	0.455	5.48×10^{-6}	8.74×10^{-6}	2.16×10^{-5}	2.5	1.25	8.63×10^{-8}	1.82×10^{-6}	1.98×10^{-5}	2.11×10^{1}
4	0.100	24.30	0.481	5.80×10^{-6}	8.73×10^{-6}	2.88×10^{-5}	3.3	1.12	7.77×10^{-8}	2.14×10^{-6}	2.67×10^{-5}	2.76×10^{1}
5	0.125	24.33	0.503	6.06×10^{-6}	8.72×10^{-6}	3.60×10^{-5}	4.1	1.03	7.12×10^{-8}	2.42×10^{-6}	3.36×10^{-5}	3.40×10^{1}
6	0.150	24.35	0.522	6.29×10^{-6}	8.71×10^{-6}	4.32×10^{-5}	5.0	0.95	6.59×10^{-8}	2.66×10^{-6}	4.05×10^{-5}	4.03×10^{1}

RM947-3

Titration						
Entry	$V_{tot,\,LB}$ (mL)	V (mL)	A	$[Ar_2CH^+]$ (M)	$A_0*(V_0/V)$-A	$[LB]_0$ (M)
1	–	24.12	**1.046**	1.26×10^{-5}		
2	0.08	24.20	**0.340**	4.10×10^{-6}	0.703	8.61×10^{-6}

Entry	$V_{tot,\,Ar2I+}$ (mL)	V (mL)	A	$[Ar_2CH^+]$ (M)	$[LB]_0(V_0/V)$ (M)	$[Ar_2I^+]_{0,i}$ (M)	$[Ar_2I^+]_0$/ $[LB]_0(V_0/V)$	$(A_0*(V_0/V)\text{-}A)/A$	[LB] (M)	$[Ar_2I\text{-}LB]$ (M)	$[Ar_2I^+]$ (M)	$[Ar_2I\text{-}LB]$/ [LB]
1	0.03	24.23	0.410	4.94×10^{-6}	8.60×10^{-6}	7.23×10^{-6}	0.8	1.54	1.07×10^{-7}	8.84×10^{-7}	6.35×10^{-6}	8.29
2	0.05	24.25	0.453	5.46×10^{-6}	8.59×10^{-6}	1.44×10^{-5}	1.7	1.30	8.97×10^{-8}	1.42×10^{-6}	1.30×10^{-5}	1.59×10^{1}
3	0.08	24.28	0.483	5.82×10^{-6}	8.58×10^{-6}	2.16×10^{-5}	2.5	1.15	7.97×10^{-8}	1.80×10^{-6}	1.98×10^{-5}	2.26×10^{1}
4	0.10	24.30	0.510	6.14×10^{-6}	8.57×10^{-6}	2.88×10^{-5}	3.4	1.04	7.17×10^{-8}	2.14×10^{-6}	2.67×10^{-5}	2.98×10^{1}
5	0.13	24.33	0.532	6.41×10^{-6}	8.56×10^{-6}	3.60×10^{-5}	4.2	0.95	6.57×10^{-8}	2.41×10^{-6}	3.36×10^{-5}	3.67×10^{1}
6	0.15	24.35	0.552	6.65×10^{-6}	8.55×10^{-6}	4.32×10^{-5}	5.0	0.88	6.07×10^{-8}	2.66×10^{-6}	4.05×10^{-5}	4.39×10^{1}

RM947-4

Titration						
Entry	$V_{tot,\,LB}$ (mL)	V (mL)	A	$[Ar_2CH^+]$ (M)	$A_0*(V_0/V)$-A	$[LB]_0$ (M)
1	–	24.12	**1.053**	1.27×10^{-5}		
2	0.08	24.20	**0.343**	4.13×10^{-6}	0.707	8.65×10^{-6}

Entry	$V_{tot,\,Ar2I+}$ (mL)	V (mL)	A	$[Ar_2CH^+]$ (M)	$[LB]_0(V_0/V)$ (M)	$[Ar_2I^+]_{0,i}$ (M)	$[Ar_2I^+]_0/[LB]_0(V_0/V)$	$(A_0*(V_0/V)-A)/A$	[LB] (M)	$[Ar_2I$-LB] (M)	$[Ar_2I^+]$ (M)	$[Ar_2I$-LB]/[LB]
1	0.03	24.23	0.409	4.93×10^{-6}	8.65×10^{-6}	7.23×10^{-6}	0.8	1.56	1.08×10^{-7}	8.34×10^{-7}	6.40×10^{-6}	7.71
2	0.05	24.25	0.449	5.41×10^{-6}	8.64×10^{-6}	1.44×10^{-5}	1.7	1.33	9.22×10^{-8}	1.34×10^{-6}	1.31×10^{-5}	1.45×10^{1}
3	0.08	24.28	0.480	5.78×10^{-6}	8.63×10^{-6}	2.16×10^{-5}	2.5	1.18	8.16×10^{-8}	1.72×10^{-6}	1.99×10^{-5}	2.11×10^{1}
4	0.10	24.30	0.506	6.10×10^{-6}	8.62×10^{-6}	2.88×10^{-5}	3.3	1.07	7.37×10^{-8}	2.05×10^{-6}	2.68×10^{-5}	2.78×10^{1}
5	0.13	24.33	0.528	6.36×10^{-6}	8.61×10^{-6}	3.60×10^{-5}	4.2	0.98	6.76×10^{-8}	2.32×10^{-6}	3.37×10^{-5}	3.44×10^{1}
6	0.15	24.35	0.547	6.59×10^{-6}	8.60×10^{-6}	4.32×10^{-5}	5.0	0.91	6.27×10^{-8}	2.56×10^{-6}	4.06×10^{-5}	4.08×10^{1}

2b + 3e (20 °C) - RM835

BIMT experiment (MeCN, 20 °C) for the *p*-nitrophenolate ion (**3e**) with **2b** (stock solution: 3.64 mM) competing against the benzhydrylium ion **B2** (605 nm, ε = 1.66×10^5 M^{-1} cm^{-1}, $K = 1.45 \times 10^7$ M^{-1} from LA and LB).

RM835-1

Titration						
Entry	$V_{tot,\,LB}$ (mL)	V (mL)	A	$[Ar_2CH^+]$ (M)	$A_0*(V_0/V)$-A	$[LB]_0$ (M)
1	–	24.12	**0.959**	1.16×10^{-5}		
2	0.03	24.15	**0.361**	4.35×10^{-6}	0.597	7.30×10^{-6}

Entry	$V_{tot,\,Ar2I+}$ (mL)	V (mL)	A	$[Ar_2CH^+]$ (M)	$[LB]_0(V_0/V)$ (M)	$[Ar_2I^+]_{0,i}$ (M)	$[Ar_2I^+]_0/[LB]_0(V_0/V)$	$(A_0*(V_0/V)-A)/A$	[LB] (M)	$[Ar_2I$-LB] (M)	$[Ar_2I^+]$ (M)	$[Ar_2I$-LB]/[LB]
1	0.01	24.16	0.413	4.98×10^{-6}	7.30×10^{-6}	1.51×10^{-6}	0.2	1.32	9.12×10^{-8}	6.51×10^{-7}	8.55×10^{-7}	7.14
2	0.02	24.17	0.446	5.37×10^{-6}	7.30×10^{-6}	3.01×10^{-6}	0.4	1.15	7.93×10^{-8}	1.06×10^{-6}	1.95×10^{-6}	1.34×10^{1}
3	0.03	24.18	0.472	5.69×10^{-6}	7.30×10^{-6}	4.52×10^{-6}	0.6	1.03	7.10×10^{-8}	1.39×10^{-6}	3.13×10^{-6}	1.95×10^{1}
4	0.04	24.19	0.492	5.93×10^{-6}	7.29×10^{-6}	6.02×10^{-6}	0.8	0.94	6.53×10^{-8}	1.63×10^{-6}	4.38×10^{-6}	2.50×10^{1}
5	0.05	24.20	0.509	6.13×10^{-6}	7.29×10^{-6}	7.52×10^{-6}	1.0	0.88	6.07×10^{-8}	1.85×10^{-6}	5.67×10^{-6}	3.04×10^{1}

RM835-2

Titration						
Entry	$V_{tot,\,LB}$ (mL)	V (mL)	A	$[Ar_2CH^+]$ (M)	$A_0*(V_0/V)$-A	$[LB]_0$ (M)
1	–	24.12	**0.977**	1.18×10^{-5}		
2	0.03	24.15	**0.269**	3.24×10^{-6}	0.707	8.70×10^{-6}

Entry	$V_{tot,\,Ar2I+}$ (mL)	V (mL)	A	$[Ar_2CH^+]$ (M)	$[LB]_0(V_0/V)$ (M)	$[Ar_2I^+]_{0,i}$ (M)	$[Ar_2I^+]_0/[LB]_0(V_0/V)$	$(A_0*(V_0/V)-A)/A$	[LB] (M)	$[Ar_2I$-LB] (M)	$[Ar_2I^+]$ (M)	$[Ar_2I$-LB]/[LB]
1	0.01	24.16	0.327	3.94×10^{-6}	8.69×10^{-6}	1.51×10^{-6}	0.2	1.98	1.37×10^{-7}	7.45×10^{-7}	7.62×10^{-7}	5.43
2	0.02	24.17	0.370	4.46×10^{-6}	8.69×10^{-6}	3.01×10^{-6}	0.3	1.64	1.13×10^{-7}	1.29×10^{-6}	1.72×10^{-6}	1.14×10^{1}
3	0.03	24.18	0.401	4.83×10^{-6}	8.69×10^{-6}	4.52×10^{-6}	0.5	1.43	9.90×10^{-8}	1.68×10^{-6}	2.84×10^{-6}	1.69×10^{1}
4	0.04	24.19	0.425	5.12×10^{-6}	8.68×10^{-6}	6.02×10^{-6}	0.7	1.29	8.94×10^{-8}	1.98×10^{-6}	4.04×10^{-6}	2.21×10^{1}
5	0.05	24.20	0.445	5.36×10^{-6}	8.68×10^{-6}	7.52×10^{-6}	0.9	1.19	8.22×10^{-8}	2.23×10^{-6}	5.29×10^{-6}	2.71×10^{1}

RM835-3

Titration						
Entry	$V_{tot,\,LB}$ (mL)	V (mL)	A	$[Ar_2CH^+]$ (M)	$A_0*(V_0/V)$-A	$[LB]_0$ (M)
1	–	24.12	**0.966**	1.16×10^{-5}		
2	0.03	24.15	**0.302**	3.64×10^{-6}	0.663	8.14×10^{-6}

Entry	$V_{tot,\,Ar2I+}$ (mL)	V (mL)	A	$[Ar_2CH^+]$ (M)	$[LB]_0(V_0/V)$ (M)	$[Ar_2I^+]_{0,i}$ (M)	$[Ar_2I^+]_0/[LB]_0(V_0/V)$	$(A_0*(V_0/V)-A)/A$	[LB] (M)	$[Ar_2I$-LB] (M)	$[Ar_2I^+]$ (M)	$[Ar_2I$-LB]/[LB]
1	0.01	24.16	0.360	4.34×10^{-6}	8.13×10^{-6}	1.51×10^{-6}	0.2	1.68	1.16×10^{-7}	7.36×10^{-7}	7.71×10^{-7}	6.34
2	0.02	24.17	0.400	4.82×10^{-6}	8.13×10^{-6}	3.01×10^{-6}	0.4	1.41	9.75×10^{-8}	1.24×10^{-6}	1.77×10^{-6}	1.27×10^{1}
3	0.03	24.18	0.428	5.16×10^{-6}	8.13×10^{-6}	4.52×10^{-6}	0.6	1.25	8.66×10^{-8}	1.59×10^{-6}	2.93×10^{-6}	1.83×10^{1}
4	0.04	24.19	0.450	5.42×10^{-6}	8.12×10^{-6}	6.02×10^{-6}	0.7	1.14	7.89×10^{-8}	1.86×10^{-6}	4.16×10^{-6}	2.36×10^{1}
5	0.05	24.20	0.467	5.63×10^{-6}	8.12×10^{-6}	7.52×10^{-6}	0.9	1.06	7.35×10^{-8}	2.07×10^{-6}	5.45×10^{-6}	2.82×10^{1}

2c + 3e (20 °C) - RM836

BIMT experiment (MeCN, 20 °C) for the *p*-nitrophenolate ion (**3e**) with **2c** (stock solution: 13.0 mM) competing against the benzhydrylium ion **B2** (605 nm, ε = 1.66×10^5 M^{-1} cm^{-1}, $K = 1.45 \times 10^7$ M^{-1} from LA and LB).

RM836-1

Titration						
Entry	$V_{tot,\,LB}$ (mL)	V (mL)	A	$[Ar_2CH^+]$ (M)	$A_0*(V_0/V)$-A	$[LB]_0$ (M)
1	–	24.12	**0.992**	1.20×10^{-5}		
2	0.03	24.15	**0.361**	4.35×10^{-6}	0.630	7.71×10^{-6}

Entry	$V_{tot,\,Ar2I+}$ (mL)	V (mL)	A	$[Ar_2CH^+]$ (M)	$[LB]_0(V_0/V)$ (M)	$[Ar_2I^+]_{0,i}$ (M)	$[Ar_2I^+]_0$/ $[LB]_0(V_0/V)$	$(A_0*(V_0/V)$-A)/A	[LB] (M)	$[Ar_2I$-LB] (M)	$[Ar_2I^+]$ (M)	$[Ar_2I$-LB]/ [LB]
1	0.10	24.25	0.394	4.75×10^{-6}	7.68×10^{-6}	5.37×10^{-5}	7.0	1.50	1.04×10^{-7}	4.32×10^{-7}	5.33×10^{-5}	4.15
2	0.20	24.35	0.426	5.13×10^{-6}	7.64×10^{-6}	1.07×10^{-4}	14.0	1.31	9.04×10^{-8}	8.48×10^{-7}	1.06×10^{-4}	9.38
3	0.30	24.45	0.456	5.49×10^{-6}	7.61×10^{-6}	1.60×10^{-4}	21.0	1.15	7.93×10^{-8}	1.24×10^{-6}	1.59×10^{-4}	1.56×10^{1}
4	0.40	24.55	0.484	5.83×10^{-6}	7.58×10^{-6}	2.12×10^{-4}	28.0	1.01	7.01×10^{-8}	1.60×10^{-6}	2.11×10^{-4}	2.28×10^{1}
5	0.50	24.65	0.513	6.18×10^{-6}	7.55×10^{-6}	2.64×10^{-4}	35.0	0.89	6.17×10^{-8}	1.98×10^{-6}	2.62×10^{-4}	3.20×10^{1}

RM836-2

Titration						
Entry	$V_{tot,\,LB}$ (mL)	V (mL)	A	$[Ar_2CH^+]$ (M)	$A_0*(V_0/V)$-A	$[LB]_0$ (M)
1	–	24.12	**1.002**	1.21×10^{-5}		
2	0.03	24.15	**0.360**	4.34×10^{-6}	0.641	7.84×10^{-6}

Entry	$V_{tot,\,Ar2I+}$ (mL)	V (mL)	A	$[Ar_2CH^+]$ (M)	$[LB]_0(V_0/V)$ (M)	$[Ar_2I^+]_{0,i}$ (M)	$[Ar_2I^+]_0$/ $[LB]_0(V_0/V)$	$(A_0*(V_0/V)$-A)/A	[LB] (M)	$[Ar_2I$-LB] (M)	$[Ar_2I^+]$ (M)	$[Ar_2I$-LB]/ [LB]
1	0.10	24.25	0.393	4.73×10^{-6}	7.81×10^{-6}	5.37×10^{-5}	6.9	1.54	1.06×10^{-7}	4.32×10^{-7}	5.33×10^{-5}	4.06
2	0.20	24.35	0.423	5.10×10^{-6}	7.78×10^{-6}	1.07×10^{-4}	13.7	1.35	9.31×10^{-8}	8.24×10^{-7}	1.06×10^{-4}	8.84
3	0.30	24.45	0.452	5.45×10^{-6}	7.75×10^{-6}	1.60×10^{-4}	20.6	1.19	8.21×10^{-8}	1.20×10^{-6}	1.59×10^{-4}	1.46×10^{1}
4	0.40	24.55	0.480	5.78×10^{-6}	7.72×10^{-6}	2.12×10^{-4}	27.5	1.05	7.27×10^{-8}	1.56×10^{-6}	2.11×10^{-4}	2.15×10^{1}
5	0.50	24.65	0.507	6.11×10^{-6}	7.68×10^{-6}	2.64×10^{-4}	34.4	0.93	6.46×10^{-8}	1.92×10^{-6}	2.62×10^{-4}	2.96×10^{1}

RM836-3

Titration						
Entry	$V_{tot,\,LB}$ (mL)	V (mL)	A	$[Ar_2CH^+]$ (M)	$A_0*(V_0/V)$-A	$[LB]_0$ (M)
1	–	24.12	**0.987**	1.19×10^{-5}		
2	0.03	24.15	**0.323**	3.89×10^{-6}	0.663	8.13×10^{-6}

Entry	$V_{tot,\,Ar2I+}$ (mL)	V (mL)	A	$[Ar_2CH^+]$ (M)	$[LB]_0(V_0/V)$ (M)	$[Ar_2I^+]_{0,i}$ (M)	$[Ar_2I^+]_0/[LB]_0(V_0/V)$	$(A_0*(V_0/V)-A)/A$	[LB] (M)	$[Ar_2I$-LB] (M)	$[Ar_2I^+]$ (M)	$[Ar_2I$-LB]/[LB]
1	0.10	24.25	0.358	4.31×10^{-6}	8.09×10^{-6}	5.37×10^{-5}	6.6	1.74	1.21×10^{-7}	4.59×10^{-7}	5.32×10^{-5}	3.80
2	0.20	24.35	0.389	4.69×10^{-6}	8.06×10^{-6}	1.07×10^{-4}	13.3	1.51	1.05×10^{-7}	8.63×10^{-7}	1.06×10^{-4}	8.25
3	0.30	24.45	0.421	5.07×10^{-6}	8.03×10^{-6}	1.60×10^{-4}	19.9	1.31	9.08×10^{-8}	1.28×10^{-6}	1.58×10^{-4}	1.41×10^{1}
4	0.40	24.55	0.451	5.43×10^{-6}	7.99×10^{-6}	2.12×10^{-4}	26.5	1.15	7.96×10^{-8}	1.67×10^{-6}	2.10×10^{-4}	2.09×10^{1}
5	0.50	24.65	0.481	5.80×10^{-6}	7.96×10^{-6}	2.64×10^{-4}	33.2	1.01	6.97×10^{-8}	2.05×10^{-6}	2.62×10^{-4}	2.94×10^{1}

1a + 3f (20 °C) - RM790

BIMT experiment (MeCN, 20 °C) for the pyridine **3f** with **1a** (stock solution: 32.1 mM) competing against the benzhydrylium ion **B1** (632 nm, ε = 1.45×10^5 M^{-1} cm^{-1}, K = 5.08×10^4 M^{-1} from ref. 15).

RM790-2

Titration						
Entry	$V_{tot,\,LB}$ (mL)	V (mL)	A	$[Ar_2CH^+]$ (M)	$A_0*(V_0/V)$-A	$[LB]_0$ (M)
1	–	24.10	**1.041**	1.44×10^{-5}		
2	0.06	24.16	**0.546**	7.53×10^{-6}	0.492	2.45×10^{-5}

Entry	$V_{tot,\,Ar2I+}$ (mL)	V (mL)	A	$[Ar_2CH^+]$ (M)	$[LB]_0(V_0/V)$ (M)	$[Ar_2I^+]_{0,i}$ (M)	$[Ar_2I^+]_0/[LB]_0(V_0/V)$	$(A_0*(V_0/V)-A)/A$	[LB] (M)	$[Ar_2I$-LB] (M)	$[Ar_2I^+]$ (M)	$[Ar_2I$-LB]/[LB]
1	0.20	24.36	0.550	7.59×10^{-6}	2.43×10^{-5}	2.63×10^{-4}	10.8	0.87	1.72×10^{-5}	5.49×10^{-7}	2.63×10^{-4}	3.19×10^{-2}
2	0.50	24.66	0.553	7.63×10^{-6}	2.40×10^{-5}	6.50×10^{-4}	27.0	0.84	1.65×10^{-5}	1.11×10^{-6}	6.49×10^{-4}	6.73×10^{-2}
3	1.00	25.16	0.559	7.71×10^{-6}	2.36×10^{-5}	1.28×10^{-3}	54.1	0.78	1.54×10^{-5}	2.10×10^{-6}	1.27×10^{-3}	1.36×10^{-1}
4	1.50	25.66	0.564	7.78×10^{-6}	2.31×10^{-5}	1.88×10^{-3}	81.1	0.73	1.44×10^{-5}	2.96×10^{-6}	1.87×10^{-3}	2.05×10^{-1}

RM790-3

Titration						
Entry	$V_{tot,\,LB}$ (mL)	V (mL)	A	$[Ar_2CH^+]$ (M)	$A_0*(V_0/V)$-A	$[LB]_0$ (M)
1	–	24.10	**1.052**	1.45×10^{-5}		
2	0.06	24.16	**0.552**	7.61×10^{-6}	0.497	2.46×10^{-5}

Entry	$V_{tot,\,Ar2I+}$ (mL)	V (mL)	A	$[Ar_2CH^+]$ (M)	$[LB]_0(V_0/V)$ (M)	$[Ar_2I^+]_{0,i}$ (M)	$[Ar_2I^+]_0/[LB]_0(V_0/V)$	$(A_0*(V_0/V)-A)/A$	[LB] (M)	$[Ar_2I$-LB] (M)	$[Ar_2I^+]$ (M)	$[Ar_2I$-LB]/[LB]
1	0.20	24.36	0.554	7.64×10^{-6}	2.44×10^{-5}	2.63×10^{-4}	10.8	0.88	1.73×10^{-5}	3.86×10^{-7}	2.63×10^{-4}	2.23×10^{-2}
2	0.50	24.66	0.556	7.67×10^{-6}	2.41×10^{-5}	6.50×10^{-4}	27.0	0.85	1.67×10^{-5}	8.72×10^{-7}	6.50×10^{-4}	5.22×10^{-2}
3	1.00	25.16	0.563	7.77×10^{-6}	2.36×10^{-5}	1.28×10^{-3}	54.0	0.79	1.55×10^{-5}	1.94×10^{-6}	1.27×10^{-3}	1.25×10^{-1}
4	1.50	25.66	0.568	7.83×10^{-6}	2.32×10^{-5}	1.88×10^{-3}	81.0	0.74	1.46×10^{-5}	2.81×10^{-6}	1.87×10^{-3}	1.93×10^{-1}

RM790-5 (as before but with a 34.4 mM stock solution for **1a**)

Titration						
Entry	$V_{tot,\,LB}$ (mL)	V (mL)	A	$[Ar_2CH^+]$ (M)	$A_0*(V_0/V)$-A	$[LB]_0$ (M)
1	–	24.10	**1.047**	1.44×10^{-5}		
2	0.06	24.16	**0.552**	7.61×10^{-6}	0.492	2.44×10^{-5}

Entry	$V_{tot,\,Ar2I+}$ (mL)	V (mL)	A	$[Ar_2CH^+]$ (M)	$[LB]_0(V_0/V)$ (M)	$[Ar_2I^+]_{0,i}$ (M)	$[Ar_2I^+]_0/[LB]_0(V_0/V)$	$(A_0*(V_0/V)-A)/A$	[LB] (M)	$[Ar_2I$-LB] (M)	$[Ar_2I^+]$ (M)	$[Ar_2I$-LB]/[LB]
1	0.20	24.36	0.556	7.67×10^{-6}	2.42×10^{-5}	2.82×10^{-4}	11.7	0.86	1.70×10^{-5}	5.45×10^{-7}	2.82×10^{-4}	3.21×10^{-2}
2	0.50	24.66	0.559	7.71×10^{-6}	2.39×10^{-5}	6.97×10^{-4}	29.2	0.83	1.63×10^{-5}	1.11×10^{-6}	6.96×10^{-4}	6.77×10^{-2}
3	1.00	25.16	0.564	7.78×10^{-6}	2.34×10^{-5}	1.37×10^{-3}	58.4	0.78	1.53×10^{-5}	2.01×10^{-6}	1.36×10^{-3}	1.31×10^{-1}
4	1.50	25.66	0.570	7.86×10^{-6}	2.29×10^{-5}	2.01×10^{-3}	87.6	0.73	1.43×10^{-5}	2.95×10^{-6}	2.01×10^{-3}	2.07×10^{-1}

1c + 3f (20 °C) - RM796

BIMT experiment (MeCN, 20 °C) for the pyridine **3f** with **1c** (stock solution: 22.8 mM) competing against the benzhydrylium ion **B1** (632 nm, ε = 1.45 × 10^5 M^{-1} cm^{-1}, K = 5.08 × 10^4 M^{-1} from ref. 15).

RM796-1

Titration						
Entry	$V_{tot,\,LB}$ (mL)	V (mL)	A	$[Ar_2CH^+]$ (M)	$A_0*(V_0/V)$-A	$[LB]_0$ (M)
1	–	24.10	**1.046**	1.44×10^{-5}		
2	0.05	24.15	**0.428**	5.90×10^{-6}	0.616	3.68×10^{-5}

Entry	$V_{tot,\,Ar2I+}$ (mL)	V (mL)	A	$[Ar_2CH^+]$ (M)	$[LB]_0(V_0/V)$ (M)	$[Ar_2I^+]_{0,i}$ (M)	$[Ar_2I^+]_0$/ $[LB]_0(V_0/V)$	$(A_0*(V_0/V)-A)/A$	[LB] (M)	[Ar$_2$I-LB] (M)	$[Ar_2I^+]$ (M)	[Ar$_2$I-LB]/ [LB]
1	0.20	24.35	0.443	6.11×10^{-6}	3.65×10^{-5}	1.88×10^{-4}	5.1	1.34	2.63×10^{-5}	2.03×10^{-6}	1.86×10^{-4}	7.71×10^{-2}
2	0.40	24.55	0.450	6.21×10^{-6}	3.62×10^{-5}	3.72×10^{-4}	10.3	1.28	2.52×10^{-5}	3.03×10^{-6}	3.69×10^{-4}	1.20×10^{-1}
3	0.60	24.75	0.455	6.28×10^{-6}	3.59×10^{-5}	5.54×10^{-4}	15.4	1.24	2.44×10^{-5}	3.77×10^{-6}	5.50×10^{-4}	1.55×10^{-1}
4	0.80	24.95	0.460	6.34×10^{-6}	3.56×10^{-5}	7.32×10^{-4}	20.6	1.20	2.36×10^{-5}	4.49×10^{-6}	7.28×10^{-4}	1.91×10^{-1}
5	1.00	25.15	0.464	6.40×10^{-6}	3.54×10^{-5}	9.08×10^{-4}	25.7	1.16	2.28×10^{-5}	5.09×10^{-6}	9.03×10^{-4}	2.23×10^{-1}

RM796-2

Titration						
Entry	$V_{tot,\,LB}$ (mL)	V (mL)	A	$[Ar_2CH^+]$ (M)	$A_0*(V_0/V)$-A	$[LB]_0$ (M)
1	–	24.10	**1.049**	1.45×10^{-5}		
2	0.05	24.15	**0.420**	5.79×10^{-6}	0.627	3.80×10^{-5}

Entry	$V_{tot,\,Ar2I+}$ (mL)	V (mL)	A	$[Ar_2CH^+]$ (M)	$[LB]_0(V_0/V)$ (M)	$[Ar_2I^+]_{0,i}$ (M)	$[Ar_2I^+]_0$/ $[LB]_0(V_0/V)$	$(A_0*(V_0/V)-A)/A$	[LB] (M)	[Ar$_2$I-LB] (M)	$[Ar_2I^+]$ (M)	[Ar$_2$I-LB]/ [LB]
1	0.20	24.35	0.432	5.96×10^{-6}	3.77×10^{-5}	1.88×10^{-4}	5.0	1.40	2.76×10^{-5}	1.73×10^{-6}	1.86×10^{-4}	6.25×10^{-2}
2	0.40	24.55	0.438	6.04×10^{-6}	3.74×10^{-5}	3.72×10^{-4}	10.0	1.35	2.66×10^{-5}	2.65×10^{-6}	3.70×10^{-4}	9.95×10^{-2}
3	0.60	24.75	0.442	6.10×10^{-6}	3.71×10^{-5}	5.54×10^{-4}	14.9	1.31	2.58×10^{-5}	3.30×10^{-6}	5.50×10^{-4}	1.28×10^{-1}
4	0.80	24.95	0.446	6.15×10^{-6}	3.68×10^{-5}	7.32×10^{-4}	19.9	1.27	2.50×10^{-5}	3.94×10^{-6}	7.29×10^{-4}	1.58×10^{-1}
5	1.00	25.15	0.450	6.21×10^{-6}	3.65×10^{-5}	9.08×10^{-4}	24.9	1.23	2.43×10^{-5}	4.57×10^{-6}	9.04×10^{-4}	1.88×10^{-1}

RM796-3

Titration						
Entry	$V_{tot,\,LB}$ (mL)	V (mL)	A	$[Ar_2CH^+]$ (M)	$A_0*(V_0/V)$-A	$[LB]_0$ (M)
1	–	24.10	**1.063**	1.47×10^{-5}		
2	0.05	24.15	**0.430**	5.93×10^{-6}	0.631	3.76×10^{-5}

Entry	$V_{tot,\,Ar2I+}$ (mL)	V (mL)	A	$[Ar_2CH^+]$ (M)	$[LB]_0(V_0/V)$ (M)	$[Ar_2I^+]_{0,i}$ (M)	$[Ar_2I^+]_0/[LB]_0(V_0/V)$	$(A_0*(V_0/V)\text{-}A)/A$	[LB] (M)	$[Ar_2I\text{-}LB]$ (M)	$[Ar_2I^+]$ (M)	$[Ar_2I\text{-}LB]/[LB]$
1	0.20	24.35	0.443	6.11×10^{-6}	3.73×10^{-5}	1.88×10^{-4}	5.0	1.37	2.71×10^{-5}	1.80×10^{-6}	1.86×10^{-4}	6.66×10^{-2}
2	0.40	24.55	0.449	6.19×10^{-6}	3.70×10^{-5}	3.72×10^{-4}	10.1	1.32	2.61×10^{-5}	2.70×10^{-6}	3.69×10^{-4}	1.04×10^{-1}
3	0.60	24.75	0.454	6.26×10^{-6}	3.67×10^{-5}	5.54×10^{-4}	15.1	1.28	2.52×10^{-5}	3.46×10^{-6}	5.50×10^{-4}	1.37×10^{-1}
4	0.80	24.95	0.458	6.32×10^{-6}	3.64×10^{-5}	7.32×10^{-4}	20.1	1.24	2.44×10^{-5}	4.08×10^{-6}	7.28×10^{-4}	1.67×10^{-1}
5	1.00	25.15	0.462	6.37×10^{-6}	3.61×10^{-5}	9.08×10^{-4}	25.2	1.20	2.37×10^{-5}	4.69×10^{-6}	9.04×10^{-4}	1.98×10^{-1}

1d + 3f (20 °C) - RM795

BIMT experiment (MeCN, 20 °C) for the pyridine **3f** with **1d** (stock solution: 18.1 mM) competing against the benzhydrylium ion **B1** (632 nm, ε = 1.45×10^5 M^{-1} cm^{-1}, K = 5.08×10^4 M^{-1} from ref. 15).

RM795-2

Titration						
Entry	$V_{tot,\,LB}$ (mL)	V (mL)	A	$[Ar_2CH^+]$ (M)	$A_0*(V_0/V)$-A	$[LB]_0$ (M)
1	–	24.10	**1.044**	1.44×10^{-5}		
2	0.05	24.15	**0.430**	5.93×10^{-6}	0.612	3.64×10^{-5}

Entry	$V_{tot,\,Ar2I+}$ (mL)	V (mL)	A	$[Ar_2CH^+]$ (M)	$[LB]_0(V_0/V)$ (M)	$[Ar_2I^+]_{0,i}$ (M)	$[Ar_2I^+]_0/[LB]_0(V_0/V)$	$(A_0*(V_0/V)\text{-}A)/A$	[LB] (M)	$[Ar_2I\text{-}LB]$ (M)	$[Ar_2I^+]$ (M)	$[Ar_2I\text{-}LB]/[LB]$
1	0.10	24.25	0.451	6.22×10^{-6}	3.63×10^{-5}	7.45×10^{-5}	2.1	1.30	2.56×10^{-5}	2.61×10^{-6}	7.19×10^{-5}	1.02×10^{-1}
2	0.20	24.35	0.461	6.36×10^{-6}	3.61×10^{-5}	1.48×10^{-4}	4.1	1.24	2.44×10^{-5}	3.82×10^{-6}	1.45×10^{-4}	1.56×10^{-1}
3	0.30	24.45	0.470	6.48×10^{-6}	3.60×10^{-5}	2.22×10^{-4}	6.2	1.19	2.34×10^{-5}	4.88×10^{-6}	2.17×10^{-4}	2.08×10^{-1}
4	0.40	24.55	0.481	6.63×10^{-6}	3.59×10^{-5}	2.95×10^{-4}	8.2	1.13	2.23×10^{-5}	6.10×10^{-6}	2.88×10^{-4}	2.74×10^{-1}
5	0.50	24.65	0.495	6.83×10^{-6}	3.57×10^{-5}	3.67×10^{-4}	10.3	1.06	2.09×10^{-5}	7.55×10^{-6}	3.59×10^{-4}	3.61×10^{-1}

RM795-3

Titration						
Entry	$V_{tot,\,LB}$ (mL)	V (mL)	A	$[Ar_2CH^+]$ (M)	$A_0*(V_0/V)$-A	$[LB]_0$ (M)
1	–	24.10	**1.046**	1.44×10^{-5}		
2	0.05	24.15	**0.428**	5.90×10^{-6}	0.616	3.68×10^{-5}

Entry	$V_{tot,\,Ar2I+}$ (mL)	V (mL)	A	$[Ar_2CH^+]$ (M)	$[LB]_0(V_0/V)$ (M)	$[Ar_2I^+]_{0,i}$ (M)	$[Ar_2I^+]_0/[LB]_0(V_0/V)$	$(A_0*(V_0/V)-A)/A$	[LB] (M)	$[Ar_2I$-LB] (M)	$[Ar_2I^+]$ (M)	$[Ar_2I$-LB]/[LB]
1	0.10	24.25	0.450	6.21×10^{-6}	3.67×10^{-5}	7.45×10^{-5}	2.0	1.31	2.58×10^{-5}	2.75×10^{-6}	7.18×10^{-5}	1.06×10^{-1}
2	0.20	24.35	0.461	6.36×10^{-6}	3.65×10^{-5}	1.48×10^{-4}	4.1	1.25	2.45×10^{-5}	4.07×10^{-6}	1.44×10^{-4}	1.66×10^{-1}
3	0.30	24.45	0.470	6.48×10^{-6}	3.64×10^{-5}	2.22×10^{-4}	6.1	1.19	2.35×10^{-5}	5.13×10^{-6}	2.17×10^{-4}	2.18×10^{-1}
4	0.40	24.55	0.482	6.65×10^{-6}	3.62×10^{-5}	2.95×10^{-4}	8.1	1.13	2.23×10^{-5}	6.45×10^{-6}	2.88×10^{-4}	2.90×10^{-1}
5	0.50	24.65	0.494	6.81×10^{-6}	3.61×10^{-5}	3.67×10^{-4}	10.2	1.07	2.11×10^{-5}	7.71×10^{-6}	3.59×10^{-4}	3.66×10^{-1}

RM795-4

Titration						
Entry	$V_{tot,\,LB}$ (mL)	V (mL)	A	$[Ar_2CH^+]$ (M)	$A_0*(V_0/V)$-A	$[LB]_0$ (M)
1	–	24.10	**1.054**	1.45×10^{-5}		
2	0.05	24.15	**0.424**	5.85×10^{-6}	0.628	3.78×10^{-5}

Entry	$V_{tot,\,Ar2I+}$ (mL)	V (mL)	A	$[Ar_2CH^+]$ (M)	$[LB]_0(V_0/V)$ (M)	$[Ar_2I^+]_{0,i}$ (M)	$[Ar_2I^+]_0/[LB]_0(V_0/V)$	$(A_0*(V_0/V)-A)/A$	[LB] (M)	$[Ar_2I$-LB] (M)	$[Ar_2I^+]$ (M)	$[Ar_2I$-LB]/[LB]
1	0.10	24.25	0.447	6.17×10^{-6}	3.77×10^{-5}	7.45×10^{-5}	2.0	1.34	2.64×10^{-5}	2.92×10^{-6}	7.16×10^{-5}	1.11×10^{-1}
2	0.20	24.35	0.457	6.30×10^{-6}	3.75×10^{-5}	1.48×10^{-4}	4.0	1.28	2.52×10^{-5}	4.16×10^{-6}	1.44×10^{-4}	1.65×10^{-1}
3	0.30	24.45	0.467	6.44×10^{-6}	3.73×10^{-5}	2.22×10^{-4}	5.9	1.22	2.41×10^{-5}	5.35×10^{-6}	2.16×10^{-4}	2.22×10^{-1}
4	0.40	24.55	0.477	6.58×10^{-6}	3.72×10^{-5}	2.95×10^{-4}	7.9	1.17	2.30×10^{-5}	6.48×10^{-6}	2.88×10^{-4}	2.82×10^{-1}
5	0.50	24.65	0.488	6.73×10^{-6}	3.70×10^{-5}	3.67×10^{-4}	9.9	1.11	2.19×10^{-5}	7.68×10^{-6}	3.59×10^{-4}	3.51×10^{-1}

1e + 3f (20 °C) - RM794

BIMT experiment (MeCN, 20 °C) for the pyridine **3f** with **1e** (stock solution: 13.5 mM) competing against the benzhydrylium ion **B1** (632 nm, ε = 1.45 × 10^5 M^{-1} cm^{-1}, K = 5.08 × 10^4 M^{-1} from ref. 15).

RM794-1

Titration						
Entry	$V_{tot,\,LB}$ (mL)	V (mL)	A	$[Ar_2CH^+]$ (M)	$A_0*(V_0/V)$-A	$[LB]_0$ (M)
1	–	24.10	**1.033**	1.42×10^{-5}		
2	0.05	24.15	**0.477**	6.58×10^{-6}	0.554	3.05×10^{-5}

Entry	$V_{tot,\,Ar2I+}$ (mL)	V (mL)	A	$[Ar_2CH^+]$ (M)	$[LB]_0(V_0/V)$ (M)	$[Ar_2I^+]_{0,i}$ (M)	$[Ar_2I^+]_0/[LB]_0(V_0/V)$	$(A_0*(V_0/V)-A)/A$	[LB] (M)	[Ar$_2$I-LB] (M)	$[Ar_2I^+]$ (M)	[Ar$_2$I-LB]/[LB]
1	0.05	24.20	0.583	8.04×10^{-6}	3.04×10^{-5}	2.79×10^{-5}	0.9	0.76	1.51×10^{-5}	9.24×10^{-6}	1.87×10^{-5}	6.14×10^{-1}
2	0.10	24.25	0.616	8.50×10^{-6}	3.04×10^{-5}	5.57×10^{-5}	1.8	0.67	1.31×10^{-5}	1.16×10^{-5}	4.41×10^{-5}	8.83×10^{-1}
3	0.15	24.30	0.641	8.84×10^{-6}	3.03×10^{-5}	8.33×10^{-5}	2.7	0.60	1.18×10^{-5}	1.32×10^{-5}	7.01×10^{-5}	1.12
4	0.20	24.35	0.661	9.12×10^{-6}	3.02×10^{-5}	1.11×10^{-4}	3.7	0.55	1.08×10^{-5}	1.45×10^{-5}	9.64×10^{-5}	1.35
5	0.25	24.40	0.679	9.37×10^{-6}	3.02×10^{-5}	1.38×10^{-4}	4.6	0.50	9.89×10^{-6}	1.56×10^{-5}	1.23×10^{-4}	1.57

RM794-2

Titration						
Entry	$V_{tot,\,LB}$ (mL)	V (mL)	A	$[Ar_2CH^+]$ (M)	$A_0*(V_0/V)$-A	$[LB]_0$ (M)
1	–	24.10	**1.031**	1.42×10^{-5}		
2	0.05	24.15	**0.472**	6.51×10^{-6}	0.557	3.09×10^{-5}

Entry	$V_{tot,\,Ar2I+}$ (mL)	V (mL)	A	$[Ar_2CH^+]$ (M)	$[LB]_0(V_0/V)$ (M)	$[Ar_2I^+]_{0,i}$ (M)	$[Ar_2I^+]_0/[LB]_0(V_0/V)$	$(A_0*(V_0/V)-A)/A$	[LB] (M)	[Ar$_2$I-LB] (M)	$[Ar_2I^+]$ (M)	[Ar$_2$I-LB]/[LB]
1	0.05	24.20	0.573	7.90×10^{-6}	3.08×10^{-5}	2.79×10^{-5}	0.9	0.79	1.56×10^{-5}	9.00×10^{-6}	1.89×10^{-5}	5.77×10^{-1}
2	0.10	24.25	0.601	8.29×10^{-6}	3.08×10^{-5}	5.57×10^{-5}	1.8	0.70	1.39×10^{-5}	1.11×10^{-5}	4.46×10^{-5}	7.97×10^{-1}
3	0.15	24.30	0.624	8.61×10^{-6}	3.07×10^{-5}	8.33×10^{-5}	2.7	0.64	1.26×10^{-5}	1.26×10^{-5}	7.07×10^{-5}	1.01
4	0.20	24.35	0.641	8.84×10^{-6}	3.07×10^{-5}	1.11×10^{-4}	3.6	0.59	1.17×10^{-5}	1.38×10^{-5}	9.71×10^{-5}	1.18
5	0.25	24.40	0.659	9.09×10^{-6}	3.06×10^{-5}	1.38×10^{-4}	4.5	0.55	1.07×10^{-5}	1.49×10^{-5}	1.23×10^{-4}	1.39

RM794-3

Titration						
Entry	$V_{tot,\,LB}$ (mL)	V (mL)	A	$[Ar_2CH^+]$ (M)	$A_0*(V_0/V)$-A	$[LB]_0$ (M)
1	–	24.10	**1.042**	1.44×10^{-5}		
2	0.05	24.15	**0.483**	6.66×10^{-6}	0.557	3.04×10^{-5}

Entry	$V_{tot,\,Ar2I+}$ (mL)	V (mL)	A	$[Ar_2CH^+]$ (M)	$[LB]_0(V_0/V)$ (M)	$[Ar_2I^+]_{0,i}$ (M)	$[Ar_2I^+]_0/[LB]_0(V_0/V)$	$(A_0*(V_0/V)\text{-}A)/A$	[LB] (M)	$[Ar_2I\text{-}LB]$ (M)	$[Ar_2I^+]$ (M)	$[Ar_2I\text{-}LB]/[LB]$
1	0.05	24.20	0.597	8.23×10^{-6}	3.03×10^{-5}	2.79×10^{-5}	0.9	0.74	1.45×10^{-5}	9.70×10^{-6}	1.82×10^{-5}	6.68×10^{-1}
2	0.10	24.25	0.628	8.66×10^{-6}	3.02×10^{-5}	5.57×10^{-5}	1.8	0.65	1.28×10^{-5}	1.19×10^{-5}	4.38×10^{-5}	9.28×10^{-1}
3	0.15	24.30	0.652	8.99×10^{-6}	3.02×10^{-5}	8.33×10^{-5}	2.8	0.59	1.15×10^{-5}	1.34×10^{-5}	6.99×10^{-5}	1.16
4	0.20	24.35	0.672	9.27×10^{-6}	3.01×10^{-5}	1.11×10^{-4}	3.7	0.53	1.05×10^{-5}	1.46×10^{-5}	9.62×10^{-5}	1.39
5	0.25	24.40	0.691	9.53×10^{-6}	3.01×10^{-5}	1.38×10^{-4}	4.6	0.49	9.63×10^{-6}	1.58×10^{-5}	1.23×10^{-4}	1.64

1f + 3f (20 °C) - RM792

BIMT experiment (MeCN, 20 °C) for the pyridine **3f** with **1f** (stock solution: 34.7 mM) competing against the benzhydrylium ion **B1** (632 nm, ε = 1.45×10^5 M^{-1} cm^{-1}, $K = 5.08 \times 10^4$ M^{-1} from ref. 15).

RM792-1

Titration						
Entry	$V_{tot,\,LB}$ (mL)	V (mL)	A	$[Ar_2CH^+]$ (M)	$A_0*(V_0/V)$-A	$[LB]_0$ (M)
1	–	24.10	**1.033**	1.42×10^{-5}		
2	0.04	24.14	**0.556**	7.67×10^{-6}	0.475	2.34×10^{-5}

Entry	$V_{tot,\,Ar2I+}$ (mL)	V (mL)	A	$[Ar_2CH^+]$ (M)	$[LB]_0(V_0/V)$ (M)	$[Ar_2I^+]_{0,i}$ (M)	$[Ar_2I^+]_0/[LB]_0(V_0/V)$	$(A_0*(V_0/V)\text{-}A)/A$	[LB] (M)	$[Ar_2I\text{-}LB]$ (M)	$[Ar_2I^+]$ (M)	$[Ar_2I\text{-}LB]/[LB]$
1	0.20	24.34	0.588	8.11×10^{-6}	2.32×10^{-5}	2.85×10^{-4}	12.3	0.74	1.46×10^{-5}	2.64×10^{-6}	2.83×10^{-4}	1.81×10^{-1}
2	0.40	24.54	0.601	8.29×10^{-6}	2.30×10^{-5}	5.66×10^{-4}	24.6	0.69	1.35×10^{-5}	3.76×10^{-6}	5.62×10^{-4}	2.77×10^{-1}
3	0.60	24.74	0.611	8.43×10^{-6}	2.28×10^{-5}	8.42×10^{-4}	36.9	0.65	1.27×10^{-5}	4.63×10^{-6}	8.37×10^{-4}	3.63×10^{-1}
4	0.80	24.94	0.619	8.54×10^{-6}	2.26×10^{-5}	1.11×10^{-3}	49.2	0.61	1.21×10^{-5}	5.34×10^{-6}	1.11×10^{-3}	4.43×10^{-1}
5	1.00	25.14	0.626	8.63×10^{-6}	2.25×10^{-5}	1.38×10^{-3}	61.5	0.58	1.15×10^{-5}	5.97×10^{-6}	1.38×10^{-3}	5.22×10^{-1}

RM792-2

Titration						
Entry	$V_{tot,\,LB}$ (mL)	V (mL)	A	$[Ar_2CH^+]$ (M)	$A_0*(V_0/V)$-A	$[LB]_0$ (M)
1	–	24.10	**1.027**	1.42×10^{-5}		
2	0.04	24.14	**0.537**	7.41×10^{-6}	0.488	2.46×10^{-5}

Entry	$V_{tot,\,Ar2I+}$ (mL)	V (mL)	A	$[Ar_2CH^+]$ (M)	$[LB]_0(V_0/V)$ (M)	$[Ar_2I^+]_{0,i}$ (M)	$[Ar_2I^+]_0/[LB]_0(V_0/V)$	$(A_0*(V_0/V)\text{-}A)/A$	[LB] (M)	$[Ar_2I\text{-}LB]$ (M)	$[Ar_2I^+]$ (M)	$[Ar_2I\text{-}LB]/[LB]$
1	0.20	24.34	0.565	7.79×10^{-6}	2.44×10^{-5}	2.85×10^{-4}	11.7	0.80	1.57×10^{-5}	2.46×10^{-6}	2.83×10^{-4}	1.56×10^{-1}
2	0.40	24.54	0.577	7.96×10^{-6}	2.42×10^{-5}	5.66×10^{-4}	23.4	0.75	1.47×10^{-5}	3.56×10^{-6}	5.62×10^{-4}	2.42×10^{-1}
3	0.60	24.74	0.586	8.08×10^{-6}	2.40×10^{-5}	8.42×10^{-4}	35.0	0.71	1.39×10^{-5}	4.40×10^{-6}	8.38×10^{-4}	3.16×10^{-1}
4	0.80	24.94	0.593	8.18×10^{-6}	2.38×10^{-5}	1.11×10^{-3}	46.7	0.67	1.33×10^{-5}	5.08×10^{-6}	1.11×10^{-3}	3.83×10^{-1}
5	1.00	25.14	0.600	8.28×10^{-6}	2.37×10^{-5}	1.38×10^{-3}	58.4	0.64	1.26×10^{-5}	5.74×10^{-6}	1.38×10^{-3}	4.55×10^{-1}

RM792-3

Titration						
Entry	$V_{tot,\,LB}$ (mL)	V (mL)	A	$[Ar_2CH^+]$ (M)	$A_0*(V_0/V)$-A	$[LB]_0$ (M)
1	–	24.10	**1.032**	1.42×10^{-5}		
2	0.04	24.14	**0.548**	7.56×10^{-6}	0.482	2.40×10^{-5}

Entry	$V_{tot,\,Ar2I+}$ (mL)	V (mL)	A	$[Ar_2CH^+]$ (M)	$[LB]_0(V_0/V)$ (M)	$[Ar_2I^+]_{0,i}$ (M)	$[Ar_2I^+]_0/[LB]_0(V_0/V)$	$(A_0*(V_0/V)\text{-}A)/A$	[LB] (M)	$[Ar_2I\text{-}LB]$ (M)	$[Ar_2I^+]$ (M)	$[Ar_2I\text{-}LB]/[LB]$
1	0.20	24.34	0.579	7.99×10^{-6}	2.38×10^{-5}	2.85×10^{-4}	12.0	0.76	1.51×10^{-5}	2.62×10^{-6}	2.83×10^{-4}	1.74×10^{-1}
2	0.40	24.54	0.592	8.17×10^{-6}	2.36×10^{-5}	5.66×10^{-4}	24.0	0.71	1.40×10^{-5}	3.76×10^{-6}	5.62×10^{-4}	2.68×10^{-1}
3	0.60	24.74	0.601	8.29×10^{-6}	2.34×10^{-5}	8.42×10^{-4}	36.0	0.67	1.32×10^{-5}	4.58×10^{-6}	8.38×10^{-4}	3.46×10^{-1}
4	0.80	24.94	0.609	8.40×10^{-6}	2.32×10^{-5}	1.11×10^{-3}	48.0	0.64	1.25×10^{-5}	5.30×10^{-6}	1.11×10^{-3}	4.23×10^{-1}
5	1.00	25.14	0.616	8.50×10^{-6}	2.30×10^{-5}	1.38×10^{-3}	60.0	0.61	1.19×10^{-5}	5.94×10^{-6}	1.38×10^{-3}	4.98×10^{-1}

1h + 3f (20 °C) - RM797

BIMT experiment (MeCN, 20 °C) for the pyridine **3f** with **1h** (stock solution: 28.8 mM) competing against the benzhydrylium ion **B1** (632 nm, ε = 1.45 × 10^5 M^{-1} cm^{-1}, K = 5.08 × 10^4 M^{-1} from ref. 15).

RM797-1

Titration						
Entry	$V_{tot,\,LB}$ (mL)	V (mL)	A	$[Ar_2CH^+]$ (M)	$A_0*(V_0/V)$-A	$[LB]_0$ (M)
1	–	24.10	**1.041**	1.44×10^{-5}		
2	0.05	24.15	**0.425**	5.86×10^{-6}	0.614	3.69×10^{-5}

Entry	$V_{tot,\,Ar2I+}$ (mL)	V (mL)	A	$[Ar_2CH^+]$ (M)	$[LB]_0(V_0/V)$ (M)	$[Ar_2I^+]_{0,i}$ (M)	$[Ar_2I^+]_0/[LB]_0(V_0/V)$	$(A_0*(V_0/V)-A)/A$	[LB] (M)	$[Ar_2I$-LB] (M)	$[Ar_2I^+]$ (M)	$[Ar_2I$-LB]/[LB]
1	0.20	24.35	0.443	6.11×10^{-6}	3.66×10^{-5}	2.37×10^{-4}	6.5	1.33	2.61×10^{-5}	2.40×10^{-6}	2.34×10^{-4}	9.19×10^{-2}
2	0.40	24.55	0.452	6.23×10^{-6}	3.63×10^{-5}	4.69×10^{-4}	12.9	1.26	2.49×10^{-5}	3.56×10^{-6}	4.66×10^{-4}	1.43×10^{-1}
3	0.60	24.75	0.458	6.32×10^{-6}	3.60×10^{-5}	6.98×10^{-4}	19.4	1.21	2.39×10^{-5}	4.46×10^{-6}	6.94×10^{-4}	1.87×10^{-1}
4	0.80	24.95	0.463	6.39×10^{-6}	3.57×10^{-5}	9.24×10^{-4}	25.9	1.17	2.31×10^{-5}	5.17×10^{-6}	9.18×10^{-4}	2.24×10^{-1}
5	1.00	25.15	0.468	6.46×10^{-6}	3.54×10^{-5}	1.15×10^{-3}	32.3	1.13	2.23×10^{-5}	5.85×10^{-6}	1.14×10^{-3}	2.63×10^{-1}

RM797-2

Titration						
Entry	$V_{tot,\,LB}$ (mL)	V (mL)	A	$[Ar_2CH^+]$ (M)	$A_0*(V_0/V)$-A	$[LB]_0$ (M)
1	–	24.10	**1.038**	1.43×10^{-5}		
2	0.05	24.15	**0.423**	5.83×10^{-6}	0.613	3.70×10^{-5}

Entry	$V_{tot,\,Ar2I+}$ (mL)	V (mL)	A	$[Ar_2CH^+]$ (M)	$[LB]_0(V_0/V)$ (M)	$[Ar_2I^+]_{0,i}$ (M)	$[Ar_2I^+]_0/[LB]_0(V_0/V)$	$(A_0*(V_0/V)-A)/A$	[LB] (M)	$[Ar_2I$-LB] (M)	$[Ar_2I^+]$ (M)	$[Ar_2I$-LB]/[LB]
1	0.20	24.35	0.439	6.06×10^{-6}	3.67×10^{-5}	2.37×10^{-4}	6.5	1.34	2.64×10^{-5}	2.17×10^{-6}	2.34×10^{-4}	8.24×10^{-2}
2	0.40	24.55	0.446	6.15×10^{-6}	3.64×10^{-5}	4.69×10^{-4}	12.9	1.28	2.53×10^{-5}	3.18×10^{-6}	4.66×10^{-4}	1.26×10^{-1}
3	0.60	24.75	0.451	6.22×10^{-6}	3.61×10^{-5}	6.98×10^{-4}	19.4	1.24	2.44×10^{-5}	3.93×10^{-6}	6.94×10^{-4}	1.61×10^{-1}
4	0.80	24.95	0.456	6.29×10^{-6}	3.58×10^{-5}	9.24×10^{-4}	25.8	1.20	2.36×10^{-5}	4.65×10^{-6}	9.19×10^{-4}	1.97×10^{-1}
5	1.00	25.15	0.460	6.34×10^{-6}	3.55×10^{-5}	1.15×10^{-3}	32.3	1.16	2.29×10^{-5}	5.25×10^{-6}	1.14×10^{-3}	2.29×10^{-1}

RM797-3

Titration						
Entry	$V_{tot,\,LB}$ (mL)	V (mL)	A	$[Ar_2CH^+]$ (M)	$A_0*(V_0/V)$-A	$[LB]_0$ (M)
1	–	24.10	**1.042**	1.44×10^{-5}		
2	0.05	24.15	**0.418**	5.77×10^{-6}	0.622	3.79×10^{-5}

Entry	$V_{tot,\,Ar2I+}$ (mL)	V (mL)	A	$[Ar_2CH^+]$ (M)	$[LB]_0(V_0/V)$ (M)	$[Ar_2I^+]_{0,i}$ (M)	$[Ar_2I^+]_0/[LB]_0(V_0/V)$	$(A_0*(V_0/V)-A)/A$	[LB] (M)	$[Ar_2I$-LB] (M)	$[Ar_2I^+]$ (M)	$[Ar_2I$-LB]/[LB]
1	0.20	24.35	0.433	5.97×10^{-6}	3.76×10^{-5}	2.37×10^{-4}	6.3	1.38	2.72×10^{-5}	2.10×10^{-6}	2.34×10^{-4}	7.71×10^{-2}
2	0.40	24.55	0.440	6.07×10^{-6}	3.72×10^{-5}	4.69×10^{-4}	12.6	1.32	2.61×10^{-5}	3.13×10^{-6}	4.66×10^{-4}	1.20×10^{-1}
3	0.60	24.75	0.445	6.14×10^{-6}	3.69×10^{-5}	6.98×10^{-4}	18.9	1.28	2.52×10^{-5}	3.89×10^{-6}	6.94×10^{-4}	1.54×10^{-1}
4	0.80	24.95	0.449	6.19×10^{-6}	3.66×10^{-5}	9.24×10^{-4}	25.2	1.24	2.44×10^{-5}	4.52×10^{-6}	9.19×10^{-4}	1.85×10^{-1}
5	1.00	25.15	0.454	6.26×10^{-6}	3.64×10^{-5}	1.15×10^{-3}	31.5	1.20	2.36×10^{-5}	5.24×10^{-6}	1.14×10^{-3}	2.22×10^{-1}

1j + 3f (20 °C) - RM800

BIMT experiment (MeCN, 20 °C) for the pyridine **3f** with **1j** (stock solution: 40.4 mM) competing against the benzhydrylium ion **B1** (632 nm, ε = 1.45×10^5 M^{-1} cm^{-1}, K = 5.08×10^4 M^{-1} from ref. 15).

RM800-1

Titration						
Entry	$V_{tot,\,LB}$ (mL)	V (mL)	A	$[Ar_2CH^+]$ (M)	$A_0*(V_0/V)$-A	$[LB]_0$ (M)
1	–	24.10	**1.037**	1.43×10^{-5}		
2	0.05	24.15	**0.422**	5.82×10^{-6}	0.613	3.70×10^{-5}

Entry	$V_{tot,\,Ar2I+}$ (mL)	V (mL)	A	$[Ar_2CH^+]$ (M)	$[LB]_0(V_0/V)$ (M)	$[Ar_2I^+]_{0,i}$ (M)	$[Ar_2I^+]_0/[LB]_0(V_0/V)$	$(A_0*(V_0/V)-A)/A$	[LB] (M)	$[Ar_2I$-LB] (M)	$[Ar_2I^+]$ (M)	$[Ar_2I$-LB]/[LB]
1	0.20	24.35	0.432	5.96×10^{-6}	3.67×10^{-5}	3.32×10^{-4}	9.0	1.38	2.71×10^{-5}	1.46×10^{-6}	3.30×10^{-4}	5.37×10^{-2}
2	0.40	24.55	0.440	6.07×10^{-6}	3.64×10^{-5}	6.58×10^{-4}	18.1	1.31	2.59×10^{-5}	2.61×10^{-6}	6.55×10^{-4}	1.01×10^{-1}
3	0.60	24.75	0.446	6.15×10^{-6}	3.61×10^{-5}	9.79×10^{-4}	27.1	1.26	2.49×10^{-5}	3.48×10^{-6}	9.75×10^{-4}	1.40×10^{-1}
4	0.80	24.95	0.452	6.23×10^{-6}	3.59×10^{-5}	1.29×10^{-3}	36.1	1.22	2.39×10^{-5}	4.33×10^{-6}	1.29×10^{-3}	1.81×10^{-1}
5	1.00	25.15	0.458	6.32×10^{-6}	3.56×10^{-5}	1.61×10^{-3}	45.1	1.17	2.30×10^{-5}	5.15×10^{-6}	1.60×10^{-3}	2.24×10^{-1}

RM800-2

Titration						
Entry	$V_{tot,\,LB}$ (mL)	V (mL)	A	$[Ar_2CH^+]$ (M)	$A_0*(V_0/V)$-A	$[LB]_0$ (M)
1	–	24.10	**1.040**	1.43×10^{-5}		
2	0.05	24.15	**0.418**	5.77×10^{-6}	0.620	3.77×10^{-5}

Entry	$V_{tot,\,Ar2I+}$ (mL)	V (mL)	A	$[Ar_2CH^+]$ (M)	$[LB]_0(V_0/V)$ (M)	$[Ar_2I^+]_{0,i}$ (M)	$[Ar_2I^+]_0/[LB]_0(V_0/V)$	$(A_0*(V_0/V)-A)/A$	[LB] (M)	$[Ar_2I$-LB] (M)	$[Ar_2I^+]$ (M)	$[Ar_2I$-LB]/[LB]
1	0.20	24.35	0.429	5.92×10^{-6}	3.74×10^{-5}	3.32×10^{-4}	8.9	1.40	2.75×10^{-5}	1.60×10^{-6}	3.30×10^{-4}	5.82×10^{-2}
2	0.40	24.55	0.436	6.01×10^{-6}	3.71×10^{-5}	6.58×10^{-4}	17.7	1.34	2.65×10^{-5}	2.59×10^{-6}	6.55×10^{-4}	9.78×10^{-2}
3	0.60	24.75	0.441	6.08×10^{-6}	3.68×10^{-5}	9.79×10^{-4}	26.6	1.30	2.55×10^{-5}	3.42×10^{-6}	9.75×10^{-4}	1.34×10^{-1}
4	0.80	24.95	0.447	6.17×10^{-6}	3.65×10^{-5}	1.29×10^{-3}	35.4	1.25	2.46×10^{-5}	4.29×10^{-6}	1.29×10^{-3}	1.75×10^{-1}
5	1.00	25.15	0.453	6.25×10^{-6}	3.62×10^{-5}	1.61×10^{-3}	44.3	1.20	2.36×10^{-5}	5.12×10^{-6}	1.60×10^{-3}	2.17×10^{-1}

RM800-3

Titration						
Entry	$V_{tot,\,LB}$ (mL)	V (mL)	A	$[Ar_2CH^+]$ (M)	$A_0*(V_0/V)$-A	$[LB]_0$ (M)
1	–	24.10	**1.049**	1.45×10^{-5}		
2	0.05	24.15	**0.426**	5.88×10^{-6}	0.621	3.73×10^{-5}

Entry	$V_{tot,\,Ar2I+}$ (mL)	V (mL)	A	$[Ar_2CH^+]$ (M)	$[LB]_0(V_0/V)$ (M)	$[Ar_2I^+]_{0,i}$ (M)	$[Ar_2I^+]_0/[LB]_0(V_0/V)$	$(A_0*(V_0/V)-A)/A$	[LB] (M)	$[Ar_2I$-LB] (M)	$[Ar_2I^+]$ (M)	$[Ar_2I$-LB]/[LB]
1	0.20	24.35	0.435	6.00×10^{-6}	3.69×10^{-5}	3.32×10^{-4}	9.0	1.39	2.73×10^{-5}	1.33×10^{-6}	3.30×10^{-4}	4.86×10^{-2}
2	0.40	24.55	0.442	6.09×10^{-6}	3.66×10^{-5}	6.58×10^{-4}	18.0	1.33	2.62×10^{-5}	2.30×10^{-6}	6.56×10^{-4}	8.77×10^{-2}
3	0.60	24.75	0.448	6.18×10^{-6}	3.63×10^{-5}	9.79×10^{-4}	26.9	1.28	2.52×10^{-5}	3.24×10^{-6}	9.75×10^{-4}	1.29×10^{-1}
4	0.80	24.95	0.454	6.26×10^{-6}	3.61×10^{-5}	1.29×10^{-3}	35.9	1.23	2.43×10^{-5}	4.04×10^{-6}	1.29×10^{-3}	1.66×10^{-1}
5	1.00	25.15	0.460	6.34×10^{-6}	3.58×10^{-5}	1.61×10^{-3}	44.9	1.19	2.34×10^{-5}	4.86×10^{-6}	1.60×10^{-3}	2.08×10^{-1}

1l + 3f (20 °C) - RM798

BIMT experiment (MeCN, 20 °C) for the pyridine **3f** with **1l** (stock solution: 22.4 mM) competing against the benzhydrylium ion **B1** (632 nm, ε = 1.45 × 10^5 M^{-1} cm^{-1}, K = 5.08 × 10^4 M^{-1} from ref. 15).

RM798-1

Titration						
Entry	$V_{tot,\,LB}$ (mL)	V (mL)	A	$[Ar_2CH^+]$ (M)	$A_0*(V_0/V)$-A	$[LB]_0$ (M)
1	–	24.10	**1.054**	1.45×10^{-5}		
2	0.05	24.15	**0.426**	5.88×10^{-6}	0.626	3.76×10^{-5}

Entry	$V_{tot,\,Ar2I+}$ (mL)	V (mL)	A	$[Ar_2CH^+]$ (M)	$[LB]_0(V_0/V)$ (M)	$[Ar_2I^+]_{0,i}$ (M)	$[Ar_2I^+]_0$/ $[LB]_0(V_0/V)$	$(A_0*(V_0/V)$-A)/A	[LB] (M)	[Ar$_2$I-LB] (M)	$[Ar_2I^+]$ (M)	[Ar$_2$I-LB]/ [LB]
1	0.20	24.35	0.441	6.08×10^{-6}	3.72×10^{-5}	1.84×10^{-4}	4.9	1.37	2.69×10^{-5}	2.06×10^{-6}	1.82×10^{-4}	7.65×10^{-2}
2	0.40	24.55	0.451	6.22×10^{-6}	3.69×10^{-5}	3.65×10^{-4}	9.9	1.29	2.55×10^{-5}	3.41×10^{-6}	3.61×10^{-4}	1.34×10^{-1}
3	0.60	24.75	0.459	6.33×10^{-6}	3.66×10^{-5}	5.43×10^{-4}	14.8	1.24	2.43×10^{-5}	4.48×10^{-6}	5.38×10^{-4}	1.84×10^{-1}
4	0.80	24.95	0.467	6.44×10^{-6}	3.63×10^{-5}	7.18×10^{-4}	19.7	1.18	2.32×10^{-5}	5.52×10^{-6}	7.12×10^{-4}	2.37×10^{-1}
5	1.00	25.15	0.474	6.54×10^{-6}	3.61×10^{-5}	8.90×10^{-4}	24.7	1.13	2.23×10^{-5}	6.40×10^{-6}	8.84×10^{-4}	2.88×10^{-1}

RM798-2

Titration						
Entry	$V_{tot,\,LB}$ (mL)	V (mL)	A	$[Ar_2CH^+]$ (M)	$A_0*(V_0/V)$-A	$[LB]_0$ (M)
1	–	24.10	**1.037**	1.43×10^{-5}		
2	0.05	24.15	**0.419**	5.78×10^{-6}	0.616	3.74×10^{-5}

Entry	$V_{tot,\,Ar2I+}$ (mL)	V (mL)	A	$[Ar_2CH^+]$ (M)	$[LB]_0(V_0/V)$ (M)	$[Ar_2I^+]_{0,i}$ (M)	$[Ar_2I^+]_0$/ $[LB]_0(V_0/V)$	$(A_0*(V_0/V)$-A)/A	[LB] (M)	[Ar$_2$I-LB] (M)	$[Ar_2I^+]$ (M)	[Ar$_2$I-LB]/ [LB]
1	0.20	24.35	0.436	6.01×10^{-6}	3.71×10^{-5}	1.84×10^{-4}	5.0	1.35	2.67×10^{-5}	2.32×10^{-6}	1.82×10^{-4}	8.72×10^{-2}
2	0.40	24.55	0.447	6.17×10^{-6}	3.68×10^{-5}	3.65×10^{-4}	9.9	1.28	2.51×10^{-5}	3.80×10^{-6}	3.61×10^{-4}	1.51×10^{-1}
3	0.60	24.75	0.456	6.29×10^{-6}	3.65×10^{-5}	5.43×10^{-4}	14.9	1.21	2.39×10^{-5}	4.98×10^{-6}	5.38×10^{-4}	2.08×10^{-1}
4	0.80	24.95	0.464	6.40×10^{-6}	3.62×10^{-5}	7.18×10^{-4}	19.8	1.16	2.28×10^{-5}	6.00×10^{-6}	7.12×10^{-4}	2.63×10^{-1}
5	1.00	25.15	0.471	6.50×10^{-6}	3.59×10^{-5}	8.90×10^{-4}	24.8	1.11	2.18×10^{-5}	6.88×10^{-6}	8.83×10^{-4}	3.15×10^{-1}

RM798-3

Titration						
Entry	$V_{tot,\,LB}$ (mL)	V (mL)	A	$[Ar_2CH^+]$ (M)	$A_0*(V_0/V)$-A	$[LB]_0$ (M)
1	–	24.10	**1.031**	1.42×10^{-5}		
2	0.05	24.15	**0.423**	5.83×10^{-6}	0.606	3.66×10^{-5}

Entry	$V_{tot,\,Ar2I+}$ (mL)	V (mL)	A	$[Ar_2CH^+]$ (M)	$[LB]_0(V_0/V)$ (M)	$[Ar_2I^+]_{0,i}$ (M)	$[Ar_2I^+]_0/[LB]_0(V_0/V)$	$(A_0*(V_0/V)-A)/A$	[LB] (M)	$[Ar_2I$-LB] (M)	$[Ar_2I^+]$ (M)	$[Ar_2I$-LB]/[LB]
1	0.20	24.35	0.443	6.11×10^{-6}	3.63×10^{-5}	1.84×10^{-4}	5.1	1.30	2.57×10^{-5}	2.63×10^{-6}	1.81×10^{-4}	1.02×10^{-1}
2	0.40	24.55	0.454	6.26×10^{-6}	3.60×10^{-5}	3.65×10^{-4}	10.1	1.23	2.42×10^{-5}	4.06×10^{-6}	3.61×10^{-4}	1.68×10^{-1}
3	0.60	24.75	0.463	6.39×10^{-6}	3.57×10^{-5}	5.43×10^{-4}	15.2	1.17	2.30×10^{-5}	5.21×10^{-6}	5.37×10^{-4}	2.26×10^{-1}
4	0.80	24.95	0.471	6.50×10^{-6}	3.54×10^{-5}	7.18×10^{-4}	20.3	1.11	2.19×10^{-5}	6.20×10^{-6}	7.11×10^{-4}	2.83×10^{-1}
5	1.00	25.15	0.478	6.59×10^{-6}	3.51×10^{-5}	8.90×10^{-4}	25.4	1.07	2.10×10^{-5}	7.06×10^{-6}	8.83×10^{-4}	3.36×10^{-1}

1m + 3f (20 °C) - RM799

BIMT experiment (MeCN, 20 °C) for the pyridine **3f** with **1m** (stock solution: 26.5 mM) competing against the benzhydrylium ion **B1** (632 nm, ε = 1.45×10^5 M^{-1} cm^{-1}, K = 5.08×10^4 M^{-1} from ref. 15).

RM799-1

Titration						
Entry	$V_{tot,\,LB}$ (mL)	V (mL)	A	$[Ar_2CH^+]$ (M)	$A_0*(V_0/V)$-A	$[LB]_0$ (M)
1	–	24.10	**1.045**	1.44×10^{-5}		
2	0.05	24.15	**0.428**	5.90×10^{-6}	0.615	3.68×10^{-5}

Entry	$V_{tot,\,Ar2I+}$ (mL)	V (mL)	A	$[Ar_2CH^+]$ (M)	$[LB]_0(V_0/V)$ (M)	$[Ar_2I^+]_{0,i}$ (M)	$[Ar_2I^+]_0/[LB]_0(V_0/V)$	$(A_0*(V_0/V)-A)/A$	[LB] (M)	$[Ar_2I$-LB] (M)	$[Ar_2I^+]$ (M)	$[Ar_2I$-LB]/[LB]
1	0.20	24.35	0.454	6.26×10^{-6}	3.65×10^{-5}	2.17×10^{-4}	6.0	1.28	2.52×10^{-5}	3.29×10^{-6}	2.14×10^{-4}	1.31×10^{-1}
2	0.40	24.55	0.475	6.54×10^{-6}	3.62×10^{-5}	4.31×10^{-4}	11.9	1.16	2.29×10^{-5}	5.68×10^{-6}	4.26×10^{-4}	2.48×10^{-1}
3	0.60	24.75	0.495	6.83×10^{-6}	3.59×10^{-5}	6.42×10^{-4}	17.9	1.06	2.08×10^{-5}	7.88×10^{-6}	6.34×10^{-4}	3.79×10^{-1}
4	0.80	24.95	0.515	7.10×10^{-6}	3.56×10^{-5}	8.49×10^{-4}	23.9	0.96	1.89×10^{-5}	9.86×10^{-6}	8.39×10^{-4}	5.22×10^{-1}
5	1.00	25.15	0.536	7.39×10^{-6}	3.53×10^{-5}	1.05×10^{-3}	29.8	0.87	1.71×10^{-5}	1.18×10^{-5}	1.04×10^{-3}	6.90×10^{-1}

RM799-2

Titration						
Entry	$V_{tot,\,LB}$ (mL)	V (mL)	A	$[Ar_2CH^+]$ (M)	$A_0*(V_0/V)$-A	$[LB]_0$ (M)
1	–	24.10	**1.042**	1.44×10^{-5}		
2	0.05	24.15	**0.424**	5.85×10^{-6}	0.616	3.71×10^{-5}

Entry	$V_{tot,\,Ar2I+}$ (mL)	V (mL)	A	$[Ar_2CH^+]$ (M)	$[LB]_0(V_0/V)$ (M)	$[Ar_2I^+]_{0,i}$ (M)	$[Ar_2I^+]_0/[LB]_0(V_0/V)$	$(A_0*(V_0/V)-A)/A$	[LB] (M)	$[Ar_2I$-LB] (M)	$[Ar_2I^+]$ (M)	$[Ar_2I$-LB]/[LB]
1	0.20	24.35	0.450	6.21×10^{-6}	3.68×10^{-5}	2.17×10^{-4}	5.9	1.29	2.54×10^{-5}	3.33×10^{-6}	2.14×10^{-4}	1.31×10^{-1}
2	0.40	24.55	0.470	6.48×10^{-6}	3.65×10^{-5}	4.31×10^{-4}	11.8	1.18	2.32×10^{-5}	5.70×10^{-6}	4.26×10^{-4}	2.46×10^{-1}
3	0.60	24.75	0.490	6.76×10^{-6}	3.62×10^{-5}	6.42×10^{-4}	17.7	1.07	2.11×10^{-5}	7.87×10^{-6}	6.34×10^{-4}	3.74×10^{-1}
4	0.80	24.95	0.510	7.03×10^{-6}	3.59×10^{-5}	8.49×10^{-4}	23.6	0.97	1.92×10^{-5}	9.88×10^{-6}	8.39×10^{-4}	5.16×10^{-1}
5	1.00	25.15	0.530	7.31×10^{-6}	3.56×10^{-5}	1.05×10^{-3}	29.6	0.88	1.74×10^{-5}	1.17×10^{-5}	1.04×10^{-3}	6.75×10^{-1}

RM799-3

Titration						
Entry	$V_{tot,\,LB}$ (mL)	V (mL)	A	$[Ar_2CH^+]$ (M)	$A_0*(V_0/V)$-A	$[LB]_0$ (M)
1	–	24.10	**1.034**	1.43×10^{-5}		
2	0.05	24.15	**0.423**	5.83×10^{-6}	0.609	3.67×10^{-5}

Entry	$V_{tot,\,Ar2I+}$ (mL)	V (mL)	A	$[Ar_2CH^+]$ (M)	$[LB]_0(V_0/V)$ (M)	$[Ar_2I^+]_{0,i}$ (M)	$[Ar_2I^+]_0/[LB]_0(V_0/V)$	$(A_0*(V_0/V)-A)/A$	[LB] (M)	$[Ar_2I$-LB] (M)	$[Ar_2I^+]$ (M)	$[Ar_2I$-LB]/[LB]
1	0.20	24.35	0.448	6.18×10^{-6}	3.64×10^{-5}	2.17×10^{-4}	6.0	1.28	2.53×10^{-5}	3.21×10^{-6}	2.14×10^{-4}	1.27×10^{-1}
2	0.40	24.55	0.468	6.46×10^{-6}	3.61×10^{-5}	4.31×10^{-4}	11.9	1.17	2.30×10^{-5}	5.58×10^{-6}	4.26×10^{-4}	2.42×10^{-1}
3	0.60	24.75	0.488	6.73×10^{-6}	3.58×10^{-5}	6.42×10^{-4}	17.9	1.06	2.09×10^{-5}	7.76×10^{-6}	6.34×10^{-4}	3.71×10^{-1}
4	0.80	24.95	0.507	6.99×10^{-6}	3.56×10^{-5}	8.49×10^{-4}	23.9	0.97	1.91×10^{-5}	9.68×10^{-6}	8.39×10^{-4}	5.07×10^{-1}
5	1.00	25.15	0.528	7.28×10^{-6}	3.53×10^{-5}	1.05×10^{-3}	29.8	0.88	1.73×10^{-5}	1.16×10^{-5}	1.04×10^{-3}	6.74×10^{-1}

2a + 3f (20 °C) - RM793

BIMT experiment (MeCN, 20 °C) for the pyridine **3f** with **2a** (stock solution: 21.1 mM) competing against the benzhydrylium ion **B1** (632 nm, ε = 1.45 × 10^5 M^{-1} cm^{-1}, K = 5.08 × 10^4 M^{-1} from ref. 15).

RM793-1

Titration						
Entry	$V_{tot,\,LB}$ (mL)	V (mL)	A	$[Ar_2CH^+]$ (M)	$A_0*(V_0/V)$-A	$[LB]_0$ (M)
1	–	24.10	**1.031**	1.42×10^{-5}		
2	0.04	24.14	**0.543**	7.49×10^{-6}	0.486	2.43×10^{-5}

Entry	$V_{tot,\,Ar2I+}$ (mL)	V (mL)	A	$[Ar_2CH^+]$ (M)	$[LB]_0(V_0/V)$ (M)	$[Ar_2I^+]_{0,i}$ (M)	$[Ar_2I^+]_0$/ $[LB]_0(V_0/V)$	$(A_0*(V_0/V)$-A)/A	[LB] (M)	[Ar$_2$I-LB] (M)	$[Ar_2I^+]$ (M)	[Ar$_2$I-LB]/ [LB]
1	0.10	24.24	0.579	7.99×10^{-6}	2.42×10^{-5}	8.69×10^{-5}	3.6	0.77	1.52×10^{-5}	2.92×10^{-6}	8.40×10^{-5}	1.92×10^{-1}
2	0.20	24.34	0.592	8.17×10^{-6}	2.41×10^{-5}	1.73×10^{-4}	7.2	0.72	1.43×10^{-5}	3.96×10^{-6}	1.69×10^{-4}	2.78×10^{-1}
3	0.30	24.44	0.603	8.32×10^{-6}	2.40×10^{-5}	2.59×10^{-4}	10.8	0.69	1.35×10^{-5}	4.83×10^{-6}	2.54×10^{-4}	3.58×10^{-1}
4	0.40	24.54	0.612	8.44×10^{-6}	2.39×10^{-5}	3.43×10^{-4}	14.3	0.65	1.29×10^{-5}	5.53×10^{-6}	3.38×10^{-4}	4.30×10^{-1}
5	0.50	24.64	0.620	8.55×10^{-6}	2.38×10^{-5}	4.27×10^{-4}	17.9	0.63	1.23×10^{-5}	6.15×10^{-6}	4.21×10^{-4}	4.99×10^{-1}

RM793-2

Titration						
Entry	$V_{tot,\,LB}$ (mL)	V (mL)	A	$[Ar_2CH^+]$ (M)	$A_0*(V_0/V)$-A	$[LB]_0$ (M)
1	–	24.10	**1.025**	1.41×10^{-5}		
2	0.04	24.14	**0.542**	7.48×10^{-6}	0.481	2.41×10^{-5}

Entry	$V_{tot,\,Ar2I+}$ (mL)	V (mL)	A	$[Ar_2CH^+]$ (M)	$[LB]_0(V_0/V)$ (M)	$[Ar_2I^+]_{0,i}$ (M)	$[Ar_2I^+]_0$/ $[LB]_0(V_0/V)$	$(A_0*(V_0/V)$-A)/A	[LB] (M)	[Ar$_2$I-LB] (M)	$[Ar_2I^+]$ (M)	[Ar$_2$I-LB]/ [LB]
1	0.10	24.24	0.587	8.10×10^{-6}	2.40×10^{-5}	8.69×10^{-5}	3.6	0.74	1.45×10^{-5}	3.57×10^{-6}	8.33×10^{-5}	2.46×10^{-1}
2	0.20	24.34	0.602	8.30×10^{-6}	2.39×10^{-5}	1.73×10^{-4}	7.2	0.69	1.35×10^{-5}	4.72×10^{-6}	1.68×10^{-4}	3.50×10^{-1}
3	0.30	24.44	0.615	8.48×10^{-6}	2.38×10^{-5}	2.59×10^{-4}	10.9	0.64	1.27×10^{-5}	5.70×10^{-6}	2.53×10^{-4}	4.50×10^{-1}
4	0.40	24.54	0.625	8.62×10^{-6}	2.37×10^{-5}	3.43×10^{-4}	14.5	0.61	1.20×10^{-5}	6.44×10^{-6}	3.37×10^{-4}	5.36×10^{-1}
5	0.50	24.64	0.634	8.74×10^{-6}	2.36×10^{-5}	4.27×10^{-4}	18.1	0.58	1.14×10^{-5}	7.10×10^{-6}	4.20×10^{-4}	6.21×10^{-1}

RM793-3

Titration						
Entry	$V_{tot,\,LB}$ (mL)	V (mL)	A	$[Ar_2CH^+]$ (M)	$A_0*(V_0/V)$-A	$[LB]_0$ (M)
1	–	24.10	**1.035**	1.43×10^{-5}		
2	0.04	24.14	**0.545**	7.52×10^{-6}	0.488	2.44×10^{-5}

Entry	$V_{tot,\,Ar2I+}$ (mL)	V (mL)	A	$[Ar_2CH^+]$ (M)	$[LB]_0(V_0/V)$ (M)	$[Ar_2I^+]_{0,i}$ (M)	$[Ar_2I^+]_0/[LB]_0(V_0/V)$	$(A_0*(V_0/V)-A)/A$	[LB] (M)	$[Ar_2I$-LB] (M)	$[Ar_2I^+]$ (M)	$[Ar_2I$-LB]/[LB]
1	0.10	24.24	0.584	8.06×10^{-6}	2.43×10^{-5}	8.69×10^{-5}	3.6	0.76	1.50×10^{-5}	3.13×10^{-6}	8.38×10^{-5}	2.09×10^{-1}
2	0.20	24.34	0.598	8.25×10^{-6}	2.42×10^{-5}	1.73×10^{-4}	7.2	0.71	1.40×10^{-5}	4.24×10^{-6}	1.69×10^{-4}	3.01×10^{-1}
3	0.30	24.44	0.610	8.41×10^{-6}	2.41×10^{-5}	2.59×10^{-4}	10.7	0.67	1.33×10^{-5}	5.12×10^{-6}	2.53×10^{-4}	3.86×10^{-1}
4	0.40	24.54	0.620	8.55×10^{-6}	2.40×10^{-5}	3.43×10^{-4}	14.3	0.64	1.26×10^{-5}	5.92×10^{-6}	3.37×10^{-4}	4.70×10^{-1}
5	0.50	24.64	0.629	8.67×10^{-6}	2.39×10^{-5}	4.27×10^{-4}	17.9	0.61	1.20×10^{-5}	6.56×10^{-6}	4.21×10^{-4}	5.46×10^{-1}

1a + 3g (at −10 °C) - RM1041

BIMT experiment (MeCN, –10 °C) for quinuclidine (**3g**) with **1a** (stock solution: 30.0 mM) competing against the benzhydrylium ion **B2** (605 nm, ε = 1.66×10^5 M^{-1} cm^{-1}, at –10 °C: $K = 7.15 \times 10^6$ M^{-1} from this work).

RM1041-M10-1

Titration							
Entry	$V_{tot,\,LB}$ (mL)	V (mL)	V_{corr} (mL)	A	$[Ar_2CH^+]$ (M)	$A_0*(V_0/V)$-A	$[LB]_0$ (M)
1	–	24.15	23.17	**1.131**	1.36×10^{-5}		
2	0.03	24.18	23.20	**0.088**	1.06×10^{-6}	1.042	1.42×10^{-5}

Entry	$V_{tot,\,Ar2I+}$ (mL)	V (mL)	V_{corr} (mL)	A	$[Ar_2CH^+]$ (M)	$[LB]_0(V_0/V)$ (M)	$[Ar_2I^+]_{0,i}$ (M)	$[Ar_2I^+]_0/[LB]_0(V_0/V)$	$(A_0*(V_0/V)-A)/A$	[LB] (M)	$[Ar_2I$-LB] (M)	$[Ar_2I^+]$ (M)	$[Ar_2I$-LB]/[LB]
1	0.20	24.38	23.39	0.104	1.25×10^{-6}	1.41×10^{-5}	2.56×10^{-4}	18.2	9.77	1.37×10^{-6}	4.77×10^{-7}	2.56×10^{-4}	3.49×10^{-1}
2	0.40	24.58	23.58	0.122	1.47×10^{-6}	1.40×10^{-5}	5.09×10^{-4}	36.4	8.11	1.13×10^{-6}	9.21×10^{-7}	5.08×10^{-4}	8.12×10^{-1}
3	0.60	24.78	23.78	0.140	1.69×10^{-6}	1.39×10^{-5}	7.57×10^{-4}	54.6	6.87	9.61×10^{-7}	1.31×10^{-6}	7.55×10^{-4}	1.36
4	0.80	24.98	23.97	0.157	1.89×10^{-6}	1.37×10^{-5}	1.00×10^{-3}	72.8	5.96	8.34×10^{-7}	1.63×10^{-6}	9.99×10^{-4}	1.96
5	1.00	25.18	24.16	0.176	2.12×10^{-6}	1.36×10^{-5}	1.24×10^{-3}	91.0	5.16	7.22×10^{-7}	1.97×10^{-6}	1.24×10^{-3}	2.73

RM1041-M10-2

Titration							
Entry	$V_{tot,\,LB}$ (mL)	V (mL)	V_{corr} (mL)	A	$[Ar_2CH^+]$ (M)	$A_0*(V_0/V)$-A	$[LB]_0$ (M)
1	–	24.15	23.17	**1.156**	1.39×10^{-5}		
2	0.03	24.18	23.20	**0.089**	1.07×10^{-6}	1.066	1.45×10^{-5}

Entry	$V_{tot,\,Ar2I+}$ (mL)	V (mL)	V_{corr} (mL)	A	$[Ar_2CH^+]$ (M)	$[LB]_0(V_0/V)$ (M)	$[Ar_2I^+]_{0,i}$ (M)	$[Ar_2I^+]_0/[LB]_0(V_0/V)$	$(A_0*(V_0/V)\text{-}A)/A$	[LB] (M)	$[Ar_2I\text{-}LB]$ (M)	$[Ar_2I^+]$ (M)	$[Ar_2I\text{-}LB]/[LB]$
1	0.20	24.38	23.39	0.107	1.29×10^{-6}	1.44×10^{-5}	2.56×10^{-4}	17.8	9.70	1.36×10^{-6}	5.30×10^{-7}	2.56×10^{-4}	3.90×10^{-1}
2	0.40	24.58	23.58	0.123	1.48×10^{-6}	1.43×10^{-5}	5.09×10^{-4}	35.6	8.23	1.15×10^{-6}	9.23×10^{-7}	5.08×10^{-4}	8.01×10^{-1}
3	0.60	24.78	23.78	0.142	1.71×10^{-6}	1.42×10^{-5}	7.57×10^{-4}	53.4	6.93	9.70×10^{-7}	1.33×10^{-6}	7.55×10^{-4}	1.37
4	0.80	24.98	23.97	0.162	1.95×10^{-6}	1.40×10^{-5}	1.00×10^{-3}	71.3	5.90	8.25×10^{-7}	1.71×10^{-6}	9.99×10^{-4}	2.07
5	1.00	25.18	24.16	0.182	2.19×10^{-6}	1.39×10^{-5}	1.24×10^{-3}	89.1	5.09	7.12×10^{-7}	2.06×10^{-6}	1.24×10^{-3}	2.89

RM1041-M10-3

Titration							
Entry	$V_{tot,\,LB}$ (mL)	V (mL)	V_{corr} (mL)	A	$[Ar_2CH^+]$ (M)	$A_0*(V_0/V)$-A	$[LB]_0$ (M)
1	–	24.15	23.17	**1.162**	1.40×10^{-5}		
2	0.03	24.18	23.20	**0.104**	1.25×10^{-6}	1.057	1.42×10^{-5}

Entry	$V_{tot,\,Ar2I+}$ (mL)	V (mL)	V_{corr} (mL)	A	$[Ar_2CH^+]$ (M)	$[LB]_0(V_0/V)$ (M)	$[Ar_2I^+]_{0,i}$ (M)	$[Ar_2I^+]_0/[LB]_0(V_0/V)$	$(A_0*(V_0/V)\text{-}A)/A$	[LB] (M)	$[Ar_2I\text{-}LB]$ (M)	$[Ar_2I^+]$ (M)	$[Ar_2I\text{-}LB]/[LB]$
1	0.20	24.38	23.39	0.125	1.51×10^{-6}	1.40×10^{-5}	2.56×10^{-4}	18.3	8.21	1.15×10^{-6}	5.24×10^{-7}	2.56×10^{-4}	4.57×10^{-1}
2	0.40	24.58	23.58	0.144	1.73×10^{-6}	1.39×10^{-5}	5.09×10^{-4}	36.5	6.93	9.69×10^{-7}	9.31×10^{-7}	5.08×10^{-4}	9.61×10^{-1}
3	0.60	24.78	23.78	0.165	1.99×10^{-6}	1.38×10^{-5}	7.57×10^{-4}	54.8	5.86	8.20×10^{-7}	1.33×10^{-6}	7.55×10^{-4}	1.62
4	0.80	24.98	23.97	0.184	2.22×10^{-6}	1.37×10^{-5}	1.00×10^{-3}	73.1	5.11	7.14×10^{-7}	1.67×10^{-6}	9.99×10^{-4}	2.33
5	1.00	25.18	24.16	0.206	2.48×10^{-6}	1.36×10^{-5}	1.24×10^{-3}	91.3	4.41	6.17×10^{-7}	2.03×10^{-6}	1.24×10^{-3}	3.29

1a + 3g (0 °C) - RM1041

BIMT experiment (MeCN, 0 °C) for quinuclidine (**3g**) with **1a** (stock solution: 30.0 mM) competing against the benzhydrylium ion **B2** (605 nm, ε = 1.66 × 10^5 M^{-1} cm^{-1}, at 0 °C: K = 2.39 × 10^6 M^{-1} from this work).

RM1041-0-1

Titration							
Entry	$V_{tot,\,LB}$ (mL)	V (mL)	V_{corr} (mL)	A	$[Ar_2CH^+]$ (M)	$A_0*(V_0/V)$-A	$[LB]_0$ (M)
1	–	24.15	23.49	**1.089**	1.31×10^{-5}		
2	0.03	24.18	23.52	**0.266**	3.20×10^{-6}	0.822	1.12×10^{-5}

Entry	$V_{tot,\,Ar2I+}$ (mL)	V (mL)	V_{corr} (mL)	A	$[Ar_2CH^+]$ (M)	$[LB]_0(V_0/V)$ (M)	$[Ar_2I^+]_{0,i}$ (M)	$[Ar_2I^+]_0$/ $[LB]_0(V_0/V)$	$(A_0*(V_0/V)$-A)/A	[LB] (M)	$[Ar_2I$-LB] (M)	$[Ar_2I^+]$ (M)	$[Ar_2I$-LB]/ [LB]
1	0.20	24.38	23.71	0.311	3.75×10^{-6}	1.11×10^{-5}	2.53×10^{-4}	22.8	2.47	1.03×10^{-6}	8.17×10^{-7}	2.52×10^{-4}	7.91×10^{-1}
2	0.40	24.58	23.91	0.334	4.02×10^{-6}	1.10×10^{-5}	5.02×10^{-4}	45.6	2.20	9.22×10^{-7}	1.22×10^{-6}	5.01×10^{-4}	1.32
3	0.60	24.78	24.10	0.351	4.23×10^{-6}	1.09×10^{-5}	7.47×10^{-4}	68.4	2.02	8.47×10^{-7}	1.52×10^{-6}	7.45×10^{-4}	1.79
4	0.80	24.98	24.29	0.364	4.39×10^{-6}	1.08×10^{-5}	9.87×10^{-4}	91.1	1.89	7.92×10^{-7}	1.74×10^{-6}	9.86×10^{-4}	2.20
5	1.00	25.18	24.49	0.376	4.53×10^{-6}	1.07×10^{-5}	1.22×10^{-3}	113.9	1.78	7.44×10^{-7}	1.95×10^{-6}	1.22×10^{-3}	2.62

RM1041-0-2

Titration							
Entry	$V_{tot,\,LB}$ (mL)	V (mL)	V_{corr} (mL)	A	$[Ar_2CH^+]$ (M)	$A_0*(V_0/V)$-A	$[LB]_0$ (M)
1	–	24.15	23.49	**1.100**	1.33×10^{-5}		
2	0.03	24.18	23.52	**0.139**	1.67×10^{-6}	0.960	1.45×10^{-5}

Entry	$V_{tot,\,Ar2I+}$ (mL)	V (mL)	V_{corr} (mL)	A	$[Ar_2CH^+]$ (M)	$[LB]_0(V_0/V)$ (M)	$[Ar_2I^+]_{0,i}$ (M)	$[Ar_2I^+]_0$/ $[LB]_0(V_0/V)$	$(A_0*(V_0/V)$-A)/A	[LB] (M)	$[Ar_2I$-LB] (M)	$[Ar_2I^+]$ (M)	$[Ar_2I$-LB]/ [LB]
1	0.20	24.38	23.71	0.154	1.86×10^{-6}	1.43×10^{-5}	2.53×10^{-4}	17.6	6.08	2.54×10^{-6}	5.17×10^{-7}	2.52×10^{-4}	2.04×10^{-1}
2	0.40	24.58	23.91	0.169	2.04×10^{-6}	1.42×10^{-5}	5.02×10^{-4}	35.3	5.40	2.26×10^{-6}	9.73×10^{-7}	5.01×10^{-4}	4.31×10^{-1}
3	0.60	24.78	24.10	0.182	2.19×10^{-6}	1.41×10^{-5}	7.47×10^{-4}	52.9	4.89	2.05×10^{-6}	1.33×10^{-6}	7.45×10^{-4}	6.51×10^{-1}
4	0.80	24.98	24.29	0.196	2.36×10^{-6}	1.40×10^{-5}	9.87×10^{-4}	70.6	4.43	1.85×10^{-6}	1.68×10^{-6}	9.86×10^{-4}	9.10×10^{-1}
5	1.00	25.18	24.49	0.210	2.53×10^{-6}	1.39×10^{-5}	1.22×10^{-3}	88.2	4.02	1.68×10^{-6}	2.01×10^{-6}	1.22×10^{-3}	1.20

RM1041-0-4

Titration							
Entry	$V_{tot,\,LB}$ (mL)	V (mL)	V_{corr} (mL)	A	$[Ar_2CH^+]$ (M)	$A_0*(V_0/V)$-A	$[LB]_0$ (M)
1	–	24.15	23.49	**1.061**	1.28×10^{-5}		
2	0.03	24.18	23.52	**0.124**	1.49×10^{-6}	0.936	1.44×10^{-5}

Entry	$V_{tot,\,Ar2I+}$ (mL)	V (mL)	V_{corr} (mL)	A	$[Ar_2CH^+]$ (M)	$[LB]_0(V_0/V)$ (M)	$[Ar_2I^+]_{0,i}$ (M)	$[Ar_2I^+]_0/[LB]_0(V_0/V)$	$(A_0*(V_0/V)\text{-}A)/A$	[LB] (M)	$[Ar_2I\text{-}LB]$ (M)	$[Ar_2I^+]$ (M)	$[Ar_2I\text{-}LB]/[LB]$
1	0.20	24.38	23.71	0.138	1.66×10^{-6}	1.43×10^{-5}	2.53×10^{-4}	17.7	6.62	2.77×10^{-6}	5.44×10^{-7}	2.52×10^{-4}	1.97×10^{-1}
2	0.40	24.58	23.91	0.151	1.82×10^{-6}	1.42×10^{-5}	5.02×10^{-4}	35.3	5.90	2.47×10^{-6}	9.85×10^{-7}	5.01×10^{-4}	3.99×10^{-1}
3	0.60	24.78	24.10	0.163	1.96×10^{-6}	1.41×10^{-5}	7.47×10^{-4}	53.0	5.34	2.24×10^{-6}	1.35×10^{-6}	7.45×10^{-4}	6.04×10^{-1}
4	0.80	24.98	24.29	0.177	2.13×10^{-6}	1.40×10^{-5}	9.87×10^{-4}	70.7	4.80	2.01×10^{-6}	1.74×10^{-6}	9.86×10^{-4}	8.65×10^{-1}
5	1.00	25.18	24.49	0.190	2.29×10^{-6}	1.39×10^{-5}	1.22×10^{-3}	88.4	4.36	1.82×10^{-6}	2.06×10^{-6}	1.22×10^{-3}	1.13

1a + 3g (10 °C) - RM1035

BIMT experiment (MeCN, 10 °C) for quinuclidine (**3g**) with **1a** (stock solution: 31.1 mM) competing against the benzhydrylium ion **B2** (605 nm, ε = 1.66×10^5 M^{-1} cm^{-1}, at 10 °C: $K = 8.92 \times 10^5$ M^{-1} from this work).

RM1035-10-1

Titration							
Entry	$V_{tot,\,LB}$ (mL)	V (mL)	V_{corr} (mL)	A	$[Ar_2CH^+]$ (M)	$A_0*(V_0/V)$-A	$[LB]_0$ (M)
1	–	24.15	23.82	**1.039**	1.25×10^{-5}		
2	0.04	24.19	23.86	**0.119**	1.43×10^{-6}	0.918	1.97×10^{-5}

Entry	$V_{tot,\,Ar2I+}$ (mL)	V (mL)	V_{corr} (mL)	A	$[Ar_2CH^+]$ (M)	$[LB]_0(V_0/V)$ (M)	$[Ar_2I^+]_{0,i}$ (M)	$[Ar_2I^+]_0/[LB]_0(V_0/V)$	$(A_0*(V_0/V)\text{-}A)/A$	[LB] (M)	$[Ar_2I\text{-}LB]$ (M)	$[Ar_2I^+]$ (M)	$[Ar_2I\text{-}LB]/[LB]$
1	0.20	24.39	24.05	0.126	1.52×10^{-6}	1.96×10^{-5}	2.59×10^{-4}	13.2	7.16	8.03×10^{-6}	6.44×10^{-7}	2.58×10^{-4}	8.01×10^{-2}
2	0.40	24.59	24.25	0.134	1.61×10^{-6}	1.94×10^{-5}	5.13×10^{-4}	26.5	6.61	7.42×10^{-6}	1.30×10^{-6}	5.12×10^{-4}	1.75×10^{-1}
3	0.60	24.79	24.45	0.142	1.71×10^{-6}	1.92×10^{-5}	7.63×10^{-4}	39.7	6.13	6.87×10^{-6}	1.88×10^{-6}	7.61×10^{-4}	2.74×10^{-1}
4	0.80	24.99	24.64	0.150	1.81×10^{-6}	1.91×10^{-5}	1.01×10^{-3}	52.9	5.69	6.38×10^{-6}	2.41×10^{-6}	1.01×10^{-3}	3.78×10^{-1}
5	1.00	25.19	24.84	0.159	1.92×10^{-6}	1.89×10^{-5}	1.25×10^{-3}	66.1	5.26	5.90×10^{-6}	2.94×10^{-6}	1.25×10^{-3}	4.99×10^{-1}

RM1035-10-2

Titration													
Entry	$V_{tot,\,LB}$ (mL)	V (mL)	V_{corr} (mL)	A	$[Ar_2CH^+]$ (M)	$A_0*(V_0/V)$-A	$[LB]_0$ (M)						
1	–	24.15	23.82	**1.040**	1.25×10^{-5}								
2	0.04	24.19	23.86	**0.128**	1.54×10^{-6}	0.910	1.89×10^{-5}						
Entry	$V_{tot,\,Ar2I+}$ (mL)	V (mL)	V_{corr} (mL)	A	$[Ar_2CH^+]$ (M)	$[LB]_0(V_0/V)$ (M)	$[Ar_2I^+]_{0,i}$ (M)	$[Ar_2I^+]_0/[LB]_0(V_0/V)$	$(A_0*(V_0/V)-A)/A$	[LB] (M)	$[Ar_2I$-LB] (M)	$[Ar_2I^+]$ (M)	$[Ar_2I$-LB]/[LB]
1	0.20	24.39	24.05	0.138	1.66×10^{-6}	1.88×10^{-5}	2.59×10^{-4}	13.8	6.46	7.24×10^{-6}	7.96×10^{-7}	2.58×10^{-4}	1.10×10^{-1}
2	0.40	24.59	24.25	0.147	1.77×10^{-6}	1.86×10^{-5}	5.13×10^{-4}	27.5	5.95	6.67×10^{-6}	1.43×10^{-6}	5.12×10^{-4}	2.14×10^{-1}
3	0.60	24.79	24.45	0.156	1.88×10^{-6}	1.85×10^{-5}	7.63×10^{-4}	41.3	5.49	6.16×10^{-6}	1.99×10^{-6}	7.61×10^{-4}	3.24×10^{-1}
4	0.80	24.99	24.64	0.165	1.99×10^{-6}	1.83×10^{-5}	1.01×10^{-3}	55.1	5.09	5.71×10^{-6}	2.50×10^{-6}	1.01×10^{-3}	4.39×10^{-1}
5	1.00	25.19	24.84	0.174	2.10×10^{-6}	1.82×10^{-5}	1.25×10^{-3}	68.8	4.73	5.30×10^{-6}	2.97×10^{-6}	1.25×10^{-3}	5.60×10^{-1}

RM1035-10-3

Titration													
Entry	$V_{tot,\,LB}$ (mL)	V (mL)	V_{corr} (mL)	A	$[Ar_2CH^+]$ (M)	$A_0*(V_0/V)$-A	$[LB]_0$ (M)						
1	–	24.15	23.82	**1.079**	1.30×10^{-5}								
2	0.04	24.19	23.86	**0.131**	1.58×10^{-6}	0.946	1.95×10^{-5}						
Entry	$V_{tot,\,Ar2I+}$ (mL)	V (mL)	V_{corr} (mL)	A	$[Ar_2CH^+]$ (M)	$[LB]_0(V_0/V)$ (M)	$[Ar_2I^+]_{0,i}$ (M)	$[Ar_2I^+]_0/[LB]_0(V_0/V)$	$(A_0*(V_0/V)-A)/A$	[LB] (M)	$[Ar_2I$-LB] (M)	$[Ar_2I^+]$ (M)	$[Ar_2I$-LB]/[LB]
1	0.20	24.39	24.05	0.139	1.67×10^{-6}	1.93×10^{-5}	2.59×10^{-4}	13.4	6.69	7.50×10^{-6}	6.45×10^{-7}	2.58×10^{-4}	8.60×10^{-2}
2	0.40	24.59	24.25	0.147	1.77×10^{-6}	1.92×10^{-5}	5.13×10^{-4}	26.7	6.21	6.96×10^{-6}	1.22×10^{-6}	5.12×10^{-4}	1.76×10^{-1}
3	0.60	24.79	24.45	0.156	1.88×10^{-6}	1.90×10^{-5}	7.63×10^{-4}	40.1	5.74	6.43×10^{-6}	1.81×10^{-6}	7.62×10^{-4}	2.81×10^{-1}
4	0.80	24.99	24.64	0.165	1.99×10^{-6}	1.89×10^{-5}	1.01×10^{-3}	53.5	5.32	5.96×10^{-6}	2.33×10^{-6}	1.01×10^{-3}	3.92×10^{-1}
5	1.00	25.19	24.84	0.174	2.10×10^{-6}	1.87×10^{-5}	1.25×10^{-3}	66.9	4.95	5.54×10^{-6}	2.81×10^{-6}	1.25×10^{-3}	5.07×10^{-1}

1a + 3g (20 °C) - RM1035

BIMT experiment (MeCN, 20 °C) for quinuclidine (**3g**) with **1a** (stock solution: 31.1 mM) competing against the benzhydrylium ion **B2** (605 nm, ε = 1.66 × 10^5 M^{-1} cm^{-1}, at 20 °C: K = 3.55 × 10^5 M^{-1} from this work).

RM1035-20-1

Titration						
Entry	$V_{tot,\,LB}$ (mL)	V (mL)	A	$[Ar_2CH^+]$ (M)	$A_0*(V_0/V)$-A	$[LB]_0$ (M)
1	–	24.15	**1.077**	1.30×10^{-5}		
2	0.04	24.19	**0.266**	3.20×10^{-6}	0.809	1.83×10^{-5}

Entry	$V_{tot,\,Ar2I+}$ (mL)	V (mL)	A	$[Ar_2CH^+]$ (M)	$[LB]_0(V_0/V)$ (M)	$[Ar_2I^+]_{0,i}$ (M)	$[Ar_2I^+]_0$/ $[LB]_0(V_0/V)$	$(A_0*(V_0/V)$-A)/A	[LB] (M)	[Ar$_2$I-LB] (M)	$[Ar_2I^+]$ (M)	[Ar$_2$I-LB]/ [LB]
1	0.20	24.39	0.275	3.31×10^{-6}	1.82×10^{-5}	2.55×10^{-4}	14.0	2.88	8.11×10^{-6}	5.27×10^{-7}	2.55×10^{-4}	6.51×10^{-2}
2	0.40	24.59	0.282	3.40×10^{-6}	1.80×10^{-5}	5.06×10^{-4}	28.1	2.75	7.75×10^{-6}	9.26×10^{-7}	5.05×10^{-4}	1.20×10^{-1}
3	0.60	24.79	0.291	3.51×10^{-6}	1.79×10^{-5}	7.53×10^{-4}	42.1	2.61	7.34×10^{-6}	1.40×10^{-6}	7.51×10^{-4}	1.91×10^{-1}
4	0.80	24.99	0.300	3.61×10^{-6}	1.77×10^{-5}	9.96×10^{-4}	56.2	2.47	6.96×10^{-6}	1.85×10^{-6}	9.94×10^{-4}	2.66×10^{-1}
5	1.00	25.19	0.309	3.72×10^{-6}	1.76×10^{-5}	1.23×10^{-3}	70.2	2.34	6.60×10^{-6}	2.28×10^{-6}	1.23×10^{-3}	3.45×10^{-1}

RM1035-20-2

Titration						
Entry	$V_{tot,\,LB}$ (mL)	V (mL)	A	$[Ar_2CH^+]$ (M)	$A_0*(V_0/V)$-A	$[LB]_0$ (M)
1	–	24.15	**1.094**	1.32×10^{-5}		
2	0.04	24.19	**0.270**	3.25×10^{-6}	0.822	1.85×10^{-5}

Entry	$V_{tot,\,Ar2I+}$ (mL)	V (mL)	A	$[Ar_2CH^+]$ (M)	$[LB]_0(V_0/V)$ (M)	$[Ar_2I^+]_{0,i}$ (M)	$[Ar_2I^+]_0$/ $[LB]_0(V_0/V)$	$(A_0*(V_0/V)$-A)/A	[LB] (M)	[Ar$_2$I-LB] (M)	$[Ar_2I^+]$ (M)	[Ar$_2$I-LB]/ [LB]
1	0.20	24.39	0.274	3.30×10^{-6}	1.83×10^{-5}	2.55×10^{-4}	13.9	2.95	8.32×10^{-6}	2.63×10^{-7}	2.55×10^{-4}	3.16×10^{-2}
2	0.40	24.59	0.280	3.37×10^{-6}	1.82×10^{-5}	5.06×10^{-4}	27.8	2.84	7.99×10^{-6}	6.20×10^{-7}	5.05×10^{-4}	7.75×10^{-2}
3	0.60	24.79	0.288	3.47×10^{-6}	1.80×10^{-5}	7.53×10^{-4}	41.7	2.70	7.61×10^{-6}	1.06×10^{-6}	7.52×10^{-4}	1.39×10^{-1}
4	0.80	24.99	0.297	3.58×10^{-6}	1.79×10^{-5}	9.96×10^{-4}	55.7	2.56	7.21×10^{-6}	1.52×10^{-6}	9.94×10^{-4}	2.11×10^{-1}
5	1.00	25.19	0.306	3.69×10^{-6}	1.78×10^{-5}	1.23×10^{-3}	69.6	2.43	6.84×10^{-6}	1.96×10^{-6}	1.23×10^{-3}	2.87×10^{-1}

RM1035-20-3 (as before but with a 34.1 mM stock solution for **1a**)

Titration						
Entry	$V_{tot,\,LB}$ (mL)	V (mL)	A	$[Ar_2CH^+]$ (M)	$A_0*(V_0/V)$-A	$[LB]_0$ (M)
1	–	24.15	**1.037**	1.25×10^{-5}		
2	0.04	24.19	**0.238**	2.87×10^{-6}	0.797	1.90×10^{-5}

Entry	$V_{tot,\,Ar2I+}$ (mL)	V (mL)	A	$[Ar_2CH^+]$ (M)	$[LB]_0(V_0/V)$ (M)	$[Ar_2I^+]_{0,i}$ (M)	$[Ar_2I^+]_0/[LB]_0(V_0/V)$	$(A_0*(V_0/V)-A)/A$	[LB] (M)	$[Ar_2I$-LB] (M)	$[Ar_2I^+]$ (M)	$[Ar_2I$-LB]/[LB]
1	0.20	24.39	0.245	2.95×10^{-6}	1.89×10^{-5}	2.79×10^{-4}	14.8	3.19	8.99×10^{-6}	4.78×10^{-7}	2.79×10^{-4}	5.32×10^{-2}
2	0.40	24.59	0.252	3.04×10^{-6}	1.87×10^{-5}	5.54×10^{-4}	29.6	3.04	8.57×10^{-6}	9.31×10^{-7}	5.53×10^{-4}	1.09×10^{-1}
3	0.60	24.79	0.260	3.13×10^{-6}	1.86×10^{-5}	8.24×10^{-4}	44.4	2.89	8.13×10^{-6}	1.41×10^{-6}	8.23×10^{-4}	1.74×10^{-1}
4	0.80	24.99	0.268	3.23×10^{-6}	1.84×10^{-5}	1.09×10^{-3}	59.1	2.74	7.72×10^{-6}	1.87×10^{-6}	1.09×10^{-3}	2.42×10^{-1}
5	1.00	25.19	0.276	3.33×10^{-6}	1.83×10^{-5}	1.35×10^{-3}	73.9	2.60	7.33×10^{-6}	2.30×10^{-6}	1.35×10^{-3}	3.14×10^{-1}

1d + 3g (20 °C) - RM1038

BIMT experiment (MeCN, 20 °C) for quinuclidine (**3g**) with **1d** (stock solution: 11.7 mM) competing against the benzhydrylium ion **B2** (605 nm, ε = 1.66×10^5 M^{-1} cm^{-1}, K = 3.55×10^5 M^{-1} from this work).

RM1038-1

Titration						
Entry	$V_{tot,\,LB}$ (mL)	V (mL)	A	$[Ar_2CH^+]$ (M)	$A_0*(V_0/V)$-A	$[LB]_0$ (M)
1	–	24.15	**1.025**	1.23×10^{-5}		
2	0.04	24.19	**0.244**	2.94×10^{-6}	0.779	1.84×10^{-5}

Entry	$V_{tot,\,Ar2I+}$ (mL)	V (mL)	A	$[Ar_2CH^+]$ (M)	$[LB]_0(V_0/V)$ (M)	$[Ar_2I^+]_{0,i}$ (M)	$[Ar_2I^+]_0/[LB]_0(V_0/V)$	$(A_0*(V_0/V)-A)/A$	[LB] (M)	$[Ar_2I$-LB] (M)	$[Ar_2I^+]$ (M)	$[Ar_2I$-LB]/[LB]
1	0.20	24.39	0.263	3.17×10^{-6}	1.82×10^{-5}	9.63×10^{-5}	5.3	2.86	8.05×10^{-6}	1.12×10^{-6}	9.52×10^{-5}	1.39×10^{-1}
2	0.40	24.59	0.279	3.36×10^{-6}	1.81×10^{-5}	1.91×10^{-4}	10.6	2.61	7.35×10^{-6}	1.97×10^{-6}	1.89×10^{-4}	2.69×10^{-1}
3	0.60	24.79	0.293	3.53×10^{-6}	1.79×10^{-5}	2.84×10^{-4}	15.8	2.41	6.78×10^{-6}	2.66×10^{-6}	2.82×10^{-4}	3.92×10^{-1}
4	0.80	24.99	0.305	3.67×10^{-6}	1.78×10^{-5}	3.76×10^{-4}	21.1	2.25	6.33×10^{-6}	3.21×10^{-6}	3.73×10^{-4}	5.06×10^{-1}
5	1.00	25.19	0.317	3.82×10^{-6}	1.77×10^{-5}	4.66×10^{-4}	26.4	2.10	5.92×10^{-6}	3.72×10^{-6}	4.62×10^{-4}	6.29×10^{-1}

RM1038-2

Titration						
Entry	$V_{tot,\,LB}$ (mL)	V (mL)	A	$[Ar_2CH^+]$ (M)	$A_0*(V_0/V)$-A	$[LB]_0$ (M)
1	–	24.15	**1.053**	1.27×10^{-5}		
2	0.04	24.19	**0.251**	3.02×10^{-6}	0.800	1.86×10^{-5}

Entry	$V_{tot,\,Ar2I+}$ (mL)	V (mL)	A	$[Ar_2CH^+]$ (M)	$[LB]_0(V_0/V)$ (M)	$[Ar_2I^+]_{0,i}$ (M)	$[Ar_2I^+]_0/[LB]_0(V_0/V)$	$(A_0*(V_0/V)-A)/A$	[LB] (M)	$[Ar_2I$-LB] (M)	$[Ar_2I^+]$ (M)	$[Ar_2I$-LB]/[LB]
1	0.20	24.39	0.271	3.27×10^{-6}	1.85×10^{-5}	9.63×10^{-5}	5.2	2.85	8.02×10^{-6}	1.15×10^{-6}	9.51×10^{-5}	1.44×10^{-1}
2	0.40	24.59	0.287	3.46×10^{-6}	1.83×10^{-5}	1.91×10^{-4}	10.4	2.60	7.33×10^{-6}	1.98×10^{-6}	1.89×10^{-4}	2.71×10^{-1}
3	0.60	24.79	0.301	3.63×10^{-6}	1.82×10^{-5}	2.84×10^{-4}	15.6	2.41	6.78×10^{-6}	2.66×10^{-6}	2.82×10^{-4}	3.92×10^{-1}
4	0.80	24.99	0.314	3.78×10^{-6}	1.80×10^{-5}	3.76×10^{-4}	20.9	2.24	6.31×10^{-6}	3.24×10^{-6}	3.73×10^{-4}	5.13×10^{-1}
5	1.00	25.19	0.326	3.93×10^{-6}	1.79×10^{-5}	4.66×10^{-4}	26.1	2.10	5.91×10^{-6}	3.74×10^{-6}	4.62×10^{-4}	6.34×10^{-1}

RM1038-3

Titration						
Entry	$V_{tot,\,LB}$ (mL)	V (mL)	A	$[Ar_2CH^+]$ (M)	$A_0*(V_0/V)$-A	$[LB]_0$ (M)
1	–	24.15	**1.009**	1.22×10^{-5}		
2	0.04	24.19	**0.233**	2.81×10^{-6}	0.774	1.87×10^{-5}

Entry	$V_{tot,\,Ar2I+}$ (mL)	V (mL)	A	$[Ar_2CH^+]$ (M)	$[LB]_0(V_0/V)$ (M)	$[Ar_2I^+]_{0,i}$ (M)	$[Ar_2I^+]_0/[LB]_0(V_0/V)$	$(A_0*(V_0/V)-A)/A$	[LB] (M)	$[Ar_2I$-LB] (M)	$[Ar_2I^+]$ (M)	$[Ar_2I$-LB]/[LB]
1	0.20	24.39	0.251	3.02×10^{-6}	1.85×10^{-5}	9.63×10^{-5}	5.2	2.98	8.40×10^{-6}	1.13×10^{-6}	9.52×10^{-5}	1.34×10^{-1}
2	0.40	24.59	0.266	3.20×10^{-6}	1.84×10^{-5}	1.91×10^{-4}	10.4	2.73	7.68×10^{-6}	1.98×10^{-6}	1.89×10^{-4}	2.57×10^{-1}
3	0.60	24.79	0.280	3.37×10^{-6}	1.82×10^{-5}	2.84×10^{-4}	15.6	2.51	7.07×10^{-6}	2.70×10^{-6}	2.81×10^{-4}	3.81×10^{-1}
4	0.80	24.99	0.292	3.52×10^{-6}	1.81×10^{-5}	3.76×10^{-4}	20.8	2.34	6.59×10^{-6}	3.27×10^{-6}	3.73×10^{-4}	4.97×10^{-1}
5	1.00	25.19	0.303	3.65×10^{-6}	1.79×10^{-5}	4.66×10^{-4}	26.0	2.19	6.18×10^{-6}	3.77×10^{-6}	4.62×10^{-4}	6.10×10^{-1}

1e + 3g (20 °C) - RM1042

BIMT experiment (MeCN, 20 °C) for quinuclidine (**3g**) with **1e** (stock solution: 4.03 mM) competing against the benzhydrylium ion **B2** (605 nm, ε = 1.66 × 10^5 M^{-1} cm^{-1}, K = 3.55 × 10^5 M^{-1} from this work).

RM1042-1

Titration						
Entry	$V_{tot,\,LB}$ (mL)	V (mL)	A	$[Ar_2CH^+]$ (M)	$A_0*(V_0/V)$-A	$[LB]_0$ (M)
1	–	24.15	**1.048**	1.26×10^{-5}		
2	0.04	24.19	**0.252**	3.04×10^{-6}	0.794	1.84×10^{-5}

Entry	$V_{tot,\,Ar2I+}$ (mL)	V (mL)	A	$[Ar_2CH^+]$ (M)	$[LB]_0(V_0/V)$ (M)	$[Ar_2I^+]_{0,i}$ (M)	$[Ar_2I^+]_0$/ $[LB]_0(V_0/V)$	$(A_0*(V_0/V)$-A)/A	[LB] (M)	$[Ar_2I$-LB] (M)	$[Ar_2I^+]$ (M)	$[Ar_2I$-LB]/ [LB]
1	0.03	24.22	0.303	3.65×10^{-6}	1.84×10^{-5}	4.16×10^{-6}	0.2	2.45	6.90×10^{-6}	2.59×10^{-6}	1.57×10^{-6}	3.75×10^{-1}
2	0.05	24.24	0.346	4.17×10^{-6}	1.84×10^{-5}	8.31×10^{-6}	0.5	2.02	5.68×10^{-6}	4.32×10^{-6}	4.00×10^{-6}	7.59×10^{-1}
3	0.08	24.27	0.381	4.59×10^{-6}	1.84×10^{-5}	1.25×10^{-5}	0.7	1.74	4.89×10^{-6}	5.52×10^{-6}	6.94×10^{-6}	1.13
4	0.10	24.29	0.409	4.93×10^{-6}	1.84×10^{-5}	1.66×10^{-5}	0.9	1.55	4.36×10^{-6}	6.39×10^{-6}	1.02×10^{-5}	1.47
5	0.13	24.32	0.432	5.20×10^{-6}	1.84×10^{-5}	2.07×10^{-5}	1.1	1.41	3.97×10^{-6}	7.05×10^{-6}	1.37×10^{-5}	1.77

RM1042-2

Titration						
Entry	$V_{tot,\,LB}$ (mL)	V (mL)	A	$[Ar_2CH^+]$ (M)	$A_0*(V_0/V)$-A	$[LB]_0$ (M)
1	–	24.15	**1.017**	1.23×10^{-5}		
2	0.04	24.19	**0.241**	2.90×10^{-6}	0.774	1.84×10^{-5}

Entry	$V_{tot,\,Ar2I+}$ (mL)	V (mL)	A	$[Ar_2CH^+]$ (M)	$[LB]_0(V_0/V)$ (M)	$[Ar_2I^+]_{0,i}$ (M)	$[Ar_2I^+]_0$/ $[LB]_0(V_0/V)$	$(A_0*(V_0/V)$-A)/A	[LB] (M)	$[Ar_2I$-LB] (M)	$[Ar_2I^+]$ (M)	$[Ar_2I$-LB]/ [LB]
1	0.03	24.22	0.288	3.47×10^{-6}	1.84×10^{-5}	4.16×10^{-6}	0.2	2.52	7.10×10^{-6}	2.51×10^{-6}	1.65×10^{-6}	3.53×10^{-1}
2	0.05	24.24	0.327	3.94×10^{-6}	1.83×10^{-5}	8.31×10^{-6}	0.5	2.10	5.91×10^{-6}	4.16×10^{-6}	4.15×10^{-6}	7.04×10^{-1}
3	0.08	24.27	0.360	4.34×10^{-6}	1.83×10^{-5}	1.25×10^{-5}	0.7	1.81	5.10×10^{-6}	5.36×10^{-6}	7.10×10^{-6}	1.05
4	0.10	24.29	0.387	4.66×10^{-6}	1.83×10^{-5}	1.66×10^{-5}	0.9	1.61	4.54×10^{-6}	6.24×10^{-6}	1.04×10^{-5}	1.37
5	0.13	24.32	0.411	4.95×10^{-6}	1.83×10^{-5}	2.07×10^{-5}	1.1	1.46	4.11×10^{-6}	6.96×10^{-6}	1.38×10^{-5}	1.70

RM1042-3

Titration						
Entry	$V_{tot,\,LB}$ (mL)	V (mL)	A	$[Ar_2CH^+]$ (M)	$A_0*(V_0/V)$-A	$[LB]_0$ (M)
1	–	24.15	**1.027**	1.24×10^{-5}		
2	0.04	24.19	**0.257**	3.10×10^{-6}	0.768	1.77×10^{-5}

Entry	$V_{tot,\,Ar2I+}$ (mL)	V (mL)	A	$[Ar_2CH^+]$ (M)	$[LB]_0(V_0/V)$ (M)	$[Ar_2I^+]_{0,i}$ (M)	$[Ar_2I^+]_0/[LB]_0(V_0/V)$	$(A_0*(V_0/V)-A)/A$	[LB] (M)	$[Ar_2I$-LB] (M)	$[Ar_2I^+]$ (M)	$[Ar_2I$-LB]/[LB]
1	0.03	24.22	0.309	3.72×10^{-6}	1.77×10^{-5}	4.16×10^{-6}	0.2	2.31	6.52×10^{-6}	2.52×10^{-6}	1.64×10^{-6}	3.87×10^{-1}
2	0.05	24.24	0.352	4.24×10^{-6}	1.76×10^{-5}	8.31×10^{-6}	0.5	1.91	5.37×10^{-6}	4.18×10^{-6}	4.13×10^{-6}	7.79×10^{-1}
3	0.08	24.27	0.391	4.71×10^{-6}	1.76×10^{-5}	1.25×10^{-5}	0.7	1.61	4.55×10^{-6}	5.47×10^{-6}	6.99×10^{-6}	1.20
4	0.10	24.29	0.421	5.07×10^{-6}	1.76×10^{-5}	1.66×10^{-5}	0.9	1.43	4.02×10^{-6}	6.36×10^{-6}	1.02×10^{-5}	1.58
5	0.13	24.32	0.447	5.39×10^{-6}	1.76×10^{-5}	2.07×10^{-5}	1.2	1.28	3.61×10^{-6}	7.07×10^{-6}	1.36×10^{-5}	1.96

1f + 3g (20 °C) - RM1036

BIMT experiment (MeCN, 20 °C) for quinuclidine (**3g**) with **1f** (stock solution: 28.6 mM) competing against the benzhydrylium ion **B2** (605 nm, ε = 1.66×10^5 M^{-1} cm^{-1}, K = 3.55×10^5 M^{-1} from this work).

RM1036-1

Titration						
Entry	$V_{tot,\,LB}$ (mL)	V (mL)	A	$[Ar_2CH^+]$ (M)	$A_0*(V_0/V)$-A	$[LB]_0$ (M)
1	–	24.15	**1.050**	1.27×10^{-5}		
2	0.04	24.19	**0.252**	3.04×10^{-6}	0.796	1.85×10^{-5}

Entry	$V_{tot,\,Ar2I+}$ (mL)	V (mL)	A	$[Ar_2CH^+]$ (M)	$[LB]_0(V_0/V)$ (M)	$[Ar_2I^+]_{0,i}$ (M)	$[Ar_2I^+]_0/[LB]_0(V_0/V)$	$(A_0*(V_0/V)-A)/A$	[LB] (M)	$[Ar_2I$-LB] (M)	$[Ar_2I^+]$ (M)	$[Ar_2I$-LB]/[LB]
1	0.20	24.39	0.279	3.36×10^{-6}	1.83×10^{-5}	2.34×10^{-4}	12.8	2.73	7.68×10^{-6}	1.50×10^{-6}	2.33×10^{-4}	1.95×10^{-1}
2	0.40	24.59	0.302	3.64×10^{-6}	1.82×10^{-5}	4.65×10^{-4}	25.6	2.41	6.80×10^{-6}	2.61×10^{-6}	4.62×10^{-4}	3.83×10^{-1}
3	0.60	24.79	0.323	3.89×10^{-6}	1.80×10^{-5}	6.92×10^{-4}	38.3	2.17	6.10×10^{-6}	3.51×10^{-6}	6.88×10^{-4}	5.75×10^{-1}
4	0.80	24.99	0.341	4.11×10^{-6}	1.79×10^{-5}	9.15×10^{-4}	51.1	1.98	5.57×10^{-6}	4.22×10^{-6}	9.11×10^{-4}	7.58×10^{-1}
5	1.00	25.19	0.359	4.33×10^{-6}	1.78×10^{-5}	1.13×10^{-3}	63.9	1.80	5.08×10^{-6}	4.88×10^{-6}	1.13×10^{-3}	9.59×10^{-1}

RM1036-2

Titration						
Entry	$V_{tot,\,LB}$ (mL)	V (mL)	A	$[Ar_2CH^+]$ (M)	$A_0*(V_0/V)$-A	$[LB]_0$ (M)
1	–	24.15	**1.052**	1.27×10^{-5}		
2	0.04	24.19	**0.251**	3.02×10^{-6}	0.799	1.86×10^{-5}

Entry	$V_{tot,\,Ar2I+}$ (mL)	V (mL)	A	$[Ar_2CH^+]$ (M)	$[LB]_0(V_0/V)$ (M)	$[Ar_2I^+]_{0,i}$ (M)	$[Ar_2I^+]_0/[LB]_0(V_0/V)$	$(A_0*(V_0/V)-A)/A$	[LB] (M)	$[Ar_2I$-LB] (M)	$[Ar_2I^+]$ (M)	$[Ar_2I$-LB]/[LB]
1	0.20	24.39	0.278	3.35×10^{-6}	1.84×10^{-5}	2.34×10^{-4}	12.7	2.75	7.74×10^{-6}	1.51×10^{-6}	2.33×10^{-4}	1.95×10^{-1}
2	0.40	24.59	0.301	3.63×10^{-6}	1.83×10^{-5}	4.65×10^{-4}	25.4	2.43	6.85×10^{-6}	2.62×10^{-6}	4.62×10^{-4}	3.83×10^{-1}
3	0.60	24.79	0.322	3.88×10^{-6}	1.81×10^{-5}	6.92×10^{-4}	38.1	2.18	6.15×10^{-6}	3.53×10^{-6}	6.88×10^{-4}	5.75×10^{-1}
4	0.80	24.99	0.341	4.11×10^{-6}	1.80×10^{-5}	9.15×10^{-4}	50.8	1.98	5.58×10^{-6}	4.28×10^{-6}	9.11×10^{-4}	7.67×10^{-1}
5	1.00	25.19	0.358	4.31×10^{-6}	1.79×10^{-5}	1.13×10^{-3}	63.5	1.82	5.12×10^{-6}	4.90×10^{-6}	1.13×10^{-3}	9.58×10^{-1}

RM1036-3

Titration						
Entry	$V_{tot,\,LB}$ (mL)	V (mL)	A	$[Ar_2CH^+]$ (M)	$A_0*(V_0/V)$-A	$[LB]_0$ (M)
1	–	24.15	**1.037**	1.25×10^{-5}		
2	0.04	24.19	**0.248**	2.99×10^{-6}	0.787	1.84×10^{-5}

Entry	$V_{tot,\,Ar2I+}$ (mL)	V (mL)	A	$[Ar_2CH^+]$ (M)	$[LB]_0(V_0/V)$ (M)	$[Ar_2I^+]_{0,i}$ (M)	$[Ar_2I^+]_0/[LB]_0(V_0/V)$	$(A_0*(V_0/V)-A)/A$	[LB] (M)	$[Ar_2I$-LB] (M)	$[Ar_2I^+]$ (M)	$[Ar_2I$-LB]/[LB]
1	0.20	24.39	0.276	3.33×10^{-6}	1.83×10^{-5}	2.34×10^{-4}	12.8	2.72	7.66×10^{-6}	1.57×10^{-6}	2.33×10^{-4}	2.05×10^{-1}
2	0.40	24.59	0.300	3.61×10^{-6}	1.81×10^{-5}	4.65×10^{-4}	25.6	2.39	6.75×10^{-6}	2.73×10^{-6}	4.62×10^{-4}	4.04×10^{-1}
3	0.60	24.79	0.320	3.86×10^{-6}	1.80×10^{-5}	6.92×10^{-4}	38.5	2.16	6.08×10^{-6}	3.59×10^{-6}	6.88×10^{-4}	5.91×10^{-1}
4	0.80	24.99	0.339	4.08×10^{-6}	1.78×10^{-5}	9.15×10^{-4}	51.3	1.96	5.51×10^{-6}	4.34×10^{-6}	9.11×10^{-4}	7.87×10^{-1}
5	1.00	25.19	0.357	4.30×10^{-6}	1.77×10^{-5}	1.13×10^{-3}	64.1	1.78	5.03×10^{-6}	4.99×10^{-6}	1.13×10^{-3}	9.93×10^{-1}

2a + 3g (20 °C) - RM1037

BIMT experiment (MeCN, 20 °C) for quinuclidine (**3g**) with **2a** (stock solution: 16.3 mM) competing against the benzhydrylium ion **B2** (605 nm, ε = 1.66 × 10^5 M^{-1} cm^{-1}, K = 3.55 × 10^5 M^{-1} from this work).

RM1037-1

Titration						
Entry	$V_{tot,\,LB}$ (mL)	V (mL)	A	$[Ar_2CH^+]$ (M)	$A_0*(V_0/V)$-A	$[LB]_0$ (M)
1	–	24.15	**1.040**	1.25×10^{-5}		
2	0.04	24.19	**0.244**	2.94×10^{-6}	0.794	1.87×10^{-5}

Entry	$V_{tot,\,Ar2I+}$ (mL)	V (mL)	A	$[Ar_2CH^+]$ (M)	$[LB]_0(V_0/V)$ (M)	$[Ar_2I^+]_{0,i}$ (M)	$[Ar_2I^+]_0$/ $[LB]_0(V_0/V)$	$(A_0*(V_0/V)$-A)/A	[LB] (M)	[Ar$_2$I-LB] (M)	$[Ar_2I^+]$ (M)	[Ar$_2$I-LB]/ [LB]
1	0.20	24.39	0.260	3.13×10^{-6}	1.86×10^{-5}	1.34×10^{-4}	7.2	2.96	8.34×10^{-6}	9.72×10^{-7}	1.33×10^{-4}	1.16×10^{-1}
2	0.40	24.59	0.272	3.28×10^{-6}	1.84×10^{-5}	2.65×10^{-4}	14.4	2.76	7.76×10^{-6}	1.64×10^{-6}	2.64×10^{-4}	2.12×10^{-1}
3	0.60	24.79	0.285	3.43×10^{-6}	1.83×10^{-5}	3.95×10^{-4}	21.6	2.55	7.20×10^{-6}	2.32×10^{-6}	3.92×10^{-4}	3.22×10^{-1}
4	0.80	24.99	0.299	3.60×10^{-6}	1.81×10^{-5}	5.22×10^{-4}	28.8	2.36	6.65×10^{-6}	2.98×10^{-6}	5.19×10^{-4}	4.48×10^{-1}
5	1.00	25.19	0.314	3.78×10^{-6}	1.80×10^{-5}	6.47×10^{-4}	36.0	2.18	6.13×10^{-6}	3.64×10^{-6}	6.43×10^{-4}	5.94×10^{-1}

RM1037-2

Titration						
Entry	$V_{tot,\,LB}$ (mL)	V (mL)	A	$[Ar_2CH^+]$ (M)	$A_0*(V_0/V)$-A	$[LB]_0$ (M)
1	–	24.15	**1.051**	1.27×10^{-5}		
2	0.04	24.19	**0.253**	3.05×10^{-6}	0.796	1.85×10^{-5}

Entry	$V_{tot,\,Ar2I+}$ (mL)	V (mL)	A	$[Ar_2CH^+]$ (M)	$[LB]_0(V_0/V)$ (M)	$[Ar_2I^+]_{0,i}$ (M)	$[Ar_2I^+]_0$/ $[LB]_0(V_0/V)$	$(A_0*(V_0/V)$-A)/A	[LB] (M)	[Ar$_2$I-LB] (M)	$[Ar_2I^+]$ (M)	[Ar$_2$I-LB]/ [LB]
1	0.20	24.39	0.268	3.23×10^{-6}	1.83×10^{-5}	1.34×10^{-4}	7.3	2.88	8.12×10^{-6}	8.77×10^{-7}	1.33×10^{-4}	1.08×10^{-1}
2	0.40	24.59	0.281	3.39×10^{-6}	1.82×10^{-5}	2.65×10^{-4}	14.6	2.67	7.53×10^{-6}	1.58×10^{-6}	2.64×10^{-4}	2.10×10^{-1}
3	0.60	24.79	0.295	3.55×10^{-6}	1.80×10^{-5}	3.95×10^{-4}	21.9	2.47	6.96×10^{-6}	2.27×10^{-6}	3.92×10^{-4}	3.26×10^{-1}
4	0.80	24.99	0.309	3.72×10^{-6}	1.79×10^{-5}	5.22×10^{-4}	29.2	2.29	6.44×10^{-6}	2.91×10^{-6}	5.19×10^{-4}	4.52×10^{-1}
5	1.00	25.19	0.324	3.90×10^{-6}	1.77×10^{-5}	6.47×10^{-4}	36.5	2.11	5.94×10^{-6}	3.55×10^{-6}	6.44×10^{-4}	5.97×10^{-1}

RM1037-3

Titration						
Entry	$V_{tot,\ LB}$ (mL)	V (mL)	A	$[Ar_2CH^+]$ (M)	$A_0*(V_0/V)$-A	$[LB]_0$ (M)
1	–	24.15	**1.060**	1.28×10^{-5}		
2	0.04	24.19	**0.257**	3.10×10^{-6}	0.801	1.84×10^{-5}

Entry	$V_{tot,\ Ar2I+}$ (mL)	V (mL)	A	$[Ar_2CH^+]$ (M)	$[LB]_0(V_0/V)$ (M)	$[Ar_2I^+]_{0,i}$ (M)	$[Ar_2I^+]_0/[LB]_0(V_0/V)$	$(A_0*(V_0/V)-A)/A$	[LB] (M)	$[Ar_2I$-LB] (M)	$[Ar_2I^+]$ (M)	$[Ar_2I$-LB]/[LB]
1	0.20	24.39	0.279	3.36×10^{-6}	1.83×10^{-5}	1.34×10^{-4}	7.3	2.76	7.78×10^{-6}	1.22×10^{-6}	1.32×10^{-4}	1.57×10^{-1}
2	0.40	24.59	0.294	3.54×10^{-6}	1.81×10^{-5}	2.65×10^{-4}	14.6	2.54	7.16×10^{-6}	1.98×10^{-6}	2.63×10^{-4}	2.76×10^{-1}
3	0.60	24.79	0.309	3.72×10^{-6}	1.80×10^{-5}	3.95×10^{-4}	21.9	2.34	6.60×10^{-6}	2.67×10^{-6}	3.92×10^{-4}	4.05×10^{-1}
4	0.80	24.99	0.324	3.90×10^{-6}	1.78×10^{-5}	5.22×10^{-4}	29.2	2.16	6.09×10^{-6}	3.32×10^{-6}	5.19×10^{-4}	5.45×10^{-1}
5	1.00	25.19	0.341	4.11×10^{-6}	1.77×10^{-5}	6.47×10^{-4}	36.6	1.98	5.58×10^{-6}	3.99×10^{-6}	6.43×10^{-4}	7.15×10^{-1}

6.7 Direct Titration (PT Method)

Summary – Photometric Titrations

Initial experiments were performed with the potassium salt of **3e**. Identical equilibrium constants (within experimental error) were observed with the tetrabutylammonium salt of **3e**. All measurements were performed in acetonitrile.

Lewis Acid	Lewis Base	*T* (°C)	Titration	K_I (M^{-1})
1b	**3e**-K^+	10.0	CYL018-1	9.47×10^3
1b	**3e**-K^+	10.0	CYL018-2	9.53×10^3
1b	**3e**-K^+	10.0	CYL018-3	9.29×10^3
1b	**3e**-K^+	10.0	CYL018-4	9.68×10^3
			Average	$(9.49 \pm 0.17) \times 10^3$
1b	**3e**-K^+	20.0	CYL017-1	7.21×10^3
1b	**3e**-K^+	20.0	CYL017-2	8.21×10^3
1b	**3e**-K^+	20.0	CYL017-3	8.11×10^3
1b	**3e**-K^+	20.0	CYL017-4	8.13×10^3
			Average	$(7.91 \pm 0.42) \times 10^3$
1b	**3e**-K^+	30.0	CYL019-1	6.82×10^3
1b	**3e**-K^+	30.0	CYL019-2	6.67×10^3
1b	**3e**-K^+	30.0	CYL019-3	6.78×10^3
1b	**3e**-K^+	30.0	CYL020-1	6.66×10^3
1b	**3e**-K^+	30.0	CYL020-2	6.52×10^3
			Average	$(6.69 \pm 0.12) \times 10^3$
1b	**3e**-K^+	40.0	CYL021-1	5.40×10^3
1b	**3e**-K^+	40.0	CYL021-2	5.07×10^3
1b	**3e**-K^+	40.0	CYL021-3	5.48×10^3
1b	**3e**-K^+	40.0	CYL021-4	5.32×10^3
			Average	$(5.32 \pm 0.18) \times 10^3$
1b	**3e**-NBu_4^+	20.0	CYL032-1	8.64×10^3
1b	**3e**-NBu_4^+	20.0	CYL032-2	7.62×10^3
1b	**3e**-NBu_4^+	20.0	CYL032-3	7.09×10^3
			Average	$(7.78 \pm 0.65) \times 10^3$
1a	**3e**-K^+	20.0	CYL029-1	8.60×10^3
1a	**3e**-K^+	20.0	CYL029-2	9.09×10^3
1a	**3e**-K^+	20.0	CYL029-3	7.96×10^3
			Average	$(8.55 \pm 0.47) \times 10^3$
1a	**3e**-NBu_4^+	20.0	CYL030-1	8.48×10^3
1a	**3e**-NBu_4^+	20.0	CYL030-2	7.84×10^3
1a	**3e**-NBu_4^+	20.0	CYL030-3	7.73×10^3
			Average	$(8.02 \pm 0.33) \times 10^3$
1c	**3e**-NBu_4^+	20.0	CYL046-1	3.10×10^4
1c	**3e**-NBu_4^+	20.0	CYL046-2	3.34×10^4
1c	**3e**-NBu_4^+	20.0	CYL046-3	3.11×10^4
			Average	$(3.18 \pm 0.12) \times 10^4$
1d	**3e**-NBu_4^+	20.0	CYL033-1	1.30×10^5
1d	**3e**-NBu_4^+	20.0	CYL033-2	1.48×10^5
1d	**3e**-NBu_4^+	20.0	CYL033-3	1.35×10^5

			Average	$(1.37 \pm 0.08) \times 10^5$
1f	**3e**-NBu_4^+	20.0	CYL044-1	2.51×10^4
1f	**3e**-NBu_4^+	20.0	CYL044-2	1.88×10^4
1f	**3e**-NBu_4^+	20.0	CYL044-3	2.02×10^4
			Average	$(2.14 \pm 0.28) \times 10^4$
1g	**3e**-NBu_4^+	20.0	RM860-1	4.67×10^3
1g	**3e**-NBu_4^+	20.0	RM860-2	4.99×10^3
1g	**3e**-NBu_4^+	20.0	RM860-3	4.88×10^3
			Average	$(4.85 \pm 0.14) \times 10^3$
1h	**3e**-NBu_4^+	20.0	CYL045-1	1.84×10^4
1h	**3e**-NBu_4^+	20.0	CYL045-2	2.14×10^4
1h	**3e**-NBu_4^+	20.0	CYL045-3	2.06×10^4
			Average	$(2.01 \pm 0.13) \times 10^4$
1i	**3e**-NBu_4^+	20.0	RM833a-1	2.72×10^3
1i	**3e**-NBu_4^+	20.0	RM833a-2	1.56×10^3
1i	**3e**-NBu_4^+	20.0	RM833a-3	2.30×10^3
			Average	$(2.20 \pm 0.48) \times 10^3$
1j	**3e**-NBu_4^+	20.0	CYL047-1	4.76×10^3
1j	**3e**-NBu_4^+	20.0	CYL047-2	4.62×10^3
1j	**3e**-NBu_4^+	20.0	CYL047-3	4.49×10^3
			Average	$(4.62 \pm 0.11) \times 10^3$
1k	**3e**-NBu_4^+	20.0	RM833b-1	8.22×10^3
1k	**3e**-NBu_4^+	20.0	RM833b-2	8.33×10^3
1k	**3e**-NBu_4^+	20.0	RM833b-3	8.30×10^3
			Average	$(8.28 \pm 0.05) \times 10^3$
1l	**3e**-NBu_4^+	20.0	CYL049-1	4.40×10^4
1l	**3e**-NBu_4^+	20.0	CYL049-2	4.27×10^4
1l	**3e**-NBu_4^+	20.0	CYL049-3	4.40×10^4
			Average	$(4.36 \pm 0.07) \times 10^4$
1m	**3e**-NBu_4^+	20.0	CYL048-1	2.31×10^4
1m	**3e**-NBu_4^+	20.0	CYL048-2	2.39×10^4
1m	**3e**-NBu_4^+	20.0	CYL048-3	2.35×10^4
			Average	$(2.35 \pm 0.03) \times 10^4$
1n	**3e**-NBu_4^+	20.0	RM1226-1	9.82×10^3
1n	**3e**-NBu_4^+	20.0	RM1226-2	8.41×10^3
1n	**3e**-NBu_4^+	20.0	RM1226-3	7.57×10^3
			Average	$(8.60 \pm 1.14) \times 10^3$

Van't Hoff analysis for the reaction of **1b** with **3e**:

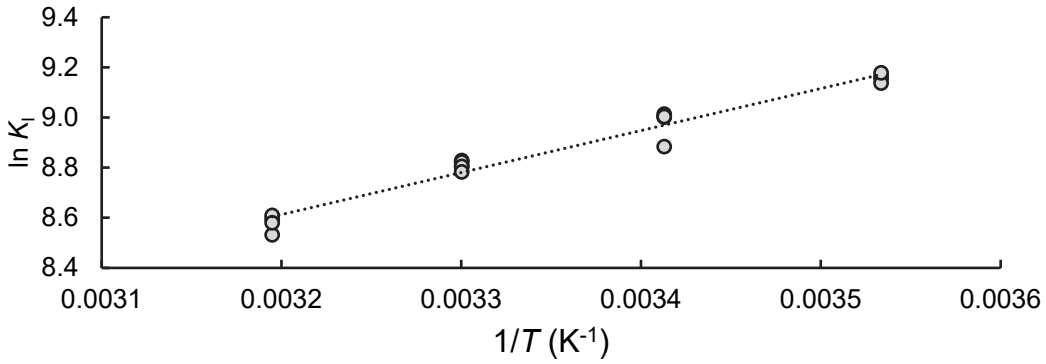

ln K_I = (1.68 ± 0.08) × 10^3 1/T + (3.24 ± 0.27), R^2 = 0.968

ΔH = (−14.0 ± 0.6) kJ mol^{-1}

ΔS = (26.9 ± 2.2) J mol^{-1} K^{-1}

6.8 Isothermal Titration Calorimetry (ITC)

Summary of ITC experiments in acetonitrile.

Experiment	Ar_2I^+	LB	$[Ar_2I^+]$ (mM)	[LB] (mM)	T (°C)	K (M^{-1})	ΔG (kJ mol^{-1})	ΔH (kJ mol^{-1})	$T\Delta S$ (kJ mol^{-1})	n
RM853e1	**1a**	**3a**	0.937	10.00	20.0	1.96×10^5	-29.7	-18.7	11.0	1.00
RM853e2	**1a**	**3a**	0.937	10.00	20.0	1.74×10^5	-29.4	-18.1	11.3	1.01
RM853e3	**1a**	**3a**	0.937	10.00	20.0	1.59×10^5	-29.2	-17.4	11.8	1.01
						$(1.76 \pm 0.16) \times 10^5$	-29.4 ± 0.2	-18.1 ± 0.5	11.4 ± 0.3	
RM951e4	**1a**	**3a**	1.01	10.00	30.0	1.36×10^5	-29.8	-18.6	11.2	1.03
RM951e5	**1a**	**3a**	1.12	10.10	30.0	1.54×10^5	-30.1	-20.0	10.1	0.99
RM951e6	**1a**	**3a**	1.12	10.10	30.0	1.74×10^5	-30.4	-20.2	10.2	1.01
						$(1.55 \pm 0.16) \times 10^5$	-30.1 ± 0.2	-19.6 ± 0.7	10.5 ± 0.5	
RM951e10	**1a**	**3a**	1.04	10.10	40.0	1.31×10^5	-30.7	-19.4	11.2	0.98
RM951e11	**1a**	**3a**	1.04	10.10	40.0	1.31×10^5	-30.7	-19.4	11.3	0.99
RM951e12	**1a**	**3a**	1.04	10.10	40.0	1.24×10^5	-30.5	-19.0	11.5	0.97
						$(1.29 \pm 0.04) \times 10^5$	-30.6 ± 0.1	-19.3 ± 0.2	11.3 ± 0.1	
RM951e13	**1a**	**3a**	1.04	10.10	50.0	9.91×10^4	-30.9	-18.1	12.8	0.95
RM951e14	**1a**	**3a**	1.04	10.10	50.0	1.08×10^5	-31.1	-19.1	12.0	0.84
RM951e15	**1a**	**3a**	1.04	10.10	50.0	1.13×10^5	-31.3	-18.8	12.5	0.85
						$(1.07 \pm 0.06) \times 10^5$	-31.1 ± 0.2	-18.7 ± 0.4	12.4 ± 0.3	
RM954e10	**1a**	**3e**	0.993	10.10	20.0	6.94×10^3	-21.6	-16.4	5.2	1.11
RM954e11	**1a**	**3e**	0.993	10.10	20.0	7.58×10^3	-21.8	-17.3	4.5	1.03
RM954e12	**1a**	**3e**	0.993	10.10	20.0	7.19×10^3	-22.4	-16.9	5.4	1.05
						$(7.24 \pm 0.26) \times 10^3$	-21.9 ± 0.3	-16.9 ± 0.4	5.0 ± 0.4	

RM954e4	**1a**	**3e**	1.03	10.00	30.0	6.28×10^3	-22.0	-17.1	4.9	1.02
RM954e5	**1a**	**3e**	1.03	10.00	30.0	5.85×10^3	-21.9	-17.3	4.6	1.03
RM954e6	**1a**	**3e**	1.03	10.00	30.0	5.88×10^3	-21.9	-16.3	5.5	1.03
						$(6.00 \pm 0.20) \times 10^3$	-21.9 ± 0.1	-16.9 ± 0.4	5.0 ± 0.4	
RM954e7	**1a**	**3e**	1.00	10.10	40.0	5.70×10^3	-22.5	-16.9	5.6	1.09
RM954e8	**1a**	**3e**	1.00	10.10	40.0	5.06×10^3	-22.2	-16.5	5.7	1.10
RM954e9	**1a**	**3e**	1.00	10.10	40.0	4.89×10^3	-22.1	-16.8	5.3	1.10
						$(5.22 \pm 0.35) \times 10^3$	-22.3 ± 0.2	-16.7 ± 0.2	5.5 ± 0.2	
RM831e1	**1a**	**3i**	0.821	10.00	20.0	6.88×10^4	-27.1	-11.6	15.5	0.96
RM831e2	**1a**	**3i**	0.821	10.00	20.0	6.07×10^4	-26.8	-11.0	15.9	0.96
RM831e3	**1a**	**3i**	0.821	10.00	20.0	5.93×10^4	-26.8	-11.1	15.7	0.95
						$(6.29 \pm 0.42) \times 10^4$	-26.9 ± 0.1	-11.2 ± 0.3	15.7 ± 0.2	
RM956e1	**1a**	**3i**	1.05	10.00	30.0	5.78×10^4	-27.6	-11.5	16.1	0.99
RM956e2	**1a**	**3i**	1.05	10.00	30.0	5.57×10^4	-27.5	-11.6	16.0	0.96
RM956e3	**1a**	**3i**	1.05	10.00	30.0	5.53×10^4	-27.5	-11.5	16.1	0.97
						$(5.63 \pm 0.11) \times 10^4$	-27.6 ± 0.1	-11.5 ± 0.1	16.1 ± 0.1	
RM956e4	**1a**	**3i**	1.05	10.00	40.0	4.85×10^4	-28.1	-11.1	17.0	0.95
RM956e5	**1a**	**3i**	1.05	10.00	40.0	4.76×10^4	-28.0	-11.2	16.8	0.95
RM956e6	**1a**	**3i**	1.05	10.00	40.0	4.92×10^4	-28.1	-11.0	17.1	0.96
						$(4.84 \pm 0.07) \times 10^4$	-28.1 ± 0.1	-11.1 ± 0.1	17.0 ± 0.1	
RM956e7	**1a**	**3i**	1.05	10.00	50.0	4.36×10^4	-28.7	-10.6	18.1	0.93
RM956e8	**1a**	**3i**	1.05	10.00	50.0	4.39×10^4	-28.7	-10.4	18.3	0.94
RM956e9	**1a**	**3i**	1.05	10.00	50.0	4.37×10^4	-28.7	-10.6	18.1	0.93
						$(4.37 \pm 0.02) \times 10^4$	-28.7 ± 0.0	-10.5 ± 0.1	18.2 ± 0.1	

RM842e1	**1a**	**3j**	1.07	10.00	20.0	2.33×10^4	-24.5	-10.8	13.7	1.10
RM842e2	**1a**	**3j**	1.07	10.00	20.0	2.39×10^4	-24.6	-10.8	13.8	1.11
RM842e3	**1a**	**3j**	1.07	10.00	20.0	2.25×10^4	-24.4	-11.0	13.5	1.11
						$(2.32 \pm 0.06) \times 10^4$	-24.5 ± 0.1	-10.8 ± 0.1	13.7 ± 0.1	
RM848e1	**1a**	**3k**	0.835	10.00	20.0	4.44×10^3	-20.4	-10.0	10.4	0.977
RM848e2	**1a**	**3k**	0.835	10.00	20.0	4.89×10^3	-20.7	-9.4	11.3	1.01
RM848e3	**1a**	**3k**	0.835	10.00	20.0	3.83×10^3	-20.1	-10.0	10.1	1.01
						$(4.39 \pm 0.44) \times 10^3$	-20.4 ± 0.2	-9.8 ± 0.3	10.6 ± 0.5	
RM839e1	**1d**	**3i**	1.02	10.00	20.0	5.76×10^5	-32.3	-10.5	21.8	1.04
RM839e2	**1d**	**3i**	1.02	10.00	20.0	6.11×10^5	-32.5	-10.7	21.8	1.03
RM839e3	**1d**	**3i**	1.02	10.00	20.0	5.98×10^5	-32.4	-10.5	22.0	1.04
						$(5.95 \pm 0.14) \times 10^5$	-32.4 ± 0.1	-10.5 ± 0.1	21.9 ± 0.1	
RM832e1	**1f**	**3i**	0.92	10.00	200.	4.45×10^5	-31.7	-12.2	19.5	1.09
RM832e2	**1f**	**3i**	0.92	10.00	20.0	3.99×10^5	-31.4	-12.2	19.2	1.06
RM832e3	**1f**	**3i**	0.92	10.00	20.0	4.24×10^5	-31.6	-12.1	19.5	1.06
						$(4.23 \pm 0.19) \times 10^5$	-31.6 ± 0.1	-12.2 ± 0.1	19.4 ± 0.1	
RM843e1	**1f**	**3j**	0.896	10.00	20.0	9.94×10^4	-28.0	-12.6	15.5	1.01
RM843e2	**1f**	**3j**	0.896	10.00	20.0	1.09×10^5	-28.3	-12.6	15.7	1.02
RM843e3	**1f**	**3j**	0.896	10.00	20.0	1.00×10^5	-28.1	-12.5	15.6	0.992
						$(1.03 \pm 0.05) \times 10^5$	-28.1 ± 0.1	-12.6 ± 0.1	15.6 ± 0.1	
RM849e1	**1f**	**3k**	0.842	9.94	20.0	2.18×10^4	-24.3	-10.7	13.6	1
RM849e2	**1f**	**3k**	0.842	9.94	20.0	2.30×10^4	-24.5	-10.5	13.9	1
RM849e3	**1f**	**3k**	0.842	9.94	20.0	2.15×10^4	-24.3	-10.9	13.4	1
						$(2.21 \pm 0.07) \times 10^4$	-24.4 ± 0.1	-10.7 ± 0.2	13.6 ± 0.2	

RM837e1	**1i**	**3i**	1.02	10.00	20.0	1.22×10^4	-22.9	-9.9	13.0	0.98
RM837e3	**1i**	**3i**	1.02	10.00	20.0	1.17×10^4	-22.8	-10.2	12.6	1.01
RM837e4	**1i**	**3i**	1.02	10.00	20.0	1.09×10^4	-22.7	-10.4	12.3	0.99
						$(1.16 \pm 0.06) \times 10^4$	-22.8 ± 0.1	-10.2 ± 0.2	12.6 ± 0.3	
RM841e2	**1i**	**3j**	1.03	9.96	20.0	4.35×10^3	-20.4	-9.1	11.3	1.03
RM841e3	**1i**	**3j**	1.03	9.96	20.0	3.85×10^3	-20.1	-9.6	10.5	0.99
RM841e4	**1i**	**3j**	1.05	9.96	20.0	3.91×10^3	-20.2	-9.7	10.4	1.02
						$(4.04 \pm 0.22) \times 10^3$	-20.2 ± 0.1	-9.5 ± 0.3	10.7 ± 0.4	
RM847e1	**1i**	**3k**	0.834	10.00	20.0	8.04×10^2	-16.3	-11.3	5.0	1.00
RM847e2	**1i**	**3k**	0.834	10.00	20.0	8.39×10^2	-16.4	-10.7	5.6	1.00
RM847e3	**1i**	**3k**	0.834	10.00	20.0	1.27×10^3	-17.4	-7.4	10.0	1.11
						$(9.71 \pm 2.12) \times 10^2$	-16.7 ± 0.5	-9.8 ± 1.7	6.9 ± 2.2	
RM1228e3	**1n**	**3i**	1.02	10.07	20.0	1.64×10^4	-23.7	-12.1	11.6	0.922
RM1228e4	**1n**	**3i**	1.02	10.07	20.0	1.71×10^4	-23.8	-11.8	12.0	0.924
RM1228e5	**1n**	**3i**	1.02	10.07	20.0	1.68×10^4	-23.7	-11.5	12.2	0.925
						$(1.68 \pm 0.03) \times 10^4$	-23.7 ± 0.1	-11.8 ± 0.2	11.9 ± 0.2	
RM840e1	**2a**	**3i**	0.329	3.50	20.0	2.35×10^6	-35.8	-13.8	22.0	0.94
RM840e2	**2a**	**3i**	0.329	3.50	20.0	2.08×10^6	-35.5	-13.2	22.3	0.95
RM840e3	**2a**	**3i**	0.329	3.50	20.0	2.39×10^6	-35.8	-13.5	22.3	0.98
						$(2.27 \pm 0.14) \times 10^6$	-35.7 ± 0.1	-13.5 ± 0.2	22.2 ± 0.1	
RM845e1	**2a**	**3j**	0.367	3.50	20.0	7.42×10^5	-32.9	-14.2	18.7	1.00
RM845e2	**2a**	**3j**	0.367	3.50	20.0	7.39×10^5	-32.9	-14.4	18.5	1.02
RM845e3	**2a**	**3j**	0.367	3.50	20.0	7.49×10^5	-32.9	-14.3	18.6	1.03
						$(7.43 \pm 0.05) \times 10^5$	-32.9 ± 0.0	-14.3 ± 0.1	18.6 ± 0.1	

RM850e1	**2a**	**3k**	0.353	3.90	20.0	1.24×10^5	-28.5	-12.4	16.1	0.95
RM850e2	**2a**	**3k**	0.353	3.90	20.0	1.35×10^5	-28.8	-12.5	16.3	0.95
RM850e3	**2a**	**3k**	0.353	3.90	20.0	1.47×10^5	-29.0	-12.5	16.5	0.95
						$(1.35 \pm 0.10) \times 10^5$	-28.8 ± 0.2	-12.5 ± 0.1	16.3 ± 0.1	

Summary of ITC experiments in dichloromethane.

Experiment	Ar_2I^+	LB	$[Ar_2I^+]$ (mM)	[LB] (mM)	*T* (°C)	*K* (M^{-1})	Δ*G* (kJ mol^{-1})	Δ*H* (kJ mol^{-1})	*T*Δ*S* (kJ mol^{-1})	*n*
RM1216e1	**1a**	**3a**	1.01	10.07	20.0	9.16×10^5	-33.5	-16.8	16.6	1
RM1216e2	**1a**	**3a**	1.01	10.07	20.0	1.44×10^6	-34.6	-14.8	19.8	1.03
RM1216e3	**1a**	**3a**	1.01	10.07	20.0	1.98×10^6	-35.3	-13.4	22.0	1.04
						$(1.45 \pm 0.44) \times 10^6$	-34.5 ± 0.8	-15.0 ± 1.4	19.5 ± 2.2	

Summary of ITC experiments in THF.

Experiment	Ar_2I^+	LB	$[Ar_2I^+]$ (mM)	[LB] (mM)	*T* (°C)	*K* (M^{-1})	Δ*G* (kJ mol^{-1})	Δ*H* (kJ mol^{-1})	*T*Δ*S* (kJ mol^{-1})	*n*
RM1220e1	**1a**	**3a**	1.02	10.29	20.0	3.65×10^6	-36.8	-21.6	15.2	1
RM1220e2	**1a**	**3a**	1.02	10.29	20.0	3.73×10^6	-36.9	-21.1	15.8	0.989
RM1220e3	**1a**	**3a**	1.02	10.29	20.0	3.36×10^6	-36.6	-21.4	15.2	0.946
						$(3.58 \pm 0.16) \times 10^6$	-36.8 ± 0.1	-21.4 ± 0.3	15.4 ± 0.3	

Van't Hoff Analysis based on ITC Data

1a + 3a

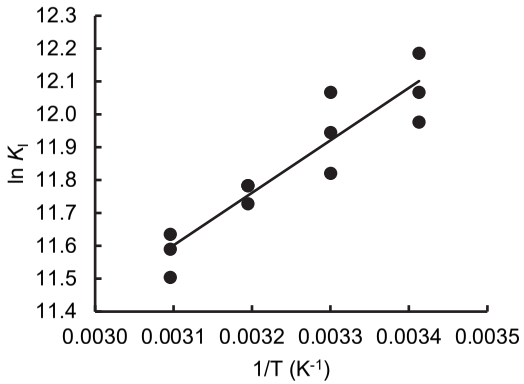

$\ln K_I = (1.59 \pm 0.22) \times 10^3\ 1/T + (6.69 \pm 0.66)$

$R^2 = 0.861$

$\Delta_r H = (-13.2 \pm 1.6)$ kJ mol^{-1}

$\Delta_r S = (55.6 \pm 5.3)$ J mol^{-1} K^{-1}

1a + 3e

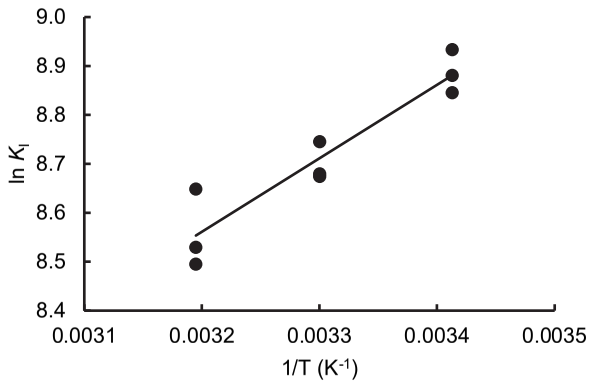

$\ln K_I = (1.51 \pm 0.21) \times 10^3\ 1/T + (3.73 \pm 0.67)$

$R^2 = 0.888$

$\Delta_r H = (-14.3 \pm 2.0)$ kJ mol^{-1}

$\Delta_r S = (25.5 \pm 6.5)$ J mol^{-1} K^{-1}

1a + 3i

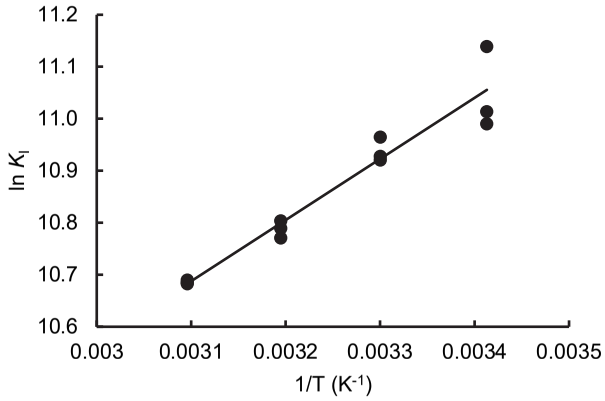

$\ln K_I = (1.17 \pm 0.10) \times 10^3\ 1/T + (7.07 \pm 0.32)$

$R^2 = 0.936$

$\Delta_r H = (-9.7 \pm 0.8)$ kJ mol^{-1}

$\Delta_r S = (58.3 \pm 2.6)$ J mol^{-1} K^{-1}

6.9 NMR Titrations in CD_3CN

1a+ 3f (RM1232)

^1H NMR titration experiment (CD_3CN, 20 °C) of $Ph_2I^+TfO^-$ (**1a**) with **3f**.

Entry	**1a** (M)	**3f** (M)	δ (ppm)	Δδ (ppm)
1	5.0×10^{-3}	0.0	7.7250	0.0000
2	5.0×10^{-3}	2.5×10^{-3}	7.7192	0.0058
3	5.0×10^{-3}	5.0×10^{-3}	7.7140	0.0110
4	5.0×10^{-3}	7.5×10^{-3}	7.7098	0.0152
5	5.0×10^{-3}	1.25×10^{-2}	7.7018	0.0232
6	5.0×10^{-3}	2.0×10^{-2}	7.6917	0.0333
7	5.0×10^{-3}	3.0×10^{-2}	7.6816	0.0434
8	5.0×10^{-3}	5.0×10^{-2}	7.6722	0.0528

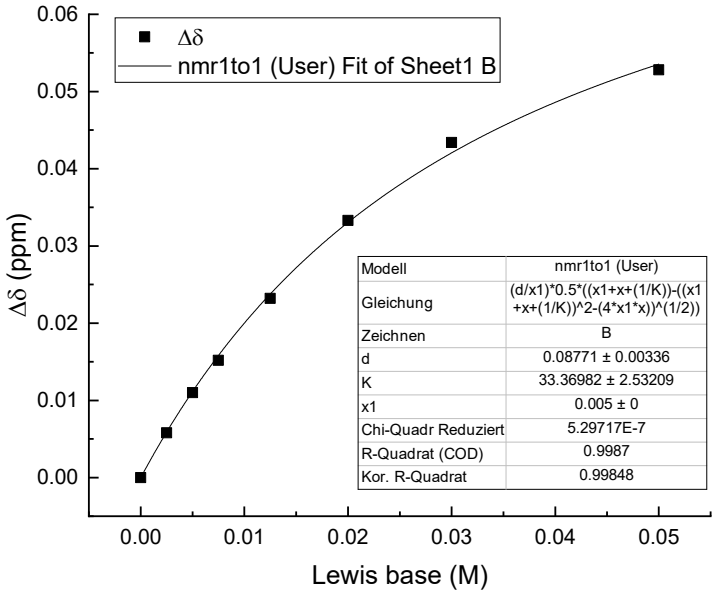

6.10 Kinetics

Determination of the Nucleophilicity of Benzoate (3a) in MeCN at 20 °C

3a-NBu_4^+ + **B1** in MeCN (stopped-flow, detection at 632 nm)

$[\mathbf{B1}]_0$ (M)	$[\mathbf{3a}]_0$ (M)	k_{obs} (s^{-1})
3.53×10^{-6}	1.00×10^{-4}	4.21
3.53×10^{-6}	2.00×10^{-4}	8.78
3.53×10^{-6}	3.00×10^{-4}	13.9
3.53×10^{-6}	4.00×10^{-4}	17.7
3.53×10^{-6}	5.00×10^{-4}	21.9

$k_2 = 4.43 \times 10^4\ M^{-1}\ s^{-1}$

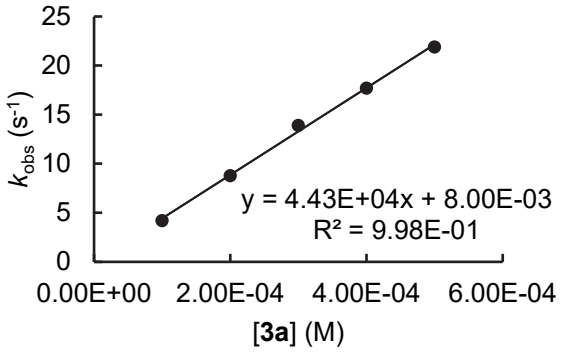

3a-NBu_4^+ + **B3** in MeCN (stopped-flow, detection at 635 nm)

$[\mathbf{B3}]_0$ (M)	[**3a**] (M)	k_{obs} (s^{-1})
2.48×10^{-6}	1.00×10^{-4}	9.64
2.48×10^{-6}	2.00×10^{-4}	17.8
2.48×10^{-6}	3.00×10^{-4}	27.7
2.48×10^{-6}	4.00×10^{-4}	33.5
2.48×10^{-6}	5.00×10^{-4}	44.3

$k_2 = 8.50 \times 10^4\ M^{-1}\ s^{-1}$

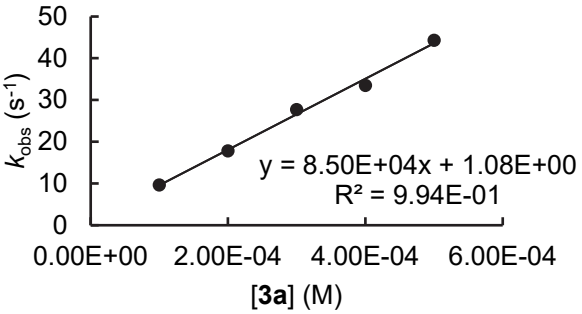

3a-NBu_4^+ + **B4** in MeCN (stopped-flow, detection at 616 nm)

$[\mathbf{B4}]_0$ (M)	$[\mathbf{3a}]_0$ (M)	k_{obs} (s^{-1})
5.03×10^{-6}	1.00×10^{-4}	30.5
5.03×10^{-6}	2.00×10^{-4}	67.0
5.03×10^{-6}	3.00×10^{-4}	105
5.03×10^{-6}	4.00×10^{-4}	142
5.03×10^{-6}	5.00×10^{-4}	179

$k_2 = 3.72 \times 10^5\ M^{-1}\ s^{-1}$

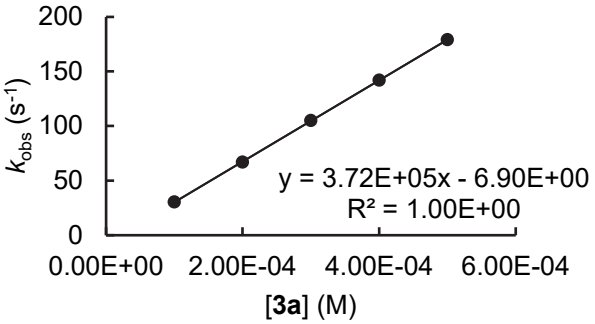

3a-NBu_4^+ + **B5** in MeCN (stopped-flow, detection at 620 nm)

$[\mathbf{B5}]_0$ (M)	$[\mathbf{3a}]_0$ (M)	k_{obs} (s^{-1})
3.85×10^{-6}	1.00×10^{-4}	81.7
3.85×10^{-6}	2.00×10^{-4}	174
3.85×10^{-6}	3.00×10^{-4}	267
3.85×10^{-6}	4.00×10^{-4}	307
3.85×10^{-6}	5.00×10^{-4}	410

$k_2 = 7.90 \times 10^5\ M^{-1}\ s^{-1}$

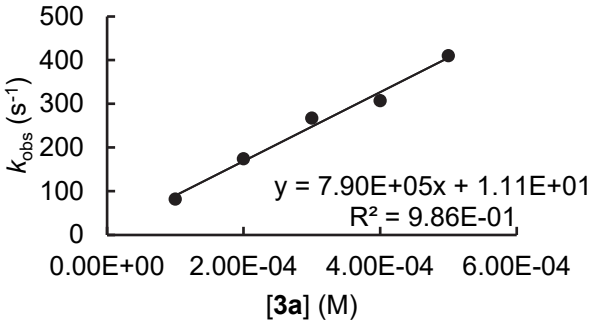

Determination of N and s_N parameters for **3a**-NBu_4^+ in MeCN.

Reference Electrophile	Electrophilicity E	k_2 ($M^{-1}\ s^{-1}$)	lg k_2
B1	−10.04	4.43×10^4	4.65
B3	−9.45	8.50×10^4	4.93
B4	−8.76	3.72×10^5	5.57
B5	−8.22	7.90×10^5	5.90

$N = 16.45$

$s_N = 0.72$

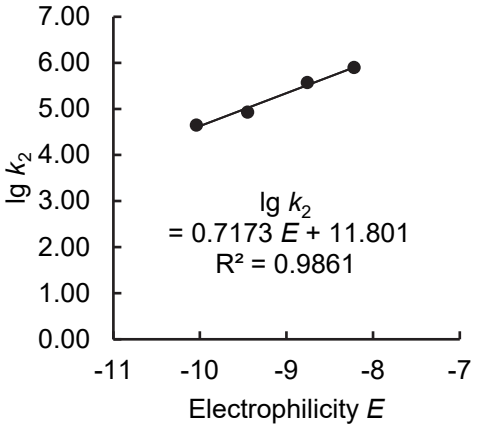

Kinetics for the Reaction of Benzhydryl Benzoate B2-3a in the Presence of Diaryliodonium Ions 1e

The kinetics for the heterolysis reaction were measured under similar conditions that were used for the BIMT titration: A mixture of the benzhydrylium tetrafluoroborate **B2** and ca. 0.7 equiv tetrabutylammonium benzoate (**3a**) was mixed with a solution of the $Ph(C_6F_5)I^+\ PF_6^-$ (**1e**) in acetonitrile at 20 °C. The resulting liberation of the benzhydrylium ion was followed by stopped-flow UV/Vis spectroscopy by monitoring the increase of the absorption at 605 nm.

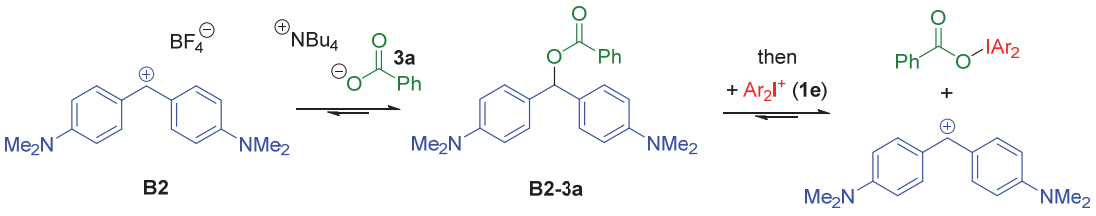

$[\mathbf{B2}]_0$ (M)	[**B2**] (M)	[**1e**] (M)	k_{obs} (s^{-1})
8.65×10^{-6}	2.45×10^{-6}	1.00×10^{-4}	0.101
8.65×10^{-6}	2.45×10^{-6}	2.00×10^{-4}	0.108
8.65×10^{-6}	2.45×10^{-6}	3.00×10^{-4}	0.108
8.65×10^{-6}	2.45×10^{-6}	4.00×10^{-4}	0.113
8.65×10^{-6}	2.45×10^{-6}	5.00×10^{-4}	0.113

6.11 References

[1] Bugaenko, D. I.; Yurovskaya, M. A.; Karchava, A. V. *Org. Lett.* **2018**, *20*, 6389-6393.

[2] Alcock, N. W.; Countryman, R. M. *J. Chem. Soc., Dalton Trans.* **1977**, 217-219

[3] Labattut, A.; Tremblay, P.-L.; Moutounet, O.; Legault, C. Y. *J. Org. Chem.* **2017**, *82*, 11891-11896.

[4] Mayer, R. J.; Hampel, N.: Mayer, P.; Ofial, A. R.; Mayr, H. *Eur. J. Org. Chem.* **2019**, 412-421.

[5] Fulmer, G. R.; Miller, A. J. M.; Sherden, N. H.; Gottlieb, H. E.; Nudelman, A.; Stoltz, B. M.; Bercaw, J. E.; Goldberg, K. I. *Organometallics* **2010**, *29*, 2176-2179.

[6] Wu, Y. C.; Koch, W. F.; Pratt, K. W. *J. Res. Natl. Inst. Stand. Technol.* **1991**, *96*, 191-201.

[7] *SAINT*, Bruker AXS Inc., Madison, Wisconsin, USA, 2012.

[8] *SADABS,* Sheldrick, G. M., University of Göttingen, Germany, 2016.

[9] Sheldrick, G. M. *Acta Cryst.* **2015**, *A71*, 3-8.

[10] *CrysAlis PRO*, Agilent Technologies Ltd, Yarnton, UK, 2014.

[11] Altomare, A., Burla, M. C., Camalli, M., Cascarano, G. L., Giacovazzo, C., Guagliardi, A., Moliterni, A. G. G., Polidori, G., Spagna, R. *J. Appl. Cryst.* **1999***, 32*, 115-119.

[12] Sheldrick, G. M. *Acta Cryst.* **2015***, C71*, 3-8.

[13] Farrugia, L. J. *J. Appl. Cryst.* **2012***, 45*, 849-854.

[14] Grant-Taylor, D.; Macdonald, D. D. *Can. J. Chem.* **1976**, *54*, 2813-1819.

[15] Mayr, H.; Ammer, J.; Baidya, M.; Maji, B.; Nigst, T. A.; Ofial, A. R.; Singer, T. *J. Am. Chem. Soc.* **2015**, *137*, 2580-2599.

[16] Piñeiro, A.; Muñoz, E.; Sabín, J.; Costas, M.; Bastos, M.; Velázquez-Campoy, A.; Garrido, P. F.; Dumas, P.; Ennifar, E.; García-Río, L.; Rial, J.; Pérez, D.; Fraga, P.; Rodríguez, A.; Cotelo, C. *Anal. Biochem.* **2019**, *577*, 117-134.

[17] Schaller, H. F.; Tishkov, A. A.; Feng, X.; Mayr, H. *J. Am. Chem. Soc.* **2008**, *130*, 3012-3022.

[18] Mayr, H.; Bug, T.; Gotta, M. F.; Hering, N.; Irrgang, B.; Janker, B.; Kempf, B.; Loos, R.; Ofial, A. R.; Remennikov, G.; Schimmel, H. *J. Am. Chem. Soc.* **2001**, *123*, 9500-9512.

[19] Thordarson, P. Binding Constants and Their Measurement. In Supramolecular Chemistry, Gale, P. A.; Steed, J. W., Ed., Wiley: Chichester, UK, 2012, vol. 2, pp 461-522.

[20] Fearnly, A. F.; An, J.; Jackson, M.; Lindovska, P.; Denton, R. M. *Chem. Commun.* **2016**, *52*, 4987-4990.

[21] Seidl, T. L.; Sundalam, S. K.; McCullough, B.; Stuart, D. R. *J. Org. Chem.* **2016**, *81*, 1998-2009.

Chapter 7. Lewis Adduct Formations: Lewis Basicity Scales Toward Boranes

Robert J. Mayer, Nathalie Hampel, Armin R. Ofial, ***2020**, submitted.*

Author Contributions

R.J.M. conceived the overall research with A.R.O. providing guidance. R.J.M performed all the experiments and computations. N.H. assisted in the determination of equilibrium constants and the synthesis of precursors. R.J.M and A.R.O. wrote the manuscript.

The complete supporting information (SI) for this work is provided starting with section 7.1.

Lewis Adduct Formations: Lewis Basicity Scales Toward Boranes

Robert J. Mayer, Nathalie Hampel, Armin R. Ofial*

Department Chemie, Ludwig-Maximilians-Universität München, Butenandtstr. 5-13, 81377 München, Germany

ABSTRACT: Knowledge of the Lewis acidity is key to for the development of Lewis acid catalyzed reactions. In this study, experimental equilibrium constants for the reactions of a series of triarylboranes with various Lewis basic pyridines, carbonyl compounds, and phosphines were determined in dichloromethane at 20 °C. The experimental data were used to construct Lewis acidity/basicity scales which allow to calculate equilibrium constants for borane/Lewis base combinations by the sum of two descriptors, one for Lewis acidity (LA_B) and one for Lewis basicity (LB_B). Correlations of LA_B and LB_B with Hammett substituent parameters, known reaction enthalpies, and results of quantum-chemical calculations are discussed. We demonstrate that the Lewis acidity/basicity scales in this work are easily extendable, widely applicable in organic synthesis, and enable chemists to rationally design borane-catalyzed reactions.

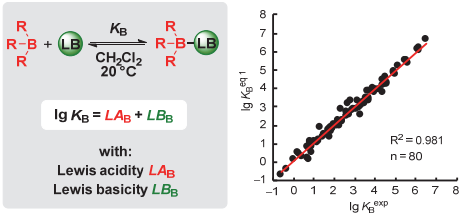

Introduction

Organoboranes have multiple applications in chemistry due to their strong electron deficient nature. Typically, their Lewis acidic properties are used to catalyze reactions through coordination at Lewis basic centers of organic compounds.[1-6] The association of triarylboranes with sterically hindered Lewis bases yields uniquely active catalysts (so called frustrated Lewis pairs, FLPs) that are able to activate even small, inert molecules, such as molecular hydrogen or carbon dioxide.[7-9] The degree of Lewis acid/base association in a certain solvent can gradually span the energetic spectrum from formation of a covalent bond down to only weakly attractive dispersion interactions. Quantitative information is derived from the equilibrium constant of the Lewis adduct formation, which primarily depends on the electron-accepting ability of the boranes (that is, their Lewis acidity) and the electron-donating properties of the Lewis base (that is, their Lewis basicity) but can substantially be diminished by repulsive steric effects.[10-12]

The search for even stronger Lewis acids is still ongoing[13-17] and understanding the Lewis acidity of triarylboranes would foster the rational design of borane-catalyzed reactions.[5-12] Quantum chemistry allows to calculate descriptive properties such as orbital energies or Gibbs energies for the association of Lewis acids with a reference Lewis base, e.g. fluoride.[10] However, few equilibrium constants for the association of free triarylboranes with Lewis bases have been determined experimentally, and only Lewis adduct formations of $B(C_6F_5)_3$ with benzaldehyde, acetophenone, ethyl benzoate (in d_6-benzene),[18,19] lutidine (in CD_2Cl_2),[20] and trimesitylphosphine (in d_6-benzene)[21] have been studied in more detail. To characterize Lewis acidity experimentally, it is more common to follow the changes in the spectroscopic features of selected reference Lewis bases upon their conversion from the free to the bound state.[22,23] The infinite number of potential reference Lewis bases gives rise to an ongoing evolvement of new spectroscopic methods that supplement the existing repertoire of methods for the construction of Lewis acidity scales.[24-27] It has been shown that the Lewis acidity rankings determined by NMR based methods can be used to rationalize certain Lewis acid catalyzed reactions.[25] However, the so far established Lewis acidity scales generally suffer from the fact that each uses only one particular reference Lewis base,[24] which does not necessarily represent the manifold of Lewis bases met in synthesis. Furthermore, spectroscopic as well as quantum-chemically calculated acidity scales may give the correct ordering of the strength of the Lewis acids, but missing calibration to experimental thermodynamics severely limits their ability to predict whether the association of a certain Lewis acid with a certain Lewis base will be possible. We, therefore, envisioned to construct a quantitative Lewis basicity scale by using a set of Lewis acidic triarylboranes and experimental equilibrium constants of their reactions with a diverse set of weak, moderate, and strong Lewis bases with oxygen, nitrogen, or phosphorus as the reactive sites.

Results and Discussion

Constructing a Quantitative Lewis Acidity/Basicity Scale. First, we determined the equilibrium constants for the formation of adducts of the triarylboranes **1** with the substituted pyridines **2**, the nitriles **3**, the carbonyl compounds **5**-**9**, and triethylphosphine oxide (**10**) in anhydrous dichloromethane at 20 °C (Figure 1a,b).

Known X-ray structures indicate that these Lewis bases do not interact with the aryl rings of the boranes in the emerging Lewis adducts.[18] Hence, we anticipated that electronic effects control the Lewis adduct formation for the investigated Lewis acid/base combinations (except for **2n**). For the less Lewis acidic boranes **1a**-**1e** isothermal titration calorimetry (ITC) revealed the thermodynamics of the adduct formation at first hand and afforded equilibrium constants $K_B > 10^3$ M^{-1} (Figure 2). Equilibrium constants $K_B < 10^3$ M^{-1} as well as associations of Lewis bases with highly reactive

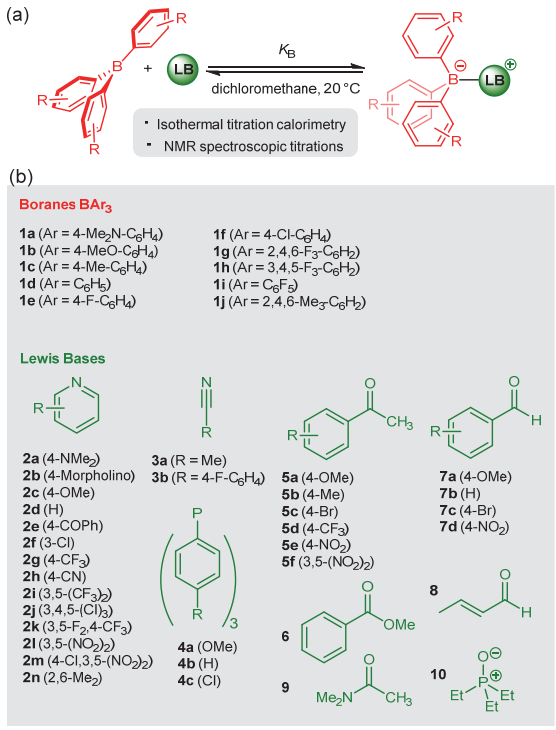

Figure 1. (a) Equilibrium for the adduct formation between a triarylborane and a Lewis base. (b) Lewis acids and bases used for the equilibrium studies in this work.

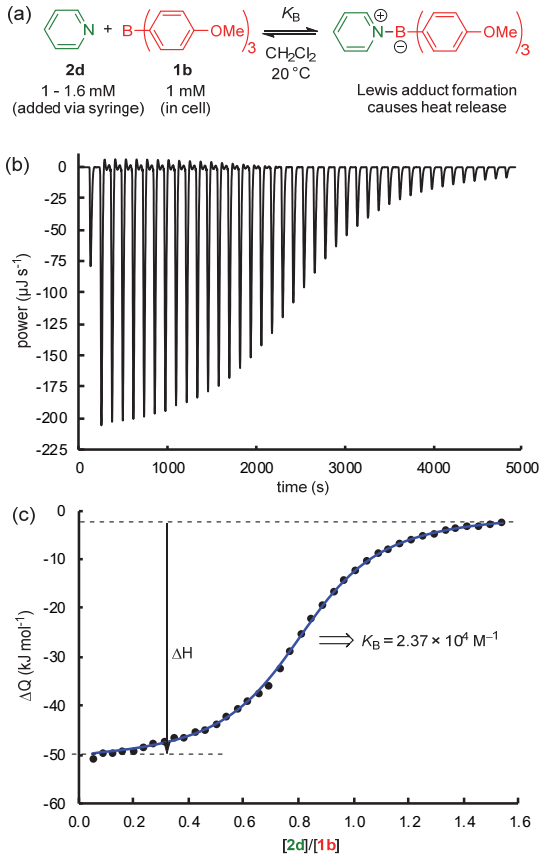

Figure 2. (a) ITC based determination of equilibrium constants illustrated for the reaction between tris(*p*-anisyl)borane (**1b**) and pyridine (**2d**). (b) Heat flow during the titration of a tris(*p*-anisyl)borane (**1b**) solution in dichloromethane with pyridine (**2d**). (c) Integrated heat flow vs. the molar ratio of the Lewis base/borane (black dots) and fitted curve (blue line) giving K_B for the individual measurement.

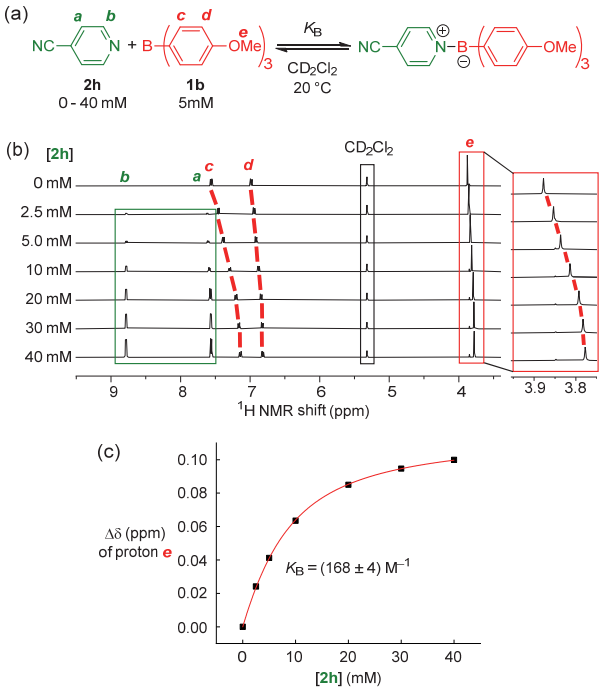

Figure 3. (a) NMR based determination of equilibrium constants shown for the reaction between 4-cyanopyridine (**2h**) and tris(*p*-anisyl)borane (**1b**). (b) ^{1}H NMR spectra (400 MHz, CD_2Cl_2) of borane **1b** in the presence of variable concentrations of **2h**. (c) Plot of the chemical shift difference of the methoxy groups of **1b** (with reference to the shift in the absence of **2h**) at different concentrations of **2h** and the correlation line used to derive K_B by numerical fitting (red).

boranes were studied by ^{1}H NMR spectroscopic titrations under an atmosphere of dry argon (Figure 3). All equilibrium constants are gathered in Table 1. For an individual Lewis base, equilibrium constants in the range of $0.3 < K_B < 10^7$ M^{-1} can be determined by combining the ITC and NMR methods.

Yet, a single reference Lewis base is not sufficient to compare boranes of widely differing Lewis acidities: the moderately Lewis basic 3,4,5-trichloropyridine (**2j**) establishes equilibria for Lewis adduct formation with the donor- and weakly acceptor-substituted triarylboranes **1b**-**f**. However, selecting the Lewis base **2j** as the reference would neither allow to study the association equilibria with the less Lewis acidic **1a** nor with the stronger Lewis acids **1g**-**i**.

Hence, we decided to use a floating scale of Lewis basic reference compounds, which relies on combining Lewis acids with overlapping sets of differently strong Lewis bases. Thus, strong Lewis bases were used to characterize weak Lewis acids, while weaker Lewis bases were used to study equilibria of Lewis adduct formation with stronger Lewis acids. Overall, we determined a set of 88 equilibrium constants for various combinations of boranes and Lewis bases (see Table 1 and Supporting Information for the individual measurements).

Table 1: Equilibrium Constants K_B (M^{-1}) for the Reactions of Boranes 1 and Lewis Bases 2–10 in Dichloromethane at 20 °C and Comparison with the Equilibrium Constants $K_B^{eq\,1}$ Derived by Applying Equation (1)

Lewis Base	R =		LB_B		LA_B	K_B^{exp} (M^{-1})	Method	$K_B^{eq\,1}$ (M^{-1})	$K_B^{eq\,1}/K_B^{exp}$
	4-NMe_2	**2a**	8.63	**1j**	-8.97	4.54×10^{-1}	NMR	4.54×10^{-1}	
	4-NMe_2	**2a**	8.63	**1a**	-4.28	3.53×10^{4}	ITC	2.20×10^{4}	0.62
	4-NMe_2	**2a**	8.63	**1b**	-1.92	3.21×10^{6}	ITC	5.15×10^{6}	1.60
	4-Morpholino	**2b**	8.13	**1a**	-4.28	9.35×10^{3}	ITC	7.07×10^{3}	0.76
	4-Morpholino	**2b**	8.13	**1b**	-1.92	1.25×10^{6}	ITC	1.65×10^{6}	1.32
	4-OMe	**2c**	7.16	**1a**	-4.28	1.01×10^{3}	NMR	7.52×10^{2}	0.74
	4-OMe	**2c**	7.16	**1b**	-1.92	1.31×10^{5}	ITC	1.76×10^{5}	1.34
	H	**2d**	6.13	**1a**	-4.28	7.81×10^{1}	NMR	7.05×10^{1}	0.90
	H	**2d**	6.13	**1b**	-1.92	2.22×10^{4}	ITC	1.65×10^{4}	0.74
	H	**2d**	6.13	**1c**	-0.57	3.40×10^{5}	ITC	3.68×10^{5}	1.08
	H	**2d**	6.13	**1d**	0.00	1.39×10^{6}	ITC	1.36×10^{6}	0.98
	H	**2d**	6.13	**1e**	0.13	1.30×10^{6}	ITC	1.83×10^{6}	1.41
	4-COPh	**2e**	5.42	**1a**	-4.28	9.93	NMR	1.37×10^{1}	1.38
	4-COPh	**2e**	5.42	**1b**	-1.92	3.25×10^{3}	ITC	3.20×10^{3}	0.99
	4-COPh	**2e**	5.42	**1c**	-0.57	7.86×10^{4}	ITC	7.14×10^{4}	0.91
	4-COPh	**2e**	5.42	**1d**	0.00	3.86×10^{5}	ITC	2.64×10^{5}	0.68
	4-COPh	**2e**	5.42	**1e**	0.13	3.01×10^{5}	ITC	3.56×10^{5}	1.18
	3-Cl	**2f**	4.83	**1a**	-4.28	1.52	NMR	3.48	2.29
	3-Cl	**2f**	4.83	**1b**	-1.92	7.99×10^{2}	NMR	8.14×10^{2}	1.02
	3-Cl	**2f**	4.83	**1c**	-0.57	3.31×10^{4}	ITC	1.81×10^{4}	0.55
	3-Cl	**2f**	4.83	**1d**	0.00	9.33×10^{4}	ITC	6.70×10^{4}	0.72
	3-Cl	**2f**	4.83	**1e**	0.13	8.30×10^{4}	ITC	9.05×10^{4}	1.09
	4-CF_3	**2g**	4.52	**1b**	-1.92	4.88×10^{2}	NMR	4.07×10^{2}	0.83
	4-CF_3	**2g**	4.52	**1c**	-0.57	1.43×10^{4}	ITC	9.06×10^{3}	0.63
	4-CF_3	**2g**	4.52	**1d**	0.00	2.42×10^{4}	ITC	3.35×10^{4}	1.38
	4-CF_3	**2g**	4.52	**1e**	0.13	3.31×10^{4}	ITC	4.53×10^{4}	1.37
	4-CN	**2h**	3.92	**1b**	-1.92	1.68×10^{2}	NMR	9.99×10^{1}	0.59
	4-CN	**2h**	3.92	**1c**	-0.57	3.60×10^{3}	ITC	2.23×10^{3}	0.62
	4-CN	**2h**	3.92	**1d**	0.00	4.27×10^{3}	ITC	8.22×10^{3}	1.93
	4-CN	**2h**	3.92	**1e**	0.13	7.87×10^{3}	ITC	1.11×10^{4}	1.41
	3,5-$(CF_3)_2$	**2i**	1.76	**1c**	-0.57	1.62×10^{1}	NMR	1.57×10^{1}	0.97
	3,5-$(CF_3)_2$	**2i**	1.76	**1d**	0.00	5.04×10^{1}	NMR	5.81×10^{1}	1.15
	3,5-$(CF_3)_2$	**2i**	1.76	**1e**	0.13	6.37×10^{1}	NMR	7.85×10^{1}	1.23
	3,5-$(CF_3)_2$	**2i**	1.76	**1f**	1.33	1.71×10^{3}	NMR	1.24×10^{3}	0.73
	3,4,5-$(Cl)_3$	**2j**	2.67	**1b**	-1.92	6.06	NMR	5.75	0.95
	3,4,5-$(Cl)_3$	**2j**	2.67	**1c**	-0.57	1.22×10^{2}	NMR	1.28×10^{2}	1.05
	3,4,5-$(Cl)_3$	**2j**	2.67	**1d**	0.00	4.33×10^{2}	NMR	4.73×10^{2}	1.09
	3,4,5-$(Cl)_3$	**2j**	2.67	**1e**	0.13	7.56×10^{2}	NMR	6.39×10^{2}	0.85
	3,4,5-$(Cl)_3$	**2j**	2.67	**1f**	1.33	9.29×10^{3}	NMR	1.01×10^{4}	1.09
	3,5-$(F)_2$-4-CF_3	**2k**	1.43	**1c**	-0.57	7.11	NMR	7.24	1.02
	3,5-$(F)_2$-4-CF_3	**2k**	1.43	**1d**	0.00	5.35×10^{1}	NMR	2.68×10^{1}	0.50
	3,5-$(F)_2$-4-CF_3	**2k**	1.43	**1e**	0.13	2.96×10^{1}	NMR	3.62×10^{1}	1.22
	3,5-$(F)_2$-4-CF_3	**2k**	1.43	**1f**	1.33	3.56×10^{2}	NMR	5.72×10^{2}	1.61
	3,5-$(NO_2)_2$	**2l**	-0.75	**1e**	0.13	2.38×10^{-1}	NMR	2.43×10^{-1}	1.02
	3,5-$(NO_2)_2$	**2l**	-0.75	**1f**	1.33	7.91	NMR	3.84	0.49
	3,5-$(NO_2)_2$	**2l**	-0.75	**1g**	4.08	4.50×10^{3}	NMR	2.18×10^{3}	0.48
	3,5-$(NO_2)_2$	**2l**	-0.75	**1h**	3.98	4.10×10^{2}	NMR	1.71×10^{3}	4.18
	4-Cl-3,5-$(NO_2)_2$	**2m**	-1.07	**1f**	1.33	4.87	NMR	1.81	0.37

	4-Cl-3,5-$(NO_2)_2$	**2m**	-1.07	**1g**	4.08	1.60×10^3	NMR	1.03×10^3	0.64
	4-Cl-3,5-$(NO_2)_2$	**2m**	-1.07	**1h**	3.98	1.94×10^2	NMR	8.10×10^2	4.18
	2,6-$(Me)_2$	**2n**	-5.50	**1i**	7.24	5.47×10^1	NMR	5.47×10^1	
	Me	**3a**	-0.48	**1f**	1.33	4.93	NMR	7.15	1.45
	Me	**3a**	-0.48	**1h**	3.98	4.63×10^3	NMR	3.19×10^3	0.69
R-CN	4-F-C_6H_4	**3b**	-0.81	**1f**	1.33	1.87	NMR	3.33	1.78
	4-F-C_6H_4	**3b**	-0.81	**1g**	4.08	2.39×10^3	NMR	1.89×10^3	0.79
	4-F-C_6H_4	**3b**	-0.81	**1h**	3.98	2.10×10^3	NMR	1.49×10^3	0.71
	4-OMe	**4a**	2.43	**1e**	0.13	3.60×10^2	NMR	3.60×10^2	
	4-OMe	**4a**	2.43	**1f**	1.33	too high	NMR	5.69×10^3	
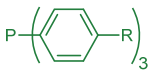	4-OMe	**4a**	2.43	**1g**	4.08	(8.61×10^2)	NMR	3.23×10^6	
	4-OMe	**4a**	2.43	**1h**	3.98	too high	NMR	2.54×10^6	
	H	**4b**	0.87	**1f**	1.33	1.58×10^2	NMR	1.58×10^2	
	H	**4b**	0.87	**1h**	3.98	too high	NMR	7.06×10^4	
	4-Cl	**4c**	-0.11	**1f**	1.33	1.67×10^1	NMR	1.67×10^1	
	4-OMe	**5a**	-1.99	**1f**	1.33	too low	NMR	2.19×10^{-1}	
	4-OMe	**5a**	-1.99	**1g**	4.08	9.79×10^1	NMR	1.24×10^2	1.27
	4-OMe	**5a**	-1.99	**1h**	3.98	1.24×10^2	NMR	9.78×10^1	0.79
	4-Me	**5b**	-2.57	**1g**	4.08	2.97×10^1	NMR	3.24×10^1	1.09
	4-Me	**5b**	-2.57	**1h**	3.98	2.78×10^1	NMR	2.55×10^1	0.92
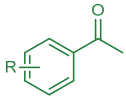	4-Br	**5c**	-2.99	**1g**	4.08	6.22	NMR	1.23×10^1	1.98
	4-Br	**5c**	-2.99	**1i**	7.24	3.51×10^4	NMR	1.77×10^4	0.50
	4-CF_3	**5d**	-3.29	**1g**	4.08	5.42	NMR	6.17	1.14
	4-CF_3	**5d**	-3.29	**1i**	7.24	1.01×10^4	NMR	8.87×10^3	0.88
	4-NO_2	**5e**	-3.90	**1g**	4.08	5.02	NMR	1.51	0.30
	4-NO_2	**5e**	-3.90	**1i**	7.24	6.53×10^2	NMR	2.17×10^3	3.33
	3,5-$(NO_2)_2$	**5f**	-6.12	**1i**	7.24	1.31×10^1	NMR	1.31×10^1	
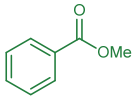		**6**	-5.38	**1i**	7.24	7.31×10^1	NMR	7.31×10^1	
	4-OMe	**7a**	-0.18	**1f**	1.33	6.75	NMR	1.42×10^1	2.10
	4-OMe	**7a**	-0.18	**1g**	4.08	4.90×10^3	NMR	8.04×10^3	1.64
	4-OMe	**7a**	-0.18	**1h**	3.98	2.18×10^4	NMR	6.33×10^3	0.29
	H	**7b**	-1.78	**1g**	4.08	1.41×10^2	NMR	2.00×10^2	1.42
	H	**7b**	-1.78	**1h**	3.98	2.24×10^2	NMR	1.58×10^2	0.70
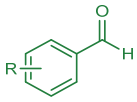	4-Br	**7c**	-2.25	**1g**	4.08	5.34×10^1	NMR	6.78×10^1	1.27
	4-Br	**7c**	-2.25	**1h**	3.98	6.78×10^1	NMR	5.34×10^1	0.79
	4-Br	**7c**	-2.25	**1i**	7.24	too high	NMR	9.75×10^4	
	4-NO_2	**7d**	-3.76	**1g**	4.08	2.31	NMR	2.10	0.91
	4-NO_2	**7d**	-3.76	**1h**	3.98	1.02	NMR	1.66	1.62
	4-NO_2	**7d**	-3.76	**1i**	7.24	4.46×10^3	NMR	3.02×10^3	0.68
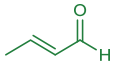		**8**	-0.73	**1g**	4.08	1.38×10^3	NMR	2.23×10^3	1.62
		8	-0.73	**1h**	3.98	2.84×10^3	NMR	1.76×10^3	0.62
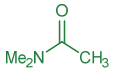		**9**	0.97	**1d**	0.00	7.60	NMR	9.43	1.24
		9	0.97	**1f**	1.33	2.50×10^2	NMR	2.01×10^2	0.81
$Et_3P{=}O$		**10**	2.51	**1c**	-0.57	1.90×10^1	NMR	8.68×10^1	4.57
		10	2.51	**1e**	0.13	1.98×10^3	NMR	4.33×10^2	0.22

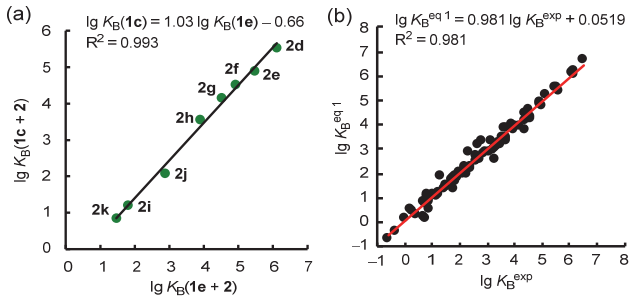

Figure 4. Correlations showing the internal consistency of the Lewis acidity/basicity scales derived by using eq. (1). (a) Correlation of the decadic logarithm of the experimental equilibrium constants K_B for the reactions of **1c** with pyridines with those for the reactions of **1e** with pyridines **2**. (b) Correlation of the decadic logarithm of the equilibrium constants $K_B^{eq\,1}$ predicted calculated using eq. (1) with the experimental equilibrium constants K_B^{exp} for reactions between boranes and Lewis bases.

As illustrated by the linear correlation of the equilibrium constants K_B for boranes **1c** and **1e** with a series of pyridines (slope = 1.03), the relative values of the equilibrium constants are the same for the Lewis base-association with different triarylboranes (Figure 4a).

Similar correlations have previously been observed for equilibrium constants of Lewis bases with carbenium ions, which are isoelectronic with BR_3 compounds, for example with diarylcarbenium ions (Ar_2CH^+) which are reliable reference electrophiles for reactivity studies.[28] In analogy to the formation of Lewis adducts with diarylcarbenium ions, we found that the two-parameter equation (1) is sufficient to calculate the equilibrium constants for the triarylborane/Lewis base combinations determined in this work.

lg K_B = LA_B + LB_B (in dichloromethane at 20 °C) (1)

For Lewis acid/base reactions in dichloromethane solution eq. (1) relates the decadic logarithm of an equilibrium constant K_B with a Lewis acidity parameter LA_B specific for a certain triarylborane and an LB_B parameter referring to a specific Lewis base. By defining the Lewis acidity of triphenylborane LA_B(**1d**) = 0 and subsequently performing a least-squares minimization, a set of 10 Lewis acidity parameters and 32 Lewis basicity parameters was obtained, which affords calculated equilibrium constants $K_B^{eq\,1}$ that deviate at maximum by a factor of 4.5 from K_B^{exp} determined by experiment (Figure 4b).

The parallel correlation lines obtained by plotting lg K_B versus LB_B as shown in Figure 5 illustrate eq. (1) graphically, furnishing LA_B as the negative intercepts with the abscissa. The thus established Lewis acidity/basicity scales (Figure 6) both cover 15 orders of magnitude and, by applying the descriptors for Lewis acidity and Lewis basicity in eq. (1), they provide a reliable tool to predict absolute equilibrium constants for arbitrary combinations of triarylboranes with Lewis bases except when steric impositions become effective. Structure-affinity relationships can now be discussed on an experimentally relevant, quantitative basis.

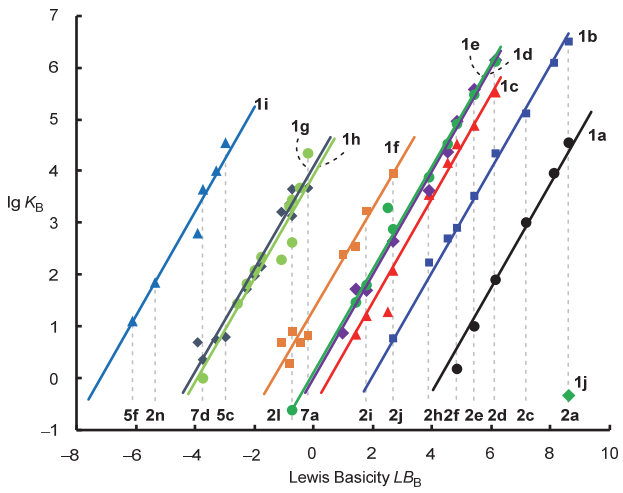

Figure 5. Least squares minimization of the equilibrium constants (lg K_B) generates Lewis acidity and basicity scales.

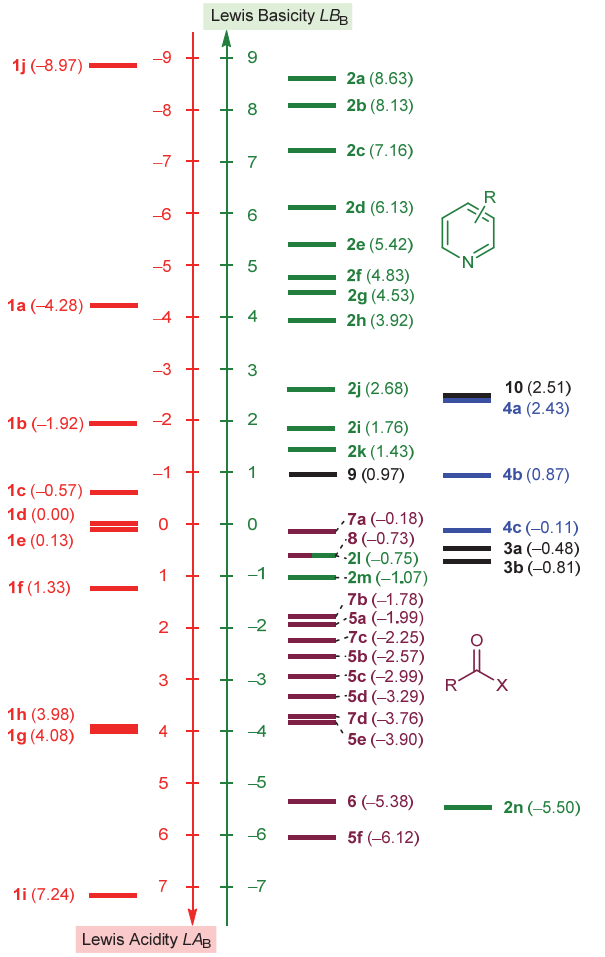

Figure 6. Experimental Lewis acidity and basicity scales for boranes and N-, O- and P-centered Lewis bases derived on the basis of eq. (1). Compounds on the same level combine with an equilibrium constant K_B = 1 M^{-1} in dichloromethane at 20 °C.

Applicability of Computational Methods. First, we tested whether quantum-chemical calculations of the Gibbs reaction energies reproduce the experimental values for a representative set of B-N, B-O, and B-P Lewis acid/base combinations (that is, **1d**/**2d**, **1f**/**3a**, **1h**/**7b**, and **1f**/**4b**) by using density functional theory methods. Good agreement

with the experiments was obtained at the SMD(DCM)/MN15/def2-TZVP level of theory[29] (average deviation: −5.4 ± 2.4 kJ/mol, see the Supporting Information for details). The use of isodesmic reactions, such as the transfer of a Lewis base between two boranes, allows to reference quantum-chemical calculations to an experimental basis point.[10,30] Starting from the experimental data for the formation of Lewis adducts of **1d**/**2d**, **1f**/**3a**, and **1h**/**7b**, the Lewis acidity of further boranes was investigated by studying isodesmic reactions for the transfer of pyridine (**2d**), acetonitrile (**3a**), and benzaldehyde (**7b**). In this way, we estimated the Lewis acidities for BF_3 (LA_B = 8.4 ± 2.0), BCl_3 (LA_B = 9.3 ± 1.8), and BBr_3 (LA_B = 10.1 ± 1.3) in dichloromethane (see Supporting Information for a detailed procedure).

Access to Further Lewis Acidity Parameters by Correlations. The Lewis acidity parameters LA_B for para/meta-substituted triarylboranes correlate excellently with the sum of the Hammett substituent parameters Σσ,[31] which allows to extrapolate LA_B for further triarylboranes with various substitution patterns (Figure 7).

Gas-phase fluoride ion affinities (FIA) are often used as a measure for Lewis acidity,[10] and we found a good correlation of LA_B with gas-phase FIA for para-substituted boranes (Figure 8a, data from Table 2). Boranes with ortho-fluoro substituents (**1i**, **1g**) deviate from the correlation, however, and the quantum-chemically estimated LA_B values for BX_3 (X = F, Cl, Br) depart even more. Calculated FIAs considering solvent effects for dichloromethane (FIA^{DCM}) gave a more general relationship, and LA_B for all types of boranes **1a**-**1i** studied in this work correlated linearly with FIA^{DCM} (Figure 8d).

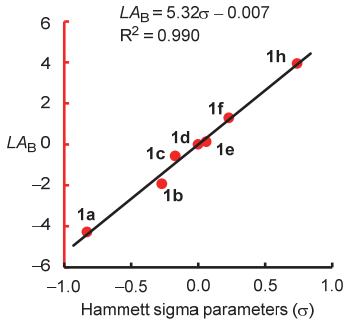

Figure 7. Correlation of LA_B parameters with Hammett σ parameters.

The LA_B parameters for triarylboranes correlate linearly with LUMO energies and global electrophilicity indices (GEI) calculated for the gas-phase and dichloromethane solution, which were both proposed as alternative measure of Lewis acidity.[6,10,32] However, both quantum-chemical descriptors are not generally applicable to a broader scope of boranes, e.g. for BX_3 (X = F, Cl, Br) (Figure 8b,c,e,f). Within the set of triarylboranes, the correlation of LA_B with sterically unbiased parameters can be used to quantify the effects of steric hindrance on acidity. The experimentally determined Lewis acidity of trimesitylborane (**1j**) is 8-9 orders of magnitude lower than that predicted by its electronic properties (i.e., GEI or ε_{LUMO}) (Figure 8e,f), and we assume that adducts of trimesitylborane (**1j**) with Lewis basic phosphines are mainly stabilized by weak dispersive rather than by specific acid/base interactions, in analogy to the trimesitylphosphine/$B(C_6F_5)_3$ combination previously characterized by NMR spectroscopic methods.[21]

Table 2: Lewis Acidity Parameters LA_B and Further Acidity Descriptors for Boranes

Borane		LA_B	σ[a]	FIA (Δ*H*, kJ/mol)[b]	ε_{LUMO} (Hartree)	GEI (eV)	FIA (ΔG, kJ/mol)	ε_{LUMO} (Hartree)	GEI (eV)
				at the BP86-D3BJ/def2-SVP level in gas-phase			at the SMD(DCM)/MN15/def2-TZVP in dichloromethane		
$B(4\text{-}Me_2N\text{-}C_6H_4)_3$	**1a**	-4.28	-0.83	-292.1	-0.06001	1.65	-96.7	-0.02941	1.10
$B(4\text{-}MeO\text{-}C_6H_4)_3$	**1b**	-1.92	-0.27	-330.0	-0.08069	2.27	-127.1	-0.04147	1.39
$B(4\text{-}Me\text{-}C_6H_4)_3$	**1c**	-0.57	-0.17	-347.3	-0.09261	2.63	-141.2	-0.04908	1.57
$B(C_6H_5)_3$	**1d**	0.00	0	-359.7	-0.10049	2.88	-147.7	-0.05429	1.69
$B(4\text{-}F\text{-}C_6H_4)_3$	**1e**	0.13	0.06	-376.7	-0.10466	3.06	-154.1	-0.05390	1.68
$B(4\text{-}Cl\text{-}C_6H_4)_3$	**1f**	1.33	0.23	-396.1	-0.11260	3.44	-163.7	-0.06249	1.84
$B(2,4,6\text{-}(F)_3\text{-}C_6H_2)_3$	**1g**	4.08		-396.5	-0.12108	3.83	-185.1	-0.07655	2.14
$B(3,4,5\text{-}(F)_3\text{-}C_6H_2)_3$	**1h**	3.98	0.74	-440.3	-0.12913	4.14	-197.2	-0.07260	2.07
$B(C_6F_5)_3$	**1i**	7.24		-458.8	-0.14437	5.31	-231.7	-0.09589	2.61
$B(2,4,6\text{-}(Me)_3\text{-}C_6H_2)_3$	**1j**	(-8.97)		-323.8	-0.09395	2.78	-87.4	-0.04968	1.54
BF_3		(8.4)		-343.9	-0.01084	1.34	-239.7	0.06314	1.09
BCl_3		(9.3)		-408.7	-0.08770	2.39	-259.6	-0.04009	1.71
BBr_3		(10.1)		-446.1	-0.10629	2.98	-263.2	-0.05910	1.90

[a] Hammett σ values taken from ref. 31. [b] Calculated according to the procedure outlined in ref. 10 and anchored to the dissociation of fluorotrimethylsilane calculated at the G3 level in ref. 30.

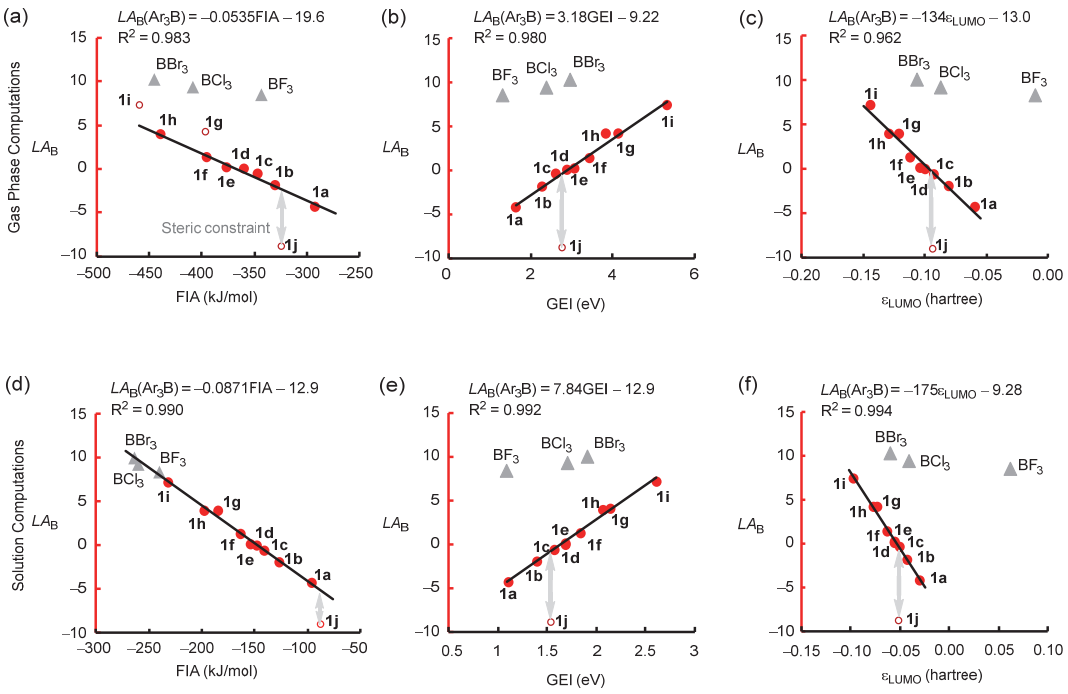

Figure 8. Correlation of LA_B with different quantum-chemically calculated acidity descriptors for boranes in gas phase and solution. (a)-(c): Correlation of LA_B with fluoride ion affinities FIA (a), global electrophilicity indices GEI (b) and LUMO energies ε_{LUMO} (c) obtained at the BP86-D3BJ/def2-SVP level of theory in gas phase (all values from Table 2). (d)-(f): Correlation of LA_B with fluoride ion affinities FIA (d), global electrophilicity indices GEI (e) and LUMO energies ε_{LUMO} (f) obtained considering dichloromethane solvation at the SMD(DCM)/MN15/def2-TZVP level of theory (all values from Table 2). The data for BF_3, BCl_3 and BBr_3 (grey triangles) were not used for the calculation of the correlation lines.

Lewis acidity rankings based on NMR chemical shift differences like the Childs method,[22] which uses the resonance of the 3-H proton in *trans*-crotonaldehyde (**8**), cannot be directly correlated with the values described in this work as they – in theory – require quantitative adduct formation (Figure 9): while reactions of **8** with highly Lewis acidic boranes **1h**-**1i** lead to a change in the 3-H resonance due to almost quantitative adduct formation ($K_B^{eq\,1} = 10^3$–10^6 M^{-1}, calculated with the LA_B and LB_B values in Figure 6), the reaction with triphenylborane (**1d**) is endergonic ($K_B^{eq\,1}$ = 0.19 M^{-1}). The Gutmann-Beckett method follows the ^{31}P NMR chemical shift of triethylphosphine oxide (**10**),[23] which is a stronger Lewis base toward boranes than **8**. Therefore, it would allow the characterization of many weaker Lewis acids. However, significant scatter in published data of ^{31}P NMR chemical shifts for Lewis adducts of **10** hamper meaningful correlations.[11]

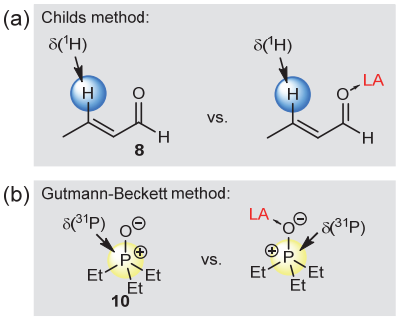

Figure 9. Lewis acidity scales based on NMR chemical shift differences of probe molecules. (a) The Childs method[22] determines the strength of Lewis acids by comparing the NMR chemical shift of the proton at the β-carbon of the free *trans*-crotonaldehyde (**8**) with that for the same proton in the corresponding Lewis adduct. (b) The Gutmann-Beckett method[23] measures Lewis acidity by comparing the ^{31}P NMR chemical shift of free triethylphosphine oxide (**10**) with that of the Lewis adduct.

Accessing Further Lewis Basicities LB_B and Quantification of Steric Effects. The Lewis basicity parameters LB_B cover almost 15 orders of magnitude from highly basic pyridines to weakly basic aldehydes and ketones. The Lewis basicities LB_B of pyridines, triarylphosphines, benzaldehydes, and acetophenones with substituents at 3- and 4-position of their aromatic rings yield individual linear correlations with Hammett σ constants (Figure 10, data from Table 3).

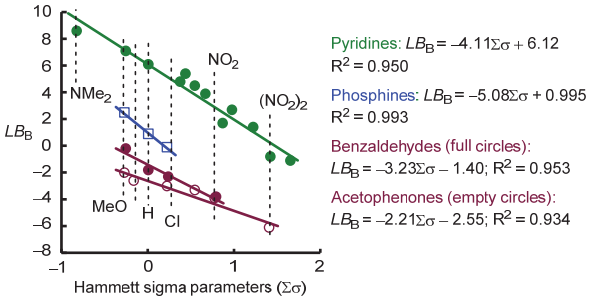

Figure 10. Correlation of LB_B with the sum of Hammett substituent parameters σ[31] for the different classes of compounds investigated in this study with data from Table 3.

Table 3. Lewis Basicity Parameters LB_B and Further Basicity Descriptors for Pyridines, Nitriles, Phosphines, Carbonyl Compounds and Triethylphosphine Oxide

Lewis Base	R =		LB_B	Σσ[a]	LB (vs Ar_2CH^+)[b]	pK_{aH}(H_2O)	ΔH_{BF3}[c]	BA[d]
	4-NMe_2	**2a**	8.63	-0.83	16.42	9.39 (ref. 33)	151.55	-155.3
	4-Morpholino	**2b**	8.13		15.04	8.53 (ref. 33)	144.47	-152.2
	4-MeO	**2c**	7.16	-0.27	11.99	6.58 (ref. 34)	135.27	-146.5
	H	**2d**	6.13	0	10.02	5.21 (ref. 34)	128.08	-141.7
	4-COPh	**2e**	5.42	0.43	8.78	3.35 (ref. 34)		-134.9
	3-Cl	**2f**	4.83	0.37	7.44	2.81 (ref. 34)	118.79	-131.1
	4-CF_3	**2g**	4.52	0.54	6.71	2.63 (ref. 35)	115.75	-130.7
	4-CN	**2h**	3.92	0.66	6.08	1.86 (ref. 34)	113.27	-129.3
	3,5-$(CF_3)_2$	**2i**	1.76	0.86		--		-118.8
	3,4,5-$(Cl)_3$	**2j**	2.67	0.97		--		-117.5
	3,5-$(F)_2$-4-CF_3	**2k**	1.43	1.22		--		-114.5
	3,5-$(NO_2)_2$	**2l**	-0.75	1.42		--		-106.2
	4-Cl-3,5-$(NO_2)_2$	**2m**	-1.07	1.65		--		-102.9
	2,6-$(Me)_2$	**2n**	(-5.50)	--		6.72 (ref. 36)	97.73	-125.5
R-CN	Me	**3a**	-0.48	--			60.39	-98.8
	4-F-C_6H_4	**3b**	-0.81	--		--		-93.4
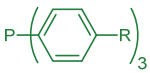	4-MeO	**4a**	(2.43)	-0.27	17.00	4.57 (ref. 37)		-145.3
	H	**4b**	(0.87)	0	14.27	2.73 (ref. 38)		-138.4
	4-Cl	**4c**	(-0.11)	0.23	11.65	1.03 (ref. 37)		-132.7
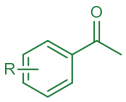	4-MeO	**5a**	-1.99	-0.27			83.01	-88.5
	4-Me	**5b**	-2.57	-0.17			77.82	-85.4
	4-Br	**5c**	-2.99	0.23			73.09	-79.9
	4-CF_3	**5d**	-3.29	0.54				-75.8
	4-NO_2	**5e**	-3.90	0.78			67.07	-73.9
	3,5-$(NO_2)_2$	**5f**	-6.12	1.42				-67.9
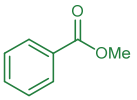		**6**	-5.38	--			59.40	-49.4
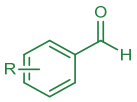	4-MeO	**7a**	-0.18	-0.27			84.81	-88.7
	H	**7b**	-1.78	0			74.88	-80.8
	4-Br	**7c**	-2.25	0.23				-77.7
	4-NO_2	**7d**	-3.76	0.78			62.32	-70.6
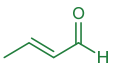		**8**	-0.73	--				-88.9
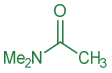		**9**	0.97	--			112.14	-105.7
Et_3P=O		**10**	2.51	--			119.28	-121.9

[a] Sum of Hammett σ parameters, from ref. 31. [b] Lewis basicities LB (in dichloromethane) toward diarylcarbenium ions from ref. 28. [c] Experimental BF_3 affinities (in kJ/mol), from ref. 12. [d] Calculated borane (BH_3) affinities BA in dichloromethane (BA = ΔG_{BH3} in kJ/mol, this work, Supporting Information).

A general correlation of Lewis basicities LB_B is found with Gal's experimental enthalpies for boron trifluoride-complexation (Figure 11a).[12] For Lewis bases that lack these experimental data, quantum-chemically calculated borane affinities BA, defined as the Gibbs reaction energy for the addition of BH_3 to a Lewis base in dichloromethane (Supporting Information), provide an equally reliable tool for estimating LB_B parameters (Figure 11b).

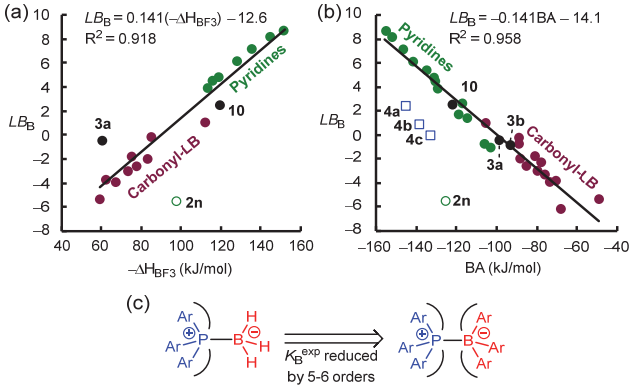

Figure 11. Correlation of LB_B parameters with further types of experimental or quantum-chemically calculated basicity descriptors (open data points not used for the construction of the correlation line). (a) Correlation of LB_B parameters with experimental BF_3 affinities in dichloromethane ($-\Delta H_{BF3}$) from ref. 12. (b) Correlation of LB_B parameters with quantum-chemically calculated BH_3 affinities BA (at the SMD(DCM)/MN15/def2-TZVP level of theory, referenced to the experimental $\Delta_r G$ of the reaction of **1d** with **2d** as outlined in the Supporting Information). (c) The association constants of bulky triarylphosphines depend on the steric demand of the Lewis acidic partner.

Moreover, the relationship in Figure 11b illustrates the effect of repulsive forces when formation of sterically crowded Lewis adducts with adjacent quaternary sp^3 centers is intended. Formation of hexaaryl phosphonium-boronates (Figurer 11c), which are isoelectronic to the hypothetical hexaphenylethane,[39] by combining the Lewis acids **1** with the triarylphosphines **4a-c** proceeded with equilibrium constants 5 to 6 powers of ten lower than expected based on the correlation for the formation of less strained Ar_3P-BH_3 adducts in Figure 11b.

Nevertheless, LB_B parameters for pyridines and phosphines correlate linearly with Lewis basicity parameters determined in the reactions with diarylcarbenium ions (Figure 12a), which are sterically less demanding than triarylboranes. Though phosphines and pyridines follow different correlations, the similar slopes of 0.45 indicate a weaker bonding of Lewis bases toward boron-centered than toward carbon-centered Lewis acids in accord with the generally lower bond dissociation energies for B-N and B-P bonds in comparison to C-N and C-P bonds.[40]

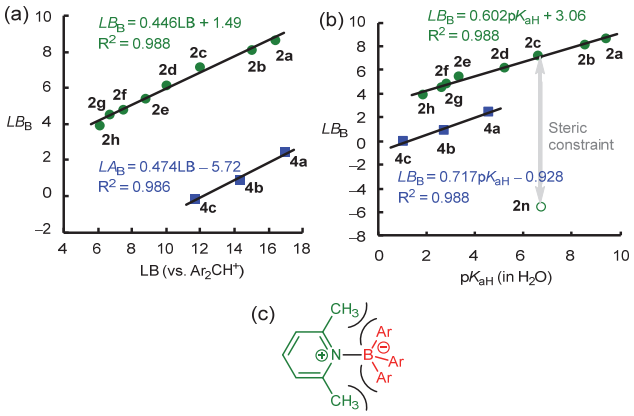

Figure 12. (a) Correlation of LB_B with the Lewis basicities LB derived from the equilibrium constants for Lewis adduct formation between Lewis bases and diarylcarbenium ions (Ar_2CH^+) in dichloromethane.[28] (b) Correlation of LB_B for pyridines and triarylphosphines with their pK_{aH} values (values in Table 3). (c) Repulsive steric interactions in Lewis adducts of 2,6-lutidine (**2n**).

Analogous correlations were found for LB_B parameters with the Brønsted basicities of pyridines and phosphines (Figure 12b). The linear LB_B vs pK_{aH} relationship for pyridines predicts LB_B = 7.3 for 2,6-lutidine (**2n**). The experimentally observed Lewis basicity LB_B = –5.5 shows that adduct formation of **2n** with $B(C_6F_5)_3$ (**1i**) is attenuated by almost 13 orders of magnitude (or by 8 orders of magnitude when calculated borane affinities BA are considered, Figure 11b) because of the steric imposition of the pyridine's methyl substituents with the aryl groups of the BAr_3 fragment (Figure 12c). Release of this 'frustration' (45 to 73 kJ/mol) is then able to deliver a considerable part of the driving force for FLP activity of $B(C_6F_5)_3$/2,6-lutidine, in accord with reports that this Lewis acid/base combination is able to add to alkynes or activate molecular hydrogen.[20]

While the almost identical Lewis acidities of **1g** (LA_B = 4.08) and **1h** (LA_B = 3.98) indicate that the pattern of fluoro-substitution at the borane has a negligible impact on the acidity toward sp- or sp^2-centered (rod-like) reference Lewis bases, this is not true toward the sterically more challenging phosphines. For the reaction of tris(*p*-anisyl)phosphine (**4a**) with the borane **1e** (*p*-F) we determined K_B = 360 M^{-1}, which was used to estimate LB_B = 2.43 for **4a**. Accordingly, the association of **4a** with the 3,4,5-fluorinated borane **1h** proceeded quantitatively ($K_B^{eq\ 1}$ = 2.4 × 10^6 M^{-1}). The analogous reaction of **4a** with the 2,4,6-trifluoro-substituted triphenylborane **1g**, however, gave an experimental K_B^{exp} = 861 M^{-1} which is more than 3 logarithmic units lower than predicted by eq. (1) for this Lewis adduct formation ($K_B^{eq\ 1}$ = 3.3 × 10^6 M^{-1}). The latter finding indicates that ortho-fluorine atoms in boranes can cause repulsive effects toward bulky Lewis basic counterparts.

Applying Quantitative Acidities and Basicities in Synthesis. Next, we tested the applicability of the Lewis acidity scale to systematically investigate Nazarov cyclizations, which were reported to be catalyzed by 5-mol% of $B(C_6F_5)_3$ (**1i**) while BPh_3 (**1d**, $LA_B = 0$) was ineffective (Figure 13).[41] The quantum-chemically calculated BA of the divinyl ketone educt in combination with the correlation in Figure 11b gives a Lewis basicity LB_B of −3.0, which suggests that bonding might only occur with Lewis acids with $LA_B > 3$. This is in line with our experimental results (10 mol-% BX_3 or BAr_3, CD_2Cl_2, 25 °C), which show that conversion to the cyclopentenone product was observed for BBr_3, BCl_3 and the triarylboranes **1i** (LA_B = 7.2), **1g** (LA_B = 4.1) and **1h** (LA_B = 3.9), but not when **1f** (LA_B = 1.3) was used as the catalyst (Figure 13a). The Lewis acidities determined in this work also reflect the different efficacies of boranes to catalyze the Diels-Alder reaction of methyl vinyl ketone with cyclopentadiene (Figure 13b) and the Michael addition of 1-methylindole to methyl vinyl ketone (Figure 12c). The quantum-chemically calculated BA allowed to estimate the Lewis basicity of methyl vinyl ketone (LB_B = −2.7). Accordingly, minor conversion was still obtained with the catalyst **1f**, for which $K_B^{eq\,1} = 4.3 \times 10^{-2}\ M^{-1}$ is calculated, suggesting that permille levels of Lewis adduct are sufficient to enable the reactions. While faster Diels-Alder reactions and Michael additions were observed with borane catalysts that are more Lewis acidic than **1f**, the less acidic triphenylborane (**1d**) was inapt to catalyze both reactions even after extended reaction times (Figure 13b,c).

Notably, not only highly Lewis acidic fluorinated triarylboranes are applied as catalysts. Already triphenylborane (**1d**) forms adducts with tertiary amides, such as *N*,*N*-dimethylacetamide (**9**, LB_B = 0.97) (K_B^{exp} = 7.6 M^{-1}), enabling their selective reduction with hydrosilanes as hydride donors in acetonitrile (LB_B = –0.48), which is only a slightly weaker Lewis base than the amide **9**.[43] Less Lewis acidic boranes as catalysts may be beneficial in future applications because of their advantageous chemoselectivity in reactions at highly functionalized substrates, which tend to react unselectively when highly Lewis acidic boranes are used as catalysts.[43-45]

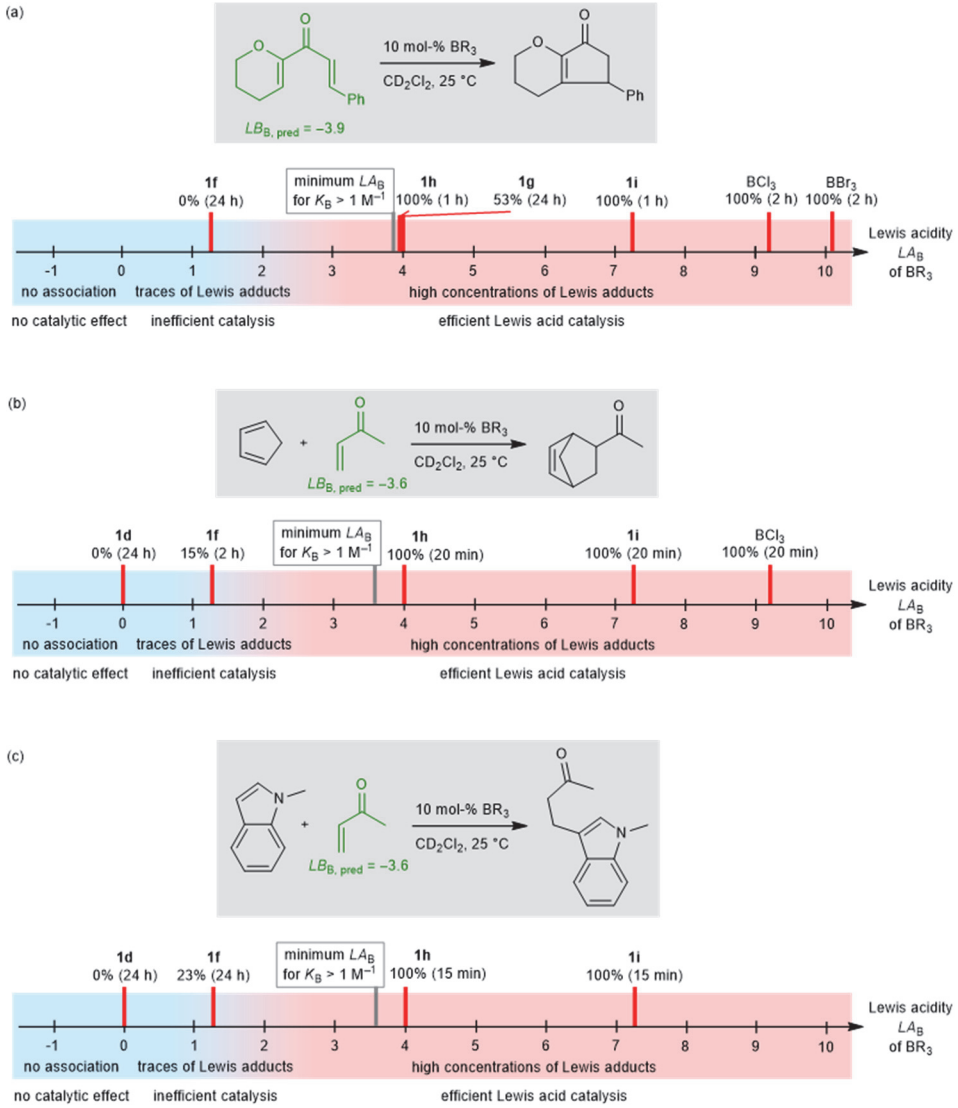

Figure 13: Application of the Lewis acidity parameters LA_B in borane catalyzed reactions. (a) Nazarov cyclizations. Borane **1g** (with ortho-fluorine atoms) is a less efficient catalyst than the equally Lewis acidic **1h** (with only ortho-hydrogen atoms). (b) Diels-Alder reactions of methyl vinyl ketone with cyclopentadiene. (c) Michael additions of 1-methylindole to methyl vinyl ketone (ref. 42 reports catalysis of this Michael addition by 5 mol-% **1i** in $CHCl_3$ at 80 °C)

Conclusions

In this work we constructed Lewis acidity/basicity scales that allow the quantitative prediction of the association between triarylboranes and various O-, N-, and P-centered Lewis bases covering 15 orders of magnitude in acidity/basicity. As a consequence, eq (1) enables chemists to predict whether at all and if 'yes', to which extent Lewis adduct formation of a certain Lewis acidic borane with a certain Lewis base in dichloromethane will be possible (Figure 14).

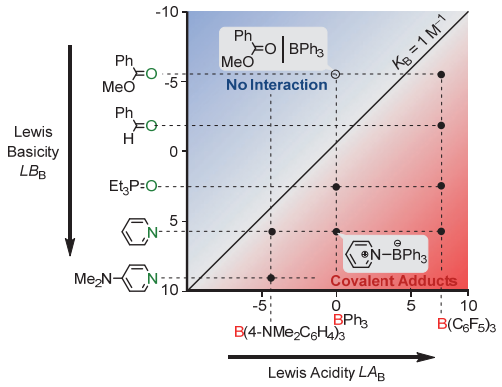

Figure 14. The two-dimensional arrangement of Lewis acidity and Lewis basicity scales illustrates which Lewis acid/base combination forms a Lewis adduct.

Physical organic descriptors like Hammett σ-parameters, tabulated reaction enthalpies as well as quantum-chemically calculated thermodynamics offer direct avenues for chemists to introduce new substrates to the Lewis acidity/basicity scales presented herein. Future developments in Lewis acid catalysis as well as in the chemistry of frustrated Lewis pairs can now be carried out more purposefully by using quantitative predictions of the thermodynamics of adduct formations, which are strongly linked to experimentally investigated equilibria and borane catalyst efficacy in solution.

ACKNOWLEDGMENT

We thank Amalina Buda for experimental assistance at the beginning of the project and Prof. Herbert Mayr (LMU) for helpful discussion. R.J.M. is grateful to the Fonds der Chemischen Industrie for a Kekulé fellowship.

REFERENCES

(1) Ishihara, K., Yamamoto, H. Arylboron Compounds as Acid Catalysts in Organic Synthetic Transformations. *Eur. J. Org. Chem.* **1999**, 527-538.
(2) Ishihara, K. Achiral B(III) Lewis Acids. In: H. Yamamoto (Ed.), Lewis Acids in Organic Synthesis, Wiley-VCH, New York, 2000, 89-133.
(3) Ishihara, K. Chiral B(III) Lewis Acids. In: H. Yamamoto (Ed.), Lewis Acids in Organic Synthesis, Wiley-VCH, New York, 2000, 135-190.
(4) Hatano, M., Ishihara, K. Lewis Acids. In: A. Coca (Ed.) Boron Reagents in Synthesis (ACS Symposium Series, Vol. 1236), American Chemical Society, Washington, DC, 2016, 27-66.
(5) Lawson, J. R.; Melen, R. L. Tris(pentafluorophenyl)borane and Beyond: Modern Advances in Borylation Chemistry. *Inorg. Chem.* **2017**, *56*, 8627-8643.
(6) Carden, J. L.; Dasgupta, A.; Melen, R. L. Halogenated triarylboranes: synthesis, properties and applications in catalysis. *Chem. Soc. Rev.* **2020**, *49,* 1706-1725.
(7) Stephan, D. W., Erker, G. Frustrated Lewis Pair Chemistry: Development and Perspectives. *Angew. Chem. Int. Ed.* **2015, 54**, 6400-6441.
(8) Stephan, D. W. The broadening reach of frustrated Lewis pair chemistry. *Science* **2016**, *354*, aaf7229.
(9) Jupp, A. R., Stephan, D. W. New Directions for Frustrated Lewis Pair Chemistry. *Trends Chem.* **2019**, *1*, 35-48.
(10) Greb, L. Lewis Superacids: Classifications, Candidates, and Applications. *Chem. Eur. J.* **2018**, *24*, 17881-17896.
(11) Sivaev, I. B., Bregadze, V. I. Lewis acidity of boron compounds. *Coord. Chem. Rev*. **2014**, *270-271*, 75-88.
(12) Laurence, C., Gal, J.-F. Lewis Basicity and Affinity Scales: Data and Measurement; Wiley: Chichester, UK, 2010.
(13) Chase, P. A., Piers, W. A., Patrick, B. O. New Fluorinated 9-Borafluorene Lewis Acids. *J. Am. Chem. Soc.* **2000**, *122*, 12911-12912.
(14) Ashley, A. E., Herrington, T. A., Wildgoose, G. G., Zaher, H., Thompson, A. L., Rees, N. H., Krämer, T., O'Hare, D. Separating Electrophilicity and Lewis Acidity: The Synthesis, Characterization, and Electrochemistry of the Electron Deficient Tris(aryl)boranes $B(C_6F_5)_{3-n}(C_6Cl_5)_n$ (n = 1-3). *J. Am. Chem. Soc.* **2011**, *133*, 14727-14740.
(15) Houghton, A. Y., Karttunen, V. A., Piers, W. E., Tuononen, H. M. Hydrogen activation with perfluorinated organoboranes: 1,2,3-tris(pentafluorophenyl)-4,5,6,7-tetrafluoro-1-boraindene. *Chem. Commun.* **2014**, *50*, 1295-1298.
(16) Saida, A. B., Chardon, A., Osi, A., Tumanov, N., Wouters, J., Adjieufack, A. I., Champagne, B., Berionni, G. Pushing the Lewis Acidity Boundaries of Boron Compounds With Non-Planar Triarylboranes Derived from Triptycenes. *Angew. Chem. Int. Ed.* **2019**, *58*, 16889-16893.
(17) Chardon, A., Osi, A., Mahaut, D., Doan, T. H., Tumanov, N., Wouters, J., Fusaro, L., Champagne, B., Berionni, G. Controlled Generation of 9-Boratriptycene by Lewis Adduct Dissociation: Accessing a Unique Non-Planar Triarylborane. *Angew. Chem. Int. Ed.* **2020**, doi: 10.1002/anie.202003119.
(18) Parks, D. J., Piers, W. E. Tris(pentafluorophenyl)boron-Catalyzed Hydrosilation of Aromatic Aldehydes, Ketones, and Esters. *J. Am. Chem. Soc.* **1996**, *118*, 9440-9441.
(19) Morgan, M. M.; Marwitz, A. J. V., Piers, W. E., Parvez, M. Comparative Lewis Acidity in Fluoroarylboranes: $B(o\text{-}HC_6F_4)_3$, $B(p\text{-}HC_6F_4)_3$, and $B(C_6F_5)_3$. *Organometallics* **2013**, *32*, 317-322.
(20) Geier, S. J., Stephan, D. W. Lutidine/$B(C_6F_5)_3$: At the Boundary of Classical and Frustrated Lewis Pair Reactivity. *J. Am. Chem. Soc.* **2009**, *131*, 3476-3477.
(21) Rocchigiani, L., Ciancaleoni, G., Zuccaccia, C., Macchioni, A. Probing the Association of Frustrated Phosphine−Borane Lewis Pairs in Solution by NMR Spectroscopy. *J. Am. Chem. Soc.* **2014**, *136*, 112-115.
(22) Childs, R. F., Mulholland, D. L., Nixon, A. The Lewis acid complexes of α,β-unsaturated carbonyl and nitrile compounds. A nuclear magnetic resonance study. *Can. J. Chem* **1982**, *60,* 801–808.
(23) Beckett, M. A., Strickland, G. C., Holland, J. R., Varma, K. S. A convenient n.m.r. method for the measurement of Lewis acidity at boron centres: correlation of reaction rates of Lewis acid initiated epoxide polymerizations with Lewis acidity. *Polymer* **1996**, 4629-4631.
(24) Laurence, C., Graton, J., Gal, J.-F. An Overview of Lewis Basicity and Affinity Scales. *J. Chem. Educ.* **2011**, *88*, 1651-1657.
(25) Hilt, G., Pünner, F., Möbus, J., Naseri, V., Bohn, M. A. A Lewis Acidity Scale in Relation to Rate Constants of Lewis Acid Catalyzed Organic Reactions. *Eur. J. Org. Chem.* **2011**, 5962-5966.
(26) Gaffen, J. R., Bentley, J. N., Torres, L. C, Chu, C., Baumgartner, T., Caputo, C. B. A Simple and Effective Method of Determining Lewis Acidity by Using Fluorescence. *Chem* **2019**, *5*, 1567-1583.
(27) Hanson, C. S., Psaltakis, M. C., Cortes, J. J., Siddiqi, S. S., Devery III, J. J. Investigation of Lewis Acid-Carbonyl Solution

Interactions via Infrared-Monitored Titration, *J. Org. Chem*. **2020**, *85*, 820-832.
(28) Mayr, H., Ammer, J., Baidya, M., Maji, B., Nigst, T. A., Ofial, A. R., Singer, T. Scales of Lewis Basicity toward C-Centered Lewis Acids (Carbocations). *J. Am. Chem. Soc.* **2015***, 137*, 2580-2599.
(29) Verma, P., Truhlar, D. G. Status and Challenges of Density Functional Theory, *Trends Chem*. **2020**, *2*, 302-318.
(30) Böhrer, H.; Trapp, N.; Himmel, D.; Schleep, M.; Krossing, I. From unsuccessful H_2-activation with FLPs containing $B(Ohfip)_3$ to a systematic evaluation of the Lewis acidity of 33 Lewis acids based on fluoride, chloride, hydride and methyl ion affinities. *Dalton Trans.* **2015***, 44*, 7489-7499.
(31) Hansch, C., Leo, A., Hoekman, D. Exploring QSAR – Hydrophobic, Electronic, and Steric Constants (ACS Professional Reference Book); American Chemical Society, Washington, DC, 1995.
(32) Jupp, A. R., Johnstone, T. C., Stephan, D. W. The global electrophilicity index as a metric for Lewis acidity. *Dalton Trans.* **2018**, *47*, 7029-7034.
(33) Jameson, G. W., Lawlor, J. M. Aminolysis of N-phosphorylated pyridines. *J. Chem. Soc. B* **1970***,* 53-57.
(34) Fischer, A., Galloway, W. J., Vaughan, J. Structure and reactivity in the pyridine series. Part I. Acid dissociation constants of pyridinium ions. *J. Chem. Soc.* **1964***,* 3591-3596.
(35) Taagepera, M., Henderson, W. G., Brownlee, R. T. C., Beauchamp, J. L., Holtz, D., Taft, R. W. Gas-Phase Basicities and Pyridine Substituent Effects. *J. Am. Chem. Soc*. **1972**, *94*, 1369-1370.
(36) Andon, R. L.; Cox, J. D.; Herington, E. F. G. The ultra-violet absorption spectra and dissociation constants of certain pyridine bases in aqueous solution. *Trans. Faraday Soc.* **1954***, 50,* 918-927.
(37) Allman, T., Goel, R. G. The basicity of phosphines. *Can. J. Chem.* **1982**, *60*, 716-722.
(38) Henderson, W. A., Jr.; Streuli, C. A. The Basicity of Phosphines. *J. Am. Chem. Soc.* **1960**, *82*, 5791-5794.
(39) Grimme, S, Schreiner, P. R. Steric Crowding Can Stabilize a Labile Molecule: Solving the Hexaphenylethane Riddle. *Angew. Chem. Int. Ed.* **2011**, *50*, 12639-12642.
(40) Luo, Y. R., Comprehensive Handbook of Chemical Bond Energies, CRC Press, Boca Raton, FL, 2007.
(41) Süsse, L., Vogler, M., Mewald, M., Kemper, B., Irran, E., Oestreich, M. Enantioselective Nazarov Cyclizations Catalyzed by an Axial Chiral C_6F_5-Substituted Boron Lewis Acid. *Angew. Chem. Int. Ed.* **2018**, *57*, 11441-11444.
(42) Li, W., Werner, T. $B(C_6F_5)_3$-Catalyzed Michael Reactions: Aromatic C−H as Nucleophiles. *Org. Lett.* **2017**, *19*, 2568-2571.
(43) Mukherjee, D., Shirase, S., Mashima, K., Okuda, J. Chemoselective Reduction of Tertiary Amides to Amines Catalyzed by Triphenylborane. *Angew. Chem. Int. Ed.* **2016**, *55*, 13326-13329.
(44) Andrea, K. A., Kerton, F. M. Triarylborane-Catalyzed Formation of Cyclic Organic Carbonates and Polycarbonates. *ACS Catal.* **2019***, 9*, 1799-1809.
(45) Brar, A., Unruh, D. K., Ling, N., Krempner, C. BPh_3-Catalyzed [2+3] Cycloaddition of Ph_3PCCO with Aldonitrones: Access to 5-Isoxazolidinones with Exocyclic Phosphonium Ylide Moieties. *Org. Lett.* **2019**, *21*, 6305-6309.

7.1 Supporting Information - General

Solvents, Reagents, and Analytics. Triarylboranes were prepared according to the modified literature procedures as outlined below using commercially available chemicals purchased from Sigma Aldrich, ABCR or TCI. Trimesitylborane (**1j**) was purchased from EGA-Chemie KG and used without further purification. $Ph_3B{\cdot}NaOH$ was purchased from TCI. All boranes were stored in an argon-filled glove box at –35 °C. Hydrazine monohydrate (purum, > 99%) was purchased from Fluka.

Dichloromethane for isothermal titration calorimetry (ITC) measurements was purchased from Merck (HPLC grade) and stirred over concentrated H_2SO_4 for 2 weeks to remove olefinic stabilizers. Subsequently, distillation over calcium hydride provided anhydrous material which was stored for 24 h over activated molecular sieves (3 Å).

Deuterated dichloromethane (CD_2Cl_2) was purchased from Eurisotop and stored for 24 h over activated molecular sieves (3 Å).

Melting points were acquired on Büchi Melting Point M-560 devices and are not corrected.

Nuclear magnetic resonance (NMR) spectra were acquired on 400 MHz spectrometers. The following abbreviations and their combinations were used in the analysis of NMR spectra: s = singlet, d = doublet, t = triplet, q = quartet, m = multiplet, br s = broad singlet, app = apparent. NMR signals were assigned based on information from additional 2D NMR experiments (COSY, gHSQC, gHMBC, NOESY). Chemical shifts are given in ppm. Internal reference was set to the residual solvent signals (for CD_2Cl_2: δ_H = 5.32, δ_C = 54.00, $CDCl_3$: δ_H = 7.26, δ_C = 77.16; for d_6-DMSO: δ_H = 2.50, δ_C = 39.52).[1] The ^{13}C NMR spectra (101 MHz) were recorded under broad-band proton-decoupling.

High resolution (HRMS) mass spectra were recorded on a Finnigan MAT 95 sectorfield mass spectrometer where samples were vaporized on a platinum wire from 20 to 1600 °C at a rate of 120 °C/min. For ionization of the samples, electron-impact ionization (EI) was applied.

Isothermal Titration Calorimetry (ITC). The ITC measurements were performed on a Microcal VP-ITC instrument with solutions maintained under an atmosphere of dry nitrogen. The reference cell was filled with dichloromethane and the sample cell was filled with a solution of the borane in the same solvent. The syringe was filled with a solution of the Lewis base in dichloromethane, which was then gradually injected (6 µL/injection, 40 steps, 120 s spacing between injections) into the sample cell. The ITC raw data were processed and analyzed with the AFFINImeter ITC software (v.2.1710) assuming a 1:1 interaction model.[2]

NMR Spectroscopic Titrations. NMR spectroscopic titration experiments were performed with a series of NMR tubes that were handled in an argon filled glovebox and filled with anhydrous CD_2Cl_2 solutions. In most cases, the borane was used as the minor component. Only in case of tris(pentafluorophenyl)borane (**1i**), the Lewis base was used as minor component and treated with an excess of **1i**. ^1H NMR measurements were performed on a 400 MHz NMR spectrometer at 22 °C. The resulting dependency of the chemical shift difference Δδ (in ppm, referenced to the residual solvent signal in d_2-dichloromethane) of the resonance of the Lewis acid (or Lewis base) vs. the concentration of the excess component was analyzed according to the equation (S1) by non-linear fitting with Origin software.[3] For the detailed derivation of eq. (S1) see ref. 4. The only variable in (S1) is K_B, all other quantities are known from the concentrations used in the titrations.

$$\Delta\delta = \frac{\Delta\delta_{max}}{[LA]}\left(\frac{1}{2}\left\{\left([LA]+[LB]+\frac{1}{K_B}\right)-\sqrt{\left([LA]+[LB]+\frac{1}{K_B}\right)^2+4[LA][LB]}\right\}\right) \quad \text{(S1)}$$

7.2 Synthesis

Tris(4-dimethylaminophenyl)borane (1a)

Synthesis according to the modified procedure in ref. 5.

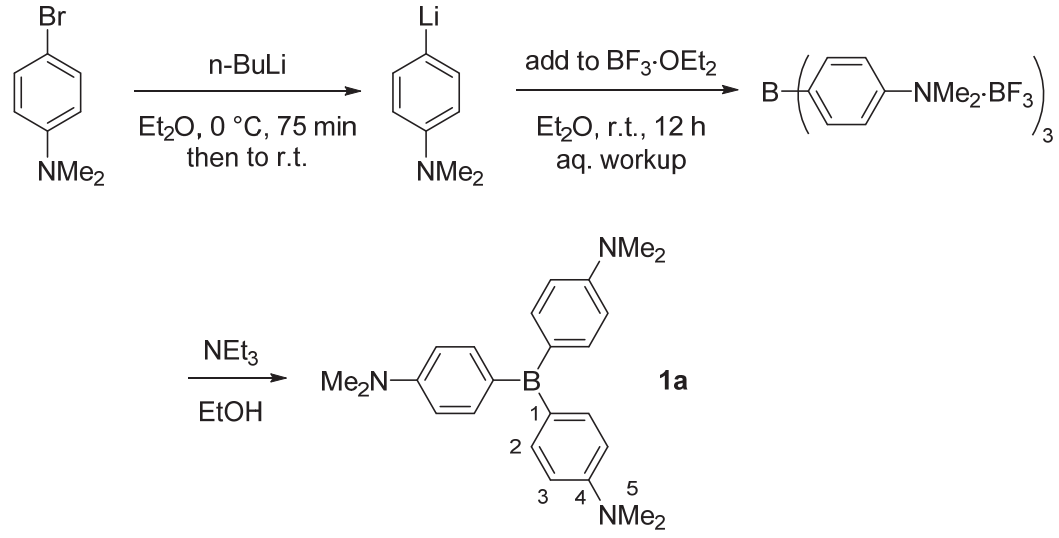

(RNH408)

To a flame dried 100 mL Schlenk flask under nitrogen was added diethyl ether (27 mL) and 4-(dimethylamino)bromobenzene (3.58 g, 17.9 mmol). The resulting solution was cooled to 0 °C. Under stirring n-BuLi (2.3 M, 7.78 mL, 17.9 mmol) was added. Then the mixture was stirred for further 75 min at 0 °C and subsequently allowed to warm to room temperature.

In a separate flame dried 100 mL Schlenk flask under nitrogen was dissolved freshly distilled $BF_3{\cdot}OEt_2$ (2.62 mL, 21.3 mmol) in diethyl ether (25 mL). Under stirring, the solution of the above prepared aryl lithium species was added dropwise causing the formation of a cloudy, yellowish precipitate. After stirring overnight, water (20 mL) was added. The organic layer was separated, and the aqueous phase placed on a rotary evaporator (40 °C, 300 mbar) to remove residual diethyl ether. The aqueous phase was filtrated, and a solution of triethylamine (1.80 g, 17.8 mmol) in ethanol (5 mL) was added. The resulting yellow precipitate was separated, washed several times with water and then methanol, and finally dried under reduced pressure (crude yield: 605 mg).

For purification, that crude material was suspended in acetone (10 mL), heated under reflux for 2.5 h and the hot mixture filtrated. The solution was concentrated to dryness and the residue recrystallized from acetone to give the borane (148 mg, 7%) as yellow, fluorescent solid.

Though borane **1a** is not particularly sensitive towards moisture, we stored it in an argon filled glovebox at −35 °C. Under nitrogen, initially colorless diluted solutions of **1a** in dichloromethane turned intense yellow after exposure to light.

Mp.: 199-221 °C (ref. 5: 209-212 °C)

^{1}H NMR (400 MHz, CD_2Cl_2) δ = 7.51–7.49 (m, 6 H), 6.77–6.75 (m, 6 H), 3.04 (s, 18 H).

$^{13}C\{^{1}H\}$ NMR (101 MHz, CD_2Cl_2) δ = 152.5 (C_q, C-4), 140.8 (CH, C-2), 137.9 (C_q, C-1), 111.2 (CH, C-3), 40.4 (CH_3, C-5).

HRMS (EI^+) calcd *m/z* for $C_{24}H_{30}BN_3^{\bullet+}$ ($M^{\bullet+}$) 371.2527; found 371.2538.

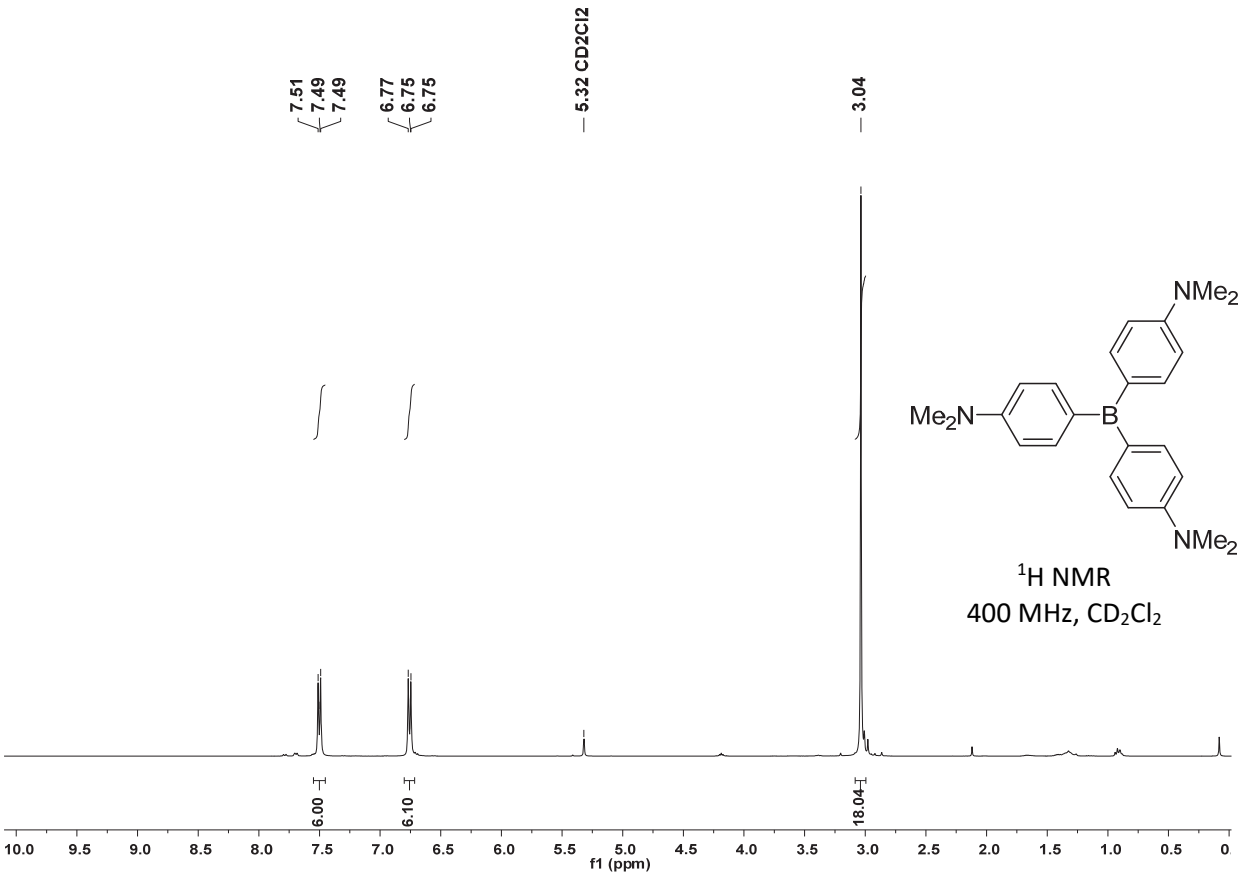

^{1}H NMR
400 MHz, CD_2Cl_2

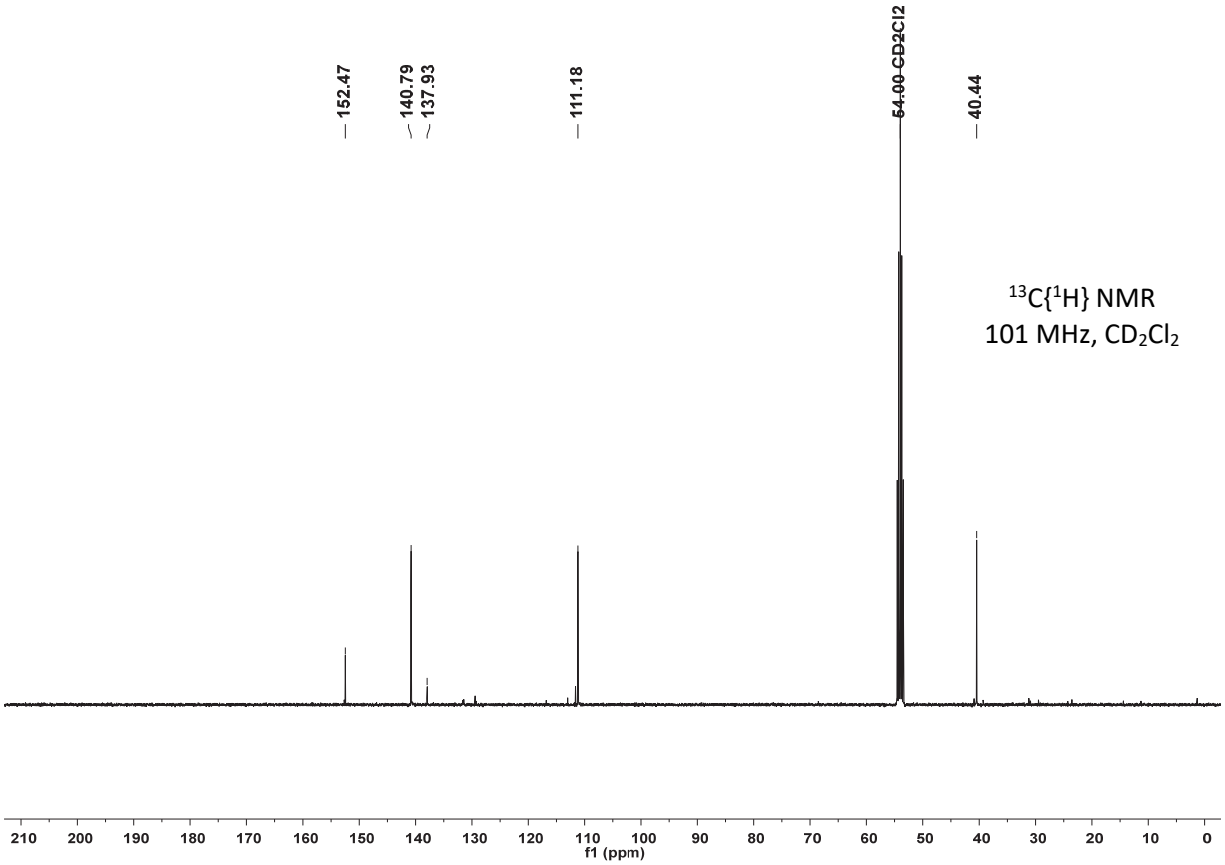

^{13}C{^{1}H} NMR
101 MHz, CD_2Cl_2

Tris(4-methoxyphenyl)borane (1b)

Synthesis according to the modified procedure in ref. 6.

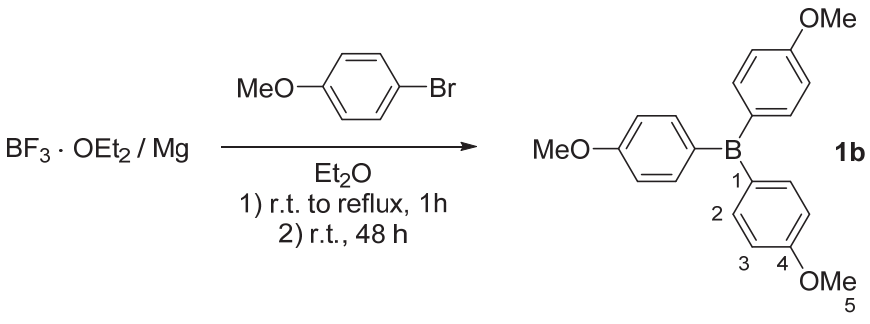

(RM1070)

A 100 mL Schlenk flask with reflux condenser was charged with magnesium turnings (854 mg, 35.1 mmol), flame dried under vacuum, and filled with dry nitrogen. Diethyl ether (20 mL) and freshly distilled $BF_3{\cdot}OEt_2$ (1.26 mL, 10.0 mmol) were added. To the vigorously stirred mixture, a solution of 4-bromoanisole (3.78 mL, 30.2 mmol) in diethyl ether (20 mL) was added. The Grignard reaction was initiated by the addition of 2 drops of iodomethane and careful heating to reflux causing the suspension to turn yellow. The mixture was heated to reflux for 3 h, allowed to cool to room temperature, and then stirred for another 64 h. All volatiles were subsequently removed under reduced pressure. The residue was suspended in n-hexane (50 mL) and filtered through a Schlenk-frit. The resulting yellow solution was concentrated under reduced pressure to leave a yellow solid residue, which was recrystallized from n-hexane to afford the product (1.22 g, 37%) as yellowish, crystalline solid.

Mp.: 80-95 °C (ref. 7: 128 °C)

^{1}H NMR (400 MHz, $CDCl_3$) δ = 7.62–7.59 (m, 6 H, 2-H), 7.01–6.97 (m, 6 H, 3-H), 3.90 (s, 9 H, 5-H).

$^{13}C\{^{1}H\}$ NMR (101 MHz, $CDCl_3$) δ = 162.2 (C_q, C-4), 140.7 (CH, C-2), 135.9 (br, C_q, C-1), 113.0 (CH, C-3), 55.3 (CH_3, C-5).

^{11}B NMR (128 MHz, $CDCl_3$) δ = 64.8.

HRMS (EI^+) calcd *m/z* for $C_{21}H_{21}BO_3^{\bullet+}$ ($M^{\bullet+}$) 332.1578; found 332.1571.

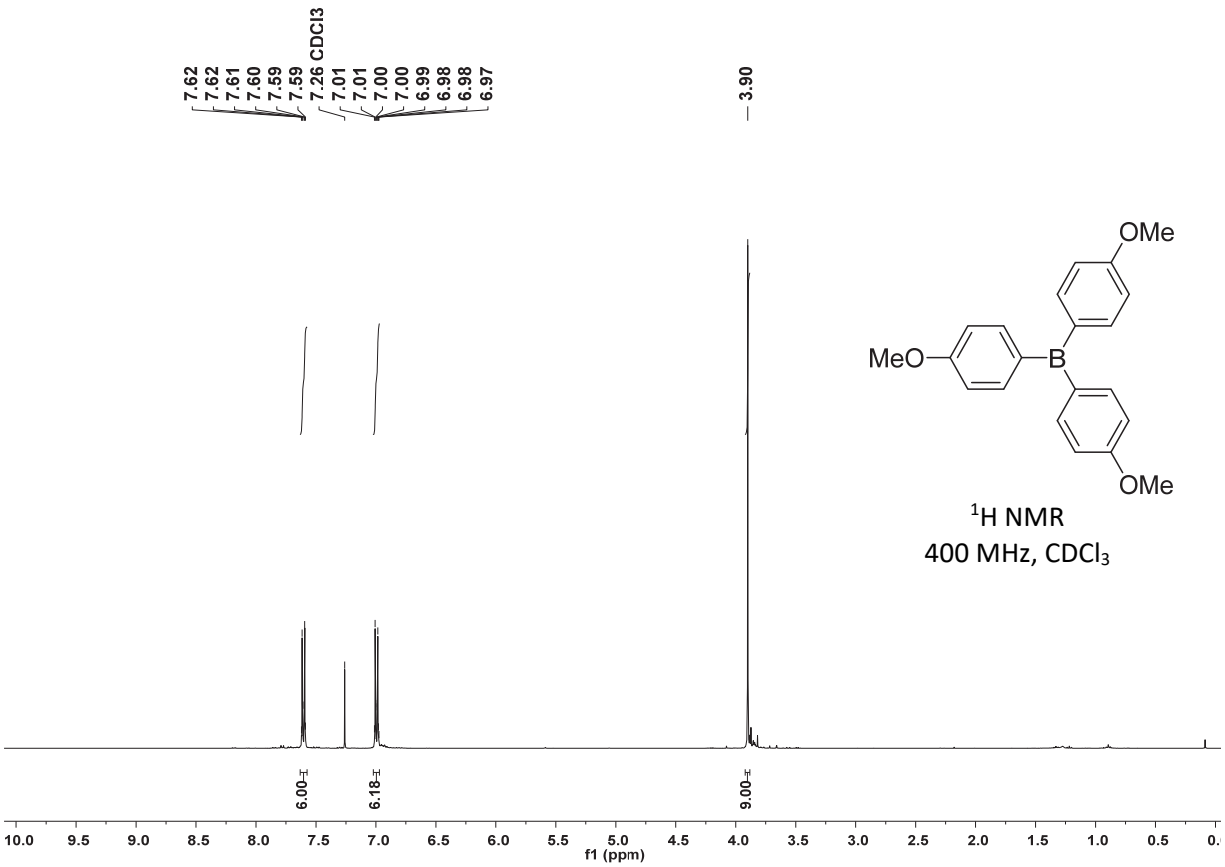

^{1}H NMR
400 MHz, $CDCl_3$

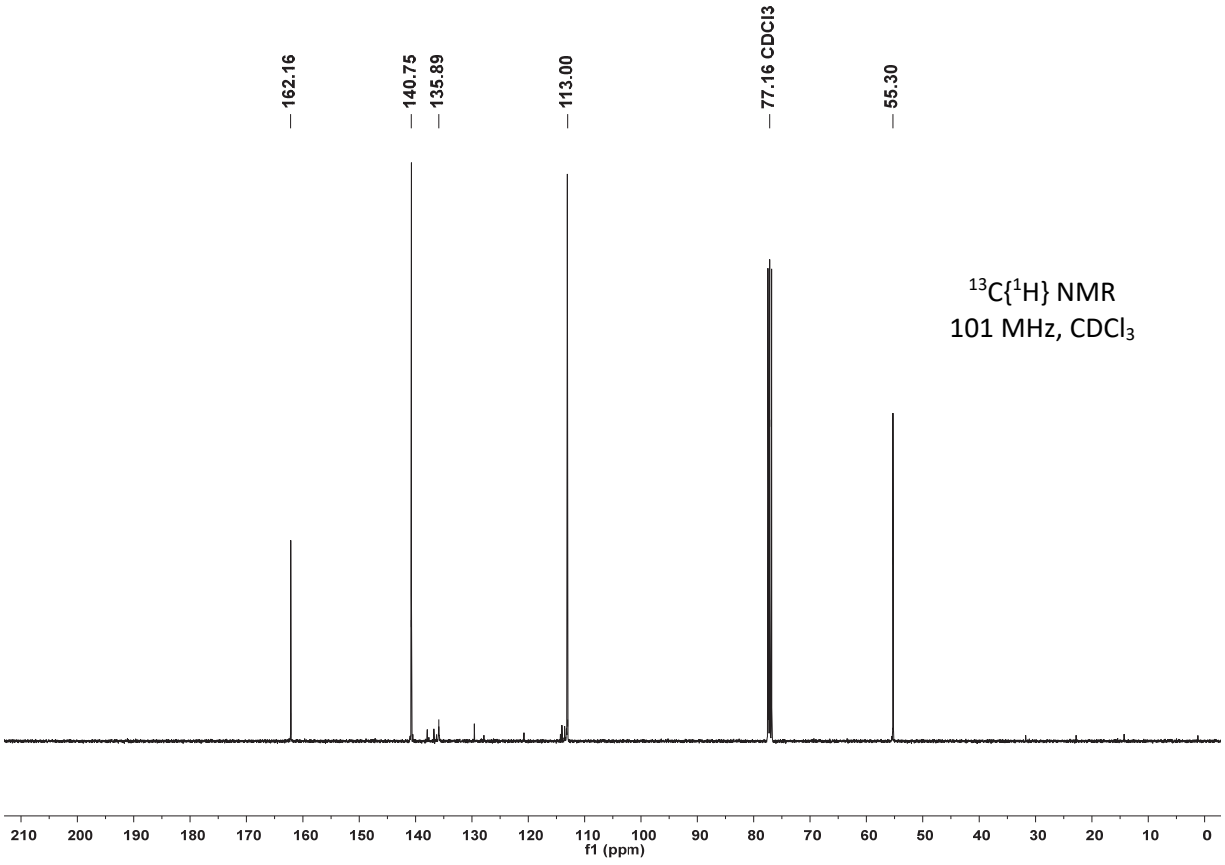

$^{13}C\{^{1}H\}$ NMR
101 MHz, $CDCl_3$

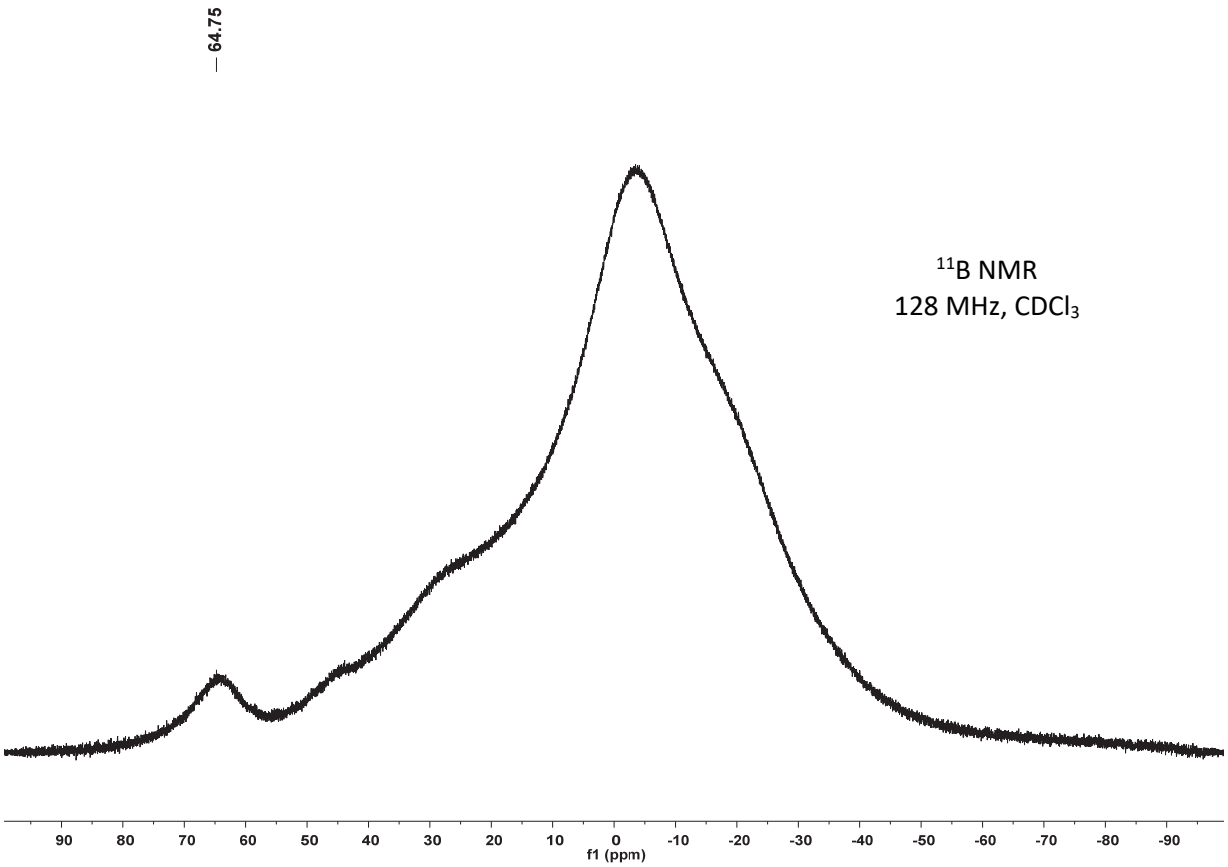
64.75
^{11}B NMR
128 MHz, $CDCl_3$
90 80 70 60 50 40 30 20 10 0 -10 -20 -30 -40 -50 -60 -70 -80 -90
f1 (ppm)

Tris(4-methylphenyl)borane (1c)

Synthesis according to the modified procedure in ref. 6.

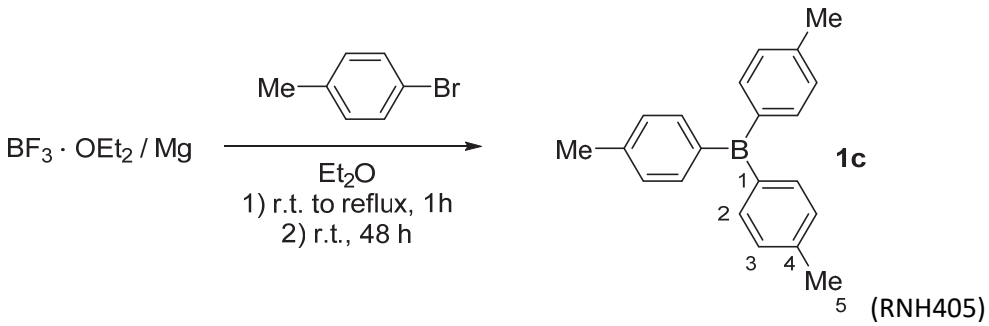

(RNH405)

A 100 mL Schlenk flask with reflux condenser was charged with magnesium turnings (853 mg, 35.1 mmol), flame dried under vacuum, and filled with dry nitrogen. Diethyl ether (20 mL), a crystal of iodine and freshly distilled $BF_3{\cdot}OEt_2$ (1.26 mL, 10.0 mmol) were added. To the vigorously stirred mixture, a solution of 4-bromotoluene (3.74 mL, 30.2 mmol) in diethyl ether (20 mL) was added. The Grignard reaction was initiated by careful heating causing the suspension to turn yellow. The mixture was stirred for another 12 h. Volatiles were removed under reduced pressure. The residue was suspended in n-hexane (40 mL) and stirred for 30 minutes or until the residue was finely suspended. The suspension was filtered through a Schlenk-frit. The solid was washed with n-hexane (10 mL), and the clear filtrate concentrated to dryness. The crude product was recrystallized from n-hexane to give the borane (646 mg, 23%) as colorless, crystalline solid. Further concentration of the mother liquor afforded additional material of lower quality, which was not used in our experiments.

Mp.: 150 °C (ref. 5: 142-144 °C)

^{1}H NMR (400 MHz, CD_2Cl_2) δ = 7.51–7.49 (m, 6 H, 2-H), 7.29–7.27 (m, 6 H, 3-H), 2.45 (s, 9 H, 5-H).

$^{13}C\{^{1}H\}$ NMR (101 MHz, CD_2Cl_2) δ = 142.1 (C_q, C-4), 140.8 (br, C_q, C-1), 139.2 (CH, C-2), 128.7 (CH, C-3), 22.0 (CH_3, C-5).

^{11}B NMR (128 MHz, CD_2Cl_2) δ = 66.8.

HRMS (EI^+) calcd *m/z* for $C_{21}H_{21}B^{\bullet+}$ ($M^{\bullet+}$) 284.1731; found 284.1717.

NMR data agree with those reported in ref. 8.

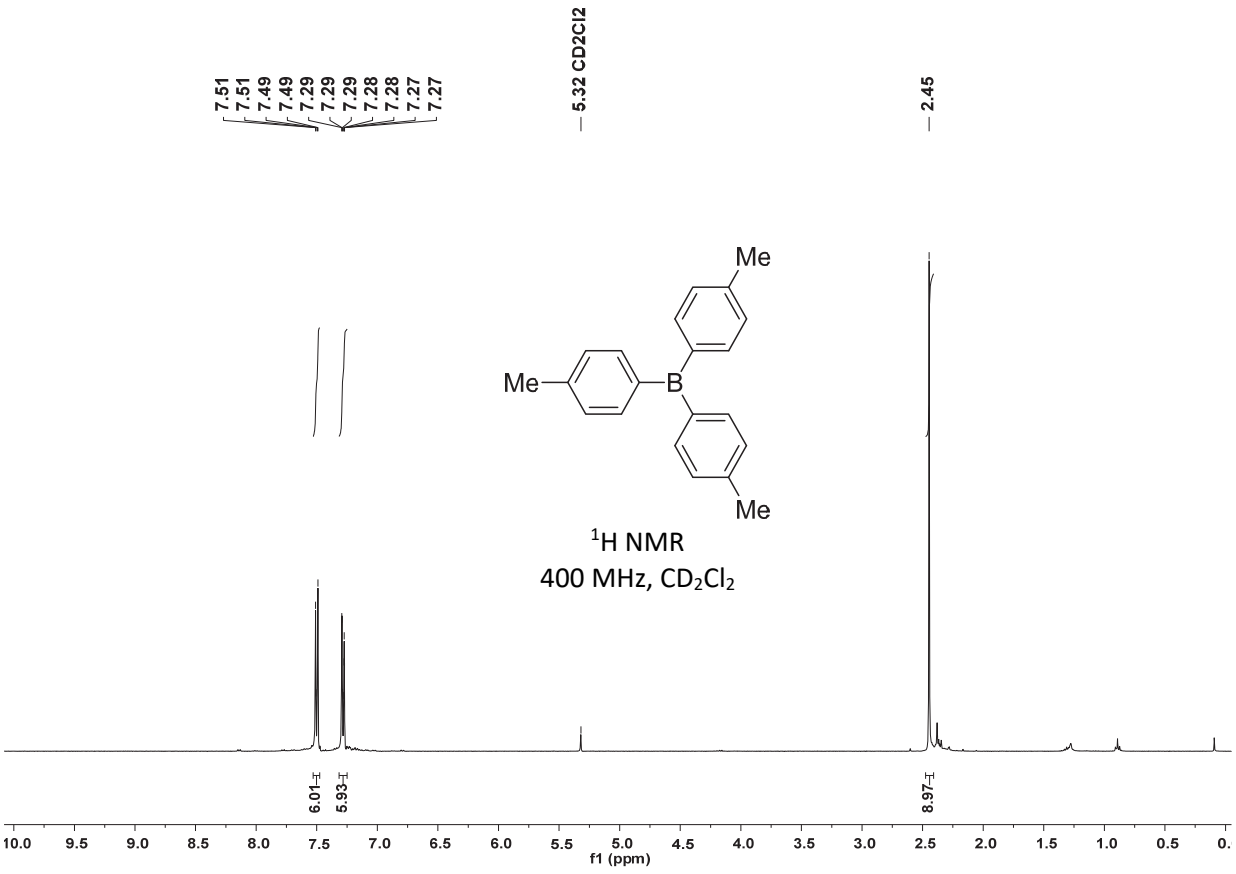

^{1}H NMR
400 MHz, CD_2Cl_2

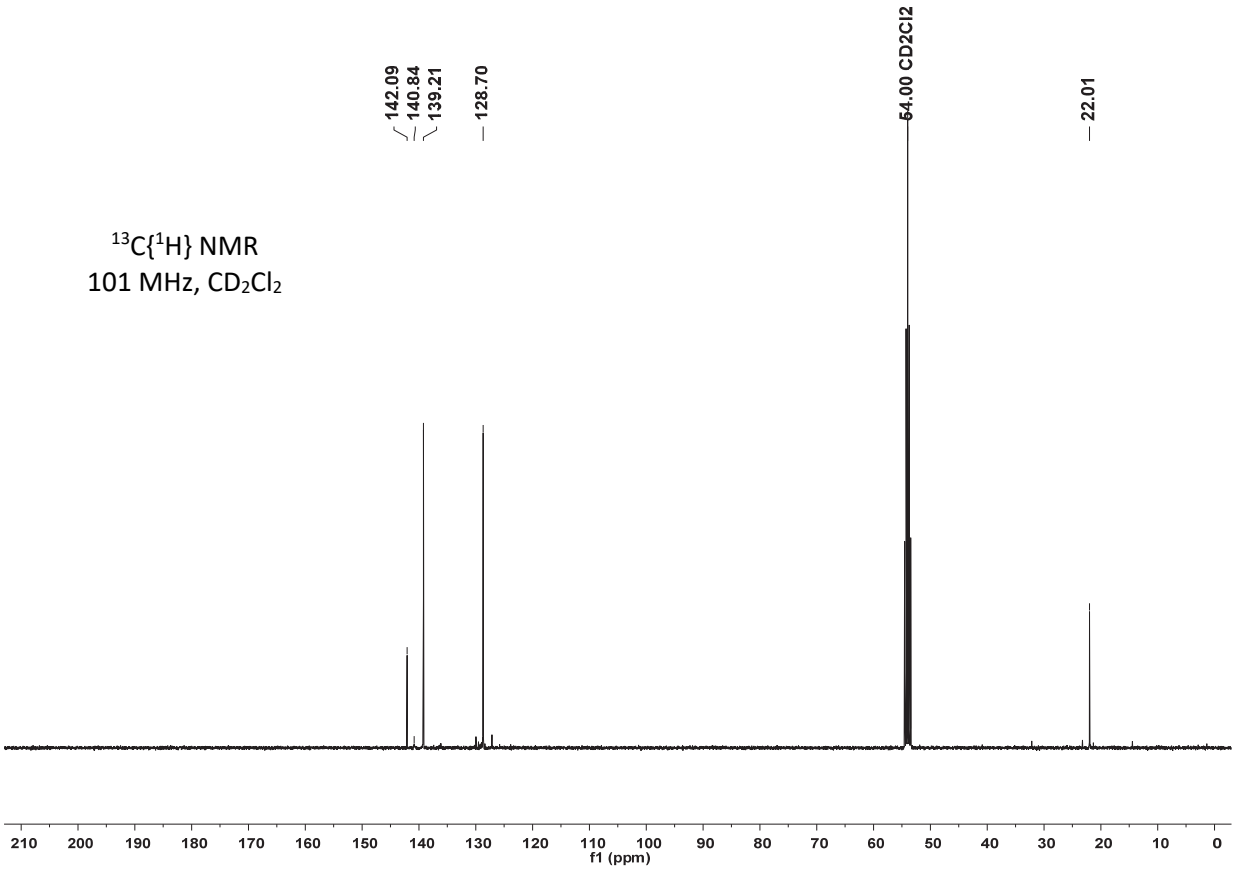

$^{13}C\{^{1}H\}$ NMR
101 MHz, CD_2Cl_2

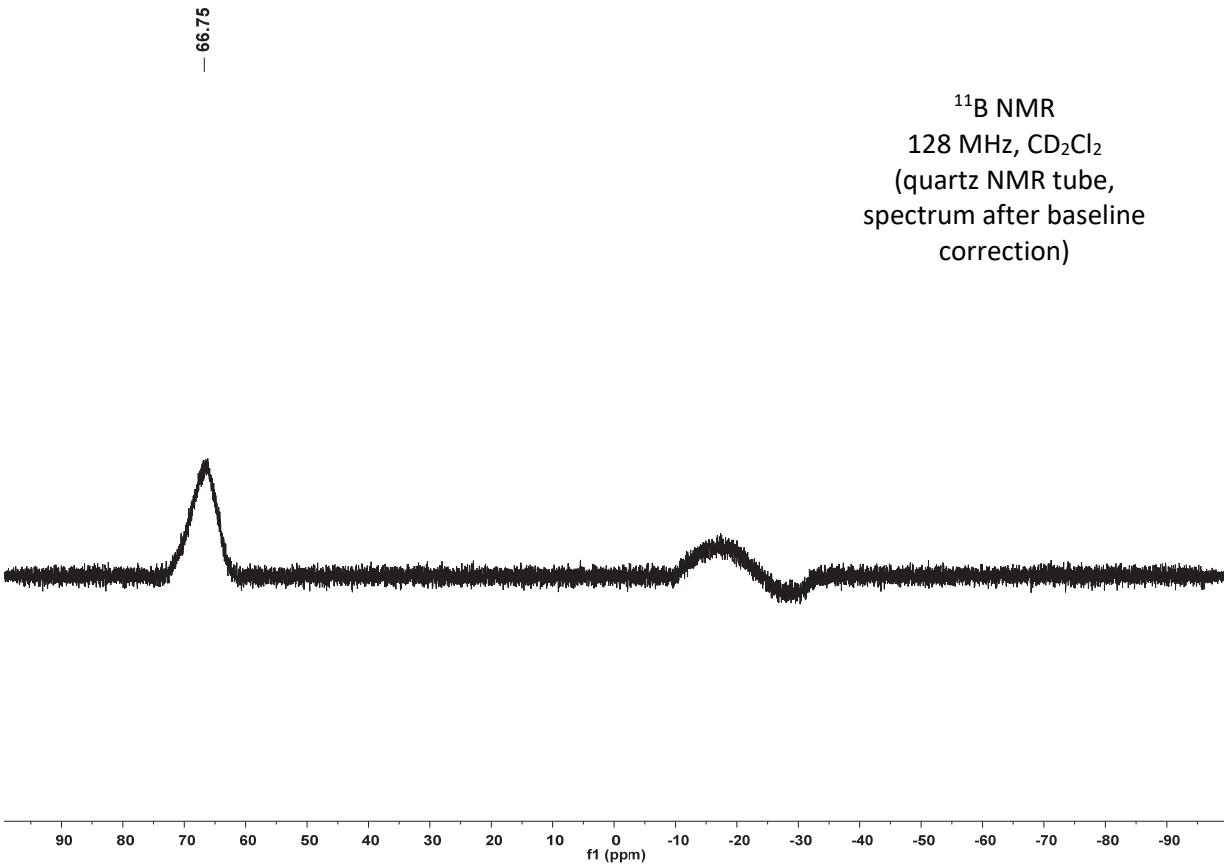

^{11}B NMR
128 MHz, CD_2Cl_2
(quartz NMR tube,
spectrum after baseline
correction)

Triphenylborane (1d)

Triphenylborane from various commercial sources was not of sufficient quality for our experiments. Starting from an aqueous solution of the adduct $Ph_3B{\cdot}NaOH$ and following the procedure described in ref. 9 yielded pure **1d**.

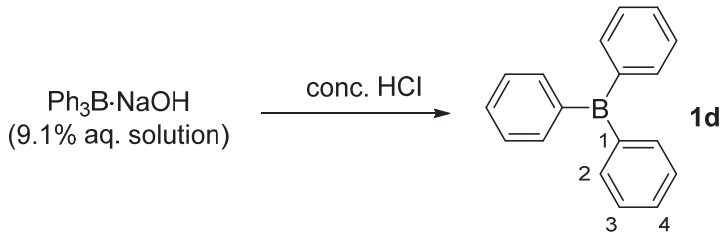

(AB014/AB023/AB026)

In a 100 mL Schlenk flask under nitrogen was placed a commercial solution of 9.1 w% aq $Ph_3B{\cdot}NaOH$ (25 g, 8.1 mmol). Careful addition of conc. hydrochloric acid (ca. 3 mL in total, pH 1) caused the formation of a colorless precipitate, which was isolated immediately by filtration through a Schlenk-frit under nitrogen (according to the literature, the freshly formed Ph_3B is highly oxygen sensitive and decomposes rapidly in acidic aq solution[9b]). The solid material was washed with water and dried under reduced pressure. The crude product was recrystallized from n-heptane (7 mL) to give **1d** (1.65 g, 84%) as colorless, crystalline needles which were further purified by sublimation (120 °C, 1×10^{-2} mbar).

Ph_3B was found to be highly air and moisture sensitive. Already during the time needed for NMR characterization small amounts of decomposed material were observed.

Mp.: 128-133 °C (ref. 10: 142 °C)

^{1}H NMR (400 MHz, CD_2Cl_2) δ = 7.65–7.63 (m, 2 H, 2-H), 7.60–7.56 (m, 1 H, 4-H), 7.50–7.46 (m, 2 H, 3-H).

$^{13}C\{^1H\}$ NMR (101 MHz, CD_2Cl_2) δ = 143.7 (br, C_q, C-1), 139.1 (CH, C-2), 131.8 (CH, C-4), 127.9 (CH, C-3).

^{11}B NMR (128 MHz, CD_2Cl_2) δ = 67.9.

HRMS (EI^+) calcd *m/z* for $C_{18}H_{15}B^{\bullet+}$ ($M^{\bullet+}$) 242.1261; found 242.1249.

NMR data agree with those reported in ref. 11.

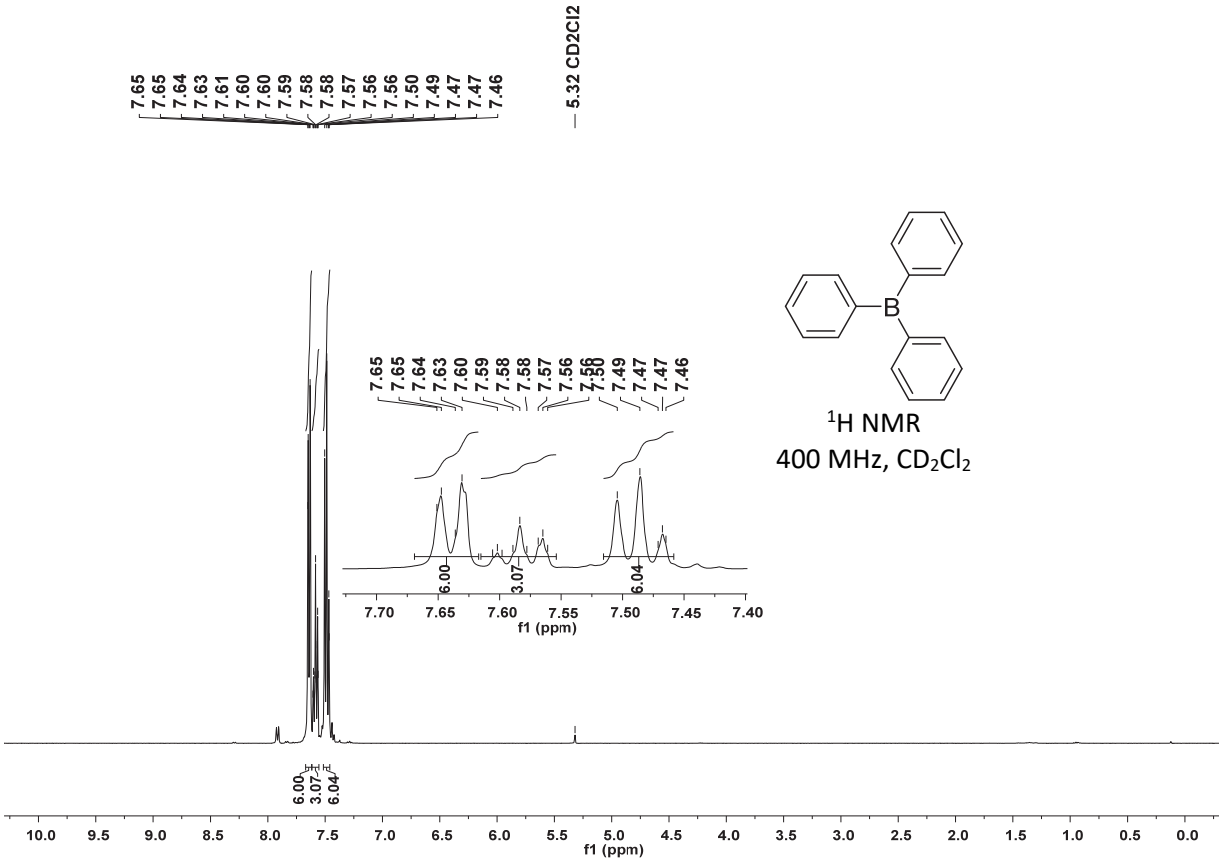
7.65
7.65
7.64
7.63
7.61
7.60
7.60
7.59
7.58
7.58
7.57
7.56
7.56
7.50
7.49
7.47
7.47
7.46
5.32 CD2Cl2
6.00
3.07
6.04
7.70
7.65
7.60
7.55
7.50
7.45
7.40
f1 (ppm)
B
^{1}H NMR
400 MHz, CD_2Cl_2
10.0
9.5
9.0
8.5
8.0
7.5
7.0
6.5
6.0
5.5
5.0
4.5
4.0
3.5
3.0
2.5
2.0
1.5
1.0
0.5
0.0
f1 (ppm)

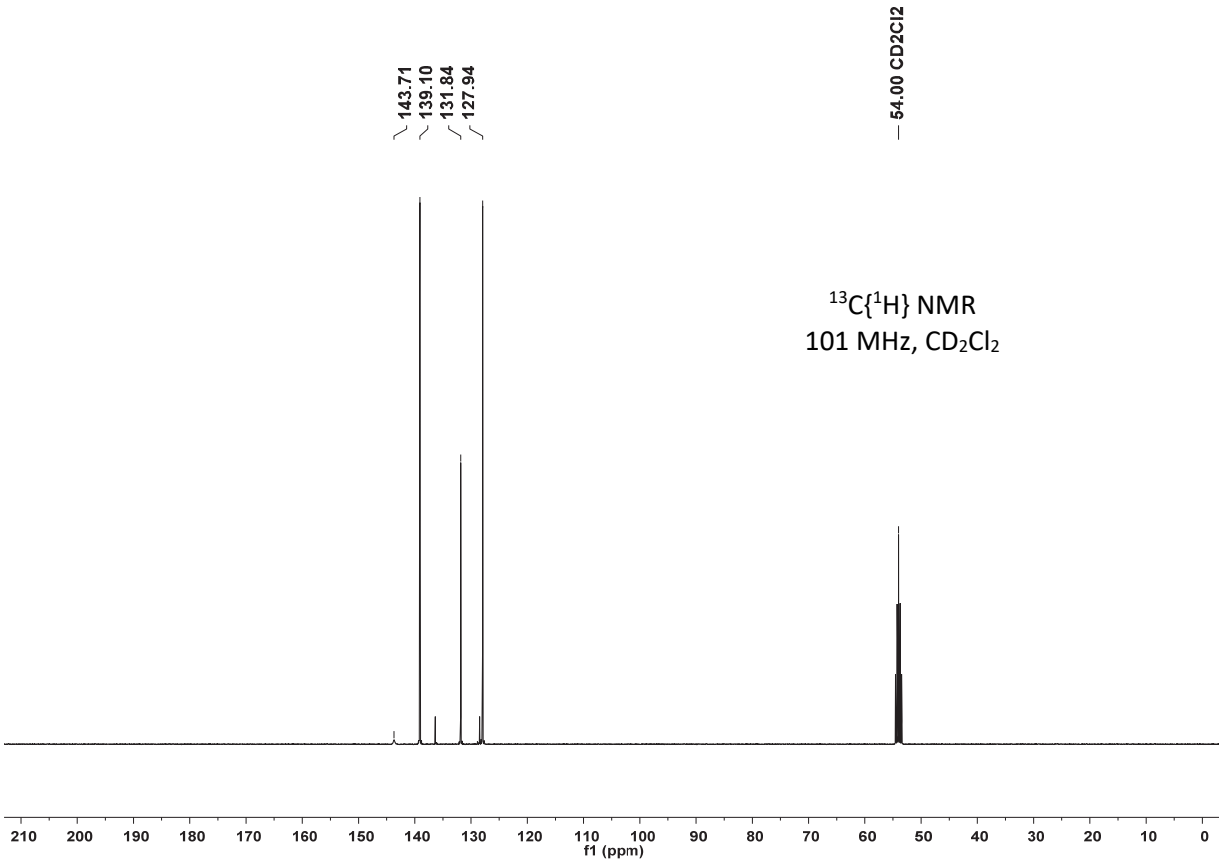
143.71
139.10
131.84
127.94
54.00 CD2Cl2
^{13}C{^{1}H} NMR
101 MHz, CD_2Cl_2
210
200
190
180
170
160
150
140
130
120
110
100
90
80
70
60
50
40
30
20
10
0
f1 (ppm)

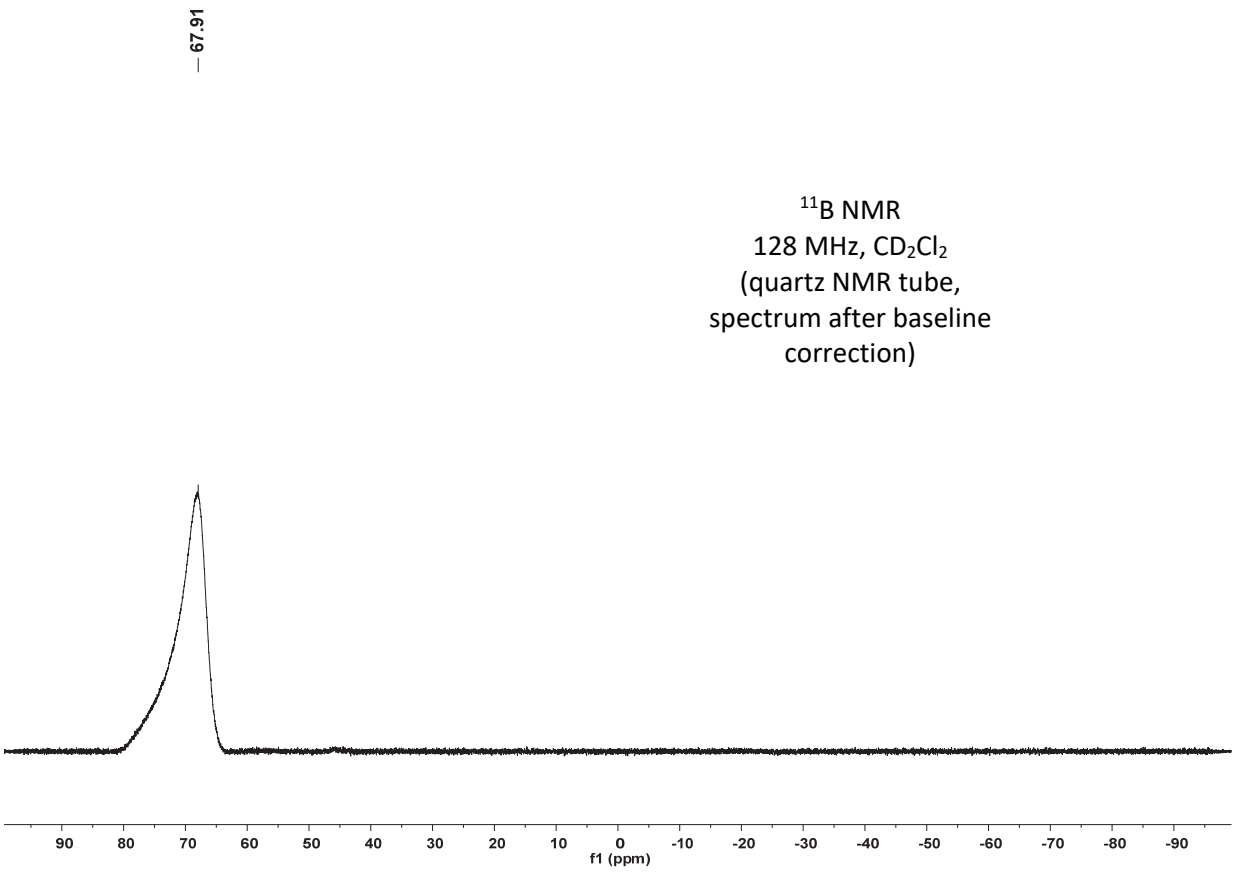

^{11}B NMR
128 MHz, CD_2Cl_2
(quartz NMR tube,
spectrum after baseline
correction)

Tris(4-fluorophenyl)borane (1e)

Synthesis according to the modified procedure in ref. 6.

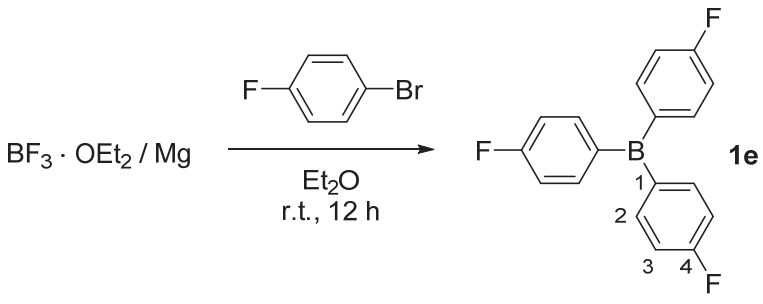

(RM1069)

A 100 mL Schlenk flask with reflux condenser was charged with magnesium turnings (854 mg, 35.1 mmol), flame dried under vacuum, and filled with dry nitrogen. Diethyl ether (20 mL) and freshly distilled $BF_3{\cdot}OEt_2$ (1.26 mL, 10.0 mmol) were added. To the vigorously stirred mixture, a solution of 4-bromo-1-fluorobenzene (3.30 mL, 30.2 mmol) in diethyl ether (20 mL) was added. The Grignard reaction was initiated by heating causing the suspension to turn brownish. The mixture was stirred for another 12 h to give a mixture of liquid two phases, whereupon all volatiles were removed under reduced pressure to form a solid. The residue was suspended in n-hexane (40 mL) and filtered through a Schlenk-frit and washed with n-hexane (10 mL) to give a clear filtrate, which was concentrated to dryness to give a solid residue. The crude product was recrystallized from n-hexane to give the borane **1e** (955 mg, 32%) as a soft yellow, crystalline solid.

Mp.: 99-113 °C

^{1}H NMR (400 MHz, CD_2Cl_2) δ = 7.63–7.59 (m, 6 H, 2-H), 7.21–7.15 (m, 6 H, 3-H).

^{13}C{^{1}H} NMR (101 MHz, CD_2Cl_2) δ = 165.9 (d, C_q, $J_{C,F}$ = 252.0 Hz, C-4), 141.5 (d, CH, $J_{C,F}$ = 8.4 Hz, C-2), 139.4 (br, C_q, C-1), 115.2 (d, CH, $J_{C,F}$ = 20.0 Hz, C-3).

^{11}B NMR (128 MHz, CD_2Cl_2) δ = 63.2.

^{19}F NMR (377 MHz, CD_2Cl_2) δ = -108.75 (tt, *J* = 9.3, 6.3 Hz)

HRMS (EI^{+}) calcd *m/z* for $C_{18}H_{12}F_3B^{\bullet+}$ ($M^{\bullet+}$) 296.0979; found 296.0984.

NMR data agree with those reported in ref. 12.

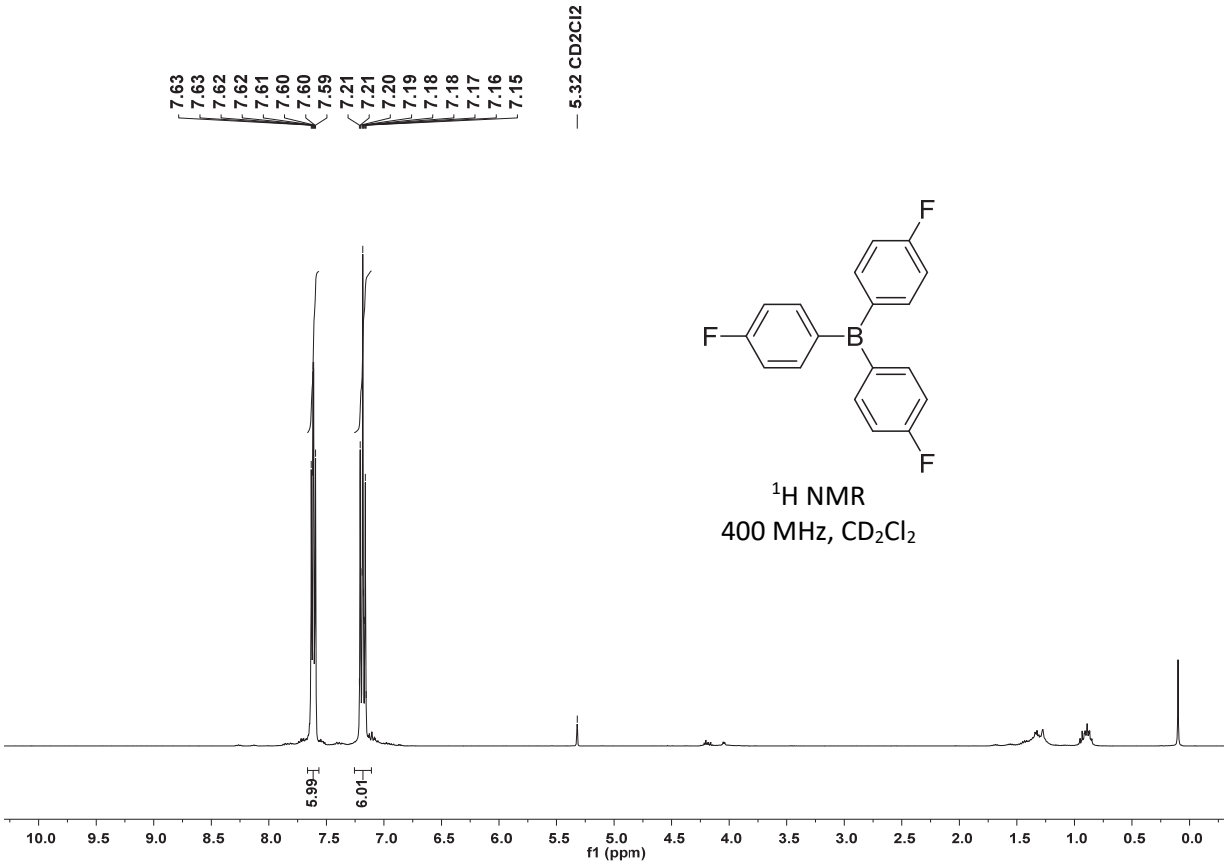

^{1}H NMR
400 MHz, CD_2Cl_2

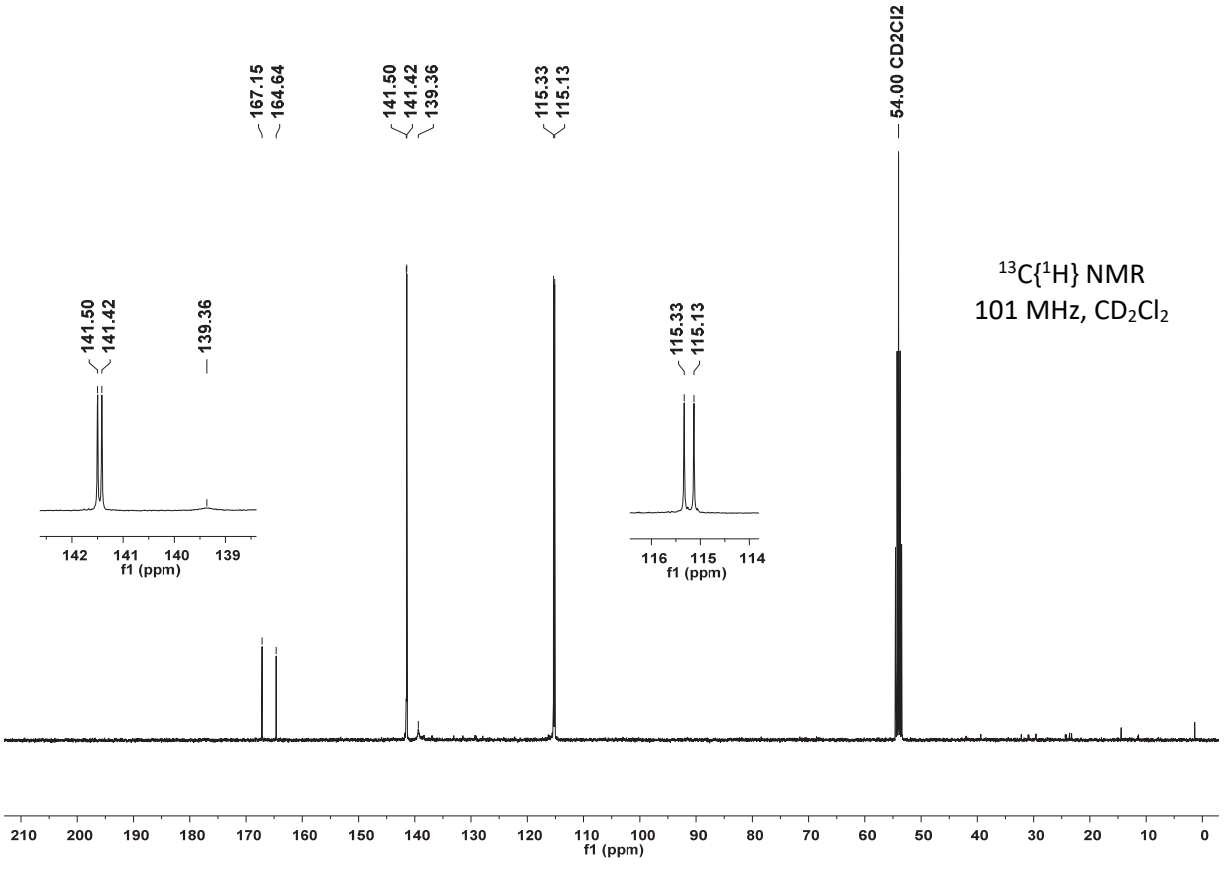

^{13}C{^{1}H} NMR
101 MHz, CD_2Cl_2

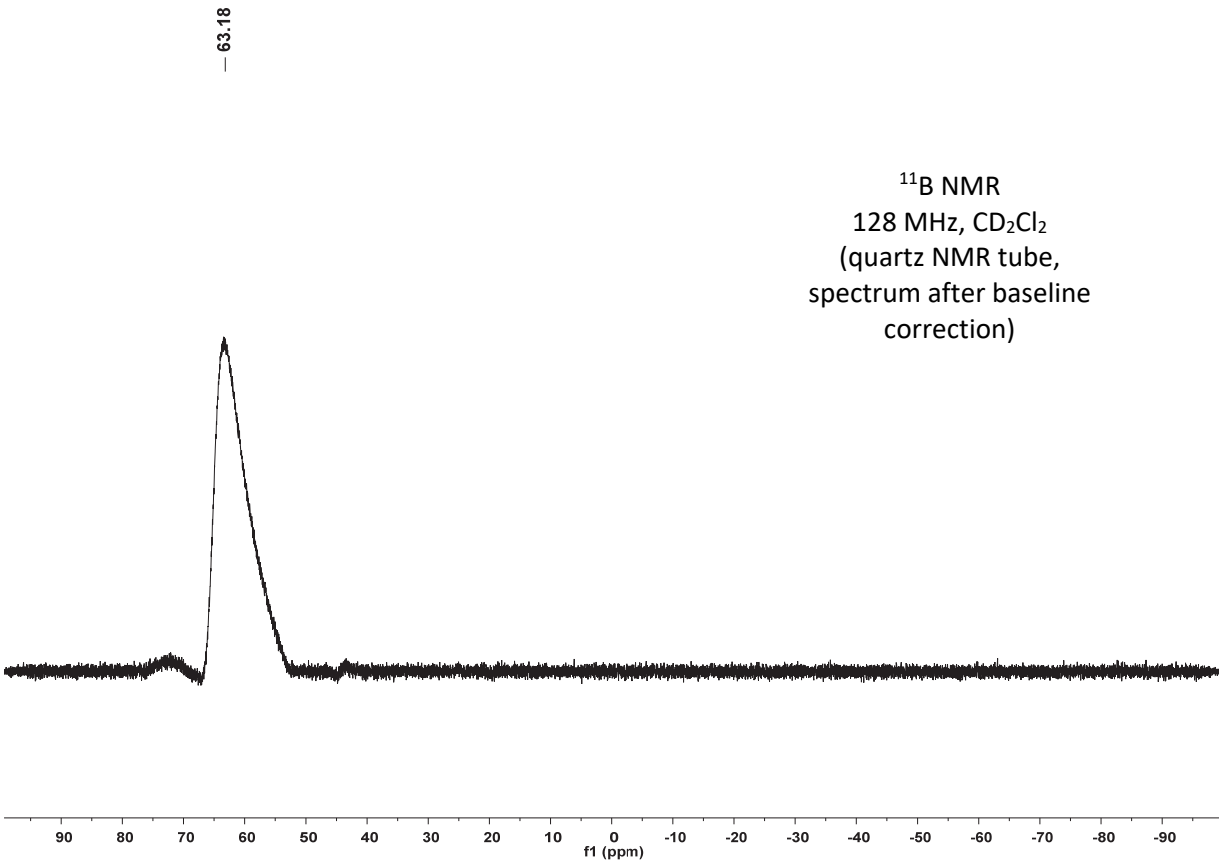

^{11}B NMR
128 MHz, CD_2Cl_2
(quartz NMR tube,
spectrum after baseline
correction)

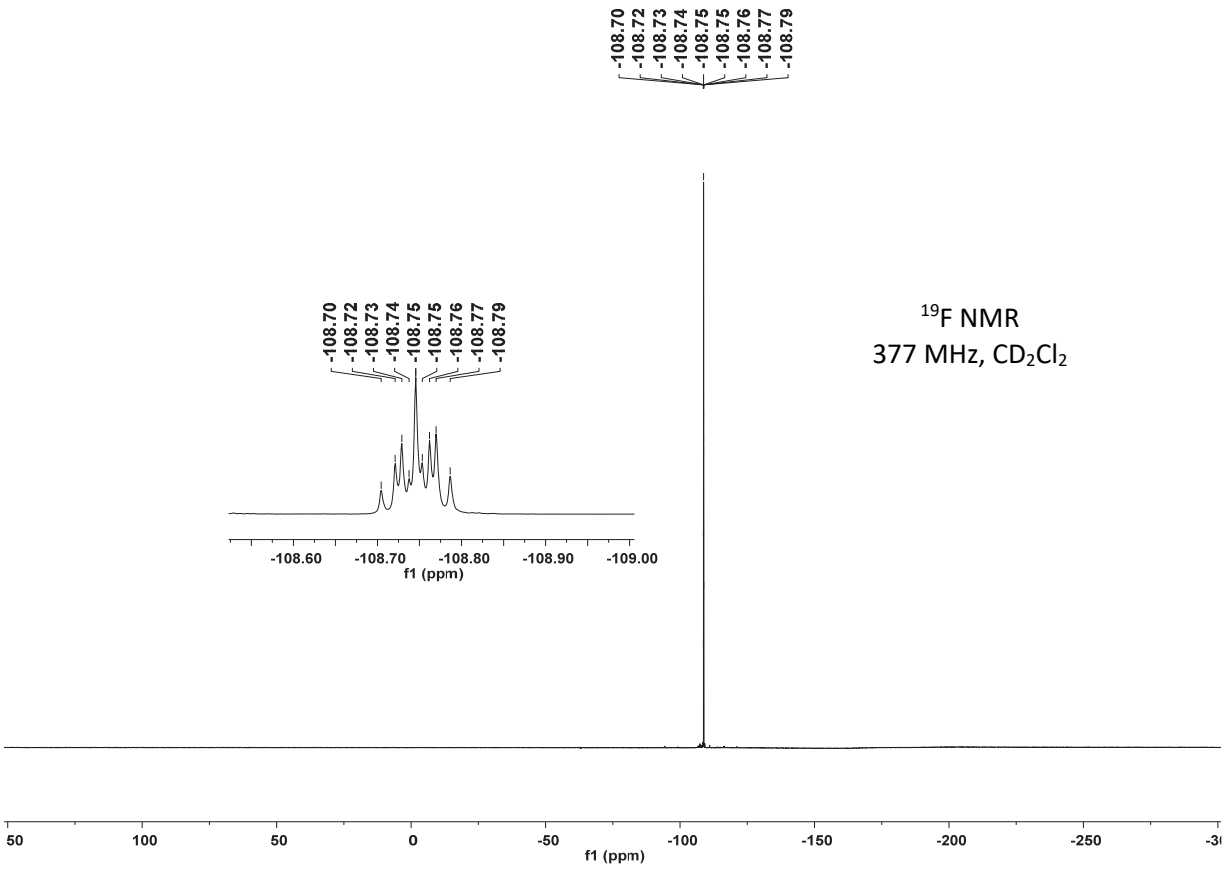

^{19}F NMR
377 MHz, CD_2Cl_2

Tris(4-chlorophenyl)borane (1f)

Synthesis according to the modified procedure in ref. 6.

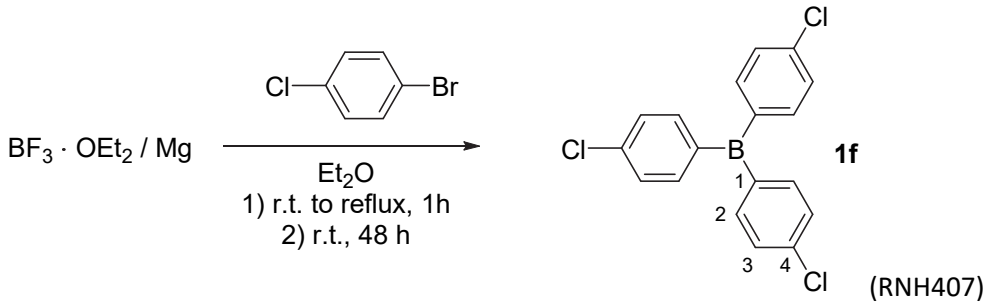

(RNH407)

A 100 mL Schlenk flask with reflux condenser was charged with magnesium turnings (853 mg, 35.1 mmol), flame dried under vacuum, and filled with dry nitrogen. Diethyl ether (20 mL) and freshly distilled $BF_3{\cdot}OEt_2$ (1.26 mL, 10.0 mmol) were added. To the vigorously stirred mixture, a solution of 4-bromo-1-chlorobenzene (5.78 g, 30.2 mmol) in diethyl ether (20 mL) was added. After about 10 mL of the bromoarene solution was added, heat was applied to initiate the Grignard reaction. Then the remaining 4-bromo-1-chlorobenzene solution was added. The mixture was stirred for another 12 h. Then volatiles were removed under reduced pressure. The residue was suspended in dichloromethane (40 mL) and filtrated through a Schlenk-frit. The clear solution was concentrated to dryness and the residue purified by sublimation (191 °C, 1.6×10^{-2} mbar) to give **1e** (885 mg, 26%) as colorless to pale yellow crystals.

Mp.: 166 °C (ref. 13: 197-202 °C)

^{1}H NMR (400 MHz, CD_2Cl_2) δ = 7.54–7.52 (m, 6 H), 7.48–7.46 (m, 6 H).

$^{13}C\{^1H\}$ NMR (101 MHz, CD_2Cl_2) δ = 141.2 (br, C_q, C-4), 140.3 (CH), 138.8 (C_q, C-1), 128.4 (CH).

^{11}B NMR (128 MHz, $CDCl_3$) δ = 66.3.

HRMS (EI^+) calcd *m/z* for $C_{18}H_{12}BCl_3^{\bullet+}$ ($M^{\bullet+}$) 344.0092; found 344.0093.

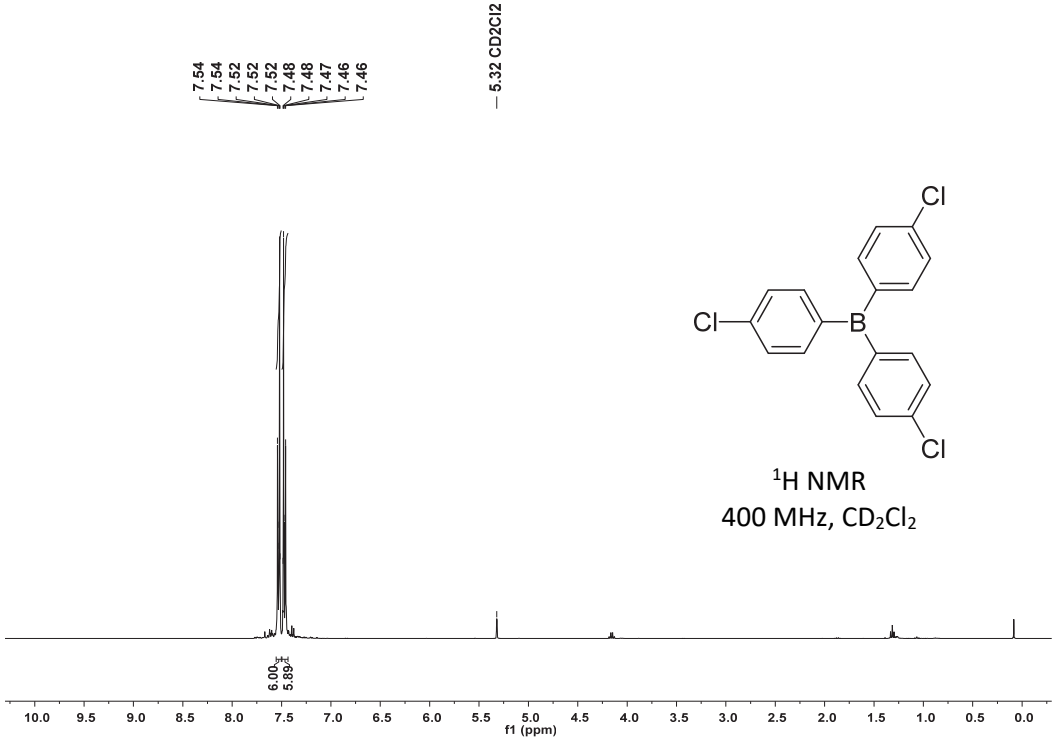

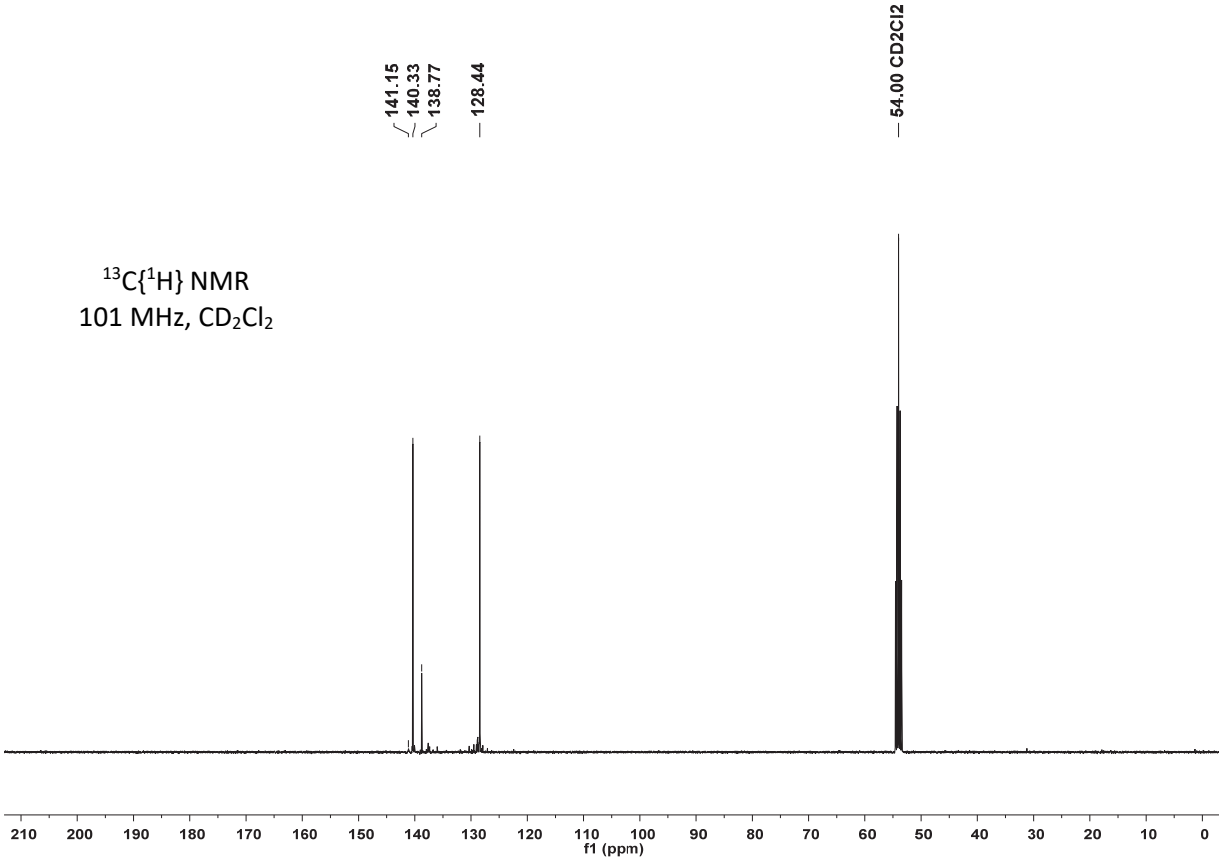

$^{13}C\{^{1}H\}$ NMR
101 MHz, CD_2Cl_2

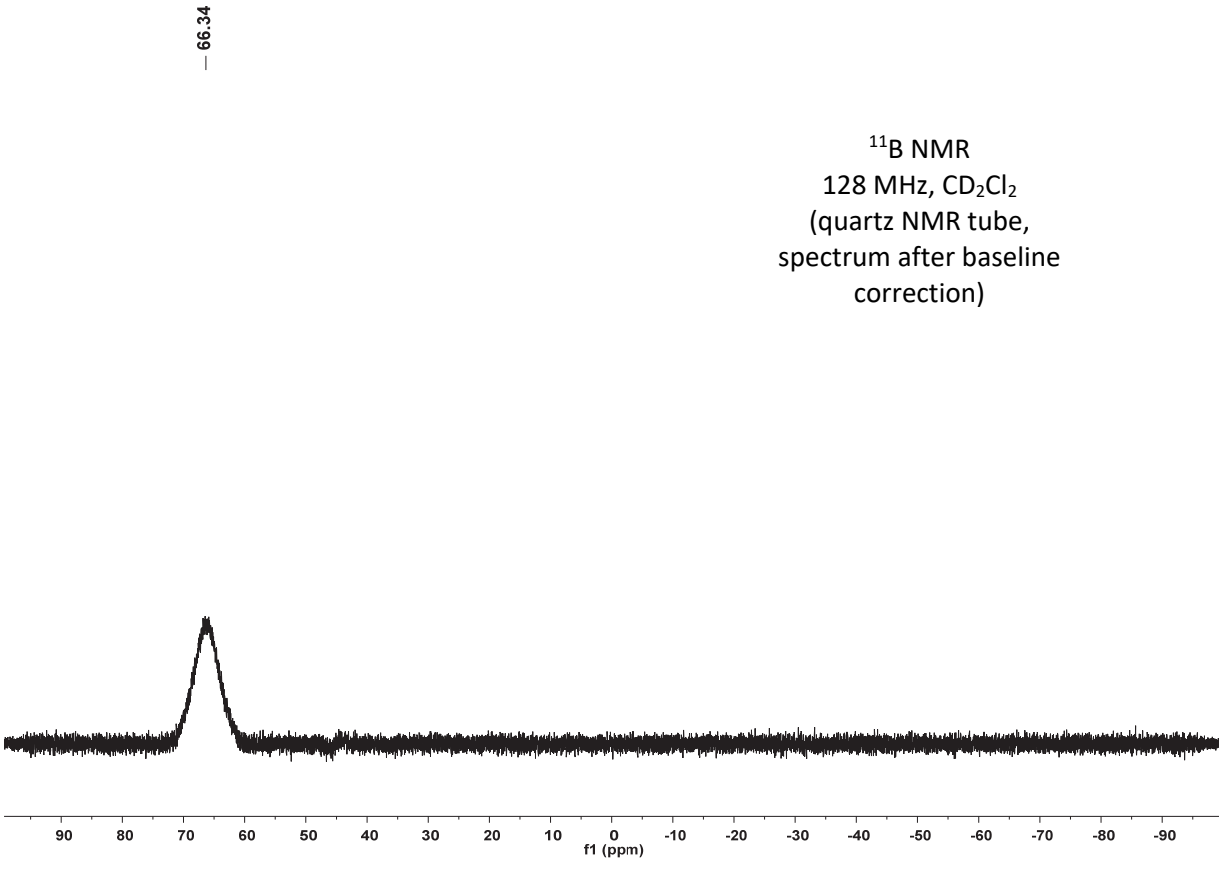

^{11}B NMR
128 MHz, CD_2Cl_2
(quartz NMR tube,
spectrum after baseline
correction)

Tris(2,4,6-trifluorophenyl)borane (1g)

Synthesis according to the modified procedure in ref. 14.

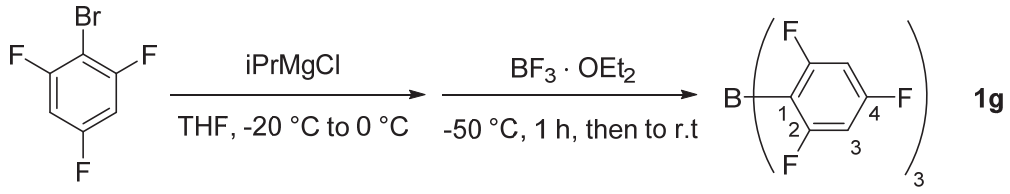

1g

(RM1072)

In a 100 mL flame dried Schlenk flask under nitrogen was dissolved 1-bromo-2,4,6-trifluorobenzene (3.50 mL, 30 mmol) in THF (100 mL). The solution was cooled to -20 °C and isopropylmagnesium chloride (2.0 M solution in THF, 15 mL, 30 mmol) was added in portions. The solution was allowed to warm to 0 °C over a period of 1 h and subsequently cooled to -50 °C. At -50 °C, freshly distilled $BF_3{\cdot}OEt_2$ (1.26 mL, 10.0 mmol) was added. The solution was stirred at -50°C for another 60 min. The solution was subsequently allowed to warm up to room temperature within 2 d. Next, all volatiles were removed. The residue was suspended in n-hexane (40 mL) and filtered through a Schlenk-frit. After washing of the solid with n-hexane (20 mL) and concentration of the filtrate the crude product was furnished as a colorless solid. Purification by sublimation (120 °C, 1×10^{-3} mbar) afforded **1g** (524 mg, 13%) as colorless, crystalline solid.

Mp.: 106-111 °C

^{1}H NMR (400 MHz, CD_2Cl_2) δ = 6.72–6.65 (m, 6 H).

^{13}C NMR (101 MHz, CD_2Cl_2) δ = 167.1 (C_q, dt, *J* = 256.0 Hz, 16.6 Hz, C-4), 166.6 (C_q, dt, $J_{C,F}$ = 252.2 Hz, *J* = 14.9 Hz, C-2), 101.3–100.5 (m, CH, C-3). The resonance for C-1 was not detected.

^{11}B NMR (128 MHz, $CDCl_3$) δ = 59.5.

^{19}F NMR (377 MHz, CD_2Cl_2) δ = -96.4 (app t, *J* = 8.2 Hz, 6 F, 2-F), -100.9 (app pent, *J* = 9.8 Hz, 3 F, 4-F).

HRMS (EI^+) calcd *m/z* for $C_{18}H_6BF_9^{\bullet+}$ ($M^{\bullet+}$) 404.0413; found 404.0398.

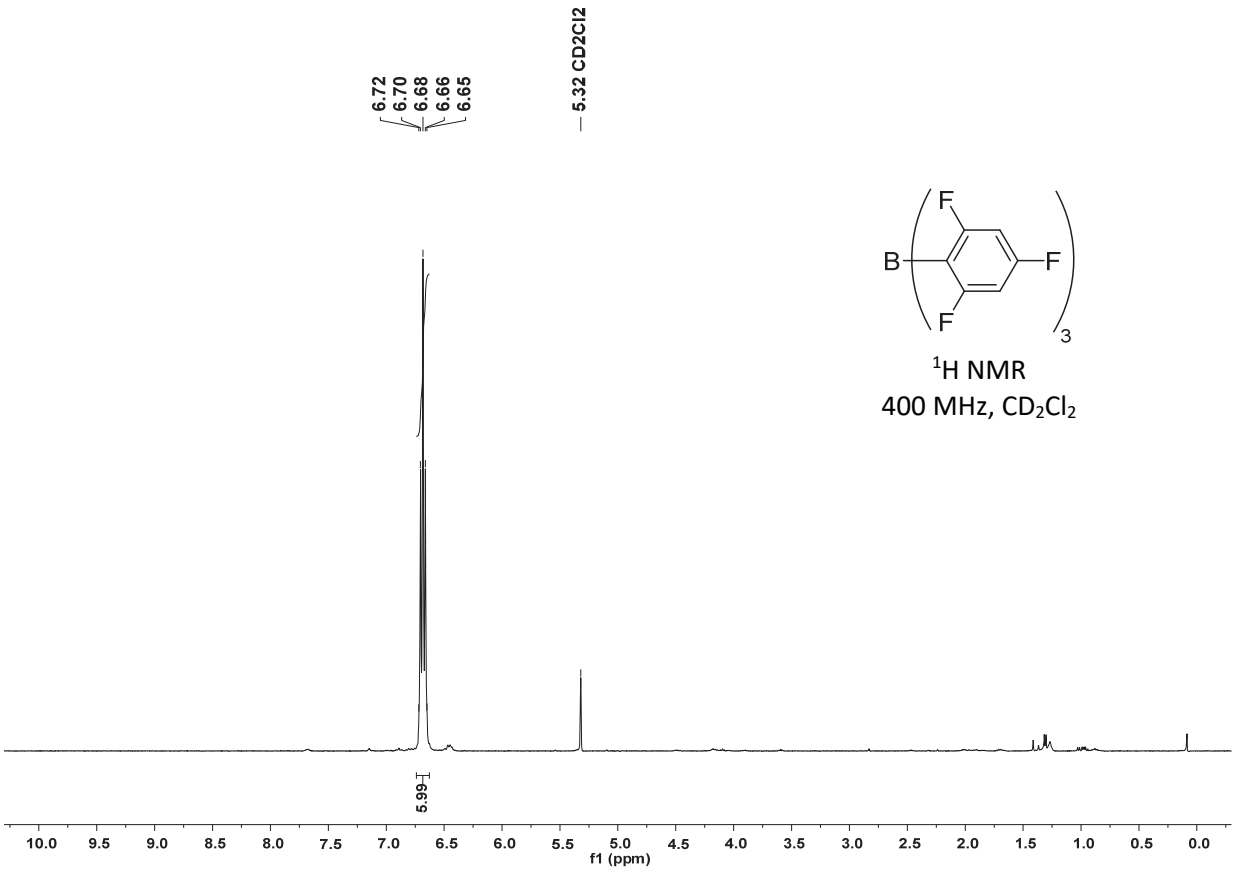

^{1}H NMR
400 MHz, CD_2Cl_2

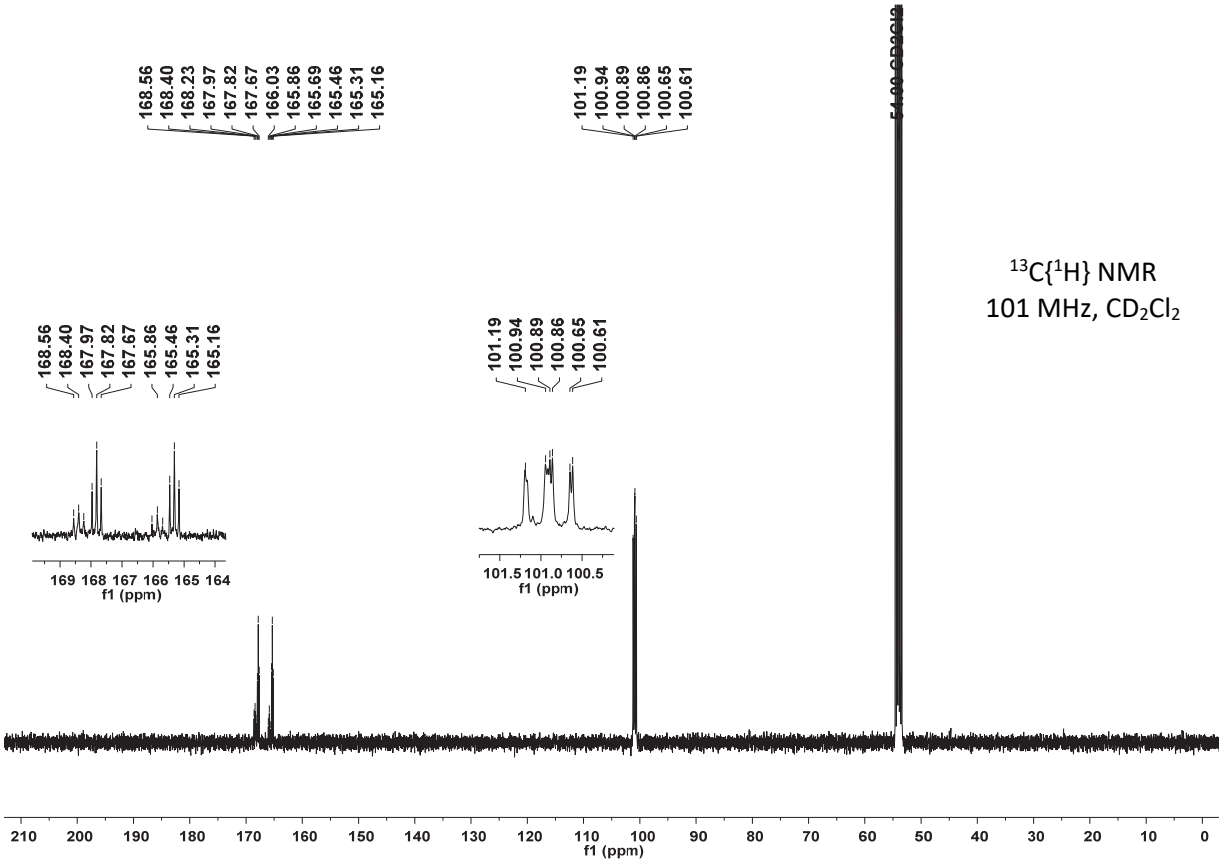

$^{13}C\{^{1}H\}$ NMR
101 MHz, CD_2Cl_2

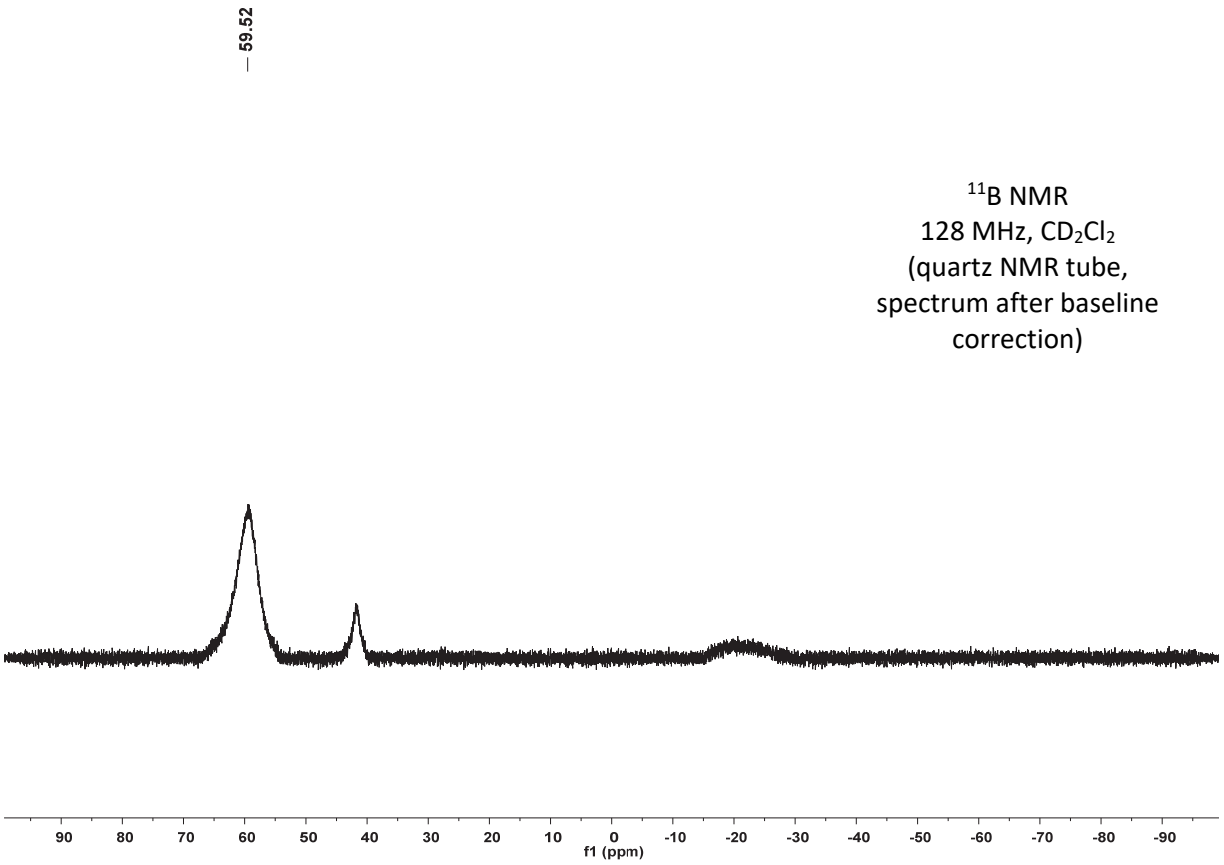

^{11}B NMR
128 MHz, CD_2Cl_2
(quartz NMR tube,
spectrum after baseline
correction)

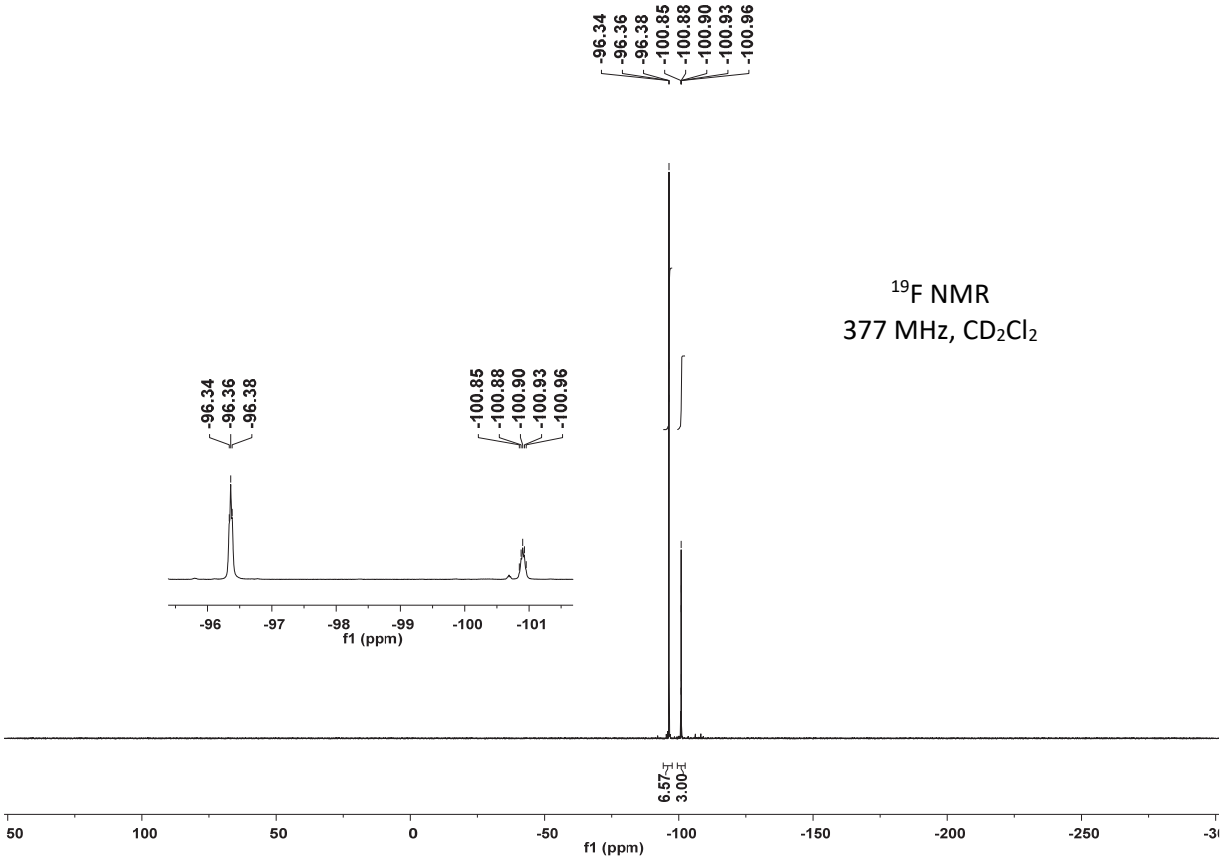

^{19}F NMR
377 MHz, CD_2Cl_2

Tris(3,4,5-trifluorophenyl)borane (1h)

Synthesis according to the modified procedure in ref. 14.

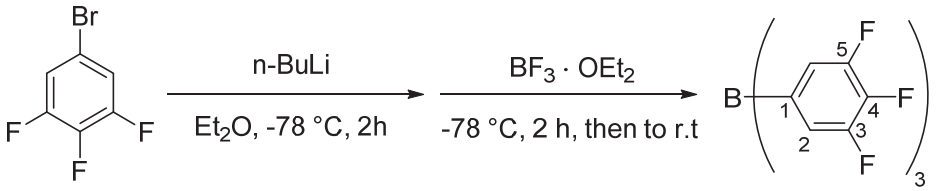

(RNH415)

In a 250 mL flame dried Schlenk flask under nitrogen was added 1-bromo-3,4,5-fluorobenzene (7.02 mL, 58.8 mmol) and diethyl ether (100 mL). The solution was cooled to -78 °C and n-BuLi (2.3 M, 25.6 mL, 58.8 mmol) was added slowly to give a milky suspension. Stirring was continued for 2 h at -78 °C whereupon freshly distilled $BF_3{\cdot}OEt_2$ (2.39 mL, 19.4 mmol) was added and the mixture stirred for an additional 2 h at -78 °C. The mixture was allowed to warm up to room temperature overnight and all volatiles were removed under reduced pressure. The residue was suspended in pentane, the solvent again removed and the crude product purified by sublimation (150 °C, 8×10^{-3} mbar) to give the borane as yellowish, oily crystals. The sublimated material was suspended in n-hexane (5 mL) and the solvent removed with a Pasteur pipette (repeated two more times) to give the borane as colorless solid (2.20 g, 28%).

Mp.: 160-177 °C

^{1}H NMR (400 MHz, CD_2Cl_2) δ = 7.24–7.16 (m, 6 H, 2-H).

$^{13}C\{^{1}H\}$ NMR (101 MHz, CD_2Cl_2) δ = 151.5 (C_q, ddd, *J* = 252.8 Hz, 9.6 Hz, 2.9 Hz, C-3), 143.2 (C_q, dt, *J* = 259.0 Hz, 15.2 Hz, C-4), 137.0–136.8 (C_q, m, C-1), 122.5 (CH, dd, *J* = 13.7 Hz, 5.0 Hz, C-2).

^{11}B NMR (128 MHz, CD_2Cl_2) δ = 64.7.

^{19}F NMR (377 MHz, CD_2Cl_2) δ = (-134.6) – (-134.7) (m, 6 F, 3-F and 5-F), (-154.1) – (-154.2) (m, 3 F, 4-F).

HRMS (EI^+) calcd *m/z* for $C_{18}H_6BF_9^{\bullet+}$ ($M^{\bullet+}$) 404.0413; found 404.0409.

NMR data agree with those reported in ref. 14.

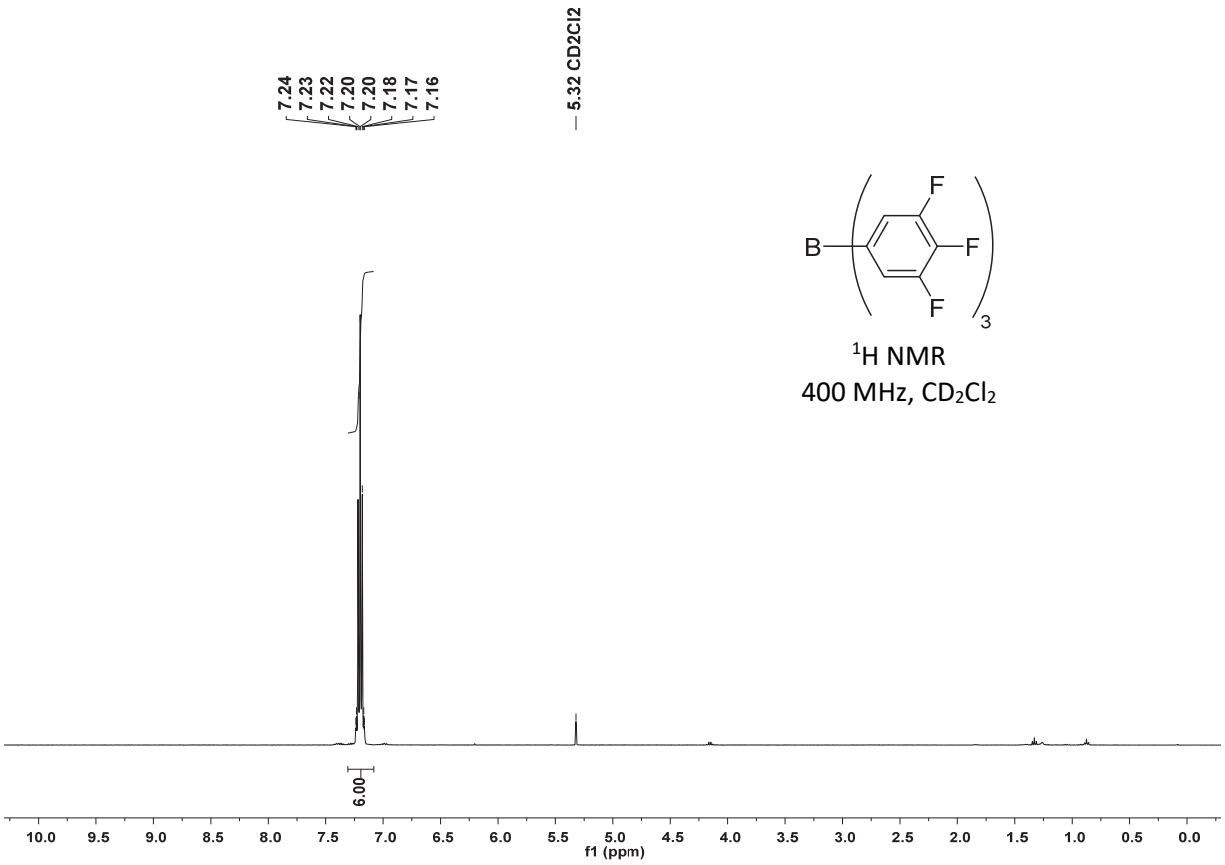

^{1}H NMR
400 MHz, CD_2Cl_2

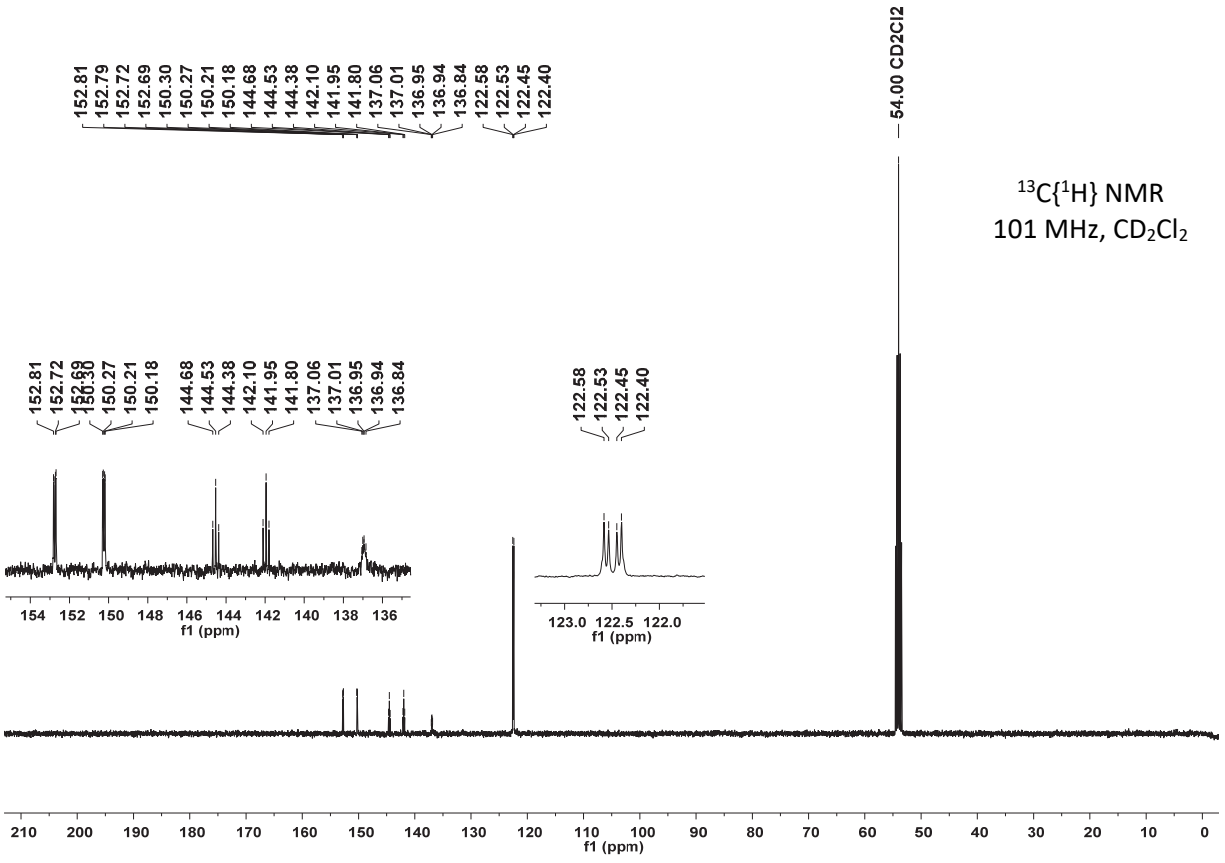

^{13}C{^{1}H} NMR
101 MHz, CD_2Cl_2

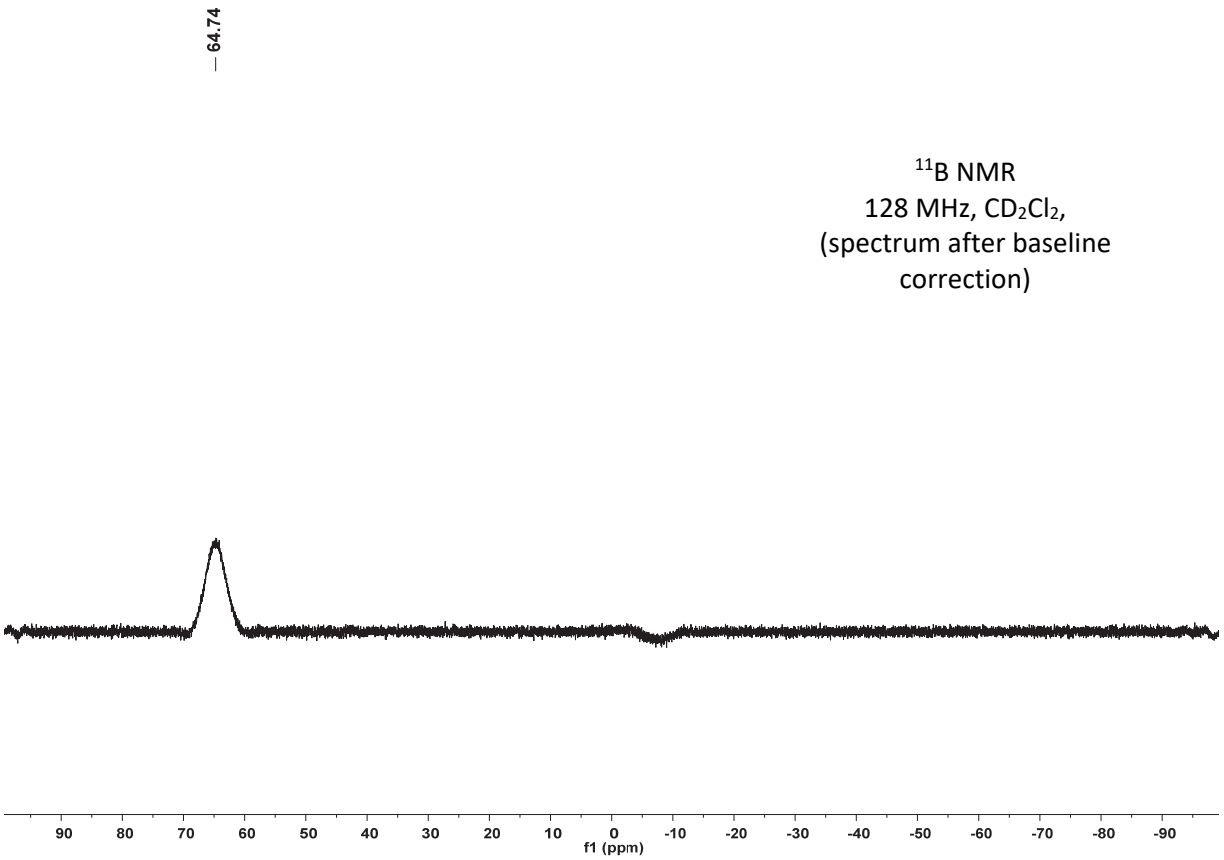

^{11}B NMR
128 MHz, CD_2Cl_2,
(spectrum after baseline correction)

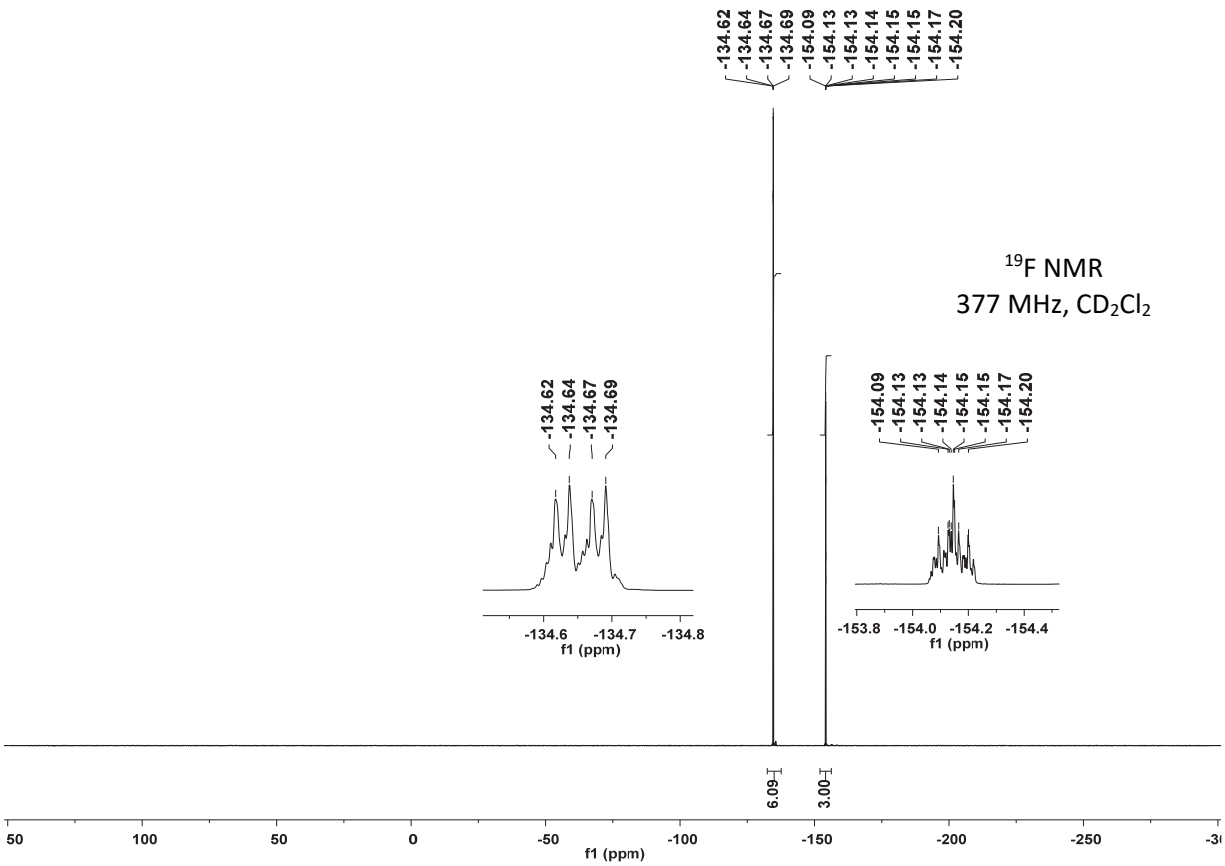

^{19}F NMR
377 MHz, CD_2Cl_2

Tris(pentafluorophenyl)borane (1i)

Synthesis according to the modified procedure in ref. 15.

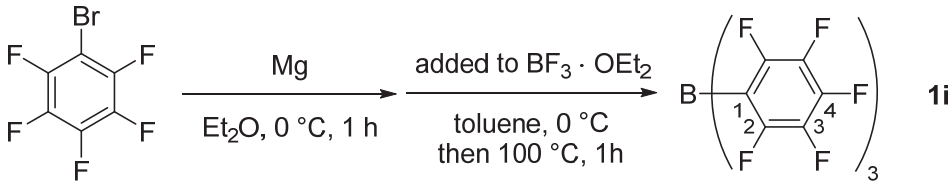

1i

(RNH344)

In a flame dried 500 mL three necked round bottom flask with nitrogen inlet and reflux condenser under nitrogen was added magnesium turnings (2.43 g, 0.100 mol) and diethyl ether (167 mL). Bromopentafluorobenzene (12.5 mL, 0.100 mol) was added dropwise under stirring. After the initiation of the Grignard reaction the reaction mixture was cooled with an ice-bath. After stirring for another 60 min at 0 °C, the Grignard solution was transferred via syringe techniques into a separate flame dried flask containing a solution of $BF_3{\cdot}OEt_2$ (4.10 mL, 0.033 mol) in toluene (67 mL) at 0 °C. After the transfer of the Grignard reagent was complete, the reaction mixture was allowed to warm at room temperature while diethyl ether was removed under reduced pressure. The remaining toluene solution was heated to 100 °C for 1 h. Then concentration to dryness yielded a beige solid residue. n-Hexane (200 mL) was added and the mixture was heated to 45 °C under vigorous stirring. The suspension was filtrated through a pre-heated Schlenk frit. The clear filtrate was cooled to 5 °C causing the formation of feathery, colorless crystals. Filtration through a Schlenk frit, washing with n-hexane (20 mL) and drying gave pure **1i** (8.74 g, 52%).

Mp.: 133-134 °C (ref. 16: 197-202 °C)

$^{13}C\{^1H\}$ NMR (101 MHz, CD_2Cl_2) δ = 150.3–147.6 (m), 147.1–144.1 (m), 139.6–136.7 (m), 113.9–113.3 (m, C_q, C-1).

^{11}B NMR (128 MHz, CD_2Cl_2) δ = 58.8.

^{19}F NMR (377 MHz, CD_2Cl_2) δ = -128.2 (s, 2 F, 2-F), -143.9 (s, 1 F, 4-F), (-161.0) – (-161.1) (m, 2 F, 3-F).

HRMS (EI^+) calcd *m/z* for $C_{18}BF_{15}^{\bullet+}$ ($M^{\bullet+}$) 511.9848; found 511.9846.

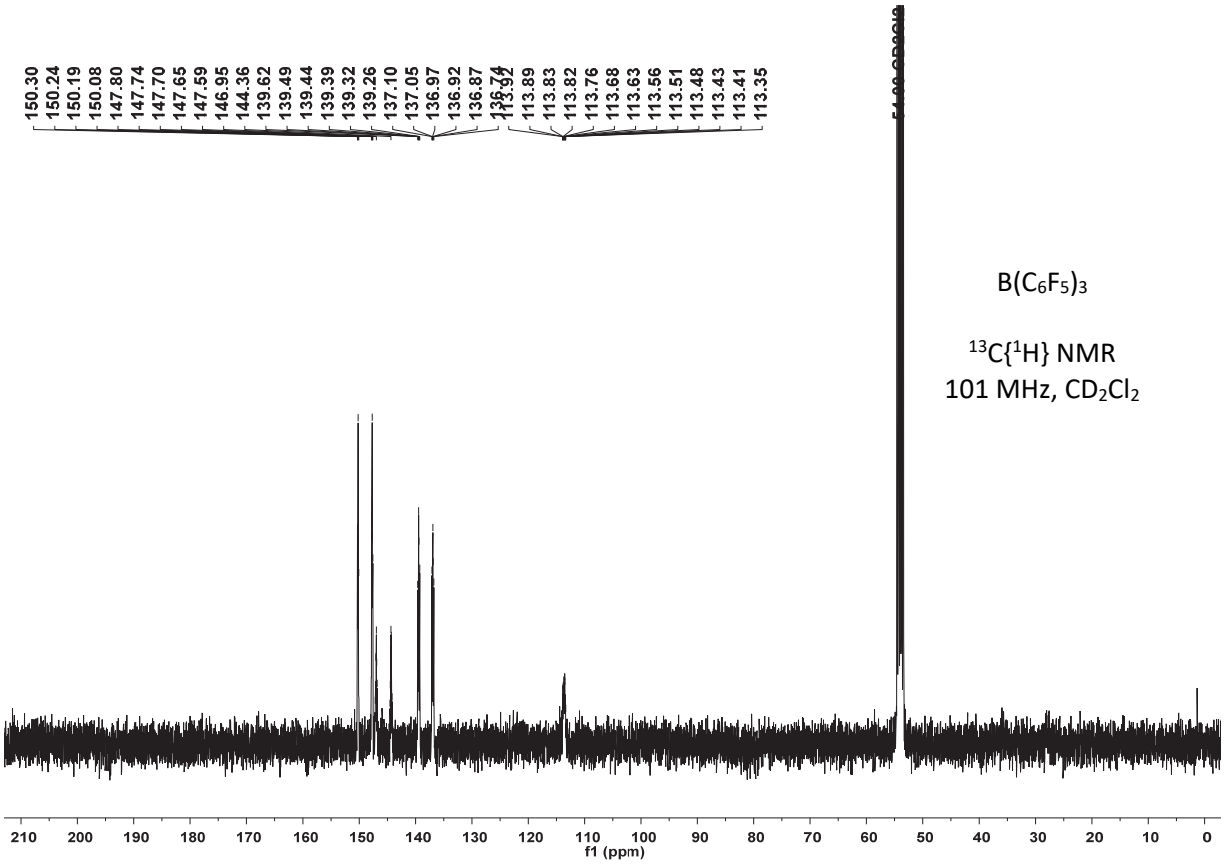

$B(C_6F_5)_3$

$^{13}C\{^1H\}$ NMR
101 MHz, CD_2Cl_2

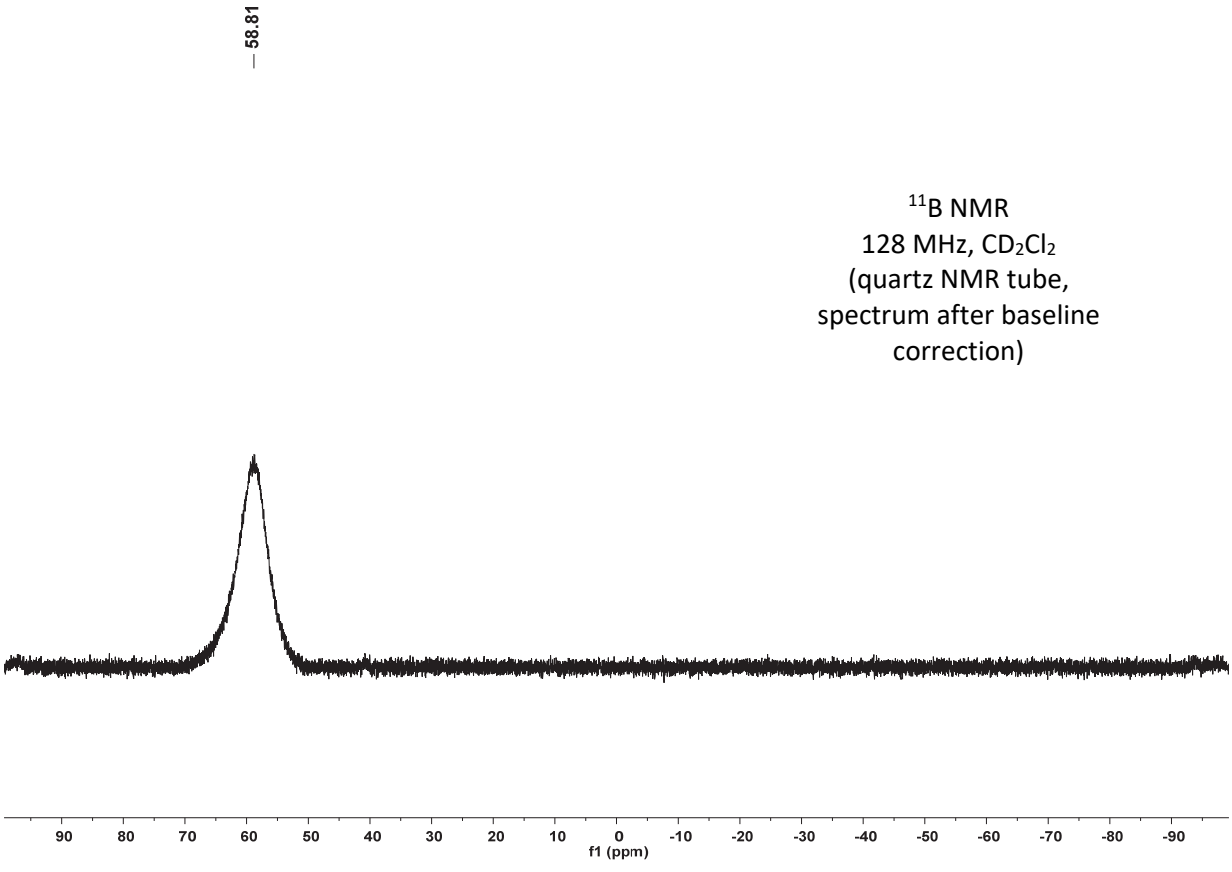

^{11}B NMR
128 MHz, CD_2Cl_2
(quartz NMR tube,
spectrum after baseline
correction)

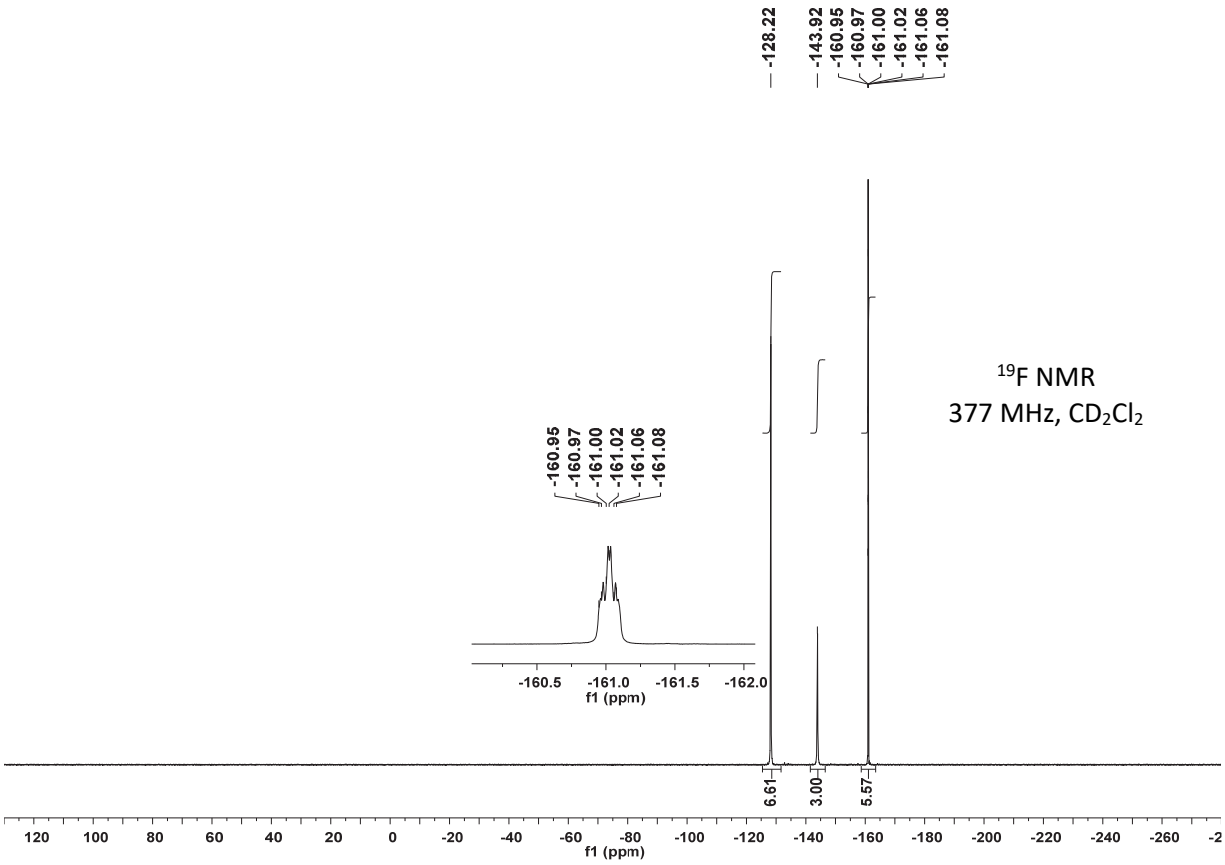
-128.22
-143.92
-160.95
-160.97
-161.00
-161.02
-161.06
-161.08
^{19}F NMR
377 MHz, CD_2Cl_2
-160.5
-161.0
-161.5
-162.0
f1 (ppm)
6.61
3.00
5.57
120 100 80 60 40 20 0 -20 -40 -60 -80 -100 -120 -140 -160 -180 -200 -220 -240 -260
f1 (ppm)

3,5-Dinitropyridine (2l)

Synthesis according to the modified procedure in ref. 17.

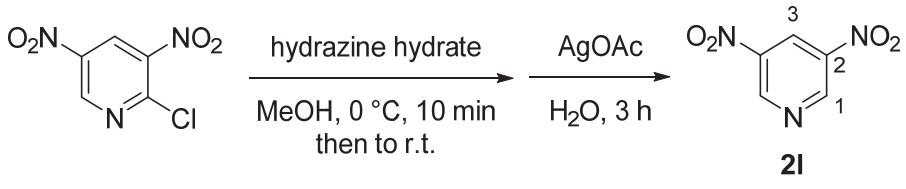

2l (RNH414)

In a 100 mL round-bottom flask was dissolved 2-chloro-3,5-dinitropyridine (2.00 g, 9.83 mmol) in methanol (20 mL). The resulting yellow solution was cooled at 0 °C and hydrazine monohydrate (0.77 mL, 15.8 mmol) was added dropwise over a period of 10 min causing the formation of a dark-brown precipitate. Stirring was continued overnight at room temperature and gave a red suspension. The suspension was filtrated. The collected solid material was washed with MeOH (2 × 10 mL) and dried to give a red-brownish solid (1.61 g), which was used without further purification.

The solid was suspended in water (53 mL), and silver acetate (4.83 g, 28.9 mmol) was added. The brown suspension was heated for 3 h under reflux which led to decolorization. After cooling to room temperature a pH 9 was adjusted with 25% aq NaOH. Then the mixture was extracted with diethyl ether (3 x 100 mL). The combined organic phases were dried over Na_2SO_4, filtrated and concentrated under reduced pressure. The crude product was recrystallized from ethanol to yield pyridine **2l** (487 mg, 29%) as a yellow-orange crystalline solid.

Mp.: 105-107 °C (ref. 17: 106 °C)

^{1}H NMR (400 MHz, DMSO-d_6) δ = 9.74 (d, *J* = 2.3 Hz, 2 H, 1-H), 9.13 (t, *J* = 2.3 Hz, 1 H, 3-H).

^{13}C{^{1}H} NMR (101 MHz, d_6-DMSO) δ = 149.5 (CH, C-1), 144.1 (C_q, C-2), 127.0 (CH, C-3).

HRMS (EI$^+$) calcd *m/z* for $C_5H_3N_3O_4^{\bullet+}$ ($M^{\bullet+}$) 169.0118; found 169.0120.

NMR data agree with those reported in ref. 18.

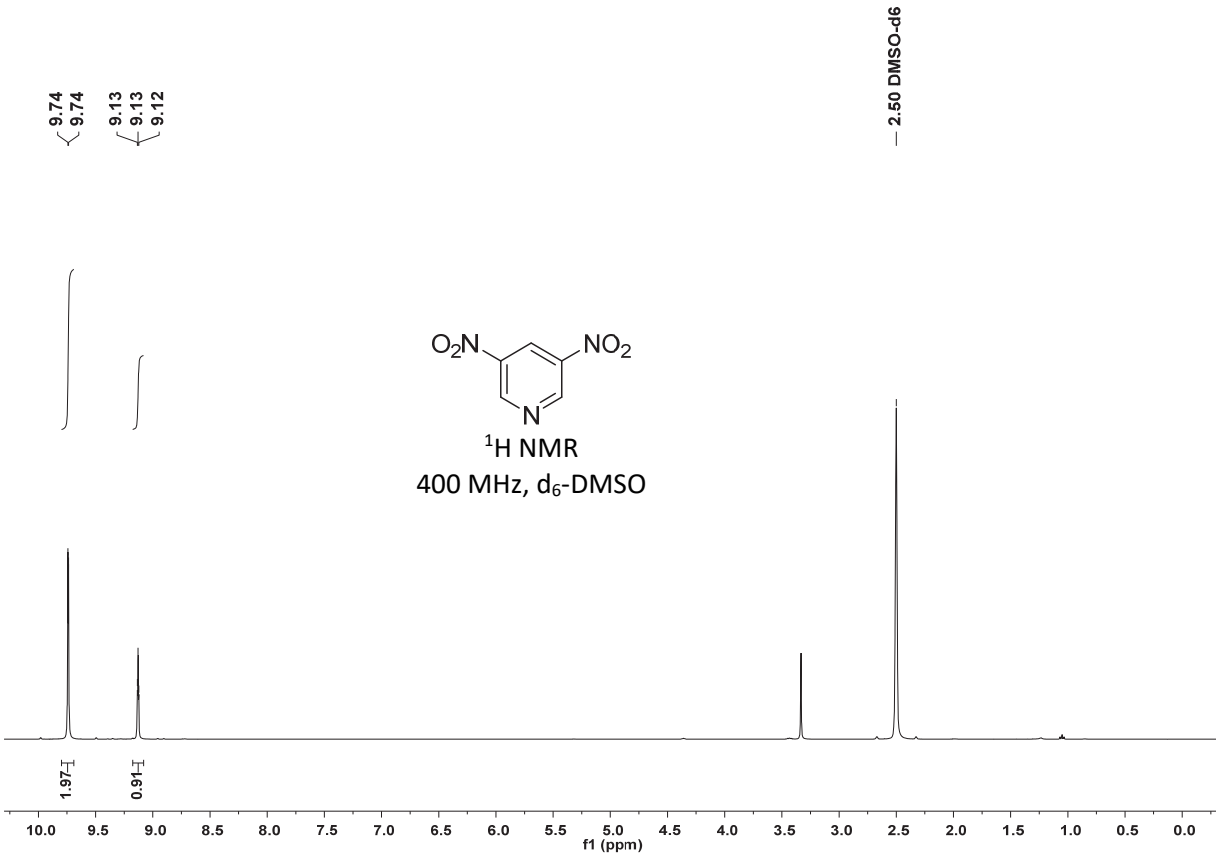
9.74
9.74
9.13
9.13
9.12
2.50 DMSO-d6
O_2N
NO_2
N
^{1}H NMR
400 MHz, d_6-DMSO
1.97
0.91
f1 (ppm)

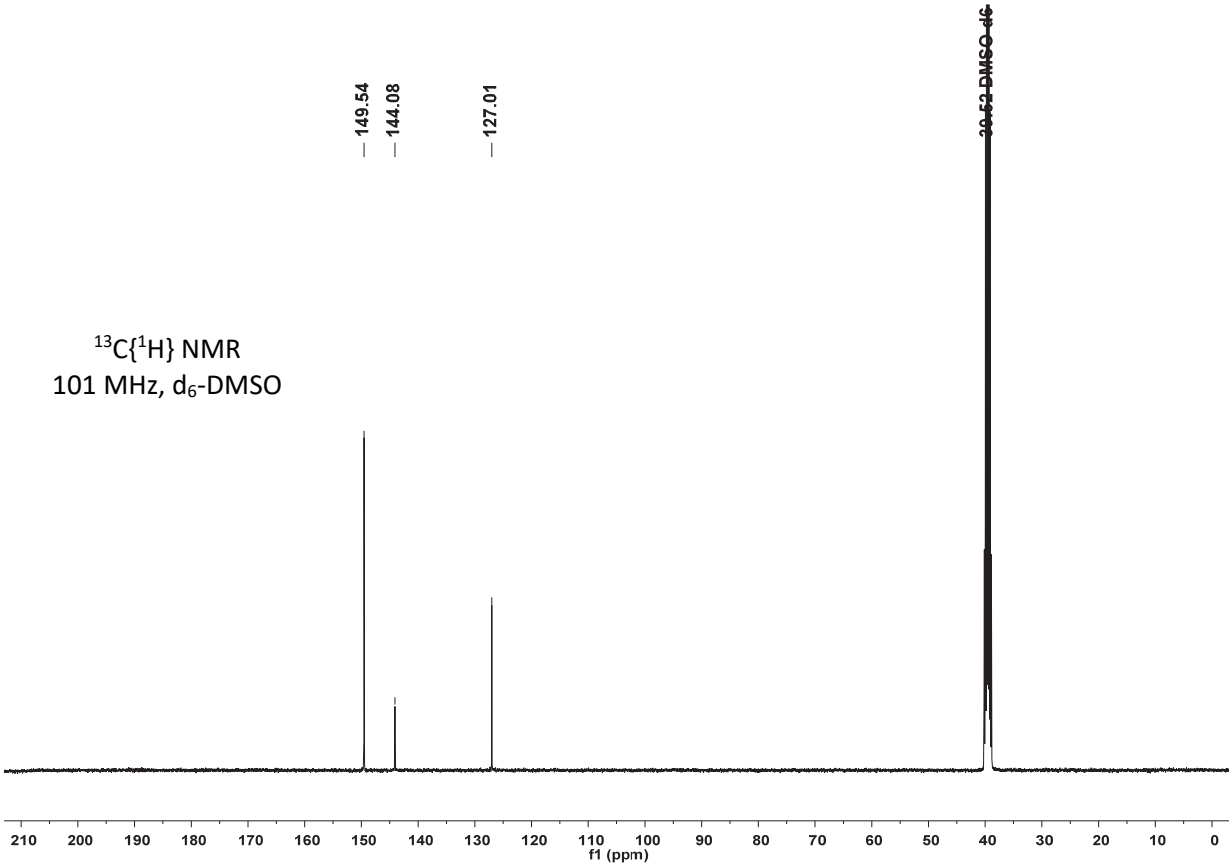
149.54
144.08
127.01
39.52 DMSO-d6
^{13}C{^{1}H} NMR
101 MHz, d_6-DMSO
f1 (ppm)

4-Chloro-3,5-dinitropyridine (2m)

Caution: *This reaction uses highly corrosive chemicals and produces large amounts of nitrous oxides. The reaction has to be carried out in a well ventilated fume hood.*

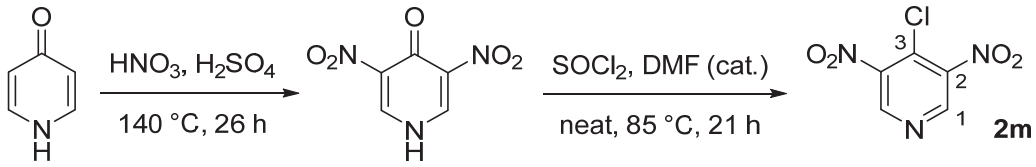

(RM1159,RM1161)

The pyridine **2m** was prepared according to the modified procedure in ref.[19] A 100 mL round bottom flask with reflux condenser and drying tube ($CaCl_2$) was charged with H_2SO_4 (96%, 25 mL). 4-Pyridone (2.0 g, 21 mmol) was added, followed by HNO_3 (100%, 7 mL). The resulting solution was heated under stirring to 140 °C for 26 h (progress monitored by NMR spectroscopy). The reaction mixture was poured into ice cold water (100 mL) causing the precipitation of the product, which was collected by filtration. The crude product was recrystallized from an 1:1 mixture of acetic acid/water (100 mL) to give the product as colorless needles (2.12 g, 55%).

Synthesis according to the modified procedure in ref. 20. In a 20 × 1.5 cm pressure tube (Ace glassware) was added 3,5-dinitro-4-pyridone (2.12 g, 11.5 mmol), thionyl chloride (1.66 mL, 22.9 mmol) and DMF (2 drops). The pressure tube was sealed under nitrogen and heated at 85 °C overnight. The initially solid mixture slowly converted to a suspension and yielded a clear yellow solution after 21 h. After cooling to room temperature the mixture was transferred into a Schlenk flask, washed with dichloromethane (2 mL), and all volatiles were removed under reduces pressure to give a pale yellow solid. The crude product was recrystallized from cyclohexane to yield **2m** (1.02 g, 44%) as colorless crystalline solid.

Pyridine **2m** is highly moisture sensitive and was stored at -35 °C in an argon filled glovebox.

Mp.: 69-71 °C (ref. 21: 68-70 °C)

^{1}H NMR (400 MHz, $CDCl_3$) δ = 9.22 (s, 2 H, 1-H).

$^{13}C\{^1H\}$ NMR (101 MHz, $CDCl_3$) δ =148.4 (CH, C-1), 145.4 (C_q, C-3), 131.4 (C_q, C-2).

HRMS (EI^+) calcd *m/z* for $C_5H_2ClN_3O_4^{\bullet+}$ ($M^{\bullet+}$) 202.9728; found 202.9725.

NMR data agree with those reported in ref. 20.

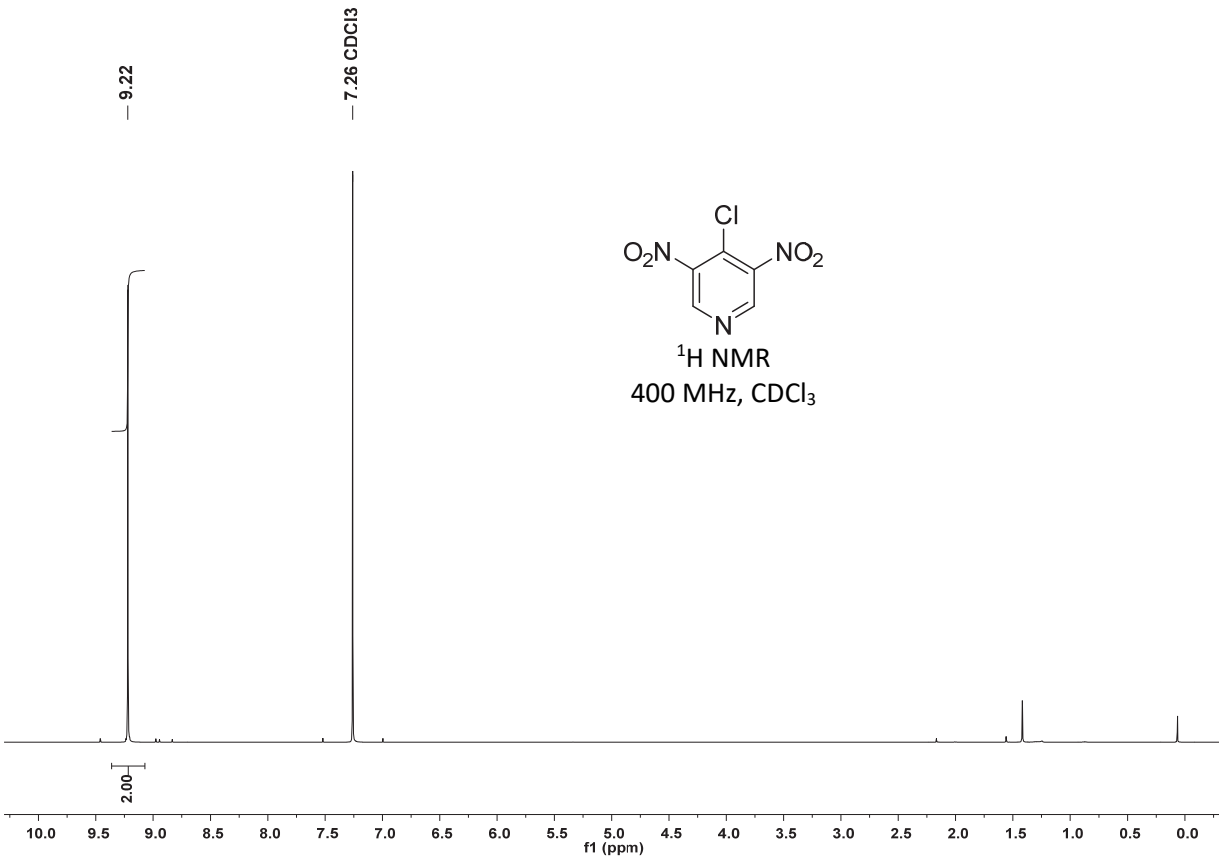

^{1}H NMR
400 MHz, $CDCl_3$

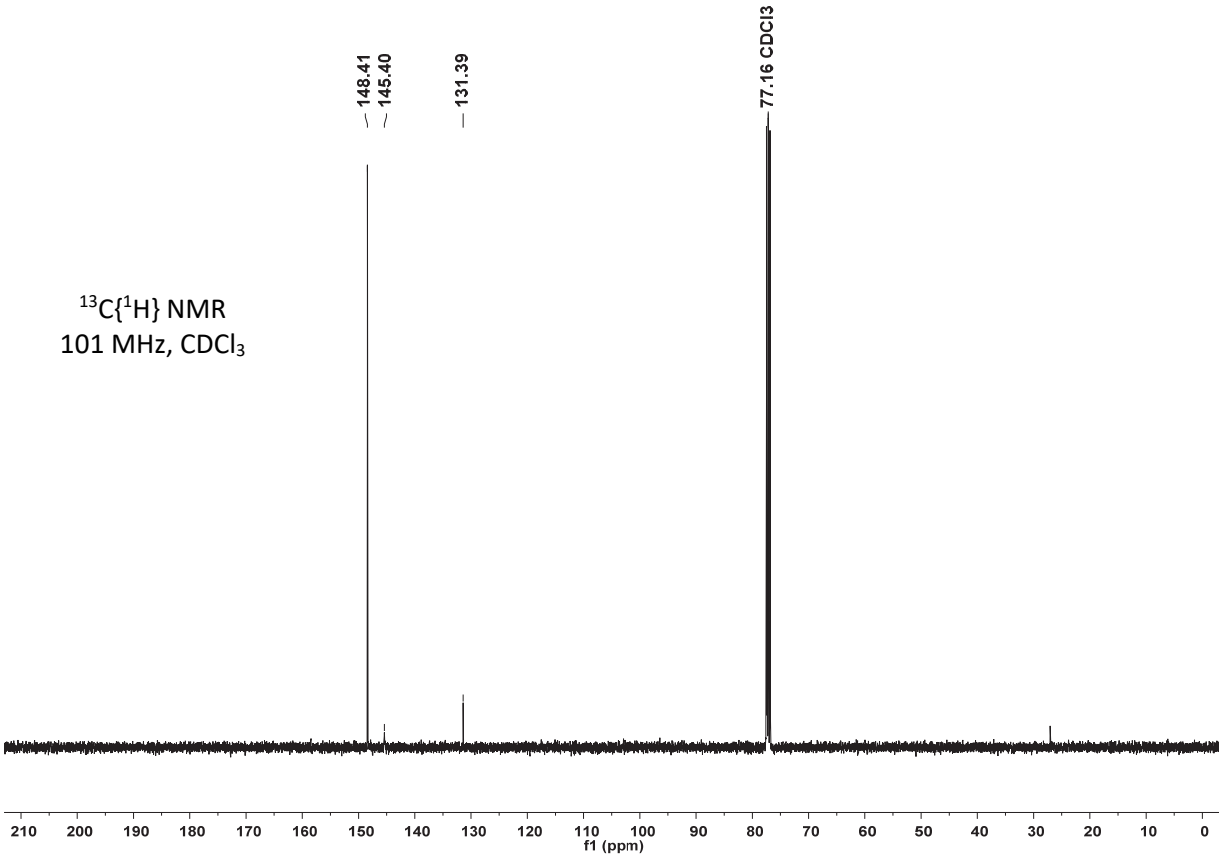

$^{13}C\{^{1}H\}$ NMR
101 MHz, $CDCl_3$

7.3 Application of Lewis Acidity Parameters in Borane Catalyzed Reactions

Nazarov Cyclization (RNH426)

Under an atmosphere of dry argon a solution of the Nazarov precursor (6.0 mg, 0.028 mmol) in CD_2Cl_2 (0.35 mL) was added to a solution of the borane (0.0028 mmol) in CD_2Cl_2 (0.35 mL). The reaction mixture was transferred into an NMR tube which was sealed with a rubber septum. The progress of the Nazarov cyclization was monitored by ^{1}H NMR (400 MHz) spectroscopy.

Conversion to the cyclopentenone product[22,23] was observed for BBr_3, BCl_3 and the triarylboranes **1i**, **1g** within 1–2 h. After 24 h reaction time partial conversion to the product was observed with **1h** but not when **1f** was used as the catalyst.

Diels-Alder Reaction of Methyl Vinyl Ketone with Cyclopentadiene

Under an atmosphere of dry argon CD_2Cl_2 solutions of methyl vinyl ketone (0.028 mmol), cyclopentadiene (freshly prepared by thermal decomposition of its dimer and subsequent distillation, 0.028 mmol), and the borane (0.0028 mmol) in CD_2Cl_2 (0.75 mL) were transferred into an NMR tube, which was sealed with a rubber septum. The reaction mixtures were analyzed by ^{1}H NMR spectroscopy (200 MHz) after 20 min reaction time at room temperature (25 °C).

Quantitative conversion of the educts to the Diels-Alder adduct[24] was observed after 20 min for solutions that contained 10 mol% of the boranes **1h**, **1i** and BCl_3. With borane **1f**, traces of the product (15%) were observed after 2 h reaction time.

Michael Addition of 1-Methylindole to Methyl Vinyl Ketone

Under an atmosphere of dry argon CD_2Cl_2 solutions of methyl vinyl ketone (0.028 mmol), 1-methylindole (0.028 mmol) and the borane (0.0028 mmol) in CD_2Cl_2 (0.75 mL) were transferred into an NMR tube which was sealed with a rubber septum. The reaction mixtures were analyzed by ^{1}H NMR spectroscopy (200 MHz) after 20 min reaction time at room temperature (25 °C).

Quantitative conversion of the educts to the Michael adduct[25] was observed after 20 min for solutions that contained 10 mol% of boranes **1h**, **1i**. With borane **1f**, traces of the product (24%) were observed after 24 h reaction time.

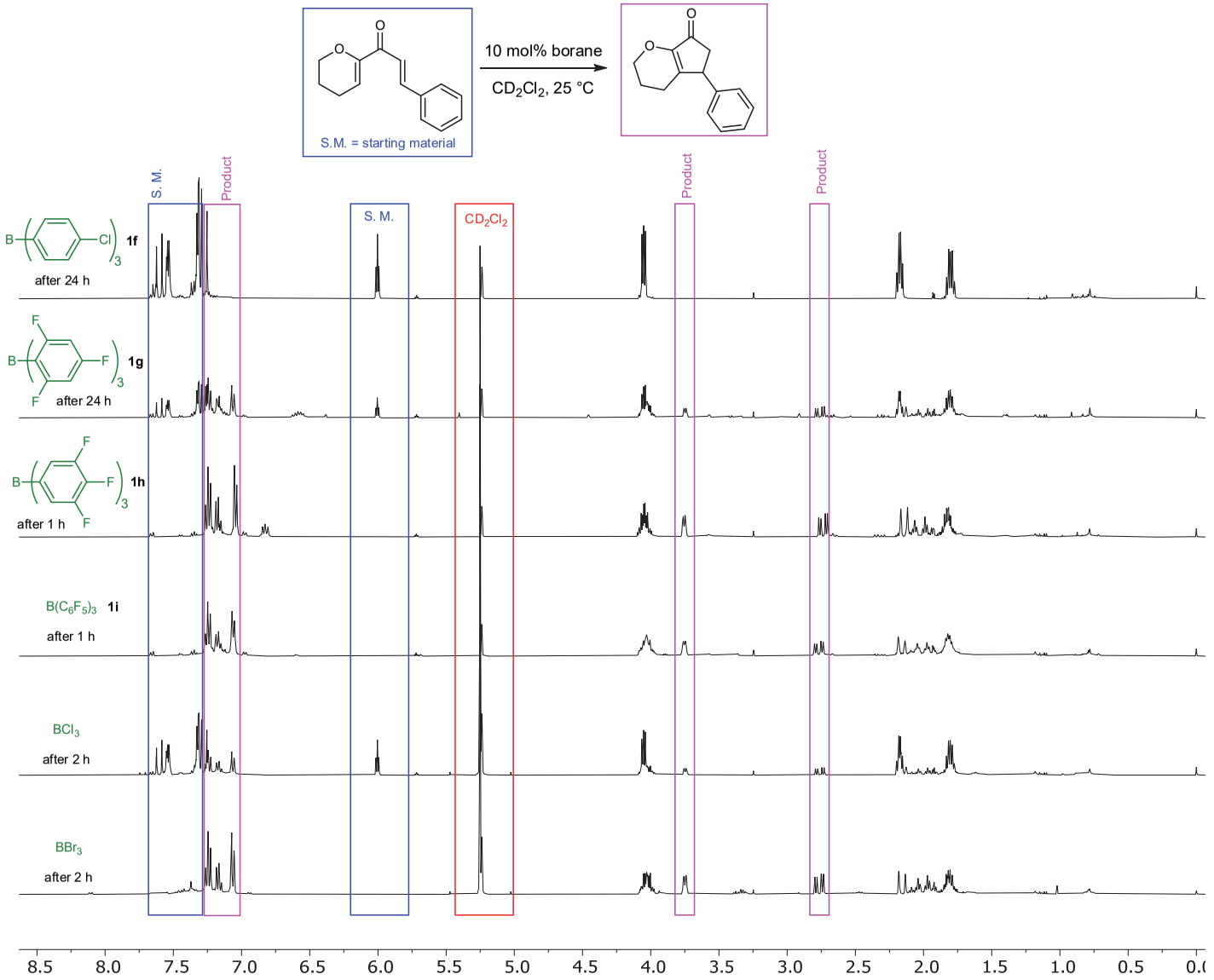

Figure S1: ^{1}H NMR spectra (400 MHz) in CD_2Cl_2 of the borane catalyzed Nazarov reaction.

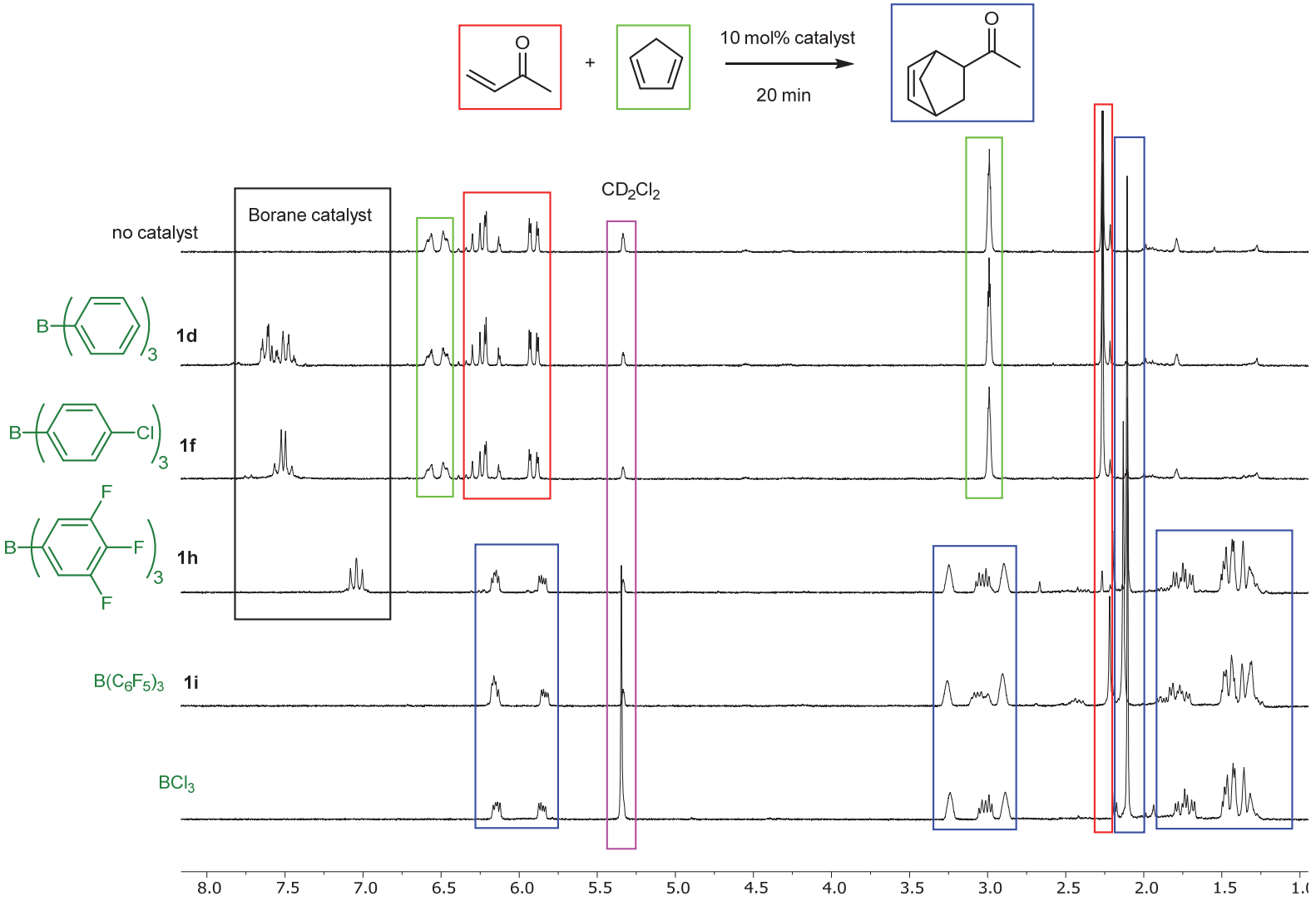

Figure S2: ^{1}H NMR spectra (200 MHz) in CD_2Cl_2 of the borane catalyzed Diels-Alder reaction of methyl vinyl ketone with cyclopentadien.

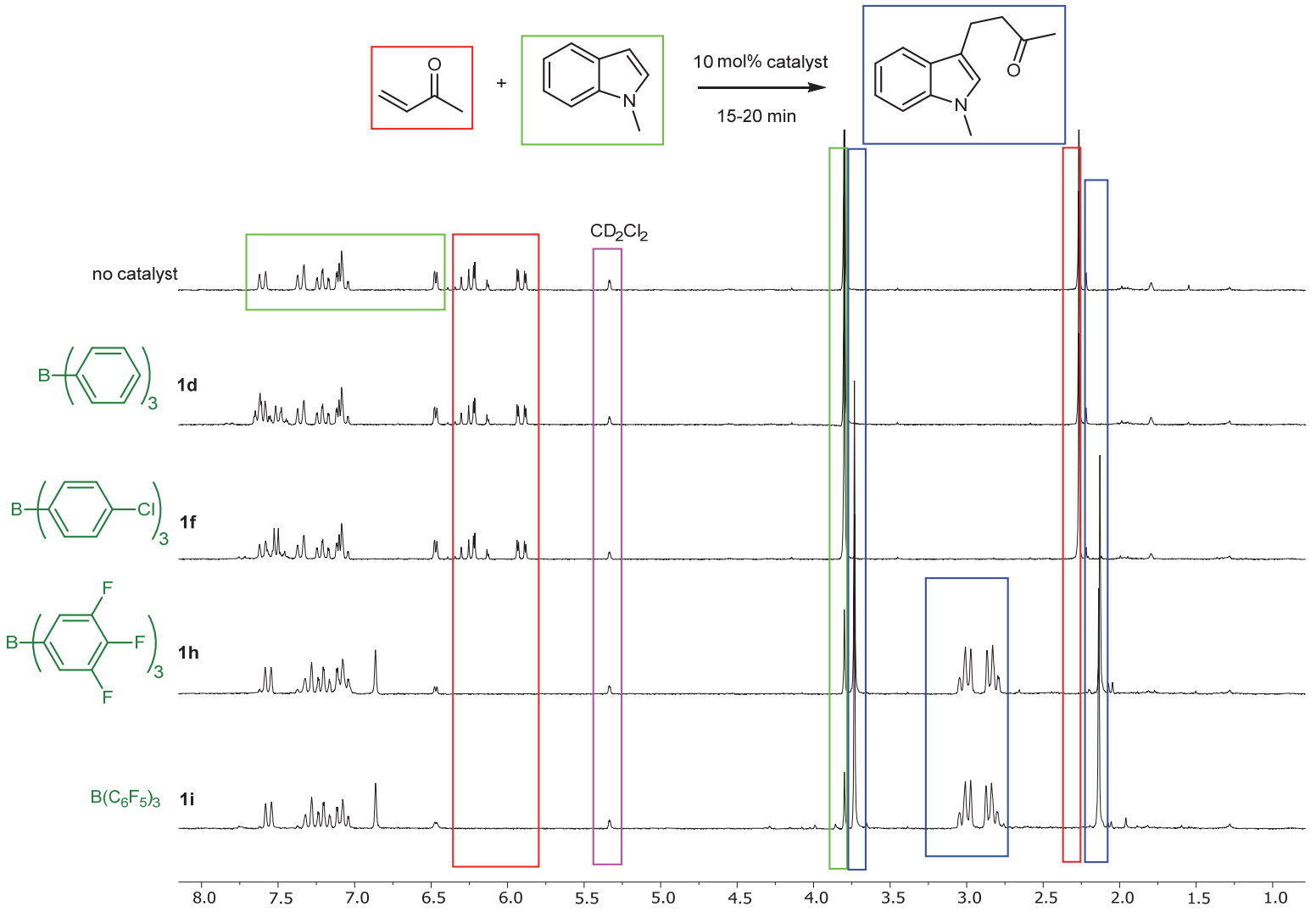

Figure S3: ^{1}H NMR spectra (200 MHz) in CD_2Cl_2 of the borane catalyzed Michael addition of 1-methylindole at methyl vinyl ketone.

7.4 Determination of Equilibrium Constants by Isothermal Titration Calorimetry (ITC)

Summary of ITC experiments in dichloromethane

Reported errors are standard deviations from the averaged results of three experiments under identical conditions at 20 °C.

Table S1: Summary of ITC titration experiments of boranes **1** with Lewis bases in dichloromethane at 20 °C.

Experiment	Ar_3B	LB	[Ar_3B] (mM)	[LB] (mM)	T (°C)	K (M^{-1})	ΔG (kJ mol^{-1})	ΔH (kJ mol^{-1})	$T\Delta S$ (kJ mol^{-1})	n
RM1087e1	**1a**	**2a**	0.996	11.7	20.0	3.74×10^4	-25.7	-55.2	-29.5	0.928
RM1087e2	**1a**	**2a**	0.996	11.7	20.0	3.46×10^4	-25.5	-54.8	-29.3	0.656
RM1087e3	**1a**	**2a**	0.97	11.7	20.0	3.39×10^4	-25.4	-56.8	-31.4	0.775
						$(3.53 \pm 0.16) \times 10^4$	-25.5 ± 0.1	-55.6 ± 0.9	-30.1 ± 1.0	
RM1089e1	**1a**	**2b**	1.02	11.0	20.0	9.28×10^3	-22.3	-54.8	-32.5	0.821
RM1089e2	**1a**	**2b**	0.996	10.1	20.0	9.12×10^3	-22.2	-58.1	-35.9	0.734
RM1089e3	**1a**	**2b**	0.996	10.1	20.0	9.64×10^3	-22.4	-57.3	-34.9	0.691
						$(9.35 \pm 0.22) \times 10^3$	-22.3 ± 0.1	-56.7 ± 1.4	-34.4 ± 1.4	
RM1091e1	**1b**	**2a**	0.963	11.4	20.0	2.31×10^6	-35.7	-64.8	-29.1	0.763
RM1091e2	**1b**	**2a**	0.963	11.4	20.0	5.06×10^6	-37.6	-66.5	-28.8	0.754
RM1091e3	**1b**	**2a**	0.963	11.4	20.0	2.27×10^6	-35.7	-66.5	-30.8	0.749
						$(3.21 \pm 1.31) \times 10^6$	-36.3 ± 0.9	-65.9 ± 0.8	-29.6 ± 0.9	
RM1081e1	**1b**	**2b**	0.993	10.3	20.0	1.18×10^6	-34.1	-70.2	-36.1	0.749
RM1081e2	**1b**	**2b**	0.993	10.3	20.0	1.47×10^6	-34.6	-68.6	-33.9	0.71
RM1081e3	**1b**	**2b**	0.993	10.3	20.0	1.09×10^6	-33.9	-70.2	-36.3	0.68
						$(1.25 \pm 0.17) \times 10^6$	-34.2 ± 0.3	-69.7 ± 0.8	-35.5 ± 1.1	
RM1078e1	**1b**	**2c**	1.32	14.0	20.0	1.33×10^5	-28.8	-58.1	-29.3	0.809
RM1078e2	**1b**	**2c**	1.32	14.0	20.0	1.39×10^5	-28.9	-58.1	-29.2	0.782
RM1078e3	**1b**	**2c**	1.32	14.0	20.0	1.22×10^5	-28.5	-59.8	-31.2	0.744
						$(1.31 \pm 0.08) \times 10^5$	-28.7 ± 0.1	-58.7 ± 0.8	-29.9 ± 0.9	

RM1075e3	**1b**	**2d**	1.50	13.2	20.0	2.02×10^4	-24.2	-51.8	-27.7	0.871
RM1075e4	**1b**	**2d**	1.50	13.2	20.0	2.37×10^4	-24.6	-51.0	-26.4	0.821
RM1075e5	**1b**	**2d**	1.50	13.2	20.0	2.27×10^4	-24.4	-53.9	-29.5	0.797
						$(2.22 \pm 0.15) \times 10^4$	-24.4 ± 0.2	-52.3 ± 1.2	-27.9 ± 1.2	
RM1077e2	**1b**	**2e**	1.50	15.0	20.0	2.89×10^3	-19.4	-57.7	-38.3	0.691
RM1077e3	**1b**	**2e**	1.50	15.0	20.0	3.51×10^3	-19.9	-52.3	-32.4	0.674
RM1077e4	**1b**	**2e**	1.50	15.0	20.0	3.34×10^3	-19.8	-53.1	-33.3	0.657
						$(3.25 \pm 0.27) \times 10^3$	-19.7 ± 0.2	-54.3 ± 2.4	-34.6 ± 2.6	
RM1114e1	**1c**	**2b**	1.02	10.3	20.0	6.62×10^5	-32.7	-69.0	-36.3	0.852
RM1114e2	**1c**	**2b**	0.95	10.3	20.0	3.66×10^5	-31.2	-75.2	-44.0	0.975
RM1114e3	**1c**	**2b**	1.02	10.3	20.0	3.42×10^5	-31.1	-75.7	-44.6	0.901
						$(4.57 \pm 1.46) \times 10^5$	-31.7 ± 0.7	-73.3 ± 3.1	-41.6 ± 3.8	
RM1085e1	**1c**	**2c**	1.09	9.41	20.0	6.87×10^5	-32.8	-70.2	-37.5	0.739
RM1085e2	**1c**	**2c**	1.06	9.41	20.0	5.15×10^5	-32.1	-69.0	-36.9	0.786
RM1085e3	**1c**	**2c**	1.09	9.41	20.0	5.46×10^5	-32.2	-69.8	-37.6	0.817
						$(5.83 \pm 0.75) \times 10^5$	-32.3 ± 0.3	-69.7 ± 0.5	-37.3 ± 0.3	
RM1079e2	**1c**	**2d**	1.06	10.8	20.0	3.18×10^5	-30.9	-69.0	-38.1	0.857
RM1080e1	**1c**	**2d**	1.06	10.1	20.0	2.29×10^5	-30.1	-74.0	-43.9	0.754
RM1116e1	**1c**	**2d**	1.02	9.62	20.0	3.69×10^5	-31.2	-67.7	-36.5	0.781
RM1116e2	**1c**	**2d**	1.02	9.62	20.0	4.43×10^5	-31.7	-69.4	-37.7	0.763
						$(3.40 \pm 0.78) \times 10^5$	-31.0 ± 0.6	-70.0 ± 2.4	-39.0 ± 2.9	
RM1083e1	**1c**	**2e**	1.06	9.72	20.0	9.41×10^4	-27.9	-76.5	-48.6	0.716
RM1086e1	**1c**	**2e**	1.09	9.95	20.0	6.42×10^4	-27.0	-64.4	-37.4	0.773
RM1086e2	**1c**	**2e**	1.09	9.95	20.0	7.75×10^4	-27.4	-69.0	-41.5	0.74
						$(7.86 \pm 1.22) \times 10^4$	-27.4 ± 0.4	-69.9 ± 5.0	-42.5 ± 4.6	

RM1084e1	**1c**	**2f**	1.06	10.7	20.0	2.14×10^4	-24.3	-79.8	-55.5	0.772
RM1084e3	**1c**	**2f**	1.06	10.7	20.0	2.94×10^4	-25.1	-78.2	-53.1	0.763
RM1084e4	**1c**	**2f**	1.09	10.7	20.0	4.86×10^4	-26.3	-76.1	-49.8	0.618
						$(3.31 \pm 1.14) \times 10^4$	-25.2 ± 0.4	-79.0 ± 0.8	-54.3 ± 1.2	
RM1124e1	**1c**	**2g**	1.06	10.1	20.0	1.08×10^4	-22.6	-71.9	-49.3	0.766
RM1124e2	**1c**	**2g**	0.985	10.1	20.0	1.58×10^4	-23.6	-70.6	-47.1	0.759
RM1124e3	**1c**	**2g**	1.06	9.94	20.0	1.63×10^4	-23.6	-71.9	-48.3	0.812
						$(1.43 \pm 0.25) \times 10^4$	-23.3 ± 0.5	-71.5 ± 0.6	-48.2 ± 0.9	
RM1125e2	**1c**	**2h**	1.06	10.8	20.0	3.30×10^3	-19.7	-65.2	-45.5	0.681
RM1125e3	**1c**	**2h**	0.985	10.8	20.0	3.66×10^3	-20.0	-63.5	-43.5	0.723
RM1125e4	**1c**	**2h**	1.06	10.8	20.0	3.83×10^3	-20.1	-68.6	-48.4	0.657
						$(3.60 \pm 0.23) \times 10^3$	-20.0 ± 0.2	-65.8 ± 2.1	-45.8 ± 2.0	
RM968e1	**1d**	**2d**	1.13	10.1	20.0	1.39×10^6	-34.5	-70.2	-35.7	1.1
RM968e3	**1d**	**2d**	1.13	10.1	20.0	1.43×10^6	-34.5	-74.0	-39.4	1.0
RM968e5	**1d**	**2d**	1.05	10.1	20.0	1.34×10^6	-34.4	-76.1	-41.7	1.07
						$(1.39 \pm 0.04) \times 10^6$	-34.5 ± 0.1	-73.4 ± 2.4	-39.0 ± 2.4	
RM1118e1	**1d**	**2e**	1.03	10.6	20.0	4.20×10^5	-31.6	-74.4	-42.8	0.918
RM1118e2	**1d**	**2e**	1.20	10.6	20.0	3.69×10^5	-31.2	-75.7	-44.4	0.936
RM1118e3	**1d**	**2e**	1.24	10.6	20.0	3.70×10^5	-31.3	-73.2	-41.9	0.861
						$(3.86 \pm 0.24) \times 10^5$	-31.4 ± 0.1	-74.4 ± 1.0	-43.1 ± 1.0	
AB037e2	**1d**	**2f**	1.13	10.1	20.0	8.81×10^4	-27.8	-71.9	-44.1	1.12
AB037e3	**1d**	**2f**	1.05	10.1	20.0	8.39×10^4	-27.6	-74.0	-46.4	0.84
RM1121e1	**1d**	**2f**	1.12	10.1	20.0	1.08×10^5	-28.2	-66.9	-38.6	1.01
						$(9.33 \pm 1.05) \times 10^4$	-27.9 ± 0.3	-70.9 ± 3.0	-43.0 ± 3.2	
AB035e3	**1d**	**2g**	1.13	10.1	20.0	2.82×10^4	-25.0	-67.3	-42.3	1.0
AB035e4	**1d**	**2g**	1.05	10.1	20.0	2.43×10^4	-24.6	-64.0	-39.3	1.22

AB035e5	**1d**	**2g**	1.05	10.1	20.0	2.01×10^4	-24.2	-63.1	-39.0	0.89
						$(2.42 \pm 0.34) \times 10^4$	-24.6 ± 0.3	-64.8 ± 1.8	-40.2 ± 1.5	
RM974e1	**1d**	**2h**	1.13	10.1	20.0	3.87×10^3	-20.1	-81.9	-61.8	0.95
RM974e2	**1d**	**2h**	1.13	10.1	20.0	4.64×10^3	-20.6	-80.3	-59.7	0.99
RM974e3	**1d**	**2h**	1.05	10.1	20.0	4.31×10^3	-20.4	-80.7	-60.3	0.93
						$(4.27 \pm 0.32) \times 10^3$	-20.4 ± 0.2	-81.0 ± 0.7	-60.6 ± 0.9	
RM1094e1	**1e**	**2d**	1.01	10.0	20.0	1.34×10^6	-34.4	-68.1	-33.7	0.96
RM1094e2	**1e**	**2d**	1.08	10.0	20.0	1.31×10^6	-34.3	-70.2	-35.9	0.894
RM1094e3	**1e**	**2d**	1.01	9.67	20.0	1.25×10^6	-34.2	-71.9	-37.7	0.997
						$(1.30 \pm 0.04) \times 10^6$	-34.3 ± 0.1	-70.1 ± 1.5	-35.8 ± 1.6	
RM1092e1	**1e**	**2e**	1.01	10.4	20.0	2.72×10^5	-30.5	-71.9	-41.4	0.409
RM1092e2	**1e**	**2e**	1.01	10.4	20.0	2.73×10^5	-30.5	-73.6	-43.1	0.904
RM1092e3	**1e**	**2e**	1.08	10.4	20.0	3.58×10^5	-31.2	-69.8	-38.6	0.857
						$(3.01 \pm 0.41) \times 10^5$	-30.7 ± 0.3	-71.8 ± 1.5	-41.0 ± 1.8	
RM1096e1	**1e**	**2f**	0.979	10.7	20.0	8.41×10^4	-27.6	-68.1	-40.5	0.88
RM1096e2	**1e**	**2f**	1.05	10.7	20.0	8.37×10^4	-27.6	-68.1	-40.5	0.864
RM1096e3	**1e**	**2f**	1.01	10.7	20.0	8.11×10^4	-27.6	-68.1	-40.6	0.921
						$(8.30 \pm 0.14) \times 10^4$	-27.6 ± 0.0	-68.1 ± 0.0	-40.5 ± 0.1	
RM1097e1	**1e**	**2g**	1.05	9.93	20.0	3.55×10^4	-25.5	-61.4	-35.9	0.914
RM1097e2	**1e**	**2g**	1.01	10.3	20.0	3.35×10^4	-25.4	-64.4	-39.0	0.848
RM1097e3	**1e**	**2g**	0.979	10.3	20.0	3.03×10^4	-25.2	-66.0	-40.9	1.03
						$(3.31 \pm 0.22) \times 10^4$	-25.4 ± 0.2	-64.0 ± 1.9	-38.6 ± 2.1	
RM1099e1	**1e**	**2h**	0.946	11.1	20.0	6.95×10^3	-21.6	-66.5	-44.9	0.948
RM1099e2	**1e**	**2h**	0.912	11.1	20.0	7.30×10^3	-21.7	-64.8	-43.1	0.996
RM1099e3	**1e**	**2h**	0.979	11.1	20.0	9.36×10^3	-22.3	-61.9	-39.6	0.988
						$(7.87 \pm 1.06) \times 10^3$	-21.8 ± 0.3	-64.4 ± 1.9	-42.5 ± 2.2	

7.5 Determination of Equilibrium Constants by NMR Chemical Shift Changes

Summary

For the determination of equilibrium constants, typically 6 to 9 individual NMR samples with a constant Lewis acid concentration and a variable (excess) concentration of the Lewis base were prepared. NMR spectra were acquired for each individual sample in CD_2Cl_2 at 22°C, and the chemical shift changes of one resonance that is unequivocally assigned to the Lewis acid was evaluated. Errors correspond to the standard deviations of variables in the least-squares fitting of Eq (S1).

Table S2: Summary of equilibrium constants obtained from NMR titration experiments of boranes **1** with Lewis bases (CD_2Cl_2, 22 °C)

BAr_3	LB	Experiment	K_B (M^{-1})
1a	**2c**	RM1102	$(1.01 \pm 0.06) \times 10^3$
1a	**2d**	RM1110	$(7.81 \pm 0.04) \times 10^1$
1a	**2e**	RM1111	9.93 ± 0.42
1a	**2f**	RM1123	1.52 ± 0.29
1b	**2f**	RM1120	$(7.99 \pm 1.81) \times 10^2$
1b	**2g**	RM1106	$(4.88 \pm 0.43) \times 10^2$
1b	**2h**	RM1122	$(1.68 \pm 0.04) \times 10^2$
1b	**2j**	RM1131	6.06 ± 0.30
1c	**2i**	RM1146	$(1.62 \pm 0.07) \times 10^1$
1c	**2j**	RM1129	$(1.22 \pm 0.11) \times 10^2$
1c	**2k**	RM1170	7.11 ± 0.61
1c	**9**	RM1262	$(1.90 \pm 0.12) \times 10^1$
1d	**2i**	RM1147	$(5.04 \pm 0.71) \times 10^1$
1d	**2j**	RM1130	$(4.33 \pm 0.85) \times 10^2$
1d	**2k**	RM1169	$(5.35 \pm 1.07) \times 10^1$
1d	**10**	RM1270	7.60 ± 0.18
1e	**2i**	RM1144	$(6.37 \pm 0.19) \times 10^1$
1e	**2j**	RM1128	$(7.56 \pm 0.56) \times 10^2$
1e	**2k**	RM1167	$(2.96 \pm 0.13) \times 10^1$
1e	**2l**	RM1157	$(2.38 \pm 0.51) \times 10^{-1}$
1e	**4a**	RM1260	$(3.60 \pm 0.36) \times 10^2$
1e	**9**	RM1261	$(1.98 \pm 0.33) \times 10^3$
1f	**2i**	RM1145	$(1.71 \pm 0.75) \times 10^3$
1f	**2j**	RM1133	$(9.29 \pm 0.22) \times 10^3$
1f	**2k**	RM1168	$(3.56 \pm 0.08) \times 10^2$
1f	**2l**	RM1155	7.91 ± 0.28
1f	**2m**	RM1166	4.87 ± 0.12
1f	**7a**	RM1188	6.75 ± 0.21
1f	**3a**	RM1258	4.93 ± 0.16
1f	**3b**	RM1195	1.87 ± 0.04
1f	**4b**	RM1259	$(1.58 \pm 0.04) \times 10^2$
1f	**4c**	RM1254	$(1.67 \pm 0.08) \times 10^1$
1e	**10**	RM1271	$(2.50 \pm 0.19) \times 10^2$

1g	**2l**	RM1239	$(4.50 \pm 1.11) \times 10^{3}$
1g	**2m**	RM1165	$(1.60 \pm 0.22) \times 10^{3}$
1g	**3b**	RM1238	$(2.39 \pm 0.28) \times 10^{3}$
1g	**4a**	RM1237	$(8.61 \pm 0.75) \times 10^{2}$
1g	**5a**	RM1148	$(9.79 \pm 0.32) \times 10^{1}$
1g	**5b**	RM1141	$(2.97 \pm 0.34) \times 10^{1}$
1g	**5c**	RM1177	6.22 ± 0.92
1g	**5d**	RM1153	5.42 ± 0.58
1g	**5e**	RM1158	5.02 ± 0.82
1g	**7a**	RM1187	$(4.90 \pm 2.02) \times 10^{3}$
1g	**7b**	RM1214	$(1.41 \pm 0.05) \times 10^{2}$
1g	**7c**	RM1186	$(5.34 \pm 0.12) \times 10^{1}$
1g	**7d**	RM1185	2.31 ± 0.28
1g	**8**	RM1184	$(1.38 \pm 0.21) \times 10^{3}$
1h	**2l**	RM1174	$(4.10 \pm 0.35) \times 10^{2}$
1h	**2m**	RM1173	$(1.94 \pm 0.07) \times 10^{2}$
1h	**3a**	RM1211	$(4.63 \pm 0.25) \times 10^{3}$
1h	**3b**	RM1201	$(2.10 \pm 0.38) \times 10^{3}$
1h	**5a**	RM1172	$(1.24 \pm 0.04) \times 10^{2}$
1h	**5b**	RM1163	$(2.78 \pm 0.25) \times 10^{1}$
1h	**7a**	RM1198	$(2.18 \pm 1.10) \times 10^{4}$
1h	**7b**	RM1257	$(2.24 \pm 0.06) \times 10^{2}$
1h	**7c**	RM1197	$(6.78 \pm 0.03) \times 10^{1}$
1h	**7d**	RM1196	1.02 ± 0.13
1h	**8**	RM1199	$(2.84 \pm 0.42) \times 10^{3}$
1i	**2n**	RM1240	$(5.47 \pm 1.02) \times 10^{1}$
1i	**5c**	RM1241	$(3.51 \pm 1.82) \times 10^{4}$
1i	**5d**	RM1251	$(1.01 \pm 0.60) \times 10^{4}$
1i	**5e**	RM1143	$(6.53 \pm 0.92) \times 10^{2}$
1i	**5f**	RM1150	$(1.31 \pm 0.37) \times 10^{1}$
1i	**6**	RM1200	$(7.31 \pm 2.19) \times 10^{1}$
1i	**7d**	RM1180	$(4.46 \pm 1.41) \times 10^{3}$
1j	**2a**	RM1256	$(4.54 \pm 0.26) \times 10^{-1}$

Individual NMR titrations

NMR titration of tris(4-dimethylaminophenyl)borane (1a) with 4-methoxypyridine (2c)

Entry	Borane (M)	LB (M)	δ (ppm)	Δδ (ppm)
1	5.0×10^{-3}	0.0	7.498	0.000
3	5.0×10^{-3}	5.0×10^{-3}	7.211	0.287
4	5.0×10^{-3}	7.5×10^{-3}	7.149	0.349
6	5.0×10^{-3}	2.0×10^{-2}	7.085	0.413
7	5.0×10^{-3}	3.0×10^{-2}	7.070	0.428
8	5.0×10^{-3}	4.0×10^{-2}	7.062	0.436

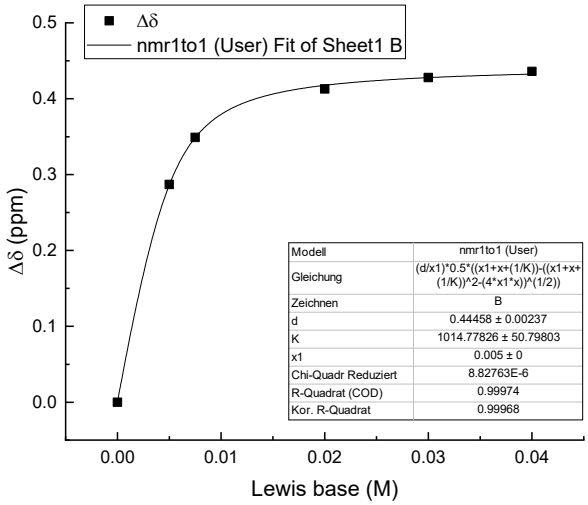

(RM1102)

NMR titration of tris(4-dimethylaminophenyl)borane (1a) with pyridine (1d)

Entry	Borane (M)	LB (M)	δ (ppm)	Δδ (ppm)
1	3.0×10^{-3}	0.0	3.0350	0.0000
2	3.0×10^{-3}	1.5×10^{-3}	3.0201	0.0149
3	3.0×10^{-3}	3.0×10^{-3}	3.0084	0.0266
4	3.0×10^{-3}	4.5×10^{-3}	2.9983	0.0367
5	3.0×10^{-3}	6.0×10^{-3}	2.9898	0.0452
6	3.0×10^{-3}	1.2×10^{-2}	2.9630	0.0720
7	3.0×10^{-3}	1.8×10^{-2}	2.9452	0.0898

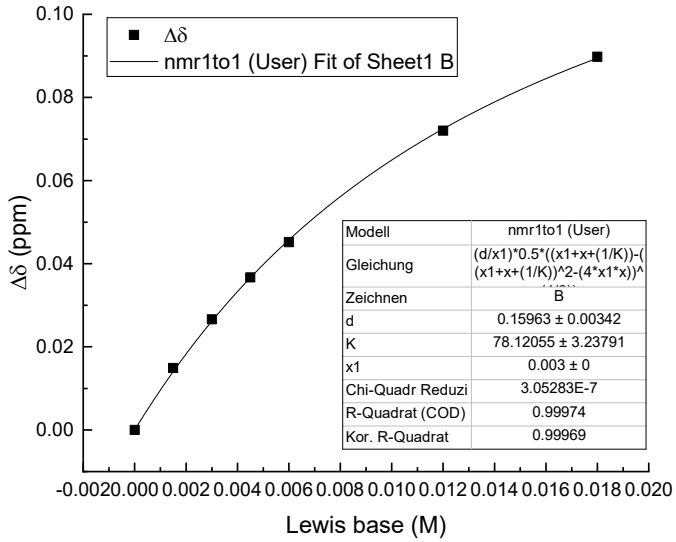

(RM1110)

NMR titration of tris(4-dimethylaminophenyl)borane (1a) with 4-benzoylpyridine (2e)

Entry	Borane (M)	LB (M)	δ (ppm)	Δδ (ppm)
1	3.0×10^{-3}	0.0	3.0351	0.0000
2	3.0×10^{-3}	3.0×10^{-3}	3.0293	0.0058
3	3.0×10^{-3}	7.5×10^{-3}	3.0234	0.0117
4	3.0×10^{-3}	1.5×10^{-2}	3.0139	0.0212
5	3.0×10^{-3}	3.0×10^{-2}	2.9981	0.0370
6	3.0×10^{-3}	6.0×10^{-2}	2.9744	0.0607
7	3.0×10^{-3}	1.2×10^{-1}	2.9455	0.0896

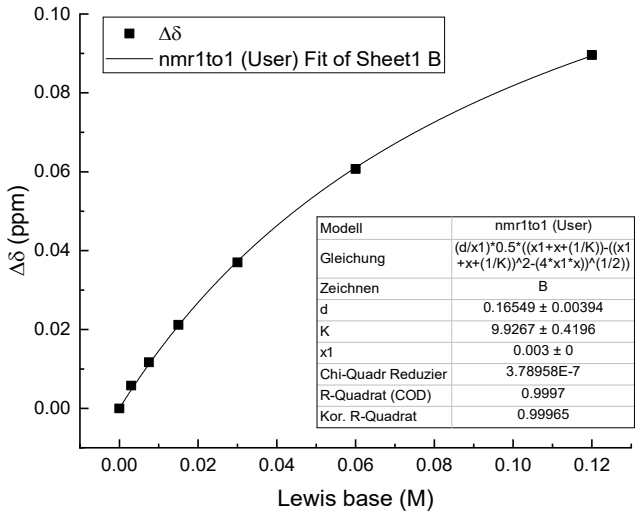

(RM1111)

NMR titration of tris(4-dimethylaminophenyl)borane (1a) with 3-chloropyridine (2f)

Entry	Borane (M)	LB (M)	δ (ppm)	Δδ (ppm)
1	5.0×10^{-3}	0.0	3.0347	0.0000
2	5.0×10^{-3}	5.0×10^{-2}	3.0239	0.0108
3	5.0×10^{-3}	1.0×10^{-1}	3.0110	0.0237
4	5.0×10^{-3}	2.0×10^{-1}	2.9905	0.0442
5	5.0×10^{-3}	3.0×10^{-1}	2.9719	0.0628
6	5.0×10^{-3}	4.0×10^{-1}	2.9634	0.0713
7	5.0×10^{-3}	5.0×10^{-1}	2.9539	0.0808

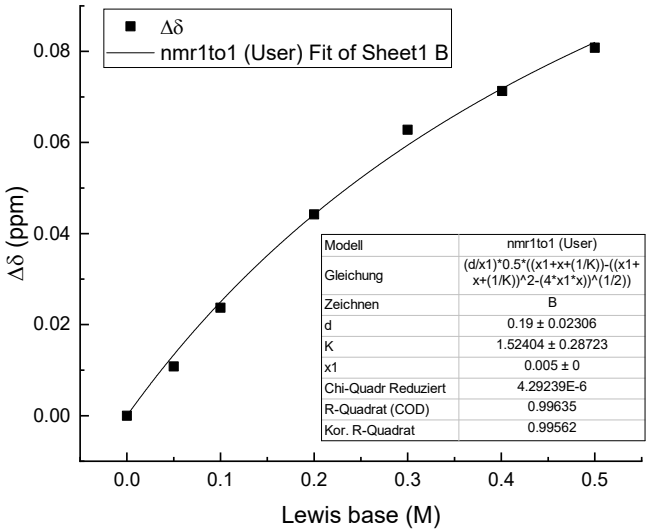

(RM1123)

NMR titration of tris(p-anisyl)borane (1b) with 3-chloropyridine (2f)

Entry	Borane (M)	LB (M)	δ (ppm)	Δδ (ppm)
1	5.0×10^{-3}	0.0	3.8777	0.0000
2	5.0×10^{-3}	2.5×10^{-3}	3.8322	0.0455
3	5.0×10^{-3}	5.0×10^{-3}	3.8093	0.0684
4	5.0×10^{-3}	7.5×10^{-3}	3.7970	0.0807
5	5.0×10^{-3}	1.0×10^{-2}	3.7864	0.0913
6	5.0×10^{-3}	1.5×10^{-2}	3.7775	0.1002
7	5.0×10^{-3}	2.0×10^{-2}	3.7735	0.1042

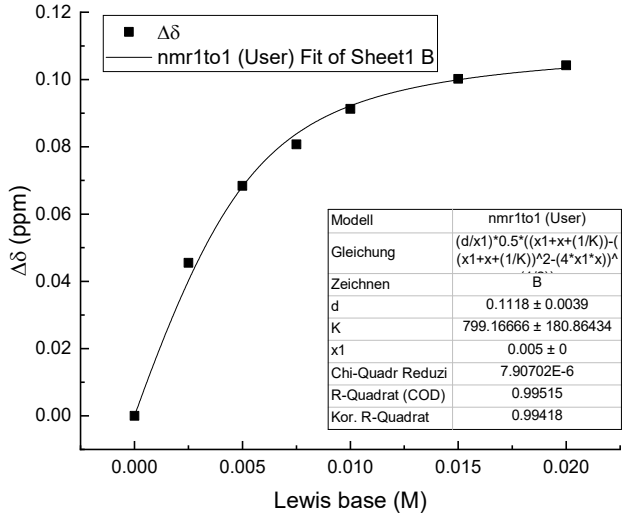

(RM1120)

NMR titration of tris(p-anisyl)borane (1b) with 4-(trifluoromethyl)pyridine (2g)

Entry	Borane (M)	LB (M)	δ (ppm)	Δδ (ppm)
1	5.0×10^{-3}	0.0	7.560	0.000
2	5.0×10^{-3}	2.5×10^{-3}	7.416	0.144
3	5.0×10^{-3}	5.0×10^{-3}	7.313	0.247
4	5.0×10^{-3}	7.5×10^{-3}	7.249	0.311
5	5.0×10^{-3}	1.0×10^{-2}	7.194	0.366
6	5.0×10^{-3}	2.0×10^{-2}	7.145	0.415
7	5.0×10^{-3}	3.0×10^{-2}	7.127	0.433

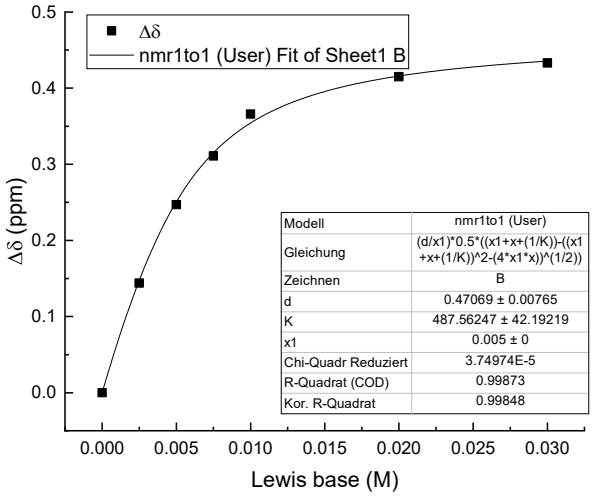

(RM1106)

NMR titration of tris(p-anisyl)borane (1b) with 4-cyanopyridine (2h)

Entry	Borane (M)	LB (M)	δ (ppm)	Δδ (ppm)
1	5.0×10^{-3}	0.0	3.8777	0.0000
2	5.0×10^{-3}	2.5×10^{-3}	3.8536	0.0241
3	5.0×10^{-3}	5.0×10^{-3}	3.8365	0.0412
4	5.0×10^{-3}	1.0×10^{-2}	3.8142	0.0635
5	5.0×10^{-3}	2.0×10^{-2}	3.7927	0.0850
6	5.0×10^{-3}	3.0×10^{-2}	3.7830	0.0947
7	5.0×10^{-3}	4.0×10^{-2}	3.7778	0.0999

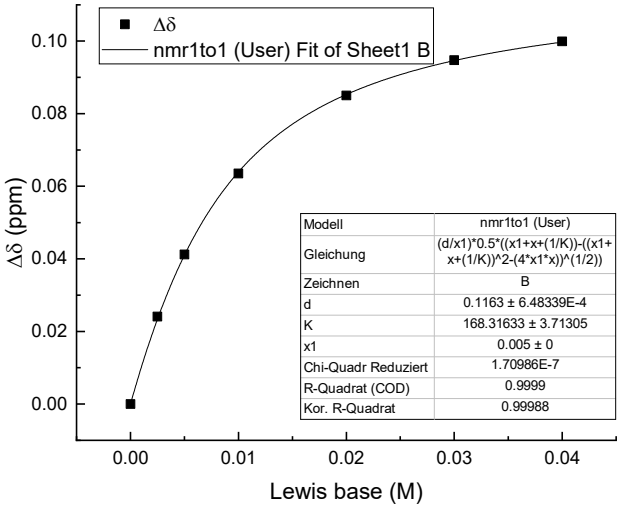

(RM1122)

NMR titration of tris(p-anisyl)borane (1b) with 3,4,5-trichloropyridine (2j)

Entry	Borane (M)	LB (M)	δ (ppm)	Δδ (ppm)
1	3.0×10^{-3}	0.0	3.8777	0.0000
2	3.0×10^{-3}	3.0×10^{-3}	3.8759	0.0018
3	3.0×10^{-3}	7.5×10^{-3}	3.8731	0.0046
4	3.0×10^{-3}	1.5×10^{-2}	3.8685	0.0092
5	3.0×10^{-3}	3.0×10^{-2}	3.8606	0.0171
6	3.0×10^{-3}	6.0×10^{-2}	3.8471	0.0306
7	3.0×10^{-3}	1.2×10^{-1}	3.8301	0.0476

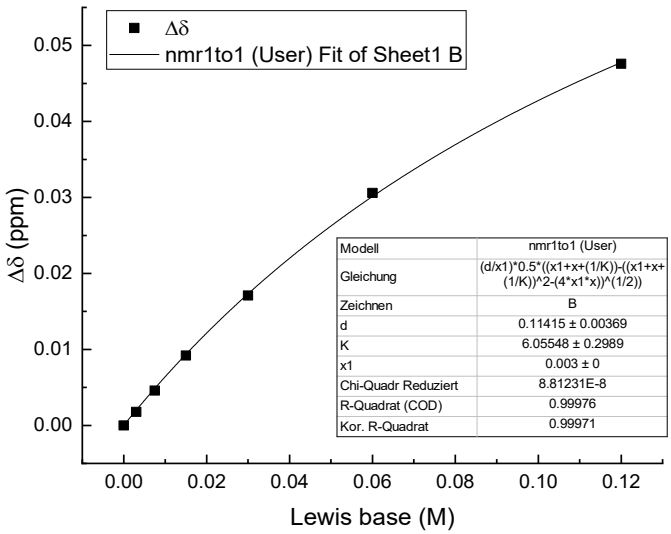

(RM1131)

NMR titration of tris(p-tolyl)borane (1c) with 3,5-bis(trifluoromethyl)pyridine (2i)

Entry	Borane (M)	LB (M)	δ (ppm)	Δδ (ppm)
1	5.0×10^{-3}	0.0	2.4378	0.0000
2	5.0×10^{-3}	5.0×10^{-3}	2.4278	0.0100
3	5.0×10^{-3}	1.0×10^{-2}	2.4186	0.0192
4	5.0×10^{-3}	2.0×10^{-2}	2.4040	0.0338
5	5.0×10^{-3}	4.0×10^{-2}	2.3834	0.0544
6	5.0×10^{-3}	7.5×10^{-2}	2.3584	0.0794
7	5.0×10^{-3}	1.26×10^{-1}	2.3420	0.0958

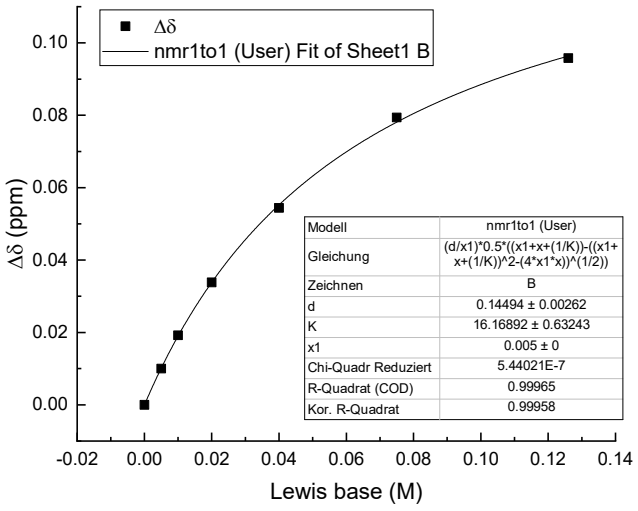

(RM1146)

NMR titration of tris(p-tolyl)borane (1c) with 3,4,5-trichloropyridine (2j)

Entry	Borane (M)	LB (M)	δ (ppm)	Δδ (ppm)
1	5.0×10^{-3}	0.0	7.489	0.000
2	5.0×10^{-3}	2.5×10^{-3}	7.421	0.068
3	5.0×10^{-3}	5.0×10^{-3}	7.359	0.130
4	5.0×10^{-3}	7.5×10^{-3}	7.317	0.172
5	5.0×10^{-3}	1.0×10^{-2}	7.285	0.204
6	5.0×10^{-3}	1.5×10^{-2}	7.229	0.260
7	5.0×10^{-3}	2.0×10^{-2}	7.205	0.284

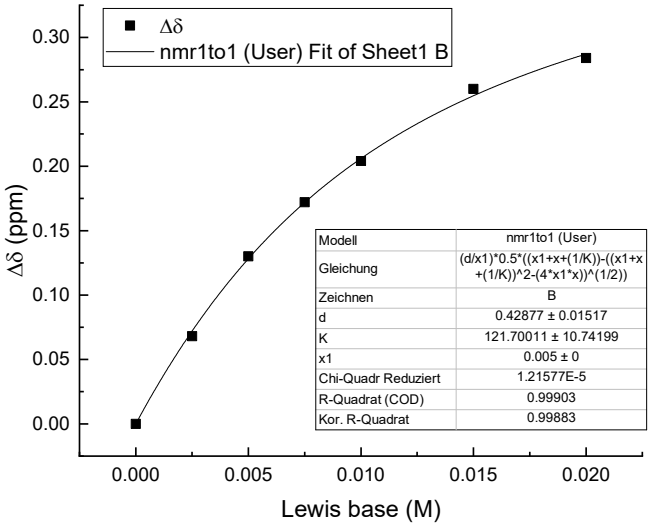

(RM1129)

NMR titration of tris(p-tolyl)borane (1c) with 3,5-difluoro-4-(trifluoromethyl)pyridine (2k)

Entry	Borane (M)	LB (M)	δ (ppm)	Δδ (ppm)
1	5.0×10^{-3}	0.0	7.490	0.000
2	5.0×10^{-3}	5.10×10^{-2}	7.372	0.118
3	5.0×10^{-3}	9.75×10^{-2}	7.294	0.196
4	5.0×10^{-3}	1.49×10^{-1}	7.243	0.247
5	5.0×10^{-3}	2.02×10^{-1}	7.211	0.279
6	5.0×10^{-3}	2.50×10^{-1}	7.190	0.300

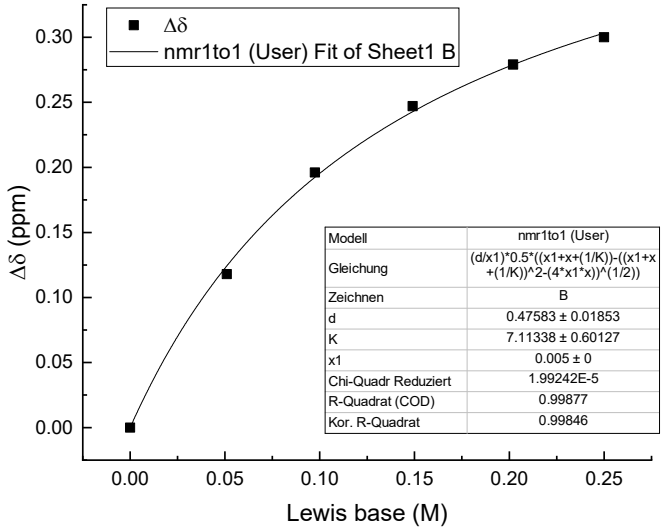

(RM1170)

NMR titration of tris(p-tolyl)borane (1c) with triethylphosphine oxide (10)

Entry	Borane (M)	LB (M)	δ (ppm)	Δδ (ppm)
1	5.0×10^{-3}	0.0	2.4381	0.0000
2	5.0×10^{-3}	2.5×10^{-3}	2.4299	0.0082
3	5.0×10^{-3}	5.0×10^{-3}	2.4220	0.0161
4	5.0×10^{-3}	7.5×10^{-3}	2.4140	0.0241
5	5.0×10^{-3}	1.0×10^{-2}	2.4076	0.0305
6	5.0×10^{-3}	1.5×10^{-2}	2.3947	0.0434
7	5.0×10^{-3}	2.5×10^{-2}	2.3750	0.0631

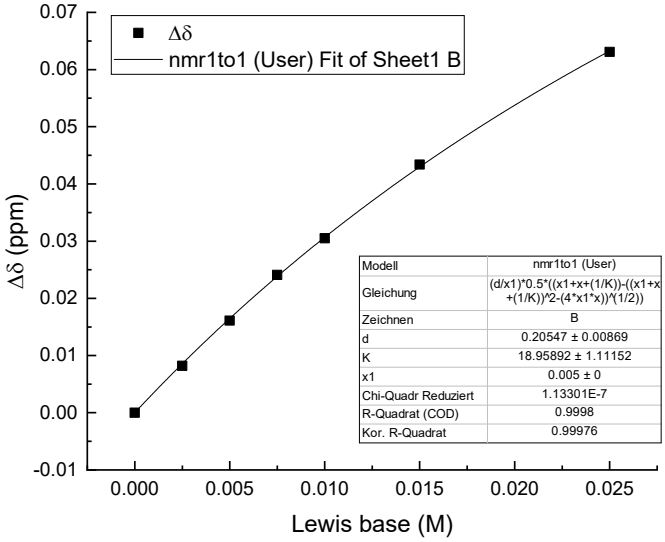

(RM1262)

NMR titration of triphenylborane (1d) with 3,5-bis(trifluoromethyl)pyridine (2i)

Entry	Borane (M)	LB (M)	δ (ppm)	Δδ (ppm)
1	5.0×10^{-3}	0.0	7.4669	0.0000
2	5.0×10^{-3}	2.5×10^{-3}	7.4342	0.0327
3	5.0×10^{-3}	5.0×10^{-3}	7.4070	0.0599
4	5.0×10^{-3}	7.5×10^{-3}	7.3907	0.0762
5	5.0×10^{-3}	1.0×10^{-2}	7.3707	0.0962
6	5.0×10^{-3}	1.5×10^{-2}	7.3354	0.1315
7	5.0×10^{-3}	2.0×10^{-2}	7.3123	0.1546

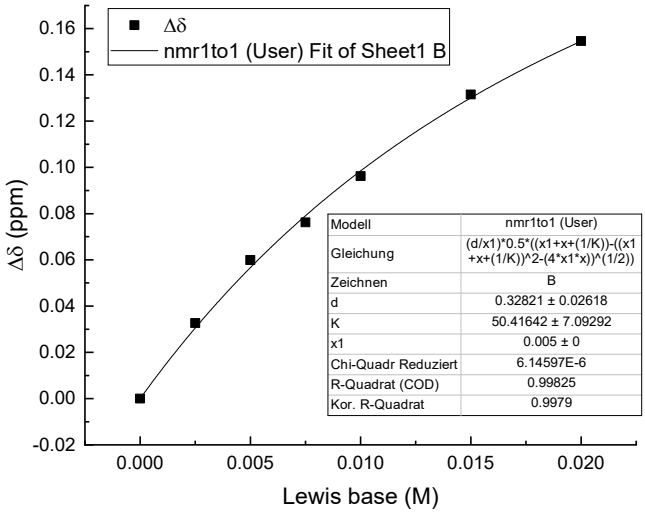

(RM1147)

NMR titration of triphenylborane (1d) with 3,4,5-trichloropyridine (2j)

Entry	Borane (M)	LB (M)	δ (ppm)	Δδ (ppm)
1	5.0×10^{-3}	0.0	7.4671	0.0000
2	5.0×10^{-3}	2.5×10^{-3}	7.3958	0.0713
3	5.0×10^{-3}	5.0×10^{-3}	7.3258	0.1413
4	5.0×10^{-3}	7.5×10^{-3}	7.2833	0.1838
5	5.0×10^{-3}	1.0×10^{-2}	7.2591	0.2080
6	5.0×10^{-3}	1.5×10^{-2}	7.2387	0.2284
7	5.0×10^{-3}	2.0×10^{-2}	7.2292	0.2379

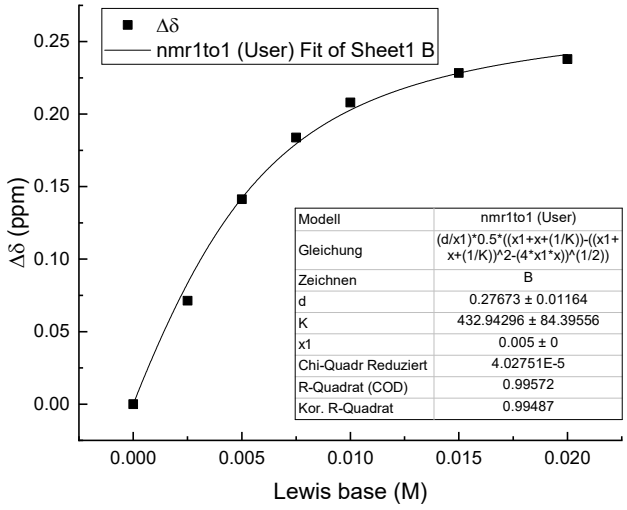

(RM1130)

NMR titration of triphenylborane (1d) with 3,5-difluoro-4-(trifluoromethyl)pyridine (2k)

Entry	Borane (M)	LB (M)	δ (ppm)	Δδ (ppm)
1	5.0×10^{-3}	0.0	7.4662	0.0000
2	5.0×10^{-3}	5.0×10^{-3}	7.4193	0.0469
3	5.0×10^{-3}	1.25×10^{-2}	7.3735	0.0927
4	5.0×10^{-3}	2.50×10^{-2}	7.3459	0.1203
5	5.0×10^{-3}	5.10×10^{-2}	7.3138	0.1524
6	5.0×10^{-3}	7.35×10^{-2}	7.2830	0.1832
7	5.0×10^{-3}	1.00×10^{-1}	7.2643	0.2019

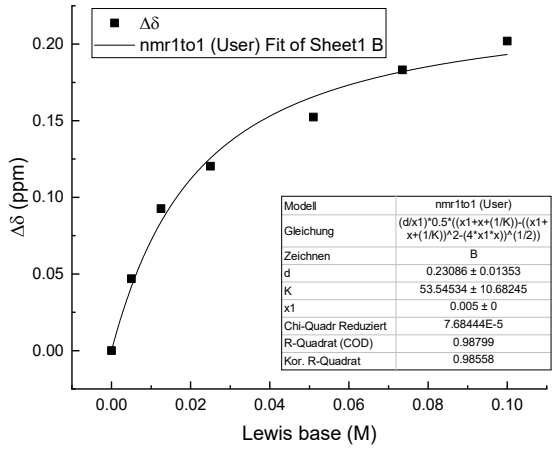

(RM1169)

NMR titration of triphenylborane (1d) with dimethylacetamide (9)

Entry	Borane (M)	LB (M)	δ (ppm)	Δδ (ppm)
1	5.0×10^{-3}	0.0	7.4670	0.0000
2	5.0×10^{-3}	2.5×10^{-3}	7.4608	0.0062
3	5.0×10^{-3}	5.0×10^{-3}	7.4539	0.0131
4	5.0×10^{-3}	7.5×10^{-3}	7.4477	0.0193
5	5.0×10^{-3}	1.0×10^{-2}	7.4412	0.0258
6	5.0×10^{-3}	1.5×10^{-2}	7.4304	0.0366
7	5.0×10^{-3}	2.5×10^{-2}	7.4089	0.0581
8	5.0×10^{-3}	5.0×10^{-2}	7.3695	0.0975
9	5.0×10^{-3}	1.0×10^{-1}	7.3117	0.1553
10	5.0×10^{-3}	1.5×10^{-1}	7.2732	0.1938

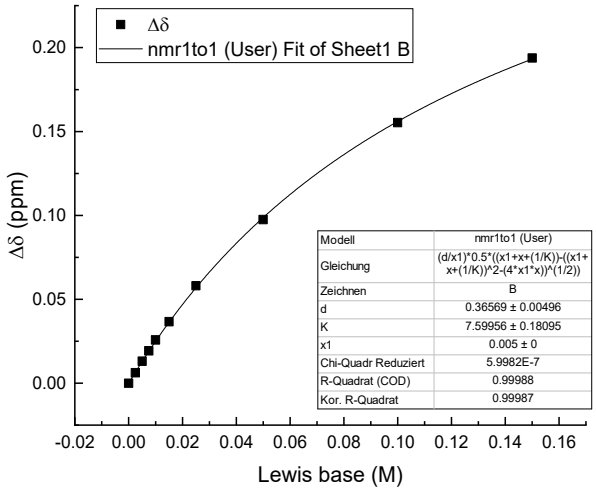

(RM1270)

NMR titration of tris(4-fluorophenyl)borane (1e) with 3,5-bis(trifluoromethyl)pyridine (2i)

Entry	Borane (M)	LB (M)	δ (ppm)	Δδ (ppm)
1	5.0×10^{-3}	0.0	7.1794	0.0000
2	5.0×10^{-3}	2.5×10^{-3}	7.1559	0.0235
3	5.0×10^{-3}	5.0×10^{-3}	7.1351	0.0443
4	5.0×10^{-3}	7.5×10^{-3}	7.1180	0.0614
5	5.0×10^{-3}	1.0×10^{-2}	7.1046	0.0748
6	5.0×10^{-3}	1.5×10^{-2}	7.0813	0.0981
7	5.0×10^{-3}	2.0×10^{-2}	7.0651	0.1143

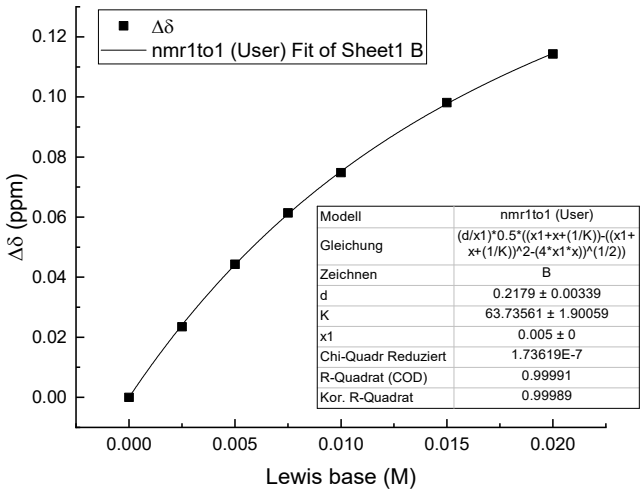

(RM1144)

NMR titration of tris(4-fluorophenyl)borane (1e) with 3,4,5-trichloropyridine (2j)

Entry	Borane (M)	LB (M)	δ (ppm)	Δδ (ppm)
1	5.0×10^{-3}	0.0	7.605	0.000
2	5.0×10^{-3}	2.5×10^{-3}	7.429	0.176
3	5.0×10^{-3}	5.0×10^{-3}	7.319	0.286
4	5.0×10^{-3}	7.5×10^{-3}	7.255	0.350
5	5.0×10^{-3}	1.0×10^{-2}	7.220	0.385
6	5.0×10^{-3}	1.5×10^{-2}	7.181	0.424
7	5.0×10^{-3}	2.0×10^{-2}	7.166	0.439

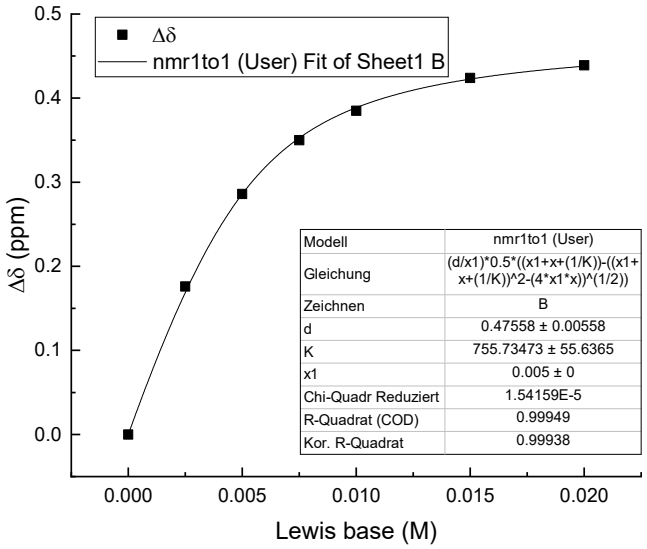

(RM1128)

NMR titration of tris(4-fluorophenyl)borane (1e) with 3,5-difluoro-4-(trifluoromethyl)pyridine (2k)

Entry	Borane (M)	LB (M)	δ (ppm)	Δδ (ppm)
1	5.0×10^{-3}	0.0	7.1794	0.0000
2	5.0×10^{-3}	2.5×10^{-3}	7.1666	0.0128
3	5.0×10^{-3}	5.0×10^{-3}	7.1540	0.0254
4	5.0×10^{-3}	7.5×10^{-3}	7.1434	0.0360
5	5.0×10^{-3}	1.0×10^{-2}	7.1336	0.0458
6	5.0×10^{-3}	1.5×10^{-2}	7.1165	0.0629
7	5.0×10^{-3}	2.0×10^{-2}	7.1030	0.0764

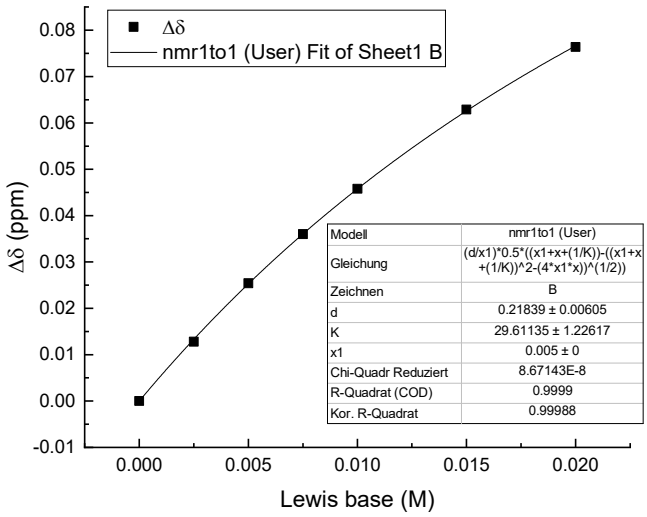

(RM1167)

NMR titration of tris(4-fluorophenyl)borane (1e) with 3,5-dinitropyridine (2l)

Entry	Borane (M)	LB (M)	δ (ppm)	Δδ (ppm)
1	2.5×10^{-3}	0.0	7.1787	0.0000
2	2.5×10^{-3}	1.25×10^{-2}	7.1764	0.0023
3	2.5×10^{-3}	2.50×10^{-2}	7.1733	0.0054
4	2.5×10^{-3}	5.05×10^{-2}	7.1674	0.0113
5	2.5×10^{-3}	1.01×10^{-1}	7.1574	0.0213
6	2.5×10^{-3}	2.00×10^{-1}	7.1360	0.0427
7	2.5×10^{-3}	3.77×10^{-1}	7.1021	0.0766

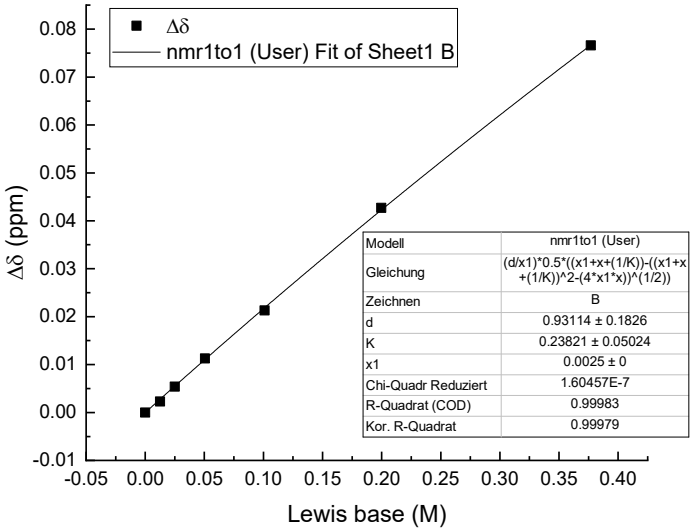

(RM1157)

NMR titration of tris(4-fluorophenyl)borane (1e) with tris(4-methoxyphenyl)phosphine (4a)

Entry	Borane (M)	LB (M)	δ (ppm)	Δδ (ppm)
1	5.0×10^{-3}	0.0	7.605	0.000
2	5.0×10^{-3}	2.5×10^{-3}	7.458	0.147
3	5.0×10^{-3}	5.0×10^{-3}	7.336	0.269
4	5.0×10^{-3}	7.5×10^{-3}	7.266	0.339
5	5.0×10^{-3}	1.0×10^{-2}	7.219	0.386
6	5.0×10^{-3}	1.5×10^{-2}	7.167	0.438

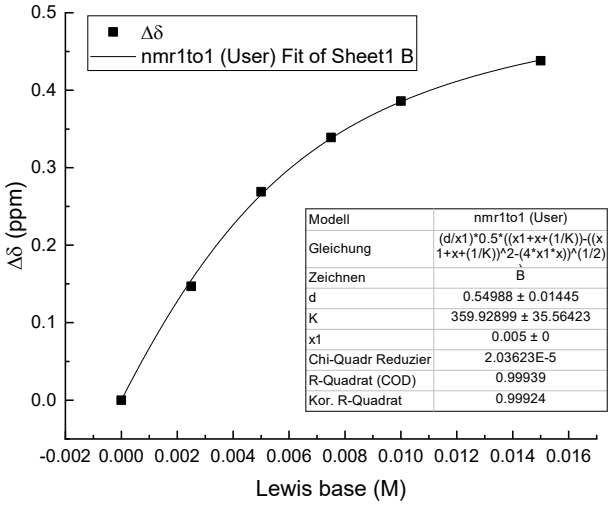

(RM1260)

NMR titration of tris(4-fluorophenyl)borane (1e) with triethylphosphine oxide (10)

Entry	Borane (M)	LB (M)	δ (ppm)	Δδ (ppm)
1	5.0×10^{-3}	0.0	7.604	0.000
2	5.0×10^{-3}	2.5×10^{-3}	7.483	0.121
3	5.0×10^{-3}	5.0×10^{-3}	7.404	0.200
4	5.0×10^{-3}	7.5×10^{-3}	7.374	0.230
5	5.0×10^{-3}	1.0×10^{-2}	7.360	0.244
6	5.0×10^{-3}	1.5×10^{-2}	7.347	0.257
7	5.0×10^{-3}	2.5×10^{-2}	7.336	0.268

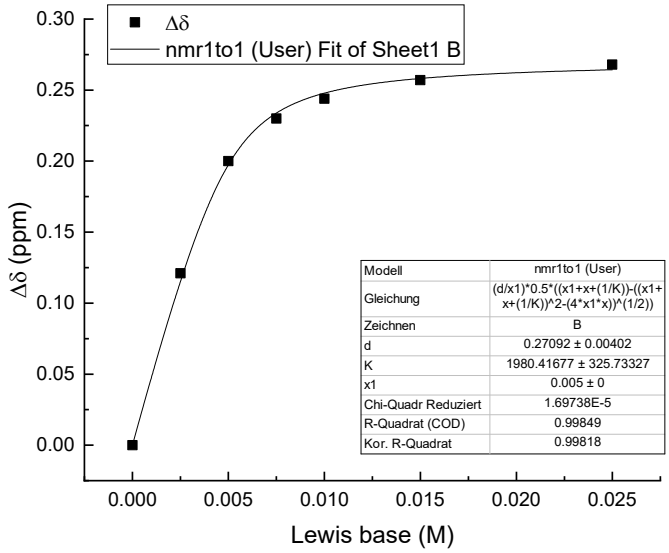

(RM1261)

NMR titration of tris(4-chlorophenyl)borane (1f) with 3,5-bis(trifluoromethyl)pyridine (2i)

Entry	Borane (M)	LB (M)	δ (ppm)	Δδ (ppm)
1	5.0×10^{-3}	0.0	7.529	0.000
2	5.0×10^{-3}	2.5×10^{-3}	7.398	0.131
3	5.0×10^{-3}	5.0×10^{-3}	7.344	0.185
4	5.0×10^{-3}	7.5×10^{-3}	7.313	0.216
5	5.0×10^{-3}	1.0×10^{-2}	7.298	0.231
6	5.0×10^{-3}	1.5×10^{-2}	7.280	0.249
7	5.0×10^{-3}	2.0×10^{-2}	7.272	0.257

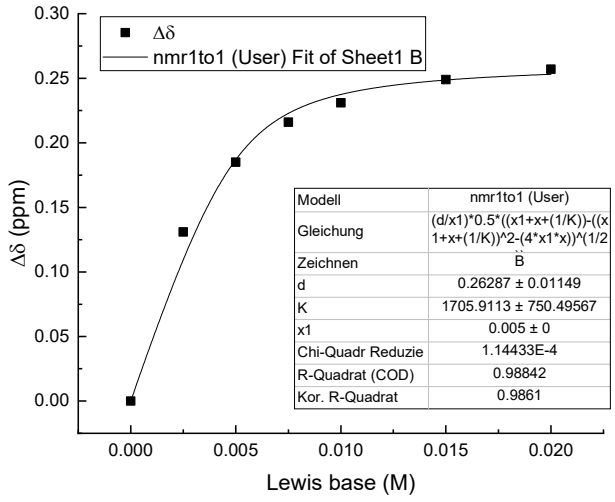

(RM1145)

NMR titration of tris(4-chlorophenyl)borane (1f) with 3,4,5-trichloropyridine (2j)

Entry	Borane (M)	LB (M)	δ (ppm)	Δδ (ppm)
1	5.0×10^{-3}	0.0	7.465	0
2	5.0×10^{-3}	2.5×10^{-3}	7.284	0.181
3	5.0×10^{-3}	5.0×10^{-3}	7.139	0.326
4	5.0×10^{-3}	7.5×10^{-3}	7.103	0.362
5	5.0×10^{-3}	1.0×10^{-2}	7.096	0.369
6	5.0×10^{-3}	1.5×10^{-2}	7.092	0.373
7	5.0×10^{-3}	2.0×10^{-2}	7.090	0.375

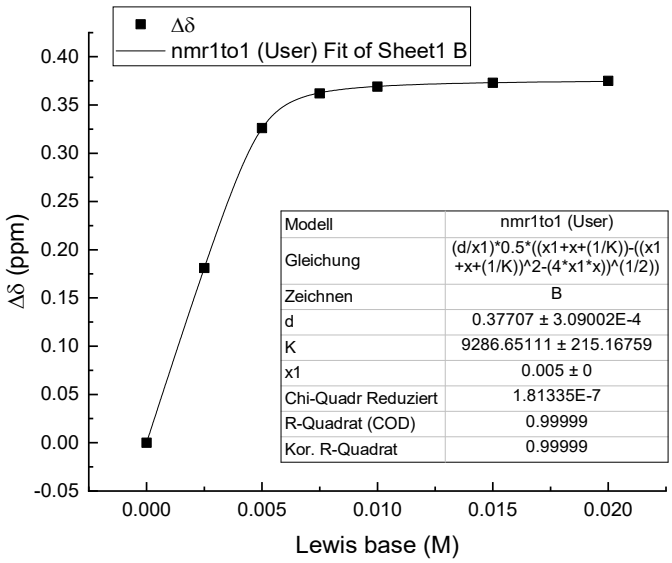

(RM1133)

NMR titration of tris(4-chlorophenyl)borane (1f) with 3,5-difluoro-4-(trifluoromethyl)pyridine (2k)

Entry	Borane (M)	LB (M)	δ (ppm)	Δδ (ppm)
1	5.0×10^{-3}	0.0	7.500	0.000
2	5.0×10^{-3}	2.5×10^{-3}	7.408	0.092
3	5.0×10^{-3}	5.0×10^{-3}	7.343	0.157
4	5.0×10^{-3}	7.5×10^{-3}	7.298	0.202
5	5.0×10^{-3}	1.0×10^{-2}	7.272	0.228
6	5.0×10^{-3}	1.5×10^{-2}	7.238	0.262
7	5.0×10^{-3}	2.0×10^{-2}	7.222	0.278

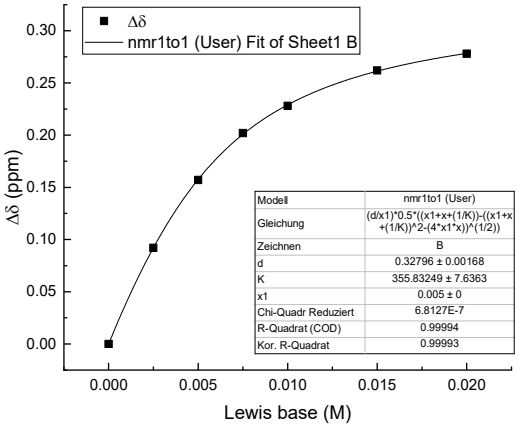

(RM1168)

NMR titration of tris(4-chlorophenyl)borane (1f) with 3,5-dinitropyridine (2l)

Entry	Borane (M)	LB (M)	δ (ppm)	Δδ (ppm)
1	5.0×10^{-3}	0.0	7.495	0.000
2	5.0×10^{-3}	2.5×10^{-3}	7.488	0.007
3	5.0×10^{-3}	5.0×10^{-3}	7.482	0.013
4	5.0×10^{-3}	7.5×10^{-3}	7.477	0.018
5	5.0×10^{-3}	1.0×10^{-2}	7.471	0.024
6	5.0×10^{-3}	1.5×10^{-2}	7.461	0.034
7	5.0×10^{-3}	2.0×10^{-2}	7.447	0.048
8	5.0×10^{-3}	2.5×10^{-2}	7.440	0.055
9	5.0×10^{-3}	5.0×10^{-2}	7.404	0.091
10	5.0×10^{-3}	1.0×10^{-1}	7.347	0.148
11	5.0×10^{-3}	2.0×10^{-1}	7.289	0.206

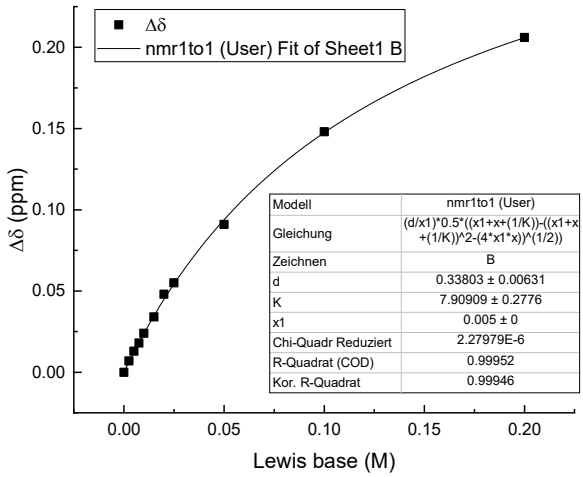

(RM1155)

NMR titration of tris(4-chlorophenyl)borane (1f) with 4-chloro-3,5-dinitropyridine (2m)

Entry	Borane (M)	LB (M)	δ (ppm)	Δδ (ppm)
1	3.0×10^{-3}	0.0	7.499	0.000
2	3.0×10^{-3}	3.0×10^{-2}	7.451	0.048
3	3.0×10^{-3}	7.5×10^{-2}	7.403	0.096
4	3.0×10^{-3}	1.5×10^{-1}	7.345	0.154
5	3.0×10^{-3}	3.0×10^{-1}	7.281	0.218
6	3.0×10^{-3}	4.5×10^{-1}	7.249	0.250
7	3.0×10^{-3}	6.0×10^{-1}	7.225	0.274

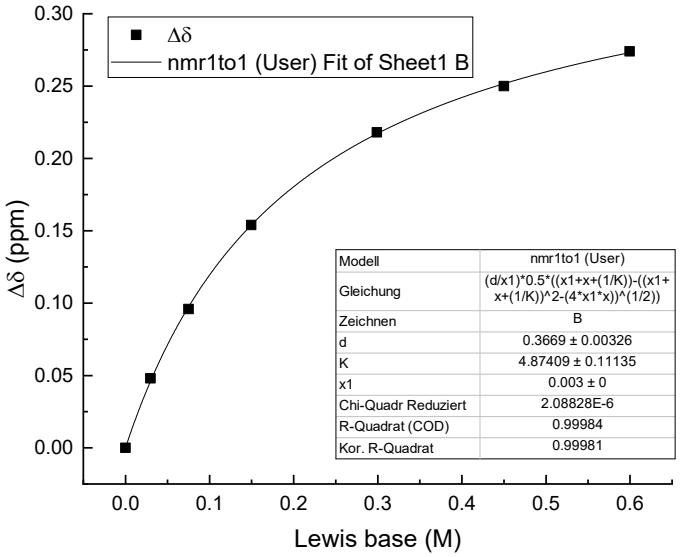

(RM1166)

NMR titration of tris(4-chlorophenyl)borane (1f) with 4-methoxybenzaldehyde (7a)

Entry	Borane (M)	LB (M)	δ (ppm)	Δδ (ppm)
1	5.0×10^{-3}	0.0	7.460	0.000
2	5.0×10^{-3}	5.00×10^{-2}	7.406	0.054
3	5.0×10^{-3}	1.25×10^{-1}	7.363	0.097
4	5.0×10^{-3}	2.00×10^{-1}	7.338	0.122
5	5.0×10^{-3}	3.00×10^{-1}	7.316	0.144

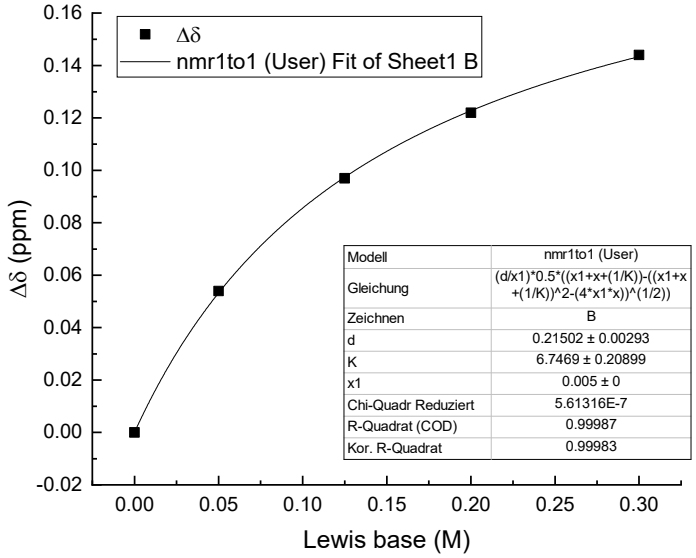

(RM1188)

NMR titration of tris(4-chlorophenyl)borane (1f) with acetonitrile (3a)

Entry	Borane (M)	LB (M)	δ (ppm)	Δδ (ppm)
1	5.0×10^{-3}	0.0	7.498	0.000
2	5.0×10^{-3}	5.0×10^{-2}	7.423	0.075
3	5.0×10^{-3}	1.0×10^{-1}	7.379	0.119
4	5.0×10^{-3}	2.0×10^{-1}	7.320	0.178
5	5.0×10^{-3}	3.5×10^{-1}	7.269	0.229
6	5.0×10^{-3}	5.0×10^{-1}	7.238	0.260
7	5.0×10^{-3}	7.5×10^{-1}	7.210	0.288

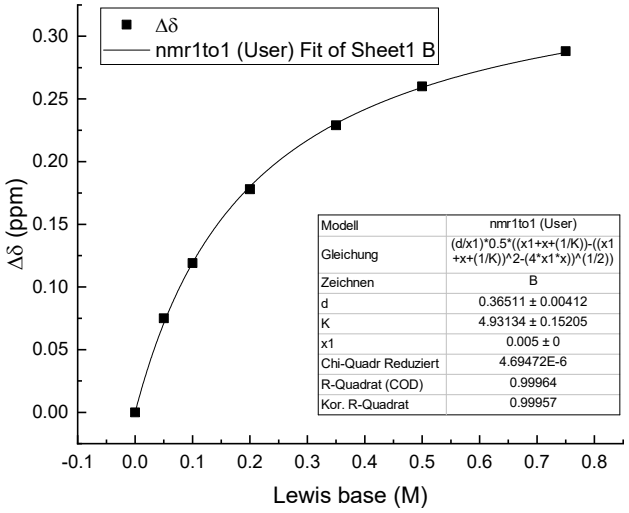

(RM1258)

NMR titration of tris(4-chlorophenyl)borane (1f) with 4-fluorobenzonitrile (3b)

Entry	Borane (M)	LB (M)	δ (ppm)	Δδ (ppm)
1	5.0×10^{-3}	0.0	7.499	0.000
2	5.0×10^{-3}	5.0×10^{-2}	7.473	0.026
3	5.0×10^{-3}	1.0×10^{-1}	7.450	0.049
4	5.0×10^{-3}	2.0×10^{-1}	7.416	0.083
5	5.0×10^{-3}	3.0×10^{-1}	7.388	0.111
6	5.0×10^{-3}	4.0×10^{-1}	7.367	0.132
7	5.0×10^{-3}	5.0×10^{-1}	7.350	0.149

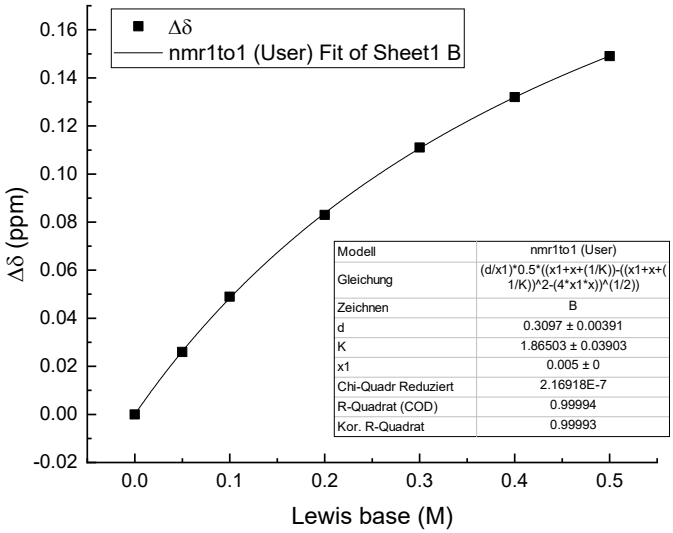

(RM1195)

NMR titration of tris(4-chlorophenyl)borane (1f) with triphenylphosphine (4b)

Entry	Borane (M)	LB (M)	δ (ppm)	Δδ (ppm)
1	5.0×10^{-3}	0.0	7.496	0.000
2	5.0×10^{-3}	2.5×10^{-3}	7.406	0.090
3	5.0×10^{-3}	5.0×10^{-3}	7.340	0.156
4	5.0×10^{-3}	7.5×10^{-3}	7.295	0.201
5	5.0×10^{-3}	1.0×10^{-2}	7.259	0.237
6	5.0×10^{-3}	1.5×10^{-2}	7.206	0.290
7	5.0×10^{-3}	2.0×10^{-2}	7.178	0.318
8	5.0×10^{-3}	5.0×10^{-2}	7.102	0.394
9	5.0×10^{-3}	1.0×10^{-1}	7.079	0.417

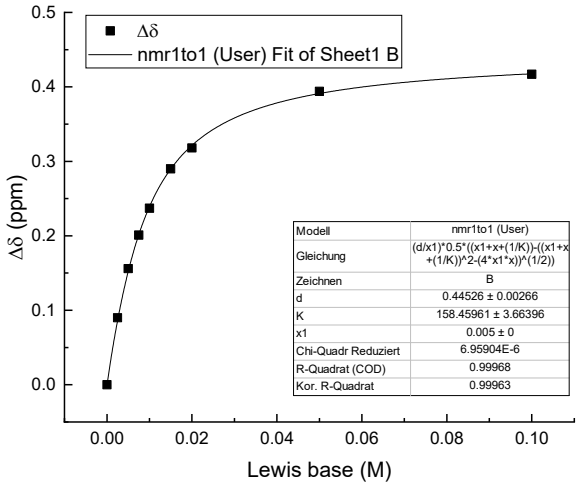

(RM1259)

NMR titration of tris(4-chlorophenyl)borane (1f) with tris(4-chlorophenyl)phosphine (4c)

Entry	Borane (M)	LB (M)	δ (ppm)	Δδ (ppm)
1	5.3×10^{-3}	0.0	7.499	0.000
2	5.3×10^{-3}	2.5×10^{-3}	7.484	0.015
3	5.3×10^{-3}	5.0×10^{-3}	7.471	0.028
4	5.3×10^{-3}	7.5×10^{-3}	7.457	0.042
5	5.3×10^{-3}	1.0×10^{-2}	7.446	0.053
6	5.3×10^{-3}	1.5×10^{-2}	7.424	0.075
7	5.3×10^{-3}	2.5×10^{-2}	7.387	0.112

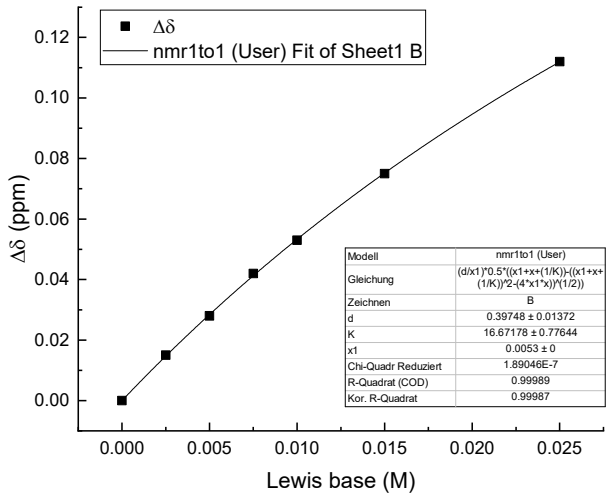

(RM1254)

NMR titration of tris(4-chlorophenyl)borane (1f) with *N*,*N*-dimethylacetamide (9)

Entry	Borane (M)	LB (M)	δ (ppm)	Δδ (ppm)
1	5.0×10^{-3}	0.0	7.499	0.000
2	5.0×10^{-3}	2.5×10^{-3}	7.433	0.066
3	5.0×10^{-3}	5.0×10^{-3}	7.374	0.125
4	5.0×10^{-3}	7.5×10^{-3}	7.337	0.162
5	5.0×10^{-3}	1.0×10^{-2}	7.310	0.189
6	5.0×10^{-3}	1.5×10^{-2}	7.280	0.219
7	5.0×10^{-3}	2.5×10^{-2}	7.252	0.247

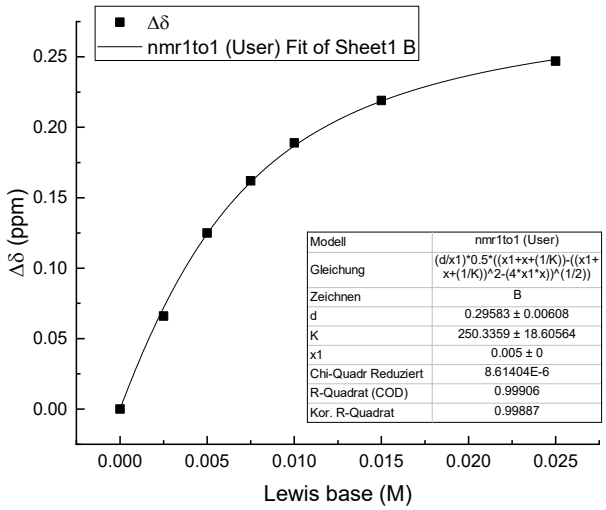

(RM1271)

NMR titration of tris(2,4,6-trifluorophenyl)borane (1g) with 3,5-dinitropyridine (2l)

Entry	Borane (M)	LB (M)	δ (ppm)	Δδ (ppm)
1	5.0×10^{-3}	0.0	6.6768	0.0000
2	5.0×10^{-3}	2.5×10^{-3}	6.6184	0.0584
3	5.0×10^{-3}	5.0×10^{-3}	6.5812	0.0956
4	5.0×10^{-3}	7.5×10^{-3}	6.5687	0.1081
5	5.0×10^{-3}	1.0×10^{-2}	6.5642	0.1126
6	5.0×10^{-3}	1.5×10^{-2}	6.5612	0.1156
7	5.0×10^{-3}	2.0×10^{-2}	6.5598	0.1170

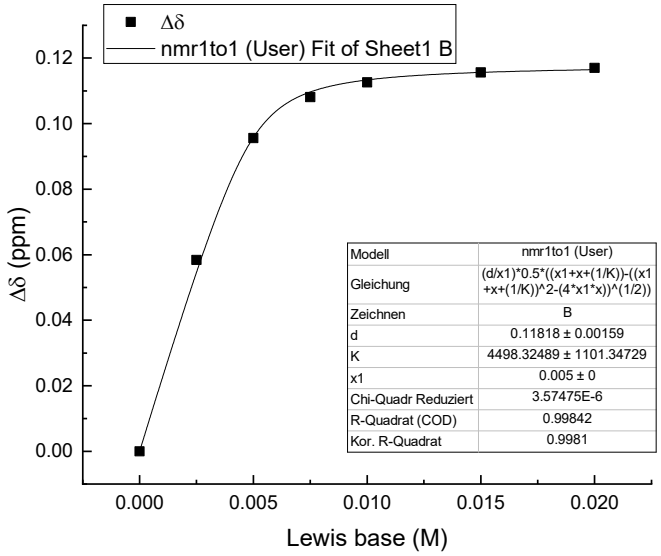

(RM1239)

NMR titration of tris(2,4,6-trifluorophenyl)borane (1g) with 4-chloro-3,5-dinitropyridine (2m)

Entry	Borane (M)	LB (M)	δ (ppm)	Δδ (ppm)
1	5.0×10^{-3}	0.0	6.6811	0.0000
2	5.0×10^{-3}	2.5×10^{-3}	6.6269	0.0542
3	5.0×10^{-3}	5.0×10^{-3}	6.5945	0.0866
4	5.0×10^{-3}	7.5×10^{-3}	6.5790	0.1021
5	5.0×10^{-3}	1.0×10^{-2}	6.5722	0.1089
6	5.0×10^{-3}	2.0×10^{-2}	6.5631	0.1180
7	5.0×10^{-3}	3.0×10^{-2}	6.5603	0.1208

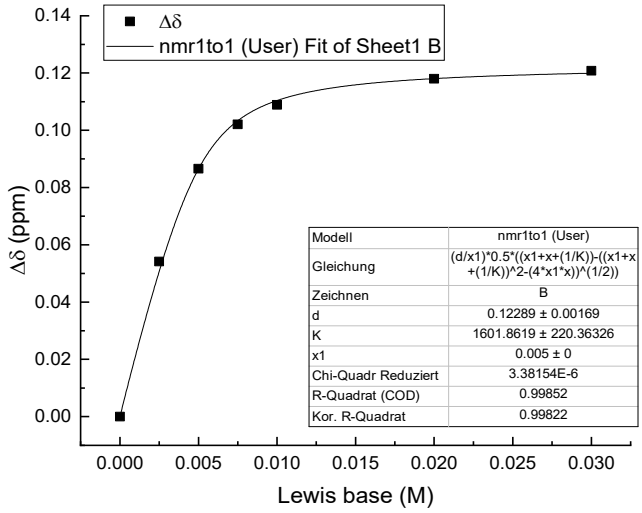

(RM1165)

NMR titration of tris(2,4,6-trifluorophenyl)borane (1g) with 4-fluorobenzonitrile (3b)

Entry	Borane (M)	LB (M)	δ (ppm)	Δδ (ppm)
1	5.0×10^{-3}	0.0	6.6766	0.0000
2	5.0×10^{-3}	2.5×10^{-3}	6.6168	0.0598
3	5.0×10^{-3}	5.0×10^{-3}	6.5771	0.0995
4	5.0×10^{-3}	7.5×10^{-3}	6.5618	0.1148
5	5.0×10^{-3}	1.0×10^{-2}	6.5541	0.1225
6	5.0×10^{-3}	1.5×10^{-2}	6.5495	0.1271
7	5.0×10^{-3}	2.0×10^{-2}	6.5475	0.1291

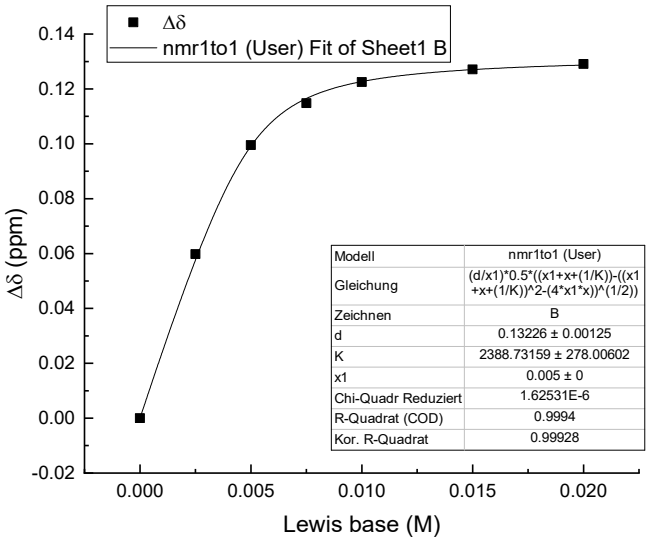

(RM1238)

NMR titration of tris(2,4,6-trifluorophenyl)borane (1g) with tris(4-methoxyphenyl)phosphine (4a)

Entry	Borane (M)	LB (M)	δ (ppm)	Δδ (ppm)
1	5.0×10^{-3}	0.0	6.6759	0.0000
2	5.0×10^{-3}	2.5×10^{-3}	6.5364	0.1395
3	5.0×10^{-3}	5.0×10^{-3}	6.4241	0.2518
4	5.0×10^{-3}	7.5×10^{-3}	6.3767	0.2992
5	5.0×10^{-3}	1.0×10^{-2}	6.3449	0.3310
6	5.0×10^{-3}	1.5×10^{-2}	6.3187	0.3572
7	5.0×10^{-3}	2.0×10^{-2}	6.3065	0.3694

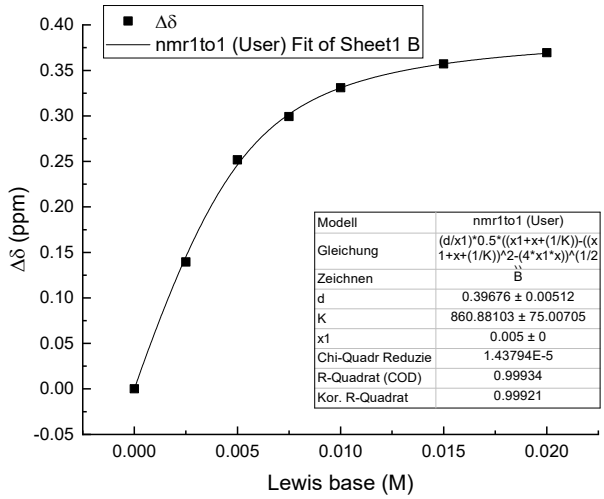

(RM1237)

NMR titration of tris(2,4,6-trifluorophenyl)borane (1g) with 4-methoxyacetophenone (5a)

Entry	Borane (M)	LB (M)	δ (ppm)	Δδ (ppm)
1	5.0×10^{-3}	0.0	6.6790	0.0000
2	5.0×10^{-3}	2.5×10^{-3}	6.6506	0.0284
3	5.0×10^{-3}	5.0×10^{-3}	6.6296	0.0494
4	5.0×10^{-3}	7.5×10^{-3}	6.6124	0.0666
5	5.0×10^{-3}	1.0×10^{-2}	6.5985	0.0805
6	5.0×10^{-3}	1.5×10^{-2}	6.5769	0.1021
7	5.0×10^{-3}	2.0×10^{-2}	6.5627	0.1163

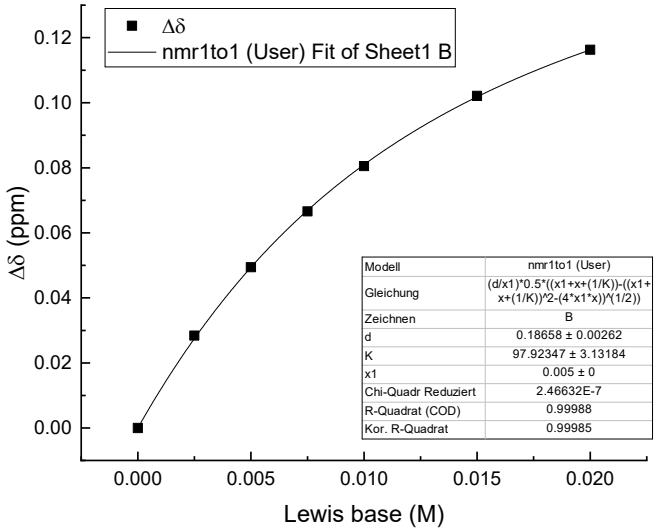

(RM1148)

NMR titration of tris(2,4,6-trifluorophenyl)borane (1g) with 4-methylacetophenone (5b)

Entry	Borane (M)	LB (M)	δ (ppm)	Δδ (ppm)
1	5.0×10^{-3}	0.0	6.6823	0.0000
2	5.0×10^{-3}	2.5×10^{-3}	6.6657	0.0166
3	5.0×10^{-3}	5.0×10^{-3}	6.6608	0.0215
4	5.0×10^{-3}	7.5×10^{-3}	6.6484	0.0339
5	5.0×10^{-3}	1.0×10^{-2}	6.6353	0.0470
6	5.0×10^{-3}	2.0×10^{-2}	6.6138	0.0685
7	5.0×10^{-3}	3.0×10^{-2}	6.5817	0.1006
8	5.0×10^{-3}	6.0×10^{-2}	6.5557	0.1266
9	5.0×10^{-3}	1.0×10^{-1}	6.5252	0.1571

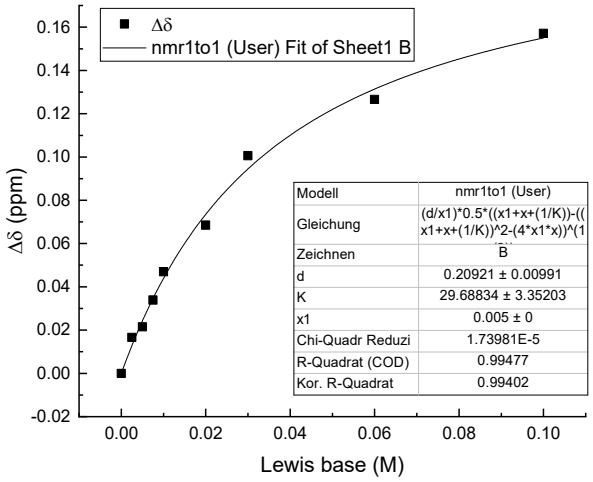

(RM1141)

NMR titration of tris(2,4,6-trifluorophenyl)borane (1g) with 4-bromoacetophenone (5c)

Entry	Borane (M)	LB (M)	δ (ppm)	Δδ (ppm)
1	3.0×10^{-3}	0.0	6.6815	0.0000
2	3.0×10^{-3}	3.00×10^{-2}	6.6619	0.0196
3	3.0×10^{-3}	5.95×10^{-2}	6.6381	0.0434
4	3.0×10^{-3}	1.12×10^{-1}	6.6168	0.0647
5	3.0×10^{-3}	1.81×10^{-1}	6.5958	0.0857
6	3.0×10^{-3}	2.41×10^{-1}	6.5891	0.0924
7	3.0×10^{-3}	3.00×10^{-1}	6.5828	0.0987

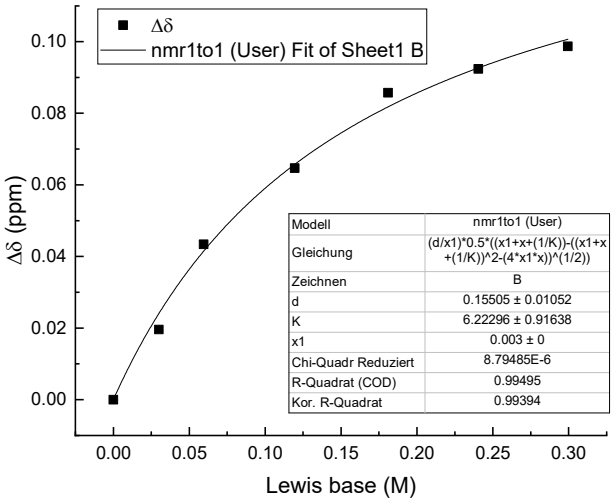

(RM1177)

NMR titration of tris(2,4,6-trifluorophenyl)borane (1g) with 4-(trifluoromethyl)acetophenone (5d)

Entry	Borane (M)	LB (M)	δ (ppm)	Δδ (ppm)
1	3.0×10^{-3}	0.0	6.6783	0.0000
2	3.0×10^{-3}	3.0×10^{-3}	6.6779	0.0004
3	3.0×10^{-3}	7.5×10^{-3}	6.6777	0.0006
4	3.0×10^{-3}	1.5×10^{-2}	6.6751	0.0032
5	3.0×10^{-3}	3.0×10^{-2}	6.6730	0.0053
6	3.0×10^{-3}	6.1×10^{-2}	6.6682	0.0101
7	3.0×10^{-3}	1.2×10^{-1}	6.6618	0.0165
8	3.0×10^{-3}	2.8×10^{-1}	6.6538	0.0245

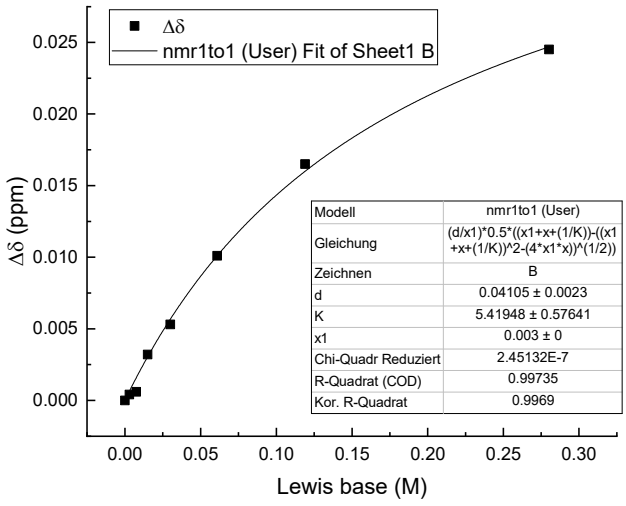

(RM1153)

NMR titration of tris(2,4,6-trifluorophenyl)borane (1g) with 4-nitroacetophenone (5e)

Entry	Borane (M)	LB (M)	δ (ppm)	Δδ (ppm)
1	4.0×10^{-3}	0.0	6.6807	0.0000
2	4.0×10^{-3}	4.00×10^{-2}	6.6721	0.0086
3	4.0×10^{-3}	1.00×10^{-1}	6.6645	0.0162
4	4.0×10^{-3}	2.00×10^{-1}	6.6597	0.0210
5	4.0×10^{-3}	4.00×10^{-1}	6.6493	0.0314
6	4.0×10^{-3}	6.01×10^{-1}	6.6459	0.0348

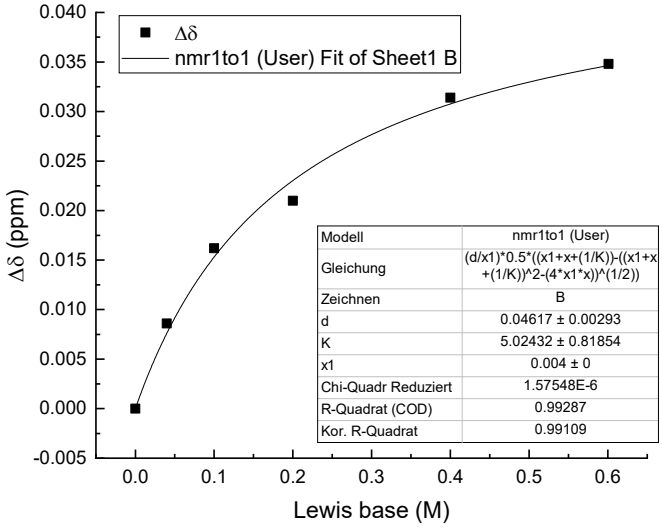

(RM1158)

NMR titration of tris(2,4,6-trifluorophenyl)borane (1g) with 4-methoxybenzaldehyde (7a)

Entry	Borane (M)	LB (M)	δ (ppm)	Δδ (ppm)
1	4.3×10^{-3}	0.0	6.6481	0.0000
2	4.3×10^{-3}	2.5×10^{-3}	6.5750	0.0731
3	4.3×10^{-3}	5.0×10^{-3}	6.5432	0.1049
4	4.3×10^{-3}	7.5×10^{-3}	6.5307	0.1174
5	4.3×10^{-3}	1.0×10^{-2}	6.5279	0.1202
6	4.3×10^{-3}	1.5×10^{-2}	6.5257	0.1224
7	4.3×10^{-3}	2.5×10^{-2}	6.5239	0.1242

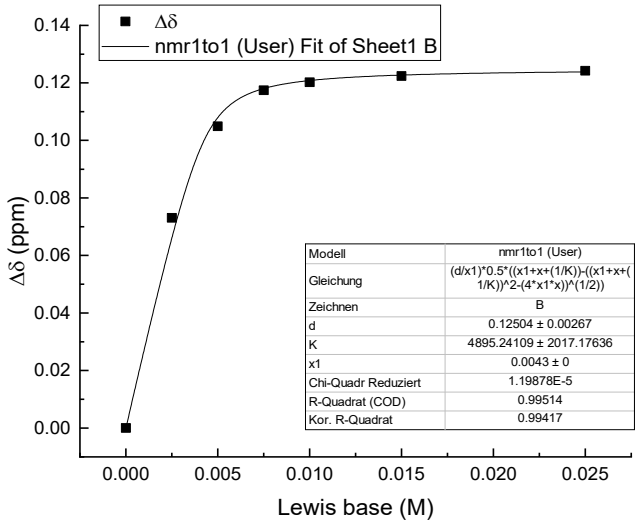

(RM1187)

NMR titration of tris(2,4,6-trifluorophenyl)borane (1g) with benzaldehyde (7b)

Entry	Borane (M)	LB (M)	δ (ppm)	Δδ (ppm)
1	5.0×10^{-3}	0.0	6.6803	0.0000
2	5.0×10^{-3}	2.5×10^{-3}	6.6548	0.0255
3	5.0×10^{-3}	5.0×10^{-3}	6.6339	0.0464
4	5.0×10^{-3}	7.5×10^{-3}	6.6177	0.0626
5	5.0×10^{-3}	1.0×10^{-2}	6.6059	0.0744
6	5.0×10^{-3}	1.5×10^{-2}	6.5892	0.0911
7	5.0×10^{-3}	2.5×10^{-2}	6.5722	0.1081

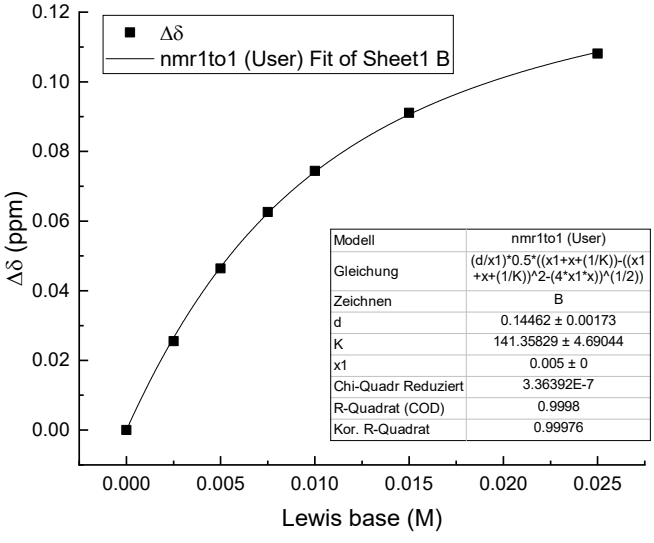

(RM1214)

NMR titration of tris(2,4,6-trifluorophenyl)borane (1g) with 4-bromobenzaldehyde (7c)

Entry	Borane (M)	LB (M)	δ (ppm)	Δδ (ppm)
1	5.0×10^{-3}	0.0	6.6507	0.0000
2	5.0×10^{-3}	5.0×10^{-3}	6.6293	0.0214
3	5.0×10^{-3}	1.5×10^{-2}	6.6034	0.0473
4	5.0×10^{-3}	2.5×10^{-2}	6.5878	0.0629
5	5.0×10^{-3}	4.0×10^{-2}	6.5731	0.0776
6	5.0×10^{-3}	5.5×10^{-2}	6.5652	0.0855
7	5.0×10^{-3}	7.5×10^{-2}	6.5588	0.0919

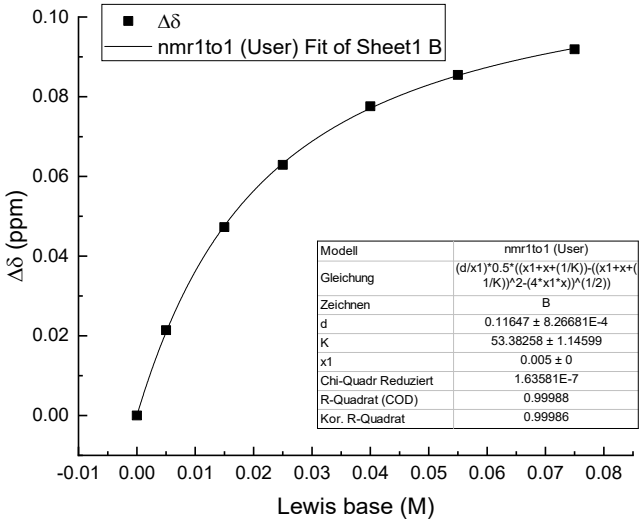

(RM1186)

NMR titration of tris(2,4,6-trifluorophenyl)borane (1g) with 4-nitrobenzaldehyde (7d)

Entry	Borane (M)	LB (M)	δ (ppm)	Δδ (ppm)
1	5.0×10^{-3}	0.0	10.1462	0.0000
2	5.0×10^{-3}	1.65×10^{-2}	10.1248	0.0214
3	5.0×10^{-3}	3.30×10^{-2}	10.1049	0.0413
4	5.0×10^{-3}	5.05×10^{-2}	10.0826	0.0636
5	5.0×10^{-3}	7.50×10^{-2}	10.0560	0.0902
6	5.0×10^{-3}	1.175×10^{-1}	10.0178	0.1284

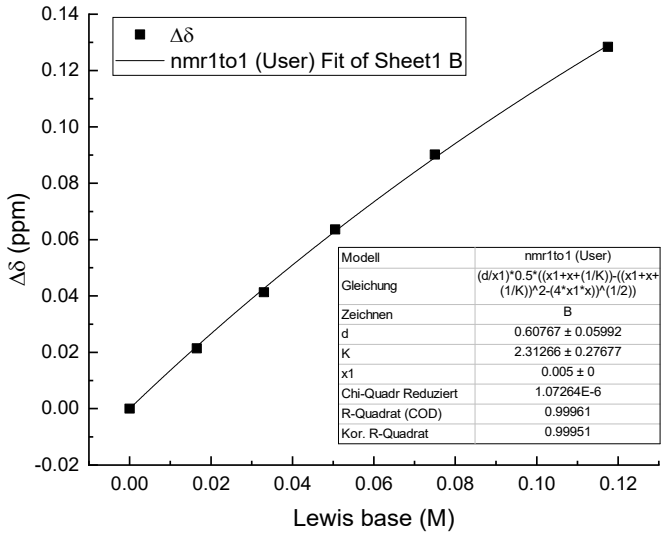

(RM1185)

NMR titration of tris(2,4,6-trifluorophenyl)borane (1g) with trans-crotonaldehyde (8)

Entry	Borane (M)	LB (M)	δ (ppm)	Δδ (ppm)
1	5.0×10^{-3}	0.0	6.6572	0.0000
2	5.0×10^{-3}	2.5×10^{-3}	6.5982	0.0590
3	5.0×10^{-3}	5.0×10^{-3}	6.5627	0.0945
4	5.0×10^{-3}	7.5×10^{-3}	6.5454	0.1118
5	5.0×10^{-3}	1.0×10^{-2}	6.5377	0.1195
6	5.0×10^{-3}	1.5×10^{-2}	6.5295	0.1277
7	5.0×10^{-3}	2.5×10^{-2}	6.5231	0.1341

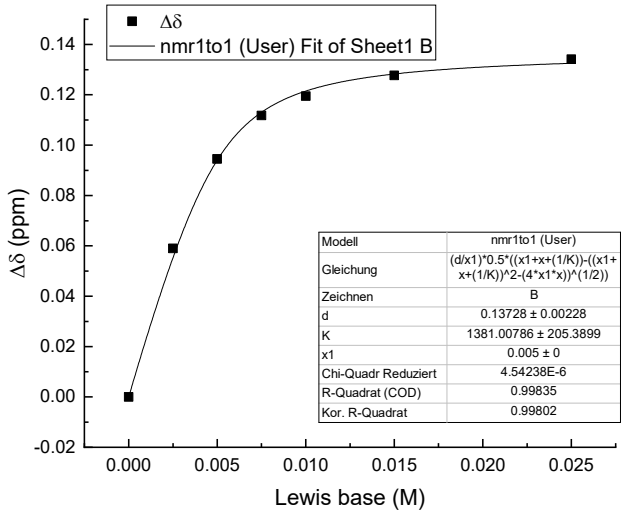

(RM1184)

NMR titration of tris(3,4,5-trifluorophenyl)borane (1h) with 3,5-dinitropyridine (2l)

Entry	Borane (M)	LB (M)	δ (ppm)	Δδ (ppm)
1	4.0×10^{-3}	0.0	7.1927	0.0000
2	4.0×10^{-3}	1.32×10^{-3}	7.1036	0.0891
3	4.0×10^{-3}	2.64×10^{-3}	7.0273	0.1654
4	4.0×10^{-3}	4.00×10^{-3}	6.9675	0.2252
5	4.0×10^{-3}	5.32×10^{-2}	6.9280	0.2647
6	4.0×10^{-3}	6.64×10^{-2}	6.8935	0.2992
7	4.0×10^{-3}	8.00×10^{-2}	6.8640	0.3287

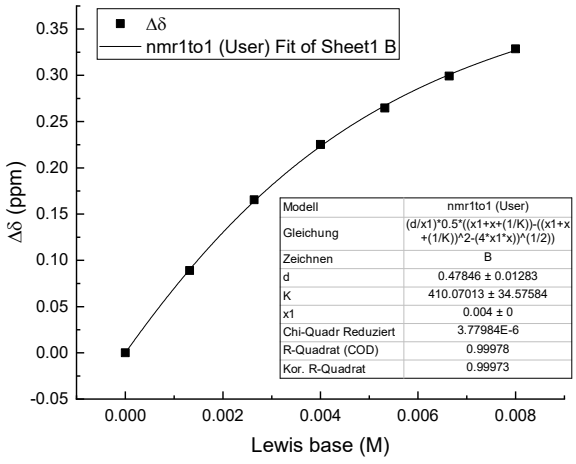

(RM1174)

NMR titration of tris(3,4,5-trifluorophenyl)borane (1h) with 4-chloro-3,5-dinitropyridine (2m)

Entry	Borane (M)	LB (M)	δ (ppm)	Δδ (ppm)
1	5.0×10^{-3}	0.0	7.1864	0.0000
2	5.0×10^{-3}	2.5×10^{-3}	7.0850	0.1014
3	5.0×10^{-3}	5.0×10^{-3}	7.0136	0.1728
4	5.0×10^{-3}	7.5×10^{-3}	6.9547	0.2317
5	5.0×10^{-3}	1.0×10^{-2}	6.9175	0.2689
6	5.0×10^{-3}	1.5×10^{-2}	6.8637	0.3227
7	5.0×10^{-3}	2.0×10^{-2}	6.8341	0.3523

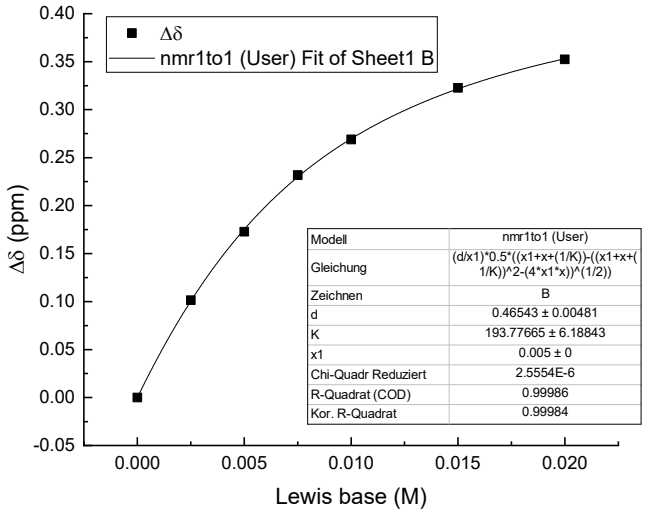

(RM1173)

NMR titration of tris(3,4,5-trifluorophenyl)borane (1h) with acetonitrile (3a)

Entry	Borane (M)	LB (M)	δ (ppm)	Δδ (ppm)
1	5.0×10^{-3}	0.0	7.1920	0.0000
2	5.0×10^{-3}	2.5×10^{-3}	6.9743	0.2177
3	5.0×10^{-3}	5.0×10^{-3}	6.8132	0.3788
4	5.0×10^{-3}	7.5×10^{-3}	6.7617	0.4303
5	5.0×10^{-3}	1.0×10^{-2}	6.7465	0.4455
6	5.0×10^{-3}	1.5×10^{-2}	6.7362	0.4558
7	5.0×10^{-3}	2.0×10^{-2}	6.7325	0.4595

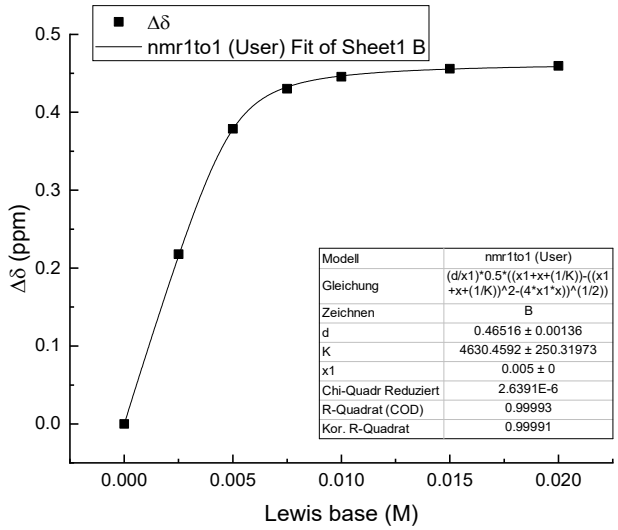

(RM1211)

NMR titration of tris(3,4,5-trifluorophenyl)borane (1h) with 4-fluorobenzonitrile (3b)

Entry	Borane (M)	LB (M)	δ (ppm)	Δδ (ppm)
1	5.0×10^{-3}	0.0	7.1654	0.0000
2	5.0×10^{-3}	2.5×10^{-3}	7.0004	0.1650
3	5.0×10^{-3}	5.0×10^{-3}	6.9005	0.2649
4	5.0×10^{-3}	7.5×10^{-3}	6.8572	0.3082
5	5.0×10^{-3}	1.0×10^{-2}	6.8378	0.3276
6	5.0×10^{-3}	1.5×10^{-2}	6.8210	0.3444
7	5.0×10^{-3}	2.0×10^{-2}	6.8142	0.3512

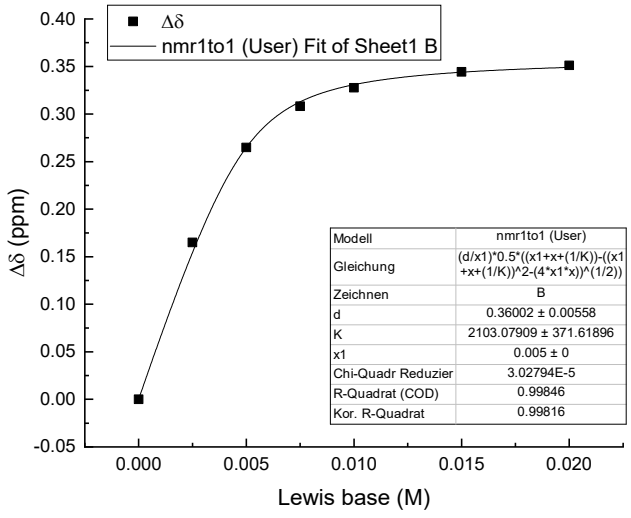

(RM1201)

NMR titration of tris(3,4,5-trifluorophenyl)borane (1h) with 4-methoxyacetophenone (5a)

Entry	Borane (M)	LB (M)	δ (ppm)	Δδ (ppm)
1	5.0×10^{-3}	0.0	7.1869	0.0000
2	5.0×10^{-3}	5.0×10^{-3}	7.0956	0.0913
3	5.0×10^{-3}	1.0×10^{-2}	7.0429	0.1440
4	5.0×10^{-3}	1.75×10^{-2}	6.9944	0.1925
5	5.0×10^{-3}	2.50×10^{-2}	6.9704	0.2165
6	5.0×10^{-3}	3.75×10^{-2}	6.9427	0.2442
7	5.0×10^{-3}	5.0×10^{-2}	6.9333	0.2536

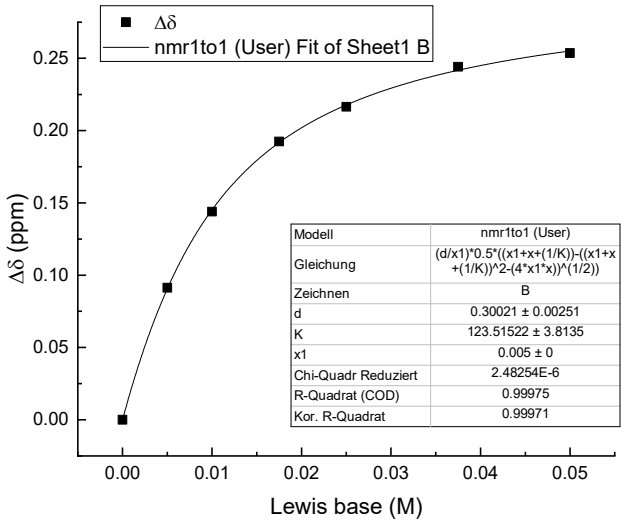

(RM1172)

NMR titration of tris(3,4,5-trifluorophenyl)borane (1h) with 4-methylacetophenone (5b)

Entry	Borane (M)	LB (M)	δ (ppm)	Δδ (ppm)
1	5.0×10^{-3}	0.0	7.193	0.000
2	5.0×10^{-3}	2.5×10^{-3}	7.176	0.017
3	5.0×10^{-3}	5.0×10^{-3}	7.164	0.029
4	5.0×10^{-3}	7.5×10^{-3}	7.150	0.043
5	5.0×10^{-3}	1.0×10^{-2}	7.139	0.054
6	5.0×10^{-3}	2.0×10^{-2}	7.088	0.105
7	5.0×10^{-3}	3.0×10^{-2}	7.047	0.146
8	5.0×10^{-3}	7.41×10^{-2}	6.985	0.208
9	5.0×10^{-3}	1.59×10^{-1}	6.944	0.249

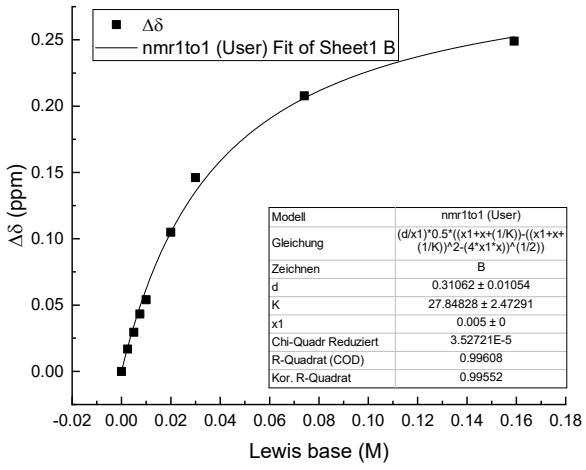

(RM1163)

NMR titration of tris(3,4,5-trifluorophenyl)borane (1h) with *p*-anisaldehyde (7a)

Entry	Borane (M)	LB (M)	δ (ppm)	Δδ (ppm)
1	5.0×10^{-3}	0.0	6.6584	0.0000
2	5.0×10^{-3}	2.5×10^{-3}	6.5893	0.0691
3	5.0×10^{-3}	5.0×10^{-3}	6.5609	0.0975
4	5.0×10^{-3}	7.5×10^{-3}	6.5529	0.1055
5	5.0×10^{-3}	1.0×10^{-2}	6.5493	0.1091
6	5.0×10^{-3}	1.5×10^{-2}	6.5465	0.1119
7	5.0×10^{-3}	2.0×10^{-2}	6.5466	0.1118

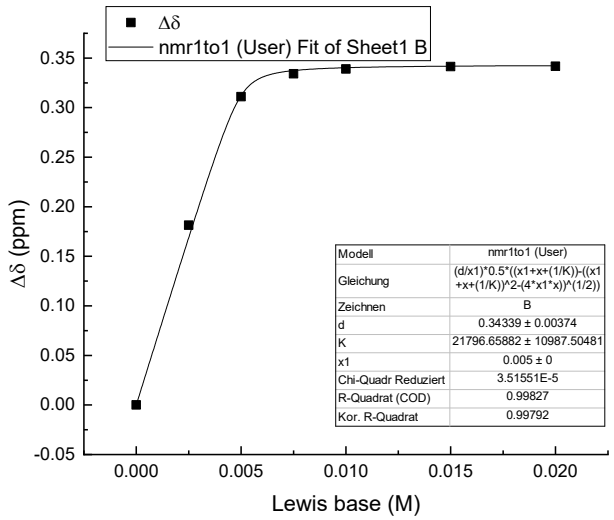

(RM1198)

NMR titration of tris(3,4,5-trifluorophenyl)borane (1h) with benzaldehyde (7b)

Entry	Borane (M)	LB (M)	δ (ppm)	Δδ (ppm)
1	5.0×10^{-3}	0.0	7.1840	0.0000
2	5.0×10^{-3}	2.5×10^{-3}	7.1075	0.0765
3	5.0×10^{-3}	5.0×10^{-3}	7.0470	0.1370
4	5.0×10^{-3}	7.5×10^{-3}	7.0076	0.1764
5	5.0×10^{-3}	1.0×10^{-2}	6.9774	0.2066
6	5.0×10^{-3}	1.5×10^{-2}	6.9415	0.2425
7	5.0×10^{-3}	2.5×10^{-2}	6.9052	0.2788

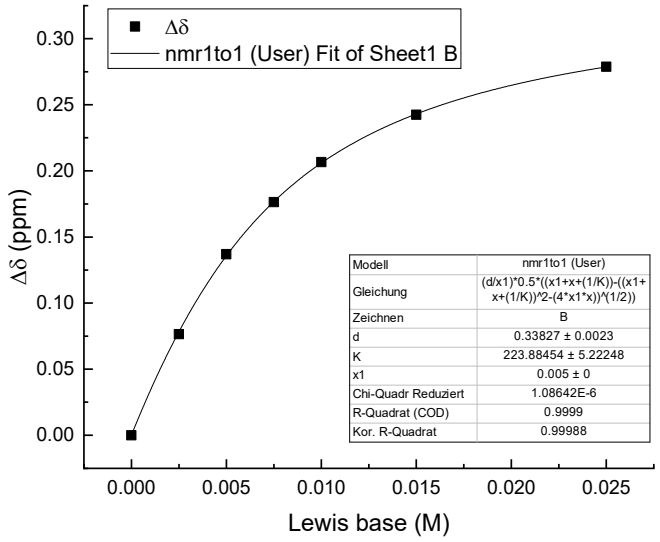

(RM1257)

NMR titration of tris(3,4,5-trifluorophenyl)borane (1h) with 4-bromobenzaldehyde (7c)

Entry	Borane (M)	LB (M)	δ (ppm)	Δδ (ppm)
1	5.0×10^{-3}	0.0	7.1720	0.0000
2	5.0×10^{-3}	5.0×10^{-2}	7.0955	0.0765
3	5.0×10^{-3}	1.5×10^{-1}	7.0154	0.1566
4	5.0×10^{-3}	2.5×10^{-1}	6.9667	0.2053
5	5.0×10^{-3}	4.0×10^{-1}	6.9269	0.2451
6	5.0×10^{-3}	5.5×10^{-1}	6.9053	0.2667
7	5.0×10^{-3}	7.5×10^{-1}	6.8869	0.2851

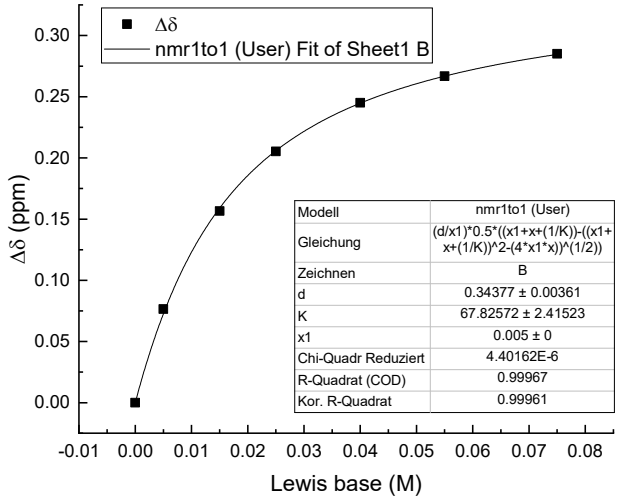

(RM1197)

NMR titration of tris(3,4,5-trifluorophenyl)borane (1h) with 4-nitrobenzaldehyde (7d)

Entry	Borane (M)	LB (M)	δ (ppm)	Δδ (ppm)
1	5.0×10^{-3}	0.0	10.1462	0.0000
2	5.0×10^{-3}	2.45×10^{-2}	10.1236	0.0226
3	5.0×10^{-3}	6.26×10^{-2}	10.0860	0.0602
4	5.0×10^{-3}	1.25×10^{-1}	10.0338	0.1124
5	5.0×10^{-3}	2.005×10^{-1}	9.9778	0.1684

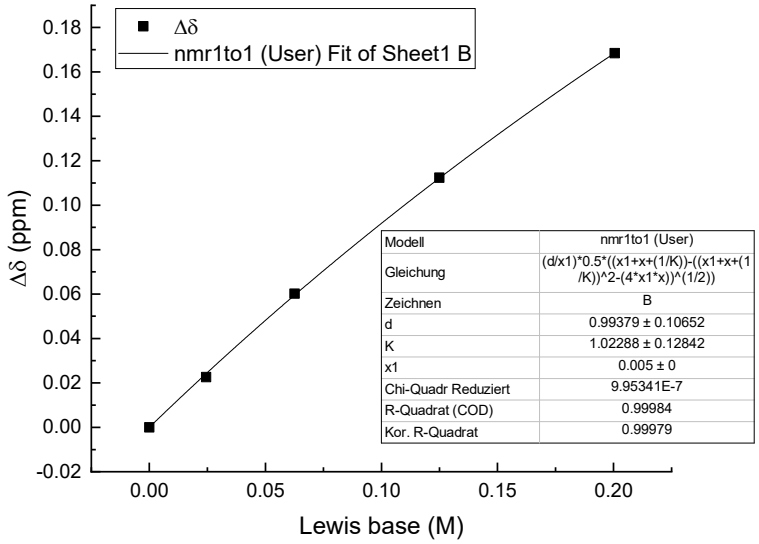

(RM1196)

NMR titration of tris(3,4,5-trifluorophenyl)borane (1h) with trans-crotonaldehyde (8)

Entry	Borane (M)	LB (M)	δ (ppm)	Δδ (ppm)
1	5.0×10^{-3}	0.0	7.1816	0.0000
2	5.0×10^{-3}	2.5×10^{-3}	6.9953	0.1863
3	5.0×10^{-3}	5.0×10^{-3}	6.8664	0.3152
4	5.0×10^{-3}	7.5×10^{-3}	6.8256	0.3560
5	5.0×10^{-3}	1.0×10^{-2}	6.8015	0.3801
6	5.0×10^{-3}	1.5×10^{-2}	6.7889	0.3927
7	5.0×10^{-3}	2.5×10^{-2}	6.7803	0.4013

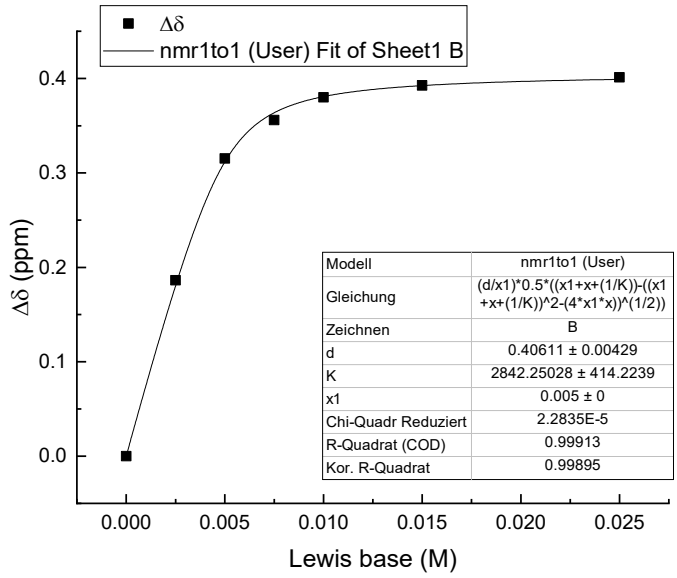

(RM1199)

NMR titration of 2,6-lutidine (2n) with tris(pentafluorophenyl)borane (1i)

Entry	LB (M)	Borane (M)	δ (ppm)	Δδ (ppm)
1	5.0×10^{-3}	0.0	2.4587	0.0000
2	5.0×10^{-3}	5.0×10^{-3}	2.5026	0.0439
3	5.0×10^{-3}	2.0×10^{-2}	2.5667	0.1080
4	5.0×10^{-3}	3.0×10^{-2}	2.5888	0.1301
5	5.0×10^{-3}	4.0×10^{-2}	2.6004	0.1417
6	5.0×10^{-3}	5.0×10^{-2}	2.6224	0.1637

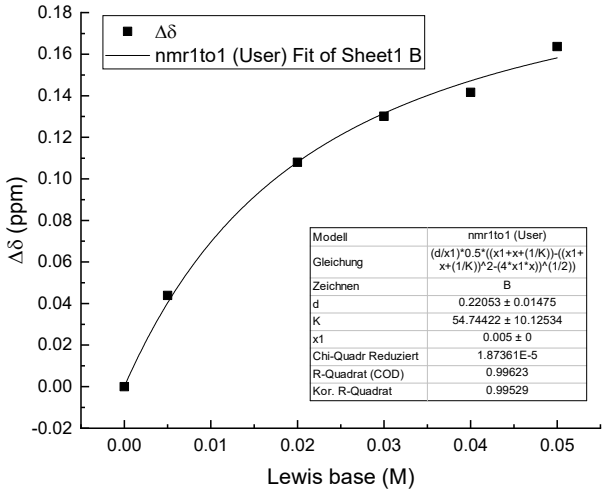

(RM1240)

NMR titration of 4-bromoacetophenone (5c) with tris(pentafluorophenyl)borane (1i)

Entry	LB (M)	Borane (M)	δ (ppm)	Δδ (ppm)
1	5.0×10^{-3}	0.0	7.722	0.000
2	5.0×10^{-3}	2.0×10^{-3}	7.791	0.069
3	5.0×10^{-3}	3.75×10^{-3}	7.854	0.132
4	5.0×10^{-3}	5.0×10^{-3}	7.906	0.184
5	5.0×10^{-3}	6.25×10^{-3}	7.929	0.207
6	5.0×10^{-3}	7.50×10^{-3}	7.935	0.213
7	5.0×10^{-3}	1.0×10^{-2}	7.941	0.219
8	5.0×10^{-3}	1.5×10^{-2}	7.941	0.219

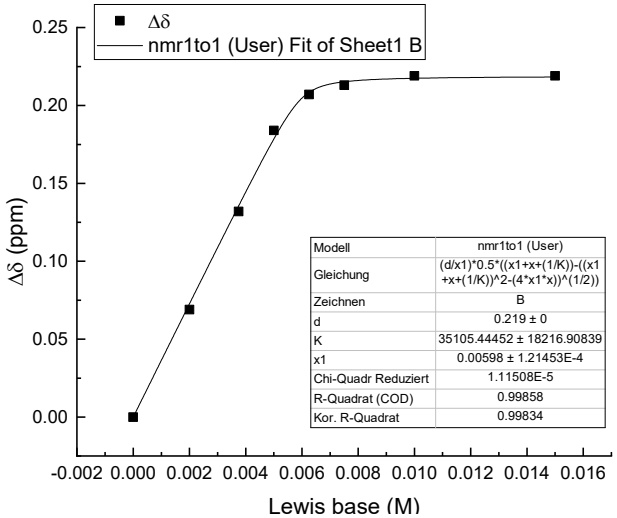

(RM1176/RM1241)

The value of x1 (that is, the LB concentration) was allowed to vary in the fitting process.

NMR titration of 4-(trifluoromethyl)acetophenone (5d) with tris(pentafluorophenyl)borane (1i)

Entry	LB (M)	Borane (M)	δ (ppm)	Δδ (ppm)
1	5.0×10^{-3}	0.00	2.6261	0.0000
2	5.0×10^{-3}	1.65×10^{-3}	2.6860	0.0599
3	5.0×10^{-3}	3.30×10^{-3}	2.7559	0.1298
4	5.0×10^{-3}	5.00×10^{-3}	2.8257	0.1996
5	5.0×10^{-3}	6.65×10^{-3}	2.8625	0.2364
6	5.0×10^{-3}	1.00×10^{-2}	2.8844	0.2583
7	5.0×10^{-3}	1.50×10^{-2}	2.8912	0.2651

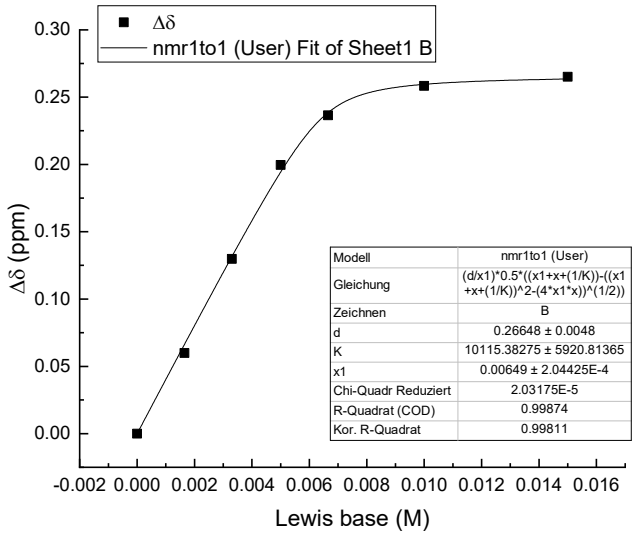

(RM1251)

NMR titration of 4-nitroacetophenone (5e) with tris(pentafluorophenyl)borane (1i)

Entry	LB (M)	Borane (M)	δ (ppm)	Δδ (ppm)
1	5.0×10^{-3}	0.0	2.6542	0.0000
2	5.0×10^{-3}	2.5×10^{-3}	2.7437	0.0895
3	5.0×10^{-3}	5.0×10^{-3}	2.8238	0.1696
4	5.0×10^{-3}	7.5×10^{-3}	2.8638	0.2096
5	5.0×10^{-3}	1.0×10^{-2}	2.8800	0.2258
6	5.0×10^{-3}	1.5×10^{-2}	2.9036	0.2494
7	5.0×10^{-3}	2.0×10^{-2}	2.9161	0.2619

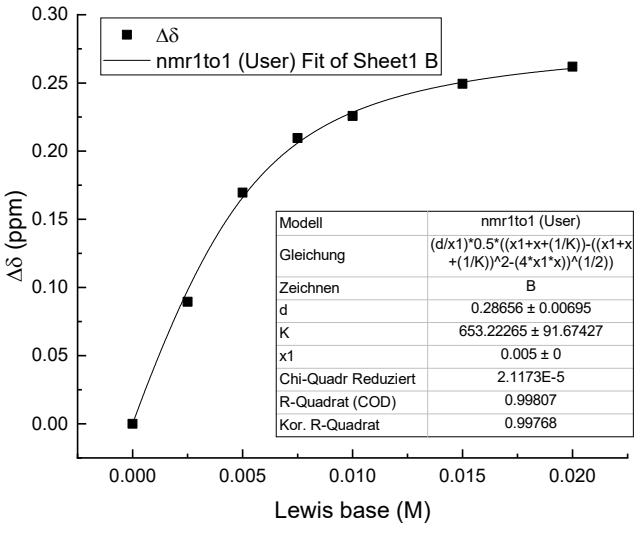

(RM1143)

NMR titration of 3,5-dinitroacetophenone (5f) with tris(pentafluorophenyl)borane (1i)

Entry	LB (M)	Borane (M)	δ (ppm)	Δδ (ppm)
1	5.0×10^{-3}	0.0	9.2197	0.0000
2	5.0×10^{-3}	2.5×10^{-3}	9.2282	0.0085
3	5.0×10^{-3}	5.0×10^{-3}	9.2411	0.0214
4	5.0×10^{-3}	7.5×10^{-3}	9.2500	0.0303
5	5.0×10^{-3}	1.0×10^{-2}	9.2573	0.0376
6	5.0×10^{-3}	1.5×10^{-2}	9.2738	0.0541
7	5.0×10^{-3}	2.0×10^{-2}	9.2891	0.0694

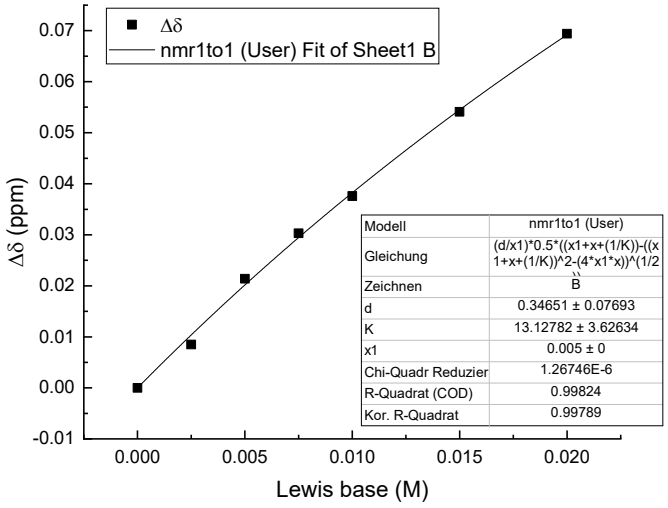

(RM1150)

NMR titration of methyl benzoate (6) with tris(pentafluorophenyl)borane (1i)

Entry	LB (M)	Borane (M)	δ (ppm)	Δδ (ppm)
1	5.0×10^{-3}	0.0	8.018	0.000
2	5.0×10^{-3}	2.5×10^{-3}	7.983	0.035
3	5.0×10^{-3}	5.0×10^{-3}	7.973	0.045
4	5.0×10^{-3}	7.5×10^{-3}	7.954	0.064
5	5.0×10^{-3}	1.0×10^{-2}	7.923	0.095
6	5.0×10^{-3}	1.5×10^{-2}	7.907	0.111
7	5.0×10^{-3}	2.5×10^{-2}	7.876	0.142

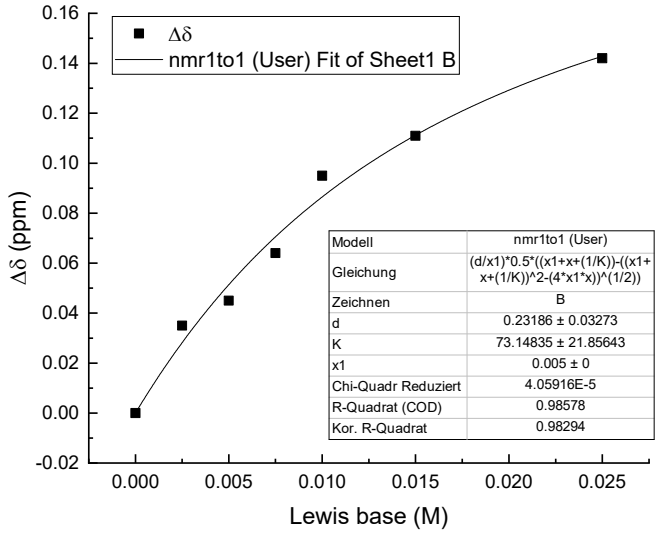

(RM1200)

NMR titration of 4-nitrobenzaldehyde (7d) with tris(pentafluorophenyl)borane (1i)

Entry	LB (M)	Borane (M)	δ (ppm)	Δδ (ppm)
1	5.0×10^{-3}	0.0	10.1462	0.0000
2	5.0×10^{-3}	2.5×10^{-3}	9.8925	0.2537
3	5.0×10^{-3}	5.0×10^{-3}	9.6528	0.4934
4	5.0×10^{-3}	7.5×10^{-3}	9.5759	0.5703
5	5.0×10^{-3}	1.0×10^{-2}	9.5604	0.5858
6	5.0×10^{-3}	1.5×10^{-2}	9.5534	0.5928
7	5.0×10^{-3}	2.0×10^{-2}	9.5510	0.5952

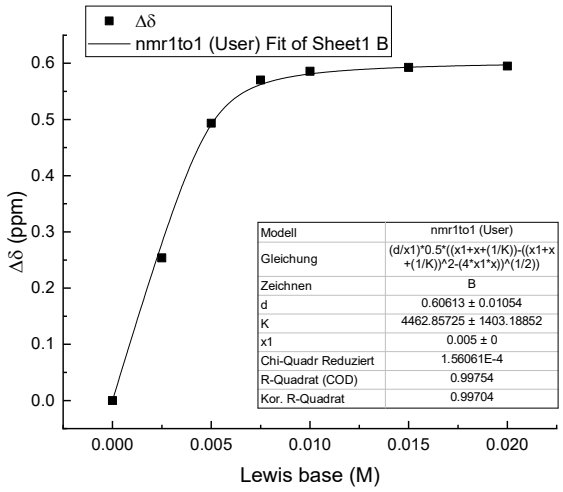

(RM1180)

NMR titration of 4-(dimethylamino)pyridine (2a) with tris(2,4,6-trimethylphenyl)borane (1j)

Entry	LB (M)	Borane (M)	δ (ppm)	Δδ (ppm)
1	5.0×10^{-3}	0.0	1.9521	0.0000
2	5.0×10^{-3}	5.0×10^{-3}	1.9522	0.0001
3	5.0×10^{-3}	1.5×10^{-2}	1.9526	0.0005
4	5.0×10^{-3}	2.5×10^{-2}	1.9528	0.0007
5	5.0×10^{-3}	2.5×10^{-1}	1.9575	0.0054
6	5.0×10^{-3}	5.0×10^{-1}	1.9619	0.0098
7	5.0×10^{-3}	7.5×10^{-1}	1.9657	0.0136
8	5.0×10^{-3}	1.0	1.9687	0.0166

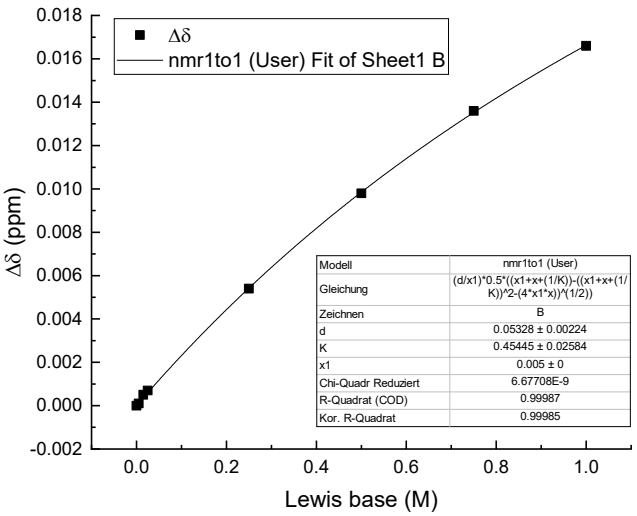

(RM1256)

7.6 Computation Details

General

Initially, all structures were subjected to a conformational search using the OPLS3[26] force field as implemented in Macromodel.[27] All conformers were then optimized at the corresponding level of theory (see respective sections below) with the Gaussian 16 software package.[28] Frequency analyses were performed to confirm that all structures correspond to minima.

Test of DFT Functionals

We tested the overall quality of different commonly employed DFT functionals for the prediction of equilibrium constants for Lewis adduct formation in comparison to a set of experimental equilibrium constants determined in this work. To avoid a bias for a certain type of Lewis base, the set of Lewis adducts **1d**/**2d**, **1f**/**3a**, **1h**/**7b**, and **1f**/**4b** was selected under the aspect of diversity to reflect the formation of B-N, B-O, and B-P adducts. At the same time, the experimentally determined equilibrium constants for these four Lewis adducts cover the experimentally relevant range from 1.4×10^6 to 4.9 M^{-1}.

Within the test set, conformers of the Lewis adducts depicted below were first optimized at SMD(DCM)[29]/B3LYP[30]-D3BJ[31]/def2-SVP[32] level of theory. The minimum conformer of each species was subsequently optimized with further DFT methods. Thermochemical corrections were obtained at the same level using the rigid rotor harmonic oscillator (RRHO) model as implemented in Gaussian. Alternatively, we tested the Grimme's quasi-harmonic RRHO approximation.[33] A free energy change of +7.91 kJ/mol (= R · 298 K · ln(22.46 L mol^{-1}/L mol^{-1})) was applied to all free energies for their conversion from gas phase (1 atm) to liquid phase (1 M).

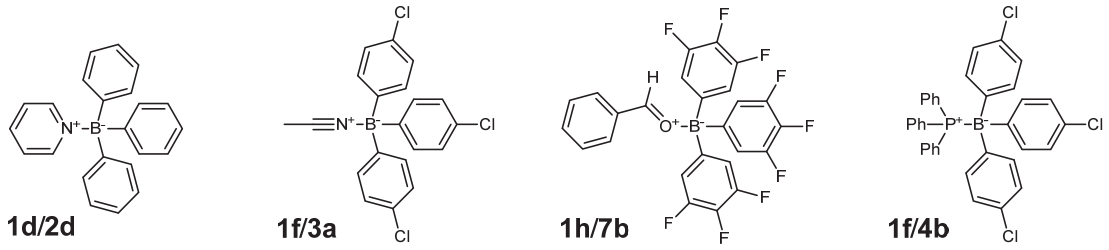

Table S3: Gibbs reaction energies $\Delta_r G$ calculated at different DFT levels with thermochemical analysis based on the RRHO model.

	1d/2d	1f/3a	1h/7b	1f/4b	1d/2d	1f/3a	1h/7b	1f/4b	MUE	Error
	$\Delta_r G$ (kJ/mol)				deviation from experiment (kJ/mol)					
Experimental	-34.5	-3.9	-13.2	-12.3	0.0	0.0	0.0	0.0		
B3LYP-D3BJ/def2-SVP	-42.5	-19.6	-23.1	-39.8	8.0	15.7	9.9	27.5	15.3	15.3 ± 7.6
B3LYP-D3BJ/def2-TZVP	-21.7	-1.3	-4.8	-23.4	-12.7	-2.5	-8.4	11.0	8.7	-3.2 ± 9.0
M06-2X/def2-TZVP	-31.3	-11.5	-17.9	10.6	-3.2	7.6	4.7	-22.9	9.6	-3.4 ± 11.9
wb97xd/def2-TZVP	-24.4	-2.7	-10.1	-18.1	-10.0	-1.2	-3.1	5.8	5.0	-2.1 ± 5.6
PBE-D3BJ/def2-TZVP	-35.3	-17.5	-14.5	-29.3	0.8	13.6	1.3	16.9	8.2	8.2 ± 7.2
PBE0-D3BJ/def2-TZVP	-38.0	-15.3	-14.7	-33.0	3.5	11.4	1.5	20.7	9.3	9.3 ± 7.5
M06/def2-TZVP	-13.4	-1.1	3.3	9.4	-21.1	-2.8	-16.5	-21.7	15.5	-15.5 ± 7.6
M06-L/def2-TZVP	-12.4	1.5	5.4	9.0	-22.0	-5.4	-18.6	-21.3	16.8	-16.8 ± 6.7
MN15/def2-TZVP	-33.2	-12.5	-20.8	-7.7	-1.3	8.6	7.6	-4.7	5.5	2.6 ± 5.7
BP86-D3BJ/def2-TZVP	-42.5	-11.9	-13.7	-57.1	8.1	8.0	0.5	44.7	15.3	15.3 ± 17.2
B97D3/def2-TZVP	-20.7	-1.7	1.7	-28.4	-13.8	-2.1	-14.9	16.1	11.7	-3.7 ± 12.5

MUE = mean unassigned error

Table S4: Gibbs reaction energies ΔG calculated at different DFT levels with thermochemical analysis based on Grimme's quasi-harmonic RRHO approximation.

	1d/2d	1f/3a	1h/7b	1f/4b	1d/2d	1f/3a	1h/7b	1f/4b	MUE	Error
	ΔG (kJ/mol)				deviation from experiment (kJ/mol)					
Experimental	-34.5	-3.9	-13.2	-12.3	0.0	0.0	0.0	0.0		
B3LYP-D3BJ/def2-SVP	-38.1	-10.6	-13.8	-34.3	3.7	6.7	0.6	21.9	8.2	8.2 ± 8.2
B3LYP-D3BJ/def2-TZVP	-17.3	9.4	5.0	-18.5	-17.1	-13.2	-18.2	6.2	13.7	-10.6 ± 9.9
M06-2X/def2-TZVP	-26.5	-0.5	-5.6	10.8	-7.9	-3.4	-7.6	-23.1	10.5	-10.5 ± 7.5
wb97xd/def2-TZVP	-21.1	6.4	2.0	-13.6	-13.3	-10.3	-15.2	1.2	10.0	-9.4 ± 6.4
PBE-D3BJ/def2-TZVP	-30.8	-6.8	-2.8	-24.4	-3.7	2.9	-10.4	12.1	7.3	0.2 ± 8.3
PBE0-D3BJ/def2-TZVP	-33.6	-5.9	-4.8	-29.2	-0.9	2.0	-8.4	16.9	7.0	2.4 ± 9.2
M06/def2-TZVP	-9.6	8.4	12.9	15.5	-24.9	-12.3	-26.1	-27.9	22.8	-22.8 ± 6.1
M06-L/def2-TZVP	-6.6	12.0	16.9	13.0	-27.8	-15.9	-30.1	-25.4	24.8	-24.8 ± 5.4
MN15/def2-TZVP	**-28.4**	**-1.9**	**-8.2**	**-3.9**	**-6.0**	**-2.0**	**-5.0**	**-8.4**	**5.4**	**-5.4 ± 2.4**
BP86-D3BJ/def2-TZVP	-38.1	-3.5	-4.0	-53.4	3.6	-0.4	-9.2	41.1	13.6	8.8 ± 19.2
B97D3/def2-TZVP	-16.0	11.0	12.3	-24.0	-18.5	-14.9	-25.5	11.7	17.6	-11.8 ± 14.1

MUE = mean unassigned error

The accuracy of the different DFT methods in predicting the experimental Gibbs energies of reaction for the Lewis adduct formations **1d/2d**, **1f/3a**, **1h/7b**, and **1d/4b** is illustrated in Figure S4. The best agreement of computed and experimental $\Delta_r G$ with the lowest scattering was obtained for the MN15 functional using the quasi-harmonic approximation by Grimme. By using the MN15 functional ΔG values are on average by −5.4 ± 2.4 kJ/mol lower than those determined by experiment. All other methods show a significantly stronger scattering and/or enhanced errors.

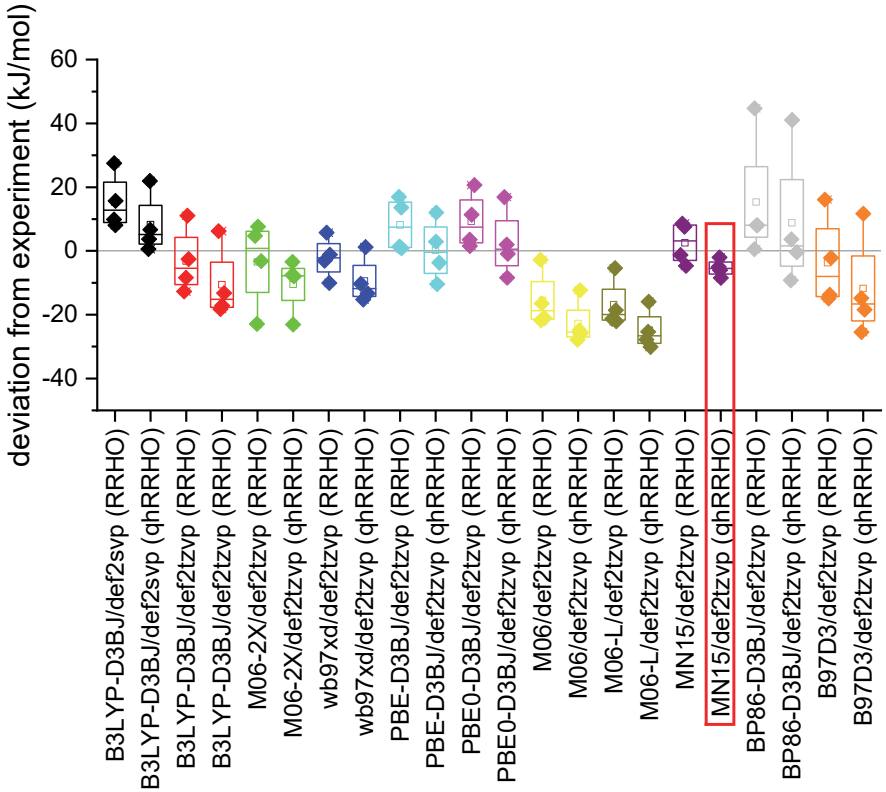

Figure S4. Comparison of the predictive power of the tested DFT methods.

Table S5: Raw computational data at different levels of theory in dichloromethane.

Species	Filename	E_{tot} (hartree)	$G_{298,\ RRHO}$ (hartree)	$G_{298,\ qHRRHO}$ (hartree)
	SMD(DCM)/B3LYP-D3BJ/def2-SVP			
1d-2d	1d_2d_b3lyp_svp.log	-967.580904	-967.261964	-967.257686
1d	1d_b3lyp_svp.log	-719.411898	-719.178108	-719.175492
1f-3a	1f_3a_b3lyp_svp.log	-2230.516442	-2230.280204	-2230.272777
1f-4b	1f_4b_b3lyp_svp.log	-3133.687340	-3133.234860	-3133.224625
1f	1f_b3lyp_svp.log	-2097.826879	-2097.628483	-2097.624492
1h-7b	1h_7b_b3lyp_svp.log	-1957.187909	-1956.937739	-1956.929423
1h	1h_b3lyp_svp.log	-1611.800125	-1611.650875	-1611.646157
1d	2d_b3lyp_svp.log	-248.132100	-248.070679	-248.070681
3a	3a_b3lyp_svp.log	-132.668240	-132.647276	-132.647277
4b	4b_b3lyp_svp.log	-1035.821657	-1035.594213	-1035.590088
7b	7b_b3lyp_svp.log	-345.360643	-345.281089	-345.281040
	SMD(DCM)/B3LYP-D3BJ/def2-TZVP			
1d-2d	1d_2d_b3lyp.log	-968.619918	-968.302046	-968.297641
1d	1d_b3lyp.log	-720.184081	-719.951320	-719.948593
1f-3a	1f_3a_b3lyp.log	-2231.916474	-2231.682054	-2231.673940
1f-4b	1f_4b_b3lyp.log	-3135.801163	-3135.349237	-3135.339261
1f	1f_b3lyp.log	-2099.078392	-2098.880774	-2098.876735
1h-7b	1h_7b_b3lyp.log	-1959.441112	-1959.193556	-1959.184953
1h	1h_b3lyp.log	-1613.676211	-1613.528486	-1613.523710
1d	2d_b3lyp.log	-248.406839	-248.345462	-248.345465
3a	3a_b3lyp.log	-132.824924	-132.803781	-132.803783
4b	4b_b3lyp.log	-1036.689409	-1036.462575	-1036.458481
7b	7b_b3lyp.log	-345.745387	-345.666256	-345.666178
	SMD(DCM)/M06-2X/def2-TZVP			
1d-2d	1d_2d_m062x.log	-968.100562	-967.779940	-967.775479
1d	1d_m062x.log	-719.791317	-719.556428	-719.553786
1f-3a	1f_3a_m062x.log	-2231.382375	-2231.145307	-2231.137190
1f-4b	1f_4b_m062x.log	-3134.901979	-3134.443477	-3134.434943
1f	1f_m062x.log	-2098.608465	-2098.408712	-2098.404788
1h-7b	1h_7b_m062x.log	-1958.616550	-1958.366699	-1958.357276
1h	1h_m062x.log	-1613.026267	-1612.875443	-1612.870786
1d	2d_m062x.log	-248.276759	-248.214604	-248.214606
3a	3a_m062x.log	-132.756869	-132.735240	-132.735243
4b	4b_m062x.log	-1036.269873	-1036.041797	-1036.037265
7b	7b_m062x.log	-345.567578	-345.487449	-345.487360
	SMD(DCM)/wb97xd/def2-TZVP			
1d-2d	1d_2d_wb97xd.log	-968.168956	-967.847063	-967.842849
1d	1d_wb97xd.log	-719.843274	-719.608527	-719.605569
1f-3a	1f_3a_wb97xd.log	-2231.464208	-2231.225314	-2231.217923
1f-4b	1f_4b_wb97xd.log	-3135.048309	-3134.590520	-3134.580953
1f	1f_wb97xd.log	-2098.682607	-2098.482187	-2098.478264
1h-7b	1h_7b_wb97xd.log	-1958.709887	-1958.460350	-1958.450821
1h	1h_wb97xd.log	-1613.097827	-1612.947456	-1612.942642
1d	2d_wb97xd.log	-248.294468	-248.232249	-248.232251
3a	3a_wb97xd.log	-132.766630	-132.745101	-132.745102
4b	4b_wb97xd.log	-1036.334240	-1036.104451	-1036.100536
7b	7b_wb97xd.log	-345.592189	-345.512061	-345.511966
	SMD(DCM)/PBE-D3BJ/def2-TZVP			
1d-2d	1d_2d_pbe.log	-967.293236	-966.986715	-966.982117
1d	1d_pbe.log	-719.181463	-718.957143	-718.954274
1f-3a	1f_3a_pbe.log	-2230.165310	-2229.940207	-2229.931922
1f-4b	1f_4b_pbe.log	-3133.095328	-3132.660591	-3132.650168
1f	1f_pbe.log	-2097.498537	-2097.308682	-2097.304458
1h-7b	1h_7b_pbe.log	-1957.244910	-1957.009102	-1956.999658

1h	1h_pbe.log	-1611.923522	-1611.782716	-1611.777824
1d	2d_pbe.log	-248.077896	-248.019138	-248.019141
3a	3a_pbe.log	-132.647717	-132.627882	-132.627884
4b	4b_pbe.log	-1035.561851	-1035.343774	-1035.339435
7b	7b_pbe.log	-345.299640	-345.223866	-345.223777
	SMD(DCM)/PBE0-D3BJ/def2-TZVP			
1d-2d	1d_2d_pbe0.log	-967.387272	-967.067805	-967.063415
1d	1d_pbe0.log	-719.256980	-719.023109	-719.020394
1f-3a	1f_3a_pbe0.log	-2230.344786	-2230.108025	-2230.100235
1f-4b	1f_4b_pbe0.log	-3133.366539	-3132.912014	-3132.902272
1f	1f_pbe0.log	-2097.671216	-2097.472801	-2097.468589
1h-7b	1h_7b_pbe0.log	-1957.292343	-1957.042154	-1957.033463
1h	1h_pbe0.log	-1611.949681	-1611.800098	-1611.795266
1d	2d_pbe0.log	-248.095085	-248.033246	-248.033249
3a	3a_pbe0.log	-132.653753	-132.632424	-132.632426
4b	4b_pbe0.log	-1035.657668	-1035.429656	-1035.425561
7b	7b_pbe0.log	-345.319088	-345.239458	-345.239378
	SMD(DCM)/M06/def2-TZVP			
1d-2d	1d_2d_m06.log	-967.733609	-967.417800	-967.413369
1d	1d_m06.log	-719.516036	-719.284990	-719.282007
1f-3a	1f_3a_m06.log	-2231.046586	-2230.812920	-2230.805035
1f-4b	1f_4b_m06.log	-3134.336287	-3133.885260	-3133.876500
1f	1f_m06.log	-2098.313635	-2098.117557	-2098.113308
1h-7b	1h_7b_m06.log	-1958.250996	-1958.001934	-1957.993539
1h	1h_m06.log	-1612.770727	-1612.621481	-1612.616817
1d	2d_m06.log	-248.191668	-248.130716	-248.130719
3a	3a_m06.log	-132.719081	-132.697950	-132.697951
4b	4b_m06.log	-1036.003773	-1035.778522	-1035.774321
7b	7b_m06.log	-345.463559	-345.384724	-345.384645
	SMD(DCM)/M06L/def2-TZVP			
1d-2d	1d_2d_m06l.log	-968.357473	-968.039917	-968.035239
1d	1d_m06l.log	-719.988165	-719.754203	-719.751730
1f-3a	1f_3a_m06l.log	-2231.628541	-2231.393246	-2231.385488
1f-4b	1f_4b_m06l.log	-3135.308322	-3134.855736	-3134.846200
1f	1f_m06l.log	-2098.818832	-2098.620140	-2098.616394
1h-7b	1h_7b_m06l.log	-1959.037087	-1958.790129	-1958.781018
1h	1h_m06l.log	-1613.359921	-1613.211214	-1613.206559
1d	2d_m06l.log	-248.345402	-248.283996	-248.283998
3a	3a_m06l.log	-132.798126	-132.776694	-132.776695
4b	4b_m06l.log	-1036.468976	-1036.242020	-1036.237784
7b	7b_m06l.log	-345.663250	-345.583981	-345.583913
	SMD(DCM)/MN15/def2-TZVP			
1d-2d	1d_2d.log	-967.288983	-966.970440	-966.966127
1d	1d.log	-719.183183	-718.949547	-718.947039
1f-3a	1f_3a.log	-2230.425035	-2230.189357	-2230.181409
1f-4b	1f_4b.log	-3133.375826	-3132.922388	-3132.913002
1f	1f.log	-2097.759858	-2097.561415	-2097.557514
1h-7b	1h_7b.log	-1957.359664	-1957.112128	-1957.102630
1h	1h.log	-1612.040717	-1611.891398	-1611.886781
1d	2d.log	-248.073066	-248.011268	-248.011271
3a	3a.log	-132.647673	-132.626196	-132.626199
4b	4b.log	-1035.588730	-1035.361063	-1035.357020
7b	7b.log	-345.295354	-345.215818	-345.215736
	SMD(DCM)/BP86-D3BJ/def2-TZVP			
1d-2d	1d_2d_bp86.log	-968.575732	-968.269541	-968.264937
1d	1d_bp86.log	-720.140941	-719.917037	-719.914119
1f-3a	1f_3a_bp86.log	-2231.976088	-2231.749547	-2231.742032
1f-4b	1f_4b_bp86.log	-3135.864960	-3135.429199	-3135.419395
1f	1f_bp86.log	-2099.138799	-2098.949652	-2098.945347
1h-7b	1h_7b_bp86.log	-1959.411206	-1959.174476	-1959.165771

1h	1h_bp86.log	-1613.654461	-1613.514177	-1613.509268
1d	2d_bp86.log	-248.397924	-248.339318	-248.339321
3a	3a_bp86.log	-132.818123	-132.798366	-132.798368
4b	4b_bp86.log	-1036.679163	-1036.460823	-1036.456723
7b	7b_bp86.log	-345.733688	-345.658084	-345.657994
	SMD(DCM)/B97D3/def2-TZVP			
1d-2d	1d_2d.log	-967.863511	-967.554716	-967.549973
1d	1d.log	-719.614698	-719.388593	-719.385636
1f-3a	1f_3a.log	-2231.291166	-2231.065370	-2231.056388
1f-4b	1f_4b.log	-3134.713161	-3134.273861	-3134.263638
1f	1f.log	-2098.549749	-2098.358103	-2098.353959
1h-7b	1h_7b.log	-1958.191922	-1957.953159	-1957.944221
1h	1h.log	-1612.682208	-1612.539965	-1612.535138
1d	2d.log	-248.220603	-248.161254	-248.161257
3a	3a.log	-132.729784	-132.709617	-132.709618
4b	4b.log	-1036.128072	-1035.907940	-1035.903554
7b	7b.log	-345.493445	-345.416856	-345.416770

Isodesmic Reactions as Tool to Calculate Equilibrium Constants

Isodesmic reactions are appropriate tools to reduce the errors of computational methods. The MN15 DFT level was identified to reproduce experimental equilibrium constants of Lewis adduct formation in this work with acceptable accuracy, and we used the following Scheme for the computation of Gibbs energies of association of boranes and Lewis bases. By combining the experimental Δ_rG values from Eq (II) with the computationally accessible Δ_rG for the isodesmic reaction in Eq (I), we arrive at ΔG_{iso} which is founded on the experimental equilibrium constants for a certain Lewis base.

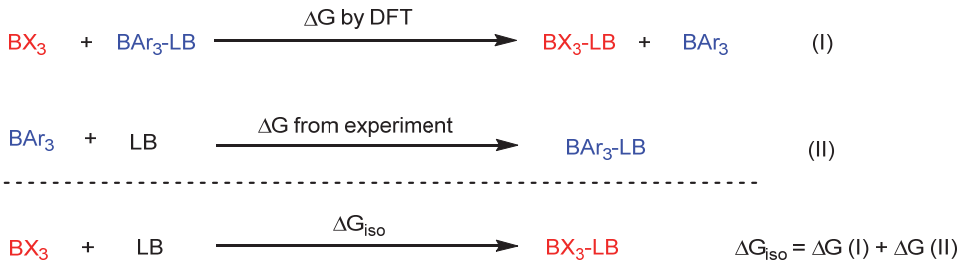

Next, we set out to assess the Lewis acidity LA_B of BBr_3, BCl_3, and BF_3. Pyridine (**2d**), acetonitrile (**3a**), and benzaldehyde (**7b**) were chosen as reference Lewis bases which were optimized at the SMD(DCM)[29]/MN15[34]/def2-TZVP[32] level of theory. Thermochemical corrections were calculated using Grimme's quasi-harmonic approximation.[33]

Table S6: Energies of the reaction of boron halides with pyridine (**1d**) at the SMD(DCM)/MN15/def2-TZVP level of theory and calculation of LA_B via an isodesmic reaction.

Species		E_{tot} (hartree)	G_{298} (hartree)	Δ_rG(I) (kJ/mol)	Δ_rG(II)[a] (kJ/mol)	ΔG_{iso} (kJ/mol)	K_B (M^{-1})[b]	LA_B[b]
1d-Pyridine	1d_2d.log	-967.288983	-966.966127					
1d	1d.log	-719.183183	-718.947039					
BBr_3	bbr3.log	-7748.408212	-7748.434048					
BBr_3-Pyridine	bbr3_2d.log	-7996.538426	-7996.478099	-65.5	-34.5	-100.0	6.85×10^{17}	11.7
BCl_3	bcl3.log	-1405.317291	-1405.338254					
BCl_3-Pyridine	bcl3_2d.log	-1653.446263	-1653.381447	-63.3	-34.5	-97.8	2.72×10^{17}	11.3
BF_3	bf3.log	-324.456841	-324.470180					
BF_3-Pyridine	bf3_2d.log	-572.582190	-572.511173	-57.5	-34.5	-92.0	2.54×10^{16}	10.3

[a] Experimental K_B for the reaction of **1d** with **2d** (see Extended Data Table 1) converted to Δ_rG with $\Delta_rG = -RT \ln K_B$. [b] At 20 °C.

Table S7: Energies of the reaction of boron halides with benzaldehyde (**7b**) at the SMD(DCM)/MN15/def2-TZVP level of theory and calculation of LA_B via an isodesmic reaction.

Species		E_{tot} (hartree)	G_{298} (hartree)	Δ_rG(I) (kJ/mol)	Δ_rG(II)[a] (kJ/mol)	ΔG_{iso} (kJ/mol)	K_B (M^{-1})[b]	LA_B[b]
1h-PhCHO	1h_7b.log	-1957.359664	-1957.102630					
1h	1h.log	-1612.040717	-1611.886781					
BBr_3	bbr3.log	-7748.408212	-7748.434048					
BBr_3-PhCHO	bbr3_7b.log	-8093.740174	-8093.662573	-33.3	-13.2	-46.5	1.94×10^8	10.1
BCl_3	bcl3.log	-1405.317291	-1405.338254					
BCl_3-PhCHO	bcl3_7b.log	-1750.647924	-1750.566009	-31.3	-13.2	-44.5	8.44×10^7	9.7
BF_3	bf3.log	-324.456841	-324.470180					
BF_3-PhCHO	bf3_7b.log	-669.786167	-669.697911	-31.2	-13.2	-44.4	8.23×10^7	9.7

[a]: Experimental K_B for the reaction of **1h** with **7b** (see Extended Data Table 1) converted to Δ_rG with $\Delta_rG = -RT \ln K_B$. [b] At 20 °C.

Table S8: Energies of the reaction of boron halides with acetonitrile (**3a**) at the SMD(DCM)/MN15/def2-TZVP level of theory and calculation of LA_B via an isodesmic reaction.

Species		E_{tot} (hartree)	G_{298} (hartree)	Δ_rG(I) (kJ/mol)	Δ_rG(II)[a] (kJ/mol)	ΔG_{iso} (kJ/mol)	K_B (M^{-1})[b]	LA_B[b]
1f-MeCN	1f_3a.log	-2230.425035	-2230.181409					
1f	1f.log	-2097.759858	-2097.557514					
BBr_3	bbr3.log	-7748.408212	-7748.434048					
BBr_3-MeCN	bbr3_3a.log	-7881.089538	-7881.073402	-40.6	-3.9	-44.5	8.53×10^7	8.4
BCl_3	bcl3.log	-1405.317291	-1405.338254					
BCl_3-MeCN	bcl3_3a.log	-1537.995002	-1537.974251	-31.8	-3.9	-35.7	2.29×10^6	6.8
BF_3	bf3.log	-324.456841	-324.470180					
BF_3-MeCN	bf3_3a.log	-457.130481	-457.103044	-23.5	-3.9	-27.4	7.82×10^4	5.4

[a]: Experimental K_B for the reaction of **1f** with **3a** (see Extended Data Table 1) converted to Δ_rG with $\Delta_rG = -RT \ln K_B$. [b] At 20 °C.

Table S9: LA_B from the three reference reactions and averaged LA_B

Lewis Acid	LA_B from Pyridine	LA_B from Benzaldehyde	LA_B from MeCN	LA_B Average
BBr_3	11.7	10.1	8.4	10.1 ± 1.3
BCl_3	11.3	9.7	6.8	9.3 ± 1.8
BF_3	10.3	9.7	5.4	8.4 ± 2.0

Fluoride Ion Affinities (FIA)

First, we calculated gas-phase FIA (as ΔH) following the procedure outlined in ref. 35 at the BP86-D3BJ/def2-SVP level of theory. As suggested, we used the isodesmic reaction of $Me_3Si^+ + F^- \rightarrow Me_3SiF$ (with ΔH at the G3 level as suggested in ref. 36) as anchor point. Therefore, all geometries were optimized in gas phase at the BP86[37]-D3BJ[31]/def2-SVP[32] level of theory and confirmed to be energetic minima by frequency analyses.

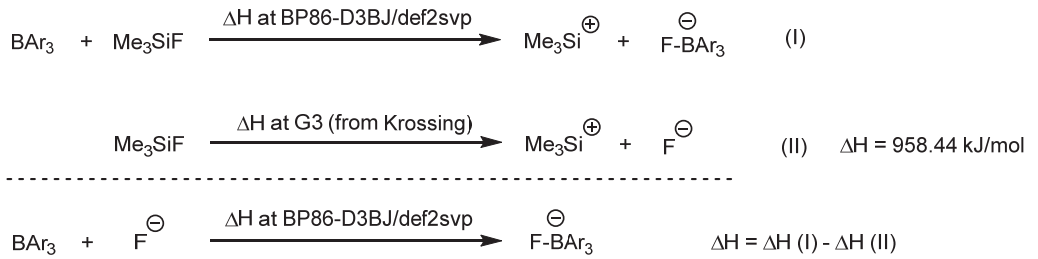

Table S10: Gas-phase FIA at the BP86-D3BJ/def2-SVP level of theory anchored to the $Me_3SiF/Me_3Si^+ + F^-$ reaction (with ΔH at the G3 level from ref. 36).

Compound	Name	E_{tot} (hartree)	ΔH (hartree)	ΔH(I) (kJ/mol)	FIA = ΔH – ΔH (II) (kJ/mol)
Me_3SiF	tms_cation.log	-408.832819	-408.718535		
Me_3Si^+	tms_f.log	-508.947655	-508.828343		
1a	1a.log	-1121.022940	-1120.512056		
1a-F^-	1a_f.log	-1220.879285	-1220.368078	666.3	-292.1
1b	1b.log	-1062.706045	-1062.317768		
1b-F^-	1b_f.log	-1162.577430	-1162.188214	628.4	-330.0
1c	1c.log	-837.236925	-836.866150		
1c-F^-	1c_f.log	-937.115155	-936.743194	611.1	-347.3
1d	1d.log	-719.359926	-719.073788		
1d-F^-	1d_f.log	-819.242997	-818.955556	598.7	-359.7
1e	1e.log	-1016.851796	-1016.586953		
1e-F^-	1e_f.log	-1116.741597	-1116.475206	581.7	-376.7
1f	1f.log	-2097.875931	-2097.614239		
1f-F^-	1f_f.log	-2197.773400	-2197.509855	562.4	-396.1
1g	1g.log	-1611.827482	-1611.605375		
1g-F^-	1g_f.log	-1711.725270	-1711.501146	562.0	-396.5
1h	1h.log	-1611.783601	-1611.560989		
1h-F^-	1h_f.log	-1711.698201	-1711.473463	518.1	-440.3
1i	1i.log	-2206.709158	-2206.528720		
1i-F^-	1i_f.log	-2306.630948	-2306.448215	499.7	-458.8
1j	1j.log	-1072.981077	-1072.440991		
1j-F^-	1j_f.log	-1172.850930	-1172.309088	634.6	-323.8
BF_3	bf3.log	-324.301595	-324.284934		
BF_3-F^-	bf3_f.log	-424.180170	-424.160668	614.6	-343.9
BCl_3	bcl3.log	-1405.258983	-1405.246111		
BCl_3-F^-	bcl3_f.log	-1505.162885	-1505.146538	549.7	-408.7
BBr_3	bbr3.log	-7747.298444	-7747.286611		
BBr_3-F^-	bbr3_f.log	-7847.216865	-7847.201283	512.3	-446.1

Fluoride Ion Affinities in Dichloromethane (FIA^{DCM})

Fluoride ion affinities (as ΔG_{298}) in dichloromethane solution were calculated at the SMD(DCM)[29]/MN15[34]/def2-TZVP[32] level of theory with thermochemical corrections calculated using Grimme's quasi-harmonic approximation.[33] A free energy change of +7.91 kJ/mol (= R · 298 K · ln(22.46 L mol^{-1}/L mol^{-1})) was applied to all free energies for their conversion from gas phase (1 atm) to liquid phase (1 M).

$$BAr_3 + F^{\ominus} \xrightarrow{\Delta G \text{ at SMD(DCM)/MN15/def2tzvp}} F\text{-}BAr_3^{\ominus}$$

In contrast to gas-phase FIA, there is no reliable anchor reaction for fluoride association with a borane in dichloromethane solution, and due to ion pairing in organic solution it is also unlikely to exist. Therefore, the absolute FIA^{DCM} values reported herein should not be overinterpreted.

Table S11: FIA in dichloromethane solutions (FIA^{DCM}) at the SMD(DCM)/MN15/def2-TZVP level of theory.

Compound	Name	E_{tot} (hartree)	ΔG (hartree)	FIA^{DCM} (kJ/mol)
F^-	fluoride.log	-99.922600	-99.936759	
1a	1a.log	-1120.757210	-1120.317861	
1a-F^-	1a_f.log	-1220.727944	-1220.288428	-96.7
1b	1b.log	-1062.545388	-1062.218981	
1b-F^-	1b_f.log	-1162.525919	-1162.201148	-127.1
1c	1c.log	-837.018675	-836.707329	
1c-F^-	1c_f.log	-937.004045	-936.694851	-141.2
1d	1d.log	-719.183183	-718.947039	
1d-F^-	1d_f.log	-819.172812	-818.937033	-147.7
1e	1e.log	-1016.820334	-1016.611786	
1e-F^-	1e_f.log	-1116.811692	-1116.604241	-154.1
1f	1f.log	-2097.759858	-2097.557514	
1f-F^-	1f_f.log	-2197.755352	-2197.553620	-163.7
1g	1g.log	-1612.079522	-1611.925116	
1g-F^-	1g_f.log	-1712.084355	-1711.929353	-185.1
1h	1h.log	-1612.040717	-1611.886781	
1h-F^-	1h_f.log	-1712.048259	-1711.895637	-197.2
1i	1i.log	-2207.247423	-2207.146808	
1i-F^-	1i_f.log	-2307.270349	-2307.168786	-231.7
1j	1j.log[a]	-1072.672657	-1072.205711	
1j-F^-	1j_f.log	-1172.642414	-1172.172727	-87.4
BF_3	bf3.log	-324.456841	-324.470180	
BF_3-F^-	bf3_f.log	-424.481810	-424.495205	-239.7
BCl_3	bcl3.log	-1405.317291	-1405.338254	
BCl_3-F^-	bcl3_f.log	-1505.350042	-1505.370892	-259.6
BBr_3	bbr3.log	-7748.408212	-7748.434048	
BBr_3-F^-	bbr3_f.log	-7848.442427	-7848.468054	-263.2

[a] Structure has one imaginary frequency (−13.2 cm^{-1}) as convergence showed to be problematic.

Orbital Energies

Both LUMO energies as well as global electrophilicity indices (GEI) were proposed to be a suitable descriptor for Lewis acidity.[35,38] Parr global electrophilicity indices can be calculated from the electronic chemical potential (μ), chemical hardness (η) and the global electrophilicity index (ω) as follows:[39]

$$\mu \approx \frac{E_{HOMO} + E_{LUMO}}{2}$$

$$\eta \approx E_{LUMO} - E_{HOMO}$$

$$\omega = \frac{\mu^2}{2\eta}$$

The following two tables list HOMO and LUMO energies, chemical potential (μ), chemical hardness (η) and the global electrophilicity index (ω) for both gas-phase optimized boranes (BP86-D3BJ/def2-SVP, Table S12) as well as the ones in dichloromethane solution (SMD(DCM)/MN15/def2-TZVP, Table S13). The corresponding correlation with experimental Lewis acidities is shown in Extended Figure 4.

Table S12: Orbital energies and GEI analysis for boranes optimized in the gas-phase at the BP86-D3BJ/def2-SVP level of theory.

Compound	Name	ε_{HOMO} (hartree)	ε_{LUMO} (hartree)	Chemical Potential (hartree)	Chemical Hardness (hartree)	Global Electrophilicity (eV)
1a	1a.log	-0.15683	-0.06001	-0.10842	0.09682	1.65
1b	1b.log	-0.19166	-0.08069	-0.13618	0.11097	2.27
1c	1c.log	-0.21392	-0.09261	-0.15327	0.12131	2.63
1d	1d.log	-0.22686	-0.10049	-0.16368	0.12637	2.88
1e	1e.log	-0.22650	-0.10466	-0.16558	0.12184	3.06
1f	1f.log	-0.22634	-0.11260	-0.16947	0.11374	3.44
1g	1g.log	-0.23176	-0.12108	-0.17642	0.11068	3.83
1h	1h.log	-0.24254	-0.12913	-0.18584	0.11341	4.14
1i	1i.log	-0.23790	-0.14437	-0.19114	0.09353	5.31
1j	1j.log	-0.19839	-0.09395	-0.14617	0.10444	2.78
BF_3	bf3.log	-0.35988	-0.01084	-0.18536	0.34904	1.34
BCl_3	bcl3.log	-0.27814	-0.08770	-0.18292	0.19044	2.39
BBr_3	bbr3.log	-0.25686	-0.10629	-0.18158	0.15057	2.98

Table S13: Orbital energies and GEI analysis for boranes optimized in dichloromethane solution at the SMD(DCM)/MN15/def2-TZVP level of theory.

Compound	Name	ε_{HOMO} (hartree)	ε_{LUMO} (hartree)	Chemical Potential (hartree)	Chemical Hardness (hartree)	Global Electrophilicity (eV)
1a	1a.log	-0.21710	-0.02941	-0.12326	0.18769	1.10
1b	1b.log	-0.25312	-0.04147	-0.14730	0.21165	1.39
1c	1c.log	-0.27054	-0.04908	-0.15981	0.22146	1.57
1d	1d.log	-0.28319	-0.05429	-0.16874	0.22890	1.69
1e	1e.log	-0.28154	-0.05390	-0.16772	0.22764	1.68
1f	1f.log	-0.28062	-0.06249	-0.17156	0.21813	1.84
1g	1g.log	-0.29157	-0.07655	-0.18406	0.21502	2.14
1h	1h.log	-0.29536	-0.07260	-0.18398	0.22276	2.07
1i	1i.log	-0.29833	-0.09589	-0.19711	0.20244	2.61
1j	1j.log	-0.25626	-0.04968	-0.15297	0.20658	1.54
BF_3	bf3.log	-0.48092	0.06314	-0.20889	0.54406	1.09
BCl_3	bcl3.log	-0.36253	-0.04009	-0.20131	0.32244	1.71
BBr_3	bbr3.log	-0.33101	-0.05910	-0.19506	0.27191	1.90

Borane (BH_3) Affinities (BA)

For the calculation of borane affinities BA (= ΔG_{BH3}, in kJ/mol), all structures were optimized at the SMD(DCM)[29]/MN15[34]/def2-TZVP[32] level of theory. Frequency calculations including Grimme's quasi-harmonic RRHO approximation[33] were obtained at the same level and converted from gas phase (1 atm) to liquid phase (1 M) by adding a free energy change of +7.91 kJ/mol (= R · 298 K · ln(22.46 L mol^{-1}/L mol^{-1})) to all free energies. To reference borane affinities to experimental values, we used two isodesmic reactions as basis: the reaction of BH_3 with pyridine (**2d**), which can be connected with an isodesmic reaction to the experimental value for the reaction of pyridine (**2d**) with triphenylborane (**1d**) (see above), was taken as anchor point as described in equations (I)–(IV):

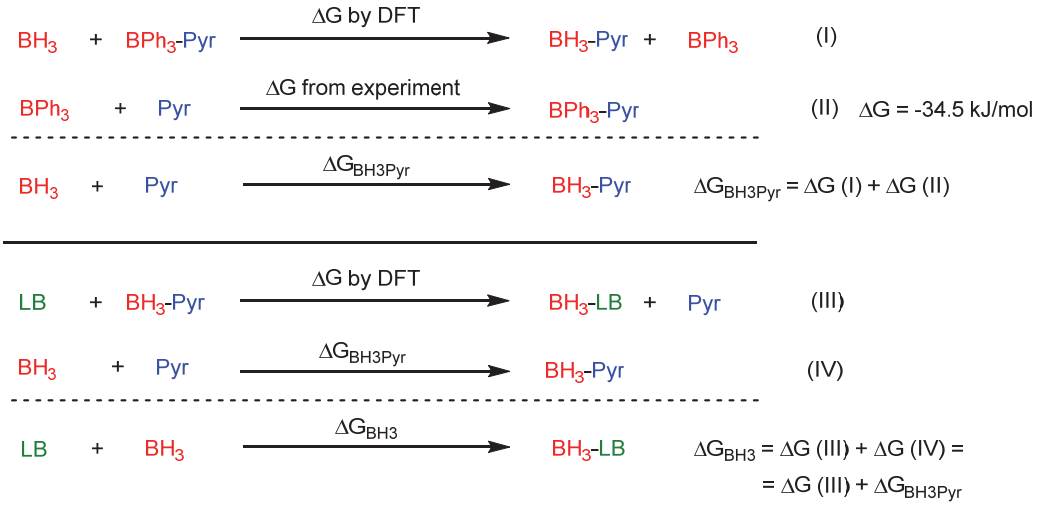

Table S14: Borane affinities in dichloromethane at the SMD(DCM)/MN15/def2-TZVP level of theory.

Compound	Name	E_{tot} (hartree)	ΔG (hartree)
BH_3	bh3.log	-26.571987	-26.564324
BH_3-2d	bh3_2d.log	-274.716247	-274.624257
1d	1d.log	-719.183183	-718.947039
2d	2d.log	-248.073066	-248.011271
1d-2d	1d_2d.log	-967.288983	-966.966127
		ΔG_I (kJ/mol):	-107.2
		$\Delta G_{II, exp}$ (kJ/mol):	-34.5
		ΔG_{BH3Py} (kJ/mol):	-141.7

Compound	R =		Name	E_{tot} (hartree)	ΔG (hartree)
	4-NMe_2	**2a**	2a.log	-381.934671	-381.805184
			bh3_2a.log	-408.583729	-408.423337
				ΔG_{BH3} (kJ/mol):	-155.3
	4-Morpholino	**2b**	2b.log	-534.464827	-534.295128
			bh3_2b.log	-561.112566	-560.912079
				ΔG_{BH3} (kJ/mol):	-152.2
	4-MeO	**2c**	2c.log	-362.528691	-362.437424
			bh3_2c.log	-389.173948	-389.052228
				ΔG_{BH3} (kJ/mol):	-146.5
	H	**2d**	2d.log	-248.073066	-248.011271
			bh3_2d.log	-274.716247	-274.624257
				ΔG_{BH3} (kJ/mol):	-141.7
	4-COPh	**2e**	2e.log	-592.183945	-592.040244
			bh3_2e.log	-618.825044	-618.650624
				ΔG_{BH3} (kJ/mol):	-134.9
	3-Cl	**2f**	2f.log	-707.596035	-707.546045
			bh3_2f.log	-734.235338	-734.154962
				ΔG_{BH3} (kJ/mol):	-131.1

	4-CF_3	**2g**	2g.log	-584.999106	-584.938099
			bh3_2g.log	-611.638527	-611.546893
				ΔG_{BH3} (kJ/mol):	-130.7
	4-CN	**2h**	2h.log	-340.246417	-340.188790
			bh3_2h.log	-366.884992	-366.797051
				ΔG_{BH3} (kJ/mol):	-129.3
	3,5-$(CF_3)_2$	**2i**	2i.log	-921.923968	-921.863313
			bh3_2i.log	-948.558534	-948.467577
				ΔG_{BH3} (kJ/mol):	-118.8
	3,4,5-$(Cl)_3$	**2j**	2j.log	-1626.635341	-1626.608150
			bh3_2j.log	-1653.269439	-1653.211890
				ΔG_{BH3} (kJ/mol):	-117.5
	3,5-$(F)_2$-4-CF_3	**2k**	2k.log	-783.403845	-783.361163
			bh3_2k.log	-810.036760	-809.963770
				ΔG_{BH3} (kJ/mol):	-114.5
	3,5-$(NO_2)_2$	**2l**	2l.log	-656.846806	-656.787791
			bh3_2l.log	-683.476479	-683.387257
				ΔG_{BH3} (kJ/mol):	-106.2
	4-Cl-3,5-$(NO_2)_2$	**2m**	2m.log	-1116.348325	-1116.300644
			bh3_2m.log	-1142.976501	-1142.898845
				ΔG_{BH3} (kJ/mol):	-102.9
	2,6-Me	**2n**	2n.log	-326.635224	-326.523532
			bh3_2n.log	-353.275512	-353.130321
				ΔG_{BH3} (kJ/mol):	-125.5
	Me	**3a**	3a.log	-132.647673	-132.626199
			bh3_3a.log	-159.272603	-159.222836
				ΔG_{BH3} (kJ/mol):	-98.8
	4-F-C_6H_4	**3b**	3b.log	-423.427299	-423.367386
			bh3_3b.log	-450.051296	-449.961957
				ΔG_{BH3} (kJ/mol):	-93.4
	4-MeO	**4a**	4a.log	-1378.946594	-1378.625288
			bh3_4a.log	-1405.591504	-1405.239627
				ΔG_{BH3} (kJ/mol):	-145.3
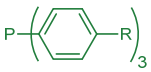	H	**4b**	4b.log	-1035.588730	-1035.357020
			bh3_4b.log	-1062.230358	-1061.968738
				ΔG_{BH3} (kJ/mol):	-138.4
	4-Cl	**4c**	4c.log	-2414.163212	-2413.965711
			bh3_4c.log	-2440.803224	-2440.575235
				ΔG_{BH3} (kJ/mol):	-132.7
	4-MeO	**5a**	5a.log	-499.035065	-498.899400
			bh3_5a.log	-525.657975	-525.492098
				ΔG_{BH3} (kJ/mol):	-88.5
	4-Me	**5b**	5b.log	-423.859519	-423.728844
			bh3_5b.log	-450.481111	-450.320387
				ΔG_{BH3} (kJ/mol):	-85.4
	4-Br	**5c**	5c.log	-2958.474380	-2958.381682
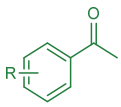			bh3_5c.log	-2985.093870	-2984.971115
				ΔG_{BH3} (kJ/mol):	-79.9
	4-CF_3	**5d**	5d.log	-721.508489	-721.403174
			bh3_5d.log	-748.126799	-747.991046
				ΔG_{BH3} (kJ/mol):	-75.8
	4-NO_2	**5e**	5e.log	-588.972745	-588.867934
			bh3_5e.log	-615.589804	-615.455082
				ΔG_{BH3} (kJ/mol):	-73.9
	3,5-NO_2	**5f**	5f.log	-793.360191	-793.255962
			bh3_5f.log	-819.974823	-819.840805

				ΔG_{BH3} (kJ/mol):	-67.9
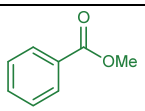		**6**	6.log bh3_6.log	-459.778391 -486.385602 ΔG_{BH3} (kJ/mol):	-459.668022 -486.245820 -49.4
	4-MeO	**7a**	7a.log bh3_7a.log	-459.750289 -486.373253 ΔG_{BH3} (kJ/mol):	-459.640878 -486.233653 -88.7
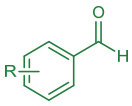	H	**7b**	7b.log bh3_7b.log	-345.295354 -371.915384 ΔG_{BH3} (kJ/mol):	-345.215736 -371.805519 -80.8
	4-Br	**7c**	7c.log bh3_7c.log	-2919.188659 -2945.807705 ΔG_{BH3} (kJ/mol):	-2919.122201 -2945.710780 -77.7
	4-NO_2	**7d**	7d.log bh3_7d.log	-549.686430 -576.302788 ΔG_{BH3} (kJ/mol):	-549.607758 -576.193642 -70.6
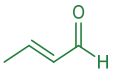		**8**	8.log bh3_8.log	-231.051410 -257.674619 ΔG_{BH3} (kJ/mol):	-230.990400 -257.583270 -88.9
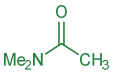		**9**	9.log bh3_9.log	-287.605958 -314.235888 ΔG_{BH3} (kJ/mol):	-287.506926 -314.106202 -105.7
$Et_3P{=}O$		**10**	10.log bh3_10.log	-653.944244 -680.580453 ΔG_{BH3} (kJ/mol):	-653.776810 -680.382227 -121.9

For the evaluation of experimental borane-catalyzed reactions, the BH_3 affinity ΔG_{BH3} (kJ/mol) of the divinyl ketone educt for the Nazarov cyclization and for methyl vinyl ketone (educt for the Diels-Alder and the Michael addition) were calculated.

Table S15: Borane affinities in dichloromethane at the SMD(DCM)/MN15/def2-TZVP level of theory for additional compounds.

Compound	Name	E_{tot} (hartree)	ΔG (hartree)
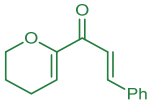	nazarov_starting.log bh3_nazarov_starting.log	-691.778042 -718.397500	-691.571430 -718.160161
		ΔG_{BH3} (kJ/mol):	-78.1
	methylvinylketon.log bh3_methylvinylketon.log	-231.053607 -257.673518	-230.992865 -257.582480
		ΔG_{BH3} (kJ/mol):	-80.4

7.7 References

[1] Fulmer, G. R.; Miller, A. J. M.; Sherden, N. H.; Gottlieb, H. E.; Nudelman, A.; Stoltz, B. M.; Bercaw, J. E.; Goldberg, K. I. NMR Chemical Shifts of Trace Impurities: Common Laboratory Solvents, Organics, and Gases in Deuterated Solvents Relevant to the Organometallic Chemist. *Organometallics* **2010**, *29*, 2176-2179.

[2] Piñeiro, A.; Muñoz, E.; Sabín, J.; Costas, M.; Bastos, M.; Velázquez-Campoy, A.; Garrido, P. F.; Dumas, P.; Ennifar, E.; García-Río, L.; Rial, J.; Pérez, D.; Fraga, P.; Rodríguez, A.; Cotelo, C. AFFINImeter: A software to analyze molecular recognition processes from experimental data. *Anal. Biochem.* **2019**, *577*, 117-134.

[3] Origin(Pro), Version 2018b. OriginLab Corporation, Northampton, MA, USA.

[4] Thordarson, P. Binding Constants and Their Measurement. In *Supramolecular Chemistry*, Gale, P. A.; Steed, J. W., Ed., Wiley: Chichester, UK, 2012, Vol. 2, pp 461-522.

[5] Wittig, G.; Herwig, W. Über neue Triaryl-bor-Verbindungen und ihre Tetraarylo-borat-Komplexe (V. Mitteil.). *Chem. Ber.* **1955**, ***88***, 962-976.

[6] Brown, H. C.; Racherla, U. S. Organoboranes. 43. A Convenient, Highly Efficient Synthesis of Triorganylboranes via a Modified Organometallic Route. *J. Org. Chem.* **1986**, *51*, 427-432.

[7] Krause, N.; Nobbe, P. Experimentelle Beiträge zum Valenz-Problem des Bors, VI.: Die Valenz-Äußerungen des Bors im Tri-p-anisyl-, tri-tert.-butyl- und Tri-sek.-propyl-bor, sowie Versuche über die Existenzfähigkeit gemischter Trialkylborverbindungen. *Chem. Ber.* **1931**, *64*, 2112-2116.

[8] Osseili, H.; Mukherjee, D.; Beckerle, K.; Spaniol T. P.; Okuda, J. Me_6TREN-Supported Alkali Metal Hydridotriphenylborates [(L)M][$HBPh_3$] (M = Li, Na, K): Synthesis, Structure, and Reactivity. *Organometallics* **2017**, *36*, 3029-3034.

[9] a) Yoon, N. M.; Kim, K. W. Reaction of potassium triphenylborohydride with selected organic compounds containing representative functional groups. *J. Org. Chem.* **1987**, *52*, 5564-5570; b) Nazarenko, N., Seidel, W. C. Process for the preparation of triarylborane. US Patent 4076756, **1975**.

[10] Krause, N. Über intensive gefärbtes Triphenylboryl-natrium, ein merkwürdiges Analogon zum Triphenylmethyl-natrium (Vorläufige Mitteilung). *Chem. Ber.* **1924**, *57*, 216-217.

[11] Borger, J. E.; Ehlers, A. W.; Lutz, M.; Slootweg, J. C.; Lammertsma, K. Stabilization and Transfer of the Transient [Mes*P4]− Butterfly Anion Using BPh3. *Angew. Chem. Int. Ed*. **2016**, *55*, 613-617.

[12] Santi, M.; Ould, D. M. C.; Wenz, J.; Soltani, Y.; Melen, R. L.; Wirth, T. Metal-Free Tandem Rearrangement/Lactonization: Access to 3,3-Disubstituted Benzofuran-2-(3H)-ones. *Angew. Chem. Int. Ed*. **2019**, *58*, 7861-7865.

[13] Leffler, J. E.; Watts, G. B.; Tanigaki, T.; Dolan, E.; Miller, D. S. Triarylboron anion radicals and the reductive cleavage of boron compounds. *J. Am. Chem. Soc.* **1970**, *92*, 6825-6830.

[14] Yin, Q.; Soltani, Y.; Melen, R. L.; Oestreich, M. $BArF_3$-Catalyzed Imine Hydroboration with Pinacolborane Not Requiring the Assistance of an Additional Lewis Base. *Organometallics* **2017**, *36*, 2381-2384.

[15] Lancaster, S. Alkylation of boron trifluoride with pentafluorphenyl Grignard reagent; Tri(pentafluorophenyl)boron; borane. *ChemSpider,* Synthetic Page 215, doi: 10.1039/SP215.

[16] Govorchin, S. W.; Kana'an, A. S.; Kanamueller, J. M. Sublimation study of triphenyl boron and the bond-dissociation enthalpy of B-C6H5. *J. Chem. Thermodyn*. **1984**, *16*, 703-710.

[17] Plažek, E. Ueber eine Synthese des 3,5-Dinitropyridins. *Recl. Trav. Chim. Pays-Bas* **1953***, 72*, 569-575.

[18] Winkler, M.; Cakir, B.; Sander, W. 3,5-Pyridyne – A Heterocyclic *meta*-Benzyne Derivative. *J. Am. Chem. Soc.* **2004**, *126*, 6135-6149.

[19] Brignell, P. J.; Katritzky, A. R.; Tarhan, H. O. The kinetics and mechanism of electrophilic substitution of heteroaromatic compounds. Part XVII. The nitration of pyridines. *J. Chem. Soc. B* **1968**, 1477-1484.

[20] De Rycke, N; Berionni, G.; Couty, F.; Mayr, H.; Goumont, R.; David, O. R. P. Synthesis and Reactivity of Highly Nucleophilic Pyridines. *Org. Lett.* **2011**, *13*, 530-533.

[21] Bailey, A. S.; Heaton, M. W.; Murphy, J. I. The preparation of a nitropyrido[3,4-c]furoxan: 7-nitro[1,2,5]oxadiazolo-[3,4-c]pyridine 3-oxide. *J. Chem. Soc. C* **1971**, 1211-1213.

[22] Liang, G., Gradl, S. N., Trauner, D. Efficient Nazarov Cyclizations of 2-Alkoxy-1,4-pentadien-3-ones. *Org. Lett*. **2003**, *5*, 4931-4934.

[23] Koenig, J. J., Arndt, T., Gildemeister, N., Neudörfl, J.-M., Breugst, M. Iodine-Catalyzed Nazarov Cyclizations. *J. Org. Chem*. **2019**, *84***,** 7587-7605.

[24] Schmidt, R. K., Müther, K., Mück-Lichtenfeld, C., Grimme, S., Oestreich, M. Silylium Ion-Catalyzed Challenging Diels-Alder Reactions: The Danger of Hidden Proton Catalysis with Strong Lewis Acids. *J. Am. Chem. Soc.* **2012**, *134*, 4421-4428.

[25] Li, W., Werner, T. $B(C_6F_5)_3$-Catalyzed Michael Reactions: Aromatic C−H as Nucleophiles. *Org. Lett*. **2017**, *19*, 2568-2571.

[26] Harder, E.; Damm, W.; Maple, J.; Wu, C.; Reboul, M.; Xiang, J. Y.; Wang, L.; Lupyan, D.; Dahlgren, M. K.; Knight, J.L.; Kaus, J. W.; Cerutti, D. S.; Krilov, G.; Jorgensen, W. L.; Abel, R.; Friesner, R. A. OPLS3: A Force Field Providing Broad Coverage of Drug-like Small Molecules and Proteins. *J. Chem. Theory Comput.* **2016**, *12*, 281–296.

[27] Schrödinger Release 2019-4: MacroModel, Schrödinger, LLC, New York, NY (2019).

[28] Gaussian 16, Revision A.03, Frisch, M. J.; Trucks, G. W.; Schlegel, H. B.; Scuseria, G. E.; Robb, M. A.; Cheeseman, J. R.; Scalmani, G.; Barone, V.; Petersson, G. A.; Nakatsuji, H.; Li, X.; Caricato, M.; Marenich, A. V.; Bloino, J.; Janesko, B. G.; Gomperts, R.; Mennucci, B.; Hratchian, H. P.; Ortiz, J. V.; Izmaylov, A. F.; Sonnenberg, J. L.; Williams-Young, D.; Ding, F.; Lipparini, F.; Egidi, F.; Goings, J.; Peng, B.; Petrone, A.; Henderson, T.; Ranasinghe, D.; Zakrzewski, V. G.; Gao, J.; Rega, N.; Zheng, G.; Liang, W.; Hada, M.; Ehara, M.; Toyota, K.; Fukuda, R.; Hasegawa, J.; Ishida, M.; Nakajima, T.; Honda, Y.; Kitao, O.; Nakai, H.; Vreven, T.; Throssell, K.; Montgomery, J. A., Jr.; Peralta, J. E.; Ogliaro, F.; Bearpark, M. J.; Heyd, J. J.; Brothers, E. N.; Kudin, K. N.; Staroverov, V. N.; Keith, T. A.; Kobayashi, R.; Normand, J.; Raghavachari, K.; Rendell, A. P.; Burant, J. C.; Iyengar, S. S.; Tomasi, J.; Cossi, M.; Millam, J. M.; Klene, M.; Adamo, C.; Cammi, R.; Ochterski, J. W.; Martin, R. L.; Morokuma, K.; Farkas, O.; Foresman, J. B.; Fox, D. J. Gaussian, Inc., Wallingford CT (2016).

[29] Marenich, A. V.; Cramer, C. J.; Truhlar, D. G. Universal Solvation Model Based on Solute Electron Density and on a Continuum Model of the Solvent Defined by the Bulk Dielectric Constant and Atomic Surface Tensions. *J. Phys. Chem. B* **2009**, *113*, 6378–6396.

[30] Becke, A. D. Density-functional thermochemistry. III. The role of exact exchange. *J. Chem. Phys.* **1993**, *98*, 5648–5652.

[31] S. Grimme, S. Ehrlich, L. Goerigk, Effect of the damping function in dispersion corrected density functional theory. *J. Comput. Chem.* **2011**, *32*, 1456-1465.

[32] Weigend, F.; Ahlrichs, R. Balanced basis sets of split valence, triple zeta valence and quadruple zeta valence quality for H to Rn: Design and assessment of accuracy. *Phys. Chem. Chem. Phys.* **2005**, *7*, 3297-3305.

[33] Grimme, S. Supramolecular Binding Thermodynamics by Dispersion-Corrected Density Functional Theory. *Chem. Eur. J.* **2012**, *18*, 9955-9964.

[34] Yu, H. S.; He, X.; Li, Shaohong L.; Truhlar, D. G. MN15: A Kohn–Sham global-hybrid exchange–correlation density functional with broad accuracy for multi-reference and single-reference systems and noncovalent interactions. *Chem. Sci.* **2016**, *7*, 5032-5051.

[35] Greb, L. Lewis Superacids: Classifications, Candidates, and Applications. *Chem. Eur. J.* **2018**, *24*, 17881-17896.

[36] Böhrer, H.; Trapp, N.; Himmel, D.; Schlepp, M.; Krossing, I. From unsuccessful H_2-activation with FLPs containing $B(Ohfip)_3$ to a systematic evaluation of the Lewis acidity of 33 Lewis acids based on fluoride, chloride, hydride and methyl ion affinities. *Dalton Trans.* **2015**, *44*, 7489-7499.

[37] a) Becke, A. D. Density-functional exchange-energy approximation with correct asymptotic behavior. *Phys. Rev. A* **1988**, *38*, 3098-3100; b) Perdew. J. P. Density-functional approximation for the correlation energy of the inhomogeneous electron gas. *Phys. Rev. B* **1986**, *33*, 8822-8824; c) Perdew, J. P. Erratum: Density-functional approximation for the correlation energy of the inhomogeneous electron gas. *Phys. Rev. B* **1986**, *34*, 7406-7406.

[38] Jupp, A. R., Johnstone, T. C., Stephan, D. W. The global electrophilicity index as a metric for Lewis acidity. *Dalton Trans.* **2018**, *47*, 7029-7035.

[39] Parr, R. G., v. Szentpály, L., Liu, S. Electrophilicity Index. *J. Am. Chem. Soc.* **1999**, *121*, 1922-1924.